

Casein kinases in human diseases

Edited by

Andrea Venerando, Giorgio Cozza, Victor Bustos
and Lorenzo Alberto Pinna

Published in

Frontiers in Molecular Biosciences
Frontiers in Cell and Developmental Biology



FRONTIERS EBOOK COPYRIGHT STATEMENT

The copyright in the text of individual articles in this ebook is the property of their respective authors or their respective institutions or funders. The copyright in graphics and images within each article may be subject to copyright of other parties. In both cases this is subject to a license granted to Frontiers.

The compilation of articles constituting this ebook is the property of Frontiers.

Each article within this ebook, and the ebook itself, are published under the most recent version of the Creative Commons CC-BY licence. The version current at the date of publication of this ebook is CC-BY 4.0. If the CC-BY licence is updated, the licence granted by Frontiers is automatically updated to the new version.

When exercising any right under the CC-BY licence, Frontiers must be attributed as the original publisher of the article or ebook, as applicable.

Authors have the responsibility of ensuring that any graphics or other materials which are the property of others may be included in the CC-BY licence, but this should be checked before relying on the CC-BY licence to reproduce those materials. Any copyright notices relating to those materials must be complied with.

Copyright and source acknowledgement notices may not be removed and must be displayed in any copy, derivative work or partial copy which includes the elements in question.

All copyright, and all rights therein, are protected by national and international copyright laws. The above represents a summary only. For further information please read Frontiers' Conditions for Website Use and Copyright Statement, and the applicable CC-BY licence.

ISSN 1664-8714
ISBN 978-2-83251-067-4
DOI 10.3389/978-2-83251-067-4

About Frontiers

Frontiers is more than just an open access publisher of scholarly articles: it is a pioneering approach to the world of academia, radically improving the way scholarly research is managed. The grand vision of Frontiers is a world where all people have an equal opportunity to seek, share and generate knowledge. Frontiers provides immediate and permanent online open access to all its publications, but this alone is not enough to realize our grand goals.

Frontiers journal series

The Frontiers journal series is a multi-tier and interdisciplinary set of open-access, online journals, promising a paradigm shift from the current review, selection and dissemination processes in academic publishing. All Frontiers journals are driven by researchers for researchers; therefore, they constitute a service to the scholarly community. At the same time, the *Frontiers journal series* operates on a revolutionary invention, the tiered publishing system, initially addressing specific communities of scholars, and gradually climbing up to broader public understanding, thus serving the interests of the lay society, too.

Dedication to quality

Each Frontiers article is a landmark of the highest quality, thanks to genuinely collaborative interactions between authors and review editors, who include some of the world's best academicians. Research must be certified by peers before entering a stream of knowledge that may eventually reach the public - and shape society; therefore, Frontiers only applies the most rigorous and unbiased reviews. Frontiers revolutionizes research publishing by freely delivering the most outstanding research, evaluated with no bias from both the academic and social point of view. By applying the most advanced information technologies, Frontiers is catapulting scholarly publishing into a new generation.

What are Frontiers Research Topics?

Frontiers Research Topics are very popular trademarks of the *Frontiers journals series*: they are collections of at least ten articles, all centered on a particular subject. With their unique mix of varied contributions from Original Research to Review Articles, Frontiers Research Topics unify the most influential researchers, the latest key findings and historical advances in a hot research area.

Find out more on how to host your own Frontiers Research Topic or contribute to one as an author by contacting the Frontiers editorial office: frontiersin.org/about/contact

Casein kinases in human diseases

Topic editors

Andrea Venerando — University of Udine, Italy

Giorgio Cozza — University of Padua, Italy

Victor Bustos — The Rockefeller University, United States

Lorenzo Alberto Pinna — Institute of Neuroscience, National Research Council, Italy

Citation

Venerando, A., Cozza, G., Bustos, V., Pinna, L. A., eds. (2023). *Casein kinases in human diseases*. Lausanne: Frontiers Media SA. doi: 10.3389/978-2-83251-067-4

Table of contents

- 06 **Editorial: Casein kinases in human diseases**
Andrea Venerando, Victor H. Bustos, Lorenzo A. Pinna and Giorgio Cozza
- 12 **Fam20C in Human Diseases: Emerging Biological Functions and Therapeutic Implications**
Rongsheng Xu, Huidan Tan, Jiahui Zhang, Zhaoxin Yuan, Qiang Xie and Lan Zhang
- 21 **Identification of the Host Substratome of *Leishmania*-Secreted Casein Kinase 1 Using a SILAC-Based Quantitative Mass Spectrometry Assay**
Despina Smirlis, Florent Dingli, Valentin Sabatet, Aileen Roth, Uwe Knippschild, Damarys Loew, Gerald F. Späth and Najma Rachidi
- 35 **Inhibition of Protein Kinase CK2 Affects Thymidylate Synthesis Cycle Enzyme Level and Distribution in Human Cancer Cells**
Patrycja Wińska, Łukasz Widło, Elżbieta Senkara, Mirosława Koronkiewicz, Jarosław M. Cieśla, Alicja Krzyśko, Katarzyna Skierka and Joanna Cieśla
- 48 **CIGB-300-Regulated Proteome Reveals Common and Tailored Response Patterns of AML Cells to CK2 Inhibition**
Mauro Rosales, Arielis Rodríguez-Ulloa, George V. Pérez, Vladimir Besada, Thalia Soto, Yassel Ramos, Luis J. González, Katharina Zettl, Jacek R. Wiśniewski, Ke Yang, Yasser Perera and Silvio E. Perea
- 60 **Structural and Enzymological Evidence for an Altered Substrate Specificity in Okur-Chung Neurodevelopmental Syndrome Mutant CK2 $\alpha^{Lys198Arg}$**
Christian Werner, Alexander Gast, Dirk Lindenblatt, Anna Nickelsen, Karsten Niefind, Joachim Jose and Jennifer Hochscherf
- 74 **The Okur-Chung Neurodevelopmental Syndrome Mutation CK2 $K198R$ Leads to a Rewiring of Kinase Specificity**
Danielle M. Caefer, Nhat Q. Phan, Jennifer C. Liddle, Jeremy L. Balsbaugh, Joseph P. O'Shea, Anastasios V. Tzingounis and Daniel Schwartz
- 83 **Comparing Two Neurodevelopmental Disorders Linked to CK2: Okur-Chung Neurodevelopmental Syndrome and Poirier-Bienvenu Neurodevelopmental Syndrome—Two Sides of the Same Coin?**
Demetra Ballardín, Jose M. Cruz-Gamero, Thierry Bienvenu and Heike Rebholz
- 98 **Mechanism of CK2 Inhibition by a Ruthenium-Based Polyoxometalate**
Simone Fabbian, Gabriele Giachin, Massimo Bellanda, Christian Borgo, Maria Ruzzene, Giacomo Spuri, Ambra Campofelice, Laura Veneziano, Marcella Bonchio, Mauro Carraro and Roberto Battistutta

- 113 **Casein Kinase 1 and Human Disease: Insights From the Circadian Phosphoswitch**
Joel C. Francisco and David M. Virshup
- 121 **Copper Modulates the Catalytic Activity of Protein Kinase CK2**
John E. Chojnowski, Rongrong Li, Tiffany Tsang, Fatimah H. Alfaran, Alexej Dick, Simon Cocklin, Donita C. Brady and Todd I. Storchlic
- 132 **Chemical Genetic Validation of CSNK2 Substrates Using an Inhibitor-Resistant Mutant in Combination with Triple SILAC Quantitative Phosphoproteomics**
Laszlo Gyenis, Daniel Menyhart, Edward S. Cruise, Kristina Jurcic, Scott E. Roffey, Darren B. Chai, Flaviu Trifoi, Sam R. Fess, Paul J. Desormeaux, Teresa Núñez de Villavicencio Díaz, Adam J. Rabalski, Stephanie A. Zukowski, Jacob P. Turowec, Paula Pittock, Gilles Lajoie and David W. Litchfield
- 150 **Comprehensive Characterization of CK1 δ -Mediated Tau Phosphorylation in Alzheimer's Disease**
Aileen Roth, Annabelle Sander, Marleen Silke Oswald, Fabian Gärtner, Uwe Knippschild and Joachim Bischof
- 166 **CK2 β Is a Gatekeeper of Focal Adhesions Regulating Cell Spreading**
Odile Filhol, Anne-Marie Hesse, Anne-Pascale Bouin, Corinne Albigès-Rizo, Florian Jeanneret, Christophe Battail, Delphine Pflieger and Claude Cochet
- 180 **Implementing a Scoring Function Based on Interaction Fingerprint for Autogrow4: Protein Kinase CK1 δ as a Case Study**
Matteo Pavan, Silvia Menin, Davide Bassani, Mattia Sturlese and Stefano Moro
- 197 **Casein Kinase 2 Signaling in White Matter Stroke**
Hung Nguyen, Wenbin Zhu and Selva Baltan
- 208 **Protein Kinase CK2 represents a new target to boost Ibrutinib and Venetoclax induced cytotoxicity in mantle cell lymphoma**
Sabrina Manni, Maria Pesavento, Zaira Spinello, Lara Saggin, Arash Arjomand, Anna Fregnani, Laura Quotti Tubi, Greta Scapinello, Carmela Gurrieri, Gianpietro Semenzato, Livio Trentin and Francesco Piazza
- 221 **The protein kinase CK1: Inhibition, activation, and possible allosteric modulation**
Yashoda Krishna Sunkari, Laurent Meijer and Marc Flajolet

- 231 **CK2 and protein kinases of the CK1 superfamily as targets for neurodegenerative disorders**
Andrea Baier and Ryszard Szyszka
- 259 **Predictive functional, statistical and structural analysis of *CSNK2A1* and *CSNK2B* variants linked to neurodevelopmental diseases**
Prasida Unni, Jack Friend, Janice Weinberg, Volkan Okur, Jennifer Hochscherf and Isabel Dominguez



OPEN ACCESS

EDITED BY

William C. Cho,
QEH, Hong Kong SAR, China

REVIEWED BY

Sourav Banerjee,
University of Dundee, United Kingdom
Zheng Ruan,
Van Andel Research Institute (VARI),
United States
David Litchfield,
Western University, Canada

*CORRESPONDENCE

Andrea Venerando,
andrea.venerando@unipd.it
Victor H. Bustos,
vbustos@rockefeller.edu
Lorenzo A. Pinna,
lorenzo.pinna@unipd.it
Giorgio Cozza,
giorgio.cozza@unipd.it

SPECIALTY SECTION

This article was submitted to Molecular
Diagnostics and Therapeutics,
a section of the journal
Frontiers in Molecular Biosciences

RECEIVED 10 November 2022

ACCEPTED 24 November 2022

PUBLISHED 02 December 2022

CITATION

Venerando A, Bustos VH, Pinna LA and
Cozza G (2022), Editorial: Casein kinases
in human diseases.
Front. Mol. Biosci. 9:1094922.
doi: 10.3389/fmolb.2022.1094922

COPYRIGHT

© 2022 Venerando, Bustos, Pinna and
Cozza. This is an open-access article
distributed under the terms of the
[Creative Commons Attribution License](#)
(CC BY). The use, distribution or
reproduction in other forums is
permitted, provided the original
author(s) and the copyright owner(s) are
credited and that the original
publication in this journal is cited, in
accordance with accepted academic
practice. No use, distribution or
reproduction is permitted which does
not comply with these terms.

Editorial: Casein kinases in human diseases

Andrea Venerando^{1*}, Victor H. Bustos^{2*}, Lorenzo A. Pinna^{3*}
and Giorgio Cozza^{4*}

¹Department of Comparative Biomedicine and Food Science, Agripolis Campus, University of Padova, Legnaro, Italy, ²Fisher Drug Discovery Resource Center, The Rockefeller University, New York, NY, United States, ³CNR Neuroscience Institute, Padova, Italy, ⁴Department of Molecular Medicine, University of Padova, Padova, Italy

KEYWORDS

casein kinase, CK1, CK2, Fam20C, protein kinase, phosphorylation, G-CK

Editorial on the Research Topic

Casein kinases in human diseases

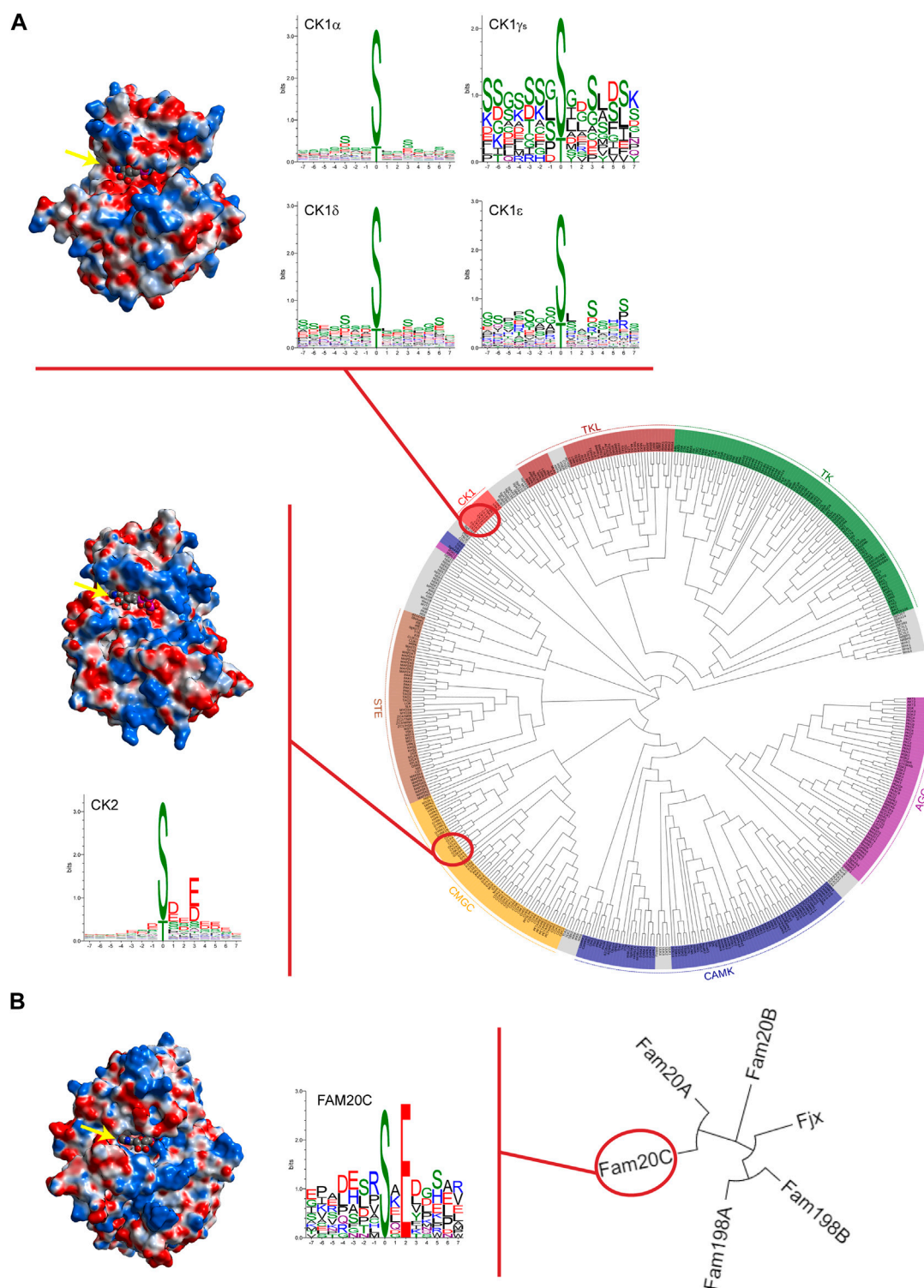
Introduction

140 years after the discovery of the first phosphoprotein (i.e., casein), the research on protein kinases (in humans about 500 enzymes that catalyse the transfer of phosphate from ATP to proteins) represents an evergreen field in the scientific landscape and the journey into the dissection of their crucial biological roles continues to unveil new breath-taking scenarios.

In such a context, so called “casein kinases,” a heterogeneous category of phylogenetically distant acidophilic protein kinases (namely CK1, CK2, and Fam20C, see [Figure 1](#) for an overview) that share the ability to phosphorylate casein *in vitro*, represent an appealing Research Topic in which unanticipated pathophysiological aspects of these enzymes are continuously emerging.

The extraordinary pleiotropicity of casein kinases reflects their involvement in a wide variety of both physiological and pathological processes. Indeed, the dramatic effects of casein kinases dysregulation have been observed in several pathologies, including cancer, neurodegenerative disorders, viral and parasite infections, and biomineralization diseases among others ([Venerando et al., 2014](#)). Therefore, the specific tuning of casein kinases is considered instrumental to counteract many pathological conditions.

This Research Topic, composed of thirteen original research papers, five review articles, and one mini review, provides an up-to-date snapshot of the ongoing research in the casein kinases field shedding light on their implication in human diseases as well as on innovative strategies to modulate their activity.

**FIGURE 1**

Casein kinases at a glance. **(A)** Phylogenetic dendrogram of the human kinome in which major groups of canonical protein kinases are labelled and coloured. Protein kinases CK1 and CK2 are highlighted. In the upper part, CK1δ tridimensional structure (PDB code 7P7H) is reported as an illustrative example of the CK1 family comprising six different isoforms and WebLogos for each isoform are depicted. For CK1γ isoforms (namely CK1γ1, CK1γ2, and CK1γ3), a single WebLogo of merged substrate sequences phosphorylated by the three isoforms is displayed. In the lower part, crystal structure of a catalytic subunit of protein kinase CK2 (PDB code 3WOW) and WebLogo analysis of CK2 holoenzyme's known substrates are reported. **(B)** Phylogenetic tree of the Four-Jointed family of atypical protein kinases. Due to their altered amino acid sequences in respect to the

(Continued)

FIGURE 1 (Continued)

canonical kinases, none of these atypical kinases has been included in the human kinome. On the left, Fam20C crystal structure (PDB code 4KQB) and its own WebLogo. Fam20C is the Genuine Casein Kinase (G-CK) responsible for phosphorylating the majority of secreted proteins. WebLogo analysis was performed on human protein sequences phosphorylated by casein kinases as reported on PhosphositePlus[®] database (www.phosphosite.org). Note that WebLogos evidence the acidophilic nature of casein kinases as suggested by the residues surrounding the phosphorylation site (in position "0"), either downstream or upstream. Analytic Connolly's electrostatic charge distribution surface was obtained through the MOE 2020.09 software. Blue colour indicates positive surface charges whereas red colour indicates negative surface charges. It is worth to note that in the case of CK2, an extensive basic region (in blue) is present both above and below the ATP binding site (indicated by yellow arrow) protruding towards the right side. Conversely, in the case of Fam20C and CK1 δ , the basic region is much less extensive and is located, in both cases, in a region underlying the ATP pocket; in addition, for CK1 only, a positively charged region is present on the upper left side. The trend of the arrangement of the basic residues evidenced by the electrostatic surfaces are in perfect agreement with the consensus sequences revealed by the WebLogos. Phylogenetic trees were drawn using EvolView program (www.evolgenius.info).

Protein kinase CK1

Casein kinase 1 (CK1 or CKI) is a family of protein kinases of the human kinome (Figure 1A) that function in diverse biological pathways, and the regulation of which is just beginning to be understood.

In this Research Topic, novel information on the role of CK1 in Alzheimer's disease, in the circadian rhythm, and in Leishmaniasis is provided, as well as a review on the role of casein kinases in neurodegenerative diseases. Finally, cutting-edge methods to generate isoform specific CKI modulators are proposed.

Alzheimer's disease is a degenerative disease that affects the brain. One of the main pathological events in Alzheimer's disease is the generation of neurofibrillary tangles that are formed when the tau protein becomes hyperphosphorylated and aggregates. It is suspected that members of the protein kinase CK1 family are involved in the pathogenesis of Alzheimer's disease, as they can phosphorylate tau. Roth et al. analysed recombinant tau441 phosphorylated *in vitro* by CK1 δ via mass spectrometry and identified ten potential phosphorylation sites, five of which are associated with Alzheimer's disease. *In vitro* kinase assays and two-dimensional phosphopeptide analyses were performed with tau441 phospho-mutants confirming that Alzheimer's disease-associated residues Ser68/Thr71 and Ser289 are CK1 δ -specific phosphorylation sites. Finally, the use of an *in vitro* tau aggregation assay suggested that CK1 δ represents a good target for the prevention of Alzheimer's disease.

An overview of the impact of CK1, TTBK, and CK2 kinases on neurodegenerative diseases as well as a summary of their substrates and inhibitors has been presented by Baier and Szyszka.

An interesting observation is reviewed by Francisco and Virshup. The authors highlighted that, among kinases, CK1 is unique in that substrate specificity is altered by its own phosphorylation state. A telling example is provided by the PERIOD2 (PER2) phosphoswitch: in this case, CK1 δ/ϵ kinase activity can be varied between three different substrate motifs to regulate the circadian clock.

Compelling novel results are presented by Smirlis et al., which developed a technology that allows efficient identification of substrates in the context of Leishmaniasis. Leishmaniasis is a severe public health problem caused by the protozoan *Leishmania*. To get insights into the functions of L-CK1.2 in the macrophage, the systematic identification of its host substrates was performed, leading to the identification of 225 host substrates as well as a potential novel phosphorylation motif for CK1. The L-CK1.2 substratome is enriched upon *Leishmania* infection, suggesting that L-CK1.2 might be a master regulator of this process.

Sunkari et al. offer a cutting-edge proposal to find isoform specific modulators, an especially thorny issue considering the high degree of conservation of the ATP-binding site among CK1 isoforms and the fact that all available CK1 inhibitors are ATP site-directed. The authors proposed that the DNA-encoded library (DEL) technology might represent a valuable approach to uncover allosteric modulators instead of ATP competitors.

Finally, in the research scenario of computational methodologies for the identification of novel molecules with therapeutic potential, Pavan et al. investigated CK1 δ as a target for the development of an implemented version of Autogrow4 docking software with an alternative scoring function based on protein-ligand interaction fingerprints.

Protein kinase CK2

The constitutively active casein kinase 2 (CK2 or CKII) has been among the first identified protein kinases (Venerando et al., 2017). CK2, belonging to the class of CMGC protein kinases, is part of the human kinome. The CK2 hetero-tetrameric enzyme, composed of two catalytic (α and/or α') and two regulatory (β) subunits encoded by CSNK2A1 (and/or CSNK2A2) and CSNK2B genes, respectively, is considered a "lateral player" in several signaling pathways (Borgo et al., 2021). Notably, the "regulatory" functions of β subunits are not restricted at preserving the enzyme stability and driving the substrates

specificity. Conversely, it has been proposed that unbalanced expression of CK2 subunits prompts epithelial to mesenchymal transition fostering cancer invasion and spreading. In particular, [Filhol et al.](#) showed that CK2 β loss promotes focal adhesion formation and invasion by triggering pTyr signaling and activation of the FAK1-Src-PAX1 pathway suggesting a key role of CK2 β in controlling cancer progression and metastasis formation.

An interesting role of copper as an enhancer of CK2 activity has recently emerged. [Chojnowski et al.](#) suggested that the ability of copper to increase CK2 activity occurs only if the phosphate donor is ATP and not GTP. This effect is counteracted by the copper chelator Cu-ATSM and increases or decreases of intracellular copper level raises or reduces CK2 signaling. Note that the two identified residues essential for copper-binding (Met153 and His154) are conserved in many kinases and consequently further systematic studies are required to assess the possible role of copper as a physiological regulator of other kinases.

Although CK2 malfunctions have been described in many different pathologies, its role in the pathogenesis of various cancers deserves special attention, as it appears to correlate to almost all malignant hallmarks. CK2 is overexpressed in many cancer cells where it potentiates other oncogenic signals and overall sustains tumorigenesis. Especially in haematological malignancies, overexpression and pro-oncogenic functions of CK2 have been widely reported. As an example, [Manni et al.](#) demonstrated that in mantle cell lymphoma, overexpressed CK2 sustains BCR signaling and Bcl-2 family proteins. Note that BCR signaling and Bcl-2 related pro-survival pathways are considered rational therapeutic targets in B cell derived lymphomas; most importantly, CK2 inhibition enhances cytotoxicity induced by the combination of chemical inhibitors directed against both pathways.

Downregulating a constitutively active enzyme generally overexpressed in malignant cells, represents a reasonable strategy to treat related diseases ([Borgo et al., 2021](#)) and during the last decades several CK2 inhibitors have been proposed. Two of them, namely CX-4945 and CIGB-300, are already in human clinical trials as anticancer drugs. In this respect, the research on the peptide-based inhibitor CIGB-300 by [Rosales et al.](#) has disclosed its antileukemic effect. Coupling LC-MS/MS data and bioinformatics in two human cell lines (HL-60 and OCI-AML3), the authors revealed that CIGB-300 promotes oxidative stress and ROS production, which might play a relevant role on CIGB-300-induced apoptosis.

From a different point of view, metal-oxide polyanionic clusters called polyoxometalates (POMs) have been previously identified as CK2 inhibitors in the nanomolar range. Nevertheless, their mechanism of action was a matter of study until today. In fact, a recent study by [Fabbian et al.](#) on ruthenium-based polyoxometalate (Ru4POM) has deciphered the mechanism of action of these unconventional inhibitors

demonstrating that it involves both CK2 α and CK2 α 2 β 2 tetramer with which the inhibitor forms stable complexes by interacting with the substrate binding site.

The employment of specific CK2 inhibitors has found an additional application for the identification and validation of CK2 substrates. [Gyenis et al.](#), using quantitative phosphoproteomics of cells expressing inhibitor-resistant CK2 α mutant in comparison with its wild type counterpart, have been able to identify *bona fide* targets among CK2 putative substrates, thus overcoming the caveat that ATP site-directed inhibitors invariably display off-target effect given the high conservation of the ATP site among protein kinases. Interestingly, this strategy has the potential to be successfully applied also to the identification of *bona fide* substrates of other protein kinases.

A different perspective is given by the recent discovery that thymidylate synthase (TS) and dihydrofolate reductase (DHFR) are phosphorylated by CK2, paving the road toward an in-depth study of the role of CK2 in the di- and trimolecular complexes formation between TS, DHFR and hydroxymethyltransferase (SHMT), responsible for the thymidylate synthesis. In particular, [Wińska et al.](#) demonstrated that CK2 inhibition by CX-4945 leads to increased level of DHFR and SHMT possibly through a decrease of their ubiquitination; on the contrary, CK2 inhibition has an opposite impact on TS causing a decrease of the protein level. Moreover, the phosphorylation of TS increases the stability of its complex with SHMT1 and DHFR in comparison to non-phosphorylated TS.

Considering the high number of substrates and the ubiquity of CK2, it appears clear that CK2 regulates many cellular functions and its activity is considered essential for cellular homeostasis in different tissues. It has been suggested that CK2 (at least its α subunit) is more abundant in brain than in other tissues and its role in the brain is recognized as vital for neurological development and functioning. As an example, [Nguyen et al.](#) proposed that CK2 signaling is responsible for the activation of a spatiotemporal cascade pathway that mediates ischemic injury in white matter.

It should be stressed that several neurodegeneration-related CK2 targets have been identified so far suggesting a link (either pathogenic or protective) between CK2 and different well-acknowledged neurodegenerative diseases. Recently, two newly identified rare neurodevelopmental disorders have been associated to mutations in the genes encoding either the α catalytic (in the Okur-Chung neurodevelopmental syndrome, OCNDS) or the β regulatory (in the Poirier-Bienvenu neurodevelopmental syndrome, POBINDS) subunits of CK2. In OCNDS patients, one of the most frequently observed mutation is lysine-198 to arginine exchange (K198R) in the P+1 activation loop of CK2 α . [Caefer et al.](#) demonstrated that K198R mutant is still an active enzyme even though it presents a different substrate specificity in comparison to the wild type kinase. The change in the kinase specificity is mainly due to a

shift of the anion binding site harboured by the P+1 loop rather than by an altered interaction between the catalytic with the non-catalytic subunits in the CK2 holoenzyme, as revealed by the K198R mutant crystal structure presented by [Werner et al.](#)

Although the two syndromes display very similar clinical manifestations, it has been possible to rationalize the diagnosis based on clinical symptomatology in comparison with preclinical and biochemical CK2 characterization, as described by [Ballardin et al.](#) Finally, [Unni et al.](#), integrating information on the CK2 genes mutations discovered in OCNDs and POBIND patients with experimental data, have provided useful predictive tools that allow a better understanding of the functional and structural consequences of such mutations.

Atypical protein kinase Fam20C

Family with sequence similarity 20 member C also known as Fam20C or DMP4 is a protein, recently identified as the Genuine Casein Kinase (G-CK or GEF-CK), especially abundant in the Golgi apparatus of the lactating mammary gland ([Tagliabracci et al., 2012](#)). Fam20C is an atypical serine protein kinase that possess little sequence similarity to canonical protein kinases present in the human kinome. Fam20C phosphorylates not only casein but also highly acidic secreted proteins with the common consensus motif S-x-E/pS ([Lasa-Benito et al., 1996](#)). Although Fam20C is far from the other two casein kinases both structurally and phylogenetically ([Figure 1](#)), it shares with them the extraordinary pleiotropicity. Indeed, Fam20C is the major contributor in the generation of the human phosphosecretome, the pool of phosphorylated secreted proteins ([Tagliabracci et al., 2015](#)). From this point of view, [Xu et al.](#) reviewed the structure and biological functions of Fam20C with special reference to its ability to phosphorylate secreted proteins. The important role of Fam20C in biomineralization has been addressed being Fam20C implicated in the phosphorylation of the small integrin binding ligand-N-linked glycoproteins (SIBLINGs), dentin matrix protein 1, matrix extracellular phosphoglycoprotein, osteopontin, bone sialoprotein, and dentin sialophosphoprotein. The best-known and dramatic consequence of Fam20C aberrant function in biomineralization is epitomized by the Raine syndrome, a lethal osteosclerotic bone dysplasia. However, the phosphorylation of multiple substrates by Fam20C justifies its role in many other life processes and its implication in several diseases, such as in smooth muscle cell calcification and frontotemporal dementia, have been discovered recently. In addition, cardiovascular implications of Fam20C is inferred from the phosphorylation of calsequestrin 2, matrix interacting molecule 1, and fibroblast growth factor 23, connecting this atypical protein kinase to heart and neurovascular diseases. Finally, the phosphorylation by Fam20C of insulin-like growth factor binding proteins and osteopontin reveals the role of Fam20C in tumorigenesis. Notwithstanding, the regulation mechanism of Fam20C activity is still a matter of study and, unfortunately, no contributions have been submitted to

this Research Topic to shed additional light on this intricate matter. In the past, two possible mechanisms not mutually exclusive have been proposed. One is the association of Fam20C with Fam20A, a Fam20C paralog with no kinase activity by itself but able to increase the activity of Fam20C ([Cui et al., 2015](#)); another mechanism appears to exploit sphingosine and some related compounds to stimulate Fam20C kinase activity ([Cozza et al., 2017](#)). In this respect, it should be noted that stimulation rather than inhibition of this atypical protein kinase appears to represent a valuable pharmacological strategy. Indeed, Fam20C-linked diseases are generally a consequence of its defective expression or activity. We hope that this review stimulates the scientific community to deepen the research on Fam20C as an important therapeutic target.

Author contributions

All authors listed have made a substantial, direct, and intellectual contribution to the work and approved it for publication.

Funding

We acknowledge support from Fondazione AIRC per la Ricerca sul Cancro (grant IG18756 to LP), Supporting TAlent in ReSearch (grant COZZ_STARS20_01 to GC) and the Italian Cystic Fibrosis Research Foundation (grant FFC#4/2019 to GC).

Acknowledgments

We are deeply indebted with all the authors and reviewers for their valuable contribution to this Research Topic. Finally, we would like to acknowledge Luca Cesaro (University of Padova) for his technical support.

Conflict of interest

The authors declare that the research was conducted in the absence of any commercial or financial relationships that could be construed as a potential conflict of interest.

Publisher's note

All claims expressed in this article are solely those of the authors and do not necessarily represent those of their affiliated organizations, or those of the publisher, the editors and the reviewers. Any product that may be evaluated in this article, or claim that may be made by its manufacturer, is not guaranteed or endorsed by the publisher.

References

- Borgo, C., D'Amore, C., Sarno, S., Salvi, M., and Ruzzene, M. (2021). Protein kinase CK2: A potential therapeutic target for diverse human diseases. *Signal Transduct. Target. Ther.* 6, 183. doi:10.1038/s41392-021-00567-7
- Cozza, G., Salvi, M., Tagliabracci, V. S., and Pinna, L. A. (2017). Fam20C is under the control of sphingolipid signaling in human cell lines. *FEBS J.* 284, 1246–1257. doi:10.1111/febs.14052
- Cui, J., Xiao, J., Tagliabracci, V. S., Wen, J., Rahdar, M., and Dixon, J. E. (2015). A secretory kinase complex regulates extracellular protein phosphorylation. *eLife* 4, e06120. doi:10.7554/eLife.06120
- Lasa-Benito, M., Marin, O., Meggio, F., and Pinna, L. A. (1996). Golgi apparatus mammary gland casein kinase: Monitoring by a specific peptide substrate and definition of specificity determinants. *FEBS Lett.* 382, 149–152. doi:10.1016/0014-5793(96)00136-6
- Tagliabracci, V. S., Engel, J. L., Wen, J., Wiley, S. E., Worby, C. A., Kinch, L. N., et al. (2012). Secreted kinase phosphorylates extracellular proteins that regulate biomineralization. *Science* 336, 1150–1153. doi:10.1126/science.1217817
- Tagliabracci, V. S., Wiley, S. E., Guo, X., Kinch, L. N., Durrant, E., Wen, J., et al. (2015). A single kinase generates the majority of the secreted phosphoproteome. *Cell* 161, 1619–1632. doi:10.1016/j.cell.2015.05.028
- Venerando, A., Cesaro, L., and Pinna, L. A. (2017). From phosphoproteins to phosphoproteomes: A historical account. *FEBS J.* 284, 1936–1951. doi:10.1111/febs.14014
- Venerando, A., Ruzzene, M., and Pinna, L. A. (2014). Casein kinase: The triple meaning of a misnomer. *Biochem. J.* 460, 141–156. doi:10.1042/BJ20140178



Fam20C in Human Diseases: Emerging Biological Functions and Therapeutic Implications

Rongsheng Xu¹, Huidan Tan², Jiahui Zhang², Zhaoxin Yuan^{2,3}, Qiang Xie^{2*} and Lan Zhang^{3*}

¹Department of Stomatology, Zigong First People's Hospital, Zigong, China, ²State Key Laboratory of Biotherapy and Cancer Center, West China Hospital, Sichuan University, Chengdu, China, ³Sichuan Engineering Research Center for Biomimetic Synthesis of Natural Drugs, School of Life Science and Engineering, Southwest Jiaotong University, Chengdu, China

OPEN ACCESS

Edited by:

Andrea Venerando,
University of Padua, Italy

Reviewed by:

Valeria De Pasquale,
University of Naples Federico II, Italy
Qinzhe Wang,
University of Utah, United States

*Correspondence:

Lan Zhang
zhanglan299@swjtu.edu.cn
Qiang Xie
dentistqiangxie@163.com

Specialty section:

This article was submitted to
Molecular Diagnostics and
Therapeutics,
a section of the journal
Frontiers in Molecular Biosciences

Received: 06 October 2021

Accepted: 08 November 2021

Published: 20 December 2021

Citation:

Xu R, Tan H, Zhang J, Yuan Z, Xie Q
and Zhang L (2021) Fam20C in Human
Diseases: Emerging Biological
Functions and
Therapeutic Implications.
Front. Mol. Biosci. 8:790172.
doi: 10.3389/fmolb.2021.790172

Fam20C, a typical member of Fam20 family, has been well-known as a Golgi casein kinase, which is closely associated with Raine Syndrome (RS). It can phosphorylate many secreted proteins and multiple substrates, and thereby plays a crucial role in biological functions. More importantly, Fam20C has also been found to enhance the metastasis of several types of human cancers, such as breast cancer, indicating that Fam20C may be a promising therapeutic target. Accordingly, some small-molecule inhibitors of Fam20C have been reported in cancer. Taken together, these inspiring findings would shed new light on exploiting Fam20C as a potential therapeutic target and inhibiting Fam20C with small-molecule compounds would provide a clue on discovery of more candidate small-molecule drugs for fighting with human diseases.

Keywords: casein kinase, FAM20c, phosphorylation, diseases, inhibitors

INTRODUCTION

Hitherto, more and more proteins have been found to play important physiological functions in various life processes after being phosphorylated. Therefore, protein phosphorylation, as a fundamental regulatory modification of proteins, has gradually become an important research content and has come into people's sight (Cohen, 2002; Taliabracci et al., 2012; Klement and Medzihradszky, 2017). The first sign of protein kinases' existence was in 1883, when stoichiometric amounts of phosphate were found in the secreted protein casein. This casein was therefore identified as the first phosphoprotein, but the responsible kinase responsible for it was not clear until 2013 (Tagliabracci et al., 2012). The emergence of a novel atypical protein kinase family, the Fam20 family, solved these problems to a certain extent. These protein kinases are secreted in the Golgi apparatus and seem to be able to phosphorylate many extracellular proteins including casein (Tagliabracci et al., 2013). Protein kinase phosphorylates the substrate through phosphorylation, thus changing the activity of the substrate and mediating most of the signal transduction and cell processes, including transcriptional regulation and metabolic regulation (Manning et al., 2002). Therefore, abnormal protein phosphorylation is the cause of many diseases.

Fam20C, this kinase, and its family members Fam20A and Fam20B define a new family of secretory proteins that collectively regulate a diverse network of secretory pathway components (Palma-Lara et al., 2021). As the most widely studied member of the Fam20 family, Fam20C is a secreted protein with kinase activity. In the process of evolution, Fam20C not only obtained new substrate specificity, but also gained the ability to form evolutionarily conserved homodimers or heterodimers with Fam20A to regulate protein conformation and kinase activity. Although the other two members have a high degree of sequence homology, their biochemical activities are completely

different. Fam20B has a unique active site that can recognize Gal β 1-4Xyl β 1 and is able to regulate the synthesis of proteoglycans by acting as a glycan kinase phosphorylating xylose residues and triggers peptidoglycan biosynthesis. At the same time, all Fam20B subfamily members function as monomers and do not need to form homologous or heterodimers. Fam20A, which did not appear until spinal animals, is a pseudokinase because it lacks active site residues that are essential for kinase activity and binds ATP in a catalytically incapable way, but it also obtains a more optimized ability to form dimers with Fam20C and activate Fam20C (Xiao et al., 2013; Zhang et al., 2018a; Worby et al., 2021).

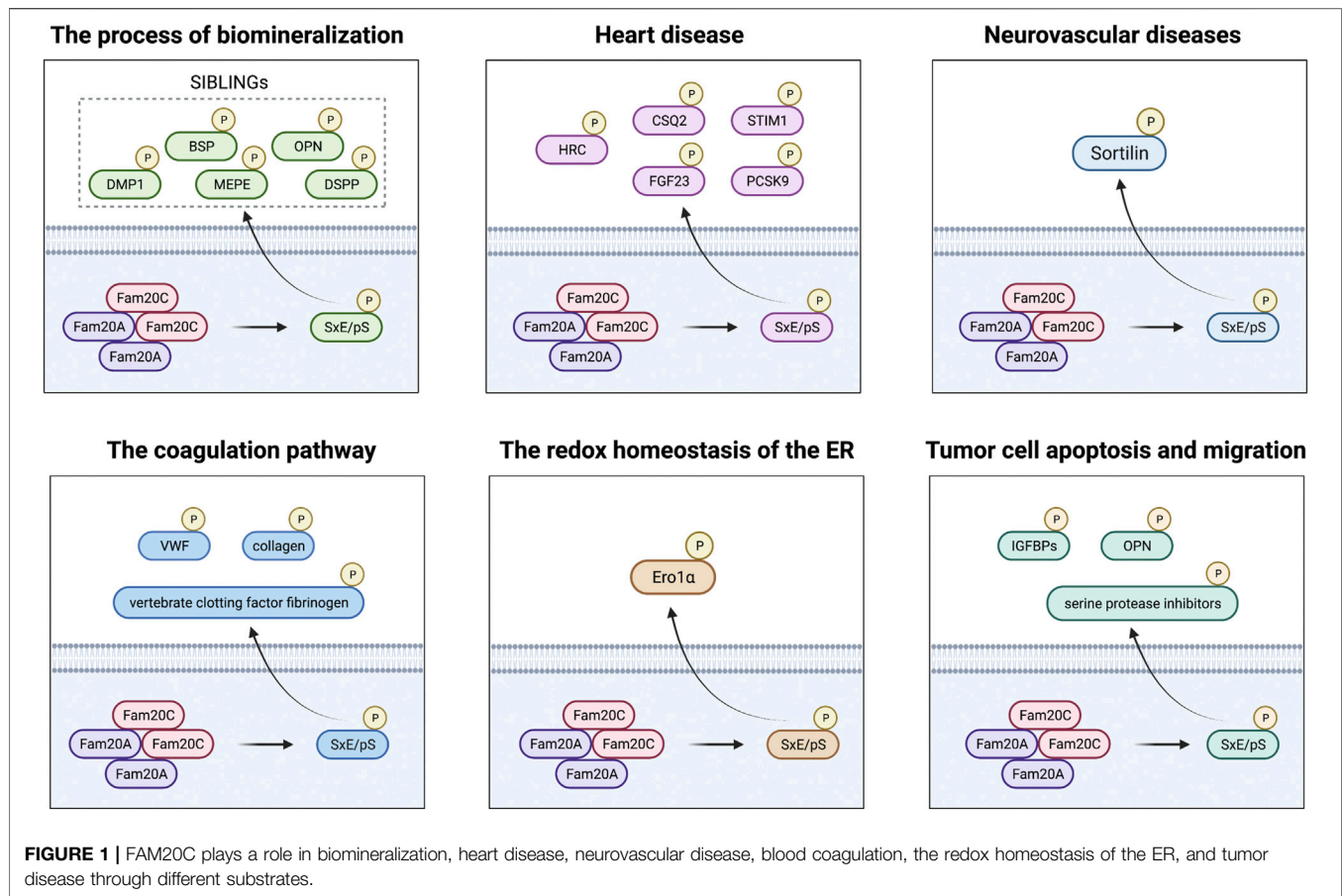
Fam20C, originally named as Golgi-enriched-fraction casein kinase (GEF-CK) and discovered in 1972, is confirmed by Tagliabracci et al. and Ishikawa et al. as a protein kinase that can phosphorylate the S-x-E/pS (S is serine, x is any one amino acid, E/pS is glutamate or phosphoserine) motif of secreted proteins (Bingham et al., 1972; Tagliabracci et al., 2012). In addition, Fam20C can also recognize amino acid sequences other than the typical S-x-E/pS motif, such as S-x-Q-x-D-E-E motif, which indicates that Fam20C-dependent phosphorylation is more extensive than indicated by only those substrates that are phosphorylated within the canonical motif (Brunati et al., 2000). Moreover, FAM20C, expressed in a variety of tissues, has been shown by functional annotation of substrates that it not only is involved in biomineralization but also plays an important role in cell migration and adhesion, wound healing, endopeptidase inhibitor activity, and lipid metabolism disorders (Tagliabracci et al., 2015). Such rich and useful functions have established Fam20C as a major protein kinase. Here, we have summarized the structure and function of Fam20C, discussed its important role in various diseases, and further discussed its potential diagnosis and therapeutic effect. Through an in-depth understanding of these relationships, the biological functions of Fam20C will be further developed, laying a new foundation for studying the role of protein phosphorylation in life processes and diseases.

STRUCTURE AND BIOLOGICAL FUNCTION OF FAM20C

The Fam20C gene is located on chromosome 7, with a full length of 72,410 bp and contains 10 exons (Nalbant et al., 2005). The Fam20C protein sequence includes 584 amino acids, of which the C-terminal contains 350 amino acids that are highly conserved regions and is called conserved C-terminal domain (CCD), and the N-terminal has a signal peptide targeting the secretory pathway, a total of 22 amino acids. Its kinase domain (KD) spans 222 amino acids, from residue 354 to 565 (Cozza and Pinna, 2016). Fam20C is considered an atypical protein kinase and is therefore not included in the “typical” group of human kinases. The kinase core of Fam20C has a two-lobe structure (N-lobe and C-lobe), which is characteristic of all protein kinases. The crystal structure of the *C. elegans* homolog of human

Fam20C (ceFam20) displays a large kinase domain and a protein kinase-like fold characterized by being contained in a shell-like structure formed by an N-terminal segment and a novel insertion domain. The N-terminal segment wraps around the lower half of the molecule, forming the base of the C-lobe. The insertion domain has a novel fold and forms a cap-like structure that covers the N-lobe. Therefore, sequence analyses usually failed to identify the Fam20 family as kinases because this domain is hidden in the N-lobe (Xiao et al., 2013). In addition, the Mn/ADP-bound structure is important for nucleotide binding and catalysis as the critical residues. Therefore, the unique architecture of the kinase suggests that Fam20C is an efficient catalyst as opposed to a dynamically regulated enzyme (Cozza and Pinna, 2016). Activation of Fam20C requires the formation of either an evolutionarily conserved homodimer or a heterodimer with Fam20A. Compared with Fam20C itself, Fam20A has a more effective Fam20C binding surface and is a special Fam20C allosteric activator. For example, Ile214A, Ile255A, and Leu365A are unique to Fam20A, and contribute to the formation of an optimized hydrophobic surface for interacting with Fam20C (Zhang et al., 2018a). In a word, the structure of Fam20C is distinct to other “typical” kinases, which makes it more druggable. Therefore, further studying of Fam20C structure can help us understand their biological functions, which can promote the development of more effective new drugs to treat diseases.

Fam20C is not a specific kinase dedicated to phosphorylation of casein, but a ubiquitous protein kinase, which mostly acts on the phosphorylation of many secreted proteins within the Sx-E/pS motif (Zhou et al., 2009; Salvi et al., 2010). Chromosome 4 harbors a cluster of genes encoding small integrin binding ligand-N-linked glycoproteins (SIBLINGs). The proteins encoded by these genes are involved in binding calcium and are the substrates of Fam20C, mainly five members of the secretory calcium binding phosphoprotein (SCPP) family, namely, dentin matrix protein 1 (DMP1), matrix extracellular phosphoglycoprotein (MEPE), osteopontin (OPN), bone sialoprotein (BSP), and dentin sialophosphoprotein (DSPP), indicating that Fam20C plays an important role in the process of biomineralization (Tagliabracci et al., 2012). Histidine-rich calcium binding protein (HRC) was the first sarcoplasmic reticulum (SR) protein to be discovered as a substrate of Fam20 (Pollak et al., 2017). In addition, other proteins involved in Ca²⁺ signaling include calsequestrin 2 (CSQ2) and matrix interacting molecule 1 (STIM1), as well as fibroblast growth factor 23 (FGF23), which directly causes cardiovascular problems in patients, and proprotein convertase subtilisin 9 (PCSK9), which is related to LDL-cholesterol disorders, which are all key links in the process of Fam20C affecting heart disease (Ezumba et al., 2014; Pollak et al., 2017; Pollak et al., 2018; Ben Djoudi Ouadda et al., 2019). Sortilin is not limited to the expression of a single tissue and is another unique target for Fam20C because of its versatility and its important role in the pathogenesis of a variety of diseases, especially neurovascular diseases. (Xu et al., 2019). Besides, in phosphorylated proteomics screening, the main proteins in



plasma and serum such as vertebrate clotting factor fibrinogen, von Willebrand factor (VWF), and collagen were determined as potential substrates for Fam20C. Therefore, the role of Fam20C and its key substrate phosphorylation in the coagulation pathway is also worthy of further study (Tagliabracci et al., 2015; Qiu et al., 2018; Da et al., 2019). Studies have also found that the endoplasmic reticulum (ER) sulfhydryl oxidase ER oxidoreductin 1α (Ero1α), which can regulate the redox homeostasis of the ER, can also be phosphorylated by Fam20C, thereby establishing a new connection between phosphorylation modification and oxidative folding (Zhang et al., 2018b). Finally, many Fam20C phosphorylated substrates are also related to tumor cell apoptosis and migration, including insulin-like growth factor binding proteins (IGFBPs), OPN, and serine protease inhibitors (Rangaswami et al., 2006; Baxter, 2014; Tagliabracci et al., 2015). In short, Fam20C plays an important role in various life processes through phosphorylation of multiple substrates (Figure 1; Supplementary Table S1).

DISEASES ASSOCIATED WITH FAM20C

Given the important role of FAM20C in biomineralization and phosphorylating secretory proteins, mutations of FAM20C gene

and aberrant function of fam20c kinase are responsible for many diseases, including Raine Syndrome (RS), cancer, and other diseases.

Raine Syndrome

RS is a bone dysplasia with characteristic features of generalized osteosclerosis, craniofacial anomalies, and intracerebral calcifications (Vishwanath et al., 2014), which is caused by mutations of Fam20C. Hitherto, 42 variants of Fam20C gene have been summarized to be responsible for RS, and they cause either lethal or non-lethal cases (Palma-Lara et al., 2021). For example, mutations of FAM20C gene (MIM *611061) are reported to impair splicing process, leading to the functional loss of proteins and causing disease phenotype (Simpson et al., 2007). More recently, new mutations of Fam20C have been detected to cause lethal RS in two Mexican family siblings, with a duplicated cytosine at position 456 and a deleted cytosine at position 704 in exon 1 (Hernández-Zavala et al., 2020). In addition, whole exome sequencing reveals a non-lethal case of a middle-aged woman with a frameshift insertion c.1107_1108insTACTG (p.Tyr369fs) and a missense substitution c.1375C > G (p.Arg459Gly) in Fam20C gene (Mamedova et al., 2019). Another non-lethal case of RS happens in a Brazil patient carrying a homozygous

missense variant c.1487C > T at exon 9 of FAM20C (NM_020223.4), who displays mild facial dysmorphism, without hypoplastic nose, micrognathia, low set ears, or depressed nasal bridge (Ferreira et al., 2021).

FGF23-related hypophosphatemia is reported in non-lethal RS patients and is found to be associated with FAM20C mutations (Simpson et al., 2009; Rafaelsen et al., 2013). Given the causative role of mutant Fam20C gene in RS pathogenesis, some researchers have investigated detailed pathogenetic mechanism of mutant Fam20C in preclinical experiments (Cozza and Pinna, 2016). Six mutant Fam20C proteins (T268M, P328S, R408W, D451N, D478A, and R549W) responsible for RS were demonstrated to cause impaired kinase activity and hinder DMP1 transcription, ultimately leading to FGF-related hypophosphatemia in rat osteosarcoma UMR-106 cells (Kinoshita et al., 2014). Recently, mice that were knocked out of Fam20C showed vertebral abnormalities and decreased β -catenin, indicating that Fam20C loss of function may affect vertebral development through modulating Wnt/ β -catenin pathway (Huang et al., 2021).

Cancer

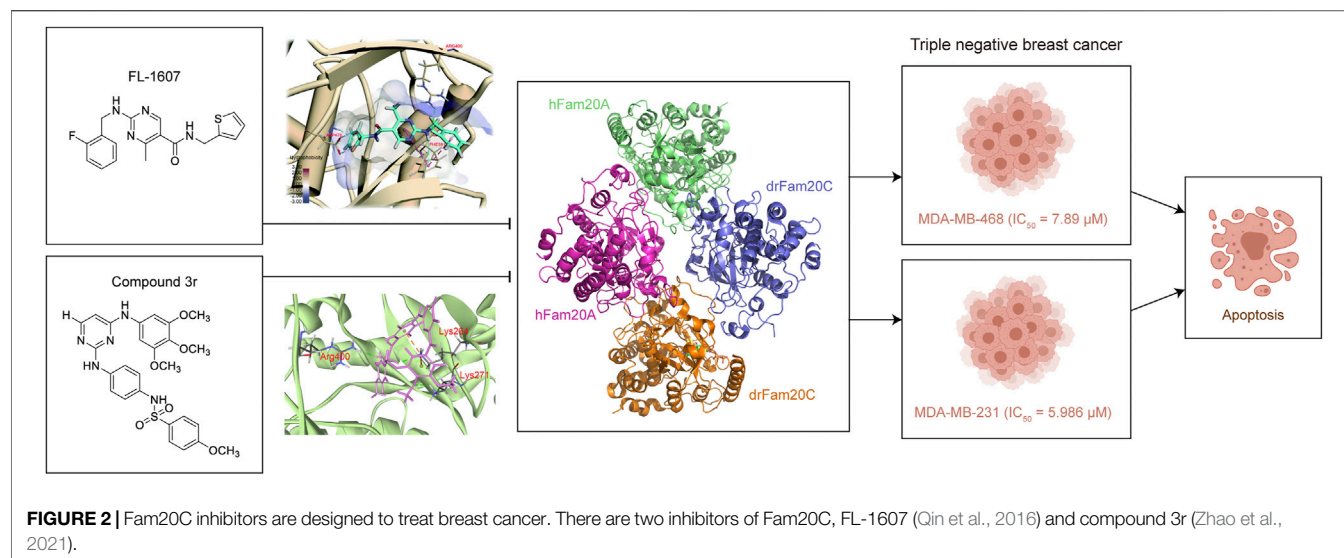
Recently, the role of Fam20C in tumorigenesis has been illuminated and widely reported, making it a possible biomarker and potentially therapeutic target for diverse cancers (Simpson et al., 2009).

Its association with triple-negative breast cancer (TNBC) was first reported in 2015 (Tagliabracci et al., 2015), as the phosphorylation of a large number of its substrates was identified to play a role in adhesion and migration of MDA-MB-231 cells and U2OS cells, such as IGFBP7 and cadherin-2 (CDH2). Fam20C knockout (KO) MDA-MB-231 cells were demonstrated with less malignant invasion and the phosphorylation of its substrate IGFBP7 was responsible for the changes. In a later study, Fam20C knockdown with siRNA also impaired the metastasis of MDA-MB-231 cells while mildly affecting cell proliferation, indicating the possible oncogenic effect of Fam20C in TNBC (Zhao et al., 2021). More recently, a genome-wide analysis uncovered that high expression and hypomethylation of Fam20C were correlated with poor prognosis in hypoxia-related lung adenocarcinoma (LUAD), in which hypoxia condition promoted FAM20C gene expression, making Fam20C a potential biomarker of LUAD (Li et al., 2020). Subsequently, a study has revealed the expression patterns of Fam20C in pan-cancer, of which increased expressions were correlated with poor prognosis in bladder urothelial carcinoma (BLCA), brain lower grade glioma (LGG), and stomach adenocarcinoma (STAD), making Fam20C a potential prognostic biomarker in those tumors. Particularly, high expression of FAM20C was found to affect lymphatic metastasis of STAD (Liu et al., 2021). The altered infiltration levels of immune cells, including B cells, CD8⁺T cells, CD4⁺T cells, macrophages, neutrophils, and dendritic cells were considered to be responsible for its correlation with cancers, while the expression of FAM20C also assisted the polarization of tumor-associated

macrophages (TAM), activation of Treg cells and T helper cells, and induction of T-cell exhaustion (Liu et al., 2021). Moreover, augmented Fam20C expression was found to be positively correlated with the malignancy of gliomas, which makes the expression of Fam20C a possibly diagnostic marker of malignant gliomas. Also, patients with higher Fam20C expression were more resistant to radiotherapy and chemotherapy. In line with the bioinformatics analysis, Fam20C knockdown significantly impaired the invasion and migration of human glioblastoma LN229 cells (Du et al., 2020). More importantly, a wide range of secreted proteins phosphorylated by Fam20C were found to be associated with different cancers (Zhao et al., 2021). Fibronectin 1 (FN1) was identified to interact with Fam20C and promote tumor cell migration (Du et al., 2020). OPN, a substrate of Fam20C involved in cell differentiation (Zhao et al., 2018), was overexpressed in bladder cancer tissues and OPN knockdown could suppress proliferation and invasion of human bladder cancer T24 cell *via* the JAK1/STAT1 pathway (Zhang et al., 2020). In addition, myeloid Fam20C phosphorylates OPN and decreases its secretion, thereby regulating osteoclast differentiation and decelerating breast cancer bone metastasis *in vivo* (Zuo et al., 2021). Another substrate, BMP4, is also involved in breast cancer bone metastasis, in which Fam20C facilitates the growth of human breast cancer MDA-MB-231 cells and its bone metastasis through phosphorylation of BMP4 to induce osteoclast differentiation (Zuo et al., 2021). IGFBPs 3 and 7, which are both substrates of Fam20C (Liu et al., 2018), were reported to enhance the metastasis of colorectal cancer (CRC) sW480 and Caco2 cells (Georges et al., 2011; **Supplementary Table S2**).

Other Human Diseases

Besides IGFBP7 and CDH2, which play an important role in TNBC metastasis, the comprehensive article in 2015 identified many other substrates of Fam20C that were involved in other diseases, including Fetuin A (FetA) and histidine-rich calcium binding protein (HRC) (Tagliabracci et al., 2015). Phosphorylated FetA was reported to play a part in insulin resistance in type 2 diabetes mellitus (T2DM) through binding the β -subunit of the insulin receptor and hindering insulin signaling (Ochieng et al., 2018). A study showed that the phosphorylation of FetA at Ser 312 is time-dependent on Fam20C, whereas the biological function of FAM20C-dependent FetA phosphorylation remains unknown (Kovářová et al., 2021). Another study originally revealed the possible regulatory effects of Fam20C on (pro)insulin production and correlative secretory pathway trafficking, establishing connections between Fam20C function and the development of diabetes (Kang et al., 2019). HRC is a 170-kDa protein with high capacity for Ca^{2+} binding and is critical in the modulation of cardiomyocyte SR Ca^{2+} homeostasis (Arvanitis et al., 2018). Recently, the relationship between Fam20C and SR Ca^{2+} handling machinery has been illuminated, demonstrating that the phosphorylation of HRC at Ser96 by Fam20C regulates the interactions of HRC



and triadin and sarco/endoplasmic reticulum Ca^{2+} adenosine triphosphatase-2a (SERCA2a), maintains the SR Ca^{2+} homeostasis, and finally protects patients from cardiac arrhythmias (Pollak et al., 2017). A follow-up study identified Stim1 and CSQ2 as new substrates of Fam20C, which are important in controlling the SR Ca^{2+} homeostasis. The loss of Fam20C-dependent phosphorylation of these two proteins may underlie the development of heart failure in Fam20C KO mice (Pollak et al., 2018). In addition, the possible pathogenesis of Fam20C in coronary artery disease has been revealed, of which the Fam20C-dependent phosphorylation of sortlin at Ser825 is integral in the process of smooth muscle cell (SMC) calcification (Goettsch et al., 2016). One latest study reported the decreased expression of Fam20C in behavioral variant frontotemporal dementia (bvFTD) with autoimmune disease (Bright et al., 2021).

THERAPEUTIC POTENTIAL FOR TARGETING FAM20C

Considering the important role of Fam20C in various diseases, especially its role in tumorigenesis, targeting Fam20C is a potential treatment for diseases including cancer in the future (Wu et al., 2021). Some attempts to design inhibitors of Fam20C for treating cancer, focused in TNBC, have emerged. For the first time, FL-1607 was identified through virtual screening and interacted well with Fam20C, with better stability (RMSD reached its dynamic equilibrium after 2 ns simulation) and compactness (RG of 1.462 ± 0.0073 nm), as well as lower flexibility (RMSF of 0.0805 ± 0.0353 nm; mean \pm SD) when binding with Fam20C. Meanwhile, it showed good antiproliferative property in human breast cancer MCF-7, MDA-MB-231 and MDA-MB-468 cells, with the best IC_{50}

of $7.89 \mu\text{M}$ in MDA-MB-468 cells. Moreover, FL-1607 was shown to induce apoptosis and suppress migration of MDA-MB-468 cells. The researchers found that Fam20C harbored unique amino acids residues in ATP-binding sites, which makes Fam20C more possible to be selectively target by small molecules (Qin et al., 2016). Encouraged by this study and the x-ray crystal structure of Fam20C (Zhang et al., 2018a), a new inhibitor of Fam20C was identified in 2021 (Zhao et al., 2021). Optimized from F2078-0064, compound **3r** showed good kinase inhibitory ability against Fam20C ($6.243 \mu\text{M}$), with IC_{50} of $5.986 \mu\text{M}$ in MDA-MB-231 cells. **3r** killed cancer cells through apoptosis induction and could significantly block migration of MDA-MB-231 cells. In addition, **3r** inhibited tumor growth in MDA-MB-231 xenograft mouse model through inducing apoptosis (Zhao et al., 2021) (Figure 2).

Two inhibitors of Fam20C mentioned above shed light on the therapeutic potential for targeting Fam20C in cancer, providing successful examples for future discovery of new Fam20C inhibitors. However, in-depth investigations of therapies targeting Fam20C remain limited, and no studies illuminated its therapeutic effects in heart diseases and diabetes, in which experimental evidence confirmed the important pathogenetic role of Fam20C. The two existing inhibitors may be good tools for studying biological and pathogenetic functions of Fam20C while their application for treating other diseases associated with Fam20C warrants further investigations. Additionally, the wide distribution of Fam20C in bone, heart, kidney, etc. may make therapeutics targeting Fam20C easily cause side effects in unexpected organs or tissues, thus requiring more comprehensive understanding of Fam20C functions in different tissues and calling for precise delivery of therapeutics. Moreover, molecular subtyping of diseases, especially of cancers with aberrant expression of Fam20C, represents a future direction.

CONCLUSION

Of note, the Fam20 family is composed of three secreted proteins, including Fam20A, Fam20B, and Fam20C; among them, Fam20C could phosphorylate a series of downstream secreted proteins. Fam20C is a typical member of Fam20 family, which has been well-known as a Golgi casein kinase that can be identified during hematopoietic differentiation (Nalbant et al., 2005). Interestingly, the other two members Fam20A and Fam20B have a high sequence homology with Fam20C, but their biological activities are completely different. Thus, Fam20C has its unique biological function in several cellular processes (Worby et al., 2021).

Recently, Fam20C, which is closely associated with RS, has been reported to phosphorylate more than 100 types of secreted proteins and more multiple substrates, thereby playing a key role in regulation of their complicated biological function (Tagliabracci et al., 2015). Accordingly, accumulating evidence has been demonstrating that Fam20C has several links to many types of human diseases, such as RS, cancer, and others. More importantly, Fam20C has also been found to enhance the metastasis of several types of human cancers, such as breast cancer and CRC, indicating that Fam20C may be a promising therapeutic target for the current drug development. More recently, some small-molecule inhibitors of Fam20C (e.g., FL-1607 and 3r) have been reported to induce apoptosis as well as to prevent metastasis in breast cancer, which may reveal Fam20C as a druggable target for cancer therapy (Qin et al., 2016; Zhao et al., 2021).

With the rapid development of structure biology and artificial intelligence (AI), the tertiary structure of Fam20C and even the quaternary structure of Fam20C-Fam20A have been elucidated (Zhang et al., 2018a). Therefore, the structure-guided design of Fam20C inhibitors will provide more precisely small-molecule inhibitors for potential therapy. Also, some AI technologies, such as AlphaFold2 would also provide more potential selectively small-molecule inhibitors for possible pharmaceutical

applications. Especially when the experimental structure is not available, AlphaFold2 may provide more accurate model for virtual screening (Cramer, 2021). In a nutshell, these inspiring findings would shed new light on exploiting Fam20C as a potential therapeutic target and inhibiting Fam20C with small-molecule compounds will provide a new clue on discovery of more candidate drugs in the treatment of human diseases in the future.

AUTHOR CONTRIBUTIONS

QX and LZ conceived, formatted, and submitted this manuscript. RX and HT wrote the manuscript. JZ and ZY searched and archived the literature.

FUNDING

This work was supported by grants from Sichuan Science and Technology Program (Grant Nos. 2020JDR0053, 2019YFSY0038, and 2020YJ0085) and Fundamental Research Funds for the Central Universities (Grant No. 2682020CX56).

ACKNOWLEDGMENTS

We are grateful to Wenke Jin and Shiou Zhu for their good discussion on this manuscript.

SUPPLEMENTARY MATERIAL

The Supplementary Material for this article can be found online at: <https://www.frontiersin.org/articles/10.3389/fmolb.2021.790172/full#supplementary-material>.

REFERENCES

- Arvanitis, D. A., Vafiadaki, E., Johnson, D. M., Kranias, E. G., and Sanoudou, D. (2018). The Histidine-Rich Calcium Binding Protein in Regulation of Cardiac Rhythmicity. *Front. Physiol.* 9, 1379. doi:10.3389/fphys.2018.01379
- Baxter, R. C. (2014). IGF Binding Proteins in Cancer: Mechanistic and Clinical Insights. *Nat. Rev. Cancer* 14, 329–341. doi:10.1038/nrc3720
- Ben Djoudi Ouadda, A., Gauthier, M.-S., Susan-Resiga, D., Girard, E., Essalmani, R., Black, M., et al. (2019). Ser-Phosphorylation of PCSK9 (Proprotein Convertase Subtilisin-Kexin 9) by Fam20C (Family with Sequence Similarity 20, Member C) Kinase Enhances its Ability to Degrade the LDLR (Low-Density Lipoprotein Receptor). *Atvb* 39, 1996–2013. doi:10.1161/ATVBAHA.119.313247
- Bingham, E. W., Farrell, H. M., and Basch, J. J. (1972). Phosphorylation of Casein. *J. Biol. Chem.* 247, 8193–8194. doi:10.1016/s0021-9258(20)81827-4
- Bright, F., Katzeff, J. S., Hodges, J. R., Piguet, O., Kril, J. J., Halliday, G. M., et al. (2021). Glycoprotein Pathways Altered in Frontotemporal Dementia with Autoimmune Disease. *Front. Immunol.* 12, 736260. doi:10.3389/fimmu.2021.736260
- Brunati, A. M., Marin, O., Bisinella, A., Salvati, A., and Pinna, L. A. (2000). Novel Consensus Sequence for the Golgi Apparatus Casein Kinase, Revealed Using
- Proline-Rich Protein-1 (PRP1)-Derived Peptide Substrates. *Biochem. J.* 351, 765–768. doi:10.1042/bj3510765
- Cohen, P. (2002). The Origins of Protein Phosphorylation. *Nat. Cell Biol.* 4, E127–E130. doi:10.1038/ncb0502-e127
- Cozza, G., and Pinna, L. A. (2016). Casein Kinases as Potential Therapeutic Targets. *Expert Opin. Ther. Targets* 20, 319–340. doi:10.1517/14728222.2016.1091883
- Cramer, P. (2021). AlphaFold2 and the Future of Structural Biology. *Nat. Struct. Mol. Biol.* 28, 704–705. doi:10.1038/s41594-021-00650-1
- Da, Q., Han, H., Valladolid, C., Fernández, M., Khatlani, T., Pradhan, S., et al. (2019). In vitrophosphorylation of von Willebrand factor by FAM20c enhances its ability to support platelet adhesion. *J. Thromb. Haemost.* 17, 866–877. doi:10.1111/jth.14426
- Du, S., Guan, S., Zhu, C., Cao, J., Guan, G., et al. (2020). Secretory Pathway Kinase FAM20C, a Marker for Glioma Invasion and Malignancy, Predicts Poor Prognosis of Glioma. *Ott* 13, 11755–11768. doi:10.2147/OTT.S275452
- Ezumba, I., Quarles, L. D., and Kovesdy, C. P. (2014). FGF23 and the Heart. *G Ital. Nefrol* 31, gin/31.6.12
- Ferreira, L. D., Leal, G. F., and De Oliveira, J. R. M. (2021). Non-lethal Raine Syndrome Report Lacking Characteristic Clinical Features. *J. Mol. Neurosci.* 71, 2482–2486. doi:10.1007/s12031-021-01873-z

- Georges, R. B., Adwan, H., Hamdi, H., Hielscher, T., Linnemann, U., and Berger, M. R. (2011). The Insulin-like Growth Factor Binding Proteins 3 and 7 Are Associated with Colorectal Cancer and Liver Metastasis. *Cancer Biol. Ther.* 12, 69–79. doi:10.4161/cbt.12.1.15719
- Goettsch, C., Hutcheson, J. D., Aikawa, M., Iwata, H., Pham, T., Nykjaer, A., et al. (2016). Sortilin Mediates Vascular Calcification via its Recruitment into Extracellular Vesicles. *J. Clin. Invest.* 126, 1323–1336. doi:10.1172/JCI80851
- Hernández-Zavala, A., Cortés-Camacho, F., Palma-Lara, I., Godínez-Aguilar, R., Espinosa, A. M., Pérez-Durán, J., et al. (2020). Two Novel FAM20C Variants in A Family with Raine Syndrome. *Genes* 11, 222. doi:10.3390/genes11020222
- Huang, Y., Chen, H., Zhang, H., Lu, Y., and Qin, C. (2021). FAM20C Plays a Critical Role in the Development of Mouse Vertebra. *Spine J.* S1529–9430 (1521), 00846–00849. doi:10.1016/j.spinee.2021.07.022
- Kang, T., Boland, B. B., Alarcon, C., Grimsby, J. S., Rhodes, C. J., and Larsen, M. R. (2019). Proteomic Analysis of Restored Insulin Production and Trafficking in Obese Diabetic Mouse Pancreatic Islets Following Euglycemia. *J. Proteome Res.* 18, 3245–3258. doi:10.1021/acs.jproteome.9b00160
- Kinoshita, Y., Hori, M., Taguchi, M., and Fukumoto, S. (2014). Functional Analysis of Mutant FAM20C in Raine Syndrome with FGF23-Related Hypophosphatemia. *Bone* 67, 145–151. doi:10.1016/j.bone.2014.07.009
- Klement, E., and Medzihradsky, K. F. (2017). Extracellular Protein Phosphorylation, the Neglected Side of the Modification. *Mol. Cell Proteomics* 16, 1–7. doi:10.1074/mcp.O116.064188
- Kovářová, M., Kalbacher, H., Peter, A., Häring, H.-U., Didangelos, T., Stefan, N., et al. (2021). Detection and Characterization of Phosphorylation, Glycosylation, and Fatty Acid Bound to Fetuin A in Human Blood. *Jcm* 10, 411. doi:10.3390/jcm10030411
- Li, H., Tong, L., Tao, H., and Liu, Z. (2020). Genome-wide Analysis of the Hypoxia-Related DNA Methylation-Driven Genes in Lung Adenocarcinoma Progression. *Biosci. Rep.* 40, BSR20194200. doi:10.1042/BSR20194200
- Liu, C., Zhang, H., Jani, P., Wang, X., Lu, Y., Li, N., et al. (2018). FAM20C Regulates Osteoblast Behaviors and Intracellular Signaling Pathways in a Cell-Autonomous Manner. *J. Cell Physiol* 233, 3476–3486. doi:10.1002/jcp.26200
- Liu, X., Zhan, Y., Xu, W., Liu, X., Geng, Y., Liu, L., et al. (2021). Prognostic and Immunological Role of Fam20C in Pan-Cancer. *Biosci. Rep.* 41, BSR20201920. doi:10.1042/BSR20201920
- Mamedova, E., Dimitrova, D., Przhivalkovskaya, E., Buryakina, S., Vasilyev, E., Tiulpakov, A., et al. (2019). Non-lethal Raine Syndrome in a Middle-Aged Woman Caused by a Novel FAM20C Mutation. *Calcif Tissue Int.* 105, 567–572. doi:10.1007/s00223-019-00599-w
- Manning, G., Whyte, D. B., Martinez, R., Hunter, T., and Sudarsanam, S. (2002). The Protein Kinase Complement of the Human Genome. *Science* 298, 1912–1934. doi:10.1126/science.1075762
- Nalbant, D., Youn, H., Nalbant, S. I., Sharma, S., Cobos, E., Beale, E. G., et al. (2005). FAM20: an Evolutionarily Conserved Family of Secreted Proteins Expressed in Hematopoietic Cells. *BMC Genomics* 6, 11. doi:10.1186/1471-2164-6-11
- Ochieng, J., Nangami, G., Sakwe, A., Moye, C., Alvarez, J., Whalen, D., et al. (2018). Impact of Fetuin-A (AHSG) on Tumor Progression and Type 2 Diabetes. *Ijms* 19, 2211. doi:10.3390/ijms19082211
- Palma-Lara, I., Pérez-Ramírez, M., García Alonso-Themann, P., Espinosa-García, A. M., Godínez-Aguilar, R., Bonilla-Delgado, J., et al. (2021). FAM20C Overview: Classic and Novel Targets, Pathogenic Variants and Raine Syndrome Phenotypes. *Ijms* 22, 8039. doi:10.3390/ijms22158039
- Pollak, A. J., Haghighi, K., Kunduri, S., Arvanitis, D. A., Bidwell, P. A., Liu, G.-S., et al. (2017). Phosphorylation of Serine96 of Histidine-Rich Calcium-Binding Protein by the Fam20C Kinase Functions to Prevent Cardiac Arrhythmia. *Proc. Natl. Acad. Sci. USA* 114, 9098–9103. doi:10.1073/pnas.1706441114
- Pollak, A. J., Liu, C., Gudlur, A., Mayfield, J. E., Dalton, N. D., Gu, Y., et al. (2018). A Secretory Pathway Kinase Regulates Sarcoplasmic Reticulum Ca²⁺ Homeostasis and Protects against Heart Failure. *Elife* 7, e41378. doi:10.7554/eLife.41378
- Qin, Z., Wang, P., Li, X., Zhang, S., Tian, M., Dai, Y., et al. (2016). Systematic Network-Based Discovery of a Fam20C Inhibitor (FL-1607) with Apoptosis Modulation in Triple-Negative Breast Cancer. *Mol. Biosyst.* 12, 2108–2118. doi:10.1039/C6MB00111D
- Qiu, Y., Poppleton, E., Mekkat, A., Yu, H., Banerjee, S., Wiley, S. E., et al. (2018). Enzymatic Phosphorylation of Ser in a Type I Collagen Peptide. *Biophysical J.* 115, 2327–2335. doi:10.1016/j.bpj.2018.11.012
- Rafaelsen, S. H., Raeder, H., Fagerheim, A. K., Knappskog, P., Carpenter, T. O., Johansson, S., et al. (2013). Exome Sequencing Reveals FAM20c Mutations Associated with Fibroblast Growth Factor 23-related Hypophosphatemia, Dental Anomalies, and Ectopic Calcification. *J. Bone Miner. Res.* 28, 1378–1385. doi:10.1002/jbmr.1850
- Rangaswami, H., Bulbule, A., and Kundu, G. C. (2006). Osteopontin: Role in Cell Signaling and Cancer Progression. *Trends Cell Biol.* 16, 79–87. doi:10.1016/j.tcb.2005.12.005
- Salvi, M., Cesaro, L., Tibaldi, E., and Pinna, L. A. (2010). Motif Analysis of Phosphosites Discloses a Potential Prominent Role of the Golgi Casein Kinase (GCK) in the Generation of Human Plasma Phospho-Proteome. *J. Proteome Res.* 9, 3335–3338. doi:10.1021/pr100058r
- Simpson, M. A., Hsu, R., Keir, L. S., Hao, J., Sivapalan, G., Ernst, L. M., et al. (2007). Mutations in FAM20C Are Associated with Lethal Osteosclerotic Bone Dysplasia (Raine Syndrome), Highlighting a Crucial Molecule in Bone Development. *Am. J. Hum. Genet.* 81, 906–912. doi:10.1086/522240
- Simpson, M., Scheuerle, A., Hurst, J., Patton, M., Stewart, H., and Crosby, A. (2009). Mutations in FAM20C Also Identified in Non-lethal Osteosclerotic Bone Dysplasia. *Clin. Genet.* 75, 271–276. doi:10.1111/j.1399-0004.2008.01118.x
- Tagliabracci, V. S., Engel, J. L., Wen, J., Wiley, S. E., Worby, C. A., Kinch, L. N., et al. (2012). Secreted Kinase Phosphorylates Extracellular Proteins that Regulate Biomineralization. *Science* 336, 1150–1153. doi:10.1126/science.1217817
- Tagliabracci, V. S., Pinna, L. A., and Dixon, J. E. (2013). Secreted Protein Kinases. *Trends Biochem. Sci.* 38, 121–130. doi:10.1016/j.tibs.2012.11.008
- Tagliabracci, V. S., Wiley, S. E., Guo, X., Kinch, L. N., Durrant, E., Wen, J., et al. (2015). A Single Kinase Generates the Majority of the Secreted Phosphoproteome. *Cell* 161, 1619–1632. doi:10.1016/j.cell.2015.05.028
- Vishwanath, B., Srinivasa, K., and Shankar, M. V. (2014). Raine Syndrome. *Indian J. Hum. Genet.* 20, 72–74. doi:10.4103/0971-6866.132761
- Worby, C. A., Mayfield, J. E., Pollak, A. J., Dixon, J. E., and Banerjee, S. (2021). The ABCs of the Atypical Fam20 Secretory Pathway Kinases. *J. Biol. Chem.* 296, 100267. doi:10.1016/j.jbc.2021.100267
- Wu, Y., Wang, H., and Liu, C. (2021). From Biomineralization to Tumorigenesis—The Expanding Insight of the Physiological and Pathological Roles of Fam20C. *Biosci. Rep.* 41, BSR20210040. doi:10.1042/BSR20210040
- Xiao, J., Tagliabracci, V. S., Wen, J., Kim, S.-A., and Dixon, J. E. (2013). Crystal Structure of the Golgi Casein Kinase. *Proc. Natl. Acad. Sci.* 110, 10574–10579. doi:10.1073/pnas.1309211110
- Xu, S.-Y., Zhang, Q.-L., Zhang, Q., Wan, L., Jiang, J., Tu, T., et al. (2019). Regional and Cellular Mapping of Sortilin Immunoreactivity in Adult Human Brain. *Front. Neuroanat.* 13, 31. doi:10.3389/fnana.2019.00031
- Zhang, H., Zhu, Q., Cui, J., Wang, Y., Chen, M. J., Guo, X., et al. (2018a). Structure and Evolution of the Fam20 Kinases. *Nat. Commun.* 9, 1218. doi:10.1038/s41467-018-03615-z
- Zhang, J., Zhu, Q., Wang, X. e., Yu, J., Chen, X., Wang, J., et al. (2018b). Secretory Kinase Fam20C Tunes Endoplasmic Reticulum Redox State via Phosphorylation of Ero1a. *EMBO J.* 37, e98699. doi:10.15252/embj.201798699
- Zhang, N., Li, F., Gao, J., Zhang, S., and Wang, Q. (2020). Osteopontin Accelerates the Development and Metastasis of Bladder Cancer via Activating JAK1/STAT1 Pathway. *Genes Genom* 42, 467–475. doi:10.1007/s13258-019-00907-6
- Zhao, H., Chen, Q., Alam, A., Cui, J., Suen, K. C., Soo, A. P., et al. (2018). The Role of Osteopontin in the Progression of Solid Organ Tumour. *Cell Death Dis* 9, 1–15. doi:10.1038/s41419-018-0391-6
- Zhao, R., Fu, L., Yuan, Z., Liu, Y., Zhang, K., Chen, Y., et al. (2021). Discovery of a Novel Small-Molecule Inhibitor of Fam20C that Induces Apoptosis and

- Inhibits Migration in Triple Negative Breast Cancer. *Eur. J. Med. Chem.* 210, 113088. doi:10.1016/j.ejmech.2020.113088
- Zhou, W., Ross, M. M., Tessitore, A., Ornstein, D., Vanmeter, A., Liotta, L. A., et al. (2009). An Initial Characterization of the Serum Phosphoproteome. *J. Proteome Res.* 8, 5523–5531. doi:10.1021/pr900603n
- Zuo, H., Yang, D., and Wan, Y. (2021). Fam20C Regulates Bone Resorption and Breast Cancer Bone Metastasis through Osteopontin and BMP4. *Cancer Res.* 81, 5242–5254. doi:10.1158/0008-5472.CAN-20-3328

Conflict of Interest: The authors declare that the research was conducted in the absence of any commercial or financial relationships that could be construed as a potential conflict of interest.

Publisher's Note: All claims expressed in this article are solely those of the authors and do not necessarily represent those of their affiliated organizations, or those of the publisher, the editors, and the reviewers. Any product that may be evaluated in this article, or claim that may be made by its manufacturer, is not guaranteed or endorsed by the publisher.

Copyright © 2021 Xu, Tan, Zhang, Yuan, Xie and Zhang. This is an open-access article distributed under the terms of the Creative Commons Attribution License (CC BY). The use, distribution or reproduction in other forums is permitted, provided the original author(s) and the copyright owner(s) are credited and that the original publication in this journal is cited, in accordance with accepted academic practice. No use, distribution or reproduction is permitted which does not comply with these terms.

GLOSSARY

AI artificial intelligence

BLCA bladder urothelial carcinoma

BSP bone sialoprotein

bvFTD behavioral variant frontotemporal dementia

CRC colorectal cancer

CDH2 cadherin-2

CSQ2 calsequestrin 2

DMP1 dentin matrix protein 1

DSPP dentin sialophosphoprotein

ER endoplasmic reticulum

Ero1 α ER oxidoreductin 1 α

FetA Fetuin A

FGF23 fibroblast growth factor 23

FN1 fibronectin 1

GEF-CK Golgi-enriched-fraction casein kinase

HRC histidine-rich calcium binding protein

IGFBP insulin-like growth factor binding protein

KD kinase domain

KO knockout

LGG brain lower grade glioma

LUAD lung adenocarcinoma

MEPE matrix extracellular phosphoglycoprotein

OPN osteopontin

PCSK9 proprotein convertase subtilisin 9

RS Raine syndrome

SCPP secretory calcium binding phosphoprotein

SERCA2a sarco/endoplasmic reticulum Ca²⁺ adenosine triphosphatase-2a

SIBLING small integrin binding ligand-N-linked glycoprotein

SMC smooth muscle cell

SR sarcoplasmic reticulum

STAD stomach adenocarcinoma

STIM1 matrix interacting molecule 1

T2DM type 2 diabetes mellitus

TAM tumor-associated macrophages

TNBC triple-negative breast cancer

VWF von Willebrand factor



Identification of the Host Substratome of *Leishmania*-Secreted Casein Kinase 1 Using a SILAC-Based Quantitative Mass Spectrometry Assay

Despina Smirlis^{1,2}, Florent Dingli³, Valentin Sabatet³, Aileen Roth⁴, Uwe Knippschild⁴, Damarys Loew³, Gerald F. Späth¹ and Najma Rachidi^{1*}

¹Institut Pasteur, Université de Paris, Institut National de Santé et Recherche Médicale INSERM U1201, Unité de parasitologie Moléculaire et Signalisation, Paris, France, ²Hellenic Pasteur Institute, Athens, Greece, ³Laboratoire de Spectrométrie de Masse Protéomique (LSMP), Centre de Recherche, Institut Curie, PSL Research University, Paris, France, ⁴Department of General and Visceral Surgery, Centre of Surgery, University Hospital Ulm, Ulm, Germany

OPEN ACCESS

Edited by:

Andrea Venerando,
University of Padua, Italy

Reviewed by:

Leonard James Foster,
University of British Columbia, Canada
Kathleen Gould,
Vanderbilt University, United States

*Correspondence:

Najma Rachidi
najma.rachidi@pasteur.fr

Specialty section:

This article was submitted to
Cellular Biochemistry,
a section of the journal
Frontiers in Cell and Developmental
Biology

Received: 22 October 2021

Accepted: 13 December 2021

Published: 03 January 2022

Citation:

Smirlis D, Dingli F, Sabatet V, Roth A, Knippschild U, Loew D, Späth GF and Rachidi N (2022) Identification of the Host Substratome of *Leishmania*-Secreted Casein Kinase 1 Using a SILAC-Based Quantitative Mass Spectrometry Assay. *Front. Cell Dev. Biol.* 9:800098. doi: 10.3389/fcell.2021.800098

Leishmaniasis is a severe public health problem, caused by the protozoan *Leishmania*. This parasite has two developmental forms, extracellular promastigote in the insect vector and intracellular amastigote in the mammalian host where it resides inside the phagolysosome of macrophages. Little is known about the virulence factors that regulate host-pathogen interactions and particularly host signalling subversion. All the proteomes of *Leishmania* extracellular vesicles identified the presence of *Leishmania* casein kinase 1 (L-CK1.2), a signalling kinase. L-CK1.2 is essential for parasite survival and thus might be essential for host subversion. To get insights into the functions of L-CK1.2 in the macrophage, the systematic identification of its host substrates is crucial, we thus developed an easy method to identify substrates, combining phosphatase treatment, *in vitro* kinase assay and Stable Isotope Labelling with Amino acids in Cell (SILAC) culture-based mass spectrometry. Implementing this approach, we identified 225 host substrates as well as a potential novel phosphorylation motif for CK1. We confirmed experimentally the enrichment of our substratome in bona fide L-CK1.2 substrates and showed they were also phosphorylated by human CK1δ. L-CK1.2 substratome is enriched in biological processes such as “viral and symbiotic interaction,” “actin cytoskeleton organisation” and “apoptosis,” which are consistent with the host pathways modified by *Leishmania* upon infection, suggesting that L-CK1.2 might be the missing link. Overall, our results generate important mechanistic insights into the signalling of host subversion by these parasites and other microbial pathogens adapted for intracellular survival.

Keywords: Casein kinase I, Substrate screen, *Leishmania*, Host-pathogen interactions, Cancer, SARS-CoV2

INTRODUCTION

Leishmania causes immuno-pathological diseases including cutaneous, muco-cutaneous, and visceral leishmaniasis, leading to severe morbidity and mortality. This parasite has two developmental stages, in the insect vector as an extracellular promastigote form, and in the mammalian host as an intracellular amastigote form where it resides inside the phagolysosome of macrophages. Our understanding of host-*Leishmania* interactions was very limited until the discovery of the *Leishmania* exo-proteome, revealing potential mechanisms by which the parasite subverts its host cell (Silverman et al., 2010) (Atayde et al., 2015; Rachidi et al., 2021). Among the proteins released by *Leishmania*, casein kinase 1.2 (LmjF35.1010, L-CK1.2) is particularly remarkable. Indeed CK1 family members as signalling kinases are involved in the regulation of multiple processes, such as apoptosis or cell cycle. Moreover, manipulation of the host cell CK1-signalling pathways is common to many intracellular pathogens, from viruses to eukaryote pathogens (Jayaswal et al., 2010; Xia et al., 2018; Rachidi et al., 2021; Dorin-Semblat et al., 2015), suggesting that the release of L-CK1.2 might be essential for macrophage subversion by *Leishmania*. Similarly to its human orthologs, *Leishmania* CK1.2 has a ubiquitous distribution in the parasite and is detected in the flagellum, flagellar pocket, the cytoplasm, or strongly associated with the cytoskeleton (Martel et al., 2020). The localisation of L-CK1.2, but not its activity requires its C-terminus domain (Martel et al., 2020), which might mostly mediate the interaction of L-CK1.2 to interacting partners (Knippschild et al., 2014). L-CK1.2 was shown to be part of the core cargo of exosomal proteins (Silverman et al., 2011; Silverman et al., 2010), present in exosomes released by promastigotes in the insect vector (Atayde et al., 2015) and enriched in exosomes released by amphotericin B-resistant parasites but not in that released by miltefosine- or antimony-resistant parasites (Douanne et al., 2020; Rachidi et al., 2021), suggesting that it has an important role for parasite survival in the insect and mammalian hosts. We and others have shown that L-CK1.2 is essential for intracellular parasite survival (Rachidi et al., 2014; Baker et al., 2021) and could be evolutionary selected for its capacity to interact with and phosphorylate host proteins to modulate macrophage biological and immune processes (Rachidi et al., 2021; Rachidi et al., 2014). Indeed, L-CK1.2 phosphorylates the human IFNAR1 receptor, which leads to the attenuation of the cellular response to interferon α/β (Liu et al., 2009). Altogether, these findings are consistent with L-CK1.2 being a master regulator of *Leishmania* intracellular survival. To determine its contribution to the regulation of host-pathogen interactions, identification of the host pathways it regulates through the systematic identification of substrates is crucial. However, the low stoichiometry of protein phosphorylation, the presence of endogenous kinases as well as the reversibility of the phosphorylation by phosphatases render systematic mapping of the cellular substratome extremely challenging. This is particularly true when handling pleiotropic signalling

kinases such as CK1 family members, able to phosphorylate hundreds of substrates (Knippschild et al., 2014). We thus developed a technology, easily applicable to other protein kinases, that allows efficient identification of substrates. Applying this pipeline on L-CK1.2, we identified 225 host substrates that shed important new lights on parasite immune and biological subversion of its host. Furthermore, we validated our approach, which might become a powerful new tool to study mechanisms of host-pathogen interactions and might provide host targets for host-directed therapy against Leishmaniasis.

MATERIAL AND METHODS

SILAC Labelling and Lysate Preparation

For labelling cells by SILAC, equal numbers of THP-1 monocytes ($2 \times 10^5 \text{ ml}^{-1}$) were seeded in RPMI 1640 without Lysine and Arginine (Thermo Fisher Scientific), supplemented either with natural amino acids (L-Lysine, 0.274 mM; L-Lysine, 1.15 mM; Arginine, 1.15 mM) or with the same concentrations of amino acid isotopes 2H4-Lysine (Lys4) and 13C6--Arginine (Arg6) (Thermo Scientific). The medium was supplemented with 50 μM β -mercaptoethanol, 50U mL^{-1} penicillin, 50 $\mu\text{g mL}^{-1}$ streptomycin and 10% (v/v) of dialysed Fetal Bovine Serum (Sigma). Cells were split and seeded before reaching a concentration of 10^6 ml^{-1} in fully supplemented SILAC medium, for a period of at least 15 days 0.75 to 1×10^8 cells were then differentiated for 48 h into macrophages by the addition of 10 ng mL^{-1} PMA. Cells cultivated in SILAC medium were washed three times in PBS and lysed in RIPA lysis and extraction buffer (Thermo Scientific) containing one tablet per 10 ml of cOmplete™ protease Inhibitor Cocktail tablets (Sigma). Cell extracts were incubated on ice 30 min, sonicated 5 min, and centrifuged 15 min at 14,000 g to eliminate cell debris. Proteins were quantified in the supernatants using the RC DC™ protein assay kit (Bio-Rad), according to the manufacturer's instructions. For free ATP depletion, protein extracts were dialyzed overnight at 4°C in 1 L of dialysis solution (1× PBS, 1 mM EDTA, 1 mM dithiothreitol) in a Slide-A-Lyzer dialysis cassette (Pierce).

Expression and Purification of L-CK1.2 and L-CK1.2-K40A

Bacterial expression plasmid for L-CK1.2 was generated as previously described (Rachidi et al., 2014). Bacterial expression plasmid carrying L-CK1.2-K40A (kinase dead) was generated by site-directed mutagenesis as previously reported (Rachidi et al., 2014). Recombinant proteins were induced in Rosetta™ (DE3) Competent Cells (Novagen) with 0.02% (w/v) L-arabinose for 3 h at 25°C. Cells were harvested and resuspended in lysis buffer as previously described (Rachidi et al., 2014). Briefly recombinant kinases were purified on co-nitrilotriacetic acid agarose (Pierce) and eluted in 300 mM imidazole in PBS containing 60 mM

β -glycerophosphate, 1 mM sodium vanadate, 1 mM sodium fluoride and 1 mM disodium phenylphosphate. Protein eluates were supplemented with 15% glycerol and stored at -80°C .

Expression and Purification of Human GST-CK1 δ^{TV1}

Bacterial expression of GST-CK1 δ^{TV1} was induced with 0.5 mM IPTG at an OD₆₀₀ of 0.6 AU in *E. coli* SoluBL21TM (Genlantis) and incubated for 18 h at 18°C . Cells were harvested and resuspended in lysis buffer containing 20 mM Tris-HCl (pH 7.6), 150 mM NaCl, 0.5% NP-40, 10% glycerol, 1 mM EDTA, 1 mM EGTA, 1 mM benzamidazine, 0.25 $\mu\text{g}/\text{ml}$ aprotinin and 1 mM DTT. The lysate was centrifuged at $15,000 \times g$ for 30 min. The cleared lysate was incubated with 300 μL of glutathione sepharose suspension (50% Glutathione Sepharose[®] 4 Fast Flow (Cytiva) in PBS) for 2 h at 4°C . Afterwards, glutathione sepharose beads were washed three times in lysis buffer containing 300 mM NaCl and twice in washing buffer (20 mM Tris-HCl (pH 7.6), 50 mM NaCl, 0.25 $\mu\text{g}/\mu\text{L}$ aprotinin, 1 mM EDTA). The bound proteins were eluted with 1 ml elution buffer containing 50 mM Tris-HCl (pH 7.6), 1 mM EDTA and 5 mM reduced glutathione. Proteins were stored in 10% glycerol at -80°C after shock freezing in liquid nitrogen.

Protein Kinase Assay and Phosphatase Treatment

For phosphatase treatment, 500 μg of “heavy” or “light” THP-1 protein extract were dephosphorylated with 50 U of Antarctic phosphatase (NEB) in Antarctic phosphatase buffer (NEB) for 30 min at 37°C . Phosphatase activity was heat inactivated at 65°C for 15 min. The kinase assay for the “heavy” or “light” protein extracts (500 μg) were performed in buffer C (60 mM β -glycerophosphate, 30 mM *p*-nitrophenyl phosphate, 25 mM MOPS [morpholinepropanesulfonic acid], 5 mM EGTA, 15 mM MgCl_2 , 1 mM dithiothreitol, 0.1 mM sodium vanadate; pH 7.0) in the presence of 15 μM ATP and 200 ng of recombinant L-CK1.2 or kinase dead L-CK1.2-K40A. The reaction was performed in triplicate at 30°C for 45 min. For mock reactions no kinases were added. Reactions were stopped with the addition of 10 μM of D4476 {4- [4-(2,3-dihydro- 1,4-benzodioxin-6-yl)- 5- 2-pyridinyl)- 1*H*- imidazol-2-yl]} benzamide, a specific inhibitor of CK1 known to inhibit L-CK1.2 activity (Rachidi et al., 2014), followed by heat inactivation at 65°C for 15 min. Next, kinase inactivation heavy and light protein samples were mixed in a 1:1 ratio, and precipitated in 80 (v/v) % ice-cold acetone and stored at -80°C prior to LC/MS-MS analysis. For IVKA with L-CK1.2, 15 μg of total THP-1 protein extracts or 0.5–1.0 μg of recombinant proteins, GST-14-3-3 γ (Enzo #BML-SE313-0100), RCN2-6XHis (Abcam #ab125644) Glo1 (Abcam # ab206792), SNAP23 (Abnova #H00008773-P01) and TAF7 (Abnova #H00006879-P01), were assayed with 0.2 μg of L-CK1.2 or L-CK1.2-K40A, as described in Rachidi et al. (2014). Incorporated ^{32}P was monitored by SDS-PAGE and

autoradiography. For IVKA with human GST-CK1 δ^{TV1} , 6 ng of kinase was incubated with the 0.5–1.0 μg of recombinant proteins (see above) in 1x kinase buffer (250 mM Tris-HCl (pH 7.0), 100 mM MgCl_2 , 1 mM EDTA) and 15 μM ^{32}P - γATP in 30 μL final volume for 30 min at 30°C . All kinase assays were performed at least three times.

Phospho-Peptide Enrichment

Phosphorylated peptides were enriched using TitansphereTM Phos-TiO kit centrifuge columns (3 mg/200 μL , cat. No. 5010-21312, GL Sciences), as described by the manufacturer. After elution from the Spin tips, phospho-peptides were vacuum concentrated to dryness and reconstituted in 0.1% formic acid. Samples were then loaded onto a custom-made C18 StageTips packed by stacking one AttractSPE[®] disk (#SPE-Disks-Bio-C18-100.47.20 Affinisep) and 2 mg beads (#186004521 SepPak C18 Cartridge Waters) into a 200 μL micropipette tip for desalting. Enriched phospho-peptides were eluted using 40/60 MeCN/H₂O + 0.1% formic acid and vacuum concentrated to dryness.

Liquid Chromatography-Tandem Mass Spectrometry

LC was performed with an RSLC nano system (Ultimate 3000, Thermo Scientific) coupled online to an Orbitrap Fusion Tribrid mass spectrometer (Thermo Scientific). Peptides were first trapped on a C18 column (75 μm inner diameter \times 2 cm; nanoViper Acclaim PepMapTM 100, Thermo Scientific) with buffer A (2/98 MeCN/H₂O in 0.1% formic acid) at a flow rate of 2.5 $\mu\text{L}/\text{min}$ over 4 min. Separation was then performed on a 50 cm \times 75 μm C18 column (nanoViper Acclaim PepMapTM RSLC, 2 μm , 100 \AA , Thermo Scientific) regulated to a temperature of 55°C with a linear gradient of 2–25% buffer B (100% MeCN in 0.1% formic acid) at a flow rate of 350 nL/min over 211 min. Separation of phospho-peptide samples without phosphatase was performed with buffer A' (5/98 DMSO/H₂O in 0.1% formic acid) and B' (5/95 DMSO/MeCN in 0.1% formic acid) by using a linear gradient of 2–30% with the same time and flow rate as previous gradient. Full-scan MS was acquired in the Orbitrap analyzer with a resolution set to 240,000, a mass range of *m/z* 400–1500 and a 4×10^5 ion count target. Ions from each full scan were isolated and further HCD fragmented with normalized collision energy of 30% and rapid scan MS analysed in the linear ion trap. The MS² ion count target was set to 2×10^4 and only those precursors with charge state from 2 to 7 were sampled for MS² acquisition.

Data Analysis

For identification, the data were searched against the *Homo sapiens* (UP000005640) UniProt database using Sequest-HT through Proteome Discoverer (PD, version 2.4). Enzyme specificity was set to trypsin and a maximum of two-missed cleavage sites was allowed. Oxidized methionine, Met-loss, Met-loss-Acetyl, Ser/Thr/Tyr phosphorylation, N-terminal acetylation, heavy $^2\text{H}_4$ -Lysine (Lys4) and $^{13}\text{C}_6$ -Arginine (Arg6) were set as variable modifications. Carbamidomethyl

of cysteines were set as fixed modification. Maximum allowed mass deviation was set to 10 ppm for monoisotopic precursor ions and 0.6 Da for MS/MS peaks. The resulting files were further processed using myProMS v3.9.2 (Poullet et al., 2007). The Sequest-HT target and decoy search result were validated at 1% false discovery rate (FDR) with Percolator at the peptide level. Technical replicates ($n = 3$) were merged using the MSF files node and a SILAC-based phospho-peptides quantification was performed by computing peptides XICs (Extracted Ion Chromatograms). The phosphosite localization accuracy was estimated by using the PtmRS node in PD (version 2.4), in PhosphoRS mode only. Phosphosites with a localization site probability greater than 75% and with at least two SILAC measurements per peptide were quantified at the peptide level. Mass spectrometry proteomics data have been deposited to the ProteomeXchange Consortium via the PRIDE (Perez-Riverol et al., 2019) partner repository with the dataset identifier PXD026220.

Motif Discovery

Unique phospho-peptides sequences, matching the strict selection criteria, were aligned on phosphorylated serine and threonine with 5 flanking amino acids. PhosphoSitePlus phosphosite plus [https://www.phosphosite.org/homeAction.action (Hornbeck et al., 2015)] was used to compute motif analysis enrichment (automatic background selection; significance of $1e-6$; support threshold of 0.1) and to generate corresponding sequence logo (automatic background selection; frequency change algorithm (Vacic et al., 2006)).

STRING Network Visualization and Gene Ontology Enrichment Analysis

The dataset was analyzed for protein-protein interactions and visualized using the STRING plugin [string, https://string-db.org/ (Szklarczyk et al., 2019)] of the Cytoscape software package [version 3.8.2, https://cytoscape.org/ (Shannon et al., 2003)]. Each node represents a substrate and each edge represents a protein-protein interaction. Functional enrichment analysis of the dataset was performed using the g:profiler web server (https://biit.cs.ut.ee/gprofiler/gost) and the following criteria: only annotated genes, with a significance threshold of 0.05, select GO terms of less than 5,000 genes, and only focusing on GO “biological process.” Results were visualized using the EnrichmentMap plugin of the Cytoscape software package [version 3.3, http://apps.cytoscape.org/apps/enrichmentmap (Merico et al., 2010)], with a p-value and a Q-value above 0.05 and an edge cut-off of 0.375. Node color represents the enrichment p-value (see legend Figure 4). Node size is proportional to the total number of genes belonging to the corresponding gene-set. The edge corresponds to the Annotation shared between two nodes, with edge thickness corresponding to the number of shared genes. Node clusters were identified and annotated by the AutoAnnotate plugin of cytoscape (version 1.3.3 https://autoannotate.readthedocs.io/en/latest/).

RESULTS

Strategy and Establishment of the Experimental Protocol

To identify the L-CK1.2 host-substratome, we implemented an experimental workflow designed to quantify TiO_2 -enriched phospho-peptide stoichiometry by LC-MS/MS in metabolically-labelled, heat inactivated THP-1 macrophage protein lysates after their phosphorylation by recombinant L-CK1.2 (Figure 1A). In order to increase the number of sites available for *de novo* L-CK1.2 phosphorylation prior *in vitro* kinase assay (IVKA), we depleted the lysates in ATP before treating them with Antarctic phosphatase. However, since CK1 recognises, as a main consensus site, the following motif [S/T] X_{2-3} [pS/pT], where the second S/T residue is only accessible for CK1 phosphorylation if the first S/T residue is primed (a.k.a. phosphorylated) by other kinases, we also performed an experiment without phosphatase treatment. TiO_2 -enriched phospho-peptide stoichiometry was calculated from technical triplicate as a ratio of Heavy_{L-CK1.2}/Light_{L-CK1.2-K40A} and comparisons were made to phospho-peptide ratios of Heavy/Light mock reactions without kinases.

For establishing appropriate experimental conditions, several pilot experiments were carried out. To decrease the background activity of endogenous kinases, the lysate of THP-1 macrophages was pulse-heated to denature endogenous kinases (Supplementary Figure S1). Denaturation efficiency was demonstrated by the absence of ^{32}P incorporation in the background control (Supplementary Figure S1, lane 2). In contrast, the *de novo* phosphorylation of denatured THP-1 proteins by active L-CK1.2 was detected, showing that L-CK1.2 phosphorylates proteins present in the macrophage lysate (Supplementary Figure S1, lane 1). To increase the number of sites available for *de novo* phosphorylation in the macrophage lysate, two steps were added to the pipeline (Figure 1A). The protein lysates were dephosphorylated by Antarctic phosphatase and depleted of free ATP by dialysis to prevent any additional phosphorylation. Similar patterns of total protein staining (Supplementary Figure S1, right panel) and phosphorylation profile (Supplementary Figure S1, left panel) were observed between samples treated or not with phosphatase and thus dialysed or not, suggesting that protein degradation following dialysis was minimal under our experimental conditions. The increase of ^{32}P incorporation into substrates following phosphatase treatment (Supplementary Figure S1, lane 3) confirms that previously many sites were inaccessible to *de novo* phosphorylation. To reduce technical errors during phospho-peptides enrichment, to limit missing values and to perform quantitative analyses, we used Stable Isotope Labelling with Amino acids in Cell culture (SILAC). This method relies on the metabolic incorporation of either “Heavy” [2H_4 -Lysine (Lys⁴) and $^{13}C_6$ -Arginine (Arg⁶)] or natural (“Light”) [lysine (Lys⁰) and arginine (Arg⁰)] amino acids (Ong et al., 2002; Ong and Mann, 2006; Basken et al., 2018). We validated the percentage of Lys4 incorporation in THP-1 macrophage

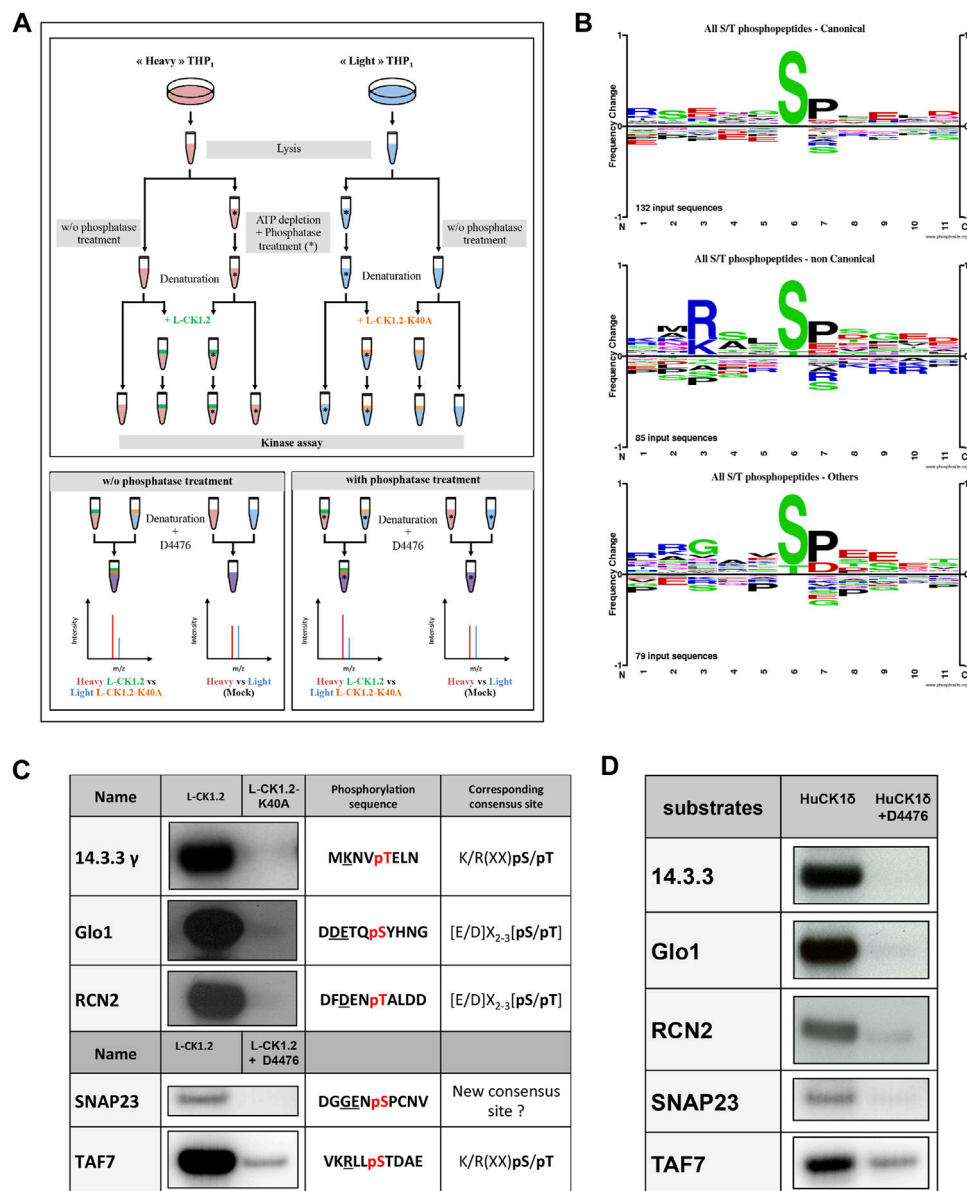


FIGURE 1 | Experimental workflow and validation of substrate dataset. **(A)** Upper Panel. Workflow diagram showing the experimental strategy used to reveal L-CK1.2 substratome derived from THP-1 lysates. THP1 cells were cultured and differentiated in the presence of natural amino acids (light, blue) or stable amino acid isotopes (heavy, red). Equal amounts per reaction (0.5 mg) of heavy or light lysates were treated with phosphatase and ATP depleted (*) or not and denatured by heat inactivation to remove endogenous kinase activities. The phosphatase reactions were stopped by heat inactivation. Lysates were then subjected to IVKA in presence of recombinant L-CK1.2 (green), L-CK1.2-K40A (kinase-dead, orange), or were mock treated with equal amounts of kinase elution buffer, in triplicate. The reactions were stopped with heat inactivation and addition of 10 μM D4476. Lower panel. Equal amounts (0.5 mg) of heavy (L-CK1.2) and light (L-CK1.2-K40A) samples were mixed. In addition, mock heavy and light samples were mixed in a 1:1 ratio and used as a control. The four samples were reduced, alkylated and digested and the resulting phospho-peptides were enriched by TiO₂-affinity chromatography, and processed by LC-MS/MS analysis on an Orbitrap fusion mass spectrometer. **(B)** Sequence logos analysis of unique phospho-sites (five amino acids before and after the phosphorylation residues) matching strict selection criteria. Upper panel, for canonical consensus sites; middle panel, for non-canonical sites; and lower panel, for others. The amino acids are labelled according to their chemical properties: green for polar amino acids (G, S, T, Y, C, Q, N), blue for basic amino acids (K, R, H), red for acidic amino acids (D, E), and black for hydrophobic amino acids (A, V, L, I, P, W, F, M). **(C)** Autoradiogram representing IVKA using selected recombinant human proteins and inactive L-CK1.2-K40A (kinase-dead), active L-CK1.2 alone or in presence of the CK1-specific small molecule inhibitor D4476 (10 μM). **(D)** Autoradiogram representing IVKA using selected recombinant human proteins and recombinant CK1δ^{TV1} alone or in the presence of D4476.

proteins by LC-MS/MS analysis, which was over 99%. Finally, to reduce the risk of selecting false positive signals, we performed mock kinase assays using the “light” and “heavy”

macrophage lysates without adding the kinases, to discard sites already differentially phosphorylated prior to the kinase assays.

TABLE 1 | Phospho-peptides.

	W/o phosphatase treatment	With phosphatase treatment	Total phospho-sites	%
Total phospho-peptides	99	158	257	
Consensus site for CK1				
Canonical sites	42	84	126	72
Non-canonical sites	31	43	74	
Others sites	31	46	77	28
Sites phosphorylated by huCK1s				
Site phosphorylated <i>in vitro</i>	14	9	19	7
Sites detected in human cell phospho-proteomes				
Site phosphorylated <i>in vivo</i>	92	149	241	94
SARS-coV2 infection				
Sites phosphorylated during SARS-coV2 infection	20	28	52	20
Tumorigenesis				
Site phosphorylated in cancer cells	83	146	229	89
Sites mutated during tumorigenesis	10	16	26	10

Identification of L-CK1.2 Host Cell Substrates

Three independent reactions for each condition were carried out, and two independent protein extracts treated or not with phosphatase were used. In the absence of phosphatase treatment, 7,752 unique enriched phospho-peptides belonging to 3,544 unique proteins were identified of which 65% were quantified (see **Supplementary Figures S2A, B** for Venn diagrams). The same analysis was performed with samples pre-treated with phosphatase, and 15,852 enriched phospho-peptides (5,158 proteins) were identified of which 66% were quantified (**Supplementary Figures S2C, D**), demonstrating the efficiency of the phosphatase treatment. However, the increase in phospho-peptides also in the H/L control (**Supplementary Figures S2A, B**) suggests that the pulse-heating step did not completely abrogate but only reduced the activity of endogenous kinases to levels undetectable by autoradiography (**Supplementary Figure S1**).

To determine *L-CK1.2* substrates, the following selection criteria were applied: 1) A probability of correct localisation of the phosphorylation site on validated peptides greater than 75%, as calculated by PtmRS software (see Data analysis of Material and methods), 2) the ratio $\text{Heavy}_{L-CK1.2}/\text{Light}_{L-CK1.2-K40A}$ equal or above two to select the sites phosphorylated by *L-CK1.2* (Sugiyama et al., 2019); and/or 3) the ratio $\text{Heavy}_{L-CK1.2}/\text{Light}_{L-CK1.2-K40A}$ at least twofold higher than that of the control Heavy/Light to only select the newly phosphorylated sites. As we detected a high number of unique peptides identified in the presence of active kinase and not in that of inactive kinase, p-value could not be used, as statistical analyses either lacked power or were not available depending if a unique phosphopeptide was identified in one or more replicates of one state, respectively. We chose not to use data imputation to force statistical analyses, as current methods are not really suitable for phospho-proteomics, and they often add noise. We chose a stringent fold-change cut-off of 2, similar to the approach of Sugiyama et al., 2019 using for the discovery of the substrates of human kinases (Sugiyama et al., 2019). In addition, to strengthen our selection process, and considering that the overlap between

replicates is about 25% at best, we considered reproducibility between replicates and we validated phosphopeptides solely if criteria 1), 2) and 3) were validated at least in two out of three replicates.

Using the above criteria, 99 phospho-peptides (81 proteins) and 158 phospho-peptides (144 proteins) were selected as potential substrates of *L-CK1.2* in absence or in presence of phosphatase, respectively (**Table 1**). Noticeably, only proteins expressed in non-infected macrophages could be detected in our experimental setting. We missed potential substrates exclusively expressed in infected macrophages. Only fifteen proteins were common to the two datasets. Although consistent with the variability of the data dependent acquisition (DDA) LC-MS/MS analysis, this finding suggests that the phosphatase treatment greatly improves the access of *L-CK1.2* to new substrates for which it has more affinity.

Validation of the Substratome

Because our approach is *in vitro*, we first checked whether the sites we identified are phosphorylated *in vivo*. To this end, we compared our dataset with existing human phosphoproteomes (**Table 1** and **Supplementary Table S1**, <https://www.phosphosite.org/homeAction.action>). We found that 94% of the 257 phosphosites were phosphorylated *in vivo* suggesting they are physiologically relevant and accessible *in vivo*. Next, three levels of validation were used to demonstrate that the dataset containing 225 proteins are *bona fide* host *L-CK1.2* substrates (**Table 2**). First, we showed that our dataset contains 55% of known mammalian CK1 substrates or interacting partners: 11 known substrates, including the interferon-alpha/beta receptor alpha chain (IFNAR1/2) (Liu et al., 2009), Sprouty 2 (SPRY2) (Yim et al., 2015) and Fam83H (Fulcher et al., 2018); 46 potential new substrates obtained by Sugiyama et al. using a similar method (**Supplementary Table S2**) (Sugiyama et al., 2019); as well as 66 known interacting partners, which thus might also be substrates (Buljan et al., 2020). Second, the phospho-peptides, we identified, were highly enriched in known CK1 consensus sites (Xu et al., 2019). Hundred and twenty-six sites display the

TABLE 2 | Proteins.

	W/o phosphatase treatment	With phosphatase treatment	Total proteins	%
Total proteins	81	144	225	—
Known human CK1 substrates or binding partners				
Substrates	32	30	57	55
Binding partners	19	47	66	
<i>Leishmania</i> infection				
Proteins differentially regulated during infection	25	47	72	60
Transcripts differentially regulated during infection	20	48	68	
Tumorigenesis				
Prognosis markers				76
Favourable	17	23	40	
Unfavourable	34	57	91	
Both depending on the cancer type	12	28	40	
SARS-coV2 infection				
Proteins phosphorylated during infection	37	78	115	51

canonical CK1-phosphorylation motif, [S/T]X₂₋₃ [pS/pT] or [E/D]X₂₋₃ [pS/pT] (Table 1; Figure 1B top panel), consistent with the affinity of CK1 for these two motifs (Xu et al., 2019). Seventy-four sites display the non-canonical consensus SLS-Xn-(E/D)n (Ha et al., 2004; Marin et al., 2002; Marin et al., 2003; Marin et al., 1994) or resemble to K/R(X)K/R (XX)pS/pT, a CK1 consensus site identified in cholesterol and sulfatide binding proteins (Table 1; Figure 1B middle panel) (Kawakami et al., 2008). Surprisingly, this motif was present in only 10 phosphopeptides while the remaining 58 peptides contained a shorter version, K/R (XX)pS/pT. Finally, seventy-seven phospho-sites did not contain any known CK1 motif (others, Table 1), and might represent novel CK1 phosphorylation motifs (Table 1). We searched for motif enrichment using PhosphoSitePlus and identified [G]XX [pS] in 20 phospho-peptides with a p-value of 8.02E-11 (Figure 1B bottom panel and Table 3) and variants of this site: [G]XX [pS]XX [E] (7 sites) and [G]XX [pS]P (10 sites). Noticeably, all the motifs generated for L-CK1.2 in this study highlight the presence of a proline residue adjacent to the phosphorylated S or T (Figure 1B, position 7), which has not been described for human CK1 motifs (Sugiyama et al., 2019). It might reflect the specificity in the substrate recognition motif of L-CK1.2. Third, we performed an *in vitro* kinase assay using recombinant L-CK1.2 to experimentally validate our substratome data. We included five proteins that might be important for *Leishmania* intracellular survival based on their potential to modulate macrophage functions and/or inflammation. The selected recombinant proteins, namely reticulocalbin 2 (RCN2, Q14257), 14-3-3γ (YWHAG, P61981), lactoylglutathione lyase 1 (Glo1, Q04760), synaptosomal-associated prot 23 (SNAP23, O00161) and transcription initiation factor TFIID subunit 7 (TAF7, Q15545) were subjected to a kinase assay using inactive L-CK1.2-K40A (kinase-dead), active L-CK1.2 alone or in presence of the CK1-specific small molecule inhibitor D4476 (Rachidi et al., 2014). All recombinant proteins were phosphorylated by L-CK1.2, but no phosphorylation was observed in the D4476 and L-CK1.2-K40A controls (Figure 1C). We performed a similar experiment using recombinant human CK1δ and showed that the five substrates were also phosphorylated by the human kinase, confirming the

relevance of our substratome for human CK1s (Figure 1D). Altogether, these results confirm that our dataset identified bona fide L-CK1.2 host cell substrates, which validate our approach. Furthermore, these substrates are also targeted by human CK1δ, which is consistent with data obtained by Sugiyama et al. showing that 24 L-CK1.2 phospho-sites are also targeted by human CK1s (Table 4).

Relevance of the Substratome for *Leishmania* Infection

Next, we asked whether the phosphorylation of these host substrates by L-CK1.2 might be relevant for *Leishmania* intracellular survival. Although, many studies described host pathways modified upon *Leishmania* infection, little is known about host proteins regulated by excreted *Leishmania* proteins and particularly excreted kinases (Isnard et al., 2012; Nandan and Reiner, 2005). Thus, we asked whether L-CK1.2 host substrates were differentially regulated during *Leishmania* infection and whether pathways enriched in our dataset were consistent with those modified during infection. Indeed, during *Leishmania* infection, 32% of L-CK1.2 substrates are differentially regulated at protein level (Smirlis et al., 2020; Singh et al., 2015; da Silva Santos et al., 2015; Negrão et al., 2019), and 30% differentially expressed at transcript level during infection (Fernandes et al., 2016; Dillon et al., 2015; Frank et al., 2015; Rabhi et al., 2013) (Table 2). These findings suggest that 60% of the proteins targeted by L-CK1.2 might be important for *Leishmania* infection. To determine the biological processes enriched in our dataset, we used Enrichment map app from cytoscape. We identified functional enrichment for nine GO terms relative to apoptosis, actin cytoskeleton organisation or RNA processing and splicing, which is consistent with *Leishmania* inhibiting host apoptosis (Moore and Matlashewski, 1994; Gupta et al., 2016), altering F-actin dynamics (de Menezes et al., 2017), or modifying the host transcriptome, respectively (Fortéa et al., 2009; Fernandes et al., 2016) (Figure 2). Moreover, several key biological processes, preferentially targeted by *Leishmania* CK1.2, are associated with host-pathogen interactions such as “viral and

TABLE 3 | Motifs identified in category “others.”

Motif	ZScore	p-value	Foreground matches	Foreground size
...G...sP...	8.64	0.00E+00	10	69
...G...s...E	8.24	0.00E+00	7	69
...G...s...	6.4	8.02E-11	20	69
...sP...	9.94	0.00E+00	34	69
...sD.E	8.43	0.00E+00	8	69
...sD...	8.73	0.00E+00	11	69
...s...E	5.03	2.43E-07	16	69

TABLE 4 | Residues also phosphorylated by huCK1s.

Substrate/Uniprot ID	Uniprot	huCK1 paralogs	Phosphorylated by huCK1s and L-CK1.2	Protein description
CLIC1_HUMAN	O00299	CK1e	S221	Chloride intracellular channel protein 1
ARC1B_HUMAN	O15143	CK1d	S311	Actin-related protein 2/3 complex subunit 1B
ANXA2_HUMAN	P07355	CK1d/e/g1/g2/g3	S12/S184	Annexin A2
GRP78_HUMAN	P11021	CK1d/g2	S311	78 kDa glucose-regulated protein
PDIA4_HUMAN	P13667	CK1d/e	S468	Protein disulfide-isomerase A4
KAP2_HUMAN	P13861	CK1d/g2	S80	cAMP-dependent protein kinase type II- α regulatory subunit
1433T_HUMAN	P27348	CK1d/e	T30	14-3-3 protein theta
1433B_HUMAN	P31946	CK1d	T32	14-3-3 protein beta/alpha
MDHC_HUMAN	P40925	CK1d/g1/g2/g3	T321/S332	Malate dehydrogenase, cytoplasmic
BAT2_HUMAN	P48634	CK1d/g1	S1092	Large proline-rich protein BAT2
TERA_HUMAN	P55072	CK1e	S37	Transitional endoplasmic reticulum ATPase
1433G_HUMAN	P61981	CK1d/e	T31	14-3-3 protein gamma
1433Z_HUMAN	P63104	CK1d/e/g1/g2/g3	S28/T30	14-3-3 protein zeta/delta
LGUL_HUMAN	Q04760	CK1d/g3	S114	Lactoylglutathione lyase
1433F_HUMAN	Q04917	CK1e/g2	T31	14-3-3 protein eta
C1QBP_HUMAN	Q07021	CK1d/e/g1/g3	S205	Complement component 1 Q subcomponent -binding protein, mitochondrial
RCN2_HUMAN	Q14257	CK1d/e/g1	T137	Reticulocalbin-2
SEPT9_HUMAN	Q9UHD8	CK1d/e	S247	Septin-9
UTP18_HUMAN	Q9Y5J1	CK1d	S121/S124/S210	U3 small nucleolar RNA-associated protein 18 homolog

symbiotic interactions” or “response to stimulus” (**Figure 2, Supplementary Table S3**), suggesting that despite the use of non-infected macrophages as experimental system, pathways activated during infection were identified in our dataset. Altogether, this functional enrichment study suggests that the pathways targeted by L-CK1.2 *in vitro* might have some relevance *in vivo*. Further experiments will be required to determine the respective importance of all these substrates for *Leishmania* infection.

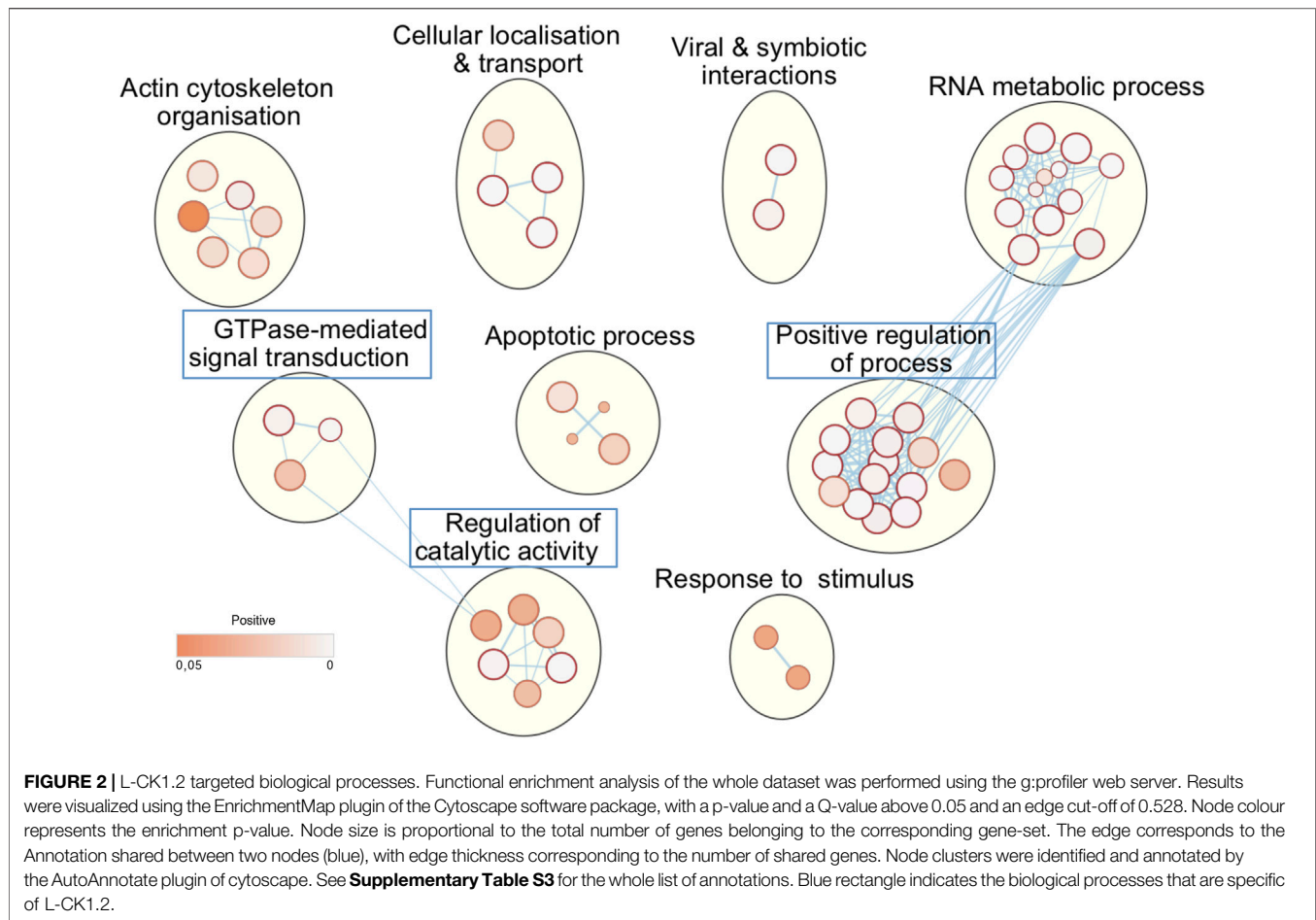
L-CK1.2 Substratome Versus Human CK1s Substratome

It is expected that L-CK1.2 and the host CK1s would target the same substrates, as they are closely related, but we have shown that they have structural differences in their ATP binding pocket (Durieu et al., 2016) and in their primary sequence with the presence of three additional amino acids between domain III and IV (Rachidi et al., 2014). These differences might lead to differences in substrate affinity. To examine this hypothesis and to take in account the variability of DDA of LC-MS/MS analyses, instead of comparing substrates, we compared biological process enrichments to deduce the

ability of L-CK1.2 to regulate host CK1-related pathways. To this end, we took advantage of the recent substratome of human CK1s (CK1 α , δ , ϵ , γ 1, γ 2 and γ 3) obtained by Sugiyama et al. Sugiyama et al. (2019) using HeLa cells, and performed a biological process enrichment map, which we compared to that of L-CK1.2 (**Figure 3, Supplementary Table S4**). We identified 19 groups, including “DNA metabolic process,” “cell cycle” and “catabolic process,” among which 6 are common with L-CK1.2. Noticeably, three biological processes are enriched only in L-CK1.2 dataset: “GTPase-mediated signal transduction,” “positive regulation of process” and “regulation of catalytic activity.”

L-CK1.2 Substrates for Human Diseases

CK1 family members have been implicated in the physiopathology of several human diseases such as cancer or infectious diseases (Knippschild et al., 2014; Xu et al., 2019). Indeed, defect in CK1 regulation is associated with cancer, while survival of intracellular pathogens relies on the manipulation of host CK1-pathways (Jayaswal et al., 2010; Cegielska and Virshup, 1993; Zhang et al., 2017). One intriguing possibility would be that the modification of similar CK1 pathways might contribute to the pathology of

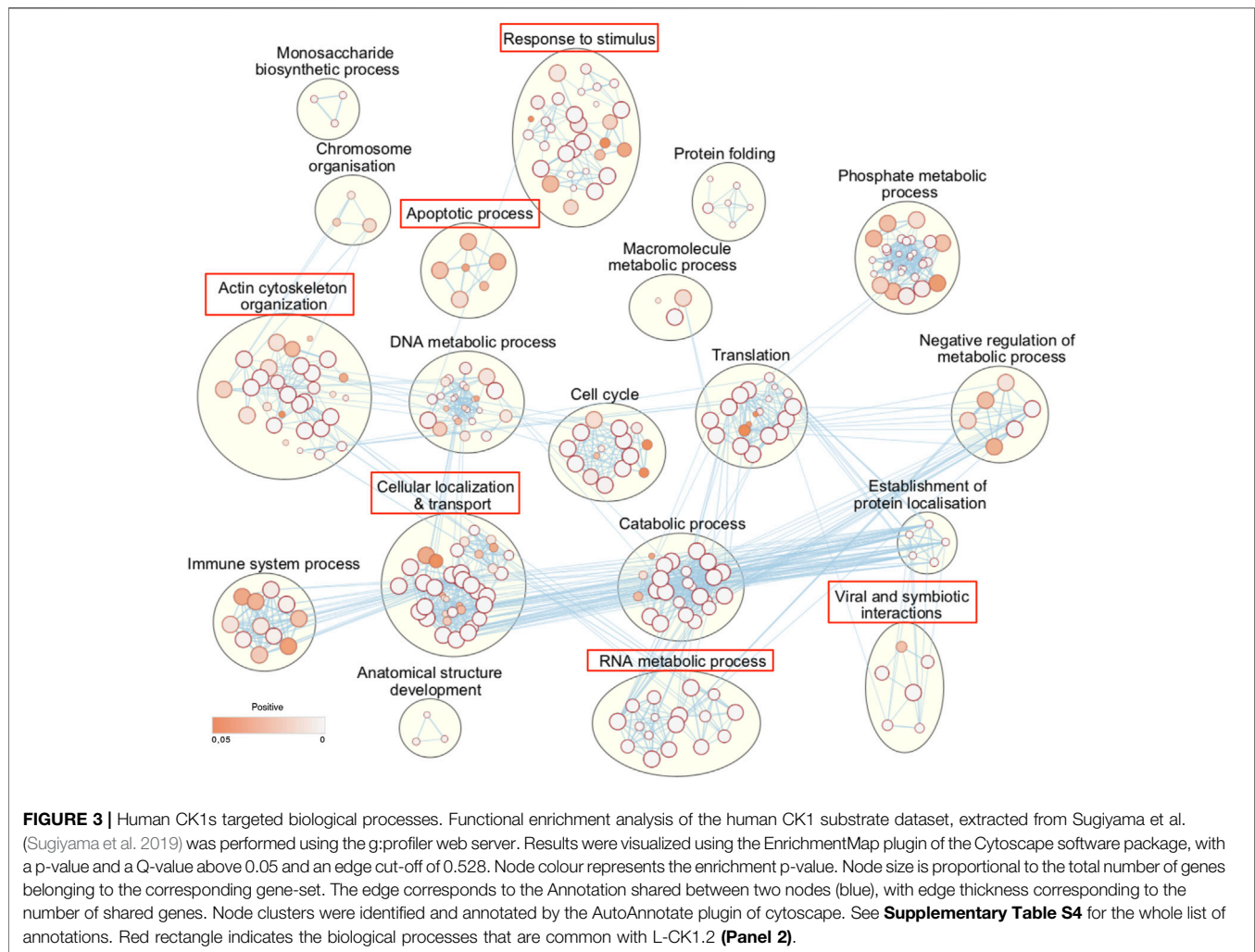


these different diseases. To support this hypothesis, we investigated whether any of L-CK1.2 substrates might be important for other human diseases, focusing on cancer and viral infection. First, we showed using PhosphoSitePlus that 1) 76% of the L-CK1.2 substrates are considered as prognosis markers for various cancer types (**Supplementary Table S1**), 2) 89% of L-CK1.2 phosphosites are phosphorylated in cancer cells (**Table 1**; **Supplementary Table S1** and **Figure 4**, round shape), and 3) 10% of L-CK1.2 phosphosites are mutated during tumorigenesis (**Table 1**; **Supplementary Table S1** and **Figure 4**, red border). These data are consistent with the fact that human CK1s are overexpressed in cancer cells (Xu et al., 2019). Second, we showed that 51% of L-CK1.2 substrates are phosphorylated during SARS-CoV2 infection (**Figure 4**, green, **Table 2** and **Supplementary Table S1**), and 20% on the same sites as those phosphorylated by L-CK1.2 (**Table 1** and **Supplementary Table S1**) (Bouhaddou et al., 2020). Only two biological processes, “RNA splicing” and “cellular localisation and transport,” are commonly enriched (**Supplementary Figure S3** and **Supplementary Tables S5, S6**). Interestingly, L-CK1.2 substratome contains eight proteins that interact with SARS-CoV2 proteins, suggesting similar regulations (Gordon et al., 2020). Altogether, our data

point to similar pathways being altered in different human diseases.

DISCUSSION

Increasing the knowledge on released parasite proteins is crucial to better understand host-pathogen interactions. Even more when studying host cell signalling pathways exploited by pathogens during infection through the release of their kinases, hence the importance of finding their host substrates in an unbiased manner. Here, we developed a method, applicable to other kinases, combining SILAC-based quantitative mass spectrometry, pulsed heating and IVKA that allows direct detection of phosphorylation and does not require the modification of the kinase (Shah et al., 1997). We applied this method to L-CK1.2, as, despite its essentialness for intracellular parasite survival, little is known on the host functions of this signalling kinase released by *Leishmania*, except its phosphorylation of host IFNAR1, the receptor to interferon α/β (Liu et al., 2009). We identified 257 phospho-sites corresponding to 225 substrates. Although our approach has limitations inherent to the variability of the DDA of mass



spectrometry analyses or to the IVKA, we validated them as *bona fide* CK1 substrates, suggesting that the above limitations did not compromised our ability to identify true L-CK1.2 substrates. Regarding the physiological relevance of those substrates, we cannot exclude that the pulsed heating might have altered protein structure and revealed sites that would normally not be accessible. However, we do not favour this hypothesis for two reasons. First, most of the phosphosites in our dataset are phosphorylated *in vivo* (PhosphoSitePlus), suggesting that they are accessible even integrated into protein complexes. Second, we validated experimentally some of these substrates even when correctly folded. These results will need experimental confirmation in a cellular model, nonetheless they provide pathways to prioritise for further characterisation. We showed that only few substrates are common to the two datasets, + and - phosphatase treatment, which can be explained as follows. 1) Substrates carrying the following consensus site, [S/T]pX₂₋₃ [pS/pT], might have been lost from the “+ phosphatase” dataset, as it requires priming. 2) Phospho-peptides were lost as a consequence of the variability in TiO₂ purification, of DDA LC-MS/MS analysis. 3)

Dephosphorylation might have made accessible residues for which L-CK1.2 has more affinity and thus might phosphorylate preferentially when available, explaining why some residues targeted efficiently in absence of phosphatase treatment were no longer identified after the treatment. These variabilities led to the lost of a substantial number of common substrates, as they were above threshold in only one of the three replicates, which is not sufficient to be considered as a substrate.

From our large dataset, we showed that L-CK1.2 phosphorylates the known canonical and non-canonical CK1 recognition motifs, which is consistent with previous observations (Rachidi et al., 2014). The only differences are first linked to the motif identified by Kawakami et al. K/R(X) K/R (XX)pS/pT (Kawakami et al., 2008), as our results suggest a shorter motif, K/R (XX)pS/pT. Our analysis is based on a bigger number of substrates, which might explain the difference with Kawakami et al. (2008). The second difference is the presence of a proline residue adjacent to the phosphorylated S/T ([pS/pT][P]). Sugiyama et al. identified 507 substrates for human CK1α, δ, ε, γ1, γ2, γ3, and found similar CK1 phosphorylation motifs to those

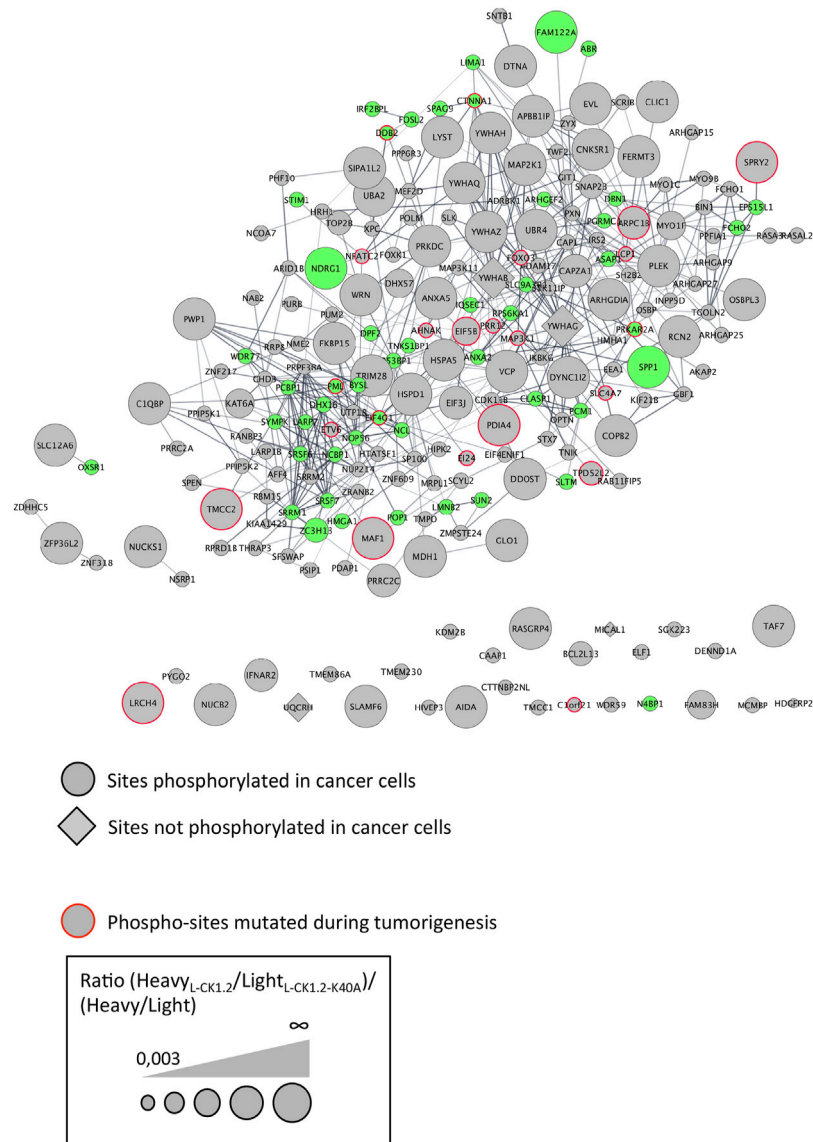


FIGURE 4 | Protein-protein interaction network of L-CK1.2 substrates. The dataset was analyzed for protein-protein interactions and visualized using the STRING plugin of the Cytoscape software package. Each node represents a substrate and each edge represents a protein-protein interaction. Round shape represents sites phosphorylated in cancer cells; Diamond shape represents sites not phosphorylated in cancer cells; Red border indicates phospho-sites mutated during tumorigenesis; Green fill color indicates proteins phosphorylated during SARS-CoV2 infection. The labeling indicates the UniProt human name. The size of the node represents the ratio $(Heavy_{L-CK1.2}/Light_{L-CK1.2-K40A})/(Heavy/Light \text{ mock})$.

we identified with the exception of the proline in +1 (Sugiyama et al., 2019). L-CK1.2 might have more affinity for consensus sites containing a proline adjacent to the S/T, which might be a way to restrict the host CK1 substrates targeted. Its requirement and its importance for L-CK1.2 substrate affinity remain to be confirmed experimentally. Furthermore, we identified a potential new CK1 consensus site, $[G]X_{2-3} [pS/pT]$, which was validated experimentally with L-CK1.2 and CK1 δ (SNAP23, **Figures 1C,D**). Further analyses, including mutagenesis, will be required to confirm this new consensus, as we cannot exclude the possibility that SNAP23 was phosphorylated on another site. L-CK1.2, not only targets similar consensus sites as mammalian

CK1s but also similar biological processes (BP), as we showed that five human CK1 BP were also enriched in L-CK1.2 dataset. Noticeably, L-CK1.2 seems to target fewer pathways than human CK1s. Although we cannot rule out that it might be the consequence of the variability inherent to proteomic analyses, L-CK1.2 and human CK1s might have differences in substrate affinity despite high level of identity. Indeed, structural differences (Rachidi et al., 2014; Durieu et al., 2016) and a potentially more restricted consensus site (presence of a proline, this work) might explain this specificity. Further analyses will be required to distinguish between these two possibilities.

Numerous publications described host pathways modified during *Leishmania* infection but only few established a link between these pathways and parasite effectors. Our study by determining the host substrates of *Leishmania* CK1.2 highlight, for the first time, the pathways it may regulate in the host cell, providing a potential new link between a parasite effector and the host pathways it modifies. These pathways are consistent with those modified during *Leishmania* infection. For instance, several studies have shown that *Leishmania* infection inhibits macrophage apoptosis, which might contribute to the spread of the infection and parasite transmission (Moore and Matlashewski, 1994; Gupta et al., 2016). Indeed, we identified 41 L-CK1.2 host substrates involved in apoptosis, such as BCL2L13, which regulates the role of mitochondria-mediated cell death pathway and can be pro- or anti-apoptotic (Meng et al., 2021), or FOXO3, which is a transcription factor inducing transcription of genes involved in apoptosis. There are other examples with host pathways such as “actin cytoskeleton organisation” or RNA metabolic process” that are both targeted by L-CK1.2 and modified during *Leishmania* infection (Fernandes et al., 2016; de Menezes et al., 2017; Smirlis et al., 2020; Bichiou et al., 2021). Extensive work remains to be done to ascertain the link between L-CK1.2 and host pathways modified during *Leishmania* infection. Nevertheless, the biological processes enriched among L-CK1.2 host substrates provide a starting point to prioritize pathways that should be characterised to reveal L-CK1.2 functions in the host cell. Furthermore, our dataset provides a list of potential host targets for host-targeted therapy against leishmaniasis (Lamotte et al., 2017).

Finally, although seemingly different, Visceral Leishmaniasis (VL), COVID-19 and cancer have manifestations that are to some extent common. For example, the uncontrolled overproduction of cytokines, namely the cytokine storm, is a common feature of terminal VL (Santos-Oliveira et al., 2011), SARS-CoV-2 infection and cancer (Turnquist et al., 2020). At the cellular level, similar pathways are regulated in infected or cancer cells. For instance, apoptosis is inhibited in *Leishmania* infected macrophages as well as in cancer cells (Knippschild et al., 2014; Gupta et al., 2016). The immune response is attenuated, preventing infected or cancer cells from being destroyed by the immune system (Knippschild et al., 2014; Figueiredo et al., 2016). CK1 is involved in the regulation of these two pathways, suggesting that it might be important for disease development (Knippschild et al., 2014; Xu et al., 2019; Rachidi et al., 2021). Indeed, human CK1 has cancer-associated functions linked to its involvement in the Wnt (Wingless/Int-1), Hh (Hedgehog), and Hippo signalling pathways (Knippschild et al., 2014; Xu et al., 2019), as well as an involvement in viral, bacterial and parasitic infections (Cegielska and Virshup, 1993; Jayaswal et al., 2010; Durieu et al., 2016; Zhang et al., 2017). Therefore CK1 substrates, including those identified in this work, might be similarly altered in different diseases. For instance, inactivation of FOXO3 is associated with the initiation and progression of cancer (Liu et al., 2018) and has a role in infectious diseases through regulation of IL-10 (Kane and Mosser, 2001; Bouzeyer et al., 2019). Understanding these molecular connections between

infectious diseases and cancer may help health care providers discover new therapies for combatting these diseases.

DATA AVAILABILITY STATEMENT

The datasets presented in this study can be found in online repositories. The names of the repository/repositories and accession number(s) can be found below: <https://www.ebi.ac.uk/pride/archive/>, PXD026220.

AUTHOR CONTRIBUTIONS

Conceptualization: DS and NR; Investigation: DS, FD, AR, UK and NR; Formal analysis: DS, FD, VS, DL and NR; Writing –original draft: DS, NR; Writing –review and Editing: DS, FD, VS, AR, UK, DL, GS and NR; Funding acquisition: GS and NR; Supervision DL, UK and NR.

FUNDING

This work was supported by the Institut Pasteur grant, PTR539 and by the ANR-13-ISV3-000.

ACKNOWLEDGMENTS

The authors would like to thank Olivier Leclercq for its graphical contribution and Victor Laigle for fruitful discussions.

SUPPLEMENTARY MATERIAL

The Supplementary Material for this article can be found online at: <https://www.frontiersin.org/articles/10.3389/fcell.2021.800098/full#supplementary-material>

Supplementary Figure S1 | Increase of accessible residues for *de novo* phosphorylation following phosphatase treatment. Left panel Autoradiogram representing IVKA using THP-1 cell extracts treated (lane 3 and 4) or not (lane 1 and 2) with Antarctic phosphatase, and active L-CK1.2 (lane 1 and 3) or inactive L-CK1.2-K40A (lane 2 and 4). Right Panel Same gel stained with coomassie blue.

Supplementary Figure S2 | Comparison of the different experimental conditions. Venn diagrams showing the numbers and overlaps of phospho-peptides (A,C) or proteins (B,D) in the following four experiments: Heavy_{L-CK1.2}/Light_{L-CK1.2-K40A} and Heavy/Light mock, treated (A,B) or not with Antarctic phosphatase (C,D).

Supplementary Figure S3 | Common pathways targeted by L-CK1.2 and phosphorylated during SARS-CoV2 infection. Functional enrichment analysis of the proteins phosphorylated by L-CK1.2 and also during SARS-CoV2 infection was performed using the g:profiler web server. Results were visualized using the EnrichmentMap plugin of the Cytoscape software package, with a p-value and a Q-value above 0.03 and an edge cut-off of 0.375. Node colour represents the enrichment p-value. Node size is proportional to the total number of genes belonging to the corresponding gene-set. The edge corresponds to the Annotation shared between two nodes (blue), with edge thickness corresponding to the number of shared genes. Node clusters were identified and annotated by the AutoAnnotate plugin of cytoscape. See Table 2 (RNA splicing and processing) and 3 (cellular localisation & transport) for the list of annotations.

REFERENCES

- Atayde, V. D., Aslan, H., Townsend, S., Hassani, K., Kamhawi, S., and Olivier, M. (2015). Exosome Secretion by the Parasitic Protozoan *Leishmania* within the Sand Fly Midgut. *Cel Rep.* 13 (5), 957–967. doi:10.1016/j.celrep.2015.09.058
- Baker, N., Catta-Preta, C. M. C., Neish, R., Sadlova, J., Powell, B., Alves-Ferreira, E. V. C., et al. (2021). Systematic Functional Analysis of *Leishmania* Protein Kinases Identifies Regulators of Differentiation or Survival. *Nat. Commun.* 12 (1), 1244. doi:10.1038/s41467-021-21360-8
- Basken, J., Stuart, S. A., Kavran, A. J., Lee, T., Ebmeier, C. C., Old, W. M., et al. (2018). Specificity of Phosphorylation Responses to Mitogen Activated Protein (MAP) Kinase Pathway Inhibitors in Melanoma Cells. *Mol. Cell Proteomics* 17 (4), 550–564. doi:10.1074/mcp.RA117.000335
- Bichou, H., Bouabid, C., Rabhi, I., and Guizani-Tabbane, L. (2021). Transcription Factors Interplay Orchestrates the Immune-Metabolic Response of *Leishmania* Infected Macrophages. *Front. Cel. Infect. Microbiol.* 11, 660415. doi:10.3389/fcimb.2021.660415
- Bouhaddou, M., Memon, D., Meyer, B., White, K. M., Rezeli, V. V., Correa Marrero, M., et al. (2020). The Global Phosphorylation Landscape of SARS-CoV-2 Infection. *Cell* 182 (3), 685–712. e19. doi:10.1016/j.cell.2020.06.034
- Bouzeyen, R., Haoues, M., Barbouche, M.-R., Singh, R., and Essafi, M. (2019). FOXO3 Transcription Factor Regulates IL-10 Expression in Mycobacteria-Infected Macrophages, Tuning Their Polarization and the Subsequent Adaptive Immune Response. *Front. Immunol.* 10, 2922. doi:10.3389/fimmu.2019.02922
- Buljan, M., Ciuffa, R., van Drogen, A., Vichalkovski, A., Mehnert, M., Rosenberger, G., et al. (2020). Kinase Interaction Network Expands Functional and Disease Roles of Human Kinases. *Mol. Cel.* 79 (3), 504–520. e9. doi:10.1016/j.molcel.2020.07.001
- Cegielska, A., and Virshup, D. M. (1993). Control of Simian Virus 40 DNA Replication by the HeLa Cell Nuclear Kinase Casein Kinase I. *Mol. Cel. Biol.* 13, 1202–1211. doi:10.1128/mcb.13.2.1202
- da Silva Santos, C., Attarha, S., Saini, R. K., Boaventura, V., Costa, J., Khouri, R., et al. (2015). Proteome Profiling of Human Cutaneous Leishmaniasis Lesion. *J. Invest. Dermatol.* 135 (2), 400–410. doi:10.1038/jid.2014.396
- Dacher, M., Morales, M. A., Pescher, P., Leclercq, O., Rachidi, N., Prina, E., et al. (2014). Probing Druggability and Biological Function of Essential Proteins in *Leishmania* combining Facilitated Null Mutant and Plasmid Shuffle Analyses. *Mol. Microbiol.* 93, 146–166. doi:10.1111/mmi.12648
- de Menezes, J. P. B., Koushik, A., Das, S., Guven, C., Siegel, A., Laranjeira-Silva, M. F., et al. (2017). *Leishmania* infection Inhibits Macrophage Motility by Altering F-Actin Dynamics and the Expression of Adhesion Complex Proteins. *Cell Microbiol.* 19 (3), e12668. doi:10.1111/cmi.12668
- Dillon, L. A. L., Suresh, R., Okrah, K., Corrada Bravo, H., Mosser, D. M., and El-Sayed, N. M. (2015). Simultaneous Transcriptional Profiling of *Leishmania* Major and its Murine Macrophage Host Cell Reveals Insights into Host-Pathogen Interactions. *BMC genomics* 16, 1108. doi:10.1186/s12864-015-2237-2
- Dorin-Semlat, D., Demarta-Gatsi, C., Hamelin, R., Armand, F., Carvalho, T. G., Moniatte, M., et al. (2015). Malaria Parasite-Infected Erythrocytes Secrete PfCK1, the Plasmodium Homologue of the Pleiotropic Protein Kinase Casein Kinase I. *PLOS ONE* 10 (12), e0139591. doi:10.1371/journal.pone.0139591
- Douanne, N., Dong, G., Douanne, M., Olivier, M., and Fernandez-Prada, C. (2020). Unravelling the Proteomic Signature of Extracellular Vesicles Released by Drug-Resistant *Leishmania Infantum* Parasites. *Plos Negl. Trop. Dis.* 14 (7), e0008439. doi:10.1371/journal.pntd.0008439
- Durieu, E., Prina, E., Leclercq, O., Oumata, N., Gaboriaud-Kolar, N., Vougiannopoulou, K., et al. (2016). From Drug Screening to Target Deconvolution: a Target-Based Drug Discovery Pipeline Using *Leishmania* Casein Kinase I Isoform 2 to Identify Compounds with Antileishmanial Activity. *Antimicrob. Agents Chemother.* 60 (5), 2822–2833. doi:10.1128/AAC.00021-16
- Fernandes, M. C., Dillon, L. A. L., Belew, A. T., Bravo, H. C., Mosser, D. M., and El-Sayed, N. M. (2016). Dual Transcriptome Profiling of *Leishmania* -Infected Human Macrophages Reveals Distinct Reprogramming Signatures. *mBio* 7 (3), e00027–16. doi:10.1128/mBio.00027-16
- Figueiredo, A. B. d., Souza-Testasica, M. C., and Afonso, L. C. C. (2016). Purinergic Signaling and Infection by *Leishmania* : A New Approach to Evasion of the Immune Response. *Biomed. J.* 39 (4), 244–250. doi:10.1016/j.bj.2016.08.004
- Forté, J. O. y., de La Llave, E., Regnault, B., Coppée, J.-Y., Milon, G., Lang, T., et al. (2009). Transcriptional Signatures of BALB/c Mouse Macrophages Housing Multiplying *Leishmania Amazonensis* Amastigotes. *BMC genomics* 10, 119. doi:10.1186/1471-2164-10-119
- Frank, B., Marcu, A., de Oliveira Almeida Petersen, A. L., Weber, H., Stigloher, C., Mottram, J. C., et al. (2015). Autophagic Digestion of *Leishmania* Major by Host Macrophages Is Associated with Differential Expression of BNIP3, CTSE, and the miRNAs miR-101c, miR-129, and miR-210. *Parasites Vectors* 8, 404. doi:10.1186/s13071-015-0974-3
- Fulcher, L. J., Bozatz, P., Tachie-Menson, T., Wu, K. Z. L., Cummins, T. D., Bufton, J. C., et al. (2018). The DUF1669 Domain of FAM83 Family Proteins Anchor Casein Kinase I Isoforms. *Sci. Signal.* 11, 531. doi:10.1126/scisignal.aao2341
- Gordon, D. E., Jang, G. M., Bouhaddou, M., Xu, J., Obernier, K., White, K. M., et al. (2020). A SARS-CoV-2 Protein Interaction Map Reveals Targets for Drug Repurposing. *Nature* 583 (7816), 459–468. doi:10.1038/s41586-020-2286-9
- Gupta, P., Srivastav, S., Saha, S., Das, P. K., and Ukil, A. (2016). *Leishmania* Donovanii Inhibits Macrophage Apoptosis and Pro-inflammatory Response through AKT-Mediated Regulation of β -catenin and FOXO-1. *Cell Death Differ* 23 (11), 1815–1826. doi:10.1038/cdd.2016.101
- Ha, N.-C., Tonzok, T., Stamos, J. L., Choi, H.-J., and Weis, W. I. (2004). Mechanism of Phosphorylation-dependent Binding of APC to β -Catenin and its Role in β -Catenin Degradation. *Mol. Cel.* 15 (4), 511–521. doi:10.1016/j.molcel.2004.08.010
- Hornbeck, P. V., Zhang, B., Murray, B., Kornhauser, J. M., Latham, V., and Skrzypek, E. (2015). PhosphoSitePlus, 2014: Mutations, PTMs and Recalibrations. *Nucleic Acids Res.* 43, D512–D520. Database issue. doi:10.1093/nar/gku1267
- Isnard, A., Shio, M. T., and Olivier, M. (2012). Impact of *Leishmania* Metalloprotease GP63 on Macrophage Signaling. *Front. Cel. Inf. Microbio.* 2, 72. doi:10.3389/fcimb.2012.00072
- Jayaswal, S., Kamal, M. A., Dua, R., Gupta, S., Majumdar, T., Das, G., et al. (2010). Identification of Host-dependent Survival Factors for Intracellular *Mycobacterium tuberculosis* through an siRNA Screen. *Plos Pathog.* 6 (4), e1000839. doi:10.1371/journal.ppat.1000839
- Kane, M. M., and Mosser, D. M. (2001). The Role of IL-10 in Promoting Disease Progression in *Leishmaniasis*. *J. Immunol.* 166 (2), 1141–1147. doi:10.4049/jimmunol.166.2.1141
- Kawakami, F., Suzuki, K., and Ohtsuki, K. (2008). A Novel Consensus Phosphorylation Motif in Sulfatide- and Cholesterol-3-Sulfate-Binding Protein Substrates for CK1 *In Vitro*. *Biol. Pharm. Bull.* 31 (2), 193–200. doi:10.1248/bpb.31.193
- Knippschild, U., KrÄ¼ger, M., Richter, J., Xu, P., GarcÄa-Reyes, B., Peifer, C., et al. (2014). The CK1 Family: Contribution to Cellular Stress Response and its Role in Carcinogenesis. *Front. Oncol.* 4, 96. doi:10.3389/fonc.2014.00096
- Lamotte, S., SpÄth, G. F., Rachidi, N., and Prina, E. (2017). The Enemy within: Targeting Host-Parasite Interaction for Antileishmanial Drug Discovery. *Plos Negl. Trop. Dis.* 11 (6), e0005480. doi:10.1371/journal.pntd.0005480
- Liu, J., Carvalho, L. P., Bhattacharya, S., Carbone, C. J., Kumar, K. G. S., Leu, N. A., et al. (2009). Mammalian Casein Kinase 1 α and its *Leishmania* Ortholog Regulate Stability of IFNAR1 and Type I Interferon Signaling. *Mol. Cel Biol* 29 (24), 6401–6412. doi:10.1128/mcb.00478-09
- Liu, Y., Ao, X., Ding, W., Ponnusamy, M., Wu, W., Hao, X., et al. (2018). Critical Role of FOXO3a in Carcinogenesis. *Mol. Cancer* 17 (1), 104. doi:10.1186/s12943-018-0856-3
- Marin, O., Burzio, V., Boschetti, M., Meggio, F., Allende, C. C., Allende, J. E., et al. (2002). Structural Features Underlying the Multisite Phosphorylation of the A Domain of the NF-AT4 Transcription Factor by Protein Kinase CK1. *Biochemistry* 41 (2), 618–627. doi:10.1021/bi0112309
- Marin, O., Bustos, V. H., Cesaro, L., Meggio, F., Pagano, M. A., Antonelli, M., et al. (2003). A Noncanonical Sequence Phosphorylated by Casein Kinase 1 in β -catenin May Play a Role in Casein Kinase 1 Targeting of Important Signaling Proteins. *Proc. Natl. Acad. Sci.* 100 (18), 10193–10200. doi:10.1073/pnas.1733909100

- Marin, O., Meggio, F., Sarno, S., Andretta, M., and Pinna, L. A. (1994). Phosphorylation of Synthetic Fragments of Inhibitor-2 of Protein Phosphatase-1 by Casein Kinase-1 and -2. Evidence that Phosphorylated Residues Are Not Strictly Required for Efficient Targeting by Casein Kinase-1. *Eur. J. Biochem.* 223 (2), 647–653. doi:10.1111/j.1432-1033.1994.tb19037.x
- Martel, D., Pine, S., Bartsch, K., Clos, J., Späth, G. F., and Rachidi, N. (2020). The Low Complexity Regions in the C-Terminus Are Essential for the Subcellular Localisation of Leishmania Casein Kinase 1 but Not for its Activity. *bioRxiv*. doi:10.1101/2020.02.28.969741
- Meng, F., Sun, N., Liu, D., Jia, J., Xiao, J., and Dai, H. (2021). BCL2L13: Physiological and Pathological Meanings. *Cell. Mol. Life Sci.* 78 (6), 2419–2428. doi:10.1007/s00018-020-03702-9
- Merico, D., Isserlin, R., Stueker, O., Emili, A., and Bader, G. D. (2010). Enrichment Map: a Network-Based Method for Gene-Set Enrichment Visualization and Interpretation. *PLoS One* 5 (11), e13984. doi:10.1371/journal.pone.0013984
- Moore, K. J., and Matlashewski, G. (1994). Intracellular Infection by Leishmania Donovanii Inhibits Macrophage Apoptosis. *J. Immunol.* 152 (6), 2930–2937.
- Nandan, D., and Reiner, N. E. (2005). Leishmania Donovanii Engages in Regulatory Interference by Targeting Macrophage Protein Tyrosine Phosphatase SHP-1. *Clin. Immunol.* 114 (3), 266–277. doi:10.1016/j.clim.2004.07.017
- Negrão, F., Fernandez-Costa, C., Zorzi, N., Giorgio, S., Nogueira Eberlin, M., and Yates, J. R., 3rd (2019). Label-Free Proteomic Analysis Reveals Parasite-specific Protein Alterations in Macrophages Following Leishmania Amazonensis, Leishmania Major, or Leishmania Infantum Infection. *ACS Infect. Dis.* 5 (6), 851–862. doi:10.1021/acscinfdis.8b00338
- Ong, S.-E., Blagoev, B., Kratchmarova, I., Kristensen, D. B., Steen, H., Pandey, A., et al. (2002). Stable Isotope Labeling by Amino Acids in Cell Culture, SILAC, as a Simple and Accurate Approach to Expression Proteomics. *Mol. Cell Proteomics* 1 (5), 376–386. doi:10.1074/mcp.m200025-mcp200
- Ong, S.-E., and Mann, M. (2006). A Practical Recipe for Stable Isotope Labeling by Amino Acids in Cell Culture (SILAC). *Nat. Protoc.* 1 (6), 2650–2660. doi:10.1038/nprot.2006.427
- Perez-Riverol, Y., Csordas, A., Bai, J., Bernal-Llinares, M., Hewapathirana, S., Kundu, D. J., et al. (2019). The PRIDE Database and Related Tools and Resources in 2019: Improving Support for Quantification Data. *Nucleic Acids Res.* 47 (D1), D442–D450. doi:10.1093/nar/gky1106
- Poulet, P., Carpentier, S., and Barillot, E. (2007). myProMS, a Web Server for Management and Validation of Mass Spectrometry-Based Proteomic Data. *Proteomics* 7 (15), 2553–2556. doi:10.1002/pmic.200600784
- Rabhi, I., Rabhi, S., Ben-Othman, R., Aniba, M. R., Trentin, B., Piquemal, D., et al. (2013). Comparative Analysis of Resistant and Susceptible Macrophage Gene Expression Response to Leishmania Major parasite. *BMC genomics* 14, 723. doi:10.1186/1471-2164-14-723
- Rachidi, N., Taly, J. F., Durieu, E., Leclercq, O., Aulner, N., Prina, E., et al. (2014). Pharmacological Assessment Defines Leishmania Donovanii Casein Kinase 1 as a Drug Target and Reveals Important Functions in Parasite Viability and Intracellular Infection. *Antimicrob. Agents Chemother.* 58 (3), 1501–1515. doi:10.1128/AAC.02022-13
- Rachidi, N., Knippschild, U., and Späth, G. F. (2021). Dangerous Duplicity: The Dual Functions of Casein Kinase 1 in Parasite Biology and Host Subversion. *Front. Cel. Infect. Microbiol.* 11, 230. doi:10.3389/fcimb.2021.655700
- Santos-Oliveira, J. R., Regis, E. G., Leal, C. R. B., Cunha, R. V., Bozza, P. T., and Da-Cruz, A. M. (2011). Evidence that Lipopolysaccharide May Contribute to the Cytokine Storm and Cellular Activation in Patients with Visceral Leishmaniasis. *Plos Negl. Trop. Dis.* 5 (7), e1198. doi:10.1371/journal.pntd.0001198
- Shah, K., Liu, Y., Deirmengian, C., and Shokat, K. M. (1997). Engineering Unnatural Nucleotide Specificity for Rous Sarcoma Virus Tyrosine Kinase to Uniquely Label its Direct Substrates. *Proc. Natl. Acad. Sci.* 94 (8), 3565–3570. doi:10.1073/pnas.94.8.3565
- Shannon, P., Markiel, A., Ozier, O., Baliga, N. S., Wang, J. T., Ramage, D., et al. (2003). Cytoscape: a Software Environment for Integrated Models of Biomolecular Interaction Networks. *Genome Res.* 13 (11), 2498–2504. doi:10.1101/gr.1239303
- Silverman, J. M., Clos, J., deOliveira, C. C., Shirvani, O., Fang, Y., Wang, C., et al. (2010). An Exosome-Based Secretion Pathway Is Responsible for Protein export from Leishmania and Communication with Macrophages. *J. Cell Sci* 123 (Pt 6), 842–852. doi:10.1242/jcs.056465
- Silverman, J. M., Clos, J., Horakova, E., Wang, A. Y., Wiesgigl, M., Kelly, I., et al. (2011). Leishmania Exosomes Modulate Innate and Adaptive Immune Responses through Effects on Monocytes and Dendritic Cells. *J. Immunol.* 185 (9), 5011–5022. doi:10.4049/jimmunol.1000541
- Singh, A. K., Pandey, R. K., Siqueira-Neto, J. L., Kwon, Y.-J., Freitas-Junior, L. H., Shaha, C., et al. (2015). Proteomic-based Approach to Gain Insight into Reprogramming of THP-1 Cells Exposed to Leishmania Donovanii over an Early Temporal Window. *Infect. Immun.* 83 (5), 1853–1868. doi:10.1128/IAI.02833-14
- Smirlis, D., Dingli, F., Pescher, P., Prina, E., Loew, D., Rachidi, N., et al. (2020). SILAC-based Quantitative Proteomics Reveals Pleiotropic, Phenotypic Modulation in Primary Murine Macrophages Infected with the Protozoan Pathogen Leishmania Donovanii. *J. Proteomics* 213, 103617. doi:10.1016/j.jprot.2019.103617
- Sugiyama, N., Imamura, H., and Ishihama, Y. (2019). Large-scale Discovery of Substrates of the Human Kinome. *Sci. Rep.* 9 (1), 10503. doi:10.1038/s41598-019-46385-4
- Szklarczyk, D., Gable, A. L., Lyon, D., Junge, A., Wyder, S., Huerta-Cepas, J., et al. (2019). STRING V11: Protein-Protein Association Networks with Increased Coverage, Supporting Functional Discovery in Genome-wide Experimental Datasets. *Nucleic Acids Res.* 47 (D1), D607–D613. doi:10.1093/nar/gky1131
- Turnquist, C., Ryan, B. M., Horikawa, I., Harris, B. T., and Harris, C. C. (2020). Cytokine Storms in Cancer and COVID-19. *Cancer cell* 38 (5), 598–601. doi:10.1016/j.ccell.2020.09.019
- Vacic, V., Iakoucheva, L. M., and Radivojac, P. (2006). Two Sample Logo: a Graphical Representation of the Differences between Two Sets of Sequence Alignments. *Bioinformatics* 22 (12), 1536–1537. doi:10.1093/bioinformatics/btl151
- Xia, C., Wolf, J. J., Vijayan, M., Studstill, C. J., Ma, W., and Hahm, B. (2018). Casein Kinase 1 α Mediates the Degradation of Receptors for Type I and Type II Interferons Caused by Hemagglutinin of Influenza A Virus. *J. Virol.* 92 (7), e00006–18. doi:10.1128/JVI.00006-18
- Xu, P., Ianes, C., Gärtner, F., Liu, C., Burster, T., Bakulev, V., et al. (2019). Structure, Regulation, and (Patho-)physiological Functions of the Stress-Induced Protein Kinase CK1 delta (CSNK1D). *Gene* 715, 144005. doi:10.1016/j.gene.2019.144005
- Yim, D. G. R., Ghosh, S., Guy, G. R., and Virshup, D. M. (2015). Casein Kinase 1 Regulates Sprouty2 in FGF-ERK Signaling. *Oncogene* 34 (4), 474–484. doi:10.1038/onc.2013.564
- Zhang, L., Li, H., Chen, Y., Gao, X., Lu, Z., Gao, L., et al. (2017). The Down-Regulation of Casein Kinase 1 Alpha as a Host Defense Response against Infectious Bursal Disease Virus Infection. *Virology* 512, 211–221. doi:10.1016/j.virol.2017.08.007

Conflict of Interest: The authors declare that the research was conducted in the absence of any commercial or financial relationships that could be construed as a potential conflict of interest.

Publisher's Note: All claims expressed in this article are solely those of the authors and do not necessarily represent those of their affiliated organizations, or those of the publisher, the editors, and the reviewers. Any product that may be evaluated in this article, or claim that may be made by its manufacturer, is not guaranteed or endorsed by the publisher.

Copyright © 2022 Smirlis, Dingli, Sabatet, Roth, Knippschild, Loew, Späth and Rachidi. This is an open-access article distributed under the terms of the Creative Commons Attribution License (CC BY). The use, distribution or reproduction in other forums is permitted, provided the original author(s) and the copyright owner(s) are credited and that the original publication in this journal is cited, in accordance with accepted academic practice. No use, distribution or reproduction is permitted which does not comply with these terms.



Inhibition of Protein Kinase CK2 Affects Thymidylate Synthesis Cycle Enzyme Level and Distribution in Human Cancer Cells

Patrycja Wińska^{1*}, Łukasz Widło¹, Elżbieta Senkara¹, Mirosława Koronkiewicz², Jarosław M. Cieśla³, Alicja Krzyśko¹, Katarzyna Skierka¹ and Joanna Cieśla^{1*}

¹Chair of Drug and Cosmetics Biotechnology, Faculty of Chemistry, Warsaw University of Technology, Warsaw, Poland,

²Department of Biomedical Research, National Medicines Institute, Warsaw, Poland, ³Institute of Biochemistry and Biophysics, Polish Academy of Sciences, Warsaw, Poland

OPEN ACCESS

Edited by:

Giorgio Cozza,
University of Padua, Italy

Reviewed by:

Hannu Myllykallio,
Laboratoire d'optique et Biosciences,
France
Giovanni Ribaudo,
University of Brescia, Italy

*Correspondence:

Patrycja Wińska
pwinska@ch.pw.edu.pl
Joanna Cieśla
jcieśla@ch.pw.edu.pl

Specialty section:

This article was submitted to
Cellular Biochemistry,
a section of the journal
Frontiers in Molecular Biosciences

Received: 03 January 2022

Accepted: 31 January 2022

Published: 25 February 2022

Citation:

Wińska P, Widło Ł, Senkara E, Koronkiewicz M, Cieśla JM, Krzyśko A, Skierka K and Cieśla J (2022) Inhibition of Protein Kinase CK2 Affects Thymidylate Synthesis Cycle Enzyme Level and Distribution in Human Cancer Cells. *Front. Mol. Biosci.* 9:847829. doi: 10.3389/fmolb.2022.847829

Thymidylate synthase (TS), dihydrofolate reductase (DHFR), and serine hydroxymethyltransferase (SHMT) constitute the thymidylate synthesis cycle providing thymidylate for DNA synthesis and repair. Our previous studies indicated that TS and DHFR are the substrates of protein kinase CK2. This work has been aimed at the elucidation of the effect of CK2 activity on cell cycle progression, thymidylate synthesis enzyme expression and localization, and the role of CK2-mediated TS phosphorylation in *in vitro* di- and trimolecular complex formation. The results were obtained by means of western blot, confocal microscopy, flow cytometry, quantitative polymerase chain reaction (QPCR), quartz crystal microbalance with dissipation monitoring (QCM-D), and microthermophoresis (MST). Our research indicates that CK2 inhibition does not change the levels of the transcripts; however, it affects the protein levels of DHFR and TS in both tested cell lines, i.e., A549 and CCRF-CEM, and the level of SHMT1 in CCRF-CEM cells. Moreover, we show that CK2-mediated phosphorylation of TS enables the protein (pTS) interaction with SHMT1 and leads to the stability of the tri-complex containing SHMT1, DHFR, and pTS. Our results suggest an important regulatory role of CK2-mediated phosphorylation for inter- and intracellular protein level of enzymes involved in the thymidylate biosynthesis cycle.

Keywords: protein kinase CK2, CX-4945, thymidylate synthase, dihydrofolate reductase, serine hydroxymethyltransferase, acute lymphoblastic leukemia cells CCRF-CEM, protein-protein interaction

INTRODUCTION

CK2 (formerly known as casein kinase II) is a protein kinase involved in regulation of many processes such as transcription (Lüscher et al., 1990; Cabrejos et al., 2004) and translation (Riera et al., 1999; Szebeni et al., 2003; Borgo et al., 2015; Gandin et al., 2016), control of protein stability (Zhang et al., 2002; Patsoukis et al., 2013; Niechi et al., 2015) and degradation (Shen et al., 2001; Scaglioni et al., 2009), cell cycle progression (Homma and Homma, 2008), cell survival (Ahmed et al., 2002; Piazza et al., 2006; Duncan et al., 2011), and circadian rhythms (Tsuchiya et al., 2009). The role of this conserved, constitutively active serine-threonine kinase in a cell regulatory network is highly complex, and the extensive interplay between CK2-mediated phosphorylation and other post-translational modifications has been suggested (Nuñez de Villavicencio-Díaz et al., 2017). Moreover,

an increased level/activity of CK2 kinase has been observed in several tumor types (Trembley et al., 2009; Borgo and Ruzzene, 2021).

Most of the CK2 substrates play important roles in the regulation of metabolic processes, cell signaling or apoptosis, including protecting the integrity of DNA (Chapman and Jackson, 2008; Siddiqui-Jain et al., 2012). Among those substrates are also three enzymes, namely, thymidylate synthase (TS), dihydrofolate reductase (DHFR), and serine hydroxymethyltransferase (SHMT), involved in the metabolic cycle resulting in *de novo* synthesis of thymidylate, a crucial substrate for DNA synthesis and repair. The *in vitro* CK2-mediated phosphorylation of TS was shown by Frączyk et al. (Frączyk et al., 2010; Frączyk et al., 2015) and Ludwiczak et al., 2016. The phosphorylation lowered TS catalytic activity and affected binding of the TS inhibitor, 5-fluorodeoxyuridylate (FdUMP). The results of molecular dynamics simulations have shown that CK2-mediated phosphorylation of serine 124 residue of the human TS leads to a protein conformational change, resulting in an unfavorable position of the substrate (dUMP) and cofactor (methylene-THF) in the active center (Jarmuła et al., 2010). In addition, a stiffening of certain protein fragments, especially the loop closing the active center pocket, has been shown (Frączyk et al., 2010). High-resolution structures provided evidence that the native human TS can have two major conformations: active and inactive, which depends on the location of the loop 182–297 (Lovelace et al., 2009). Mutant TS, M190K, with loop 182–297 stabilized in inactive conformation, was highly phosphorylated by CK2 in contrast to the active-conformation-stabilized mutant R163K (Luo et al., 2011). This may indicate the physiological relevance for the conformational switching of TS activity with possible stabilization of the inactive form by phosphorylation. The *in vitro* phosphorylation by CK2 of the second enzyme of the thymidylate synthesis cycle, DHFR, has been demonstrated recently by us (Skierka et al., 2019), while the third enzyme of the cycle, SHMT, has been indicated as the CK2 substrate in phosphoproteomics studies on mitotic HEK 293T cells (Rusin et al., 2017).

Both TS and DHFR are well-known molecular targets in anti-cancer chemotherapy, whereas CK2 has recently emerged as a target (Borgo et al., 2021), and the enzyme inhibitor, CX-4945 (5-(3-chlorophenylamino)benzo [c][2,6]naphthyridine-8-carboxylic acid), also known as silmitasertib (Pierre et al., 2011; Kim and Kim, 2012; Chon et al., 2015) undergoes phase I and phase II clinical studies for cancer treatment. This small molecule, ATP-competitive inhibitor, demonstrates an excellent profile of selectivity. Testing CX-4945 at 500 nM against a panel of 235 kinases revealed that this compound is able to affect the activity of only 49 kinases to an extent greater than 50% (D'Amore et al., 2020). It shows efficacy both *in vitro* in cells and *in vivo* in animal models and has a suitable pharmacokinetic profile (long half-life, oral bioavailability, and no toxicity). CX-4945 has been found to show an extensive anti-proliferative activity, i.e., to promote cell cycle arrest, and to induce caspase activity and apoptosis in various cancer cell lines (D'Amore et al., 2020).

Taking into account that CK2 regulates many oncogenic pathways and processes, we have recently undertaken the studies on simultaneous treatment of cancer cells with inhibitors of TS and CK2 (Wińska et al., 2018; Wińska et al., 2020) or DHFR and CK2 (Wińska et al., 2019) searching for the synergistic effect. The obtained results demonstrate the ability of CK2 inhibitors to enhance the efficacy of 5-fluorouracil (FU, TS inhibitor) or methotrexate (MTX, DHFR inhibitor) in cancer cells. The molecular mechanism of the observed synergistic effect that occurred in MCF-7 cells after CX-4945 and FU simultaneous treatment was not clear; however, the synergistic effect seemed to be related to the delay of FU-induced S-phase arrest recovery. In the MTX and CX-4945 case, we have observed cell accumulation in both the S-phase and G2/M-phase of the cell cycle after the combined treatment of CCRF-CEM cells, which seems to result from an additive effect, since MTX and CX-4945 used separately led to G2/M-phase arrest and S-phase arrest, respectively. Additionally, we have observed a significant increase in the DHFR level in acute lymphoblastic leukemia cells (CCRF-CEM) after treatment with CX-4945 (Wińska et al., 2019), which might indicate the possible involvement of CK2 in the regulation of thymidylate synthesis and, therefore, may affect CX-4945 therapy outcome.

In this follow-up study, we investigate the effect of CK2 inhibition on DHFR and TS expression in two different cancer cell lines, A549 (adenocarcinomic human alveolar basal epithelial cells) and CCRF-CEM (human acute lymphoblastic leukemia cells), while the expression of two forms of serine hydroxymethyltransferase, cytosolic (SHMT1) and mitochondrial (SHMT2), was studied in the CCRF-CEM cell line. The effect of CX-4945 on cell cycle progression and DHFR and TS localization has been investigated in A-549 cells. Additionally, the effect of CK2-mediated TS phosphorylation on the formation of di- and trimolecular complexes with SHMT1 and DHFR was studied by means of quartz crystal microbalance with dissipation monitoring (QCM-D) and microthermophoresis (MST). The obtained results suggest an important regulatory role of CK2-mediated phosphorylation in the stability of SHMT/DHFR/TS in cells, cellular localization of DHFR and TS, and the ability of the three enzymes to interact with each other.

MATERIALS AND METHODS

Reagents and Antibodies

Dimethyl sulphoxide (DMSO), molecular biology grade, used as a solvent for all stocks of chemical agents, was obtained from Roth (Karlsruhe, Germany). All reagents used in flow cytometry analysis were purchased from BD Biosciences Pharmingen (San Diego, CA, United States). The following primary antibodies were used: anti-GAPDH (Merck Millipore, #MAB374, 1:20000, 30 min, RT), anti-p65 (Ser529) (Biorbyt, # orb 14916, 1:500, overnight, +4°C), anti-DHFR (BD Biosciences), and anti-TS (Merck Millipore, #MAB4130, 1:500, overnight, +4°C). Secondary goat anti-rabbit IgG-HRP (Dako, #P0448, 1:2000, 1h, RT) and anti-mouse IgG-HRP (Dako, #P0447, 1:1000, 1h, RT) were used. Hoechst 33342 (Life

Technologies, #H3569) and anti-mouse Alexa Fluor 555 were used in the IF study. Protease inhibitors (#11 836 153 001) were from Roche Applied Science (Mannheim Germany). The nitrocellulose membrane was from GE Healthcare Life Sciences (Freiburg, Germany), solvents for HRP reaction (Western Bright Peroxide and Western Bright Quantum) were purchased from Advantia, ECL reagent was from Millipore (United States), and CX-4945 was obtained from Biorbyt. Other solvents, reagents, and chemicals were purchased from POCH (Avantor Performance Materials, Gliwice, Poland), Merck, and Sigma-Aldrich Chemical Company (St. Louis, MO, United States).

Cell Culture and Treatment of Agents

CCRF-CEM (ECACC 85112105) human Caucasian acute lymphoblastic leukaemia was purchased from ECACC, whereas A-549 (ATCC CCL-185) human lung carcinoma was purchased from ATCC. A-549 cell line was cultured in high-glucose DMEM (Lonza, Basel, Switzerland) supplemented with 10% fetal bovine serum (EuroClone), 2 mM L-glutamine, and antibiotics (100 U/ml penicillin and 100 µg/ml streptomycin). CCRF-CEM was cultured in RPMI 1640 supplemented with 10% fetal bovine serum (EuroClone), 2 mM L-glutamine, and antibiotics (100 U/ml penicillin and 100 µg/ml streptomycin). Cells were grown in 75 cm² cell culture flasks (Sarstedt, Nümbrecht, Germany), in a humidified atmosphere of CO₂/air (5/95%) at 37°C. All the experiments were performed in exponentially growing cultures. Stock solution of CX-4945 was prepared in DMSO and stored in -80°C for maximum 1 month. For the cytotoxicity studies, the stock solution of CX-4945 was diluted 200-fold with the proper culture medium to obtain the final concentration. For cytotoxicity studies, 2-fold serial dilutions of CX-4945 were prepared in the proper medium containing 0.5% DMSO.

3-(4,5-Dimethylthiazol-2-yl)-2,5-diphenyltetrazolium bromide (MTT)-based viability assay: after incubation with the test compounds, an MTT test was performed as described previously (Wińska et al., 2020). Optical densities were measured at 570 nm using a BioTek microplate reader. All measurements were carried out in a minimum of three replicates.

Cell Cycle Analysis

A-549 cells were cultured in 25 cm² culture flasks and treated with the tested compounds as it was described above. After exposure to CX-4945, the cells were trypsinized, collected, and washed with cold PBS and fixed at -20°C in 70% ethanol for at least 24 h. Subsequently, the cells were washed in PBS and stained with 50 µg/ml PI (propidium iodide) and 100 µg/ml RNase solution in PBS supplemented with 0.1% v/v Triton X-100 for 30 min in the dark at the RT. Cellular DNA content was determined by flow cytometry employing a CyFlow Cube 8 (Sysmex, Norderstedt, Germany) flow cytometer. The DNA histograms obtained were analyzed using FCS Express 5 Flow software (De Novo Software, Glendale, CA, United States) for evaluation of distribution of the cells in different phases of the cell cycle.

Western Blotting

Adherent cells growing exponentially were seeded at 4.8×10^5 cells in 6 cm diameter plates, whereas CCRF-CEM cells were seeded in a concentration of 2×10^5 cells/ml in 25 cm² flasks (Sarstedt). Subsequently, CX-4945 was added in a final concentration of 0.5% DMSO in concentrations corresponding to 0.5 IC₅₀, IC₅₀, and 1.5 IC₅₀ for adherent cells and 0.5 IC₅₀, IC₅₀, and 2 IC₅₀ for CCRF-CEM. After incubation, the suspension cells were collected by centrifugation at 260 RCF and washed 3 times with ice-cold PBS and supernatants were discarded and pellets were storage at -20°C up to 1 month. In order to obtain lysates, RIPA buffer (50 mM Tris-HCl pH 7.4, 1% NP-40, 0.5% sodium deoxycholate, 0.1% SDS, 150 mM NaCl, 2 mM EDTA, 50 mM NaF, 0.2 mM sodium orthovanadate, and protease inhibitors cocktail, Roche) was added as it was described elsewhere (Wińska et al., 2020). Adherent monolayer cells were washed three times in ice-cold PBS, and the cells were scraped and lysed in RIPA as it was described previously (Wińska et al., 2020). Cellular lysates were analyzed by western blotting as it was described previously (Wińska et al., 2019).

Densitometry

For densitometry, immunoblots were scanned using G Box Chemi (Syngene), and the density of each lane of phosphorylated and total protein was quantified, using Image J software. Phosphorylated protein densities were normalized to GAPDH densities, assuming 1 for untreated cells, and then, they were converted to a percent of the appropriate control.

Statistical Evaluation

Results are represented as mean ± s.e.m. of at least three independent experiments performed in triplicate. Statistical analysis was performed using the GraphPad Prism 5.0 software (GraphPad Software Inc., San Diego, CA, United States). Significance was determined using a *t*-test. The statistical significance of differences was indicated in figures by asterisks as follows: **p* ≤ 0.05, ***p* ≤ 0.01, and ****p* ≤ 0.001.

Immunocytochemical Staining and Microscopy Analysis

Cells were seeded in 4-well dishes (35/10 mm; Greiner Bio-One North America, Inc.) and cultured in respective conditions. After 18 h culturing, cells were treated with 0.5% DMSO (control) or 15.5, 31, or 46.6 µM CX-4945 for indicated incubation time. Subsequently, cells were washed twice with PBS, fixed with 3.7% paraformaldehyde solution (PFA) for 20 min, washed twice with PBS, and incubated for 30 min at the room temperature with permeabilization and blocking solution (5% BSA, 0.1% Triton X 100, and 0.5% Tween 20 in PBS). Subsequently, the solution was discarded, and the cells were washed three times with PBST (0.1% Tween 20 in PBS) and incubated with the primary antibodies (anti-DHFR or anti-TS, both 1:100) in PBST for 24 h at 4°C. After washing with PBST (0.5 ml/compartments), the cells were protected from light and incubated with Alexa Fluor 546-conjugated anti-mouse diluted 1:500 (ThermoFisher Scientific, United States) for 1 h at the room

temperature. After washing, the cells were incubated in 1 μ M Hoechst 33342 in PBST for 15 min. The dye solution was discarded, and the cells were washed with PBST (0.5 ml/compartment). Pictures were taken using the Olympus Fluoview FV1000 confocal laser scanning microscope (CLSM, Olympus, Center Valley, PA, United States).

Total RNA Isolation and Quantitative Polymerase Chain Reaction

Total RNA isolation was performed with the use of RNeasy TRI RNA extraction reagent (GenoPlast Biochemicals), and reverse transcription was conducted using a High Capacity cDNA Reverse Transcription Kit (Applied Biosystems™) according to the protocols of manufacturers. The obtained cDNA was a template in quantitative polymerase chain reaction (QPCR), which has been performed virtually as described previously (Wińska et al., 2019). The primers used for the amplification of SHMT1 were 5' CCTGTCCAGGTGACAGAAG 3' (forward) and 5' TGCCAGTCTCTCCTTGAAC 3' (reverse) and for SHMT2 amplification were 5' AGCTCATTGCCTCAGAGAC 3' (forward) and 5' TGCAGGATCCAGGTCAAAG 3' (reverse). The primers were designed using the Kalign tool available at www.ebi.ac.uk (Chojnacki et al., 2017) and ordered from the DNA Sequencing and Oligonucleotides Synthesis Laboratory at the Institute of Biochemistry and Biophysics (Warsaw, Poland). QPCR was performed with the use of Real-Time 2xHS-PCR Master Mix SYBR® A (A&A Biotechnology Gdynia, Poland) as it was previously described (Borkiewicz et al., 2019). The amount of target mRNA was calculated by the Δ Ct method (Vandesompele et al., 2002) with the geometric mean of Cts of two reference genes, β -glucuronidase (GUSB, NM_000181) and TATA-binding protein (TBP, NM_003194). Relative SHMT1 and SHMT2 gene expression in control cells (RE) was set at a value of 1, and the relative SHMT1 or SHMT2 gene expression after treatment with the inhibitor (RE + I) was calculated as the ratio RE + I/RE. Values of experimental measurements were considered as independent variables. Rare outlying results were omitted in further calculations. In the next step, the ratio of each relative gene expression in the sample from the cells treated with the inhibitor versus each relative gene expression in the sample from the untreated cells was calculated. This yielded a two-dimensional matrix of values comparing gene expression in untreated and treated cells. If compared expressions are the same, these ratios should equal 1. Therefore, it was possible to apply the chi-square test with 1 as the expected value and the average of all results from the matrix as the observed value. Significantly outlying quantiles from the matrix were omitted in this test. The result of the chi-square test is the probability that the gene expression in treated cells is equal to the gene expression in untreated cells. Expression in both groups of cells was considered different when the probability of this equality was lower than 0.05 ($p \leq 0.05$).

Protein Preparations

Recombinant His-tagged DHFR and TS were overexpressed and purified as described previously (Antosiewicz et al., 2015; Skierka

et al., 2019). Recombinant SHMT1 was overexpressed and purified with the following modifications. The Ni-NTA binding solution contained 50 mM phosphate buffer pH 7.5, 300 mM NaCl, 10 mM imidazole, 50 μ M pyridoxal phosphate (PLP), 2 μ g/ml aprotinin, 2 μ g/ml leupeptin, and 15 μ g/ml PMSF. The column was washed with 50 mM phosphate buffer containing 300 mM NaCl, 50 μ M PLP, and 50 mM imidazole and eluted with the same buffer except that 250 mM imidazole was used. The purest fractions were pooled, dialyzed against 20 mM Tris-HCl pH 7.5, 500 mM NaCl, 50 μ M PLP, and 10% glycerol, and stored at -20°C .

For His-tag removal, the Thrombin CleanCleave Kit (Sigma-Aldrich) was used according to the manufacturer's recommendations.

TS was phosphorylated using CK2 α enzyme preparation. The reaction was conducted in 4 ml of 20 mM Tris-HCl buffer, pH 7.5 containing 98 μ M His-tagged human TS, a 2.8 μ M CK2 α subunit, 15 mM MgCl₂, 280 μ M ATP, and 6 mM 2-mercaptoethanol at 30°C for 1 h. Phosphorylated and non-phosphorylated fractions were separated using the method of Wolschin et al. (Wolschin et al., 2005). Fractions containing phosphorylated and non-phosphorylated proteins were adjusted to contain 50 mM phosphate buffer pH 7.6, 300 mM NaCl, and 10 mM imidazole and uploaded onto Ni-NTA columns in order to purify them from CK α ' and concentrate. Eluted His-tagged TS and PTS were dialyzed against 50 mM phosphate buffer pH 7.6 and 10% glycerol.

The protein concentrations in all preparations were assayed using the Bradford method (Bradford, 1976).

QCM-D Assay

The protein-protein interactions were assayed according to the work of Antosiewicz et al., 2015, using commercial His-tag capturing sensors QX340, with slight modifications. A His-tagged protein was immobilized on the sensor and served as a receptor, whereas the ligand protein (or proteins) was introduced into the measuring chamber. Before the immobilization of the His-tagged protein, the sensor alone was measured to exclude non-specific adsorption of the tagless ligand protein. Additionally, the binding of the His-tagged ligand to the sensor surface already functionalized with His-tagged receptor was excluded.

For the study of two-protein interactions of SHMT1 with TS, pTS, or DHFR, 5 μ M His-tagged SHMT was immobilized on the sensor surface, whereas the tagless ligand protein was introduced into the chamber in various concentrations (in the range of 0.1–1.0 μ M or 0.5–7.0 μ M in case of TS, pTS, or DHFR, respectively).

For the study of three-protein interactions, 5 μ M His-tagged SHMT1 was immobilized on the sensor surface followed by the introduction of mixture containing a fixed concentration of TS or pTS (1.0 μ M) and various concentrations of DHFR (in the range of 0.25–2.0 μ M).

All measurements were conducted in 20 mM Tris-HCl (pH 7.6) containing 100 mM, 10 mM MgCl₂, and 0.05% Tween 20 at 25°C and 200 μ l/min flow rate.

The K_d values were obtained by fitting the experimental data to the Langmuir isotherm model using QTools software.

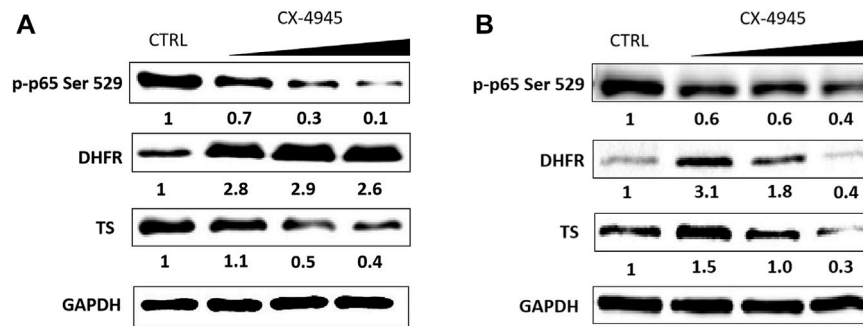


FIGURE 1 | The effect of CX-4945 on the level of p-p65 Ser 529 (nuclear factor kappa-light-chain-enhancer of activated B cells), DHFR, and TS in CCRF-CEM (A) and in A-549 (B). Western blot analysis of the following proteins in the crude extracts obtained from the tested cell lines after 48 h of treatment with CX-4945 used in the concentrations of 15.54, 31.08, and 46.62 μM for A-549 and 2, 4, and 8 μM for CCRF-CEM. GAPDH was used as a loading control for each sample. Preparation of cell extracts and protein detection are described in *Materials and Methods*. Densitometry quantifications for each tested protein, given under each cell line panel, were calculated with untreated cells (CTRL) serving as the reference point.

The diagram illustrating the QCM-D method is given in **Supplementary Figure S1**.

MST Assay

The microthermophoresis assays were optimized and performed as previously described (Antosiewicz et al., 2015) using the MST Monolith.115 instrument, courtesy of NanoTemper Technologies company. Di- and tri-complex formation was monitored using Premium MST capillaries. The diagram of the MST procedure is shown in **Supplementary Figure S2**. The temperature-induced fluorescent change as a function of the titrant concentrations enables the determination of the strength of interactions occurring. The SHMT–DHFR interaction was measured using fluorescently labeled DHFR protein and various concentrations of SHMT in the range of 157 μM–4.79 nM. For SHMT–TS and SHMT–pTS interactions, either SHMT or pTS was labeled and the other protein was used as a titrant (TS in the range of 62.0 μM–1.9 nM and SHMT in the range of 157 μM–4.79 nM). For tri-complex formation assay, DHFR was labeled and samples containing constant concentrations of labeled DHFR and TS or pTS (9.0 μM) and SHMT titrant concentration in the range of 157 μM–4.79 nM were used. The dissociation constant K_d is obtained by fitting the binding curve with the quadratic solution for the fraction of fluorescent molecules that formed the complex, calculated from the law of mass action. We used DLScreening Analysis software (NanoTemper) to fit the K_d model which allows to determine the strength of molecular interactions occurring with either 1:1 stoichiometry or where several molecules A bind to one molecule B independently, i.e., with no cooperativity (**Supplementary Figure S5**).

RESULTS

The Effect of CK2 Inhibition on the Level of DHFR, TS, SHMT1, and SHMT2 in Cellular Lysates

DHFR and TS protein levels were measured by means of western blot in A-549 and CCRF-CEM, whereas the levels of SHMT1 and

SHMT2 were measured in CCRF-CEM cells. The cells were treated with the increasing concentrations of CX-4945 within the range from 0.5 IC_{50} to 1.5 IC_{50} (A-549) or 0.5 IC_{50} to 2 IC_{50} (CCRF-CEM) determined after 48 h of incubation. IC_{50} values for CX-4945 are 4 and 31 μM for CCRF-CEM and A-549, respectively (**Supplementary Figure S3**). To confirm the intracellular inhibition of CK2, we evaluated a site-specific phosphorylation of Ser 529 in p65NF-κB. Dose-dependent CK2 inhibition was obtained in both tested cell lines with the highest efficiency in CCRF-CEM (**Figure 1A**). The obtained results indicate that inhibition of CK2 affects the level of the tested proteins, but the correlation between the effect and dose of CX-4945 is not simple and depends on a cell line. The relative level of DHFR increases in both tested cell lines up to 3.1 in A-549, with the exception of the highest concentration of CX-4945 (**Figure 1B**). The relative protein level of TS varies in the range from 0.3 to 1.5 in A-549 and from 0.4 to 1.1 in CCRF-CEM, respectively, at the highest and lowest concentration of CX-4945 (**Figure 1**).

In the next step of our investigation, we studied the effect of CK2 inhibition on the relative level of TS, DHFR, and two forms of SHMT, i.e., cytosolic (SHMT1) and mitochondrial (SHMT2) forms, in CCRF-CEM after different times of incubation with CX-4945. The research was conducted after 6, 16, 24, 48, and 72 h of incubation in cells treated with three concentrations of CX-4945, corresponding to 0.5 IC_{50} , IC_{50} , and 2 IC_{50} . An efficient and dose-dependent CK2 inhibition was obtained in CCRF-CEM cells after 6, 16, 48, and 72 h of incubation with CX-4945 (**Figure 2A**) with the weakest inhibition, i.e., 74% phosphorylation of Ser529 in p65, detected in cells treated with 2 μM CX-4945 for 48 h. GAPDH was used as a loading control for each sample (**Figure 2B**).

The relative expression of DHFR increases in CCRF-CEM after treatment with CX-4945 up to 4.3 after 72 h of incubation and in a dose-dependent manner after 6 and 24 h of treatment (**Figure 2C**). The relative protein level of TS increases in lower concentrations of CX-4945 up to 2 after 24 h of incubation, with the exception of 16 h of incubation and decreases in higher doses of CX-4945 with the lowest relative expression of 0.13 after 16 h

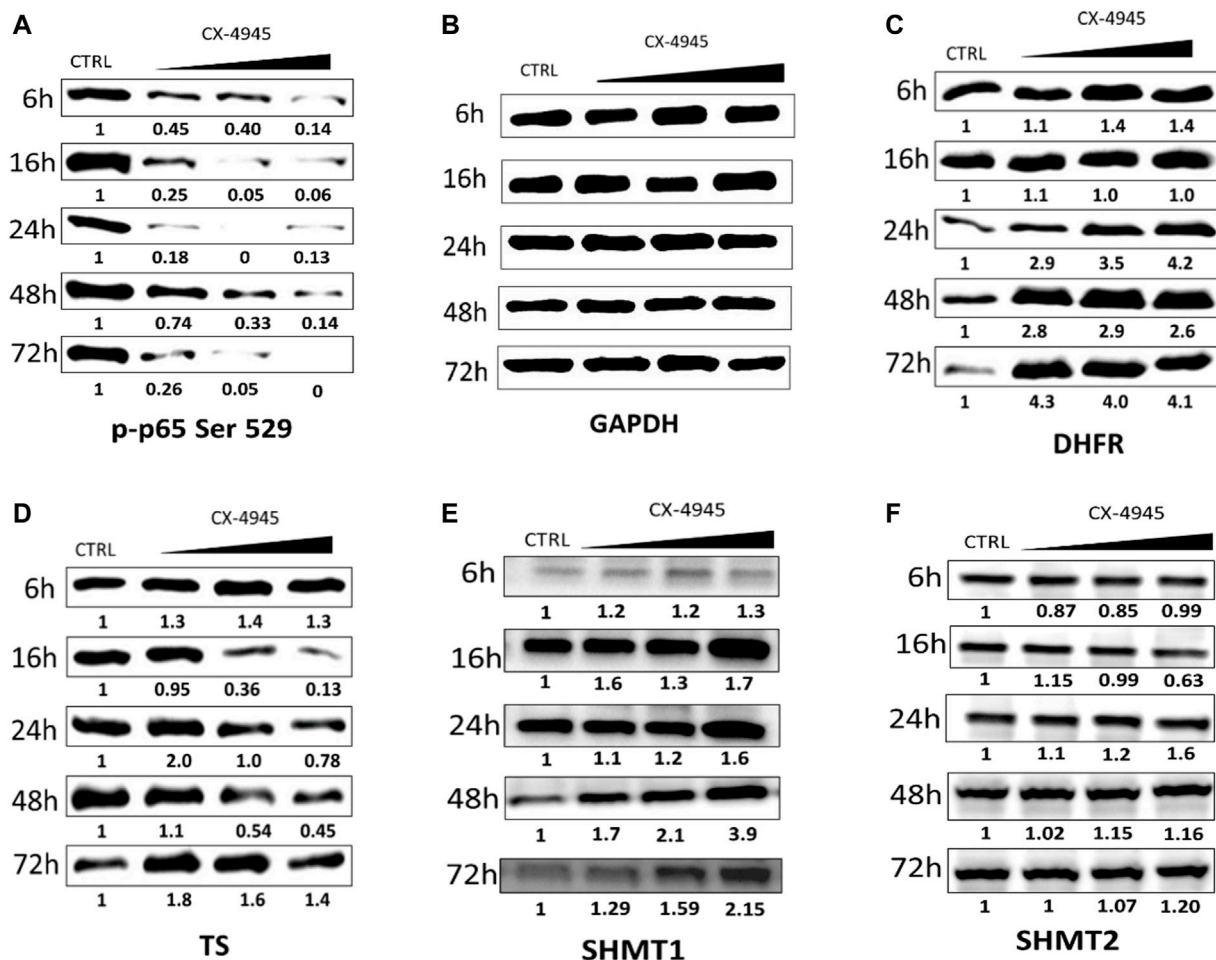


FIGURE 2 | The effect of CX-4945 on the level of p-p65 Ser 529 (nuclear factor kappa-light-chain-enhancer of activated B cells), DHFR, TS, SHMT1, and SHMT2 in CCRF-CEM. Western blot analysis of the following proteins in the crude extracts obtained from CCRF-CEM after 6, 16, 24, 48, and 72 h of treatment with 2, 4, and 8 μ M CX-4945: **(A)** p-p65 Ser 529; **(B)** GAPDH was used as a loading control for each sample; **(C)** DHFR; **(D)** TS; **(E)** SHMT1; and **(F)** SHMT2. Preparation of cell extracts and protein detection are described in *Materials and Methods*. Densitometry quantifications for each tested protein were calculated with untreated cells (CTRL) serving as the reference point showing relative protein levels.

(Figure 2D). The relative protein levels of SHMT1 and SHMT2 change in a different way with the bigger changes visible for SHMT1 with the relative expression up to 3.9 at the highest concentration of CX-4945 after 48 h of treatment (Figure 2E), whereas the relative level of SHMT2 increases the most after 24 h of treatment up to 2.02 at the highest concentration of CX-4945 (Figure 2F).

mRNA Levels in CCRF-CEM Cells Treated With CX-4945

In order to examine whether the observed level of SHMT1 and SHMT2 proteins in CCRF-CEM upon treatment with CX-4945 correlate with the cytosolic SHMT1 and/or mitochondrial SHMT2 transcript levels, QPCR was employed. The SHMT1 and SHMT2 gene expression as the ratio of relative gene expression in cells treated with the inhibitor (RE + I) and the relative gene expression in untreated cells (RE) is shown in

Figure 3. The expression of DHFR and TS genes on the mRNA level, measured by QPCR, has been previously described, and the observed changes were insignificant in a majority (Wińska et al., 2019). The results obtained in this study indicate that the changes in SHMT1 and SHMT2 transcript levels upon the treatment with CX-4945 are statistically insignificant, except for the increase in SHMT1 expression in cells treated for 24 h with 6 μ M inhibitor and decrease in SHMT2 gene expression in cells treated for 72 h with 3 μ M inhibitor. However, the changes are small, below 2-fold in both cases.

SHMT1 mRNA level in CCRF-CEM cells treated for 24 h with 3 μ M CX-4945 seems to increase only slightly when compared to untreated cells; however, this level increases more clearly in cells treated with higher (6 μ M) CK2 inhibitor concentration (Figure 3). This corresponds to the same trend in the dependence of SHMT1 protein level on CX-4945 concentration (Figure 2E). In case of SHMT2, mRNA level in

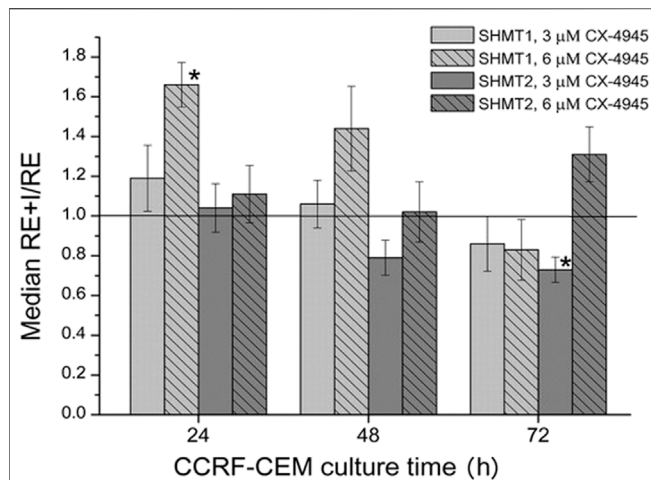


FIGURE 3 | The effect of CX-4945 on the mRNA level of cytosolic (SHMT1) and mitochondrial (SHMT2) serine hydroxymethyltransferases. The cells were treated with 3 μ M or 6 μ M CX-4945 for 24, 48, and 72 h. The RE + I/RE value equal to 1.0 means that the mRNA level in cells treated with the inhibitor is the same as in untreated cells. The asterisk indicates statistically significant results.

cells treated with 3 and 6 μ M for 24 and 48 h do not change or decrease, whereas protein level slightly increases with the concentration of CK2 inhibitor (comparing **Figure 2F**, 24 and 48 h, and **Figure 3**).

The Effect of CX-4945 Treatment on Localization of DHFR and TS in A-549 Cells

To explain the regulatory role of presumed CK2-mediated phosphorylation of DHFR and TS, we investigated the effect of CK2 inhibition on the distribution and localization of DHFR and TS in A-549 cells. Immunofluorescence was used to detect both enzymes in A-549 cells after 24, 48, and 72 h treatment with CX-4945 used in 15.5 μ M (0.5 IC_{50}), 31 μ M (IC_{50}), and 46.5 μ M (1.5 IC_{50}) concentrations, and the results are shown in **Figure 4**. The comparison of the investigated thymidylate synthesis cycle enzyme distribution in the untreated lung carcinoma cells shows that DHFR is quite evenly spread in whole cells (in the cytoplasm and nuclei) and stays that way after 24, 48, and 72 h treatment (**Figure 4A**), while TS is found mainly in the nuclei. Upon treatment with CX-4945, DHFR localization changes with CX-4945 concentration, but it is not a simple correlation. After 24 h treatment, there is a higher immunodetection of DHFR in the nuclei as compared to control cells, especially at 0.5 IC_{50} and 1 IC_{50} concentrations of the CK2 inhibitor. Additionally, the significant increase of DHFR signal is observed in the treated cells after 48 and 72 h (with the exception of the highest concentration of CX-4945) in comparison to the untreated cells. These results correlate with the DHFR protein levels assayed by western blot analysis (**Figure 1B**). The highest immunodetection of TS, localized mainly in the nuclei, is demonstrated in cells treated with 15.5 μ M CX-4945 (0.5 IC_{50}) for all incubation times (**Figure 4B**). The higher inhibitor

concentration causes a decrease in TS signal. The immunodetection of TS corresponds to the western blot analysis that shows an increase in TS protein level in A-549 treated with the lowest concentration of CX-4945 and its decrease in cells treated for 48 h with higher concentrations of CX-4945 (**Figure 1B**).

The Effect of CX-4945 Treatment on Cell Cycle Progression in A-549 Cells

In order to explain the observed differences in the expression and distribution of DHFR and TS in A-549 cells, the effect of 15.5, 31, and 46.5 μ M CX-4945 on cell cycle progression was tested by flow cytometry after 24, 48, and 72 h of treatment. The representative plots with the calculations of cell percentages in each phase of the cell cycle are shown in **Figure 5**. Distribution of control cells in each phase changes during the cell cycle progression, with the highest difference occurred for the S-phase with 12% less cells in this phase after 72 h of incubation in comparison to 24 h of incubation. Interestingly, the results correspond to confocal microscopy studies that demonstrated the decrease in TS in control nuclei with the time of incubation (**Figure 4**). Furthermore, the obtained results indicate that CX-4945 leads to prolongation of the G2/M-phase in A-549 cells up to a maximum of 20% more cells in this phase than in control after 24 h of treatment with the highest concentration of CX-4945 (statistically significant result, $p = 0.004$). Additionally, S-phase arrest is detected in the treated cells after 48 and 72 h of treatment with CX-4945. There are up to 19% more cells treated with 31 μ M CX-4945 than in control for 48 h.

The Effect of CK2-Mediated TS Phosphorylation on the Formation of Di- and Tri-Protein Thymidylate Cycle Enzyme Complexes

We have previously described the strong *in vitro* interaction occurring between TS and DHFR proteins (Antosiewicz et al., 2015) and their co-localization in normal and cancer cells (Antosiewicz et al., 2017). In this follow-up study, we show the interactions between the pairs TS and SHMT1, DHFR, and SHMT1 and the formation of the tri-molecular complex consisting of all three thymidylate synthesis proteins, TS, DHFR, and SHMT1. The effect of CK2-mediated TS phosphorylation on the formation and stability of both di- and tri-protein complexes has turned out to be particularly interesting.

Both methods used, QCM-D and MST, showed that the non-phosphorylated TS did not interact with SHMT1 (**Table 1**, **Supplementary Figures S1–S5**). However, experiments conducted with CK2 α -phosphorylated TS fraction (pTS) confirmed the formation of a strong SHMT1/pTS complex with a dissociation constant $K_d = 5.35 \pm 0.87 \mu$ M obtained from QCM-D studies (**Figure 6**) and $0.219 \pm 0.02 \mu$ M given by MST studies. Thus, in this case, phosphorylation of TS seems to determine the formation of the studied complex. The influence of this post-translational modification of TS molecule is also significant in the case of tri-enzymatic complex formation. Our

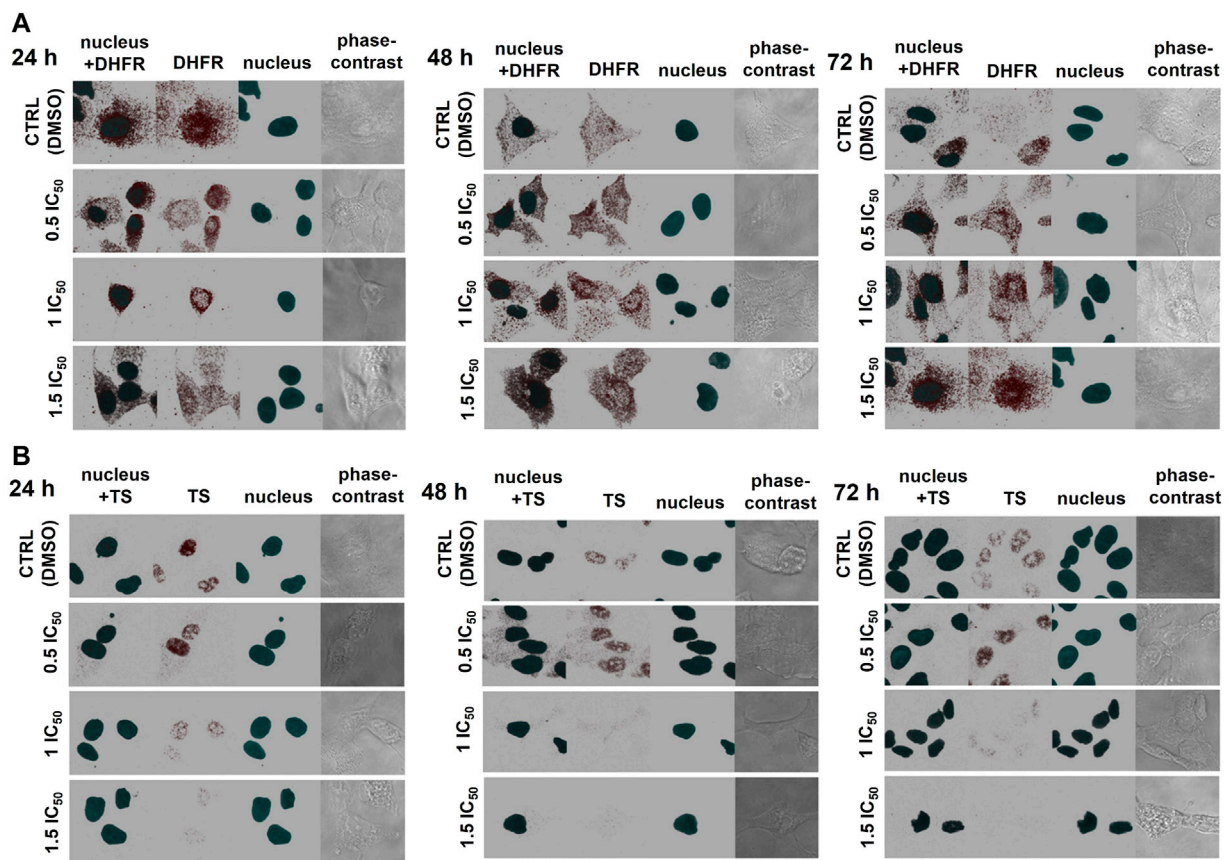


FIGURE 4 | The effect of CX-4945 on the localization and protein levels of DHFR and TS in A-549 cells. The cells were treated with CX-4945 used in concentrations corresponding to 0.5 IC₅₀, 1 IC₅₀, and 1.5 IC₅₀, fixed after incubation for 24, 48, and 72 h; after blocking, they were probed with the primary anti-DHFR (A) or anti-TS antibodies (B). Subsequently, the cells were treated with Alexa Fluor 555-conjugated secondary antibody (red fluorescence) and Hoechst 33342 (nuclei, blue fluorescence). The presented pictures of DHFR, TS, nucleus, and combined are 3D pictures of at least 15 z-stack photos visualized together to show the full three-dimensional distribution of the examined proteins. The pictures in the fourth column of each panel are 2D phase contrast photographs. Each picture is shot with the same zoom settings. Photographs represent 65 × 65 μm pictures.

studies show that although the presence of DHFR enables the formation of SHMT1/DHFR/TS tri-complex, it is weaker than the one formed in the presence of the phosphorylated TS fraction (Figure 6; Supplementary Figure S5). Dissociation constants for di- and tri-protein complexes obtained using QCM-D and MST methods are gathered in Table 1.

DISCUSSION

There are reports indicating the occurrence of CK2-mediated phosphorylation of TS, DHFR, and SHMT (Frączyk et al., 2010; Frączyk et al., 2015; Ludwiczak et al., 2016; Rusin et al., 2017; Skierka et al., 2019); however, to this date, there have been no studies showing the physiological role of CK2-mediated phosphorylation of thymidylate synthesis cycle enzymes. Our previous (Wińska et al., 2019) and present qPCR results indicate that inhibition of CK2 in CCRF-CEM cells treated with a specific CX-4945 inhibitor does not significantly influence the mRNA levels. The only statistically significant results showing

some changes are the increase in DHFR (Wińska et al., 2019) and SHMT1 transcripts in cells treated with 6 μM CX-4945 for 24 h, decrease in TS and SHMT2 in cells treated with 3 μM CX-4945 for 72 h, and decrease in DHFR in cells treated with 6 μM inhibitor for 72 h. In each case, the change was well below 2-fold, so it can hardly be considered meaningful. Therefore, the intracellular increase of DHFR and SHMT1 protein levels upon CK2 inhibitor treatment may be attributed to the disturbance of some regulatory roles of CK2. Regarding this discrepancy between the mRNA and protein level of enzymes involved in the thymidylate biosynthesis cycle in cells after CX-4945 treatment, we concluded that CK2-mediated phosphorylation affects their stability in cells. Both DHFR and SHMT1 have been shown to undergo polyubiquitination and degradation in proteasome (Johnston et al., 1995; Anderson et al., 2012); moreover, proteasome inhibition stabilizes SHMT1 and increases ubiquitinated SHMT1 levels in a cell. It has been shown that the stability and localization of SHMT1 is regulated by competitive modification by Ubc-9 and Ubc-13. The former triggers SHMT1 nuclear degradation, whereas the latter increases SHMT1 stability (Anderson et al., 2012). Since there

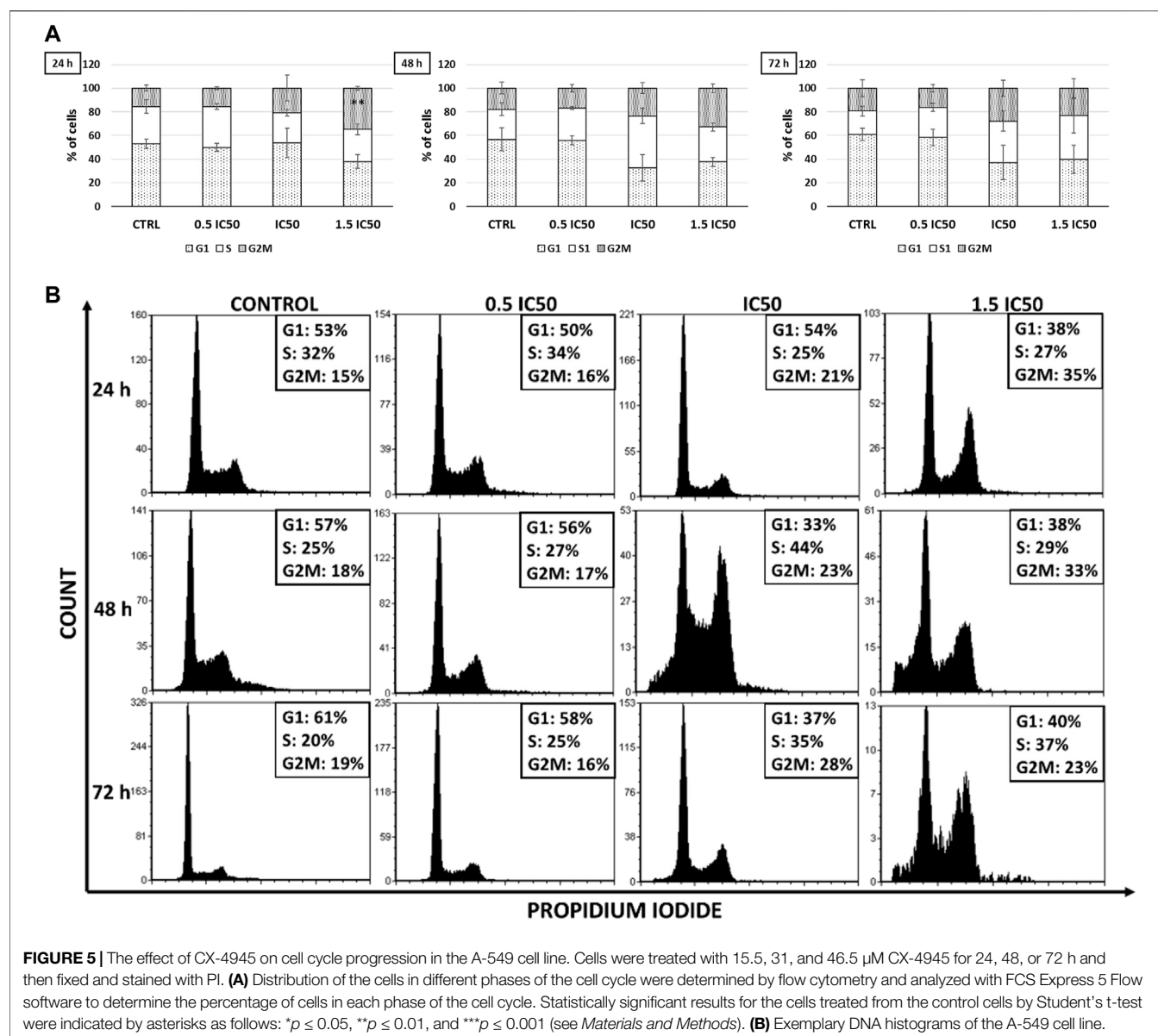


TABLE 1 | QCM-D and MST analyses of protein complex formation.

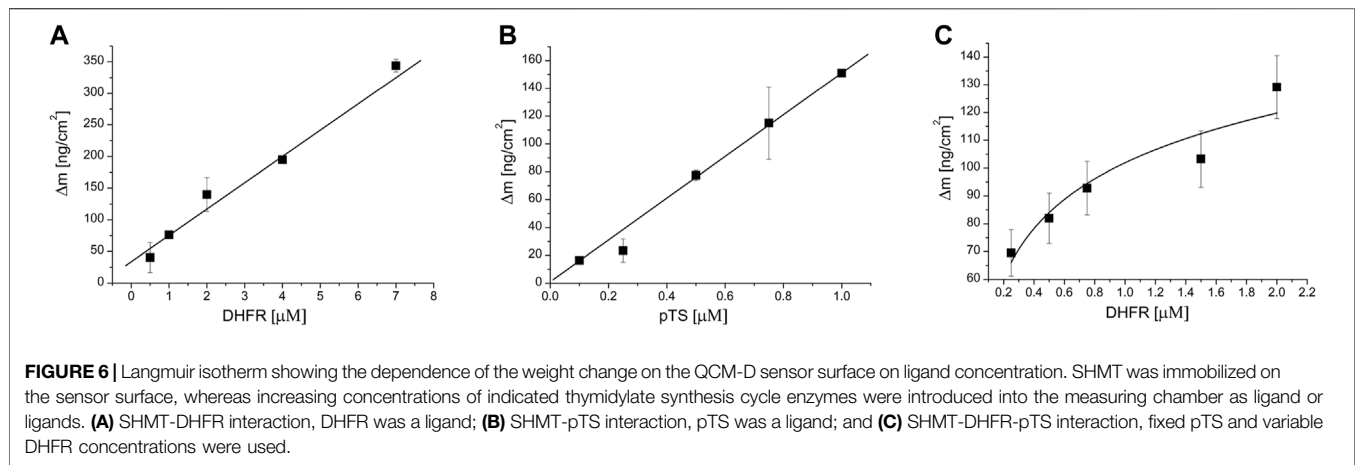
Enzyme complex	Kd [μM] QCM-D	Kd [μM] MST
TS/DHFR ^a	7.6 \pm 0.7	2.8 \pm 0.4
SHMT1/TS	No interactions	No interactions
SHMT1/pTS	5.35 \pm 0.87	0.219 \pm 0.02
SHMT1/DHFR	12.11 \pm 7.86	12.60 \pm 0.66
SHMT1/DHFR/TS	NA	5.04 \pm 0.5
SHMT1/DHFR/pTS	0.28 \pm 0.23	0.32 \pm 0.05

^aAntosiewicz et al., 2015; NA, not analyzed.

are examples for targeting CK2-phosphorylated proteins for ubiquitination and degradation, it cannot be excluded that the inhibition of CK2 may lead to the decrease of ubiquitination and, subsequently, the decrease of DHFR and SHMT1 as observed by us increased the levels of both proteins.

Interestingly, our results indicate that CK2 inhibition has a different impact on TS level compared with DHFR and SHMT1 protein levels. Our western experiments show that, in CCRF-CEM cells treated with the CK2 inhibitor, TS protein level decreases with the increase in concentrations of CX-4945, which is in contrast to DHFR and SHMT1 behavior. Considering that TS is a non-ubiquitinated proteasome substrate and undergoes only ubiquitin-independent proteasomal degradation (Erales and Coffino, 2014), the obtained results may confirm the possible role of CK2-mediated phosphorylation in the regulation of the ubiquitin-dependent degradation of DHFR and SHMT1.

Taking into account that DHFR is an important molecular target in anti-cancer therapy and CX-4945 is a potential anti-cancer agent, the significant elevation of DHFR concentration and its resulting activity increase in cells may contribute to the



vast reduction in the effectiveness of treatment. There is a lot of evidence showing that the increased DHFR level makes the therapy ineffective. Among the drug resistance mechanisms in DHFR-targeted anti-cancer therapy, the best known is the amplification of the DHFR gene which leads to the increase in DHFR level after a prolonged methotrexate MTX treatment (Carman et al., 1984; Banerjee et al., 2002). In addition, since DHFR protein binds its own mRNA when its active site is unoccupied and, thereby, autoregulates its translation, binding of MTX to DHFR inhibits DHFR activity and also disrupts the interaction between DHFR and its own mRNA, relieving the repressed DHFR translation and leading to increased DHFR protein levels and, thus, to MTX resistance (Johnston et al., 1995). Considering that CX-4945 is a potential anti-cancer therapeutic agent, in view of our data showing the inhibition of CK2 activity causes the increase of DHFR and SHMT1 protein levels, a possible increased survival of cancer cells should be taken into consideration. However, further studies are needed to determine if prolonged inhibition of CK2 will not lead to resistance to cancer cells *via* increasing the level of thymidylate biosynthesis cycle enzymes.

The obtained results indicate that CK2-mediated phosphorylation of enzymes involved in the thymidylate biosynthesis cycle can be important for not only their stability within the cells but also for their distribution and ability to form complexes. Our studies involving immunodetection of DHFR and TS within A-549 cells confirmed that both protein levels and localizations in control cells are cell cycle dependent. It is known that TS mRNA level increases up to 20-fold in the S-phase (Navalgund et al., 1980), which is driven by the E2F transcription factor (DeGregori et al., 1995). On the other hand, the transcription of DHFR in the S-phase is driven by the E2F transcription factor working in concert with the Sp1 transcription factor (Abali et al., 2008). The decrease of immunodetection of both enzymes in untreated cells during incubation corresponds to the exit of the cells from the S phase. The obtained results indicate that CX-4945 treatment leads to the prolongation of the G2/M phase, which is in good agreement with the studies demonstrating the effect of CX-4945 on the cell cycle progression in different cell lines

(Gray et al., 2014; Wińska et al., 2018). Moreover, the TS immunodetection results obtained in A-549 cells treated with CX-4945 correspond well to the western blot data for the same line, demonstrating the highest increase of TS protein level in cells treated with 0.5 IC₅₀ CX-4945 and the decrease of this level at 1.5 IC₅₀. It is worth noting that the significant decrease of TS in A-549 at IC₅₀ and 1.5 IC₅₀ CX-4945 corresponds to G2/M arrest in the cells. Interestingly, an immunodetection of DHFR in A-549 cells partially corresponds with the western blot data, since an increase in DHFR is detected in all CX-4945-treated cells in comparison to the control cells after 48 h of treatment; however, a decrease in the DHFR level in A-549 treated with the highest concentration of CX-4945 corresponding to the western blot data is detected after 72 h.

Using two methods, QCM-D and MST, we have shown the *in vitro* interactions of TS, SHMT1, and DHFR. In the QCM-D method, one protein is immobilized while the other serves as a ligand, whereas MST allows protein-protein interaction measurement with two or three proteins free in solution. Our results clearly show that TS interacts with DHFR and DHFR interacts with SHMT1; however, TS does not interact with SHMT1. Interestingly, all three proteins present in the solution interact and form a tri-complex measured with the MST method. Phosphorylation of TS by CK2 enables the interaction of the enzyme with SHMT1, and the tri-complex of pTS with SHMT1 and DHFR is more stable than the complex with non-phosphorylated TS. The obtained results suggest that phosphorylation of TS may act as a molecular switch, initiating a tri-enzymatic complex formation.

Taking into account that CK2 is a pleiotropic kinase and its inhibition affects different signaling pathways within the cells, the effects we detect do not have a simple explanation. However, considering that enzymes involved in the thymidylate biosynthesis cycle are key members of proliferation machinery, whereas CK2 is a potential anti-cancer molecular target, the obtained results may be relevant in the development of new anti-cancer therapies, based on CK2 inhibition. It should be taken into account that CK2 inhibition may affect folate and thymidylate

metabolism in cells contributing to cell resistance to such therapies. Therefore, further detailed studies on the impact of CK2 inhibition on enzymes involved in the thymidylate biosynthesis cycle should be conducted.

CONCLUSIONS

Many studies demonstrated that phosphorylation can affect the stability, the activity, and even the location of a protein within the cell. Our results suggest the potential regulatory role of CK2-mediated phosphorylation of enzymes involved in the thymidylate biosynthesis cycle in their stability, nuclear location, and ability to complex formation. Considering that CK2 is a potential anti-cancer target, whereas both TS and DHFR are well-established targets in chemotherapy, the obtained results seem to be important in developing new anti-cancer strategies. Therefore, further in-depth research should be carried out in order to clarify the physiological role of CK2-mediated phosphorylation of TS/DHFR/SHMT.

DATA AVAILABILITY STATEMENT

The original contributions presented in the study are included in the article/**Supplementary Material**, further inquiries can be directed to the corresponding authors.

REFERENCES

- Abali, E. E., Skacel, N. E., Celikkaya, H., and Hsieh, Y. C. (2008). Chapter 9 Regulation of Human Dihydrofolate Reductase Activity and Expression. *Vitam Horm.* 79, 267–292. doi:10.1016/S0083-6729(08)00409-3
- Ahmed, K., Gerber, D. A., and Cochet, C. (2002). Joining the Cell Survival Squad: An Emerging Role for Protein Kinase CK2. *Trends Cell Biol.* 12, 226–230. doi:10.1016/S0962-8924(02)02279-1
- Anderson, D. D., Eom, J. Y., and Stover, P. J. (2012). Competition between Sumoylation and Ubiquitination of Serine Hydroxymethyltransferase 1 Determines its Nuclear Localization and its Accumulation in the Nucleus. *J. Biol. Chem.* 287, 4790–4799. doi:10.1074/jbc.M111.302174
- Antosiewicz, A., Jarmuła, A., Przybylska, D., Mosieniak, G., Szczepanowska, J., Kowalkowska, A., et al. (2017). Human Dihydrofolate Reductase and Thymidylate Synthase Form a Complex *In Vitro* and Co-Localize in normal and Cancer Cells. *J. Biomol. Struct. Dyn.* 35, 1474–1490. doi:10.1080/07391102.2016.1186560
- Antosiewicz, A., Senkara, E., and Cieśla, J. (2015). Quartz crystal Microbalance with Dissipation and Microscale Thermophoresis as Tools for Investigation of Protein Complex Formation between Thymidylate Synthesis Cycle Enzymes. *Biosens. Bioelectron.* 64, 36–42. doi:10.1016/j.bios.2014.08.031
- Banerjee, D., Mayer-Kuckuk, P., Capiiaux, G., Budak-Alpdogan, T., Gorlick, R., and Bertino, J. R. (2002). Novel Aspects of Resistance to Drugs Targeted to Dihydrofolate Reductase and Thymidylate Synthase. *Biochim. Biophys. Acta (Bba) - Mol. Basis Dis.* 1587, 164–173. doi:10.1016/S0925-4439(02)00079-0
- Borgo, C., D'Amore, C., Sarno, S., Salvi, M., and Ruzzene, M. (2021). Protein Kinase CK2: A Potential Therapeutic Target for Diverse Human Diseases. *Sig Transduct Target. Ther.* 6, 183. doi:10.1038/s41392-021-00567-7
- Borgo, C., Franchin, C., Salizzato, V., Cesaro, L., Arrigoni, G., Matricardi, L., et al. (2015). Protein Kinase CK2 Potentiates Translation Efficiency by Phosphorylating eIF3j at Ser127. *Biochim. Biophys. Acta (Bba) - Mol. Cell Res.* 1853, 1693–1701. doi:10.1016/j.bbamer.2015.04.004

AUTHOR CONTRIBUTIONS

Conceptualization: PW and JC; methodology: PW and JC; investigation: PW, ŁW, ES, MK, JMC, AK, and KS; writing—original draft preparation: PW; and writing—review and editing: JC. All authors have read and agreed to the published version of the manuscript.

FUNDING

This research was funded by the Warsaw University of Technology.

ACKNOWLEDGMENTS

We wish to thank NanoTemper Technologies (www.nanotemper-technologies.com) for providing the MonolithNT.115 instrument and to Dr. Piotr Wardęga for his expert assistance.

SUPPLEMENTARY MATERIAL

The Supplementary Material for this article can be found online at: <https://www.frontiersin.org/articles/10.3389/fmolb.2022.847829/full#supplementary-material>.

- Borgo, C., and Ruzzene, M. (2021). Protein Kinase CK2 Inhibition as a Pharmacological Strategy. *Adv. Protein Chem. Struct. Biol.* 124, 23–46. doi:10.1016/bs.apcsb.2020.09.003
- Borkiewicz, L., Polkowska-Kowalczyk, L., Cieśla, J., Sowiński, P., Jończyk, M., Rymaszewski, W., et al. (2019). Expression of maize Calcium-dependent Protein Kinase (ZmCPK11) Improves Salt Tolerance in Transgenic Arabidopsis Plants by Regulating Sodium and Potassium Homeostasis and Stabilizing Photosystem II. *Physiol. Plantarum* 168, 38–57. doi:10.1111/ppl.12938
- Bradford, M. M. (1976). A Rapid and Sensitive Method for the Quantitation of Microgram Quantities of Protein Utilizing the Principle of Protein-Dye Binding. *Anal. Biochem.* 72, 248–254. doi:10.1006/abio.1976.9999
- Cabrejos, M. E., Allende, C. C., and Maldonado, E. (2004). Effects of Phosphorylation by Protein Kinase CK2 on the Human Basal Components of the RNA Polymerase II Transcription Machinery. *J. Cel. Biochem.* 93, 2–10. doi:10.1002/jcb.20209
- Carman, M. D., Schornagel, J. H., Rivest, R. S., Srmatkandada, S., Portlock, C. S., Duffy, T., et al. (1984). Resistance to Methotrexate Due to Gene Amplification in a Patient with Acute Leukemia. *J. Clin. Oncol.* 2, 16–20. doi:10.1200/JCO.1984.2.1.16
- Chapman, J. R., and Jackson, S. P. (2008). Phospho-dependent Interactions between NBS1 and MDC1 Mediate Chromatin Retention of the MRN Complex at Sites of DNA Damage. *EMBO Rep.* 9, 795–801. doi:10.1038/embor.2008.103
- Chojnacki, S., Cowley, A., Lee, J., Foix, A., and Lopez, R. (2017). Programmatic Access to Bioinformatics Tools from EMBL-EBI Update: 2017. *Nucleic Acids Res.* 45, W550–W553. doi:10.1093/nar/gkx273
- Chon, H. J., Bae, K. J., Lee, Y., and Kim, J. (2015). The Casein Kinase 2 Inhibitor, CX-4945, as an Anti-Cancer Drug in Treatment of Human Hematological Malignancies. *Front. Pharmacol.* 6, 70. doi:10.3389/fphar.2015.00070
- D'Amore, C., Borgo, C., Sarno, S., and Salvi, M. (2020). Role of CK2 Inhibitor CX-4945 in Anti-Cancer Combination Therapy - Potential Clinical Relevance. *Cell Oncol.* 43, 1003–1016. doi:10.1007/s13402-020-00566-w

- DeGregori, J., Kowalik, T., and Nevins, J. R. (1995). Cellular Targets for Activation by the E2F1 Transcription Factor Include DNA Synthesis- and G1/S-Regulatory Genes. *Mol. Cell Biol.* 15, 4215–4224. doi:10.1128/mcb.15.8.4215
- Duncan, J. S., Turowec, J. P., Duncan, K. E., Vilks, G., Wu, C., Lüscher, B., et al. (2011). A Peptide-Based Target Screen Implicates the Protein Kinase CK2 in the Global Regulation of Caspase Signaling. *Sci. Signal.* 4, ra30. doi:10.1126/scisignal.2001682
- Erales, J., and Coffino, P. (2014). Ubiquitin-Independent Proteasomal Degradation. *Biochim. Biophys. Acta (Bba) - Mol. Cell Res.* 1843, 216–221. doi:10.1016/j.bbamcr.2013.05.008
- Frączyk, T., Kubiński, K., Maslyk, M., Cieśla, J., Hellman, U., Shugar, D., et al. (2010). Phosphorylation of Thymidylate Synthase from Various Sources by Human Protein Kinase CK2 and its Catalytic Subunits. *Bioorg. Chem.* 38, 124–131. doi:10.1016/j.bioorg.2010.02.001
- Frączyk, T., Ruman, T., Wilk, P., Palmowski, P., Rogowska-Wrzesinska, A., Cieśla, J., et al. (2015). Properties of Phosphorylated Thymidylate Synthase. *Biochim. Biophys. Acta (Bba) - Proteins Proteomics* 1854, 1922–1934. doi:10.1016/j.bbapap.2015.08.007
- Gandin, V., Masvidal, L., Cargnello, M., Gyenis, L., McLaughlan, S., Cai, Y., et al. (2016). mTORC1 and CK2 Coordinate Ternary and eIF4F Complex Assembly. *Nat. Commun.* 7, 11127. doi:10.1038/ncomms11127
- Gray, G. K., McFarland, B. C., Rowse, A. L., Gibson, S. A., and Benveniste, E. N. (2014). Therapeutic CK2 Inhibition Attenuates Diverse Prosurvival Signaling Cascades and Decreases Cell Viability in Human Breast Cancer Cells. *Oncotarget* 5, 6484–6496. doi:10.18632/oncotarget.2248
- Homma, M. K., and Homma, Y. (2008). Cell Cycle and Activation of CK2. *Mol. Cell Biochem.* 316, 49–55. doi:10.1007/s11010-008-9823-4
- Jarmuła, A., Frączyk, T., Cieplak, P., and Rode, W. (2010). Mechanism of Influence of Phosphorylation on Serine 124 on a Decrease of Catalytic Activity of Human Thymidylate Synthase. *Bioorg. Med. Chem.* 18, 3361–3370. doi:10.1016/j.bmc.2010.04.019
- Johnston, J. A., Johnson, E. S., Waller, P. R. H., and Varshavsky, A. (1995). Methotrexate Inhibits Proteolysis of Dihydrofolate Reductase by the N-End Rule Pathway. *J. Biol. Chem.* 270, 8172–8178. doi:10.1074/jbc.270.14.8172
- Kim, J., and Kim, S. H. (2012). Druggability of the CK2 Inhibitor CX-4945 as an Anticancer Drug and beyond. *Arch. Pharm. Res.* 35, 1293–1296. doi:10.1007/s12272-012-0800-9
- Lovellace, L. L., Johnson, S. R., Gibson, L. M., Bell, B. J., Berger, S. H., and Lebiada, L. (2009). Variants of Human Thymidylate Synthase with Loop 181–197 Stabilized in the Inactive Conformation. *Protein Sci.* 18, 1628–1636. doi:10.1002/pro.171
- Ludwiczak, J., Maj, P., Wilk, P., Frączyk, T., Ruman, T., Kierdaszuk, B., et al. (2016). Phosphorylation of Thymidylate Synthase Affects Slow-Binding Inhibition by 5-Fluoro-dUMP and N4-Hydroxy-dCMP. *Mol. Biosyst.* 12, 1333–1341. doi:10.1039/c6mb00026f
- Luo, B., Repalli, J., Yousef, A.-M., Johnson, S. R., Lebiada, L., and Berger, S. H. (2011). Human Thymidylate Synthase with Loop 181–197 Stabilized in an Inactive Conformation: Ligand Interactions, Phosphorylation, and Inhibition Profiles. *Protein Sci.* 20, 87–94. doi:10.1002/pro.539
- Lüscher, B., Christenson, E., Litchfield, D. W., Krebs, E. G., and Eisenman, R. N. (1990). Myb DNA Binding Inhibited by Phosphorylation at a Site Deleted during Oncogenic Activation. *Nature* 344, 517–522. doi:10.1038/344517a0
- Navalgund, L. G., Rossana, C., Muench, A. J., and Johnson, L. F. (1980). Cell Cycle Regulation of Thymidylate Synthetase Gene Expression in Cultured Mouse Fibroblasts. *J. Biol. Chem.* 255, 7386–7390. doi:10.1016/s0021-9258(20)79715-2
- Niechi, I., Silva, E., Cabello, P., Huerta, H., Carrasco, V., Villar, P., et al. (2015). Colon Cancer Cell Invasion Is Promoted by Protein Kinase CK2 through Increase of Endothelin-Converting Enzyme-1c Protein Stability. *Oncotarget* 6, 42749–42760. doi:10.18632/oncotarget.5722
- Núñez de Villavicencio-Díaz, T., Rabalski, A., and Litchfield, D. (2017). Protein Kinase CK2: Intricate Relationships within Regulatory Cellular Networks. *Pharmaceuticals* 10 (1), 27. doi:10.3390/ph10010027
- Patsoukis, N., Li, L., Sari, D., Petkova, V., and Boussiotis, V. A. (2013). PD-1 Increases PTEN Phosphatase Activity while Decreasing PTEN Protein Stability by Inhibiting Casein Kinase 2. *Mol. Cell Biol.* 33, 3091–3098. doi:10.1128/MCB.00319-13
- Piazza, F. A., Ruzzene, M., Gurrieri, C., Montini, B., Bonanni, L., Chioetto, G., et al. (2006). Multiple Myeloma Cell Survival Relies on High Activity of Protein Kinase CK2. *Blood* 108, 1698–1707. doi:10.1182/blood-2005-11-013672
- Pierre, F., Chua, P. C., O'Brien, S. E., Siddiqui-Jain, A., Bourbon, P., Haddach, M., et al. (2011). Discovery and SAR of 5-(3-Chlorophenylamino)benzo[c][2,6]naphthyridine-8-Carboxylic Acid (CX-4945), the First Clinical Stage Inhibitor of Protein Kinase CK2 for the Treatment of Cancer. *J. Med. Chem.* 54, 635–654. doi:10.1021/jm101251q
- Riera, M., Roher, N., Miró, F., Gil, C., Trujillo, R., Aguilera, J., et al. (1999). Association of Protein Kinase CK2 with Eukaryotic Translation Initiation Factor eIF-2 and with Grp94/endoplasmic. *Mol. Cell Biochem.* 191, 97–104. doi:10.1023/A:1006810311743
- Rusin, S. F., Adamo, M. E., and Kettenbach, A. N. (2017). Identification of Candidate Casein Kinase 2 Substrates in Mitosis by Quantitative Phosphoproteomics. *Front. Cell Dev. Biol.* 5, 97. doi:10.3389/fcell.2017.00097
- Scaglioni, P. P., Yung, T. M., Choi, S., Baldini, C., Konstantinidou, G., Pandolfi, P. P., et al. (2009). CK2 Mediates Phosphorylation and Ubiquitin-Mediated Degradation of the PML Tumor Suppressor. *Mol. Cell Biochem.* 327, 279. doi:10.1007/s11010-009-0122-5
- Shen, J., Channavajhala, P., Seldin, D. C., and Sonenshein, G. E. (2001). Phosphorylation by the Protein Kinase CK2 Promotes Calpain-Mediated Degradation of IκBα. *J. Immunol.* 167, 4919–4925. doi:10.4049/jimmunol.167.9.4919
- Siddiqui-Jain, A., Bliesath, J., Macalino, D., Omori, M., Huser, N., Streiner, N., et al. (2012). CK2 Inhibitor CX-4945 Suppresses DNA Repair Response Triggered by DNA-Targeted Anticancer Drugs and Augments Efficacy: Mechanistic Rationale for Drug Combination Therapy. *Mol. Cancer Ther.* 11, 994–1005. doi:10.1158/1535-7163.mct-11-0613
- Skierka, K., Wilamowski, P., Wielechowska, M., Cysewski, D., Senkara, E., Wińska, P., et al. (2019). Human Dihydrofolate Reductase Is a Substrate of Protein Kinase CK2α. *Biochem. Biophysical Res. Commun.* 513, 368–373. doi:10.1016/j.bbrc.2019.03.186
- Szebeni, A., Hingorani, K., Negi, S., and Olson, M. O. J. (2003). Role of Protein Kinase CK2 Phosphorylation in the Molecular Chaperone Activity of Nucleolar Protein B23. *J. Biol. Chem.* 278, 9107–9115. doi:10.1074/jbc.M204411200
- Trembley, J. H., Wang, G., Unger, G., Slaton, J., and Ahmed, K. (2009). Protein Kinase CK2 in Health and Disease: CK2: A Key Player in Cancer Biology. *Cell. Mol. Life Sci.* 66, 1858–1867. doi:10.1007/s00018-009-9154-y
- Tsuchiya, Y., Akashi, M., Matsuda, M., Goto, K., Miyata, Y., Node, K., et al. (2009). Involvement of the Protein Kinase CK2 in the Regulation of Mammalian Circadian Rhythms. *Sci. Signal.* 2, ra26. doi:10.1126/scisignal.2000305
- Vandesompele, J., De Preter, K., Pattyn, F., Poppe, B., Van Roy, N., De Paepe, A., et al. (2002). Accurate Normalization of Real-Timequantitative RT-PCR Data by Geometric Averaging of Multiple Internal Control Genes. *Genome Biol.* 3, research0034.1. doi:10.1186/gb-2002-3-7-research0034
- Wińska, P., Karatsai, O., Staniszevska, M., Koronkiewicz, M., Chojnacki, K., and Rędowicz, M. J. (2020). Synergistic Interactions of 5-Fluorouracil with Inhibitors of Protein Kinase CK2 Correlate with P38 MAPK Activation and FAK Inhibition in the Triple-Negative Breast Cancer Cell Line. *Int. J. Mol. Sci.* 21, E6234. doi:10.3390/ijms21176234
- Wińska, P., Skierka, K., Łukowska-chojnacka, E., Koronkiewicz, M., Cieśla, J., and Bretner, M. (2018). Effect of Simultaneous Inhibition of Protein Kinase Ck2 and Thymidylate Synthase in Leukemia and Breast Cancer Cells. *Anticancer Res.* 38, 4617–4627. doi:10.21873/anticancer.12766
- Wińska, P., Widlo, L., Skierka, K., Krzyśko, A., Koronkiewicz, M., Cieśla, J. M., et al. (2019). Simultaneous Inhibition of Protein Kinase CK2 and Dihydrofolate Reductase Results in Synergistic Effect on Acute Lymphoblastic Leukemia Cells. *Anticancer Res.* 39, 3531–3542. doi:10.21873/anticancer.13499
- Wolschin, F., Wienkoop, S., and Weckwerth, W. (2005). Enrichment of Phosphorylated Proteins and Peptides from Complex Mixtures Using Metal Oxide/hydroxide Affinity Chromatography (MOAC). *Proteomics* 5, 4389–4397. doi:10.1002/pmic.200402049

Zhang, C., Vilks, G., Canton, D. A., and Litchfield, D. W. (2002). Phosphorylation Regulates the Stability of the Regulatory CK2 β Subunit. *Oncogene* 21, 3754–3764. doi:10.1038/sj.onc.1205467

Conflict of Interest: The authors declare that the research was conducted in the absence of any commercial or financial relationships that could be construed as a potential conflict of interest.

Publisher's Note: All claims expressed in this article are solely those of the authors and do not necessarily represent those of their affiliated organizations, or those of the publisher, the editors, and the reviewers. Any product that may be evaluated in

this article, or claim that may be made by its manufacturer, is not guaranteed or endorsed by the publisher.

Copyright © 2022 Wińska, Widło, Senkara, Koronkiewicz, Cieśla, Krzyśko, Skierka and Cieśla. This is an open-access article distributed under the terms of the Creative Commons Attribution License (CC BY). The use, distribution or reproduction in other forums is permitted, provided the original author(s) and the copyright owner(s) are credited and that the original publication in this journal is cited, in accordance with accepted academic practice. No use, distribution or reproduction is permitted which does not comply with these terms.



CIGB-300-Regulated Proteome Reveals Common and Tailored Response Patterns of AML Cells to CK2 Inhibition

Mauro Rosales^{1,2†}, Arielis Rodríguez-Ulloa^{3†}, George V. Pérez², Vladimir Besada³, Thalía Soto^{1,2}, Yassel Ramos³, Luis J. González³, Katharina Zettl⁴, Jacek R. Wiśniewski⁴, Ke Yang^{5*}, Yasser Perera^{2,5*} and Silvio E. Perea^{2*}

OPEN ACCESS

Edited by:

Giorgio Cozza,
University of Padua, Italy

Reviewed by:

Wei Zhou,
National Neuroscience Institute (NNI),
Singapore
Alessandra Gianoncelli,
University of Brescia, Italy

*Correspondence:

Ke Yang
young@ccbji.com
Yasser Perera
ypereranegrin@ccbji.com
Silvio E. Perea
silvio.perea@cigb.edu.cu

[†]These authors have contributed
equally to this work

Specialty section:

This article was submitted to
Cellular Biochemistry,
a section of the journal
Frontiers in Molecular Biosciences

Received: 13 December 2021

Accepted: 01 February 2022

Published: 11 March 2022

Citation:

Rosales M, Rodríguez-Ulloa A,
Pérez GV, Besada V, Soto T, Ramos Y,
González LJ, Zettl K, Wiśniewski JR,
Yang K, Perera Y and Perea SE (2022)
CIGB-300-Regulated Proteome
Reveals Common and Tailored
Response Patterns of AML Cells to
CK2 Inhibition.
Front. Mol. Biosci. 9:834814.
doi: 10.3389/fmolb.2022.834814

¹Department of Animal and Human Biology, Faculty of Biology, University of Havana (UH), Havana, Cuba, ²Molecular Oncology Group, Department of Pharmaceuticals, Biomedical Research Division, Center for Genetic Engineering and Biotechnology (CIGB), Havana, Cuba, ³Mass Spectrometry Laboratory, Proteomics Group, Department of System Biology, Biomedical Research Division, CIGB, Havana, Cuba, ⁴Biochemical Proteomics Group, Department of Proteomics and Signal Transduction, Max-Planck Institute of Biochemistry, Munich, Germany, ⁵China-Cuba Biotechnology Joint Innovation Center (CCBJIC), Yongzhou Zhong Gu Biotechnology Co., Ltd., Yongzhou, China

Protein kinase CK2 is a highly pleiotropic and ubiquitously expressed Ser/Thr kinase with instrumental roles in normal and pathological states, including neoplastic phenotype in solid tumor and hematological malignancies. In line with previous reports, CK2 has been suggested as an attractive prognostic marker and molecular target in acute myeloid leukemia (AML), a blood malignant disorder that remains as an unmet medical need. Accordingly, this work investigates the complex landscape of molecular and cellular perturbations supporting the antileukemic effect exerted by CK2 inhibition in AML cells. To identify and functionally characterize the proteomic profile differentially modulated by the CK2 peptide-based inhibitor CIGB-300, we carried out LC-MS/MS and bioinformatic analysis in human cell lines representing two differentiation stages and major AML subtypes. Using this approach, 109 and 129 proteins were identified as significantly modulated in HL-60 and OCI-AML3 cells, respectively. In both proteomic profiles, proteins related to apoptotic cell death, cell cycle progression, and transcriptional/translational processes appeared represented, in agreement with previous results showing the impact of CIGB-300 in AML cell proliferation and viability. Of note, a group of proteins involved in intracellular redox homeostasis was specifically identified in HL-60 cell-regulated proteome, and flow cytometric analysis also confirmed a differential effect of CIGB-300 over reactive oxygen species (ROS) production in AML cells. Thus, oxidative stress might play a relevant role on CIGB-300-induced apoptosis in HL-60 but not in OCI-AML3 cells. Importantly, these findings provide first-hand insights concerning the CIGB-300 antileukemic effect and draw attention to the existence of both common and tailored response patterns triggered by CK2 inhibition in different AML backgrounds, a phenomenon of particular relevance with regard to the pharmacologic blockade of CK2 and personalized medicine.

Keywords: protein kinase CK2, kinase inhibitor, CIGB-300, acute myeloid leukemia, proteomics

INTRODUCTION

Protein kinases are biological messengers that control multiple processes in cell physiology through reversible phosphorylation of thousands of proteins encoded by the human genome. In fact, phosphorylation is a pivotal mechanism for cell homeostasis, and its deregulation may result in aberrant signaling pathways implicated in a variety of human disorders (Cohen, 2002; Ardito et al., 2017).

Protein kinase CK2 (formerly known as casein kinase 2) is a ubiquitously expressed and constitutively active enzyme that exists as tetrameric complexes composed by two catalytic (α or α') and two regulatory subunits (β) (Meggio and Pinna, 2003; Venerando et al., 2014). This highly pleiotropic Ser/Thr kinase is responsible for roughly 25% of cellular phosphoproteome, thus playing instrumental roles in normal and pathological states (Meggio and Pinna, 2003; Borgo et al., 2021). Of note, CK2 stands among the most studied kinases in recent years, and its contribution to the malignant phenotype and cancer progression has been suggested by mounting pieces of evidence (Trembley et al., 2009; Chua et al., 2017; Zonta et al., 2021). In particular, CK2 modulates signaling pathways critical for hematopoietic cell survival and function, and its high expression and activity in acute myeloid leukemia (AML) have been associated with worse prognosis and reduced overall survival (Kim et al., 2007; Quotti Tubi et al., 2017). Hence, in the past few years, CK2 has emerged as a promising candidate for molecular-targeted therapy in AML, a disease often characterized by poor long-term outcomes and resistance towards standard chemotherapy (Buontempo et al., 2018; Rosales et al., 2021a; Klink et al., 2021).

Importantly, the development of highly specific inhibitors has represented a major advance for CK2 substrate identification and elucidation of its roles in cell regulation (Gyenis et al., 2011). A number of CK2 inhibitors have been described so far, including small molecules targeting the ATP-binding site on the CK2 α catalytic subunit (Sarno et al., 2011), several flavonoids characterized by a planar structure and hydroxylations at the 7 and 4' positions (McCarty et al., 2020), and two synthetic peptides designed to antagonize the interaction between the CK2 α and β subunits (Laudet et al., 2007) and bind the conserved acidic phosphoacceptor domain in CK2 substrates (Perea et al., 2018). The majority of such inhibitors have exhibited *in vitro* antiproliferative and proapoptotic activity, and some of them have also shown antitumor properties in animal models (Borgo and Ruzzene, 2021). In spite of the foregoing, only the ATP-competitive CK2 inhibitor CX-4945 and the synthetic peptide CIGB-300 have reached clinical trials in humans (Borgo and Ruzzene, 2021).

CIGB-300 is a peptidic inhibitor originally conceived to block the protein kinase CK2 activity through binding to the conserved acidic phosphoacceptor domain of substrates (Perea et al., 2004). The peptide is able to impair proliferation and viability of a variety of human cancer cells, including AML cells lines and primary cells from AML patients (Perea et al., 2008; Rosales et al., 2021a). However, pull-down assays and phosphoproteomic analysis have suggested that CIGB-300 is able to directly interact with the CK2 α catalytic subunit and modulate the

CK2-dependant phosphoproteome (Perera et al., 2020a; Perera et al., 2020b). Thus, CIGB-300 antineoplastic effect appears to be more complex than originally thought, owing to the convergence of both substrate binding mechanism and direct blockade of CK2 enzymatic activity. Considering the above, here we performed quantitative proteomic analysis in order to explore the molecular and cellular perturbations promoted by CK2 inhibition with CIGB-300 in two relevant AML backgrounds.

MATERIALS AND METHODS

Cell Culture

Human leukemia cell lines HL-60 (American Type Culture Collection, Manassas, VA, United States) and OCI-AML3 (German Collection of Microorganisms and Cell Cultures, Braunschweig, Germany) were cultured in RPMI 1640 medium (Invitrogen, Carlsbad, CA, United States) supplemented with 10% (v/v) heat-inactivated fetal bovine serum (FBS) (Invitrogen, Carlsbad, CA, USA) and 50 μ g/ml gentamicin (Sigma, St. Louis, MO, United States). Cells were maintained under standard cell culture conditions at 37°C and 5% CO₂.

Sample Preparation

For proteomic analysis, HL-60 and OCI-AML3 cells (10⁷ cells per each condition, three biological replicates) were incubated with 40 μ M of the peptide CIGB-300 for 30 min and 3 h. Parallel to CIGB-300-treated groups, non-treated HL-60 and OCI-AML3 were incubated for 30 min and 3 h with vehicle and used as normalization control. Proteins from each replicate of CIGB-300-treated and non-treated AML cell groups were extracted with 1.5% SDS, 50 mM DTT, and boiling conditions for 10 min. Protein extracts were then processed by multienzyme digestion filter-aided sample preparation (MED-FASP) with overnight Lys-C and tryptic digestions (Wiśniewski and Mann, 2012). Protein and peptide concentrations were estimated by a tryptophan fluorescence-based assay previously described by Wiśniewski and Gaugaz (2015). Finally, 1 ng of peptides for each sample were injected for nanoLC-MS/MS analysis.

NanoLC-MS/MS

A NanoLC EASY-nLC 1200 system coupled to a Q-exactive HF mass spectrometer (Thermo Scientific, Waltham, MA, USA) was used. Chromatographic runs for Lys-C and trypsin-derived peptides were performed in a home-made column (Dr. Maisch ReproSil-Pur C18-AQ 1.9 μ m, 75 μ m ID, 20 cm length) thermostated at 60°C. Peptides were eluted at 300 nl/min with a 120-min solution B (A: 0.1% formic acid in water and B: 0.1% formic acid in acetonitrile) gradient, starting at 5% solution B up to 30% in 95 min, then increased to 60% in 5 min, and finally up to 95% in 5 min more. A voltage of 2 kV was applied to the column tip to induce the nanospray and the mass range 300–1,650 *m/z* was scanned for data-dependent acquisition. Each mass spectrum obtained at 60,000 resolutions (20-ms injection time) was followed by 15 MS/MS spectra (28-ms injection time) at 15,000 resolutions. Proteins were only

TABLE 1 | Proteomic profile of AML cells treated with CIGB-300 peptide.

Proteome dataset	HL-60		OCI-AML3	
	30 min	3 h	30 min	3 h
Identified proteins	6,270	6,181	6,382	6,422
Significantly modulated proteins	25	85	74	58
	Total: 109; Overlap: 1		Total: 129; Overlap: 3	
Down-regulated	16	4	6	3
Up-regulated	9	81	68	55
—	Total: 233; overlap: 5			

considered when detected in at least two replicates in any of the groups.

Data Processing

Identification of peptides and proteins was based on the match-between-runs procedure using MaxQuant software (v1.6.2.10) (Cox et al., 2014), considering oxidation (M), deamidation (NQ), and N-terminal acetylation as variable modifications. Alignment of chromatographic runs was allowed with default parameters (20-min time window and a matching of 0.7 min between runs). Filtering and quantification were performed in Perseus computational platform (v1.6.2.2) (Tyanova et al., 2016). Student's *t* test was employed to identify statistically significant changes (*p*-values lower than 0.05) in protein levels, after filtering for two valid values in at least one group. An additional cutoff of 1.5-fold change between CIGB-300-treated AML cells and the non-treated control was also applied.

Bioinformatic Analysis

Differentially modulated proteins were tested for enrichment of Gene Ontology (GO Biological Processes) terms using Metascape gene annotation and analysis resource (<https://metascape.org/>), a web-based tool that computes the accumulative hypergeometric distribution and enrichment factors to identify significantly enriched biological processes through statistical analysis (*p*-value <0.01, enrichment factor >1.5) (Zhou et al., 2019). For either HL-60 or OCI-AML3 proteomic profiles, the Metascape Custom Analysis option was selected, and all identified proteins were used as background, and differentially modulated proteins at 30 min and 3 h after CIGB-300 treatment were combined and used as input dataset for meta-analysis. In addition, to represent the interaction networks associated with AML cell proteomic profiles, interactions among differentially modulated proteins were retrieved using Metascape, which compiles information from different integrative databases and applies the MCODE algorithm to extract highly connected regions embedded in each network (Bader and Hogue, 2003; Zhou et al., 2019). Finally, functional classification of CIGB-300-modulated proteins was based on the information retrieved through literature search and database curation, and protein interaction networks were visualized using Cytoscape software (v. 3.5.0) (Shannon et al., 2003).

Reactive Oxygen Species Detection

For detection of reactive oxygen species (ROS) levels in AML cells treated with the peptide, HL-60 and OCI-AML3 cells were

incubated with 40 μ M CIGB-300 during 30 min, 3 h, and 5 h. Following incubation, cells were collected by centrifugation, washed with PBS, and stained with the fluorescent probe dihydroethidium (DHE) (Sigma, MO, United States) for 30 min at 37°C in the dark. Finally, stained cells were analyzed in the Partec CyFlow Space flow cytometer (Sysmex Partec GmbH, Gorlitz, Germany), and FlowJo software (v7.6.1) (BD, Ashland, OR, USA) was used for data analysis and visualization. In all experiments, 5 mM H₂O₂ and 5 mM N-acetyl cysteine (NAC) anti-oxidant were used as controls.

Annexin V/PI Staining

The viability of HL-60 cells treated with CIGB-300 in the presence or absence of NAC antioxidant was assessed using the FITC Annexin V Apoptosis Detection Kit I (BD Biosciences, San Jose, CA, United States). Briefly, cells were incubated with 40 μ M CIGB-300 alone or in combination with 5 mM NAC for 30 min and 5 h. Cells were then washed twice with cold PBS and resuspended in binding buffer (1 \times) at 1 \times 10⁶ cells/ml. Next, 5 μ l of FITC Annexin V and 5 μ l of propidium iodide (PI) were added, and cell suspensions were incubated for additional 15 min at room temperature in the dark. Analysis of stained cells and data processing/visualization were performed in the abovementioned Partec CyFlow Space flow cytometer and FlowJo software.

Statistical Analysis

Differences between groups were determined using one-way ANOVA followed by Tukey's multiple comparisons test. Analyses were performed in GraphPad Prism (v6.01) software for Windows (GraphPad Software, Inc, San Diego, CA, United States).

RESULTS

Profiling CIGB-300-Regulated Proteome in AML Cells

To identify the array of proteins regulated by CIGB-300 in AML cells, we performed quantitative proteomic analysis of HL-60 and OCI-AML3 cells treated or not with 40 μ M of this peptide inhibitor. A total of 6,270 and 6,181 proteins were identified in HL-60 after 30 min and 3 h of CIGB-300 treatment, respectively (Table 1; Supplementary Table S1).

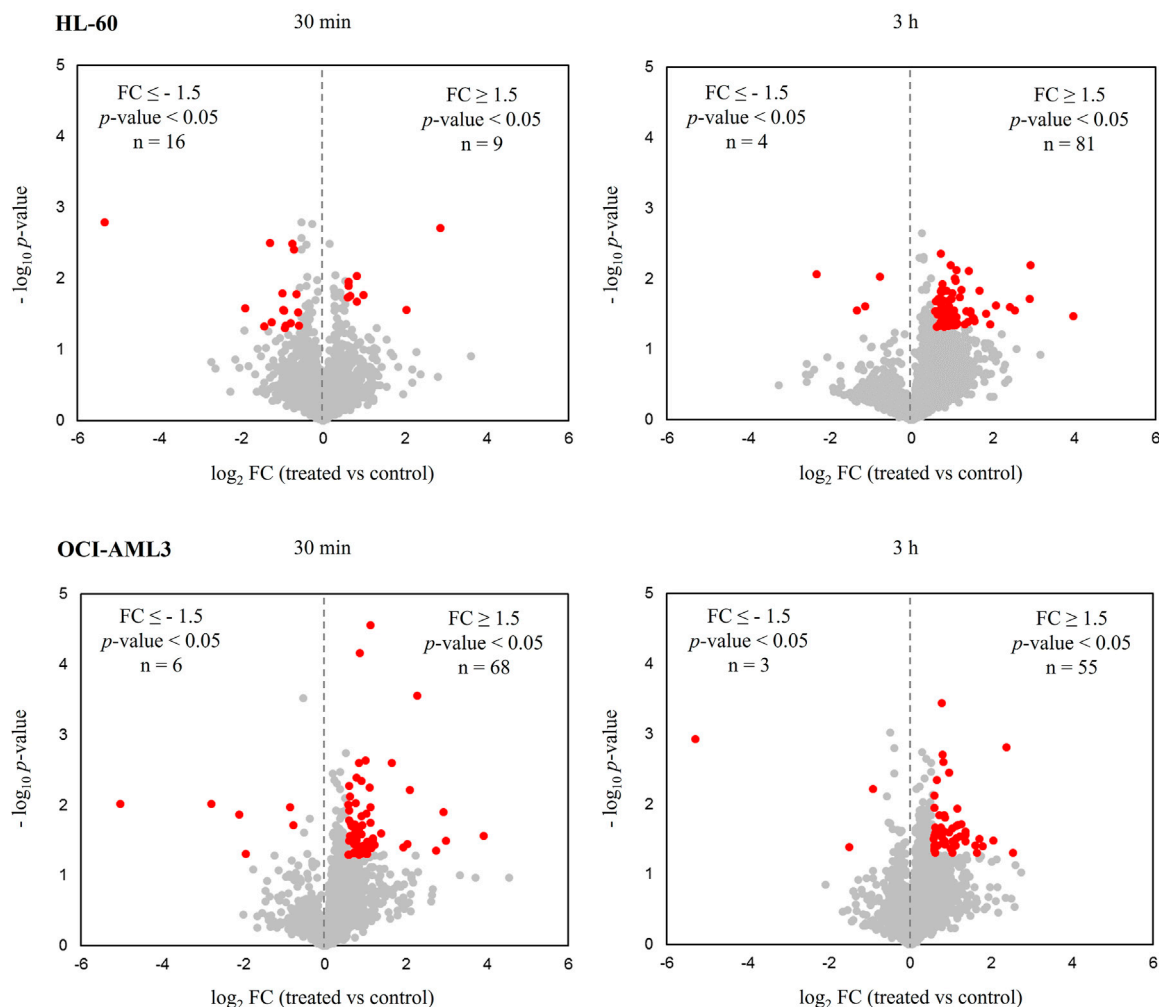


FIGURE 1 | Proteomic profiles of human acute myeloid leukemia (AML) cells treated with the CK2 inhibitor CIGB-300. Volcano plots correspond to quantified proteins from HL-60 and OCI-AML3 cells after treatment with 40 μ M of CIGB-300 for 30 min and 3 h. Red points indicate proteins that met the statistical significance cut-off ($|FC| \geq 1.5$, p -value < 0.05).

Likewise, 6,382 and 6,422 proteins were identified in OCI-AML3 cells at the same incubation periods (**Table 1; Supplementary Table S1**).

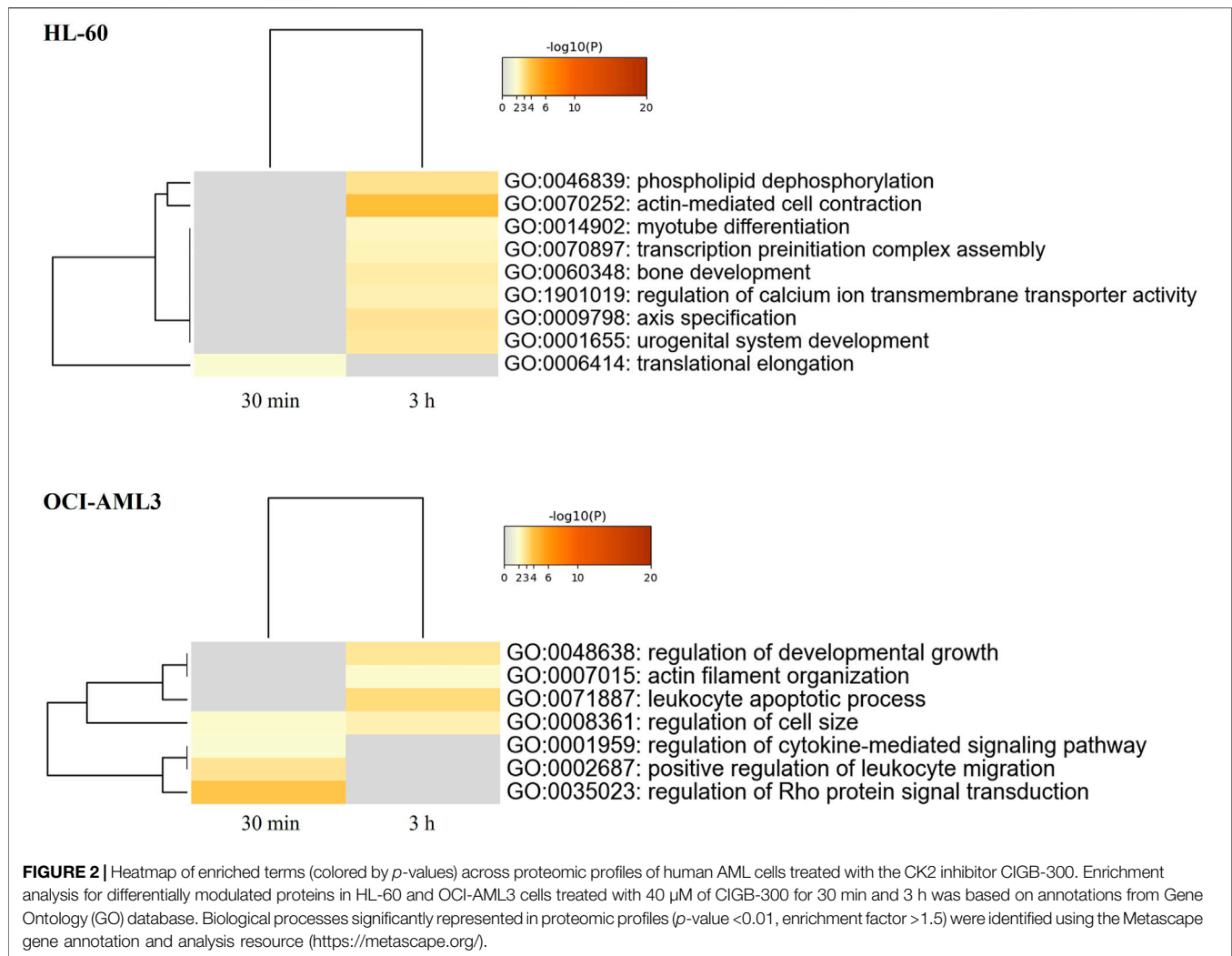
Changes in protein levels between CIGB-300-treated and untreated cells were assessed using Student's *t* test, and *p*-values below 0.05 were considered statistically significant. A fold-change threshold of 1.5 ($|FC| \geq 1.5$) in treated vs control was also applied in order to define the down- and up-regulated proteins. As a result, in HL-60 cells, 25 and 85 proteins were identified as significantly modulated at 30 min and 3 h, while in OCI-AML3 cells, 74 and 58 proteins appeared differentially modulated in response to CIGB-300 treatment (**Table 1; Supplementary Table S2**).

Of note, in practically all conditions, most of the differentially modulated proteins were up-regulated after CK2 inhibition with CIGB-300 as determined by distribution of down- and up-regulated proteins in volcano plots (**Figure 1; Table 1**). Exceptionally, in HL-60 cells treated

with the peptide for 30 min, the number of down-regulated proteins was higher than the up-regulated ones (**Figure 1; Table 1**). Overall, a total of 109 and 129 proteins were differentially modulated in HL-60 and OCI-AML3 cells, respectively, with an overlap of one (MRPL52) and three (DCTPP1, GORASP2, and RAC1) proteins that appeared modulated at 30 min and 3 h after CIGB-300 treatment (**Table 1; Supplementary Table S2**). Besides, among all differentially modulated proteins, a total of five (CD53, HMGN1, NDUFC1, RCN2, and TPM3) overlapped between both cellular backgrounds (**Table 1; Supplementary Table S2**).

Functional Characterization of CIGB-300-Regulated Proteome

Functional enrichment analysis of CIGB-300-regulated proteome in AML cells was performed using the Metascape

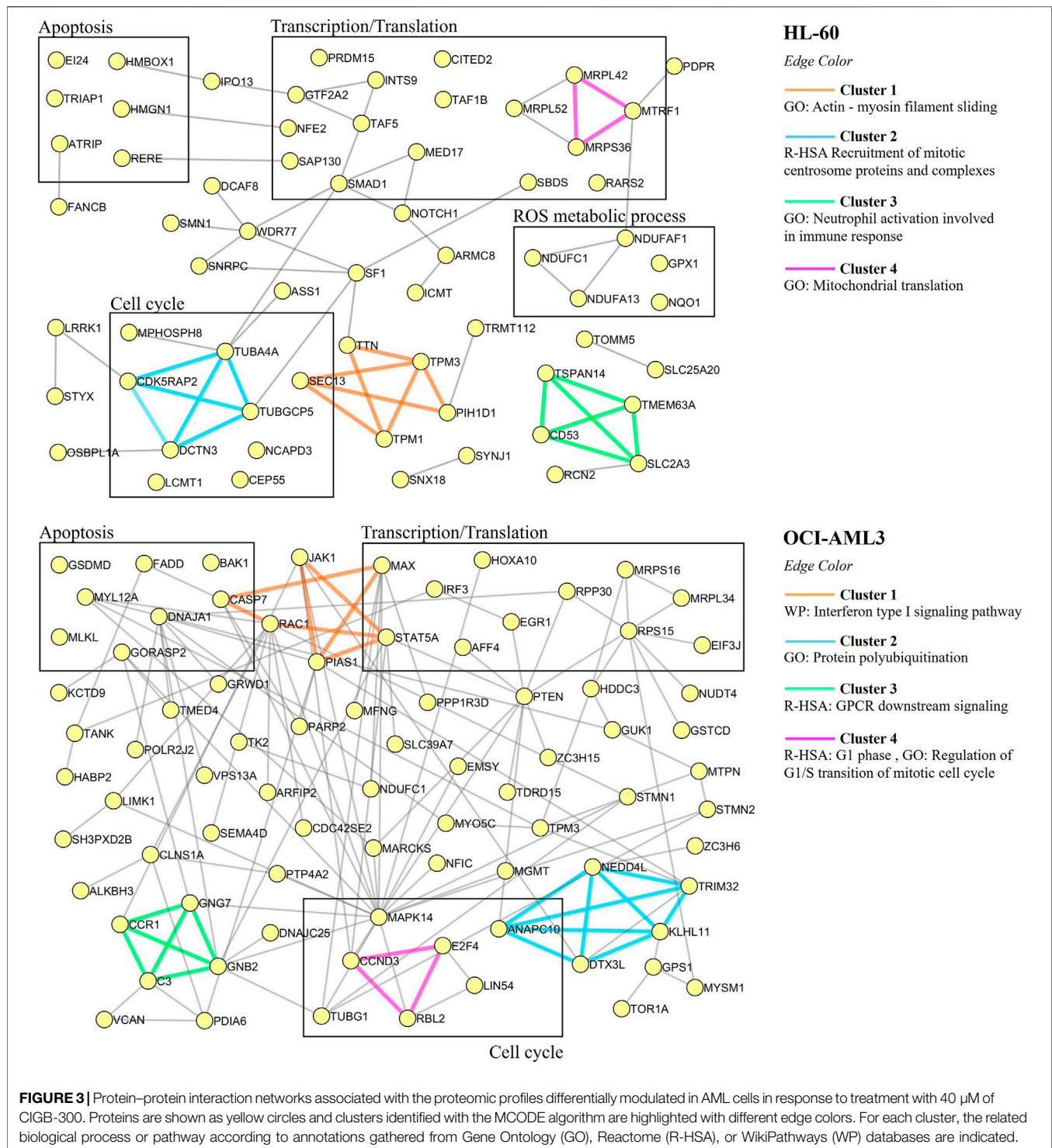


bioinformatic tool (Zhou et al., 2019). In such analysis, actin-mediated cell contraction, phospholipid dephosphorylation, transcription preinitiation complex assembly, translational regulation, regulation of calcium ion transmembrane transport activity, and others were identified as biological processes significantly represented in HL-60 proteomic profile after CK2 inhibition with CIGB-300 (**Figure 2; Supplementary Table S3**). Besides, proteins involved in the regulation of Rho protein signal transduction, leukocyte migration, cytokine-mediated signaling pathway, developmental growth, and cell size, as well as leukocyte apoptotic process and actin filament organization, appeared differentially modulated in CIGB-300-treated OCI-AML3 cells (**Figure 2; Supplementary Table S3**).

To further characterize the proteomic profile regulated by CIGB-300, the interaction networks among differentially modulated proteins in HL-60 or OCI-AML3 cells were represented using Metascape tool, and highly connected regions in such networks were identified using the MCODE

algorithm (Bader and Hogue, 2003; Zhou et al., 2019). As shown in **Figure 3**, clusters of proteins related to actin-myosin filament sliding (cluster 1), cell cycle (cluster 2), neutrophil activation (cluster 3), and mitochondrial translation (cluster 4) were differentially modulated in HL-60 cells after treatment with CIGB-300. Besides, the HL-60 proteomic profile also includes proteins related to apoptotic cell death, transcription, and ROS metabolic process (**Figure 3**). Similar results were obtained by functional enrichment analysis in which the biological processes of translation elongation, actin-mediated cell contraction, and transcription preinitiation complex assembly were found significantly represented in the proteomic profile of HL-60 cells (**Figure 2; Supplementary Table S3**).

On the other hand, network analysis of OCI-AML3 cell proteomic dataset evidenced that clusters of proteins related to interferon type I signaling (cluster 1), protein polyubiquitination (cluster 2), GPCR downstream signaling (cluster 3), and cell cycle (cluster 4) were differentially



modulated in response to CK2 inhibition with CIGB-300 peptide (Figure 3). Furthermore, proteins related to apoptotic cell death were also identified in OCI-AML3-modulated proteome (Figure 3). In line with such result, cytokine-mediated signaling pathway and leukocyte apoptotic process were identified through functional enrichment analysis (Figure 2; Supplementary Table S3).

Similar to HL-60 proteomic profile, besides proteins involved in cell cycle and apoptosis regulation, an array of proteins related to transcription and translation appeared modulated in CIGB-300-treated OCI-AML3 cells (Figure 3). Therefore, CK2 inhibition with CIGB-300 has an impact over these biological processes independently of the genetic background of these AML cell lines. Conversely,

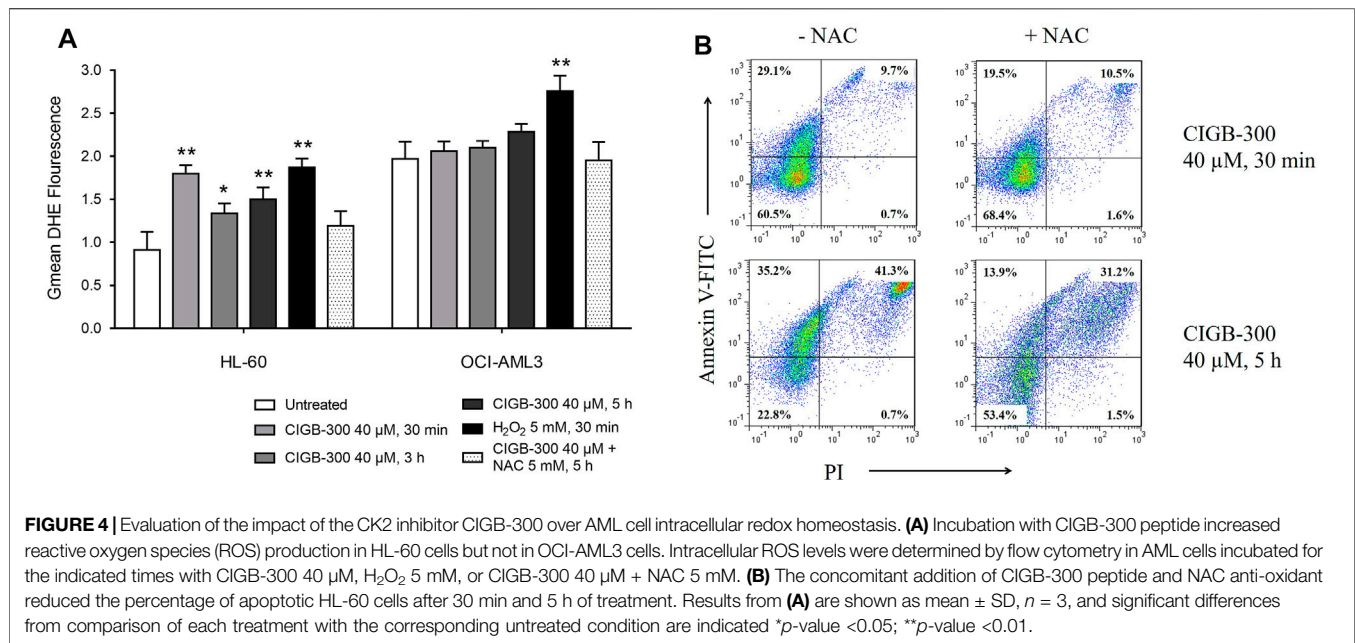


FIGURE 4 | Evaluation of the impact of the CK2 inhibitor CIGB-300 over AML cell intracellular redox homeostasis. **(A)** Incubation with CIGB-300 peptide increased reactive oxygen species (ROS) production in HL-60 cells but not in OCI-AML3 cells. Intracellular ROS levels were determined by flow cytometry in AML cells incubated for the indicated times with CIGB-300 40 μ M, H₂O₂ 5 mM, or CIGB-300 40 μ M + NAC 5 mM. **(B)** The concomitant addition of CIGB-300 peptide and NAC anti-oxidant reduced the percentage of apoptotic HL-60 cells after 30 min and 5 h of treatment. Results from **(A)** are shown as mean \pm SD, $n = 3$, and significant differences from comparison of each treatment with the corresponding untreated condition are indicated * p -value <0.05; ** p -value <0.01.

proteins involved in ROS metabolic process did not appear represented in OCI-AML3 proteomic profile.

Differential Effect of CIGB-300 Over AML Cell ROS Production

Considering that proteomic analysis suggested a differential effect of CIGB-300 over ROS metabolic process in AML cells (**Figure 3**), we sought to elucidate if intracellular ROS accumulation could be related to CIGB-300 anti-leukemic effect. To determine ROS levels in HL-60 and OCI-AML3 cells after CK2 inhibition with CIGB-300, we use DHE as fluorescent probe for flow cytometry analysis. As a result, CIGB-300 treatment significantly increased ROS levels at all the assessed incubation times on HL-60 cells, with the highest intracellular ROS levels at 30 min of incubation (**Figure 4A**). Besides, H₂O₂ increased ROS levels and NAC anti-oxidant control abrogated ROS production in HL-60 cells treated with CIGB-300 (**Figure 4A**). On the contrary, in OCI-AML3 cells, CK2 inhibition with CIGB-300 did not induce any alteration of ROS homeostasis, which is in agreement with results from proteomic analysis (**Figure 4A**).

Of note, the potential connection between ROS de-regulation and CIGB-300-induced apoptosis was explored in HL-60 cells. Importantly, Annexin V/PI staining evidenced that the addition of NAC anti-oxidant reduced not only the accumulation of intracellular ROS but also the percentage of HL-60 cells undergoing apoptosis after 30 min and 5 h of treatment with the peptide (**Figure 4B**).

DISCUSSION

In the protein kinase landscape that has emerged as attractive targets for cancer treatment, CK2 stands among the most studies

in recent years. This highly pleiotropic enzyme controls a number of signaling networks playing essential roles for malignant phenotype maintenance, and cancer cells often develop an excessive “addiction” to CK2 activity (Ruzzene and Pinna, 2010). The abovementioned has fostered the investigation of several CK2 inhibitors (Borgo and Ruzzene, 2021), including the clinical-grade synthetic peptide CIGB-300 (Perea et al., 2004). Accordingly, here we use quantitative proteomics to identify the CIGB-300-regulated proteome and explore the molecular perturbations promoted by this CK2 inhibitor in HL-60 and OCI-AML3 cells following 30 min and 3 h of treatment. These human cell lines derived from two relevant AML subtypes (i.e., acute promyelocytic and acute myelomonocytic leukemia), together accounting for roughly two thirds of all AML cases (Hanson et al., 2002). Of note, in proteomic profiles from both AML cell lines, CIGB-300 significantly modulated proteins related to apoptosis, cell cycle, transcription, and translation, while proteins involved in intracellular redox homeostasis were only identified in HL-60 cells.

Accumulated evidence demonstrates that CIGB-300 induces apoptosis in cancer cells, including AML cell lines and primary cells (Perea et al., 2004; Rosales et al., 2021a). In agreement with such results, mediators of intrinsic and extrinsic apoptotic pathways were both identified in the proteomic profile regulated by the peptide in AML cells. The pro-apoptotic proteins etoposide-induced 2.4 (EI24) and arginine-glutamic acid dipeptide repeats (RERE) were down-regulated at 30 min in HL-60 cells. EI24 is a p53 and E2F target gene that inhibits tumor progression through attenuation of NF- κ B signaling (Choi et al., 2013; Sung et al., 2013), while RERE protein colocalizes with the pro-apoptotic protein BAX and triggers caspase-3 activation (Waerner et al., 2001). It is known that to counteract pro-apoptotic stimuli, cancer cells might activate pro-survival

mechanisms, an event that could explain the decreased expression levels of E124 and RERE proteins in response to CK2 inhibition with CIGB-300.

In line with these findings, TP53-regulated inhibitor of apoptosis 1 (TRIAP1) and ATR interacting protein (ATRIP) were up-regulated in HL-60 cells at 30 min and 3 h, respectively. TRIAP1 mediates the transport of phosphatidic acid across the intermembrane space for cardiolipin synthesis and inhibits the release of cytochrome-c from mitochondria during apoptosis (Potting et al., 2013). Furthermore, to inhibit apoptosis and allow DNA damage repair under low levels of genotoxic stress, TRIAP1 interacts with heat shock protein 70 (HSP70) and impairs the formation of the apoptosome complex (Park and Nakamura, 2005; Fook-Alves et al., 2016). On the other hand, ATRIP is an essential mediator of the DNA damage response, which inhibits replicative stress and TP53-dependent cell death (Matos-Rodrigues et al., 2020). As we mentioned before, proteomic data suggests that HL-60 cells treated with CIGB-300 seem to be subjected to increased levels of ROS, a known source of genotoxic stress, which could lead to apoptotic cell death (Srinivas et al., 2019). In such context, a pro-survival response could be based on the activation of DNA repair mechanisms to mitigate the accumulation of DNA damage.

In case of OCI-AML3 cell proteomic profile, the pro-apoptotic protein BCL2 antagonist/killer 1 (BAK) was up-regulated after 3 h. BAK1 promotes the formation of mitochondrial voltage-dependent anion channels leading to loss in membrane potential and release of cytochrome-c (Wei et al., 2001). Besides, as earlier as 30 min following CIGB-300 treatment, the expression of Fas-associated death domain protein (FADD) increased in OCI-AML3 cells. Such modulation of FADD protein abundance is of great relevance for CIGB-300 chemotherapeutic potentialities, since previous data indicate that absent or low FADD protein expression in leukemic cells is a prognostic factor for poor response of AML cells to chemotherapy (Tourneur et al., 2004). FADD activates pro-caspase-8 and the subsequent caspase signaling cascade in response to apoptotic signals initiated by activation of death receptors belonging to the family of tumor necrosis factor (TNF) receptors (Marín-Rubio et al., 2019). In addition to increased levels of BAK and FADD, the augmented abundance of caspase-7 and gasdermin-D (GSDMD) supports the pro-apoptotic effect of CIGB-300 in OCI-AML3 cells. Caspase-7 is an apoptotic executioner caspase, while the N-terminal fragment of GSDMD, which is cleaved by caspase-1, permeabilizes the mitochondrial membrane and leads to cytochrome-c release (Sborgi et al., 2016; Rogers et al., 2019).

Among proteins significantly regulated by the CK2 inhibitor CIGB-300, proteins related to cell cycle appeared represented in AML proteomic profiles. For instance, in HL-60 cells, differentially expressed proteins include a cluster (CDK5RAP2, DCTN3, TUBA4A, and TUBGCP5) involved in the recruitment of mitotic centrosome proteins and complexes. Other proteins related to transition through mitotic cell cycle like centrosomal protein of 55 kDa (CEP55) (Jeffery et al., 2016) and the heterochromatin

component M-phase phosphoprotein 8 (MPHOSPH8) (Tchassovnikarova et al., 2015) were modulated in the presence of CIGB-300. The expression of leucine carboxyl methyltransferase one protein (LCMT1), which methylates the catalytic subunit of protein phosphatase 2A (PP2A) (Lee and Pallas, 2007), was increased after 3 h of CIGB-300 treatment. PP2A regulates G2/M transition of cell cycle and contributes to mitotic chromosome assembly by promoting chromosomal association of condensin-2 complex (Takemoto et al., 2009; Li et al., 2020). Of note, the condensin-2 regulatory subunit D3 (NCAPD3) was up-regulated at 3 h in HL-60 cells. Similarly, proteins differentially modulated in OCI-AML3 cells include a cluster (CCND3, E2F4, and RBL2) specifically involved in the G1/S transition. Cyclin D3 (CCND3), which functions as a regulatory subunit of CDK4 or CDK6, was up-regulated at 3 h after CIGB-300 treatment. Also, the transcription factor E2F4, a repressor member of the E2F family, its partner the retinoblastoma-like protein 2 (RBL2/p130), and the protein Lin-54 homolog (LIN54) were up-regulated in OCI-AML3 cells. Such proteins are subcomponents of the LIN complex (LINC), which represses G1/S and G2/M genes during G0 and early G1 phase of the cell cycle (Fischer and Müller, 2017).

The impact of CK2 inhibition over cell cycle in AML was previously corroborated using the ATP-competitive inhibitor CX-4945 and CIGB-300 peptide. In such studies, flow cytometry and phosphoproteomic analysis of AML cells evidenced an impairment of cell cycle progression in response to CK2 inhibition (Rosales et al., 2021a; Rosales et al., 2021b). In fact, the filament-forming cytoskeletal GTPase SEPTIN2 and the MCM2 subunit of the replicative helicase complex (MCM complex), both well-documented CK2 substrates related to cell cycle progression, were down-phosphorylated in CIGB-300-treated AML cells (Rosales et al., 2021a). Furthermore, as a downstream consequence of CK2 inhibition by CIGB-300, a significant number of down-phosphorylated phosphosites in AML cells were attributed to the CDK family, thus suggesting a functional impairment of such kinases (Rosales et al., 2021a).

Likewise, proteins related to transcription and translation were differentially modulated in both HL-60 and OCI-AML3 cells treated with CIGB-300. In agreement, previous results have evidenced an impact of CIGB-300 on such biological processes (Perera et al., 2015), and in AML cells, the peptide not only interacts with proteins from the small and the large ribosome subunits but also down-phosphorylates proteins required for transcription, ribosome biogenesis, and initiation of protein synthesis (Rosales et al., 2021a). Accordingly, several components of the transcription pre-initiation complex (TAF5, TAF1B, GTF2A, INTS9, and MED17) were modulated by CIGB-300 in HL-60 cells. Nuclear factor-erythroid 2 (NFE2), a transcription factor overexpressed in myeloproliferative neoplasms and important for hematopoietic stem cell maintenance and differentiation (Wang et al., 2010; Di Tullio et al., 2017; Peeken et al., 2018), was down-regulated in HL-60 cells. Furthermore, the transcriptional regulator Cbp/p300-interacting transactivator 2 (CITED2), which functions in

stem cell maintenance and promotes leukemic cell survival (Korthuis et al., 2015; Mattes et al., 2017), was differentially modulated in HL-60 proteomic profile in response to CIGB-300 treatment. The modulation of such proteins suggests a potential role of CIGB-300 in regulating the self-renewal of leukemic stem cells.

In line with this hypothesis, the expression of the transmembrane receptor Notch1 was increased in HL-60, and tetraspanin 14 (TSPAN14) and manic fringe glycosyltransferase (MFNG), which function as positive regulators of Notch signaling pathway (Taylor et al., 2014; Jouannet et al., 2016), were up-regulated by CIGB-300 treatment in HL-60 and OCI-AML3 cells, respectively. The classical view sustains that Notch signaling keeps cells in an undifferentiated state and plays oncogenic roles in many cancers, including hematological malignancies (Ntziachristos et al., 2014). However, specifically in AML, accumulating pieces of evidence suggest that Notch signaling pathway has a tumor suppressor role (Kannan et al., 2013; Lobry et al., 2013). In such respect, Notch1 is down-regulated in AML cell lines and patient samples and impairs leukemogenesis of AML by increasing the expression of the transcriptional factor PU.1, which mediates myeloid differentiation (Yang et al., 1992; Tohda and Nara, 2001). Since leukemic stem cell maintenance has been associated with AML relapse and resistant phenotypes to chemotherapy, a modulation of Notch signaling pathway by CIGB-300 could add a benefit to the standard antileukemic therapies.

Similar to HL-60 proteomic profile, CIGB-300 modulates the abundance levels of several transcription factors in OCI-AML3 cells including the Myc interacting factor X (MAX) and the AF4/FMR2 family member 4 (AFF4) (Lin et al., 2010; Diolaiti et al., 2015). In addition, the transcription factor homeobox A10 (HOXA10), a protein related to leukemogenesis and chemoresistance that has been proposed as a prognostic marker for AML patients (Yi et al., 2016; Guo et al., 2020), was also differentially modulated. Of note, the early growth response protein 1 (EGR1), which functions as a tumor suppressor in AML (Gibbs et al., 2008; Tian et al., 2016), was up-regulated in OCI-AML3 cells in response CIGB-300. EGR1 promotes myeloid differentiation and suppresses the leukemic phenotype driven by the oncogenes c-Myc or E2F-1 (Gibbs et al., 2008). This transcription factor is known to activate the expression of other tumor suppressor genes including p53 and the phosphatase and tensin homolog (PTEN), promoting growth arrest or cell death in cancer cells (Wang et al., 2021). Interestingly, the abundance of PTEN, which is an essential tumor suppressor in human myeloid malignancies (Morotti et al., 2015), was increased in OCI-AML3 cells. Noteworthy, sustained activation of AKT by PTEN deficiency mediates the chemoresistance of AML cells to idarubicin and cytarabine anticancer drugs (Ryu et al., 2019). Therefore, the up-regulation of PTEN in response to CIGB-300 treatment supports the benefit of combining CIGB-300 with standard chemotherapy drugs.

Remarkably, an array of proteins related to oxidative phosphorylation was only identified in HL-60 cells. Among these proteins, two subunits of the NADH:ubiquinone

oxidoreductase/complex I (NDUFA13 and NDUFC1) were up-regulated in response to CIGB-300. The complex I catalyzes the electron transfer from NADH to ubiquinone in the first step of the mitochondrial respiratory chain, and its subunit NDUFA13, in addition to be required for electron transfer (Lu and Cao, 2008), functions as a tumor suppressor that binds to STAT3 and inhibits its transcriptional activity (Nallar et al., 2010). Together with NDUFA13 and NDUFC1 subunits, complex I intermediate-associated protein 30 (NDUFAF1), a mitochondrial chaperone involved in the assembly and stability of complex I (Vogel et al., 2005), was also up-regulated. The concomitant up-regulation of these proteins suggests that complex I could have an increased activity in CIGB-300-treated HL-60 cells, which could lead to an over-production of ROS since complex I is one of the main sources of mitochondrial oxidative stress (Brand, 2016). Importantly, such finding was corroborated by flow cytometry using the fluorescent probe DHE to determine ROS levels in AML cells.

Along with increased ROS levels, the cellular antioxidant defenses can be activated as a compensatory mechanism. In line with this, glutathione peroxidase (GPX1) and NAD(P)H dehydrogenase [quinone] 1 (NQO1) were up-regulated in HL-60 cells. The enzyme GPX1 detoxifies the hydrogen peroxide (H₂O₂) generated by superoxide dismutase (Arthur, 2001), while NQO1 reduces quinones to hydroquinones, preventing the generation of radical oxygen species (Ross and Siegel, 2021). Notably, AML cells have a reduced spare respiratory capacity in comparison with normal hematopoietic cells, and increasing electron flux through the respiratory chain preferentially promotes oxidative stress and induces cell death (Srisanthadevan et al., 2015). Accordingly, we demonstrated that the reduction of intracellular ROS production by NAC anti-oxidant was accompanied by a reduced percentage of HL-60 cells undergoing apoptosis following treatment with CIGB-300. Thus, the modulation of proteins related to oxidative phosphorylation could mediate the antileukemic effect of CIGB-300 and promote apoptosis in HL-60 cells. Nevertheless, the addition of the antioxidant does not completely abrogate the pro-apoptotic effect of CIGB-300, evidencing that other molecular mechanisms different from intracellular ROS production could also be responsible for the induction of apoptosis in HL-60 cells. The foregoing is confirmed by the induction of apoptosis observed in OCI-AML3 cells (Rosales et al., 2021a), in spite of the absence of ROS accumulation when treated with CIGB-300.

Altogether, our proteomic analysis supports previous results evidencing that the proapoptotic effect and the impact of CIGB-300 over cell cycle regulation and transcriptional/translational processes are a common denominator for CK2 inhibition in AML cells (Rosales et al., 2021a). Conversely, modulation of proteins involved in redox homeostasis was only observed in HL-60 cells. Such findings not only provide fresh clues related to CIGB-300 antileukemic effect but also highlight that CK2 inhibition with the CIGB-300 triggered common and tailored response patterns in different AML backgrounds.

DATA AVAILABILITY STATEMENT

The original contributions presented in the study are included in the article/**Supplementary File**, further inquiries can be directed to the corresponding authors.

AUTHOR CONTRIBUTIONS

Conceptualization, SP, YP and LG; methodology, VB, YR, JW, and KZ; formal analysis, MR, AR-U, and VB; investigation, MR, GP, and TS; writing—original draft preparation, MR and AR-U; writing—review and editing, SP, YP, and VB; supervision, SP, YP, and YK; project administration, SP; funding acquisition, JW, VB, LG, SP, YP, and YK. All authors contributed to the article and approved the submitted version.

REFERENCES

- Ardito, F., Giuliani, M., Perrone, D., Troiano, G., and Muzio, L. L. (2017). The Crucial Role of Protein Phosphorylation in Cell Signaling and its Use as Targeted Therapy (Review). *Int. J. Mol. Med.* 40 (2), 271–280. doi:10.3892/ijmm.2017.3036
- Arthur, J. R. (2001). The Glutathione Peroxidases. *Cmls, Cel. Mol. Life Sci.* 57 (13–14), 1825–1835. doi:10.1007/pl00000664
- Bader, G. D., and Hogue, C. W. (2003). An Automated Method for Finding Molecular Complexes in Large Protein Interaction Networks. *BMC bioinformatics* 4, 2. doi:10.1186/1471-2105-4-2
- Borgo, C., D'Amore, C., Sarno, S., Salvi, M., and Ruzzene, M. (2021). Protein Kinase CK2: a Potential Therapeutic Target for Diverse Human Diseases. *Sig Transduct Target. Ther.* 6 (1), 183. doi:10.1038/s41392-021-00567-7
- Borgo, C., and Ruzzene, M. (2021). Protein Kinase CK2 Inhibition as a Pharmacological Strategy. *Adv. Protein Chem. Struct. Biol.* 124, 23–46. doi:10.1016/bs.apcsb.2020.09.003
- Brand, M. D. (2016). Mitochondrial Generation of Superoxide and Hydrogen Peroxide as the Source of Mitochondrial Redox Signaling. *Free Radic. Biol. Med.* 100, 14–31. doi:10.1016/j.freeradbiomed.2016.04.001
- Buontempo, F., McCubrey, J. A., Orsini, E., Ruzzene, M., Cappellini, A., Lonetti, A., et al. (2018). Therapeutic Targeting of CK2 in Acute and Chronic Leukemias. *Leukemia* 32 (1), 1–10. doi:10.1038/leu.2017.301
- Choi, J.-M., Devkota, S., Sung, Y. H., and Lee, H.-W. (2013). E124 Regulates Epithelial-To-Mesenchymal Transition and Tumor Progression by Suppressing TRAF2-Mediated NF- κ B Activity. *Oncotarget* 4 (12), 2383–2396. doi:10.18632/oncotarget.1434
- Chua, M., Ortega, C., Sheikh, A., Lee, M., Abdul-Rassoul, H., Hartshorn, K., et al. (2017). CK2 in Cancer: Cellular and Biochemical Mechanisms and Potential Therapeutic Target. *Pharmaceuticals* 10 (1), 18. doi:10.3390/ph10010018
- Cohen, P. (2002). Protein Kinases - the Major Drug Targets of the Twenty-First century. *Nat. Rev. Drug Discov.* 1 (4), 309–315. doi:10.1038/nrd773
- Cox, J., Hein, M. Y., Lubner, C. A., Paron, I., Nagaraj, N., and Mann, M. (2014). Accurate Proteome-wide Label-free Quantification by Delayed Normalization and Maximal Peptide Ratio Extraction, Termed MaxLFQ. *Mol. Cell Proteomics* 13 (9), 2513–2526. doi:10.1074/mcp.M113.031591
- Di Tullio, A., Passaro, D., Rouault-Pierre, K., Purewal, S., and Bonnet, D. (2017). Nuclear Factor Erythroid 2 Regulates Human HSC Self-Renewal and T Cell Differentiation by Preventing NOTCH1 Activation. *Stem Cel. Rep.* 9 (1), 5–11. doi:10.1016/j.stemcr.2017.05.027
- Diolaiti, D., McFerrin, L., Carroll, P. A., and Eisenman, R. N. (2015). Functional Interactions Among Members of the MAX and MLX Transcriptional Network during Oncogenesis. *Biochim. Biophys. Acta (Bba) - Gene Regul. Mech.* 1849 (5), 484–500. doi:10.1016/j.bbagr.2014.05.016

FUNDING

This work was supported by grants from the German Ministry of Education and Science (01DN18015), the Cuban National Program on Biotechnology, Pharmaceutical Industry and Medical Technology (PN385LH007-013), the Science and Technology Innovation Program of Hunan Province (2020RC5035), and the Hunan Provincial Base for Scientific and Technological Innovation Cooperation (2019CB1012).

SUPPLEMENTARY MATERIAL

The Supplementary Material for this article can be found online at: <https://www.frontiersin.org/articles/10.3389/fmolb.2022.834814/full#supplementary-material>

- Fischer, M., and Müller, G. A. (2017). Cell Cycle Transcription Control: DREAM/ MuvB and RB-E2f Complexes. *Crit. Rev. Biochem. Mol. Biol.* 52 (6), 638–662. doi:10.1080/10409238.2017.1360836
- Fook-Alves, V. L., de Oliveira, M. B., Zanatta, D. B., Strauss, B. E., and Colleoni, G. W. B. (2016). TP53 Regulated Inhibitor of Apoptosis 1 (TRIP1) Stable Silencing Increases Late Apoptosis by Upregulation of Caspase 9 and APAF1 in RPMI8226 Multiple Myeloma Cell Line. *Biochim. Biophys. Acta (Bba) - Mol. Basis Dis.* 1862 (6), 1105–1110. doi:10.1016/j.bbadis.2016.03.011
- Gibbs, J. D., Liebermann, D. A., and Hoffman, B. (2008). Leukemia Suppressor Function of Egr-1 Is Dependent on Transforming Oncogene. *Leukemia* 22 (10), 1909–1916. doi:10.1038/leu.2008.189
- Guo, C., Ju, Q.-q., Zhang, C.-x., Gong, M., Li, Z.-l., and Gao, Y.-y. (2020). Overexpression of HOXA10 Is Associated with Unfavorable Prognosis of Acute Myeloid Leukemia. *BMC Cancer* 20 (1), 586. doi:10.1186/s12885-020-07088-6
- Gyenis, L., Duncan, J. S., Turowec, J. P., Bretner, M., and Litchfield, D. W. (2011). Unbiased Functional Proteomics Strategy for Protein Kinase Inhibitor Validation and Identification of Bona Fide Protein Kinase Substrates: Application to Identification of EEF1D as a Substrate for CK2. *J. Proteome Res.* 10 (11), 4887–4901. doi:10.1021/pr2008994
- Hanson, C. A., and Alkan, S. (2002). “Acute Leukemias and Myelodysplastic Syndromes,” in *Clinical Laboratory Medicine*. Editor K. D. McClatchey. 2nd ed. (Philadelphia, PA, USA: Lippincott Williams & Wilkins), 909.
- Jeffery, J., Sinha, D., Srihari, S., Kalimutho, M., and Khanna, K. K. (2016). Beyond Cytokinesis: the Emerging Roles of CEP55 in Tumorigenesis. *Oncogene* 35 (6), 683–690. doi:10.1038/ncr.2015.128
- Jouannet, S., Saint-Pol, J., Fernandez, L., Nguyen, V., Charrin, S., Boucheix, C., et al. (2016). TspanC8 Tetraspanins Differentially Regulate the Cleavage of ADAM10 Substrates, Notch Activation and ADAM10 Membrane Compartmentalization. *Cell. Mol. Life Sci.* 73 (9), 1895–1915. doi:10.1007/s00018-015-2111-z
- Kannan, S., Sutphin, R. M., Hall, M. G., Golfman, L. S., Fang, W., Nolo, R. M., et al. (2013). Notch Activation Inhibits AML Growth and Survival: a Potential Therapeutic Approach. *J. Exp. Med.* 210 (2), 321–337. doi:10.1084/jem.20121527
- Kim, J. S., Eom, J. I., Cheong, J.-W., Choi, A. J., Lee, J. K., Yang, W. I., et al. (2007). Protein Kinase CK2 α as an Unfavorable Prognostic Marker and Novel Therapeutic Target in Acute Myeloid Leukemia. *Clin. Cancer Res.* 13 (3), 1019–1028. doi:10.1158/1078-0432.Ccr-06-1602
- Klink, M., Rahman, M. A., Song, C., Dhanyamraju, P. K., Ehudin, M., Ding, Y., et al. (2021). Mechanistic Basis for *In Vivo* Therapeutic Efficacy of CK2 Inhibitor CX-4945 in Acute Myeloid Leukemia. *Cancers* 13 (5), 1127. doi:10.3390/cancers13051127
- Korthuis, P. M., Berger, G., Bakker, B., Rozenveld-Geugien, M., Jaques, J., de Haan, G., et al. (2015). CITED2-mediated Human Hematopoietic Stem Cell

- Maintenance Is Critical for Acute Myeloid Leukemia. *Leukemia* 29 (3), 625–635. doi:10.1038/leu.2014.259
- Laudet, B., Barette, C., Dulery, V., Renaudet, O., Dumy, P., Metz, A., et al. (2007). Structure-based Design of Small Peptide Inhibitors of Protein Kinase CK2 Subunit Interaction. *Biochem. J.* 408 (3), 363–373. doi:10.1042/bj20070825
- Lee, J. A., and Pallas, D. C. (2007). Leucine Carboxyl Methyltransferase-1 Is Necessary for normal Progression through Mitosis in Mammalian Cells. *J. Biol. Chem.* 282 (42), 30974–30984. doi:10.1074/jbc.M704861200
- Li, F., Kozono, D., Deraska, P., Branigan, T., Dunn, C., Zheng, X.-F., et al. (2020). CHK1 Inhibitor Blocks Phosphorylation of FAM122A and Promotes Replication Stress. *Mol. Cell.* 80 (3), 410–422. e6. doi:10.1016/j.molcel.2020.10.008
- Lin, C., Smith, E. R., Takahashi, H., Lai, K. C., Martin-Brown, S., Florens, L., et al. (2010). AFF4, a Component of the ELL/P-TFEB Elongation Complex and a Shared Subunit of MLL Chimeras, Can Link Transcription Elongation to Leukemia. *Mol. Cell.* 37 (3), 429–437. doi:10.1016/j.molcel.2010.01.026
- Lobry, C., Ntziachristos, P., Ndiaye-Lobry, D., Oh, P., Cimmino, L., Zhu, N., et al. (2013). Notch Pathway Activation Targets AML-Initiating Cell Homeostasis and Differentiation. *J. Exp. Med.* 210 (2), 301–319. doi:10.1084/jem.20121484
- Lu, H., and Cao, X. (2008). GRIM-19 Is Essential for Maintenance of Mitochondrial Membrane Potential. *MBoC* 19 (5), 1893–1902. doi:10.1091/mbc.e07-07-0683
- Marín-Rubio, J. L., Vela-Martín, L., Fernández-Piqueras, J., and Villa-Morales, M. (2019). FADD in Cancer: Mechanisms of Altered Expression and Function, and Clinical Implications. *Cancers* 11 (10), 1462. doi:10.3390/cancers11101462
- Matos-Rodrigues, G. E., Grigaravicius, P., Lopez, B. S., Hofmann, T. G., Frappart, P.-O., and Martins, R. A. P. (2020). ATRIP Protects Progenitor Cells against DNA Damage *In Vivo*. *Cell Death Dis* 11 (10), 923. doi:10.1038/s41419-020-03090-9
- Mattes, K., Berger, G., Geugien, M., Vellenga, E., and Schepers, H. (2017). CITED2 Affects Leukemic Cell Survival by Interfering with P53 Activation. *Cell Death Dis* 8 (10), e3132. doi:10.1038/cddis.2017.548
- McCarty, M. F., Assanga, S. I., and Lujan, L. L. (2020). Flavones and Flavonols May Have Clinical Potential as CK2 Inhibitors in Cancer Therapy. *Med. hypotheses* 141, 109723. doi:10.1016/j.mehy.2020.109723
- Meggio, F., and Pinna, L. A. (2003). One-thousand-and-one Substrates of Protein Kinase CK2. *FASEB J.* 17 (3), 349–368. doi:10.1096/fj.02-0473rev
- Morotti, A., Panuzzo, C., Crivellaro, S., Carra', G., Torti, D., Guerrasio, A., et al. (2015). The Role of PTEN in Myeloid Malignancies. *Hematol. Rep.* 7 (4), 5844. doi:10.4081/hr.2015.6027
- Nallar, S. C., Kalakonda, S., Sun, P., Ohmori, Y., Hiroi, M., Mori, K., et al. (2010). Identification of a Structural Motif in the Tumor-Suppressive Protein GRIM-19 Required for its Antitumor Activity. *Am. J. Pathol.* 177 (2), 896–907. doi:10.2353/ajpath.2010.091280
- Ntziachristos, P., Lim, J. S., Sage, J., and Aifantis, I. (2014). From Fly Wings to Targeted Cancer Therapies: a Centennial for Notch Signaling. *Cancer cell* 25 (3), 318–334. doi:10.1016/j.ccr.2014.02.018
- Park, W.-R., and Nakamura, Y. (2005). p53CSV, a Novel P53-Inducible Gene Involved in the P53-dependent Cell-Survival Pathway. *Cancer Res.* 65 (4), 1197–1206. doi:10.1158/0008-5472.Can-04-3339
- Peeken, J. C., Jutzi, J. S., Wehrle, J., Koellerer, C., Staehle, H. F., Becker, H., et al. (2018). Epigenetic Regulation of NFE2 Overexpression in Myeloproliferative Neoplasms. *Blood* 131 (18), 2065–2073. doi:10.1182/blood-2017-10-810622
- Perea, S. E., Baladrón, I., Valenzuela, C., and Perera, Y. (2018). CIGB-300: A Peptide-Based Drug that Impairs the Protein Kinase CK2-Mediated Phosphorylation. *Semin. Oncol.* 45 (1-2), 58–67. doi:10.1053/j.seminoncol.2018.04.006
- Perea, S. E., Reyes, O., Baladrón, I., Perera, Y., Farina, H., Gil, J., et al. (2008). CIGB-300, a Novel Proapoptotic Peptide that Impairs the CK2 Phosphorylation and Exhibits Anticancer Properties Both *In Vitro* and *In Vivo*. *Mol. Cell Biochem* 316 (1-2), 163–167. doi:10.1007/s11010-008-9814-5
- Perea, S. E., Reyes, O., Puchades, Y., Mendoza, O., Vispo, N. S., Torrens, I., et al. (2004). Antitumor Effect of a Novel Proapoptotic Peptide that Impairs the Phosphorylation by the Protein Kinase 2 (Casein Kinase 2). *Cancer Res.* 64 (19), 7127–7129. doi:10.1158/0008-5472.Can-04-2086
- Perera, Y., Melão, A., Ramón, A. C., Vázquez, D., Ribeiro, D., Perea, S. E., et al. (2020). Clinical-Grade Peptide-Based Inhibition of CK2 Blocks Viability and Proliferation of T-ALL Cells and Counteracts IL-7 Stimulation and Stromal Support. *Cancers* 12 (6), 1377. doi:10.3390/cancers12061377
- Perera, Y., Pedrosa, S., Borrás-Hidalgo, O., Vázquez, D. M., Miranda, J., Villareal, A., et al. (2015). Pharmacologic Inhibition of the CK2-Mediated Phosphorylation of B23/NPM in Cancer Cells Selectively Modulates Genes Related to Protein Synthesis, Energetic Metabolism, and Ribosomal Biogenesis. *Mol. Cell Biochem* 404 (1-2), 103–112. doi:10.1007/s11010-015-2370-x
- Perera, Y., Ramos, Y., Padrón, G., Caballero, E., Guirrola, O., Caligiuri, L. G., et al. (2020). CIGB-300 Anticancer Peptide Regulates the Protein Kinase CK2-dependent Phosphoproteome. *Mol. Cell Biochem* 470 (1-2), 63–75. doi:10.1007/s11010-020-03747-1
- Potting, C., Tatsuta, T., König, T., Haag, M., Wai, T., Aaltonen, M. J., et al. (2013). TRIAP1/PRELI Complexes Prevent Apoptosis by Mediating Intramitochondrial Transport of Phosphatidic Acid. *Cell Metab.* 18 (2), 287–295. doi:10.1016/j.cmet.2013.07.008
- Quotti Tubi, L., Canovas Nunes, S., Brancalion, A., Doriguzzi Breatta, E., Manni, S., Mandato, E., et al. (2017). Protein Kinase CK2 Regulates AKT, NF-Kb and STAT3 Activation, Stem Cell Viability and Proliferation in Acute Myeloid Leukemia. *Leukemia* 31 (2), 292–300. doi:10.1038/leu.2016.209
- Rogers, C., Erkes, D. A., Nardone, A., Aplin, A. E., Fernandes-Alnemri, T., and Alnemri, E. S. (2019). Gasdermin Pores Permeabilize Mitochondria to Augment Caspase-3 Activation during Apoptosis and Inflammation Activation. *Nat. Commun.* 10 (1), 1689. doi:10.1038/s41467-019-09397-2
- Rosales, M., Pérez, G. V., Ramón, A. C., Cruz, Y., Rodríguez-Ulloa, A., Besada, V., et al. (2021). Targeting of Protein Kinase CK2 in Acute Myeloid Leukemia Cells Using the Clinical-Grade Synthetic-Peptide CIGB-300. *Biomedicine* 9 (7), 766. doi:10.3390/biomedicine9070766
- Rosales, M., Rodríguez-Ulloa, A., Besada, V., Ramón, A. C., Pérez, G. V., Ramos, Y., et al. (2021). Phosphoproteomic Landscape of AML Cells Treated with the ATP-Competitive CK2 Inhibitor CX-4945. *Cells* 10 (2), 338. doi:10.3390/cells10020338
- Ross, D., and Siegel, D. (2021). The Diverse Functionality of NQO1 and its Roles in Redox Control. *Redox Biol.* 41, 101950. doi:10.1016/j.redox.2021.101950
- Ruzzene, M., and Pinna, L. A. (2010). Addiction to Protein Kinase CK2: a Common Denominator of Diverse Cancer Cells. *Biochim. Biophys. Acta (Bba) - Proteins Proteomics* 1804 (3), 499–504. doi:10.1016/j.bbapap.2009.07.018
- Ryu, M., Han, J., Kim, S., Lee, M., Ju, X., Lee, Y., et al. (2019). PTEN/AKT Signaling Mediates Chemoresistance in Refractory Acute Myeloid Leukemia through Enhanced Glycolysis. *Oncol. Rep.* 42 (5), 2149–2158. doi:10.3892/or.2019.7308
- Sarno, S., Papinutto, E., Franchin, C., Bain, J., Elliott, M., Meggio, F., et al. (2011). ATP Site-Directed Inhibitors of Protein Kinase CK2: an Update. *Ctmc* 11 (11), 1340–1351. doi:10.2174/156802611795589638
- Sborgi, L., Rühl, S., Mulvihill, E., Pipercevic, J., Heilig, R., Stahlberg, H., et al. (2016). GSDMD Membrane Pore Formation Constitutes the Mechanism of Pyroptotic Cell Death. *Embo J.* 35 (16), 1766–1778. doi:10.15252/embj.2016194696
- Shannon, P., Markiel, A., Ozier, O., Baliga, N. S., Wang, J. T., Ramage, D., et al. (2003). Cytoscape: a Software Environment for Integrated Models of Biomolecular Interaction Networks. *Genome Res.* 13 (11), 2498–2504. doi:10.1101/gr.1239303
- Srinivas, U. S., Tan, B. W. Q., Vellayappan, B. A., and Jeyasekharan, A. D. (2019). ROS and the DNA Damage Response in Cancer. *Redox Biol.* 25, 101084. doi:10.1016/j.redox.2018.101084
- Sriskanthadevan, S., Jeyaraju, D. V., Chung, T. E., Prabha, S., Xu, W., Skrtic, M., et al. (2015). AML Cells Have Low Spare reserve Capacity in Their Respiratory Chain that Renders Them Susceptible to Oxidative Metabolic Stress. *Blood* 125 (13), 2120–2130. doi:10.1182/blood-2014-08-594408
- Sung, Y. H., Jin, Y., Kang, Y., Devkota, S., Lee, J., Roh, J.-i., et al. (2013). Ei24, a Novel E2F Target Gene, Affects P53-independent Cell Death upon Ultraviolet C Irradiation. *J. Biol. Chem.* 288 (43), 31261–31267. doi:10.1074/jbc.M113.477570
- Takemoto, A., Maeshima, K., Ikehara, T., Yamaguchi, K., Murayama, A., Imamura, S., et al. (2009). The Chromosomal Association of Condensin II Is Regulated by a Noncatalytic Function of PP2A. *Nat. Struct. Mol. Biol.* 16 (12), 1302–1308. doi:10.1038/nsmb.1708
- Taylor, P., Takeuchi, H., Sheppard, D., Chillakuri, C., Lea, S. M., Haltiwanger, R. S., et al. (2014). Fringe-mediated Extension of O-Linked Fucose in the Ligand-Binding Region of Notch1 Increases Binding to Mammalian Notch Ligands. *Proc. Natl. Acad. Sci.* 111 (20), 7290–7295. doi:10.1073/pnas.1319683111

- Tchavosnikarova, I. A., Timms, R. T., Matheson, N. J., Wals, K., Antrobus, R., Göttgens, B., et al. (2015). Epigenetic Silencing by the HUSH Complex Mediates Position-Effect Variegation in Human Cells. *Science* 348 (6242), 1481–1485. doi:10.1126/science.aaa7227
- Tian, J., Li, Z., Han, Y., Jiang, T., Song, X., and Jiang, G. (2016). The Progress of Early Growth Response Factor 1 and Leukemia. *Ird* 5 (2), 76–82. doi:10.5582/ird.2015.01049
- Tohda, S., and Nara, N. (2001). Expression of Notch1 and Jagged1 Proteins in Acute Myeloid Leukemia Cells. *Leuk. Lymphoma* 42 (3), 467–472. doi:10.3109/10428190109064603
- Tourneur, L., Delluc, S., Lévy, V., Valensi, F., Radford-Weiss, I., Legrand, O., et al. (2004). Absence or Low Expression of Fas-Associated Protein with Death Domain in Acute Myeloid Leukemia Cells Predicts Resistance to Chemotherapy and Poor Outcome. *Cancer Res.* 64 (21), 8101–8108. doi:10.1158/0008-5472.Can-04-2361
- Trembley, J. H., Wang, G., Unger, G., Slaton, J., and Ahmed, K. (2009). Protein Kinase CK2 in Health and Disease. *Cel. Mol. Life Sci.* 66 (11–12), 1858–1867. doi:10.1007/s00018-009-9154-y
- Tyanova, S., Temu, T., Sinitcyn, P., Carlson, A., Hein, M. Y., Geiger, T., et al. (2016). The Perseus Computational Platform for Comprehensive Analysis of (Prote) omics Data. *Nat. Methods* 13 (9), 731–740. doi:10.1038/nmeth.3901
- Venerando, A., Ruzzene, M., and Pinna, L. A. (2014). Casein Kinase: the Triple Meaning of a Misnomer. *Biochem. J.* 460 (2), 141–156. doi:10.1042/bj20140178
- Vogel, R. O., Janssen, R. J. R. J., Ugalde, C., Grovenstein, M., Huijbens, R. J., Visch, H.-J., et al. (2005). Human Mitochondrial Complex I Assembly Is Mediated by NDUFAF1. *FEBS J.* 272 (20), 5317–5326. doi:10.1111/j.1742-4658.2005.04928.x
- Waerner, T., Gardellin, P., Pfizenmaier, K., Weith, A., and Kraut, N. (2001). Human RERE Is Localized to Nuclear Promyelocytic Leukemia Oncogenic Domains and Enhances Apoptosis. *Mol. Cancer Res.* 12 (4), 201–210.
- Wang, B., Guo, H., Yu, H., Chen, Y., Xu, H., and Zhao, G. (2021). The Role of the Transcription Factor EGR1 in Cancer. *Front. Oncol.* 11, 642547. doi:10.3389/fonc.2021.642547
- Wang, W., Schwemmers, S., Hexner, E. O., and Pahl, H. L. (2010). AML1 Is Overexpressed in Patients with Myeloproliferative Neoplasms and Mediates JAK2V617F-independent Overexpression of NF-E2. *Blood* 116 (2), 254–266. doi:10.1182/blood-2009-11-254664
- Wei, M. C., Zong, W.-X., Cheng, E. H.-Y., Lindsten, T., Panoutsakopoulou, V., Ross, A. J., et al. (2001). Proapoptotic BAX and BAK: a Requisite Gateway to Mitochondrial Dysfunction and Death. *Science* 292 (5517), 727–730. doi:10.1126/science.1059108
- Wiśniewski, J. R., and Gaugaz, F. Z. (2015). Fast and Sensitive Total Protein and Peptide Assays for Proteomic Analysis. *Anal. Chem.* 87 (8), 4110–4116. doi:10.1021/ac504689z
- Wiśniewski, J. R., and Mann, M. (2012). Consecutive Proteolytic Digestion in an Enzyme Reactor Increases Depth of Proteomic and Phosphoproteomic Analysis. *Anal. Chem.* 84 (6), 2631–2637. doi:10.1021/ac300006b
- Yang, M.-H., Yen, C. C., Wang, W. S., Lin, Y. J., Chu, C. J., Chiou, T. J., et al. (1992). Down-regulation of Notch-1 Expression Decreases PU.1-mediated Myeloid Differentiation Signaling in Acute Myeloid Leukemia. *Int. J. Oncol.* 32 (6), 1335–1341. doi:10.3892/ijo.32.6.1335
- Yi, Y.-J., Jia, X.-H., Wang, J.-Y., Li, Y.-J., Wang, H., and Xie, S.-Y. (2016). Knockdown of HOXA10 Reverses the Multidrug Resistance of Human Chronic Myelogenous Leukemia K562/ADM Cells by Downregulating P-Gp and MRP-1. *Int. J. Mol. Med.* 37 (5), 1405–1411. doi:10.3892/ijmm.2016.2539
- Zhou, Y., Zhou, B., Pache, L., Chang, M., Khodabakhshi, A. H., Tanaseichuk, O., et al. (2019). Metascape Provides a Biologist-Oriented Resource for the Analysis of Systems-Level Datasets. *Nat. Commun.* 10 (1), 1523. doi:10.1038/s41467-019-09234-6
- Zonta, F., Borgo, C., Quezada Meza, C. P., Masgras, I., Rasola, A., Salvi, M., et al. (2021). Contribution of the CK2 Catalytic Isoforms α and α' to the Glycolytic Phenotype of Tumor Cells. *Cells* 10 (1), 181. doi:10.3390/cells10010181

Conflict of Interest: The authors declare that the research was conducted in the absence of any commercial or financial relationships that could be construed as a potential conflict of interest.

Publisher's Note: All claims expressed in this article are solely those of the authors and do not necessarily represent those of their affiliated organizations, or those of the publisher, the editors and the reviewers. Any product that may be evaluated in this article, or claim that may be made by its manufacturer, is not guaranteed or endorsed by the publisher.

Copyright © 2022 Rosales, Rodríguez-Ulloa, Pérez, Besada, Soto, Ramos, González, Zettl, Wiśniewski, Yang, Perera and Perea. This is an open-access article distributed under the terms of the Creative Commons Attribution License (CC BY). The use, distribution or reproduction in other forums is permitted, provided the original author(s) and the copyright owner(s) are credited and that the original publication in this journal is cited, in accordance with accepted academic practice. No use, distribution or reproduction is permitted which does not comply with these terms.



Structural and Enzymological Evidence for an Altered Substrate Specificity in Okur-Chung Neurodevelopmental Syndrome Mutant CK2 α ^{Lys198Arg}

Christian Werner¹, Alexander Gast², Dirk Lindenblatt¹, Anna Nickelsen², Karsten Niefind¹, Joachim Jose² and Jennifer Hochscherf^{1*}

¹Department of Chemistry, Institute of Biochemistry, University of Cologne, Cologne, Germany, ²Institute of Pharmaceutical and Medicinal Chemistry, University of Münster, Münster, Germany

OPEN ACCESS

Edited by:

Andrea Venerando,
University of Padua, Italy

Reviewed by:

David Litchfield,
Western University, Canada
Andrea Dalle Vedove,
University of Trento, Italy
Marco Mazzorana,
Diamond Light Source,
United Kingdom

*Correspondence:

Jennifer Hochscherf
J.Hochscherf@uni-koeln.de

Specialty section:

This article was submitted to
Cellular Biochemistry,
a section of the journal
Frontiers in Molecular Biosciences

Received: 08 December 2021

Accepted: 28 February 2022

Published: 04 April 2022

Citation:

Werner C, Gast A, Lindenblatt D, Nickelsen A, Niefind K, Jose J and Hochscherf J (2022) Structural and Enzymological Evidence for an Altered Substrate Specificity in Okur-Chung Neurodevelopmental Syndrome Mutant CK2 α ^{Lys198Arg}.
Front. Mol. Biosci. 9:831693.
doi: 10.3389/fmolb.2022.831693

Specific *de novo* mutations in the CSNK2A1 gene, which encodes CK2 α , the catalytic subunit of protein kinase CK2, are considered as causative for the Okur-Chung neurodevelopmental syndrome (OCNDS). OCNDS is a rare congenital disease with a high phenotypic diversity ranging from neurodevelopmental disabilities to multi-systemic problems and characteristic facial features. A frequent OCNDS mutation is the exchange of Lys198 to Arg at the center of CK2 α 's P+1 loop, a key element of substrate recognition. According to preliminary data recently made available, this mutation causes a significant shift of the substrate specificity of the enzyme. We expressed the CK2 α ^{Lys198Arg} recombinantly and characterized it biophysically and structurally. Using isothermal titration calorimetry (ITC), fluorescence quenching and differential scanning fluorimetry (Thermofluor), we found that the mutation does not affect the interaction with CK2 β , the non-catalytic CK2 subunit, and that the thermal stability of the protein is even slightly increased. However, a CK2 α ^{Lys198Arg} crystal structure and its comparison with wild-type structures revealed a significant shift of the anion binding site harboured by the P+1 loop. This observation supports the notion that the Lys198Arg mutation causes an alteration of substrate specificity which we underpinned here with enzymological data.

Keywords: okur-chung neurodevelopmental syndrome (OCNDS), protein kinase CK2, casein kinase 2, CSNK2A1 gene, acidophilic substrate specificity, substrate recognition, P+1 loop, anion binding site

INTRODUCTION

The serine/threonine kinase CK2, a member of the CMGC branch within the superfamily of eukaryotic protein kinases (EPKs) (Manning et al., 2002), is a heterotetrametric holoenzyme consisting of a central dimer of non-catalytic subunits (CK2 β) to which two separate catalytic subunits (CK2 α or CK2 α' encoded in *Homo sapiens* by the genes CSNK2A1 or CSNK2A2, respectively) are attached (Niefind et al., 2001). Unlike many other EPKs—in particular its closest relatives within the CMGC family—, CK2 it is constitutively active (Niefind et al., 2007) in the sense that it does not require a phosphorylation or any other posttranslational modification for activation; alternatively, salt- and polycation-dependent self-interactions of CK2 $\alpha_2\beta_2$ holoenzyme complexes were proposed as a regulatory mechanism (Niefind and Issinger, 2005; Poole et al., 2005;

Schnitzler et al., 2014) and experimental evidence of such interactions in the cell was provided (Hübner et al., 2014).

CK2 is involved in important cellular processes such as pro-survival signaling (St-Denis and Litchfield, 2009; Zheng et al., 2013; Castello et al., 2017), cell proliferation (Lebrin et al., 2001; St-Denis and Litchfield, 2009) and DNA-damage repair (Loizou et al., 2004; Montenarh, 2016). CK2 is extremely pleiotropic with more than 300 protein substrates reported already in 2003 (Meggio and Pinna, 2003). From these substrates as well as from peptide studies (Marchiori et al., 1988; Sarno et al., 1997), the consensus sequence S/T-D/E-X-D/E for CK2 substrate recognition was derived. The extraordinary pleiotropy of CK2 was emphasized later by Salvi et al. (2009) who extracted 2,275 potential CK2 sites out of 10,899 phospho sites altogether in a database analysis and validated some of the newly detected CK2 sites experimentally. In a review of phosphoproteomic studies, Needham et al. (2019) collected even 671 substrate proteins of CK2 α or CK2 α' , 445 of them being functionally annotated.

CK2 is expressed in various tissues (Faust and Montenarh, 2000) and particularly highly in the mammalian brain (Blanquet, 2000; Castello et al., 2017). Fitting to this, it was linked to neurodegenerative disorders such as Parkinson's disease (Ryu et al., 2008; Borgo et al., 2021) and Alzheimer's disease (Greenwood et al., 1994; Rosenberger et al., 2016) as well as to brain tumours like glioblastoma (Nitta et al., 2015; Rowse et al., 2017). The Okur-Chung neurodevelopmental syndrome (OCNDS) is a recent addition to CK2-associated pathologies of the nervous system. OCNDS is a rare disease observed predominantly in children and affects the patients' behavior, facial structures, physical, intellectual and psychological development as well as their overall health status (Okur et al., 2016; Trinh et al., 2017; Akahira-Azuma et al., 2018; Chiu et al., 2018; Owen et al., 2018; Nakashima et al., 2019; Xu et al., 2020). Currently, about 120 OCNDS patients are known worldwide (<https://www.csnk2a1foundation.org/>, retrieved at 21st of June 2021).

OCNDS is considered as linked to *de novo* mutations in one allele of the *CSNK2A1* gene as revealed by whole exome sequencing (Okur et al., 2016; Akahira-Azuma et al., 2018; Chiu et al., 2018; Owen et al., 2018; Nakashima et al., 2019; Xu et al., 2020). In a recent review, 35 different *CSNK2A1* mutations relevant for OCNDS are listed (Wu et al., 2021), among them the most common one, which is Lys198Arg (Nakashima et al., 2019). Lys198 is located in the P+1 loop, the C-terminal part of the activation segment. The P+1 loop is typically used in EPKs for substrate recognition. In CK2 α , Lys198 plus two further basic residues (Arg191 and Arg195) impart a positively charged character to the P+1 loop fitting to the enzyme's preference for a negatively charged side chain one position downstream from the phosphorylated substrate residue. This functionality of CK2 α 's P+1 loop was disclosed by a mutational study (Sarno et al., 1997); its structural basis was revealed by crystal structures of human CK2 α with two sulfate ions (one of them harboured at the P+1 loop) (Niefind et al., 2007) and with the polyanionic substrate-competitive inhibitor heparin (Schnitzler and Niefind, 2021).

Typically, the CK2 α mutations occurring in OCNDS are mentioned in clinical reports together with phenotypic features (Trinh et al., 2017; Akahira-Azuma et al., 2018; Chiu et al., 2018; Owen et al., 2018; Xu et al., 2020), while investigations on the protein level are rare so far. Recently, Dominguez et al. (2021) observed a general loss of catalytic activity for 15 OCNDS-found CK2 α mutants (among them CK2 α ^{Lys198Arg}) expressed as GST-fusion proteins in bacteria, however, only with a standard peptide substrate and without an enzymologically stringent distinction in K_M - and k_{cat} -values. Cafer et al. (2021) performed a sophisticated phosphoproteomics study in a bacterial system (Chou et al., 2012; Lubner et al., 2018) and published preliminary evidence that the critical effect of the Lys198Arg mutation might concern the substrate specificity of CK2 α rather than the overall activity. To supplement these data and to attempt to resolve the discrepancy, we report here the results of a crystallographic, biophysical and enzymological investigation of the Lys198Arg mutant of CK2 α .

MATERIALS AND METHODS

Preparation of CK2 α and CK2 β Variants

Synthetic genes for human CK2 α , CK2 α ¹⁻³³⁵, CK2 α ^{Lys198Arg}, and CK2 α ^{1-335,Lys198Arg} embedded in pET-28a (+) plasmids and thus prepared to carry an N-terminal (His)₆-tag were purchased from BioCat, Heidelberg; here, CK2 α ¹⁻³³⁵ and CK2 α ^{1-335,Lys198Arg} were included as backups because CK2 α ¹⁻³³⁵—in contrast to the full-length enzyme—does not tend to degrade C-terminally (Niefind et al., 2000), but it is functionally fully competent with respect to catalytic activity (Ermakova et al., 2003) and interaction with CK2 β (Raaf et al., 2008). Competent *Escherichia coli* BL21 (DE3) cells were transformed with those plasmids and plated onto agar plates containing 100 μ g/ml kanamycin. Grown colonies were picked and used for precultures containing 100 ml of lysogeny broth (LB) medium (10 g/L yeast extract, 20 g/L tryptone, 20 g/L sodium chloride) endowed with 100 μ g/ml kanamycin. The precultures were grown over night at 37°C under shaking at 180 rpm. They were used to inoculate main cultures of 5 L slightly modified terrific broth medium (10 g/L yeast extract, 20 g/L tryptone, 2 g/L potassium dihydrogen phosphate, 8 g/L dipotassium hydrogen phosphate and 0.4 g/L magnesium sulfate) supplemented with 100 μ g/ml kanamycin.

Each main culture was shaken at 37°C with 180 rpm until an OD₆₀₀ between 1.0 and 1.5 was reached. Then, gene expression was induced by adding IPTG (Anatrace) to a final concentration of 0.5 mM. After incubating overnight at 20°C, the cells were harvested by centrifugation at 6,200 \times g and 4°C for 30 min. The resulting cell pellets were frozen at -80°C after washing once with 0.9% (w/v) NaCl. The cells were lysed by incubation in lysis buffer (500 mM NaCl, 25 mM TRIS/HCl, pH 8.5, 1 mg/ml lysozyme and 10 μ g/ml DNaseI) for 30 min at 4°C and subsequent cautious sonification (2 min, 2 s on/2 s off, 4°C, 40% power). The cell lysate was centrifuged at 186,000 \times g and 4°C for 30 min to remove cell debris. The supernatant was filtered and then applied onto Ni-NTA affinity chromatography column (HisTrapTM FF 5 ml, GE Healthcare) mounted on an ÄKTA Prime chromatography

system. The buffer A for sample application and washing was composed of 500 mM NaCl, 25 mM TRIS/HCl, pH 8.5 and 40 mM imidazole while the buffer B for gradient elution contained 250 mM rather than 40 mM imidazole. The protein was eluted using a linear gradient of 15 column volumes. Fractions with high absorption at 280 nm were analyzed more precisely by TRIS-glycine SDS-PAGE; those containing the desired protein were pooled and then concentrated by ultrafiltration using AMICON® ultra tubes (cutoff 30 kDa). Simultaneously, the protein was rebuffed into its standard background and storage buffer (500 mM NaCl, 25 mM TRIS/HCl, pH 8.5).

Human CK2 β was prepared as full-length protein and as a C-terminal truncation construct CK2 β^{1-193} which can interact with CK2 α to form a CK2 $\alpha_2\beta_2$ holoenzyme (Boldyreff et al., 1993; Raaf et al., 2008). The pT7-7 plasmid containing the gene for CK2 β^{1-193} without any tag was transformed into *Escherichia coli* BL21 (DE3) cells. The expression, harvesting and lysing procedure was analogue to the CK2 α variants with the exception that LB medium with 100 μ g/ml ampicillin was used for the pre- and main culture and that at an OD₆₀₀ of 0.7, IPTG was added to a final concentration of 0.5 mM. Recombinant CK2 β^{1-193} was prepared with a two-step chromatographic protocol: anion exchange chromatography on a HiTrap Sepharose Q column (GE Healthcare) followed by affinity chromatography with a heparin column (GE Healthcare). For both chromatographic steps, the low-salt buffer contained 150 mM NaCl 25 mM TRIS/HCl, pH 8.5 and the high-salt buffer contained 1 M NaCl 25 mM TRIS/HCl, pH 8.5. The protocol for the chromatography, analysis of the fractions and rebuffing was analogous to the CK2 α variants.

To determine enzymatic parameters, CK2 $\alpha_2\beta_2$ holoenzyme variants consisting of either CK2 α or CK2 $\alpha^{\text{Lys198Arg}}$ in complex with CK2 β^{1-193} were prepared. For this, the mentioned pET-28a (+) vector with the CK2 α and CK2 $\alpha^{\text{Lys198Arg}}$ genes as well as a pT7-7 vector with the coding sequence for CK2 β^{1-193} with an N-terminal (His)₆-tag were used. Transformation of competent *Escherichia coli* BL21 (DE3) cells, expression, harvesting, and cell lysis were performed in a similar manner as described above. For the expression of CK2 β^{1-193} , ampicillin was substituted for carbenicillin as selection marker in bacterial culture. LB agar plates, 50 ml LB medium precultures and 0.5 L LB medium main cultures contained 50 μ g/ml kanamycin or carbenicillin.

Gene expression was induced at an OD₅₇₈ between 0.5 and 0.6 by adding IPTG to a final concentration of 1 mM. After incubation for 4 h at 30°C, cells were harvested by centrifugation at 5,000 x g and 4°C for 10 min. To constitute the respective CK2 $\alpha_2\beta_2$ holoenzyme variants upon cell lysis, cell pellets for either CK2 α or CK2 $\alpha^{\text{Lys198Arg}}$ plus such for CK2 β^{1-193} were merged at a mass ratio of 1:1 and frozen at -80°C. Mixed cells were lysed in 30 ml lysis buffer (500 mM NaCl, 25 mM TRIS/HCl, pH 8.5, 1.3 mg/ml lysozyme, 13.3 μ g/ml DNaseI, 2 mM PMSF, 0.5 μ g/ml leupeptin, 0.7 μ g/ml pepstatin A) and incubated for 30 min at 4°C before subsequent cautious sonification (6 cycles, 20 s on/20 s off, 4°C, 50% power). After centrifugation at 100,000 x g at 4°C for 30 min and filtration, the cleared lysate was applied to a Ni-NTA affinity chromatography

column (self-packed, 2 ml). Subsequently, the column was washed first with 5 column volumes of 500 mM NaCl, 25 mM TRIS/HCl, pH 8.5, and then with 10 column volumes of 500 mM NaCl, 25 mM Tris/HCl, pH 8.5, 25 mM imidazole. Finally, bound protein was eluted by addition of 5 column volumes of 500 mM NaCl, 25 mM Tris/HCl, pH 8.5, 250 mM imidazole. Fractions of 1 ml were analysed by SDS-PAGE and those containing the expected CK2 $\alpha_2\beta_2$ holoenzyme variant were pooled and applied to a gel filtration column (Cytiva HiLoad™ 26/600 Superdex™ 200 pg, 320 ml, Thermo Fisher Scientific, Braunschweig, Germany) using an Äkta Start System (GE Healthcare Europe, Freiburg, Germany) to remove further impurities as well as excess CK2 subunits not incorporated in the CK2 holoenzyme. The gel filtration column was equilibrated in 500 mM NaCl, 25 mM Tris/HCl, pH 8.5, serving subsequently as storage buffer. Again, fractions were analyzed by SDS-PAGE and the fractions containing the CK2 $\alpha_2\beta_2$ holoenzyme variants were pooled and stored at -80°C.

Fluorescence-labelled CK2 β^{1-193} was prepared to determine the CK2 β interaction with either wild-type CK2 α or CK2 $\alpha^{\text{Lys198Arg}}$ by specific fluorescence quenching. For this purpose, the unnatural amino acid *para*-azidophenylalanine (pAzF) purchased from Bachem AG (Bubendorf, Switzerland) was incorporated at position 108 of CK2 β^{1-193} following an adapted protocol described before for a CK2 α -pAzF construct (Nienberg et al., 2016). The essential modification here was that a CK2 β^{1-193} encoding DNA sequence within the plasmid pT7-7 was subjected to site-directed mutagenesis to obtain an amber stop codon at position 108. The resulting plasmid for CK2 $\beta^{1-193,\text{Tyr108Stop}}$ and the plasmid pEVOL-pAzF (Chin et al., 2002), which encodes for the amber suppressor tRNA/aminoacyl-tRNA synthetase, were transformed into *E. coli* BL21 (DE3) cells to allow the incorporation of pAzF during translation. The details of the expression procedure were performed as described by Nienberg et al. (2016). Harvested cells were lysed and the lysate was centrifuged at 100,000 x g. The supernatant was filtered using a 0.22 μ m filter to remove leftover cell debris and applied to a Ni-NTA affinity chromatography column (self-packed, 2 ml). The column was washed with 20 column volumes of 500 mM NaCl, 25 mM Tris/HCl, pH 8.5, 50 mM imidazole. Finally, CK2 β^{1-193} -pAzF was eluted by the addition of 5 column volumes of 500 mM NaCl, 25 mM Tris/HCl, pH 8.5, 250 mM imidazole. Fractions of 1 ml were dialyzed against standard storage buffer (500 mM NaCl, 25 mM Tris/HCl, pH 8.5) and analysed by SDS-PAGE. Those containing CK2 β^{1-193} -pAzF were pooled and labelled with dibenzylcyclooctyne-Sulfo-Cy5 (DBCO-Sulfo-Cy5) in a Strain Promoted Azide-Alkyne Cycloaddition (SPAAC) reaction as described before (Agard et al., 2006; Nienberg et al., 2016).

Isothermal Titration Calorimetry

The procedure previously described (Raaf et al., 2013) was adapted to perform ITC measurements. In this work, C-terminally truncated variants of the CK2 subunits were used which previously had been demonstrated to be fully competent to perform the CK2 α /CK2 β interaction (Raaf et al., 2008). The standard background buffer (500 mM NaCl, 25 mM TRIS/HCl, pH 8.5) was used to dilute the stock solutions of either CK2 α^{1-335}

or the mutant CK2 $\alpha^{1-335, \text{Lys198Arg}}$ to a concentration of 7 μM and that of CK2 β^{1-193} to 149 μM . The latter was filled into the injection syringe. The measurements were carried out using a VP-ITC (Microcal) at 35°C. In each run, 25 injections of CK2 β^{1-193} solution with a volume of 2 μL for the first, and 10 μL for all subsequent injections were applied; the off-time between two single injections was 300 s. Three independent measurements were performed for the CK2 α^{1-335} /CK2 β^{1-193} interaction and two for the CK2 $\alpha^{1-335, \text{Lys198Arg}}$ /CK2 β^{1-193} interaction.

The raw ITC data were processed with ORIGIN (version 7), Origin Lab (OriginLab Corporation, Northampton, MA, United States), assuming a binding model of a single set of sites, and with the “ligand is present in the cell” option. For curve fitting, the stoichiometry between CK2 α and CK2 β was fixed to 1 according to the structure of the CK2 $\alpha_2\beta_2$ holoenzyme (Niefind et al., 2001).

Fluorescence-Based Assay for Determination of Dissociation Constant

A fluorescence-based assay was used to determine dissociation constants (K_D values) for the interaction of either CK2 α or CK2 $\alpha^{\text{Lys198Arg}}$ with CK2 β^{1-193} -pAzF after coupling the latter with DBCO-Sulfo-Cy5. For detection of fluorescence, a Monolith NT.115 device (Nanotemper, München, Germany) was used. Increasing amounts of either CK2 α or CK2 $\alpha^{\text{Lys198Arg}}$ to give final concentrations from 0.3 nM to 5 μM were mixed to probes of CK2 β^{1-193} -DBCO-Sulfo-Cy5 with a constant concentration of 30 nM. Samples were dissolved in 500 mM NaCl, 25 mM TRIS/HCl, pH 8.5, 0.05% Tween[®]20. The fluorescence intensity was determined at 25°C by excitation with a LED-lamp (LED Power: 95%, DBCO-Sulfo-Cy5: $\lambda_{\text{abs, max}} = 646 \text{ nm}$; $\lambda_{\text{em, max}} = 661 \text{ nm}$). Based on the CK2 α - or CK2 $\alpha^{\text{Lys198Arg}}$ -dependent quenching of fluorescence, K_D values were determined using the mode “initial fluorescence” in the software MO. Affinity Analysis v2.1.3 (Nanotemper, München, Germany).

Differential Scanning Fluorimetry

Differential scanning fluorimetry (DSF) (Niesen et al., 2007; Boivin et al., 2013) was applied to probe the effect of the Lys198Arg mutation on the thermal stability of monomeric (unbound) and CK2 β -bound CK2 α . For these studies, full-length as well as C-terminally truncated versions of CK2 α were used together with CK2 β^{1-193} , the C-terminally truncated form of CK2 β (Raaf et al., 2008).

20 μM stock solutions of four different CK2 α variants (CK2 α , CK2 $\alpha^{\text{Lys198Arg}}$, CK2 α^{1-335} , CK2 $\alpha^{1-335, \text{Lys198Arg}}$) and a 50 μM stock solution of CK2 β^{1-193} were prepared. In addition, 3 μL of the commercial dye solution 5,000X SYPRO Orange (Sigma Aldrich) were diluted with 237 μL water. For a DSF scan with an unbound subunit, 2 μL of the diluted dye solution was mixed with 21 μL standard buffer (500 mM NaCl, 25 mM TRIS/HCl, pH 8.5) and with 2 μL stock solution of either CK2 β^{1-193} or one of the CK2 α variants. To analyze the effect of the CK2 α /CK2 β interaction on thermostability *via* DSF, 2 μL CK2 β^{1-193} stock solution were mixed with 2 μL stock solution of one of the CK2 α variants;

this mixture was then incubated for 5 min at room temperature and finally supplemented with 19 μL standard buffer and 2 μL diluted SYPRO Orange dye solution.

DSF measurements were performed with the BioRad CFX96[™] RT-PCR system using a temperature gradient from 4 to 95°C with a slope of 1°C per minute, an excitation wavelength of 485 nm, and an emission wavelength of 530 nm. All melting curves were measured as triplicates. Raw data were collected with the CFX Manager[™] software (BioRad) and processed with OriginPro 2021 (OriginLab Corporation, Northampton, MA, United States). To determine the inflection points of the direct melting curves (defined as the melting temperatures T_m), we calculated their first derivatives, modelled the derivative curves with the Gauss-Fit option of OriginPro 2021 and calculated their minima.

Crystallization and Crystal Structure Determination

Protein crystallization experiments were performed at 20°C using the sitting-drop variant of the vapour diffusion technique. Crystallization conditions for CK2 $\alpha^{\text{Lys198Arg}}$ and CK2 $\alpha^{1-335, \text{Lys198Arg}}$ were searched with the “Index Screen” and the “Crystal Screen” collections purchased from Hampton Research. The most attractive crystals were found with the full-length construct CK2 $\alpha^{\text{Lys198Arg}}$ and the condition G3 of the Index Screen. This combination was selected for subsequent optimization and macroseeding.

The final crystallization droplets were composed of a 1:1 mixture of protein solution (5 mg/ml CK2 $\alpha^{\text{Lys198Arg}}$ in 500 mM NaCl, 25 mM TRIS/HCl, pH 8.5) and of reservoir solution (0.2 M lithium sulfate, 25% w/v PEG 3350 and 0.1 M Bis-TRIS/HCl, pH 6.5); to these droplets, single crystals from the screening plates were transferred as macro seeds. After equilibration at 20°C, suitable crystals were harvested, shortly transferred to a cryoprotectant mixture composed of 70 μL reservoir solution and 30 μL ethylene glycol, and subsequently vitrified in liquid nitrogen.

X-ray diffraction data of the CK2 $\alpha^{\text{Lys198Arg}}$ crystals were collected at beamline ID23-2 of the European Synchrotron Radiation Facility (ESRF) in Grenoble (France) equipped with a PILATUS3 X 2M detector. The temperature of data collection was 100 K and the wavelength 0.8731 Å. The raw diffraction data were processed with the AutoPROC pipeline (Vonrhein et al., 2011) which utilized XDS (Kabsch, 2010), POINTLESS and AIMLESS (Evans and Murshudov, 2013) from the CCP4 suite (Winn et al., 2011) and finally STARANISO (Tickle et al., 2018) to improve the data set by anisotropy correction. The structure was solved by molecular replacement with PHASER (McCoy et al., 2007) integrated in the PHENIX package (Adams et al., 2010) and using the CK2 α^{1-335} structure with PDB_ID 2PVR (Niefind et al., 2007) as a search model. The refinement was performed with the phenix.refine module (Afonine et al., 2012) of PHENIX (Adams et al., 2010) in combination with COOT (Emsley et al., 2010) for manual corrections.

Enzyme Kinetics

To determine enzymatic parameters (K_M , k_{cat} , k_{cat}/K_M) of the different enzyme variants, a capillary electrophoresis (CE) based

kinase assay was performed (Gratz et al., 2010). Four different CK2 substrate peptides (RRRDDSDDD, RRRDDDTDDD, RRRDDDSGGD, and RRREDEYDDD) were purchased from GenScript (Leiden, Netherlands). The enzyme reaction rate was determined with these substrates at varying concentrations from 50 to 750 μ M. A constant concentration of 500 μ M ATP was applied throughout all experiments. Phosphorylation of substrates was performed by addition of CK2 $\alpha_2\beta_2$ holoenzyme variants with a final concentration of either 18.5 nM for (CK2 α)₂(CK2 β^{1-193})₂, if the peptides RRRDDSDDD or RRRDDDTDDD were the substrates, or 92.4 nM for (CK2 α)₂(CK2 β^{1-193})₂, if the peptides RRRDDDSGGD or RRREDEYDDD were the substrates, as well as for all reactions with (CK2 $\alpha^{\text{Lys198Arg}}$)₂(CK2 β^{1-193})₂. The significantly higher enzyme concentration for some of the reactions was chosen to compensate for low base activity and improve the detection limit. For each setup, the kinase reaction was performed at 37°C and samples for CE were taken at different time points (3, 6, 9, and 12 min). Initial reaction rates were determined by linear regression.

Substrate and product peptides were separated by CE on a ProteomeLab PA800 System (Beckman Coulter, Krefeld, Germany). For instrument control and analysing of the results the 32 karat 9.1 software (Beckman Coulter, Krefeld, Germany) was used. CE was performed with 2 M acetic acid (pH 2) as an electrolyte, a constant current of 30 μ A and UV detection at 195 nm.

K_M and v_{\max} were determined from Lineweaver-Burk diagrams using GraphPad Prism 5 (GraphPad, La Jolla, CA, United States). Finally, turnover numbers k_{cat} and catalytic efficiencies k_{cat}/K_M were calculated from these values.

RESULTS AND DISCUSSION

The Lys198Arg Mutation in CK2 α Does Not Reduce the Affinity to CK2 β

The CK2 β interacting region of CK2 α is located exclusively at the N-terminal lobe of the kinase domain (Niefind et al., 2001) with Leu41 and Phe54 being the interaction hotspots on the side of CK2 α (Raaf et al., 2011). The P+1 loop of CK2 α with Lys198 at its center is relatively far away from this region; therefore and because of the conservative nature of the mutation, we did not expect a significant loss of affinity as a consequence of the mutation.

To probe this quantitatively, we performed ITC experiments, in which CK2 β^{1-193} was titrated against either CK2 α^{1-335} (Figure 1A) or CK2 $\alpha^{1-335,\text{Lys198Arg}}$ (Figure 1B), and processed these data to obtain dissociation constants K_D plus thermodynamic profiles (Figure 1C). The resulting K_D value of 5.4 nM for the CK2 α^{1-335} /CK2 β^{1-193} interaction is in a similar range as reported previously (Raaf et al., 2008; Bischoff et al., 2011; Raaf et al., 2011; Raaf et al., 2013). Significantly, the K_D value of the CK2 $\alpha^{1-335,\text{Lys198Arg}}$ /CK2 β^{1-193} interaction is nearly identical (6.1 nM). The same is true for the enthalpic and the entropic term of the thermodynamic profile (Figure 1C); in either case, the interaction is driven strongly enthalpically, partially balanced by enthalpy-entropy compensation.

To validate these CK2 α /CK2 β interaction results with an alternative method a fluorescence-based assay was used (Figure 2). Increasing amounts of CK2 α , CK2 $\alpha^{\text{Lys198Arg}}$ or the negative control protein BSA were mixed to fluorescently labelled CK2 β^{1-193} -DBCO-Sulfo-Cy5. The quenching of fluorescence proved specific binding for CK2 α (Figure 2A) and for CK2 $\alpha^{\text{Lys198Arg}}$ (Figure 2B) to the CK2 β construct while for BSA no effect on fluorescence was detected (data not shown). Quantitative processing of these data resulted in K_D values of 13.6 nM for the CK2 α /CK2 β^{1-193} -DBCO-Sulfo-Cy5 interaction (Figure 2A) and 6.2 nM for the CK2 $\alpha^{\text{Lys198Arg}}$ /CK2 β^{1-193} -DBCO-Sulfo-Cy5 interaction (Figure 2B) which were not significantly different from each other ($p > 0.05$, One-way-ANOVA). Furthermore, the K_D values are in a similar range as those determined with ITC (Figure 1C) or reported for using Microscale thermophoresis (MST; 12 nM; (Pietsch et al., 2020)). This indicates that measuring of fluorescence quenching of CK2 β^{1-193} -DBCO-Sulfo-Cy5 has the potential to become a novel methods to determine K_D values of the interaction of CK2 β with variants of CK2 α .

In summary, the CK2 α /CK2 β interaction data determined *via* ITC and fluorescence quenching are largely consistent with the expectation that the CK2 α mutation Lys198Arg has no significant effect on the interaction with CK2 β .

The Thermostability of CK2 α and of the CK2 $\alpha_2\beta_2$ Holoenzyme Is Not Affected by the Lys198Arg Mutation

CK2 β is not only significantly more thermostable than CK2 α , but its interaction with the latter has also a strong stabilizing impact against thermal stress (Boldyreff et al., 1993; Raaf et al., 2008). These facts known from differential scanning calorimetry experiments (Raaf et al., 2008) could be confirmed here with DSF (Figure 3): the T_M value of CK2 β^{1-193} was determined as 58.2°C while the melting temperature of unbound CK2 α was almost 14° lower (44.8°C), irrespective if the full-length versions of CK2 α were tested (Figure 3A) or the C-terminally truncated constructs (Figure 3B). After binding to CK2 β^{1-193} , however, the T_M values of the CK2 α variants increased to 52°C (full-length CK2 α) and to 53.2°C (CK2 α^{1-335}).

A comparable thermostabilization effect by CK2 β^{1-193} should exist if—as the ITC (Figure 1) and fluorescence quenching (Figure 3) data suggest—the CK2 α mutation Lys198Arg does not impair the assembly of the CK2 $\alpha_2\beta_2$ holoenzyme. In fact, according to the DSF data, the T_M value of CK2 $\alpha^{\text{Lys198Arg}}$ increases from 46°C (unbound) to 53°C (CK2 β^{1-193} -bound) and the T_M value of CK2 $\alpha^{1-335,\text{Lys198Arg}}$ from 46.4°C (unbound) to 53.9°C (CK2 β^{1-193} -bound). Thus, the ITC/fluorescence evidence that the Lys198Arg mutation of CK2 α does not affect the CK2 α /CK2 β interaction is emphasized by the DSF results.

Noteworthy, the T_M value of CK2 $\alpha^{\text{Lys198Arg}}$ is about 1° higher than that of wild-type CK2 α regardless whether CK2 β^{1-193} is bound or not. A similar increase is visible if the C-terminally truncated variants are compared. Thus, the mutation Lys198Arg itself causes a slight, but significant thermostabilization of CK2 α ,

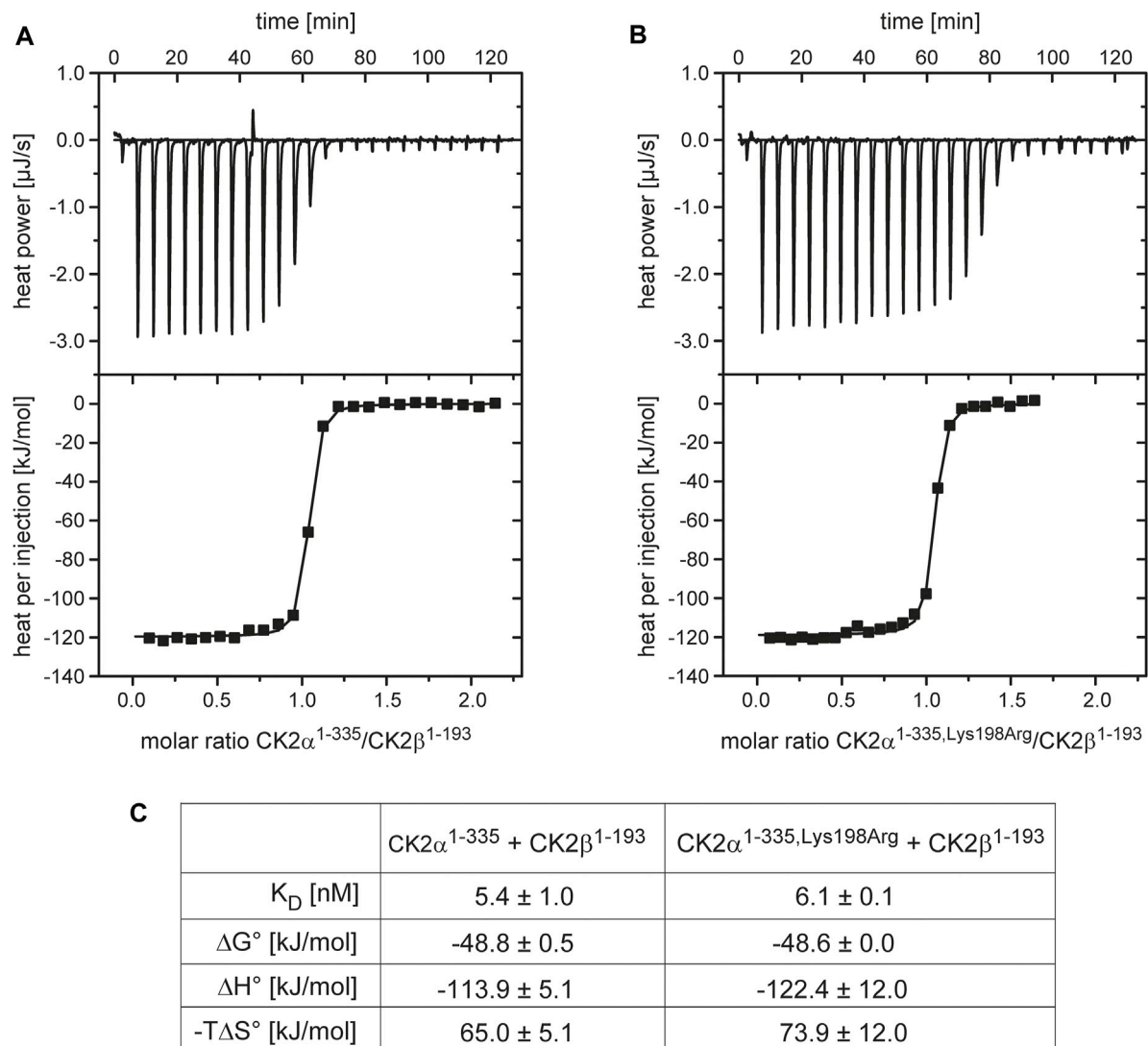


FIGURE 1 | ITC characterization of the effect of the Lys198Arg mutation on the CK2 α /CK2 β interaction. (A/B) Representative direct and integrated ITC curves for the interaction of CK2 β^{1-193} with CK2 α^{1-335} (A) and CK2 $\alpha^{1-335, \text{Lys198Arg}}$ (B) generated with ORIGIN. (C) Thermodynamic data after processing of ITC curves. The numbers represent mean values plus corresponding standard deviations for triplicate measurements.

an observation that is consistent with the conservative nature of the mutation.

The Lys198Arg Mutation in CK2 α Causes a Shift of the Anion Binding Site at the P+1 Loop

The structure of CK2 $\alpha^{\text{Lys198Arg}}$ was solved by molecular replacement and refined to a resolution of 1.77 Å (Table 1). The asymmetric unit of the tetragonal CK2 $\alpha^{\text{Lys198Arg}}$ crystal contains two protein molecules. While their C-terminal segments were not visible in the electron density, both CK2 $\alpha^{\text{Lys198Arg}}$ chains were largely well defined from residue 2 to 333 and in particular in the region of the P+1 loop, which contains the mutated position 198.

During structure refinement, a number of large and approximately tetrahedrally formed pieces of electron density emerged at positively charged surface areas of the enzyme molecules known to be relevant for substrate recognition. We filled them with sulfate ions because of the relatively high sulfate content in the crystallization solution (200 mM) and the absence of alternative anionic candidates (Figure 4A).

Sulfate ions are substrate-competitive CK2 inhibitors (Niefind et al., 2007). Some of the bound sulfate ions are coordinated by a part of the N-terminal kinase domain that receives its positive charge largely by a CK2 α -typical, lysine-rich sequence motif K⁷⁴KKIKR⁸⁰ located at the beginning of the helix αC (Figure 4B). This surface patch is referred to as “extended substrate-recognition region” in Figure 4A because it supports the binding of acidic substrates as demonstrated by mutational analyses (Sarno et al., 1995; Sarno et al.,

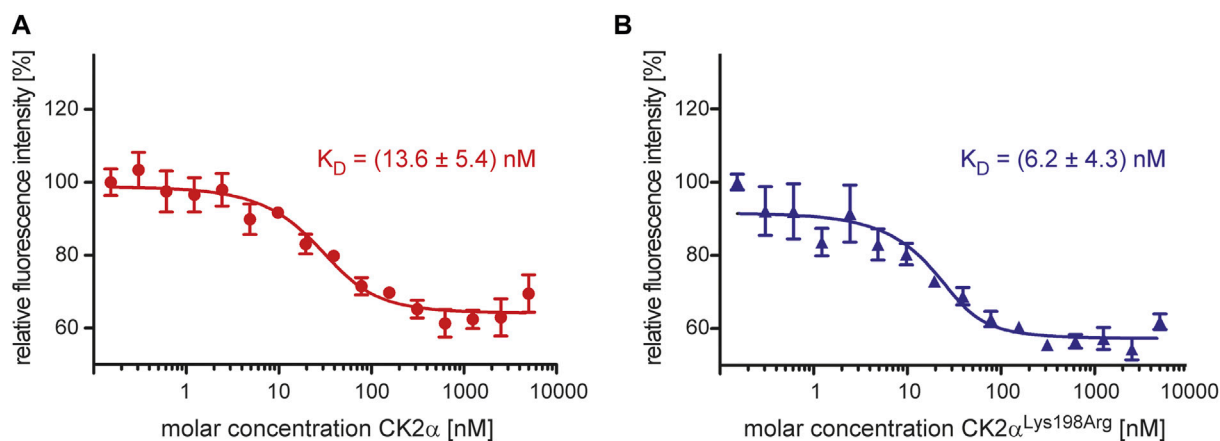
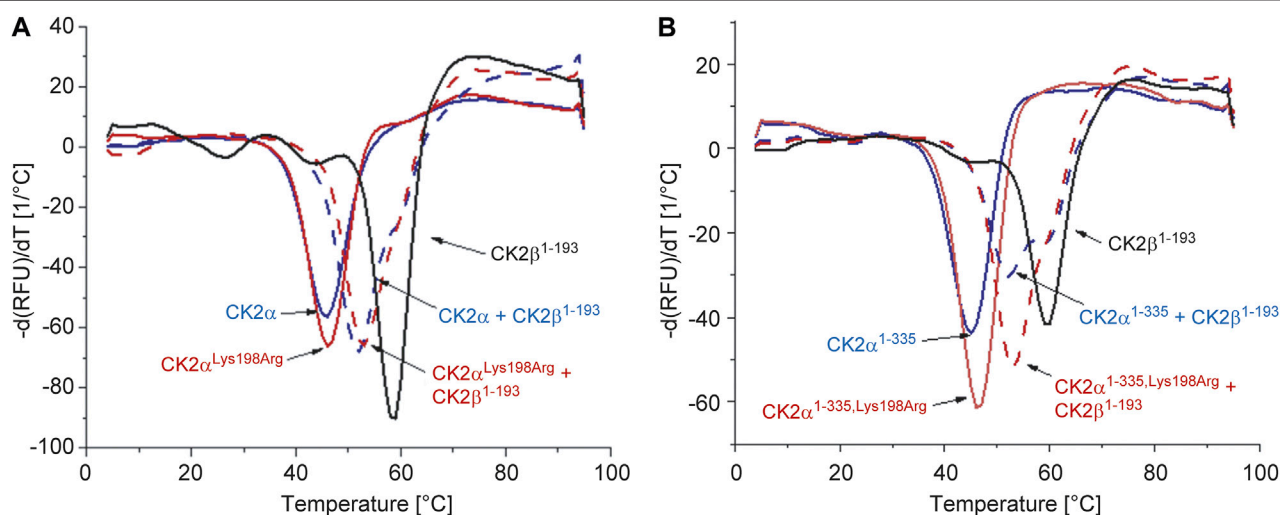


FIGURE 2 | Characterization of the effect of the Lys198Arg mutation on the CK2 α /CK2 β interaction using a fluorescence-based assay. The fluorescence of CK2 β ¹⁻¹⁹³-DBCO-Sulfo-Cy5 quenched by increasing concentrations of CK2 α (**A**) or CK2 α ^{Lys198Arg} (**B**) in the range from 0.3 to 5,000 nM was measured. The binding curves were generated and processed using the software MO. Affinity Analysis v2.1.3 (Nanotemper, München, Germany). The K_D values given in the graphs are averages from three independent experiments.



		full-length CK2 α		C-terminally truncated CK2 α	
		CK2 α	CK2 α ^{Lys198Arg}	CK2 α ¹⁻³³⁵	CK2 α ^{1-335,Lys198Arg}
- CK2 β ¹⁻¹⁹³	---	44.8 ± 0.2	46.0 ± 0.1	44.8 ± 0.2	46.4 ± 0.1
+ CK2 β ¹⁻¹⁹³	58.2 ± 0.2	52.0 ± 0.3	53.0 ± 0.3	53.2 ± 0.7	53.9 ± 0.3

FIGURE 3 | Differential scanning fluorimetry to determine the thermal stability of the CK2 α variants of this study and its change by CK2 β ¹⁻¹⁹³. (**A/B**) Negative first derivatives of representative melting curves of either full-lengths CK2 α variants (**A**) or C-terminally truncated CK2 α variants (**B**) in the absence of CK2 β ¹⁻¹⁹³ (solid blue and red lines) and in the presence of CK2 β ¹⁻¹⁹³ (dashed blue and red lines). For comparison, the curve measured with unbound CK2 β ¹⁻¹⁹³ is drawn as black solid line in both panels. (**C**) Melting temperatures derived from DSF curves as visible in panels A and B. Averages and standard deviations of three independent measurements, respectively, are given.

1997) and by the identification of an interface to the substrate-competitive inhibitor heparin, a highly sulfated, negatively charged carbohydrate (Schnitzler and Niefind, 2021).

In the context of this study, two sulfate ions located at the “central substrate-recognition region” (**Figure 4A**) are particularly relevant because their binding sites are the P+1

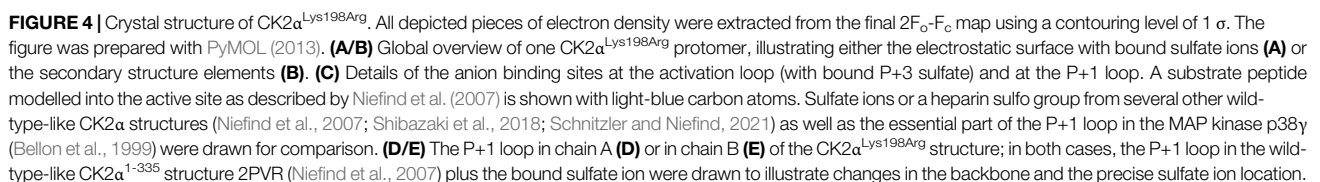


TABLE 1 | X-ray data and refinement statistics of a CK2 α ^{Lys198Arg} structure.

X-ray diffraction data quality	
Wavelength [Å]	0.87313
Synchrotron (beamline)	ESRF (ID23-2)
Space group	P4 ₃ 2 ₁ 2
Unit cell: a, b, c [Å]	127.824, 127.824, 123.180
α , β , γ [°]	90.0, 90.0, 90.0
Protomers per asymmetric unit	2
Resolution [Å] (highest shell)	88.698–1.774 (1.980–1.774) ^a
R _{sym} [%]	58.7 (281.4) ^a
CC1/2	0.990 (0.709) ^a
Signal-to-noise ratio (I/ σ)	18.1 (1.8) ^a
No. of unique reflections	65,649 (3,280) ^a
Completeness (spherical) [%]	66.5 (12.0) ^a
Completeness (ellipsoidal) [%] ^b	96.3 (80.1) ^a
Multiplicity	44.4 (38.1) ^a
Wilson B-factor [Å ²]	3.97
Refinement and structure quality	
No. of reflections for R _{work} /R _{free}	64,295/1,332
R _{work} /R _{free} [%]	18.0/21.8
Number of non-H-atoms	6,395
Protein	5,620
Ligand/ion	84
Water	691
Average B-factor [Å ²]	20.34
Protein	19.25
Ligand/ion	32.33
water	27.75
RMS deviations	
Bond lengths [Å]	0.004
Bond angles [°]	0.65
Ramachandran plot	
Favoured [%]	98.18
Allowed [%]	1.82
Outliers [%]	0.00

^aThe values in brackets refer to the highest resolution shell.

^bAfter anisotropic analysis with STARANISO (Tickle et al., 2018).

loop, which harbors the critical Lys198Arg mutation, and the activation loop (**Figure 4B**). At these two cavities, sulfate ions have been found several times before (**Figure 4C**) (Niefind et al., 2007; Shibazaki et al., 2018; Schnitzler and Niefind, 2021); in a recent high-resolution structure of a CK2 α ¹⁻³³⁵/heparin complex, one of them—the P+1 loop site—even harbors a sulfo moiety of a heparin disulfo-glucosamine residue (**Figure 4C**) (Schnitzler and Niefind, 2021). The most striking feature of the CK2 α ^{Lys198Arg}/sulfate complex structure is that the position of the sulfate ion at the activation loop, which is designated as “P+3 sulfate” in **Figure 4A/B/C** for reasons explained below, is identical compared to the wild-type structures while the sulfate ion at the mutated P+1 loop was shifted by 3.5 Å in the direction of Arg195, one of the selectivity determinants of the P+1 loop (**Figure 4C**). Noteworthy, a similar displacement of the P+1 loop anion binding site was described previously when CK2 α was structurally compared with its closest relatives in the CMGC kinase family (Niefind et al., 2007); it is illustrated in **Figure 4C** for p38 γ which like other MAP kinases requires two phosphorylations for activation and harbors the resulting terminal anionic phospho groups at the activation loop and

the P+1 loop (see phospho-Tyr185 of p38 γ in **Figure 4C**) (Bellon et al., 1999). Significantly, p38 γ such as most CMGC kinases possesses an arginine at the center of the P+1 loop, meaning equivalent to Lys198 of CK2 α ; this arginine residue is so typical that it was entitled “CMGC arginine” in a comprehensive evolutionary study (Kannan and Neuwald, 2004). Thus, an arginine at the centre of the P+1 loop can be canonically present as in most CMGC kinases or it can be the result of a mutation as in CK2 α ^{Lys198Arg}, but in both cases it shifts the binding site for anionic moieties within the P+1 loop significantly compared to wild-type CK2 α .

The relocation of the P+1 sulfate ion is visible in both protomers of the CK2 α ^{Lys198Arg} structure (**Figure 4D/E**). It is accompanied by an evasion of the Asn238 side chain and additionally in chain A (but not in chain B) by a flip of the peptide group linking Val192 and Ala193 (**Figure 4D**). The latter detail was never observed before: normally in CK2 α structures, this peptide group is turned in such a way that a close hydrogen bond between the carbonyl O-atom of Val192 and the terminal amino group of Lys198 can be formed (depicted as green dotted line in **Figure 4D/E**) with the consequence of structural tension in the peptide backbone at Ala193, indicated by an unfavourable ϕ/ψ -combination in a Ramachandran graph (Niefind et al., 2007), but released by a peptide flip as visible in chain A. Thus, the tendency to turn the Val192/Ala193 peptide to a relaxed conformation leads to less backbone strain in the P+1 loop of CK2 α ^{Lys198Arg} compared to wild-type CK2 α , an observation that fits to the gain of thermostability mentioned above (**Figure 3C**).

Relation to Substrate Specificity and Cushing's Syndrome

The question arises what the relocation of the P+1 sulfate visible in **Figures 4C–E** could mean in a functional sense. For the wild-type construct CK2 α ¹⁻³³⁵, the binding sites for sulfate ions at the P+1 loop and the activation loop were functionally interpreted by Niefind et al. (2007) who modelled—due to the absence of an experimental CK2 α /substrate peptide complex structure—a short CK2 substrate peptide (sequence DSDDD) into the active site of CK2 α . The structure of the CK2 α -relative cyclin-dependent kinase 2 in complex with cyclin A plus a peptide substrate (Brown et al., 1999) served as a template for this *in silico* modelling. Significantly, the side chain carboxylates of Asp1 and Asp3 of the modelled peptide, which represent the positions P+1 and P+3 of typical CK2 substrates (consensus sequence for substrate recognition: S/T-D/E-X-D/E), coincide well with the two sulfate ions as visible in **Figure 4C**.

If this overlap is compromised as for the P+1 loop of CK2 α ^{Lys198Arg}, no complete loss of function should be expected, but a disturbance of the canonical substrate recognition. The sulfate shift of 3.5 Å illustrated in **Figure 4C** suggests that CK2 α ^{Lys198Arg} still favours substrates with an acidic P+1 residue, but that glutamate with its longer side chain should be boosted compared to aspartate. The preliminary data of Caefer et al. (2021), for which bacterial phosphoproteomes were artificially established by the Proteomic Peptide Library

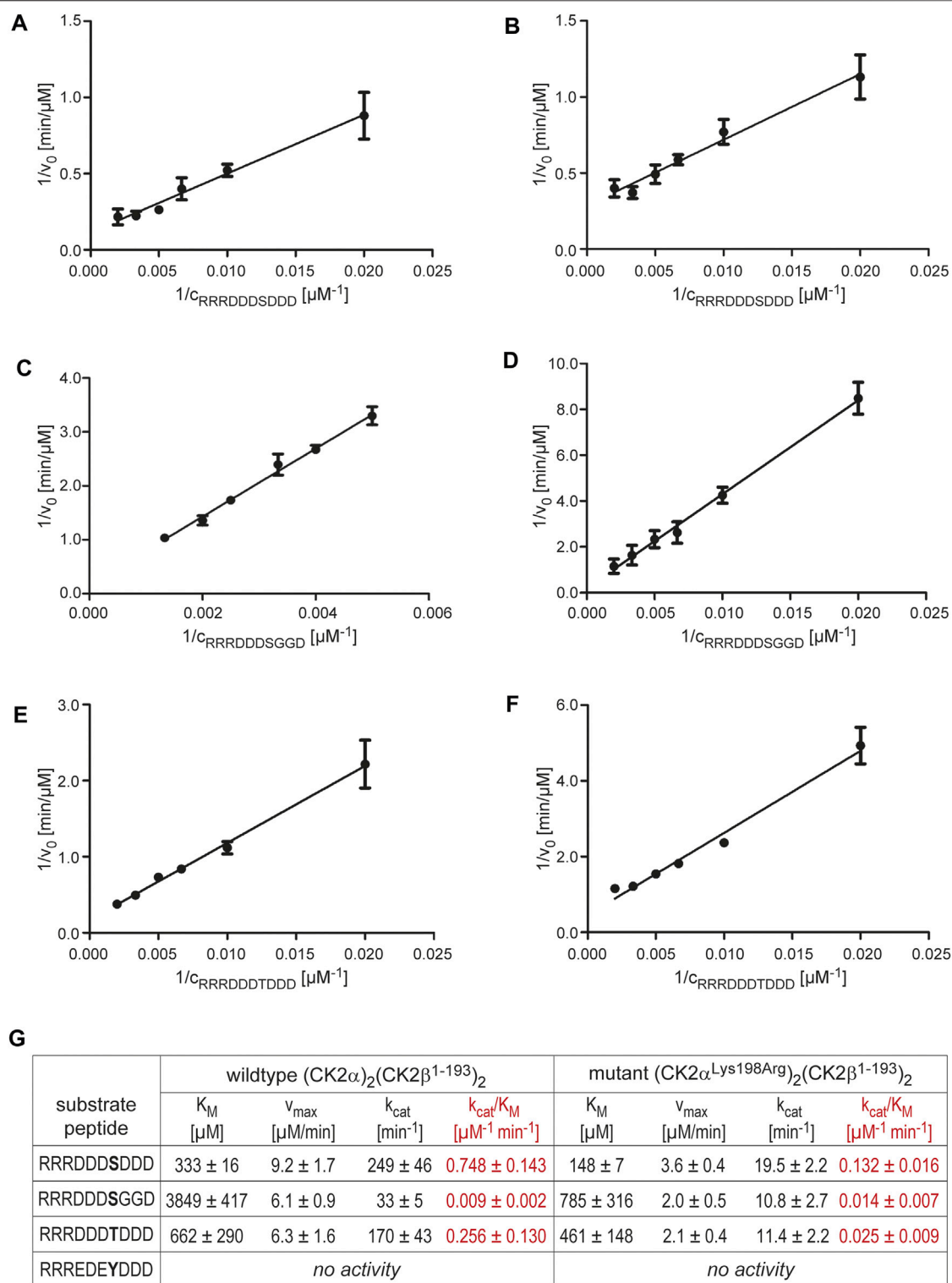


FIGURE 5 | Michaelis-Menten kinetics with varying substrate concentrations to examine changes in substrate specificity caused by the CK2 α mutation Lys198Arg. **(A/C/E)** Lineweaver-Burk plots for wild-type (CK2 α)₂(CK2 β)₂ and the substrates RRRDDSDDD **(A)**, RRRDDSSGGD **(C)**, or RRRDDTDDD **(E)**. **(B/D/F)** Lineweaver-Burk plots for the mutant (CK2 α ^{Lys198Arg})₂(CK2 β)₂ and the substrates RRRDDSDDD **(B)**, RRRDDSSGGD **(D)**, or RRRDDTDDD **(F)**. **(G)** Overview of the enzymological data derived from the Lineweaver-Burk plots in panels **(A–F)**. The catalytic efficiency values (k_{cat}/K_M) are highlighted in red colour.

(ProPeL) approach of Lubner et al. (2018), indicate a decreased preference of CK2 $\alpha^{\text{Lys198Arg}}$ for acidic residues at the P+1 position of substrates, but a detailed analysis of the identified phosphopeptide motifs shows a more differentiated picture: 699 motifs found exclusively with wild-type CK2 α disclose a pronounced specificity for aspartate (but not glutamate) at the P+1 position. In 373 motifs unique for CK2 $\alpha^{\text{Lys198Arg}}$, glycine followed at a clear distance by alanine and leucine is the preferred P+1 residue while acidic residues are no longer represented significantly. In a subset of 651 overlapping motifs (found with wild-type CK2 α as well as CK2 $\alpha^{\text{Lys198Arg}}$), aspartate is the most frequent P+1 residue closely followed by glutamate. Insofar, a selectivity shift at the P+1 position of substrates from aspartate to glutamate, which is consistent with our structural data, is indeed visible from the preliminary results of Caefer et al. (2021). Simultaneously, however, the Lys198Arg mutation seems to be accompanied by an overall decrease of P+1 preference for acidic residues and a general loss of relevance of the P+1 loop for substrate recognition. These tendencies are not apparent from the CK2 $\alpha^{\text{Lys198Arg}}$ /sulfate structure presented here. Crystal structures of CK2 α and CK2 $\alpha^{\text{Lys198Arg}}$ in complex with substrate peptides are required in the future to explain these changes of substrate specificity.

Interestingly, the ProPeL method was also applied to investigate the mutation Leu205Arg of protein kinase A (PKA) (Lubner et al., 2017) which is a central driver of Cushing's syndrome caused by cortisol-secreting adenomas (Cao et al., 2014; Berthon et al., 2015; Walker et al., 2019). Leu205 of PKA is equivalent to Lys198 of CK2 α , meaning it is the central residue of the P+1 loop in PKA and one of determinants of the enzyme's preference for hydrophobic residues like Phe, Leu, Ile or Val at the P+1 position of substrates. For PKA $^{\text{Leu205Arg}}$, Lubner et al. (2017) determined still a certain P+1 preference for Leu, but Asp, Asn and Gln emerged as new strongly acceptable P+1 residues in substrate proteins. Thus, again a subtle shift of protein kinase selectivity—caused by a mutation in the P+1 loop—rather than a loss of function seems to be a genetic background of a protein kinase-linked disease.

Michaelis-Menten Kinetics

Potential selectivity changes caused by the Lys198Arg mutation were examined. To this end, we performed comparative Michaelis-Menten kinetics to determine K_M - and k_{cat} -values (and out of them catalytic efficiencies) of CK2 $\alpha_2\beta_2$ -holoenzyme complexes with either wild-type CK2 α or CK2 $\alpha^{\text{Lys198Arg}}$ for the phosphorylation of four different peptide substrates (Figure 5). An established CK2 standard substrate with the sequence RRRDDDSDDD served as positive control (Figure 5A/B). The other substrate peptides with sequences RRRDDDSGGD (Figure 5C/D), RRRDDDTDDD (Figure 5E/F), and RRREDEYDDD were inspired by the preliminary results of Caefer et al. (2021). With CK2 $\alpha^{\text{Lys198Arg}}$, these authors had observed selectivity changes at the P+1 position as mentioned above and a decreased preference for Thr phosphorylation, but an increased propensity for phosphorylation at Tyr, in particular if the Tyr phosphorylation site is preceded by acidic residues at the P-2 and the P-1 position.

With the peptide RRREDEYDDD, we could not detect any significant tyrosine phosphorylation, either with the wild-type CK2 $\alpha_2\beta_2$ holoenzyme or with the mutant (CK2 $\alpha^{\text{Lys198Arg}}$) $_2$ (CK2 β) $_2$. Thus, no conclusions concerning changes in phosphoacceptor specificity and no comparison with the corresponding preliminary results of Caefer et al. (2021) can be drawn. Possible reasons for this failure are the nature of the peptide or the limited sensitivity of the assay read-out (or a combination of both). According to an early *in vitro* study by Marin et al. (1999) with various substrates peptides, the Tyr phosphorylation of CK2 depends extremely on the sequence environment; for instance, the peptides RRRADDYDDDDDD, EEEEEEEEEEEEE, and PEGDYEEEELE remained completely unphosphorylated in spite of acidic residues at the P+1 and P+3 positions, and even for peptides with detectable Tyr phosphorylation by CK2, the catalytic efficiencies for the phosphorylation of equivalent Ser peptides were higher by a factor of at least 10,000 (Marin et al., 1999).

In contrast to an increased propensity for Tyr phosphorylation, other tendencies mentioned in the preliminary report of Caefer et al. (2021) are confirmed by the enzymological data summarized in Figure 5G. For the standard peptide RRRDDDSDDD (Figure 5A/B), the Lys198Arg mutation decreased the catalytic efficiency by a factor of 5.7, but for Thr phosphorylation (peptide RRRDDDTDDD; Figure 5E/F), the loss of catalytic efficiency is even higher (factor 10.2). Thus, the phosphoacceptor propensity of Thr compared to Ser is reduced by the Lys198Arg mutation as found by Caefer et al. (2021).

Likewise, the catalytic efficiencies we determined for the peptide RRRDDDSGGD (Figure 5C/D/G) are consistent with the preliminary data of Caefer et al. (2021). As mentioned above, these authors reported an increase of phosphopeptide motifs with glycine at the P+1 position when CK2 $\alpha^{\text{Lys198Arg}}$ rather than the wild-type was used to generate a bacterial phosphoproteome. In line with this, we observed no loss of catalytic efficiency by the Lys198Arg mutation for peptide RRRDDDSGGD in contrast to RRRDDDSDDD, but even a slight, albeit statistically not significant increase from $0.009 \mu\text{M}^{-1} \text{min}^{-1}$ to $0.014 \mu\text{M}^{-1} \text{min}^{-1}$ (factor 1.6). This shows that glycine is in fact a preferred P+1 residue in substrates of CK2 $\alpha^{\text{Lys198Arg}}$, and it supports the notion of Caefer et al. (2021) that CK2 $\alpha^{\text{Lys198Arg}}$ might have decidedly new and unique substrate proteins not phosphorylated under the catalysis of wild-type CK2.

CONCLUSION

In summary, the enzymological data of this work fit to its central structural finding that the Lys198Arg mutation causes a shift of the anion binding site at the P+1 loop. Furthermore, they support the conclusion drawn in the preliminary report of Caefer et al. (2021) that the CK2 α mutant Lys198Arg does not primarily lead to a loss of function, but to alterations of the phosphoacceptor preference and the substrate specificity. Taylor et al. (2012) emphasized that EPKs principally differ from metabolic enzymes because they are not evolutionarily optimized for substrate turnover and because the physiological

concentrations of their protein substrates are typically low and often in the same range as the enzyme concentrations themselves. Insofar, the general reduction of the catalytic activity of an EPK is perhaps less detrimental than subtle changes in substrate specificity which disturb regulatory networks. Since OCNDs is a neurodevelopmental disease and Lys198Arg the most frequent OCNDs mutation (Nakashima et al., 2019), specific proteins of the nervous system are probably differentially phosphorylated by CK2 α and the mutant CK2 $\alpha^{\text{Lys198Arg}}$. Caefer et al. (2021) predicted a number of ion channels localized in the axon of neurons as candidates for such a differential phosphorylation. It remains to be shown if these predictions are valid, which other changes of the CK2-dependent phosphoproteome (in particular in neurons) are caused by the mutation Lys198Arg and how these are linked to neurodevelopmental processes leading to the OCNDs phenotype. Such an understanding of the molecular basis of OCNDs may finally result in translational approaches and therapies.

DATA AVAILABILITY STATEMENT

The crystallographic data (atomic coordinates and structure factors) of the CK2 $\alpha^{\text{Lys198Arg}}$ /sulfate complex structure are available from the Protein Data Bank (PDB) under the accession code 7PSU : <https://doi.org/10.2210/pdb7PSU/pdb>.

REFERENCES

- Adams, P. D., Afonine, P. V., Bunkóczi, G., Chen, V. B., Davis, I. W., Echols, N., et al. (2010). PHENIX: A Comprehensive Python-Based System for Macromolecular Structure Solution. *Acta Crystallogr. D Biol. Cryst.* 66, 213–221. doi:10.1107/S0907444909052925
- Afonine, P. V., Grosse-Kunstleve, R. W., Echols, N., Headd, J. J., Moriarty, N. W., Mustyakimov, M., et al. (2012). Towards Automated Crystallographic Structure Refinement with phenix.refine. *Acta Crystallogr. D Biol. Cryst.* 68, 352–367. doi:10.1107/S0907444912001308
- Agard, N. J., Baskin, J. M., Prescher, J. A., Lo, A., and Bertozzi, C. R. (2006). A Comparative Study of Bioorthogonal Reactions with Azides. *ACS Chem. Biol.* 1, 644–648. doi:10.1021/cb6003228
- Akahira-Azuma, M., Tsurusaki, Y., Enomoto, Y., Mitsui, J., and Kurosawa, K. (2018). Refining the Clinical Phenotype of Okur-Chung Neurodevelopmental Syndrome. *Hum. Genome Var.* 5, 18011. doi:10.1038/hgv.2018.11
- Belloni, S., Fitzgibbon, M. J., Fox, T., Hsiao, H.-M., and Wilson, K. P. (1999). The Structure of Phosphorylated P38 γ Is Monomeric and Reveals a Conserved Activation-Loop Conformation. *Structure* 7, 1057–1065. doi:10.1016/s0969-2126(99)80173-7
- Berthon, A. S., Szarek, E., and Stratakis, C. (2015). PRKACA: The Catalytic Subunit of Protein Kinase A and Adrenocortical Tumors. *Front. Cell Dev. Biol.* 3, 26. doi:10.3389/fcell.2015.00026
- Bischoff, N., Olsen, B., Raaf, J., Bretner, M., Issinger, O.-G., and Niefind, K. (2011). Structure of the Human Protein Kinase CK2 Catalytic Subunit CK2 α' and Interaction Thermodynamics with the Regulatory Subunit CK2 β . *J. Mol. Biol.* 407, 1–12. doi:10.1016/j.jmb.2011.01.020
- Blanquet, P. R. (2000). Casein Kinase 2 as a Potentially Important Enzyme in the Nervous System. *Prog. Neurobiol.* 60, 211–246. doi:10.1016/s0304-0082(99)00026-x
- Boivin, S., Kozak, S., and Meijers, R. (2013). Optimization of Protein Purification and Characterization Using Thermofluor Screens. *Protein Expr. Purif.* 91, 192–206. doi:10.1016/j.pep.2013.08.002

AUTHOR CONTRIBUTIONS

JH and JJ designed the project. CW, DL, and JH solved the crystal structure and determined thermostabilities (DSF) as well as ITC-based affinities. AG and AN performed fluorescence quenching and enzyme kinetic measurements. All authors wrote the manuscript and approved its final version.

FUNDING

This work was kindly funded by the CSNK2A1 Foundation, San Francisco, United States, www.csnk2a1foundation.org (grant from October 26, 2020), and by the Deutsche Forschungsgemeinschaft (DFG) (grant NI 643/4-2).

ACKNOWLEDGMENTS

We are grateful for access to the protein crystallography facility (c2f.uni-koeln.de) and to the protein/protein interaction platform of the University of Cologne (pipc.uni-koeln.de). We thank the staff of the European Synchrotron Radiation Facility (ESRF), Grenoble, France, for assistance with X-ray diffraction data collection. The authors would like to express their special thanks and appreciation to the CSNK2A1 Foundation and its President and Founder Jennifer Sills.

- Boldyreff, B., Meggio, F., Pinna, L. A., and Issinger, O. G. (1993). Reconstitution of normal and Hyperactivated Forms of Casein Kinase-2 by Variably Mutated β -subunits. *Biochemistry* 32, 12672–12677. doi:10.1021/bi00210a016
- Borgo, C., D'Amore, C., Sarno, S., Salvi, M., and Ruzzene, M. (2021). Protein Kinase CK2: a Potential Therapeutic Target for Diverse Human Diseases. *Sig. Transduct. Target. Ther.* 6, 183. doi:10.1038/s41392-021-00567-7
- Brown, N. R., Noble, M. E. M., Endicott, J. A., and Johnson, L. N. (1999). The Structural Basis for Specificity of Substrate and Recruitment Peptides for Cyclin-dependent Kinases. *Nat. Cell Biol.* 1, 438–443. doi:10.1038/15674
- Caefer, D. M., Phan, N. Q., Liddle, J. C., Balsbaugh, J. L., O'Shea, J. P., Tzingounis, A. V., et al. (2021). The Okur-Chung Neurodevelopmental Syndrome (OCNDs) Mutation CK2 α^{K198R} Leads to a Rewiring of Kinase Specificity. *bioRxiv*. doi:10.1101/2021.04.05.438522
- Cao, Y., He, M., Gao, Z., Peng, Y., Li, Y., Li, L., et al. (2014). Activating Hotspot L205R Mutation in PRKACA and Adrenal Cushing's Syndrome. *Science* 344, 913–917. doi:10.1126/science.1249480
- Castello, J., Ragnauth, A., Friedman, E., and Rebholz, H. (2017). CK2-A New Emerging Target for Neurological and Psychiatric Disorders. *Pharmaceuticals* 10, 7. doi:10.3390/ph10010007
- Chin, J. W., Santoro, S. W., Martin, A. B., King, D. S., Wang, L., and Schultz, P. G. (2002). Addition of P-Azido-L-Phenylalanine to the Genetic Code of *Escherichia coli*. *J. Am. Chem. Soc.* 124, 9026–9027. doi:10.1021/ja027007w
- Chiu, A. T. G., Pei, S. L. C., Mak, C. C. Y., Leung, G. K. C., Yu, M. H. C., Lee, S. L., et al. (2018). Okur-Chung Neurodevelopmental Syndrome: Eight Additional Cases with Implications on Phenotype and Genotype Expansion. *Clin. Genet.* 93, 880–890. doi:10.1111/cge.13196
- Chou, M. F., Priscic, S., Lubner, J. M., Church, G. M., Husson, R. N., and Schwartz, D. (2012). Using Bacteria to Determine Protein Kinase Specificity and Predict Target Substrates. *PLoS One* 7, e52747. doi:10.1371/journal.pone.0052747
- Dominguez, I., Cruz-Gamero, J. M., Corasolla, V., Dacher, N., Rangasamy, S., Urbani, A., et al. (2021). Okur-Chung Neurodevelopmental Syndrome-Linked CK2 α Variants Have Reduced Kinase Activity. *Hum. Genet.* 140, 1077–1096. doi:10.1007/s00439-021-02280-5

- Emsley, P., Lohkamp, B., Scott, W. G., and Cowtan, K. (2010). Features and Development of Coot. *Acta Crystallogr. D Biol. Cryst.* 66, 486–501. doi:10.1107/S0907444910007493
- Ermakova, I., Boldyreff, B., Issinger, O.-G., and Niefind, K. (2003). Crystal Structure of a C-Terminal Deletion Mutant of Human Protein Kinase CK2 Catalytic Subunit. *J. Mol. Biol.* 330, 925–934. doi:10.1016/S0022-2836(03)00638-7
- Evans, P. R., and Murshudov, G. N. (2013). How Good Are My Data and what Is the Resolution? *Acta Crystallogr. D Biol. Cryst.* 69, 1204–1214. doi:10.1107/S0907444913000061
- Faust, M., and Montenarh, M. (2000). Subcellular Localization of Protein Kinase CK2. *Cel Tissue Res.* 301, 329–340. doi:10.1007/s004410000256
- Gratz, A., Götz, C., and Jose, J. (2010). A CE-Based Assay for Human Protein Kinase CK2 Activity Measurement and Inhibitor Screening. *Electrophoresis* 31, 634–640. doi:10.1002/elps.200900514
- Greenwood, J. A., Scott, C. W., Spreen, R. C., Caputo, C. B., and Johnson, G. V. (1994). Casein Kinase II Preferentially Phosphorylates Human Tau Isoforms Containing an Amino-Terminal Insert. Identification of Threonine 39 as the Primary Phosphate Acceptor. *J. Biol. Chem.* 269, 4373–4380. doi:10.1016/s0021-9258(17)41790-x
- Hübner, G. M., Larsen, J. N., Guerra, B., Niefind, K., Vrecl, M., and Issinger, O.-G. (2014). Evidence for Aggregation of Protein Kinase CK2 in the Cell: a Novel Strategy for Studying CK2 Holoenzyme Interaction by BRET². *Mol. Cell Biochem.* 397, 285–293. doi:10.1007/s11010-014-2196-y
- Kabsch, W. (2010). XDS. *Acta Crystallogr. D Biol. Cryst.* 66, 125–132. doi:10.1107/S0907444909047337
- Kannan, N., and Neuwald, A. F. (2004). Evolutionary Constraints Associated with Functional Specificity of the CMGC Protein Kinases MAPK, CDK, GSK, SRPK, DYRK, and CK2 α . *Protein Sci.* 13, 2059–2077. doi:10.1110/ps.04637904
- Lebrin, F., Chambaz, E. M., and Bianchini, L. (2001). A Role for Protein Kinase CK2 in Cell Proliferation: Evidence Using a Kinase-Inactive Mutant of CK2 Catalytic Subunit α . *Oncogene* 20, 2010–2022. doi:10.1038/sj.onc.1204307
- Loizou, J. I., El-Khamisy, S. F., Zlatanou, A., Moore, D. J., Chan, D. W., Qin, J., et al. (2004). The Protein Kinase CK2 Facilitates Repair of Chromosomal DNA Single-Strand Breaks. *Cell* 117, 17–28. doi:10.1016/s0092-8674(04)00206-5
- Lubner, J. M., Dodge-Kafka, K. L., Carlson, C. R., Church, G. M., Chou, M. F., and Schwartz, D. (2017). Cushing's Syndrome Mutant PKA L 205R Exhibits Altered Substrate Specificity. *FEBS Lett.* 591, 459–467. doi:10.1002/1873-3468.12562
- Lubner, J. M., Balsbaugh, J. L., Church, G. M., Chou, M. F., and Schwartz, D. (2018). Characterizing Protein Kinase Substrate Specificity Using the Proteomic Peptide Library (ProPeL) Approach. *Curr. Protoc. Chem. Biol.* 10, e38. doi:10.1002/cpch.38
- Manning, G., Whyte, D. B., Martinez, R., Hunter, T., and Sudarsanam, S. (2002). The Protein Kinase Complement of the Human Genome. *Science* 298, 1912–1934. doi:10.1126/science.1075762
- Marchiori, F., Meggio, F., Marin, O., Borin, G., Calderan, A., Ruzza, P., et al. (1988). Synthetic Peptide Substrates for Casein Kinase 2. Assessment of Minimum Structural Requirements for Phosphorylation. *Biochim. Biophys. Acta Bioenerg.* 971, 332–338. doi:10.1016/0167-4889(88)90149-810.1016/s0005-2728(88)80048-3
- Marin, O., Meggio, F., Sarno, S., Cesaro, L., Pagano, M. A., and Pinna, L. A. (1999). Tyrosine versus Serine/Threonine Phosphorylation by Protein Kinase Casein Kinase-2. *J. Biol. Chem.* 274, 29260–29265. doi:10.1074/jbc.274.41.29260
- McCoy, A. J., Grosse-Kunstleve, R. W., Adams, P. D., Winn, M. D., Storoni, L. C., and Read, R. J. (2007). Phaser crystallographic Software. *J. Appl. Cryst.* 40, 658–674. doi:10.1107/S0021889807021206
- Meggio, F., and Pinna, L. A. (2003). One-thousand-and-one Substrates of Protein Kinase CK2? *FASEB J.* 17, 349–368. doi:10.1096/fj.02-0473rev
- Montenarh, M. (2016). Protein Kinase CK2 in DNA Damage and Repair. *Transl. Cancer Res.* 5, 49–63. doi:10.3978/j.issn.2218-676X.2016.01.09
- Nakashima, M., Tohyama, J., Nakagawa, E., Watanabe, Y., Siew, C. n. G., Kwong, C. S., et al. (2019). Identification of De Novo CSNK2A1 and CSNK2B Variants in Cases of Global Developmental Delay with Seizures. *J. Hum. Genet.* 64, 313–322. doi:10.1038/s10038-018-0559-z
- Needham, E. J., Parker, B. L., Burykin, T., James, D. E., and Humphrey, S. J. (2019). Illuminating the Dark Phosphoproteome. *Sci. Signal.* 12, eaau8645. doi:10.1126/scisignal.aau8645
- Niefind, K., and Issinger, O.-G. (2005). Primary and Secondary Interactions between CK2 α and CK2 β lead to Ring-like Structures in the Crystals of the CK2 Holoenzyme. *Mol. Cell. Biochem.* 274, 3–14. doi:10.1007/s11010-005-3114-0
- Niefind, K., Guerra, B., Ermakova, I., and Issinger, O.-G. (2000). Crystallization and Preliminary Characterization of Crystals of Human Protein Kinase CK2. *Acta Crystallogr. D Biol. Cryst.* 56, 1680–1684. doi:10.1107/s0907444900013627
- Niefind, K., Guerra, B., Ermakova, I., and Issinger, O. (2001). Crystal Structure of Human Protein Kinase CK2: Insights into Basic Properties of the CK2 Holoenzyme. *EMBO J.* 20, 5320–5331. doi:10.1093/emboj/20.19.5320
- Niefind, K., Yde, C. W., Ermakova, I., and Issinger, O.-G. (2007). Evolved to Be Active: Sulfate Ions Define Substrate Recognition Sites of CK2 α and Emphasise its Exceptional Role within the CMGC Family of Eukaryotic Protein Kinases. *J. Mol. Biol.* 370, 427–438. doi:10.1016/j.jmb.2007.04.068
- Nienberg, C., Retterath, A., Becher, K.-S., Saenger, T., Mootz, H., and Jose, J. (2016). Site-Specific Labeling of Protein Kinase CK2: Combining Surface Display and Click Chemistry for Drug Discovery Applications. *Pharmaceuticals* 9, 36. doi:10.3390/ph9030036
- Niesen, F. H., Berglund, H., and Vedadi, M. (2007). The Use of Differential Scanning Fluorimetry to Detect Ligand Interactions that Promote Protein Stability. *Nat. Protoc.* 2, 2212–2221. doi:10.1038/nprot.2007.321
- Nitta, R. T., Gholamin, S., Feroze, A. H., Agarwal, M., Cheshier, S. H., Mitra, S. S., et al. (2015). Casein Kinase 2 α Regulates Glioblastoma Brain Tumor-Initiating Cell Growth through the β -catenin Pathway. *Oncogene* 34, 3688–3699. doi:10.1038/onc.2014.299
- Okur, V., Cho, M. T., Henderson, L., Retterer, K., Schneider, M., Sattler, S., et al. (2016). De Novo mutations in CSNK2A1 Are Associated with Neurodevelopmental Abnormalities and Dysmorphic Features. *Hum. Genet.* 135, 699–705. doi:10.1007/s00439-016-1661-y
- Owen, C. I., Bowden, R., Parker, M. J., Patterson, J., Patterson, J., Price, S., et al. (2018). Extending the Phenotype Associated with the CSNK2A1-Related Okur-Chung Syndrome-A Clinical Study of 11 Individuals. *Am. J. Med. Genet.* 176, 1108–1114. doi:10.1002/ajmg.a.38610
- Pietsch, M., Viht, K., Schnitzler, A., Ekambaram, R., Steinkrüger, M., Enkvist, E., et al. (2020). Unexpected CK2 β -Antagonistic Functionality of Bisubstrate Inhibitors Targeting Protein Kinase CK2. *Bioorg. Chem.* 96, 103608. doi:10.1016/j.bioorg.2020.103608
- Poole, A., Poore, T., Bandhakavi, S., McCann, R. O., Hanna, D. E., and Glover, C. V. C. (2005). A Global View of CK2 Function and Regulation. *Mol. Cell. Biochem.* 274, 163–170. doi:10.1007/s11010-005-2945-z
- PyMOL (2013). *The PyMOL Molecular Graphics System*. Version 1.7. New York, NY: Schrödinger, LLC.
- Raaf, J., Brunstein, E., Issinger, O. G., and Niefind, K. (2008). The Interaction of CK2 α and CK2 β , the Subunits of Protein Kinase CK2, Requires CK2 β in a Preformed Conformation and Is Enthalpically Driven. *Protein Sci.* 17, 2180–2186. doi:10.1110/ps.037770.108
- Raaf, J., Bischoff, N., Klopffleisch, K., Brunstein, E., Olsen, B. B., Vilk, G., et al. (2011). Interaction between CK2 α and CK2 β , the Subunits of Protein Kinase CK2: Thermodynamic Contributions of Key Residues on the CK2 α Surface. *Biochemistry* 50, 512–522. doi:10.1021/bi1013563
- Raaf, J., Guerra, B., Neundorff, I., Bopp, B., Issinger, O.-G., Jose, J., et al. (2013). First Structure of Protein Kinase CK2 Catalytic Subunit with an Effective CK2 β -Competitive Ligand. *ACS Chem. Biol.* 8, 901–907. doi:10.1021/cb3007133
- Rosenberger, A. F. N., Morrema, T. H. J., Gerritsen, W. H., van Haastert, E. S., Snkhchyan, H., Hilhorst, R., et al. (2016). Increased Occurrence of Protein Kinase CK2 in Astrocytes in Alzheimer's Disease Pathology. *J. Neuroinflammation* 13, 4. doi:10.1186/s12974-015-0470-x
- Rowe, A. L., Gibson, S. A., Meares, G. P., Rajbhandari, R., Nozell, S. E., Dees, K. J., et al. (2017). Protein Kinase CK2 Is Important for the Function of Glioblastoma Brain Tumor Initiating Cells. *J. Neurooncol.* 132, 219–229. doi:10.1007/s11060-017-2378-z
- Ryu, M. Y., Kim, D. W., Arima, K., Mouradian, M. M., Kim, S. U., and Lee, G. (2008). Localization of CKII β Subunits in Lewy Bodies of Parkinson's Disease. *J. Neurol. Sci.* 266, 9–12. doi:10.1016/j.jns.2007.08.027
- Salvi, M., Sarno, S., Cesaro, L., Nakamura, H., and Pinna, L. A. (2009). Extraordinary Pleiotropy of Protein Kinase CK2 Revealed by Weblogo Phosphoproteome Analysis. *Biochim. Biophys. Acta Mol. Cell Res.* 1793, 847–859. doi:10.1016/j.bbamcr.2009.01.013

- Sarno, S., Boldyreff, B., Marin, O., Guerra, B., Meggio, F., Issinger, O. G., et al. (1995). Mapping the Residues of Protein Kinase CK2 Implicated in Substrate Recognition: Mutagenesis of Conserved Basic Residues in the α -Subunit. *Biochem. Biophys. Res. Commun.* 206, 171–179. doi:10.1006/bbrc.1995.1024
- Sarno, S., Vaglio, P., Marin, O., Issinger, O.-G., Ruffato, K., and Pinna, L. A. (1997). Mutational Analysis of Residues Implicated in the Interaction between Protein Kinase CK2 and Peptide Substrates. *Biochemistry* 36, 11717–11724. doi:10.1021/bi9705772
- Schnitzler, A., and Niefind, K. (2021). Structural Basis for the Design of Bisubstrate Inhibitors of Protein Kinase CK2 provided by Complex Structures with the Substrate-Competitive Inhibitor Heparin. *Eur. J. Med. Chem.* 214, 113223. doi:10.1016/j.ejmech.2021.113223
- Schnitzler, A., Olsen, B. B., Issinger, O.-G., and Niefind, K. (2014). The Protein Kinase CK2^{Andante} Holoenzyme Structure Supports Proposed Models of Autoregulation and Trans-Autophosphorylation. *J. Mol. Biol.* 426, 1871–1882. doi:10.1016/j.jmb.2014.02.018
- Shibazaki, C., Arai, S., Shimizu, R., Saeki, M., Kinoshita, T., Ostermann, A., et al. (2018). Hydration Structures of the Human Protein Kinase CK2 α Clarified by Joint Neutron and X-ray Crystallography. *J. Mol. Biol.* 430, 5094–5104. doi:10.1016/j.jmb.2018.09.018
- St-Denis, N. A., and Litchfield, D. W. (2009). Protein Kinase CK2 in Health and Disease. *Cell. Mol. Life Sci.* 66, 1817–1829. doi:10.1007/s00018-009-9150-2
- Taylor, S. S., Keshwani, M. M., Steichen, J. M., and Kornev, A. P. (2012). Evolution of the Eukaryotic Protein Kinases as Dynamic Molecular Switches. *Phil. Trans. R. Soc. B* 367, 2517–2528. doi:10.1098/rstb.2012.0054
- Tickle, I. J., Flensburg, C., Keller, P., Paciorek, W., Sharff, A., Vornrhein, C., et al. (2018). STARANISO. Cambridge, United Kingdom: Global Phasing Ltd.
- Trinh, J., Hüning, I., Budler, N., Hingst, V., Lohmann, K., and Gillessen-Kaesbach, G. (2017). A Novel De Novo Mutation in CSNK2A1: Reinforcing the Link to Neurodevelopmental Abnormalities and Dysmorphic Features. *J. Hum. Genet.* 62, 1005–1006. doi:10.1038/jhg.2017.73
- Vornrhein, C., Flensburg, C., Keller, P., Sharff, A., Smart, O., Paciorek, W., et al. (2011). Data Processing and Analysis with the autoPROC toolbox. *Acta Crystallogr. D Biol. Cryst.* 67, 293–302. doi:10.1107/S0907444911007773
- Walker, C., Wang, Y., Olivieri, C., Karamafrooz, A., Casby, J., Bathon, K., et al. (2019). Cushing's Syndrome Driver Mutation Disrupts Protein Kinase A Allosteric Network, Altering Both Regulation and Substrate Specificity. *Sci. Adv.* 5, eaaw9298. doi:10.1126/sciadv.aaw9298
- Winn, M. D., Ballard, C. C., Cowtan, K. D., Dodson, E. J., Emsley, P., Evans, P. R., et al. (2011). Overview of the CCP4 Suite and Current Developments. *Acta Crystallogr. D Biol. Cryst.* 67, 235–242. doi:10.1107/S0907444910045749
- Wu, R.-h., Tang, W.-t., Qiu, K.-y., Li, X.-j., Tang, D.-x., Meng, Z., et al. (2021). Identification of Novel CSNK2A1 Variants and the Genotype-Phenotype Relationship in Patients with Okur-Chung Neurodevelopmental Syndrome: a Case Report and Systematic Literature Review. *J. Int. Med. Res.* 49, 030006052110170. doi:10.1177/03000605211017063
- Xu, S., Lian, Q., Wu, J., Li, L., and Song, J. (2020). Dual Molecular Diagnosis of Tricho-Rhino-Phalangeal Syndrome Type I and Okur-Chung Neurodevelopmental Syndrome in One Chinese Patient: a Case Report. *BMC Med. Genet.* 21, 158. doi:10.1186/s12881-020-01096-w
- Zheng, Y., McFarland, B. C., Drygin, D., Yu, H., Bellis, S. L., Kim, H., et al. (2013). Targeting Protein Kinase CK2 Suppresses Prosurvival Signaling Pathways and Growth of Glioblastoma. *Clin. Cancer Res.* 19, 6484–6494. doi:10.1158/1078-0432.Ccr-13-0265

Conflict of Interest: The authors declare that the research was conducted in the absence of any commercial or financial relationships that could be construed as a potential conflict of interest.

Publisher's Note: All claims expressed in this article are solely those of the authors and do not necessarily represent those of their affiliated organizations, or those of the publisher, the editors and the reviewers. Any product that may be evaluated in this article, or claim that may be made by its manufacturer, is not guaranteed or endorsed by the publisher.

Copyright © 2022 Werner, Gast, Lindenblatt, Nickelsen, Niefind, Jose and Hochscherf. This is an open-access article distributed under the terms of the Creative Commons Attribution License (CC BY). The use, distribution or reproduction in other forums is permitted, provided the original author(s) and the copyright owner(s) are credited and that the original publication in this journal is cited, in accordance with accepted academic practice. No use, distribution or reproduction is permitted which does not comply with these terms.



The Okur-Chung Neurodevelopmental Syndrome Mutation CK2^{K198R} Leads to a Rewiring of Kinase Specificity

Danielle M. Caefer¹, Nhat Q. Phan¹, Jennifer C. Liddle², Jeremy L. Balsbaugh², Joseph P. O'Shea¹, Anastasios V. Zingounis¹, Daniel Schwartz^{1*}

¹Department of Physiology and Neurobiology, University of Connecticut, Storrs, CT, United States, ²Center for Open Research Resources and Equipment, Proteomics and Metabolomics Facility, University of Connecticut, Storrs, CT, United States

OPEN ACCESS

Edited by:

Andrea Venerando,
University of Padua, Italy

Reviewed by:

Jun Mitsui,
The University of Tokyo, Japan
Stefania Sarno,
University of Padua, Italy

*Correspondence:

Daniel Schwartz
daniel.schwartz@uconn.edu

Specialty section:

This article was submitted to
Cellular Biochemistry,
a section of the journal
Frontiers in Molecular Biosciences

Received: 08 January 2022

Accepted: 22 March 2022

Published: 19 April 2022

Citation:

Caefer DM, Phan NQ, Liddle JC, Balsbaugh JL, O'Shea JP, Zingounis AV and Schwartz D (2022) The Okur-Chung Neurodevelopmental Syndrome Mutation CK2^{K198R} Leads to a Rewiring of Kinase Specificity. *Front. Mol. Biosci.* 9:850661. doi: 10.3389/fmolb.2022.850661

Okur-Chung Neurodevelopmental Syndrome (OCNDS) is caused by heterozygous mutations to the *CSNK2A1* gene, which encodes the alpha subunit of protein kinase CK2. The most frequently occurring mutation is lysine 198 to arginine (K198R). To investigate the impact of this mutation, we first generated a high-resolution phosphorylation motif of CK2^{WT}, including the first characterization of specificity for tyrosine phosphorylation activity. A second high resolution motif representing CK2^{K198R} substrate specificity was also generated. Here we report the impact of the OCNDS associated CK2^{K198R} mutation. Contrary to prior speculation, the mutation does not result in a complete loss of function, but rather shifts the substrate specificity of the kinase. Broadly speaking the mutation leads to 1) a decreased preference for acidic residues in the +1 position, 2) a decreased preference for threonine phosphorylation, 3) an increased preference for tyrosine phosphorylation, and 4) an alteration of the tyrosine phosphorylation specificity motif. To further investigate the result of this mutation we have developed a probability-based scoring method, allowing us to predict shifts in phosphorylation in the K198R mutant relative to the wild type kinase. As an initial step we have applied the methodology to the set of axonally localized ion channels in an effort to uncover potential alterations of the phosphoproteome associated with the OCNDS disease condition.

Keywords: CK2, Okur-Chung neurodevelopmental syndrome, kinase specificity, proteomics, ProPeL, phosphorylation, mass spectrometry

INTRODUCTION

Okur-Chung Neurodevelopmental Syndrome (OCNDS) is broadly characterized by delayed psychomotor development and intellectual disability (Okur et al., 2016). The disorder has been linked to various heterozygous mutations on the *CSNK2A1* gene, which encodes the alpha subunit of protein kinase CK2, a well-characterized and conserved serine/threonine protein kinase (Pinna, 1990, 2003; Meggio and Pinna, 2003). Of the mutations associated with OCNDS, the mutation of lysine-198 to arginine (K198R) has been most frequently observed. The K198R mutation has been speculated to result in a loss of kinase function (Chiu et al., 2018), and this speculation was more recently thought to be confirmed (Dominguez et al., 2021). Interestingly however, lysine-198 is located in the activation segment of CK2 and had been previously implicated in the acidic residue preference of CK2 at the +1 position relative to the phosphoacceptor (Sarno et al., 1997).

Furthermore, Sarno et al. demonstrated that while the K198A mutation reduced phosphorylation of substrates with a +1 acidic residue, it allowed for efficient phosphorylation of substrates with a +1 alanine (Sarno et al., 1996). Taken together, we posited that the CK2^{K198R} mutation may not result in a complete loss of kinase activity, but rather a shift in substrate specificity. To determine the impact on specificity of the CK2^{K198R} mutation we implemented the ProPeL method (Lubner et al., 2018) to generate a high-resolution motif of CK2^{WT} and CK2^{K198R}. Additionally, we utilized a probabilistic strategy to determine the differential likelihood of modification for serine, threonine, and tyrosine residues on axonally localized ion channels under wild type and mutant kinase conditions.

MATERIALS AND METHODS

Plasmids

For bacterial expression, a plasmid containing the human CSNK2A1 gene in an Invitrogen Gateway donor vector (pDONR223) was provided by The Broad Institute and was transferred to the pDEST17 backbone following the standard Gateway Protocol (Life Technologies). Generation of the CK2^{K198R} mutant was done using the Q5[®] Site-Directed Mutagenesis Kit (New England BioLabs).

ProPeL Experiments for Motif Determination

The Proteomic Peptide Library (ProPeL) approach is a mass spectrometry-based method to experimentally determine high-resolution kinase specificity motifs. In this method, an exogenous kinase of interest is expressed in *Escherichia coli* and phosphorylates the endogenous proteome according to its native substrate preferences. These phosphorylated proteins can then be identified by LC-MS/MS to create a list of phosphorylation sites to be used to visualize substrate specificity. ProPeL experiments were carried out as previously described (Chou et al., 2012; Lubner et al., 2018) with the following conditions for *in vivo* proteome phosphorylation: all CK2 constructs were expressed in *E. coli* OverExpress C43 (DE3) cells (Lucigen) by IPTG induction. Optimal expression conditions were determined to be mid-log induction followed by expression for 24 h at 37°C in TB media (data not shown).

Western Blotting

Comparable expression of CK2^{WT} and CK2^{K198R} was confirmed by western blotting using the primary antibody Anti-CSNK2A1 antibody (Abcam ab10466) at a 1/5,000 dilution and the secondary antibody IRDye[®] 680RD Donkey anti-Rabbit IgG at a 1/5,000 dilution.

Untargeted Protein Identification via Tandem Mass Spectrometry

Peptide samples were subjected to mass analysis using a Thermo Scientific Ultimate 3000 RSLCnano ultra-high performance

liquid chromatography (UPLC) system coupled to a high-resolution Thermo Scientific Q Exactive HF mass spectrometer. An aliquot of each peptide preparation in Solvent A (0.1% formic acid in H₂O) was injected onto a Waters nanoEase M/Z Peptide BEH C18 analytical column (130Å, 1.7 µm, 75 µm × 250 mm) and separated by reversed-phase UPLC using a gradient of 4–30% Solvent B (0.1% formic acid in acetonitrile) over a 100-min gradient at 300 nL/min flow. Peptides were eluted directly into the Q Exactive HF using positive mode nanoflow electrospray ionization and 1.5 kV capillary voltage. MS scan acquisition parameters included 60,000 resolution, 1e6 AGC target, maximum inject time of 60 ms, and a 300–1800 m/z mass range. Data-dependent MS/MS scan acquisition parameters included 15,000 resolution, 1e5 AGC target, maximum ion time of 40 ms, loop count of 15, isolation window of 2.0 m/z, dynamic exclusion window of 30 s, normalized collision energy of 27, and charge exclusion “on” for all unassigned, +1, and >+8 charged species.

Peptides were identified using MaxQuant (v1.6.10.43) and the embedded Andromeda search engine (Cox and Mann, 2008). The raw data was searched against three databases: an in-house-generated protein database consisting of 6xHis-tagged CK2 wildtype and mutant sequences, the complete UniProt *E. coli* reference proteome (identifier UP0000068040, accessed 11 September 2020), and the MaxQuant contaminants database. Variable modifications were oxidation of Met, acetylation of protein N- termini, deamidation of Asn/Gln, and for enriched samples, phosphorylation of Ser/Thr/Tyr. Carbamidomethylation of Cys was set as a fixed modification. Protease specificity was set to trypsin, allowing a maximum of two missed cleavages. LFQ quantification was enabled. All results were filtered to a 1% false discovery rate at the peptide spectrum match and protein levels; all other parameters were kept at default values. MaxQuant-derived output was further analyzed in accordance with the ProPeL method (Chou et al., 2012).

Probability-Based Prediction of CK2^{WT} and CK2^{K198R} Phosphorylation Sites

Given that the ProPeL methodology for kinase motif determination is carried out in the context of a closed system (the *E. coli* expressed proteome) the scoring of phosphorylated and unphosphorylated serine, threonine, and tyrosine residues in *E. coli* could be used to convert motif scores to probabilities of modification. Specifically, phosphorylated 15mers (for either the wild type or K198R data set) were mapped back onto the UniProt reference K12 *E. coli* proteome to generate a list of expressed proteins phosphorylated by CK2 in *E. coli*. These proteins were then subjected to a full trypsin digestion *in silico* and resultant peptides with a length up to 50 residues were retained to generate a list of all potential phosphorylation sites that could have been hypothetically observed in our experiments. Seven residues upstream and downstream from each serine, threonine, and tyrosine residue in these peptides was extracted to create a complete list of serine, threonine, and

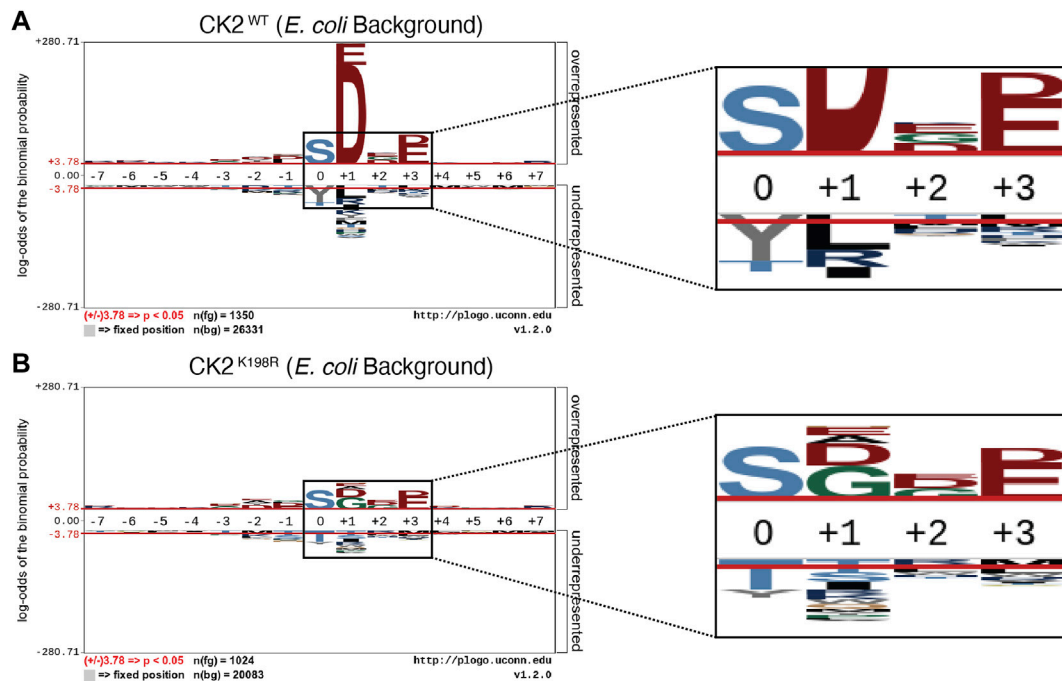


FIGURE 1 | CK2^{K198R} mutation shifts overall specificity motif. Substrate specificity of CK2^{WT} (A) and CK2^{K198R} (B). The CK2^{K198R} mutation results in a decreased preference for acidic (D/E) residues in the +1 position as well as a reordering of phosphoacceptor preference. In CK2^{K198R}, a decreased preference for threonine is paired with an increase in preference for tyrosine.

tyrosine-centered 15mers. Each 15mer was labeled as either positive or negative depending on whether it was observed to be phosphorylated in our ProPeL experiments, resulting in 1,350 positive (phosphorylated) and 26,331 negative (not observed to be phosphorylated) 15mers in the CK2^{WT} data set, and 1,024 positive and 20,083 negative 15mers in the CK2^{K198R} data set. Every peptide was scored using the appropriate wild type or K198R serine, threonine, or tyrosine-centered position weight matrix derived from the log-odds binomial probabilities observed in the corresponding serine, threonine, or tyrosine-centered pLogo, as we have shown previously (Schwartz et al., 2009). Note, the value for the central phosphorylated residue was derived from pLogo containing phosphorylated serine, threonine, and tyrosine-centered 15mers relative to presumed unphosphorylated serine, threonine, and tyrosine-centered 15mers (i.e., the pLogo with the unfixed central residue, see **Figure 1**). The complete set of scored 15mers was sorted in descending order and was used as a reference table to determine probabilities of modification based on score - specifically by taking the number of positive peptides above a score threshold divided by the total number of positive and negative peptides above a score threshold. Complete reference tables for CK2^{WT} and CK2^{K198R} are available in **Supplementary Tables S5, S6**. This methodology was utilized to score and assign probabilities of modification to all serine, threonine, and tyrosine residues in human axonally localized ion channels (see **Table 1, Supplementary Table S7**).

RESULTS

CK2^{K198R} is an Active Kinase

To obtain a higher resolution motif than we previously published in 2012 (Chou et al., 2012) for CK2^{WT}, several new ProPeL experiments were carried out utilizing more sensitive instrumentation that allowed confident identification of low abundance phosphorylated peptides that escaped identification previously. Experiments with CK2^{WT} identified 3,894 tryptic phosphopeptides (**Supplementary Table S1**) with 2,845 phosphopeptides classified as high confidence (i.e., containing at least one phosphorylation site with greater than 0.9 probability of localization determined by MaxQuant/Andromeda). Parallel ProPeL experiments with CK2^{K198R} identified 3,322 (**Supplementary Table S2**) tryptic phosphopeptides with 2,439 phosphopeptides classified as high confidence. Each high confidence phosphorylation site was mapped back to the UniProt reference K12 *E. coli* proteome and extended to create lists of unique 15mers as previously described (Lubner et al., 2018). Finally, 312 phosphorylation sites detected by our group and others as endogenous to *E. coli* (Macek et al., 2008; Chou et al., 2012; Soares et al., 2013; Lubner et al., 2016) were removed from each list prior to motif analysis. This process yielded a data set comprised of 1,350 unique phosphorylation sites (818 pS, 422 pT, 110 pY) for CK2^{WT} (**Supplementary Table S3**) and 1,024 unique phosphorylation sites (619 pS, 251 pT, 154 pY) for CK2^{K198R} (**Supplementary Table S4**).

Taken together these results indicate that CK2^{K198R} is an active kinase able to phosphorylate substrates under *in vivo* conditions. Furthermore, given that the CK2^{WT} and CK2^{K198R} ProPeL experiments were carried out under identical conditions, and western blotting revealed comparable levels of protein expression (**Supplementary Figure S1**), the number of non-unique phosphorylation sites identified could be used as a proxy for kinase activity. We identified 5,362 non-unique phosphorylation sites attributed to CK2^{WT} and 4,146 non-unique phosphorylation sites attributed to CK2^{K198R}. When considering the total amount of material analyzed by LC-MS/MS for each kinase (1570 ng for CK2^{WT}, 1430 ng for CK2^{K198R}) the overall kinase activity of CK2^{K198R} can be approximated at 85% of CK2^{WT}, thus suggesting that the OCNDS CK2^{K198R} mutation results in only a slight decrease in kinase activity relative to wild type CK2. This observed activity of CK2^{K198R} stands in contrast to previous results indicating that the mutation results in a loss of activity (Dominguez et al., 2021).

CK2^{K198R} Exhibits an Altered Substrate Specificity

The generation of pLogos (O'Shea et al., 2013) provides a visual representation of the relative statistical significance of amino acids (represented by single letter abbreviations) at positions within a 15-residue window of a central phosphoacceptor residue. Amino acid preferences at each position are stacked and sized according to significance relative to the background data set. The most significant residues are displayed with the largest size and are positioned closest to the *x*-axis. Background data sets representing unphosphorylated residues were created independently for CK2^{WT} and CK2^{K198R}. Each background was generated through the *in silico* tryptic digestion of proteins identified by the presence of at least one phosphorylated peptide in either the CK2^{WT} or CK2^{K198R} experiments. Background lists included serine, threonine, and tyrosine sites in proteins known to be expressed that could potentially have been observed *via* MS/MS but were never detected in a phosphorylated state. These sites were subsequently extended seven amino acids upstream and downstream of each phosphorylatable residue to generate two unique background lists for use in pLogo generation.

The overall pLogo generated with the current CK2^{WT} data set (**Figure 1A**) recapitulated our previously published CK2^{WT} pLogo (Chou et al., 2012); namely a strong preference for acidic residues (D/E) at the +1 and +3 positions with the +1 position being the most statistically significant position in the pLogo overall. Consistent with our prior hypothesis that the K198R mutation would impact the specificity of the +1 position, the pLogo generated for CK2^{K198R} indicated a massively decreased preference for acidic (D/E) residues in the +1 position, as well as an increased preference for both glycine and alanine, with glycine superseding aspartate to become the most statistically significant residue at the +1 position (**Figure 1B**). Interestingly, the reduction in

significance was limited to the +1 position, as the preference for acidic residues at the +3 position was maintained at nearly identical levels (compare **Figures 1A,B**).

Further comparison of the CK2^{WT} and CK2^{K198R} derived pLogos indicated an unexpected reordering of phosphoacceptor preference. Though both mutant and wild type CK2 strongly favored serine phosphorylation over threonine or tyrosine phosphorylation, CK2^{WT} strongly disfavored tyrosine as a phosphoacceptor and was relatively neutral towards threonine as a phosphoacceptor (**Figure 1A**), while CK2^{K198R} strongly disfavored threonine as a phosphoacceptor and was relatively neutral towards tyrosine as a phosphoacceptor. It is important to note that although CK2^{K198R} did not display a preference for tyrosine phosphorylation (i.e., it was not phosphorylated by CK2^{K198R} at a level greater than its relative frequency among phosphorylatable residues), its shift is significant as it represents a near doubling of the proportion of phosphorylated tyrosine residues in the K198R data set (15%) relative to wild type (8.1%).

CK2^{K198R} Exhibits Altered Substrate Specificity at the Phosphoacceptor Level

We next investigated whether the decreased preference for acidic residues at the +1 position observed in the overall CK2^{K198R} pLogo was consistent among each individual phosphoacceptor. To investigate this question, we fixed each central residue (serine, threonine, and tyrosine) to generate phosphoacceptor specific pLogos as shown in **Figure 2**. As was observed in the overall pLogo, the serine and threonine centered CK2^{WT} pLogos indicated a preference for acidic residues at the +1 and +3 positions (**Figures 2A,B**). The preference for acidic residues was only significant at the +1 position of the tyrosine centered pLogo (**Figure 2C**). In the CK2^{K198R} serine, threonine, and tyrosine centered pLogos (**Figures 2D–F**), the decreased preference for acidic residues at the +1 position was preserved. Interestingly however, the tyrosine centered pLogo suggested a modest increased preference for acidic residues at the –1 and –2 positions (**Figure 2F**). Importantly, the pLogos shown in **Figures 2C,F** represent the first-ever documentation of a tyrosine motif specificity for CK2.

CK2^{K198R} Mutation Substantially Alters the Landscape of CK2 Phosphorylation at the Site Level

The ProPeL methodology, carried out in living *E. coli*, provided a unique opportunity to explore the gain/loss of CK2^{WT} and CK2^{K198R} substrates at the site level. Specifically, we were interested in investigating whether our observed decreased preference for acidic residues at the +1 position in CK2^{K198R} resulted from the loss of existing *E. coli* substrates, the addition of completely new substrates, or a combination of the two. **Figure 3A** shows a Venn diagram representing phosphorylation site overlap between CK2^{WT} and CK2^{K198R}

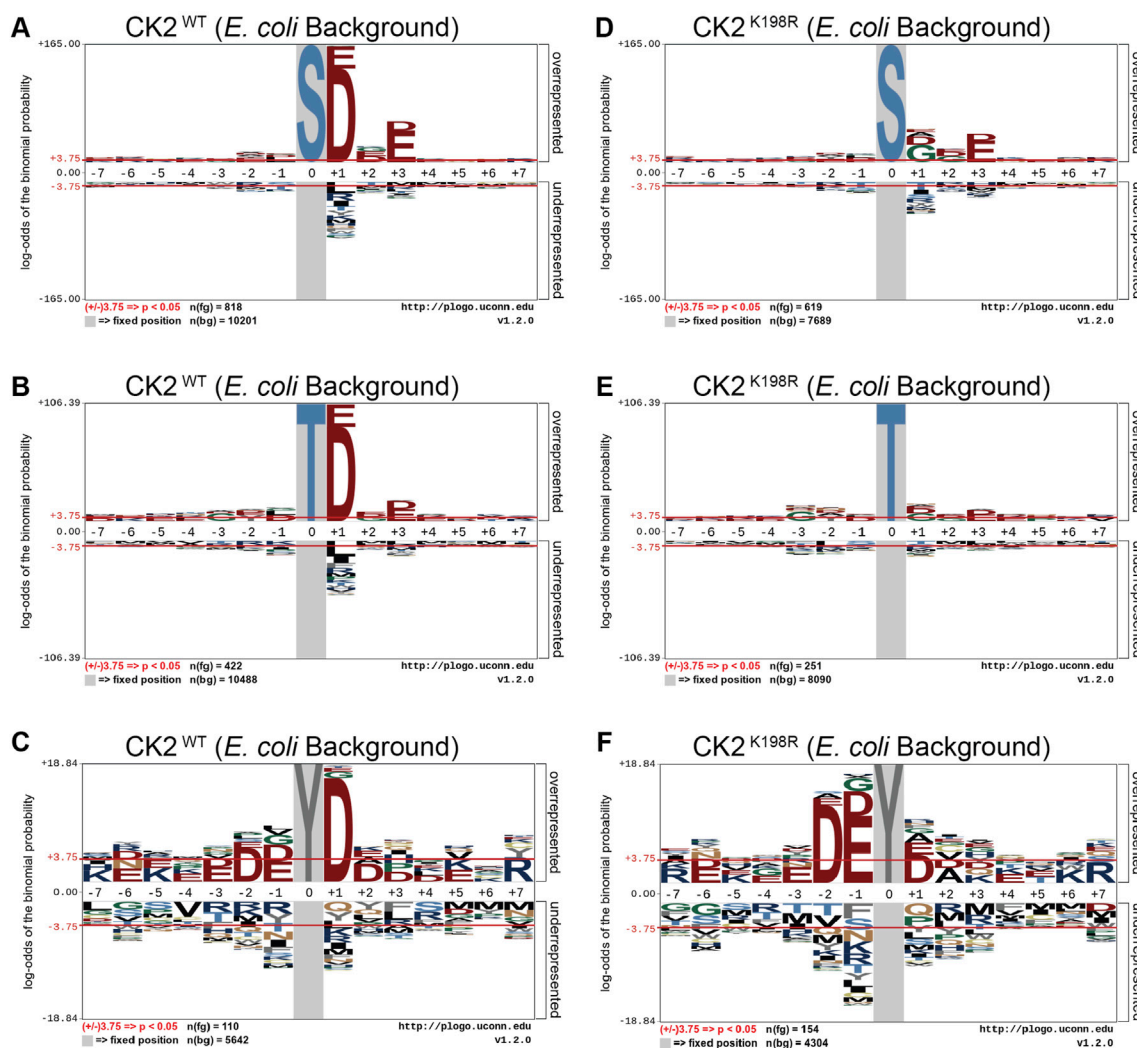


FIGURE 2 | CK2^{K198R} exhibits altered +1 substrate specificity. Substrate specificity of CK2^{WT} (A–C) and CK2^{K198R} (D–F). The CK2^{K198R} mutation results in a decreased preference for acidic (D/E) residues in the +1 position for S and T centered phosphorylation sites. For Y centered phosphorylation sites, the preference for acidic residues is shifted to the –2 and –1 positions.

indicating the latter; namely, approximately half of the CK2^{WT} sites were detected in the CK2^{K198R} mutant, yet over a third of the sites detected in the K198R mutant were not observed in the wild type kinase data set.

To further explore motif differences between the three subsets noted in the Venn diagram, pLogos were generated for each subset (Figures 3B–D). The pLogo generated from the set of phosphorylation sites unique to CK2^{WT} included a highly pronounced +1 aspartate specificity that became more attenuated in the overlapping data set and was entirely replaced by glycine (and to a lesser extent, alanine and leucine) in the sites unique to CK2^{K198R}. The +3 acidic residues were similarly attenuated in the mutant kinase data set. Finally, with regard to the phosphoacceptor residue, the phosphorylation sites unique to CK2^{WT} showed a highly significant disfavoring of tyrosine residues relative to serine residues that was lost in the CK2^{K198R}

mutant (which displayed a general neutrality to the phosphoacceptor residue).

Taken together these results point to a significant shift at the substrate level for the K198R mutant kinase, whereby the most canonical wild type CK2 phosphorylation sites are either lost or phosphorylated with decreased efficiency, coupled with a large increase in previously unphosphorylated sites.

Predictions of CK2^{WT} and CK2^{K198R} Phosphorylation Sites

CK2^{K198R} is the most frequently occurring mutation in patients with OCNDs (Chiu et al., 2018; Owen et al., 2018). Substrate rewiring in this mutant, indicated by our specificity and *E. coli* substrate analyses, is likely to contribute to the etiology of OCNDs. In an effort to offer a potential mechanism for the role of CK2^{K198R} in OCNDs pathology we

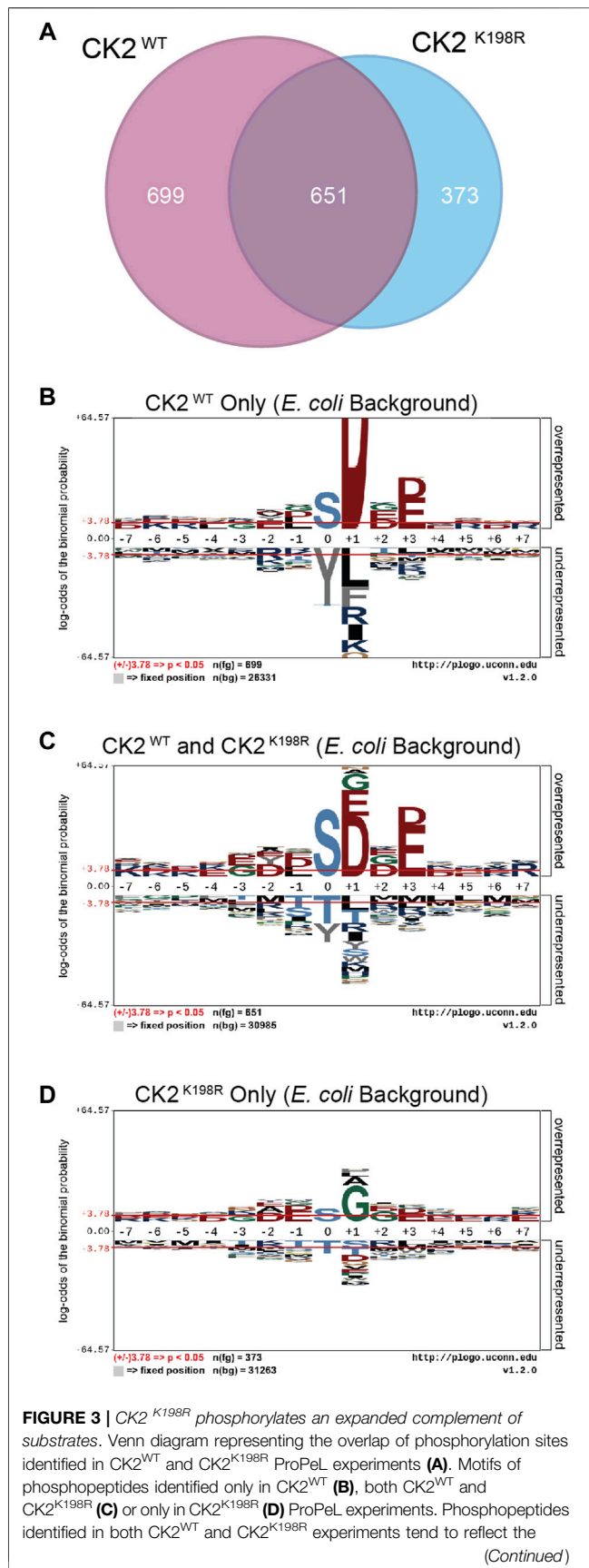


FIGURE 3 | canonical CK2^{WT} motif. Those identified only in CK2^{K198R} experiments have a much wider complement of amino acids in the +1 position, indicating increased promiscuity in this position. The phosphoacceptor abundance is also altered, reflecting an increased preference for tyrosine in the K198R mutant.

developed a predictive strategy for determining CK2^{WT} and CK2^{K198R} phosphorylation sites on human proteins based on our prior *scan-x* post-translational modification predictor (Schwartz et al., 2009), but with the advantage of calculated probabilities of modification (see Methods). Due to the neurodevelopmental nature of OCNDS, in the present study we focused our predictions of potential CK2^{WT} and CK2^{K198R} phosphorylation sites to ion channels localized to the axon. The top ten predicted sites (from a list of over 3,000 total sites) with the greatest change in probability between CK2^{WT} and CK2^{K198R} are listed in **Table 1** (a complete list of predicted sites is available in **Supplementary Table S7**). Of the sites listed, two have an increased probability of modification by CK2^{K198R} and the remaining eight are less likely to be phosphorylated by CK2^{K198R}. Additionally, four of the ten sites included in **Table 1** have been previously shown to be phosphorylated (with two additional sites being paralogs of phosphorylation sites). We have created a website Located at <https://okurchung.com> that provides users with an interactive view of our predictive results.

DISCUSSION

Contrary to prior speculation and findings, it is clear from our experiments that the CK2^{K198R} mutation does not simply cause a loss of function, or an inability to recognize substrates (Chiu et al., 2018; Dominguez et al., 2021). We demonstrate that the K198R mutation results in a substantial shift in specificity by reducing the overall preference for acidic (D/E) residues at the +1 position, and by increasing preference for glycine residues at the same position. Differences from prior results (Dominguez et al., 2021) can be attributed to the approach used. In Dominguez et al. the authors utilized a single peptide, RRRADDSDDDDD, to assay the activity of CK2 and its mutant form. Though the peptide would be readily phosphorylated by CK2^{WT}, our results predict significantly reduced phosphorylation by CK2^{K198R}. Our findings highlight the limitations of individual peptide based approaches to assessing kinase activity, and the importance of implementing unbiased methods such as ProPeL in the study of kinase mutations to gain a more complete understanding of their impact.

While wild type CK2 has previously been shown to be capable of phosphorylating tyrosine residues (Marin et al., 1999; Vilk et al., 2008; Basnet et al., 2014) the study also marks the first time a tyrosine phosphorylation motif has been identified for CK2, and, to our knowledge, the first time that a tyrosine phosphorylation motif has been identified for any kinase previously characterized as primarily phosphorylating serine and threonine residues. Interestingly, our study also revealed a

TABLE 1 | Top ten phosphorylation sites predicted to be most differentially phosphorylated by CK2^{WT} and CK2^{K198R} in axonally localized human ion channels.

Protein name	Position	Sequence	CK2 ^{WT} probability (%)	CK2 ^{K198R} probability (%)	Probability difference	Known phosphorylation site
SCN1A	510	KRKQKEQS*GGEEKDE	34	100	66%	Paralog to known SCN2A S514 site
SCN2A	514	KKKQKEQS*GEEKKND	35	100	65%	^b Yes, Human
KCNA1	438	VSSPNLAS*DSLRSR	64	23	-40%	^b Yes, Human
SCN2A	1,126	TEEFSSSES*DMESKE	83	44	-39%	^a Yes, Human
CACNA1H	1,027	AEGDANRS*DTDEDKT	64	25	-39%	No
CACNA1D	1,266	FKPKGYFS*DAWNTFD	61	23	-39%	No
SCN1A	1,136	TEDFSSSES*DLSESKE	83	44	-38%	Paralog to known SCN2A S1126 site
CACNA1H	2,094	GGEEAEAS*DPADDEEV	61	24	-37%	No
CACNA1D	2,138	QDFGPGYS*DEEPDPG	81	44	-37%	No
KCNQ2	839	PYIAEGES*DTSDSLC	58	22	-36%	^b Yes, Mouse

^aSites were considered to be known if they appeared on PhosphoSitePlus.

^bSites were identified in fewer than three high throughput experiments.

highly significant shift in phosphoacceptor preference, with tyrosine residues being shifted from a disfavored state in CK2^{WT} to a neutral state in the CK2^{K198R} mutant, while threonine residues move in the precise opposite direction. Though the detection of a tyrosine phosphorylation motif for a kinase that disfavors tyrosine phosphoacceptors may appear to be a contradiction, it is important to note that the favoring and/or disfavoring of residues is calculated in the context of the background frequency of those residues. Thus, a phosphoacceptor may still experience significant phosphorylation, while being at a level far below what one would expect due to chance if all phosphoacceptors were phosphorylated at their expected background frequencies. Finally, our work highlights the importance of assessing phosphoacceptor specificity independently, as the shift in the specificity motif from CK2^{WT} to CK2^{K198R} differed between serine/threonine (both of which exhibited similar changes) and tyrosine, which added additional preferences for acidic residues upstream of the modification site in the mutant.

Among the advantages of our ProPeL methodology in assessing kinase specificity over alternate approaches is the fact that the method is carried out under physiological conditions in *E. coli*, thus allowing researchers to assess shifts in phosphorylation at the site level between kinases bearing different characteristics and/or mutations. Utilizing this strategy here we have shown that there exists overlap between CK2^{WT} to CK2^{K198R} at the substrate level, as well as considerable extension to new atypical CK2 substrates by the mutant kinase. Another advantage of ProPeL in the present study is that the closed and finite system (i.e., living bacterial proteomes) allowed us to readily associate *scan-x* phosphorylation scores (Schwartz et al., 2009) with actual probabilities of modification based on the observed modification state of all phosphorylatable residues in *E. coli*. Thus, for any score obtained for any peptide sequence, we could utilize the *E. coli* expressed proteome as a lookup table to correlate scores with probabilities. It is important to note that probabilities obtained utilizing this strategy represent an approximate lower bound on the probability as it is likely that many phosphorylatable sites in the *E. coli* lookup table are considered “negative” when they are indeed phosphorylated,

while the converse is unlikely to be true due to our use of conservative peptide identification thresholds (i.e., “absence of proof is not proof of absence”). Most kinases have multiple substrates throughout the cell, only a few of which will directly relate to a phenotype of interest. To investigate signaling changes that may underlie neurodevelopmental phenotypes associated with OCNDs, we focused on neuronal signaling in axonally localized ion channels, as CK2 has been shown to be highly enriched in the axon (Bréchet et al., 2008) and is known to interact with axonal sodium and potassium channels (Hien et al., 2014; Kang et al., 2014; Xu and Cooper, 2015). Further, these ion channels are found to be frequently mutated in both epilepsies and neurodevelopmental disorders (Allen et al., 2020; Malerba et al., 2020), with one recent study reporting 5% of 8,565 participants carrying a mutation in axonally localized voltage gated sodium channels (Lindy et al., 2018; Brunklaus and Lal, 2020). Of 3,000+ sites predicted to be differentially phosphorylated by CK2^{WT} and CK2^{K198R}, the ten sites with the greatest differences present several interesting candidates for hypothesis generation. One site of particular interest is S839 on KCNQ2, as this site falls in the ankyrin-G (AnkG) binding motif, and is a known CK2 phosphorylation site (Xu and Cooper, 2015). Our predictions indicate that CK2^{K198R} is 36% less likely to phosphorylate S839 than CK2^{WT}. Phosphorylation of S839 by CK2 is essential for the accumulation of KCNQ2 in the axon through interaction with AnkG (Kang et al., 2014; Xu and Cooper, 2015) and a loss of this accumulation could be relevant to the pathology of OCNDs patients possessing the CK2^{K198R} mutation. Additional investigation of the interaction between CK2^{K198R} and KCNQ2 is clearly warranted. Though we have produced a website at <https://okurchung.com> that highlights our predictive results on axonally localized ion channels, it is our intention to eventually make publicly available a global proteomic CK2^{K198R} versus CK2^{WT} phosphorylation predictor, as the underlying mechanism by which OCNDs leads to disease is almost certain to be multifactorial given the phenotype is not limited to the central nervous system (Okur et al., 2016; Chiu et al., 2018; Owen et al., 2018).

It is worth noting that while the work presented here demonstrates the impact of the CK2^{K198R} mutation, the most

frequently observed mutation in OCDNS patients, to date more than 20 additional OCNDS-associated mutations identified in patients have been described in literature, including both splice variants (Okur et al., 2016; Colavito et al., 2018) and nonsense variants (Nakashima et al., 2019), many of which likely result in a reduction of functional CK2 protein. Though our results present evidence that the CK2^{K198R} mutation results in an active kinase, there is still a potential shared mechanism amongst these variants. Both loss-of-function CK2 mutations and the rewiring of substrate specificity caused by the CK2^{K198R} mutation could lead to the reduced phosphorylation of essential CK2 phosphorylation sites (particularly those where threonine is the phosphoacceptor or an acidic (D/E) residue is present in the +1 position). The additional effects of the CK2^{K198R} mutation, namely increased tyrosine phosphorylation and increased promiscuity towards the +1 position, could contribute in part to the heterogeneity observed in symptoms of OCNDS patients.

Finally, as our group and others previously demonstrated that the Cushing's Syndrome mutation PKA^{L205R} results in altered substrate specificity (Lubner et al., 2017; Bathon et al., 2019; Walker et al., 2019), the present study provides another data point to suggest that there exists a subset of disease-linked kinase mutations whose deleterious effects can be traced to subtle shifts in substrate specificity rather than broad alterations of kinase activity. The genomic revolution is likely to reveal that we are only at the tip of the proverbial iceberg, as patients with novel mutations are more frequently being identified. By coupling simple experimental strategies for kinase specificity determination with computational approaches to predict substrates, our hope is to generate testable hypotheses regarding underlying mechanisms of disease that can lead us to potential therapeutics faster than ever before.

DATA AVAILABILITY STATEMENT

The datasets presented in this study can be found in online repositories. The mass spectrometry proteomics data have been deposited to the ProteomeXchange Consortium (<http://proteomecentral.proteomexchange.org>) via the PRIDE partner

repository (Perez-Riverol et al., 2019) with the dataset identifier PXD030823.

AUTHOR CONTRIBUTIONS

AT and DS conceived of the study. DC and DS designed the ProPeL experiments. DS designed the computational scoring methodology. DC and JL performed the experiments. NP and JO, implemented the computational scoring methods. DC analyzed the data. AT, JB, JL and DS contributed materials, resources, and/or analysis tools. DC and DS wrote the manuscript. All authors helped edit the final manuscript.

FUNDING

This work was funded in part by grants awarded to DS by the National Institute of Neurological Disorders and Stroke (1R21NS096516) and the University of Connecticut Office of the Vice President for Research, Research Excellence Program.

ACKNOWLEDGMENTS

The authors wish to acknowledge other members of the Schwartz Lab, including Ben Norris, Kalin Kochnev, and Jared Poulsen who assisted with the design and implementation of the phosphorylation prediction results website described in the manuscript. This work previously appeared online as a preprint on bioRxiv (Caefer et al., 2021), uploaded April 5, 2021.

SUPPLEMENTARY MATERIAL

The Supplementary Material for this article can be found online at: <https://www.frontiersin.org/articles/10.3389/fmolb.2022.850661/full#supplementary-material>

REFERENCES

- Allen, N. M., Weckhuysen, S., Gorman, K., King, M. D., and Lerche, H. (2020). Genetic Potassium Channel-Associated Epilepsies: Clinical Review of the Kv Family. *Eur. J. Paediatr. Neurol.* 24, 105–116. doi:10.1016/j.ejpn.2019.12.002
- Basnet, H., Su, X. B., Tan, Y., Meisenhelder, J., Merkurjev, D., Ohgi, K. A., et al. (2014). Tyrosine Phosphorylation of Histone H2A by CK2 Regulates Transcriptional Elongation. *Nature* 516, 267–271. doi:10.1038/nature13736
- Bathon, K., Weigand, I., Vanselow, J. T., Ronchi, C. L., Sbiera, S., Schlosser, A., et al. (2019). Alterations in Protein Kinase A Substrate Specificity as a Potential Cause of Cushing Syndrome. *Endocrinology* 160, 447–459. doi:10.1210/en.2018-00775
- Bre'chet, A., Fache, M.-P., Brachet, A., Ferracci, G., Baude, A., Irondelle, M., et al. (2008). Protein Kinase CK2 Contributes to the Organization of Sodium Channels in Axonal Membranes by Regulating Their Interactions with Ankyrin G. *J. Cell Biol.* 183, 1101–1114. doi:10.1083/jcb.200805169
- Brunklaus, A., and Lal, D. (2020). Sodium Channel Epilepsies and Neurodevelopmental Disorders: from Disease Mechanisms to Clinical Application. *Dev. Med. Child. Neurol.* 62, 784–792. doi:10.1111/dmcn.14519
- Caefer, D. M., Phan, N. Q., Liddle, J. C., Balsbaugh, J. L., O'Shea, J. P., Tzingounis, A. V., et al. (2021). The Okur-Chung Neurodevelopmental Syndrome (OCNDS) Mutation CK2K198R Leads to a Rewiring of Kinase Specificity. *bioRxiv*. doi:10.1101/2021.04.05.438522
- Chiu, A. T. G., Pei, S. L. C., Mak, C. C. Y., Leung, G. K. C., Yu, M. H. C., Lee, S. L., et al. (2018). Okur-Chung Neurodevelopmental Syndrome: Eight Additional Cases with Implications on Phenotype and Genotype Expansion. *Clin. Genet.* 93, 880–890. doi:10.1111/cge.13196
- Chou, M. F., Priscic, S., Lubner, J. M., Church, G. M., Husson, R. N., and Schwartz, D. (2012). Using Bacteria to Determine Protein Kinase Specificity and Predict Target Substrates. *PLOS ONE* 7, e2747. doi:10.1371/journal.pone.0052747
- Colavito, D., Del Giudice, E., Ceccato, C., Dalle Carbonare, M., Leon, A., and Suppiej, A. (2018). Are CSNK2A1 Gene Mutations Associated with Retinal

- Dystrophy? Report of a Patient Carrier of a Novel De Novo Splice Site Mutation. *J. Hum. Genet.* 63, 779–781. doi:10.1038/s10038-018-0434-y
- Cox, J., and Mann, M. (2008). MaxQuant Enables High Peptide Identification Rates, Individualized p.p.b.-range Mass Accuracies and Proteome-wide Protein Quantification. *Nat. Biotechnol.* 26, 1367–1372. doi:10.1038/nbt.1511
- Dominguez, I., Cruz-Gamero, J. M., Corasolla, V., Dacher, N., Rangasamy, S., Urbani, A., et al. (2021). Okur-Chung Neurodevelopmental Syndrome-Linked CK2a Variants Have Reduced Kinase Activity. *Hum. Genet.* 140, 1077–1096. doi:10.1007/s00439-021-02280-5
- Hien, Y. E., Montersino, A., Castets, F., Leterrier, C., Filhol, O., Vacher, H., et al. (2014). CK2 Accumulation at the Axon Initial Segment Depends on Sodium Channel Nav1. *FEBS Lett.* 588, 3403–3408. doi:10.1016/j.febslet.2014.07.032
- Kang, S., Xu, M., Cooper, E. C., and Hoshi, N. (2014). Channel-anchored Protein Kinase CK2 and Protein Phosphatase 1 Reciprocally Regulate KCNQ2-Containing M-Channels via Phosphorylation of Calmodulin. *J. Biol. Chem.* 289, 11536–11544. doi:10.1074/jbc.M113.528497
- Lindy, A. S., Stosser, M. B., Butler, E., Downtain-Pickersgill, C., Shanmugham, A., Retterer, K., et al. (2018). Diagnostic Outcomes for Genetic Testing of 70 Genes in 8565 Patients with Epilepsy and Neurodevelopmental Disorders. *Epilepsia* 59, 1062–1071. doi:10.1111/epi.14074
- Lubner, J. M., Balsbaugh, J. L., Church, G. M., Chou, M. F., and Schwartz, D. (2018). Characterizing Protein Kinase Substrate Specificity Using the Proteomic Peptide Library (ProPeL) Approach. *Curr. Protoc. Chem. Biol.* 10, e38. doi:10.1002/cpch.38
- Lubner, J. M., Church, G. M., Chou, M. F., and Schwartz, D. (2016). Reprogramming Protein Kinase Substrate Specificity through Synthetic Mutations. *bioRxiv*, 091892. doi:10.1101/091892
- Lubner, J. M., Dodge-Kafka, K. L., Carlson, C. R., Church, G. M., Chou, M. F., and Schwartz, D. (2017). Cushing's Syndrome Mutant PKA L205R Exhibits Altered Substrate Specificity. *FEBS Lett.* 591, 459–467. doi:10.1002/1873-3468.12562
- Macek, B., Gnad, F., Soufi, B., Kumar, C., Olsen, J. V., Mijakovic, I., et al. (2008). Phosphoproteome Analysis of *E. coli* Reveals Evolutionary Conservation of Bacterial Ser/Thr/Tyr Phosphorylation. *Mol. Cell Proteomics* 7, 299–307. doi:10.1074/mcp.M700311-MCP200
- Malerba, F., Alberini, G., Balagura, G., Marchese, F., Amadori, E., Riva, A., et al. (2020). Genotype-phenotype Correlations in Patients with De Novo KCNQ2 Pathogenic Variants. *Neurol. Genet.* 6, e528. doi:10.1212/NXG.0000000000000528
- Marin, O., Meggio, F., Sarno, S., Cesaro, L., Pagano, M. A., and Pinna, L. A. (1999). Tyrosine versus Serine/Threonine Phosphorylation by Protein Kinase Casein Kinase-2. *J. Biol. Chem.* 274, 29260–29265. doi:10.1074/jbc.274.41.29260
- Meggio, F., and Pinna, L. A. (2003). One-thousand-and-one Substrates of Protein Kinase CK2? *FASEB j.* 17, 349–368. doi:10.1096/fj.02-0473rev
- Nakashima, M., Tohyama, J., Nakagawa, E., Watanabe, Y., Siew, C. n. G., Kwong, C. S., et al. (2019). Identification of De Novo CSNK2A1 and CSNK2B Variants in Cases of Global Developmental Delay with Seizures. *J. Hum. Genet.* 64, 313–322. doi:10.1038/s10038-018-0559-z
- O'Shea, J. P., Chou, M. F., Quader, S. A., Ryan, J. K., Church, G. M., and Schwartz, D. (2013). pLogo: a Probabilistic Approach to Visualizing Sequence Motifs. *Nat. Methods* 10, 1211–1212. doi:10.1038/nmeth.2646
- Okur, V., Cho, M. T., Henderson, L., Retterer, K., Schneider, M., Sattler, S., et al. (2016). De Novo mutations in CSNK2A1 Are Associated with Neurodevelopmental Abnormalities and Dysmorphic Features. *Hum. Genet.* 135, 699–705. doi:10.1007/s00439-016-1661-y
- Owen, C. I., Bowden, R., Parker, M. J., Patterson, J., Patterson, J., Price, S., et al. (2018). Extending the Phenotype Associated with the CSNK2A1- Related Okur-Chung Syndrome-A Clinical Study of 11 Individuals. *Am. J. Med. Genet.* 176, 1108–1114. doi:10.1002/ajmg.a.38610
- Perez-Riverol, Y., Csordas, A., Bai, J., Bernal-Llinares, M., Hewapathirana, S., Kundu, D. J., et al. (2019). The PRIDE Database and Related Tools and Resources in 2019: Improving Support for Quantification Data. *Nucleic Acids Res.* 47, D442–D450. doi:10.1093/nar/gky1106
- Pinna, L. A. (1990). Casein Kinase 2: An 'eminence Grise' in Cellular Regulation? *Biochim. Biophys. Acta (Bba) - Mol. Cel Res.* 1054, 267–284. doi:10.1016/0167-4889(90)90098-X
- Pinna, L. A. (2003). The Raison D'Être of Constitutively Active Protein Kinases: The Lesson of CK2. *Acc. Chem. Res.* 36, 378–384. doi:10.1021/ar020164f
- Sarno, S., Vaglio, P., Marin, O., Issinger, O.-G., Ruffato, K., and Pinna, L. A. (1997). Mutational Analysis of Residues Implicated in the Interaction between Protein Kinase CK2 and Peptide Substrates. *Biochemistry* 36, 11717–11724. doi:10.1021/bi9705772
- Sarno, S., Vaglio, P., Meggio, F., Issinger, O.-G., and Pinna, L. A. (1996). Protein Kinase CK2 Mutants Defective in Substrate Recognition. *J. Biol. Chem.* 271, 10595–10601. doi:10.1074/jbc.271.18.10595
- Schwartz, D., Chou, M. F., and Church, G. M. (2009). Predicting Protein Post-translational Modifications Using Meta-Analysis of Proteome Scale Data Sets. *Mol. Cell Proteomics* 8, 365–379. doi:10.1074/mcp.M800332-MCP200
- Soares, N. C., Spät, P., Krug, K., and Macek, B. (2013). Global Dynamics of the *Escherichia coli* Proteome and Phosphoproteome during Growth in Minimal Medium. *J. Proteome Res.* 12, 2611–2621. doi:10.1021/pr3011843
- Vilk, G., Weber, J. E., Turowec, J. P., Duncan, J. S., Wu, C., Derksen, D. R., et al. (2008). Protein Kinase CK2 Catalyzes Tyrosine Phosphorylation in Mammalian Cells. *Cell Signal.* 20, 1942–1951. doi:10.1016/j.cellsig.2008.07.002
- Walker, C., Wang, Y., Olivieri, C., Karamafrooz, A., Casby, J., Bathon, K., et al. (2019). Cushing's Syndrome Driver Mutation Disrupts Protein Kinase A Allosteric Network, Altering Both Regulation and Substrate Specificity. *Sci. Adv.* 5, eaaw9298. doi:10.1126/sciadv.aaw9298
- Xu, M., and Cooper, E. C. (2015). An Ankyrin-G N-Terminal Gate and Protein Kinase CK2 Dually Regulate Binding of Voltage-Gated Sodium and KCNQ2/3 Potassium Channels. *J. Biol. Chem.* 290, 16619–16632. doi:10.1074/jbc.M115.638932

Conflict of Interest: The authors declare that the research was conducted in the absence of any commercial or financial relationships that could be construed as a potential conflict of interest.

Publisher's Note: All claims expressed in this article are solely those of the authors and do not necessarily represent those of their affiliated organizations, or those of the publisher, the editors and the reviewers. Any product that may be evaluated in this article, or claim that may be made by its manufacturer, is not guaranteed or endorsed by the publisher.

Copyright © 2022 Caefer, Phan, Liddle, Balsbaugh, O'Shea, Tzingounis and Schwartz. This is an open-access article distributed under the terms of the Creative Commons Attribution License (CC BY). The use, distribution or reproduction in other forums is permitted, provided the original author(s) and the copyright owner(s) are credited and that the original publication in this journal is cited, in accordance with accepted academic practice. No use, distribution or reproduction is permitted which does not comply with these terms.



Comparing Two Neurodevelopmental Disorders Linked to CK2: Okur-Chung Neurodevelopmental Syndrome and Poirier-Bienvenu Neurodevelopmental Syndrome—Two Sides of the Same Coin?

Demetra Ballardini^{1,2}, Jose M. Cruz-Gamero¹, Thierry Bienvenu^{1,3} and Heike Rebholz^{1,2,4*}

¹INSERM U1266, Institute of Psychiatry and Neuroscience of Paris, Université de Paris, Paris, France, ²GHU-Paris Psychiatrie et Neurosciences, Hôpital Sainte Anne, Paris, France, ³Service de Médecine Génomique des Maladies de Système et d'organe, Hôpital Cochin, APHP, Centre Université de Paris, Paris, France, ⁴Center of Neurodegeneration, Faculty of Medicine, Danube Private University, Krems, Austria

OPEN ACCESS

Edited by:

Andrea Venerando,
University of Padua, Italy

Reviewed by:

Christian Borgo,
University of Padua, Italy
Francisca Millan,
GeneDx, United States

*Correspondence:

Heike Rebholz
heike.rebholz@inserm.fr

Specialty section:

This article was submitted to
Cellular Biochemistry,
a section of the journal
Frontiers in Molecular Biosciences

Received: 07 January 2022

Accepted: 01 March 2022

Published: 26 May 2022

Citation:

Ballardini D, Cruz-Gamero JM,
Bienvenu T and Rebholz H (2022)
Comparing Two Neurodevelopmental
Disorders Linked to CK2: Okur-Chung
Neurodevelopmental Syndrome and
Poirier-Bienvenu Neurodevelopmental
Syndrome—Two Sides of the Same
Coin?
Front. Mol. Biosci. 9:850559.
doi: 10.3389/fmolb.2022.850559

In recent years, variants in the catalytic and regulatory subunits of the kinase CK2 have been found to underlie two different, yet symptomatically overlapping neurodevelopmental disorders, termed Okur-Chung neurodevelopmental syndrome (OCNDS) and Poirier-Bienvenu neurodevelopmental syndrome (POBINDS). Both conditions are predominantly caused by *de novo* missense or nonsense mono-allelic variants. They are characterized by a generalized developmental delay, intellectual disability, behavioral problems (hyperactivity, repetitive movements and social interaction deficits), hypotonia, motricity and verbalization deficits. One of the main features of POBINDS is epilepsies, which are present with much lower prevalence in patients with OCNDS. While a role for CK2 in brain functioning and development is well acknowledged, these findings for the first time clearly link CK2 to defined brain disorders. Our review will bring together patient data for both syndromes, aiming to link symptoms with genotypes, and to rationalize the symptoms through known cellular functions of CK2 that have been identified in preclinical and biochemical contexts. We will also compare the symptomatology and elaborate the specificities that distinguish the two syndromes.

Keywords: OCNDS, POBINDS, NDD-neurodevelopmental disorder, CK2 (casein kinase II), autism-spectrum disorders (ASD)

INTRODUCTION

Nearly 15% of children in industrialized countries are affected by neurodevelopmental disorders (NDDs) as estimated by the World Health Organization (World Health Organization, 2013). NDDs are a group of conditions characterized by delayed or impaired functions and maturation of the central nervous system, including disorders such as autism spectrum disorder (ASD), intellectual disability (ID) and learning disorders (LD) (Gilissen et al., 2014). Even though some cases have been linked to environmental exposures (Dietrich et al., 2005), most NDDs likely result from the combination of genetic and environmental risk factors; and the role of genetics, especially of

single-gene variants, has gathered the attention (Soden et al., 2014). Until recently, diagnoses have been mainly phenotype-driven, however, enhanced use of sequencing technologies such as targeted gene panels, whole-exome (WES) and whole-genome sequencing (WGS) have enabled an unbiased genotype-driven diagnosis (Aronson and Rehm, 2015; Fitzgerald et al., 2015).

WES analysis linked several *de novo* variants in the gene *CSNK2A1*, located on chromosome 20 (20p13), which encodes for the catalytic subunit of CK2 (CK2 α) to a novel neurodevelopmental syndrome, now termed Okur-Chung Neurodevelopmental Syndrome (OCNDS) (Okur et al., 2016; OMIM #617062), characterized by developmental delay, intellectual disability, hypotonia, behavioral problems (social interaction deficits, hyperactivity, and repetitive movements), language/verbalization deficits, and, in some cases, epilepsy (Trinh et al., 2017; Akahira-Azuma et al., 2018; Chiu et al., 2018; Colavito et al., 2018; Owen et al., 2018; Nakashima et al., 2019; Martinez-Monseny et al., 2020; Xu et al., 2020; Wu et al., 2021). To date, 35 cases are described in the literature. Shortly after the first report of OCNDS, Poirier et al. linked variants of the regulatory subunit of CK2 (*CSNK2B*) to a neurodevelopmental disorder characterized by early-onset seizures, mainly generalized tonic-clonic seizures (GTCS), and ID, growth retardation and other clinical features (Poirier et al., 2017; OMIM #618732). This syndrome, linked to the *CSNK2B* gene located on chromosome 6 (6p21.33), now termed the Poirier-Bienvenu Neurodevelopmental Syndrome (POBINDS), has been described in 51 patients (Sakaguchi et al., 2017; Li et al., 2019; Nakashima et al., 2019; Bonanni et al., 2021; Ernst et al., 2021; Wilke et al., 2022).

Casein kinase 2 (CK2) is a ubiquitous, highly conserved and constitutively active serine/threonine protein kinase which can utilize ATP or GTP as phosphate donor (Niefind et al., 1999). In eukaryotic cells, CK2 is a tetrameric complex composed of two α and/or α' and two β subunits, all of which are encoded by different genes (Niefind et al., 2001). In the brain, CK2 α is more abundant than in other tissues, with a predominance of the α subunit over α' (Ceglia et al., 2011). CK2 is localized in different cellular compartments, is involved in diverse processes such as signal transduction, replication, translation, and metabolism (Roffey and Litchfield, 2021), as well as roles in angiogenesis (Montenarh, 2014), development and differentiation (Götz and Montenarh, 2017), and the immune system (Hong and Benveniste, 2021). Moreover, it is upregulated in many cancers (Ahmad et al., 2005; Ruzzene and Pinna, 2010; Rowse et al., 2017). Interestingly, CK2 has been implicated in SARS-CoV2 infection since mass spectrometric analysis revealed an upregulation of CK2 mediated phosphorylation events in response to virus infection in Vero E6 kidney cells (Bouhaddou et al., 2020).

Various mouse models with altered CK2 expression attest to the indispensability of this kinase in mammalian brain development and function: CK2 $\alpha^{-/-}$ mice are not viable and die at E11.5 due to heart and brain maldevelopment, while CK2 $\alpha^{+/-}$ mice did not show any overt gross phenotype (Lou et al., 2008; Seldin et al., 2008). Mice with a conditional CK2 α KO in dopamine D1 receptor (D1R) expressing neurons, exhibit hyperlocomotion and motor deficiencies which were linked to

elevated D1R activity (Rebholz et al., 2013). Loss of CK2 β has an even more deleterious effect on survival since CK2 $\beta^{-/-}$ embryos are absorbed very early during embryogenesis, at E7.5 (Buchou et al., 2003). Heterozygous CK2 β mice are generally healthy and reproductive, however they are born at a lower-than-expected ratio, with a 30% reduction of heterozygous live offspring and 20% of live mice exhibiting stunted growth and malformations (Blond et al., 2005).

COMPARISON OF SYMPTOM PROFILE

Being classified as NDDs, it is not surprising that both, OCNDS and POBINDS, share many phenotypic similarities with other NDDs and between themselves. Indeed, around 80% of OCNDS and POBINDS patients present growth deficits, in terms of microcephaly, stature and weight, and a high prevalence of dysmorphic features (Table 1). In both syndromes, this is accompanied by developmental delay in terms of motor and speech milestones; however, while POBINDS patients achieve walking and talking on average around the second year of life (22.5 and 24.5 months, respectively), these milestones are more delayed in OCNDS patients, with walking achieved on average at 27.6 months and talking at 42.9 months (Table 1). Moreover, intellectual disability seems to be more prominent in OCNDS compared to POBINDS patients, with 94 and 85% of patients affected, respectively. Patients from both syndromes present neurological and behavioral problems with similar prevalence: hypotonia (77% for both OCNDS and POBINDS) and autistic features (55 and 56%, for OCNDS and POBINDS, respectively); hyperactivity (17% compared to 13% of POBINDS), or ADHD-like features (38 and 44%). 58% of OCNDS patients present stereotyped movements, a phenotype that was not noticed in POBINDS patients (based on seven cases where this symptom was specifically addressed). The most striking phenotypic difference clearly is epilepsy. While only 38% of OCNDS patients suffer from seizures, mainly absences or febrile types, 90% of POBINDS patients present epilepsy and 42% of those suffer from generalized tonic-clonic seizures (GTCS). This correlates well with 60% of POBINDS patients having an abnormal EEG, while MRI anomalies were more prominent in OCNDS patients (52% compared to 37%). Notably, 31% of OCNDS patients of whom MRI was undertaken, exhibit anomalies in the pituitary gland. Interestingly, 77 and 58% of OCNDS patients were reported having sleeping and gastrointestinal problems (i.e., feeding difficulties, constipation), respectively, which were not reported by parents of POBINDS patients.

VARIANTS IN FUNCTIONAL DOMAINS

Okur-Chung Neurodevelopmental Syndrome

The CK2 α protein consists of 391 amino acids (AA) and contains five main regions of interest, all located within the kinase domain: the N-terminal domain (AA 1–38) (Niefind et al., 1998, 2001;

TABLE 1 | Comparison of OCNDS and POBINDS: types of variants and symptoms.

		OCNDS		POBINDS	
		Cases	%	Cases	%
Mutation	Missense	32/35	91	20/48	41
	Nonsense	0/35	0	8/48	17
	In-frame duplication	0/35	0	1/48	2
	Frameshift	0/35	0	7/48	15
	Start loss	1/35	3	3/48	6
	Splice site	2/35	6	9/48	19
Growth	Microcephaly	8/10	80	12/14	86
	Short stature	27/31	87	21/23	91
	Underweight	23/27	85	11/13	85
	Delayed bone age	4/8	50	1/3	*
Development	Walking onset	Average 27.6 mo (based on 27 cases)		Average 22.5 mo (based on 24 cases)	
	Speech onset	Average 42.9 mo (based on 14 cases)		Average 24.5 mo (based on 12 cases)	
—	Dysmorphic features	18/21	86	18/20	90
—	ID	15/16	94	34/40	85
Neurological or behavioural problems	Hypotonia	17/22	77	15/20	75
	Autistic features	6/11	55	9/16	56
	Stereotyped behaviour	7/12	58	0/7	0
	Hyperactivity	1/6	17	1/8	13
	ADHD features	3/8	38	4/9	44
	Seizures	8/22	36	41/45	91
	Seizures: GTCS	0/8	0	18/41	44
Problems	Sleep	10/13	77	1/1	*
	Eating/gastro	14/24	58	5/5	*
	Musculo-skeletal	5/5	*	3/3	*
Anomalies	EEG	1/3	*	12/20	60
	MRI	12/23	52	10/25	40
	Pituitary gland	4/13	31	—	—

For OCNDS, 35 and for POBINDS, 48 patient profiles were published. The respective publications are referenced in **Tables 2A, 2B, Supplementary Tables S1, S2**. The percentages of occurring symptoms were calculated as number of cases with symptoms divided by the number of cases where the particular symptom was tested. Therefore, we decided to not calculate the incidence ratio if a symptom was assessed in five or less patients, since this clearly would have skewed the ratio towards a misleading high percentage. These cases are marked with *. Abbreviations: mo: months; ID: intellectual disability; ADHD: attention deficit hyperactivity disorder; GTCS: generalized tonic-clonic seizure; EEG: electroencephalography; MRI: magnetic resonance imaging.

Sarno et al., 2002), the ATP/GTP binding loop (AA 45–53) (Jakobi and Traugh, 1992; Niefind et al., 1998), basic cluster (AA 68–80) (Sarno et al., 1996; Niefind et al., 1998), active site (D156) (Niefind et al., 1998), and activation segment (AA 175–201) (Niefind et al., 1998) (**Supplementary Table S1**).

OCNDS-linked *CSNK2A1* variants can be found along the whole amino acid sequence and along the whole kinase domain with the exception of $\beta 4/\beta 5$ region that is located between the basic cluster and the active site, and the extreme C-terminus. The lack of variants in these regions could either indicate that the variants have a more deleterious effect on protein function or more probably have no impact. Indeed, variants in the C-terminus exist, but were designated as benign or of uncertain significance (GnomAD.broadinstitute.org). Furthermore, a C-terminally deleted CK2 α protein is fully functional *in vitro* (Olsen et al., 2008). For almost all patients, variants are *de novo* missense and mono-allelic. One case of a patient with a full *CSNK2A1* gene deletion is known ([https://](https://www.sfari.org)

www.sfari.org). The N-terminal domain (AA 1–38) of CK2 α closely interacts with the activation segment and contributes to its activity (Niefind et al., 1998; Niefind et al., 2001; Sarno et al., 2002). One patient has a missense variant p.(E27K) in this domain. Eight children carry variants in the ATP/GTP binding domain: three patients with p.(R47Q), three patients with variants at AA position 50 [p.(Y50C) or p.(Y50S)] and two at AA position 51 [p.(S51R) or p.(S51N)]. All variants in this domain were associated with delays in growth, motor and speech development and, in general, patients had dysmorphic features and hypotonia. A short basic cluster (AA 74–80) interacts with the N-terminal region and the activation segment and is known as the substrate recognition site (Niefind et al., 1998). Variants in two positions in three patients, in or adjacent to this region, have been found at positions 73 and 80 [p.(V73E), p.(R80C), p.(R80H)] leading to different degrees of symptom severity. Interestingly, one patient exhibits a variant in the active site, p.(D156H). He has

microcephaly and brachycephaly, and delayed motor development and ID. The activation segment (AA 175–201) contains the basic “p + 1 loop” that helps to recognize acidic residues of the substrate. Two patients carry the p.(D175G) variant in the “p + 1 loop”. Despite an identical amino acid change, the symptomatology and severity differ between the two patients (**Table 2A** and **Supplementary Table S1**). 12 other patients had a variant in the “p + 1 loop” of which the p.(K198R) is the most commonly described thus far (nine patients). Maybe these patients exemplify best the variability in terms of symptoms: while they share abnormalities such as delayed growth, motor and speech development, and dysmorphic features, only four had ID, six had hypotonia, three experienced seizures, one sleep apnea and one needed a G-tube and had severe gastroesophageal reflux disease (GERD). Such clinical heterogeneity clearly highlights the complexity of genotype–phenotype correlations and may point towards unknown additional modifiers that are either environmental or genetic, such as expression level variations of the different isoforms. Indeed, five different *CSNK2A1* isoforms have been identified: NM_001895.4 (13 exons, 12 coding and one uncoding exon), NM_177559.3 (12 exons with initiation codon in exon 5) that could lead to a difference of phenotype between patients carrying variants before or after exon 5, NM_001362777.2 (14 exons with an additional exon 15), NM_001362771.2 (15 exons with an additional uncoding exon 2 and uncoding exon 15), and NM_177560.3 (14 exons with an additional uncoding exon 2). Two pathogenic variants also exist at the C-terminal end of the kinase domain: R312Q and R312W. When proteins carrying these variants are expressed in mammalian cells, they express a punctuate pattern within the cytosol, unlike other OCNDS-linked CK2 α mutants and wild type CK2 α . Furthermore, they are expressed at significantly lower levels than wild type CK2 α (Dominguez et al., 2021). Another variant that is expressed at lower protein levels compared to wild type is the CK2 α p.(R47Q), while the p.(R47G) (patient not published) expresses normally (Dominguez et al., 2021). These findings of altered expression and localization indicate that the heterogeneity of the condition may in part be caused by different variants, which may trigger different cellular responses that may participate in disease etiology. However, as described above, even when patients share the exact same variants, there is clinical heterogeneity. The C-terminus of CK2 α , starting at AA 351, is phosphorylated in a cell cycle-dependent manner by Cdk1 (St-Denis et al., 2009), however, no mutants were described thus far in this domain.

Poirier-Bienvenu Neurodevelopmental Syndrome

POBINDS-linked variants in *CSNK2B* can be found along the exonic as well as intronic sequences, and no clear variant hotspots can be identified. While for CK2 α the predominant type of variant was missense (91%), for CK2 β , various variant types are present: eight splicing site variants were thus far identified, compared to only two in OCNDS. Generally, such variants may lead to retention of large segments of intronic DNA, or to entire exons being spliced out of the mRNA, resulting in the production of a nonfunctional

protein. Three POBINDS and one OCNDS patients have start loss variants, resulting either in loss of the protein entirely or a N-terminally truncated protein if an alternative start codon is used. Interestingly, while two of these patients suffered from seizures, none of them suffered from GTCS.

The CK2 β protein consists of 215 AA and contains three major domains: the Asp/Glu-rich acidic domain (AA 54–64) (Li et al., 1996; Litchfield et al., 1996), metal binding (zinc finger domain) (AA 105–146) (Chantalat, 1999), and C-terminal alpha subunit interaction domain (AA 171–end) (Marin et al., 1997; Chantalat, 1999; Sarno et al., 1999) (**Supplementary Table S1**).

Several nonsense variants are predicted to lead to an early termination after amino acids 5, 9, 20, 47, 61 or 101. Like with OCNDS, there is heterogeneity in the clinical phenotypes. No *CSNK2B* full gene deletion mutant has yet been described. Missense and other in-frame variants are found along the whole protein sequence: one patient carries an in-frame duplication p.(G27D28dup) in the highly acidic N-terminal domain of CK2 β (AA 1–104) which contains docking sites for various proteins (Bojanowski et al., 1993; Appel et al., 1995; Li et al., 1997; Romero-Oliva and Allende, 2001; Theis-Febvre et al., 2003; Tapia et al., 2004). The patient has mild ID and GTCS seizures (**Table 2B** and **Supplementary Table S2**). Seven patients were described having variants in the KEN box, a sequence motif with the consensus KENxxxN (AA 32–40) that is targeted by the ubiquitin protein ligase APC (Pfleger and Kirschner, 2000). All of them presented with delayed speech, dysmorphic features and mild/moderate ID, four with seizures, but none of them with GTCS (**Table 2B** and **Supplementary Table S2**). Another motif, the D- or destruction box-like motif analogous to sequences found in cyclins (AA 47–55), that is recognized by the ubiquitin proteolysis machinery (Allende and Allende, 1995), was the location of variants in two POBINDS cases (**Table 2B** and **Supplementary Table S2**). However, the variants are predicted to lead to premature termination of the polypeptide chain, and therefore the phenotype of the patients cannot inform us about the functional effect of a D-box variant. The acidic loop (AA 55–64) can bind to the basic cluster of the CK2 α subunit that is important for substrate binding and recognition. Thus, the acidic loop could be seen as pseudo-substrate region, that competitively hinders the access of negatively charged substrates to the active site, thereby essentially down-regulating CK2 activity (Boldyreff et al., 1994; Marin et al., 1997). The acidic loop is also necessary for the creation of inactive supramolecular structures of CK2 (Lolli et al., 2017). One *de novo* nonsense variant p.(E61*) has been described in the acidic loop resulting in the insertion of a premature stop codon at p.61. Four missense variants were described further C-terminal, in a region that has been shown to interact with Topoisomerase II (AA 51–110) (Leroy et al., 1999), with clinical phenotypes varying from mild to severe, from absence to presence of GTCS.

The central part of CK2 β protein consists of the juxta-dimer interface region, which contains the zinc-finger region (AA 105–146). Four conserved cysteine residues (C109, C114, C137 and C140) coordinate Zn²⁺ ions, which are necessary for β - β subunit dimerization (Chantalat, 1999). Nine patients exhibit variants in this region. Variant at position C137 is present in four patients and thus could be considered a variant hotspot (**Table 2B** and **Supplementary Table S2**). The clinical phenotype is

TABLE 2A | OCNDS patients and their symptom profiles.

Structural domain				Kinase domain																				
N-Term												Active site		p+1 loop							C-term			
				ATP/GTP binding domain					Basic cluster					Activation segment										
Variant p.(...)				M1?	E27K	R47Q	Y50S	Y50C	S51N	S51R	V73E	R80H	D156H	H160R	I174M	D175G	R191Q	R191*	F197I	K198R	P231R	R312W	R312Q	Splice site variants
Growth delay	-	+	+/?	+	+	+	+	+	+	+	+	+	+	+	+	+	+	+/-	+	+	+	+/-/?		
Developmental delay	Motor: walking onset (mo)	?	22	+	20	+	24	30	+	+	22	18	30	+/?	18	18	24	+/?	+	27	20	+		
	Speech onset (mo)	?	36	+	12	+	36	+	+	+	+	12	18	+/?	36	+	48	+/?	+	14	54	?		
Dysmorphic features		?	+	+/?	+	+/?	?	+	?	+/?	+	+	?	+	?	?	-	?	+/?	+	?	+	-	
ID/LD		+	?	+/?	+	+/?	?	?	+	?	+	+	?	+/?	?	?	?	+/-/?	?	?	+	+/?		
Neurological and behavioural problems	Hypotonia	+	?	+/-	+	?	-	+	?	+/?	?	?	?	+/?	?	?	+	-	+/-/?	+	+	?	+/?	
	Autistic features	+	+	-/?	?	?	-	?	?	+/?	?	?	+	?	?	?	?	-	+/-/?	?	+	?	?	
	Stereotyped behaviour	?	+	-/?	?	+/?	-	?	?	?	+	?	+	+/?	?	?	-	+/-/?	?	?	?	+/?		
	Hyperactivity	?	?	-/?	?	?	-	?	?	?	?	?	?	?	?	?	?	-	+/-/?	?	?	?	?	
	ADHD features	?	?	+/-/?	?	?	-	+	?	?	?	?	?	?	?	?	?	-	-/?	?	?	?	+/?	
Problems	Seizures	?	?	-/?	+	?	-	+	?	-/?	-	+	-	+/?	-	+	-	+/-/?	?	-	?	-/?		
	Sleep	+	+	-/?	-	-/?	?	+	+	?	+	?	?	+	?	?	?	+/-/?	?	?	?	+		
	Eating/gastro intestinal	+	+	+/-	+	+/?	-	+	+	-/?	-	?	+	+	+	?	?	-	+/-/?	?	-	?	+/?	
Anomalies	EEG	?	?	?	-	?	?	?	?	?	?	+	?	?	?	?	?	?	?	?	?	?	-/?	
	MRI	-		+/-	-	+/?	?	?	-	+/-	+	+	?	+/?	-	-	+	+/-/?	-	?	?	-		

All patients whose symptoms were published thus far are ordered by the position of their amino acid alteration, from left to right: N-terminus to the C-terminus. Patients with the same variant are grouped in one column. "+" indicates that symptom is present, "-" that it is absent, "+/-" is used when patients were described who had or had not the specific phenotype, "?" is used when the specific phenotype was not discussed in the corresponding publication. When possible, age indications (in months) for symptom onset/detection are given. Abbreviations: ATP: adenosine triphosphate; GTP: guanosine triphosphate; ID: intellectual disability; LD: learning disability; ADHD: attention deficit hyperactivity disorder; GTCS: generalized tonic-clonic seizure; GERD: gastroesophageal reflux disease; G-tube: Gastrostomy tube; EEG: electroencephalography; MRI: Magnetic resonance imaging. For more details, **Supplementary Table S1**. Information derived from (Trinh et al., 2017; Akahira-Azuma et al., 2018; Chiu et al., 2018; Colavito et al., 2018; Owen et al., 2018; Nakashima et al., 2019; Martinez-Monseny et al., 2020; Xu et al., 2020; Wu et al., 2021).

TABLE 2B | POBINDS patients and their symptom profiles.

	Structural domain	N-Term				Zinc finger domain										C-Term																																																																																																																																																																																																																																																																																																																																																																																																																																																																																																																																																																																																																																																																																																																																																																																																																																																																																																																																																																																																																																																																																																																																																																																																																																																																																																																																																																																																																																																																																																																																																																																																																																																	
																																																																																																																																																																																																																																																																																																																																																																																																																																																																																																																																																																																																																																																																																																																																																																																																																																																																																																																																																																																																																																																																																																																																																																																																																																																																																																																																																																																																																																																																																																																																																																																																																																																																	</

All patients whose symptoms were published thus far are ordered by the position of their amino acid alteration, from left to right: N-terminus to the C-terminus. Patients with the same variant are grouped in one column. "+" indicates that symptom is present, "-" that it is absent, "+/-" is used when patients were described who had or had not the specific phenotype, "?" is used when the specific phenotype was not discussed in the corresponding publication. When possible, age indications (in months) for symptom onset/detection are given. Abbreviations: ATP: adenosine triphosphate; GTP: guanosine triphosphate; ID: intellectual disability; LD: learning disability; ADHD: attention deficit hyperactivity disorder; GTCS: generalized tonic-clonic seizure; GERD: gastroesophageal reflux disease; G-tube: Gastrostomy tube; EEG: electroencephalography; MRI: Magnetic resonance imaging. For more details, **Supplementary Table S2**. Information derived from (Sakaguchi et al., 2017; Li et al., 2019; Nakashima et al., 2019; Bonanni et al., 2021; Ernst et al., 2021; Wilke et al., 2022).

relatively homogeneous: 8/9 patients were reported with delayed growth, and 7/9 with various degrees of motor and speech development delay, 4/9 with mild dysmorphic features and 6/9 with mild ID. All nine patients have seizures, with 7/9 presenting GTCS. Two patients with the missense variant p.(R111P) (Li et al., 2019) were diagnosed with motor and speech delay, ID and GTCS. The C-terminal region (starting at AA 171), containing the positive regulatory region, contributes to CK2 β dimerization but is also necessary for interaction with CK2 α/α' (Meggio et al., 1995; Marin et al., 1997; Chantalat 1999; Sarno et al., 1999; Niefind et al., 2001). The crystal structure of the holoenzyme indicates that the C-terminus of CK2 β is in direct contact with the CK2 α , stabilizes the β/β and α/β contacts and points away from the enzyme body and also stimulates kinase activity. However, in the β dimer (CK2 α absent) it acts in a destabilizing manner (Niefind et al., 2001). One can therefore hypothesize that variants in the C-terminal region affect formation of a stable holoenzyme, somewhat like a variant in the zinc finger domain would do. Interestingly, all seven patients with variants in this region had ID and suffered from epilepsy, with 5/7 having GTCS. One may speculate that a deleterious effect on β/β dimerization will negatively impact on holoenzyme formation and that reduced amount of holoenzyme has a striking effect on the appearance of GTCS.

Ten patients carry seven nonsense variants [p.(G5*), p.(W9*), p.(E20*), p.(Q42*), p.(R47*), p.(E61*) and p.(Y101*)] predicted to ablate the formation of full length CK2 β protein. The patients present delayed growth, motor development and speech, with two patients being nonverbal. 8/10 present ID, with three of these eight having profound ID, and 4/10 present dysmorphic features. Half of the patients present hypotonia and autistic features, and all of them suffer from epilepsy, with 3/10 having GTCS and other three presenting myotonic-atonic seizures. Interestingly, four patients present eating/gastrointestinal issues, symptoms that are more often found in OCNDs patients.

EFFECT OF VARIANTS ON CK2 ACTIVITY

The most obvious result of any pathogenic variant in all CK2 subunits that does not abolish protein expression/translation, is to alter the activity of an enzyme, either by enhancing or, more probably, reducing it. Our group has studied the *in vitro* activity of 16 different *CSNK2A1* missense mutants and found that the activity towards a consensus peptide is significantly reduced for all. This is the case when CK2 α proteins are bacterially expressed, purified, and tested in the presence and absence of purified CK2 β , or when mutants are overexpressed in mammalian cells and immunoprecipitated (Dominguez et al., 2021). However, it has been recently suggested that the *CSNK2A1* p.(K198R) variant does not lead to a generic reduction in overall activity, but to a change in substrate specificity towards reduced preference for acidic residues at position +1, for T as phosphoacceptor and a novel preference for Y (Caefer et al., 2021). This hypothesis, generated on the basis of mass spectrometry of bacterial lysates expressing the CK2 mutant, however, awaits confirmation in mammalian cells since the bacterial phosphoproteome may not

correctly reflect the situation in mammalian cells, where several levels of CK2 activity regulation exist, starting from holoenzyme and multi-protein-complex formation, substrate recruitment, compartmentalization within a cell, and, in particular, post-translational modifications, such as hierarchical phosphorylation.

It is very surprising to observe no loss-of-function variant such as nonsense, frameshift and only two splice site consensus variants. However, taking into consideration the one OCNDs patient with full gene loss and one patient with pathogenic variant of the active site p.(D156H), it is plausible that a loss-of-function rather than a gain-of-function mechanism is present.

Whether missense variants could act in a dominant-negative manner, by competitively binding to *in vivo* substrates, or by preventing the formation of an active holoenzyme, or whether a haplo-insufficient effect underlies the phenotypes whereby the reduced amount of active wildtype CK2 α is insufficient, cannot be clearly stated at this point. It is also possible that both mechanisms are at play, and even that different mutants exert their effects through either mechanism.

Could there be compensatory upregulation of wild type CK2 α , CK2 α' or CK2 β in OCNDs and POBINDS? We have tested the expression of both catalytic isoforms in OCNDs patient-derived fibroblasts [CK2 α p.(R47G), p.(D156E) and p.(K198R)] and have not detected enhanced amounts of CK2 α or α' in patient fibroblasts compared to parental control lines. In contrast, we found that CK2 β protein is upregulated in these lines (Dominguez et al., 2021). Such regulation however could be cell-type dependent and thus further studies should shed light on this question.

CK2 β -dependent Mechanisms

CK2 β modulates CK2's biological functions through enabling the formation of a holotetramer (Boldyreff et al., 1996) (1), formation of higher-order multimers (Lolli et al., 2012) (2), recruitment of substrates (Guerra and Issinger, 1999) (3) and modulation of activity towards certain substrates (Meggio et al., 1992) (4). Finally, it is important to note that CK2 β also has roles in the cell that are independent of CK2 α (Guerra and Issinger, 1999) (5).

- 1) The zinc finger domain mediates β - β dimerization which can occur in the absence of CK2 α and is a prerequisite for the incorporation of catalytic CK2 subunits into tetrameric complexes (Niefind and Issinger 2005). The CK2 β homodimer is the building block for the holoenzyme, by bridging the two catalytic subunits. Thus, CK2 β missense variants within the zinc finger motif, especially the conserved cysteines, may result in loss of CK2 β dimers and ultimately, CK2 heterotetramers. The importance of CK2 β dimerization was demonstrated in *Drosophila* by expression of mutagenized CK2 β transgenes in a CK2 β null mutant background. Variants of either cysteine residue pair (109/114 or 137/140) resulted in a CK2 β protein which was unable to rescue the lethality of the CK2 β null mutant (Canton et al., 2001). Generally, in POBINDS patients, variants in the zinc finger domain and/or the C-terminal domain seem to have a severe phenotype. Some variants in the more N-terminal region do not show ID and/or epilepsy. For example, 100% of the patients with missense variants in the acidic loop or

more N-terminal to it, do not exhibit GTCS (**Supplementary Table S2**). However, variants in the more central region, within the Topoisomerase interaction region, or more or C-terminal to it are generally characterized by seizures, mainly of GTCS type (**Supplementary Table S2**).

- 2) Supramolecular assemblies of CK2 that are driven by inter-molecular interactions between the acidic loop of CK2 β and the p+1 loop of CK2 α of two different holoenzymes (Lolli et al., 2012) were identified. They are thought to be inactive forms that, when needed, can disassemble into the active tetrameric form of CK2. These oligomers form *in vitro* at low salt concentrations in linear or circular organization complexes (Niefind and Issinger, 2005), but also in *E. coli* as shown by native mass spectrometry (Seetoh et al., 2016). 12 patients with variants in the CK2 α p+1 loop are described in the literature [9 of which have the p.(K198R) variant], and it would be interesting to determine in patient-derived cells whether the formation of CK2 multimers is present and altered.
- 3) CK2 β confers to the holoenzyme the ability to interact with certain substrates, such as p53 (Appel et al., 1995) and topoisomerase II (Bojanowski et al., 1993). The purified isolated CK2 α subunit by itself is unable to bind to both enzymes, thus the CK2 β subunit mediates the recruitment, which, for interaction with p53 has been narrowed down to CK2 β AA 72-149 and for topoisomerase II to AA 51-110, a region in which several POBINDS-linked variants are present. Phosphorylation of p53 at position serine 392 by CK2 activates the site-specific DNA-binding function and tetramerization of p53. Mice expressing p53 proteins p.(S389A), the mouse equivalent of human S392 exhibit susceptibility to various tumors (Meek and Cox, 2011). A KSSR motif (AA 147–150), located at the interface of the β - β dimer, has been shown to be required for two other CK2 substrates, the Epstein-Barr virus EBNA1 protein and C18orf25/ARKL1 (Cao et al., 2014), however no such variants have been identified in POBINDS patients.

Another relevant example of CK2 β dependent substrate recruitment is the transcription factor Olig2 in the developing mouse brain (Xu et al., 2020). Disruption of CK2 β leads to inhibition of neuronal stem cell proliferation and loss of differentiation in oligodendrocyte precursor cells (OPCs) in mice. Olig2 is required for OPCs development and was identified *in vitro* as a strict CK2 β -dependent CK2 substrate (Huillard et al., 2010). Other binding partners of CK2 that are recruited *via* the β isoform are discussed in the review by Bibby and Litchfield (Bibby and Litchfield, 2005).

- 4) CK2 β modulates kinase specificity towards CK2 substrates. *In vitro* studies, performed in the presence or absence of CK2 β , generally showed that some substrates are phosphorylated equally with or without CK2 β while others are less phosphorylated in the absence of CK2 β (Meggio et al., 1992). Only a limited number of protein substrates are phosphorylated by CK2 α alone but not the holoenzyme, such as Calmodulin (Meggio et al., 1992). Presumably, in

these instances, the β subunit does not turn off catalytic activity, since CK2 is constitutively “on”, but mediates its effect through specific interactions with the protein substrates (Pinna, 2002). Phosphorylation of Calmodulin by CK2 alters the interaction with various downstream effectors such as CaM-dependent cyclic nucleotide phosphodiesterase, Ca²⁺-ATPase, Ca²⁺/CaM-dependent protein kinase II, myosin light chain kinase, and NO synthase (Arrigoni et al., 2004). It could be hypothesized that POBINDS mutants that are expected to prevent holoenzyme formation, will elevate the proportion of CK2 α monomers over the holoenzyme and alter CaM phosphorylation and its function. This may have an impact on several neural processes, such as synaptic plasticity via glutamate receptor homeostasis (Sanz-Clemente et al., 2013).

- 5) Recently, muscle cell clones (C2C12) that are devoid of either α , α' or β subunits were generated, and phosphoproteomic analysis revealed that lack of the β subunit affected grossly the same phosphosites than knockout of CK2 α/α' , however many phosphosites that do not conform to the CK2 consensus were also altered, strengthening the argumentation for roles of CK2 β that are independent of CK2 activity (Borgo et al., 2019). CK2 β dimers, in the absence of CK2 α , were found in mouse testis and brain (Guerra and Issinger, 1999) and appear to have regulatory function on several other protein kinases, such as A-Raf (Hagemann et al., 1997), c-Mos (Chen et al., 1997) and Chk1 (Guerra et al., 2003). A-Raf belongs to a family of cytoplasmic S/T protein kinases within the MAPK pathway (Chong et al., 2003). In two independent yeast screens (Boldyreff et al., 1996; Hagemann et al., 1997), CK2 β was found to specifically interact with A-Raf, which resulted in a 10-fold enhancement of its activity towards MEK in co-expression studies in insect cells. Interestingly, expression of CK2 α results in abolished MEK activation observed in the presence of CK2 β , suggesting that CK2 α might be competing with A-Raf for binding to CK2 β (Hagemann et al., 1997). CK2 β , by direct binding, inhibits Mos, an activator of MAPK, that is highly expressed in germ cells (Sagata et al., 1988). CK2 β binds Mos via its C-terminus, leading to reduced MAPK activation (Chen et al., 1997; Lieberman and Ruderman, 2004). It was suggested that regulation of Mos activity by CK2 β occurs during early stages of *Xenopus* oocyte maturation, and that, during later developmental stages this inhibition abates due to upregulated expression of Mos molecules that outnumber CK2 β molecules (Chen et al., 1997). Chk1 is a cell cycle checkpoint kinase (G2) that is required for ES cell viability (Takai et al., 2000). CK2 β binds Chk1 via its C-terminus *in vitro* and *in vivo*, to activate Chk1 activity (Guerra et al., 2003).

CK2-DEPENDENT BIOLOGICAL PROCESSES THAT MAY UNDERLIE SYMPTOMS

Based on our mass spectrometry results using patient fibroblasts (Dominguez et al., 2021), we hypothesize that OCNDS-linked variants will lead to overall reduced phosphorylation of *in vivo*

substrates, of which several have been linked to functions such as synaptic transmission and plasticity, neuritogenesis which are crucial for neural development and homeostasis, as reviewed (Blanquet, 2000; Castello et al., 2018). In this section, we will discuss pathways that involve CK2 activity and appear most pertinent in respect to patient symptoms.

1) Changes in cell growth and apoptosis pathways affect growth and morphogenesis

CK2 is implicated in the Akt/GSK3 β pathway, an anti-apoptotic, pro-survival pathway that is important in tumorigenesis and tumor growth by directly phosphorylating Akt at position S129 in immortalized mammalian cells (Di Maira et al., 2005). Recently CK2, especially the CK2 β and α' subunit, have been attributed a role in cell migration and adhesion (Lettieri et al., 2019). In the brain, by interaction with mammalian/mechanistic target of rapamycin (mTOR), Akt regulates neuronal processes like morphogenesis, synapse formation, plasticity, and dendritic development (Hers et al., 2011). Since autism spectrum disorders have been associated with alterations in brain connectivity in mouse models and autistic children (Ellegood et al., 2015), it could be possible that CK2 α variants cause modifications in the Akt pathway that could contribute to the ASD-like symptoms in OCNDS. In OCNDS-derived fibroblasts, however, we did not detect a reduction of pS129 Akt or pS473 Akt which suggests, again, that the regulation of signaling pathways may be cell-type dependent and different in immortalized versus primary cells (Dominguez et al., 2021).

As cells rapidly undergo mitosis during neural development, it is as important that a controlled portion of cells undergoes apoptosis, in a process called pruning, and the balance between these processes underlies correct neural and organ development (Putcha and Johnson, 2004). A role of CK2 in the cell cycle was first deduced due to cell-cycle dependent phosphorylation of CK2 α and CK2 β (Litchfield, 2003). To date, many more substrates and binding partners, such as p53, Akt, topo2, clearly involve CK2 in both of these processes (Filhol et al., 1992; Bojanowski et al., 1993; Di Maira et al., 2005).

Since a detailed discussion of CK2's role in apoptosis and the cell cycle would be too lengthy here, we refer to reviews on cell cycle regulation (St-Denis et al., 2009), survival and apoptosis (Duncan et al., 2010; Hanif and Pervaiz, 2011).

Wnt signaling is an important regulator of development, acting through a canonical and a non-canonical pathway to affect cell fate determination, polarity, and early morphogenetic movements. CK2 has been shown to modulate Wnt signaling in *Drosophila* and mammalian cells, since CK2 phosphorylates and stabilizes Dbl (downstream of Wnt-activated frizzled receptors), the transcriptional co-factor β -catenin and the transcription factor TCF/LEF itself, leading to the transcriptional activation of target genes (Song et al., 2003; Seldin et al., 2005). Interestingly, functional coupling of Wnt3a to Frizzled-1 receptor produces transient enhanced activity of CK2 and increased accumulation of β -catenin (Gao and Wang, 2006). Thus, a reduction in CK2 activity may lead to reduced target gene

expression and improper development. Canonical Wnt signaling in the ventral diencephalon regulates the formation of the pituitary gland (Osmundsen et al., 2017), which could explain the abnormalities found in four MRI out of the 35 OCNDS patients described (MRI was taken in 23 patients). If the pituitary gland is affected in OCNDS, it could lead to altered secretion of hormones, such as the growth hormone (GH) (Chinoy and Murray, 2016), resulting in retarded growth.

Recently, CK2 α has been linked to trafficking of cilia, microtubule-projections mediating morphogenic and mitogenic signals during development, that, when dysfunctional, cause ciliopathies characterized by intellectual disability and brain malformations (Valente et al., 2014). CK2 α localizes at the mother centriole and mediates cilia structure and stability. It interacts with a key regulator of ciliogenesis, the kinase TTBK2. Expression of OCNDS-linked mutants CSNK2A1 p.(R80H), p.(D156H) and p.(R191Q) mutants results in structural defects of cilia in mouse embryonic fibroblasts (MEFs) (Loukil et al., 2021). It still remains to be determined if this effect is dependent on CK2 activity, and, if yes, which substrates mediate this effect.

2) Changes in synaptic plasticity affect motor abilities, learning/memory and seizure propensity

CK2 is not only localized to the nucleus and cytoplasm of neurons, but was also detected at the plasma membrane (Rebholz et al., 2009), more precisely at the post-synaptic density in rat hippocampal and cortical preparations (Soto et al., 2004). CK2 activity is enriched in synaptosomes (Girault et al., 1990) and a whole set of CK2 substrates identified *in vitro* or *in vivo* clearly link CK2 to the control of synaptic activity, as discussed in a previous review (Castello et al., 2017). CK2 α modulates the homeostasis of neurotransmitter receptors, such as ion channel receptors (Montenarh and Götz, 2020) and GPCRs that are coupled *via* G α_q (Castello et al., 2018). As an example of an ion channel, the NMDA glutamate receptor, a cation channel for Ca²⁺, Na⁺ and K⁺ with crucial roles in synaptic plasticity, memory, and learning, shall be mentioned here. CK2 phosphorylates the NR2B subunit of the NMDAR, leading to a disruption of the interaction with PSD-95 and to decreased receptor surface expression in neurons (Chung et al., 2004), in a process driven by synaptic activity and CamKII (Sanz-Clemente et al., 2013). This seems to be of a particular importance during mouse development, in the early postnatal period, where CK2-mediated NR2B-endocytosis resulted in a switch from NR2B to NR2A expression at cortical synapses (Sanz-Clemente et al., 2010). Thus, the integrity of such synapses might be compromised due to insufficient CK2 activity.

Seizures are disorders of neuronal network excitability, which is accompanied by pronounced changes in intracellular and extracellular ion concentrations involving a multitude of ion channels (Raimondo et al., 2015). SK channels provide the hyperpolarizing K⁺ conductance that is fundamental for a wide range of physiological processes, including neuronal excitability (Stocker et al., 1999). They are gated by Ca²⁺ ions

via the Ca^{2+} sensing protein calmodulin that is bound to the intracellular C-terminal chain of the SK channel. CK2 has been detected in complex with calmodulin, to phosphorylate it at T80 and reduce its Ca^{2+} sensitivity, thereby accelerating SK channel deactivation (Bildl et al., 2004). Indeed, a CK2 inhibitor (TBB) enhanced K^+ currents and hyperpolarization in a seizure model (Pilocarpine) and blocked spontaneous epileptic activity in an acute slice model (Brehme et al., 2014). This finding, on the first glance seems at odds with the high seizure incidence in POBINDS patients, however, TBB acts on CK2 kinase activity, whereas we hypothesize that it is plausible for the high seizure incidence in POBINDS to be caused by an activity-independent mechanism. Several other ion channels (Ca^{2+} , Na^+ , Cl^- , K^+) have been shown to be CK2 substrates or binding partners and altered function of these channels will affect physiological neuronal excitability, and may result in neurological disorders such as epilepsy (Montenarh and Götz, 2020).

Another link between CK2 and neural network synchrony and epilepsy is the Mdm2-p53-Nedd4-2 pathway. Both p53 and Mdm2 are CK2 substrates (Filhol et al., 1992; Allende-Vega et al., 2005), and inhibition of CK2 leads to enhanced p53 activity (Dixit et al., 2012). In a kainic acid-induced seizure model in mice, inhibition of p53 reduced seizure susceptibility through modulation of neural network synchrony (Jewett et al., 2018). In the context of OCNDS/POBINDS, it is plausible to speculate that reduced CK2 activity therefore could exert an enhancing effect in the kainic acid seizure model.

In the case of GPCRs, reduced CK2 activity is predicted to delay agonist-induced desensitization and endocytosis of these receptors, similarly to what was observed for dopamine D1 and serotonin HTR4 receptors after knockdown or pharmacological inhibition of CK2 (Rebholz et al., 2013; Castello et al., 2018). A role for the dopamine D1 receptor in the OCNDS/POBINDS phenotype is further made conceivable by the motor behaviors of conditional *Drd1a-Cre* CK2 KO mice: they are hyperactive and exhibit stereotypies, and both phenotypes are normalized upon administration of D1 antagonist SCH23390. Furthermore, these mice also have defects in motor performance and learning in the rotarod.

3) Hypotonia

A majority of patients (OCNDS: 77%; POBINDS 75%, **Tables 2A, 2B**) suffers from hypotonia early in life, which contributes to feeding difficulties as well as delays in motor development. CK2 phosphorylates or interacts with several proteins that are involved in myogenesis or play a role at the neuromuscular junction, as recently reviewed (Hashemolhosseini, 2020).

CRISPR-mediated knockdown of either the catalytic or the regulatory subunits showed that in particular the lack/absence of CK2 β severely impairs the growth of C2C12 cells (Borgo et al., 2017, 2019), hinting towards an important role for CK2 β in muscle cells. Interestingly, CK2 β conditional knockout mice with CK2 β lacking in skeletal muscle display reduced muscle strength. Skeletal muscle cell lysates derived from these mice have reduced

activity towards Tomm22, a component of the translocase complex of the outer mitochondrial membrane, termed Tomm complex, paralleled by enhanced mitochondrial degradation through mitophagy. Phosphorylation of Tomm22 in a CK2 β -dependent manner thus protects mitochondria in skeletal muscle from degradation (Kravic et al., 2018).

Myosins are a family of actin-binding cytoskeletal motor proteins that, as a complex of heavy and light myosin chains, hydrolyze ATP during muscle contraction. During myogenesis, myosins need to assemble into long thick filaments. It was shown that phosphorylation of myosin-IIA heavy chain by PKC or CK2 inhibits the assembly of into filaments. CK2 phosphorylation of the myosin-IIA heavy chain reduced binding of the Mts1 calcium-binding protein, thereby inhibiting mts1-induced filament disassembly and assembly (Dulyaninova et al., 2005).

CK2-dependent phosphorylation is important for myogenesis and muscle homeostasis. CK2 is present at the neuromuscular junction to regulate acetylcholine receptor stability, as recently reviewed (Hashemolhosseini, 2020). Conditional CK2 β KO mice with lack of CK2 β in skeletal muscle showed reduced muscle strength and abnormal metabolic activity of oxidative muscle fibers. This was linked to deficient phosphorylation of an outer mitochondrial membrane protein, Tomm 22 (Kravic et al., 2018). CK2 α was further found to be involved in activation of muscle-specific genes, as its inhibition leads to a significant reduction in muscle-specific genes in C2C12 cells (Salizzato et al., 2019).

Taken together, CK2 activity is necessary for muscle genesis and homeostasis, both of which could be impacted by variants of either of the CK2 subunits.

4) Autistic features

55% of OCNDS and 56% of POBINDS patients have been diagnosed with ASD, and several fields of study, from genetics to biochemistry, deliver arguments for a role of CK2 in this disorder. ASD has both genetic and environmental origins. One predisposing environmental factor is the prenatal exposure to valproic acid (VPA) that increases the risk of ASD in children (Nicolini and Fahnstock, 2018). In rats, CK2 α was found to be upregulated after prenatal VPA exposure, however these results are based solely on western blotting and require further confirmation (Santos-Terra et al., 2021).

We already mentioned that in *Drd1a-Cre* conditional CK2 KO mice dopamine D1 receptor signaling is upregulated and that endocytosis of this receptor is modulated by CK2 (Rebholz et al., 2013). Indeed, several genes of the DA network have been linked to ASD, such as the genes encoding syntaxin 1 (STX1) (Nakamura et al., 2008) or dopamine transporter (DAT) (Hamilton, 2013). Autism-associated variants of these two genes show decreased phosphorylation of STX1 (at S14) by CK2, resulting in reduced STX1/DAT interaction and disruption of the reverse transport of DA (Cartier-Z et al., 2015). This functional interaction was tested in the locomotive response to amphetamine in *Drosophila*. Both, STX1A-R26Q and hDAT-R51W variants responded less to amphetamine, similarly to *Drosophila* expressing a dominant negative form of CK2 (Cartier-Z et al., 2015).

It is known that CK2 activity alters transcription via phosphorylation of a set of transcription factors such as e.g. TFIIA, IIE, or IIF, as reviewed in (St-Denis et al., 2009). The protein encoded by the ASD susceptibility gene *AUTS2* was found bound to CK2 β within the large Polycomb Repressive Complex 1 (PRC1) (Gao et al., 2014). This complex normally catalyzes the monoubiquitination of histone H2A (at K119) and leads to compaction of chromatin and transcriptional repression. CK2, through phosphorylation of another member of this complex, RING1B, inhibits PRC1-AUTS2-mediated monoubiquitination of H2A, thereby turning a transcriptional repressor into an activator and affecting the transcriptional profile of cells (Gao et al., 2014).

On the level of translation, the fragile X mental retardation protein (FMRP) is a mRNA-binding translational repressor that associates with 4–6% of brain transcripts, with autism risk gene transcripts being overrepresented. Absence or severe reduction of FMRP are responsible for fragile X syndrome, the most common monogenic cause of autism spectrum disorder (Verkerk et al., 1991). CK2 phosphorylates murine FMRP at the site S499, a site which is required for its repressor activity, and thereby primes for further phosphorylation at nearby sites by other kinases (Bartley et al., 2016).

CONCLUSION

OCNDS and POBINDS are two distinct newly described NDDs with causative variants in the genes coding for *Csnk2a1* and *Csnk2b*. The symptom overlap is large, and the most striking difference is the elevated propensity to seizures in POBINDS. CK2 β has specific roles in the cells, such as regulating kinases other than CK2, that could be at the origin of the seizure phenotype in POBINDS.

Due to its ubiquitous expression (<https://www.proteinatlas.org/ENSG00000101266-CSNK2A1/tissue>), its promiscuity, based on a non-stringent consensus (S/TxxD/E) (Meggio et al., 1994), it is most plausible that CK2 acts through many pathways and substrates to lead to the symptom profiles of both NDDs.

Clearly, experimental studies are missing and through the use of patient derived cells, especially iPS cells, as well as mouse models of both diseases more mechanistic knowledge has to be

obtained. These models can also be used for the search of potentially druggable targets and to test therapeutic approaches that could be transferred from treatment of other NDDs.

AUTHOR CONTRIBUTIONS

DB, JC-G, TB, and HR wrote the manuscript.

FUNDING

This work has been supported by the CSNK2A1 Foundation and a H2020-MSCA-IF-2019 (No 894207) (to HR).

SUPPLEMENTARY MATERIAL

The Supplementary Material for this article can be found online at: <https://www.frontiersin.org/articles/10.3389/fmolb.2022.850559/full#supplementary-material>

Supplementary Table S1 | Detailed table of OCNDS patients and their symptom profiles. All patients whose symptoms were published thus far are ordered by the position of the gene variation, position within the gene structure as well as the effect on amino acid sequence, as far as it could be predicted. More detailed information about the different symptoms is given in this table. Abbreviations: ATP: Adenosine triphosphate; GTP: Guanosine triphosphate; yo: years old; mo: months old; ID: Intellectual Disability; LD: Learning disability; ADHD: Attention deficit hyperactivity disorder; GTCS: generalized tonic-clonic seizure; GERD: Gastroesophageal reflux disease; G-tube: Gastrostomy tube; EEG: Electroencephalography; MRI: Magnetic resonance imaging.

Supplementary Table S2 | Detailed table of POBINDS patients and their symptom profiles. All patients whose symptoms were published thus far are ordered by the position of the gene variation, position within the gene structure as well as the effect on amino acid sequence, as far as it could be predicted. More detailed information about the different symptoms is given in this table. Abbreviations: D Box: Destruction box; yo: years old; mo: months old; ID: Intellectual Disability; LD: Learning disability; ADHD: Attention deficit hyperactivity disorder; GTCS: generalized tonic-clonic seizure; GERD: Gastroesophageal reflux disease; G-tube: Gastrostomy tube; EEG: Electroencephalography; MRI: Magnetic resonance imaging.

REFERENCES

- Ahmad, K. A., Wang, G., Slaton, J., Unger, G., and Ahmed, K. (2005). Targeting CK2 for Cancer Therapy. *Anti-Cancer Drugs* 16, 1037–1043. doi:10.1097/00001813-200511000-00001
- Akahira-Azuma, M., Tsurusaki, Y., Enomoto, Y., Mitsui, J., and Kurosawa, K. (2018). Refining the Clinical Phenotype of Okur-Chung Neurodevelopmental Syndrome. *Hum. Genome* 5, 18011. doi:10.1038/hgv.2018.11
- Allende, J. E., and Allende, C. C. (1995). Protein Kinase CK2: an Enzyme with Multiple Substrates and a Puzzling Regulation. *FASEB j.* 9, 313–323. doi:10.1096/fasebj.9.5.7896000
- Allende-Vega, N., Dias, S., Milne, D., and Meek, D. (2005). Phosphorylation of the Acidic Domain of Mdm2 by Protein Kinase CK2. *Mol. Cell. Biochem.* 274, 85–90. doi:10.1007/s11010-005-3074-4
- Appel, P., Wagner, P., Boldyreff, B., Issinger, O. G., and Montenarh, M. (1995). Mapping of the Interaction Sites of the Growth Suppressor Protein P53 with the Regulatory Beta-Subunit of Protein Kinase CK2. *Oncogene* 11, 1971–1978.
- Aronson, S. J., and Rehms, H. L. (2015). Building the Foundation for Genomics in Precision Medicine. *Nature* 526, 336–342. doi:10.1038/nature15816
- Arrigoni, G., Marin, O., Pagano, M. A., Settimo, L., Paolin, B., Meggio, F., et al. (2004). Phosphorylation of Calmodulin Fragments by Protein Kinase CK2. Mechanistic Aspects and Structural Consequences. *Biochemistry* 43, 12788–12798. doi:10.1021/bi049365c
- Bartley, C. M., O'Keefe, R. A., Blice-Baum, A., Mihailescu, M.-R., Gong, X., Miyares, L., et al. (2016). Mammalian FMRP S499 Is Phosphorylated by CK2 and Promotes Secondary Phosphorylation of FMRP. *eNeuro* 3, 0092–116. doi:10.1523/ENEURO.0092-16.2016
- Bibby, A. C., and Litchfield, D. W. (2005). The Multiple Personalities of the Regulatory Subunit of Protein Kinase CK2: CK2 Dependent and CK2 Independent Roles Reveal a Secret Identity for CK2 β . *Int. J. Biol. Sci.* 1, 67–79. doi:10.7150/ijbs.1.67
- Bildl, W., Strassmaier, T., Thurm, H., Andersen, J., Eble, S., Oliver, D., et al. (2004). Protein Kinase CK2 Is Coassembled with Small Conductance Ca²⁺-Activated K⁺ Channels and Regulates Channel Gating. *Neuron* 43, 847–858. doi:10.1016/j.neuron.2004.08.033

- Blanquet, P. R. (2000). Casein Kinase 2 as a Potentially Important Enzyme in the Nervous System. *Prog. Neurobiol.* 60, 211–246. doi:10.1016/s0301-0082(99)00026-x
- Blond, O., Jensen, H. H., Buchou, T., Cochet, C., Issinger, O.-G., and Boldyreff, B. (2005). Knocking Out the Regulatory Beta Subunit of Protein Kinase CK2 in Mice: Gene Dosage Effects in ES Cells and Embryos. *Mol. Cell. Biochem.* 274, 31–37. doi:10.1007/s11010-005-3117-x
- Bojanowski, K., Filhol, O., Cochet, C., Chambaz, E. M., and Larsen, A. K. (1993). DNA Topoisomerase II and Casein Kinase II Associate in a Molecular Complex that Is Catalytically Active. *J. Biol. Chem.* 268, 22920–22926. doi:10.1016/s0021-9258(18)41614-6
- Boldyreff, B., Meggio, F., Pinna, L. A., and Issinger, O. G. (1994). Protein Kinase CK2 Structure-Function Relationship: Effects of the Beta Subunit on Reconstitution and Activity. *Cell. Mol. Biol. Res.* 40, 391–399.
- Boldyreff, B., Mietens, U., and Issinger, O.-G. (1996). Structure of Protein Kinase CK2: Dimerization of the Human β -subunit. *FEBS Lett.* 379, 153–156. doi:10.1016/0014-5793(95)01497-7
- Bonanni, P., Baggio, M., Duma, G. M., Negrin, S., Danieli, A., and Giorda, R. (2021). Developmental and Epilepsy Spectrum of Poirier-Bienvenu Neurodevelopmental Syndrome: Description of a New Case Study and Review of the Available Literature. *Seizure* 93, 133–139. doi:10.1016/j.seizure.2021.10.019
- Borgo, C., Franchin, C., Cesaro, L., Zaramella, S., Arrigoni, G., Salvi, M., et al. (2019). A Proteomics Analysis of CK2 β (–/–) C2C12 Cells Provides Novel Insights into the Biological Functions of the Non-catalytic β Subunit. *FEBS J.* 286, 1561–1575. doi:10.1111/febs.14799
- Borgo, C., Franchin, C., Scalco, S., Bosello-Travain, V., Donella-Deana, A., Arrigoni, G., et al. (2017). Generation and Quantitative Proteomics Analysis of CK2 α' (–/–) Cells. *Sci. Rep.* 7, 42409. doi:10.1038/srep42409
- Bouhaddou, M., Memon, D., Meyer, B., White, K. M., Rezeli, V. V., Correa Marrero, M., et al. (2020). The Global Phosphorylation Landscape of SARS-CoV-2 Infection. *Cell* 182, 685–712. e19. doi:10.1016/j.cell.2020.06.034
- Brehme, H., Kirschstein, T., Schulz, R., and Köhling, R. (2014). *In Vivo* treatment with the Casein Kinase 2 Inhibitor 4,5,6,7-tetrabromotriazole Augments the Slow Afterhyperpolarizing Potential and Prevents Acute Epileptiform Activity. *Epilepsia* 55, 175–183. doi:10.1111/epi.12474
- Buchou, T., Vernet, M., Blond, O., Jensen, H. H., Pointu, H., Olsen, B. B., et al. (2003). Disruption of the Regulatory β Subunit of Protein Kinase CK2 in Mice Leads to a Cell-Autonomous Defect and Early Embryonic Lethality. *Mol. Cell. Biol.* 23, 908–915. doi:10.1128/MCB.23.3.908-915.2003
- Caefer, D. M., Phan, N. Q., Liddle, J. C., Balsbaugh, J. L., O'Shea, J. P., Tzingounis, A. V., et al. (2021). The Okur-Chung Neurodevelopmental Syndrome (OCNDS) Mutation CK2K198R Leads to a Rewiring of Kinase Specificity. *Biorxiv*. doi:10.1101/2021.04.05.438522
- Canton, D. A., Zhang, C., and Litchfield, D. W. (2001). Assembly of Protein Kinase CK2: Investigation of Complex Formation between Catalytic and Regulatory Subunits Using a zinc-finger-deficient Mutant of CK2 β . *Biochem. J.* 358, 87–94. doi:10.1042/0264-6021:3580087
- Cao, J. Y., Shire, K., Landry, C., Gish, G. D., Pawson, T., and Frappier, L. (2014). Identification of a Novel Protein Interaction Motif in the Regulatory Subunit of Casein Kinase 2. *Mol. Cell. Biol.* 34, 246–258. doi:10.1128/MCB.00968-13
- Cartier, E., Hamilton, P. J., Belovich, A. N., Shekar, A., Campbell, N. G., Saunders, C., et al. (2015). Rare Autism-Associated Variants Implicate Syntaxin 1 (STX1 R26Q) Phosphorylation and the Dopamine Transporter (hDAT R51W) in Dopamine Neurotransmission and Behaviors. *EBioMedicine* 2, 135–146. doi:10.1016/j.ebiom.2015.01.007
- Castello, J., LeFrancois, B., Flajolet, M., Greengard, P., Friedman, E., and Rebholz, H. (2018). CK2 Regulates 5-HT₄ Receptor Signaling and Modulates Depressive-like Behavior. *Mol. Psychiatry* 23, 872–882. doi:10.1038/mp.2017.240
- Castello, J., Ragnauth, A., Friedman, E., and Rebholz, H. (2017). CK2-An Emerging Target for Neurological and Psychiatric Disorders. *Pharmaceuticals* 10, 7. doi:10.3390/ph10010007
- Ceglia, I., Flajolet, M., and Rebholz, H. (2011). Predominance of CK2 α over CK2 α' in the Mammalian Brain. *Mol. Cell. Biochem.* 356, 169–175. doi:10.1007/s11010-011-0963-6
- Chantalat, L. (1999). Crystal Structure of the Human Protein Kinase CK2 Regulatory Subunit Reveals its Zinc finger-mediated Dimerization. *EMBO J.* 18, 2930–2940. doi:10.1093/emboj/18.11.2930
- Chen, M., Li, D., Krebs, E. G., and Cooper, J. A. (1997). The Casein Kinase II Beta Subunit Binds to Mos and Inhibits Mos Activity. *Mol. Cell. Biol.* 17, 1904–1912. doi:10.1128/MCB.17.4.1904
- Chinoy, A., and Murray, P. G. (2016). Diagnosis of Growth Hormone Deficiency in the Paediatric and Transitional Age. *Best Pract. Res. Clin. Endocrinol. Metab.* 30, 737–747. doi:10.1016/j.beem.2016.11.002
- Chiu, A. T. G., Pei, S. L. C., Mak, C. C. Y., Leung, G. K. C., Yu, M. H. C., Lee, S. L., et al. (2018). Okur-Chung Neurodevelopmental Syndrome: Eight Additional Cases with Implications on Phenotype and Genotype Expansion. *Clin. Genet.* 93, 880–890. doi:10.1111/cge.13196
- Chong, H., Vikis, H. G., and Guan, K.-L. (2003). Mechanisms of Regulating the Raf Kinase Family. *Cell Signal.* 15, 463–469. doi:10.1016/s0898-6568(02)00139-0
- Chung, H. J., Huang, Y. H., Lau, L.-F., and Haganir, R. L. (2004). Regulation of the NMDA Receptor Complex and Trafficking by Activity-dependent Phosphorylation of the NR2B Subunit PDZ Ligand. *J. Neurosci.* 24, 10248–10259. doi:10.1523/JNEUROSCI.0546-04.2004
- Colavito, D., Del Giudice, E., Ceccato, C., Dalle Carbonare, M., Leon, A., and Suppiej, A. (2018). Are CSNK2A1 Gene Mutations Associated with Retinal Dystrophy? Report of a Patient Carrier of a Novel De Novo Splice Site Mutation. *J. Hum. Genet.* 63, 779–781. doi:10.1038/s10038-018-0434-y
- Di Maira, G., Salvi, M., Arrigoni, G., Marin, O., Sarno, S., Brustolon, F., et al. (2005). Protein Kinase CK2 Phosphorylates and Upregulates Akt/PKB. *Cell Death Differ* 12, 668–677. doi:10.1038/sj.cdd.4401604
- Dietrich, K. N., Eskenazi, B., Schantz, S., Yolton, K., Rauh, V. A., Johnson, C. B., et al. (2005). Principles and Practices of Neurodevelopmental Assessment in Children: Lessons Learned from the Centers for Children's Environmental Health and Disease Prevention Research. *Environ. Health Perspect.* 113, 1437–1446. doi:10.1289/ehp.7672
- Dixit, D., Sharma, V., Ghosh, S., Mehta, V. S., and Sen, E. (2012). Inhibition of Casein Kinase-2 Induces P53-dependent Cell Cycle Arrest and Sensitizes Glioblastoma Cells to Tumor Necrosis Factor (TNF α)-Induced Apoptosis through SIRT1 Inhibition. *Cell Death Dis* 3, e271. doi:10.1038/cddis.2012.10
- Dominguez, I., Cruz-Gamero, J. M., Corasolla, V., Dacher, N., Rangasamy, S., Urbani, A., et al. (2021). Okur-Chung Neurodevelopmental Syndrome-Linked CK2 α Variants Have Reduced Kinase Activity. *Hum. Genet.* 140, 1077–1096. doi:10.1007/s00439-021-02280-5
- Dulyaninova, N. G., Malashkevich, V. N., Almo, S. C., and Bresnick, A. R. (2005). Regulation of Myosin-IIA Assembly and Mts1 Binding by Heavy Chain Phosphorylation. *Biochemistry* 44, 6867–6876. doi:10.1021/bi0500776
- Duncan, J. S., Turowec, J. P., Vilk, G., Li, S. S. C., Gloor, G. B., and Litchfield, D. W. (2010). Regulation of Cell Proliferation and Survival: Convergence of Protein Kinases and Caspases. *Biochim. Biophys. Acta (Bba) - Proteins Proteomics* 1804, 505–510. doi:10.1016/j.bbapap.2009.11.001
- Ellegood, J., Anagnostou, E., Babineau, B. A., Crawley, J. N., Lin, L., Genestine, M., et al. (2015). Clustering Autism: Using Neuroanatomical Differences in 26 Mouse Models to Gain Insight into the Heterogeneity. *Mol. Psychiatry* 20, 118–125. doi:10.1038/mp.2014.98
- Ernst, M. E., Baugh, E. H., Thomas, A., Bier, L., Lippa, N., Stong, N., et al. (2021). CSNK2B : A Broad Spectrum of Neurodevelopmental Disability and Epilepsy Severity. *Epilepsia* 62. doi:10.1111/epi.16931
- Filhol, O., Baudier, J., Delphin, C., Loue-Mackebach, P., Chambaz, E. M., and Cochet, C. (1992). Casein Kinase II and the Tumor Suppressor Protein P53 Associate in a Molecular Complex that Is Negatively Regulated upon P53 Phosphorylation. *J. Biol. Chem.* 267, 20577–20583. doi:10.1016/S0021-9258(19)36725-0
- Fitzgerald, T., Gerety, S., Jones, W., van Kogelenberg, M., King, D., McRae, J., et al. (2015). Large-scale Discovery of Novel Genetic Causes of Developmental Disorders. *Nature* 519, 223–228. doi:10.1038/nature14135
- Gao, Y., and Wang, H.-y. (2006). Casein Kinase 2 Is Activated and Essential for Wnt/ β -Catenin Signaling. *J. Biol. Chem.* 281, 18394–18400. doi:10.1074/jbc.M601112200
- Gao, Z., Lee, P., Stafford, J. M., von Schimmelmman, M., Schaefer, A., and Reinberg, D. (2014). An AUTS2-Polycomb Complex Activates Gene Expression in the CNS. *Science* 345, 349–354. doi:10.1126/science.1251391
- Gillissen, C., Hehir-Kwa, J. Y., Thung, D. T., van de Vorst, M., van Bon, B. W. M., Willemsen, M. H., et al. (2014). Genome Sequencing Identifies Major Causes of Severe Intellectual Disability. *Nature* 511, 344–347. doi:10.1038/nature13394

- Girault, J.-A., Hemmings, H. C., Zorn, S. H., Gustafson, E. L., and Greengard, P. (1990). Characterization in Mammalian Brain of a DARPP-32 Serine Kinase Identical to Casein Kinase II. *J. Neurochem.* 55, 1772–1783. doi:10.1111/j.1471-4159.1990.tb04968.x
- Götz, C., and Montenarh, M. (2017). Protein Kinase CK2 in Development and Differentiation. *Biomed. Rep.* 6, 127–133. doi:10.3892/br.2016.829
- Guerra, B., and Issinger, O.-G. (1999). Protein Kinase CK2 and its Role in Cellular Proliferation, Development and Pathology. *Electrophoresis*, 20, 391–408. doi:10.1002/(sici)1522-2683(19990201)20:2<391::aid-elps391>3.0.co;2-n
- Guerra, B., Issinger, O.-G., and Wang, J. Y. (2003). Modulation of Human Checkpoint Kinase Chk1 by the Regulatory β -subunit of Protein Kinase CK2. *Oncogene* 22, 4933–4942. doi:10.1038/sj.onc.1206721
- Hagemann, C., Kalmes, A., Wixler, V., Wixler, L., Schuster, T., and Rapp, U. R. (1997). The Regulatory Subunit of Protein Kinase CK2 Is a Specific A-Raf Activator. *FEBS Lett.* 403, 200–202. doi:10.1016/S0014-5793(97)00011-2
- Hamilton, A. F. d. C. (2013). Reflecting on the Mirror Neuron System in Autism: a Systematic Review of Current Theories. *Developmental Cogn. Neurosci.* 3, 91–105. doi:10.1016/j.dcn.2012.09.008
- Hashemolhosseini, S. (2020). The Role of Protein Kinase CK2 in Skeletal Muscle: Myogenesis, Neuromuscular Junctions, and Rhabdomyosarcoma. *Neurosci. Lett.* 729, 135001. doi:10.1016/j.neulet.2020.135001
- Hers, I., Vincent, E. E., and Tavaré, J. M. (2011). Akt Signalling in Health and Disease. *Cell Signal.* 23, 1515–1527. doi:10.1016/j.cellsig.2011.05.004
- Hong, H., and Benveniste, E. N. (2021). The Immune Regulatory Role of Protein Kinase CK2 and its Implications for Treatment of Cancer. *Biomedicine* 9, 1932. doi:10.3390/biomedicine9121932
- Huillard, E., Ziercher, L., Blond, O., Wong, M., Deloulme, J.-C., Souchelnytskyi, S., et al. (2010). Disruption of CK2 β in Embryonic Neural Stem Cells Compromises Proliferation and Oligodendrogenesis in the Mouse Telencephalon. *Mol. Cell. Biol.* 30, 2737–2749. doi:10.1128/MCB.01566-09
- Jakobi, R., and Traugh, J. A. (1992). Characterization of the Phosphotransferase Domain of Casein Kinase II by Site-Directed Mutagenesis and Expression in *Escherichia coli*. *J. Biol. Chem.* 267, 23894–23902. doi:10.1016/s0021-9258(18)35921-0
- Jewett, K. A., Lee, K. Y., Eagleman, D. E., Soriano, S., and Tsai, N.-P. (2018). Dysregulation and Restoration of Homeostatic Network Plasticity in Fragile X Syndrome Mice. *Neuropharmacology* 138, 182–192. doi:10.1016/j.neuropharm.2018.06.011
- Kravic, B., Harbauer, A. B., Romanello, V., Simeone, L., Vögtle, F.-N., Kaiser, T., et al. (2018). In Mammalian Skeletal Muscle, Phosphorylation of TOMM22 by Protein Kinase CSNK2/CK2 Controls Mitophagy. *Autophagy* 14, 311–335. doi:10.1080/15548627.2017.1403716
- Leroy, D., Alghisi, G. C., Roberts, E., Filhol-Cochet, O., and Gasser, S. M. (1999). Mutations in the C-Terminal Domain of Topoisomerase II Affect Meiotic Function and Interaction with the Casein Kinase 2 β Subunit. *Mol. Cell. Biochem.* 191, 85–95. doi:10.1007/978-1-4419-8624-5_11
- Lettieri, A., Borgo, C., Zanieri, L., D'Amore, C., Oleari, N., Paganoni, A., et al. (2019). Protein Kinase CK2 Subunits Differentially Perturb the Adhesion and Migration of GN11 Cells: A Model of Immature Migrating Neurons. *Ijms* 20, 5951. doi:10.3390/ijms20235951
- Li, D., Dobrowolska, G., and Krebs, E. G. (1996). The Physical Association of Casein Kinase 2 with Nucleolin. *J. Biol. Chem.* 271, 15662–15668. doi:10.1074/jbc.271.26.15662
- Li, D., Meier, U. T., Dobrowolska, G., and Krebs, E. G. (1997). Specific Interaction between Casein Kinase 2 and the Nucleolar Protein Nopp140. *J. Biol. Chem.* 272, 3773–3779. doi:10.1074/jbc.272.6.3773
- Li, J., Gao, K., Cai, S., Liu, Y., Wang, Y., Huang, S., et al. (2019). Germline De Novo Variants in CSNK2B in Chinese Patients with Epilepsy. *Sci. Rep.* 9, 17909. doi:10.1038/s41598-019-53484-9
- Lieberman, S. L., and Ruderman, J. V. (2004). CK2 β , Which Inhibits Mos Function, Binds to a Discrete Domain in the N-Terminus of Mos. *Developmental Biol.* 268, 271–279. doi:10.1016/j.ydbio.2003.12.009
- Litchfield, D. W. (2003). Protein Kinase CK2: Structure, Regulation and Role in Cellular Decisions of Life and Death. *Biochem. J.* 369, 1–15. doi:10.1042/BJ20021469
- Litchfield, D. W., Slominski, E., Lewenza, S., Narvey, M., Bosc, D. G., and Gietz, R. D. (1996). Analysis of Interactions between the Subunits of Protein Kinase CK2. *Biochem. Cell Biol.* 74, 541–547. doi:10.1139/o96-458
- Lolli, G., Naressi, D., Sarno, S., and Battistutta, R. (2017). Characterization of the Oligomeric States of the CK2 $\alpha 2\beta 2$ Holoenzyme in Solution. *Biochem. J.* 474, 2405–2416. doi:10.1042/BCJ20170189
- Lolli, G., Pinna, L. A., and Battistutta, R. (2012). Structural Determinants of Protein Kinase CK2 Regulation by Autoinhibitory Polymerization. *ACS Chem. Biol.* 7, 1158–1163. doi:10.1021/cb300054n
- Lou, D. Y., Dominguez, I., Toselli, P., Landesman-Bollag, E., O'Brien, C., and Seldin, D. C. (2008). The Alpha Catalytic Subunit of Protein Kinase CK2 Is Required for Mouse Embryonic Development. *Mol. Cell. Biol.* 28, 131–139. doi:10.1128/MCB.01119-07
- Loukil, A., Barrington, C., and Goetz, S. C. (2021). A Complex of Distal Appendage-Associated Kinases Linked to Human Disease Regulates Ciliary Trafficking and Stability. *Proc. Natl. Acad. Sci. USA* 118, e2018740118. doi:10.1073/pnas.2018740118
- Marin, O., Meggio, F., Sarno, S., and Pinna, L. A. (1997). Physical Dissection of the Structural Elements Responsible for Regulatory Properties and Intersubunit Interactions of Protein Kinase CK2 β -Subunit. *Biochemistry* 36, 7192–7198. doi:10.1021/bi962885q
- Martinez-Monseny, A. F., Casas-Alba, D., Arjona, C., Bolasell, M., Casano, P., Muchart, J., et al. (2020). Okur-Chung Neurodevelopmental Syndrome in a Patient from Spain. *Am. J. Med. Genet.* 182, 20–24. doi:10.1002/ajmg.a.61405
- Meek, D. W., and Cox, M. (2011). Induction and Activation of the P53 Pathway: a Role for the Protein Kinase CK2? *Mol. Cell. Biochem.* 356, 133–138. doi:10.1007/s11010-011-0966-3
- Meggio, F., Marin, O., and Pinna, L. A. (1994). Substrate Specificity of Protein Kinase CK2. *Cell. Mol. Biol. Res.* 40, 401–409.
- Meggio, F., Boldyreff, B., Marin, O., Issinger, O.-G., and Pinna, L. A. (1995). Phosphorylation and Activation of Protein Kinase CK2 by P34cdc2 Are Independent Events. *Eur. J. Biochem.* 230, 1025–1031. doi:10.1111/j.1432-1033.1995.tb02651.x
- Meggio, F., Boldyreff, B., Marin, O., Pinna, L. A., and Issinger, O.-G. (1992). Role of the Beta Subunit of Casein Kinase-2 on the Stability and Specificity of the Recombinant Reconstituted Holoenzyme. *Eur. J. Biochem.* 204, 293–297. doi:10.1111/j.1432-1033.1992.tb16636.x
- Montenarh, M., and Götz, C. (2020). Protein Kinase CK2 and Ion Channels (Review). *Biomed. Rep.* 13, 1. doi:10.3892/br.2020.1362
- Montenarh, M. (2014). Protein Kinase CK2 and Angiogenesis. *Adv. Clin. Exp. Med.* 23, 153–158. doi:10.17219/acem/37040
- Muhamad Hanif, I., and Pervaiz, S. (2011). Repressing the Activity of Protein Kinase CK2 Releases Mitochondria-Mediated Apoptosis in Cancer Cells. *Cdt* 12, 902–908. doi:10.2174/138945011795528831
- Nakamura, K., Anitha, A., Yamada, K., Tsujii, M., Iwayama, Y., Hattori, E., et al. (2008). Genetic and Expression Analyses Reveal Elevated Expression of Syntaxin 1A (STX1A) in High Functioning Autism. *Int. J. Neuropsychopharm.* 11, 1073–1084. doi:10.1017/S1461145708009036
- Nakashima, M., Tohyama, J., Nakagawa, E., Watanabe, Y., Siew, C. n. G., Kwong, C. S., et al. (2019). Identification of De Novo CSNK2A1 and CSNK2B Variants in Cases of Global Developmental Delay with Seizures. *J. Hum. Genet.* 64, 313–322. doi:10.1038/s10038-018-0559-z
- Nicolini, C., and Fahnestock, M. (2018). The Valproic Acid-Induced Rodent Model of Autism. *Exp. Neurol.* 299, 217–227. doi:10.1016/j.expneurol.2017.04.017
- Niefind, K., Pütter, M., Guerra, B., Issinger, O. G., and Schomburg, D. (1999). GTP Plus Water Mimic ATP in the Active Site of Protein Kinase CK2. *Nat. Struct. Biol.* 6, 1100–1103. doi:10.1038/70033
- Niefind, K., Guerra, B., Ermakowa, I., and Issinger, O.-G. (2001). Crystal Structure of Human Protein Kinase CK2: Insights into Basic Properties of the CK2 Holoenzyme. *EMBO J.* 20, 5320–5331. doi:10.1093/emboj/20.19.5320
- Niefind, K., Guerra, B., Pinna, L. A., Issinger, O. G., and Schomburg, D. (1998). Crystal Structure of the Catalytic Subunit of Protein Kinase CK2 from Zea mays at 2.1 Å Resolution. *EMBO J.* 17, 2451–2462. doi:10.1093/emboj/17.9.2451
- Niefind, K., and Issinger, O.-G. (2005). Primary and Secondary Interactions between CK2 α and CK2 β lead to Ring-like Structures in the Crystals of the CK2 Holoenzyme. *Mol. Cell. Biochem.* 274, 3–14. doi:10.1007/s11010-005-3114-0
- Okur, V., Cho, M. T., Henderson, L., Retterer, K., Schneider, M., Sattler, S., et al. (2016). De Novo mutations in CSNK2A1 Are Associated with

- Neurodevelopmental Abnormalities and Dysmorphic Features. *Hum. Genet.* 135, 699–705. doi:10.1007/s00439-016-1661-y
- Olsen, B. B., Rasmussen, T., Niefind, K., and Issinger, O.-G. (2008). Biochemical Characterization of CK2 α and α' Paralogues and Their Derived Holoenzymes: Evidence for the Existence of a Heterotrimeric CK2 α' -Holoenzyme Forming Trimeric Complexes. *Mol. Cell. Biochem.* 316, 37–47. doi:10.1007/s11010-008-9824-3
- Osmundsen, A. M., Keisler, J. L., Taketo, M. M., and Davis, S. W. (2017). Canonical WNT Signaling Regulates the Pituitary Organizer and Pituitary Gland Formation. *Endocrinology* 158, 3339–3353. doi:10.1210/en.2017-00581
- Owen, C. I., Bowden, R., Parker, M. J., Patterson, J., Patterson, J., Price, S., et al. (2018). Extending the Phenotype Associated with the CSNK2A1- Related Okur-Chung Syndrome-A Clinical Study of 11 Individuals. *Am. J. Med. Genet.* 176, 1108–1114. doi:10.1002/ajmg.a.38610
- Pfleger, C. M., and Kirschner, M. W. (2000). The KEN Box: an APC Recognition Signal Distinct from the D Box Targeted by Cdh1. *Genes Dev.* 14, 655–665. doi:10.1101/gad.14.6.655
- Pinna, L. A. (2002). Protein Kinase CK2: a challenge to Canons. *J. Cell Sci.* 115, 3873–3878. doi:10.1242/jcs.00074
- Poirier, K., Hubert, L., Viot, G., Rio, M., Billuart, P., Besmond, C., et al. (2017). CSNK2B Splice Site Mutations in Patients Cause Intellectual Disability with or without Myoclonic Epilepsy. *Hum. Mutat.* 38, 932–941. doi:10.1002/humu.23270
- Putch, G. V., and Johnson, E. M. (2004). 'Men Are but Worms.' Neuronal Cell Death in *C. elegans* and Vertebrates. *Cell Death Differ* 11, 38–48. doi:10.1038/sj.cdd.4401352
- Raimondo, J. V., Burman, R. J., Katz, A. A., and Akerman, C. J. (2015). Ion Dynamics during Seizures. *Front. Cell. Neurosci.* 9, 419. doi:10.3389/fncel.2015.00419
- Rebholz, H., Nishi, A., Liebscher, S., Nairn, A. C., Flajolet, M., and Greengard, P. (2009). CK2 Negatively Regulates G S Signaling. *Proc. Natl. Acad. Sci.* 106, 14096–14101. doi:10.1073/pnas.0906857106
- Rebholz, H., Zhou, M., Nairn, A. C., Greengard, P., and Flajolet, M. (2013). Selective Knockout of the Casein Kinase 2 in D1 Medium Spiny Neurons Controls Dopaminergic Function. *Biol. Psychiatry* 74, 113–121. doi:10.1016/j.biopsych.2012.11.013
- Roffey, S. E., and Litchfield, D. W. (2021). CK2 Regulation: Perspectives in 2021. *Biomedicine* 9, 1361. doi:10.3390/biomedicine9101361
- Romero-Oliva, F., and Allende, J. E. (2001). Protein p21WAF1/CIP1 Is Phosphorylated by Protein Kinase CK2 *In Vitro* and Interacts with the Amino Terminal End of the CK2 Beta Subunit. *J. Cell. Biochem.* 81, 445–452. doi:10.1002/1097-4644(20010601)81:3<445::aid-jcb1058>3.0.co;2-2
- Rowe, A. L., Gibson, S. A., Meares, G. P., Rajbhandari, R., Nozell, S. E., Dees, K. J., et al. (2017). Protein Kinase CK2 Is Important for the Function of Glioblastoma Brain Tumor Initiating Cells. *J. Neurooncol.* 132, 219–229. doi:10.1007/s11060-017-2378-z
- Ruzzene, M., and Pinna, L. A. (20101804). Addiction to Protein Kinase CK2: a Common Denominator of Diverse Cancer Cells? *Biochim. Biophys. Acta (Bba) - Proteins Proteomics* 1804, 499–504. doi:10.1016/j.bbapap.2009.07.018
- Sagata, N., Oskarsson, M., Copeland, T., Brumbaugh, J., and Woude, G. F. V. (1988). Function of C-Mos Proto-Oncogene Product in Meiotic Maturation in *Xenopus* Oocytes. *Nature* 335, 519–525. doi:10.1038/335519a0
- Sakaguchi, Y., Uehara, T., Suzuki, H., Kosaki, K., and Takenouchi, T. (2017). Truncating Mutation in CSNK2B and Myoclonic Epilepsy. *Hum. Mutat.* 38, 1611–1612. doi:10.1002/humu.23307
- Salizzato, V., Zanin, S., Borgo, C., Lidron, E., Salvi, M., Rizzuto, R., et al. (2019). Protein Kinase CK2 Subunits Exert Specific and Coordinated Functions in Skeletal Muscle Differentiation and Fusogenic Activity. *FASEB j.* 33, 10648–10667. doi:10.1096/fj.201801833RR
- Santos-Terra, J., Deckmann, I., Schwingel, G. B., Paz, A. V. C., Gama, C. S., Bambini-Junior, V., et al. (2021). Resveratrol Prevents Long-Term Structural Hippocampal Alterations and Modulates Interneuron Organization in an Animal Model of ASD. *Brain Res.* 1768, 147593. doi:10.1016/j.brainres.2021.147593
- Sanz-Clemente, A., Gray, J. A., Ogilvie, K. A., Nicoll, R. A., and Roche, K. W. (2013). Activated CaMKII Couples GluN2B and Casein Kinase 2 to Control Synaptic NMDA Receptors. *Cell Rep.* 3, 607–614. doi:10.1016/j.celrep.2013.02.011
- Sanz-Clemente, A., Matta, J. A., Isaac, J. T. R., and Roche, K. W. (2010). Casein Kinase 2 Regulates the NR2 Subunit Composition of Synaptic NMDA Receptors. *Neuron* 67, 984–996. doi:10.1016/j.neuron.2010.08.011
- Sarno, S., Ghisellini, P., and Pinna, L. A. (2002). Unique Activation Mechanism of Protein Kinase CK2. *J. Biol. Chem.* 277, 22509–22514. doi:10.1074/jbc.M200486200
- Sarno, S., Vaglio, P., Cesaro, L., Marin, O., and Pinna, L. A. (1999). A Multifunctional Network of Basic Residues Confers Unique Properties to Protein Kinase CK2. *Mol. Cell. Biochem.* 191, 13–19. doi:10.1007/978-1-4419-8624-5_2
- Sarno, S., Vaglio, P., Meggio, F., Issinger, O.-G., and Pinna, L. A. (1996). Protein Kinase CK2 Mutants Defective in Substrate Recognition. *J. Biol. Chem.* 271, 10595–10601. doi:10.1074/jbc.271.18.10595
- Seetoh, W.-G., Chan, D. S.-H., Matak-Vinković, D., and Abell, C. (2016). Mass Spectrometry Reveals Protein Kinase CK2 High-Order Oligomerization via the Circular and Linear Assembly. *ACS Chem. Biol.* 11, 1511–1517. doi:10.1021/acschembio.6b00064
- Seldin, D. C., Landesman-Bollag, E., Farago, M., Currier, N., Lou, D., and Dominguez, I. (2005). CK2 as a Positive Regulator of Wnt Signalling and Tumorigenesis. *Mol. Cell. Biochem.* 274, 63–67. doi:10.1007/s11010-005-3078-0
- Seldin, D. C., Lou, D. Y., Toselli, P., Landesman-Bollag, E., and Dominguez, I. (2008). Gene Targeting of CK2 Catalytic Subunits. *Mol. Cell. Biochem.* 316, 141–147. doi:10.1007/s11010-008-9811-8
- Soden, S. E., Saunders, C. J., Willig, L. K., Farrow, E. G., Smith, L. D., Petrikin, J. E., et al. (2014). Effectiveness of Exome and Genome Sequencing Guided by Acuity of Illness for Diagnosis of Neurodevelopmental Disorders. *Sci. Transl. Med.* 6, 265ra168. doi:10.1126/scitranslmed.3010076
- Song, D. H., Dominguez, I., Mizuno, J., Kaut, M., Mohr, S. C., and Seldin, D. C. (2003). CK2 Phosphorylation of the Armadillo Repeat Region of β -Catenin Potentiates Wnt Signaling. *J. Biol. Chem.* 278, 24018–24025. doi:10.1074/jbc.M212260200
- Soto, D., Pancetti, F., Marengo, J. J., Sandoval, M., Sandoval, R., Orrego, F., et al. (2004). Protein Kinase CK2 in Postsynaptic Densities: Phosphorylation of PSD-95/SAP90 and NMDA Receptor Regulation. *Biochem. Biophysical Res. Commun.* 322, 542–550. doi:10.1016/j.bbrc.2004.07.158
- St-Denis, N. A., Derksen, D. R., and Litchfield, D. W. (2009). Evidence for Regulation of Mitotic Progression through Temporal Phosphorylation and Dephosphorylation of CK2 α . *Mol. Cell. Biol.* 29, 2068–2081. doi:10.1128/MCB.01563-08
- Stocker, M., Krause, M., and Pedarzani, P. (1999). An Apamin-Sensitive Ca²⁺-Activated K⁺ Current in Hippocampal Pyramidal Neurons. *Proc. Natl. Acad. Sci.* 96, 4662–4667. doi:10.1073/pnas.96.8.4662
- Takai, H., Tominaga, K., Motoyama, N., Minamishima, Y. A., Nagahama, H., Tsukiyama, T., et al. (2000). Aberrant Cell Cycle Checkpoint Function and Early Embryonic Death in Chk1–/– Mice. *Genes Dev.* 14, 1439–1447. doi:10.1101/gad.14.12.1439
- Tapia, J. C., Bolanos-Garcia, V. M., Sayed, M., Allende, C. C., and Allende, J. E. (2004). Cell Cycle Regulatory Protein p27KIP1 Is a Substrate and Interacts with the Protein Kinase CK2. *J. Cell. Biochem.* 91, 865–879. doi:10.1002/jcb.20027
- Theis-Febvre, N., Filhol, O., Froment, C., Cazales, M., Cochet, C., Monsarrat, B., et al. (2003). Protein Kinase CK2 Regulates CDC25B Phosphatase Activity. *Oncogene* 22, 220–232. doi:10.1038/sj.onc.1206107
- Trinh, J., Hüning, I., Budler, N., Hingst, V., Lohmann, K., and Gillesen-Kaesbach, G. (2017). A Novel De Novo Mutation in CSNK2A1: Reinforcing the Link to Neurodevelopmental Abnormalities and Dysmorphic Features. *J. Hum. Genet.* 62, 1005–1006. doi:10.1038/jhg.2017.73
- Valente, E. M., Rosti, R. O., Gibbs, E., and Gleeson, J. G. (2014). Primary Cilia in Neurodevelopmental Disorders. *Nat. Rev. Neurol.* 10, 27–36. doi:10.1038/nrneurol.2013.247
- Verkerk, A. J. M. H., Pieretti, M., Sutcliffe, J. S., Fu, Y.-H., Kuhl, D. P. A., Pizzuti, A., et al. (1991). Identification of a Gene (FMR-1) Containing a CGG Repeat Coincident with a Breakpoint Cluster Region Exhibiting Length Variation in Fragile X Syndrome. *Cell* 65, 905–914. doi:10.1016/0092-8674(91)90397-h

- Wilke, M. V. M. B., Oliveira, B. M., Pereira, A., Doriqui, M. J. R., Kok, F., and Souza, C. F. M. (2022). Two Different Presentations of De Novo Variants of CSNK2B: Two Case Reports. *J. Med. Case Rep.* 16, 4. doi:10.1186/s13256-021-03184-8
- World Health Organization (2013). Autism Spectrum Disorders & Other Developmental Disorders. From Raising Awareness to Building Capacity. World Health Organization. Available at: https://www.who.int/mental_health/maternal-child/autism_report/en/ (Accessed May 14, 2021).
- Wu, R.-h., Tang, W.-t., Qiu, K.-y., Li, X.-j., Tang, D.-x., Meng, Z., et al. (2021). Identification of Novel CSNK2A1 Variants and the Genotype-Phenotype Relationship in Patients with Okur-Chung Neurodevelopmental Syndrome: a Case Report and Systematic Literature Review. *J. Int. Med. Res.* 49, 030006052110170. doi:10.1177/03000605211017063
- Xu, S., Lian, Q., Wu, J., Li, L., and Song, J. (2020). Dual Molecular Diagnosis of Tricho-Rhino-Phalangeal Syndrome Type I and Okur-Chung Neurodevelopmental Syndrome in One Chinese Patient: a Case Report. *BMC Med. Genet.* 21, 158. doi:10.1186/s12881-020-01096-w

Conflict of Interest: The authors declare that the research was conducted in the absence of any commercial or financial relationships that could be construed as a potential conflict of interest.

Publisher's Note: All claims expressed in this article are solely those of the authors and do not necessarily represent those of their affiliated organizations, or those of the publisher, the editors and the reviewers. Any product that may be evaluated in this article, or claim that may be made by its manufacturer, is not guaranteed or endorsed by the publisher.

Copyright © 2022 Ballardin, Cruz-Gamero, Bienvenu and Rebholz. This is an open-access article distributed under the terms of the Creative Commons Attribution License (CC BY). The use, distribution or reproduction in other forums is permitted, provided the original author(s) and the copyright owner(s) are credited and that the original publication in this journal is cited, in accordance with accepted academic practice. No use, distribution or reproduction is permitted which does not comply with these terms.



Mechanism of CK2 Inhibition by a Ruthenium-Based Polyoxometalate

Simone Fabbian¹, Gabriele Giachin¹, Massimo Bellanda^{1,2}, Christian Borgo³, Maria Ruzzene^{3,4*}, Giacomo Spuri³, Ambra Campofelice¹, Laura Veneziano¹, Marcella Bonchio^{1,5}, Mauro Carraro^{1,5*} and Roberto Battistutta^{1,2*}

¹Department of Chemical Sciences, University of Padova, Padova, Italy, ²CNR Institute of Biomolecular Chemistry, University of Padova, Padova, Italy, ³Department of Biomedical Sciences, University of Padova, Padova, Italy, ⁴CNR Institute of Neurosciences, University of Padova, Padova, Italy, ⁵Institute on Membrane Technology (ITM)-CNR, University of Padova, Padova, Italy

OPEN ACCESS

Edited by:

Victor Bustos,
The Rockefeller University,
United States

Reviewed by:

Aleksandar Kondinski,
University of Cambridge,
United Kingdom
Masooma Ibrahim,
Karlsruhe Institute of Technology (KIT),
Germany

*Correspondence:

Maria Ruzzene
maria.ruzzene@unipd.it
Mauro Carraro
mauro.carraro@unipd.it
Roberto Battistutta
roberto.battistutta@unipd.it

Specialty section:

This article was submitted to
Molecular Diagnostics and
Therapeutics,
a section of the journal
Frontiers in Molecular Biosciences

Received: 28 March 2022

Accepted: 18 May 2022

Published: 02 June 2022

Citation:

Fabbian S, Giachin G, Bellanda M,
Borgo C, Ruzzene M, Spuri G,
Campofelice A, Veneziano L,
Bonchio M, Carraro M and
Battistutta R (2022) Mechanism of CK2
Inhibition by a Ruthenium-
Based Polyoxometalate.
Front. Mol. Biosci. 9:906390.
doi: 10.3389/fmolb.2022.906390

CK2 is a Ser/Thr protein kinase involved in many cellular processes such as gene expression, cell cycle progression, cell growth and differentiation, embryogenesis, and apoptosis. Aberrantly high CK2 activity is widely documented in cancer, but the enzyme is also involved in several other pathologies, such as diabetes, inflammation, neurodegeneration, and viral infections, including COVID-19. Over the last years, a large number of small-molecules able to inhibit the CK2 activity have been reported, mostly acting with an ATP-competitive mechanism. Polyoxometalates (POMs), are metal-oxide polyanionic clusters of various structures and dimensions, with unique chemical and physical properties. POMs were identified as nanomolar CK2 inhibitors, but their mechanism of inhibition and CK2 binding site remained elusive. Here, we present the biochemical and biophysical characterizing of the interaction of CK2 α with a ruthenium-based polyoxometalate, $[\text{Ru}_4(\mu\text{-OH})_2(\mu\text{-O})_4(\text{H}_2\text{O})_4(\gamma\text{-SiW}_{10}\text{O}_{36})_2]^{10-}$ (Ru_4POM), a potent inhibitor of CK2. Using analytical Size-Exclusion Chromatography (SEC), Isothermal Titration Calorimetry (ITC), and SAXS we were able to unravel the mechanism of inhibition of Ru_4POM . Ru_4POM binds to the positively-charged substrate binding region of the enzyme through electrostatic interactions, triggering the dimerization of the enzyme which consequently is inactivated. Ru_4POM is the first non-peptide molecule showing a substrate-competitive mechanism of inhibition for CK2. On the basis of SAXS data, a structural model of the inactivated $(\text{CK2}\alpha)_2(\text{Ru}_4\text{POM})_2$ complex is presented.

Keywords: CK2, inhibition, polyoxometalate, SAXS, substrate competitive

INTRODUCTION

Protein kinase CK2 (previously known as casein kinase 2 or CK2) is a eukaryotic Ser/Thr protein kinase, ubiquitous and extremely conserved throughout evolution (Pinna, 2002; Niefind and Battistutta, 2013). Despite the name, it is a “pseudo” casein kinase since casein is not a physiological substrate (Venerando et al., 2014). Indeed, CK2 phosphorylates hundreds of cellular proteins involved in practically all biological processes (St-Denis and Litchfield, 2009), and a dysregulated phosphorylation level of many of its targets has been associated with diverse human diseases (Borgo et al., 2021b). While some pathological conditions seem related to reduced CK2 activity (Dominguez et al., 2021), usually the CK2 overexpression and the resulting abnormally elevated catalytic activity have been associated to diseases. Cancer is the best-known example of this

condition, and the role of CK2 in the strengthening of several oncogenic signals has been extensively described (Duncan and Litchfield, 2008; Ruzzene and Pinna, 2010; Trembley et al., 2010; Ortega et al., 2014; Chua et al., 2017). The pharmacological inhibition of CK2 has been largely pursued, not only for cancer but also for the drug resistant phenotype (Borgo and Ruzzene, 2019), and several inhibitors have been discovered and characterized, bearing variable degrees of efficiency and specificity, recently reviewed in (Qiao et al., 2019; Borgo and Ruzzene, 2021).

In CK2, the α catalytic subunit (or its isoform α') and the β “regulatory” subunit are associated to form the $\alpha_2\beta_2$ tetrameric holoenzyme, the prevailing form of CK2 in cells (Niefind and Battistutta, 2013). CK2 is considered “intrinsically active” because the α -subunit does not undergo significant conformational changes between active and inactive conformations (which do not exist actually), as typical for other protein kinases, in which phosphorylation events or interactions with regulatory subunits shuffle the enzyme between the two states (Niefind et al., 2001). Instead, in CK2, the α -subunit is structurally locked in the active conformation, mainly because of the unique N-terminal extension and the presence of the DWG (Asp-Trp-Gly) motif, rather than the conventional DFG (Asp-Phe-Gly) one, at the beginning of the activation loop. Together, these two characteristics block the activation segment in the active conformation, hampering the movements seen in other protein kinases, with the formation of inactive structures. As a consequence, the α catalytic subunit is catalytically functional either when isolated or part of the tetrameric enzyme. However, mechanisms for the control of CK2 functions in cell should exist, but they have not been firmly established, yet. It was proposed that it is based on a self-inhibitory oligomerization process of the $\alpha_2\beta_2$ holoenzyme, which is active in the monomeric form, but inactive when it forms trimers and higher ordered assemblies, where substrate binding is hampered (Lolli et al., 2012; Lolli et al., 2014; Lolli and Battistutta, 2015; Lolli et al., 2017). This explanation takes into account the absence of a truly inactive conformation of the catalytic subunit.

Selectivity is one major issue in the development of the most studied class of kinase inhibitors, the ATP-competitive one. This because of the conservation of the structural features of the ATP-binding sites among kinases and other ATP-binding proteins, and the high concentration of ATP inside the cell, ~ 1 – 10 mM. However, despite these difficulties, effective ATP-competitive kinase inhibitors have been successfully developed, and as of 21 January 2022 there are 70 FDA-approved small molecule protein kinase inhibitors for clinical application (Roskoski, 2021) (<http://www.brimr.org/PKI/PKIs.htm>). Yet, many of these compounds show unfavorable side effects and are convenient only when conventional treatments of cancers have been ineffective (Montazeri and Bellmunt, 2020).

The class of the ATP-competitive inhibitors is the most explored also for CK2. The crystal structure of CK2 α in complex with the anthraquinone emodin was the first showing the details of the interaction between the enzyme and an ATP-competitive inhibitor (Battistutta et al., 2000). The main characteristics of the CK2 ATP-binding site were described

some time ago (De Moliner et al., 2003; Battistutta et al., 2007; Mazzorana et al., 2008; Battistutta, 2009). As CK2 is constitutively active, only the active conformation (conventionally called “DFG-in”) can be targeted and therefore only the so-called “type I inhibitors” can be developed (Mazzorana et al., 2008; Battistutta, 2009; Sarno et al., 2011; Niefind and Battistutta, 2013; Atkinson et al., 2021). One of the most studied and used type I ATP-competitive inhibitor is CX-4945 (silmitasertib) (Battistutta et al., 2011). This compound is currently in phase II clinical trials for the treatment of various tumors and was established as Orphan Drug for cholangiocarcinoma in the United States. The selectivity issue in targeting the ATP-binding site is underlined by the fact that even CX-4945, despite its potency and efficacy, is able to inhibit also 12 other kinases with nanomolar activity.

To cope with the selectivity issue, recently, other inhibition modes were identified, which target the catalytic CK2 α subunit in different sites, namely the CK2 α /CK2 β interaction site, the substrate binding site and some potential allosteric sites outside of the classic “catalytic box” (Figure 1A) (Iegre et al., 2021). Regarding the targeting of the α/β interaction site, although it could suggest high selectivity, one critical point is that the CK2 α subunit is constitutively active and CK2 β is assumed to modulate, but not to fully suppress or switch on, the catalytic activity of the enzyme. CK2 β can also regulate the substrate specificity of CK2 (Pinna, 2002; Borgo et al., 2021a). Furthermore, the binding pocket at the α/β interface, located in the N-terminal domain of the α subunit, is shallow and relatively small, and it seems quite difficult to be targeted with efficiency and potency either by peptides or small molecules. Thus, targeting the CK2 α /CK2 β interaction site does not seem a promising strategy valid for all substrates and for the full inhibition of the catalytic activity of CK2. The development of substrate-competitive molecules (peptides or peptidomimetics) appears to be a promising approach particularly regarding the selectivity issue. In fact, unlike most protein kinases, CK2 exclusively phosphorylates acidic substrates, with a minimum consensus sequence S/T-X-X-E/D/pX, often with acidic residues also in position $n + 1$ and/or $n + 2$ (Pinna, 2002). Polyglutamyl peptides were early identified as CK2 substrate-competitive inhibitors (Meggio et al., 1983). However, the lack of structural data on complexes between CK2 and substrate makes the design of effective peptide inhibitors quite difficult, along with the fact that peptide-based molecules have low pharmacological profiles.

For some compounds targeting CK2 it was proposed an allosteric mechanism of inhibition (Prudent and Cochet, 2009; Iegre et al., 2021), yet the exact mode of action was never clarified and no structural data supporting the allosteric mechanism was produced (Brear et al., 2020).

It was early noted that in the human enzyme the hinge/ α D region, located near the active site, has an unusual mobility, unique among protein kinases, with the existence of a closed and an open conformation (Figure 1B) (Battistutta and Lolli, 2011; Papinutto et al., 2012; Niefind and Battistutta, 2013). It was then anticipated that this feature could be exploited for the development of more selective ATP-competitive inhibitors

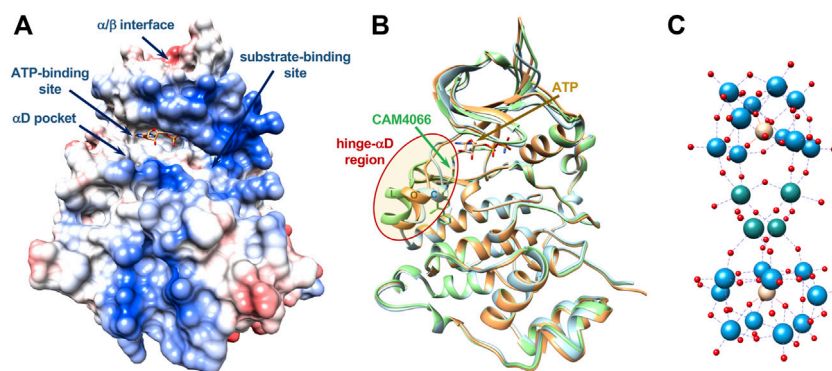


FIGURE 1 | Main interaction sites in catalytic CK2α. **(A)** Surface representation, colored according to electrostatics, of the CK2α-ATP complex (PDB-code 3NSZ); main interactions sites targeted by different classes of inhibitors discussed in the text are shown. Location of allosteric sites are uncertain as well as binding sites for POMs. **(B)** Ribbon representation of three structures of CK2α showing the conformational variability of the very mobile hinge-αD region (red oval), which can adopt a closed (C, in cyan), open (O, in orange) or large (L, in green) conformation (PDB-codes 3Q9W, 3NSZ, and 5CU3, respectively). The αD pocket is created with the “large” conformation, in presence of specific ligands such as CAM4066, shown in green. Bound ATP is shown (carbon atoms in orange). **(C)** Molecular structure of [Ru₄(H₂O)₄(μ-O)₄(μ-OH)₂(γ-SiW₁₀O₃₆)₂]¹⁰⁻ (Ru₄POM), object of this study: Ru atoms in sea-green, W atoms in light-blue, O atoms in red, Si atoms in yellow. Dimensions of Ru₄POM are around 10 × 10 × 18 Å (not in scale with CK2).

(Battistutta and Lolli, 2011; Papinutto et al., 2012). Indeed, recently, it was found that inhibitor SRPIN803-rev binds to the ATP-binding site of CK2α interacting with the open hinge/αD conformation of CK2α, with a binding mode incompatible with the closed conformation adopted by most protein kinases. This rationalizes the high selectivity of derivatives of SRPIN803-rev when tested on a panel of 320 kinases, despite the not exceptional IC₅₀, which ranges from 0.28 to 1.37 μM. Notably, the lead SRPIN803-rev derivative shows an efficacy analogous to that of CX-4945 in cells (Dalle Vedove et al., 2020).

The high mobility of the hinge/αD region, unique to CK2, is at the basis of the very interesting discovery of a new pocket near the ATP-binding site, in the C-terminal domain, the so-called “αD pocket,” corresponding to a “large” conformation of the hinge/αD region (Figure 1B). The αD pocket can be efficiently targeted by a new class of inhibitors, for instance compound CAM4066, which shows an IC₅₀ of 0.37 μM, similar to SRPIN803-rev derivatives, and a promising selectivity on a panel of selected 52 kinases (Brear et al., 2016; Iegre et al., 2018).

Polyoxometalates (POMs) are other interesting compounds explored as CK2 inhibitors. POMs are a class of polynuclear oxo-bridged transition metal complexes, which have received extensive attention due to rich topology and tunable chemical/physical properties. In addition to the application in material design (Long et al., 2010) and catalysts (Wang and Yang, 2015), their biological activity has been highlighted (Van Rompuy and Parac-Vogt, 2019). The main advantages of POMs are that their shape, acidity, surface charge distribution and redox potentials can be easily tuned to optimize the interaction with biological macromolecules. POMs were thus proved to cross cell membranes, to display anticancer, antiviral or antibacterial properties. However, their low stability at neutral pH, associated with low selectivity and relevant cytotoxicity has hampered their clinical applications. In order to overcome

these drawbacks, POMs can be encapsulated into different delivery systems (Croce et al., 2019). Moreover, their structure can be successfully strengthened by introducing different transition metals (such as Ru, Ti or Co) or by the covalent grafting of organic pendants (Bijelic et al., 2019). In this way, biomedical studies could be performed on POMs stable in solution, employing physiological conditions and concentrations (Čolović et al., 2020). The derivatization of POMs may increase both stability and bioavailability, while providing interesting opportunities for tracking and targeting (Zamolo et al., 2018; Ramezani-Aliakbari et al., 2021; Tagliavini et al., 2021).

Owing to their nano-size, POMs are able to establish various types of interactions with peptides and proteins, ranging from electrostatic interaction and hydrogen bonds, also mediated by water or cations, to other weaker types of interactions (Arefian et al., 2017). These interactions may become more important when organic counterions and appended organic molecules are also present (Zamolo et al., 2018; Tagliavini et al., 2021). POMs are also able to inhibit several enzymes (Zhao et al., 2020). Some POMs were shown to inhibit CK2 in the low nanomolar range (Prudent et al., 2008), with a mechanism of action still unclear, presumably different from that of classical small organic molecules due to their different chemical nature.

Here, we present structural and functional data regarding the CK2 inhibition by a ruthenium-based polyoxometalate, [Ru₄(H₂O)₄(μ-O)₄(μ-OH)₂(γ-SiW₁₀O₃₆)₂]¹⁰⁻ (Ru₄POM) (Figure 1C), revealing for the first time the mechanism of action of a member of the class of the POMs inhibitors. Ru₄POM has a significant biomimetic activity, fostered by the ruthenium atoms (Bonchio et al., 2019; Gobbo et al., 2020), and it has been selected for its high stability and solubility in water, even with high ionic strength, associated with a low toxicity. Moreover, its elongated structure results into dimensions (around 10 × 10 × 18 Å) which seem favorable for a better interaction. Indeed,

TABLE 1 | Inhibitory activity of different POMs.

POM compound	IC ₅₀ (nM)		
	FL-CK2 α	CK2 α	α 2 β 2
Mo ₃₆ POM	>1,000	—	—
Na (L)Trp-SiW ₁₀	18.2 \pm 1.9	—	—
Na (D)Trp-SiW ₁₀	12.8 \pm 1.7	—	—
Na Biotin-SiW ₁₀	16.4 \pm 1.3	—	—
TBA (L)Trp-SiW ₁₀	8.5 \pm 0.4	—	—
TBA (D)Trp-SiW ₁₀	11.0 \pm 0.6	—	—
TBA Biotin-SiW ₁₀	5.3 \pm 0.6	—	—
Ru ₄ POM	3.63 \pm 0.17	3.63 \pm 0.09	5.57 \pm 0.68

IC₅₀ values were determined for CK2 inhibition by means of radioactive kinase assays using the synthetic peptide CK2-tide as substrate, in the presence of increasing concentrations of the indicated POM compound. For Ru₄POM, besides full-length CK2 α (FL-CK2 α), a C-terminal truncated form of CK2 α (CK2 α) and the tetrameric holoenzyme (α 2 β 2) were tested. The other POMs were tested only on full-length CK2 α . At least two independent experiments were performed. Mean values \pm SEM are reported.

Keggin-type structures, with smaller dimension (10 Å as maximum dimension), show low inhibitory efficiency, unless organic pendants are present on the surface (Prudent et al., 2008).

RESULTS

Polyoxometalate Synthesis and Characterization

Na₁₀[Ru₄(H₂O)₄(μ -O)₄(μ -OH)₂(γ -SiW₁₀O₃₆)₂], Ru₄POM (Supplementary Figure S1), was prepared following a published procedure (Galiano et al., 2021). In order to guarantee its use in all conditions explored, its stability was confirmed by UV-vis, in buffered/saline aqueous environments, up to pH 8.5.

Since the presence of organic ligand as biotin was reported to be potentially useful for CK2 inhibition (Prudent et al., 2008), we also included in the screening some representative hybrid organic-inorganic POMs (Supplementary Figures S1, S2): [γ -SiW₁₀O₃₆{(C₅H₇N₂OS)(CH₂)₄CONH(CH₂)₃Si₂O}]⁴⁻, Biotin-SiW₁₀ (Zamolo et al., 2018) and [γ -SiW₁₀O₃₆{(C₁₆H₉)SO₂NH(CH₂)₃Si₂O}]⁴⁻, Trp-SiW₁₀ (Syrgiannis et al., 2019), which were prepared as tetrabutyl ammonium (TBA) salts, following post-functionalization strategies of the Keggin POM K₈[γ -SiW₁₀O₃₆]. The corresponding sodium salts were prepared by counterion exchange as previously described (Zamolo et al., 2018). In case of Trp-SiW₁₀, the two enantiomeric forms of tryptophan were investigated. The giant-wheel-shaped (NH₄)₁₂[Mo₃₆(NO)₄O₁₀₈(H₂O)₁₆], Mo₃₆POM, was also prepared (Amini et al., 2015) to evaluate the impact of the dimensions and shape.

In Vitro CK2 Inhibition by Ru₄POM

First, we analyzed the efficacy of different POMs in decreasing the catalytic activity of recombinant CK2 (Table 1). We found that all polyoxotungstates inhibited CK2 α , with similar IC₅₀ in the low nM range, however, the most powerful compound was Ru₄POM (IC₅₀ 3.63 nM). Concerning the hybrid polyoxotungstates, we observed a moderately higher activity for the lipophilic TBA salts.

In addition, both the nature and the configuration of the organic ligands had an impact on the inhibitory effect. The larger polyoxomolybdate showed very weak activity on CK2. Owing to these results, we focused the rest of our study on Ru₄POM.

Most inhibition assays and all the structural studies were performed with CK2 α deleted of the last 55 C-terminal residues since this deletion confers higher stability to the protein without affecting the catalytic activity (Niefind et al., 2000). Indeed, we found that the full-length monomeric enzyme (FL-CK2 α) displayed identical sensitivity to Ru₄POM (Table 1). Moreover, the presence of the β subunit only marginally reduced the efficacy of Ru₄POM, the tetrameric enzyme displaying an IC₅₀ of 5.57 nM (Table 1).

We then evaluated if the Ru₄POM inhibition efficacy depends on the kind of substrate. We observed a slightly lower inhibition when casein replaced the CK2-tide peptide as substrate; the IC₅₀, however, was still in the low nM range (18.50 \pm 1.04 nM). We then checked whether Ru₄POM competes with the substrates for the CK2 binding-site. As shown by the kinetics analysis reported in Figure 2, we found that Ru₄POM exerts a competitive inhibition towards both model substrates, since it reduced the affinity (increased K_M values for both CK2-tide peptide and casein), without decreasing the V_{max} values.

In the experiments described so far, the activity of recombinant CK2 α was evaluated at the optimal *in vitro* conditions, namely at pH 7.5 and in the absence of NaCl. Given the high negative charge of Ru₄POM, we evaluated if the inhibitory efficacy was affected by changes in pH and ionic strength. Deviation from the optimal conditions reduced the activity of the controls (see samples without Ru₄POM in Figure 3A). Nonetheless, the residual activity was sufficient to perform the experiments, which show that the percent of inhibition induced by Ru₄POM was reduced by the pH change: at 5 nM Ru₄POM, the inhibition dropped from 75% at pH 7.5% to 66% at pH 8.5 (Figure 3B). A higher variation in the inhibition values was seen varying the ionic strength, from 75% inhibition observed without NaCl to 29% and 22% in presence of NaCl at 0.2 M or 0.5 M, respectively.

Ru₄POM Inhibits Endo-Cellular CK2

Next, we wanted to assess whether Ru₄POM was able to inhibit CK2 inside intact cells. Preliminary attempts to detect inhibition of CK2 activity in Ru₄POM-treated cells failed, indicating a too small cell permeability of the compound (not shown). Therefore, we tried to treat cells with Ru₄POM in combination with increasing amounts of two different cationic transfection reagents, the stable cationic polymer polyethylenimine (PEI) and the cationic liposome JetOptimus (Figure 4). Endogenous CK2 activity was monitored by means of the phospho-antibody towards Akt1 phospho-Ser129, a well-known and specific target of CK2 (Ruzzene et al., 2010). We observed that cell treatment with Ru₄POM combined with one of the cationic compounds reduced the phosphorylation of this site (while the total amount of Akt1 protein was unchanged) and the effect was potentiated by increasing the amount of the transfecting reagents, likely due to higher amounts of Ru₄POM delivered into the cells. These results indicate that Ru₄POM is suitable for CK2 inhibition in cell, as it

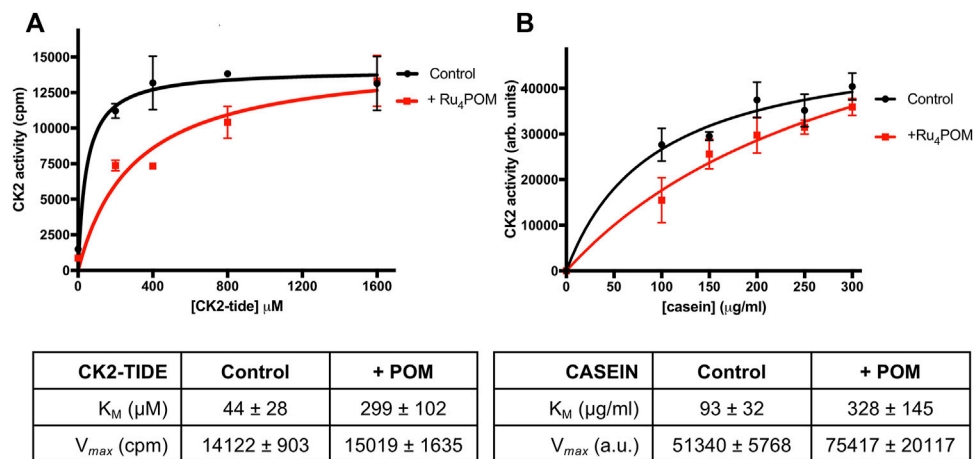


FIGURE 2 | Substrate-competitive inhibition. **(A)** CK2 activity was measured by radioactive phosphorylation assays, with increasing concentrations of CK2-tide peptide, in the absence or presence of 5 nM Ru₄POM. Radioactivity was detected by scintillation counting (cpm). **(B)** CK2 activity was measured by radioactive phosphorylation assays, with increasing concentrations of casein, in the absence or presence of 18 nM Ru₄POM. Radioactivity was detected by digital autoradiography (arbitrary units). At least two independent experiments were performed. Mean values \pm SEM are reported in the graphs; the tables on the bottom report the kinetics parameters \pm SEM calculated by Michaelis-Menten analysis.

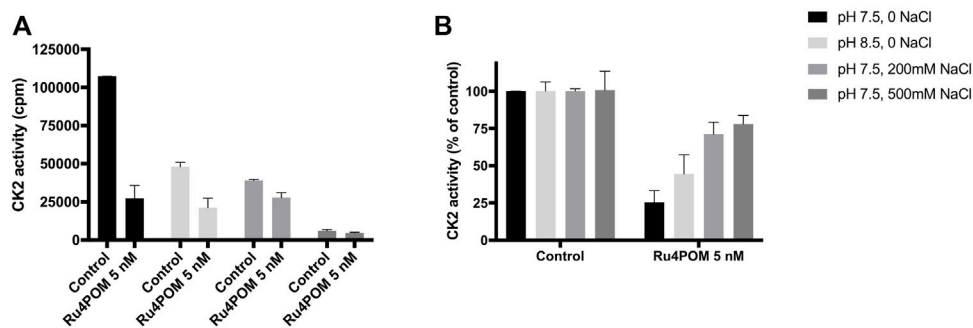


FIGURE 3 | Effect of pH and ionic strength. CK2 activity was measured by radioactive phosphorylation assays towards CK2-tide peptide, in the absence or presence of 5 nM Ru₄POM, at different conditions of pH and NaCl concentration, as indicated. Radioactivity was detected by scintillation counting (cpm) **(A)**. In **(B)**, 100% activity was assigned to each control, measured in the absence of Ru₄POM. Mean values \pm SEM of at least two independent experiments are reported.

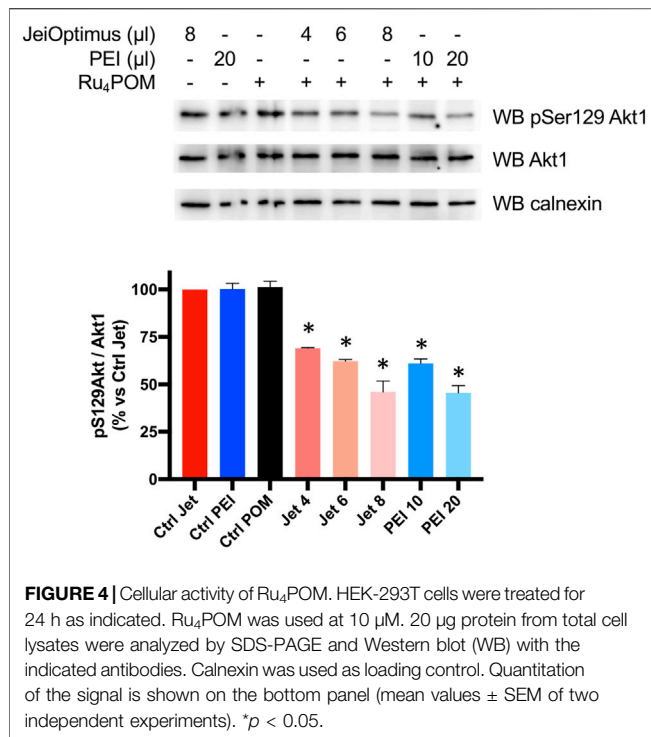
can be transferred inside intact cells, and that it is able to target endogenous CK2.

Interaction Between CK2 α and Ru₄POM by Analytical Size-Exclusion Chromatography

Analytical Size Exclusion Chromatography was then used to investigate the direct interaction between Ru₄POM and CK2 α *in vitro*. SEC elution profiles (**Supplementary Figure S3**) were monitored at 280 nm, where both protein and Ru₄POM have an absorption contribution (blue and black curve, respectively), but also at 500 nm, where only the signal of Ru₄POM is present (red curve). The lack of absorption of CK2 α at 500 nm (green curve) allows to unequivocally recognize the elution of Ru₄POM. In 25 mM Tris, 500 mM NaCl, 1 mM DTT, pH = 8.5, free CK2 α elutes at 12.6 ml retention volume, in the monomeric form (**Supplementary Figure S3**, blue curve), in accordance with the well-known notion that

CK2 α is monomeric at high salt, typically above 0.4 M NaCl, and tends to aggregate at lower ionic strengths (Niefind et al., 1998; Ermakova et al., 2003; Seetoh et al., 2016), as also confirmed by our SEC-SAXS experiments (see below). In the same running conditions, Ru₄POM elutes at higher elution volumes, at 16.0 ml (**Supplementary Figure S3**, black curve at 280 and red curve at 500 nm), corresponding to lower hydrodynamic volumes, in accordance with the smaller dimensions (MW 5 kDa).

The elution profile of samples with Ru₄POM:CK2 α in a 1:1 M ratio on a Superdex 75 column shows a unique peak at about 11.4 ml elution volume (**Figure 5A**, black curve), with the disappearance of the peaks corresponding to the isolated species (**Figure 5A**, blue curve for monomeric CK2 α). The presence of the absorption at 500 nm for the peak at 11.4 ml (red curve) confirms that all Ru₄POM are tightly bound to CK2 α , with the formation of a stable complex. From the elution volume it can be estimated that the complex is formed by two molecules

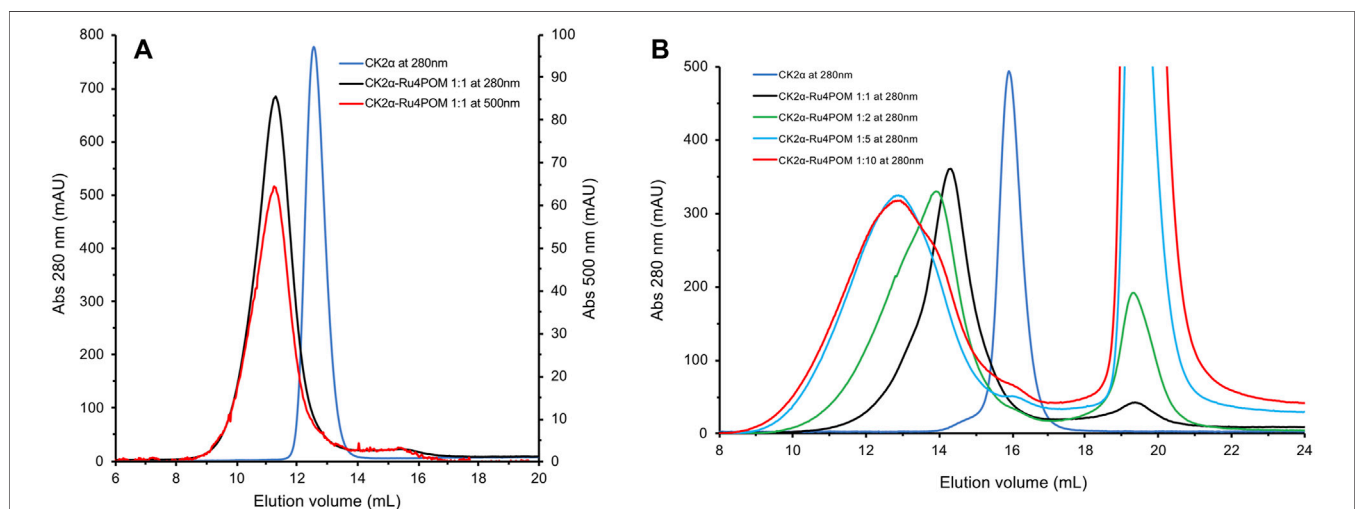


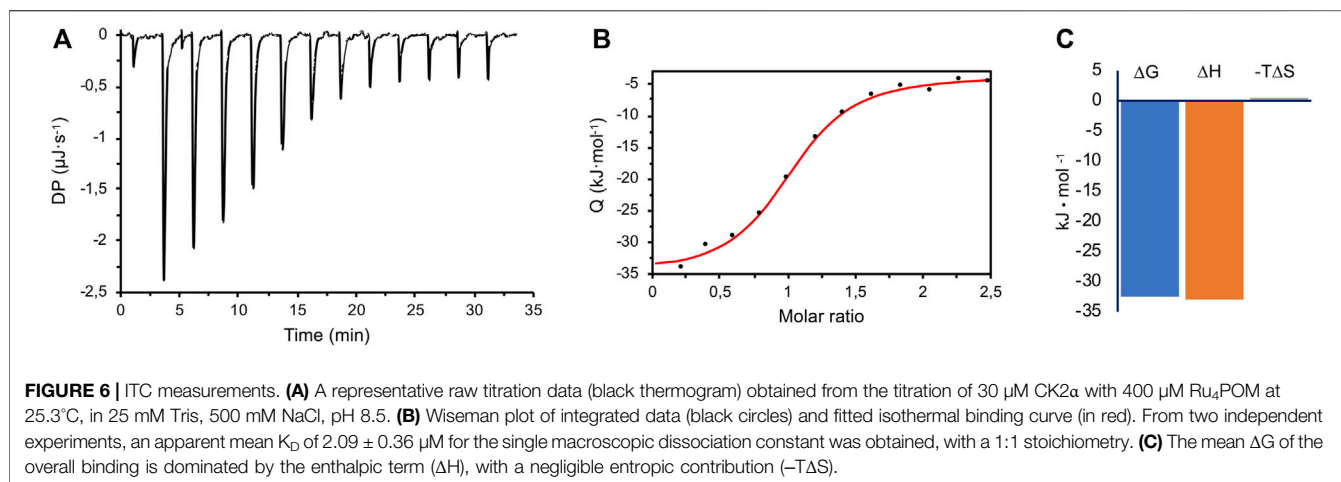
of CK2α. This, together with the 1:1 M ratio of Ru₄POM:CK2α, indicates that a complex of stoichiometry (CK2α)₂(Ru₄POM)₂ is formed.

To further investigate the interaction between CK2α and Ru₄POM, we analysed samples with increasing molar ratios in a Superdex 200 column, which has a higher MWs resolution range. The elution profiles with the unchanged buffer system, 25 mM Tris, 500 mM NaCl, 1 mM DTT, pH = 8.5, of samples with various Ru₄POM/CK2α ratios, namely 1:1, 2:1, 5:1, and 10:1, are shown in **Figure 5B**. It is evident that increasing amounts of Ru₄POM induce the formation of species with larger hydrodynamic dimensions, that is, high-order oligomeric forms of CK2α/Ru₄POM complexes. Very similar elution profiles for ratios 5:1 and 10:1 indicate that the saturation is reached for such values. The large variations in the elution volumes are explained by the formation of oligomeric forms of CK2α/Ru₄POM complexes rather than by the formation of species where monomeric CK2α (MW 40 kDa) is interacting with multiple POMs units (MW 5 kDa). Overall, the SEC experiments indicate that Ru₄POM induces the oligomerization of CK2α, with the formation of dimers when the ratio is 1:1 and of larger assemblies when the ratio is higher, with the saturation reached around 5:1 ratio.

Interaction Between CK2α and Ru₄POM by Isothermal Titration Calorimetry

To better understand the interaction between CK2α and Ru₄POM, the thermodynamic parameters of the binding were determined by isothermal titration calorimetry (ITC). In the ITC measurements, CK2α was titrated with Ru₄POM; both species were in 25 mM Tris, 500 mM NaCl, pH = 8.5. A representative experiment is shown in **Figure 6**, where the exothermic nature of





the interaction is evident. Here, the CK2 α /Ru₄POM titration produces a typical single transition, saturation-shaped thermogram, which can be fitted by the sigmoidal binding isotherm of the one binding-site model. From two independent experiments, we derived an apparent mean K_D of 2.09 ± 0.36 μM for the single macroscopic dissociation constant. The derived stoichiometry for the complex is 1:1 (1.04 ± 0.02), in accordance with the chromatographic data, thus supporting the formation of a stable (CK2 α)₂(Ru₄POM)₂ complex. The analysis of the thermodynamic signature for the binding of Ru₄POM to CK2 α reveals the dominance of the enthalpic contribution ($\Delta H = -32.99 \pm 1.42$ kJ/mol) over a negligible entropic term ($-T\Delta S = 0.50 \pm 2.43$ kJ/mol), and a final $\Delta G = -32.48 \pm 0.46$ kJ/mol (Figure 6C), evidencing the importance of electrostatics and hydrogen-bonds (which can be considered a form of electrostatic interaction) for the binding. For the sake of comparison, Keggin-type POMs as [H₂W₁₂O₄₀]⁶⁻ (H₂W₁₂) interacting with human serum albumin (HSA) were also characterized by enthalpically driven exothermic process, while bigger W-based POMs as [NaP₅W₃₀O₁₁₀]¹⁴⁻ (P₅W₃₀), showed an important endothermic component, mainly attributed to the unfolding of the protein (Zhang et al., 2008).

Interaction Between CK2 α and Ru₄POM by SAXS

Initially, we tested the protein stability at three different ionic strengths (namely 0.5, 0.3, and 0.2 M NaCl), on a SEC GE Superdex Increase 200 (3.2/300) column, equilibrated with buffer 25 mM Tris pH 8.5. The R_g and I(0) traces as functions of the SEC elution profile frames showed that the protein was monodispersed in presence of 0.5 M NaCl (Figure 7A, black curve). However, decreasing the ionic strength to 0.3 and 0.2 mM NaCl resulted in protein precipitation prior SAXS experiments, as indicated by the very low signals (green and cyan curves), in line with the known behavior of CK2 α at low salt concentration.

Primary analysis from selected scattering curves of CK2 α at 0.5 M NaCl indicated that the protein is globular, with R_g value of 2.3 nm, corresponding to an estimated molecular weight of about 39 kDa, as

expected from monomeric CK2 α , in line with the MW estimation from the previous SEC experiments. The comparison between the CK2 α crystal structure and the SAXS data showed good fitting value (χ^2 1.29) (Figure 7B) and the 3D bead model of the DAMMIF envelope overlaid well the crystal structure of CK2 α (Figure 7C), further supporting the presence of the monomeric state at 0.5 M NaCl.

We then analyzed a mixture of CK2 α :Ru₄POM at 1:1 M ratio in presence of 0.5 M NaCl, and the scattering data on the single monodisperse species displayed significant structural differences compared to the free form of CK2 α (Figure 7B). Notably, at this concentration Ru₄POM does not significantly contribute to the scattering profiles (Supplementary Figure S4A). The R_g of the complex determined by Guinier analysis showed a value of 3.1 nm (Figure 7B) and a molecular weight of about 79.7 kDa, a mass that corresponds to the formation of a stable CK2 α dimer, in accordance with the previous SEC estimations. This supports our hypothesis, based on previous SEC and ITC data, that CK2 α undergoes a Ru₄POM-mediated dimerization, with the formation of a stable (CK2 α)₂(Ru₄POM)₂ complex. Importantly, in accordance with the lack of a significant entropic contribution for the CK2 α /Ru₄POM interaction seen with ITC, SAXS data do not show any evidence of protein denaturation.

Experiments on 1:1 mixtures of CK2 α :Ru₄POM at lower ionic strengths, i.e., 0.3 and 0.2 M NaCl, caused protein precipitation of the sample, as in the case of free CK2 α , hampering the possibility of reliable SAXS analyses (Figure 7D).

Next, we monitored the effect of 2 and 10 M equivalent of Ru₄POM at 0.5 M NaCl, and the R_g and I(0) traces showed the formation of soluble complexes but in a multi-component system, with different size and molecular weight species co-existing in solution (Supplementary Figure S4B). We then tried to get more detailed structural information on the nature of the (CK2 α)₂(Ru₄POM)₂ complex from the available SAXS data. Starting from the evidence that Ru₄POM actively induces the dimerization of CK2 α , the most reasonable assumption is that Ru₄POM structurally mediate the interaction between two molecules of the enzyme. This is the simpler and more plausible explanation that globally takes into account our SEC, ITC and SAXS data.

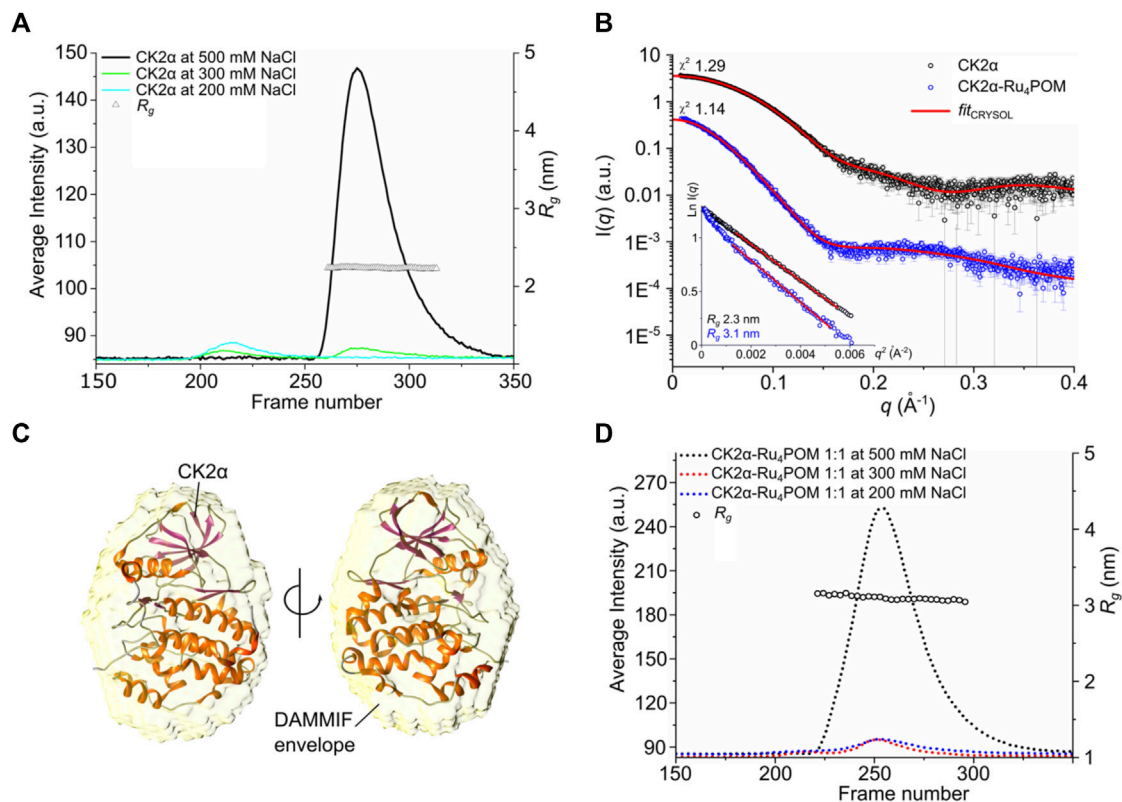


FIGURE 7 | SAXS studies on CK2α-Ru₄POM complex. **(A)** SEC-SAXS chromatograms of R_g and $I(q)$ traces as functions of frames of separated CK2α, in buffer with 0.5, 0.3, and 0.2 M NaCl (black, green, and cyan lines, respectively). Triangles represent the calculated radius of gyration, R_g in nm, in the selected frames collected in buffer containing 0.5 M NaCl. **(B)** $I(q)$ versus q experimental SAXS profiles for CK2α and CK2α-Ru₄POM (black and blue circle, respectively) with CRYSOLOG fit (red lines). χ^2 values for the CRYSOLOG fitting are indicated. The curves are shifted by an arbitrary offset for better comparison. In the inset, the Guinier fits for the two samples and the calculated radius of gyration are shown. **(C)** CK2α DAMMIF model (yellow envelope shown in transparency) overlaid with the CK2α crystal structure (PDB entry 3q04). **(D)** SEC-SAXS chromatograms of R_g and $I(q)$ traces as functions of frames of separated CK2α-Ru₄POM complex at 1:1 M ratio and increasing NaCl concentration.

Then, we first built possible structural models of the interaction between Ru₄POM and CK2α, trying to identify the binding site (**Figure 8**). The docking of Ru₄POM on monomeric CK2α was obtained using geometry-based molecular docking algorithms (Schneidman-Duhovny et al., 2005) and yielded several models with good molecular shape complementarity, where negatively charged Ru₄POM invariably interacts with CK2α along the large positively charged area present on the protein surface between the ATP binding pocket and the substrate binding site (**Figure 1A**). This result is in accordance with the biochemical data that indicates a substrate-competitive mechanism of inhibition, and with the thermodynamic signature of the interaction, largely enthalpic as deduced by ITC measurements. Since the precise location of Ru₄POM in the substrate-binding site of CK2α is not known, we generated possible dimers starting from each of the 19 plausible CK2α-Ru₄POM docking models (**Figure 8**).

First, the predicted dimers were validated based on the best χ^2 value obtained fitting the structures with the experimental SAXS data; then, only dimers stabilized by inter-molecular Ru₄POM-mediated contacts were selected (**Figure 8**; **Supplementary Figure S5**). This strategy allowed to identify a CK2α-Ru₄POM

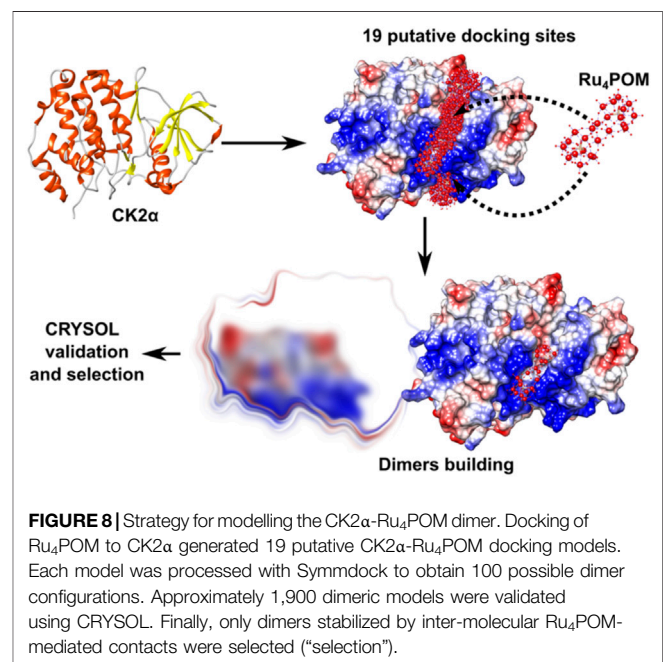


FIGURE 8 | Strategy for modelling the CK2α-Ru₄POM dimer. Docking of Ru₄POM to CK2α generated 19 putative CK2α-Ru₄POM docking models. Each model was processed with Symmdock to obtain 100 possible dimer configurations. Approximately 1,900 dimeric models were validated using CRYSOLOG. Finally, only dimers stabilized by inter-molecular Ru₄POM-mediated contacts were selected ("selection").

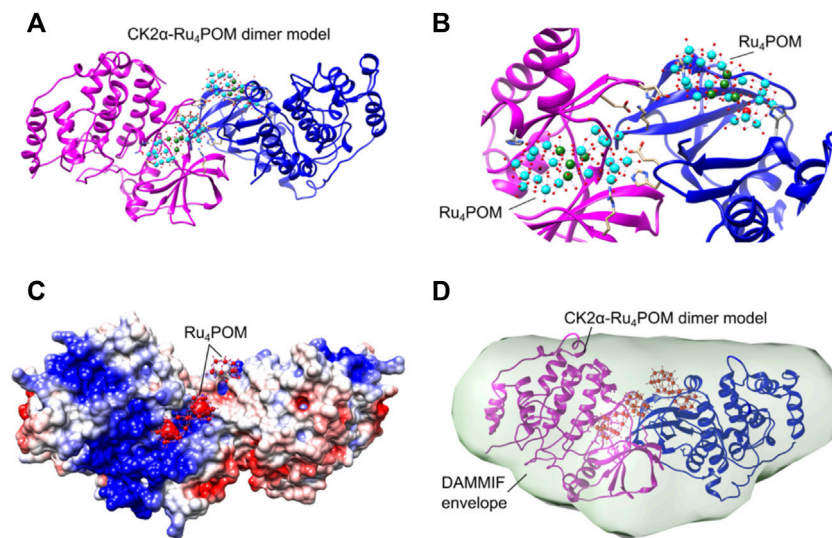


FIGURE 9 | Structural organization of the $(\text{CK2}\alpha)_2(\text{Ru}_4\text{POM})_2$ complex. **(A)** Proposed CK2 α -Ru₄POM dimer model showing two interacting CK2 α (colored in magenta and blue) and two Ru₄POM further connecting the two subunits. **(B)** Closer view on the CK2 α -Ru₄POM interface. Spheres colored in cyan represent 10 W atoms, in green 4 Ru atoms, in red O atoms and in black 2 Si atoms. **(C)** Electrostatic surface of the CK2 α -Ru₄POM dimer model. Positive and negative charges are depicted in blue and red, respectively. The potentials were calculated using programs PDB2PQR and APBS (Jurrus et al., 2018). **(D)** CK2 α -Ru₄POM DAMMIF model (light green envelope shown in transparency) overlaid with the proposed CK2 α -Ru₄POM dimer model.

dimeric configuration displaying optimal fitting to SAXS data, i.e., χ^2 value 1.14 (**Figure 9**). In this model, each of the two Ru₄POM molecules bind to each of the two CK2 α subunits, in a region adjacent to the ATP binding pocket, between the hinge- α D region and the Gly-rich loop, overlapping part of the substrate-binding site. Ru₄POM engages both intermolecular electrostatic interactions and H-bonds with polar and positively charged residues of the enzyme. In this $(\text{CK2}\alpha)_2(\text{Ru}_4\text{POM})_2$ model direct contacts between the two molecules of CK2 α are established. The predicted structural model overlays well with the DAMMIF elongated envelope obtained from CK2 α -Ru₄POM SAXS data analysis (**Figure 9D**).

DISCUSSION

It was reported that members of the family of the polyoxometalates are potent inhibitors of the CK2 activity *in vitro*. However, their mechanism of inhibition and CK2 binding site are not firmly established yet. For one of the best POM inhibitors, $[\text{P}_2\text{Mo}_{18}\text{O}_{62}]^{6-}$, steady-state kinetic analysis showed that it did not target CK2 α either at the ATP-binding site or at the protein substrate binding sites. Site-directed mutagenesis and proteolytic degradation of the CK2 α -POM complex suggested that this POM binds to domains containing key structural elements such as the Gly-rich loop, the helix α C and the activation segment. Nevertheless, the low chemical stability in an aqueous environment of this POM hampered to establish a clearly defined binding site and inhibition mechanism (Prudent et al., 2008).

Here, we confirm that different POMs are potent inhibitor of CK2 α , with IC₅₀ in the low nanomolar range, the best one being a

ruthenium-based polyoxometalate, $[\text{Ru}_4(\mu\text{-OH})_2(\mu\text{-O})_4(\text{H}_2\text{O})_4(\gamma\text{-SiW}_{10}\text{O}_{36})_2]^{10-}$. Some hybrid organic-inorganic POMs belonging to the Keggin decatungstosilicate family, which share the same $\text{SiW}_{10}\text{O}_{36}$ unit of Ru₄POM, were also shown to be promising. The variation of the inhibitory activity with the organic domains will thus deserve attention, for the possibility to anchor suitable recognition motifs and develop, for example, bi-specific inhibitors (Iegre et al., 2021). Interestingly, cell penetration of these derivative has been previously demonstrated (Zamolo et al., 2018). For now, we have focused our attention on the structurally rigid Ru₄POM.

Ru₄POM has an IC₅₀ of 3.63 nM on the catalytic subunit, either full-length or deleted of the last 55 C-terminal residues, which are flexible in solution. A very similar IC₅₀, 5.57 nM, was found on the tetrameric enzyme. This similarity in the IC₅₀ values exclude that the Ru₄POM binding region is located either at the C-terminus of CK2 α or at the α/β interface. Importantly, we showed that this compound is stable in the aqueous condition of the biochemical assays (up to pH 8.5), indicating that the full molecule and not some decomposition fragments are active on the enzyme, as instead reported for other POMs (Prudent et al., 2008).

Ru₄POM has a net negative charge, like the CK2 substrates, therefore we tested whether it works with a substrate-competitive mechanism. Indeed, we show that Ru₄POM competes with the substrates, either small peptides or casein, indicating that it interacts with CK2 at the level of the substrate-binding site. This interaction is modulated by the pH and the ionic strength, in accordance with a substrate-competitive mechanism of inhibition where the electrostatic interactions play an important role in the binding of both negative substrates and Ru₄POM to the positively charged CK2 substrate-binding site.

The physical-chemical properties of Ru₄POM seem to penalize its transport across the cellular membrane of HEK-293T cells, and, in fact, we do not detect any CK2 inhibition on intact cells treated with the free compound, in line with previously reported observations (Prudent et al., 2008). However, when applied in combination with cationic transfection reagents, we do observe inhibition of endo-cellular CK2, meaning that, with the appropriate delivery system, it can be transported inside the cells despite its dimensions and its highly negative charge. It is worth mentioning that CK2 is also present on the outer cell surface [CK2 ecto-kinase (Rodríguez et al., 2005)], with functions that are largely unknown; in this view, Ru₄POM could represent a valuable tool to discriminate between ecto- and endo-cellular CK2, according to the administration conditions.

To possibly decipher the mechanism of inhibition of Ru₄POM on CK2 we performed different biophysical analyses. Size-exclusion chromatography experiments at 0.5 M NaCl show that Ru₄POM induces the dimerization of CK2 α , with the formation of a (CK2 α)₂(Ru₄POM)₂ complex, with no residual presence of the single components, indicating the formation of a strong and stable complex. SAXS experiments confirm the presence of such a complex, with dimeric CK2 α when Ru₄POM is present in equimolar amount. According to SEC data, larger assemblies are formed at higher molar ratios, with the saturation reached at around 5:1 for Ru₄POM:CK2 α .

The specific interaction between Ru₄POM and CK2 α with the formation of a stable complex is confirmed by ITC measurements, which indicates a macroscopic apparent mean K_D of $2.09 \pm 0.36 \mu\text{M}$ and a 1:1 stoichiometry, in accordance with SEC and SAXS data. The observed thermodynamic parameters agree with literature data on the interaction between inorganic POMs and proteins, which are characterized by K_D in the μM range (Zhang et al., 2007; Zamolo et al., 2018; Vandebroek et al., 2021) and by a dominant enthalpic contribution. The exothermal process, in particular, entails the key role of the electrostatic interactions and hydrogen bonds, in line with the polar nature of the interaction between Ru₄POM and the substrate-binding site of CK2. The negligible entropic term, instead, shows that the possible stiffening of the protein structure on one hand, and the dehydration of this highly hydrophilic POM, on the other hand, are not relevant. Noteworthy, despite larger POMs may display higher free energy of binding (Zhang et al., 2007), their large surface seems to hamper the targeting of the CK2 sites involved in the inhibitory activity, as observed for Mo₃₆POM, indicating the importance of the shape complementarity between CK2 and the other tested POMs.

The structural analysis of the SAXS signal reveals the shape of the complex formed by CK2 α and Ru₄POM, with Ru₄POM connecting two CK2 α molecules, which, in turn, can interact with each other. Ru₄POM binds to CK2 α in a region adjacent to the ATP binding pocket, in between the hinge/ α D region and the Gly-rich loop, overlapping part of the substrate-binding site. The two Ru₄POM molecules do not directly interact to each other and bind CK2 α through polar interactions, likely both hydrogen-bonds and electrostatic forces.

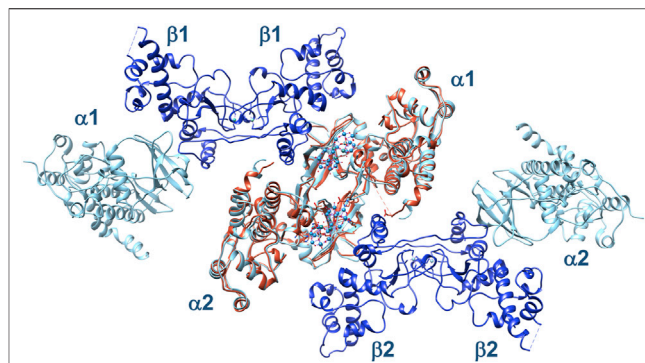


FIGURE 10 | Structural superposition of two $\alpha_2\beta_2$ tetramers, 1 and 2 (α -subunits in cyan, β -subunits in blue), on the (CK2 α)₂(Ru₄POM)₂ complex (in orange). In this arrangement, the two tetramers do not show evident steric clashes, suggesting that they can interact with Ru₄POM in a similar way to the isolated catalytic subunit.

As Ru₄POM is able to inhibit also the $\alpha_2\beta_2$ holoenzyme, we structurally superposed two molecules of $\alpha_2\beta_2$ on the (CK2 α)₂(Ru₄POM)₂ complex, to see whether the structural information derived by SAXS are valid also for the tetrameric holoenzyme (Figure 10). Indeed, we obtained a reasonable model for the hypothetical Ru₄POM-mediated dimerization of the full enzyme, with no evident steric overlaps between the two tetramers. Then, we suggest that Ru₄POM binds to $\alpha_2\beta_2$ in a very similar way to that seen for the isolated CK2 α , inhibiting the full enzyme with the same mechanism shown for the free catalytic subunit. It has been proposed that the mechanism of regulation of the enzyme relies on the self-inhibitory oligomerization of $\alpha_2\beta_2$, mediated by inter-tetrameric electrostatic interactions involving the acidic loop of the β -subunit of one tetramer (Asp55–Asp64) and the positively charged P + 1 loop of the α -subunit of the other tetramer (Arg191–Lys198). It is plausible that Ru₄POM is able to interfere with the normal regulation of the enzyme activity by affecting the oligomerization process of the tetrameric form of CK2. It is also possible that Ru₄POM affect the interaction of CK2 with at least some of the interacting partners of this kinase.

In summary, we could unravel the mechanism of inhibition of a Ru-based POM, a compound stable in aqueous solution and able to inhibit CK2 in the very low nanomolar range. Cell internalization has also been addressed by using suitable transfecting agents. Ru₄POM binds to CK2 and induces the formation of a (CK2 α)₂(Ru₄POM)₂ complex, which is inactive because the substrate-binding site and the ATP-binding site are inaccessible to substrates and ATP, respectively. This inhibition mechanism is entirely different from the common ATP-competitive one typical for most of the known protein kinase inhibitors. Ru₄POM has physical and chemical properties very different from that of conventional kinase inhibitors (small organic molecules), and this, coupled to its ability of inhibition in cell-based assays, make this compound particularly interesting for further developments. Notably, Ru₄POM is the first non-peptide molecule showing a substrate-competitive mechanism of inhibition. Atomic details of the interaction between CK2 and Ru₄POM can be unravelled by the crystallographic analysis of the

(CK2 α)₂(Ru₄POM)₂ complex, which would be useful to obtain information regarding the most relevant interactions that stabilize the complex. While many crystal structures of CK2 are available, alone or in complex with inhibitors (mainly ATP-competitive), complexes with substrate peptides have never been crystallized, suggesting that also the crystallization of CK2 in complex with POMs acting as substrate-competitive inhibitors could not be straightforward.

While a selectivity profile of Ru₄POM against a protein kinase panel is beyond the purpose of this study, our findings suggest that a remarkable specificity for CK2 is highly conceivable, being this compound able to function as a substrate-competitive inhibitor of a kinase, CK2, with the uncommon property of targeting negatively charged substrates.

MATERIALS AND METHODS

Recombinant CK2 α Production

Recombinant full-length CK2 α and tetrameric CK2 ($\alpha_2\beta_2$) [produced as in (Venerando et al., 2013)] were kindly provided by Dr. Andrea Venerando (University of Parma, Italy). Human CK2 α (residues 1-336) was produced as previously reported (Papinutto et al., 2012). Briefly, after expression in *E. coli* BL21-DE3, the protein was purified by two chromatographic steps, with heparin affinity chromatography (5 ml HiTrap Eparin HP column, GE Healthcare) and size-exclusion chromatography (HiLoad 16/60 Superdex 75 pg column, GE Healthcare). Protein eluted in 25 mM Tris, 500 mM NaCl, 1 mM DTT, pH = 8.5 was concentrated to 13.3 mg/ml, flash-frozen in liquid nitrogen and stored at -80°C.

Polyoxometalates Synthesis and Characterization

Na₁₀[Ru₄(H₂O)₄(μ -O)₄(μ -OH)₂(γ -SiW₁₀O₃₆)₂], Ru₄POM, was prepared following a published procedure (Galiano et al., 2021). Ru₄POM identity was confirmed by FTIR, while its stability was monitored by UV-vis, by using a Cary 100 instrument (Varian), in buffered aqueous environment (25 mM Tris, pH 8.5) over 24 h (Supplementary Figure S6).

(¹⁸Bu₄N)₃H[γ -SiW₁₀O₃₆{(C₅H₇N₂OS)(CH₂)₄CONH(CH₂)₃Si₂O}], Biotin-SiW₁₀ (Zamolo et al., 2018), (S,S)-(¹⁸Bu₄N)₄[γ -SiW₁₀O₃₆{(C₁₆H₉)SO₂NH(CH₂)₃Si₂O}], Trp-SiW₁₀ (Syrgiannis et al., 2019) and its (R,R) enantiomer, were prepared following previously reported procedures. The corresponding sodium salts were prepared by counterion exchange as described in (Zamolo et al., 2018). All hybrid POMs were characterized by FTIR and ESI-MS(-) to confirm their identity. (NH₄)₁₂[Mo₃₆(NO)₄O₁₀₈(H₂O)₁₆], Mo₃₆POM, was prepared as reported in (Amini et al., 2015).

Analytical Size-Exclusion Chromatography

Analytical SEC analyses on isolated CK2 α and on CK2 α /Ru₄POM mixtures were performed using a 10/30 Superdex 75 GL column (GE Healthcare) or a 10/30 Superdex 200 GL column (GE Healthcare) equilibrated with 25 mM Tris, 1 mM DTT, pH =

8.5 and NaCl at various concentrations, namely 0.5, 0.4, 0.3, and 0.2 M. For the preparation of CK2 α /POM mixtures in different ratios, a concentrated stock solution of Ru₄POM (5 mM) obtained by solubilizing dry powder in 25 mM Tris, 0.5 M NaCl, 1 mM DTT, pH = 8.5 was used. CK2 α concentration varied from 200 to 300 μ M, in accordance with SEC-SAXS experiments (see below).

Isothermal Titration Calorimetry

Isothermal titration calorimetry (ITC) experiments were performed using a Malvern PEAQ-ITC microcalorimeter, at 25°C, with a 270 μ l sample cell and a computer controlled microsyringe for titrant injections. CK2 α (20–30 μ M) and Ru₄POM (200–400 μ M) samples were in 25 mM Tris, 500 mM NaCl, pH = 8.5. After baseline stabilization, a further delay of 60 s was used before the first injection. In each individual titration, a starting Ru₄POM injection of 0.4 μ l in 0.8 s was followed by other 12 injections of 3 μ l with a duration of 6 s each. A delay of 150 s was applied between each Ru₄POM injection. Wiseman plot of integrated data was automatically obtained by software analysis (excluding the heat referred to the first 0.4 μ l injection) and then it was fitted by theoretical binding curve using the one site model.

SAXS Data Collection and Analysis

SAXS experiments were performed at the bio-SAXS beamline BM29 at ESRF, Grenoble, France (Pernot et al., 2013). The CK2 α and CK2 α /Ru₄POM mixtures were measured by SEC-SAXS approaches (Brennich et al., 2017). Samples containing 300 μ M Ru₄POM, 300 μ M CK2 α and 300 μ M CK2 α :Ru₄POM at 1:1 M ratio in buffer 25 mM Tris, 1 mM DTT, pH 8.5 and 0.5 M NaCl were loaded on a GE Superdex Increase 200 (3.2/300) column. For samples measured at 0.3 and 0.2 M NaCl (buffer 25 mM Tris, 1 mM DTT, pH 8.5) CK2 α concentration was 130 μ M. Samples with 200 μ M CK2 α with CK2 α :Ru₄POM at 1:2 and at 1:10 M ratio in buffer 25 mM Tris, 1 mM DTT, pH 8.5 and 0.5 M NaCl were loaded on a Agilent AdvanceBio SEC (4.6/300) and on a GE Superose 6 Increase (3.2/300) columns, respectively. The samples were centrifuged (16,000 g for 30 min at 4°C) prior the measurements and 50 μ l of sample were injected in the columns. The purifications were carried-out *via* a high-performance liquid chromatography device (HPLC, Shimadzu) attached directly to the sample-inlet valve of the BM29 sample changer. The columns were equilibrated with 3 CV to obtain a stable background signal before measurement. A flow rate of 0.3 ml/min was used for all sample measurements. All SAXS data were collected at a wavelength of 0.99 Å using a sample-to-detector (PILATUS 2 M, DECTRIS) distance of 2.867 m. Data reduction and preliminary data processing were performed automatically using the Dahu/FreeSAS pipeline implemented at BM29. In the SEC-SAXS chromatograms, frames in regions of stable R_g were selected with CHROMIXS and averaged using PRIMUS to yield a single averaged frame for each protein sample. Analysis of the overall parameters was carried out by PRIMUS from ATSAS 3.0.4 package (Manalastas-Cantos et al., 2021). For CK2 α and CK2 α :Ru₄POM at 1:1 the pair distance distribution functions, $P(r)$, were used to calculate *ab initio* models in P1 and P2 symmetries, respectively, with DAMMIF (Manalastas-Cantos

et al., 2021). Plots and protein models were generated using OriginPro 9.0 and UCSF Chimera software, respectively. SAXS parameters for data collection and analysis are summarized in **Supplementary Table S1** following international guidelines (Trehwella et al., 2017). SAXS data were deposited into the Small Angle Scattering Biological Data Bank (SASBDB) under accession numbers SASDNF7 for CK2 α and SASDNG7 for CK2 α :Ru₄POM 1:1.

SAXS-Based Modelling of CK2 α -Polyoxometalate Complex

The molecular docking of Ru₄POM to CK2 α was obtained exploiting Patchdock (Schneidman-Duhovny et al., 2005) using the pdb model of Ru₄POM as ligand and CK2 α (PDB 3q04) as receptor. The docking resulted in 19 plausible models of a complex formed by CK2 α monomer binding a single molecule of Ru₄POM bound in different positions along the entire positively charged cavity of CK2 α . Symmdock (Schneidman-Duhovny et al., 2005) was then used to generate CK2 α -Ru₄POM dimers using as input the 19 plausible docking models for a total of about 1,900 dimeric species (i.e., the first 100 best scored dimers obtained with Symmdock per each of the 19 docking models obtained with Patchdock). Our data showed that CK2 α never forms dimers or multimers in solution while Ru₄POM induces CK2 α dimerization at 1:1 M ratio. Based on this experimental observation, only the Symmdock-generated CK2 α :Ru₄POM dimers, where Ru₄POM mediates intermolecular contacts between two CK2 α monomer, were selected. The structures of models were ranked according to the lower χ^2 value obtained by structure comparison between the models and the SAXS data of the CK2 α -POM complex using CRY SOL (Manalastas-Cantos et al., 2021). The best model was then fitted into the DAMMIF envelope using SUPCOMB (Kozin and Svergun, 2001).

In Vitro CK2 Activity Assay

For IC₅₀ (concentrations inducing 50% inhibition) analysis, recombinant tetrameric CK2 ($\alpha_2\beta_2$), or C-terminal-deleted CK2 α (CK2 α^{1-336}), or full length CK2 α (7.5 ng) were incubated with 0.1 mM synthetic peptide substrate RRRADDSDDDDDD (CK2-tide), in a phosphorylation buffer containing 50 mM Tris-HCl pH 7.5, 10 mM MgCl₂, 20 μ M [γ -³³P]ATP (1,000–2,000 cpm/pmol), in a final volume of 20 μ l, with increasing concentrations of the inhibitor. In the case of tetrameric CK2, 0.1 M NaCl was also present in the phosphorylation mixture. Controls were performed in the absence of any inhibitor, but with equal volume of vehicle (H₂O). Reactions were performed at 30°C for 12 min and stopped by sample absorption on phospho-cellulose papers. Papers were washed three times with 75 mM phosphoric acid and counted in a scintillation counter (PerkinElmer). In the case of casein substrate (used at 0.05 mg/ml concentration), reactions were stopped by the addition of Laemmli loading buffer, samples were analyzed by 11% SDS-PAGE, and radioactive bands were detected and quantified by digital autoradiography (Cyclone plus storage phosphor system, PerkinElmer). IC₅₀ calculation was

obtained by analysis of the results with GraphPad Prism 7.0a software.

For kinetics analysis, the assays were performed with increasing concentrations of CK2-tide or casein, in the phosphorylation buffer described above, but with 100 μ M ATP concentration.

Cell Culture, Treatments, and Lysis

HEK-293T cells (human embryo kidney fibroblasts) were cultured in an atmosphere containing 5% CO₂, maintained in DMEM medium (Sigma), supplemented with 10% (v/v) fetal bovine serum (FBS), 2 mM L-glutamine, 100 U/ml penicillin, and 100 mg/ml streptomycin. Cell treatments with Ru₄POM were performed in the culture medium. When used, the cationic transfection reagents PEI (Thermo Scientific) or JetOptimus (Polyplus-transfection) were mixed with Ru₄POM and incubated for 1 h at room temperature, before adding the mix to the cells. After 24 h cells were lysed as previously described (Zanin et al., 2012). Protein concentration was determined by the Bradford method.

Endo-Cellular CK2 Activity Assay

Endo-cellular CK2 activity was evaluated by assessing the phosphorylation state of the CK2 substrate Akt phospho-Ser129 (Abcam) (Ruzzene et al., 2010). For this purpose, equal amounts of proteins from treated cells were loaded on 11% SDS-PAGE, blotted on Immobilon-P membranes (Millipore), processed in Western blot (WB), and detected by chemiluminescence.

Quantitation of the signal was obtained by chemiluminescence detection on ImageQuant LAS 500 (GE Healthcare Life Sciences) and analysis with Carestream Molecular Imaging software (Carestream).

Statistical Analysis for Kinase Activity

Statistical significance was evaluated by One-way Anova analysis using GraphPad Prism 7 program. All values are expressed as means \pm SEM. Comparisons of more than two groups were made with a one-way ANOVA using post-hoc Bonferroni's test. Comparison of two groups was obtained by the Student's t-test for unpaired data when appropriate. Differences were considered statistically significant at values of $p < 0.05$.

DATA AVAILABILITY STATEMENT

The datasets presented in this study can be found in online repositories. The names of the repository/repositories and accession number(s) can be found in the article/ **Supplementary Material**.

AUTHOR CONTRIBUTIONS

Recombinant protein production, SEC, ITC and SAXS were planned and performed by SF, GG, MBe, and RB; POMs synthesis and characterization were planned and performed by

AC, LV, MB, and MC; *in vitro* and in cell CK2 activity assays were planned and performed by CB, GS, and MR; overall design of the research by MR, MC, and RB; manuscript writing by RB; correction and approval of the manuscript by SF, GG, MBe, CB, MR, GS, AC, LV, MB, and MC.

FUNDING

This work was supported by the Department of Chemical Sciences of the University of Padova (grant number P-DISC#11NEXuS_BIRD2019-UNIPD, to MC), the Department of Biomedical Sciences of the University of Padova (grant number: BORG_BIRD2121_01, to CB) and by the University of Padova (Starting Grant STARS@UNIPD-call 2019, to GG).

REFERENCES

- Amini, M., Naslhajian, H., Farnia, S. M. F., and Holyńska, M. (2015). Selective Oxidation of Sulfides Catalyzed by the Nanocluster Polyoxomolybdate (NH₄)₁₂ [Mo₃₆ (NO)₄ O₁₀₈ (H₂ O)₁₆]. *Eur. J. Inorg. Chem.* 2015, 3873–3878. doi:10.1002/ejic.201500528
- Arefian, M., Mirzaei, M., Eshtiaq-Hosseini, H., and Frontera, A. (2017). A Survey of the Different Roles of Polyoxometalates in Their Interaction with Amino Acids, Peptides and Proteins. *Dalton Trans.* 46, 6812–6829. doi:10.1039/c7dt00894e
- Atkinson, E. L., Jegre, J., Brear, P. D., Zhabina, E. A., Hyvönen, M., and Spring, D. R. (2021). Downfalls of Chemical Probes Acting at the Kinase ATP-Site: CK2 as a Case Study. *Molecules* 26, 1977. doi:10.3390/molecules26071977
- Battistutta, R., Cozza, G., Pierre, F., Papinutto, E., Lolli, G., Sarno, S., et al. (2011). Unprecedented Selectivity and Structural Determinants of a New Class of Protein Kinase CK2 Inhibitors in Clinical Trials for the Treatment of Cancer. *Biochemistry* 50, 8478–8488. doi:10.1021/bi2008382
- Battistutta, R., and Lolli, G. (2011). Structural and Functional Determinants of Protein Kinase CK2α: Facts and Open Questions. *Mol. Cell. Biochem.* 356, 67–73. doi:10.1007/s11010-011-0939-6
- Battistutta, R., Mazzorana, M., Cendron, L., Bortolato, A., Sarno, S., Kazimierczuk, Z., et al. (2007). The ATP-Binding Site of Protein Kinase CK2 Holds a Positive Electrostatic Area and Conserved Water Molecules. *ChemBiochem* 8, 1804–1809. doi:10.1002/cbic.200700307
- Battistutta, R. (2009). Protein Kinase CK2 in Health and Disease. *Cell. Mol. Life Sci.* 66, 1868–1889. doi:10.1007/s00018-009-9155-x
- Battistutta, R., Sarno, S., De Moliner, E., Papinutto, E., Zanotti, G., and Pinna, L. A. (2000). The Replacement of ATP by the Competitive Inhibitor Emodin Induces Conformational Modifications in the Catalytic Site of Protein Kinase CK2. *J. Biol. Chem.* 275, 29618–29622. doi:10.1074/jbc.M004257200
- Bijelic, A., Aureliano, M., and Rempel, A. (2019). Polyoxometalates as Potential Next-Generation Metalloids in the Combat against Cancer. *Angew. Chem. Int. Ed.* 58, 2980–2999. doi:10.1002/anie.201803868
- Bonchio, M., Syrgiannis, Z., Burian, M., Marino, N., Pizzolato, E., Dirian, K., et al. (2019). Hierarchical Organization of Perylene Bisimides and Polyoxometalates for Photo-Assisted Water Oxidation. *Nat. Chem.* 11, 146–153. doi:10.1038/s41557-018-0172-y
- Borgo, C., D'Amore, C., Cesaro, L., Sarno, S., Pinna, L. A., Ruzzene, M., et al. (2021a). How Can a Traffic Light Properly Work if it Is Always Green? the Paradox of CK2 Signaling. *Crit. Rev. Biochem. Mol. Biol.* 56, 1–39. doi:10.1080/10409238.2021.1908951
- Borgo, C., D'Amore, C., Sarno, S., Salvi, M., and Ruzzene, M. (2021b). Protein Kinase CK2: a Potential Therapeutic Target for Diverse Human Diseases. *Sig Transduct. Target Ther.* 6, 183. doi:10.1038/s41392-021-00567-7
- Borgo, C., and Ruzzene, M. (2021). “Protein Kinase CK2 Inhibition as a Pharmacological Strategy,” in *Advances in Protein Chemistry and Structural*

ACKNOWLEDGMENTS

Authors thank Prof. Massimo Degano (IRCCS Scientific Institute San Raffaele) for organizing the Italian Bag for Structural Biology at ESRF, Dr. Mark Tully and Dr. Petra Pernot for help and assistance with data collection at the ESRF BM29 bioSAXS beamline, Haihong Yu for synthesis and characterization of Ru₄POM, Hadigheh Sadat Hosseini for preparing Mo₃₆POM.

SUPPLEMENTARY MATERIAL

The Supplementary Material for this article can be found online at: <https://www.frontiersin.org/articles/10.3389/fmolb.2022.906390/full#supplementary-material>

- Biology* (San Diego, USA: Academic Press), 23–46. doi:10.1016/bs.apscb.2020.09.003
- Borgo, C., and Ruzzene, M. (2019). Role of Protein Kinase CK2 in Antitumor Drug Resistance. *J. Exp. Clin. Cancer Res.* 38, 287. doi:10.1186/s13046-019-1292-y
- Brear, P., Ball, D., Stott, K., D'Arcy, S., and Hyvönen, M. (2020). Proposed Allosteric Inhibitors Bind to the ATP Site of CK2α. *J. Med. Chem.* 63, 12786–12798. doi:10.1021/acs.jmedchem.0c01173
- Brear, P., De Fusco, C., Hadje Georgiou, K., Francis-Newton, N. J., Stubbs, C. J., Sore, H. F., et al. (2016). Specific Inhibition of CK2α from an Anchor outside the Active Site. *Chem. Sci.* 7, 6839–6845. doi:10.1039/c6sc02335e
- Brennich, M. E., Round, A. R., and Hutin, S. (2017). Online Size-Exclusion and Ion-Exchange Chromatography on a SAXS Beamline. *J. Vis. Exp.* doi:10.3791/54861
- Chua, M. M. J., Lee, M., and Dominguez, I. (2017). Cancer-type Dependent Expression of CK2 Transcripts. *PLoS ONE* 12, e0188854. doi:10.1371/journal.pone.0188854
- Čolović, M. B., Lacković, M., Lalatović, J., Mougharbel, A. S., Kortz, U., and Krstić, D. Z. (2020). Polyoxometalates in Biomedicine: Update and Overview. *Curr. Med. Chem.* 27, 362–379. doi:10.2174/0929867326666190827153532
- Croce, M., Conti, S., Maake, C., and Patzke, G. R. (2019). Nanocomposites of Polyoxometalates and Chitosan-Based Polymers as Tuneable Anticancer Agents. *Eur. J. Inorg. Chem.* 2019, 348–356. doi:10.1002/ejic.201800268
- Dalle Vedove, A., Zonta, F., Zanforlin, E., Demitri, N., Ribaud, G., Cazzanelli, G., et al. (2020). A Novel Class of Selective CK2 Inhibitors Targeting its Open Hinge Conformation. *Eur. J. Med. Chem.* 195, 112267. doi:10.1016/j.ejmech.2020.112267
- De Moliner, E., Moro, S., Sarno, S., Zagotto, G., Zanotti, G., Pinna, L. A., et al. (2003). Inhibition of Protein Kinase CK2 by Anthraquinone-Related Compounds. *J. Biol. Chem.* 278, 1831–1836. doi:10.1074/jbc.M209367200
- Dominguez, I., Cruz-Gamero, J. M., Corasolla, V., Dacher, N., Rangasamy, S., Urbani, A., et al. (2021). Okur-Chung Neurodevelopmental Syndrome-Linked CK2α Variants Have Reduced Kinase Activity. *Hum. Genet.* 140, 1077–1096. doi:10.1007/s00439-021-02280-5
- Duncan, J. S., and Litchfield, D. W. (2008). Too Much of a Good Thing: the Role of Protein Kinase CK2 in Tumorigenesis and Prospects for Therapeutic Inhibition of CK2. *Biochimica Biophysica Acta (BBA) - Proteins Proteomics* 1784, 33–47. doi:10.1016/j.bbapap.2007.08.017
- Ermakova, I., Boldyreff, B., Issinger, O.-G., and Niefind, K. (2003). Crystal Structure of a C-Terminal Deletion Mutant of Human Protein Kinase CK2 Catalytic Subunit. *J. Mol. Biol.* 330, 925–934. doi:10.1016/s0022-2836(03)00638-7
- Galiano, F., Mancuso, R., Carraro, M., Bundschuh, J., Hoinkis, J., Bonchio, M., et al. (2021). A Polyoxometalate-Based Self-Cleaning Smart Material with Oxygenic Activity for Water Remediation with Membrane Technology. *Appl. Mater. Today* 23, 101002. doi:10.1016/j.apmt.2021.101002

- Gobbo, P., Tian, L., Pavan Kumar, B. V. V. S., Turvey, S., Cattelan, M., Patil, A. J., et al. (2020). Catalytic Processing in Ruthenium-Based Polyoxometalate Coacervate Protocells. *Nat. Commun.* 11, 41. doi:10.1038/s41467-019-13759-1
- Iegre, J., Atkinson, E. L., Brear, P. D., Cooper, B. M., Hyvönen, M., and Spring, D. R. (2021). Chemical Probes Targeting the Kinase CK2: a Journey outside the Catalytic Box. *Org. Biomol. Chem.* 19, 4380–4396. doi:10.1039/d1ob00257k
- Iegre, J., Brear, P., De Fusco, C., Yoshida, M., Mitchell, S. L., Rossmann, M., et al. (2018). Second-generation CK2a Inhibitors Targeting the α D Pocket. *Chem. Sci.* 9, 3041–3049. doi:10.1039/c7sc05122k
- Juruss, E., Engel, D., Star, K., Monson, K., Brandi, J., Felberg, L. E., et al. (2018). Improvements to the APBS Biomolecular Solvation Software Suite. *Protein Sci.* 27, 112–128. doi:10.1002/pro.3280
- Kozin, M. B., and Svergun, D. I. (2001). Automated Matching of High- and Low-Resolution Structural Models. *J. Appl. Cryst.* 34, 33–41. doi:10.1107/S0021889800014126
- Lolli, G., and Battistutta, R. (2015). “Structural Basis of CK2 Regulation by Autoinhibitory Oligomerization,” in *Protein Kinase CK2 Cellular Function In Normal and Disease States Advances in Biochemistry in Health and Disease*. Editors K. Ahmed, O.-G. Issinger, and R. Szyszka (Dordrecht, NL: Springer International Publishing), 35–47. doi:10.1007/978-3-319-14544-0_3
- Lolli, G., Naressi, D., Sarno, S., and Battistutta, R. (2017). Characterization of the Oligomeric States of the CK2 α 2 β Holoenzyme in Solution. *Biochem. J.* 474, 2405–2416. doi:10.1042/BCJ20170189
- Lolli, G., Pinna, L. A., and Battistutta, R. (2012). Structural Determinants of Protein Kinase CK2 Regulation by Autoinhibitory Polymerization. *ACS Chem. Biol.* 7, 1158–1163. doi:10.1021/cb300054n
- Lolli, G., Ranchio, A., and Battistutta, R. (2014). Active Form of the Protein Kinase CK2 α 2 β Holoenzyme Is a Strong Complex with Symmetric Architecture. *ACS Chem. Biol.* 9, 366–371. doi:10.1021/cb400771y
- Long, D.-L., Tsunashima, R., and Cronin, L. (2010). Polyoxometalates: Building Blocks for Functional Nanoscale Systems. *Angew. Chem. Int. Ed.* 49, 1736–1758. doi:10.1002/anie.200902483
- Manalastas-Cantos, K., Konarev, P. V., Hajizadeh, N. R., Kikhney, A. G., Petoukhov, M. V., Molodenskiy, D. S., et al. (2021). ATSAS 3.0: Expanded Functionality and New Tools for Small-Angle Scattering Data Analysis. *J. Appl. Cryst.* 54, 343–355. doi:10.1107/S1600576720013412
- Mazzorana, M., Pinna, L. A., and Battistutta, R. (2008). A Structural Insight into CK2 Inhibition. *Mol. Cell. Biochem.* 316, 57–62. doi:10.1007/s11010-008-9822-5
- Meggio, F., Pinna, L. A., Marchiori, F., and Borin, G. (1983). Polyglutamyl Peptides: a New Class of Inhibitors of Type-2 Casein Kinases. *FEBS Lett.* 162, 235–238. doi:10.1016/0014-5793(83)80762-5
- Montazeri, K., and Bellmunt, J. (2020). Erdafitinib for the Treatment of Metastatic Bladder Cancer. *Expert Rev. Clin. Pharmacol.* 13, 1–6. doi:10.1080/17512433.2020.1702025
- Niefind, K., and Battistutta, R. (2013). “Structural Bases of Protein Kinase CK2 Function and Inhibition,” in *Protein Kinase CK2* (Oxford, UK: John Wiley & Sons), 1–75. doi:10.1002/9781118482490.ch1
- Niefind, K., Guerra, B., Ermakowa, I., and Issinger, O.-G. (2001). Crystal Structure of Human Protein Kinase CK2: Insights into Basic Properties of the CK2 Holoenzyme. *EMBO J.* 20, 5320–5331. doi:10.1093/emboj/20.19.5320
- Niefind, K., Guerra, B., Ermakowa, I., and Issinger, O.-G. (2000). Crystallization and Preliminary Characterization of Crystals of Human Protein Kinase CK2. *Acta Crystallogr. D. Biol. Cryst.* 56, 1680–1684. doi:10.1107/S0907444900013627
- Niefind, K., Guerra, B., Pinna, L. A., Issinger, O. G., and Schomburg, D. (1998). Crystal Structure of the Catalytic Subunit of Protein Kinase CK2 from Zea mays at 2.1 Å Resolution. *EMBO J.* 17, 2451–2462. doi:10.1093/emboj/17.9.2451
- Ortega, C. E., Seidner, Y., and Dominguez, I. (2014). Mining CK2 in Cancer. *PLoS ONE* 9, e115609. doi:10.1371/journal.pone.0115609
- Papinutto, E., Ranchio, A., Lolli, G., Pinna, L. A., and Battistutta, R. (2012). Structural and Functional Analysis of the Flexible Regions of the Catalytic α -subunit of Protein Kinase CK2. *J. Struct. Biol.* 177, 382–391. doi:10.1016/j.jsb.2011.12.007
- Pernot, P., Round, A., Barrett, R., De Maria Antolinos, A., Gobbo, A., Gordon, E., et al. (2013). Upgraded ESRF BM29 Beamline for SAXS on Macromolecules in Solution. *J. Synchrotron Radiat.* 20, 660–664. doi:10.1107/S0909049513010431
- Pinna, L. A. (2002). Protein Kinase CK2: a Challenge to Canons. *J. Cell. Sci.* 115, 3873–3878. doi:10.1242/jcs.00074
- Prudent, R., and Cochet, C. (2009). New Protein Kinase CK2 Inhibitors: Jumping Out of the Catalytic Box. *Chem. Biol.* 16, 112–120. doi:10.1016/j.chembiol.2009.01.004
- Prudent, R., Moucadet, V., Laudet, B., Barette, C., Lafanechère, L., Hasenknopf, B., et al. (2008). Identification of Polyoxometalates as Nanomolar Noncompetitive Inhibitors of Protein Kinase CK2. *Chem. Biol.* 15, 683–692. doi:10.1016/j.chembiol.2008.05.018
- Qiao, Y., Chen, T., Yang, H., Chen, Y., Lin, H., Qu, W., et al. (2019). Small Molecule Modulators Targeting Protein Kinase CK1 and CK2. *Eur. J. Med. Chem.* 181, 111581. doi:10.1016/j.ejmech.2019.111581
- Ramezani-Aliakbari, M., Varshosaz, J., Sadeghi-Aliabadi, H., Hassanzadeh, F., and Rostami, M. (2021). Biotin-Targeted Nanomicellar Formulation of an Anderson-Type Polyoxomolybdate: Synthesis and *In Vitro* Cytotoxicity Evaluations. *Langmuir* 37, 6475–6489. doi:10.1021/acs.langmuir.1c00623
- Rodríguez, F., Allende, C. C., and Allende, J. E. (2005). Protein Kinase Casein Kinase 2 Holoenzyme Produced Ectopically in Human Cells Can Be Exported to the External Side of the Cellular Membrane. *Proc. Natl. Acad. Sci. U.S.A.* 102, 4718–4723. doi:10.1073/pnas.0501074102
- Roskoski, R. (2021). Properties of FDA-Approved Small Molecule Protein Kinase Inhibitors: A 2021 Update. *Pharmacol. Res.* 165, 105463. doi:10.1016/j.phrs.2021.105463
- Ruzzene, M., Di Maira, G., Tosoni, K., and Pinna, L. A. (2010). Assessment of CK2 Constitutive Activity in Cancer Cells. *Meth. Enzymol.* 484, 495–514. doi:10.1016/B978-0-12-381298-8.00024-1
- Ruzzene, M., and Pinna, L. A. (2010). Addiction to Protein Kinase CK2: a Common Denominator of Diverse Cancer Cells? *Biochimica Biophysica Acta (BBA) - Proteins Proteomics* 1804, 499–504. doi:10.1016/j.bbapap.2009.07.018
- Sarno, S., Papinutto, E., Franchin, C., Bain, J., Elliott, M., Meggio, F., et al. (2011). ATP Site-Directed Inhibitors of Protein Kinase CK2: an Update. *Ctmc* 11, 1340–1351. doi:10.2174/156802611795589638
- Schneidman-Duhovny, D., Inbar, Y., Nussinov, R., and Wolfson, H. J. (2005). PatchDock and SymmDock: Servers for Rigid and Symmetric Docking. *Nucleic Acids Res.* 33, W363–W367. doi:10.1093/nar/gki481
- Seetoh, W.-G., Chan, D. S.-H., Matak-Vinković, D., and Abell, C. (2016). Mass Spectrometry Reveals Protein Kinase CK2 High-Order Oligomerization via the Circular and Linear Assembly. *ACS Chem. Biol.* 11, 1511–1517. doi:10.1021/acscchembio.6b00064
- St-Denis, N. A., and Litchfield, D. W. (2009). Protein Kinase CK2 in Health and Disease. *Cell. Mol. Life Sci.* 66, 1817–1829. doi:10.1007/s00018-009-9150-2
- Syrgiannis, Z., Trautwein, G., Calvaresi, M., Modugno, G., Zerbetto, F., Carraro, M., et al. (2019). Controlling Size-Dispersion of Single Walled Carbon Nanotubes by Interaction with Polyoxometalates Armed with a Tryptophan Tweezer. *Eur. J. Inorg. Chem.* 2019, 374–379. doi:10.1002/ejic.201800660
- Tagliavini, V., Honisch, C., Serrati, S., Azzariti, A., Bonchio, M., Ruzza, P., et al. (2021). Enhancing the Biological Activity of Polyoxometalate-Peptide Nano-Fibrils by Spacer Design. *RSC Adv.* 11, 4952–4957. doi:10.1039/D0RA10218K
- Trembley, J. H., Chen, Z., Unger, G., Slaton, J., Kren, B. T., Van Waes, C., et al. (2010). Emergence of Protein Kinase CK2 as a Key Target in Cancer Therapy. *Biofactors* 36, 187–195. doi:10.1002/biof.96
- Trewhella, J., Duff, A. P., Durand, D., Gabel, F., Guss, J. M., Hendrickson, W. A., et al. (2017). 2017 Publication Guidelines for Structural Modelling of Small-Angle Scattering Data from Biomolecules in Solution: an Update. *Acta Cryst. Sect. D. Struct. Biol.* 73, 710–728. doi:10.1107/S2059798317011597
- Van Rompuy, L. S., and Parac-Vogt, T. N. (2019). Interactions between Polyoxometalates and Biological Systems: from Drug Design to Artificial Enzymes. *Curr. Opin. Biotechnol.* 58, 92–99. doi:10.1016/j.copbio.2018.11.013
- Vandebroek, L., Noguchi, H., Kamata, K., Tame, J. R. H., Van Meervelt, L., Parac-Vogt, T. N., et al. (2021). Shape and Size Complementarity-Induced Formation of Supramolecular Protein Assemblies with Metal-Oxo Clusters. *Cryst. Growth. Des.* 21, 1307–1313. doi:10.1021/acs.cgd.0c01571
- Venerando, A., Franchin, C., Cant, N., Cozza, G., Pagano, M. A., Tosoni, K., et al. (2013). Detection of Phospho-Sites Generated by Protein Kinase CK2 in CFTR: Mechanistic Aspects of Thr1471 Phosphorylation. *PLOS ONE* 8, e74232. doi:10.1371/journal.pone.0074232
- Venerando, A., Ruzzene, M., and Pinna, L. A. (2014). Casein Kinase: The Triple Meaning of a Misnomer. *Biochem. J.* 460, 141–156. doi:10.1042/BJ20140178

- Wang, S.-S., and Yang, G.-Y. (2015). Recent Advances in Polyoxometalate-Catalyzed Reactions. *Chem. Rev.* 115, 4893–4962. doi:10.1021/cr500390v
- Zamolo, V. A., Modugno, G., Lubian, E., Cazzolaro, A., Mancin, F., Giotta, L., et al. (2018). Selective Targeting of Proteins by Hybrid Polyoxometalates: Interaction between a Bis-Biotinylated Hybrid Conjugate and Avidin. *Front. Chem.* 6, 278. doi:10.3389/fchem.2018.00278
- Zanin, S., Borgo, C., Girardi, C., O'Brien, S. E., Miyata, Y., Pinna, L. A., et al. (2012). Effects of the CK2 Inhibitors CX-4945 and CX-5011 on Drug-Resistant Cells. *PLoS ONE* 7, e49193. doi:10.1371/journal.pone.0049193
- Zhang, G., Keita, B., Craescu, C. T., Miron, S., de Oliveira, P., and Nadjo, L. (2008). Molecular Interactions between Wells–Dawson Type Polyoxometalates and Human Serum Albumin. *Biomacromolecules* 9, 812–817. doi:10.1021/bm701120j
- Zhang, G., Keita, B., Craescu, C. T., Miron, S., de Oliveira, P., and Nadjo, L. (2007). Polyoxometalate Binding to Human Serum Albumin: a Thermodynamic and Spectroscopic Approach. *J. Phys. Chem. B* 111, 11253–11259. doi:10.1021/jp072947u
- Zhao, M., Chen, X., Chi, G., Shuai, D., Wang, L., Chen, B., et al. (2020). Research Progress on the Inhibition of Enzymes by Polyoxometalates. *Inorg. Chem. Front.* 7, 4320–4332. doi:10.1039/D0QI00860E

Conflict of Interest: The authors declare that the research was conducted in the absence of any commercial or financial relationships that could be construed as a potential conflict of interest.

Publisher's Note: All claims expressed in this article are solely those of the authors and do not necessarily represent those of their affiliated organizations, or those of the publisher, the editors and the reviewers. Any product that may be evaluated in this article, or claim that may be made by its manufacturer, is not guaranteed or endorsed by the publisher.

Copyright © 2022 Fabbian, Giachin, Bellanda, Borgo, Ruzzene, Spuri, Campofelice, Veneziano, Bonchio, Carraro and Battistutta. This is an open-access article distributed under the terms of the Creative Commons Attribution License (CC BY). The use, distribution or reproduction in other forums is permitted, provided the original author(s) and the copyright owner(s) are credited and that the original publication in this journal is cited, in accordance with accepted academic practice. No use, distribution or reproduction is permitted which does not comply with these terms.



Casein Kinase 1 and Human Disease: Insights From the Circadian Phosphoswitch

Joel C. Francisco¹ and David M. Virshup^{1,2*}

¹Program in Cancer and Stem Cell Biology, Duke-NUS Medical School, Singapore, Singapore, ²Department of Pediatrics, Duke University School of Medicine, Durham, NC, United States

OPEN ACCESS

Edited by:

Andrea Venerando,
University of Padua, Italy

Reviewed by:

Tong Wang,
Chinese Academy of Sciences (CAS),
China
Vitezslav Bryja,
Masaryk University, Czechia

*Correspondence:

David M. Virshup
david.virshup@duke-nus.edu.sg

Specialty section:

This article was submitted to
Molecular Diagnostics and
Therapeutics,
a section of the journal
Frontiers in Molecular Biosciences

Received: 03 April 2022

Accepted: 20 May 2022

Published: 03 June 2022

Citation:

Francisco JC and Virshup DM (2022)
Casein Kinase 1 and Human Disease:
Insights From the
Circadian Phosphoswitch.
Front. Mol. Biosci. 9:911764.
doi: 10.3389/fmolb.2022.911764

Biological systems operate in constant communication through shared components and feedback from changes in the environment. Casein kinase 1 (CK1) is a family of protein kinases that functions in diverse biological pathways and its regulation is beginning to be understood. The several isoforms of CK1 take part in key steps of processes including protein translation, cell-cell interactions, synaptic dopaminergic signaling and circadian rhythms. While CK1 mutations are rarely the primary drivers of disease, the kinases are often found to play an accessory role in metabolic disorders and cancers. In these settings, the dysregulation of CK1 coincides with increased disease severity. Among kinases, CK1 is unique in that its substrate specificity changes dramatically with its own phosphorylation state. Understanding the process that governs CK1 substrate selection is thus useful in identifying its role in various ailments. An illustrative example is the PERIOD2 (PER2) phosphoswitch, where CK1 δ/ϵ kinase activity can be varied between three different substrate motifs to regulate the circadian clock.

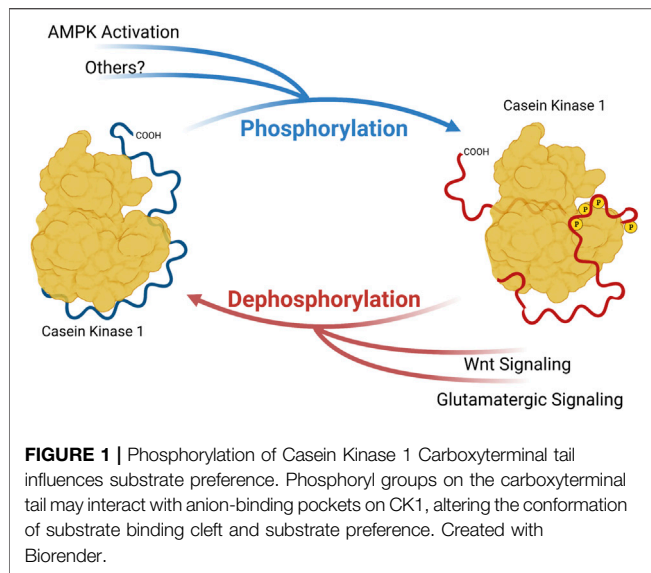
Keywords: casein kinase 1 (CK1), circadian rhythms, sleep disorder (SD), protein phosphorylation / dephosphorylation, cancer, drug addiction, alzheimer disease

THE CK1 GENE FAMILY, WITH A FOCUS ON CK1 δ/ϵ

CK1 δ and CK1 ϵ are members of a family of serine/threonine kinases that are highly conserved among eukaryotes. In humans, this group of kinases is encoded by six distinct genes, CSNK1A/D/E/G1/G2/G3 (Casein Kinase 1 α , δ , ϵ , γ -1, γ -2, and γ -3). Of these isoforms, CK1 δ and CK1 ϵ are the most closely related, sharing over 96% sequence identity in the kinase body, and have very similar carboxyterminal extensions of ~124 amino acids. CK1 δ and CK1 ϵ bind to and phosphorylate many of the same substrates, but with some subtle and important differences. The major regulation of CK1 δ/ϵ comes from their C-terminal tails. These CK1 δ/ϵ C-terminal tails are differentially phosphorylated and dephosphorylated, and it has been long known that this tail phosphorylation regulates kinase activity (Gietzen and Virshup, 1999; Graves and Roach, 1995; Rivers et al., 1998). Importantly, diverse signals, including metabotropic glutamate agonists, Wnts and the AMPK pathway regulate the activity of CK1 δ/ϵ through changes in C-terminal tail phosphorylation (Liu F. et al., 2002; Swiatek et al., 2004; Um et al., 2007) (Figure 1). Most recently, subtle changes in the phosphorylation of CK1 δ/ϵ C-terminal tails has been shown to change CK1 preference for distinct sites within one prominent substrate, PER2 (Fustin et al., 2018; Narasimamurthy et al., 2018).

CK1 Substrate Sequences

CK1 is best known for its preference to phosphorylate acidic substrates. The first-identified CK1 targets are either preceded by acidic residues, or primed by a phosphorylated serine or threonine. The acidic or phosphorylated amino acid is usually three residues upstream of a CK1 target serine/



threonine (Flotow and Roach, 1989). Repeats of this CK1 motif are found in many CK1 substrates in the pattern pSxx (S/T)xx (S/T)xx (S/T) and the phosphorylation of this upstream S/T allows propagation of the signal to multiple downstream serine/threonine residues. This phosphorylation of a primed substrate is very rapid. However, CK1 has also been shown to phosphorylate unprimed substrates. These events, while significantly slower than processive phosphorylation of a primed substrate, clearly have important regulatory functions, serving as rate-limiting steps for downstream phosphorylation. The most prominent examples of this principle of CK1 as rate limiting is the case of S45 of β -catenin (Amit et al., 2002; Liu C. et al., 2002; Marin et al., 2003) and S662 of PERIOD2 (PER2) (Toh et al., 2001). Thus, it is important to understand what leads CK1 to prioritize these different “slow” substrate motifs.

Interest in targeting CK1 for therapeutic intervention of sleep disorders, cancer and drug addiction has grown over the years. Multiple CK1 inhibitors have recently been developed and tested *in vitro* and in animal models. The modelling of how CK1 δ/ϵ selects sites on PER2 could provide a better understanding of how CK1 phosphorylate its other substrates. Here we review selected literature describing the phosphoswitch mechanism of PER2 and highlight several diseases where a similar CK1 substrate selection mechanism might be involved.

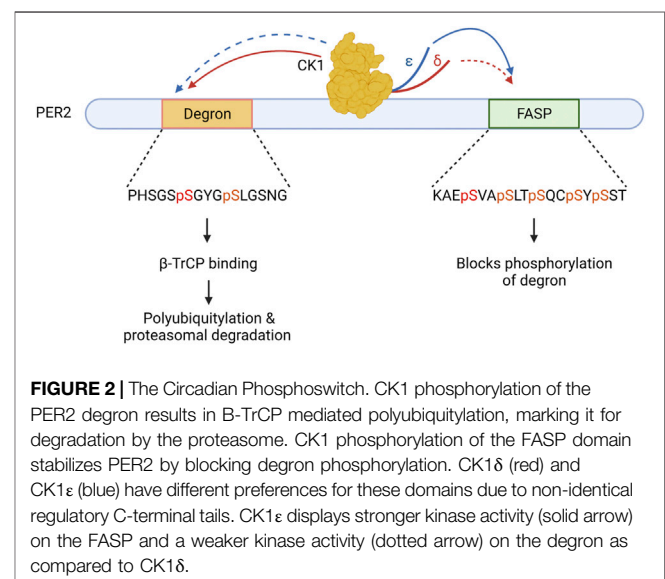
Modelling CK1 δ/ϵ Regulation: Lessons From the Circadian Phosphoswitch

While the 24-h rhythmicity of many physiological processes has been observed long before the dawn of modern biology, its genetic basis was first confirmed in 1971 by Konopka and Benzer (Konopka and Benzer, 1971). Using a forward genetic approach in *D. melanogaster*, they identified mutations in a single gene that altered both the time-of-day when flies would emerge from their pupae and locomotor rhythms in adult flies. This gene was named Period (Per) and the rise and fall of its

mRNA and protein abundance across the day results in the periodicity of animal clocks. Price, Kloss then identified that the gene Doubletime (dbt), encoding a CK1 orthologue in *Drosophila*, regulated Per degradation via direct phosphorylation (Kloss et al., 1998; Price et al., 1998). In 1999, Ptacek and others identified the first genetically linked sleep disorder in humans (Jones et al., 1999). It was characterized by an abnormally early onset of sleepiness and pre-dawn wakefulness, and so was termed Familial Advanced Sleep Phase (FASP).

The details of the mutation causing FASP has provided great insights into how CK1 interacts with the PERIOD protein. A serine to glycine substitution at residue 662 of PER2 blocked its phosphorylation by CK1 on a series of downstream serine residues, resulting in a decrease of PER2 stability (Toh et al., 2001). Thus, the multiphosphoserine region of Serine-662, -665, -668, -671, and -673, responsible for PER2 stability came to be known as the FASP domain. Phosphorylation of the FASP domain is a 2-step process where a slow priming phosphorylation of S662 creates an ideal CK1 substrate, enabling the subsequent rapid phosphorylation of the downstream serines (Narasimamurthy et al., 2018). Thus, CK1 has two types of substrate recognition in the FASP domain. First, it slowly phosphorylates S662, and then very rapidly phosphorylates the remainder of the FASP multi-serine domain.

CK1 δ/ϵ have a third type of important substrate recognition in a distant region of PER2, a domain referred to as the phosphodegron. CK1 phosphorylation of the human PER2 phosphodegron at S480 and S484 allows for binding of β -TrCP, an E3 ubiquitin ligase, which then leads to polyubiquitylation and proteasomal degradation of PER2 (Eide et al., 2005; Reischl et al., 2007). Importantly, CK1 phosphorylation of FASP domain of PER2 prevents phosphorylation of the phosphodegron. Thus, CK1 must choose—phosphorylate FASP and stabilize PER2, or phosphorylate the phosphodegron and destabilize PER2. This



mechanism, termed the phosphoswitch model of PER2 regulation (**Figure 2**), allows fine tuning of CK1 substrate specificity within the PER2 protein to increase stability or drive degradation (Zhou et al., 2015; Masuda et al., 2020).

We have seen that within the PER2 phosphoswitch, there are three distinct substrate motifs for CK1: the slow priming site of the FASP, the rapid four phosphoserine residues downstream of the FASP, and the slow phosphodegron. Using x-ray crystallography, Philpott et al. described a two-state activation loop in the CK1 δ/ϵ kinase that contributes to substrate selection (Philpott et al., 2020a). Molecular dynamics simulations of the loop found that it resided predominantly in the “Loop Down” position, but it could enter the “Loop Up” position on rare occasion. Flipping the loop up was predicted to reduce the volume of the CK1 substrate binding cleft allosterically. Importantly, the loop down versus loop up configuration could be controlled by changes in the anion environment, and in the occupancy of anion binding pockets on the kinase body. Given that phosphorylation of the CK1 carboxyterminal tail creates anionic (phospho-) patches, and that phosphorylated peptides can bind to these anion binding pockets (Gebel et al., 2020), we have proposed that phosphoresidues in the CK1 δ/ϵ tail interact with the anion binding pockets to alter activation loop conformation (Narasimamurthy and Virshup, 2021). Supporting this hypothesis, it was demonstrated that a 15 amino acid deletion from the tail of CK1 δ more than doubled its kinase activity on FASP peptide to match CK1 ϵ (Fustin 2018) (Narasimamurthy et al., 2018). Notably, this deletion removed two phosphoserine residues from the CK1 δ tail which the CK1 ϵ isoform lacks. Similarly, a splice variant of CK1 δ altering the extreme C-terminus differentially altered activity on PER2 sites (Fustin et al., 2018). Thus, changes from CK1 δ to CK1 ϵ , and changes in CK1 δ/ϵ tail phosphorylation is likely to be a mechanism to alter kinase substrate preference and give CK1 its switch-like behavior. While more insight into the control of CK1 tail phosphorylation and its subsequent interaction with the kinase domain is needed to gain a complete understanding of this process, these findings bring us closer to understanding the regulation of CK1 activity.

CK1 - Period and Sleep Disorders

The characterization of FASP syndrome demonstrates that regulation of Per2 abundance by CK1 is integral in maintaining normal sleep-wake physiology. Consistent with this, mutations in the CK1 gene also cause sleep disorders. In 1988, a mutation called Tau was identified in Syrian golden hamsters that caused a shortening of the circadian period. Heterozygous or homozygous Tau animals experienced a 22-h or 20-h biological day as compared to the standard 24-h of the wildtype controls (Ralph and Menaker, 1988). 12 years later, Lowrey and others traced the cause of this phenotype to a single R178C substitution in CK1 ϵ which abolishes one of the anion binding pockets described above. This mutation resulted in an 8-fold reduction of kinase activity on primed FASP peptide of PER2 (Lowrey et al., 2000) but increased phosphorylation of the phosphodegron (Philpott et al., 2020b). Thus, abnormalities in CK1 function could cause circadian disruption as mutations in mammals, similar to *Drosophila*.

Human mutations in CK1 δ and CK1 ϵ also alter circadian rhythms. Individuals with Delayed Sleep Phase and Non-24-Hour Sleep-Wake Disorder were half as likely to possess at least one allele of a S408N polymorphism in CK1 ϵ (Takano et al., 2004). Notably, S408 is located on the C-terminal tail of CK1 ϵ and is a known phosphorylation site. This S408N variant increased the activity of CK1 ϵ on the FASP peptide, consistent with earlier findings that S408 phosphorylation contributed to autoinhibition of CK1 ϵ (Gietzen and Virshup, 1999; Takano et al., 2004). Another family with FASP had a CK1 δ T44A mutation that caused reduced kinase activity on PER substrates (Xu et al., 2005). While the phenotype was not observed to be as dramatic as the CK1 ϵ ^{Tau} mutant, it was also linked to migraine in the same family (Brennan et al., 2013). These studies confirm that CK1 is a critical core circadian protein whose mutation leads to circadian related disorders. The dysregulation of CK1 activity has also been implicated in other diseases via additional substrates (**Table 1**).

CK1 Regulates Cell-Cell Interactions Through Connexin-43

Hyperphosphorylation of Connexin-43 (Cx-43) by CK1 may contribute to tumor metastasis in pancreatic and breast cancers. Under normal conditions, CK1 helps maintain cell-cell interfaces in part by phosphorylating Cx-43, a key structural protein of gap junctions (GJ). These structures facilitate cell-cell communication by allowing the exchange of small molecules and ions through their pore-like hemichannels. GJs are also known to transduce signals from the cell membrane to alter transcriptional programs. This includes signals that promote extravasation, cell migration, differentiation, and apoptosis. Therefore, Cx-43 can both prevent and promote tumorigenesis depending on its regulation.

Cooper et al., identified a multi-phosphoserine domain in Cx-43 that was phosphorylated by CK1 δ/ϵ (Cooper and Lampe, 2002). This phosphodomain is important for the membrane localization of Cx-43 and assembly of GJ complexes, and inhibition of CK1 δ/ϵ activity interfered with GJ formation (Cooper and Lampe, 2002). In epithelial cells, mutation of the Cx-43CK1 target serines to alanines, creating Cx-43^{CK1A}, reduced cell migration in wound healing assays. Correspondingly, serine to glutamic acid substitutions to generate phosphomimetic Cx-43 at these sites caused increased migration (Lastwika et al., 2019). This property of Cx-43 was unique to the CK1-regulated phosphodomain. Hence, dysregulation of this interaction could disrupt cell signaling and migration, both of which play important roles in cancer.

Ck1, Cx-43 and Cancer

Recent work has shown that this CK1-CX-43 axis contributes to the severity of pancreatic ductal adenocarcinomas (PDAC), a form of cancer known for its aggressive metastatic ability. In 2021, Solan et al., showed that in a KRAS^{G12D} mouse model of PDAC, phosphorylation of Cx-43 by CK1 was important for epithelial-mesenchymal transition (EMT) (Solan et al., 2021). KRAS^{G12D} mice with the Cx-43^{CK1A} mutations had reduced metastatic burden and increased overall survival compared to

TABLE 1 | CK1 target sites in PER2, Connexin-43, 4EBP1 and DARPP32.

Human CK1 target	Residues	Unprimed	Primed	Function
PER2 degron	S-480, 484	PHSGSpSGYSLGSNG	PHSGSpSGYGpSLGSNG	β -TrCP dependent polyubiquitination and proteasomal degradation
PER2 FASP	S-662, 665, 668, 671, 674	PGKAEpSVASLTQSQSYSTIVH	PGKAEpSVApSLTpSQCPsYSpSTIVH	Protein stabilization by blocking degron phosphorylation
CX-43	S-325, 328, 330	MGQAGpSTISNSHAQPF	MGQAGpSTIpSNpSHAQPF	GJ assembly and membrane localization
4EBP1	T-41, 50	TTPGGpTLFSTTPGGpTRIIYD		Release of EIF4e for cap-dependent translation
DARPP-32	S-137	PPLDEpSERDGG		Enhance PP1 inhibitory effect; facilitate switching to PKA inhibition

Amit, S., hatzubai, A., birman, Y., andersen, J.S., Ben-Shushan, E., mann, M., Ben-Neriah, Y., and Alkalay, I (2002). Axin-mediated CKI, phosphorylation of β -catenin at Ser 45: a molecular switch for the Wnt pathway. *Gene Dev* 16, 1,066–1,076.

KRAS^{G12D} alone. They also observed that primary tumors in KRAS^{G12D}; Cx-43^{CK1A} mice had less gap junctions, developed a cyst-like phenotype and maintained expression of epithelial markers, consistent with reduced EMT and less migration.

CK1-enhanced GJ activity may be a feature of other highly metastatic tumors. Rosenberg et al. found that suppressing CK1 δ activity with the potent CK1 δ/ϵ inhibitor Sr-3029 reduced the tumorigenicity of Triple Negative Breast Cancer (TNBC) cells (Rosenberg et al., 2015). In the TNBC line MDA-MB231, both CK1 δ -specific shRNA and Sr-3029 treatment led to a reduction in cell proliferation. This result was not observed in CK1 δ -low breast cancer lines like MCF7. In mouse orthotopic xenografts, Sr-3029 treatment drastically reduced the volume of MDA-MB231 tumors. Subsequent work by Bar et al. confirmed these findings (Bar et al., 2018). They similarly found that CK1 δ knockdown MDA-MB231 resulted in significantly slower growing tumors. Additionally, they showed that CK1 δ promoted MDA-MB231 cell migration. CK1 δ knockdown tumors displayed decreased ability to metastasize both *in vivo* and *ex vivo*. Although CX-43 phosphorylation was not directly assessed in this model, they noted repression of junctional proteins in these breast cancer models, making CX-43 an interesting candidate for further study.

CK1 Regulates Protein Translation via 4EBP1

There is growing interest in the use of translation inhibition as a therapy for cancer. Due to its critical role in cell growth, translation is a tightly regulated process. Most of this control takes place at the translation initiation phase and is regulated by the heterotrimeric Elongation Initiation Factor 4a Complex (EIF4A). Elongation Initiation Factor 4e (EIF4E) is a rate-limiting component of the EIF4A complex. It functions to bind the m7g cap of mRNA to recruit it to the ribosome for translation. Suppressing translation is thus accomplished through the sequestration of EIF4E by 4 E-binding protein 1 (4EBP1). 4EBP1 phosphorylation releases EIF4E to drive translation, so the kinases that phosphorylate 4EBP1 are of great interest. While initial studies on focused on the mTOR and PIK3-regulated phosphorylation, more recent studies have found that CK1 δ/ϵ also phosphorylates 4EBP1 on a distinct set of regulatory sites,

also leading to EIF4E release (Brunn et al., 1997; Gingras et al., 1999, 2001).. (Shin et al., 2014; Deng et al., 2017)

How might the activity of CK1 on 4EBP1 be regulated? One possibility is via AMP-activated protein kinase (AMPK). AMPK is a cellular energy sensor that shuts down protein translation when intracellular ATP stores are depleted. AMPK has been shown to activate CK1 ϵ by phosphorylating its regulatory tail on S389 (Um et al., 2007). Based on what we now know about CK1 δ/ϵ regulation, this suggests that phosphorylation of this site on CK1 may bias the substrate selection of the kinase. (Fustin et al., 2018; Narasimamurthy et al., 2018). We speculate that cells could also use AMPK phosphorylation of CK1 ϵ to change its substrate selection on 4EBP1.

CK1, 4EBP1 and Cancer

While CK1 is rarely the primary driver of disease, elevated CK1 δ/ϵ has been associated with highly malignant cancers (Toyoshima et al., 2012; Rosenberg et al., 2015; Bar et al., 2018). One potential target of this increased CK1 activity is the translation of c-Myc oncogene. Recent work by Deng et al. successfully utilized inhibition of CK1 ϵ to treat Myc-translocation-positive lymphomas via the suppression of protein translation (Deng et al., 2017). The MYC proto-oncogene encodes a transcription factor that influences the expression of around 15% of total human transcripts. Under normal circumstances, MYC is under tight transcriptional and translational regulation, and MYC protein is quickly degraded to prevent its accumulation. However, MYC overexpression is detected in a majority of cancers and correlates with poor treatment outcomes. MYC gene amplification and translocation cancers are particularly aggressive and challenging to treat, owing to the undruggable nature of Myc protein (Mossafa et al., 2009; Jonge et al., 2016). As part of its regulation, the 5' UTR of Myc mRNA forms complex secondary structures, making it heavily dependent on the EIF4A complex for translation (Wolfe et al., 2014). Thus, Deng and others surmised that stopping EIF4E release from 4EBP1 might be sufficient to block hypertranslation of Myc. To do this, they developed a PI3K δ (IC₅₀ = 22 nM) and CK1 ϵ (IC₅₀ = 6 μ M) dual kinase inhibitor, umbralisib (TGR-1202). Umbralisib gave promising results in reducing viability of multiple MYC-driven lymphomas. It was found to outperform idelalisib, the best-in-class approved PI3K δ inhibitor.

Umbralisib treatment greatly reduced C-MYC protein levels by effectively blocking the release of EIF4E from 4EBP1. This effect was reproduced when the lymphoma cells were treated with idelalisib in combination with the CK1 ϵ specific inhibitor PF4800567, showing that co-inhibition of PI3K δ and CK1 ϵ was required to achieve potency. Interestingly, Maharaj et al., showed that the CK1 ϵ inhibitory ability of umbralisib contributes to the safety profile of the drug (Maharaj et al., 2020). This was observed when either umbralisib alone or idelalisib with PF4800567 preserved a healthy population of regulatory T-cells (Tregs) in mice while treatment idelalisib alone did not. The authors proposed that dual-inhibition of PI3K δ and CK1 ϵ reduces immune mediated toxicities resulting in lower risks of treatment. Thus far, this method of translation inhibition has proven to be well tolerated among patients. The FDA has recently granted accelerated approval for the drug umbralisib in the treatment of Marginal Zone Lymphoma and Follicular Lymphoma while several phase 2 and 3 trials are underway for other forms of lymphoma (<https://clinicaltrials.gov>).

Bryja and coworkers recently demonstrated the potential of CK1 inhibition in Chronic Lymphocytic Leukemia (CLL) (Janovska et al., 2018). Treatment in a mouse model of CLL, E μ -TCL1, with PF670462, a dual CK1 δ/ϵ inhibitor, was found to significantly delay disease onset and extend overall survival. While the authors note that CK1 inhibition is likely non-curative in leukemia, it has strong therapeutic potential in combination with other tumor suppressive drugs. Although the role of 4EBP1 in CLL is unclear, this is a fruitful area for study given the safety and effectiveness of umbralisib in a closely related hematological malignancy.

CK1, 4EBP1, and Metabolic Disorders

Could CK1 δ/ϵ regulate translation of other important genes? A growing body of research has identified CK1 as a contributing factor to various metabolic disorders. One example is its role in promoting the maturation of pre-adipocytes in white adipose tissue (WAT) via EIF4E-dependent translation. This proliferation of WAT heightens the risk of disease by enhancing hunger signals, inducing insulin resistance, raising basal inflammation and altering sleep behavior. While PPAR γ and C/EBPs transcription factors are considered the master regulators of adipocyte differentiation, they are in turn regulated by the cellular energy sensor, AMPK (Sozio et al., 2011; Cheang et al., 2014; Mancini et al., 2017). As with MYC, PPAR γ translation is also tightly regulated by highly stable secondary structures in its 5' UTR (McClelland et al., 2009). Thus, adipogenesis is dependent on EIF4A complex activity and hence sensitive to EIF4E sequestration by 4EBP1 (Tsukiyama-Kohara et al., 2013; Tsai et al., 2016). CK1 inhibitors are therefore potential candidates for obesity intervention. Indeed, CK1 δ/ϵ inhibition with the small molecule inhibitor, PF5006739, was shown to improve glucose tolerance in both diet-induced and genetic models of obesity in mice (Wager et al., 2014; Cunningham et al., 2016), an effect that we speculate is due in part to decreased translation of PPAR γ .

Yang et al. presented additional circumstantial evidence supporting the idea that CK1 δ/ϵ activity regulates PPAR γ

translation (Yang et al., 2019). They found the soy derived compound, Orobol, reduced accumulation of WAT in mice fed with a high fat diet. It also prevented phosphorylation of 4EBP1 at serine-65 and reduced expression of PPAR γ in pre-adipocytes. Kinome screening identified CK1 ϵ (IC_{50} = 1.24 μ M) as the kinase most sensitive to Orobol treatment. However, Orobol also inhibited MAP4K5 (IC_{50} = 1.48 μ M), which also has the potential to affect 4EBP1 phosphorylation via the mTOR pathway (Gingras et al., 1999).

CK1 and DARPP-32

DARPP-32 was discovered due to its role in dopaminergic signaling, a key regulator of neuronal development, memory and learning that acts through the transcription factor CREB. This process is characterized by the stimulation of dopamine D1 receptors, activating Protein Kinase A (PKA), which in turn activates CREB through phosphorylation. Dephosphorylation of CREB by Protein Phosphatase 1 (PP1) attenuates this pathway. Another target of PKA is Dopamine- and cAMP-Regulated Neuronal Phosphoprotein of 32kDa, DARPP-32. PKA phosphorylates DARPP-32 on Threonine-34, turning it into a potent inhibitor of Protein Phosphatase 1 (PP1), thus strengthening CREB-dependent transcription. Activation of metabotropic glutamate receptors (mGluR), which are known to enhance dopaminergic signaling, decreases phosphorylation of CK1 C-terminal tail by activation of calcineurin. This increases CK1 activity on S137 of DARPP-32, which protects dephosphorylation of T-34 from Calcineurin, further strengthening suppression of PP1 (Desdouits et al., 1995; Liu F. et al., 2002). DARPP-32 is also known to be phosphorylated by CDK5 on Threonine-75 which switches it into an inhibitor of PKA. Interestingly, CK1 phosphorylation of S137 is a prerequisite for CDK5 phosphorylation of DARPP-32. This implies that CK1 plays a critical role in DARPP-32's conversion from PP1 to PKA inhibitor. Of note, S137 is situated in a highly acidic region of DARPP-32. Thus, phosphorylation of CK1 could limit its accessibility to the DARPP-32 substrate site, amplifying dopamine D1 receptor signaling and increasing drug sensitivity.

CK1, DARPP-32 and Drug Addiction

Neuroadaptations to the dopamine signaling system from substance abuse leads to drug dependence (Thomas et al., 2008). Since CK1 phosphorylation of DARPP-32 modulates dopaminergic signaling, various studies have explored its role in substance abuse. In mice, DARPP-32 phosphorylation was shown to influence addiction to the habit-forming drug, methamphetamine (MA) (Bryant et al., 2009a; 2012a). Linkage analysis performed in mice bred for high sensitivity to MA-induced locomotor activity revealed Quantitative Trait Loci (QTL) linked to CK1 ϵ overexpression. In these mice, CK1 ϵ transcript was increased by over 10-fold in the nucleus accumbens (Palmer et al., 2005). This suggests a positive relationship between CK1 ϵ activity and MA sensitivity. This was tested by the inhibition of CK1 with PF670462 (CK1 δ IC_{50} = 14 nM, CK1 ϵ IC_{50} = 7.7 nM), a dual CK1 δ/ϵ inhibitor, and this blocked MA-induced locomotor activity leading to the

conclusion that CK1 promoted drug sensitivity (Bryant et al., 2009b). However, the story got more complicated. In a follow-up study, CK1 ϵ knockout mice displayed increased sensitization to MA (Bryant et al., 2012b). This time, CK1 ϵ -specific inhibition with PF4800567 (IC₅₀ = 32 nM) enhanced MA-induced locomotor activity in the MA sensitive mice, suggesting that CK1 ϵ acts to attenuate drug addiction. The differences in substrate preference between CK1 δ and CK1 ϵ may account for this contradictory finding. Supporting this theory, Wager et al. observed a suppressive effect on drug-seeking behavior in rats treated with PF50067399 (CK1 δ IC₅₀ = 3.9 nM, CK1 ϵ IC₅₀ = 17 nM), a brain-penetrant dual CK1 δ/ϵ inhibitor (Wager et al., 2014). This molecule is four times more potent on CK1 δ than CK1 ϵ . Thus, it appears that while CK1 δ enhances drug sensitivity, CK1 ϵ acts to suppress it. Zhou et al. provided additional evidence, showing that mice with forebrain overexpression of CK1 δ were more sensitive to amphetamine and methylphenidate, which both stimulate the dopaminergic pathway (Zhou et al., 2010). This suggests that CNS-active CK1 δ inhibitors might be useful in the treatment of drug addiction.

Alzheimer Disease and CK1

Alzheimer Disease (AD) is a neurodegenerative disease characterized by a progressive decline in cognitive functions such as memory, speech, and mood regulation. While the cause of AD remains unknown, disease severity is correlated with the accumulation of hyperphosphorylated Tau protein and amyloid- β plaques (A β) which impairs proper neuronal function (Ballard et al., 2011). The failure to produce significant clinical outcomes in patients of AD after A β plaque clearance highlights the importance of understanding both Tau and A β accumulation (Sevigny et al., 2016; Selkoe, 2019). One mechanism of Tau hyperphosphorylation is the reduced activity of PP1 in AD brain tissue (Gong et al., 1993; Wang et al., 1996; Sun et al., 2003). Various studies have established that CK1 δ and CK1 ϵ protein are both highly upregulated in human AD brain tissue (Ghoshal et al., 1999; Yasojima et al., 2000). Potentially, the increase in CK1 δ/ϵ results in an accumulation of T-34

phosphorylated DARPP-32 and a pathological inhibition of PP1. This is in line with the findings of Sundaram et al., where inhibition of CK1 δ/ϵ with PF670462 improved cognitive function and reduced A β plaques in a mouse model of AD (Sundaram et al., 2019). Establishing a direct connection between CK1-mediated DARPP-32 phosphorylation and hyperphosphorylated Tau accumulation could provide new insights into developing AD therapies.

Conclusion and Future Directions

Altered regulation of CK1 δ/ϵ activity is associated with many diseases including sleep disorders, metabolic syndrome, Alzheimer Disease and cancer (Depner et al., 2014; Summa and Turek, 2014; Musiek et al., 2015; Stephenson et al., 2021). However, the molecular pathways that directly control the activity of CK1 in these diseases remain poorly understood. Insights from the regulation of circadian rhythms may expand our understanding of the role of CK1 in other processes.

Casein Kinase 1 is a key regulator of the circadian clock, determining the duration of each biological day through the phosphorylation of at least three unique PER2 domains. The ability of CK1 to choose between these three potential phosphorylation sites is a combination of several regulatory mechanisms. Firstly, the various CK1 isoforms have differing propensities for carboxyterminal tail modification. Secondly, CK1 preference for the substrates are influenced by modifications to its carboxyterminal tail. Finally, the ratio of expression between the various CK1 isoforms (and the CK1 δ splice variants) also plays a role. These mechanisms may extend to other disease-relevant substrates including Cx-43, 4EBP1 and DARPP-32. Unlocking the ability to switch CK1 activity between substrates potentially enables the precise modulation of these CK1 target proteins, offering new avenues of therapy for their respective diseases.

AUTHOR CONTRIBUTIONS

JF, DV contributed to the writing of this review.

REFERENCES

- Ballard, C., Gauthier, S., Corbett, A., Brayne, C., Aarsland, D., and Jones, E. (2011). Alzheimer's Disease. *Lancet* 377, 1019–1031. doi:10.1016/s0140-6736(10)61349-9
- Bar, I., Merhi, A., Larbanoix, L., Constant, M., Haussy, S., Laurent, S., et al. (2018). Silencing of Casein Kinase 1 Delta Reduces Migration and Metastasis of Triple Negative Breast Cancer Cells. *Oncotarget* 9, 30821–30836. doi:10.18632/oncotarget.25738
- Brennan, K. C., Bates, E. A., Shapiro, R. E., Zyuzin, J., Hallows, W. C., Huang, Y., et al. (2013). Casein Kinase I δ Mutations in Familial Migraine and Advanced Sleep Phase. *Sci. Transl. Med.* 5, 183ra56–11. doi:10.1126/scitranslmed.3005784
- Brunn, G. J., Hudson, C. C., Sekulic, A., Williams, J. M., Hosoi, H., Houghton, P. J., Jr., et al. (1997). Phosphorylation of the Translational Repressor PHAS-I by the Mammalian Target of Rapamycin. *Science* 277, 99–101. doi:10.1126/science.277.5322.99
- Bryant, C. D., Graham, M. E., Distler, M. G., Munoz, M. B., Li, D., Vezina, P., et al. (2009a). A Role for Casein Kinase 1 Epsilon in the Locomotor Stimulant Response to Methamphetamine. *Psychopharmacology* 203, 703–711. doi:10.1007/s00213-008-1417-z
- Bryant, C. D., Graham, M. E., Distler, M. G., Munoz, M. B., Li, D., Vezina, P., et al. (2009b). A Role for Casein Kinase 1 Epsilon in the Locomotor Stimulant Response to Methamphetamine. *Psychopharmacology* 203, 703–711. doi:10.1007/s00213-008-1417-z
- Bryant, C. D., Parker, C. C., Zhou, L., Olker, C., Chandrasekaran, R. Y., Wager, T. T., et al. (2012a). Csnk1e Is a Genetic Regulator of Sensitivity to Psychostimulants and Opioids. *Neuropsychopharmacol* 37, 1026–1035. doi:10.1038/npp.2011.287
- Bryant, C. D., Parker, C. C., Zhou, L., Olker, C., Chandrasekaran, R. Y., Wager, T. T., et al. (2012b). Csnk1e Is a Genetic Regulator of Sensitivity to Psychostimulants and Opioids. *Neuropsychopharmacol* 37, 1026–1035. doi:10.1038/npp.2011.287
- Cheang, W. S., Tian, X. Y., Wong, W. T., Lau, C. W., Lee, S. S.-T., Chen, Z. Y., et al. (2014). Metformin Protects Endothelial Function in Diet-Induced Obese Mice by Inhibition of Endoplasmic Reticulum Stress through 5' Adenosine Monophosphate-Activated Protein Kinase-Peroxisome Proliferator-Activated Receptor δ Pathway. *Atvb* 34, 830–836. doi:10.1161/atvbaha.113.301938

- Cooper, C. D., and Lampe, P. D. (2002). Casein Kinase 1 Regulates Connexin-43 Gap Junction Assembly*. *J. Biol. Chem.* 277, 44962–44968. doi:10.1074/jbc.m209427200
- Cunningham, P. S., Ahern, S. A., Smith, L. C., da Silva Santos, C. S., Wager, T. T., and Bechtold, D. A. (2016). Targeting of the Circadian Clock via CK1δ/ε to Improve Glucose Homeostasis in Obesity. *Sci. Rep.* 6, 29983. doi:10.1038/srep29983
- de Jonge, A. V., Roosma, T. J. A., Houtenbos, I., Vasmel, W. L. E., van de Hem, K., van de Boer, J. P., et al. (2016). Diffuse Large B-Cell Lymphoma with MYC Gene Rearrangements. *Eur. J. Cancer* 55, 140–146. doi:10.1016/j.ejca.2015.12.001
- Deng, C., Lipstein, M. R., Scotto, L., Jirau Serrano, X. O., Mangone, M. A., Li, S., et al. (2017). Silencing C-Myc Translation as a Therapeutic Strategy through Targeting PI3Kδ and CK1ε in Hematological Malignancies. *Blood* 129, 88–99. doi:10.1182/blood-2016-08-731240
- Depner, C. M., Stothard, E. R., and Wright, K. P. (2014). Metabolic Consequences of Sleep and Circadian Disorders. *Curr. Diab Rep.* 14, 507. doi:10.1007/s11892-014-0507-z
- Desdouits, F., Siciliano, J. C., Greengard, P., and Girault, J. A. (1995). Dopamine- and cAMP-Regulated Phosphoprotein DARPP-32: Phosphorylation of Ser-137 by Casein Kinase I Inhibits Dephosphorylation of Thr-34 by Calcineurin. *Proc. Natl. Acad. Sci. U.S.A.* 92, 2682–2685. doi:10.1073/pnas.92.7.2682
- Eide, E. J., Woolf, M. F., Kang, H., Woolf, P., Hurst, W., Camacho, F., et al. (2005). Control of Mammalian Circadian Rhythm by CK1ε-Regulated Proteasome-Mediated PER2 Degradation. *Mol. Cell. Biol.* 25, 2795–2807. doi:10.1128/mcb.25.7.2795-2807.2005
- Flotow, H., and Roach, P. J. (1989). Synergistic Phosphorylation of Rabbit Muscle Glycogen Synthase by Cyclic AMP-dependent Protein Kinase and Casein Kinase I. *J. Biol. Chem.* 264, 9126–9128. doi:10.1016/s0021-9258(18)60501-0
- Fustin, J.-M., Kojima, R., Itoh, K., Chang, H.-Y., Ye, S., Zhuang, B., et al. (2018). Two Ck1δ Transcripts Regulated by m6A Methylation Code for Two Antagonistic Kinases in the Control of the Circadian Clock. *Proc. Natl. Acad. Sci. U.S.A.* 115, 5980–5985. doi:10.1073/pnas.1721371115
- Gebel, J., Tuppi, M., Chaikuad, A., Hötte, K., Schröder, M., Schulz, L., et al. (2020). p63 Uses a Switch-like Mechanism to Set the Threshold for Induction of Apoptosis. *Nat. Chem. Biol.* 16, 1078–1086. doi:10.1038/s41589-020-0600-3
- Ghoshal, N., Smiley, J. F., DeMaggio, A. J., Hoekstra, M. F., Cochran, E. J., Binder, L. I., et al. (1999). A New Molecular Link between the Fibrillar and Granulovacuolar Lesions of Alzheimer's Disease. *Am. J. Pathology* 155, 1163–1172. doi:10.1016/s0002-9440(10)65219-4
- Gietzen, K. F., and Virshup, D. M. (1999). Identification of Inhibitory Autophosphorylation Sites in Casein Kinase I ε. *J. Biol. Chem.* 274, 32063–32070. doi:10.1074/jbc.274.45.32063
- Gingras, A.-C., Gygi, S. P., Raught, B., Polakiewicz, R. D., Abraham, R. T., Hoekstra, M. F., et al. (1999). Regulation of 4E-BP1 Phosphorylation: a Novel Two-step Mechanism. *Genes. & Dev.* 13, 1422–1437. doi:10.1101/gad.13.11.1422
- Gingras, A.-C., Raught, B., Gygi, S. P., Niedzwiecka, A., Miron, M., Burley, S. K., et al. (2001). Hierarchical Phosphorylation of the Translation Inhibitor 4E-BP1. *Genes. Dev.* 15, 2852–2864. doi:10.1101/gad.912401
- Gong, C.-X., Singh, T. J., Grundke-Iqbal, I., and Iqbal, K. (1993). Phosphoprotein Phosphatase Activities in Alzheimer Disease Brain. *J. Neurochem.* 61, 921–927. doi:10.1111/j.1471-4159.1993.tb03603.x
- Graves, P. R., and Roach, P. J. (1995). Role of COOH-Terminal Phosphorylation in the Regulation of Casein Kinase Iδ. *J. Biol. Chem.* 270, 21689–21694. doi:10.1074/jbc.270.37.21689
- Janovska, P., Verner, J., Kohoutek, J., Bryjova, L., Gregorova, M., Dzimkova, M., et al. (2018). Casein Kinase 1 Is a Therapeutic Target in Chronic Lymphocytic Leukemia. *Blood* 131, 1206–1218. doi:10.1182/blood-2017-05-786947
- Jones, C. R., Campbell, S. S., Zone, S. E., Cooper, F., DeSano, A., Murphy, P. J., et al. (1999). Familial Advanced Sleep-phase Syndrome: A Short-Period Circadian Rhythm Variant in Humans. *Nat. Med.* 5, 1062–1065. doi:10.1038/12502
- Kloss, B., Price, J. L., Saez, L., Blau, J., Rothenfluh, A., Wesley, C. S., et al. (1998). The Drosophila Clock Gene Double-Time Encodes a Protein Closely Related to Human Casein Kinase Iε. *Cell.* 94, 97–107. doi:10.1016/s0092-8674(00)81225-8
- Konopka, R. J., and Benzer, S. (1971). Clock Mutants of *Drosophila melanogaster*. *Proc. Natl. Acad. Sci. U.S.A.* 68, 2112–2116. doi:10.1073/pnas.68.9.2112
- Lastwika, K. J., Dunn, C. A., Solan, J. L., and Lampe, P. D. (2019). Phosphorylation of Connexin 43 at MAPK, PKC or CK1 Sites Each Distinctly Alter the Kinetics of Epidermal Wound Repair. *J. Cell. Sci.* 132, jcs234633. doi:10.1242/jcs.234633
- Liu, C., Li, Y., Semenov, M., Han, C., Baeg, G.-H., Tan, Y., et al. (2002a). Control of β-Catenin Phosphorylation/Degradation by a Dual-Kinase Mechanism. *Cell.* 108, 837–847. doi:10.1016/s0092-8674(02)00685-2
- Liu, F., Virshup, D. M., Nairn, A. C., and Greengard, P. (2002b). Mechanism of Regulation of Casein Kinase I Activity by Group I Metabotropic Glutamate Receptors. *J. Biol. Chem.* 277, 45393–45399. doi:10.1074/jbc.m204499200
- Lowrey, P. L., Shimomura, K., Antoch, M. P., Yamazaki, S., Zemenides, P. D., Ralph, M. R., et al. (2000). Positional Syntenic Cloning and Functional Characterization of the Mammalian Circadian Mutation Tau. *Science* 288, 483–491. doi:10.1126/science.288.5465.483
- Maharaj, K., Powers, J. J., Achille, A., Mediavilla-Varela, M., Gamal, W., Burger, K. L., et al. (2020). The Dual PI3Kδ/CK1ε Inhibitor Umbralisib Exhibits Unique Immunomodulatory Effects on CLL T Cells. *Blood Adv.* 4, 3072–3084. doi:10.1182/bloodadvances.2020001800
- Mancini, S. J., White, A. D., Bijland, S., Rutherford, C., Graham, D., Richter, E. A., et al. (2017). Activation of AMP-Activated Protein Kinase Rapidly Suppresses Multiple Pro-inflammatory Pathways in Adipocytes Including IL-1 Receptor-Associated Kinase-4 Phosphorylation. *Mol. Cell. Endocrinol.* 440, 44–56. doi:10.1016/j.mce.2016.11.010
- Marin, O., Bustos, V. H., Cesaro, L., Meggio, F., Pagano, M. A., Antonelli, M., et al. (2003). A Noncanonical Sequence Phosphorylated by Casein Kinase 1 in β-catenin May Play a Role in Casein Kinase 1 Targeting of Important Signaling Proteins. *Proc. Natl. Acad. Sci. U.S.A.* 100, 10193–10200. doi:10.1073/pnas.1733909100
- Masuda, S., Narasimamurthy, R., Yoshitane, H., Kim, J. K., Fukada, Y., and Virshup, D. M. (2020). Mutation of a PER2 Phosphodegron Perturbs the Circadian Phosphoswitch. *Proc. Natl. Acad. Sci. U.S.A.* 117, 10888–10896. doi:10.1073/pnas.2000266117
- McClelland, S., Shrivastava, R., and Medh, J. D. (2009). Regulation of Translational Efficiency by Disparate 5' UTRs of PPARγ Splice Variants. *Ppar Res.* 2009, 193413. doi:10.1155/2009/193413
- Mossafa, H., Damotte, D., Jenabian, A., Delarue, R., Vincenneau, A., Amouroux, I., et al. (2009). Non-Hodgkin's Lymphomas with Burkitt-like Cells Are Associated with C-Myc Amplification and Poor Prognosis. *Leukemia Lymphoma* 47, 1885–1893. doi:10.1080/10428190600687547
- Musiek, E. S., Xiong, D. D., and Holtzman, D. M. (2015). Sleep, Circadian Rhythms, and the Pathogenesis of Alzheimer Disease. *Exp. Mol. Med.* 47, e148. doi:10.1038/emmm.2014.121
- Narasimamurthy, R., Hunt, S. R., Lu, Y., Fustin, J.-M., Okamura, H., Partch, C. L., et al. (2018). CK1δ/ε Protein Kinase Primes the PER2 Circadian Phosphoswitch. *Proc. Natl. Acad. Sci. U.S.A.* 115, 5986–5991. doi:10.1073/pnas.1721076115
- Narasimamurthy, R., and Virshup, D. M. (2021). The Phosphorylation Switch that Regulates Ticking of the Circadian Clock. *Mol. Cell.* 81, 1133–1146. doi:10.1016/j.molcel.2021.01.006
- Palmer, A. A., Verbitsky, M., Suresh, R., Kamens, H. M., Reed, C. L., Li, N., et al. (2005). Gene Expression Differences in Mice Divergently Selected for Methamphetamine Sensitivity. *Mamm. Genome* 16, 291–305. doi:10.1007/s00355-004-2451-8
- Philpott, J. M., Narasimamurthy, R., Ricci, C. G., Freeberg, A. M., Hunt, S. R., Yee, L. E., et al. (2020a). Casein Kinase 1 Dynamics Underlie Substrate Selectivity and the PER2 Circadian Phosphoswitch. *Elife* 9, e52343. doi:10.7554/eLife.52343
- Philpott, J. M., Narasimamurthy, R., Ricci, C. G., Freeberg, A. M., Hunt, S. R., Yee, L. E., et al. (2020b). Casein Kinase 1 Dynamics Underlie Substrate Selectivity and the PER2 Circadian Phosphoswitch. *Elife* 9, e52343. doi:10.7554/eLife.52343
- Price, J. L., Blau, J., Rothenfluh, A., Abodeely, M., Kloss, B., and Young, M. W. (1998). Double-Time Is a Novel Drosophila Clock Gene that Regulates PERIOD Protein Accumulation. *Cell.* 94, 83–95. doi:10.1016/s0092-8674(00)81224-6
- Ralph, M. R., and Menaker, M. (1988). A Mutation of the Circadian System in Golden Hamsters. *Science* 241, 1225–1227. doi:10.1126/science.3413487
- Reischl, S., Vanselow, K., Westermarck, P. O., Thierfelder, N., Maier, B., Herzel, H., et al. (2007). β-TrCP1-Mediated Degradation of PERIOD2 Is Essential for

- Circadian Dynamics. *J. Biol. Rhythms* 22, 375–386. doi:10.1177/0748730407303926
- Rivers, A., Gietzen, K. F., Vielhaber, E., and Virshup, D. M. (1998). Regulation of Casein Kinase I ϵ and Casein Kinase I δ by Anin Vivo Futile Phosphorylation Cycle. *J. Biol. Chem.* 273, 15980–15984. doi:10.1074/jbc.273.26.15980
- Rosenberg, L. H., Lafitte, M., Quereda, V., Grant, W., Chen, W., Bibian, M., et al. (2015). Therapeutic Targeting of Casein Kinase 1 δ in Breast Cancer. *Sci. Transl. Med.* 7, 318ra202. doi:10.1126/scitranslmed.aac8773
- Selkoe, D. J. (2019). Alzheimer Disease and Aducanumab: Adjusting Our Approach. *Nat. Rev. Neurol.* 15, 365–366. doi:10.1038/s41582-019-0205-1
- Sevigny, J., Chiao, P., Bussière, T., Weinreb, P. H., Williams, L., Maier, M., et al. (2016). The Antibody Aducanumab Reduces A β Plaques in Alzheimer's Disease. *Nature* 537, 50–56. doi:10.1038/nature19323
- Shin, S., Wolgamott, L., Roux, P. P., and Yoon, S.-O. (2014). Casein Kinase 1 ϵ Promotes Cell Proliferation by Regulating mRNA Translation. *Cancer Res.* 74, 201–211. doi:10.1158/0008-5472.can-13-1175
- Solan, J. L., Hingorani, S. R., and Lampe, P. D. (2021). Cx43 Phosphorylation Sites Regulate Pancreatic Cancer Metastasis. *Oncogene* 40, 1909–1920. doi:10.1038/s41388-021-01668-x
- Sozio, M. S., Lu, C., Zeng, Y., Liangpunsakul, S., and Crabb, D. W. (2011). Activated AMPK Inhibits PPAR- α and PPAR- γ Transcriptional Activity in Hepatoma Cells. *Am. J. Physiology-Gastrointestinal Liver Physiology* 301, G739–G747. doi:10.1152/ajpgi.00432.2010
- Stephenson, E. M., Usselman, L. E. J., Tergaonkar, V., Virshup, D. M., and Dallmann, R. (2021). Cancer Clocks in Tumorigenesis: the P53 Pathway and beyond. *Endocr-Relat. Cancer* 28, R95–R110. doi:10.1530/erc-20-0475
- Summa, K. C., and Turek, F. W. (2014). Chronobiology and Obesity: Interactions between Circadian Rhythms and Energy Regulation. *Adv. Nutr. Int. Rev. J.* 5, 312S–319S. doi:10.3945/an.113.005132
- Sun, L., Liu, S. Y., Zhou, X. W., Wang, X. C., Liu, R., Wang, Q., et al. (2003). Inhibition of Protein Phosphatase 2A- and Protein Phosphatase 1-induced Tau Hyperphosphorylation and Impairment of Spatial Memory Retention in Rats. *Neuroscience* 118, 1175–1182. doi:10.1016/s0306-4522(02)00697-8
- Sundaram, S., Nagaraj, S., Mahoney, H., Portugues, A., Li, W., Millsaps, K., et al. (2019). Inhibition of Casein Kinase 1 δ Improves Cognitive-Affective Behavior and Reduces Amyloid Load in the APP-PS1 Mouse Model of Alzheimer's Disease. *Sci. Rep.* 9, 13743. doi:10.1038/s41598-019-50197-x
- Swiatek, W., Tsai, I.-C., Klimowski, L., Pepler, A., Barnette, J., Yost, H. J., et al. (2004). Regulation of Casein Kinase I ϵ Activity by Wnt Signaling. *J. Biol. Chem.* 279, 13011–13017. doi:10.1074/jbc.m304682200
- Takano, A., Uchiyama, M., Kajimura, N., Mishima, K., Inoue, Y., Kamei, Y., et al. (2004). A Missense Variation in Human Casein Kinase I Epsilon Gene that Induces Functional Alteration and Shows an Inverse Association with Circadian Rhythm Sleep Disorders. *Neuropsychopharmacol* 29, 1901–1909. doi:10.1038/sj.npp.1300503
- Thomas, M. J., Kalivas, P. W., and Shaham, Y. (2008). Neuroplasticity in the Mesolimbic Dopamine System and Cocaine Addiction. *Brit. J. Pharmacol.* 154, 327–342. doi:10.1038/bjp.2008.77
- Toh, K. L., Jones, C. R., He, Y., Eide, E. J., Hinz, W. A., Virshup, D. M., et al. (2001). An H Per2 Phosphorylation Site Mutation in Familial Advanced Sleep Phase Syndrome. *Science* 291, 1040–1043. doi:10.1126/science.1057499
- Toyoshima, M., Howie, H. L., Imakura, M., Walsh, R. M., Annis, J. E., Chang, A. N., et al. (2012). Functional Genomics Identifies Therapeutic Targets for MYC-Driven Cancer. *Proc. Natl. Acad. Sci. U.S.A.* 109, 9545–9550. doi:10.1073/pnas.1121119109
- Tsai, S.-Y., Rodriguez, A. A., Dastidar, S. G., Del Greco, E., Carr, K. L., Sitzmann, J. M., et al. (2016). Increased 4E-BP1 Expression Protects against Diet-Induced Obesity and Insulin Resistance in Male Mice. *Cell. Rep.* 16, 1903–1914. doi:10.1016/j.celrep.2016.07.029
- Tsukiyama-Kohara, K., Katsume, A., Kimura, K., Saito, M., and Kohara, M. (2013). 4E-BP1 Regulates the Differentiation of White Adipose Tissue. *Genes. cells* 18, 602–607. doi:10.1111/gtc.12059
- Um, J. H., Yang, S., Yamazaki, S., Kang, H., Viollet, B., Foretz, M., et al. (2007). Activation of 5'-AMP-Activated Kinase with Diabetes Drug Metformin Induces Casein Kinase I ϵ (CKI ϵ)-dependent Degradation of Clock Protein mPer2. *J. Biol. Chem.* 282, 20794–20798. doi:10.1074/jbc.c700070200
- Wager, T. T., Chandrasekaran, R. Y., Bradley, J., Rubitski, D., Berke, H., Mente, S., et al. (2014). Casein Kinase 1 δ / ϵ Inhibitor PF-5006739 Attenuates Opioid Drug-Seeking Behavior. *ACS Chem. Neurosci.* 5, 1253–1265. doi:10.1021/cn500201x
- Wang, J.-Z., Grundke-Iqbal, I., and Iqbal, K. (1996). Restoration of Biological Activity of Alzheimer Abnormally Phosphorylated τ by Dephosphorylation with Protein phosphatase-2A, -2B and -1. *Mol. Brain Res.* 38, 200–208. doi:10.1016/0169-328x(95)00316-k
- Wolfe, A. L., Singh, K., Zhong, Y., Drewe, P., Rajasekhar, V. K., Sanghvi, V. R., et al. (2014). RNA G-Quadruplexes Cause eIF4A-dependent Oncogene Translation in Cancer. *Nature* 513, 65–70. doi:10.1038/nature13485
- Xu, Y., Padiath, Q. S., Shapiro, R. E., Jones, C. R., Wu, S. C., Saigoh, N., et al. (2005). Functional Consequences of a CK1 δ Mutation Causing Familial Advanced Sleep Phase Syndrome. *Nature* 434, 640–644. doi:10.1038/nature03453
- Yang, H., Lee, S. H., Ji, H., Kim, J.-E., Yoo, R., Kim, J. H., et al. (2019). Orobol, an Enzyme-Convertible Product of Genistein, Exerts Anti-obesity Effects by Targeting Casein Kinase 1 Epsilon. *Sci. Rep.* 9, 8942. doi:10.1038/s41598-019-43950-9
- Yasojima, K., Kuret, J., DeMaggio, A. J., McGeer, E., and McGeer, P. L. (2000). Casein Kinase 1 Delta mRNA Is Upregulated in Alzheimer Disease Brain. *Brain Res.* 865, 116–120. doi:10.1016/s0006-8993(00)02200-9
- Zhou, M., Kim, J. K., Eng, G. W. L., Forger, D. B., and Virshup, D. M. (2015). A Period2 Phosphoswitch Regulates and Temperature Compensates Circadian Period. *Mol. Cell.* 60, 77–88. doi:10.1016/j.molcel.2015.08.022
- Zhou, M., Rebholz, H., Brocia, C., Warner-Schmidt, J. L., Fienberg, A. A., Nairn, A. C., et al. (2010). Forebrain Overexpression of CK1 δ Leads to Down-Regulation of Dopamine Receptors and Altered Locomotor Activity Reminiscent of ADHD. *Proc. Natl. Acad. Sci. U.S.A.* 107, 4401–4406. doi:10.1073/pnas.0915173107

Conflict of Interest: The authors declare that the research was conducted in the absence of any commercial or financial relationships that could be construed as a potential conflict of interest.

Publisher's Note: All claims expressed in this article are solely those of the authors and do not necessarily represent those of their affiliated organizations, or those of the publisher, the editors and the reviewers. Any product that may be evaluated in this article, or claim that may be made by its manufacturer, is not guaranteed or endorsed by the publisher.

Copyright © 2022 Francisco and Virshup. This is an open-access article distributed under the terms of the Creative Commons Attribution License (CC BY). The use, distribution or reproduction in other forums is permitted, provided the original author(s) and the copyright owner(s) are credited and that the original publication in this journal is cited, in accordance with accepted academic practice. No use, distribution or reproduction is permitted which does not comply with these terms.



Copper Modulates the Catalytic Activity of Protein Kinase CK2

John E. Chojnowski¹, Rongrong Li¹, Tiffany Tsang², Fatimah H. Alfaran¹, Alexej Dick¹, Simon Cocklin¹, Donita C. Brady² and Todd I. Storchlic^{1*}

¹Department of Biochemistry and Molecular Biology, Drexel University College of Medicine, Philadelphia, PA, United States,

²Department of Cancer Biology, Perelman School of Medicine, University of Pennsylvania, Philadelphia, PA, United States

OPEN ACCESS

Edited by:

Victor Bustos,
The Rockefeller University,
United States

Reviewed by:

Stefania Sarno,
University of Padua, Italy
Maria Pulina,
Memorial Sloan Kettering Cancer
Center, United States
David Litchfield,
Western University, Canada

*Correspondence:

Todd I. Storchlic
tis35@drexel.edu

Specialty section:

This article was submitted to
Cellular Biochemistry,
a section of the journal
Frontiers in Molecular Biosciences

Received: 18 February 2022

Accepted: 12 May 2022

Published: 09 June 2022

Citation:

Chojnowski JE, Li R, Tsang T,
Alfaran FH, Dick A, Cocklin S,
Brady DC and Storchlic TI (2022)
Copper Modulates the Catalytic
Activity of Protein Kinase CK2.
Front. Mol. Biosci. 9:878652.
doi: 10.3389/fmolb.2022.878652

Casein kinase 2 (CK2) is an evolutionarily conserved serine/threonine kinase implicated in a wide range of cellular functions and known to be dysregulated in various diseases such as cancer. Compared to most other kinases, CK2 exhibits several unusual properties, including dual co-substrate specificity and a high degree of promiscuity with hundreds of substrates described to date. Most paradoxical, however, is its apparent constitutive activity: no definitive mode of catalytic regulation has thus far been identified. Here we demonstrate that copper enhances the enzymatic activity of CK2 both *in vitro* and *in vivo*. We show that copper binds directly to CK2, and we identify specific residues in the catalytic subunit of the enzyme that are critical for copper-binding. We further demonstrate that increased levels of intracellular copper result in enhanced CK2 kinase activity, while decreased copper import results in reduced CK2 activity. Taken together, these findings establish CK2 as a copper-regulated kinase and indicate that copper is a key modulator of CK2-dependent signaling pathways.

Keywords: casein kinase 2 (CK2), copper, cell signaling, protein kinase (CK2), phosphorylation, kinase regulation

INTRODUCTION

The human kinome consists of 535 kinases capable of phosphorylating approximately 70% of the proteins expressed in human cells (Olsen et al., 2010; Sharma et al., 2014; Ardito et al., 2017; Sugiyama et al., 2019). Of these kinases, CK2 (formerly known as casein kinase 2) is predicted to be responsible for generating over 20% of the phosphoproteome (Burnett & Kennedy, 1954; Salvi et al., 2009). Due to its significant contribution to the phosphoproteome and the fact that it phosphorylates and regulates the activity of other kinases, CK2 is considered a master kinase. As such, CK2 regulates a host of critical physiologic functions, including cell division, cell survival, gene expression, and protein folding, and has been implicated in the progression of multiple diseases (Litchfield, 2003; Meggio & Pinna, 2003; Borgo et al., 2021; Salvi et al., 2021; Strum et al., 2021).

CK2 is an evolutionarily conserved serine/threonine kinase and is a heterotetramer composed of two catalytic α subunits and two regulatory β subunits. The α subunit can phosphorylate substrates as part of the tetrameric complex or as a monomer (Grankowski et al., 1991). An additional isoform of the catalytic subunit, CK2 α' is expressed in humans, is catalytically active, and shares approximately 90% identity with CK2 α in its catalytic domain (Litchfield, 2003). CK2 exhibits dual co-substrate specificity and can use either ATP or GTP to phosphorylate substrates (Niefind et al., 1999). Intriguingly, most studies to date suggest that CK2 is constitutively active and has no defined mode of catalytic regulation, a finding that is bewildering given its central role in the regulation of many core cellular processes (Pinna, 2013).

Despite CK2 being considered constitutively active, numerous studies provide solid evidence of varied enzymatic activity. Most of these reports suggest that these differences are likely due to changes in CK2 expression levels (Strum et al., 2021). However, several other studies document significant alterations in CK2 catalytic activity even when changes in expression and substrate abundance are considered, thus underscoring a likely unidentified mechanism for regulating CK2 kinase activity (Dubois et al., 2016; Purzner et al., 2018). Specifically, evidence from *in vitro* experiments suggests that polybasic molecules, such as polyamines, can increase the catalytic activity of CK2, but inconsistent catalytic enhancement was observed in cell-based assays (Leroy et al., 1997; Lawson et al., 2006; Ao et al., 2019). The binding of inositol phosphates to CK2 can enhance catalytic activity for certain substrates (Solyakov et al., 2004), and CK2 phosphorylation by Src, Lyn, and protein kinase C has also been shown to stimulate CK2 kinase activity (Donella-Deana et al., 2003; Lee et al., 2016). Furthermore, the binding of CK2 to other proteins such as fibroblast growth factor, p21, and Lamin A alters CK2 activity and promotes or inhibits the phosphorylation of specific substrates (Skjerpen et al., 2002; Jia et al., 2016; Ao et al., 2019). However, in general, most of these examples are cell-type- or context-specific, and there is currently no known universal mechanism for the catalytic regulation of CK2 kinase activity (Roffey & Litchfield, 2021).

Recent studies have uncovered a novel role for copper in modulating the activity of specific protein kinases. Copper was first identified as being essential for the activity of mitogen-activated protein kinase 1 (MEK1) and has since been demonstrated to regulate the activity of several other kinases, including Unc-51 like autophagy activating kinase (ULK1) and 3-phosphoinositide dependent protein kinase 1 (PDK1) (Brady et al., 2014; Tsang et al., 2020; Guo et al., 2021). Here, we identify CK2 as a copper-regulated kinase. We demonstrate that copper binds directly to the enzyme, enhancing its catalytic activity both *in vitro* and *in vivo*. These findings expand the repertoire of kinases regulated by copper and suggest that copper-mediated regulation is an important mechanism for modulating CK2 activity.

MATERIALS AND METHODS

Plasmids

CK2 plasmids were a gift from David Litchfield and obtained through Addgene: GST-CK2 α (pDB1-CK2 α , #27083) and CK2 α -HA (pZW6-CK2 α , #27086) (Turowec et al., 2010). The CK2 α -Met153Ala/His154Ala mutant was generated by site-directed mutagenesis using the QuikChange kit (Agilent). Mutagenic primer sequences are available upon request. All constructs were fully sequenced.

Metal Ion-Binding Site Prediction

CK2 α structures were acquired from the Protein Data Bank (<https://www.rcsb.org/>). These PDB files were uploaded to the MIB (Metal Ion-Binding site prediction and docking server)

(<http://bioinfo.cmu.edu.tw/MIB/>), and representative images were generated by the server (accessed March 2022).

Predicted copper-binding residues were included if the residues were predicted to bind copper across three independent PDB structures (3war, 3at2, 5zn0) uploaded to MIB, with all other residues excluded that did not fit the criteria. Binding potentials were normalized to the highest scoring predicted copper-binding residue.

Protein Expression and Purification

Purification of CK2 α was performed as described (Turowec et al., 2010). In brief, competent BL21 *E. coli* were transformed with plasmids encoding CK2 α -GST WT or CBM. Transformed cells were grown in Terrific Broth (TB) at 37°C until reaching an optical density of 0.6–1.0 (at 600 nM) and then protein expression was induced with 500 μ M Isopropyl β -D-1-thiogalactopyranoside (IPTG) overnight at 15°C. Cells were centrifuged at 4,000 rpm for 1 h at 4°C. Bacterial pellet was resuspended in 30 ml of lysis buffer (PBS pH 7.4, 1M NaCl) and then frozen for 24-h at –80°C. Cells were thawed on ice and 30 ml of additional lysis buffer with reagents making the final concentration of 10% TritonX-100, 1 mg/ml lysozyme, and protease inhibitors (Roche). The lysate was sonicated (QSonica) at 70% amplitude cycles for 10 s on and 20 s off pulses for 2 min total on ice. Lysates were ultracentrifuged at 45,000 rpm for 45 min at 4°C. The supernatant was filtered through 20 μ m filter and run over a gravity column with 5 ml glutathione agarose (GoldBio). The column was washed with 150 ml of PBS (pH 7.4) containing 1M NaCl, 10 mM EDTA, and 1% Triton X-100. Protein was eluted in 50 mM Tris-Cl (pH 8.0), 1 mM DTT, and glutathione ranging from 10 to 200 mM. For cleavage with Factor-Xa (New England Biolabs), protein underwent buffer exchange using a spin column with a 30 kDa molecular weight cut-off (Corning) into 20 mM Tris-Cl, 100 mM NaCl, 2 mM CaCl₂. Protein was incubated for 24 h at 4°C and subsequently applied to a gravity column with 3 ml GSH-resin. The flow-through was applied to a fast protein liquid chromatography system with a size-exclusion column HiLoad 16/60 Superdex 200 (Sigma Aldrich). Proteins eluted at the correct size were collected and underwent buffer exchange and concentration by spin column with 30 kDa molecular weight cut off (Corning) into storage buffer (15 mM MOPS pH 7.0, 0.75 mM DTT, 300 mM ammonium sulfate, with 5% glycerol). Following concentration, protein was flash-frozen and stored at –80°C.

Cell-Based Methods

HeLa, HEK293, A375, and U87 MG cells were obtained from ATCC and maintained in Dulbecco's Modified Eagle Media (DMEM) supplemented with 10% v/v fetal bovine serum (FBS) and 1% penicillin-streptomycin (P/S) at 37°C in a humidified incubator with 5% CO₂. *Ctrl*^{+/–} MEFs were generously shared by the Brady Lab (University of Pennsylvania) and maintained in Dulbecco's Modified Eagle Media (DMEM) supplemented with 10% v/v fetal bovine serum (FBS) and 1% penicillin-streptomycin (P/S) at 37°C in a humidified incubator with 5% CO₂.

For transient transfection, HEK293 cells were plated into 10 cm plates. The cells were transfected following the Lipofectamine 2000 protocol (ThermoFisher) with pZW6-CK2 α -HA-WT or CBM plasmids. Cells were lysed in 100 μ L or 500 μ L RIPA buffer (50 mM Tris-HCl, pH 7.4, 150 mM NaCl, 0.5% sodium deoxycholate, 1% NP-40) containing 20 mM EDTA and 2X EDTA-free Halt protease and phosphatase inhibitors (Thermo Fisher Scientific). Cells were scraped off the plate and transferred into microcentrifuge tubes. Lysates were subjected to homogenization by passing them twice through an insulin syringe. Samples were subsequently incubated on ice for 30 min, followed by centrifugation at 21,000 \times g at 4°C for 15 min. Following centrifugation, the supernatant was removed, and the protein concentration was determined by BCA protein assay (Pierce) using BSA as a standard.

For various treatments, HeLa, A375, or U87-MG cells were sub-cultured into a 6-well plate seeded at a density of 150,000 cells per well and allowed to grow for 48 h. After 48 h, cells were washed twice in PBS, and the media was replaced with serum-free media. After 24 h in serum-free media, 1 μ M CX-4945 (in DMSO) was added. After 24 h of growth in serum-free media with (or without) CX-4945, 10% serum, 100 μ M copper, or 100 μ M Cu-ATSM (in DMSO) was added, as indicated. After 1 h of treatment, the cells were lysed as described, followed by SDS-PAGE and immunoblot analysis.

Immunoblot Analysis

Proteins were resolved by SDS-PAGE and detected using the following primary antibodies: mouse anti-GAPDH (1:4,000 in BSA, #32233, Santa Cruz), mouse anti-CK2 α (1:2000 in BSA, #373894, Santa Cruz), mouse anti-CK2 α' (1:100 in BSA, #514403, Santa Cruz), mouse anti-CK2 β (1:2000 in BSA, #46666, Santa Cruz), mouse anti-CCS (1:500 in BSA, #55561, Santa Cruz), mouse anti-PTEN (1:500 in BSA, #7974, Santa Cruz), mouse anti-CDC37 (1:1000 in BSA, #4793, Cell Signaling), mouse anti-GST (1:2000 in BSA, #138, Santa Cruz), rabbit anti-ERK (1:1000 in BSA, #4695, Cell Signaling), rabbit anti-phospho-Thr202/Tyr204-ERK (1:1000 in BSA, #4370, Cell Signaling), rabbit anti-MEK1/2 (1:1000 in BSA, #9122, Cell Signaling), rabbit anti-phospho-Ser13-CDC37 (1:1000 in BSA, #108360, Cell Signaling), rabbit anti-phospho-PTEN (Ser380/Thr382/383) (1:500 in BSA, #9549, Cell Signaling), rabbit anti-phospho-CK2 Substrate [(pS/pT)DXE] MultiMab (1:1000 in BSA, #8738S, Cell Signaling), rabbit anti-AKT (1:1000 in BSA, #4691, Cell Signaling), rabbit anti-phospho-Ser129-AKT (1:500 in milk, #13461, Cell Signaling), rabbit anti-thiophosphate ester (1:1000 in BSA, #92570, Abcam), and rabbit-anti-HA (1:500 in BSA, #3724, Cell Signaling). Primary antibody incubation was followed by detection with secondary antibodies: IRDye® 800CW Goat anti-Mouse IgG (1:10,000 BSA, 926-32210, Licor), IRDye® 680RD Goat anti-Rabbit IgG (1:10,000, 926-68071, Licor), or anti-rabbit goat HRP-linked (1:1000, 7074, Cell Signaling) with ImmunoCruz Western Blotting Luminol (Santa Cruz) detection reagent. Immunodetection was performed using infrared imaging on the Odyssey CLx (Licor), or horseradish peroxidase, using GeneSys (Syngene). The fold-change in the ratio of

phosphorylated protein to total protein was quantified using ImageJ.

In vitro Kinase Assays

Reactions contained either 500 U of heterotetrameric CK2 (New England Biolabs) or 250 nM purified CK2 α with copper, TTM, or Cu-ATSM, as indicated. Reactions were incubated with GST-Jabba (250 μ M) or GST-AKT (60 μ M [Abcam ab62279]) and 2 mM DTT in reaction buffer (50 mM HEPES pH 7.5, 0.65 mM MgCl₂, 0.65 mM MnCl₂, 12.5 mM NaCl) for 30 min on ice prior to the addition of 500 μ M ATP γ S, GTP γ S, or ATP for 1 min @30°C. Reactions were quenched with 25 mM EDTA. Following the reaction being quenched, 2.5 mM *p*-nitrobenzyl mesylate (Abcam) was added for 1 h at room temperature. Sample buffer was then added to quench the alkylation reaction. SDS-PAGE analysis and immunoblotting were performed as described.

For the immunoprecipitation (IP)-kinase assay, HEK293 cells were transfected as described with pZW6-CK2 α -HA WT and CBM plasmids. Cells were lysed as described without EDTA in lysis buffer. Lysates were pre-cleared with 25 μ L packed A/G beads (Santa Cruz) for 1 h with rotation at 4°C. Following incubation, lysates were centrifuged at 21,000 \times g for 5 min at 4°C. Subsequently, 2.5 μ L of anti-HA antibody (Cell Signaling) was added to the supernatant and incubated overnight. The next morning, 50 μ L of packed A/G beads (Santa Cruz) were added to the tubes for 2 h with rotation at 4°C. Following incubation, samples were centrifuged at 21,000 \times g for 5 min and washed with 500 μ L RIPA buffer three times. Following the final wash, samples were resuspended in reaction buffer (50 mM HEPES pH 7.5, 0.65 mM MgCl₂, 0.65 mM MnCl₂, 12.5 mM NaCl) with GST-tagged Jabba (250 μ M) and 2 mM DTT. Reactions were incubated with 500 μ M ATP γ S for 10–30 min @30°C. Reactions were then quenched with 25 mM EDTA. Following quenching, 2.5 mM *p*-nitrobenzyl mesylate was added for 1 h at room temperature. After 1 h, sample buffer was added to quench the alkylation reaction. SDS-PAGE analysis and immunoblot were performed as described.

Resin-Binding Assays

1000 U of purified recombinant CK2 (NEB) in RIPA buffer containing 50 μ L Profinity IMAC resin (Bio-Rad) charged with no metal, Cu²⁺, Zn²⁺, or Fe³⁺, for 1-h at 4°C. Following incubation, samples were centrifuged at 1000 \times g at 4°C, and the supernatant was discarded. Samples were washed with 500 μ L of RIPA buffer and centrifuged at 1000 \times g three times. Following washes, sample buffer was added. SDS-PAGE analysis and immunoblotting were performed as described.

For resin-binding assays using cell lysate, HEK293 cells were transfected with pZW6-CK2 α -HA-WT or CBM plasmids. Cells were lysed as described. 100 μ g of cell lysate was incubated in binding buffer (RIPA buffer with 20 mM Imidazole) containing 50 μ L Profinity IMAC resin (Bio-Rad) charged with no metal, Cu²⁺ for 1-h at 4°C. Following incubation, samples were centrifuged at 1000 \times g at 4°C, and the supernatant was discarded. Samples were washed with 500 μ L of binding buffer and centrifuged at 21000 \times g three times. Following the three

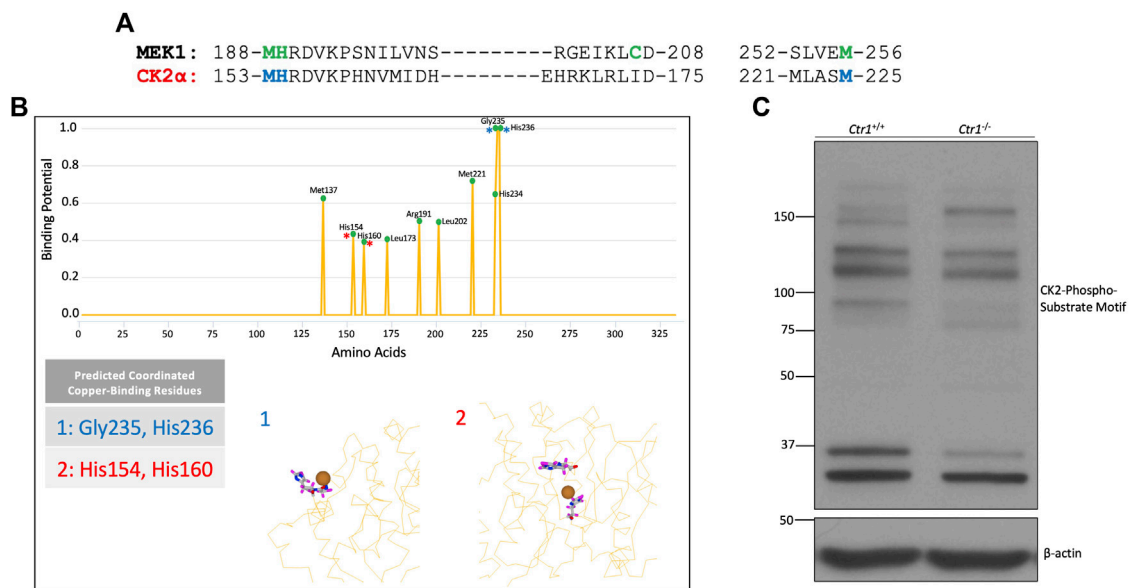


FIGURE 1 | Identification of CK2 as a putative copper-dependent kinase. **(A)** Alignment of the amino acid sequences of human MEK1 and CK2 α . The green letters represent amino acids involved in copper-binding by MEK1. The blue letters represent residues in CK2 α that share homology with MEK1 at copper-binding residues. **(B)** Prediction output by the MIB site prediction server (Lin et al., 2016) using three PDB files: 3war, 3at2, and 5zn0 (Kinoshita et al., 2011; Kinoshita et al., 2013; Shibazaki et al., 2018). Residues were only included if they were predicted to bind copper across all three structures. The top panel represents the prediction scores across CK2 α , with predicted potential binding sites denoted by a green circle. The bottom panel represents two predicted binding sites. Site 1 represents a surface-exposed binding site composed of residues Gly235 and His236, indicated by blue asterisks in the top panel. Site 2 represents a predicted binding site buried in the catalytic domain including residues His154 and His160, indicated by red asterisks in the top panel. **(C)** Immunoblot analysis of lysates from *Ctrl*^{+/+} and *Ctrl*^{-/-} MEFs probed with the indicated antibodies.

washes, sample buffer was added. SDS-PAGE analysis and immunoblotting were performed as described.

Enzyme-Linked Immunosorbent Assay (ELISA)

500 U of recombinant CK2 holoenzyme (New England Biolabs) was preincubated with 25 μ M copper sulfate and 500 μ M DTT in reaction buffer (50 mM HEPES pH 7.5, 625 μ M MgCl₂, 625 μ M MnCl₂, 12.5 mM) for 45 min on ice. Reactions were then incubated in reaction buffer with 500 μ M ATP or GTP on the ELISA plate (CycLex CK2 kit) for 30 min at 30°C. Reactions were quenched with 100 mM EDTA. Following quenching, all steps from the ELISA protocol kit were followed, and samples were read at 450 nm on a plate reader.

Inductively coupled plasma-mass spectrometry (ICP-MS)

Purified CK2 α (22.5 μ M) was incubated in the absence or presence of varying concentrations of copper sulfate (22.5 μ M, 112.5 μ M) along with varying concentrations of DTT (112.5 μ M, 675 μ M) at five times the concentration of copper. The buffer used in the reactions was 50 mM HEPES pH 8.0, 150 mM NaCl with 5% glycerol. The reaction occurred on ice for 30 min. Following incubation, samples were applied to a pre-equilibrated PD SpinTrap G-25 column to remove excess

copper. Samples were subsequently analyzed by ICP-MS at the Pennsylvania Animal Diagnostic Laboratory System at the University of Pennsylvania School of Veterinary Medicine.

RESULTS

Identification of CK2 as a Putative Copper-Regulated Kinase

To investigate if CK2 is a putative copper-dependent kinase, we analyzed the homology between CK2 α and the established copper-binding kinase MEK1 (**Figure 1A**). Alignment of the sequences of CK2 α and MEK1 confirmed that several of the critical copper-binding residues in MEK1 are indeed conserved in CK2 α . Additionally, several of these residues are conserved in two other copper-binding kinases, ULK1 and PDK1 (**Supplemental Figure S1**). To further explore the potential of CK2 regulation by copper, we took advantage of an in-silico approach: the Metal Ion-Binding Site Prediction and Docking Server (Lin et al., 2016). Through analysis of various CK2 α crystal structures in the Protein Data Bank (PDB) (Kinoshita et al., 2011; Kinoshita et al., 2013; Shibazaki et al., 2018), multiple residues predicted to be implicated in copper binding were identified (**Figure 1B**). The majority of these residues are located within the catalytic domain of CK2 α and are identical to the residues identified by homology analysis with MEK1.

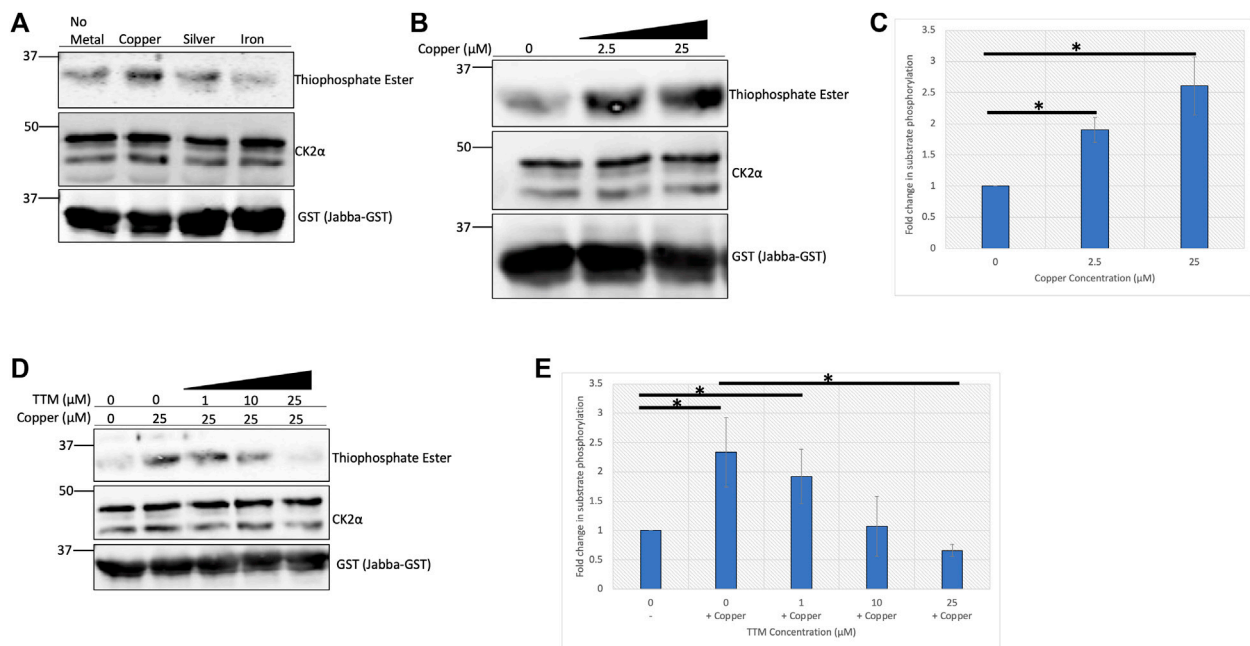


FIGURE 2 | Copper enhances CK2 activity *in vitro*. **(A)** *In vitro* kinase assay assessing CK2 activity in the presence of various metals. Recombinant heterotetrameric CK2 was incubated with GST-tagged Jabba and ATPγS in the presence or absence of the indicated metals (25 μM). Following incubation with PNBm, reactions were resolved by SDS-PAGE and analyzed by immunoblotting with the indicated antibodies. **(B)** *In vitro* kinase assay assessing CK2 activity in the presence of increasing concentrations of copper. Recombinant heterotetrameric CK2 was incubated with GST-tagged Jabba and ATPγS in the presence or absence of copper. Following incubation with PNBm, reactions were resolved by SDS-PAGE and analyzed by immunoblotting with the indicated antibodies. **(C)** Quantification of the thiophosphate ester signal detected by immunoblot analysis in panel B (n = 4). Data are represented as mean fold change ± SEM. * indicates $p < 0.05$ as calculated by a paired student *t*-test. **(D)** *In vitro* kinase assay assessing CK2 activity in the presence of copper and increasing concentrations of TTM. Recombinant heterotetrameric CK2 was incubated with GST-tagged Jabba and ATPγS in the presence or absence of copper and various TTM concentrations. Following incubation with PNBm, reactions were resolved by SDS-PAGE and analyzed by immunoblotting with the indicated antibodies. **(E)** Quantification of the thiophosphate signal detected by immunoblot in panel D (n = 3). Data are represented as mean fold change ± SEM. * indicates $p < 0.05$ as calculated by a paired student *t*-test.

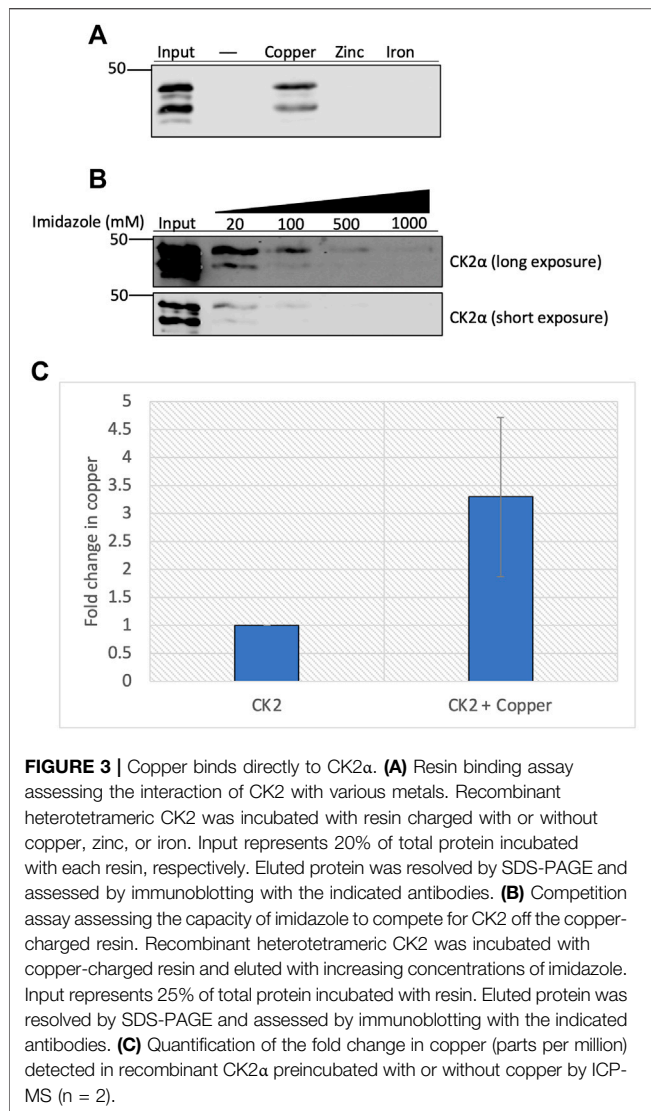
Additionally, the server generated predictions as to which residues might be capable of coordinating copper together (Figure 1B). These sites clustered in two major predicted copper-binding sites within CK2α: a binding site on the protein's surface (site 1) and a binding site within the catalytic pocket (site 2). The latter aligned with the predicted binding based on homology analysis with MEK1 (Figure 1A). Collectively, the results from this analysis suggest that CK2α has the capacity to interact with copper via residues in its catalytic domain.

To validate these findings, we investigated whether endogenous CK2 kinase activity was dependent on the expression of Ctr1, the primary copper transporter in mammalian cells (Lee et al., 2002). Knockout of *Ctr1* has been shown to modulate copper-dependent signaling by both MEK and ULK (Turski et al., 2012; Brady et al., 2014; Tsang et al., 2020). Specifically, we used mouse embryonic fibroblasts (MEFs) in which the gene encoding Ctr1 was deleted to examine if reduction in copper import influences global CK2 signaling. We assessed CK2 signaling by Western blot analysis using a pan-phospho-CK2 substrate motif antibody that demonstrated differential banding when comparing lysates from *Ctr1*^{+/+} versus *Ctr1*^{-/-} cells, suggesting an underlying difference in CK2 substrate

phosphorylation dependent on intracellular copper status (Figure 1C). Together, these data suggest that CK2 is a putative copper-regulated kinase.

Copper Enhances CK2 Kinase Activity *in vitro*

In order to directly assess the influence of copper on CK2 enzymatic activity, we performed an *in-vitro* kinase assay. A previously validated substrate of CK2, Jabba, was incubated with recombinant CK2 holoenzyme and ATPγS in the presence or absence of copper or other metals, allowing for thiophosphorylation of the substrate (McMillan et al., 2018; Chojnowski et al., 2019). Subsequent addition of the alkylating agent *p*-nitrobenzyl mesylate (PNBM) generates a thiophosphate ester moiety that can be detected with an anti-thiophosphate ester antibody by Western blotting. Copper, and to a lesser extent silver (which is isoelectric to cuprous copper), increased CK2 kinase activity as evidenced by increased phosphorylation of Jabba, whereas iron had no apparent effect (Figure 2A). Due to the observed increase in CK2 activity when incubated with copper, a titration experiment was performed that demonstrated a dose-dependent copper-mediated 2.5-fold enhancement in CK2



activity (Figure 2B,C). Copper-mediated enhancement of CK2 activity was confirmed in an independent ELISA assay using p53 as the substrate (Supplemental Figure S2). Interestingly, the enhancement seen with ATPγS or ATP was not observed when GTPγS or GTP was used in either the *in vitro* reaction or the ELISA (Supplemental Figures S2, S3), suggesting that the effect of the metal is nucleotide-specific.

To further investigate the enhancement of CK2 activity by copper, increasing concentrations of the copper-specific chelator tetrathiomolybdate (TTM) were titrated into the kinase reaction (Ogra et al., 1996). As the concentration of the chelator approached equimolar concentrations of copper in the reaction, the enhancement in CK2 activity was abolished and decreased to baseline (Figure 2D,E), and we confirmed that incubation with TTM alone had no effect on CK2 activity (Supplemental Figure S4). Together, these results indicate that cuprous copper enhances CK2 kinase activity *in vitro* and that copper chelation abrogates this effect.

CK2 Binds Directly to Copper

Given the enhanced enzymatic activity in the presence of copper, we hypothesized that CK2 directly binds to the metal. We used immobilized metal affinity chromatography (IMAC) to test this hypothesis. Recombinant heterotetrameric CK2 was incubated with uncharged resin or resin charged with various metals, and the extent of binding was assessed by elution of bound protein. Results of this experiment indicate that recombinant CK2 bound to the copper-charged resin but did not bind to the zinc- or iron-charged resins (Figure 3A). To validate the specificity of CK2 for the copper-charged resin, we conducted a competition experiment in which we assessed if CK2 could be eluted from the resin by titration of imidazole. Increasing concentrations of imidazole competed CK2 off the copper-charged resin (Figure 3B), demonstrating a specific interaction between CK2 and the copper-bound resin.

To further explore the physical capacity of CK2 to bind copper, we examined how incubating copper with the CK2α subunit influenced copper retention via inductively coupled plasma-mass spectrometry (ICP-MS). Purified CK2α was incubated with copper, excess copper was subsequently removed, and the protein was subjected to ICP-MS. The samples pre-incubated with copper demonstrated a three-fold increase in copper retention compared to control, although there was a baseline amount of copper already bound to purified CK2α prior to incubation (Figure 3C). Together, these results indicate that CK2, specifically the CK2α subunit, binds directly to copper *in vitro*.

Met153 and His154 of CK2α Are Essential for Copper-Binding

We next aimed to identify residues in CK2 that are critical for binding to copper. Here we focused on residues in MEK1 that were previously identified as being important for copper interaction and that shared substantial homology with the CK2α subunit (Figures 1A, 4A). As both MEK1 and CK2 are RD (arginine-aspartate) kinases containing an arginine immediately preceding the catalytic aspartate in the catalytic domain, we opted to mutate only the residues located directly adjacent to this region, Met153 and His154, due to their importance in regulating enzymatic activity in RD kinases (Johnson et al., 1996) (Figure 1A). To test if Met153 and His154 are indeed critical for copper-binding, we generated a mutant of CK2 (hereafter referred to as copper binding mutant, CBM) in which Met153 and His154 were mutated to alanine. We first assessed how the mutations influenced the catalytic activity of the CBM. We transiently expressed either HA-tagged CK2α^{WT} or CK2α^{CBM} in HEK293 cells and performed a subsequent immunoprecipitation (IP)-kinase assay. CK2α^{WT} or CK2α^{CBM} were immunoprecipitated using an anti-HA antibody and used in an *in vitro* kinase assay with Jabba as a substrate as previously described. While CK2α^{WT} was able to phosphorylate Jabba, the CK2α^{CBM} did not and thus appeared to be catalytically compromised (Figure 4A). To confirm that CK2α^{CBM} was not catalytically inactive due to misfolding induced by the mutations, we assessed the association of CK2α^{WT} and CK2α^{CBM} with the CK2β subunit by co-immunoprecipitation analysis. HA-tagged CK2α^{WT} and CK2α^{CBM} were immunoprecipitated, and the immunoprecipitates were probed with an anti-CK2β antibody.

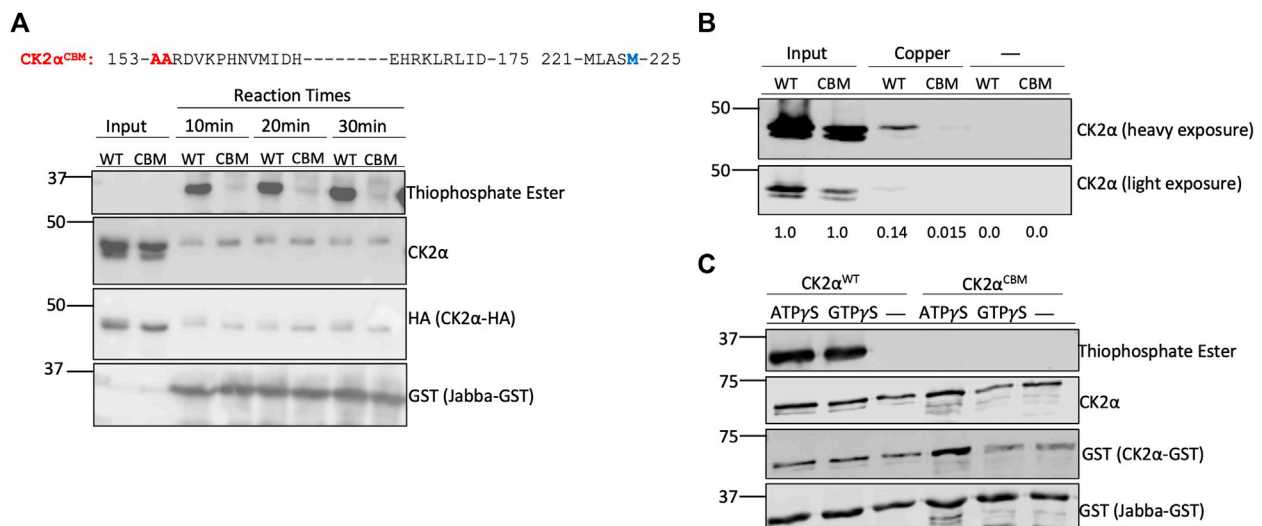


FIGURE 4 | Met153 and His154 are essential for copper-binding. **(A)** Top: Sequence of human CK2α. Blue letters represent residues in CK2α that share homology with MEK1 at copper-binding sites. Red letters represent residues Met153 and His154 that were mutated to generate the CK2α^{CBM}. Bottom: *in-vitro* kinase assay assessing CK2α^{WT} and CK2α^{CBM} enzyme activity. Constructs encoding HA-tagged CK2α^{WT} or CK2α^{CBM} were transfected into HEK293 cells. CK2α was then immunoprecipitated and incubated with GST-tagged Jabba and ATPyS. Following incubation with PNBM, reactions were resolved by SDS-PAGE and assessed by immunoblotting with the indicated antibodies. **(B)** Resin binding assay assessing the interaction of CK2α^{WT} and CK2α^{CBM} with copper-charged resin. Constructs encoding HA-tagged CK2α^{WT} or CK2α^{CBM} were transfected into HEK293 cells. Cell lysates were prepared and incubated with resin charged with or without copper. Input represents 25% total protein incubated with resin. Eluted protein was resolved by SDS-PAGE, assessed by immunoblotting with the indicated antibodies, and quantified. **(C)** *In-vitro* kinase assay assessing enzymatic activity of bacterially expressed CK2α^{WT} and CK2α^{CBM}. Constructs encoding GST-tagged CK2α^{WT} or CK2α^{CBM} were transformed into bacteria. The purified kinases were then incubated with GST-tagged Jabba and ATPyS or GTPyS. Following incubation with PNBM, reactions were resolved by SDS-PAGE and assessed by immunoblotting with the indicated antibodies.

Results from these experiments showed that both WT and CBM bind the CK2β subunit equally (**Supplemental Figure S5**), indicating that the mutations do not interfere with the interaction between CK2α and CK2β and suggest the heterotetramer is properly assembled.

We next tested if the CK2α^{CBM} had a reduced ability to bind to copper using IMAC. Lysates from HEK293 cells transiently expressing CK2α^{WT} or CK2α^{CBM} were incubated with the (IMAC) copper-charged resin. Protein bound to the resin was eluted to assess the extent of binding, and the eluates were probed for CK2α. CK2α^{CBM} demonstrated a reduction in its capacity to bind the copper-charged resin compared to CK2α^{WT} (**Figure 4B**). To further validate the influence of the mutations on CK2 enzymatic activity, we expressed and purified GST-tagged CK2α^{WT} and CK2α^{CBM} from bacteria and performed an *in vitro* kinase assay using GST-tagged Jabba as a substrate. Results from this experiment corroborated that CK2α^{CBM} appears to be catalytically impaired (**Figure 4C**). Collectively, these results indicate that residues Met153 and His154 are vital for copper binding and the enzymatic activity of CK2α.

Copper Modulates CK2 Kinase Signaling *in vivo*

To support the findings of the *in vitro* experiments, we next investigated the effect of copper on CK2 signaling in cells. We first utilized *Ctr1*^{−/−} MEFs to evaluate whether loss of copper import influenced phosphorylation of CK2-specific substrates. We validated the reduction of intracellular copper in the *Ctr1*^{−/−}

MEFs via the reduction in phosphorylation of ERK by MEK (Brady et al., 2014; Turski et al., 2012), a copper-dependent kinase, and by the increase in the expression of the copper chaperone for superoxide dismutase (CCS), which is an indirect readout for copper status: its expression is inversely proportional to intracellular copper levels (**Figure 5A**) (Bertinato and L'Abbé, 2003). Lysates from WT and *Ctr1*^{−/−} MEFs were probed with antibodies to assess CK2 signaling. We found that *Ctr1* knockout resulted in a reduction in site-specific phosphorylation of two CK2 substrates, AKT at Ser129 and CDC37 at Ser13 (Miyata & Nishida, 2004; Di Maira et al., 2005), indicating that a reduction in intracellular copper concentration reduces CK2 kinase activity (**Figure 5A**). Importantly, there were no observed changes in protein expression of CK2α, CK2α', or CK2β, that could account for these signaling differences.

We next employed a pharmacological approach to increase levels of intracellular copper. In addition to incubating cells with excess copper, we also used a copper ionophore delivery system, namely diacetyl-bis(4-methyl-3-thiosemicarbazone) copper II (Cu-ATSM). Importantly, there is evidence that Cu-ATSM facilitates the delivery of copper to cupro-enzymes, such as SOD1, by increasing the pool of metallated protein (Roberts et al., 2014). We first verified that CK2 activity is enhanced *in vitro* by Cu-ATSM (**Supplemental Figures S6, 7**), similar to incubation with copper using both Jabba and AKT as substrates. To assess the efficacy of the copper delivery methods, we then treated serum-starved HeLa cells with serum, copper, or Cu-ATSM, and then analyzed changes to the copper-modulated MAPK

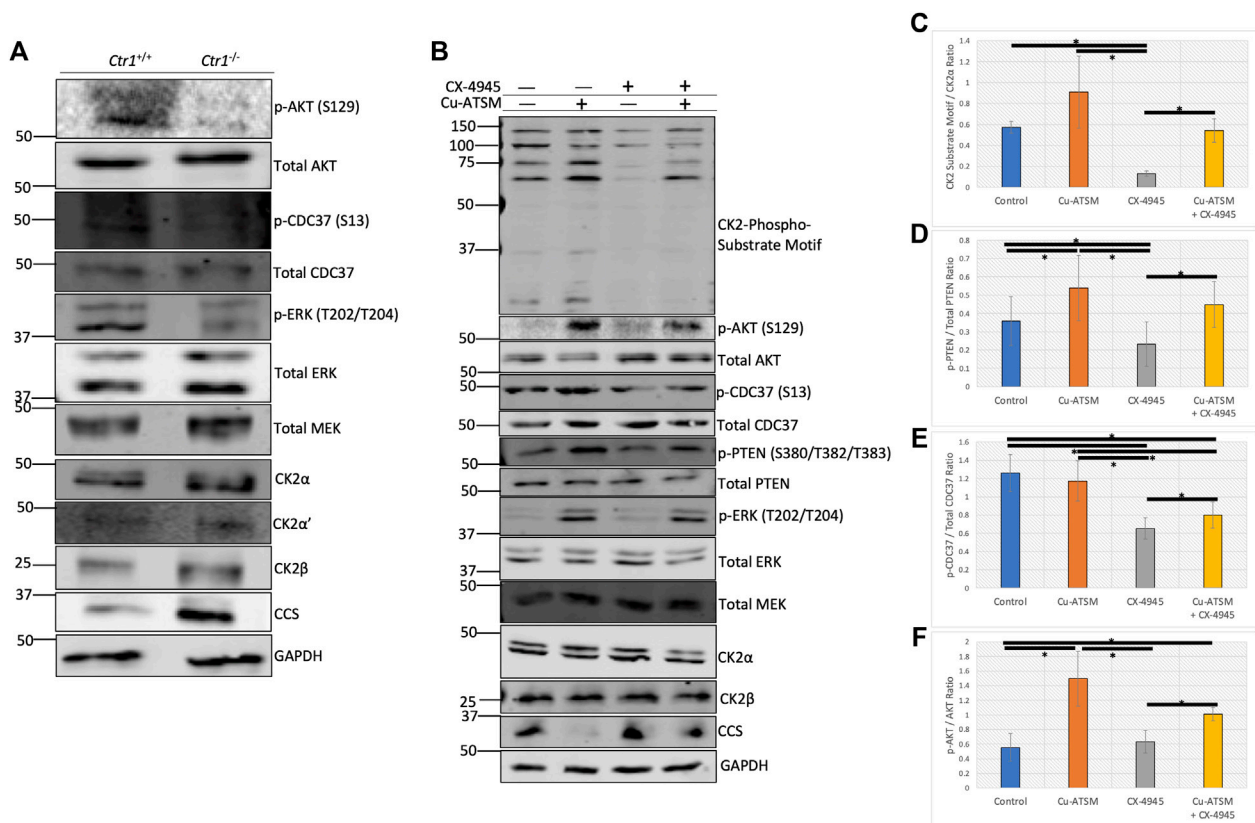


FIGURE 5 | Copper modulates cellular CK2 kinase signaling. **(A)** Lysates from *Ctrl1*^{+/+} and *Ctrl1*^{-/-} MEFs were resolved by SDS-PAGE and assessed by immunoblotting with the indicated antibodies. **(B)** Lysates from HeLa cells treated with or without Cu-ATSM and/or CX-4945 were resolved by SDS-PAGE and assessed by immunoblotting with the indicated antibodies. **(C)** Quantification of the CK2-phospho-substrate to CK2α ratio by immunoblot in panel B (n = 4). Data are represented as mean fold change ±SEM. *indicates *p* < 0.05 as calculated by a paired student *t*-test. **(D)** Quantification of the p-PTEN (S380/T382/T383) to total PTEN ratio by immunoblot in panel B (n = 4). Data are represented as mean fold change ±SEM. *indicates *p* < 0.05 as calculated by a paired student *t*-test. **(E)** Quantification of the p-CDC37 (S13) to total CDC37 ratio by immunoblot in panel B (n = 4). Data are represented as mean fold change ±SEM. *indicates *p* < 0.05 as calculated by a paired student *t*-test. **(F)** Quantification of the p-AKT (S129) to total AKT ratio by immunoblot in panel B (n = 4). Data are represented as mean fold change ±SEM. *indicates *p* < 0.05 as calculated by a paired student *t*-test.

pathway. Following treatments, cell lysates were assessed by immunoblotting. We observed a slight increase in ERK phosphorylation in response to serum and copper, whereas Cu-ATSM induced a dramatic increase in phosphorylation of ERK (Supplemental Figure S8). In addition, Cu-ATSM was able to induce an increase in CK2-specific phosphorylation of AKT at Ser129 and CDC37 at Ser13 (Miyata & Nishida, 2004; Di Maira et al., 2005), as well as slightly increase the intensity of the CK2-substrate motif antibody, which is used as a global CK2 phosphorylation readout (Supplemental Figure S8).

Given the observed increase in CK2 substrate phosphorylation upon treatment with Cu-ATSM, we next wanted to test if we could modulate these Cu-ATSM-induced changes with the ATP-competitive CK2 inhibitor CX-4945 (silmitastertib). We pre-incubated serum-starved HeLa cells with CX-4945 to ensure inhibition of CK2 prior to Cu-ATSM delivery. Following treatments, cell lysates were prepared and assessed by immunoblotting. As previously observed, treatment with Cu-ATSM increased site-specific phosphorylation of AKT at Ser129 and CDC37 at Ser13, as

well as the signal obtained with the CK2-substrate motif antibody and phosphorylated PTEN at Ser380/Thr382/Thr382, an additional CK2-specific substrate (Torres & Pulido, 2001) (Figure 5B). As expected, treatment with CX-4945 resulted in a reduction in phosphorylation of all CK2 substrates analyzed, with the exception of AKT that, at baseline, showed no detectable phosphorylation (Figure 5B). Interestingly, the combination treatment of CX-4945 and Cu-ATSM demonstrated that the reduction seen by CX-4945 could be partially rescued by the treatment of Cu-ATSM on all of the CK2 substrate readouts (Figure 5C–F). We corroborated these findings in two other cancer cell lines, U87-MG glioblastoma cells and A375 melanoma cells (Supplemental Figures S9, S10). Together, these results indicate that CK2-dependent signaling pathways are modulated by copper availability.

DISCUSSION

Despite the long-held notion that copper is predominantly a static inorganic co-factor, there is now substantial evidence that copper

plays a more dynamic role within the cell. Copper has been shown to regulate the activity of multiple kinases, including MEK1, ULK1, and PDK1 (Brady et al., 2014; Tsang et al., 2020; Guo et al., 2021), and here we demonstrate that copper also regulates CK2. Specifically, we demonstrate that copper enhances CK2 activity and that this effect can be abolished using a copper-specific chelator. We also showed that CK2 directly binds to copper and identified residues critical for copper-binding. Finally, we demonstrated that decreases in intracellular copper reduce CK2 signaling, whereas increases in intracellular copper increase CK2 signaling.

While copper enhances CK2 activity, the conditions under which this occurs are dependent on the redox state of copper. Indeed, cuprous copper is the predominant intracellular form of copper, and it has been shown that MEK and ULK also require reduced copper for catalytic enhancement. Our ICP-MS data demonstrate that a portion of purified CK2 α was copper-bound prior to incubation with additional copper, indicating a potential for reduced capacity for further copper interaction and, therefore, enzymatic enhancement (**Figure 3C**). While not directly tested, we further speculate that copper would also enhance the catalytic activity of CK2 α' based on homology of predicted copper-binding residues between CK2 α and CK2 α' .

Understanding the physiological role of copper on kinase activity has the added intricacy of determining the cellular mechanism of copper delivery. A recent study established that CCS delivers copper to MEK1, thereby modulating the signaling activity of MEK1 (Grasso et al., 2021). However, the copper delivery mechanism for CK2 is unknown, and whether CCS serves in this capacity or whether another chaperone is involved has yet to be determined. This study also identified two residues essential for copper-binding, Met153, and His154. However, these residues are conserved in many kinases across the kinome. Therefore, we cannot discount the influence of these mutations as being potentially copper-independent. Future studies will be directed at systematically identifying all putative copper-binding residues using an unbiased approach.

Two findings emerged from our work suggesting that copper-mediated regulation of CK2 may be more nuanced than simple enhancement of enzymatic activity. The first was that the enhancement in substrate phosphorylation by CK2 in the presence of copper only occurred using ATP, whereas there was no apparent enhancement with GTP (**Supplemental Figures S2, S3**). Although CK2 exhibits dual co-substrate specificity, to our knowledge, this is the first evidence suggesting that nucleotide-specific regulation may exist (Niefind et al., 1999). The second intriguing finding was the observation of differential banding patterns in lysates from the Ctr1 wildtype versus null MEFS when probed with the CK2-substrate motif antibody (**Figure 1C**). Without knowing the identity of the specific proteins

corresponding to the bands, we cannot discount changes in protein abundance due to the presence or absence of Ctr1. However, both of these findings suggest a potential underlying complexity in the enhancement of CK2 activity by copper that warrants further exploration.

Since CK2 plays a critical role in the progression of multiple types of cancer and other diseases, there has been significant interest in CK2 inhibition in the clinical setting, highlighted by several clinical trials with the CK2 inhibitor CX-4945 (clinicaltrials.gov ID# NCT02128282, NCT03897036, NCT01199718, NCT03904862, NCT00891280, NCT04668209). With inhibition as the targeted outcome, it is critical to understand any potential mechanisms that might modulate the effect of the inhibitor in a cellular context. Here we report that copper enhances CK2 activity and that treatment with Cu-ATSM appears to partially restore CK2 activity following CX-4945 treatment. These data suggest that copper may modulate the efficacy of CX-4945, suggesting the potential benefit of combining CX-4945 with copper chelation therapy to achieve the best outcome.

DATA AVAILABILITY STATEMENT

The original contributions presented in the study are included in the article/**Supplementary Material**, further inquiries can be directed to the corresponding author.

AUTHOR CONTRIBUTIONS

JC, DB, and TS conceived the work. JC, RL, TT, and FA performed experiments and generated data. AD and SC were instrumental in experimental design and data analysis. JC and TS wrote the manuscript. All authors contributed to the study and approved the submitted version of the article.

ACKNOWLEDGMENTS

The authors thank Emily McMillian and Alison Goupil for the generation of reagents. This research was funded by Drexel University College of Medicine's Dean's Fellowship for Excellence in Collaborative or Themed Research.

SUPPLEMENTARY MATERIAL

The Supplementary Material for this article can be found online at: <https://www.frontiersin.org/articles/10.3389/fmolb.2022.878652/full#supplementary-material>

REFERENCES

- Ao, Y., Zhang, J., Liu, Z., Qian, M., Li, Y., Wu, Z., et al. (2019). Lamin A Buffers CK2 Kinase Activity to Modulate Aging in a Progeria Mouse Model. *Sci. Adv.* 5 (3), eaav5078. doi:10.1126/sciadv.aav5078
- Ardito, F., Giuliani, M., Perrone, D., Troiano, G., and Muzio, L. L. (2017). The Crucial Role of Protein Phosphorylation in Cell Signaling and its Use as Targeted Therapy (Review). *Int. J. Mol. Med.* 40 (2), 271–280. doi:10.3892/ijmm.2017.3036
- Bertinato, J., and L'Abbé, M. R. (2003). Copper Modulates the Degradation of Copper Chaperone for Cu,Zn Superoxide Dismutase by the 26 S Proteasome. *J. Biol. Chem.* 278 (37), 35071–35078. doi:10.1074/jbc.m302242200
- Borgo, C., D'Amore, C., Cesaro, L., Sarno, S., Pinna, L. A., Ruzzene, M., et al. (2021). How Can a Traffic Light Properly Work if it Is Always Green? the Paradox of CK2 Signaling. *Crit. Rev. Biochem. Mol. Biol.* 56 (4), 321–359. doi:10.1080/10409238.2021.1908951
- Brady, D. C., Crowe, M. S., Turski, M. L., Hobbs, G. A., Yao, X., Chaikuad, A., et al. (2014). Copper Is Required for Oncogenic BRAF Signalling and Tumorigenesis. *Nature* 509 (7501), 492–496. doi:10.1038/nature13180
- Burnett, G., and Kennedy, E. P. (1954). The Enzymatic Phosphorylation of Proteins. *J. Biol. Chem.* 211 (2), 969–980. doi:10.1016/s0021-9258(18)71184-8
- Chojnowski, J. E., McMillan, E. A., and Stochlic, T. I. (2019). Identification of Novel CK2 Kinase Substrates Using a Versatile Biochemical Approach. *J. Vis. Exp.* 144. doi:10.3791/59037
- Di Maira, G., Salvi, M., Arrigoni, G., Marin, O., Sarno, S., Brustolon, F., et al. (2005). Protein Kinase CK2 Phosphorylates and Upregulates AKT/PKB. *Cell. Death Differ.* 12 (6), 668–677. doi:10.1038/sj.cdd.4401604
- Donella-Deana, A., Cesaro, L., Sarno, S., Ruzzene, M., Brunati, A. M., Marin, O., et al. (2003). Tyrosine Phosphorylation of Protein Kinase CK2 by Src-Related Tyrosine Kinases Correlates with Increased Catalytic Activity. *Biochem. J.* 372 (Pt 3), 841–849. doi:10.1042/BJ20021905
- Dubois, N., Willems, M., Nguyen-Khac, M.-T., Kroonen, J., Goffart, N., Deprez, M., et al. (2016). Constitutive Activation of Casein Kinase 2 in Glioblastomas: Absence of Class Restriction and Broad Therapeutic Potential. *Int. J. Oncol.* 48 (6), 2445–2452. doi:10.3892/ijo.2016.3490
- Grankowski, N., Boldyreff, B., and Issinger, O.-G. (1991). Isolation and Characterization of Recombinant Human Casein Kinase II Subunits Alpha and Beta from Bacteria. *Eur. J. Biochem.* 198 (1), 25–30. doi:10.1111/j.1432-1033.1991.tb15982.x
- Grasso, M., Bond, G. J., Kim, Y.-J., Boyd, S., Matson Dzebo, M., Valenzuela, S., et al. (2021). The Copper Chaperone CCS Facilitates Copper Binding to MEK1/2 to Promote Kinase Activation. *J. Biol. Chem.* 297 (6), 101314. doi:10.1016/j.jbc.2021.101314
- Guo, J., Cheng, J., Zheng, N., Zhang, X., Dai, X., Zhang, L., et al. (2021). Copper Promotes Tumorigenesis by Activating the PDK1-AKT Oncogenic Pathway in a Copper Transporter 1 Dependent Manner. *Adv. Sci. (Weinh)* 8 (18), e2004303. doi:10.1002/advs.202004303
- Jia, Z.-m., Ai, X., Teng, J.-f., Wang, Y.-p., Wang, B.-j., and Zhang, X. (2016). p21 and CK2 Interaction-Mediated HDAC2 Phosphorylation Modulates KLF4 Acetylation to Regulate Bladder Cancer Cell Proliferation. *Tumor Biol.* 37 (6), 8293–8304. doi:10.1007/s13277-015-4618-1
- Johnson, L. N., Noble, M. E. M., and Owen, D. J. (1996). Active and Inactive Protein Kinases: Structural Basis for Regulation. *Cell.* 85 (2), 149–158. doi:10.1016/s0092-8674(00)81092-2
- Kinoshita, T., Nakaniwa, T., Sekiguchi, Y., Sogabe, Y., Sakurai, A., Nakamura, S., et al. (2013). Crystal Structure of Human CK2α at 1.06 Å Resolution. *J. Synchrotron Radiat.* 20 (Pt 6), 974–979. doi:10.1107/S0909049513020785
- Kinoshita, T., Sekiguchi, Y., Fukada, H., Nakaniwa, T., Tada, T., Nakamura, S., et al. (2011). A Detailed Thermodynamic Profile of Cyclopentyl and Isopropyl Derivatives Binding to CK2 Kinase. *Mol. Cell. Biochem.* 356 (1–2), 97–105. doi:10.1007/s11010-011-0960-9
- Lawson, K., Larentowicz, L., Artim, S., Hayes, C. S., and Gilmour, S. K. (2006). A Novel Protein Kinase CK2 Substrate Indicates CK2 Is Not Directly Stimulated by Polyamines *In Vivo*. *Biochemistry* 45 (5), 1499–1510. doi:10.1021/bi052480i
- Lee, J., Petris, M. J., and Thiele, D. J. (2002). Characterization of Mouse Embryonic Cells Deficient in the Ctr1 High Affinity Copper Transporter. *J. Biol. Chem.* 277 (43), 40253–40259. doi:10.1074/jbc.m208002200
- Lee, Y.-H., Park, J.-W., and Bae, Y.-S. (2016). Regulation of Protein Kinase CK2 Catalytic Activity by Protein Kinase C and Phospholipase D2. *Biochimie* 121, 131–139. doi:10.1016/j.biochi.2015.12.005
- Leroy, D., Heriché, J.-K., Filhol, O., Chhabaz, E. M., and Cochet, C. (1997). Binding of Polyamines to an Autonomous Domain of the Regulatory Subunit of Protein Kinase CK2 Induces a Conformational Change in the Holoenzyme. *J. Biol. Chem.* 272 (33), 20820–20827. doi:10.1074/jbc.272.33.20820
- Lin, Y.-F., Cheng, C.-W., Shih, C.-S., Hwang, J.-K., Yu, C.-S., and Lu, C.-H. (2016). MIB: Metal Ion-Binding Site Prediction and Docking Server. *J. Chem. Inf. Model.* 56 (12), 2287–2291. doi:10.1021/acs.jcim.6b00407
- Litchfield, D. W. (2003). Protein Kinase CK2: Structure, Regulation and Role in Cellular Decisions of Life and Death. *Biochem. J.* 369 (Pt 1), 1–15. doi:10.1042/BJ20021469
- McMillan, E. A., Longo, S. M., Smith, M. D., Broskin, S., Lin, B., Singh, N. K., et al. (2018). The Protein Kinase CK2 Substrate Jabba Modulates Lipid Metabolism during *Drosophila* Oogenesis. *J. Biol. Chem.* 293 (8), 2990–3002. doi:10.1074/jbc.m117.814657
- Meggio, F., and Pinna, L. A. (2003). One-thousand-and-one Substrates of Protein Kinase CK2? *FASEB J.* 17 (3), 349–368. doi:10.1096/fj.02-0473rev
- Miyata, Y., and Nishida, E. (2004). CK2 Controls Multiple Protein Kinases by Phosphorylating a Kinase-Targeting Molecular Chaperone, CDC37. *Mol. Cell. Biol.* 24 (9), 4065–4074. doi:10.1128/mcb.24.9.4065-4074.2004
- Niefind, K., Pütter, M., Guerra, B., Issinger, O.-G., and Schomburg, D. (1999). GTP Plus Water Mimic ATP in the Active Site of Protein Kinase CK2. *Nat. Struct. Biol.* 6 (12), 1100–1103. doi:10.1038/70033
- Ogra, Y., Ohmichi, M., and Suzuki, K. T. (1996). Mechanisms of Selective Copper Removal by Tetrathiomolybdate from Metallothionein in LEC Rats. *Toxicology* 106 (1–3), 75–83. doi:10.1016/0300-483x(95)03171-b
- Olsen, J. V., Vermeulen, M., Santamaria, A., Kumar, C., Miller, M. L., Jensen, L. J., et al. (2010). Quantitative Phosphoproteomics Reveals Widespread Full Phosphorylation Site Occupancy during Mitosis. *Sci. Signal* 3 (104), ra3. doi:10.1126/scisignal.2000475
- Pinna, L. A. (2013). *Protein Kinase CK2*. Wiley-Blackwell.
- Purzner, T., Purzner, J., Buckstaff, T., Cozza, G., Gholamin, S., Rusert, J. M., et al. (2018). Developmental Phosphoproteomics Identifies the Kinase CK2 as a Driver of Hedgehog Signaling and a Therapeutic Target in Medulloblastoma. *Sci. Signal* 11 (547). doi:10.1126/scisignal.aau5147
- Roberts, B. R., Lim, N. K. H., McAllum, E. J., Donnelly, P. S., Hare, D. J., Doble, P. A., et al. (2014). Oral Treatment with CuII(atm) Increases Mutant SOD1 *In Vivo* but Protects Motor Neurons and Improves the Phenotype of a Transgenic Mouse Model of Amyotrophic Lateral Sclerosis. *J. Neurosci.* 34 (23), 8021–8031. doi:10.1523/jneurosci.4196-13.2014
- Roffey, S. E., and Litchfield, D. W. (2021). CK2 Regulation: Perspectives in 2021. *Biomedicine* 9 (10). doi:10.3390/biomedicine9101361
- Salvi, M., Borgo, C., Pinna, L. A., and Ruzzene, M. (2021). Targeting CK2 in Cancer: a Valuable Strategy or a Waste of Time? *Cell. Death Discov.* 7 (1), 325. doi:10.1038/s41420-021-00717-4
- Salvi, M., Sarno, S., Cesaro, L., Nakamura, H., and Pinna, L. A. (2009). Extraordinary Pleiotropy of Protein Kinase CK2 Revealed by Weblogo Phosphoproteome Analysis. *Biochimica Biophysica Acta (BBA) - Mol. Cell. Res.* 1793 (5), 847–859. doi:10.1016/j.bbamcr.2009.01.013
- Sharma, K., D'Souza, R. C. J., Tyanova, S., Schaab, C., Wiśniewski, J. R., Cox, J., et al. (2014). Ultradeep Human Phosphoproteome Reveals a Distinct Regulatory Nature of Tyr and Ser/Thr-Based Signaling. *Cell. Rep.* 8 (5), 1583–1594. doi:10.1016/j.celrep.2014.07.036
- Shibazaki, C., Arai, S., Shimizu, R., Saeki, M., Kinoshita, T., Ostermann, A., et al. (2018). Hydration Structures of the Human Protein Kinase CK2α Clarified by Joint Neutron and X-Ray Crystallography. *J. Mol. Biol.* 430 (24), 5094–5104. doi:10.1016/j.jmb.2018.09.018
- Skjerper, C. S., Nilsen, T., Wesche, J., and Olsnes, S. (2002). Binding of FGF-1 Variants to Protein Kinase CK2 Correlates with Mitogenicity. *EMBO J.* 21 (15), 4058–4069. doi:10.1093/emboj/cdf402
- Solyakov, L., Cain, K., Tracey, B. M., Jukes, R., Riley, A. M., Potter, B. V. L., et al. (2004). Regulation of Casein Kinase-2 (CK2) Activity by Inositol Phosphates. *J. Biol. Chem.* 279 (42), 43403–43410. doi:10.1074/jbc.m403239200
- Strum, S. W., Gyenis, L., and Litchfield, D. W. (2021). CSNK2 in Cancer: Pathophysiology and Translational Applications. *Br. J. Cancer* 126, 994–1003. doi:10.1038/s41416-021-01616-2

- Sugiyama, N., Imamura, H., and Ishihama, Y. (2019). Large-scale Discovery of Substrates of the Human Kinome. *Sci. Rep.* 9 (1), 10503. doi:10.1038/s41598-019-46385-4
- Torres, J., and Pulido, R. (2001). The Tumor Suppressor PTEN Is Phosphorylated by the Protein Kinase CK2 at its C Terminus. *J. Biol. Chem.* 276 (2), 993–998. doi:10.1074/jbc.m009134200
- Tsang, T., Posimo, J. M., Gudiel, A. A., Cicchini, M., Feldser, D. M., and Brady, D. C. (2020). Copper Is an Essential Regulator of the Autophagic Kinases ULK1/2 to Drive Lung Adenocarcinoma. *Nat. Cell. Biol.* 22 (4), 412–424. doi:10.1038/s41556-020-0481-4
- Turowec, J. P., Duncan, J. S., French, A. C., Gyenis, L., St. Denis, N. A., Vilks, G., et al. (2010). Protein Kinase CK2 Is a Constitutively Active Enzyme that Promotes Cell Survival: Strategies to Identify CK2 Substrates and Manipulate its Activity in Mammalian Cells. *Methods Enzymol.* 484, 471–493. doi:10.1016/b978-0-12-381298-8.00023-x
- Turski, M. L., Brady, D. C., Kim, H. J., Kim, B.-E., Nose, Y., Counter, C. M., et al. (2012). A Novel Role for Copper in Ras/mitogen-Activated Protein Kinase Signaling. *Mol. Cell. Biol.* 32 (7), 1284–1295. doi:10.1128/mcb.05722-11

Conflict of Interest: The authors declare that the research was conducted in the absence of any commercial or financial relationships that could be construed as a potential conflict of interest.

Publisher's Note: All claims expressed in this article are solely those of the authors and do not necessarily represent those of their affiliated organizations, or those of the publisher, the editors and the reviewers. Any product that may be evaluated in this article, or claim that may be made by its manufacturer, is not guaranteed or endorsed by the publisher.

Copyright © 2022 Chojnowski, Li, Tsang, Alfaran, Dick, Cocklin, Brady and Storchlic. This is an open-access article distributed under the terms of the Creative Commons Attribution License (CC BY). The use, distribution or reproduction in other forums is permitted, provided the original author(s) and the copyright owner(s) are credited and that the original publication in this journal is cited, in accordance with accepted academic practice. No use, distribution or reproduction is permitted which does not comply with these terms.



Chemical Genetic Validation of CSNK2 Substrates Using an Inhibitor-Resistant Mutant in Combination with Triple SILAC Quantitative Phosphoproteomics

Laszlo Gyenis^{1†}, Daniel Menyhart^{1†}, Edward S. Cruise^{1†}, Kristina Jurcic¹, Scott E. Roffey¹, Darren B. Chai¹, Flaviu Trifoi¹, Sam R. Fess¹, Paul J. Desormeaux¹, Teresa Núñez de Villavicencio Díaz¹, Adam J. Rabalski¹, Stephanie A. Zukowski¹, Jacob P. Turowec¹, Paula Pittock¹, Gilles Lajoie¹ and David W. Litchfield^{1,2*}

OPEN ACCESS

Edited by:

Andrea Venerando,
University of Padua, Italy

Reviewed by:

Emmanuel Ampofo,
Saarland University Hospital, Germany
Eduardo Silva-Pavez,
Universidad Mayor, Chile

*Correspondence:

David W. Litchfield
litchfi@uwo.ca

[†]These authors have contributed
equally to this work and share first
authorship

Specialty section:

This article was submitted to
Molecular Diagnostics and
Therapeutics,
a section of the journal
Frontiers in Molecular Biosciences

Received: 31 March 2022

Accepted: 02 May 2022

Published: 09 June 2022

Citation:

Gyenis L, Menyhart D, Cruise ES,
Jurcic K, Roffey SE, Chai DB, Trifoi F,
Fess SR, Desormeaux PJ,
Núñez de Villavicencio Díaz T,
Rabalski AJ, Zukowski SA,
Turowec JP, Pittock P, Lajoie G and
Litchfield DW (2022) Chemical Genetic
Validation of CSNK2 Substrates Using
an Inhibitor-Resistant Mutant in
Combination with Triple SILAC
Quantitative Phosphoproteomics.
Front. Mol. Biosci. 9:909711.
doi: 10.3389/fmolb.2022.909711

¹Department of Biochemistry, Schulich School of Medicine & Dentistry, Western University, London, ON, Canada, ²Department of Oncology, Schulich School of Medicine & Dentistry, Western University, London, ON, Canada

Casein Kinase 2 (CSNK2) is an extremely pleiotropic, ubiquitously expressed protein kinase involved in the regulation of numerous key biological processes. Mapping the CSNK2-dependent phosphoproteome is necessary for better characterization of its fundamental role in cellular signalling. While ATP-competitive inhibitors have enabled the identification of many putative kinase substrates, compounds targeting the highly conserved ATP-binding pocket often exhibit off-target effects limiting their utility for definitive kinase-substrate assignment. To overcome this limitation, we devised a strategy combining chemical genetics and quantitative phosphoproteomics to identify and validate CSNK2 substrates. We engineered U2OS cells expressing exogenous wild type CSNK2A1 (WT) or a triple mutant (TM, V66A/H160D/I174A) with substitutions at residues important for inhibitor binding. These cells were treated with CX-4945, a clinical-stage inhibitor of CSNK2, and analyzed using large-scale triple SILAC (Stable Isotope Labelling of Amino Acids in Cell Culture) quantitative phosphoproteomics. In contrast to wild-type CSNK2A1, CSNK2A1-TM retained activity in the presence of CX-4945 enabling identification and validation of several CSNK2 substrates on the basis of their increased phosphorylation in cells expressing CSNK2A1-TM. Based on high conservation within the kinase family, we expect that this strategy can be broadly adapted for identification of other kinase-substrate relationships.

Keywords: protein kinase CK2, CSNK2, chemical genetics, CX-4945, phosphoproteomics, SILAC, mass spectrometry, kinase-substrate relationship validation

INTRODUCTION

The coordinated phosphorylation of serine, threonine, and tyrosine residues at distinct sites within proteins enables intricate control of cellular processes (Cohen, 2002). It is estimated that up to 90% of all proteins are phosphorylated (Wilson et al., 2018). Despite an increasing wealth of information regarding phosphorylated sites in living cells, the majority have yet to be attributed to any one of the

more than 500 kinases encoded in the genome (Manning et al., 2002; Lemeer and Heck, 2009; Wilson et al., 2018). The lack of knowledge surrounding kinase-substrate relationships prevents a thorough understanding of complex signalling networks and biological processes in cells.

Casein Kinase 2 (CSNK2) is a ubiquitously expressed protein kinase with an integral role in the regulation of key cellular processes (Litchfield and Gyenis, 2015; Rabalski et al., 2016). These include cell cycle progression (Litchfield and Lüscher, 1993; St-Denis et al., 2009; St-Denis et al., 2011), transcription (Cabrejos et al., 2004), circadian rhythms (Tsuchiya et al., 2009), apoptosis (Ahmad et al., 2008; Wang et al., 2008; Duncan et al., 2010; Duncan et al., 2011; Turowec et al., 2011; Turowec et al., 2013; Turowec et al., 2014), and DNA repair (Loizou et al., 2004; Ali et al., 2009; Xu et al., 2014). With approximately 20% of the known phosphoproteome adhering to its [S/T]-X-X-[D/E] minimal recognition motif (Meggio and Pinna, 2003; Salvi et al., 2009), CSNK2 is suggested to be one of the most pleiotropic human kinases. The CSNK2-dependent phosphoproteome is likely even more expansive when considering the ability of CSNK2 to phosphorylate outside of this recognition motif (Meek et al., 1990). In mammalian cells, CSNK2 exists primarily as a tetrameric holoenzyme composed of two catalytic alpha (CSNK2A1, UniProt: P68400) and/or alpha' (CSNK2A2, UniProt: P19784) subunits complexed with two regulatory beta subunits (CSNK2B, UniProt: P67870). However, the catalytic CSNK2A1 and CSNK2A2 subunits can also function independently of the regulatory CSNK2B subunits (Litchfield, 2003). Deletion of either the CSNK2A1 or CSNK2B subunits results in an embryonic lethal phenotype in mice indicating that CSNK2 is essential for organismal development. Due to its fundamental role in regulating cellular processes, CSNK2 is also implicated in neurological disease (e.g., Alzheimers) and numerous malignancies when dysregulated (Rosenberger et al., 2016; Castello et al., 2017; Chua et al., 2017; Strum et al., 2021).

Mapping the CSNK2-dependent phosphoproteome is necessary for better characterization of its central role in cellular signalling. An increased understanding of the physiological signalling coordinated by CSNK2 will further reveal how perturbation of these pathways is implicated in disease. While several studies have attempted direct, large-scale CSNK2 substrate identification, they have done so either *in vitro* or in cell lysate. *In vitro* studies which attempt to determine *bona fide* CSNK2 substrates using purified components do not fully recapitulate kinase activity and substrate specificity in living cells, which is not only dictated by the recognition motif of substrates, but also by subcellular localization, scaffolding/adaptor protein interactions, and post-translational modification of substrates and CSNK2 itself (Pinna and Ruzzene, 1996; Good et al., 2011; Roffey and Litchfield, 2021). Although CSNK2 substrate discovery experiments performed in lysate offer some improvement over those done *in vitro*, they are unable to capture the spatiotemporal context of CSNK2 activity in living, intact cells.

Indirect methods of kinase-substrate identification better reflect the spatiotemporal context of kinase activity in living

cells and may therefore be more likely to identify true cellular substrates. For example, a chemical genetics approach in which cells are treated with a membrane-permeable kinase inhibitor is most often utilized. Those sites which demonstrate reduced phosphorylation relative to control cells not treated with inhibitor are presumed to be substrates. Combination of this method with quantitative phosphoproteomic analysis enables the large-scale identification of putative substrates (Shah and Kim, 2019; Jurcik et al., 2020). The success of this approach relies mainly on the availability of specific, potent inhibitors for the kinase of interest. Due to the central role of protein kinase CSNK2 in multiple cellular processes and malignancies (Chua et al., 2017; Strum et al., 2021), several CSNK2-directed inhibitors have been developed (Sarno et al., 2001; Pagano et al., 2004a; Pagano et al., 2004b; Cozza et al., 2006; Perea et al., 2008; Cozza et al., 2009; Sandholt et al., 2009; Siddiqui-Jain et al., 2010; Hou et al., 2012). However, these CSNK2-directed compounds exhibit variable specificity and selectivity towards their intended kinase target—this is especially true of compounds targeting the highly conserved ATP-binding site (Duncan et al., 2008; Gyenis et al., 2011; Duncan et al., 2012; Gyenis et al., 2013a; Gyenis et al., 2013b). Consequently, the differential phosphorylation of several phosphosites may be incorrectly attributed to CSNK2 activity when they are in fact due to off-target effects of the inhibitor. Moreover, CSNK2-directed inhibitors exhibit variable potency in living cells, which is not only dependent on their ability to bind CSNK2 and effectively compete with ATP and GTP, but also their ability to cross cellular and internal membranes. To achieve a sufficient level of CSNK2 inhibition, inhibitors of low potency must be utilized at high concentrations, which results in further decreased specificity (Knight and Shokat, 2005).

To overcome limitations noted above, we devised an approach for the large-scale identification and validation of CSNK2 substrates in living cells. The use of an inhibitor-resistant mutant kinase can clarify differential phosphorylation resulting from on- versus off-target effects of inhibitors. The mutant kinase remains active in the presence of the inhibitor and therefore, *bona fide* sites remain phosphorylated when compared with the inhibitor-sensitive wild-type kinase. Phosphosites which are downregulated due to off-target effects remain downregulated in cells expressing the inhibitor-resistant mutant. Previously, we had developed a Flp-In T-REx osteosarcoma (U2OS) cell line expressing a double mutant of CSNK2A1 (DM, V66A/I174A) under tetracycline control, a CSNK2 mutant which resisted inhibition by TBB and derivatives. This inhibitor-resistant mutant was instrumental in identifying and validating eukaryotic elongation factor 1 delta (EEF1D) pS162 as a *bona fide* CSNK2 phosphosite substrate (Gyenis et al., 2011). We have since developed a Flp-In T-REx U2OS cell line expressing a triple mutant of CSNK2A1 (TM, V66A/H160D/I174A) under tetracycline control. When compared with DM-CSNK2A1, TM-CSNK2A1 better resists inhibition of catalytic activity by CX-4945, a clinical stage CSNK2-directed ATP-competitive inhibitor. Therefore, we exploited this TM-CSNK2A1 in combination with a triple SILAC-based (Stable Isotope Labelling of Amino Acids in Cell Culture) quantitative

phosphoproteomics strategy for the systematic identification of *bona fide* CSNK2 substrates in living cells.

EXPERIMENTAL PROCEDURES

Reagents, Antibodies, and Immunoblotting

All reagents used in the assays were from Sigma or indicated otherwise. CSNK2 inhibitors tested in this study were TBB (4,5,6,7-Tetrabromobenzotriazole), TBBz (4,5,6,7-Tetrabromobenzimidazole), DMAT (2-Dimethylamino-4,5,6,7-tetrabromo-1H-benzimidazole; Calbiochem), Ellagic acid, Quinalizarin (1,2,5,8-Tetrahydroxy-9,10-anthraquinone; ACP Chemicals, Inc. Canada), Resorufin (7-Hydroxy-3H-phenoxazin-3-one), CSNK2 inhibitor 8 (4-(2-(4-Methoxybenzamido)thiazol-5-yl)benzoic acid), CX-4945 (5-(3-chlorophenylamino)benzo[c][2,6]naphthyridine-8-carboxylic acid; for earlier works synthesized at Department of Pharmacology, University of North Carolina at Chapel Hill; or at MedKoo Biosciences, Inc., Chapel Hill, NC, USA). Immunoblotting was done as described earlier by Gyenis et al. (2013b). Briefly, for the detection of CSNK2A1 and CSNK2A2, polyclonal rabbit antibodies were raised against the C-terminal 51 amino acid sequence of CSNK2A2 (CSK21 and CSK22, 1:2,000; BABCO, Berkley, CA) that can recognize both catalytic subunits of CSNK2 (Bosc et al., 1995). For detection of total CSK2B (1:2,000) we followed established protocols (Towbin et al., 1992) at the indicated dilutions in 3% BSA in TBST (contains 0.05% Tween 20, used for all rabbit antibodies) or PBST (contains 0.1% Tween 20, used for all mouse antibodies) for primary, and 1% BSA in TBST or PBST for secondary antibodies. For the C-terminal HA-tagged form of CSNK2A1-HA detection the monoclonal anti-HA 3F10 (1:500; Roche) antibody was used. The anti-Glyceraldehyde-3-Phosphate Dehydrogenase (GAPDH), clone 6C5 (1:1,000; Millipore) antibody was used to assess equal loading. We monitored CSNK2-dependent phosphorylation with the following commercially available phospho-specific antibodies: CSNK2 pS/pTDXE motif antibody (1:1,000; Cell Signaling), XRCC1 pS518/T519/T523 (1:2,500; Cell Signaling), CDC37 pS13 (1:25,000; Abcam). Additionally, we raised phosphospecific rabbit antibodies against eukaryotic translation initiation factor 2 subunit beta pS2 (EIF2S2; 1:10,000) using the ac-pS-GDEMIFDPTMSKC-amide peptide; against CSNK2B pS2/3/8 (CSNK2B pS2/3/8; 1:10,000) using ac-pS-pS-pS-EEVSMISWFC-amide mixed with ac-pS-pS-pS-EEV-pS-MISWFC-amide peptides (1:1); against DNA ligase 1 pS36 (LIG1, 1:5,000) using the C-Ahx-KAARVLGpSEGEED-amide peptide; and against single stranded binding protein SSB pS366 using the C-Ahx-KTKFASDDEHDEH-amide peptide (1:10,000). We also raised rabbit antibodies against the nonphosphorylated SSB protein site S366 using the C-Ahx-KTKFASDDEHDEH-amide peptide (1:5,000). All antibody production and affinity purification were done as was reported earlier (Gyenis et al., 2011) for eukaryotic elongation factor 1 delta pS162 (EEF1D pS162; 1:20,000) at YenZym Antibodies, LLC, San Francisco, CA following their proprietary company protocols. To visualize and

validate the phospho-specificity of our antibodies, we treated cell lysate +/-λ-protein phosphatase (New England Biolabs). We also immunoblotted with total EIF2S2 (1:500, Novus in **Figure 4D**; or 1:3,000; GeneTex in **Supplementary Figure S2A**). Infrared IRDye-labeled antibodies (1:10,000; LiCor) were used for immunoblot visualization and densitometry quantification on the LiCor Odyssey Infrared Imaging System with the Odyssey V3.0 software.

Peptide competition assays were performed with the visualization procedure previously stated with the exception that primary antibodies were pre-incubated for 30 min at room temperature with at least 200-fold molar excess of the non-phosphorylated peptide or phosphorylated peptide against which the antibody was raised.

Cell Culture and Cell Line Development

The human adenocarcinoma HeLa Tet-Off (HeLaT, Clontech) and osteosarcoma U2OS derived cells expressing the tetracycline responsible element (U2OS, gift from Dr. Christoph Englert, Forschungszentrum Karlsruhe, Germany (Englert et al., 1995)), or U2OS cells expressing the tetracycline responsible element of Flp-In™ T-Rex system (FT-U2OS, gift from Karmella Haynes, Arizona State University (Haynes and Silver, 2011)) were cultured in Dulbecco's Modified Eagle's medium (DMEM, Wisent) supplemented with 10% fetal bovine serum (FBS, HyClone), 100 µg/ml streptomycin and 100 units/mL penicillin (Thermo) at 37 °C with 5% CO₂ in 10 or 15 cm dishes (TPP, FroggaBio), 6- or 12-well plates (Greiner Bio-One). Following the recommendations of Flp-In™ T-Rex cell line development of Thermo Fisher Scientific (www.thermofisher.com) we developed and characterized FT-U2OS cell lines stably expressing the wild type CSNK2A1-WT (C-terminal HA tag) or inhibitor-resistant forms of triple mutant CSNK2A1-TM (V66A/H16D/I174A, C-terminal HA tag) with tight tetracycline regulation.

Inhibitor Treatment-Evaluation by Immunoblotting

Prior to the inhibitor treatments the U2OS cells were plated at 8×10^5 cells per well in 6-well dishes. The cells were challenged with CSNK2 inhibitors at 80% cell confluency using three different inhibitor concentrations (1 µM, 10 µM, or 50 µM) for 24 h. Equal volume of DMSO was used for experiment control. At the time of harvest on ice, all cells were washed three times with ice cold PBS following established protocols (Gyenis et al., 2011). One of the two DMSO controls (λ-phosphatase treated lysates) was harvested with the same lysis buffer but without any phosphatase inhibitors. Protein concentration was measured by BCA Protein Assay Kit (Pierce) using BSA as standard.

SILAC Cell Incorporation

SILAC-dropout DMEM (Wisent) lacking L-arginine and L-lysine was supplemented with isotope-encoded L-arginine (Arg-6) (13C6) and L-lysine (Lys-4) (4,4,5,5-D4) (Silantes) at respective concentrations of 86.2 mg/L (0.398 mM) and 61.16 mg/L (0.274 mM) to create a "Medium" labelled cell medium (M). "Heavy" labelled medium (H) was created by supplementing the

SILAC-dropout DMEM with isotope encoded L-arginine (Arg-10) (13C6, 15N4) and L-lysine (Lys-8) (13C6, 15N2) at respective concentrations of 87.7 mg/L (0.397 mM) and 52.4 mg/L (0.274 mM). “Light” labelled medium (L) was created using the SILAC-dropout DMEM and supplementing it with unlabeled L-arginine (R0) (83.9 mg/ml) and L-lysine (K0) (60.04 mg/ml). All media used for SILAC studies were supplemented with 10% of 10 kDa dialyzed FBS (Wisent), penicillin (100 U/mL), streptomycin (100 mg/ml) and L-proline (400 mg/ml, Cambridge Isotope Laboratories Inc.) to prevent arginine to proline conversion (Bendall et al., 2008). Cell media was filter-sterilized using 0.2 µm filter (Nalgene) prior to use for cell culture.

FT-U2OS cells expressing wild type CSNK2A1-HA were either adapted to “Light” (L) or “Medium” (M) SILAC media for 21 days and the isotope incorporation was verified by LC-MS/MS to be >95%. FT-U2OS cells expressing the inhibitor-resistant triple mutant form of CSNK2A1-HA was adapted to “Heavy” (H) SILAC media for 21 days and the isotope incorporation was verified by LC-MS/MS to be >95%. The WT (L, M) and TM (H) cell lines were treated with 1 µg/ml tetracycline for 48 h (cells were 80% confluent) to induce expression of the appropriate form of CSNK2A1. “Medium” WT and “Heavy” TM cells were treated with 30 µM CX-4945 for 4 h. “Light” WT cells were treated with equal volume of DMSO vehicle. Experiments were carried out with five biological replicates of each treatment.

Phosphoproteome and Proteome Sample Preparation

Following treatment +/-CX-4945, the cells were lysed following the protocol established by Humphrey et al. (2015). Briefly, the cell media was vacuum-aspirated and cells were washed with ice cold PBS twice followed by lysis on ice in 1 ml of buffer containing 6 M guanidinium chloride (GdmCl), 100 mM tris pH 8.5, 10 mM tris (2-carboxyethyl)phosphine (TCEP), and 40 mM 2-chloroacetamide (CAA). Lysates were then heated for 5 min at 95°C, cooled on ice for 15 min, sonicated for 2 × 15 s, and heated again at 95°C for 5 min. Lysates were cleared for 10 min at 13,000 × g at 4°C. Lysate protein concentration was determined using a NanoDrop™ (Thermo).

An equal amount (0.5 mg) of lysate from each treatment—L, M, and H—were mixed for all five biological replicates. Proteins were then precipitated by chloroform (Sigma-Aldrich) and methanol (Fisher) extraction method (Wessel and Flügge, 1984) and protein pellets were resuspended in 1 ml of digestion buffer (5% 2,2,2-trifluoroethanol (TFE) (Aldrich) and 50 mM ammonium bicarbonate (FLUKA). Trypsin/Lys-C (Promega) was added at 1:100 enzyme:protein ratio and incubated for 4 h at 37°C with gentle agitation. Subsequently, additional trypsin (Promega) was added at 1:100 enzyme:protein ratio and the sample was incubated at 37°C for 16 h with gentle agitation. For phosphoproteome analysis, phosphopeptide enrichment was performed using titanium dioxide (TiO₂) beads (Titansphere TiO Bulk 10 µm, Canadian Life Science) and styrenedivinylbenzene-reversed phase sulfonated (SDB-RPS) (3M Empore) StageTips, as described by Humphrey

et al. (2015). Enriched phosphopeptide solutions were acidified using 0.1% formic acid and peptide concentrations were determined using a NanoDrop™ (Thermo). Lastly, 1 µg was injected for LC-MS/MS analysis. For proteome analysis, digested proteins were desalted using a C18 StageTip (3M Empore) (Rappsilber et al., 2007) and the peptide concentrations were determined using a NanoDrop™. Finally, 0.7 µg was injected for LC-MS/MS analysis.

Mass Spectrometry

Phosphoproteome and proteome samples were analyzed using an Orbitrap Elite Hybrid Ion Trap-Orbitrap mass spectrometer (Thermo Scientific) connected to a NanoFlex (Thermo Electron Corp., Waltham, MA) nanospray ionization source with a source voltage of 2.4 kV. Samples were injected using a NanoAcquity UPLC (Waters) onto a Symmetry C18 trapping column (20 mm × 180 µm i. d., 5 µm, 100 Å) at a flow rate of 10 µL/min in 99% mobile phase A (0.1% FA (v/v), 1% mobile phase B (0.1% FA (v/v) in ACN) for 4 min. Samples were then separated on a NanoAcquity Peptide BEH C18 analytical column (250 mm × 75 µm i. d., 1.7 µm, 130 Å) at a flow rate of 300 nL/min by a linear gradient of increasing mobile phase B from initial condition 5%–7.5% over 1 min, followed by 7.5%–25% over 179 min, 25%–32.5% over 40 min, and culminating at 60% at 240 min. Mass spectrometer was operated by Thermo XCalibur software (version 2.7.0) in data-dependent acquisition (DDA) mode using an FT/IT/CID Top 20 scheme. MS1 survey scans were performed at 120,000 resolution from 400–1,450 m/z with full Automatic Gain Control (AGC) set to 10⁶ and an isolation window of 1.0 m/z. The top 20 most abundant ions were selected for MS2. A lock mass ion was enabled at 445.120025 m/z. Peptide ions were fragmented using a CID (Collision-Induced Dissociation) with Normalized Collision Energy (NCE) set to 35%, an activation time of 10 ms, and a Q value of 0.25. Data-dependent MS2 scans were acquired in the linear ion trap using rapid scan type, with a dynamic exclusion window of 30 s. Five biological replicates were analyzed without technical replicates.

Data Analysis

Raw mass spectrometric data of the five biological replicates were analyzed using MaxQuant (version 1.6.2.10., Max Planck Institute of Biochemistry, Munich (Cox et al., 2009; Tyanova et al., 2016a) and searched against the Human UniProtKB database (9 May 2020), which contained 20,362 entries. Default settings of MaxQuant (Tyanova et al., 2016a) were used with minor changes: multiplicity was set to 3, medium labels were selected as Arg6 and Lys4 and heavy labels were selected as Arg8 and Lys10; maximum number of 3 missed cleavages was chosen for trypsin/P; carbamidomethyl (C) was set as a fixed modification while oxidation (M), acetylation (protein N-terminal), deamidation (NQ), and phosphorylation (STY) were set as variable modifications for phosphopeptide enriched samples while the proteome data were searched using analogue modifications yet excluding the phosphorylation (STY). For quantification, unmodified peptides as well as those with fixed and variable modifications, excluding phosphorylation (STY), were included. “Re-quantify” and “Match Between

Runs" were selected using default parameters. The maximum number of variable modifications was set to 5. The minimum score for modified peptides was set to 40, and the decoy-database setting was "Revert." The False Discovery Rate (FDR) of PSM, protein and site of 0.01 was used.

Output data from MaxQuant were interpreted using Perseus software (version 1.6.14.0) (Max Planck Institute of Biochemistry, Munich) as described (Tyanova et al., 2016b) (<https://maxquant.net/perseus/>). Briefly, the light condition ("L") comprised CSNK2A1-WT subjected to DMSO treatment, the medium condition ("M") comprised CSNK2A1-WT subjected to CX-4945 treatment, and the heavy condition ("H") comprised CSNK2A1-TM subjected to CX-4945 treatment. The Phospho (STY)Sites.txt table was annotated with PTMSigDB (Krug et al., 2019). Normalized ratios of medium to light (M/L), heavy to light (H/L), and heavy to medium (H/M) intensities from the Phospho (STY)Sites.txt output were log2 transformed. Phosphorylation sites were considered for further analysis only if the localization probability was ≥ 0.75 . Reverse sequences and contaminants were removed. Our differential expression filtering workflow was the following: Phosphopeptides were considered significantly downregulated and significantly upregulated if mean M/L < 0 and mean M/L > 0, respectively (One-sample *t*-test of M/L values, Benjamini–Hochberg (BH) FDR multiple testing correction $q < 0.05$). Phosphopeptides were inhibited or upregulated to a biologically relevant level if the M/L log2 value < -0.585 or M/L log2 value > 0.585 (1.5-fold regulation), respectively.

Phosphopeptides were considered 'rescued' if $-0.585 < \text{mean H/L} < 0.585$ (One-sample *t*-test of H/M values, $q < 0.05$ BH FDR). Several phosphopeptides were significantly downregulated 1.5-fold but did not satisfy our strict biological criterion for 'rescue'. Instead, they demonstrated 'partial rescue' ($\text{H/M} > 0$) (One-sample *t*-test H/M, $q < 0.05$ BH FDR). Therefore, partially rescued phosphopeptides include those which were significantly upregulated in cells expressing exogenous CSNK2A1-TM in the presence of CX-4945 (H), but not to the same level as cells overexpressing exogenous CSNK2A1-WT in the absence of any inhibitor (L).

Proteins inhibited and upregulated—and subsequently rescued—were determined using the same criteria, except applied to the normalized log2 transformed M/L, H/L, and H/M ratios originating from the proteinGroups.txt MaxQuant output.

Further interpretation and visualization of our filtered phosphoproteomic and proteomic data were conducted using R Studio (Version 1.2.5033; RStudio Team (2020). RStudio: Integrated Development for R. RStudio, PBC, Boston, MA URL <http://www.rstudio.com/>). Sequence logo analysis of phosphopeptides was conducted using the WebLogo tool (University of California, Berkeley, <https://weblogo.berkeley.edu/logo.cgi>) (Crooks et al., 2004). Network creation was performed using the online GeneMANIA tool (University of Toronto, <https://genemania.org/>) (Warde-Farley et al., 2010). An "equal by data type" weighting method was utilized, and the following networks were utilized for network creation: physical interaction, genetic interaction, shared protein domains, co-localization, pathway, and predicted, as well as our own dataset. Protein substrates which were identified by

our rescued phosphopeptides were assigned a value of 1 to indicate an interaction. If a partially rescued phosphopeptide could have originated from several proteins (e.g., CDK1, CDK2, or CDK3), then all proteins were included in the uploaded gene list at a value of 1. Gene Ontology (GO) terms, which were enriched among the proteins depicted in the GeneMANIA network (protein substrates of CSNK2 and those implicated in relevant cellular signalling), were visualized using R Studio.

RESULTS

Comparison of CSNK2 Inhibitors by Western Blotting

To compare the potency of CSNK2 inhibitors, cells were treated with eight commercially available and previously published compounds (TBB, TBBz, DMAT, Ellagic Acid, Quinalizarin, Resorufin, Inhibitor 8, CX-4945) and lysates were analyzed by immunoblotting (**Figure 1A**). We treated human osteosarcoma (U2OS) cells with 1 μM , 10 μM , and 50 μM (**Figure 1B**) and HeLaT cells with 1 μM , 10 μM , and 20 μM (**Supplementary Figure S1**) of each inhibitor for 24 h. We subsequently compared the level of CSNK2 inhibition using a panel of commercial phospho-specific antibodies (CSNK2 pS/pTDXE motif, XRCC1 pS518/T519/T523, CDC37 pS13) as well as antibodies we developed for sites previously validated to be CSNK2-dependent (EIF2S2 pS2 (Gandin et al., 2016), EEF1D pS162 (Gyenis et al., 2011)) (**Figure 1B**, **Supplementary Figure S1**, **S2A**). Additionally, we developed a phosphospecific antibody for CSNK2B pS2/3/4/8 to monitor CSNK2A1-dependent autophosphorylation of the regulatory beta subunit (**Figure 1B**, **Supplementary Figure S1**, **S2B**). We immediately noticed disparities in potency of cellular CSNK2 inhibition. Six of eight CSNK2 inhibitors demonstrated little to no inhibition of CSNK2 at the tested concentrations in U2OS cells as indicated by our immunoblotting results (**Figure 1B** and **Supplementary Figure S1**). By comparison, Inhibitor 8 and CX-4945 showed dose-dependent inhibition of CSNK2. Inhibitor 8 demonstrated the strongest inhibition of CSNK2 at all three tested concentrations in these evaluations (**Figure 1B** and **Supplementary Figure S1**). Similar results were seen in human adenocarcinoma HeLaT cells (**Supplementary Figure S1**), confirming that our results were not restricted to U2OS cells.

Despite effective inhibition of CSNK2 by CX-4945 and Inhibitor 8, the phosphoantibody recognizing EEF1D pS162 did not demonstrate reduced phosphorylation. In our previous study in which we demonstrated EEF1D pS162 to be a *bona fide* substrate of CSNK2 in cells, *in vitro* phosphorylation by CSNK2 at this site was dramatically increased following λ -phosphatase treatment of EEF1D immunoprecipitates. This observation demonstrates high occupancy of the site in living cells suggesting that the site is not readily acted upon by phosphatases (Gyenis et al., 2011).

Although we observed Inhibitor 8 to be the most potent inhibitor of CSNK2 in these experiments, we chose CX-4945 for use in our systematic CSNK2 substrate identification and validation approach for a number of reasons. CX-4945 was

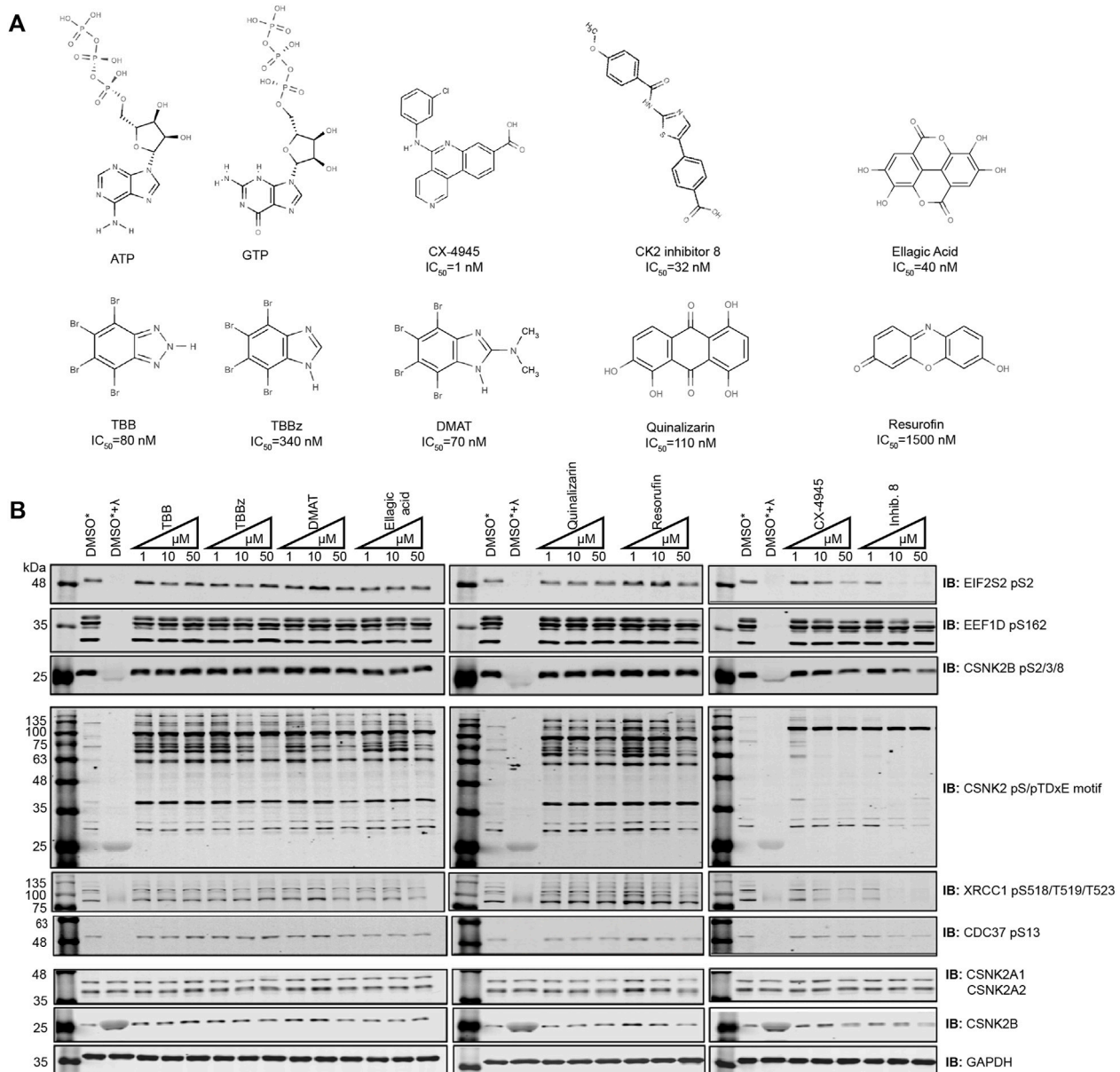


FIGURE 1 | Comparing the efficacy of CSNK2 inhibitors in U2OS cells. **(A)** Schematic illustration of the CSNK2 inhibitors that were evaluated in this study with reported *in vitro* IC_{50} values **(B)** CSNK2 inhibition was assessed by immunoblotting with the indicated phospho-specific antibodies after 24 h of inhibitor CX-4945 treatment at the indicated concentrations in U2OS cells. Lysis buffer of lysates marked with * did not contain phosphatase inhibitors. DMSO treated lysates +/-λ-phosphatase were used as immunoblotting controls for the phospho-specific antibodies. Results are representative of two independent experiments.

previously demonstrated to have a favorable specificity profile *in vitro*. When tested against a panel of 238 kinases, only 7 were inhibited greater than 90% at a concentration of 500 nmol/L. CSNK2A1 and CSNK2A2 exhibited the lowest IC_{50} of the 7 kinases inhibited at 1 nmol/L CX-4945 (Siddiqui-Jain et al., 2010). Furthermore, CX-4945 is the only small molecule CSNK2 inhibitor of those we tested which is currently in clinical trials (NCT04663737, NCT04668209, NCT03904862). CSNK2-independent cellular effects of CX-4945 have been well documented (Kim et al., 2014; Kim et al., 2016;

Lertsuwan et al., 2018), and while they may in part be responsible for clinical efficacy of the inhibitor, they are detrimental to definitive kinase-substrate assignment when employed without a robust method of validation. When utilized with CX-4945, our strategy might therefore provide some insight on the extent to which CSNK2-dependent inhibition contributes to the clinical efficacy of this inhibitor. Taken together, we reasoned CX-4945 was a suitable CSNK2 inhibitor for the development of a systematic CSNK2-substrate identification and validation workflow.

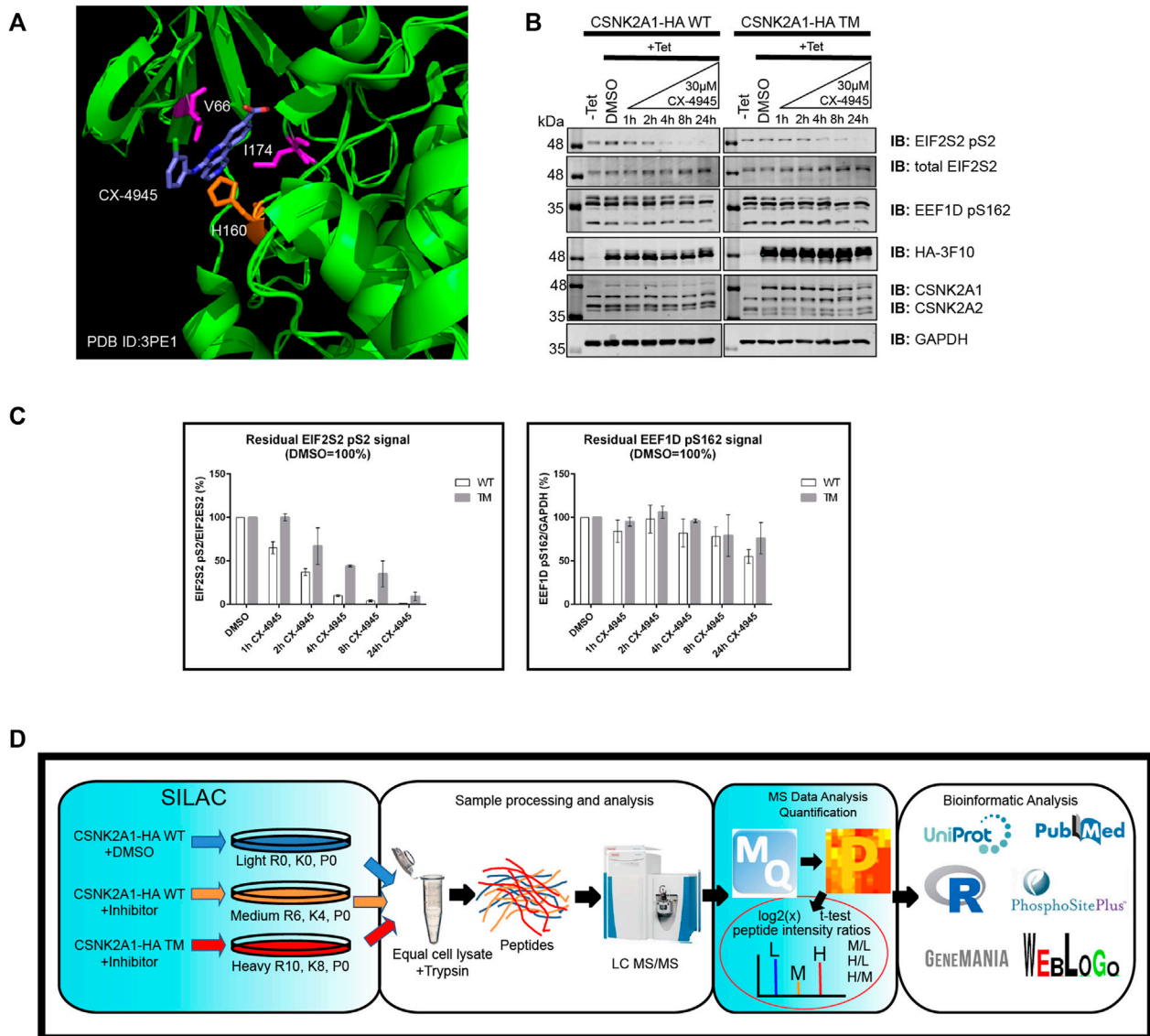


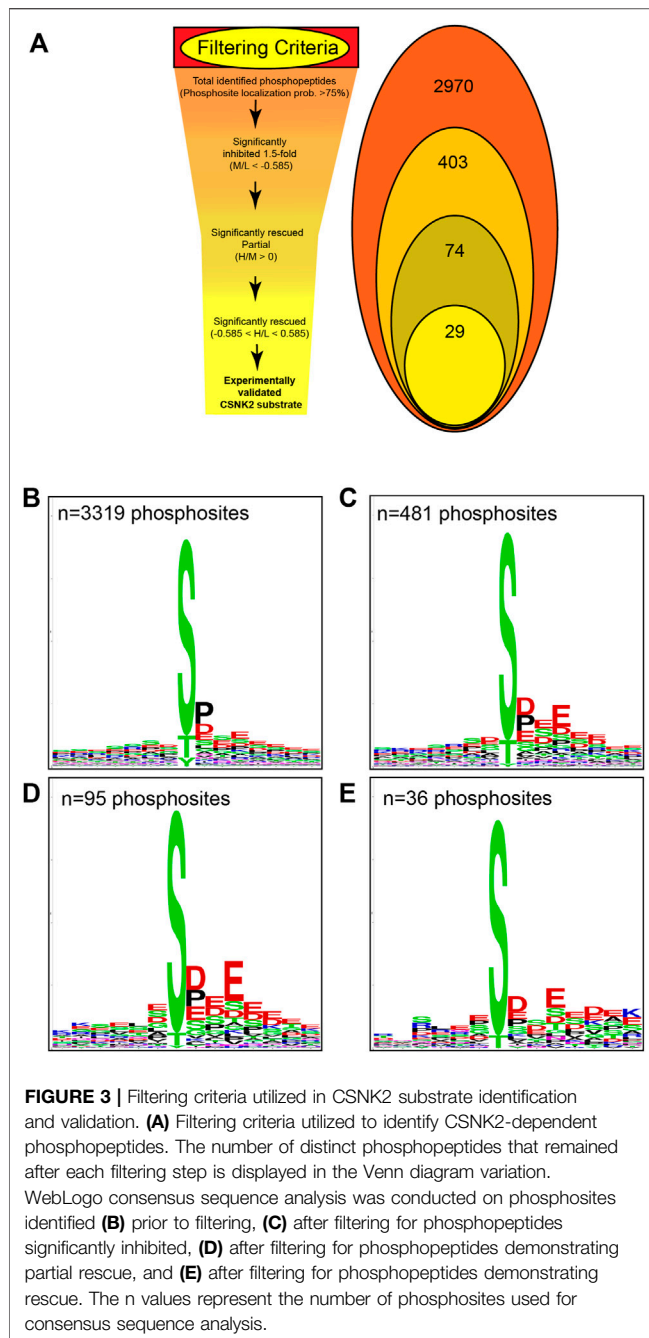
FIGURE 2 | Use of a triple mutant CSNK2A1 for validation of CSNK2 substrates. **(A)** Crystal structure of CX-4945 interacting with the ATP-binding site of CSNK2A1 (PDB ID: 3PE1). Highlighted are the residues mutated in CSNK2A1-TM (V66A/H160D/I174A) to create an inhibitor tolerant/resistant kinase. **(B)** Immunoblots demonstrate the inhibition and rescue of CSNK2-dependent phosphorylation using Flp-In T-REx U2OS cell lines stably expressing CSNK2A-HA WT or CSNK2A-HA TM with tight Tetracycline (Tet-ON) regulation. Cells were treated with 30 μ M of CX-4945 for the indicated times. **(C)** Bar charts demonstrate residual CSNK2 activity based on EIF2S2 pS2/total EIF2S2 or EEF1D pS162/GAPDH ratios, with CSNK2 activity in the DMSO control defined as 100%. Each column represents the mean value of two independent experiments with range bars displayed. Band intensities on blots were quantified with LiCor Odyssey v3.0 software. Results are representative of two independent experiments **(D)** Overview of large-scale identification and validation of CSNK2 substrates using a chemical genetics approach combined with triple SILAC quantitative phosphoproteomics.

Employing Chemical Genetics for CSNK2 Kinase Substrate Validation

To start, we developed Flp-In T-REx U2OS (FT-U2OS) cell lines expressing the CSNK2A1-HA wild-type (CSNK2A1-WT) or CSNK2A1-HA triple mutant (CSNK2A1-TM, V66A/H160D/I174A) form of the kinase with tight tetracycline regulation (Figures 2A,B; Supplementary Figure S4). When characterizing these cell lines for their response to CX-4945

treatment, we observed the earliest inhibition of CSNK2A1-WT occurred at 4 h post-treatment with 30 μ M CX-4945 using the phospho-EIF2S2 pS2 antibody (Figure 2B). This inhibitory effect on CSNK2 was then ‘rescued’ in the CSNK2A1-TM cell line under the same conditions (Figures 2B,C). Therefore, we proceeded to treat cells with 30 μ M of CX-4945 for 4 h in our phosphoproteomics evaluation (outlined in Figure 2D).

To identify phosphopeptides which were diminished following CX-4945 treatment, normalized intensity ratio



values were calculated between CSNK2A1-WT cells treated with CX-4945 and CSNK2A1-WT cells treated with DMSO (control). To validate phosphopeptides as CSNK2-dependent, normalized intensity ratio values were calculated between CSNK2A1-TM cells treated with CX-4945 and CSNK2A1-WT cells treated with DMSO (control). Those phosphopeptides which maintained phosphorylation in cells expressing CSNK2A1-TM despite the presence of CX-4945 were designated as rescued. Using this method, we could identify and validate *bona fide* CSNK2 substrates.

Identification and Validation of CSNK2 Substrates

Using the MaxQuant-Andromeda integrated computation platform, we identified 4,511 proteins and 3,319 distinct phosphosites corresponding to 2,970 distinct phosphopeptides. We performed downstream bioinformatic analyses of the MaxQuant output using Perseus (**Figure 3A**). Data tables were annotated with PTMSigDB, a database which contains curated, site-specific signature data regarding perturbation, kinase activity, and signalling pathways. Consensus sequence analysis of distinct phosphosites was performed at each filtering step using WebLogo (**Figure 3B**) (Crooks et al., 2004). Following initial removal of reverse sequences and contaminants, log₂ transformation, and localization probability filtering for >75%, 403 distinct phosphopeptides (481 distinct phosphosites) were significantly downregulated by 1.5-fold or greater ($M/L < -0.585$) following 4 h of 30 μ M CX-4945 treatment (One-sample *t*-test M/L , $q < 0.05$ BH FDR). Of these 403 phosphopeptides significantly downregulated 1.5-fold or greater, 29 distinct phosphopeptides mapping to 22 proteins (36 distinct phosphosites) demonstrated rescue according to our biological criterion ($-0.585 < H/L < 0.585$) (One-sample *t*-test H/M , $q < 0.05$ BH FDR) (**Figure 4A**; **Supplementary Figure S5**). Of the 36 distinct phosphosites identified, 30 phosphosites (~83%) adhered to the minimal CSNK2 recognition motif further reinforcing the promise of this strategy. Rescued phosphopeptides were cross referenced with proteomic analysis of the same samples to ensure that differential abundance of these phosphopeptides was not a result of differential protein expression (**Supplementary Figure S6**).

Of note, 177 distinct phosphopeptides (200 distinct phosphosites) were significantly upregulated 1.5-fold or greater ($M/L > 0.585$) following 30 μ M CX-4945 treatment (One-sample *t*-test M/L , $q < 0.05$ BH FDR). Of these 177 phosphopeptides significantly upregulated 1.5-fold or greater, nine distinct phosphopeptides (10 distinct phosphosites) demonstrated rescue ($-0.585 < H/L < 0.585$) (One-sample *t*-test H/M , $q < 0.05$ BH FDR) (**Figure 4A**, **Supplementary Table S1**).

Altogether, we were able to identify and validate 22 CSNK2 substrates which correspond to 29 phosphopeptides having demonstrated robust inhibition and rescue (**Figure 4B**). Out of 29 phosphopeptides which were identified to be CSNK2-dependent, 11 phosphopeptides were of multiplicity 1 (i.e., one phosphorylation site present on the identified peptide). Thus, our method identified 11 high-confidence CSNK2 phosphosite substrates within a subset of the proteins identified to be CSNK2-substrates.

Several phosphopeptides were significantly downregulated 1.5-fold but did not satisfy our strict biological criterion ($-0.585 < H/L < 0.585$). Instead, they demonstrated 'partial rescue' ($H/M > 0$) (One-sample *t*-test H/M , $q < 0.05$ BH FDR). Partially rescued phosphopeptides include those which were significantly upregulated in cells expressing exogenous CSNK2A1-TM in the presence of CX-4945, but not to the same level as cells overexpressing exogenous CSNK2A1-WT in the absence of any inhibitor. Considering this filtering was less

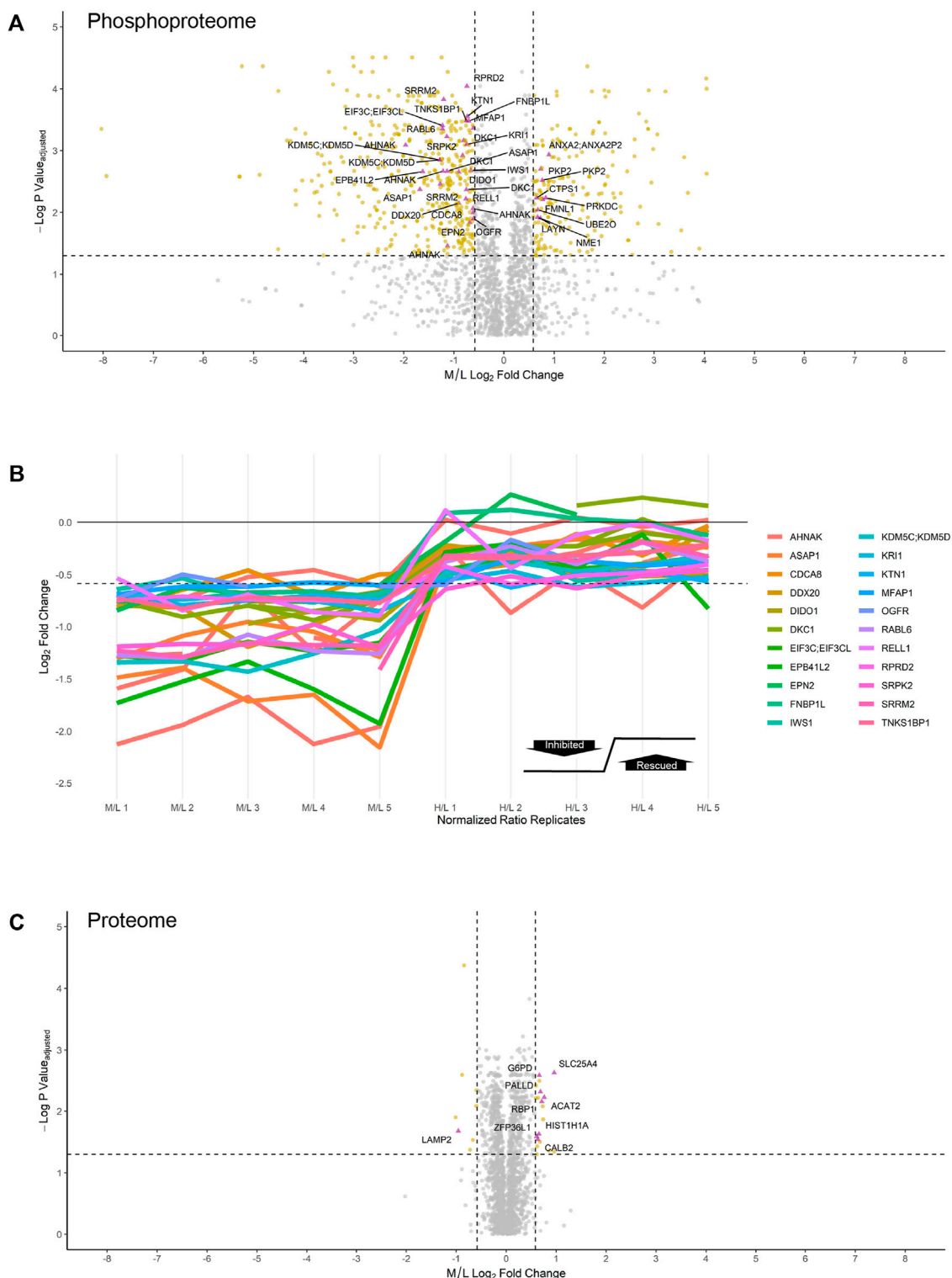


FIGURE 4 | Inhibition and rescue profile of CSNK2 substrates. Differential expression of **(A)** phosphopeptides and **(C)** proteins after treating U2OS cells expressing CSNK2A1-WT with 30uM of CX-4945 for 4 h. Phosphopeptides/proteins highlighted in gold are significantly down- or upregulated 1.5-fold. Phosphopeptides/proteins highlighted in purple demonstrate rescue in U2OS cells expressing CSNK2A1-TM with 30uM of CX-4945 for 4 h. Rescued phosphopeptides are labelled with the gene name of the corresponding protein. Vertical dashed lines (± 0.585) represent 1.5-fold down- and upregulation, respectively. The horizontal dashed line represents an adjusted p -value cutoff of 0.05 **(B)** Inhibition and rescue profiles of CSNK2 substrate phosphopeptides. The horizontal dashed line is representative of significant inhibition (-0.585).

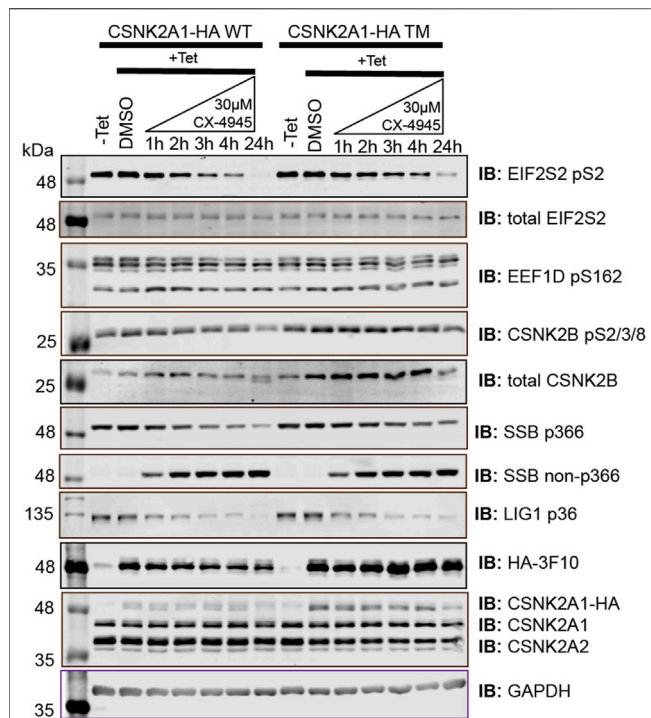


FIGURE 5 | Immunoblot evaluation of phosphospecific antibodies recognizing SSB pS366, SSB S366, and LIG1 pS36. Flp-In T-REx U2OS cell lines stably expressing CSNK2A-HA WT or CSNK2A-HA TM with tight Tetracycline (Tet-ON) regulation were treated with 30 μ M of CX-4945 for the indicated times and blotted with the indicated antibodies recognizing total protein or specific sites. Results are representative of two independent experiments.

stringent than that which was applied to our list of rescued phosphopeptides, this list of partially rescued substrates naturally also included those which were rescued ($-0.585 < H/L < 0.585$). In total, our partially rescued list of substrates identified 55 protein substrates, 74 distinct phosphopeptides, and 95 distinct phosphosites. This list warrants further attention and serves as a potential source of *bona fide* CSNK2 substrates (Supplementary Table S1).

Motif Analysis of CSNK2-dependent Phosphosites

Kinase assays performed with purified components *in vitro* have repeatedly demonstrated CSNK2 activity to highly favor the presence of acidic residues downstream of the phosphoacceptor. One notable negative sequence determinant of CSNK2-catalyzed phosphorylation has been reported to be the presence of Proline at the +1 position. We conducted consensus sequence analysis using the online WebLogo tool at each filtering step to visualize the phosphorylation landscape of cellular CSNK2 substrates (Crooks et al., 2004). The sequence generated from our list of rescued phosphopeptides closely adheres to the minimal consensus sequence of CSNK2 frequently noted in the literature—[S/T]-x-x-[D/E] (Figure 3B) (Meggio and Pinna, 2003; Salvi et al., 2009). The high frequency of aspartic acid

and glutamic acid residues downstream from the phosphoacceptor residue reflects the well-characterized acidophilic nature of CSNK2. Upstream residues do not seem to demonstrate a high level of conservation and are likely less important to CSNK2 phosphorylation, as also previously noted in the literature. Although CSNK2 has demonstrated the ability to phosphorylate tyrosine residues in previous studies (Vilk et al., 2008), we did not see phosphorylated tyrosine sites following our stringent filtering.

Despite strong adherence of identified phosphosites to the typical CSNK2 recognition motif, our WebLogo analysis demonstrated that proline is quite prevalent at position +1 despite previous studies claiming it is a negative determinant (Marin et al., 1992). While we do not suggest that proline at this position positively influences phosphorylation, it is possible that proline at the +1 position is not enough of a negative sequence determinant to absolutely prevent CSNK2 phosphorylation *in vivo*.

Characterizing the CSNK2-dependent Proteome

In comparison to the phosphoproteome, the proteome was minimally perturbed in response to CX-4945 treatment (Figures 4A,C). Only a small number of proteins were differentially regulated in a CSNK2-dependent manner. Of the 4,511 proteins identified and quantified by MaxQuant, only eight proteins were significantly downregulated 1.5-fold or greater ($M/L < -0.585$) (One-sample *t*-test M/L , $q < 0.05$ BH FDR). One of these proteins, lysosome-associated membrane glycoprotein 2 (LAMP2), demonstrated rescue ($-0.585 < H/L < 0.585$) (One-sample *t*-test H/M , $q < 0.05$ BH FDR). In contrast, proteins which were significantly upregulated 1.5-fold or greater ($M/L > 0.585$) in response to CX-4945 treatment numbered 19 (One-sample *t*-test M/L , $q < 0.05$ BH FDR). Eight of these proteins demonstrated rescue ($-0.585 < H/L < 0.585$) (One-sample *t*-test H/M , $q < 0.05$ BH FDR) (Figure 4B, Supplementary Table S2).

Development of Novel Antibodies for Bona Fide CSNK2 Substrates

To extend this work, we developed novel antibodies against a number of putative CSNK2 substrates identified by the chemical genetics strategy that we devised. When deciding on antibody candidates from those identified and validated within our MS analysis, our selection criteria also included: i) (phospho)peptide uniqueness, ii) molecular weight of the protein, iii) reported cellular abundance of the protein, iv) adherence to CSNK2 motif, and v) literature relating the site to CSNK2. We also utilized our list of partially rescued sites as a source of candidates. We developed and characterized phospho-specific antibodies for DNA ligase 1 (LIG1) pS66 (ARVLGpSEGEED) and Lupus La protein (SSB) pS366 (KTKFpSDEHD) (Supplementary Figure S3A). Each of these phosphoproteins exhibited significant inhibition and subsequent 'rescue' following 4 hours of CX-4945 treatment in the CSNK2A1-WT and CSNK2A1-TM cell lines, respectively (Figure 6). These

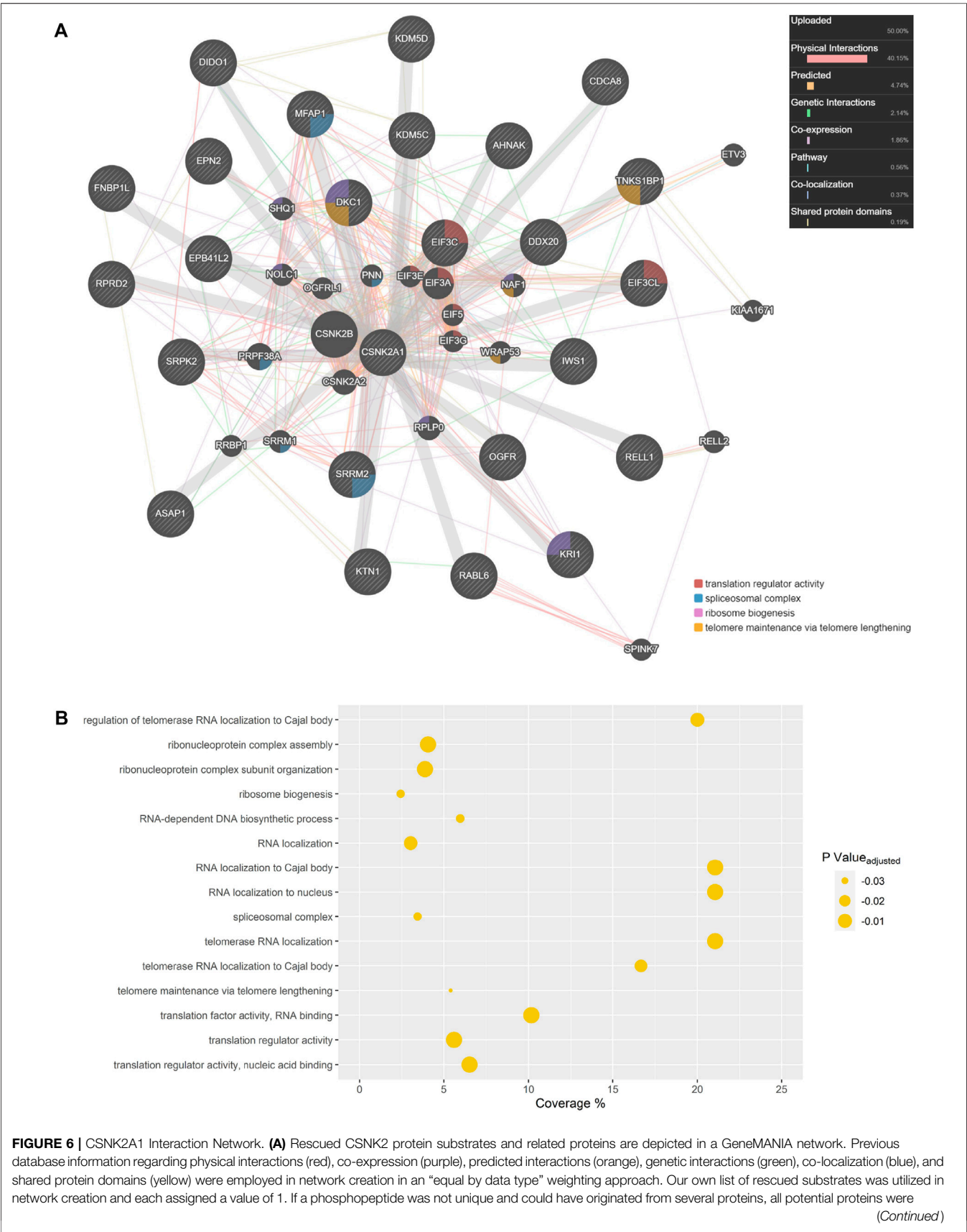


FIGURE 6 | assigned a value of 1. Hashed gene names indicate proteins included in our query list, while those with a solid background are related proteins inserted during GeneMANIA network creation. Proteins implicated in Gene Ontology (GO) biological processes are labelled. **(B)** GO terms enriched amongst proteins displayed in the GeneMANIA network. Coverage represents the proportion of displayed proteins which are annotated with a certain GO term when compared to all genes in the genome annotated with that same term.

candidates originated from the list of partially rescued sites identified by our MS analysis, thus further increasing our confidence in the *bona fide* nature of this list of substrates. During the course of phospho-specific antibody development, we also obtained an anti-SSB antibody which selectively recognizes the unphosphorylated version of the peptide (KTKFASDDEHD) (**Figure 6** and **Supplementary Figure S3B**). This antibody demonstrated a decrease in phosphorylation at S366 with increased CX-4945 incubation times, perfectly opposing the trend seen with the antibody targeting SSB pS366. With these newly developed phospho-specific antibodies, we gained additional tools to monitor CSNK2 activity and further increased confidence in our kinase-substrate identification method.

CSNK2A1 Interaction Network

Biological network representation can simultaneously display several interaction types which occur between constituents in living cells by extracting data from numerous databases and existing literature. Network depictions can also provide meaningful information and leads on potential CSNK2 interactors and downstream effector molecules. Therefore, using GeneMANIA, we generated a CSNK2A1 interaction network of the proteins which were rescued in our analysis (**Figure 6A**) (Warde-Farley et al., 2010). Previous database information regarding physical interactions, co-expression, genetic interactions, co-localization, and shared protein domains, as well as predicted interactions, were employed in network creation with an “equal by data type” weighting. Our own uploaded dataset was also utilized in network creation; rescued CSNK2A1 protein substrates were assigned a value of 1. If a phosphopeptide was not unique and could have originated from several proteins (e.g., EIF3C or EIF3CL) all potential proteins were included in the uploaded gene list at a value of 1. The network displays 26 proteins which were manually inputted and 19 proteins which were implicated by some relationship to our proteins of interest. Proteins displayed in this network were enriched for several GO terms, including numerous biological processes with which CSNK2 has previously been associated (**Figure 6B**).

DISCUSSION

Collective efforts to characterize the CSNK2-dependent phosphoproteome have resulted in no shortage of phosphoproteomic studies directed at identifying putative substrates using CSNK2-directed inhibitors. These inhibitors exhibit variable specificity, display off-target effects, and they are typically not accompanied by rigorous validation. In this study, we describe a strategy for the systematic identification and

validation of CSNK2 substrates by employing an inhibitor-resistant mutant of CSNK2 mutant in conjunction with triple SILAC phosphoproteomics.

We began by evaluating the ability of several commercially available CSNK2 inhibitors to effectively inhibit CSNK2 in U2OS and HeLaT cells. Using multiple phospho-specific antibodies recognizing previously determined *bona fide* CSNK2 substrates, we demonstrated that only two of eight CSNK2 inhibitors—CX-4945 and Inhibitor-8—were effective in inhibiting CSNK2 in cells. These observations fail to demonstrate utility of a number of these compounds for cell-based studies despite previous *in vitro* studies demonstrating strong potency of these compounds as inhibitors of CSNK2 in enzymatic assays (Sarno et al., 2001; Pagano et al., 2004a; Pagano et al., 2004b; Cozza et al., 2006; Cozza et al., 2009; Sandholt et al., 2009). The potency of small molecule inhibitors in living cells can be vastly different from their *in vitro* inhibition profiles, thereby highlighting the importance of testing inhibitors in cell-based assays using validated CSNK2 activity markers. With the increased identification of *bona fide* CSNK2 substrates in cells, our repertoire of CSNK2 activity markers will also expand to serve this purpose.

Evaluating CX-4945 with the chemical genetics validation strategy described here, we identified 29 phosphopeptides which were both inhibited in cells expressing CSNK2A1-WT in the presence of CX-4945 and also rescued (i.e., maintained) in cells expressing CSNK2A1-TM in the presence of CX-4945. This led to the identification of 22 CSNK2 protein substrates (**Supplementary Figure S5**). For some of these protein substrates, it is not exactly clear which protein isoform from which the phosphopeptide originates. For example, QPLLLpSEDEEDTKR is a multiplicity 1 CSNK2 phosphopeptide substrate which was inhibited and rescued, yet this tryptic peptide is present in both EIF3C and EIF3CL. Moreover, numerous tryptic phosphopeptides which demonstrated rescue were multiply phosphorylated (multiplicity >1), making confident identification of the CSNK2-dependent phosphosite(s) challenging. Despite these limitations, several phosphopeptides of multiplicity 1 were also rescued, and we were therefore able to definitively identify 11 CSNK2 phosphosite substrates. None of these sites have been previously validated to be CSNK2-dependent phosphosites, highlighting the utility of this strategy to identify and validate novel CSNK2 sites. While we acknowledge that some of the phosphopeptides which demonstrated inhibition and rescue may be downstream effects of CSNK2 inhibition (i.e., due to sequential phosphorylation by CSNK2-activated kinases), a high proportion (~83%) of phosphosites identified adhere to the minimal CSNK2 recognition motif.

Several phosphopeptides were significantly downregulated 1.5-fold but did not satisfy our strict biological criterion for

‘rescue’ ($-0.585 < H/L < 0.585$). Instead, they demonstrated ‘partial rescue’ ($H/M > 0$) (One-sample *t*-test H/M , $q < 0.05$ BH FDR). We successfully raised antibodies against the following sites which were identified in our list of partially rescued substrates: ARVLGpSEGE (LIG1 pS36), KTKFpSDDEHD (SSB pS366), and KTKFASDDEHD (SSB S366). A dose-dependent decrease in both phosphoproteins was observed with increasing concentrations of CX-4945 (and in the case of SSB, a coordinated increase in the unphosphorylated protein variant) using these antibodies. These effects were then rescued in cells expressing CSNK2A1-TM in the presence of CX-4945, thus confirming that these phosphosites are *bona fide* CSNK2 sites. CSNK2 was previously demonstrated to phosphorylate the N-terminal region of LIG1 *in vitro* resulting in an increase in LIG1 activity (Prigent et al., 1992). LIG1 pS66 is part of a strong CSNK2 consensus sequence and was subsequently shown to be a CSNK2 site *in vitro* (Rossi et al., 1999). To our knowledge, our systematic method of CSNK2 substrate identification and validation is the first to confirm this specific site to be a true cellular substrate of CSNK2. CSNK2-dependent phosphorylation of SSB pS366 has been extensively characterized and previously validated *in vivo* (Fan et al., 1997; Schwartz et al., 2004). SSB plays a crucial role in the termination and re-initiation of the RNA polymerase 3 complex by binding the poly Uridine 3′ tails of nascent polypeptides. With the development and characterization of these novel phospho-specific antibodies, we demonstrated the partially rescued list of substrates to be a source of *bona fide* CSK2 substrates. Remarkably, 28 phosphopeptides of multiplicity 1 are present in this list of partially rescued phosphopeptides, providing site-specific information regarding CSNK2 activity in living cells (**Supplementary Figure S7**).

Other previously known CSNK2 substrates were also identified in our list of partially rescued phosphopeptides, increasing confidence in the *bona fide* nature of this list to the same effect. The pS109 site of ATP-binding cassette 1 (ABCF1/ABC50) was identified in our analysis and has been shown to be phosphorylated by CSNK2 *in vitro*. Phosphoablative mutation of this site to alanine resulted in a marked decrease in EIF2S2 binding to 80S ribosomes and polysomal fractions, identifying a role for CSNK2 in regulation of mRNA translation (Paytubi et al., 2008). Additionally, translation initiation factors EIF2S2 and EIF5B (also identified in our list of partially rescued substrates) have also been previously reported to be *bona fide* CSNK2 substrates (Wang et al., 2001; Majumdar et al., 2002; Llorens et al., 2003; Homma et al., 2005; Gandin et al., 2016). The pS121 and pS122 sites of protein phosphatase inhibitor 2 (PPP1R2) were also identified in our analysis, and they have too been previously determined to be CSNK2 sites using radiolabeled [γ -³²P] ATP *in vitro* (Holmes et al., 1986).

To gain insight regarding the involvement of CSNK2 in cellular processes, we conducted network analysis on the list of rescued protein substrates (**Figure 6A**), and the list of partially rescued protein substrates (**Supplementary Figure S8**). The importance of these depictions is that they allow for integrative visualization of network constituents using multiple different types of interaction data including physical interactions, predicted interactions, genetic interactions, pathway information,

co-localization data, and shared protein domains. Several GO terms were enriched among the proteins depicted in the GeneMANIA network of both rescued (**Figure 6B**; **Supplementary Table S3**) and partially rescued protein substrates (**Supplementary Figure S9**; **Table S4**) including translation regulator activity, spliceosomal complex, ribosome biogenesis, telomere maintenance via telomere lengthening, and several other biological processes which have been previously associated with CSNK2. An added benefit was the ability of GeneMANIA to highlight studies which demonstrated large overlap in physical CSNK2 interactors. Numerous phosphopeptides which demonstrated partial rescue (including a few that satisfied our strict criterion for rescue) were previously identified as CSNK2 substrates in a study by Zhang and colleagues (Zhang et al., 2011). In the study by Zhang et al., proteins from HeLa cell lysate were immobilized onto solid-phase beads and phosphorylated by a recombinant CSNK2 heterotetramer composed of catalytic alpha subunits. Tryptic phosphopeptide substrates were obtained following digestion and MS analysis. The identification of thirteen phosphosites (underscore followed by number indicates the multiplicities of their respective phosphopeptides) overlapped with those identified and validated in our partially rescued list. These include the following (*Site_Multiplicity*): DHX16 *S103_2*, EIF5B *S214_1*, EXOSC9 *S306_1*, IWS *S398_2* and IWS *S400_2*, MFAP *S52_2* and MFAP *S53_2*, NOP58 *S502_1*, PRCC *S157_2*, RPRD2 *S374_1*, SSB *S366_1*, and TNKS1BP1 *S1620_2* and TNKS1BP1 *S1621_2*. The following sites identified on partially rescued phosphopeptides in our dataset also overlapped but were identified on phosphopeptides of differing multiplicities in the Zhang study: DKC1 *S451_2* and DKC1 *S453_2*, NOP56 *S519_1*, and SRRM1 *S874_1*. Such extensive overlap with this *in vitro* lysate study further demonstrates that our list of partially rescued phosphosites is a source of CSNK2 cellular substrates.

In addition to identifying numerous CSNK2 substrates which are downregulated and rescued, nine phosphopeptides were upregulated in response to CX-4945 treatment with restoration of baseline phosphorylation levels in the presence of CSNK2A1-TM. Strikingly, eight of these nine peptides presented with a CSNK2 recognition motif. Cell systems have previously been demonstrated to enact compensatory mechanisms in response to kinase inhibition. This might include upregulating other kinases which directly compensate for reduced CSNK2 activity. It is also possible that the sequences which flank these phosphosites contain positive sequence determinants for other kinases, or that the spatial regulation of these proteins is altered in response to CSNK2 inhibition such that phosphorylation by a nearby kinase is favoured. CSNK2 has also been demonstrated to prime phosphorylation by other kinases at nearby residues—and vice versa—in what is known as hierarchical phosphorylation (St-Denis et al., 2015; Nuñez de Villavicencio-Díaz et al., 2017). In this regard, one potential explanation of the apparent upregulation of phosphopeptides which contain the CSNK2 recognition motif is that phosphopeptides of higher multiplicity (e.g., 2 or 3 phosphorylated residues) may not be phosphorylated by CSNK2 when cells are treated with CX-4945, thereby resulting in an increased abundance of the same peptide

of a lower multiplicity. It is often difficult to observe this relationship given the stochastic sampling of abundant peptides by MS; the same peptide of a different multiplicity may not be identified or if it is, it may not be quantified. If this explanation holds true, it underscores the practical limitations of MS in dissecting the phosphoproteome.

CONCLUDING REMARKS AND IMPLICATIONS

By using an inhibitor-resistant CSNK2 mutant to validate on-target effects of CX-4945, we devised a strategy for the large-scale identification of CSNK2-dependent substrates in an unbiased, systematic manner. In addition to identifying *bona fide* substrates for CSNK2 that increases our understanding of the role of CSNK2 in cellular signaling, we identified a number of sites which were downregulated in response to CX-4945 treatment due to its off-target effects in cells. This information could help explain the extent to which CX-4945 exhibits its clinical efficacy in the treatment of certain diseases due to CSNK2-dependent inhibition. Considering the promise of CSNK2 as potential therapeutic target, a natural extension of this work could be to exploit this strategy in both normal cells and in cancer cells to reveal the divergence of CSNK2-dependent signaling that accompanies cancer. In a similar respect, we can envisage that the strategy could also be adapted to investigate the relationship between the two closely related isoforms of CSNK2 (ie. CSNK2A1 and CSNK2A2), particularly in terms of determining the extent to which they share overlapping substrates within cells. From this perspective, the need for isoform-specific inhibitors could be overcome by selectively generating inhibitor-resistant mutants of either isoform to elucidate signaling events requiring either CSNK2A1 or CSNK2A2.

Despite having used CX-4945, other inhibitors of CSNK2 could also be employed in this workflow for substrate discovery and characterization of inhibitor potency within cells. For example, during the preparation of this manuscript, a novel CSNK2 inhibitor, SGC-CK2-1, was described as a potent inhibitor of cellular CSNK2 with exceptional specificity *in vitro* (Wells et al., 2021). Although our focus was on CSNK2 substrate elucidation, we also expect that this validation strategy can be adapted for the study of other kinases given the high conservation within the kinase family. Overall, it is of great importance that studies employ a method of validation so that our collective understanding of cellular signalling is not limited by small molecule specificity.

DATA AVAILABILITY STATEMENT

The mass spectrometry proteomics data have been deposited to the ProteomeXchange Consortium (Deutsch et al. 2020) via the PRIDE (Perez-Riverol et al., 2022) partner repository with the dataset identifier PXD033523 and 10.6019/PXD0.

AUTHOR CONTRIBUTIONS

LG, main-coauthor, coordinated projects, contributed final figures (Figures 1, 2, 5; Supplementary Figure S1, S2),

writing and editing manuscript; DM, main-coauthor, contributed final figures (Figures 3, 4, 6; Supplementary Figure S3, S5–S9), MS data analysis, antibody development and characterization, writing and editing manuscript; EC, main-coauthor, cell experiment for MS experiment and sample processing; KJ, LC-MS/MS analysis, MS data analysis, scientific discussions; SR, experiment of Figure 5; DC, Supplementary Figure S4 characterization of cell lines using immunofluorescence; FT, antibody development and characterization, scientific discussions; SF, U2OS cell line development; PD, U2OS cell line characterization; TN, AR, SZ, and JT, scientific discussions related to experimental design and data analysis and interpretation; PP, LC-MS/MS method development and LC-MS/MS analysis, scientific discussions; GL, principal investigator of MS analysis; DL, project principal investigator.

FUNDING

This research has been supported by the Canadian Institutes of Health Research and the Natural Sciences and Engineering Research Council of Canada.

ACKNOWLEDGMENTS

We thank our colleague Victoria Clarke in the BioCORE Facility (Schulich School of Medicine and Dentistry, Western University) for her assistance with the enzymatic protein digests. Furthermore, we are grateful to Dr. Tim Haystead (Duke University) and Dr. Lee Graves (University of North Carolina) for sharing materials. We are thankful to the Litchfield and Lajoie laboratory members for the helpful discussions.

SUPPLEMENTARY MATERIAL

The Supplementary Material for this article can be found online at: <https://www.frontiersin.org/articles/10.3389/fmolb.2022.909711/full#supplementary-material>.

Supplementary Figure S1 | Comparison of CSNK2 inhibitors for their ability to inhibit cellular CSNK2 with 24 h of treatment at the indicated concentrations in human adenocarcinoma HeLa (HeLaT) cells. DMSO treated lysates +/- λ -phosphatase were used as immunoblotting controls of phospho-specific antibodies. GAPDH was used to demonstrate equal gel loading. Results are representative of two independent experiments.

Supplementary Figure S2 | Anti-EIF2S2 pS2 and anti-CSNK2B pS2/3/4/8 antibody (Ab) characterization using HeLaT cell lysates. Lysate control lanes are treated with +/- λ -phosphatase. The listed EIF2S2 pS2 (A) or CSNK2B pS2/3/4/8 (B) peptide sequences were used for phospho-antibody development. The specificity of anti-EIF2S2 pS2 (A) or anti-CSNK2B pS2/3/4/8 (B) antibodies was demonstrated in the peptide competition using 200X molar excess of phospho- or nonphospho-peptides. Equal amount of lysate loading was demonstrated with the anti-GAPDH antibody.

Supplementary Figure S3 | Anti-SSB pS366, anti-SSB non-phospho S366 and anti-LIG1 pS36 antibody characterization using U2OS cell lysates. Lysate control lanes are treated with +/- λ -phosphatase. The listed SSB pS366 (A, B) or LIG1 pS36 (C) peptide sequences were used for phospho-antibody development. The

specificity of **(A)** anti-SSB pS366 **(B)** anti-SSB non-phospho S366 or **(C)** anti-LIG1 pS36 antibodies is demonstrated in peptide competitions using 200X molar excess of phospho- or nonphospho-peptides. Equal amount of lysate loading was demonstrated with anti-GAPDH antibody.

Supplementary Figure S4 | Characterization of Flp-In T-Rex U2OS parental, CSNK2A1-HA wild type (WT) and triple mutant (TM, V66A/H160D/I174A) cell lines in immunofluorescence (IF) experiments. Exogenous CSNK2A1-HA WT or CSNK2A1-HA TM expression in the cells were induced with 1 µg/mL Tetracycline. Cells were asynchronous or cell cycle arrested with double Thymidine block (Roberts et al., 2006) before IF labelling with the indicated anti-HA/Alexa 488 (FITC, Thermo Fisher Scientific) antibody and the nucleus was stained with Hoechst 33342 (DAPI, Thermo Fisher Scientific). Scalebar indicates 50 µm on images. Figures are presenting results from two independent experiments.

Supplementary Figure S5 | Profile plots of distinct phosphopeptides which were significantly inhibited and rescued, categorized based on corresponding protein. The horizontal dashed line represents 1.5-fold significant inhibition (−0.585).

Supplementary Figure S6 | Comparison of rescued phosphopeptides with corresponding differential protein expression. Vertical and horizontal lines (−/+ 0.585) are indicative of significant down- and upregulation of phosphosites and proteins.

REFERENCES

- Ahmad, K. A., Wang, G., Unger, G., Slaton, J., and Ahmed, K. (2008). Protein Kinase CK2 - A Key Suppressor of Apoptosis. *Adv. Enzyme Regul.* 48, 179–187. doi:10.1016/j.advenzreg.2008.04.002
- Ali, A. A. E., Jukes, R. M., Pearl, L. H., and Oliver, A. W. (2009). Specific Recognition of a Multiply Phosphorylated Motif in the DNA Repair Scaffold XRCC1 by the FHA Domain of Human PNK. *Nucleic Acids Res.* 37 (5), 1701–1712. doi:10.1093/nar/gkn1086
- Bendall, S. C., Hughes, C., Stewart, M. H., Doble, B., Bhatia, M., and Lajoie, G. A. (2008). Prevention of Amino Acid Conversion in SILAC Experiments with Embryonic Stem Cells. *Mol. Cell. Proteomics* 7 (9), 1587–1597. doi:10.1074/mcp.m800113-mcp200
- Bosc, D. G., Slominski, E., Sichler, C., and Litchfield, D. W. (1995). Phosphorylation of Casein Kinase II by P34cdc2. *J. Biol. Chem.* 270 (43), 25872–25878. doi:10.1074/jbc.270.43.25872
- Cabrejos, M. a. E., Allende, C. C., and Maldonado, E. (2004). Effects of Phosphorylation by Protein Kinase CK2 on the Human Basal Components of the RNA Polymerase II Transcription Machinery. *J. Cell. Biochem.* 93 (1), 2–10. doi:10.1002/jcb.20209
- Castello, J., Ragnauth, A., Friedman, E., and Rebholz, H. (2017). CK2-An Emerging Target for Neurological and Psychiatric Disorders. *Pharm. (Basel)* 10 (1). doi:10.3390/ph10010007
- Chua, M. M. J., Lee, M., and Dominguez, I. (2017). Cancer-type Dependent Expression of CK2 Transcripts. *PLoS One* 12 (12), e0188854–e. doi:10.1371/journal.pone.0188854
- Cohen, P. (2002). Protein Kinases - the Major Drug Targets of the Twenty-first Century? *Nat. Rev. Drug Discov.* 1 (4), 309–315. doi:10.1038/nrd773
- Cox, J., Matic, I., Hilger, M., Nagaraj, N., Selbach, M., Olsen, J. V., et al. (2009). A Practical Guide to the MaxQuant Computational Platform for SILAC-Based Quantitative Proteomics. *Nat. Protoc.* 4 (5), 698–705. doi:10.1038/nprot.2009.36
- Cozza, G., Bonvini, P., Zorzi, E., Poletto, G., Pagano, M. A., Sarno, S., et al. (2006). Identification of Ellagic Acid as Potent Inhibitor of Protein Kinase CK2: a Successful Example of a Virtual Screening Application. *J. Med. Chem.* 49 (8), 2363–2366. doi:10.1021/jm060112m
- Cozza, G., Mazzorana, M., Papinutto, E., Bain, J., Elliott, M., di Maira, G., et al. (2009). Quinalizarin as a Potent, Selective and Cell-Permeable Inhibitor of Protein Kinase CK2. *Biochem. J.* 421 (3), 387–395. doi:10.1042/bj20090069
- Crooks, G. E., Hon, G., Chandonia, J.-M., and Brenner, S. E. (2004). WebLogo: A Sequence Logo Generator: Figure 1. *Genome Res.* 14 (6), 1188–1190. doi:10.1101/gr.849004
- Deutsch, E. W., Bandeira, N., Sharma, V., Perez-Riverol, Y., Carver, J. J., Kundu, D. J., et al. (2020). The ProteomeXchange Consortium in 2020: Enabling 'big Data' Approaches in Proteomics. *Nucleic Acids Res.* 48 (D1), D1145–D52. doi:10.1093/nar/gkz984
- Duncan, J. S., Turowec, J. P., Duncan, K. E., Vilks, G., Wu, C., Lüscher, B., et al. (2011). A Peptide-Based Target Screen Implicates the Protein Kinase CK2 in the Global Regulation of Caspase Signaling. *Sci. Signal* 4 (172), ra30. doi:10.1126/scisignal.2001682
- Duncan, J. S., Gyenis, L., Lenehan, J., Bretner, M., Graves, L. M., Haystead, T. A., et al. (2008). An Unbiased Evaluation of CK2 Inhibitors by Chemoproteomics. *Mol. Cell. Proteomics* 7 (6), 1077–1088. doi:10.1074/mcp.m700559-mcp200
- Duncan, J. S., Haystead, T. A. J., and Litchfield, D. W. (2012). Chemoproteomic Characterization of Protein Kinase Inhibitors Using Immobilized ATP. *Methods Mol. Biol.* 795, 119–134. doi:10.1007/978-1-61779-337-0_8
- Duncan, J. S., Turowec, J. P., Vilks, G., Li, S. S. C., Gloor, G. B., and Litchfield, D. W. (2010). Regulation of Cell Proliferation and Survival: Convergence of Protein Kinases and Caspases. *Biochimica Biophysica Acta (BBA) - Proteins Proteomics* 1804, 505–510. doi:10.1016/j.bbapap.2009.11.001
- Englert, C., Hou, X., Maheswaran, S., Bennett, P., Ngwu, C., Re, G. G., et al. (1995). WT1 Suppresses Synthesis of the Epidermal Growth factor Receptor and Induces Apoptosis. *EMBO J.* 14 (19), 4662–4675. doi:10.1002/j.1460-2075.1995.tb00148.x
- Fan, H., Sakulich, A. L., Goodier, J. L., Zhang, X., Qin, J., and Maraia, R. J. (1997). Phosphorylation of the Human La Antigen on Serine 366 Can Regulate Recycling of RNA Polymerase III Transcription Complexes. *Cell* 88 (5), 707–715. doi:10.1016/s0092-8674(00)81913-3
- Gandin, V., Masvidal, L., Cargnello, M., Gyenis, L., McLaughlan, S., Cai, Y., et al. (2016). mTORC1 and CK2 Coordinate Ternary and eIF4F Complex Assembly. *Nat. Commun.* 7 (1), 11127. doi:10.1038/ncomms11127
- Good, M. C., Zalatan, J. G., and Lim, W. A. (2011). Scaffold Proteins: Hubs for Controlling the Flow of Cellular Information. *Science* 332 (6030), 680–686. doi:10.1126/science.1198701
- Gyenis, L., Duncan, J. S., Turowec, J. P., Bretner, M., and Litchfield, D. W. (2011). Unbiased functional Proteomics Strategy for Protein Kinase Inhibitor Validation and Identification of Bona Fide Protein Kinase Substrates: Application to Identification of EEF1D as a Substrate for CK2. *J. Proteome Res.* 10 (11), 4887–4901. doi:10.1021/pr2008994
- Gyenis, L., Kuš, A., Bretner, M., and Litchfield, D. W. (2013). Functional Proteomics Strategy for Validation of Protein Kinase Inhibitors Reveals New Targets for a TBB-Derived Inhibitor of Protein Kinase CK2. *J. Proteomics* 81, 70–79. doi:10.1016/j.jpro.2012.09.017
- Gyenis, L., Turowec, J. P., Bretner, M., and Litchfield, D. W. (2013). Chemical Proteomics and functional Proteomics Strategies for Protein Kinase Inhibitor Validation and Protein Kinase Substrate Identification: Applications to Protein Kinase CK2. *Biochimica Biophysica Acta (BBA) - Proteins Proteomics* 1834 (7), 1352–1358. doi:10.1016/j.bbapap.2013.02.006

- Haynes, K. A., and Silver, P. A. (2011). Synthetic Reversal of Epigenetic Silencing. *J. Biol. Chem.* 286 (31), 27176–27182. doi:10.1074/jbc.c111.229567
- Holmes, C. F. B., Kuret, J., Chisholm, A. A. K., and Cohen, P. (1986). Identification of the Sites on Rabbit Skeletal Muscle Protein Phosphatase Inhibitor-2 Phosphorylated by Casein Kinase-II. *Biochimica Biophysica Acta (BBA) - Protein Struct. Mol. Enzym.* 870 (3), 408–416. doi:10.1016/0167-4838(86)90248-7
- Homma, M. K., Wada, I., Suzuki, T., Yamaki, J., Krebs, E. G., and Homma, Y. (2005). CK2 Phosphorylation of Eukaryotic Translation Initiation factor 5 Potentiates Cell Cycle Progression. *Proc. Natl. Acad. Sci. U.S.A.* 102 (43), 15688–15693. doi:10.1073/pnas.0506791102
- Hou, Z., Nakanishi, I., Kinoshita, T., Takei, Y., Yasue, M., Misu, R., et al. (2012). Structure-Based Design of Novel Potent Protein Kinase CK2 (CK2) Inhibitors with Phenyl-Azole Scaffolds. *J. Med. Chem.* 55 (6), 2899–2903. doi:10.1021/jm2015167
- Humphrey, S. J., Azimifar, S. B., and Mann, M. (2015). High-throughput Phosphoproteomics Reveals *In Vivo* Insulin Signaling Dynamics. *Nat. Biotechnol.* 33 (9), 990–995. doi:10.1038/nbt.3327
- Jurcik, J., Sivakova, B., Cipakova, I., Selicky, T., Stupenova, E., Jurcik, M., et al. (2020). Phosphoproteomics Meets Chemical Genetics: Approaches for Global Mapping and Deciphering the Phosphoproteome. *Ijms* 21 (20), 7637. doi:10.3390/ijms21207637
- Kim, H., Lee, K. S., Kim, A. K., Choi, M., Choi, K., Kang, M., et al. (2016). A Chemical with Proven Clinical Safety Rescues Down-Syndrome-Related Phenotypes in through DYRK1A Inhibition. *Dis. Model Mech.* 9 (8), 839–848. doi:10.1242/dmm.025668
- Kim, H., Choi, K., Kang, H., Lee, S.-Y., Chi, S.-W., Lee, M.-S., et al. (2014). Identification of a Novel function of CX-4945 as a Splicing Regulator. *PLoS One* 9 (4), e94978. doi:10.1371/journal.pone.0094978
- Knight, Z. A., and Shokat, K. M. (2005). Features of Selective Kinase Inhibitors. *Chem. Biol.* 12 (6), 621–637. doi:10.1016/j.chembiol.2005.04.011
- Krug, K., Mertins, P., Zhang, B., Hornbeck, P., Raju, R., Ahmad, R., et al. (2019). A Curated Resource for Phosphosite-specific Signature Analysis. *Mol. Cell. Proteomics* 18 (3), 576–593. doi:10.1074/mcp.tir118.000943
- Lemeer, S., and Heck, A. J. (2009). The Phosphoproteomics Data Explosion. *Curr. Opin. Chem. Biol.* 13 (4), 414–420. doi:10.1016/j.cbpa.2009.06.022
- Lertsuwan, J., Lertsuwan, K., Sawasdech, A., Tasnawijitwong, N., Lee, K. Y., Kitchen, P., et al. (2018). CX-4945 Induces Methuosis in Cholangiocarcinoma Cell Lines by a CK2-independent Mechanism. *Cancers (Basel)* 10 (9). doi:10.3390/cancers10090283
- Litchfield, D., and Gyenis, L. (2015). Protein Kinase CK2: Systematic Relationships with Other Posttranslational Modifications. *Pharm. (Basel)* 10 (1), 27. doi:10.3390/ph10010027
- Litchfield, D. W. (2003). Protein Kinase CK2: Structure, Regulation and Role in Cellular Decisions of Life and Death. *Biochem. J.* 369 (Pt 1), 1–15. doi:10.1042/BJ20021469
- Litchfield, D. W., and Lüscher, B. (1993). Casein Kinase II in Signal Transduction and Cell Cycle Regulation. *Mol. Cell Biochem.* 127–128 (1), 187–199. doi:10.1007/bf01076770
- Llorens, F., Roher, N., Miró, F. A., Sarno, S., Ruiz, F. X., Meggio, F., et al. (2003). Eukaryotic Translation-Initiation factor eIF2beta Binds to Protein Kinase CK2: Effects on CK2alpha Activity. *Biochem. J.* 375 (Pt 3), 623–631. doi:10.1042/BJ20030915
- Loizou, J. I., El-Khamisy, S. F., Zlatanou, A., Moore, D. J., Chan, D. W., Qin, J., et al. (2004). The Protein Kinase CK2 facilitates Repair of Chromosomal DNA Single-Strand Breaks. *Cell* 117 (1), 17–28. doi:10.1016/s0092-8674(04)00206-5
- Majumdar, R., Bandyopadhyay, A., Deng, H., and Maitra, U. (2002). Phosphorylation of Mammalian Translation Initiation factor 5 (eIF5) *In Vitro* and *In Vivo*. *Nucleic Acids Res.* 30 (5), 1154–1162. doi:10.1093/nar/30.5.1154
- Manning, G., Whyte, D. B., Martinez, R., Hunter, T., and Sudarsanam, S. (2002). The Protein Kinase Complement of the Human Genome. *Science* 298 (5600), 1912–1934. doi:10.1126/science.1075762
- Marin, O., Meggio, F., Draetta, G., and Pinna, L. A. (1992). The Consensus Sequences for Cdc2 Kinase and for Casein Kinase-2 Are Mutually Incompatible A Study with Peptides Derived from the β -subunit of Casein Kinase-2. *FEBS Lett.* 301 (1), 111–114. doi:10.1016/0014-5793(92)80221-2
- Meek, D. W., Simon, S., Kikkawa, U., and Eckhart, W. (1990). The P53 Tumour Suppressor Protein Is Phosphorylated at Serine 389 by Casein Kinase II. *EMBO J.* 9 (10), 3253–3260. doi:10.1002/j.1460-2075.1990.tb07524.x
- Meggio, F., and Pinna, L. A. (2003). One-thousand-and-one Substrates of Protein Kinase CK2? *FASEB J.* 17 (3), 349–368. doi:10.1096/fj.02-0473rev
- Nuñez de Villavicencio-Díaz, T., Rabalski, A. J., and Litchfield, D. W. (2017). Protein Kinase CK2: Intricate Relationships within Regulatory Cellular Networks. *Pharm. (Basel)* 10 (1), 27. doi:10.3390/ph10010027
- Pagano, M. A., Andrzejewska, M., Ruzzene, M., Sarno, S., Cesaro, L., Bain, J., et al. (2004). Optimization of Protein Kinase CK2 Inhibitors Derived from 4,5,6,7-Tetrabromobenzimidazole. *J. Med. Chem.* 47 (25), 6239–6247. doi:10.1021/jm049854a
- Pagano, M. A., Meggio, F., Ruzzene, M., Andrzejewska, M., Kazimierczuk, Z., and Pinna, L. A. (2004). 2-Dimethylamino-4,5,6,7-tetrabromo-1H-benzimidazole: a Novel Powerful and Selective Inhibitor of Protein Kinase CK2. *Biochem. Biophysical Res. Commun.* 321 (4), 1040–1044. doi:10.1016/j.bbrc.2004.07.067
- Paytubi, S., Morrice, N. A., Boudeau, J., and Proud, C. G. (2008). The N-Terminal Region of ABC50 Interacts with Eukaryotic Initiation factor eIF2 and Is a Target for Regulatory Phosphorylation by CK2. *Biochem. J.* 409 (1), 223–231. doi:10.1042/bj20070811
- Perea, S. E., Reyes, O., Baladron, I., Perera, Y., Farina, H., Gil, J., et al. (2008). CIGB-300, a Novel Proapoptotic Peptide that Impairs the CK2 Phosphorylation and Exhibits Anticancer Properties Both *In Vitro* and *In Vivo*. *Mol. Cell Biochem.* 316 (1), 163–167. doi:10.1007/s11010-008-9814-5
- Perez-Riverol, Y., Bai, J., Bandla, C., García-Seisdedos, D., Hewapathirana, S., Kamatchinathan, S., et al. (2022). The PRIDE Database Resources in 2022: a Hub for Mass Spectrometry-Based Proteomics Evidences. *Nucleic Acids Res.* 50 (D1), D543–D552. doi:10.1093/nar/gkab1038
- Pinna, L. A., and Ruzzene, M. (1996). How Do Protein Kinases Recognize Their Substrates? *Biochimica Biophysica Acta (BBA) - Mol. Cell Res.* 1314 (3), 191–225. doi:10.1016/s0167-4889(96)00083-3
- Prigent, C., Lasko, D. D., Kodama, K., Woodgett, J. R., and Lindahl, T. (1992). Activation of Mammalian DNA Ligase I through Phosphorylation by Casein Kinase II. *EMBO J.* 11 (8), 2925–2933. doi:10.1002/j.1460-2075.1992.tb05362.x
- Rabalski, A. J., Gyenis, L., and Litchfield, D. W. (2016). Molecular Pathways: Emergence of Protein Kinase CK2 (CSNK2) as a Potential Target to Inhibit Survival and DNA Damage Response and Repair Pathways in Cancer Cells. *Clin. Cancer Res.* 22 (12), 2840–2847. doi:10.1158/1078-0432.ccr-15-1314
- Rappsilber, J., Mann, M., and Ishihama, Y. (2007). Protocol for Micro-purification, Enrichment, Pre-fractionation and Storage of Peptides for Proteomics Using StageTips. *Nat. Protoc.* 2 (8), 1896–1906. doi:10.1038/nprot.2007.261
- Roberts, E. C., Hammond, K., Traish, A. M., Resing, K. A., and Ahn, N. G. (2006). Identification of G2/M Targets for the MAP Kinase Pathway by functional Proteomics. *Proteomics* 6 (16), 4541–4553. doi:10.1002/pmic.200600365
- Roffey, S. E., and Litchfield, D. W. (2021). CK2 Regulation: Perspectives in 2021. *Biomedicines* 9 (10), 1361. doi:10.3390/biomedicines9101361
- Rosenberger, A. F. N., Morrema, T. H. J., Gerritsen, W. H., van Haastert, E. S., Snkhchyan, H., Hilhorst, R., et al. (2016). Increased Occurrence of Protein Kinase CK2 in Astrocytes in Alzheimer's Disease Pathology. *J. Neuroinflammation* 13, 4. doi:10.1186/s12974-015-0470-x
- Rossi, R., Villa, A., Negri, C., Scovassi, I., Ciarrocchi, G., Biamonti, G., et al. (1999). The Replication factory Targeting sequence/PCNA-Binding Site Is Required in G1 to Control the Phosphorylation Status of DNA Ligase I. *EMBO J.* 18 (20), 5745–5754. doi:10.1093/emboj/18.20.5745
- Salvi, M., Sarno, S., Cesaro, L., Nakamura, H., and Pinna, L. A. (2009). Extraordinary Pleiotropy of Protein Kinase CK2 Revealed by Weblogo Phosphoproteome Analysis. *Biochimica Biophysica Acta (BBA) - Mol. Cell Res.* 1793 (5), 847–859. doi:10.1016/j.bbamcr.2009.01.013
- Sandholt, I. S., Olsen, B. B., Guerra, B., and Issinger, O.-G. (2009). Resorufin: a Lead for a New Protein Kinase CK2 Inhibitor. *Anticancer Drugs* 20 (4), 238–248. doi:10.1097/cad.0b013e328326472e
- Sarno, S., Reddy, H., Meggio, F., Ruzzene, M., Davies, S. P., Donella-Deana, A., et al. (2001). Selectivity of 4,5,6,7-tetrabromobenzotriazole, an ATP Site-Directed Inhibitor of Protein Kinase CK2 ('casein Kinase-2'). *FEBS Lett.* 496 (1), 44–48. doi:10.1016/s0014-5793(01)02404-8

- Schwartz, E. I., Intine, R. V., and Maraia, R. J. (2004). CK2 Is Responsible for Phosphorylation of Human La Protein Serine-366 and Can Modulate rPL37 5'-Terminal Oligopyrimidine mRNA Metabolism. *Mol. Cell Biol.* 24 (21), 9580–9591. doi:10.1128/mcb.24.21.9580-9591.2004
- Shah, K., and Kim, H. (2019). The Significant Others: Global Search for Direct Kinase Substrates Using Chemical Approaches. *IUBMB Life* 71 (6), 721–737. doi:10.1002/iub.2023
- Siddiqui-Jain, A., Drygin, D., Streiner, N., Chua, P., Pierre, F., O'Brien, S. E., et al. (2010). CX-4945, an Orally Bioavailable Selective Inhibitor of Protein Kinase CK2, Inhibits Prosurvival and Angiogenic Signaling and Exhibits Antitumor Efficacy. *Cancer Res.* 70 (24), 10288–10298. doi:10.1158/0008-5472.can-10-1893
- St-Denis, N. A., Bailey, M. L., Parker, E. L., Vilks, G., and Litchfield, D. W. (2011). Localization of Phosphorylated CK2 α to the Mitotic Spindle Requires the Peptidyl-Prolyl Isomerase Pin1. *J. Cell Sci.* 124 (Pt 14), 2341–2348. doi:10.1242/jcs.077446
- St-Denis, N. A., Derksen, D. R., and Litchfield, D. W. (2009). Evidence for Regulation of Mitotic Progression through Temporal Phosphorylation and Dephosphorylation of CK2 α . *Mol. Cell Biol.* 29 (8), 2068–2081. doi:10.1128/mcb.01563-08
- St-Denis, N., Gabriel, M., Turowec, J. P., Gloor, G. B., Li, S. S.-C., Gingras, A.-C., et al. (2015). Systematic Investigation of Hierarchical Phosphorylation by Protein Kinase CK2. *J. Proteomics* 118, 49–62. doi:10.1016/j.jpro.2014.10.020
- Strum, S. W., Gyenis, L., and Litchfield, D. W. (2021). CSNK2 in Cancer: Pathophysiology and Translational Applications. *Br. J. Cancer* 126 (7), 994–1003. doi:10.1038/s41416-021-01616-2
- Towbin, H., Staehelin, T., and Gordon, J. (1979). Electrophoretic Transfer of Proteins from Polyacrylamide Gels to Nitrocellulose Sheets: Procedure and Some Applications. *Biotechnology*. 1992 24, 145–9.
- Tsuchiya, Y., Akashi, M., Matsuda, M., Goto, K., Miyata, Y., Node, K., et al. (2009). Involvement of the Protein Kinase CK2 in the Regulation of Mammalian Circadian Rhythms. *Sci. Signal* 2 (73), ra26. doi:10.1126/scisignal.2000305
- Turowec, J. P., Duncan, J. S., Gloor, G. B., and Litchfield, D. W. (2011). Regulation of Caspase Pathways by Protein Kinase CK2: Identification of Proteins with Overlapping CK2 and Caspase Consensus Motifs. *Mol. Cell Biochem.* 356 (1–2), 159–167. doi:10.1007/s11010-011-0972-5
- Turowec, J. P., Vilks, G., Gabriel, M., and Litchfield, D. W. (2013). Characterizing the Convergence of Protein Kinase CK2 and Caspase-3 Reveals Isoform-specific Phosphorylation of Caspase-3 by CK2 α' : Implications for Pathological Roles of CK2 in Promoting Cancer Cell Survival. *Oncotarget* 4, 560–571. doi:10.18632/oncotarget.948
- Turowec, J. P., Zukowski, S. A., Knight, J. D. R., Smalley, D. M., Graves, L. M., Johnson, G. L., et al. (2014). An Unbiased Proteomic Screen Reveals Caspase Cleavage Is Positively and Negatively Regulated by Substrate Phosphorylation. *Mol. Cell. Proteomics* 13 (5), 1184–1197. doi:10.1074/mcp.m113.037374
- Tyanova, S., Temu, T., and Cox, J. (2016). The MaxQuant Computational Platform for Mass Spectrometry-Based Shotgun Proteomics. *Nat. Protoc.* 11 (12), 2301–2319. doi:10.1038/nprot.2016.136
- Tyanova, S., Temu, T., Sinitcyn, P., Carlson, A., Hein, M. Y., Geiger, T., et al. (2016). The Perseus Computational Platform for Comprehensive Analysis of (Pro)teomics Data. *Nat. Methods* 13 (9), 731–740. doi:10.1038/nmeth.3901
- Vilks, G., Weber, J. E., Turowec, J. P., Duncan, J. S., Wu, C., Derksen, D. R., et al. (2008). Protein Kinase CK2 Catalyzes Tyrosine Phosphorylation in Mammalian Cells. *Cell. Signal.* 20 (11), 1942–1951. doi:10.1016/j.cellsig.2008.07.002
- Wang, G., Ahmad, K. A., Harris, N. H., and Ahmed, K. (2008). Impact of Protein Kinase CK2 on Inhibitor of Apoptosis Proteins in Prostate Cancer Cells. *Mol. Cell Biochem.* 316 (1–2), 91–97. doi:10.1007/s11010-008-9810-9
- Wang, X., Paulin, F. E., Campbell, L. E., Gomez, E., O'Brien, K., Morrice, N., et al. (2001). Eukaryotic Initiation factor 2B: Identification of Multiple Phosphorylation Sites in the Epsilon-Subunit and Their functions *In Vivo*. *EMBO J.* 20 (16), 4349–4359. doi:10.1093/emboj/20.16.4349
- Warde-Farley, D., Donaldson, S. L., Comes, O., Zuberi, K., Badrawi, R., Chao, P., et al. (2010). The GeneMANIA Prediction Server: Biological Network Integration for Gene Prioritization and Predicting Gene function. *Nucleic Acids Res.* 38 (Web Server issue), W214–W220. doi:10.1093/nar/gkq537
- Wells, C. I., Drewry, D. H., Pickett, J. E., Tjaden, A., Krämer, A., Müller, S., et al. (2021). Development of a Potent and Selective Chemical Probe for the Pleiotropic Kinase CK2. *Cell Chem. Biol.* 28 (4), 546–558. e10. doi:10.1016/j.chembiol.2020.12.013
- Wessel, D., and Flügge, U. I. (1984). A Method for the Quantitative Recovery of Protein in Dilute Solution in the Presence of Detergents and Lipids. *Anal. Biochem.* 138 (1), 141–143. doi:10.1016/0003-2697(84)90782-6
- Wilson, L. J., Linley, A., Hammond, D. E., Hood, F. E., Coulson, J. M., MacEwan, D. J., et al. (2018). New Perspectives, Opportunities, and Challenges in Exploring the Human Protein Kinome. *Cancer Res.* 78 (1), 15–29. doi:10.1158/0008-5472.can-17-2291
- Xu, W., Chen, Q., Wang, Q., Sun, Y., Wang, S., Li, A., et al. (2014). JWA Reverses Cisplatin Resistance via the CK2-XRCC1 Pathway in Human Gastric Cancer Cells. *Cell Death Dis.* 5 (12), e1551. doi:10.1038/cddis.2014.517
- Zhang, M., Han, G., Wang, C., Cheng, K., Li, R., Liu, H., et al. (2011). A Bead-Based Approach for Large-Scale Identification of *In Vitro* Kinase Substrates. *Proteomics* 11 (24), 4632–4637. doi:10.1002/pmic.201100339

Conflict of Interest: The authors declare that the research was conducted in the absence of any commercial or financial relationships that could be construed as a potential conflict of interest.

Publisher's Note: All claims expressed in this article are solely those of the authors and do not necessarily represent those of their affiliated organizations, or those of the publisher, the editors and the reviewers. Any product that may be evaluated in this article, or claim that may be made by its manufacturer, is not guaranteed or endorsed by the publisher.

Copyright © 2022 Gyenis, Menyhart, Cruise, Jurcic, Roffey, Chai, Trifoi, Fess, Desormeaux, Núñez de Villavicencio Díaz, Rabalski, Zukowski, Turowec, Pittock, Lajoie and Litchfield. This is an open-access article distributed under the terms of the Creative Commons Attribution License (CC BY). The use, distribution or reproduction in other forums is permitted, provided the original author(s) and the copyright owner(s) are credited and that the original publication in this journal is cited, in accordance with accepted academic practice. No use, distribution or reproduction is permitted which does not comply with these terms.

NOMENCLATURE

AKT1 AKT serine/threonine kinase 1

BH Benjamini-Hochberg

CDC37 Hsp90 co-chaperone Cdc37

CSNK2 casein kinase 2

CSNK2 inhibitor 8 4-(2-(4-Methoxybenzamido)thiazol-5-yl) benzoic acid

CSNK2A1 Casein kinase II subunit alpha

CSNK2A2 Casein kinase II subunit alpha'

CSNK2B Casein kinase II subunit beta

CX-4945 5-(3-chlorophenylamino)benzo[c][2,6]naphthyridine-8-carboxylic acid

DMAT 2-Dimethylamino-4,5,6,7-tetrabromo-1H-benzimidazole

EEF1D Elongation factor 1-delta

EIF2S2 Eukaryotic translation initiation factor 2 subunit 2

Ellagic acid Ellagic acid/Benzoaric acid

FT-U2OS U2OS cells expressing the tetracycline responsible element of Flp-In™ T-Rex

GO Gene Ontology

GAPDH Glyceraldehyde-3-phosphate dehydrogenase

HA Human influenza hemagglutinin

HeLaT human adenocarcinoma HeLa Tet-Off (Clontech) expressing the tetracycline responsible element

LIG1 DNA ligase 1

PBST phosphate-buffered saline with 0.1% Tween 20

Quinalizarin 1,2,5,8-Tetrahydroxy-9,10-anthraquinone

Resorufin 7-Hydroxy-3H-phenoxazin-3-one

SILAC Stable Isotope Labeling by/with Amino acids in Cell culture

SSB Lupus La protein

TBB 4,5,6,7-Tetrabromobenzotriazole

TBBz 4,5,6,7-Tetrabromobenzimidazole

TBST Tris-buffered saline with 0.05% Tween 20

TM Triple Mutant (V66A/H160D/I174A) of CSNK2A1-HA with c-term HA tag

U2OS Human osteosarcoma cell (Tet-Off) expressing tetracycline responsible element

WT Wild Type

XRCC1 DNA repair protein XRCC1



Comprehensive Characterization of CK1 δ -Mediated Tau Phosphorylation in Alzheimer's Disease

Aileen Roth, Annabelle Sander, Marleen Silke Oswald, Fabian Gärtner, Uwe Knippschild^{*†} and Joachim Bischof^{*†}

Department of General and Visceral Surgery, University Medical Center Ulm, University of Ulm, Ulm, Germany

OPEN ACCESS

Edited by:

Lorenzo Alberto Pinna,
Institute of Neuroscience (CNR), Italy

Reviewed by:

Arne Ittner,
Flinders University, Australia
Mauro Salvi,
University of Padua, Italy

*Correspondence:

Uwe Knippschild
uwe.knippschild@uniklinik-ulm.de
Joachim Bischof
joachim.bischof@uni-ulm.de

[†]These authors share senior
authorship

Specialty section:

This article was submitted to
Cellular Biochemistry,
a section of the journal
Frontiers in Molecular Biosciences

Received: 09 February 2022

Accepted: 31 May 2022

Published: 27 June 2022

Citation:

Roth A, Sander A, Oswald MS,
Gärtner F, Knippschild U and Bischof J
(2022) Comprehensive
Characterization of CK1 δ -Mediated
Tau Phosphorylation in
Alzheimer's Disease.
Front. Mol. Biosci. 9:872171.
doi: 10.3389/fmolb.2022.872171

A main pathological event in Alzheimer's disease is the generation of neurofibrillary tangles originating from hyperphosphorylated and subsequently aggregated tau proteins. Previous reports demonstrated the critical involvement of members of the protein kinase family CK1 in the pathogenesis of Alzheimer's disease by hyperphosphorylation of tau. However, precise mechanisms and effects of CK1-mediated tau phosphorylation are still not fully understood. In this study, we analyzed recombinant tau441 phosphorylated by CK1 δ *in vitro* via mass spectrometry and identified ten potential phosphorylation sites, five of them are associated to Alzheimer's disease. To confirm these results, *in vitro* kinase assays and two-dimensional phosphopeptide analyses were performed with tau441 phosphomutants confirming Alzheimer's disease-associated residues Ser68/Thr71 and Ser289 as CK1 δ -specific phosphorylation sites. Treatment of differentiated human neural progenitor cells with PF-670462 and Western blot analysis identified Ser214 as CK1 δ -targeted phosphorylation site. The use of an *in vitro* tau aggregation assay demonstrated a possible role of CK1 δ in tau aggregation. Results obtained in this study highlight the potential of CK1 δ to be a promising target in the treatment of Alzheimer's disease.

Keywords: Alzheimer's disease, AD, casein kinase 1 δ , CK1 δ , tau phosphorylation, tau aggregation

INTRODUCTION

Alzheimer's disease (AD) is a progressive neurodegenerative disorder characterized by an irreversible process of changes involving specific neurons of the neocortex, hippocampus, and other regions of the brain, leading to a cognitive impairment followed by a mental and functional decline. Generally, AD is responsible for more than 80% of dementia cases in elderly people worldwide (Anand et al., 2014). One of the main neuropathological characteristics is the presence of intraneuronal aggregated neurofibrillary tangles (NFTs) assembled from paired helical filaments (PHF) composed of highly phosphorylated tau proteins (Buée et al., 2000; Kumar and Dogra, 2008).

Tau proteins belong to the family of microtubule-associated proteins (MAPs) (Weingarten et al., 1975) and occur mainly in the axonal compartment of neurons (Binder et al., 1985). In the central nervous system, six alternatively spliced tau isoforms in a range from 352 to 441 amino acids were identified (Goedert et al., 1989), that regulate microtubule assembly by modulating the functional organization of neurons, particularly in growth, polarity and axonal morphology (Buée et al., 2000). Extensive tau phosphorylation at various amino acid residues converts soluble tau proteins into PHF leading to the development of NFTs, which cause tau pathologies in AD and other tauopathies

(Grundke-Iqbal et al., 1986; Kosik et al., 1986; Brion et al., 1991). A wide range of proline-directed kinases (e.g., glycogen synthase kinase 3 β (GSK3 β) (Llorens-Martín et al., 2014), cyclin-dependent kinase 5 (CDK5) (Kimura et al., 2014)), nonproline-directed kinases (e.g., tau-tubulin kinases (TTBK) (Tomizawa et al., 2001)), microtubule affinity regulated kinases (e.g., MARK) (Matenia and Mandelkow, 2009) and tyrosine kinases (e.g., Fyn and Abl (Lee et al., 2004; Derkinderen et al., 2005)) have been found to phosphorylate tau and contribute to the pathophysiological hallmark of AD.

Potential kinases catalyzing the hyperphosphorylation of tau in AD also include members of the CK1 (formerly named casein kinase 1) family. Members of the CK1 family are highly conserved serine/threonine-specific, ubiquitously expressed protein kinases. So far, seven different CK1 isoforms (α , β , γ 1-3, δ and ϵ) and their splice variants were identified in mammals. CK1 is able to recognize canonical as well as noncanonical consensus sequences within a substrate resulting in over 150 different *in vitro* and *in vivo* substrates (reviewed in Knippschild et al., 2014). The role of CK1 as a potential kinase phosphorylating tau has become of particular interest, because it has been reported that levels of CK1 δ were elevated by a factor of 30 in the hippocampus in the brain of AD patients compared with equivalent controls (Ghoshal et al., 1999). Additionally, CK1 α and CK1 δ have been shown to be tightly associated with neurofibrillary lesions of AD, further implicating CK1 in PHF formation (Kuret et al., 1997; Schwab et al., 2000). CK1 δ site-specific tau phosphorylation was detected at Ser202/Thr205 and Ser396/Ser404 in non-neuronal human embryonic kidney 293 (HEK293) cells using immunodetection (Li et al., 2004). In a more comprehensive study, various CK1 δ -specific phosphorylation sites were detected analyzing recombinant tau, which was phosphorylated by CK1 δ *in vitro* by using mass spectrometry (MS). MS analysis revealed 33 CK1 δ -specific tau phosphorylation sites, while previously detected phosphorylation of Ser202/Thr205 and Ser396/Ser404 could not be confirmed (Hanger et al., 2007). In both studies, CK1 δ -specific phosphorylation of tau was verified by treating HEK293 or rat cortical neurons with IC261, which was later observed to induce CK1 δ - and ϵ -independent cytotoxic effects by its binding to tubulin leading to microtubule polymerization (Cheong and Virshup, 2011; Stöter et al., 2014; Xian et al., 2021). Because of qualitative methods used in these studies, connection between CK1-mediated tau phosphorylation identified by MS analysis or immunological methods and the role of CK1 in AD by determining the effect of CK1-mediated phosphorylation on tau aggregation has remained elusive.

Tau hyperphosphorylation and tau-phosphorylating kinases have become attractive targets in the treatment of AD. Therefore, the characterization of tau hyperphosphorylation by tau-targeting kinases, such as CK1, is necessary to understand the pathophysiological mechanisms and to provide better therapeutical approaches addressing tau pathology. Here, we characterized the contribution of CK1 δ to AD-associated tau phosphorylation sites *in vitro* by using different techniques including MS, *in vitro* kinase assays and two-dimensional phosphopeptide analysis. The results were further supported

by a cell-based assay and Western blot analysis using phospho-specific antibodies. Additionally, we demonstrated that CK1 δ co-localized with tau in neuronal cells and that CK1 δ -mediated phosphorylation led to an increased *in vitro* tau aggregation. With our data, we provide a comprehensive analysis of CK1 δ -mediated site-specific tau phosphorylation and confirm a functional influence of CK1 δ on tau aggregation.

MATERIALS AND METHODS

Plasmid Constructs for Protein Expression

The codon-optimized bacterial expression vector pET28a(+) tau441 encoding for N-terminal 6xHis-tagged human microtubule-associated protein tau (MAPT) isoform 4 (tau441) was synthesized by Biomatik (Kitchener, ON, Canada). Plasmids encoding for tau441 fragments (tau441¹⁻¹⁵⁵ and tau441²⁴³⁻⁴⁴¹) and phosphorylation site mutants of full-length tau441 (tau441^{S68A+T69A+T71A}, tau441^{S198A+S199A+S202A+T205A}, tau441^{T212A+S214A+T217A+T220A}, tau441^{S289A}, tau441^{S409A+S412A+S413A+T414A+S416A} and tau441^{S422A+T427A}) were created by using inverse PCR and the PCR primer pairs as indicated in **Supplementary Table S1** (see **Figure 1**). Subsequently, PCR products were ligated. To generate plasmid pET28a(+)tau441¹⁵⁶⁻²⁴², Gibson Assembly[®] was performed according to manufacturer's instructions (New England Biolabs Inc., Ipswich, NY, United States). Sanger DNA sequencing (Eurofins Genomics, Munich, Germany) confirmed successful introduction of mutations.

Expression and Purification of Recombinant 6xHis- and GST-Tagged Fusion Proteins

Plasmids encoding for 6xHis-tagged tau441 fragments or phosphorylation site mutants of full-length tau441 were transformed into *E. coli* SHuffle[®] T7 Express (New England Biolabs Inc., Ipswich, NY, United States). Protein production was conducted in 450 ml lysogeny broth (LB) medium supplemented with 15 μ g/ml kanamycin and induced with 0.5 mM IPTG at an OD₆₀₀ of 0.6 AU for 3 h at 30°C. Bacteria were harvested by centrifugation for 10 min at 3,200 g and 4°C. Bacteria were lysed in lysis buffer composed of 50 mM sodium phosphate buffer (pH 7.0), 350 mM NaCl, 15 mM imidazole, 0.5% NP-40, 10% glycerol, 1 mM benzamidine, 0.25 g/L aprotinin and 10 mg lysozyme. Cell lysates were cleared by centrifugation for 20 min at 15,500 g and 4°C. According to Barghorn et al. (Barghorn et al., 2005), cleared lysates were boiled for 10 min and centrifuged for 30 min at 25,000 rpm and 4°C. Supernatant was mixed with 600 μ l TALON[®] Metal Affinity Resin (Takara Bio Inc., Kyoto, Japan) (50% (v/v) in PBS) and incubated at 4°C rotating overnight. Bound proteins were washed (50 mM sodium phosphate buffer (pH 7.0), 350 mM NaCl, 15 mM imidazole, 10% glycerol, 0.25 g/L aprotinin) and eluted stepwise (50 mM Na₂PO₄ pH 7.0, 350 mM NaCl, 350 mM imidazole, 10% glycerol, 0.25 g/L aprotinin) followed by dialysis using PD-10 desalting columns (Cytiva, Freiburg, Germany). Production of GST-tagged and 6xHis-tagged kinases was carried out as described previously

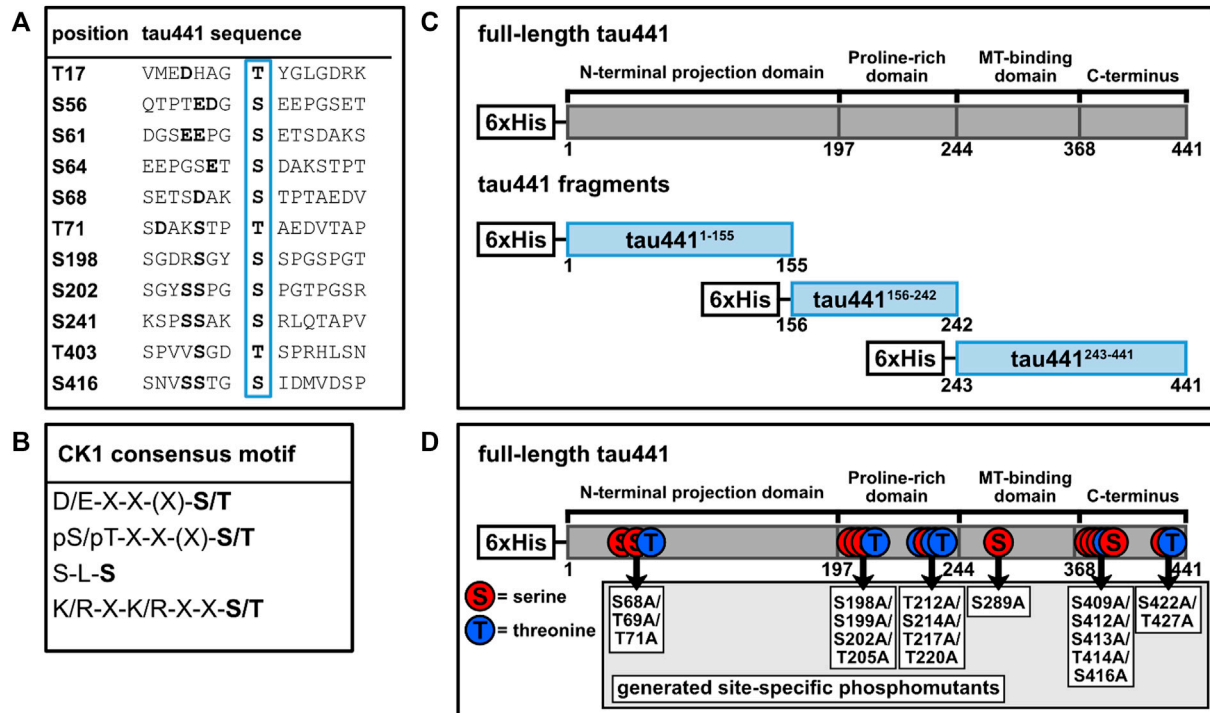


FIGURE 1 | Tau441 contains several potential target sites for CK1. **(A)** Adjacent amino acid sequences of potential phosphorylation sites for CK1 on tau441 predicted by ScanSite 4.0 at low stringency according to Krüger et al. (2021). **(B)** Consensus motifs for CK1. **(C)** Tau441 fragments were generated according to different tau domains. **(D)** Tau441 phosphomutants were generated according to the positions of the predicted CK1 phosphorylation sites or the detection via MS analysis. MT: microtubule, pS/pT: pre-phosphorylated serine or threonine, S: serine, T: threonine, X: no amino acid preference.

(Knippschild et al., 1997; Roth et al., 2021b). All protein solutions were adjusted to 10% glycerol, quick frozen and stored at -80°C for subsequent use.

In Vitro Kinase Assay and Two-Dimensional Phosphopeptide Analysis

The reaction was performed in a total volume of 15 μl containing the kinase buffer (25 mM Tris pH 7.5, 10 mM MgCl_2 , 0.1 mM EDTA, 10 μM ATP), 2 μCi [$\gamma\text{-}^{32}\text{P}$]-ATP (only for radiometric determination), 300 nM CK1 δ and 1 μg (4 μg for phosphopeptide analysis) substrate. As substrates either tau441, tau441 fragments or tau441 phosphorylation site mutants were used. Reaction was carried out for 30 min at 30°C in triplicates. Proteins were separated by SDS-PAGE on 10% gels followed by Coomassie blue staining. Radioactively labeled substrate bands were visualized on dried gels by autoradiography. For quantification of phosphorylated products, radioactively labeled substrate bands were excised from dried gels and phosphate incorporation was determined by Cherenkov counting (LC6000IC, Beckman Coulter, USA). *In vitro* phosphorylated tau441 (wild type), fragments and phosphorylation site mutants were analyzed by two-dimensional phosphopeptide analysis using standard protocols described previously (van der Geer and Hunter, 1994). *In vitro* phosphorylated proteins were separated via SDS-PAGE and transferred onto a PVDF membrane (Cytiva,

Freiburg, Germany). Protein bands of interest were incubated with 5% (w/v) polyvinylpyrrolidone (in 10 mM acetic acid) at 37°C for 30 min, washed with 50 mM ammonium bicarbonate buffer and digested with 10 μg TPCK-trypsin. Digested proteins were further oxidized with performic acid on ice for 2 h. Radioactively labeled phosphopeptides were separated on cellulose TLC plates (Merck Millipore, Darmstadt, Germany) by electrophoresis at pH 1.9 (containing 6% (v/v) formic acid, 1.25% (v/v) acetic acid and 0.25% (v/v) pyridine in dH_2O) followed by ascending chromatographic separation in buffer (composed of 37.5% (v/v) n-butanol, 7.5% (v/v) acetic acid and 25% (v/v) pyridine in dH_2O). Radioactively labeled phosphopeptides were visualized by autoradiography.

LC-MS/MS Analysis of Purified tau441

In vitro phosphorylated proteins were separated by SDS-PAGE and SDS gel pieces were in-gel digested with trypsin as described previously (Borchert et al., 2010). Extracted peptides were desalted using C18 StageTips (Rappsilber et al., 2007) and subjected to LC-MS/MS analysis. LC-MS/MS analyses were performed on an Easy-nLC 1200 UHPLC (Thermo Fisher Scientific Inc., Waltham, MA, United States) coupled to an QExactive HF Orbitrap mass spectrometer (Thermo Fisher Scientific Inc., Waltham, MA, United States) as described elsewhere (Schmitt et al., 2019). Peptides were eluted with a segmented gradient at a flow rate of 200 nl/min for 60 min,

selecting seven most intensive peaks for fragmentation with HCD. The MS data was processed with MaxQuant software suite v.1.6.7.0 (Cox and Mann, 2008). Search for variable modification phosphorylation (STY) was enabled. Database search was provided against human (96817 entries) UniProt database using the Andromeda search engine (Cox et al., 2011). Since the goal of the analysis was to identify tau phosphorylation sites targeted by CK1δ, no global normalization of phosphorylation sites to proteome was performed. The amount of the identified phosphorylation sites within the aa 1 to 155, 156 to 242 and 243 to 441 were normalized to the total amount of the detected phosphorylation sites.

Tau Aggregation and Thioflavin S Assay

Tau441 was phosphorylated *in vitro* as described above with 1,000 μM ATP and 300 nM GST-CK1δ. The reactions were incubated for 30 min at 30°C and afterwards centrifuged for 10 min at full speed and 4°C. Formation of cross-β structures of phosphorylated and non-phosphorylated tau441 (4 μM) in 100 mM Tris/HCl (pH 6.8) was induced with freshly prepared 150 μM arachidonic acid (10 mM in ethanol) as described previously (Barghorn et al., 2005; Chirita et al., 2005). Tau aggregation was detected by the addition of Thioflavin S (ThS). Changes in the emission fluorescence spectra with the excitation wavelength set at 430 nm and the emission wavelength set at 480 nm were monitored using a TriStar² LB 942 multimode plate reader (Berthold Technologies, Bad Wildbad, Germany) at intervals of 1.5 min within 30 min. Data were displayed and fit to one-phase association exponential model using Prism 8 (GraphPad, San Diego, CA, United States).

Cell Culture, Stable Transfection, and Treatment

Immortalized human neural progenitor cells (hNPCs) (ReNcell[®] VM from Merck Millipore, Darmstadt, Germany) were expanded and maintained in proliferation medium (DMEM/F12 (Gibco/Life Technologies, Carlsbad, CA, United States) supplemented with 2% (v/v) B-27 neural supplement (Gibco/Life Technologies, Carlsbad, CA, United States), 2 μg/μl heparin (Stemcell Technologies Inc., Vancouver, BC, Canada), 20 ng/ml human basic fibroblast growth factor (bFGF) (Reprocell Inc., Glasgow, UK), 20 ng/ml human epidermal growth factor (EGF) (Sigma Aldrich, St. Louis, MO, United States), and 100 U/ml penicillin-streptomycin solution (Gibco/Life Technologies, Carlsbad, CA, United States)) as described previously (Roth et al., 2021a). For co-localization experiments, 0.3×10^6 naïve hNPCs were seeded onto Matrigel-coated glass slides in a 6-well with differentiation medium (proliferation medium without growth factors) and differentiated for 2 weeks.

To generate a cell culture system for modeling the AD pathology, hNPCs were stably transfected with lentiviral DNA constructs pCSCW-APPSL-IRES-GFP and pCSCW-PSEN1(ΔE9)-IRES-mCherry, which encode full-length human APP695 with K670N/M671L/V717I (Swedish and London mutation) and GFP or human presenilin 1 with a deletion in exon 9 (PSEN1 (ΔE9)) and mCherry. The lentiviral DNA

constructs were kindly provided by Prof. Dr. Doo Kim (Massachusetts General Hospital, Harvard Medical School, Charlestown, MA, United States). Lentiviral transduction and the subsequent enrichment of high-expressing transduced hNPCs via fluorescence-activated cell sorting (FACS) was performed according to Choi et al. (2014) and Kim et al. (2015). For the analysis of CK1δ-specific tau phosphorylation, 0.9×10^6 transduced hNPCs were seeded into a Matrigel-coated 6-well and differentiated for 2 weeks. After 2 weeks, cells were treated with 1 μM PF-670462 (Sigma Aldrich, St. Louis, MO, United States) or DMSO as vehicle control for 24 h and subsequently lysed.

Cell Lysis and Western Blot Analysis

Transduced hNPCs were washed with 20 mM Tris-HCl (pH 7.6) buffer containing 140 mM NaCl. Cell lysates used for Western blot analyses were prepared in RIPA lysis buffer composed of 50 mM Tris-HCl (pH 7.4), 150 mM NaCl, 0.5% sodium deoxycholate, 1% NP-40, 1 mM EDTA, 2 mM PMSF, 2 mM PNT, 1 mM Na₃VO₄, 1 mM NaF containing fresh phosphatase inhibitor cocktail (phosSTOP[™], Roche, Basel, Switzerland) and cOmplete[™] protease inhibitor cocktail (Roche, Basel, Switzerland). Cell lysates were cleared by centrifugation at 10,000 × g for 10 min at 4°C. 10 μg of cleared lysates were separated on 10% (v/v) gels in SDS-PAGE and transferred to a 0.2 μm PVDF membrane (Hybond-P, Amersham, Buckinghamshire, United Kingdom). Membranes were blocked in 5% (w/v) BSA in TBST for 1 h and incubated with anti-tau antibody (HT7, Thermo Fisher Scientific Inc., Waltham, MA, United States; 1:1000), anti-pSer202/pThr205-tau antibody (AT8, Thermo Fisher Scientific Inc., Waltham, MA, United States; 1:1000), anti-pSer214-tau antibody (D1Q2X, Cell Signaling Technology, Danvers, MA, United States; 1:1000), anti-pSer416-tau antibody (D7U2P, Cell Signaling Technology, Danvers, MA, United States, 1:1000) and anti-β-actin antibody (AC-15, Sigma Aldrich, St. Louis, MO, United States, 1:5000) overnight. Immunocomplexes were detected using a secondary antibody (horseradish-peroxidase (HRP)-conjugated anti-mouse or anti-rabbit antibody, 1:10,000). Immunoreactivity was detected by enhanced chemiluminescence using the Fusion FX imaging system (Vilber, Collégien, France). Signal intensities were quantitatively determined by using ImageJ (Schneider et al., 2012).

Immunofluorescence Staining and Co-Localization Analysis

After differentiation and inhibitor treatment, cells were washed briefly with 1x PBS and fixed with 4% (v/v) paraformaldehyde in 1x PEM buffer (80 mM PIPES (pH 6.8), 1 mM EGTA, 5 mM MgCl₂) at 4°C for 20 min followed by permeabilization with 0.3% (v/v) Triton-X 100 in 1x PEM buffer at RT for 5 min. Cells were washed briefly with 1x PEM and blocked with 5% (w/v) BSA in 1x PEM at RT for 30 min. Thereafter, cells were incubated with anti-tau antibody (HT7, Thermo Fisher Scientific Inc., Waltham, MA, United States; 1:500) at 4°C overnight. Cells were washed three times with 1x PEM and subsequently incubated with Alexa Fluor

488 anti-mouse antibody (InvitrogenTM, Carlsbad, CA, United States; 1:250) at RT for 1 h. Then, cells were washed three times with 1x PEM. Cultures were blocked again in 5% (w/v) BSA in 1x PEM at RT for 30 min, washed three times with 1x PEM and stained with anti-CK1δ antibody (ab10877, abcam, Cambridge, UK; 1:500) or anti-MAP2 antibody (Poly18406, BioLegend, San Diego, CA, United States; 1:500). After washing the 2D grown cells, they were incubated with Alexa Fluor 647 anti-goat antibody (InvitrogenTM, Carlsbad, CA, United States; 1:250) or Alexa Fluor 633 anti-rabbit antibody (InvitrogenTM, Carlsbad, CA, United States; 1:250) at RT for 1 h. Then, cells were washed three times with 1x PEM and stained with 0.1 µg/ml DAPI (Sigma Aldrich, St. Louis, MO, United States) at RT for 5 min. Washed cells were finally mounted with ProLongTM Glass Antifade Mountant (InvitrogenTM, Carlsbad, CA, United States). Images were captured using the Leica SP8 confocal microscope (Leica Mikrosysteme Vertrieb GmbH, Wetzlar, Germany) at ×63 magnification.

Co-localization analysis was carried out using R (version 4.2.0, R Foundation for Statistical Computing, Vienna, Austria) and RStudio (version 2022.02.2, RStudio PBC, Boston, MA, United States). The required packages include imager (Barthelmé and Tschumperlé, 2019) and colocr (Ahmed et al., 2019). In brief, at least three regions of interest (ROI) were selected in the gray-scale image. The threshold value was set to 95. For evaluation of the co-localization the Pearson's correlation coefficient (PCC) and the Mander's overlap coefficient (MOC) were determined according to Ahmed et al. (2019). PCC describes the co-variance of the pixel intensities from both channels (Cy5, FITC). MOC describes the fraction of pixels from each channel (Cy5, FITC) with values above the background.

Statistical Analysis

Results are presented as the mean of experiments at least performed in triplicates. Evaluation and statistical analysis of the results were performed using Prism 8 (GraphPad, San Diego, CA, United States). Statistical significance was tested by using the nonparametric Mann-Whitney U test. *p* values ≤ 0.05 (shown as * for *p* ≤ 0.05 and ns for not significant) were considered to be statistically significant.

RESULTS

Tau441 Is Phosphorylated by CK1δ *in vitro*

Hyperphosphorylation of tau by various kinases plays an important role in the pathogenesis of AD. Previously, several studies demonstrated a potential role of CK1 in the hyperphosphorylation of tau that could be linked to the development of AD. The present study intends to demonstrate a specific involvement of CK1 in tau hyperphosphorylation and aggregation.

According to the canonical consensus sequence for CK1 substrates, the longest tau isoform (tau441) contains several putative target sites for CK1-mediated phosphorylation (Figure 1A). Initially, mass spectrometric examination of

CK1δ-phosphorylated tau441 was used to detect whether CK1δ is able to phosphorylate tau441. Therefore, full-length human N-terminal 6xHis-tagged tau441 encoded on pET28a(+) (purchased from Biomartik (Kitchener, ON, Canada)) was recombinantly expressed in *E. coli*, purified via immobilized metal affinity chromatography and subsequently phosphorylated by human recombinant CK1δ *in vitro*. LC-MS/MS data generated from *in vitro* phosphorylated and trypsin-digested tau441 revealed 91.8% and 94.1% sequence coverage of non-phosphorylated tau441 and CK1δ-phosphorylated tau441, respectively, based on the amino acid sequence of the longest human tau isoform tau441 (UniProt: P10636-8). Additionally, MS analysis did not detect any phosphorylation of non-phosphorylated tau441. In total, we detected phosphopeptides corresponding to ten different phosphorylation sites (Figure 2A; Table 1). In the majority of cases, precise phosphorylation sites could be identified. A clear identification was not possible for the residues Thr414 and Ser416, which belong to a phosphopeptide sequence containing four closely spaced potential CK1-specific phosphorylation sites (Ser412, Ser413, Thr414 and Ser416).

Most of the phosphorylation sites, which could be detected in our study, were recently identified by Hanger et al. (2007). Additionally, we found two phosphorylation sites, Ser324 and Thr427, that have not been identified so far. However, we did not detect CK1δ-mediated phosphorylation of Thr17, Ser46/Thr50, Thr95, Thr101/Thr102, Ser113, Ser131, Thr149, Thr169, Ser184, Ser208, Ser210/Thr212, Ser237/Ser238, Ser241, Ser258, Ser262, Thr263, Ser285, Ser341, Ser352/Ser356/Thr361, Thr373, Ser412/Ser413, Ser433, and Ser435, which were recently identified by using LC-MS/MS (Hanger et al., 2007). Of the ten phosphorylation sites, which we detected by LC-MS/MS analysis, five were located within the MT-binding domain, which plays a special role in the interaction of tau with the microtubule (Lee et al., 1989) (Figure 2A). CK1-specific consensus sequences were identified for Ser198, Ser214, Ser289, Ser324, Thr361 and Ser416 (Figure 2B). No typical CK1-specific consensus sequence was observed for Ser305, Thr386, Thr414 and Thr427. Interestingly, five out of ten CK1δ-specific phosphorylation sites (including Ser198, Ser214, Ser289, Thr414/Ser416 and Thr427) have been associated to AD in previous studies (see Table 1).

In order to support the results obtained by MS analysis, fragments of tau441 were generated. Therefore, the sequence of tau441 was divided into three shorter fragments (tau441¹⁻¹⁵⁵, tau441¹⁵⁶⁻²⁴² and tau441²⁴³⁻⁴⁴¹). Each of them contains a specific domain of tau441 (Figure 3). Phosphorylation by CK1δ has been observed for all fragments, indicating that phosphorylation sites for CK1δ are located within all domains of tau441 protein (Figure 3). Most intense phosphorylation could be observed for fragment tau441¹⁵⁶⁻²⁴², which contains the second most predicted CK1-specific phosphorylation sites on tau441 (Figure 4). MS analysis revealed that most of the phosphorylation sites are located on tau441²⁴³⁻⁴⁴¹, which cannot be supported by the findings obtained from the *in vitro* kinase assay measuring the transfer of radioactively labeled phosphate.

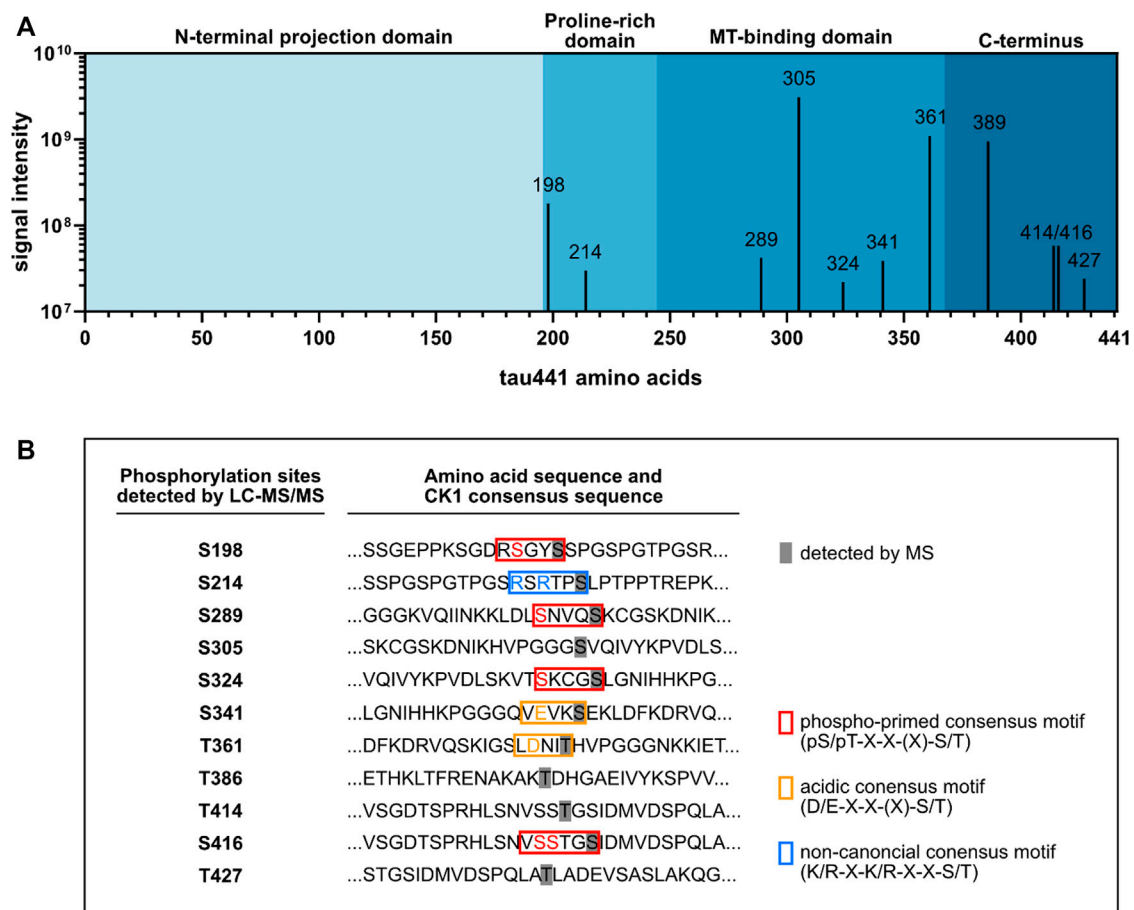


FIGURE 2 | LC-MS/MS analysis identified ten tau441 phosphorylation sites targeted by CK1δ. Tau441 was recombinantly produced and used for *in vitro* phosphorylation by CK1δ. Phosphorylated tau441 was digested with trypsin and analyzed by LC-MS/MS. **(A)** Results of the LC-MS/MS analysis identified ten tau441 phosphorylation sites targeted by CK1δ mainly located in the MT-binding domain and the C-terminus of tau441. **(B)** Sequences of tau including the detected phosphorylation sites. Detected phosphorylation sites are covered in grey. Phospho-primed, acidic or non-canonical consensus motifs of CK1 are marked in red, orange and blue, respectively.

TABLE 1 | LC-MS/MS analysis of tau441 *in vitro* phosphorylated by CK1δ. Tau441 was recombinantly expressed in *E. coli* and purified. Subsequently, tau441 was phosphorylated by CK1δ *in vitro*, digested with trypsin and analyzed by LC-MS/MS. Positions of the identified phosphorylation sites within tau441 (indicated with **p**) as well as phosphorylation probability data are shown.

Site position	Probability [%]	Modified sequence	CK1δ intensity	AD association
S198	100	SGY p SPGSPGTPGSR	1.8*10 ⁸	yes (Morishima-Kawashima et al., 1995b; Hanger et al., 1998)
S214	100	TP p SLPTPTREP	3.0*10 ⁷	yes (Hanger et al., 1998; Kinoshita et al., 2006)
S289	100	KLDLSNV p SK	4.2*10 ⁷	yes (Hanger et al., 2007)
S305	100	HVPGGG p SVQIVYKPDLSK	3.1*10 ⁹	no
S324	100	CG p SLGNIHHKPGGGQVEVK	2.2*10 ⁷	no
S341	100	P SEKLDKDR	3.9*10 ⁷	no
T361	100	IGSLDN p THVPGGGNK	1.1*10 ⁹	no
T386	100	AK p TDHGAIEIVYK	9.5*10 ⁸	no
S416/T414	60.5/34.3	HLSNVSS p T p GSIDMVDSPQLATLADEVASLAK	5.8*10 ⁷	yes/yes (Hanger et al., 2007)
T427	67.7	HLSNVSS p TGSIDMVDSPQLA p TLADEVASLAK	2.4*10 ⁷	yes (Hanger et al., 2007)

After MS analysis and *in vitro* kinase assays, two-dimensional phosphopeptide analyses were performed to confirm the results obtained from the previous experiments. Due to technical limitations, it was not possible to fully separate the protein band

of tau441 from that of CK1δ by SDS-PAGE. However, by performing phosphopeptide analysis also with CK1δ alone, phosphopeptides corresponding to the autophosphorylated kinase could be clearly identified (see **Supplementary Figure S1**,

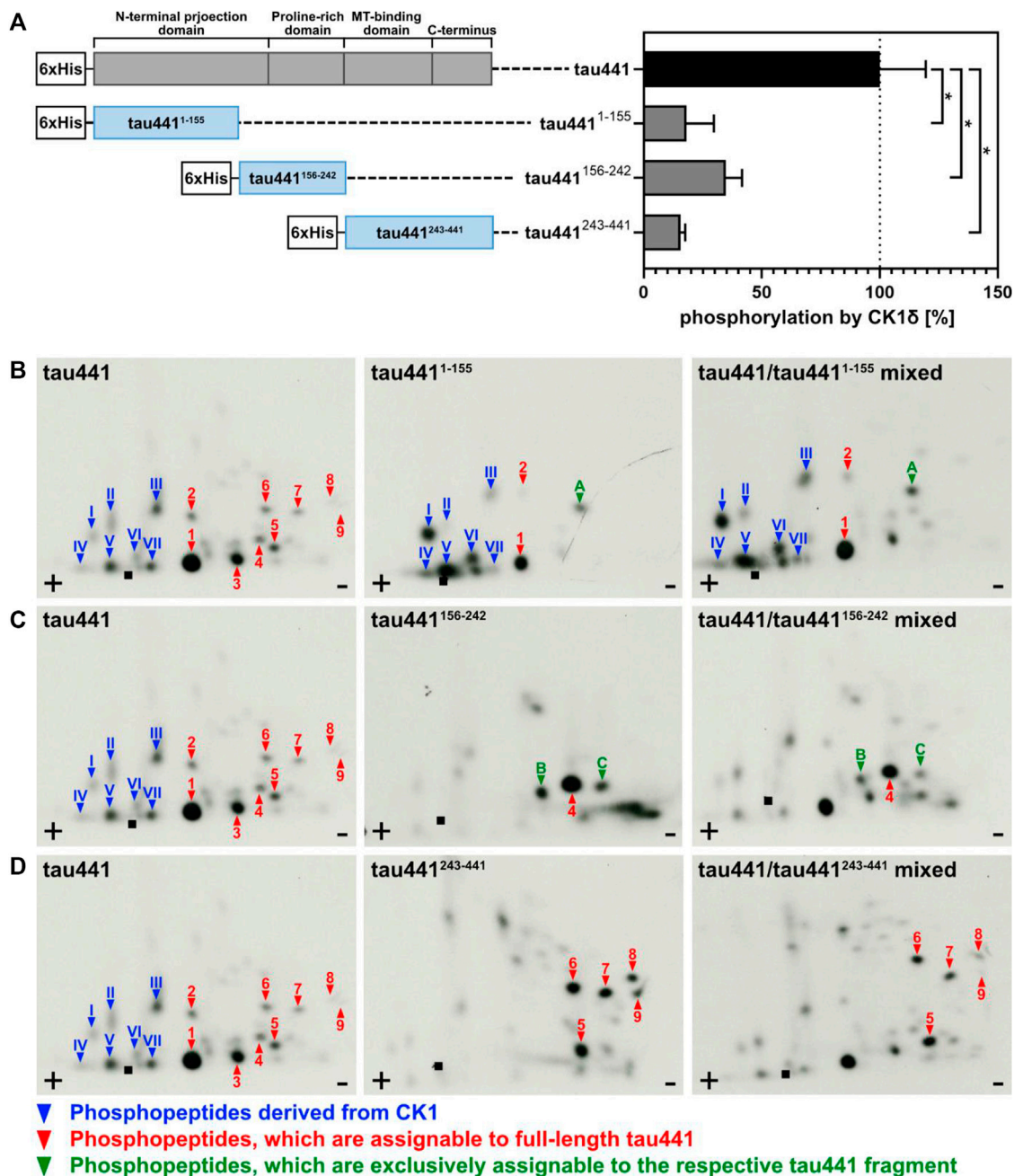


FIGURE 3 | Tau441 and tau441 fragments are phosphorylated by CK1δ *in vitro*. Tau441 as well as tau441¹⁻¹⁵⁵, tau441¹⁵⁶⁻²⁴² and tau441²⁴³⁻⁴⁴¹ fragments were phosphorylated by CK1δ *in vitro*. **(A)** After separation of phosphorylated proteins by SDS-PAGE followed by Coomassie staining, determination of phosphate incorporation into the different tau proteins was performed by Cerenkov counting. Data is shown as mean values of the experiments performed in triplicates and error bars represent the standard deviation. Data was normalized to full-length tau441. Statistical significance was tested using the nonparametric Mann-Whitney U test. * indicates $p \leq 0.05$. MT: microtubule. Full-length tau441 as well as **(B)** tau441¹⁻¹⁵⁵, **(C)** tau441¹⁵⁶⁻²⁴² and **(D)** tau441²⁴³⁻⁴⁴¹ were phosphorylated by CK1δ *in vitro*, processed and analyzed by two-dimensional phosphopeptide analysis. Arabic numerals indicate major phosphorylated peptides, which can be assigned to full-length tau441. Phosphopeptides, that are exclusively phosphorylated in the respective tau441 fragment are indicated with letters. Roman numerals indicated phosphopeptides that correspond to autophosphorylated CK1δ. ■: loading point of samples, +: anode, -: cathode.

roman numerals). Two major phosphopeptides and one additional phosphopeptide, which cannot be allocated to full-length tau441, were visible in the autoradiograph of tau441¹⁻¹⁵⁵ (peptides 1, 2 and A in **Figure 3B**). The autoradiograph of tau441¹⁵⁶⁻²⁴² showed only

one major full-length tau441-associated phosphopeptide and two additional phosphopeptides, which are exclusively phosphorylated in the fragment (peptides 4, B and C in **Figure 3C**). The phosphorylation pattern of tau441²⁴³⁻⁴⁴¹ showed most major

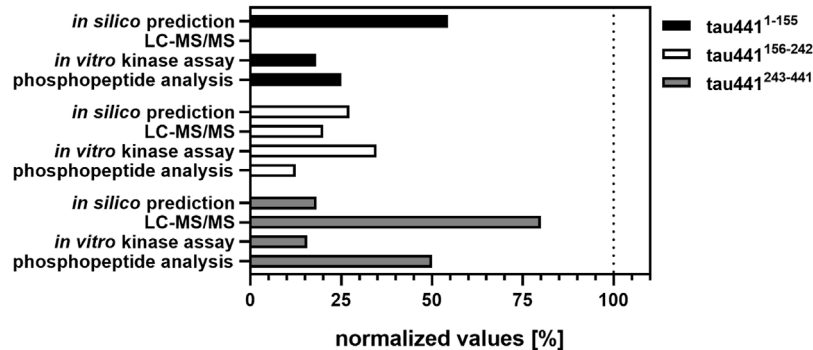


FIGURE 4 | Overview of the results obtained from *in silico* prediction, LC-MS/MS analysis, *in vitro* kinase assays and phosphopeptide analysis. Amount of the identified phosphorylation sites (*in silico* prediction of CK1-specific phosphorylation sites by ScanSite 4.0 at low stringency according to Krüger et al. (2021) and LC-MS/MS analysis) or phosphopeptides (visualized by phosphopeptide analysis) were normalized to the total amount of phosphorylation sites or phosphopeptides detected by the respective method. Data of the *in vitro* kinase assays is shown as mean values of the experiments performed in triplicates and was normalized to full-length tau441.

peptide signals that could be assigned to full-length tau441 (peptides 5 to 9 in **Figure 3D**).

In sum, data obtained from MS analysis and classical biochemical approaches provide evidence that CK1δ is able to phosphorylate tau441 at several different phosphorylation sites. Interestingly, the distribution of *in silico* predicted CK1-specific phosphorylation sites on tau441 could be verified by *in vitro* kinase assays especially for tau441¹⁵⁶⁻²⁴² and tau441²⁴³⁻⁴⁴¹ (**Figure 4**). In contrast to that, data obtained from MS analysis clearly supported the results of the phosphopeptide analysis. In conclusion, most CK1δ-specific phosphorylation sites on tau441 are located within its MT-binding and the C-terminal domain, both located on fragment tau441²⁴³⁻⁴⁴¹. To prove this right, we performed *in vitro* kinase assays and phosphopeptide analysis with tau441 phosphomutants in combination with cell-based assays, which together provide enough information about specific phosphorylation sites within the domains.

CK1δ Targets AD-Associated Phosphorylation Sites on Tau

To validate potential AD-associated phosphorylation sites predicted by the consensus motif via Scansite 4.0 or identified by MS analysis, six tau441 phosphomutants encompassing amino acids 68–71, 198–205, 212–220, 289, 409–416, and 422–427 were designed and generated by using primers given in **Supplementary Table S1**. Equal amounts of wild type tau441 and tau441 phosphomutants were then subjected to *in vitro* phosphorylation by CK1δ and phosphate incorporation was quantified. Mutation of Ser68/Thr69/Thr71, Thr212/Ser214/Thr217/Thr220, Ser289 as well as Ser409/Ser412/Ser413/Thr414/Ser416 showed major reduction of CK1δ-mediated phosphorylation by 18%, 16%, 39%, and 22% compared to wild type tau441 (see **Figure 5A**). Only minor reduction in phosphorylation was observed for Ser198/Ser199/Ser202/Thr205 and Ser422/Thr427 with 65 % and 58% compared to wild type tau441.

In addition, the significance of these results was further confirmed by phosphopeptide analysis using tau441 (wild

type) and corresponding phosphomutants tau441^{S68A+T69A+T71A}, tau441^{S198A+S199A+S202A+T205A}, tau441^{T212A+S214A+T217A+T220A}, tau441^{S289A}, tau441^{S409A+S412A+S413A+T414A+S416A} and tau441^{S422A+T427A}. As expected from *in silico* prediction (**Figure 1A**), one phosphopeptide (peptide 2) is missing in the phosphopeptide analysis of tau441^{S68A+T69A+T71A} compared to wild type tau441 (**Figure 5B**). Additionally, phosphopeptide analysis of tau441^{S289A} showed changes in the phosphorylation pattern concerning phosphopeptides 7 and 9, thereby confirming that Ser289 can be phosphorylated by CK1δ *in vitro* (**Figure 5C**). No new information has arisen from the phosphopeptide patterns of tau441^{S198A+S199A+S202A+T205A}, tau441^{T212A+S214A+T217A+T220A}, tau441^{S409A+S412A+S413A+T414A+S416A} and tau441^{S422A+T427A} (**Supplementary Figure S2**).

To determine whether CK1δ modulates tau phosphorylation in neurons, transduced hNPCs were differentiated for 2 weeks and treated with 1 μM PF-670462 or DMSO as vehicle control for 24 h. After cell lysis, site-specific tau phosphorylation was determined by Western blot and phospho-specific tau antibodies targeting pSer202/pThr205, pSer214 or pSer416. We observed that treatment with PF-670462 did not affect the expression of tau (**Figure 5D**). Additionally, tau phosphorylation in cells treated with PF-670462 was significantly decreased at Ser214 verifying the results obtained by MS analysis and *in vitro* kinase assay. However, CK1δ-specific inhibition by PF-670462 did not affect tau phosphorylation at Ser202/Thr205 and Ser416 (**Figure 5E**).

CK1δ Co-Localizes With tau441 in Neuronal Cells

We further explored whether tau and CK1δ are co-locating in human neuronal cells that were generated from hNPCs. By double immunofluorescence staining and confocal microscopy, the expression of tau and CK1δ was visualized in neuronal cells (**Figure 6A**). Control staining with secondary antibodies only is depicted in **Supplementary Figure S3**.

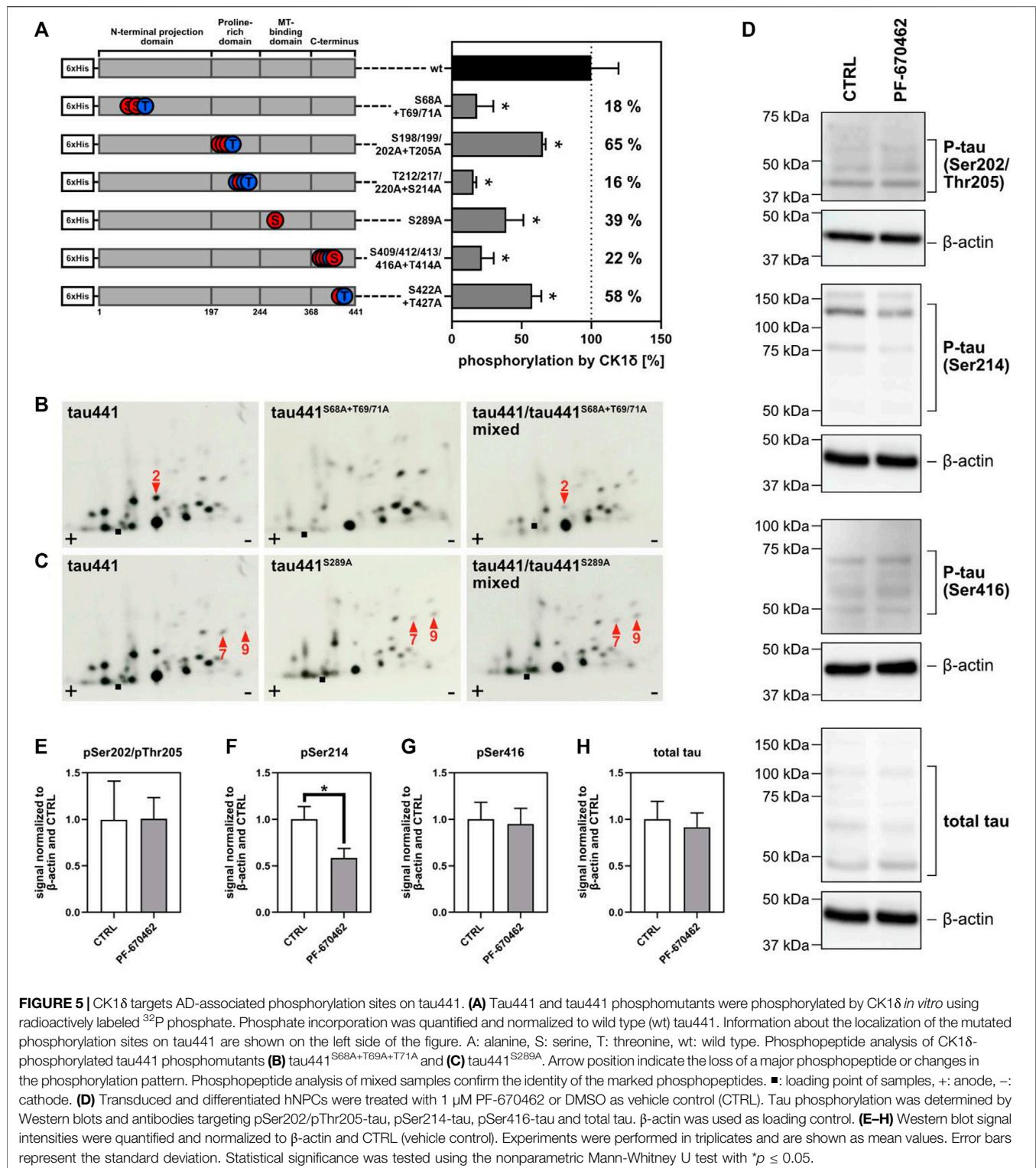


FIGURE 5 | CK1δ targets AD-associated phosphorylation sites on tau441. **(A)** Tau441 and tau441 phosphomutants were phosphorylated by CK1δ *in vitro* using radioactively labeled ^{32}P phosphate. Phosphate incorporation was quantified and normalized to wild type (wt) tau441. Information about the localization of the mutated phosphorylation sites on tau441 are shown on the left side of the figure. A: alanine, S: serine, T: threonine, wt: wild type. Phosphopeptide analysis of CK1δ-phosphorylated tau441 phosphomutants **(B)** tau441^{S68A+T69/71A} and **(C)** tau441^{S289A}. Arrow position indicate the loss of a major phosphopeptide or changes in the phosphorylation pattern. Phosphopeptide analysis of mixed samples confirm the identity of the marked phosphopeptides. ■: loading point of samples, +: anode, -: cathode. **(D)** Transduced and differentiated hNPCs were treated with 1 μM PF-670462 or DMSO as vehicle control (CTRL). Tau phosphorylation was determined by Western blots and antibodies targeting pSer202/pThr205-tau, pSer214-tau, pSer416-tau and total tau. β-actin was used as loading control. **(E-H)** Western blot signal intensities were quantified and normalized to β-actin and CTRL (vehicle control). Experiments were performed in triplicates and are shown as mean values. Error bars represent the standard deviation. Statistical significance was tested using the nonparametric Mann-Whitney U test with * $p \leq 0.05$.

Neuronal differentiation level was verified by immunofluorescence staining of the neuron-specific marker MAP2 shown in **Figure 6B**. Analysis of PCC and MOC was performed to determine the subcellular co-localization of CK1δ with tau **Figures 6C-G**.

As shown in **Figure 6A**, immunofluorescence staining of tau as well as CK1δ revealed a variety of subcellular localizations. A clear staining pattern for both proteins was especially observed around the nuclei and in the cell body. Co-localization was determined by performing PCC and MOC

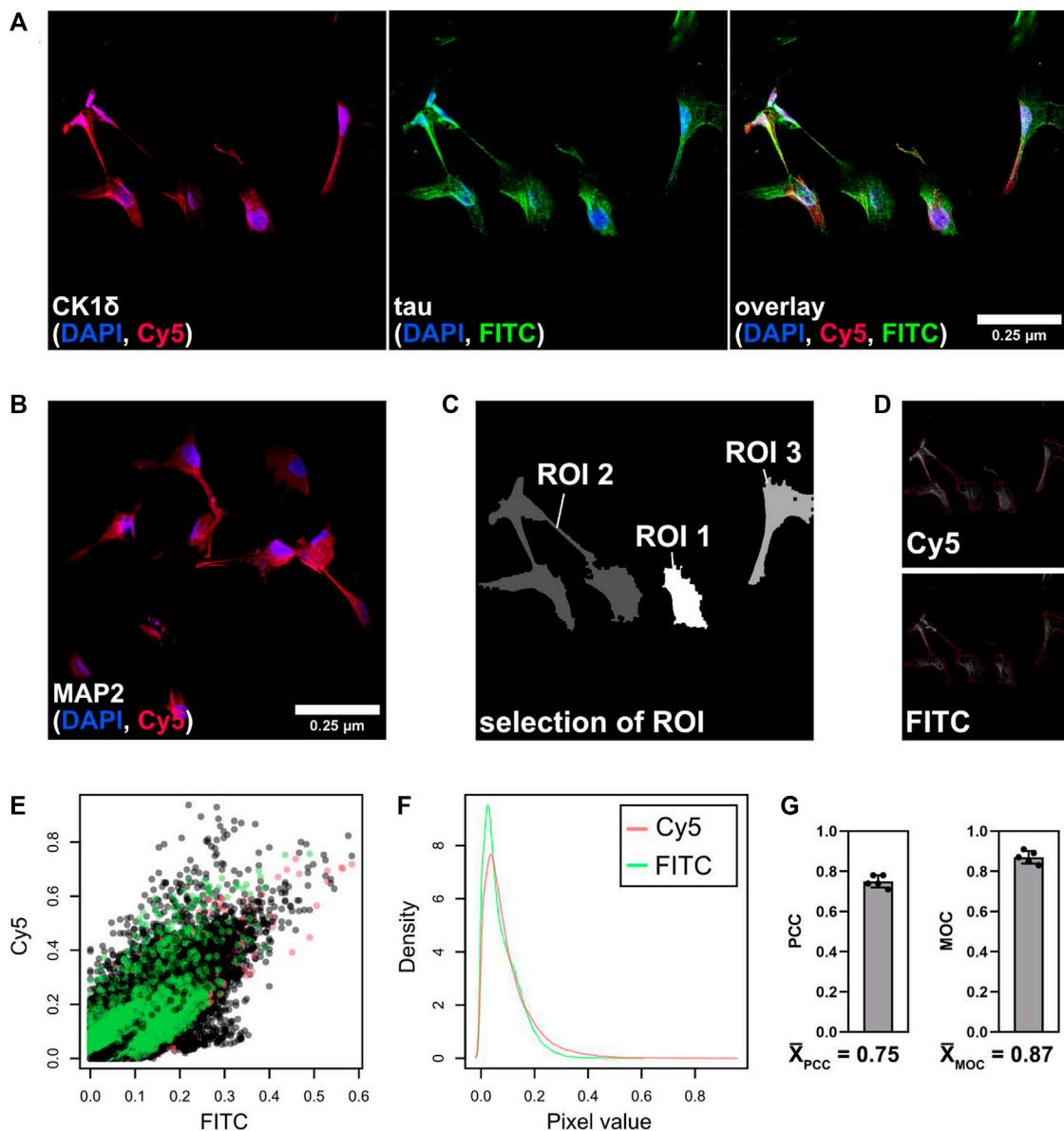


FIGURE 6 | Co-localization of tau and CK1δ in neuronal cells. Immunofluorescence was performed with differentiated human neuronal cells. **(A)** Cells were fixed and stained with DAPI (blue, nuclei), anti-CK1δ goat antibody/Alexa Fluor 647 anti-goat antibody (Cy5/red, CK1δ) and anti-tau mouse antibody/DyLight 488 anti-mouse antibody (FITC/green, tau). **(B)** Differentiation level was examined by staining of neuron-specific marker MAP2. Images were taken at ×63 magnification using the Leica SP8 confocal microscope (Leica Mikrosysteme Vertrieb GmbH, Wetzlar, Germany). Scale bar: 0.25 μm. **(C,D)** Merged images were processed and analyzed using R according to Ahmed et al. (2019). **(C)** Low-resolution image (pixel set) of the merged image with selected ROIs. **(D)** Selected ROIs are highlighted (red line) within both channels (Cy5, FITC). **(E)** Raw pixel intensities of both channels (Cy5, FITC) from three selected regions (shown in black, green, and red). **(F)** Density of the pixel values of both channels (Cy5 (red) and FITC (green)) from summarized ROIs. **(G)** Analysis of PCC and MOC according to (Ahmed et al., 2019) ($n = 5$). Values are given as mean and error bars represent the standard deviation. MOC: Mander's overlap coefficient, PCC: Pearson's correlation coefficient, ROI: region of interest.

analysis using R (Figures 6C–G). Co-localization analyses gave a PCC of 75% (0.75) and a MOC of 87% (0.87) for the overlay of CK1δ (Cy5) with tau (FITC) (Figure 6G) indicating a strong co-localization of CK1δ and tau in differentiated neuronal cells.

CK1δ-Mediated Phosphorylation has an Impact on Tau Aggregation

Hyperphosphorylation of tau by various kinases leads to the aggregation of tau into PHFs causing NFT formation and neuronal cell death in AD. We therefore considered the

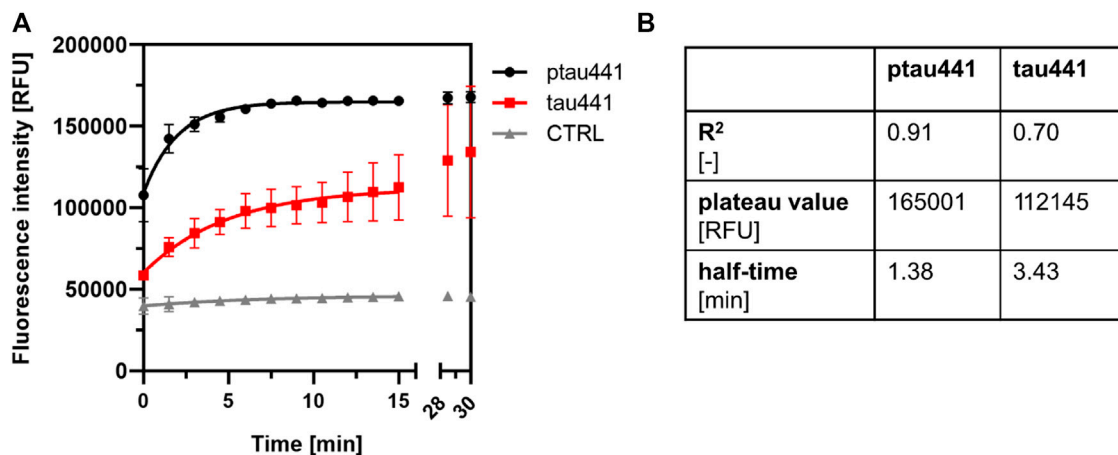


FIGURE 7 | CK1δ-mediated phosphorylation is linked to tau aggregation. **(A)** Tau aggregation assay was performed with CK1δ-phosphorylated tau441 (ptau441) and non-phosphorylated tau441 (tau441). Control reaction (CTRL) was performed with standard reaction mix without protein. Tau aggregation was measured by the ThS assay at 480 nm. Shown are the mean values of the triplicates and the error bars of the standard deviation. Data were fit to one-phase association exponential model within the first 15 min. **(B)** Amount of formed aggregates and velocity of aggregation was calculated as plateau value [RFU] and half-time [min]. CTRL: control reaction, ptau441: CK1δ-phosphorylated tau441, RFU: relative fluorescence units, tau441: non-phosphorylated tau441.

possibility that CK1δ enhances tau aggregation by phosphorylating tau at AD-associated phosphorylation sites.

Tau aggregation assay was performed with CK1δ-phosphorylated and non-phosphorylated tau441. Standard reaction mix without protein served as a negative control. The tau aggregation kinetics was strongly affected by the phosphorylation of CK1δ (Figure 7A). Phosphorylation by CK1δ highly increased the formation of tau441 aggregations (correlating with an increased plateau value) as well as the aggregation velocity (correlating with a decreased half-time of the aggregation kinetics) (Figure 7B).

DISCUSSION

Hyperphosphorylation of tau leads to the formation of PHF and can only be achieved by the activities of various kinases. A wide range of kinases have been found to phosphorylate tau and contribute to this pathophysiological hallmark of AD (Grundke-Iqbal et al., 1986; Kosik et al., 1986; Brion et al., 1991). Here, our data strongly support previous findings that CK1δ is one of the kinases specifically phosphorylating tau441 at several AD-associated residues. Furthermore, we show that CK1δ and tau are co-localized in neuronal cells and that CK1δ-mediated phosphorylation affects tau aggregation.

Initially, site-specific phosphorylation of tau441 was predicted for CK1 canonical consensus motifs using ScanSite 4.0 revealing ten potential phosphorylation sites. Complementary information was obtained via MS analysis resulting in ten potential CK1δ-specific phosphorylation sites. Classical biochemical methods (such as *in vitro* kinase assays and two-dimensional phosphopeptide analysis) revealed that CK1δ prefers to phosphorylate tau441 within the MT-binding and C-terminal domain (aa 244-441) as well as the proline-rich domain (aa 197-

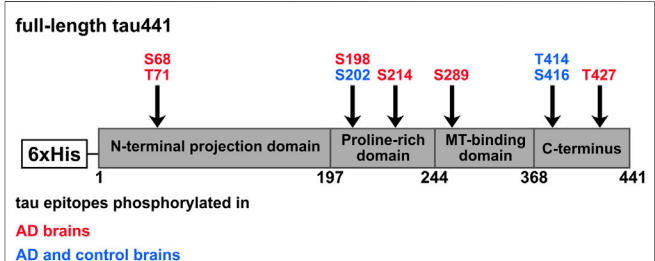


FIGURE 8 | Potential CK1δ-specific phosphorylation sites on tau protein. Tau441 phosphorylation sites were predicted *in silico* or detected experimentally via MS analysis, *in vitro* kinase assay or phosphopeptide analysis. Shown are CK1-specific phosphorylation sites, which were predicted/identified with at least two methods. Red: Tau epitopes phosphorylated in AD brain. Blue: Tau epitopes phosphorylated in AD and control brains.

244), which is in line with the findings of several other studies, demonstrating that most of the known AD-associated phosphorylation sites are located within the central region (172-251) and the C-terminal region (aa 368-441) (Liu et al., 2007; Rudrabhatla et al., 2011; Noble et al., 2013).

Combined results of *in silico* approaches and MS analysis showed that CK1δ specifically phosphorylates the AD-associated phosphorylation sites Ser68, Thr71, Ser198, Ser214, Ser289, Thr414/Ser416 and Thr427 (Figure 8; Table 2). Biochemical methods and Western blot analysis with phospho-specific antibodies of cell lysates obtained from treatment with CK1δ-specific inhibitor were used to verify these findings. Our results demonstrate that not all predicted sites, which are included in the CK1 consensus motif suggested by Krismer et al. (2021) are phosphorylated by CK1δ *in vitro*. Additionally, several CK1δ-targeted phosphorylation sites detected by MS analysis could not

TABLE 2 | AD-associated phosphorylation sites of CK1 within tau. Results were obtained from different methods including different sources of tau as indicated. Positive identified phosphorylation sites are shown as “✓” and positive results within a tau441-phosphomutant including multiple amino acid are shown as “✓*.”

	Ser68	Thr69	Thr71	Ser198	Ser199	Ser202	Thr205	Thr212	Ser214	Thr217	Thr220	Ser289	Thr403	Ser409	Ser412	Ser413	Thr414	Ser416	Ser422	Thr427
<i>in silico</i> prediction (tau441)	✓					✓			✓				✓					✓		
MS analysis (recombinant tau441)		✓		✓								✓						✓		✓
<i>in vitro</i> kinase assay (recombinant tau441)	✓*	✓*	✓*	✓	×	✓*	✓*													
phosphopeptide analysis (recombinant tau441)	✓*				×															
Western blot (endogenous tau)	×	×	×	×	×			×	✓	×	×	×	×	×	×	×	×	×	×	×

✓: positive result, ✓*: positive result with a tau441-phosphomutant including multiple amino acid changes, x: not performed.

be confirmed in other *in vitro* experiments (Ser198, S202, Thr427) and vice versa. *In vitro* experiments based on *in vitro* kinase assays confirmed that the AD-associated phosphorylation sites Ser68 and/or Thr71 and Ser289 on tau441 are targeted by CK1δ. Although Ser68 and/or Thr71 were not detected by MS analysis, *in vitro* kinase assays and phosphopeptide analysis clearly identified these phosphorylation sites as CK1δ-specific highlighting the potential of these methods. The failure to detect these phosphorylation sites by MS analysis could have been due to difficulties in separation, the loss of phosphorylation at these residues during sample preparation or reduced peptide lengths (Liu et al., 2005; Vandermarliere et al., 2013; Solari et al., 2015). Differences between *in vitro* kinase assay and phosphopeptide analysis could be explained by technical limitations within sample preparation prior to phosphopeptide mapping. For sample preparation, we performed on-membrane digestion with trypsin, that has distinct advantages over in-gel digestion. However, we experienced a loss of some (phospho)peptides, that is probably caused by peptide precipitation and unpolymerized acrylamide cross-linked to proteins interfering tryptic digestion, that leads to inefficient tryptic peptide digestion and insufficient membrane detachment (Luque-Garcia and Neubert, 2009). Phosphorylation of Thr414/Ser416 was detected *in silico* and experimentally via MS analysis and *in vitro* kinase assays, but Ser416 could not be verified by Western blot analysis indicating no physiological relevance for the phosphorylation of Ser416 by CK1δ. However, significant physiological relevant phosphorylation by CK1δ was demonstrated for Ser214. Previous studies emphasize that the combination of results obtained from different methods is essential to reliably provide evidence for the phosphorylation of certain amino acid residues (Bischof et al., 2013; Dephoure et al., 2013; Ianes et al., 2016; Meng et al., 2016; Meng et al., 2019). Considering all methods, which were performed, it is very likely that Ser68/Thr71, Ser214 and Ser289 are targeted by CK1δ.

Ser68 and/or Thr71 are newly identified CK1δ-specific phosphorylation sites, which are tightly connected to the pathogenesis of AD. Previously, comprehensive MS analysis identified phosphorylated Ser68 and Thr71 in brain tissue isolated from patients with AD (Hanger et al., 2007). So far, only a few kinases have been identified to phosphorylate Thr69 or Thr71 including GSK3 (Hanger et al., 2009) or AMP-activated protein kinase (AMPK) (Thornton et al., 2011), respectively. Interestingly, *in vitro* phosphorylation of Thr71 was observed after combining GSK3β with CK1δ indicating a potential priming role of CK1δ for GSK3β (Hanger et al., 2007). Hyperphosphorylated tau in PHFs was reported to contain several double-site phosphorylation residues, such as Thr212/Ser214. Comparable to Ser68 and Thr71, phosphorylation of Thr212/Ser214 is absent in biopsy-derived normal tau (Matsuo et al., 1994). Phosphorylation of Ser214 is of particular interest, because its phosphorylation alone potentially leads to the disruption of microtubule binding and reduces the affinity of tau for microtubules (Illenberger et al., 1998). Phosphorylation of Ser214 was detected to be mediated by PKA (Zheng-Fischhöfer et al., 1998; Hanger et al., 2007), Akt (Ksiezak-Reding et al., 2003), CDK5, GSK3 and CK1δ (Hanger et al., 2007; Hanger et al., 2009).

Among the identified CK1δ-specific phosphorylation sites, Ser289 is located within the microtubule-binding domain of tau important for its microtubule-binding property. Phosphorylation events within this domain were associated with conformational changes of tau and its disruption from microtubules (Biernat et al., 1993; Liu et al., 2007). Other kinases, which are involved in the phosphorylation of Ser289 are checkpoint kinase (Chk)1, Chk2 (Mendoza et al., 2013) and GSK3 (Hanger et al., 2009).

In addition, we provide evidence that tau co-localizes with endogenous CK1δ in differentiated neuronal cells, which was demonstrated in double immunofluorescence staining of both proteins. Co-localization is required for the interaction of both proteins and subsequent phosphorylation. These findings support the hypothesis that CK1δ has a possible role in the modulation of tau, which is further supported by the findings that CK1 is an active physiological kinase in neuronal cells and that the expression of CK1δ is strongly increased in AD brains probably leading to severe and pathological disruption of tau-MT binding (Ghoshal et al., 1999; Yasojima et al., 2000; Hanger et al., 2007).

CK1δ phosphorylates tau at specific AD-associated residues *in vitro* and in cells, it co-localizes with tau in neuronal cells and its expression is up-regulated in the brain of patients suffering from AD (Ghoshal et al., 1999). To directly demonstrate the functional effect of CK1δ-mediated phosphorylation on tau aggregation, we performed *in vitro* tau aggregation assays with pre-phosphorylated tau441 and non-phosphorylated tau441. Tau aggregation assay is not only used to study mechanisms of tau misfolding and aggregation, but it is also a robust tool for the screening of drugs, that interfere and inhibit tau aggregation. The relevance of this assay was previously demonstrated by Pickhardt et al. (2005). In this study, anthraquinone-based small molecule inhibitors were identified in an initial drug screening for their ability to prevent tau aggregation by using the tau aggregation assay. Promising compounds were further successfully identified for their ability to prevent tau aggregation in a cell-based assay using a genetically modified neuroblastoma (N2a) cell line. By using the tau aggregation assay in our experimental set-up, a remarkable increase in the aggregation kinetics of pre-phosphorylated tau441 could be observed. In aggregated PHF-tau, several amino acid residues were shown to be phosphorylated including Ser68, Ser69, Thr71, Ser184, Ser185, Ser202, Thr205, Ser208, Ser210, Thr212, Ser214, Thr231, Ser235, Ser258, Ser262, Ser289, Thr403, Ser412, Thr414/Ser416, Ser422, Thr427, Ser433 and Ser435 (Wolozin et al., 1986; Morishima-Kawashima et al., 1995a; Zheng-Fischhöfer et al., 1998; Hanger et al., 2007; Despres et al., 2017). Within this study, several phosphorylation sites, which are associated to tau aggregation, were predicted to be phosphorylated by CK1 *in silico* (Ser68, Thr71, Ser198, Ser202, Thr403, Ser416) or experimentally identified (Ser68, Thr71, Ser214, Ser289). Results obtained from our aggregation experiments demonstrated a potential role of CK1δ in tau aggregation, which has already been shown for several other kinases including TTBK1 and Fyn (Xu et al., 2010; Briner et al.,

2020). In a bi-transgenic mouse model (overexpressing TTBK1 and P301L tau mutant) enhanced tau phosphorylation at Ser202/Thr205, Ser262/Ser356, Ser396/Ser404, Ser422 was observed leading to increased accumulation of tau aggregates (Xu et al., 2010). TTBK1 is known to be a neuron-specific kinase that regulates tau phosphorylation. Interestingly, TTBK1 shares high homology and characteristics with CK1δ explaining why both kinases are assigned to the CK1 family within the phylogenetic kinase tree (Liachko et al., 2014).

In summary, we clearly identified AD-associated tau phosphorylation sites, which can be targeted by CK1δ. Furthermore, we demonstrated that CK1δ co-localizes with tau in differentiated neuronal cells. For the first time, we provide experimental proof that CK1δ-mediated phosphorylation plays an important role at least in the *in vitro* aggregation of tau. Therefore, our findings clearly support the assumption that CK1δ has an essential role in tau hyperphosphorylation and the pathogenesis of AD.

DATA AVAILABILITY STATEMENT

The original contributions presented in the study are included in the article/**Supplementary Material**, further inquiries can be directed to the corresponding author.

AUTHOR CONTRIBUTIONS

AR, UK, and JB conceived and designed the experiments. AR, AS, and MO performed the experiments. AR and AS analyzed the data. AR, FG, UK, and JB wrote the paper. All authors contributed to the article and approved the submitted version.

FUNDING

This work as well as the APC were supported by a grant from the Else Kröner-Fresenius-Stiftung awarded to JB (grant number 2017_A142) and the German Research Foundation (DFG) awarded to UK (grant number KN356/9-1). AR is a participating member of the International Graduate School in Molecular Medicine at Ulm University, which is supported by the DFG (grant number GSC 270). The sponsors had no influence on study design, on collection, analysis, and interpretation of data, on the writing of the report, and on the decision to submit the article for publication.

ACKNOWLEDGMENTS

The authors would like to thank Dr. Ana Velic (Proteome Center Tübingen, Interfaculty Institute for Cell Biology, University of Tübingen, Tübingen, Germany) for the performed mass spectrometric analyses. The authors also thank Dr. Federica Diefano and Dr. Bernd Gahr (Molecular Cardiology, Internal

Medicine II, Ulm University Hospital, Ulm, Germany) for the opportunity to use the confocal microscope for the co-localization experiment. Finally, we thank Prof. Dr. Doo Kim from the Massachusetts General Hospital (Harvard Medical School, Charlestown) for providing the lentiviral expression vectors.

REFERENCES

- Ahmed, M., Lai, T. H., and Kim, D. R. (2019). Colocr: an R Package for Conducting Co-localization Analysis on Fluorescence Microscopy Images. *PeerJ* 7, e7255. doi:10.7717/peerj.7255
- Anand, R., Gill, K. D., and Mahdi, A. A. (2014). Therapeutics of Alzheimer's Disease: Past, Present and Future. *Neuropharmacology* 76, 27–50. doi:10.1016/j.neuropharm.2013.07.004
- Barghorn, S., Biernat, J., and Mandelkow, E. (2005). Purification of Recombinant Tau Protein and Preparation of Alzheimer-Paired Helical Filaments *In Vitro*. *Methods Mol. Biol.* 299, 035–052. doi:10.1385/1-59259-874-9:035
- Barthelmé, S., and Tschumperl, D. (2019). Imager: an R Package for Image Processing Based on CImg. *JOSS* 4, 1012. doi:10.21105/joss.01012
- Biernat, J., Gustke, N., Drewes, G., Mandelkow, E., and Mandelkow, E. (1993). Phosphorylation of Ser262 Strongly Reduces Binding of Tau to Microtubules: Distinction between PHF-like Immunoreactivity and Microtubule Binding. *Neuron* 11, 153–163. doi:10.1016/0896-6273(93)90279-z
- Binder, L. I., Frankfurter, A., and Rebhun, L. I. (1985). The Distribution of Tau in the Mammalian Central Nervous System. *J. Cell Biol.* 101, 1371–1378. doi:10.1083/jcb.101.4.1371
- Bischof, J., Randoll, S.-J., Süßner, N., Henne-Bruns, D., Pinna, L. A., and Knippschild, U. (2013). CK1δ Kinase Activity Is Modulated by Chk1-Mediated Phosphorylation. *PLoS One* 8, e68803. doi:10.1371/journal.pone.0068803
- Borchert, N., Dieterich, C., Krug, K., Schütz, W., Jung, S., Nordheim, A., et al. (2010). Proteogenomics of *Pristionchus pacificus* Reveals Distinct Proteome Structure of Nematode Models. *Genome Res.* 20, 837–846. doi:10.1101/gr.103119.109
- Briner, A., Götz, J., and Polanco, J. C. (2020). Fyn Kinase Controls Tau Aggregation *In Vivo*. *Cell Rep.* 32, 108045. doi:10.1016/j.celrep.2020.108045
- Brion, J. P., Hanger, D. P., Couck, A. M., and Anderton, B. H. (1991). A68 Proteins in Alzheimer's Disease Are Composed of Several Tau Isoforms in a Phosphorylated State Which Affects Their Electrophoretic Mobilities. *Biochem. J.* 279 (Pt 3), 831–836. doi:10.1042/bj2790831
- Buée, L., Bussiére, T., Buée-Scherrer, V., Delacourte, A., and Hof, P. R. (2000). Tau Protein Isoforms, Phosphorylation and Role in Neurodegenerative disorders. These Authors Contributed Equally to This Work. *Brain Res. Rev.* 33, 95–130. doi:10.1016/s0165-0173(00)00019-9
- Cheong, J. K., and Virshup, D. M. (2011). Casein Kinase 1: Complexity in the Family. *Int. J. Biochem. Cell Biol.* 43, 465–469. doi:10.1016/j.biocel.2010.12.004
- Chirita, C. N., Congdon, E. E., Yin, H., and Kuret, J. (2005). Triggers of Full-Length Tau Aggregation: a Role for Partially Folded Intermediates. *Biochemistry* 44, 5862–5872. doi:10.1021/bi0500123
- Choi, S. H., Kim, Y. H., Hebisch, M., Sliwinski, C., Lee, S., D'Avanzo, C., et al. (2014). A Three-Dimensional Human Neural Cell Culture Model of Alzheimer's Disease. *Nature* 515, 274–278. doi:10.1038/nature13800
- Cox, J., and Mann, M. (2008). MaxQuant Enables High Peptide Identification Rates, Individualized p.p.b.-range Mass Accuracies and Proteome-wide Protein Quantification. *Nat. Biotechnol.* 26, 1367–1372. doi:10.1038/nbt.1511
- Cox, J., Neuhauser, N., Michalski, A., Scheltema, R. A., Olsen, J. V., and Mann, M. (2011). Andromeda: a Peptide Search Engine Integrated into the MaxQuant Environment. *J. Proteome Res.* 10, 1794–1805. doi:10.1021/pr101065j
- Dephoure, N., Gould, K. L., Gygi, S. P., and Kellogg, D. R. (2013). Mapping and Analysis of Phosphorylation Sites: a Quick Guide for Cell Biologists. *MBoC* 24, 535–542. doi:10.1091/mbc.e12-09-0677
- Derkinderen, P., Scales, T. M. E., Hanger, D. P., Leung, K.-Y., Byers, H. L., Ward, M. A., et al. (2005). Tyrosine 394 Is Phosphorylated in Alzheimer's Paired Helical Filament Tau and in Fetal Tau with C-Abl as the Candidate Tyrosine Kinase. *J. Neurosci.* 25, 6584–6593. doi:10.1523/JNEUROSCI.1487-05.2005
- Despres, C., Byrne, C., Qi, H., Cantrelle, F.-X., Huvent, I., Chambraud, B., et al. (2017). Identification of the Tau Phosphorylation Pattern that Drives its Aggregation. *Proc. Natl. Acad. Sci. U.S.A.* 114, 9080–9085. doi:10.1073/pnas.1708481114
- Ghoshal, N., Smiley, J. F., DeMaggio, A. J., Hoekstra, M. F., Cochran, E. J., Binder, L. I., et al. (1999). A New Molecular Link between the Fibrillar and Granulovacuolar Lesions of Alzheimer's Disease. *Am. J. Pathology* 155, 1163–1172. doi:10.1016/S0002-9440(10)65219-4
- Goedert, M., Spillantini, M. G., Jakes, R., Rutherford, D., and Crowther, R. A. (1989). Multiple Isoforms of Human Microtubule-Associated Protein Tau: Sequences and Localization in Neurofibrillary Tangles of Alzheimer's Disease. *Neuron* 3, 519–526. doi:10.1016/0896-6273(89)90210-9
- Grundke-Iqbal, I., Iqbal, K., Tung, Y. C., Quinlan, M., Wisniewski, H. M., and Binder, L. I. (1986). Abnormal Phosphorylation of the Microtubule-Associated Protein Tau (Tau) in Alzheimer Cytoskeletal Pathology. *Proc. Natl. Acad. Sci. U.S.A.* 83, 4913–4917. doi:10.1073/pnas.83.13.4913
- Hanger, D. P., Anderton, B. H., and Noble, W. (2009). Tau Phosphorylation: the Therapeutic Challenge for Neurodegenerative Disease. *Trends Mol. Med.* 15, 112–119. doi:10.1016/j.molmed.2009.01.003
- Hanger, D. P., Betts, J. C., Loviny, T. L. F., Blackstock, W. P., and Anderton, B. H. (1998). New Phosphorylation Sites Identified in Hyperphosphorylated Tau (Paired Helical Filament-Tau) from Alzheimer's Disease Brain Using Nanoelectrospray Mass Spectrometry. *J. Neurochem.* 71, 2465–2476. doi:10.1046/j.1471-4159.1998.71062465.x
- Hanger, D. P., Byers, H. L., Wray, S., Leung, K.-Y., Saxton, M. J., Seereeram, A., et al. (2007). Novel Phosphorylation Sites in Tau from Alzheimer Brain Support a Role for Casein Kinase 1 in Disease Pathogenesis. *J. Biol. Chem.* 282, 23645–23654. doi:10.1074/jbc.M703269200
- Ianes, C., Xu, P., Werz, N., Meng, Z., Henne-Bruns, D., Bischof, J., et al. (2016). CK1δ Activity Is Modulated by CDK2/E- and CDK5/p35-Mediated Phosphorylation. *Amino Acids* 48, 579–592. doi:10.1007/s00726-015-2114-y
- Illenberger, S., Zheng-Fischhöfer, Q., Preuss, U., Stamer, K., Baumann, K., Trinczek, B., et al. (1998). The Endogenous and Cell Cycle-dependent Phosphorylation of Tau Protein in Living Cells: Implications for Alzheimer's Disease. *MBoC* 9, 1495–1512. doi:10.1091/mbc.9.6.1495
- Kim, Y. H., Choi, S. H., D'Avanzo, C., Hebisch, M., Sliwinski, C., Bylykbashi, E., et al. (2015). A 3D Human Neural Cell Culture System for Modeling Alzheimer's Disease. *Nat. Protoc.* 10, 985–1006. doi:10.1038/nprot.2015.065
- Kimura, T., Ishiguro, K., and Hisanaga, S.-I. (2014). Physiological and Pathological Phosphorylation of Tau by Cdk5. *Front. Mol. Neurosci.* 7, 65. doi:10.3389/fnmol.2014.00065
- Kinoshita, E., Kinoshita-Kikuta, E., Takiyama, K., and Koike, T. (2006). Phosphate-binding Tag, a New Tool to Visualize Phosphorylated Proteins. *Mol. Cell. Proteomics* 5, 749–757. doi:10.1074/mcp.T500024-MCP200
- Knippschild, U., KrÄger, M., Richter, J., Xu, P., GarcÄ-a-Reyes, B., Peifer, C., et al. (2014). The CK1 Family: Contribution to Cellular Stress Response and its Role in Carcinogenesis. *Front. Oncol.* 4, 96. doi:10.3389/fonc.2014.00096
- Knippschild, U., Milne, D. M., Campbell, L. E., DeMaggio, A. J., Christenson, E., Hoekstra, M. F., et al. (1997). p53 Is Phosphorylated *In Vitro* and *In Vivo* by the Delta and Epsilon Isoforms of Casein Kinase 1 and Enhances the Level of

SUPPLEMENTARY MATERIAL

The Supplementary Material for this article can be found online at: <https://www.frontiersin.org/articles/10.3389/fmolb.2022.872171/full#supplementary-material>

- Casein Kinase 1 Delta in Response to Topoisomerase-Directed Drugs. *Oncogene* 15, 1727–1736. doi:10.1038/sj.onc.1201541
- Kosik, K. S., Joachim, C. L., and Selkoe, D. J. (1986). Microtubule-associated Protein Tau (Tau) Is a Major Antigenic Component of Paired Helical Filaments in Alzheimer Disease. *Proc. Natl. Acad. Sci. U.S.A.* 83, 4044–4048. doi:10.1073/pnas.83.11.4044
- Krismer, K., Bernwinkler, T., and Ehrenberger, T. (2021). Scan Protein for Motifs - Scansite 4. <https://scansite4.mit.edu/#scanProtein> (Accessed March 15, 2022).
- Ksiezak-Reding, H., Pyo, H. K., Feinstein, B., and Pasinetti, G. M. (2003). Akt/PKB Kinase Phosphorylates Separately Thr212 and Ser214 of Tau Protein *In Vitro*. *Biochimica Biophysica Acta (BBA) - Mol. Basis Dis.* 1639, 159–168. doi:10.1016/j.bbadis.2003.09.001
- Kumar, A., and Dogra, S. (2008). Neuropathology and Therapeutic Management of Alzheimer's Disease - an Update. *Drugs Fut.* 33, 433. doi:10.1358/dof.2008.033.05.1192677
- Kuret, J., Johnson, G. S., Cha, D., Christenson, E. R., DeMaggio, A. J., and Hoekstra, M. F. (1997). Casein Kinase 1 Is Tightly Associated with Paired-Helical Filaments Isolated from Alzheimer's Disease Brain. *J. Neurochem.* 69, 2506–2515. doi:10.1046/j.1471-4159.1997.69062506.x
- Lee, G., Neve, R. L., and Kosik, K. S. (1989). The Microtubule Binding Domain of Tau Protein. *Neuron* 2, 1615–1624. doi:10.1016/0896-6273(89)90050-0
- Lee, G., Thangavel, R., Sharma, V. M., Litersky, J. M., Bhaskar, K., Fang, S. M., et al. (2004). Phosphorylation of Tau by Fyn: Implications for Alzheimer's Disease. *J. Neurosci.* 24, 2304–2312. doi:10.1523/JNEUROSCI.4162-03.2004
- Li, G., Yin, H., and Kuret, J. (2004). Casein Kinase 1 Delta Phosphorylates Tau and Disrupts Its Binding to Microtubules. *J. Biol. Chem.* 279, 15938–15945. doi:10.1074/jbc.M314116200
- Liachko, N. F., McMillan, P. J., Strovass, T. J., Loomis, E., Greenup, L., Murrell, J. R., et al. (2014). The Tau Tubulin Kinases TTBK1/2 Promote Accumulation of Pathological TDP-43. *PLoS Genet.* 10, e1004803. doi:10.1371/journal.pgen.1004803
- Liu, F., Li, B., Tung, E.-J., Grundke-Iqbal, I., Iqbal, K., and Gong, C.-X. (2007). Site-specific Effects of Tau Phosphorylation on its Microtubule Assembly Activity and Self-Aggregation. *Eur. J. Neurosci.* 26, 3429–3436. doi:10.1111/j.1460-9568.2007.05955.x
- Liu, S., Zhang, C., Campbell, J. L., Zhang, H., Yeung, K. K.-C., Han, V. K. M., et al. (2005). Formation of Phosphopeptide-Metal Ion Complexes in Liquid Chromatography/electrospray Mass Spectrometry and Their Influence on Phosphopeptide Detection. *Rapid Commun. Mass Spectrom.* 19, 2747–2756. doi:10.1002/rcm.2105
- Llorens-Marà-tin, M. a., Jurado, J., Hernández, F. I., and Ávila, J. (2014). GSK-3β, a Pivotal Kinase in Alzheimer Disease. *Front. Mol. Neurosci.* 7, 46. doi:10.3389/fnmol.2014.00046
- Luque-Garcia, J. L., and Neubert, T. A. (2009). On-membrane Tryptic Digestion of Proteins for Mass Spectrometry Analysis. *Methods Mol. Biol.* 536, 331–341. doi:10.1007/978-1-59745-542-8_35
- Matenia, D., and Mandelkow, E.-M. (2009). The Tau of MARK: a Polarized View of the Cytoskeleton. *Trends Biochem. Sci.* 34, 332–342. doi:10.1016/j.tibs.2009.03.008
- Matsuo, E. S., Shin, R.-W., Billingsley, M. L., van de Voorde, A., O'Connor, M., Trojanowski, J. Q., et al. (1994). Biopsy-derived Adult Human Brain Tau Is Phosphorylated at Many of the Same Sites as Alzheimer's Disease Paired Helical Filament Tau. *Neuron* 13, 989–1002. doi:10.1016/0896-6273(94)90264-X
- Mendoza, J., Sekiya, M., Taniguchi, T., Iijima, K. M., Wang, R., and Ando, K. (2013). Global Analysis of Phosphorylation of Tau by the Checkpoint Kinases Chk1 and Chk2 *In Vitro*. *J. Proteome Res.* 12, 2654–2665. doi:10.1021/pr400008f
- Meng, Z., Bischof, J., Ianes, C., Henne-Bruns, D., Xu, P., and Knippschild, U. (2016). CK1δ Kinase Activity Is Modulated by Protein Kinase C α (PKCα)-Mediated Site-specific Phosphorylation. *Amino Acids* 48, 1185–1197. doi:10.1007/s00726-015-2154-3
- Meng, Z., Böhm, T., Xu, P., Henne-Bruns, D., Peifer, C., Witt, L., et al. (2019). Kinase Activity of Casein Kinase 1 Delta (CK1δ) Is Modulated by Protein Kinase C α (PKCα) by Site-specific Phosphorylation within the Kinase Domain of CK1δ. *Biochimica Biophysica Acta (BBA) - Proteins Proteomics* 1867, 710–721. doi:10.1016/j.bbapap.2019.05.004
- Morishima-Kawashima, M., Hasegawa, M., Takio, K., Suzuki, M., Yoshida, H., Titani, K., et al. (1995a). Proline-directed and Non-proline-directed Phosphorylation of PHF-Tau. *J. Biol. Chem.* 270, 823–829. doi:10.1074/jbc.270.2.823
- Morishima-Kawashima, M., Hasegawa, M., Takio, K., Suzuki, M., Yoshida, H., Watanabe, A., et al. (1995b). Hyperphosphorylation of Tau in PHF. *Neurobiol. Aging* 16, 365–371. doi:10.1016/0197-4580(95)00027-C
- Noble, W., Hanger, D. P., Miller, C. C. J., and Lovestone, S. (2013). The Importance of Tau Phosphorylation for Neurodegenerative Diseases. *Front. Neurol.* 4, 83. doi:10.3389/fneur.2013.00083
- Pickhardt, M., Gazova, Z., von Bergen, M., Khlistunova, I., Wang, Y., Hascher, A., et al. (2005). Anthraquinones Inhibit Tau Aggregation and Dissolve Alzheimer's Paired Helical Filaments *In Vitro* and in Cells. *J. Biol. Chem.* 280, 3628–3635. doi:10.1074/jbc.M410984200
- Rappsilber, J., Mann, M., and Ishihama, Y. (2007). Protocol for Micro-purification, Enrichment, Pre-fractionation and Storage of Peptides for Proteomics Using StageTips. *Nat. Protoc.* 2, 1896–1906. doi:10.1038/nprot.2007.261
- Roth, A., Gärtner, F., Mayer, K., Beyrle, J., König, I., Knippschild, U., et al. (2021a). CK1δ-Derived Peptides as Novel Tools Inhibiting the Interactions between CK1δ and APP695 to Modulate the Pathogenic Metabolism of APP. *Ijms* 22, 6423. doi:10.3390/ijms22126423
- Roth, A., Gihring, A., Göser, F., Peifer, C., Knippschild, U., and Bischof, J. (2021b). Assessing the Inhibitory Potential of Kinase Inhibitors *In Vitro*: Major Pitfalls and Suggestions for Improving Comparability of Data Using CK1 Inhibitors as an Example. *Molecules* 26, 4898. doi:10.3390/molecules26164898
- Rudrabhatla, P., Jaffe, H., and Pant, H. C. (2011). Direct Evidence of Phosphorylated Neuronal Intermediate Filament Proteins in Neurofibrillary Tangles (NFTs): Phosphoproteomics of Alzheimer's NFTs. *FASEB J.* 25, 3896–3905. doi:10.1096/fj.11-181297
- Schmitt, M., Sinnberg, T., Nalpas, N. C., Maass, A., Schitteck, B., and Macek, B. (2019). Quantitative Proteomics Links the Intermediate Filament Nestin to Resistance to Targeted BRAF Inhibition in Melanoma Cells. *Mol. Cell. Proteomics* 18, 1096–1109. doi:10.1074/mcp.RA119.001302
- Schwab, C., DeMaggio, A. J., Ghoshal, N., Binder, L. I., Kuret, J., and McGeer, P. L. (2000). Casein Kinase 1 Delta Is Associated with Pathological Accumulation of Tau in Several Neurodegenerative Diseases. *Neurobiol. Aging* 21, 503–510. doi:10.1016/s0197-4580(00)00110-x
- Solari, F. A., Dell'Aica, M., Sickmann, A., and Zahedi, R. P. (2015). Why Phosphoproteomics Is Still a Challenge. *Mol. Biosyst.* 11, 1487–1493. doi:10.1039/C5MB00024F
- Stöter, M., Krüger, M., Banting, G., Henne-Bruns, D., and Knippschild, U. (2014). Microtubules Depolymerization Caused by the CK1 Inhibitor IC261 May Be Not Mediated by CK1 Blockage. *PLoS One* 9, e100090. doi:10.1371/journal.pone.0100090
- Thornton, C., Bright, N. J., Sastre, M., Muckett, P. J., and Carling, D. (2011). AMP-activated Protein Kinase (AMPK) Is a Tau Kinase, Activated in Response to Amyloid β-peptide Exposure. *Biochem. J.* 434, 503–512. doi:10.1042/BJ20101485
- Tomizawa, K., Omori, A., Ohtake, A., Sato, K., and Takahashi, M. (2001). Tau-tubulin Kinase Phosphorylates Tau at Ser-208 and Ser-210, Sites Found in Paired Helical Filament-Tau. *FEBS Lett.* 492, 221–227. doi:10.1016/S0014-5793(01)02256-6
- van der Geer, P., and Hunter, T. (1994). Phosphopeptide Mapping and Phosphoamino Acid Analysis by Electrophoresis and Chromatography on Thin-Layer Cellulose Plates. *Electrophoresis* 15, 544–554. doi:10.1002/elps.1150150173
- Vandermarliere, E., Mueller, M., and Martens, L. (2013). Getting Intimate with Trypsin, the Leading Protease in Proteomics. *Mass Spec. Rev.* 32, 453–465. doi:10.1002/mas.21376
- Weingarten, M. D., Lockwood, A. H., Hwo, S. Y., and Kirschner, M. W. (1975). A Protein Factor Essential for Microtubule Assembly. *Proc. Natl. Acad. Sci. U.S.A.* 72, 1858–1862. doi:10.1073/pnas.72.5.1858
- Wolozin, B. L., Pruchnicki, A., Dickson, D. W., and Davies, P. (1986). A Neuronal Antigen in the Brains of Alzheimer Patients. *Science* 232, 648–650. doi:10.1126/science.3083509
- Xian, J., Bu, F., Wang, Y., Long, F., Zhang, Z., Wu, C., et al. (2021). A Rationale for Drug Design provided by Co-Crystal Structure of IC261 in Complex with Tubulin. *Molecules* 26, 946. doi:10.3390/molecules26040946
- Xu, J., Sato, S., Okuyama, S., Swan, R. J., Jacobsen, M. T., Strunk, E., et al. (2010). Tau-tubulin Kinase 1 Enhances Prefibrillar Tau Aggregation and Motor Neuron Degeneration in P301L FTDP-17 Tau-mutant Mice. *FASEB J.* 24, 2904–2915. doi:10.1096/fj.09-150144

- Yasojima, K., Kuret, J., DeMaggio, A. J., McGeer, E., and McGeer, P. L. (2000). Casein Kinase 1 Delta mRNA Is Upregulated in Alzheimer Disease Brain. *Brain Res.* 865, 116–120. doi:10.1016/s0006-8993(00)02200-9
- Zheng-Fischhöfer, Q., Biernat, J., Mandelkow, E.-M., Illenberger, S., Godemann, R., and Mandelkow, E. (1998). Sequential Phosphorylation of Tau by Glycogen Synthase Kinase-3beta and Protein Kinase A at Thr212 and Ser214 Generates the Alzheimer-specific Epitope of Antibody AT100 and Requires a Paired-helical-filament-like Conformation. *Eur. J. Biochem.* 252, 542–552. doi:10.1046/j.1432-1327.1998.2520542.x

Conflict of Interest: The authors declare that the research was conducted in the absence of any commercial or financial relationships that could be construed as a potential conflict of interest.

Publisher's Note: All claims expressed in this article are solely those of the authors and do not necessarily represent those of their affiliated organizations, or those of the publisher, the editors and the reviewers. Any product that may be evaluated in this article, or claim that may be made by its manufacturer, is not guaranteed or endorsed by the publisher.

Copyright © 2022 Roth, Sander, Oswald, Gärtner, Knippschild and Bischof. This is an open-access article distributed under the terms of the Creative Commons Attribution License (CC BY). The use, distribution or reproduction in other forums is permitted, provided the original author(s) and the copyright owner(s) are credited and that the original publication in this journal is cited, in accordance with accepted academic practice. No use, distribution or reproduction is permitted which does not comply with these terms.



CK2 β Is a Gatekeeper of Focal Adhesions Regulating Cell Spreading

Odile Filhol¹, Anne-Marie Hesse², Anne-Pascale Bouin³, Corinne Albigès-Rizo³, Florian Jeanneret¹, Christophe Battail¹, Delphine Pflieger^{2*} and Claude Cochet^{1*}

¹Univ. Grenoble Alpes, INSERM, CEA, UMR Biosanté, U1292, Grenoble, France, ²Univ. Grenoble Alpes, INSERM, CEA, UMR Biosanté U1292, CNRS FR 2048, Grenoble, France, ³Univ. Grenoble Alpes, INSERM U1209, CNRS 5309, Institute for Advanced Biosciences (IAB), Grenoble, France

OPEN ACCESS

Edited by:

Lorenzo Alberto Pinna,
National Research Council, Italy

Reviewed by:

Chungho Kim,
Korea University, South Korea
Jose R Bayascas,
Universidad Autónoma de Barcelona,
Spain

*Correspondence:

Claude Cochet
claude.cochet@cea.fr
Delphine Pflieger
delphine.pflieger@cea.fr

[†]These authors share senior
authorship

Specialty section:

This article was submitted to
Cellular Biochemistry,
a section of the journal
Frontiers in Molecular Biosciences

Received: 21 March 2022

Accepted: 02 May 2022

Published: 29 June 2022

Citation:

Filhol O, Hesse A-M, Bouin A-P,
Albigès-Rizo C, Jeanneret F, Battail C,
Pflieger D and Cochet C (2022) CK2 β
Is a Gatekeeper of Focal Adhesions
Regulating Cell Spreading.
Front. Mol. Biosci. 9:900947.
doi: 10.3389/fmolb.2022.900947

CK2 is a hetero-tetrameric serine/threonine protein kinase made up of two CK2 α/α' catalytic subunits and two CK2 β regulatory subunits. The free CK2 α subunit and the tetrameric holoenzyme have distinct substrate specificity profiles, suggesting that the spatiotemporal organization of the individual CK2 subunits observed in living cells is crucial in the control of the many cellular processes that are governed by this pleiotropic kinase. Indeed, previous studies reported that the unbalanced expression of CK2 subunits is sufficient to drive epithelial to mesenchymal transition (EMT), a process involved in cancer invasion and metastasis. Moreover, sub-stoichiometric expression of CK2 β compared to CK2 α in a subset of breast cancer tumors was correlated with the induction of EMT markers and increased epithelial cell plasticity in breast carcinoma progression. Phenotypic changes of epithelial cells are often associated with the activation of phosphotyrosine signaling. Herein, using phosphotyrosine enrichment coupled with affinity capture and proteomic analysis, we show that decreased expression of CK2 β in MCF10A mammary epithelial cells triggers the phosphorylation of a number of proteins on tyrosine residues and promotes the striking activation of the FAK1-Src-PAX1 signaling pathway. Moreover, morphometric analyses also reveal that CK2 β loss increases the number and the spatial distribution of focal adhesion signaling complexes that coordinate the adhesive and migratory processes. Together, our findings allow positioning CK2 β as a gatekeeper for cell spreading by restraining focal adhesion formation and invasion of mammary epithelial cells.

Keywords: CK2 β depletion, EMT, tyrosine-phosphorylated proteins, FAK1-Src-PAX1 signaling pathway, focal adhesions, epithelial cell spreading

INTRODUCTION

The serine/threonine protein kinase CK2 has been implicated in the phosphorylation of hundreds of cellular proteins, and more than 10% of the phosphoproteome matches the consensus sequence for CK2 phosphorylation (Meggio and Pinna, 2003; Salvi et al., 2009). CK2 exists as a tetrameric complex made up of two CK2 α or CK2 α' catalytic subunits and two CK2 β regulatory subunits (Litchfield, 2003). Extensive studies have established that CK2 regulates the crosstalk among multiple signaling pathways critical for cell differentiation, proliferation, and survival (Ahmed et al., 2002; Litchfield, 2003; Hong and Benveniste, 2021; Roffey and Litchfield, 2021), thereby justifying its potential as a therapeutic target in diverse human diseases (Borgo et al., 2021; Strum et al., 2021). A variety of experimental evidence supports the view that deregulated CK2 is functionally linked to cancer (Chua

et al., 2017; Nunez de Villavicencio-Diaz et al., 2017). For instance, CK2 α , whose expression is abnormally high in a wide range of tumors, operates as a cancer driver by creating the cellular environment favorable to neoplasia (Guerra and Issinger, 2008; Kreutzer et al., 2010; Schmitt et al., 2021) and the CK2 α gene (CSNK2A1) is one of 186 genes making up an “invasiveness signature” (Rozanov et al., 2008). CK2 α overexpression in human breast cancers is predictive of metastatic risk and poor outcome (Giusiano et al., 2011). In contrast to other multi-subunit protein kinases, the free CK2 α catalytic subunits possess a constitutive activity, while the homodimer of CK2 β regulatory subunits operates as a regulatory component, modifying the accessibility of binding substrates to the catalytic site of the holoenzyme (Filhol et al., 2003; Filhol and Cochet, 2009; Deshiere et al., 2011). The spatiotemporal organization of the CK2 individual subunits in living cells coupled with the observation that the free CK2 α subunit and the tetrameric holoenzyme have distinct, though overlapping, substrate specificity profiles has led to postulate that such a balance is crucial in the control of the many cellular processes that are governed by this pleiotropic kinase (Filhol et al., 2003; Filhol et al., 2004). Interestingly, a sub-stoichiometric expression of CK2 β compared to CK2 α in a subset of breast cancer tumors is correlated with the induction of hypoxia and epithelial to mesenchymal transition (EMT) markers, providing evidence that unbalanced expression of CK2 subunits may influence key cellular processes associated with epithelial cell plasticity in breast carcinoma progression (Deshiere et al., 2013; Golden and Cantley, 2014). We further demonstrate that CK2 β depletion in non-transformed mammary epithelial cells induced dissociation of cell–cell contacts, led to the acquisition of a mesenchymal cell shape (properties described for EMT-induced cells), and drove breast cell stemness (Deshiere et al., 2008; Deshiere et al., 2011; Deshiere et al., 2013; Golden and Cantley, 2014; Filhol et al., 2015; Duchemin-Pelletier et al., 2017). These disparate effects may be dependent on the levels of free CK2 α , which is markedly elevated in metastatic tumors compared to non-transformed cells (Kim et al., 2007; Laramas et al., 2007; Giusiano et al., 2011; Lin et al., 2011; Roelants et al., 2015; Choy et al., 2017; Schmitt et al., 2021). Phenotypic changes in cancer cells are controlled by a network of positive and negative regulators (Qian et al., 2015). In particular, phosphorylation-mediated signaling networks drive tumor progression and regulate inherent and acquired therapeutic resistance (Burridge, 2017). While tyrosine phosphorylation (pTyr) accounts for only 0.1–1% of the total phosphoproteome, 30% of the known oncoproteins are protein tyrosine kinases (PTKs) that regulate a vast array of cellular signaling networks necessary for processes such as survival, growth, migration, and invasion (Hunter, 1995; Blume-Jensen and Hunter, 2001; Olsen et al., 2006; Hochgrafe et al., 2010). Phenotypic changes in epithelial cells such as focal adhesion formation, cell spreading, and cytoskeletal reorganization are associated with pTyr signaling pathways. PTK activity can promote invadopodia formation, invasion, and diverse cellular processes implicated in EMT induction and subsequent steps in the metastatic cascade (Kim et al., 2014; Okayama et al., 2015). Since a CK2 β level establishes a

critical cell fate threshold in the control of epithelial cell plasticity, the purpose of this study was to evaluate the impact of an unbalanced expression of CK2 subunits on the potential activation of pTyr signaling pathways. We demonstrate that CK2 β depletion in MCF10A mammary cells (Δ CK2 β) promotes the phosphorylation on tyrosine residues of a number of proteins involved in cell migration and focal adhesion formation, including Src and focal adhesion kinase 1 (FAK1) tyrosine kinases. Our findings reveal that the unbalanced expression of the CK2 subunits, which was observed in a subset of breast tumors (Deshiere et al., 2013), may affect pTyr signaling cascades through activation of the FAK-Src-paxillin axis promoting spreading and migration of mammary epithelial cells.

MATERIAL AND METHODS

Cell Culture and Retroviral Infection

MCF10A cells from ATCC-LGS (Molsheim, France) (CRL-10317) are mammary epithelial cells derived from fibrocystic breast tissue from women with no family history of breast cancer and no evidence of disease. MCF7 cells are invasive breast cancer cells. Stable CK2 β silencing was accomplished in MCF10A or MCF7 cells by transduction with lentiviruses pLKO1 (Sigma-Aldrich, St. Louis, MO, United States) followed by puromycin selection as previously described (Deshiere et al., 2013). Stable transfected cells were maintained in puromycin-containing medium for 5–6 days before use and the silencing efficiency was evaluated at the protein level by Western blot analysis. Mock-cells are MCF10A or MCF7 cells transduced with an empty pLKO1 vector and are referred in the article as WT MCF10A cells. They were both cultured as described (Debnath et al., 2003). Transient CK2 β -siRNA transfection was performed as previously described (Deshiere et al., 2013).

Western Blot Analysis

Western blot membranes were immunostained with primary antibodies as follows: phosphotyrosine 4G10 clone, #05-321 (Merck); P-FAK1 Y576/577, #3281, P-PAX1 Y118, #2541, P-p130CAS Y410, #4011, and P-EGFR Y1173, #4407 (Cell Signaling, Danvers, MA, United States); P-Src Y418, #11091 (SAB Signaling Antibody, Maryland, United States); Src, #sc-19, and EGFR, #sc-03 (Santa Cruz Biotechnology Inc., Santa Cruz, CA, United States); PAX1, #610052, FAK1, #610088, and p130CAS, #610271 (BD Biosciences, Pont de Claix, France); P-PLC γ Y771, #ab131455, and PLC γ , #ab52200 (Abcam, Paris, France); and GAPDH, #AM4300 (Invitrogen, Thermo Fisher, France). Secondary antibodies were peroxidase-conjugated affinity pure goat anti-rabbit IgG (#111035003) and peroxidase-conjugated affinity pure goat anti-mouse IgG (#115035003) from Jackson Immuno Research. Cells were scrapped in lysis buffer (50 mM Tris-HCl pH 7.4, 150 mM NaCl, 1% Triton X-100, 0.5% NP40, 1 M EDTA, 1 mM EGTA, 10 mM NaF, 2.5 mM Na₄P₂O₇, 1 mM β -glycerophosphate, 1 mM Na₂VO₄, and protease-inhibitor cocktail, #P8340 (Sigma-Aldrich). The lysate concentrations were normalized after determination of protein concentration using the BCA protein

assay kit (Thermo Scientific, Sacle, France). SDS-PAGE was performed using pre-cast 4–12% gradient gel (Bio-Rad, Hercules, CA, United States). Separated proteins at 20–25 μ g/lane were transferred to PVDF membranes (100 V for 60 min). Blotted membranes were blocked during 1 h at room temperature with saturation buffer (1% BSA in 10 mM Tris-buffered saline, 0.1% Tween (TBST)) and then incubated with primary antibody diluted in saturation buffer, for 2 h or overnight. After three washes with TBST, appropriate secondary antibodies were added for 1 h at room temperature. Luminata Forte Western HRP substrate (Millipore, Billerica, MA, United States) was added and membranes were read with Fusion Fx7 (PerkinElmer, Waltham, MA, United States). Quantification was performed using ImageJ software.

Immunoaffinity Purification of Tyr-Phosphorylated Cellular Proteins

Subconfluent WT and Δ CK2 β MCF10A cells in two 10-cm culture dishes were washed with PBS and then lysed directly in lysis buffer (50 mM Tris-HCl pH 7.4, 150 mM NaCl, 1% Triton X-100, 0.5% NP40, 1 mM EDTA, 1 mM EGTA, 10 mM NaF, 2.5 mM $\text{Na}_4\text{P}_2\text{O}_7$, 1 mM β -glycerophosphate, 1 mM Na_2VO_4 , and protease-inhibitor cocktail) for 20 min on ice. After centrifugation at 14,000 g for 15 min, cell lysates were normalized for protein concentration and incubated overnight with 50 μ l of anti-phosphotyrosine monoclonal antibody covalently coupled to agarose beads (4G10 resin). The beads were then washed three times with lysis buffer and twice with PBS. The adsorbed proteins were eluted in four successive washes of 100 μ l containing 100 mM phenyl phosphate in 10 mM Tris-HCl pH 7.5, 50 mM NaCl, and 2% glycerol.

Phosphate Metal Affinity Chromatography of Phosphorylated Cellular Proteins

Phosphoprotein enrichment of cell extracts was performed according to the manufacturer's protocol (TALON PMAC Phosphoprotein Enrichment Kit, Clontech Laboratories, United States). Subconfluent WT and Δ CK2 β MCF10A cells in five 10-cm culture dishes were washed with PBS and then lysed directly in extraction/loading buffer A containing 10 mM NaF, 2.5 mM $\text{Na}_4\text{P}_2\text{O}_7$, 1 mM β -glycerophosphate, 1 mM Na_2VO_4 , and protease-inhibitor cocktail for 20 min on ice. After centrifugation at 14,000 g for 15 min, Na_2VO_4 which interferes with phosphoprotein binding to PMAC resin was removed by running the cell lysates through PD10 desalting columns. Samples of desalted cell lysates containing 3.5 mg protein were loaded on 1 ml of phosphoprotein affinity column (PMAC resin) and the column was agitated with the sample at 4°C for 2 h on a platform shaker. The column was then washed with 20 ml buffer A. The adsorbed proteins were eluted in three successive washes of 1 ml of buffer B (20 mM sodium phosphate and 0.5 M sodium chloride).

Immunofluorescence

A total of 10,000 cells were seeded on glass coverslips coated with 2.5 μ g vitronectin and incubated at 37°C 5% CO_2 for 24 h. The

cells were fixed with 4% PFA for 15 min at room temperature, washed three times with PBS, and permeabilized for 10 min with PBS containing 0.3% Triton X-100. After blocking with 3% BSA and 1% goat serum in PBS for 1 h, the cells were incubated with the primary antibody diluted in blocking solution for 1 h. The samples were then washed, incubated with a secondary Alexa Fluor-conjugated antibody (Thermo Fisher Scientific) for 1 h in blocking solution and Alexa-Fluor 647-phalloidin (A22287), when required, and finally washed and mounted using Mowiol-containing DAPI (Santa Cruz). Primary antibodies used for immunostaining are the following: P-tyrosine 4G10 (Millipore #05321), P-paxillin (Invitrogen #44-722G), P-FAK (Invitrogen #44-624G), and P-Src (Invitrogen #44-660G).

Images were acquired on an iMIC Andromeda (FEI, Gräfelfing, Germany) microscope at 40 \times magnification in spinning disk mode. We analyzed at least 50 cells per experiment in 3 independent experiments. Segmentation of focal adhesions was performed using Ilastik (interactive machine learning for (bio)image analysis) (Berg et al., 2019) and subsequently analyzed with Fiji software (Schindelin et al., 2012). Fiji is an open-source platform for biological image analysis. Statistics analyses were performed with R. Significant differences were evaluated by Student test.

Protein Kinase CK2 Assay

Radiometric CK2 assay was performed in a final volume of 18 μ l containing 3 μ l of cell extract, and a mixture containing 100 μ M of peptide substrate (RRREDEESDDEE), 10 mM MgCl_2 , and 100 μ M [γ - ^{32}P]-ATP (6,000 Ci/mmol). Assays were performed at room temperature for 5 min before termination by the addition of 60 μ l of 4% trichloroacetic acid. Incorporation of ^{32}P in the peptide substrate was determined as previously described (Filhol et al., 1991). All kinase assays were performed in triplicates.

Multiplex Kinase Activity Profiling

PamGene PTK multiplex activity assays were used to investigate TK activity of 196 PTKs. This platform utilizes a high-throughput peptide microarray system by measuring the phosphorylation of peptide representations of targets/substrates (referred hereafter as phosphosites) that are immobilized on the PamChip[®] microarrays. Generic fluorescent-labeled antibodies that recognize phosphorylated residues are used to visualize the phosphorylation. Whole-cell lysates of WT and Δ CK2 β MCF10A cells were prepared according to the manufacturer's instructions (PamGene International, 's-Hertogenbosch, the Netherlands). Cell samples were lysed for 30 min on ice and centrifuged for 15 min at 16,000 g at 4°C in a precooled centrifuge. After protein quantification (BCA protein determination, Pierce Scientific), aliquots of the samples were stored immediately in a -80°C freezer. Per array, 4 μ g of protein and 100 μ M ATP were loaded onto the appropriate PTK PamChip in kinase buffer. Phosphorylation of peptides was monitored by PamStation 12 following the manufacturer's protocol as described previously (Arni et al., 2017). Technical triplicates were analyzed, and sequence-specific peptide tyrosine phosphorylation was detected by the fluorescein-labeled antibody PY20 (Exalpha, Maynard, MA). Capture of peptide phosphorylation signal is

via a computer-controlled CCD camera. Kinomic profiling was performed using the Evolve software (PamGene International). Data were analyzed using the BioNavigator software version 6.3 (PamGene International) for raw data transformation into kinetic and steady-state values. Data were expressed as the average signal intensity (\pm SD) of the 196 peptide spots based on end levels of the phosphorylation curve. Prior to statistical analysis, fluorescent signal intensities were log₂-transformed to satisfy the normality assumptions. Significant differences between two conditions were determined using two-sided Student's *t*-test. The differential activity of kinases was predicted using an in-house bioinformatic approach, upstream kinase analysis (UKA) (Chirumamilla et al., 2019). Briefly, UKA identifies kinase activity based on a permutation analysis of the peptide substrate phosphorylation, by using known associations of phosphoproteins and kinases from literature and *in silico* databases. This permutation analysis gave a specificity score (mapping of peptides to kinases) and a significance score (kinase statistic that indicates the difference between treatment groups). Prior to UKA, the raw signal intensities were transformed using variance stabilizing normalization (VSN) (Huber et al., 2002).

Mass Spectrometry-Based Proteomic Analyses

After phosphoprotein enrichment (both 4G10 and PMAC), the eluates were solubilized in Laemmli buffer before stacking of proteins in the top layer of a 4–12% NuPAGE gel (Invitrogen) for separation followed by R-250 Coomassie blue staining. The gel bands were manually excised and digested using modified trypsin (sequencing grade, Promega) as previously described (Salveti et al., 2016). After peptide extraction, the samples were split into two parts before drying: one-third for proteome analysis and two-thirds for phosphopeptide enrichment. The phosphopeptides were enriched with TiO₂ beads (GL Science) in batch mode with a modified protocol from Jensen and Larsen (2007). Briefly, the samples were mixed for 1 h with 0.6 mg beads in loading buffer (1 M glycolic acid in 80% acetonitrile (v/v) and 5% TFA (v/v)). The beads were washed three times with loading buffer, 80% acetonitrile with 1% TFA (v/v), and finally 10% acetonitrile (v/v) with 0.1% TFA (v/v). The phosphopeptides were eluted with 10% ammonia solution (v/v) for 10 min. After acidification with formic acid, the peptides were desalted using C18 ultra-micro spin columns (Harvard Apparatus) and dried under vacuum. The dried extracted peptides were resuspended in 5% acetonitrile and 0.1% trifluoroacetic acid and analyzed by online nano-liquid chromatography coupled to tandem mass spectrometry (LC–MS/MS) (Ultimate 3000 RSLCnano and the Q-Exactive HF, Thermo Fisher Scientific). The peptides were sampled on a 300- μ m internal diameter, 5-mm length PepMap C18 precolumn (Thermo Fisher Scientific) and separated on a 75- μ m internal diameter, 250-mm length C18 column (Reprosil-Pur 120 C18-AQ, 1.9 μ m particles, Dr. Maisch HPLC GmbH). The column flow rate was 300 nL/min. The mobile phases consisted of solution A (water with 0.1% (v/v) formic acid) and solution B (acetonitrile with 0.1% (v/v) formic acid). For 4G10 samples, the

peptides were eluted with a gradient consisting of an increase in solvent B from 5 to 13% in 1.5 min, then from 13 to 31% over 29 min, and from 31 to 41% over 4.5 min. For data-dependent acquisition (DDA), the spray voltage was set at 2 kV and the heated capillary was adjusted to 270°C. Survey full-scan MS spectra (m/z = 400–2,000) were acquired with a resolution of 60,000 after the accumulation of 3×10^6 ions (maximum filling time 250 ms). The 12 most intense ions were fragmented by higher-energy collisional dissociation (HCD) after the accumulation of 1×10^6 ions (maximum filling time 250 ms). For PMAC samples, the nano-LC method consisted of a 120-min multilinear gradient at a flow rate of 300 nL/min (same gradient slopes as for 4G10 samples). Survey full-scan MS spectra (m/z = 400–2,000) were acquired with a resolution of 60,000 after the accumulation of 1×10^6 ions (maximum filling time 200 ms). The 20 most intense ions were fragmented by HCD after the accumulation of 1×10^5 ions (maximum filling time 50 ms). MS and MS/MS data were acquired using the software Xcalibur (Thermo Scientific).

Mass Spectrometry-Based Proteomic Data Processing

The data were processed automatically using Mascot Distiller software (version 2.7.1.0, Matrix Science). The peptides and proteins were identified using Mascot (version 2.8) through concomitant searches against Uniprot (*Homo sapiens* taxonomy, September 2021 version) and a database of 250 classical contaminants (homemade) and their corresponding reversed databases. Trypsin/P was chosen as the enzyme and two missed cleavages were allowed. Precursor and fragment mass error tolerances were set, respectively, to 10 and 20 ppm. Peptide modifications allowed during the search were cysteine carbamidomethylation (fixed), acetyl (protein N-terminal, variable), methionine oxidation (variable), and serine, threonine, tyrosine phosphorylation (variable). Proline software (version 2.1) (Bouyssi et al., 2020) was used to merge DDA results from proteome analysis and phosphopeptide enrichment. After combination, the results were filtered: conservation of rank 1 peptide-spectrum matches (PSMs) with a minimal length of 6 amino acids and a minimal score of 25. PSM score filtering was then optimized to reach a false discovery rate (FDR) of PSM identification below 1% by employing the target decoy approach. A minimum of one specific peptide per identified protein group was required. Proline was then used to perform MS1-based label-free quantification of the peptides and protein groups from the different samples with cross-assignment activated. Protein abundances were computed as a sum of specific peptide abundances, without using phosphopeptides and their counterparts. The data from 4G10 and PMAC enrichment were processed separately to obtain two different datasets.

Statistical Analysis of Mass Spectrometry-Based Proteomic Data

Statistical analysis on the proteins from 4G10 dataset was performed using ProStaR (Wieczorek et al., 2017) to

determine differentially abundant proteins between WT and Δ CK2 β MCF10A cells. Protein sets were filtered out if they were not identified and quantified in at least two biological replicates of one condition. Reverse protein sets and contaminants were also filtered out. These filters downsized the dataset to 249 proteins. After log₂ transformation, the data were normalized with VSN method. POV missing values were imputed with *slsa* method and MEC ones with 1-percentile value of each sample. Statistical testing was conducted using *limma* test. Differentially expressed proteins were sorted out using a log₂ (fold change) cut-off of 1 and a *p*-value inferior to 0.05. Proteins with more than three imputed values in the upregulated condition were invalidated. For each replicate, pTyr-phosphopeptides were declared upregulated in Δ CK2 β cells (or, respectively, WT cells) if they were detected only in this condition or if their log₂ (fold change) was higher than 1 (respectively, lower than -1). The peptides upregulated in at least two replicates were further considered. For the PMAC protein dataset, after log₂ transformation, missing values were imputed with 1-percentile value. Log₂ (fold change) was calculated and normalized.

Pathway Enrichment

Biological pathway enrichment analyses were carried out by Gene Set Enrichment Analysis (GSEA, FDR <0.05) from the 249 proteins quantified by proteomic analysis and kept during statistical analysis (Supplementary Table S1). The *enrichGO* and the *cnet* (category net plot used for visualization) functions were executed by ClusterProfiler v4.2.2 (Wu et al., 2015) (Bioconductor 3.14, <https://www.bioconductor.org/>, accessed on XX February 2022, R v4.1.2 (2021-11-01)). The enrichment analyses were performed using the biological pathway annotations from the Gene Ontology (GO, GO, db_v3.14.0 (2021-09-01), Bioconductor v3.14 Rv4.1.2 (2021-11-01), and KEGG databases (release 101, 2022/01) (Kanehisa and Goto, 2000). Gene sets consisting of at least 10 genes and less than 500 genes were retained for analysis. Thousand permutations were performed to compute *p*-values corrected by the Benjamini–Hochberg method.

RESULTS

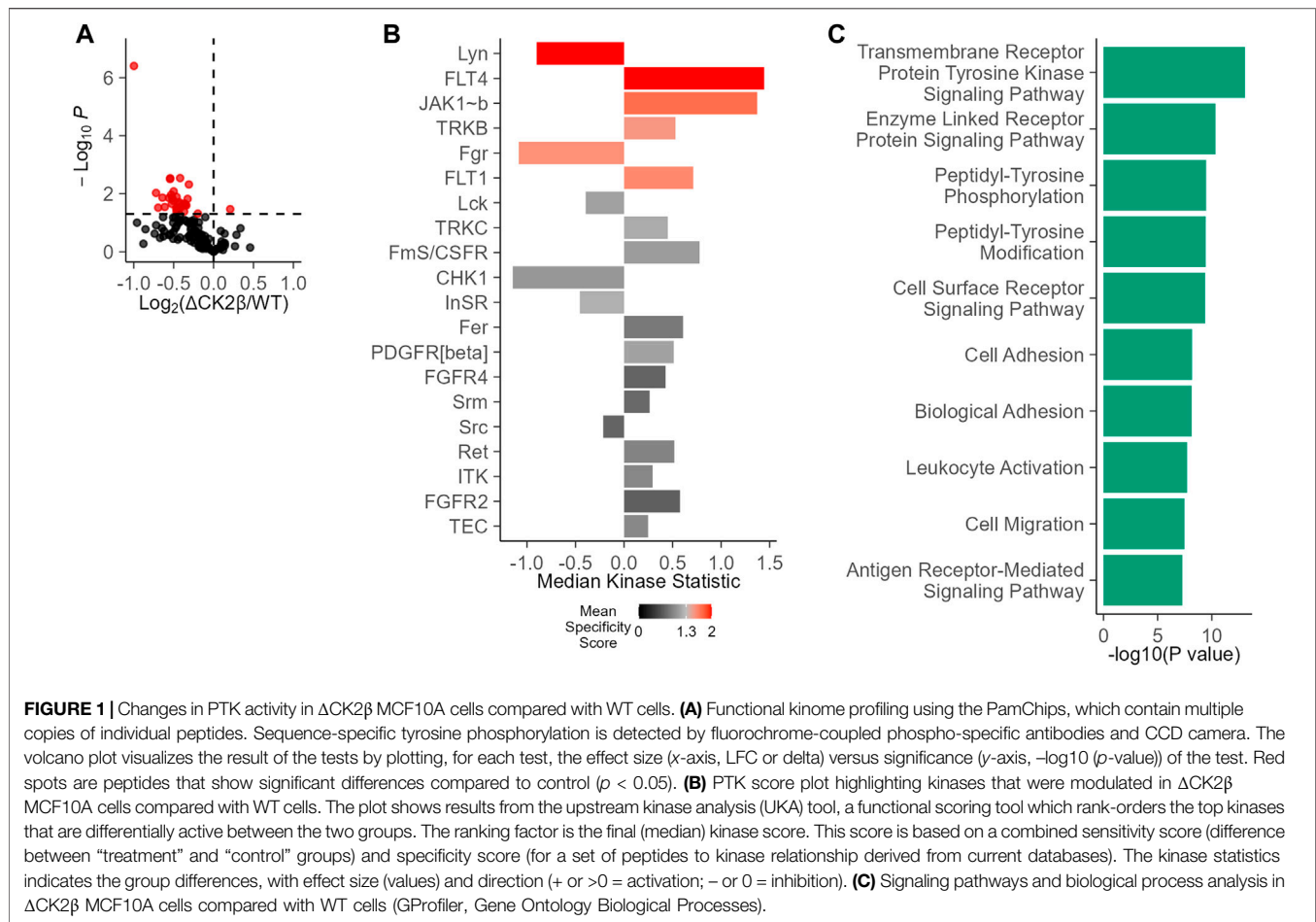
Changes in Tyrosine Kinase Activity in Extracts of WT and Δ CK2 β MCF10A Cells

Given the interplay between serine/threonine and tyrosine kinases, we evaluated the potential impact of an imbalanced expression of CK2 subunits on global tyrosine kinase activity in WT non-transformed mammary MCF10A or shRNA-mediated CK2 β -silenced MCF10A cells (Δ CK2 β) (Deshiere et al., 2013; Deshiere et al., 2011; Deshiere et al., 2008; Filhol et al., 2015; Duchemin-Pelletier et al., 2017; Golden and Cantley, 2014). For this purpose, we used the PamChip PTK multiplex activity profiling (PamGene International BV 's-Hertogenbosch, Netherlands). This methodology has been developed as a screening tool that allows for the robust analysis of kinase activity from cells and tissues

(Anderson et al., 2015; Arsenault et al., 2011). A 73% efficiency in CK2 β silencing was evaluated at the protein level in Δ CK2 β MCF10A cells (Supplementary Figure S1). Equal amounts of protein extracts of WT or Δ CK2 β MCF10A cells were then applied to peptide array chips. In a two-group comparison between these two cell lines, the deregulation of phosphorylation for each peptide represents the changes in kinase activity. There was a clear difference in the mean pattern of peptide substrate phosphorylation on comparing WT and Δ CK2 β MCF10A cells as illustrated in the volcano plot of Figure 1A, indicating that upon CK2 β silencing, the activity of certain signaling pathways driven by distinct PTK was altered (Figure 1B). Based on those phosphorylation patterns, a computational upstream kinase analysis predicted increased activity of PTKs that are known to contribute to invasive progression and metastasis of breast tumor, namely, FLT4, JAK1b, TRKB, and FLT1 (Zhang et al., 2010; Qian et al., 2015; Choy et al., 2017; Wehde et al., 2018). In contrast, the activity of other TKs (Lyn and Fgr) was decreased in Δ CK2 β MCF10A cells (Figure 1B). Thus, a significant change in the pattern of Tyr phosphorylation was noted when comparing WT and Δ CK2 β MCF10A cells. A ranked list of possible canonical pathways (and networks) responsible for the differences in the peptide phosphorylation was established. CK2 β loss induced changes in transmembrane PTK in correlation with biological events such as cell adhesion and migration (Figure 1C).

Abundant pTyr-Containing Proteins Are Identified in Δ CK2 β MCF10A Cells

To obtain an exhaustive landscape of proteins differentially modified on Tyr residues in WT *versus* Δ CK2 β MCF10A cells, we performed a proteomic analysis of pTyr-containing proteins. Since pTyr-containing proteins of low abundance might be difficult to detect within cell extracts, phosphoprotein enrichment was performed using pTyr immunoaffinity chromatography on anti-phosphotyrosine monoclonal antibody covalently coupled to agarose beads (4G10 resin). After extensive washing, the retained proteins were eluted with 100 mM phenyl phosphate, a phosphotyrosine hapten analog (Figure 2A). After trypsin digestion of the enriched proteins, a fraction of peptides was further loaded on a TiO₂ resin, to allow the selection of phosphorylated peptides. We identified 542 unique proteins (contaminants filtered) from the total tryptic digest of the proteins retained on the 4G10 resin (Figure 2B, Supplementary Table S1). In addition, by analyzing the tryptic peptides further enriched on the TiO₂ resin, 204 phosphosites were identified. Among them, 40 sites from 25 unique proteins were localized on tyrosine with a confidence higher than 75% (Supplementary Table S2). A large part of the pTyr-phosphopeptides was more abundant or specifically detected in Δ CK2 β MCF10A cells (Figure 2C, Supplementary Table S2). This was the case not only for the EPH tyrosine receptor A2 (EPHA2) but also for a number of non-receptor tyrosine kinases including FAK1, the signaling pseudokinase pragmin (PRAG1), activated CDC42 kinase 1



(ACK1), glycogen synthase kinase 3 α (GSK3A), and mitogen-activated protein kinase 1 (MK01). pTyr-phosphopeptides from signaling proteins, such as p130CAS/BCAR1, paxillin (PAX1), partitioning defective 3 (PAR3), lipoma-preferred partner (LPP), and ARF GTPase-activating protein (GIT1), that are activated by tyrosine phosphorylation, were also enriched or specifically detected in Δ CK2 β MCF10A cells (Figure 2C). Interestingly, several of these well-characterized proteins form supra-molecular complexes belonging to adhesive structures at cell membrane known under the name of focal adhesions (FAs), playing important functional roles in integrin signaling (Wozniak et al., 2004; Burridge, 2017) and coordinating the adhesive and migratory processes (Geiger and Bershadsky, 2001). Among them, FAK1 as well as GIT1, ACK1, PAX1, p130CAS, PAR3, and LPP are known substrates of Src kinase (Wang et al., 2006; Sachdev et al., 2009; Meenderink et al., 2010; Totaro et al., 2014; Wu et al., 2015; Ngan et al., 2017; Atashrazm and Ellis, 2021) (Table 1). Of note, even if we did not identify upregulated pTyr-phosphopeptides from their sequences, several proteins such as vimentin (VIME), fibronectin 1 (FINC), sortin nexin-18 (SNX18), BCAR3 adaptor protein (BCAR3), tensin 2 tyrosine protein phosphatase (TNS2), inactive-tyrosine

protein kinase PEAK (PEAK1), and growth factor receptor-bound protein 2 (GRB2) were also substantially enriched in Δ CK2 β MCF10A cell extracts (Supplementary Table S1). In contrast, pTyr-phosphopeptides from the epidermal growth factor receptor (EGFR) and the SH2 domain-containing adapter protein B (SHB) were downregulated in Δ CK2 β MCF10A cells suggesting a de-enrichment of the proliferation signature (Figure 2C, Supplementary Table S2).

A pathway enrichment analysis by GSEA was carried out to identify deregulated molecular processes from proteomics quantification data (Supplementary Table S1). The enrichment analysis was performed from the log2 (fold change) values computed according to protein abundances between both phenotypes (Δ CK2 β /WT). Figure 2D shows the seven significant cellular components enriched using the pathway annotation from the GO database (Supplementary Table S3). Significance was defined as each cellular component with a p -value less than 0.05 after the Benjamini–Hochberg correction. We observed that among them, the focal adhesion, anchoring junction, cell-substrate junction, microtubule cytoskeleton, and microtubule organizing center were significantly enriched in upregulated proteins. These

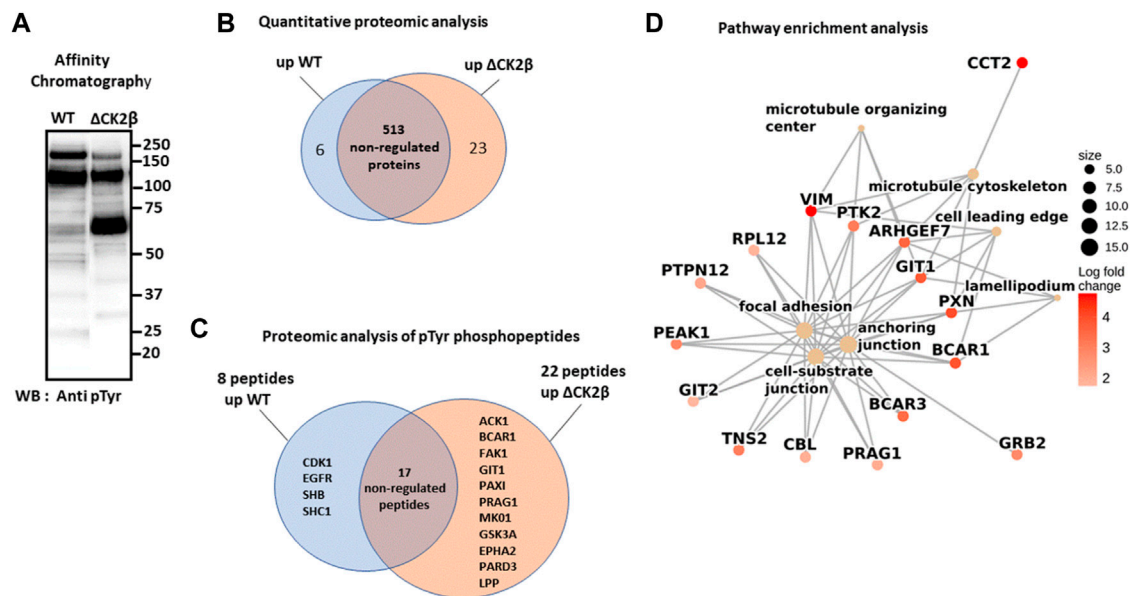


FIGURE 2 | LC-MS/MS and GSEA analysis of differentially elevated levels of Tyr-phosphorylated proteins in WT and Δ CK2 β MCF10A cells. **(A)** Proteins immunopurified from WT and Δ CK2 β MCF10A cell lysates were analyzed by Western blotting for pTyr proteins using the 4G10 antibody. **(B)** Venn diagram showing differentially abundant proteins between WT and CK2 β -depleted cells in samples obtained by immunoaffinity purification of Tyr-phosphorylated proteins (**Supplementary Table S1**). **(C)** Venn diagram showing the proteins in which differentially abundant pTyr-phosphopeptides between WT and CK2 β -depleted cells were identified (**Supplementary Table S2**). These pTyr-phosphopeptides were identified and quantified from the LC-MS/MS analyses of peptide samples coming from a double enrichment starting from the two cell types: immunoaffinity purification of Tyr-phosphorylated proteins followed by the enrichment of their tryptic peptides on a TiO₂ resin. **(D)** Significant gene ontology cellular components enriched from proteomics quantification of phosphoproteins (**Supplementary Table S3**) according to corrected *p*-values by the Benjamini–Hochberg method <0.05 . Cellular component names are displayed as yellow nodes and bound to core phosphoproteins that led to a significant enrichment by GSEA. The core phosphoproteins are the nodes colored in red according to their log2 fold change value.

TABLE 1 | pTyr proteins enriched in Δ CK2 β MCF10A and localized in adhesion complexes.

Name	pTyr Proteins	Adhesion Complex-Localized Proteins
FAK1	Focal adhesion kinase 1	Shen and Schaller (1999), Hu et al. (2014)
PRAG1	PEAK1-related kinase-activating pseudokinase	Senda et al. (2016), Abu-Thuraia et al. (2020)
ACK1	Activated CDC42 kinase	Modzelewska et al. (2006)
p130CAS	Crk-associated substrate	Harte et al. (1996), Donato et al. (2010), Machiyama et al. (2014)
PAX1	Paxillin1	Salgia et al. (1995), Brown et al. (1996)
GIT1	ARF GTPase-activating protein 1	Yin et al. (2005), Schmalzigaug et al. (2007)
Src	Proto-oncogene tyrosine protein kinase Src	Schaller et al. (1999), Volberg et al. (2001)
FLT1/4	Fms-related receptor tyrosine Kinase 1/4	Maru et al. (2001), Galvagni et al. (2010)
JAK1	Janus kinase 1	Petropoulos et al. (2016)
GSK3A	Glycogen synthase kinase 3 alpha	Kobayashi et al. (2006), Sun et al. (2013)
EPHA2	EPH receptor A2	Miao et al. (2000), Chen et al. (2018), Finney et al. (2021)
PARD3	Partitioning defective 3	Bridgewater et al. (2012), Valdivia et al. (2020)
LPP	Lipoma-preferred partner	Petit et al. (2003), Petit et al. (2005)

enrichment insights support the idea that the overabundance of phosphoproteins involved in these biological processes following CK2 β depletion leads to a revamping of the cell adhesion mechanisms. Moreover, the pathway enrichment by GSEA based on the KEGG database (**Supplementary Table S4**) reveals the upregulation of actin cytoskeleton as the only significant pathway. These results suggest that changes in phosphoprotein abundances following CK2 β downregulation may also impair the actin or microtubule cytoskeleton regulation.

Focal Adhesion Proteins Are Hyperphosphorylated in Extracts of Δ CK2 β MCF10A Cells

In line with the phosphoproteomic approach, immunoblotting of cell extracts of subconfluent WT and Δ CK2 β MCF10A cells with the 4G10 antibody confirmed the upregulation in CK2 β -depleted MCF10A cells of diverse tyrosine-phosphorylated proteins (**Figure 3A**). Notably, Western blot analysis of pTyr proteins released from immobilized phosphotyrosine antibody (4G10

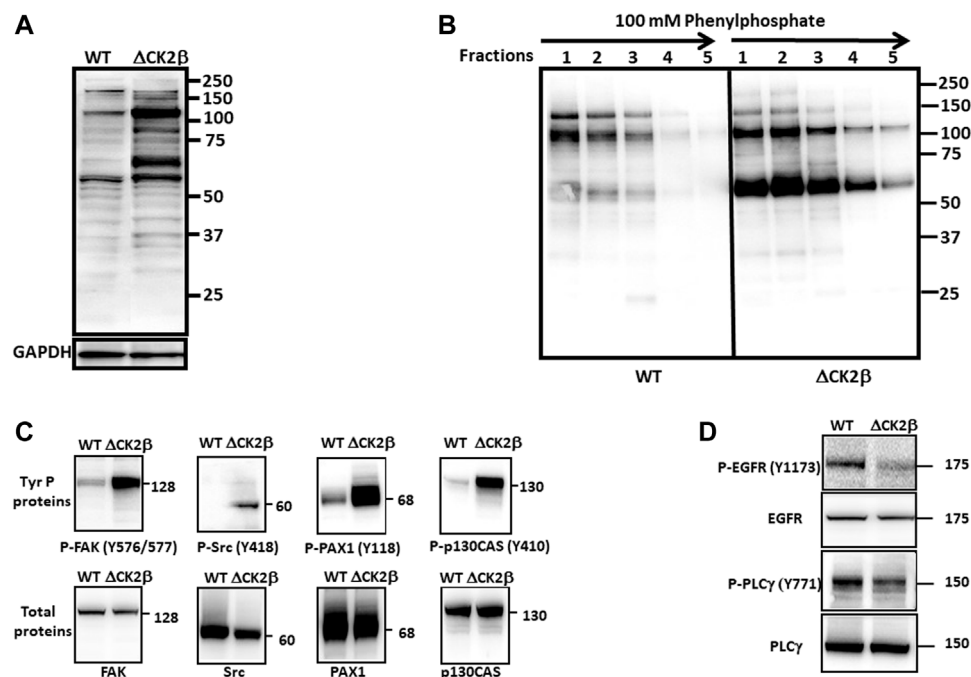


FIGURE 3 | Upregulation of pTyr proteins in lysates of Δ CK2 β MCF10A cells. **(A)** Lysates from WT and Δ CK2 β MCF10A cells were analyzed for pTyr-containing proteins using the 4G10 antibody. GAPDH was used as a loading control. **(B)** Cell extracts (500 μ g of protein) of WT and Δ CK2 β MCF10A cells were loaded on 4G10 resin. After extensive washing, the bound proteins were eluted with 100 mM phenyl phosphate. The collected fractions were analyzed by Western blotting with the 4G10 antibody. **(C)** Proteins immunopurified from WT and Δ CK2 β MCF10A cell lysates were analyzed by Western blotting for p-FAK (Y576/577), p-Src (Y418), p-PAX1 (Y118), p-p130CAS (Y410), FAK, Src, PAX1, and p130CAS and **(D)** for p-EGFR (Y1173), EGFR, p-PLC γ (Y771), and PLC γ .

resin) highlighted the enrichment of two major upregulated phosphoproteins (65 and 115 kDa), most highly phosphorylated on Tyr residues in Δ CK2 β cell extracts (Figure 3B). Similar patterns of enhanced tyrosine-phosphorylated proteins could be observed in either MCF10A cells which have been transiently depleted for CK2 β or in shRNA-mediated CK2 β -silenced MCF7 cells (Supplementary Figure 2 and Supplementary Figure S3). To go further, relevant antibodies also revealed the upregulation of additional pTyr-containing proteins in Δ CK2 β MCF10A cells. Among them, non-receptor tyrosine kinases were identified, including FAK1 and the Src kinase. Important adhesion complex proteins such as PAX1 and p130CAS were also highly tyrosine phosphorylated (Figure 3C). Immunoblotting as well as immunoprecipitation analysis in these immunoaffinity-purified proteins suggested that the major 65-kDa tyrosine-phosphorylated protein may represent the scaffolding protein PAX1 (Supplementary Figure S4). PAX1 phosphorylation on tyrosine residue (Y118) is a prominent event during EMT and cell migration, through its recruitment into adhesion sites called FAs (Nakamura et al., 2000). PAX1 is also a well-known substrate for the FAK1/Src adhesion protein complex, which phosphorylates its residues Tyr31 and Tyr118 in dynamic adhesions, thus regulating both the assembly and the turnover of FAs (Schindelin et al., 2012). Plasma membranes act as transient trapping sites for signaling molecules playing a pivotal role in biological functions, including signal transduction and cell-ECM communication. Interestingly,

it has been reported that the localization of a fraction of CK2 to the plasma membrane is controlled by cell-matrix interactions (Filhol et al., 2015). Moreover, protein-protein interaction between the scaffold protein CKIP-1 and CK2 provided evidence for CK2 targeting to the plasma membrane (Olsten et al., 2004). Therefore, selected differentially tyrosine-phosphorylated proteins known to be localized to the plasma membrane were validated using immunoblotting. This was the case for the activation of EGFR, a key driver in growth factor-dependent signal transduction, and its downstream effector PLC γ in WT and Δ CK2 β MCF10A cells. The phosphorylation of EGFR and PLC γ on Tyr1173 and Tyr771, respectively, was decreased in Δ CK2 β MCF10A cells compared to WT cells (Figure 3D). Thus, in agreement with the proteomic analysis (Figure 2D), CK2 β downregulation significantly inhibited the activated form of EGFR and reduced the activation of its downstream signaling molecule PLC γ . Collectively, these data were consistent with the proteomic analyses, highlighting the phosphorylation-dependent activation of focal adhesion markers of the FAK1-Src-PAX1 axis upon CK2 β depletion in MCF10A cells.

CK2 β Depletion Induces Cell Spreading and Increase of Focal Adhesion Number

Early evidence indicated that tyrosine phosphorylation plays an important role in the overall organization of adhesion complexes and their dynamic regulation (Craig and Johnson, 1996; Burridge

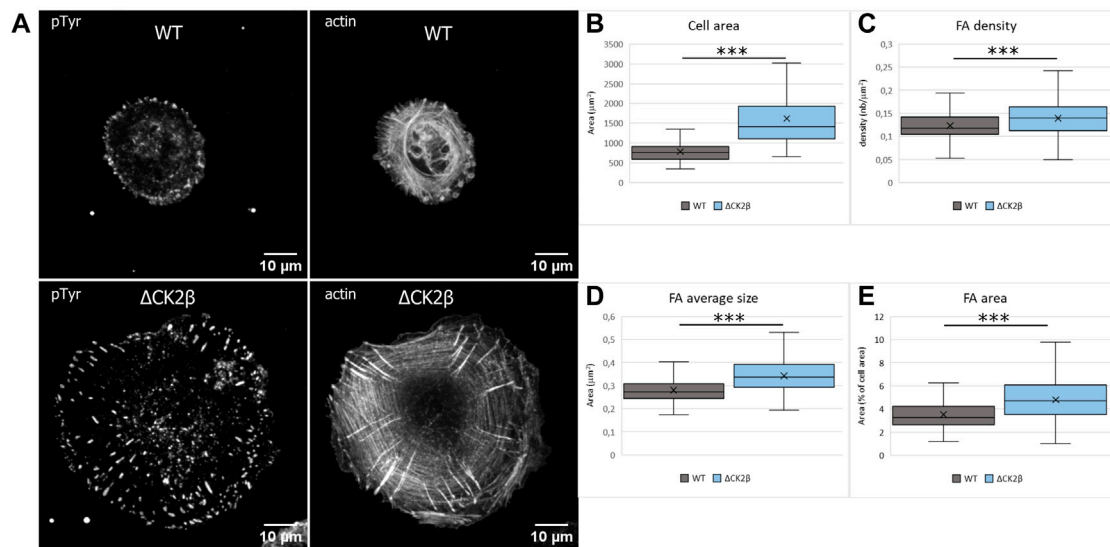


FIGURE 4 | Cell spreading and size of focal adhesions are dependent on CK2 β . **(A)** Staining of pTyr and actin was carried out on cells spread on vitronectin-coated cover glass for 24 h. Scale bar represents 10 μ m. **(B)** Quantification of the cell area. **(C)** Quantification of the number of FAs normalized to the cell area. **(D)** Quantification of the FA average area. **(E)** Quantification of the FA area, normalized to the cell area. Error bars represent standard deviation. ***p-value \leq 0.0005.

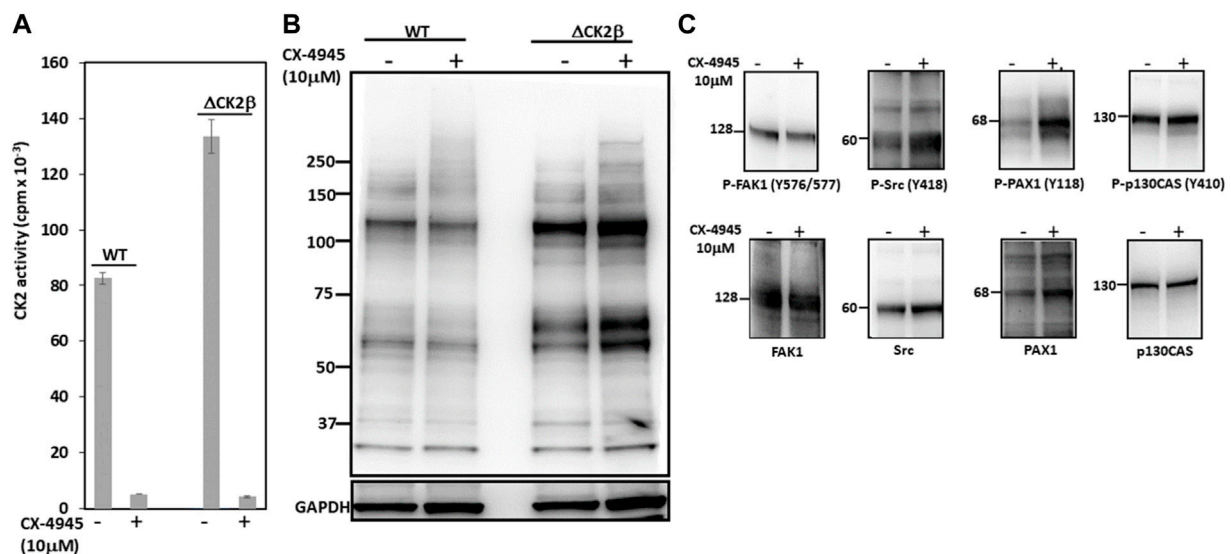


FIGURE 5 | CK2 catalytic activity does not contribute to enhanced Tyr phosphorylation in Δ CK2 β MCF10A cells. **(A)** CK2 kinase activity in cell lysates from WT or Δ CK2 β MCF10A cells treated for 5 h in the absence or presence of 10 μ M CX-4945. **(B)** Cell lysates as in **(A)** were Western blotted with 4G10 antibody for the presence of pTyr proteins. GAPDH was used as a loading control. **(C)** Δ CK2 β MCF10A cell lysates were also analyzed by Western blotting for p-FAK (Y576/577), p-Src (Y418), p-PAX1 (Y118), p-p130CAS (Y410), FAK, Src, PAX1, and p130CAS.

et al., 1988). In addition, tyrosine phosphorylation events were acknowledged to be concentrated at focal adhesions formed by the cells with the substratum (Maher et al., 1985). It has also been reported that PAX1 and FAK1 enter nascent adhesions as discrete entities and form dynamic molecular complexes within adhesion sites. Moreover, phosphorylation of PAX1 at Y31-Y118 regulates

the formation and size of the complexes (Choi et al., 2011). As these focal adhesion markers were identified in Δ CK2 β MCF10A cells after pTyr immunoaffinity chromatography, we analyzed the impact of CK2 β depletion in the distribution of focal adhesions of isolated MCF10A cells spread onto vitronectin. Vitronectin was chosen as the adhesive substrate since WT or Δ CK2 β MCF10A

cells plated on vitronectin-coated coverslips clearly display a distinguishable morphology (Deshiere et al., 2013). In particular, Δ CK2 β MCF10A cells plated on vitronectin-coated coverslips display higher cell spreading as evidenced by the projected area of actin cytoskeleton (Figure 4A and Figure 4B). This cell spreading is associated with an increase in the number (Figure 4C) and the size (Figure 4D) of focal adhesions giving rise to an increase in the total adhesive surface when compared to the cell surface (Figure 4E). FAK1 phosphorylation is one of the key steps following integrin engagement, either directly or through its role as a scaffolding protein for Src (Tapial Martinez et al., 2020). Based on the increase in cell spreading upon CK2 β loss, we investigated whether this increase might be related to a change in focal adhesion organization by immunostaining FAK1, Src, and PAX1 (Supplementary Figure S5A,F,K). Immunofluorescence analyses demonstrated that CK2 β depletion increased the Src labeling and changed the spatial distribution of FAK1 and PAX1 in focal adhesion sites. Morphometric analyses showed that CK2 β -depleted cells were much larger than WT cells. Moreover, descriptors of focal adhesion morphology such as number and mean size of the focal adhesions were strikingly upregulated in these cells (Supplementary Figure S5). It has been reported that the mean size of focal adhesions uniquely predicts cell speed independently of focal adhesion surface density and molecular composition (Kim and Wirtz, 2013). The regulation of FAs by CK2 β is consistent with our previous observations, showing that CK2 β -depleted cells displayed a mesenchymal phenotype and a loss of polarity driving a 2D-to-3D morphologic transformation (Deshiere et al., 2008; Deshiere et al., 2013).

The Catalytic Activity of CK2 Is Not Involved in Enhanced Tyr Phosphorylation in Δ CK2 β MCF10A Cells

CK2 is mostly known as a Ser/Thr kinase, yet the enzyme also exhibits tyrosine kinase activity in mammalian cells (Basnet et al., 2014; Borgo et al., 2021). To clarify the potential contribution of CK2 activity in the activation of these Tyr phosphorylations, we analyzed pTyr proteins in the extracts of WT or Δ CK2 β MCF10A cells that had been incubated for 5 h with 10 μ M of the small chemical CK2 inhibitor CX-4945. CK2 activity measured in whole-cell lysates from WT or Δ CK2 β MCF10A cells treated with CX-4945 was inhibited by more than 90% (Figure 5A). Immunoblotting analysis of protein extracts from cells treated under these conditions revealed that the inhibition of CK2 did not abrogate the Tyr phosphorylation of the 65- and 115-kDa endogenous proteins (Figure 5B). In addition, the Tyr phosphorylation of adhesion complex proteins was either not affected (FAK1, p130CAS) or enhanced (Src, PAX1) upon CX-4945 treatment (Figure 5C). The increased Tyr phosphorylation of Src and PAX1 observed in Δ CK2 β MCF10A cells after CX-4945 treatment suggests that the activation of these two components of the adhesion complexes could be similarly antagonized by CK2 β and CK2 α . This would reinforce the notion that any variation in the expression/activity of either

CK2 subunits could have significant impacts on focal adhesion signaling pathways.

DISCUSSION

In the present study, we demonstrate that CK2 β downregulation in MCF10A mammary cells triggers the phosphorylation of an array of tyrosine-phosphorylated proteins involved in cell migration and focal adhesion including Src and FAK1 tyrosine kinases. Our findings highlight a crosstalk between CK2, a serine/threonine kinase, and pTyr signaling pathways involved in phenotypic changes of epithelial cells. Such a potential link has been previously evoked. For instance, the catalytic subunits of CK2 are readily phosphorylated *in vitro* by the Src family protein tyrosine kinases Lyn and c-Fgr with a concomitant threefold increase in catalytic activity of CK2 (Donella-Deana et al., 2003). Interestingly, the presence of CK2 β decreased this Lyn/Fgr-mediated phosphorylation, suggesting that at least *in vitro*, the CK2 holoenzyme is less prone to tyrosine phosphorylation. One could speculate that, within cells, the pool of catalytic subunits that is not incorporated into the holoenzyme would acquire an increased activity toward a subset of specific targets. Indeed, it has been reported that in advanced cancers, the TGF β receptor (TGFBR) 1 kinase phosphorylated CK2 β targeting it for degradation. The resulting CK2 α /CK2 β subunit imbalance promoted the activation of CK2 and EMT induction (Kim et al., 2018). Thus, a dysregulation in CK2 subunit levels, originating either from shRNA-mediated CK2 β silencing or from TGF β -dependent decrease of CK2 β , invariably promotes EMT activation in epithelial cells (Deshiere et al., 2013; Filhol et al., 2015). Consequently, it is conceivable that signaling-mediated drop of CK2 β expression could increase intracellular CK2 activity impacting downstream signaling events such as pTyr-relayed signaling cascades. Indeed, our results reveal that spreading-coupled pTyr signaling pathways including FAK1, PAX1, ACK1, EPHA2, PARD3, and LPP are impacted by CK2 β depletion (Supplementary Table S2). Of note, the focal adhesion network (www.adhesome.org) which is involved in the regulation of cell shape and focal adhesion complexes is acting at the plasma membrane level. This is consistent with previous observations showing that in epithelial cells, the association of a fraction of CK2 to the plasma membrane is controlled by cell-matrix interactions (Deshiere et al., 2008). Phosphoproteomic analysis revealed that FAK1 is activated through membrane recruitment by growth factors, extracellular matrix, and integrin signaling followed by subsequent autophosphorylation at Tyr 397 exposing an SH2-binding domain, which in turn recruits Src and promotes phosphorylation of FAK1 at Tyr 576/577 (Robertson et al., 2015). The fully active FAK1/Src complex can then recruit, phosphorylate, and activate numerous targets including p130CAS and PAX1, which play critical roles in regulating cell spreading, cell motility, and cytoskeletal modifications (Zhang et al., 2010). In this line, it has been shown that maximal tyrosine phosphorylation of PAX1 by Src and FAK1 is required for the

induction of anchorage-independent signal transduction, a characteristic of metastatic cells (Vilk et al., 2008; Anderson et al., 2015). As a signal transducer for ECM–tumor cell interactions, FAK1 expression and/or activation has been found altered in most human epithelial cancers, resulting in enhanced invasive potential and poor overall patient survival (McLean et al., 2005; Luo and Guan, 2010). Similarly, CK2 α overexpression in a significant fraction of breast cancers is predictive of metastatic risk (Giusiano et al., 2011). Moreover, suppression of CK2 β expression in a subset of breast cancers modulates the expression of EMT-related markers (Deshiere et al., 2013). Our findings now demonstrate that a loss of CK2 β leads to changes in the size of the focal adhesions, through the activation of the well-characterized FAK1–Src–PAX1 signaling pathway.

While CK2 β is traditionally considered as a regulatory subunit of CK2, some studies also suggest that this subunit might function independently of CK2 α (Filhol et al., 2015; Borgo et al., 2019; Lettieri et al., 2019). Indeed, blocking the CK2 catalytic activity in CK2 β -depleted cells with CX-4945 did not affect the Tyr phosphorylation of FAK1 and p130CAS while triggering enhanced phosphorylation of Src and PAX1, supporting the hypothesis that CK2 β may play additional roles outside of the CK2 tetrameric holoenzyme (Bibby and Litchfield, 2005; Borgo et al., 2019). Our data show that by limiting the focal adhesion formation, CK2 β appears as a major molecular break for cell spreading. The impact of CK2 β on FAs is supported by the role of CK2 in cytoskeletal alteration (Canton and Litchfield, 2006; Lettieri et al., 2019) and in the regulation of actin and tubulin polymerization (reviewed in D'Amore et al., 2019). For instance, it has been previously reported that epithelial cell polarity and morphology might be controlled by CK2 through the phosphorylation of the Pleckstrin homology domain-containing protein (CKIP-1) and coronins, key proteins playing roles in the functional organization of actin-dependent cellular processes like protrusion formation, migration, and invasion (Canton et al., 2005; Deshiere et al., 2008; Deshiere et al., 2011; Xavier et al., 2012; Filhol et al., 2015).

We have generated proteomics data on samples enriched by PMAC (**Supplementary Table S5**), which give a global overview of the phosphoproteome, and on the 4G10 affinity resin which enriches for pTyr-modified proteins (**Supplementary Table S2**). Both approaches provided a complementary view on the phosphoproteins deregulated upon deletion of the CK2 β subunit and are also incomplete, as they missed many proteins involved in the Src pathway, for example. To follow specifically the phosphorylation state of proteins of interest, a complementary approach such as targeted proteomics on the proteolytic peptides containing the modified Ser/Thr/Tyr residues of interest or Western blot analysis using specific antibodies would be better suited. Yet targeted proteomics requires time for method development and Western blot analysis is only possible if antibodies of validated specificity are available.

In summary, the data collected here support the notion that CK2 β works by more than altering the CK2 activity: it also plays a

key role in the negative regulation of focal adhesion maturation, blocking dominant pTyr downstream signaling pathways involved in cell scattering and invasion. Further functional characterization of the molecular mechanism by which CK2 β could restrain these pathways in normal human mammary cells is the subject of ongoing work. More broadly, this analysis will cast additional insights into the specific contribution of individual CK2 subunits during breast carcinoma progression.

DATA AVAILABILITY STATEMENT

Publicly available datasets were analyzed in this study. The LC-MS/MS data have been submitted to the ProteomeXchange Consortium via the PRIDE (Perez-Riverol et al., 2019) partner repository under dataset identifier PXD030991.

AUTHOR CONTRIBUTIONS

Conceptualization: CC, OF, and DP; investigation: A-MH, OF, CC, and A-PB; formal analysis: CC, OF, DP, FJ, CB, A-MH, CA-R, and A-PB; writing original draft: CC, OF, and DP; funding acquisition: OF, CC, CA-R, and DP; supervision: OF, CC, DP, and CA-R.

FUNDING

FJ is supported by the KATY EU program Horizon 2020/H2020-SCI-FA-DTS-2020-1 (contract number 101017453). The proteomic experiments were partially supported by Agence Nationale de la Recherche under projects ProFI (Proteomics French Infrastructure, ANR-10-INBS-08) and GRAL, a program from the Chemistry Biology Health (CBH) Graduate School of University Grenoble Alpes (ANR-17-EURE-0003). This research was supported in part by Institut National de la Santé et de la Recherche Médicale (Inserm), Commissariat à l'Energie Atomique et aux Energies Alternatives (CEA), the Ligue Nationale contre le Cancer, the Ligue Comité de la Loire, and Université Grenoble-Alpes (UGA).

ACKNOWLEDGMENTS

The authors would like to thank Peter Linders for his contribution to PamGene data analysis and Mélodie Malige and Justine Cristante for their technical support.

SUPPLEMENTARY MATERIAL

The Supplementary Material for this article can be found online at: <https://www.frontiersin.org/articles/10.3389/fmolb.2022.900947/full#supplementary-material>

REFERENCES

- Abu-Thuraia, A., Goyette, M.-A., Boulais, J., Delliaux, C., Apcher, C., Schott, C., et al. (2020). AXL Confers Cell Migration and Invasion by Hijacking a PEAK1-Regulated Focal Adhesion Protein Network. *Nat. Commun.* 11, 3586. doi:10.1038/s41467-020-17415-x
- Ahmed, K., Gerber, D. A., and Cochet, C. (2002). Joining the Cell Survival Squad: An Emerging Role for Protein Kinase CK2. *Trends Cell Biol.* 12, 226–230. doi:10.1016/s0962-8924(02)02279-1
- Anderson, J. C., Willey, C. D., Mehta, A., Welaya, K., Chen, D., Duarte, C. W., et al. (2015). High Throughput Kinomic Profiling of Human Clear Cell Renal Cell Carcinoma Identifies Kinase Activity Dependent Molecular Subtypes. *PLoS One* 10, e0139267. doi:10.1371/journal.pone.0139267
- Arni, S., LE, T. H. N., DE Wijn, R., Garcia-Villegas, R., Dankers, M., Weder, W., et al. (2017). *Ex Vivo* Multiplex Profiling of Protein Tyrosine Kinase Activities in Early Stages of Human Lung Adenocarcinoma. *Oncotarget* 8, 68599–68613. doi:10.18632/oncotarget.19803
- Arsenault, R., Griebel, P., and Napper, S. (2011). Peptide Arrays for Kinome Analysis: New Opportunities and Remaining Challenges. *Proteomics* 11, 4595–4609. doi:10.1002/pmic.201100296
- Atashrazm, F., and Ellis, S. (2021). The Polarity Protein PARD3 and Cancer. *Oncogene* 40, 4245–4262. doi:10.1038/s41388-021-01813-6
- Basnet, H., Su, X. B., Tan, Y., Meisenhelder, J., Merkurjev, D., Ohgi, K. A., et al. (2014). Tyrosine Phosphorylation of Histone H2A by CK2 Regulates Transcriptional Elongation. *Nature* 516, 267–271. doi:10.1038/nature13736
- Berg, S., Kutra, D., Kroeger, T., Straehle, C. N., Kausler, B. X., Haubold, C., et al. (2019). Ilastik: Interactive Machine Learning for (Bio)Image Analysis. *Nat. Methods* 16, 1226–1232. doi:10.1038/s41592-019-0582-9
- Bibby, A. C., and Litchfield, D. W. (2005). The Multiple Personalities of the Regulatory Subunit of Protein Kinase CK2: CK2 Dependent and CK2 Independent Roles Reveal a Secret Identity for CK2 β . *Int. J. Biol. Sci.* 1, 67–79. doi:10.7150/ijbs.1.67
- Blume-Jensen, P., and Hunter, T. (2001). Oncogenic Kinase Signalling. *Nature* 411, 355–365. doi:10.1038/35077225
- Borgo, C., D'Amore, C., Sarno, S., Salvi, M., and Ruzzene, M. (2021). Protein Kinase CK2: A Potential Therapeutic Target for Diverse Human Diseases. *Sig. Transduct. Target Ther.* 6, 183. doi:10.1038/s41392-021-00567-7
- Borgo, C., Franchin, C., Cesaro, L., Zaramella, S., Arrigoni, G., Salvi, M., et al. (2019). A Proteomics Analysis of CK2 β (–/–) C2C12 Cells Provides Novel Insights into the Biological Functions of the Non-Catalytic β Subunit. *FEBS J.* 286, 1561–1575. doi:10.1111/febs.14799
- Bouyssié, D., Hesse, A.-M., Mouton-Barbosa, E., Rompais, M., Macron, C., Carapito, C., et al. (2020). Proline: An Efficient and User-Friendly Software Suite for Large-Scale Proteomics. *Bioinformatics* 36, 3148–3155. doi:10.1093/bioinformatics/btaa118
- Bridgewater, R. E., Norman, J. C., and Caswell, P. T. (2012). Integrin Trafficking at a Glance. *J. Cell Sci.* 125, 3695–3701. doi:10.1242/jcs.095810
- Brown, M. C., Perrotta, J. A., and Turner, C. E. (1996). Identification of LIM3 as the Principal Determinant of Paxillin Focal Adhesion Localization and Characterization of a Novel Motif on Paxillin Directing Vinculin and Focal Adhesion Kinase Binding. *J. Cell Biol.* 135, 1109–1123. doi:10.1083/jcb.135.4.1109
- Burridge, K., Fath, K., Kelly, T., Nuckolls, G., and Turner, C. (1988). Focal Adhesions: Transmembrane Junctions Between the Extracellular Matrix and the Cytoskeleton. *Annu. Rev. Cell Biol.* 4, 487–525. doi:10.1146/annurev.cb.04.110188.002415
- Burridge, K. (2017). Focal Adhesions: A Personal Perspective on a Half Century of Progress. *FEBS J.* 284, 3355–3361. doi:10.1111/febs.14195
- Canton, D. A., and Litchfield, D. W. (2006). The Shape of Things to Come: An Emerging Role for Protein Kinase CK2 in the Regulation of Cell Morphology and the Cytoskeleton. *Cell. Signal.* 18, 267–275. doi:10.1016/j.cellsig.2005.07.008
- Canton, D. A., Olsten, M. E. K., Kim, K., Doherty-Kirby, A., Lajoie, G., Cooper, J. A., et al. (2005). The Pleckstrin Homology Domain-Containing Protein CKIP-1 Is Involved in Regulation of Cell Morphology and the Actin Cytoskeleton and Interaction with Actin Capping Protein. *Mol. Cell Biol.* 25, 3519–3534. doi:10.1128/mcb.25.9.3519-3534.2005
- Chen, Z., Oh, D., Biswas, K. H., Yu, C. H., Zaidel-Bar, R., and Groves, J. T. (2018). Spatially Modulated ephrinA1:EphA2 Signaling Increases Local Contractility and Global Focal Adhesion Dynamics to Promote Cell Motility. *Proc. Natl. Acad. Sci. U. S. A.* 115, E5696–E5705. doi:10.1073/pnas.1719961115
- Chirumamilla, C. S., Fazil, M. H. U. T., Perez-Novo, C., Rangarajan, S., DE Wijn, R., Ramireddy, P., et al. (2019). Profiling Activity of Cellular Kinases in Migrating T-Cells. *Methods Mol. Biol.* 1930, 99–113. doi:10.1007/978-1-4939-9036-8_13
- Choi, C. K., Zareno, J., Digman, M. A., Gratton, E., and Horwitz, A. R. (2011). Cross-Correlated Fluctuation Analysis Reveals Phosphorylation-Regulated Paxillin-FAK Complexes in Nascent Adhesions. *Biophysical J.* 100, 583–592. doi:10.1016/j.bpj.2010.12.3719
- Choy, L., Hagenbeek, T. J., Solon, M., French, D., Finkle, D., Shelton, A., et al. (2017). Constitutive NOTCH3 Signaling Promotes the Growth of Basal Breast Cancers. *Cancer Res.* 77, 1439–1452. doi:10.1158/0008-5472.can-16-1022
- Chua, M. M., Ortega, C. E., Sheikh, A., Lee, M., Abdul-Rassoul, H., Hartshorn, K. L., et al. (2017). CK2 in Cancer: Cellular and Biochemical Mechanisms and Potential Therapeutic Target. *Pharm. (Basel)* 10, 18. doi:10.3390/ph10010018
- Craig, S. W., and Johnson, R. P. (1996). Assembly of Focal Adhesions: Progress, Paradigms, and Portents. *Curr. Opin. Cell Biol.* 8, 74–85. doi:10.1016/s0955-0674(96)80051-2
- D'Amore, C., Salizzato, V., Borgo, C., Cesaro, L., Pinna, L. A., and Salvi, M. (2019). A Journey Through the Cytoskeleton with Protein Kinase CK2. *Cpps* 20, 547–562. doi:10.2174/1389203720666190119124846
- Debnath, J., Muthuswamy, S. K., and Brugge, J. S. (2003). Morphogenesis and Oncogenesis of MCF-10A Mammary Epithelial Acini Grown in Three-Dimensional Basement Membrane Cultures. *Methods* 30, 256–268. doi:10.1016/s1046-2023(03)00032-x
- Deshiere, A., Duchemin-Pelletier, E., Spreux, E., Ciais, D., Combes, F., Vandenbrouck, Y., et al. (2013). Unbalanced Expression of CK2 Kinase Subunits Is Sufficient to Drive Epithelial-To-Mesenchymal Transition by Snail Induction. *Oncogene* 32, 1373–1383. doi:10.1038/nc.2012.165
- Deshiere, A., Duchemin-Pelletier, E., Spreux, E., Ciais, D., Forcet, C., Cochet, C., et al. (2011). Regulation of Epithelial to Mesenchymal Transition: CK2 β on Stage. *Mol. Cell Biochem.* 356, 11–20. doi:10.1007/s11010-011-0942-y
- Deshière, A., Theis-Febvre, N., Martel, V., Cochet, C., and Filhol, O. (2008). Protein Kinase CK2 and Cell Polarity. *Mol. Cell Biochem.* 316, 107–113. doi:10.1007/s11010-008-9845-y
- Donato, D. M., Ryzhova, L. M., Meenderink, L. M., Kaverina, I., and Hanks, S. K. (2010). Dynamics and Mechanism of p130Cas Localization to Focal Adhesions. *J. Biol. Chem.* 285, 20769–20779. doi:10.1074/jbc.m109.091207
- Donella-Deana, A., Cesaro, L., Sarno, S., Ruzzene, M., Brunati, A. M., Marin, O., et al. (2003). Tyrosine Phosphorylation of Protein Kinase CK2 by Src-Related Tyrosine Kinases Correlates with Increased Catalytic Activity. *Biochem. J.* 372, 841–849. doi:10.1042/bj20021905
- Duchemin-Pelletier, E., Baulard, M., Spreux, E., Prioux, M., Burute, M., Mograbi, B., et al. (2017). Stem Cell-Like Properties of CK2 β -Down Regulated Mammary Cells. *Cancers (Basel)* 9, 114. doi:10.3390/cancers9090114
- Filhol, O., Cochet, C., Delagoutte, T., and Chambaz, E. M. (1991). Polyamine Binding Activity of Casein Kinase II. *Biochem. Biophysical Res. Commun.* 180, 945–952. doi:10.1016/s0006-291x(05)81157-x
- Filhol, O., and Cochet, C. (2009). Protein Kinase CK2 in Health and Disease. *Cell. Mol. Life Sci.* 66, 1830–1839. doi:10.1007/s00018-009-9151-1
- Filhol, O., Giacosa, S., Wallez, Y., and Cochet, C. (2015). Protein Kinase CK2 in Breast Cancer: The CK2 β Regulatory Subunit Takes Center Stage in Epithelial Plasticity. *Cell. Mol. Life Sci.* 72, 3305–3322. doi:10.1007/s00018-015-1929-8
- Filhol, O., Martiel, J. L., and Cochet, C. (2004). Protein Kinase CK2: A New View of an Old Molecular Complex. *EMBO Rep.* 5, 351–355. doi:10.1038/sj.embor.7400115
- Filhol, O., Nueda, A., Martel, V., Gerber-Scockaert, D., Benitez, M. J., Souchier, C., et al. (2003). Live-Cell Fluorescence Imaging Reveals the Dynamics of Protein Kinase CK2 Individual Subunits. *Mol. Cell Biol.* 23, 975–987. doi:10.1128/mcb.23.3.975-987.2003
- Finney, A. C., Scott, M. L., Reeves, K. A., Wang, D., Alfaidi, M., Schwartz, J. C., et al. (2021). EphA2 Signaling within Integrin Adhesions Regulates Fibrillar

- Adhesion Elongation and Fibronectin Deposition. *Matrix Biol.* 103–104, 1–21. doi:10.1016/j.matbio.2021.09.001
- Galvagni, F., Pennacchini, S., Salameh, A., Rocchigiani, M., Neri, F., Orlandini, M., et al. (2010). Endothelial Cell Adhesion to the Extracellular Matrix Induces C-Src-Dependent VEGFR-3 Phosphorylation Without the Activation of the Receptor Intrinsic Kinase Activity. *Circulation Res.* 106, 1839–1848. doi:10.1161/circresaha.109.206326
- Geiger, B., and Bershadsky, A. (2001). Assembly and Mechanosensory Function of Focal Contacts. *Curr. Opin. Cell Biol.* 13, 584–592. doi:10.1016/s0955-0674(00)00255-6
- Giusiano, S., Cochet, C., Filhol, O., Duchemin-Pelletier, E., Secq, V., Bonnier, P., et al. (2011). Protein Kinase CK2 α Subunit Over-Expression Correlates with Metastatic Risk in Breast Carcinomas: Quantitative Immunohistochemistry in Tissue Microarrays. *Eur. J. Cancer* 47, 792–801. doi:10.1016/j.ejca.2010.11.028
- Golden, D., and Cantley, L. G. (2014). Casein Kinase 2 Prevents Mesenchymal Transformation by Maintaining Foxc2 in the Cytoplasm. *Oncogene* 34, 4702–4712. doi:10.1038/onc.2014.395
- Guerra, B., and Issinger, O.-G. (2008). Protein Kinase CK2 in Human Diseases. *Cmc* 15, 1870–1886. doi:10.2174/092986708785132933
- Harte, M. T., Hildebrand, J. D., Burnham, M. R., Bouton, A. H., and Parsons, J. T. (1996). p130Cas, a Substrate Associated with V-Src and V-Crk, Localizes to Focal Adhesions and Binds to Focal Adhesion Kinase. *J. Biol. Chem.* 271, 13649–13655. doi:10.1074/jbc.271.23.13649
- Hochgräfe, F., Zhang, L., O'Toole, S. A., Browne, B. C., Pinese, M., Porta Cubas, A., et al. (2010). Tyrosine Phosphorylation Profiling Reveals the Signaling Network Characteristics of Basal Breast Cancer Cells. *Cancer Res.* 70, 9391–9401. doi:10.1158/0008-5472.can.10-0911
- Hong, H., and Benveniste, E. N. (2021). The Immune Regulatory Role of Protein Kinase CK2 and Its Implications for Treatment of Cancer. *Biomedicine* 9, 1932. doi:10.3390/biomedicine9121932
- Hu, Y.-L., Lu, S., Szeto, K. W., Sun, J., Wang, Y., Lasheras, J. C., et al. (2014). FAK and Paxillin Dynamics at Focal Adhesions in the Protrusions of Migrating Cells. *Sci. Rep.* 4, 6024. doi:10.1038/srep06024
- Huber, W., VON Heydebreck, A., Sülthmann, H., Poustka, A., and Vingron, M. (2002). Variance Stabilization Applied to Microarray Data Calibration and to the Quantification of Differential Expression. *Bioinformatics* 18 (Suppl. 1), S96–S104. doi:10.1093/bioinformatics/18.suppl_1.s96
- Hunter, T. (1995). Protein Kinases and Phosphatases: The Yin and Yang of Protein Phosphorylation and Signaling. *Cell* 80, 225–236. doi:10.1016/0092-8674(95)90405-0
- Jensen, S. S., and Larsen, M. R. (2007). Evaluation of the Impact of Some Experimental Procedures on Different Phosphopeptide Enrichment Techniques. *Rapid Commun. Mass Spectrom.* 21, 3635–3645. doi:10.1002/rcm.3254
- Kanehisa, M., and Goto, S. (2000). KEGG: Kyoto Encyclopedia of Genes and Genomes. *Nucleic Acids Res.* 28, 27–30. doi:10.1093/nar/28.1.27
- Kim, D. H., and Wirtz, D. (2013). Focal Adhesion Size Uniquely Predicts Cell Migration. *FASEB J.* 27, 1351–1361. doi:10.1096/fj.12-220160
- Kim, H., Choi, K., Kang, H., Lee, S.-Y., Chi, S.-W., Lee, M.-S., et al. (2014). Identification of a Novel Function of CX-4945 as a Splicing Regulator. *PLoS One* 9, e94978. doi:10.1371/journal.pone.0094978
- Kim, J. S., Eom, J. I., Cheong, J.-W., Choi, A. J., Lee, J. K., Yang, W. I., et al. (2007). Protein Kinase CK2 α as an Unfavorable Prognostic Marker and Novel Therapeutic Target in Acute Myeloid Leukemia. *Clin. Cancer Res.* 13, 1019–1028. doi:10.1158/1078-0432.ccr-06-1602
- Kim, S., Ham, S., Yang, K., and Kim, K. (2018). Protein Kinase CK2 Activation Is Required for Transforming Growth Factor β -Induced Epithelial-Mesenchymal Transition. *Mol. Oncol.* 12, 1811–1826. doi:10.1002/1878-0261.12378
- Kobayashi, T., Hino, S.-i., Oue, N., Asahara, T., Zollo, M., Yasui, W., et al. (2006). Glycogen Synthase Kinase 3 and H-Prune Regulate Cell Migration by Modulating Focal Adhesions. *Mol. Cell Biol.* 26, 898–911. doi:10.1128/mcb.26.3.898-911.2006
- Kreutzer, J. N., Ruzzene, M., and Guerra, B. (2010). Enhancing Chemosensitivity to Gemcitabine via RNA Interference Targeting the Catalytic Subunits of Protein Kinase CK2 in Human Pancreatic Cancer Cells. *BMC Cancer* 10, 440. doi:10.1186/1471-2407-10-440
- Laramas, M., Pasquier, D., Filhol, O., Ringeisen, F., Descotes, J.-L., and Cochet, C. (2007). Nuclear Localization of Protein Kinase CK2 Catalytic Subunit (CK2 α) Is Associated with Poor Prognostic Factors in Human Prostate Cancer. *Eur. J. Cancer* 43, 928–934. doi:10.1016/j.ejca.2006.11.021
- Lettieri, A., Borgo, C., Zanieri, L., D'Amore, C., Oleari, R., Paganoni, A., et al. (2019). Protein Kinase CK2 Subunits Differentially Perturb the Adhesion and Migration of GN11 Cells: A Model of Immature Migrating Neurons. *Int. J. Mol. Sci.* 20, 5951. doi:10.3390/ijms20235951
- Lin, K.-Y., Tai, C., Hsu, J.-C., Li, C.-F., Fang, C.-L., Lai, H.-C., et al. (2011). Overexpression of Nuclear Protein Kinase CK2 α Catalytic Subunit (CK2 α) as a Poor Prognosticator in Human Colorectal Cancer. *PLoS One* 6, e17193. doi:10.1371/journal.pone.0017193
- Litchfield, D. W. (2003). Protein Kinase CK2: Structure, Regulation and Role in Cellular Decisions of Life and Death. *Biochem. J.* 369, 1–15. doi:10.1042/bj20021469
- Luo, M., and Guan, J.-L. (2010). Focal Adhesion Kinase: A Prominent Determinant in Breast Cancer Initiation, Progression and Metastasis. *Cancer Lett.* 289, 127–139. doi:10.1016/j.canlet.2009.07.005
- Machiyama, H., Hirata, H., Loh, X. K., Kanchi, M. M., Fujita, H., Tan, S. H., et al. (2014). Displacement of p130Cas from Focal Adhesions Links Actomyosin Contraction to Cell Migration. *J. Cell Sci.* 127, 3440–3450. doi:10.1242/jcs.143438
- Maher, P. A., Pasquale, E. B., Wang, J. Y., and Singer, S. J. (1985). Phosphotyrosine-Containing Proteins Are Concentrated in Focal Adhesions and Intercellular Junctions in Normal Cells. *Proc. Natl. Acad. Sci. U.S.A.* 82, 6576–6580. doi:10.1073/pnas.82.19.6576
- Maru, Y., Hanks, S. K., and Shibuya, M. (2001). The Tubulogenic Activity Associated with an Activated Form of Flt-1 Kinase Is Dependent on Focal Adhesion Kinase. *Biochimica Biophysica Acta (BBA) - Mol. Cell Res.* 1540, 147–153. doi:10.1016/s0167-4889(01)00127-6
- McLean, G. W., Carragher, N. O., Avizienyte, E., Evans, J., Brunton, V. G., and Frame, M. C. (2005). The Role of Focal-Adhesion Kinase in Cancer - A New Therapeutic Opportunity. *Nat. Rev. Cancer* 5, 505–515. doi:10.1038/nrc1647
- Meenderink, L. M., Ryzhova, L. M., Donato, D. M., Gochberg, D. F., Kaverina, I., and Hanks, S. K. (2010). P130Cas Src-Binding and Substrate Domains Have Distinct Roles in Sustaining Focal Adhesion Disassembly and Promoting Cell Migration. *PLoS One* 5, e13412. doi:10.1371/journal.pone.0013412
- Meggio, F., and Pinna, L. A. (2003). One-Thousand-and-One Substrates of Protein Kinase CK2? *FASEB J.* 17, 349–368. doi:10.1096/fj.02-0473rev
- Miao, H., Burnett, E., Kinch, M., Simon, E., and Wang, B. (2000). Activation of EphA2 Kinase Suppresses Integrin Function and Causes Focal-Adhesion-Kinase Dephosphorylation. *Nat. Cell Biol.* 2, 62–69. doi:10.1038/35000008
- Modzelewska, K., Newman, L. P., Desai, R., and Keely, P. J. (2006). Ack1 Mediates Cdc42-Dependent Cell Migration and Signaling to p130Cas. *J. Biol. Chem.* 281, 37527–37535. doi:10.1074/jbc.m604342200
- Nakamura, K., Yano, H., Uchida, H., Hashimoto, S., Schaefer, E., and Sabe, H. (2000). Tyrosine Phosphorylation of Paxillin α Is Involved in Temporospatial Regulation of Paxillin-Containing Focal Adhesion Formation and F-Actin Organization in Motile Cells. *J. Biol. Chem.* 275, 27155–27164. doi:10.1016/s0021-9258(19)61492-4
- Ngan, E., Stoletov, K., Smith, H. W., Common, J., Muller, W. J., Lewis, J. D., et al. (2017). LPP Is a Src Substrate Required for Invasive Podia Formation and Efficient Breast Cancer Lung Metastasis. *Nat. Commun.* 8, 15059. doi:10.1038/ncomms15059
- Nunez DE Villavicencio-Diaz, T., Rabalski, A. J., and Litchfield, D. W. (2017). Protein Kinase CK2: Intricate Relationships within Regulatory Cellular Networks. *Pharm. (Basel)* 10, 27. doi:10.3390/ph10010027
- Okayama, A., Miyagi, Y., Oshita, F., Ito, H., Nakayama, H., Nishi, M., et al. (2015). Identification of Tyrosine-Phosphorylated Proteins Upregulated During Epithelial-Mesenchymal Transition Induced with TGF- β . *J. Proteome Res.* 14, 4127–4136. doi:10.1021/acs.jproteome.5b00082
- Olsen, B. B., Boldyreff, B., Niefind, K., and Issinger, O.-G. (2006). Purification and Characterization of the CK2 α' -Based Holoenzyme, an Isozyme of CK2 α : A Comparative Analysis. *Protein Expr. Purif.* 47, 651–661. doi:10.1016/j.pep.2005.12.001
- Olsten, M. E. K., Canton, D. A., Zhang, C., Walton, P. A., and Litchfield, D. W. (2004). The Pleckstrin Homology Domain of CK2 Interacting Protein-1 Is Required for Interactions and Recruitment of Protein Kinase CK2 to the Plasma Membrane. *J. Biol. Chem.* 279, 42114–42127. doi:10.1074/jbc.m407628200

- Perez-Riverol, Y., Csordas, A., Bai, J., Bernal-Llinares, M., Hewapathirana, S., Kundu, D. J., et al. (2019). The PRIDE Database and Related Tools and Resources in 2019: Improving Support for Quantification Data. *Nucleic Acids Res.* 47, D442–D450. doi:10.1093/nar/gky1106
- Petit, M. M., Meulemans, S. M., Alen, P., Ayoubi, T. A., Jansen, E., and VAN DE Ven, W. J. (2005). The Tumor Suppressor Scrib Interacts with the Zyxin-Related Protein LPP, Which Shuttles Between Cell Adhesion Sites and the Nucleus. *BMC Cell Biol.* 6, 1. doi:10.1186/1471-2121-6-1
- Petit, M. M. R., Meulemans, S. M. P., and VAN DE Ven, W. J. M. (2003). The Focal Adhesion and Nuclear Targeting Capacity of the LIM-Containing Lipoma-Preferred Partner (LPP) Protein. *J. Biol. Chem.* 278, 2157–2168. doi:10.1074/jbc.m206106200
- Petropoulos, C., Oddou, C., Emadali, A., Hiriart-Bryant, E., Boyault, C., Faurobert, E., et al. (2016). Roles of Paxillin Family Members in Adhesion and ECM Degradation Coupling at Invadosomes. *J. Cell Biol.* 213, 585–599. doi:10.1083/jcb.201510036
- Qian, B.-Z., Zhang, H., Li, J., He, T., Yeo, E.-J., Soong, D. Y. H., et al. (2015). FLT1 Signaling in Metastasis-Associated Macrophages Activates an Inflammatory Signature that Promotes Breast Cancer Metastasis. *J. Exp. Med.* 212, 1433–1448. doi:10.1084/jem.20141555
- Robertson, J., Jacquemet, G., Byron, A., Jones, M. C., Warwood, S., Selley, J. N., et al. (2015). Defining the Phospho-Adesome Through the Phosphoproteomic Analysis of Integrin Signalling. *Nat. Commun.* 6, 6265. doi:10.1038/ncomms7265
- Roelants, C., Giacosa, S., Duchemin-Pelletier, E., Mcleer-Florin, A., Tisseyre, C., Aubert, C., et al. (2015). *Dysregulated Expression of Protein Kinase CK2 in Renal Cancer*. German: Springer.
- Roffey, S. E., and Litchfield, D. W. (2021). CK2 Regulation: Perspectives in 2021. *Biomedicine* 9, 1361. doi:10.3390/biomedicine9101361
- Rozanov, D. V., Savinov, A. Y., Williams, R., Liu, K., Golubkov, V. S., Krajewski, S., et al. (2008). Molecular Signature of MT1-MMP: Transactivation of the Downstream Universal Gene Network in Cancer. *Cancer Res.* 68, 4086–4096. doi:10.1158/0008-5472.can-07-6458
- Sachdev, S., Bu, Y., and Gelman, I. H. (2009). Paxillin-Y118 Phosphorylation Contributes to the Control of Src-Induced Anchorage-Independent Growth by FAK and Adhesion. *BMC Cancer* 9, 12. doi:10.1186/1471-2407-9-12
- Salgia, R., Li, J.-L., Lo, S. H., Brunkhorst, B., Kansas, G. S., Sobhany, E. S., et al. (1995). Molecular Cloning of Human Paxillin, a Focal Adhesion Protein Phosphorylated by P210BCR/ABL. *J. Biol. Chem.* 270, 5039–5047. doi:10.1074/jbc.270.10.5039
- Salveti, A., Couté, Y., Epstein, A., Arata, L., Kraut, A., Navratil, V., et al. (2016). Nuclear Functions of Nucleolin Through Global Proteomics and Interactomic Approaches. *J. Proteome Res.* 15, 1659–1669. doi:10.1021/acs.jproteome.6b00126
- Salvi, M., Sarno, S., Cesaro, L., Nakamura, H., and Pinna, L. A. (2009). Extraordinary Pleiotropy of Protein Kinase CK2 Revealed by Weblog Phosphoproteome Analysis. *Biochimica Biophysica Acta (BBA) - Mol. Cell Res.* 1793, 847–859. doi:10.1016/j.bbamcr.2009.01.013
- Schaller, M. D., Hildebrand, J. D., and Parsons, J. T. (1999). Complex Formation with Focal Adhesion Kinase: A Mechanism to Regulate Activity and Subcellular Localization of Src Kinases. *MBoC* 10, 3489–3505. doi:10.1091/mbc.10.10.3489
- Schindelin, J., Arganda-Carreras, I., Frise, E., Kaynig, V., Longair, M., Pietzsch, T., et al. (2012). Fiji: An Open-Source Platform for Biological-Image Analysis. *Nat. Methods* 9, 676–682. doi:10.1038/nmeth.2019
- Schmalzigaug, R., Garron, M., Roseman, J., Xing, Y., Davidson, C., Arold, S., et al. (2007). GIT1 Utilizes a Focal Adhesion Targeting-Homology Domain to Bind Paxillin. *Cell. Signal.* 19, 1733–1744. doi:10.1016/j.cellsig.2007.03.010
- Schmitt, B. M., Boewe, A. S., Gotz, C., Philipp, S. E., Urbchat, S., Oertel, J., et al. (2021). CK2 Activity Mediates the Aggressive Molecular Signature of Glioblastoma Multiforme by Inducing Nerve/Glial Antigen (NG2) Expression. *Cancers (Basel)* 13, 1678. doi:10.3390/cancers13071678
- Senda, Y., Murata-Kamiya, N., and Hatakeyama, M. (2016). C-Terminal Src Kinase-Mediated EPIYA Phosphorylation of Pragmin Creates a Feed-Forward C-Terminal Src Kinase Activation Loop that Promotes Cell Motility. *Cancer Sci.* 107, 972–980. doi:10.1111/cas.12962
- Shen, Y., and Schaller, M. D. (1999). Focal Adhesion Targeting: The Critical Determinant of FAK Regulation and Substrate Phosphorylation. *MBoC* 10, 2507–2518. doi:10.1091/mbc.10.8.2507
- Strum, S. W., Gyenis, L., and Litchfield, D. W. (2021). CSNK2 in Cancer: Pathophysiology and Translational Applications. *Br. J. Cancer* 126, 994–1003. doi:10.1038/s41416-021-01616-2
- Sun, T., Kim, B., and Kim, L. W. (2013). Glycogen Synthase Kinase 3 Influences Cell Motility and Chemotaxis by Regulating PI3K Membrane Localization in Dictyostelium. *Dev. Growth Differ.* 55, 723–734. doi:10.1111/dgd.12078
- Tapial Martínez, P., López Navajas, P., and Lietha, D. (2020). FAK Structure and Regulation by Membrane Interactions and Force in Focal Adhesions. *Biomolecules* 10. doi:10.3390/biom10020179
- Totaro, A., Astro, V., Tonoli, D., and DE Curtis, I. (2014). Identification of Two Tyrosine Residues Required for the Intramolecular Mechanism Implicated in GIT1 Activation. *PLoS One* 9, e93199. doi:10.1371/journal.pone.0093199
- Valdivia, A., Cárdenas, A., Brenet, M., Maldonado, H., Kong, M., Díaz, J., et al. (2020). Syndecan-4/PAR-3 Signaling Regulates Focal Adhesion Dynamics in Mesenchymal Cells. *Cell Commun. Signal.* 18, 129. doi:10.1186/s12964-020-00629-3
- Vilk, G., Weber, J. E., Turowec, J. P., Duncan, J. S., Wu, C., Derksen, D. R., et al. (2008). Protein Kinase CK2 Catalyzes Tyrosine Phosphorylation in Mammalian Cells. *Cell. Signal.* 20, 1942–1951. doi:10.1016/j.cellsig.2008.07.002
- Volberg, T., Romer, L., Zamir, E., and Geiger, B. (2001). pp60c-src and Related Tyrosine Kinases: A Role in the Assembly and Reorganization of Matrix Adhesions. *J. Cell Sci.* 114, 2279–2289. doi:10.1242/jcs.114.12.2279
- Wang, Y., DU, D., Fang, L., Yang, G., Zhang, C., Zeng, R., et al. (2006). Tyrosine Phosphorylated Par3 Regulates Epithelial Tight Junction Assembly Promoted by EGFR Signaling. *EMBO J.* 25, 5058–5070. doi:10.1038/sj.emboj.7601384
- Wehde, B. L., Rädler, P. D., Shrestha, H., Johnson, S. J., Triplett, A. A., and Wagner, K.-U. (2018). Janus Kinase 1 Plays a Critical Role in Mammary Cancer Progression. *Cell Rep.* 25, 2192–2207. e5. doi:10.1016/j.celrep.2018.10.063
- Wieczorek, S., Combes, F., Lazar, C., Gai Gianetto, Q., Gatto, L., Dorffer, A., et al. (2017). DAPAR & ProStaR: Software to Perform Statistical Analyses in Quantitative Discovery Proteomics. *Bioinformatics* 33, 135–136. doi:10.1093/bioinformatics/btw580
- Wozniak, M. A., Modzelewska, K., Kwong, L., and Keely, P. J. (2004). Focal Adhesion Regulation of Cell Behavior. *Biochimica Biophysica Acta (BBA) - Mol. Cell Res.* 1692, 103–119. doi:10.1016/j.bbamcr.2004.04.007
- Wu, J.-C., Chen, Y.-C., Kuo, C.-T., Wenshin Yu, H., Chen, Y.-Q., Chiou, A., et al. (2015). Focal Adhesion Kinase-Dependent Focal Adhesion Recruitment of SH2 Domains Directs SRC into Focal Adhesions to Regulate Cell Adhesion and Migration. *Sci. Rep.* 5, 18476. doi:10.1038/srep18476
- Xavier, C.-P., Rastetter, R. H., Blömacher, M., Stumpf, M., Himmel, M., Morgan, R. O., et al. (2012). Phosphorylation of CRN2 by CK2 Regulates F-Actin and Arp2/3 Interaction and Inhibits Cell Migration. *Sci. Rep.* 2, 241. doi:10.1038/srep00241
- Yin, G., Zheng, Q., Yan, C., and Berk, B. C. (2005). GIT1 Is a Scaffold for ERK1/2 Activation in Focal Adhesions. *J. Biol. Chem.* 280, 27705–27712. doi:10.1074/jbc.m502271200
- Zhang, S., Yu, H., and Zhang, L. (2010). Role of Vascular Endothelial Growth Factor Receptor-3/Flt-4 in Early-Stage Cervical Cancer. *Oncol. Lett.* 1, 453–456. doi:10.3892/ol.00000080

Conflict of Interest: The authors declare that the research was conducted in the absence of any commercial or financial relationships that could be construed as a potential conflict of interest.

Publisher's Note: All claims expressed in this article are solely those of the authors and do not necessarily represent those of their affiliated organizations, or those of the publisher, the editors, and the reviewers. Any product that may be evaluated in this article, or claim that may be made by its manufacturer, is not guaranteed or endorsed by the publisher.

Copyright © 2022 Filhol, Hesse, Bouin, Albignès-Rizo, Jeanneret, Battail, Pflieger and Cochet. This is an open-access article distributed under the terms of the Creative Commons Attribution License (CC BY). The use, distribution or reproduction in other forums is permitted, provided the original author(s) and the copyright owner(s) are credited and that the original publication in this journal is cited, in accordance with accepted academic practice. No use, distribution or reproduction is permitted which does not comply with these terms.



Implementing a Scoring Function Based on Interaction Fingerprint for Autogrow4: Protein Kinase CK1 δ as a Case Study

Matteo Pavan, Silvia Menin, Davide Bassani, Mattia Sturlese and Stefano Moro *

Molecular Modeling Section (MMS), Department of Pharmaceutical and Pharmacological Sciences, University of Padova, Padova, Italy

OPEN ACCESS

Edited by:

Victor Bustos,
The Rockefeller University,
United States

Reviewed by:

Antonio Monari,
Université de Paris, France
Marcus Scotti,
Federal University of Paraíba, Brazil

*Correspondence:

Stefano Moro
stefano.moro@unipd.it

Specialty section:

This article was submitted to
Molecular Diagnostics and
Therapeutics,
a section of the journal
Frontiers in Molecular Biosciences

Received: 31 March 2022

Accepted: 25 May 2022

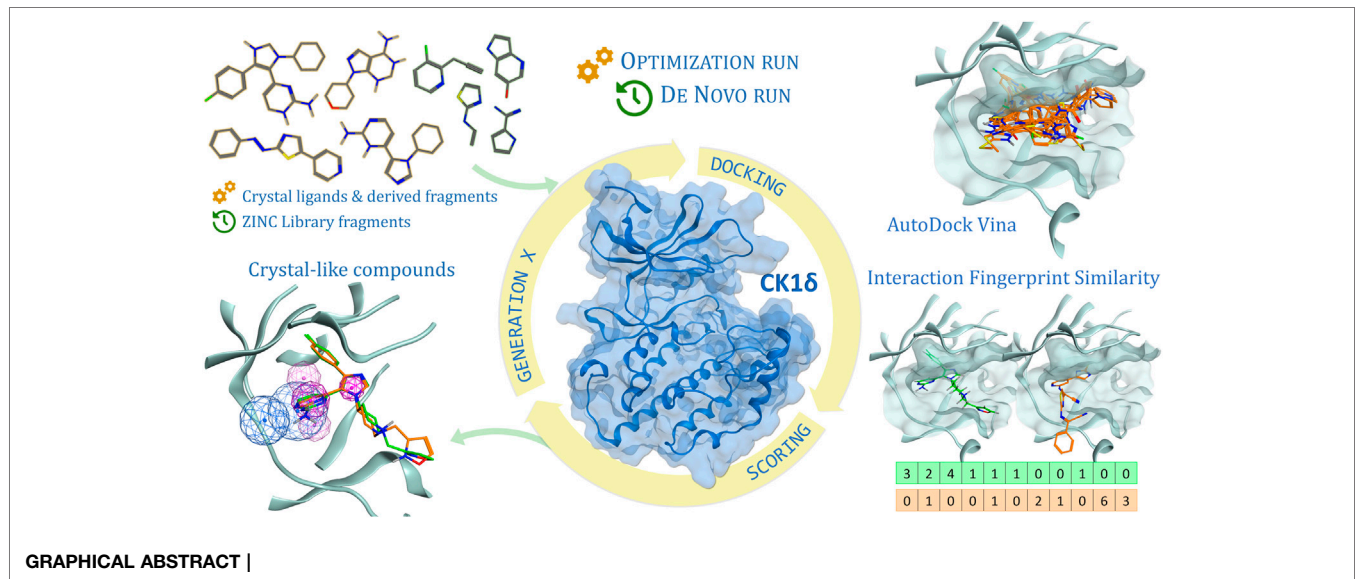
Published: 07 July 2022

Citation:

Pavan M, Menin S, Bassani D,
Sturlese M and Moro S (2022)
Implementing a Scoring Function
Based on Interaction Fingerprint for
Autogrow4: Protein Kinase CK1 δ as a
Case Study.
Front. Mol. Biosci. 9:909499.
doi: 10.3389/fmolb.2022.909499

In the last 20 years, fragment-based drug discovery (FBDD) has become a popular and consolidated approach within the drug discovery pipeline, due to its ability to bring several drug candidates to clinical trials, some of them even being approved and introduced to the market. A class of targets that have proven to be particularly suitable for this method is represented by kinases, as demonstrated by the approval of BRAF inhibitor vemurafenib. Within this wide and diverse set of proteins, protein kinase CK1 δ is a particularly interesting target for the treatment of several widespread neurodegenerative diseases, such as Alzheimer's disease, Parkinson's disease, and amyotrophic lateral sclerosis. Computational methodologies, such as molecular docking, are already routinely and successfully applied in FBDD campaigns alongside experimental techniques, both in the hit-discovery and in the hit-optimization stage. Concerning this, the open-source software Autogrow, developed by the Durrant lab, is a semi-automated computational protocol that exploits a combination between a genetic algorithm and a molecular docking software for *de novo* drug design and lead optimization. In the current work, we present and discuss a modified version of the Autogrow code that implements a custom scoring function based on the similarity between the interaction fingerprint of investigated compounds and a crystal reference. To validate its performance, we performed both a *de novo* and a lead-optimization run (as described in the original publication), evaluating the ability of our fingerprint-based protocol to generate compounds similar to known CK1 δ inhibitors based on both the predicted binding mode and the electrostatic and shape similarity in comparison with the standard Autogrow protocol.

Keywords: fragment-based drug discovery, protein kinase CK1 δ , neurodegenerative diseases, Autogrow, interaction fingerprint, *de novo* drug design, fragment growing, lead optimization



1 INTRODUCTION

Protein kinase CK1δ is a Ser/Thr protein kinase belonging to the casein kinase 1 family. In mammals, seven distinct genes encoding for casein kinase proteins are present, each producing a different isoform (α, β, γ1, γ2, γ3, δ, and ε) (Knippschild et al., 2005). CK1 family proteins use exclusively ATP as a phosphate source for their kinase activity, which is carried out by the protein in its monomeric form. Each isoform is constitutionally active and does not require the presence of a cofactor to exert its activity (Knippschild et al., 2014).

From a biological function point of view, the members of this family have been historically related to different physiological mechanisms, such as cell replication (Xu et al., 2019), DNA repair (Behrend et al., 2000), and circadian rhythm (Lee et al., 2009).

From a structural perspective, the members of the CK1 family are characterized by the typical bilobed structure of the globular Ser-Thr kinase proteins, with the N-term lobe consisting mainly of β-sheets, and a larger C-term lobe, constituted primarily of α-helices. The two domains are connected by a protein region named the “hinge region,” which forms a highly conserved pocket for ATP binding (Knippschild et al., 2014).

As for other members of the CK1 family, CK1δ recognizes the canonical phospho-primed structural motif *pSer/pThr-X₁₋₂-Ser/Thr*, where X stands for any amino acid and pSer/pThr represents the phospho-primed residue (Meggio et al., 1991). The CK1 kinases are also able to recognize non-phosphorylated sequences, as far as they contain strongly acidic residues (Asp or Glu) that can make up for the absence of the phosphorylated residue (Xu et al., 2019). The structural motif that can be recognized by the CK1 proteins is widespread in many cellular proteins and, because of this, over 140 substrates have been reported both *in vitro* and *in vivo* (Knippschild et al., 2014), underlining the pleiotropic character of this protein family. Due to the great variability of its substrates, CK1δ is involved in many

cellular pathways, among which the main ones are the Wnt-pathway, the Hippo pathway, the p53 regulation pathway, and the Hedgehog pathway (Xu et al., 2019).

The endogenous regulation of CK1δ, on the other hand, can be carried out through various mechanisms, including autophosphorylation or phosphorylation by other protein kinases (Graves and Roach, 1995; Bischof et al., 2013), interactions with other protein and/or cellular components, and subcellular sequestration (Milne et al., 2001; Xu et al., 2019). In addition, homodimerization excludes ATP from the binding site, thus inhibiting kinase activity (Longenecker et al., 1998; Hirner et al., 2012).

In recent years, several studies have highlighted the importance of CK1δ in neurodegenerative diseases, particularly tauopathies, such as Alzheimer’s disease (AD), Parkinson’s disease (PD), and amyotrophic lateral sclerosis (ALS) (Perez et al., 2011). In addition to having unknown etiology, these illnesses are all characterized by loss of neuronal function, with neurotransmitter deficiency, misfolding, and protein aggregation (Breijyeh and Karaman, 2020). Clinical symptoms are manifested differently, depending on the neuronal area involved (Lee et al., 2001).

AD is a progressive neurodegenerative disorder that mainly involves the neurons of the hippocampus (Selkoe, 2001). On the extracellular side, the main marker of the disease is represented by the accumulation of β-amyloid peptides, produced by β-secretase 1 and γ-secretase enzymes, which lead to neuronal death (J and DJ, 2002). Meanwhile, on the intracellular part, the illness presents lesions related to both cytoplasmic accumulations of vacuoles with abnormal dimensions and dense granular content and the assembly of fibrils and filaments within the neuronal body. These types of lesions are characterized by the accumulation of hyperphosphorylated Tau protein not only in the filaments, but also within the vacuoles (Ghoshal et al., 1999).

The correlation between CK1δ activity and tau protein aggregates in various neurodegenerative diseases has been confirmed by co-immunoprecipitation studies, which highlight that the presence of CK1δ is associated with hyperphosphorylated tau aggregates (Schwab et al., 2000; Li et al., 2004). CK1δ phosphorylates tau protein at the Ser202/Thr205 and Ser369/Ser404 residues *in vitro* (Li et al., 2004; Perez et al., 2011). The phosphorylation sites are the same as those involved in binding with tubulin, highlighting the key role of kinase in the pathogenesis of AD (Li et al., 2004). It is not clear whether the hyperactivity of CK1δ is due to an overtranscription of its gene, altered protein turnover, or both causes, but it has been observed that the concentration of the protein CK1δ in an AD-affected hippocampus is 30 times higher than normal (Ghoshal et al., 1999).

In PD, on the other hand, the pathology is characterized by the accumulation of Lewy bodies, consisting of aggregates of α-synuclein hyperphosphorylated by CK1δ at the level of Ser129 residues (Okochi et al., 2000). This process determines a massive loss of neuronal function at the substantia nigra level (Surmeier, 2018).

CK1δ also plays a key role in ALS, a neurodegenerative disorder in which intracellular inclusions of TDP-43 (TAR DNA-binding protein) are found in the frontotemporal lobe. It was established that TDP-43 can be phosphorylated by CK1δ at 29 different sites (Kametani et al., 2009).

These pathologies are all characterized by the absence of effective pharmacological therapy: in fact, there are no EMA-approved drugs on the market that can solve, and therefore cure, these diseases, but there are only palliative therapies for the temporary improvement of the patient's quality of life, thus resulting in a high social cost (Dementia, 2021). For these reasons, CK1δ appears as an interesting therapeutic target in the field of neurodegeneration, as witnessed by the increasing interest in the research for inhibitory candidates for this protein during the last 15 years.

Concerning the identification of novel kinase inhibitors, an approach that has proven to be particularly successful is the so-called fragment-based drug discovery (FBDD), as demonstrated by the approval of the BRAF inhibitor vemurafenib (Bollag et al., 2012) (employed in the treatment of metastatic melanoma) and by several other kinase inhibitors which are at various stages of clinical trials (Erlanson et al., 2016; Schoepfer et al., 2018).

This approach revolves around the exploitation of “fragments,” i.e., compounds that respect the “Rule of Three” (molecular weight <300, number of hydrogen bond donor/acceptor ≤ 3, log P ≤ 3), as a starting point for the rational development of novel mature, drug-like, active molecules (Hajduk, 2006; Jhoti et al., 2013). The main reason for the success of FBDD is the ability to sample a larger portion of the chemical space compared to the one occupied by drug-like molecules, thus increasing the success rate in finding novel scaffolds for targets of interest (Hall et al., 2014).

This methodology heavily relies on very sensitive biophysical methods, such as X-ray crystallography (XRC), nuclear magnetic resonance (NMR), or surface plasmon resonance (SPR), to perform large screening campaigns on libraries composed of

molecules with low molecular weight and high solubility, to find hit compounds (Erlanson et al., 2004; Murray and Rees, 2009). These hit fragments usually have a low affinity for the target, ranging from low millimolar to high micromolar (hence the need for very sensitive screening techniques), but a higher binding efficiency compared to traditional drug-like molecules, being able to establish high-quality interaction with the target (Schultes et al., 2010). Fragment hits can then be easily combined (either through a linking or a merging process) or chemically modified (growing) to increase their affinity for the target, allowing for the development of potent and selective active compounds (Rees et al., 2004).

Alongside the aforementioned experimental techniques, in the last decade, a prominent role in FBDD campaigns has been played by computer-aided drug discovery (CADD) techniques, such as molecular docking or molecular dynamics (Bissaro et al., 2020). These computational approaches have been routinely and successfully applied for performing large screening on virtual fragment libraries, for the characterization of the fragment interaction mode with the target and to aid the fragment-to-lead optimization in a less time-consuming, more rational, and more efficient way. Some examples of software specifically designed for FBDD are LUDI (Böhm, 1992), HOOK (Eisen et al., 1994), CAVEAT (Lauri and Bartlett, 1994), and RECORE (Maass et al., 2007). Moreover, commercial drug discovery suites, such as Schrödinger, MOE, and OpenEye, have implemented several tools related to the fragment optimization process.

Among the plethora of software available for FBDD, the open-source software Autogrow, developed by the Durrant lab, is particularly interesting. As thoroughly described in the work of Spiegel and Durrant (2020), the open-source software Autogrow is a Python written code that combines a genetic algorithm with docking calculation based on the Vina (Trott and Olson, 2010) docking software to perform a semi-automatized process for both *de novo* drug design and lead optimization. The latest release of the Autogrow (version 4.0.3, the one used in this work) was developed with the idea of making the codebase modular, thus allowing the third-party implementation of different conversion scripts, molecular docking programs, scoring functions, and reaction libraries, to better suit the need of different research groups.

A recent scientific work published by our laboratory led to the identification of seven novel fragment compounds that bind the hinge region of CK1δ with a low-micromolar IC₅₀ (Bolcato et al., 2021). Attracted by the idea of exploiting a semi-automatized computational protocol for the optimization of our newly discovered fragment compounds, we decided to investigate if this protocol would be suitable for our needs. Since it is notorious that molecular docking programs are usually very efficient and optimized with regard to the conformational search, but are usually lacking in the scoring phase (Chen, 2015; Chaput and Mouawad, 2017) [especially for molecules-like fragments that deviate from the drug-like chemical space on which these scoring functions have been trained (Verdonk et al., 2011; de Souza Neto et al., 2020)], we decided to investigate if the implementation of a different scoring protocol based on protein–ligand interaction

fingerprint would improve the performance of the Autogrow protocol, concerning the ability of the program to generate compounds similar to known inhibitors based on their interaction scheme and electrostatic and shape similarity.

2 MATERIALS AND METHODS

2.1 Hardware Overview

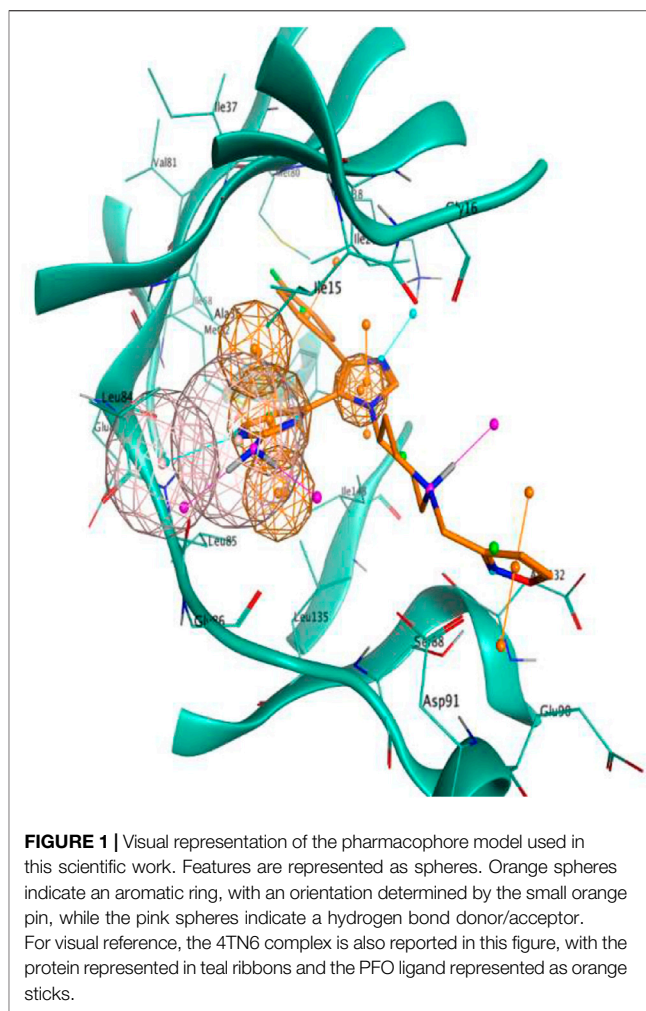
Each general molecular modeling operation has been performed on a Linux Workstation equipped with an 8 core Intel Xeon® CPU E5-1620 CPU. For more intensive calculations, such as the Autogrow runs, a 64 core AMD Opteron™ Processor 6376 CPU cluster was exploited. Both the workstation and the cluster run Ubuntu 16.04 as their operative system.

2.2 Structure Preparation

In the case of protein kinase CK1δ, 23 protein–ligand complexes between the protein and small drug-like molecules are available in the Protein Data Bank (Berman et al., 2000) (PDB ID: 3UYT, 3UZP, 4HGT, 4HNF, 4KB8, 4KBA, 4KBC, 4KBK, 4TN6, 4TW9, 4TWC, 5IH5, 5IH6, 5MQV, 5OKT, 5W4W, 6F1W, 6F26, 6GZM, 6HMP, 6HMR, 6RCG, and 6RCH). The crystals with codes 6RU6, 6RU7, and 6RU8 were not considered in this study because they contain the natural substrate adenosine-5'-diphosphate. One of the structures [PDB ID: 4KB8 (Mente et al., 2013)] is composed of two different CK1δ–ligand complexes. For this reason, the system has been separated into two different entries (namely, 4KB8A and 4KB8B). Because of this, the total number of complexes considered in our study is 24.

Each of the mentioned complexes has been downloaded and properly prepared for subsequent computational analysis with the “Structure Preparation” tool implemented in the Molecular Operating Environment (MOE) (Molecular Operating Environment (MOE), 2021) 2019.01 suite. The missing hydrogen atoms were appropriately added with the MOE “Protonate 3D” program (setting the pH for the protonation at a value of 7.4) and were then energetically minimized according to the AMBER10: EHT (Case et al., 2008) force field implemented in MOE. After the preparation phase, the protein–ligand complexes were properly aligned and superposed with the MOE dedicated tool, to make the binding site coordinates coherent among the different crystallographic structures. These complexes were saved and used at a later stage for the generation of the pharmacophore model (see Section 2.4).

Afterward, each ligand was separated from its respective protein. All the small molecules were collected in a database and prepared for docking calculations exploiting several packages from the QUACPAC OpenEye (QUACPAC, 2021) suite. For each molecule, the most probable tautomeric state was selected with the “tautomers” program, the three-dimensional coordinates were rebuilt using the “Omega” tool, the partial charges were attributed with the “MolCharge” program according to the MMFF94 force field, and finally, the dominant protonation state at pH 7.4 was determined by the “FixPka” tool.



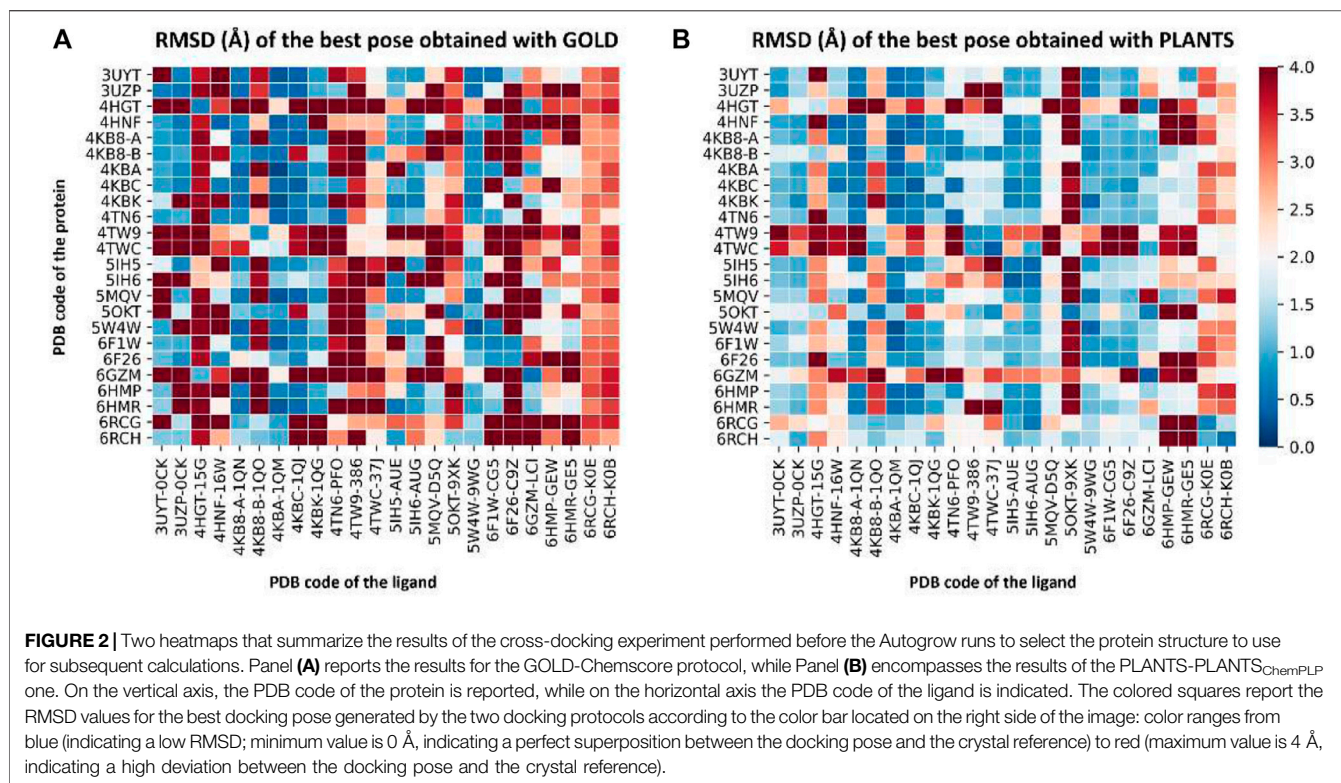
2.3 Cross-Docking

Each of the aforementioned 24 CK1δ crystallographic ligands, prepared as described in Section 2.2, was docked inside each of the correspondent 24 CK1δ protein structures exploiting two different molecular docking pieces of software, namely GOLD (Jones et al., 2002) (based on a genetic algorithm, developed and distributed with a commercial license from CCDC) and PLANTS (Korb et al., 2006) (an Ant-Colony-Optimization docking algorithm, developed by the University of Tübingen and free for use for academics).

This approach was chosen to follow the principles of “consensus docking” (Houston and Walkinshaw, 2013), which is based on the fact that data obtained by combining results coming from docking programs that operate in an orthogonal way are associated with higher robustness.

For both GOLD and PLANTS, 10 poses per molecule were collected. The default parameters were used for both protocols. Concerning the choice of the scoring function, Chemscore was selected for GOLD, while PLANTS_{ChemPLP} was selected for PLANTS.

A total of 1,152 (24 ligands × 24 proteins × 2 docking protocols) independent docking runs were performed, and the results were then



analyzed using an in-house Python script. The script collects the RMSD between each docking pose and the correspondent crystal reference pose, outputting two different plots. The first plot is a heatmap that illustrates the RMSD values for the best docking pose generated for each ligand onto each protein. The second plot is a histogram that re-elaborates the previous results to give a visual representation of the “success rate” of each protein: a successful docking run is obtained when the RMSD between the docking pose and the crystal reference is below the arbitrarily chosen 2 Å threshold value so that the “success rate” is defined by the percentage ratio of the successful docking runs for each protein (i.e., the percentage of docking experiments where the RMSD falls below the threshold value).

2.4 Pharmacophore Modeling

Based on previously published works on the same target, we took advantage of the structural information about known inhibitors of CK1 δ in the form of crystal structures of their complex with the kinase deposited in the PDB. The same 24 protein–ligand complexes mentioned in **Section 2.2** were subjected to the MOE Pharmacophore model tool: shared interaction features (with a 50% threshold value for feature retention) were then used in the generation of the pharmacophore model.

As can be seen in **Figure 1**, the final model consisted of four features (represented as spheres in the image), namely a hydrogen bond donor and a hydrogen bond acceptor interacting with Leu85, an aromatic ring in the proximity of the hinge region, and another aromatic ring adjacent to the first one in the inner part of the binding pocket.

2.5 Autogrow

Autogrow4 (AutoGrow4, 2020) is a fully open-source code written in Python and developed by the Durrant lab that combines a genetic algorithm with docking calculation based on the Vina (Eberhardt et al., 2021) docking software (version 1.2.0) to perform a semi-automatized process for both *de novo* drug design and lead optimization.

Molecules are submitted to the program in the form of SMILES strings. The genetic algorithm part of the code uses a series of synthetically feasible reactions to perform a defined number of mutation and crossover operations (i.e., growing and merging) on submitted chemical entities, creating a full population (called generation) of molecules to feed to the molecular docking program.

This generation is then docked using the Vina docking software. After the docking stage, the genetic algorithm retrieves the score for each docking pose, which it uses to rank molecules and pick the most fitted members of the generation to promote them to the next generation. This iterative process is repeated for a user-defined number of generations or until an earlier termination criterion is met.

The code is released under the Apache2 license, is freely available at <https://durrantlab.pitt.edu/autogrow4/>, and works both in Python 2.7 and ≥ 3.6 environment. A detailed description of how the latest Autogrow release works is provided in the work of Spiegel and Durrant (2020).

Two different versions of the Autogrow code were used in this scientific work. The first one was downloaded from the official repository and used as is, without any modifications to the source code. The second one was the result of an in-house

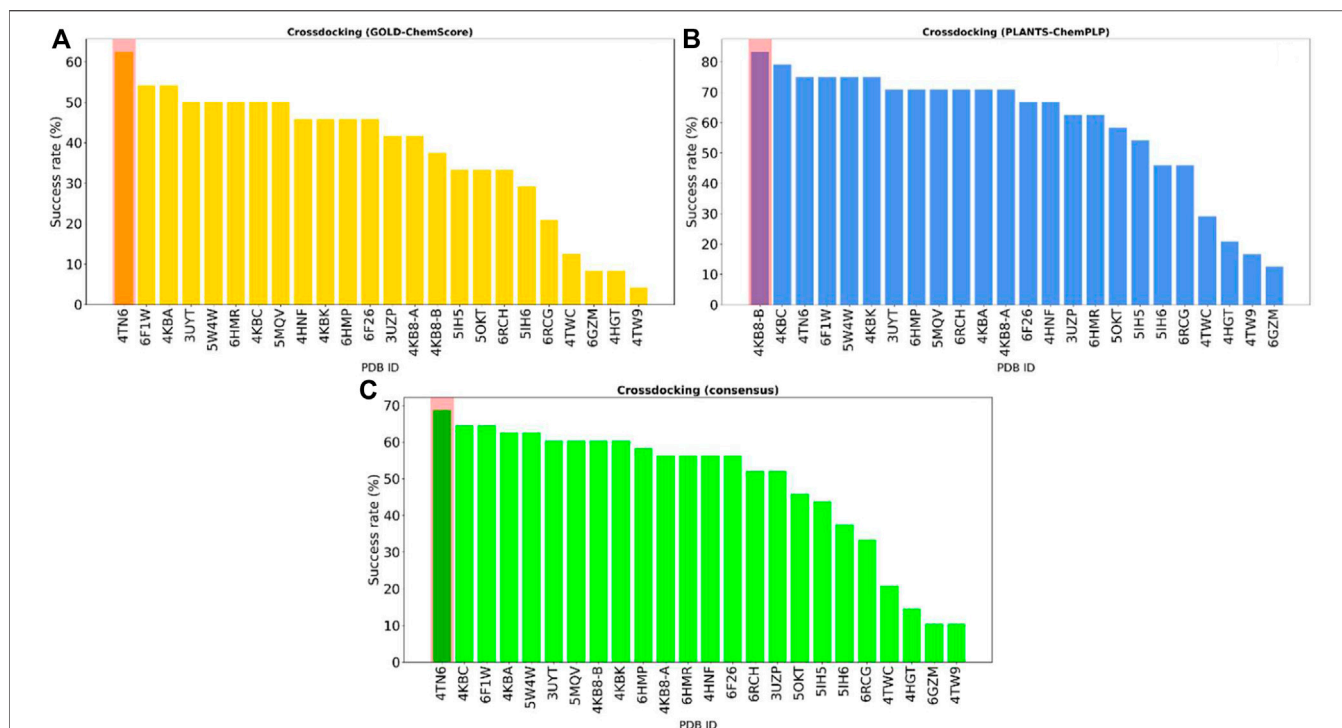


FIGURE 3 | The overall “success rate” in reproducing the correct crystallographic binding mode for each of the 24 CK1δ complexes considered in the study. The “success rate” is defined as the percentage of successful docking runs for each protein in the cross-docking experiment, where a successful docking run is defined as a docking calculation where the RMSD between the best docking pose and the crystal reference falls below an arbitrarily chosen threshold value of 2 Å. Panel (A) reports the results for the GOLD-ChemScore protocol. Panel (B) reports the results for the PLANTS-PLANTS_{ChemPLP} protocol. Panel (C) encompasses the combined “success rate” for each protein, defined as the average between the success rate for each protocol. Protein from the complex 4TN6 was chosen as the most representative CK1δ structure for successive calculations.

modification of the source code performed to customize the scoring stage of the docking process. The traditional Autogrow protocol uses the Vina standard scoring function (from now on, defined as VINA), which encompasses some elements of knowledge-based potentials and others of a typical empiric scoring function (Eberhardt et al., 2021). Instead, our modified version of the Autogrow code implements an alternative scoring function (from now on, defined as IFP_{CS}) based on the similarity between protein–ligand interaction fingerprints.

The crystal complex of a known inhibitor is chosen as reference (in our case, the ligand PFO from complex 4TN6 was chosen) and its binding mode is codified into a bit vector exploiting the InteractionFingerprint function from the fingerprint module of the Open Drug Discovery Toolkit (Wójcikowski et al., 2015) Python Library. This function converts the protein–ligand interaction into a bit array according to the residue of choice and the type of interaction. Each protein residue is represented by eight bits, one for each type of interaction considered (hydrophobic contacts, aromatic face to face, aromatic edge to face, hydrogen bond with protein acting as donor, hydrogen bond with protein acting as acceptor, salt bridge with protein acting as the positively charged member, salt bridge with protein acting as the positively negative member, and ionic

bond with a metal ion), so that the final vector will have a size of $r \times 8$, where r stands for the number of protein residues.

During the scoring phase of our custom Autogrow run, each docking pose is also codified into an Interaction Fingerprint vector, the same way as for the crystal reference. Then, the two vectors are transformed from sparse to dense, making use of the appropriate functions from the Numpy Python library, before the comparison between the reference and the query fingerprint is executed using the cosine similarity metrics, exploiting the appropriate function of the Scikit-learn Python library. The resulting score, which ranges from 1 (indicating a complete agreement and coherence between the two binding modes) to 0 (indicating that the two binding modes are not coherent), is then multiplied by -1 to comply with the selection mechanism of Autogrow genetic algorithm, which favors the most negative scores, as is usually the case for most classic scoring functions, like the one used by Vina.

$$IFP_{CS} = \frac{A \cdot B}{\|A\| \|B\|} * (-1). \quad (1)$$

Equation 1 is the mathematic formulation of the IFP_{CS} scoring function. This scoring function is the inverse of the cosine similarity between two vectors, A and B, representing the Interaction Fingerprint for the reference and the query ligand,

respectively. Values range from -1 (indicating maximum coherence between the two binding modes) to 0 (indicating the lowest possible correspondence between the two binding modes).

3 RESULTS

3.1 Cross-Docking

Since 24 different protein–ligand complexes were available for CK1δ (the target for our computational study), but only one at a given time can be used for docking calculations, we had to carefully evaluate the one most suitable for our needs. The choice of the protein structure to use for docking calculation is not trivial, for several reasons. When a ligand gets in contact with a protein, the binding event may cause a change in the structure of the protein itself (Li and Ji, 2019). These modifications are mainly depictable in the binding site and may also be extended to other regions. In a crystallographic complex, this effect is highlightable by differences in the shape of the binding site among the different crystal structures available for a single protein (Csermely et al., 2010).

One of the possible approaches to accomplish this task, the one that we used in our workflow, is known as “cross-docking” (Wierbowski et al., 2020). This technique consists in taking all the protein–ligand complexes available for a target, separating all the ligands from their respective co-crystallized structure, and docking all the different ligands in the binding site of each different protein structure. By analyzing the docking results, it is possible to define the crystallographic protein structure that has the highest tendency to correctly reproduce ligands’ crystallographic conformation.

For these reasons, we performed a cross-docking experiment on our 24 CK1δ complexes to decide which one to pick for subsequent calculation. Each ligand was docked into each protein structure using two different docking protocols, GOLD-Chemscore and PLANTS-PLANTS_{ChemPLP}, for a total of 1,152 independent docking runs. For each ligand, the root-mean-square deviation (RMSD) between each docking pose and the crystallographic conformation was calculated. The poses with the lowest RMSD in each docking run were selected and their RMSDs were plotted, obtaining the graphs represented in **Figure 2**. A detailed description of the methodology used for the cross-docking experiment is provided in **Section 2.3**.

To visualize the results more clearly, the data from the plots reported in **Figure 2** were re-elaborated to obtain a single indicator of the performance of each protein in reproducing the correct binding mode for docked ligands. We opted for calculating the “success rate” for each protein structure: a 2 Å threshold value was chosen to discriminate between successful and unsuccessful docking runs. For each protein, the percentage of successful docking runs (the “success rate”) was calculated accordingly and plotted in a histogram.

Figure 3 encompasses the results of this second analysis, reporting the success rate for both the GOLD-Chemscore and PLANTS-PLANTS_{ChemPLP} protocols. Moreover, since we

adopted the principle of “consensus docking,” as mentioned in **Section 2.3**, we decided to calculate the average success rate between the two docking protocols. As can be seen in **Figure 3**, the overall “success rate” obtained by the combination of data from the two docking protocols indicates the protein from the complex 4TN6 as the protein that is, on average, more able than the other ones to correctly reproduce the crystallographic binding mode of docked ligands. Although the difference in the success rate between the first and the second protein is low, in the context of several consequential docking runs where thousands of compounds are considered at a given time, even small differences in the percentage success rate could have a big impact on the quality of the run, considering that the prioritization of compounds from one generation to another is based upon their docking-predicted ability to retain the interaction features that characterize the binding mode of known inhibitors. For this reason, we used the protein 4TN6 as a representative CK1δ structure for our subsequent calculations with Autogrow.

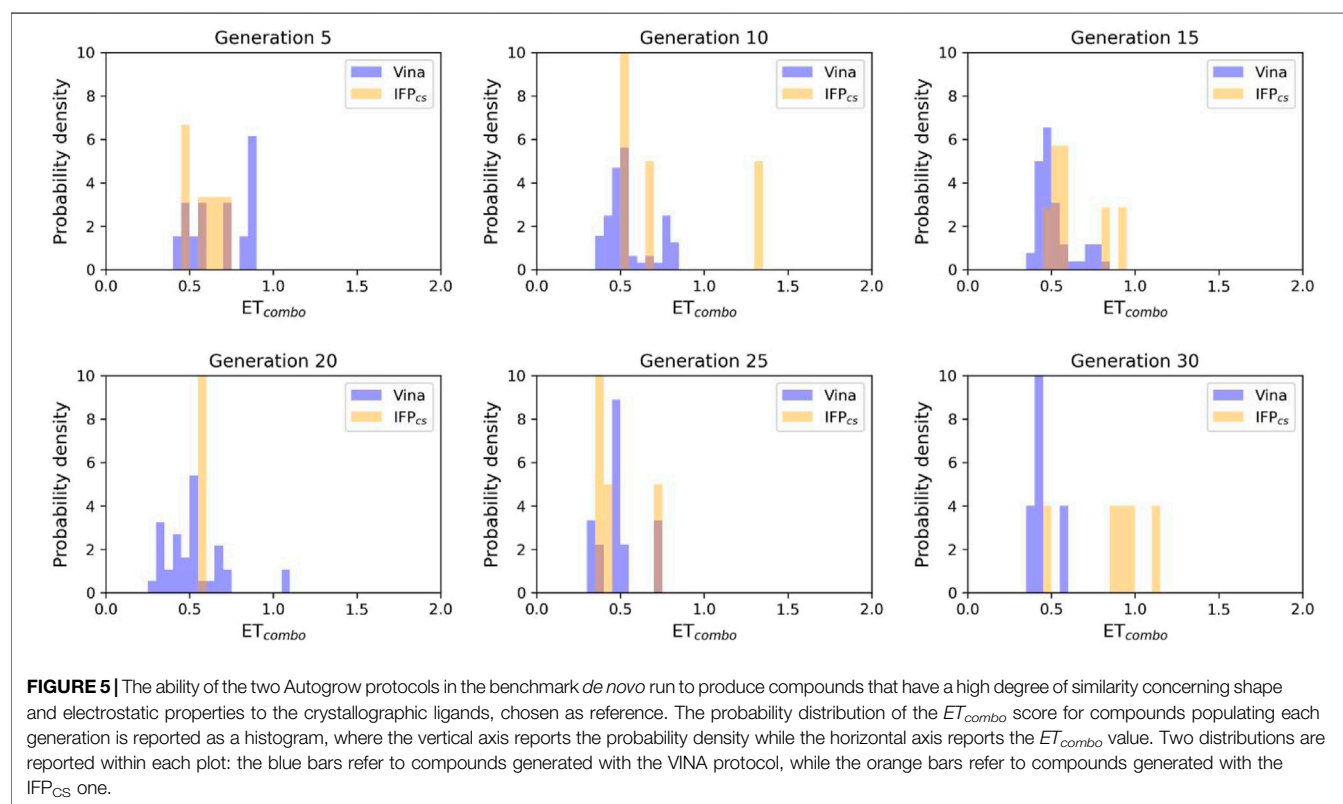
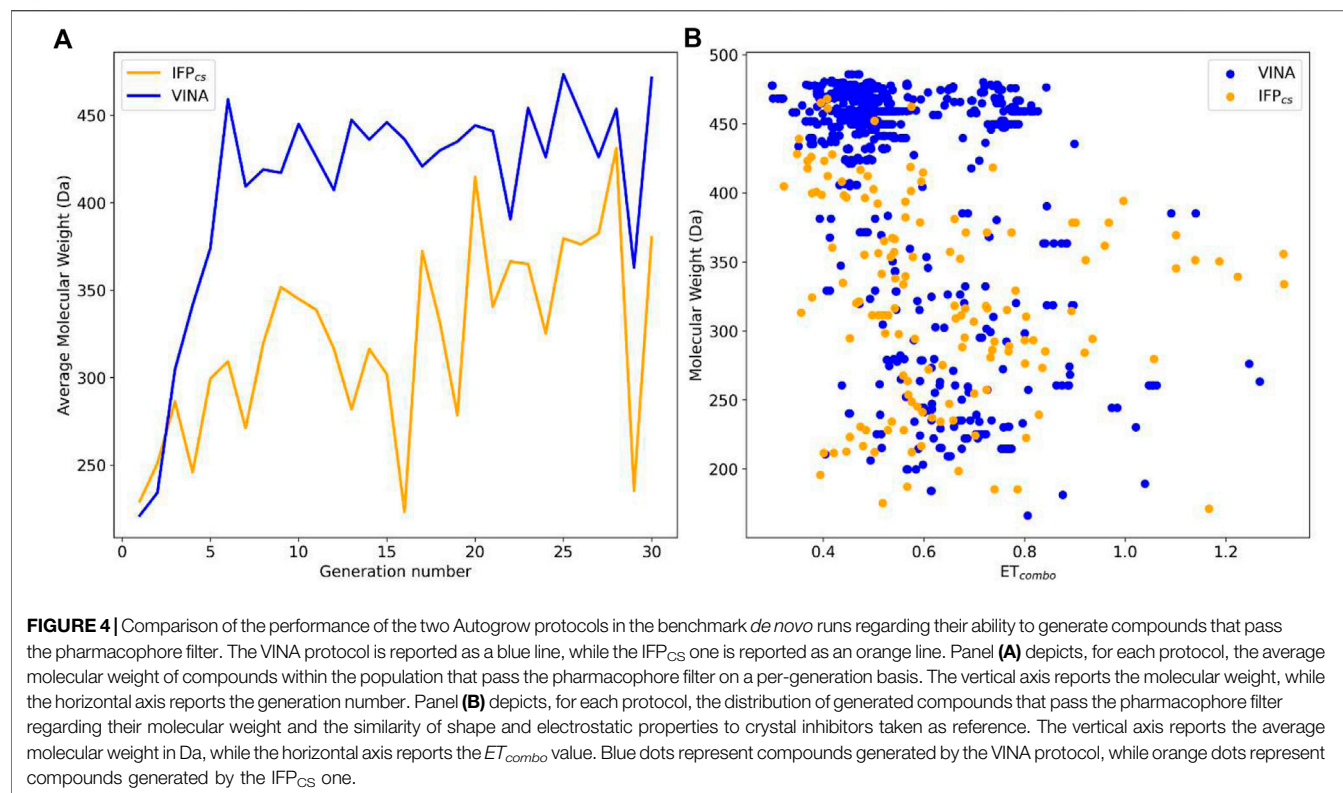
3.2 Benchmark De Novo Run

To assess the performance of our alternative, fingerprint-based, Autogrow protocol (defined as IFP_{CS}, while the traditional one is VINA), we first performed a benchmark *de novo* run, using the same conditions as the ones described in the work of Spiegel and Durrant (2020).

A 30-generation run was performed for each protocol, using the “Fragment_MW_100_to_150.sm” library provided in the Autogrow repository and described in the original publication. Configuration files for both *de novo* runs in the JSON format are available in the **Supplementary Material**, while a detailed description of both Autogrow and our alternative scoring approach is described in **Sections 2, 2.5**.

In order to validate the performance of both protocols, we opted for evaluating the quality of the generated compounds by filtering each generation of poses using a pharmacophore model. This filter, which has already been proved to identify true binders in previous related works (Cescon et al., 2020; Bolcato et al., 2021), was used to retain only those poses which complied with known requirements for binding to the CK1δ pocket. This metric was used to determine if there is any advantage in incorporating a knowledge-based element in the generation of novel potential inhibitors of CK1δ, steering the compound selection process toward the ones that assume a pharmacophore-like binding mode. These pharmacophore-like compounds were then characterized by calculating their molecular weight and the similarity of their shape and electrostatic properties to crystal CK1δ inhibitors taken as reference. For this purpose, the EON (Eberhardt et al., 2021) package from the OpenEye suite was used. Each compound passing the pharmacophore filter was compared with each crystallographic ligand, calculating the electrostatic and shape similarity (ET_{combo}). The best value for each ligand was extracted and used for the elaboration of the *a posteriori* analysis, whose results are reported in **Figures 4, 5**.

As can be seen in **Figure 4A**, which shows the average molecular weight of compounds that pass the pharmacophore filter for each generation, the VINA protocol rapidly reaches the peak of the average



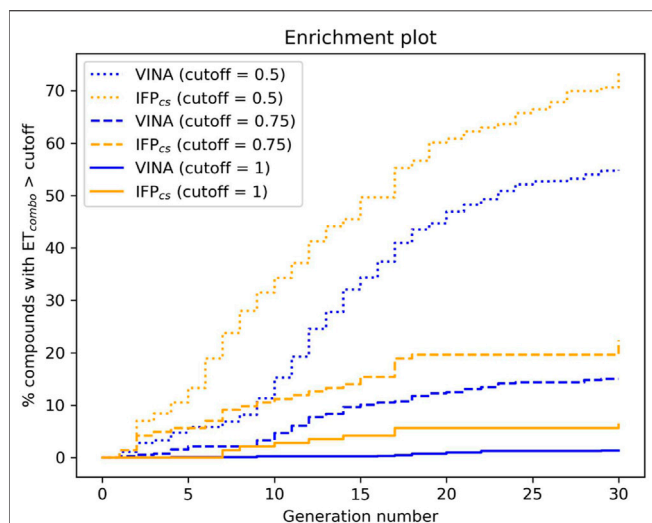


FIGURE 6 | The capability of the two different Autogrow protocols in the benchmark *de novo* run to produce compounds that have a high degree of similarity concerning shape and electrostatic properties to the crystallographic ligands, chosen as reference. For each generation, the percentage of compounds within the total population whose ET_{combo} exceeds a defined threshold value is reported. Three different cutoff values are reported: 0.50, 0.75, and 1.00, respectively.

molecular weight (around generation 6), while our IFP_{CS} protocol has a slower but regular growth that reaches values comparable to the VINA protocol from around generation 27 onwards. This difference is probably related to the fact that the VINA scoring function is biased toward the selection of larger compounds, which can make a good number of non-specific interactions with the target, while our IFP_{CS} one is biased toward the selection of compounds that have a similar interaction pattern compared to a reference compound, regardless of their dimensions.

As depicted in **Figure 4B**, which illustrates the distribution of generated compounds across all generations concerning their molecular weight and their electrostatic and shape similarity with crystal CK1δ inhibitors, this different selection process results in the production of compounds with different properties: the blue dots, which represent the compounds generated by the VINA protocol, are mostly located in the left-upper portion of the graph, indicating that most of the compounds generated by the traditional protocol have a high molecular weight but a low level of similarity with known inhibitors. On the contrary, the upper-right part of the graph (high molecular weight, high electrostatic, and shape similarity) is mostly populated with orange dots, which represent the compounds generated by our IFP_{CS} protocol.

The difference in the selection process is also highlighted in **Figure 5**, which illustrates the distribution of compounds across a representative subset of generations concerning their electrostatic and shape similarity: the graph clearly shows how the VINA protocol does not improve the similarity of generated compounds while increasing the number of generations. On the contrary, the orange population (which represents the compounds generated by the IFP_{CS} protocol) gradually shifts toward the right part of the plot passing from earlier to later stage generations, indicating that the compounds passing the pharmacophore filter

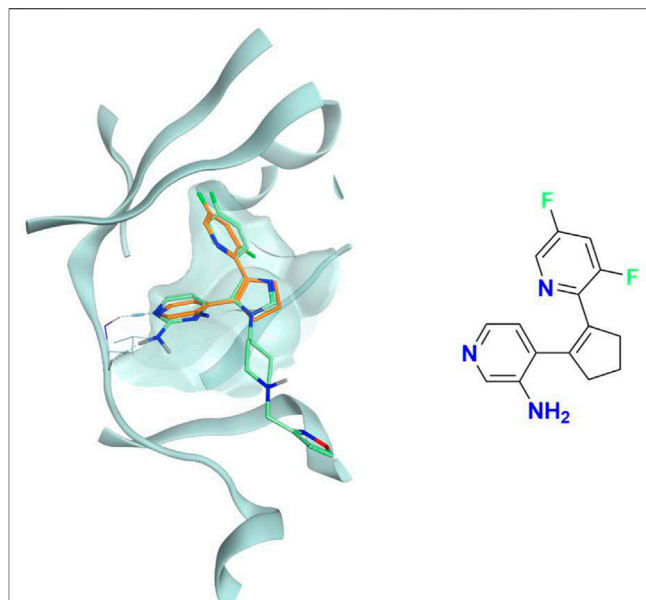


FIGURE 7 | The superposition between the docking-predicted binding mode of a high-scoring compound (MMS1) from the benchmark *de novo* run performed with the IFP_{CS} scoring protocol and the reference crystal binding pose of compound PFO from the structure deposited in the Protein Data Bank with accession code 4TN6. On the left part of the image, the protein kinase CK1δ ATP binding site is reported in teal ribbon, the pose of the compound MMS1 is shown as orange sticks, while the pose of compound PFO is shown as green sticks. On the right part of the image, the chemical structure of the compound MMS1 is reported.

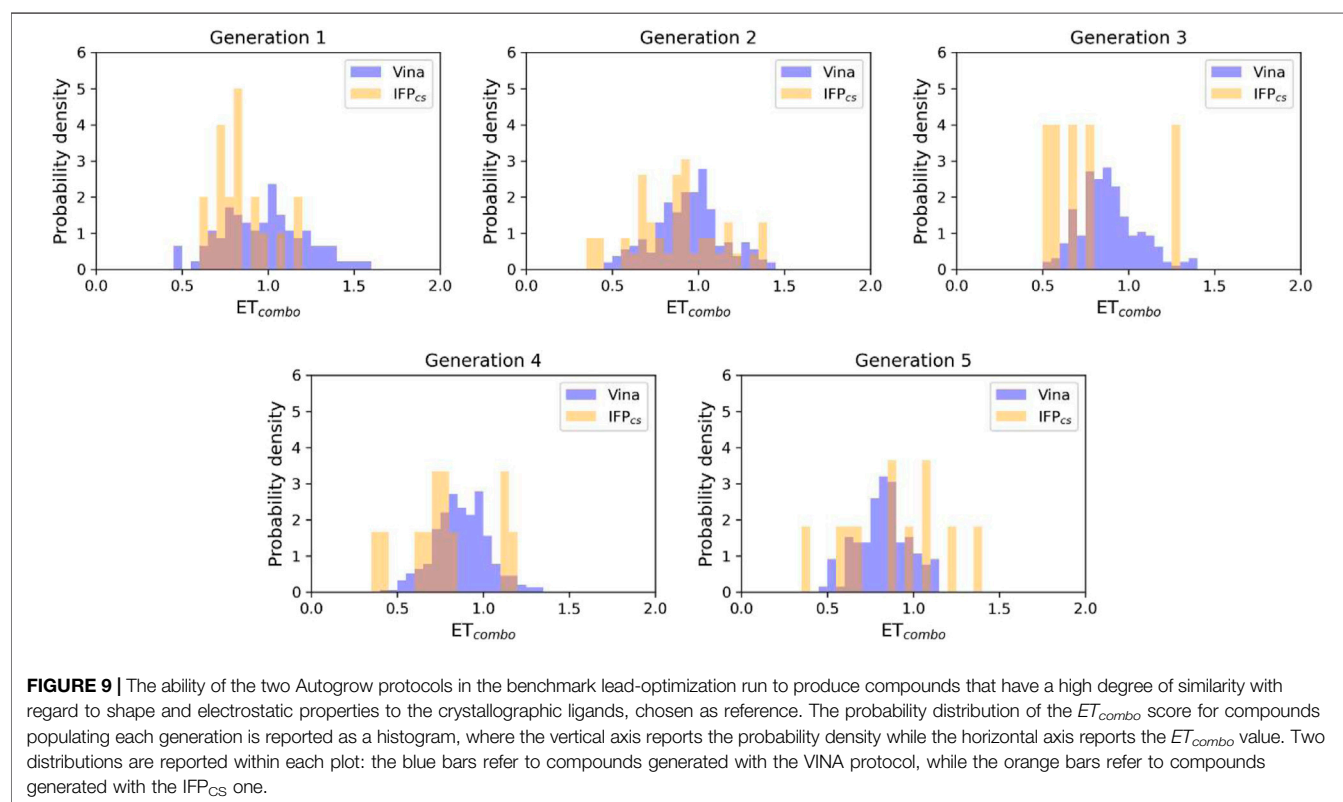
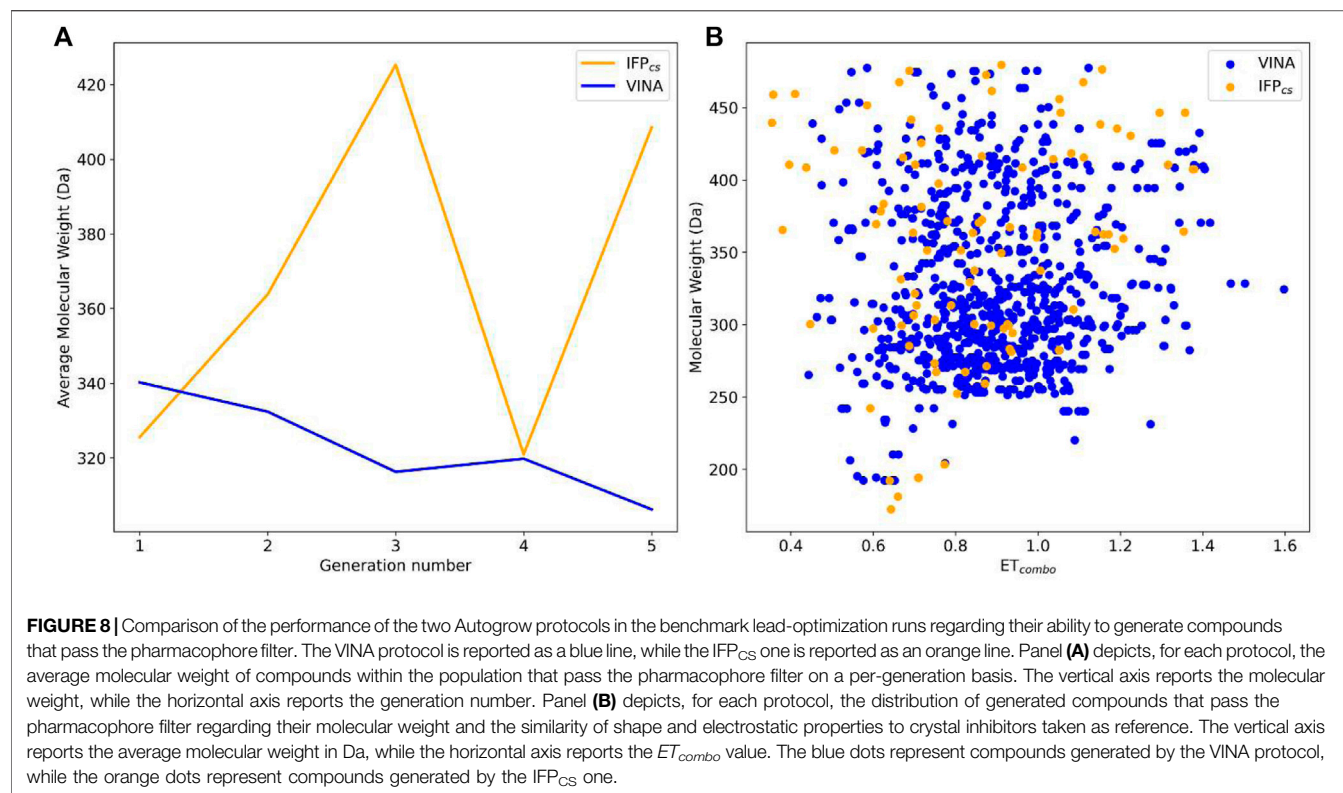
increase their electrostatic and shape similarity passing from one generation to another. Another comparison of the performances of the two protocol is given in **Figure 6**, which reports the progressive enrichment in compounds with a high degree of similarity to reference inhibitors within the total population. An example of a high-scoring compound generated by our IFP_{CS} protocol is reported in **Figure 7**, where its chemical structure and the comparison between its docking-predicted binding mode and the crystal pose of the PFO ligand from reference crystal complex 4TN6 is shown.

3.3 Benchmark Lead-Optimization Run

To further evaluate the validity of our custom scoring protocol, we also performed a benchmark lead-optimization run, using once again the same conditions as the ones reported in the work of Spiegel and Durrant (2020).

A 5-generation run was performed for each protocol, using a library composed of the 24 crystallographic ligands mentioned in the previous sections and another 316 fragments obtained from the fragmentation of crystallographic ligands exploiting the “fragmenter_of_smi_mol.py” Python script provided by the Autogrow developers, using the BRICS fragmentation rule, for a total of 340 compounds fed to the algorithm. In this case, configuration files for both benchmark runs in the JSON format are available in the **Supplementary Material**.

To assess the performance of both protocols, we applied the same criteria described previously for the *de novo* runs, focusing once again on compounds passing the pharmacophore filter



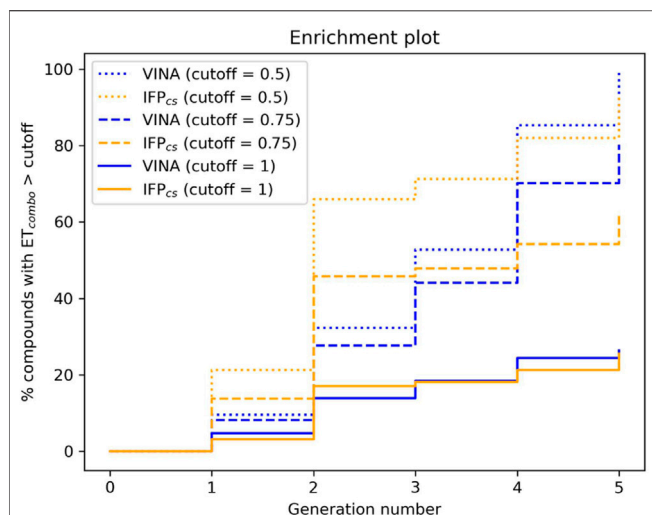


FIGURE 10 | The capability of the two different Autogrow protocols in the benchmark lead-optimization run to produce compounds that have a high degree of similarity concerning shape and electrostatic properties to the crystallographic ligands, chosen as reference. For each generation, the percentage of compounds within the total population whose ET_{combo} exceeds a defined threshold value is reported. Three different cutoff values are reported: 0.50, 0.75, and 1.00, respectively.

described in **Section 2.4** and characterizing them about their molecular weight and electrostatic and shape similarity compared to crystal CK1δ inhibitors.

Figure 8B illustrates the distribution of compounds across all five generations regarding their ET_{combo} and their molecular weight: as can be seen, there is little to no difference between the two protocols, with the two populations being practically superimposable. However, contrary to what might be suggested by this plot, there is a significant difference in the performances of the two protocols, which is highlighted in **Figures 8A, 9, 10**.

As can be noticed in **Figure 8A**, the average molecular weight of compounds passing the pharmacophore filter grows by about 90 Da, passing from the first to the last generation in the case of our IFP_{CS} protocol. On the contrary, the average molecular weight of pharmacophore-like compounds generated by the traditional VINA protocol does not increase with the number of generations, but slightly decreases over time, falling even below the average molecular weight of the first generation derived from the IFP_{CS} protocol. Furthermore, **Figure 9** illustrates how, as previously seen in the benchmark *de novo* run, the similarity of compounds passing the pharmacophore filter increases over time when the IFP_{CS} scoring protocol is adopted, while it slightly decreases and does not improve over time in the case of the traditional VINA scoring protocol. Particularly, this trend is also confirmed by **Figure 10**, which shows how the IFP_{CS} protocol can produce a quicker enrichment of the population in high-similarity compounds compared to the traditional VINA one. As for the previous case, an example of a high-scoring compound generated in the

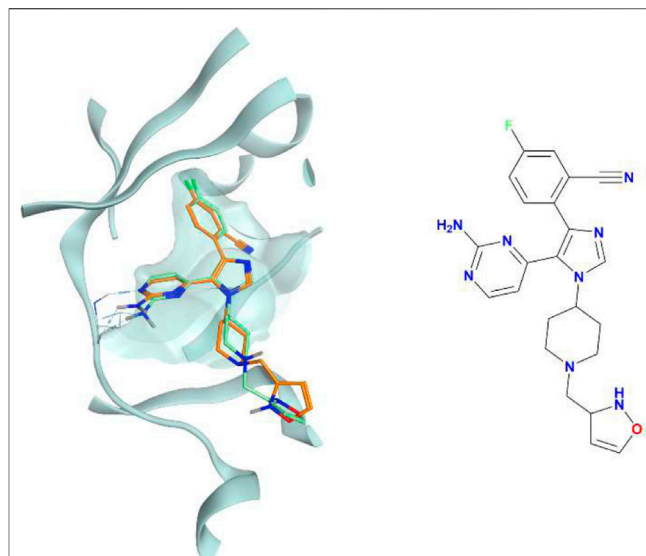


FIGURE 11 | The superposition between the docking-predicted binding mode of a high-scoring compound (MMS2) from the benchmark lead-optimization run performed with the IFP_{CS} scoring protocol and the reference crystal binding pose of compound PFO from the structure deposited in the Protein Data Bank with accession code 4TN6. On the left part of the image, the protein kinase CK1δ ATP binding site is reported in teal ribbon, the pose of the compound MMS2 is shown as orange sticks, while the pose of compound PFO is shown as green sticks. On the right part of the image, the chemical structure of the compound MMS2 is reported.

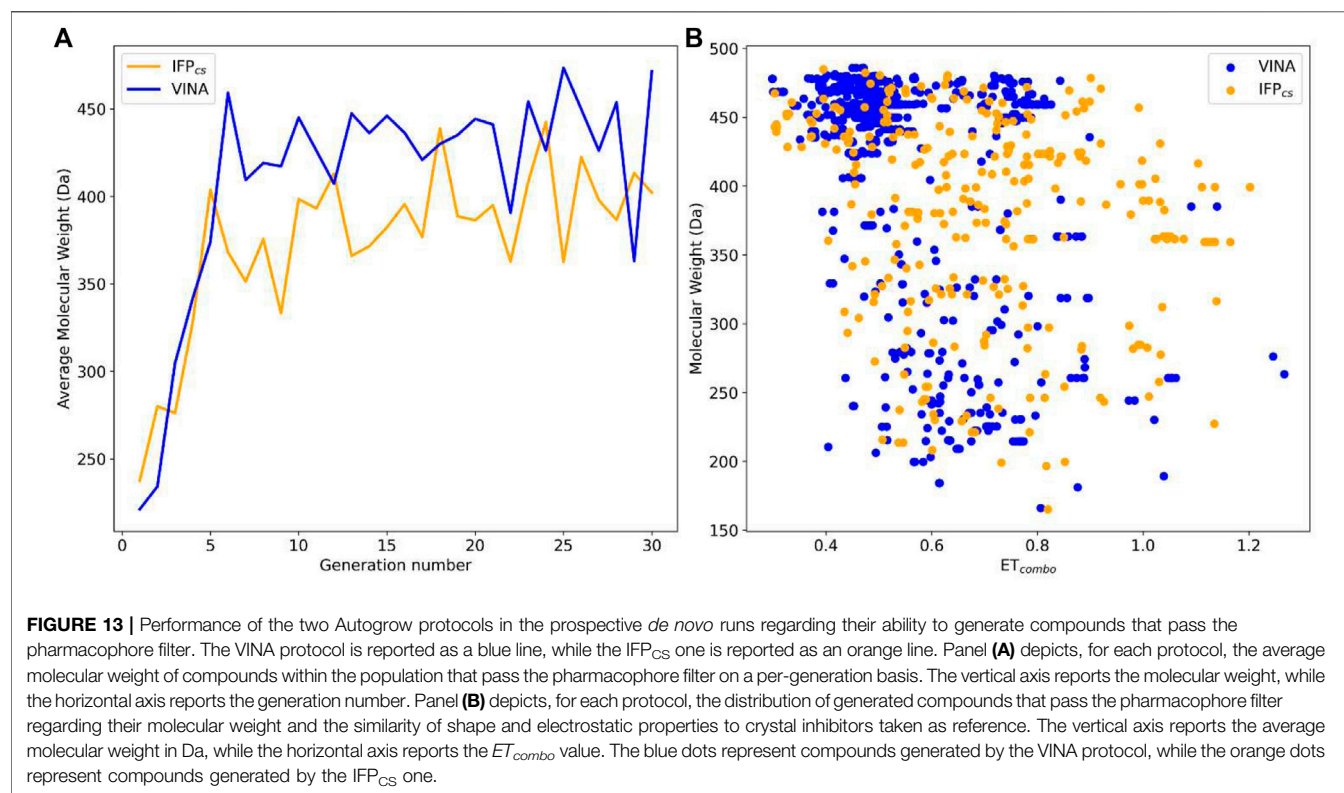
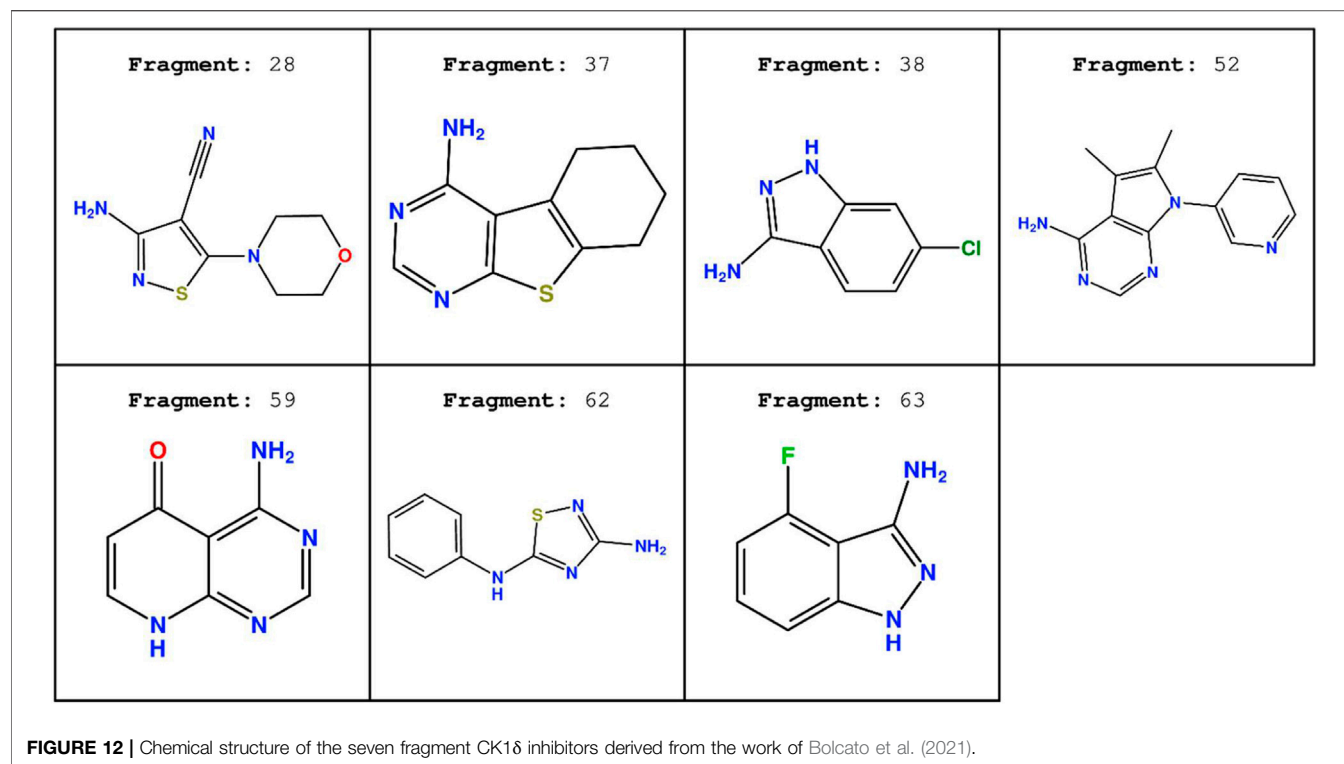
last and final generation of the IFP_{CS} run is reported in **Figure 11**.

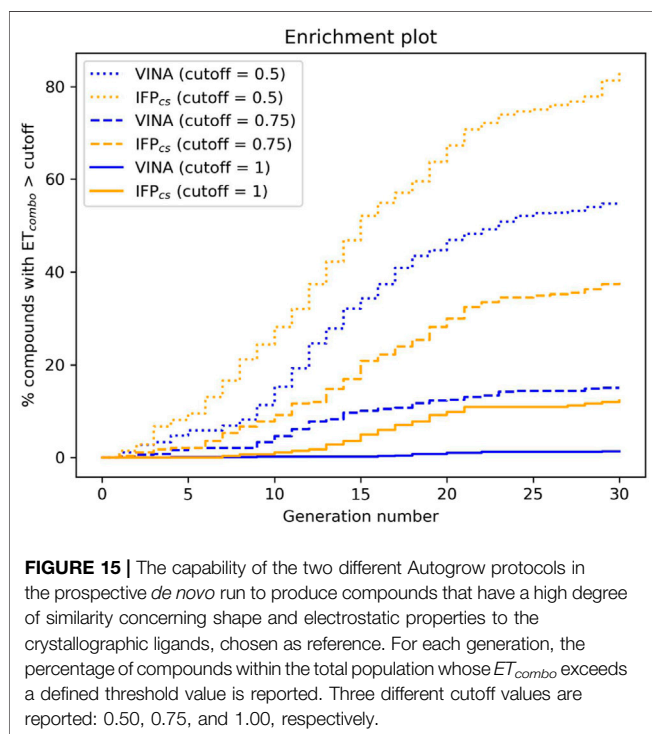
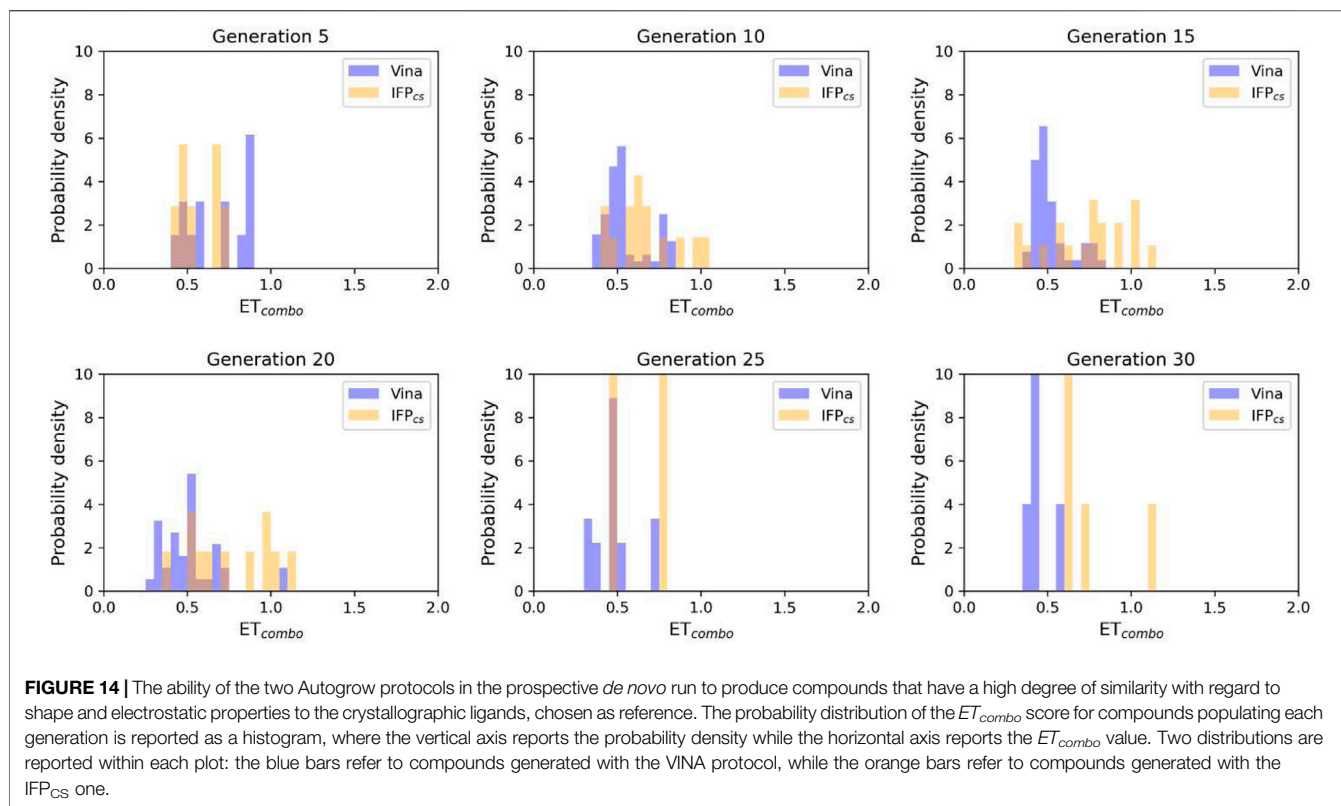
3.4 Prospective *De Novo* Run

Encouraged by the results of our benchmark runs, we decided to perform a prospective run with the IFP_{CS} protocol, applying the same operating conditions as before. This time, the starting library was modified to add to the compounds used for the benchmark runs seven fragment ATP-competitive CK1δ inhibitors identified during a previous virtual screening campaign from our laboratory (Bolcato et al., 2021). The idea behind this run was to evaluate the ability of our IFP_{CS} scoring protocol to generate interesting novel potential CK1δ inhibitors derived from in-house, readily available compounds.

The chemical structure of the seven fragments used in this run is reported in **Figure 12**.

To verify the quality of this run, we performed the same analysis as for the benchmark runs. The results of this analysis are summarized in **Figures 13–15**, respectively. As remarked in **Figure 14**, the same trend seen in the benchmark *de novo* run can also be observed in the case of this prospective run: while the VINA protocol is not able to increase the shape and electrostatic similarity to known inhibitors over time, the IFP_{CS} protocol can produce a shift of the orange population toward higher ET_{combo} values. As illustrated by **Figure 13**, which reports a comparison between the benchmark *de novo* run performed with the VINA protocol and the prospective *de novo* run carried out with the IFP_{CS} protocol, the trend in both the distribution of compounds regarding their molecular weight and ET_{combo} and the growth of molecular weight over time are similar to the benchmark *de*





novo run. **Figure 13B** clearly shows how the upper-right portion of the graph, which hosts compounds with both high molecular weight and ET_{combo} values, is populated exclusively by orange dots, which

represent compounds generated with the IFP_{CS} scoring protocol. Interestingly, **Figure 14A** highlights how there is much less difference in the growth rate of molecular weight between the IFP_{CS} run (which is contaminated by the presence of our seven CK1δ-inhibiting fragments) and the benchmark VINA run, suggesting that performances of the IFP_{CS} could improve if some high-quality pharmacophore-like fragments are included in the starting library. However, despite the quicker growth of molecular weight, the quality of generated compounds follows the same trend seen in the benchmark *de novo* run, as reported in **Figure 15**. As for the previous cases, an example of a high-scoring compound is reported in **Figure 16**.

4 DISCUSSION

The open-source software Autogrow4 (AutoGrow4, 2020) is an interesting piece of code that utilizes a combination between a genetic algorithm and the Vina (Trott and Olson, 2010) molecular docking software to semi-automatize the processes of fragment growing and lead optimization. Thanks to the modular nature of the codebase, we implemented an alternative scoring protocol (IFP_{CS}) based on the similarity of protein–ligand interaction fingerprint between a crystal reference and query compounds, exploiting the appropriate function from the open-source library Open Drug Discovery Toolkit (Wójcikowski et al., 2015), and we compared its performances with the traditional Autogrow scoring protocol (VINA), which is based on the Autodock Vina scoring function.

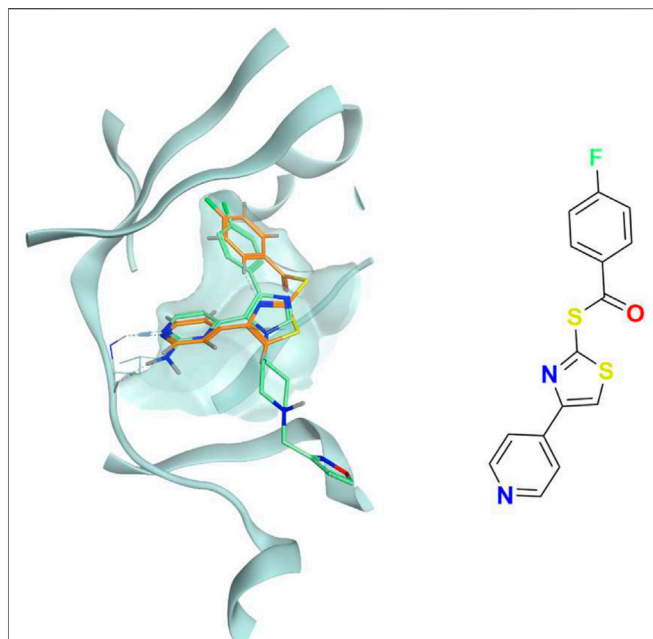


FIGURE 16 | The superposition between the docking-predicted binding mode of a high-scoring compound (MMS3) from the benchmark *de novo* run performed with the IFP_{CS} scoring protocol and the reference crystal binding pose of compound PFO from the structure deposited in the Protein Data Bank with accession code 4TN6. On the left part of the image, the protein kinase CK1δ ATP binding site is reported in teal ribbon, the pose of the compound MMS3 is shown as orange sticks, while the pose of compound PFO is shown in green sticks. On the right part of the image, the chemical structure of the compound MMS3 is reported.

The VINA protocol uses a scoring function that incorporates some elements of knowledge-based potentials and some others of empirical scoring functions. As is the case for many scoring functions, the score is biased toward higher molecular weight compounds, which can establish a higher number of non-specific interactions with the target (Chen, 2015). For this reason, usually, molecular docking programs are efficient in sampling the conformational space available for the ligand within the binding site but are weaker in prioritizing the right binding mode among a set of reasonable hypotheses generated by the search algorithm (Chaput and Mouawad, 2017). This is especially true in the case of fragments, which deviate from the drug-like properties of compounds upon which traditional scoring functions have been trained (Verdonk et al., 2011).

As thoroughly discussed in the work of Bolcato et al. (Bolcato et al., 2021), one possible solution to the scoring problem is to apply a pharmacophore filter to poses generated by the molecular docking program. When several structural pieces of information are available in the form of protein–ligand crystal complexes for a certain target (as is the case for protein kinase CK1δ, the case study for this work), a good solution to reduce the false positive rate of molecular docking programs is to build a pharmacophore model that encompasses the most prominent interaction features that are required to bind ligands to the target active site (Peach and Nicklaus, 2009). In the case of a program like Autogrow, where the selection mechanism that

determines which compounds to promote to the next generation is based on the docking score, we thought it would be interesting to incorporate a knowledge-based element in the pose selection mechanism in the form of a comparison between the interaction fingerprint of query compounds and known inhibitors, to bias the selection mechanism toward molecules that respect the required features to bind to the target.

To validate our IFP_{CS} scoring protocol, we performed both a *de novo* and a lead-optimization benchmark run, using the same operative conditions described in the original work of Spiegel and Durrant (2020) but on a different target. The protein target of choice was the protein kinase CK1δ, a pharmaceutically relevant target in the field of neurodegenerative diseases for which several crystal complexes with inhibitors are available in the PDB. The benchmark *de novo* run was performed on a library composed of 6,103 fragment compounds whose molecular weight falls between 100 and 150 Da, while the benchmark lead-optimization run was carried out on a library composed of 24 crystallographic ligands of the protein kinase CK1δ and 316 fragments derived from the fragmentation of crystallographic ligands using the BRICS rule. To compare the capabilities of the two protocols, we filtered each generation of compounds with the same pharmacophore filter already utilized in previous scientific works on the target (Cescon et al., 2020; Bolcato et al., 2021). We then proceeded to evaluate the quality of compounds that pass the pharmacophore filter, considering both the size and the similarity of shape and electrostatic properties of query compounds compared to the crystallographic ligands taken as reference.

As illustrated by the results of our analysis (Sections 3.3, 3.4, respectively), there is a substantial difference in the performances of the two protocols: while both protocols can generate a certain amount of compounds that pass the pharmacophore filter (therefore possessing the right structural features that are required for the interaction with the target), in both scenarios the IFP_{CS} scoring function outperforms the traditional VINA one regarding the ability to select and prioritize pharmacophore-like compounds that have a similar shape and electrostatic properties compared to known inhibitors of the protein kinase CK1δ. This is particularly evident in the lead-optimization scenario, where within each generation passage, the average molecular weight of compounds that pass the pharmacophore filter steadily increases, passing from the typical MW of a fragment-like compound to the MW of a grown, mature, lead candidate, while the contrary happens in the case of the VINA protocol, with the average MW of the compounds that pass the pharmacophore filter steadily decreasing, falling even below the value of the first generation from the IFP_{CS} protocol. Moreover, when poses from each generation are compared with the ones of crystallographic ligands concerning the shape and electrostatic similarity, a similar trend can be noticed. While the VINA protocol can select high-quality compounds in the first generation, compared to the IFP_{CS} one, at later stages during the run a progressive reduction in the similarity between the query and reference compounds can be noticed, contrary to what happens when the IFP_{CS} scoring protocol is utilized. This can be explained considering the different nature of the two scoring functions: the VINA protocol is biased toward bigger, therefore higher scoring, compounds, while the IFP_{CS} protocol favors compounds that respect the interaction pattern of the reference crystallographic ligand, regardless of their

size. For this reason, the IFP_{CS} protocol tends to favor smaller compounds in the first generations, as long as they are complying with the constraint imposed by the reference interaction fingerprint, increasing the possibility to maintain in the population high-quality fragment to be optimized via the mutation and crossover operation of the genetic algorithm. On the contrary, the VINA protocol selects high MW compounds in the first generation that have little to no space for meaningful chemical modifications, giving low priority to those smaller compounds that will have a lower number of interactions with the target, thus resulting in lower docking score. Overall, our IFP_{CS} protocol seems preferable in those cases where structural data are available in the form of protein–ligand complex structure, as is the case for a good number of targets nowadays, while the traditional protocol seems a valid choice in those cases where such structural information is missing.

A recent virtual screening campaign performed in our laboratory led to the identification of seven novel fragment compounds that are ATP-competitive CK1 δ inhibitors (Bolcato et al., 2021). Curious to see if our protocol would have been able to produce novel potential CK1 δ that incorporates structural features of our seven fragments, we performed a second *de novo* run, using the same conditions as for the benchmark one, except for the introduction in the starting library of those seven fragment compounds. The same analysis performed on the benchmark runs showed that the performance of our IFP_{CS} scoring protocol is even better when the Autogrow protocol is seeded with high-quality fragments that have the right structural feature to interact with the target. Usually, in a typical FBDD campaign, the identification of fragment binders either through virtual or experimental screening leads to the discovery of several potential starting points for the hit-to-lead fragment optimization phase. Our preliminary study showed that it is possible to obtain meaningful results even in those cases where the starting library is populated by fragments that are randomly selected and not specifically tuned for the target of choice, but it certainly benefits from the contamination of the starting library with fragments that are known binders, indicating that the application of the IFP_{CS} protocol could lead to some interesting results in those cases where the known binders constitute a bigger fraction of the starting library. Concerning this, this approach could be utilized to evaluate the competitiveness of newly found scaffolds with the already existing ones, based on the simplicity to derive those scaffolds with common and feasible chemical reactions, therefore producing a good number of derivatives with increased affinity for the target.

5 CONCLUSION

In the present work, we presented and benchmarked a custom version of the open-source Autogrow4 which implements an alternative scoring protocol based on the similarity between protein–ligand interaction fingerprint of query compounds compared to a crystal reference. To demonstrate the applicability of our protocol in a pharmaceutically relevant scenario, we tested its capability to generate compounds that have similar binding and structural features to known inhibitors

of the protein kinase CK1 δ , a protein that is involved in several neurodegenerative diseases, such as AD, PD, and ALS.

A benchmark *de novo* run and a lead-optimization one were both carried out to compare the performance of our IFP_{CS} scoring protocol against the traditional one implemented in the original version of the Autogrow code, using the same conditions as the one reported in the original publication by Spiegel et al. Compared to the traditional Autogrow protocol, which uses the default scoring function of the Vina docking software, our IFP_{CS} protocol was able to generate, on average, compounds that were bigger and more similar to crystallographic ligands from the point of view of the shape and electrostatic properties, while retaining the key protein–ligand interaction features required for the inhibition of CK1 δ .

The custom Autogrow version used in this work, which implements our alternative IFP_{CS} scoring protocol, along with the JSON configuration files used for each run and a YAML file to reconstitute the Python environment to run the custom version of the code, is available in the **Supplementary Material**.

DATA AVAILABILITY STATEMENT

Publicly available datasets were analyzed in this study. These data can be found here: <https://www.rcsb.org/>.

AUTHOR CONTRIBUTIONS

SMe and MS conceived the research idea and approach. SMe, MP, and DB carried out all computational simulations. SMe, MS, MP, and SMO wrote the manuscript. All authors discussed the results and reviewed the manuscript.

FUNDING

This scientific work was financially supported by MIUR (PRIN2017, no. 2017MT3993).

ACKNOWLEDGMENTS

MMS lab is very grateful to Chemical Computing Group, OpenEye, and Acellera for the scientific and technical partnership. MMS lab gratefully acknowledges the support of NVIDIA Corporation with the donation of the Titan V GPU, used for this research.

SUPPLEMENTARY MATERIAL

The Supplementary Material for this article can be found online at: <https://www.frontiersin.org/articles/10.3389/fmolb.2022.909499/full#supplementary-material>

REFERENCES

- AutoGrow4 (2020). AutoGrow4 – Durrant Lab. Available at: <https://durrantlab.pitt.edu/autogrow4/>.
- Behrend, L., Stöter, M., Kurth, M., Rutter, G., Heukeshoven, J., Deppert, W., et al. (2000). Interaction of Casein Kinase 1 Delta (CK1δ) with Post-golgi Structures, Microtubules and the Spindle Apparatus. *Eur. J. Cell. Biol.* 79, 240–251. doi:10.1078/s0171-9335(04)70027-8
- Berman, H. M., Westbrook, J., Feng, Z., Gilliland, G., Bhat, T. N., Weissig, H., et al. (2000). The Protein Data Bank. *Nucleic Acids Res.* 28, 235–242. doi:10.1093/nar/28.1.235
- Bischof, J., Randoll, S.-J., Stüßner, N., Henne-Bruns, D., Pinna, L. A., and Knippschild, U. (2013). CK1δ Kinase Activity Is Modulated by Chk1-Mediated Phosphorylation. *PLoS ONE* 8, e68803. doi:10.1371/journal.pone.0068803
- Bissaro, M., Sturlese, M., and Moro, S. (2020). The Rise of Molecular Simulations in Fragment-Based Drug Design (FBDD): an Overview. *Drug Discov. Today* 25, 1693–1701. doi:10.1016/j.drudis.2020.06.023
- Böhm, H. J. (1992). The Computer Program LUDI: a New Method for the De Novo Design of Enzyme Inhibitors. *J. Comput. Aided. Mol. Des.* 6, 61–78.
- Bolcato, G., Cescon, E., Pavan, M., Bissaro, M., Bassani, D., Federico, S., et al. (2021). A Computational Workflow for the Identification of Novel Fragments Acting as Inhibitors of the Activity of Protein Kinase CK1δ. *Ijms* 22, 9741. doi:10.3390/ijms22189741
- Bollag, G., Tsai, J., Zhang, J., Zhang, C., Ibrahim, P., Nolop, K., et al. (2012). Vemurafenib: the First Drug Approved for BRAF-Mutant Cancer. *Nat. Rev. Drug Discov.* 11, 873–886. doi:10.1038/nrd3847
- Breijyeh, Z., and Karaman, R. (2020). Comprehensive Review on Alzheimer's Disease: Causes and Treatment. *Molecules* 25, 5789. doi:10.3390/molecules25245789
- Case, D. A., Darden, T., Cheatham, T., Simmerling, C., Wang, J., and Duke, R. E. (2008). *Amber 10*. San Francisco: University of California.
- Cescon, E., Bolcato, G., Federico, S., Bissaro, M., Valentini, A., Ferlin, M. G., et al. (2020). Scaffold Repurposing of In-House Chemical Library toward the Identification of New Casein Kinase 1 δ Inhibitors. *ACS Med. Chem. Lett.* 11, 1168–1174. doi:10.1021/acsmchemlett.0c00028
- Chaput, L., and Mouawad, L. (2017). Efficient Conformational Sampling and Weak Scoring in Docking Programs? Strategy of the Wisdom of Crowds. *J. Cheminform.* 9, 37–18. doi:10.1186/s13321-017-0227-x
- Chen, Y. C. (2015). Beware of Docking!. *Trends Pharmacol. Sci.* 36, 78–95. doi:10.1016/j.tips.2014.12.001
- Csermely, P., Palotai, R., and Nussinov, R. (2010). Induced Fit, Conformational Selection and Independent Dynamic Segments: an Extended View of Binding Events. *Trends Biochem. Sci.* 35, 539–546. doi:10.1016/j.tibs.2010.04.009
- de Souza Neto, L. R., Moreira-Filho, J. T., Neves, B. J., Maidana, R. L. B. R., Guimarães, A. C. R., Furnham, N., et al. (2020). In Silico Strategies to Support Fragment-To-Lead Optimization in Drug Discovery. *Front. Chem.* 8, 93. doi:10.3389/fchem.2020.00093
- Dementia (2021). WHO. Available at: <https://www.who.int/news-room/fact-sheets/detail/dementia>.
- Eberhardt, J., Santos-Martins, D., Tillack, A. F., and Forli, S. (2021). AutoDock Vina 1.2.0: New Docking Methods, Expanded Force Field, and Python Bindings. *J. Chem. Inf. Model.* 61, 3891–3898. doi:10.1021/acs.jcim.1c00203
- Eisen, M. B., Wiley, D. C., Karplus, M., and Hubbard, R. E. (1994). HOOK: A Program for Finding Novel Molecular Architectures that Satisfy the Chemical and Steric Requirements of a Macromolecule Binding Site. *Proteins* 19, 199–221. doi:10.1002/prot.340190305
- Erlanson, D. A., Fesik, S. W., Hubbard, R. E., Jahnke, W., and Jhoti, H. (2016). Twenty Years on: The Impact of Fragments on Drug Discovery. *Nat. Rev. Drug Discov.* 15, 605–619. doi:10.1038/nrd.2016.109
- Erlanson, D. A., McDowell, R. S., and O'Brien, T. (2004). Fragment-Based Drug Discovery. *J. Med. Chem.* 47, 3463–3482. doi:10.1021/jm040031v
- Ghoshal, N., Smiley, J. F., DeMaggio, A. J., Hoekstra, M. F., Cochran, E. J., Binder, L. I., et al. (1999). A New Molecular Link between the Fibrillar and Granulovacuolar Lesions of Alzheimer's Disease. *Am. J. Pathology* 155, 1163–1172. doi:10.1016/s0002-9440(10)65219-4
- Graves, P. R., and Roach, P. J. (1995). Role of COOH-Terminal Phosphorylation in the Regulation of Casein Kinase Iδ. *J. Biol. Chem.* 270, 21689–21694. doi:10.1074/jbc.270.37.21689
- Hajduk, P. J. (2006). Fragment-based Drug Design: How Big Is Too Big? *J. Med. Chem.* 49, 6972–6976. doi:10.1021/jm060511h
- Hall, R. J., Mortenson, P. N., and Murray, C. W. (2014). Efficient Exploration of Chemical Space by Fragment-Based Screening. *Prog. Biophys. Mol. Biol.* 116, 82–91. doi:10.1016/j.pbiomolbio.2014.09.007
- Hirner, H., Günes, C., Bischof, J., Wolff, S., Grothey, A., Köhl, M., et al. (2012). Impaired CK1 Delta Activity Attenuates SV40-Induced Cellular Transformation In Vitro and Mouse Mammary Carcinogenesis In Vivo. *PLoS One* 7, e29709. doi:10.1371/journal.pone.0029709
- Houston, D. R., and Walkinshaw, M. D. (2013). Consensus Docking: Improving the Reliability of Docking in a Virtual Screening Context. *J. Chem. Inf. Model.* 53, 384–390. doi:10.1021/ci300399w
- J, H., and Dj, S. (2002). The Amyloid Hypothesis of Alzheimer's Disease: Progress and Problems on the Road to Therapeutics. *Science* 297, 353–356.
- Jhoti, H., Williams, G., Rees, D. C., and Murray, C. W. (2013). The 'rule of Three' for Fragment-Based Drug Discovery: where Are We Now? *Nat. Rev. Drug Discov.* 12, 644. doi:10.1038/nrd3926-c1
- Jones, G., Willett, P., Glen, R. C., Leach, A. R., and Taylor, R. (2002). Development and Validation of a Genetic Algorithm for Flexible Docking. *J. Mol. Biol.* 267, 727–748. doi:10.1006/jmbi.1996.0897
- Kametan, F., Nonaka, T., Suzuki, T., Arai, T., Dohmae, N., Akiyama, H., et al. (2009). Identification of Casein Kinase-1 Phosphorylation Sites on TDP-43. *Biochem. Biophysical Res. Commun.* 382, 405–409. doi:10.1016/j.bbrc.2009.03.038
- Knippschild, U., Krüger, M., Richter, J., Xu, P., García-Reyes, B., Peifer, C., et al. (2014). The CK1 Family: Contribution to Cellular Stress Response and its Role in Carcinogenesis. *Front. Oncol.* 4, 96. doi:10.3389/fonc.2014.00096
- Knippschild, U., Gocht, A., Wolff, S., Huber, N., Löhler, J., and Stöter, M. (2005). The Casein Kinase 1 Family: Participation in Multiple Cellular Processes in Eukaryotes. *Cell. Signal.* 17, 675–689. doi:10.1016/j.cellsig.2004.12.011
- Korb, O., Stützle, T., and Exner, T. E. (2006). PLANTS: Application of Ant Colony Optimization to Structure-Based Drug Design. *Ant. Colony Optim. Swarm Intelligence, Lecture Notes Comput. Sci.* 247–258. doi:10.1007/11839088_22
- Lauri, G., and Bartlett, P. A. (1994/1994). CAVEAT: A Program to Facilitate the Design of Organic Molecules. *J. Computer-Aided Mol. Des.* 8, 51–66. doi:10.1007/bf00124349
- Lee, H., Chen, R., Lee, Y., Yoo, S., and Lee, C. (2009). Essential Roles of CKIδ and CKIε in the Mammalian Circadian Clock. *Proc. Natl. Acad. Sci. U.S.A.* 106, 21359–21364. doi:10.1073/pnas.0906651106
- Lee, V. M.-Y., Goedert, M., and Trojanowski, J. Q. (2001). Neurodegenerative Tauopathies. *Annu. Rev. Neurosci.* 24, 1121–1159. doi:10.1146/annurev.neuro.24.1.1121
- Li, D., and Ji, B. (2019). Protein Conformational Transitions Coupling with Ligand Interactions: Simulations from Molecules to Medicine. *Med. Nov. Technol. Devices* 3, 100026. doi:10.1016/j.medntd.2019.100026
- Li, G., Yin, H., and Kuret, J. (2004). Casein Kinase 1 Delta Phosphorylates Tau and Disrupts its Binding to Microtubules. *J. Biol. Chem.* 279, 15938–15945. doi:10.1074/jbc.m314116200
- Longenecker, K. L., Roach, P. J., and Hurley, T. D. (1998). Crystallographic Studies of Casein Kinase I δ: toward a Structural Understanding of Auto-Inhibition. *Acta Crystallogr. D. Biol. Cryst.* 54, 473–475. doi:10.1107/s0907444997011724
- Maass, P., Schulz-Gasch, T., Stahl, M., and Rarey, M. (2007). Recore: a Fast and Versatile Method for Scaffold Hopping Based on Small Molecule Crystal Structure Conformations. *J. Chem. Inf. Model.* 47, 390–399. doi:10.1021/ci060094h
- Meggio, F., Perich, J. W., Reynolds, E. C., and Pinna, L. A. (1991). A Synthetic β-casein Phosphopeptide and Analogues as Model Substrates for Casein Kinase-1, a Ubiquitous, Phosphate Directed Protein Kinase. *FEBS Lett.* 283, 303–306. doi:10.1016/0014-5793(91)80614-9
- Mente, S., Arnold, E., Butler, T., Chakrapani, S., Chandrasekaran, R., Cherry, K., et al. (2013). Ligand-Protein Interactions of Selective Casein Kinase 1δ Inhibitors. *J. Med. Chem.* 56, 6819–6828. doi:10.1021/jm4006324
- Milne, D. M., Looby, P., and Meek, D. W. (2001). Catalytic Activity of Protein Kinase CK1δ (Casein Kinase 1δ) Is Essential for its Normal Subcellular Localization. *Exp. Cell. Res.* 263, 43–54. doi:10.1006/excr.2000.5100
- Molecular Operating Environment (MOE) (2021). 2019.01; Chemical Computing Group ULC, 1010 Sherbooke St. West, Suite #910, Montreal, QC, Canada, H3A 2R7. Available at: https://www.chemcomp.com/Research-Citing_MOE.htm.

- Murray, C. W., and Rees, D. C. (2009). The Rise of Fragment-Based Drug Discovery. *Nat. Chem.* 1, 187–192. doi:10.1038/nchem.217
- Okochi, M., Walter, J., Koyama, A., Nakajo, S., Baba, M., Iwatsubo, T., et al. (2000). Constitutive Phosphorylation of the Parkinson's Disease Associated α -Synuclein. *J. Biol. Chem.* 275, 390–397. doi:10.1074/jbc.275.1.390
- Peach, M. L., and Nicklaus, M. C. (2009). Combining Docking with Pharmacophore Filtering for Improved Virtual Screening. *J. Cheminform.* 1, 6. doi:10.1186/1758-2946-1-6
- Perez, D. I., Gil, C., and Martinez, A. (2011). Protein Kinases CK1 and CK2 as New Targets for Neurodegenerative Diseases. *Med. Res. Rev.* 31, 924–954. doi:10.1002/med.20207
- QUACPAC (2021). QUACPAC 2.1.3.0. Santa Fe, NM: OpenEye Scientific Software. Available at: <http://www.eyesopen.com>.
- Rees, D. C., Congreve, M., Murray, C. W., and Carr, R. (2004). Fragment-based Lead Discovery. *Nat. Rev. Drug Discov.* 3, 660–672. doi:10.1038/nrd1467
- Schoepfer, J., Jahnke, W., Berellini, G., Buonamici, S., Cotesta, S., Cowan-Jacob, S. W., et al. (2018). Discovery of Asciminib (ABL001), an Allosteric Inhibitor of the Tyrosine Kinase Activity of BCR-ABL1. *J. Med. Chem.* 61, 8120–8135. doi:10.1021/acs.jmedchem.8b01040
- Schultes, S., de Graaf, C., Haaksma, E. E. J., de Esch, I. J. P., Leurs, R., and Krämer, O. (2010). Ligand Efficiency as a Guide in Fragment Hit Selection and Optimization. *Drug Discov. Today Technol.* 7, e157–e162. doi:10.1016/j.ddtec.2010.11.003
- Schwab, C., DeMaggio, A. J., Ghoshal, N., Binder, L. I., Kuret, J., and McGeer, P. L. (2000). Casein Kinase 1 Delta Is Associated with Pathological Accumulation of Tau in Several Neurodegenerative Diseases. *Neurobiol. Aging* 21, 503–510. doi:10.1016/s0197-4580(00)00110-x
- Selkoe, D. J. (2001). Alzheimer's Disease: Genes, Proteins, and Therapy. *Physiol. Rev.* 81, 741–766. doi:10.1152/physrev.2001.81.2.741
- Spiegel, J. O., and Durrant, J. D. (2020). AutoGrow4: an Open-Source Genetic Algorithm for De Novo Drug Design and Lead Optimization. *J. Cheminformatics* 12112, 1–16. doi:10.1186/s13321-020-00429-4
- Surmeier, D. J. (2018). Determinants of Dopaminergic Neuron Loss in Parkinson's Disease. *FEBS J.* 285, 3657–3668. doi:10.1111/febs.14607
- Trott, O., and Olson, A. J. (2010). Vina: AutoDock Vina: Improving the Speed and Accuracy of Docking with a New Scoring Function, Efficient Optimization, and Multithreading. *J. Comput. Chem.* 31, 455–461. doi:10.1002/jcc.21334
- Verdonk, M. L., Giangreco, I., Hall, R. J., Korb, O., Mortenson, P. N., and Murray, C. W. (2011). Docking Performance of Fragments and Druglike Compounds. *J. Med. Chem.* 54, 5422–5431. doi:10.1021/jm200558u
- Wierbowski, S. D., Wingert, B. M., Zheng, J., and Camacho, C. J. (2020). Cross-docking Benchmark for Automated Pose and Ranking Prediction of Ligand Binding. *Protein Sci.* 29, 298–305. doi:10.1002/pro.3784
- Wójcikowski, M., Zielenkiewicz, P., and Siedlecki, P. (2015). Open Drug Discovery Toolkit (ODDT): a New Open-Source Player in the Drug Discovery Field. *J. Cheminform.* 7, 26. doi:10.1186/s13321-015-0078-2
- Xu, P., Ianes, C., Gärtner, F., Liu, C., Burster, T., Bakulev, V., et al. (2019). Structure, Regulation, and (Patho-)physiological Functions of the Stress-Induced Protein Kinase CK1 Delta (CSNK1D), *Gene* 715, 144005. doi:10.1016/j.gene.2019.144005

Conflict of Interest: The authors declare that the research was conducted in the absence of any commercial or financial relationships that could be construed as a potential conflict of interest.

Publisher's Note: All claims expressed in this article are solely those of the authors and do not necessarily represent those of their affiliated organizations, or those of the publisher, the editors and the reviewers. Any product that may be evaluated in this article, or claim that may be made by its manufacturer, is not guaranteed or endorsed by the publisher.

Copyright © 2022 Pavan, Menin, Bassani, Sturlese and Moro. This is an open-access article distributed under the terms of the Creative Commons Attribution License (CC BY). The use, distribution or reproduction in other forums is permitted, provided the original author(s) and the copyright owner(s) are credited and that the original publication in this journal is cited, in accordance with accepted academic practice. No use, distribution or reproduction is permitted which does not comply with these terms.



Casein Kinase 2 Signaling in White Matter Stroke

Hung Nguyen, Wenbin Zhu and Selva Baltan *

Anesthesiology and Peri-Operative Medicine (APOM), Oregon Health and Science University, Portland, OR, United States

OPEN ACCESS

Edited by:

Andrea Venerando,
University of Padua, Italy

Reviewed by:

Jason D Hinman,
University of California, Los Angeles,
United States
Byung Gon Kim,
Ajou University, South Korea

*Correspondence:

Selva Baltan
baltan@ohsu.edu

Specialty section:

This article was submitted to
Molecular Diagnostics and
Therapeutics,
a section of the journal
Frontiers in Molecular Biosciences

Received: 30 March 2022

Accepted: 21 June 2022

Published: 13 July 2022

Citation:

Nguyen H, Zhu W and Baltan S (2022)
Casein Kinase 2 Signaling in White
Matter Stroke.
Front. Mol. Biosci. 9:908521.
doi: 10.3389/fmolb.2022.908521

The growth of the aging population, together with improved stroke care, has resulted in an increase in stroke survivors and a rise in recurrent events. Axonal injury and white matter (WM) dysfunction are responsible for much of the disability observed after stroke. The mechanisms of WM injury are distinct compared to gray matter and change with age. Therefore, an ideal stroke therapeutic must restore neuronal and axonal function when applied before or after a stroke, and it must also protect across age groups. Casein kinase 2 (CK2), is expressed in the brain, including WM, and is regulated during the development and numerous disease conditions such as cancer and ischemia. CK2 activation in WM mediates ischemic injury by activating the Cdk5 and AKT/GSK3 β signaling pathways. Consequently, CK2 inhibition using the small molecule inhibitor CX-4945 (Silmitasertib) correlates with preservation of oligodendrocytes, conservation of axon structure, and axonal mitochondria, leading to improved functional recovery. Remarkably, CK2 inhibition promotes WM function when applied after ischemic injury by specifically regulating the AKT/GSK3 β pathways. The blockade of the active conformation of AKT confers post-ischemic protection to young and old WM by preserving mitochondria, implying AKT as a common therapeutic target across age groups. Using a NanoString nCounter miRNA expression profiling, comparative analyses of ischemic WM with or without CX-4945 treatment reveal that miRNAs are expressed at high levels in WM after ischemia, and CX-4945 differentially regulates some of these miRNAs. Therefore, we propose that miRNA regulation may be one of the protective actions of CX-4945 against WM ischemic injury. Silmitasertib is FDA approved and currently in use for cancer and Covid patients; therefore, it is plausible to repurpose CK2 inhibitors for stroke patients.

Keywords: mitochondria, micro RNA, CX-4945, silmitasertib, akt, post-ischemic protection, ischemia

INTRODUCTION

The Role of Casein Kinase 2 in Brain Ischemia

Casein Kinase 2 (CK2), is an unconventional protein kinase (PK) that is composed of two catalytic α -subunits (α and α') and two β -subunits (Pinna and Allende, 2009). CK2 is shown to phosphorylate numerous substrates, including other PKs, thus acting as a “master regulator” (Meggio and Pinna, 2003; Poole et al., 2005). Unlike other PKs, the catalytic activity of CK2 is not regulated by second messengers or phosphorylation (Poole et al., 2005; Vilk et al., 2008) and it is constitutively active. In addition, CK2 is recently reported to be activated *via* a polymerization/depolymerization mechanisms (Kristensen et al., 2004; Lolli et al., 2012; Franchin et al., 2018) together with reactive oxygen species (ROS) (Leslie and Downes, 2002; Cosentino-Gomes et al., 2012; Srinivasan et al., 2013). CK2 regulates many cellular functions and its activity is vital for brain

development (Lou et al., 2008) and cellular homeostasis (Blanquet, 2000; Brunet et al., 2015). For instance, direct interaction of CK2 β with the transcription factor Olig2 is required for oligodendrocyte progenitor cell development and lineage (Huillard et al., 2010). On the other hand, upregulation of CK2 signaling is linked to many diseases, such as cancers (Sarno et al., 2002), cardiac hypertrophy (Hauck et al., 2008; Eom et al., 2011), and ischemic injury (Hu et al., 1993; Hu and Wieloch, 1993; Ka et al., 2015).

CK2 is constitutively expressed in the central nervous system (CNS) including glial cells such as adult oligodendrocytes (Huillard et al., 2010) and has a complex role in cellular injury (Ka et al., 2015). A previous report has shown that CK2 is a neuroprotectant that acts by directly modulating NADPH oxidase activity during cerebral ischemia (Kim et al., 2009). On the other hand, a brief and moderate AMPA receptor activation in rat oligodendrocyte cell cultures triggers CK2 activity to mediate excitotoxic injury (Canedo-Antelo et al., 2018). Accordingly, CK2 inhibition alleviates AMPA-mediated excitotoxic oligodendrocyte death by blocking AMPA receptor activation (Canedo-Antelo et al., 2019). Although these findings propose an intriguing role for CK2 signaling in brain ischemic injury mechanisms, the role of CK2 has remained unexplored in white matter (WM) function and ischemic injury mechanisms until recently (Baltan et al., 2018; Bastian et al., 2019b). WM is composed of astrocytes, oligodendrocytes, microglia, axons, and myelin that wraps them (Fields, 2008) therefore an ideal stroke therapeutic must be directed towards neurons, axons, and glial cells across all age groups. Currently, recombinant tissue plasminogen activator or endovascular thrombectomy are effective treatments for reperfusion after ischemic stroke. However, reperfusion alone is not sufficient to rescue dying cells due to the activation of injury-related pathways. Thus, there is an unmet need for the identification of post-ischemic injury mechanisms to develop effective stroke treatment. Axonal injury is an important independent risk factor and burden for adverse outcomes following a stroke, even in intravenous thrombolysis patients (Curtze et al., 2015). It is crucial, therefore, to search for therapeutic options that protect the entire brain by treating both gray and WM components against ischemia.

Mechanisms of Ischemic White Matter Injury Are Age-Dependent

Mechanisms underlying ischemic WM injury prove to be unexpectedly complex and distinct from gray matter (GM) injury (Wrathall et al., 1994; Agrawal and Fehlings, 1997; Fern and Ransom, 1997; McDonald et al., 1998; Sanchez-Gomez and Matute, 1999; Follett et al., 2000; Tekk  k and Goldberg, 2001; Stys, 2004; Tekk  k et al., 2007). WM injury mechanisms follow a spatiotemporal sequence of events; axons are injured directly by the loss of ionic homeostasis resulting in toxic accumulation of intracellular Na⁺ and Ca²⁺ (Stys et al., 1990; Fern et al., 1995; Wolf et al., 2001; Ouardouz et al., 2003; Underhill and Goldberg, 2007), while astrocytes due to reversal of Na⁺-dependent glutamate transporters release excessive glutamate (Tekk  k et al., 2007)

leading to injury of oligodendrocytes and the myelin they produce (Matute et al., 1997; McDonald et al., 1998; Li et al., 1999; Sanchez-Gomez and Matute, 1999; Tekk  k and Goldberg, 2001; Alberdi et al., 2002; Micu et al., 2006; Tekk  k et al., 2007). Consistent with this idea, removal of extracellular Ca²⁺, blockade of AMPA/kainate receptors, or blockade of reverse glutamate transport reduces ischemic WM injury. Moreover, glutamate accumulation triggers oxidative injury pathways by competing with cysteine. Together with mitochondrial dysfunction and nitric oxide synthetase (NOS) activation, reactive oxidative stress (ROS) production increases contributing to irreversible ischemic WM injury.

Aging is the most independent risk factor for stroke. Age-related changes in the molecular structure of WM dictate injury mechanisms by surpassing the ionic pathway and initiating injury by combined excitotoxic and oxidative injury pathways. Consequently, protective interventions in young WM become ineffective at promoting recovery of, or even injurious to, aging WM (Saab et al., 2016; Bastian et al., 2019a). For instance, in the aging axons, there is a significant increase in glutamate transporter-1 (GLT-1) levels leading to excessive extracellular glutamate accumulation presumably due to an increased need for glutamate signaling in aging WM to maintain its function (Baltan, 2009; Baltan et al., 2011). However, these adaptive changes act against the tissue by causing glutamate toxicity and mitochondrial energy depletion in aging axons during an ischemic episode (Stahon et al., 2016). To maintain proper axon function, axonal mitochondria exhibit unique and complex dynamics to proficiently buffer Ca²⁺, produce sufficient ATP, and effectively scavenge ROS. Ca²⁺ overload activates eNOS to produce nitric oxide (NO) and ROS, which are proposed as diffusible second messengers to link oligodendrocyte excitotoxicity to axon injury (Matute, 2010; Voccoli et al., 2014; Bastian et al., 2018). The fusion and fission processes of mitochondria are delicately regulated to coordinate the spatiotemporal properties of mitochondrial Ca²⁺ responses and the physiological and pathophysiological consequences of Ca²⁺ signals (Baltan, 2014b). By enhancing fusion or inhibiting fission, elongated mitochondria efficiently buffer Ca²⁺, thus preventing eNOS activation and subsequent ROS production (Lugus et al., 2011; Miller et al., 2013; Baltan, 2014b; Bastian et al., 2018). In aging axons, there is an increase in mitochondrial fusion, presumably to effectively buffer increased Ca²⁺ load and ROS production, which further alters the mitochondrial dynamics and function (Baltan, 2009; Stahon et al., 2016). Therefore, an age-dependent modification in mitochondrial bioenergetics may underlie the increased vulnerability of aging axons to ischemia. The intimate link between changes in aging WM structure and response to injury complicates the development of possible therapeutic options and warrants attention to identify beneficial interventions that act on shared molecular targets between young and aging WM.

Casein Kinase 2 Mediates Ischemic White Matter Injury

The optic nerve, a purely myelinated CNS WM tract, offers several advantages to study the mechanisms of WM injury. These advantages include minimal surgical injury due to

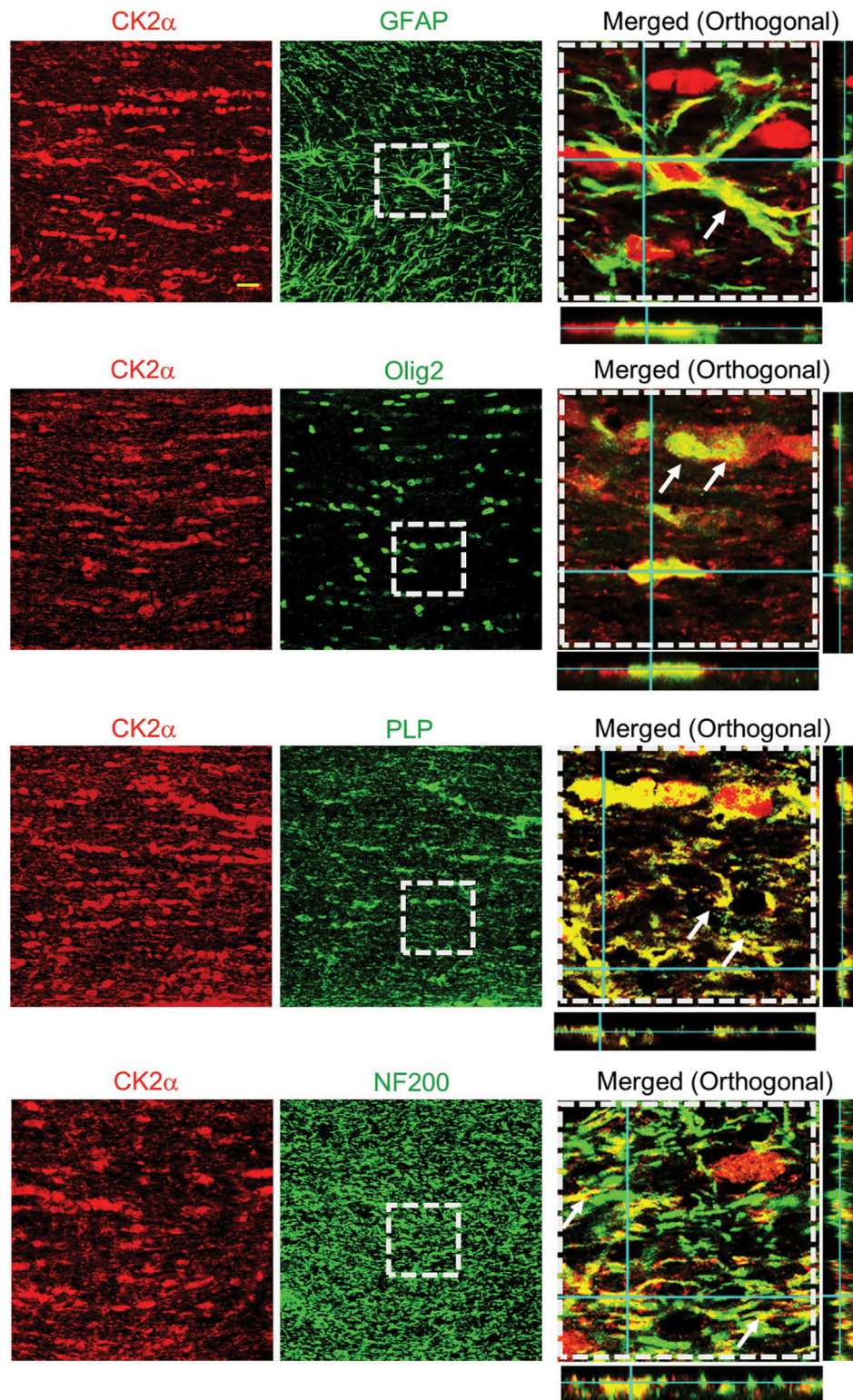
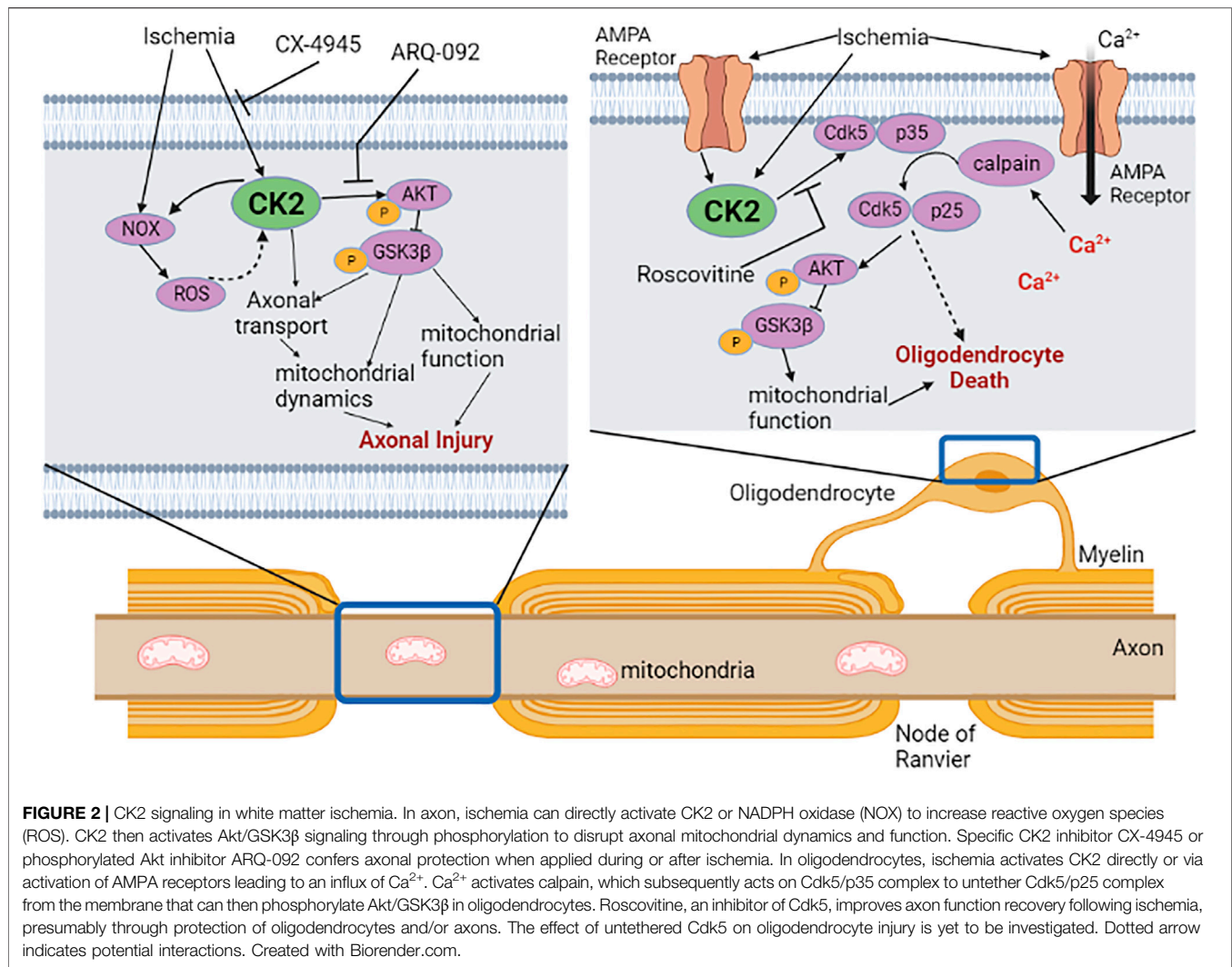


FIGURE 1 | CK2 α expression and localization in mouse optic nerves. CK2 α subunits are expressed in optic nerve astrocytes, myelin sheath, and oligodendrocytes. To identify the cellular expression of CK2 α subunits in the mouse optic nerve, CK2 α was co-immunolabeled with glial fibrillary acidic protein (GFAP, astrocytes, top row), oligodendrocyte lineage transcription factor 2 (Olig2, oligodendrocytes, second row), myelin proteolipid protein (PLP, myelin, third row), and neurofilament protein (NF200, axons, bottom row). Note that the merged images (xy, xz and yz orthogonal view) in the right panels are enlarged areas (50 μ m \times 50 μ m) indicated by the squares with dashed lines in the middle panels. Scale bar = 20 μ m. (Figure from Bastian et al., 2019).



isolation techniques, preservation of the three-dimensional structure of myelinated axons with their supporting glia, stable and quantifiable recording of action potentials for prolonged periods (Cavallotti et al., 2002; Cavallotti et al., 2003). Tissue collected at the end of the experiments can be further processed to quantify the proteins of interest. In addition, in fixed optic nerve tissue, the cellular and axonal structures can be immunolabeled with cell-specific antibodies or prepared for three-dimensional electron microscopy imaging for ultrastructural assessment. The corpus callosum (CC) is another WM tract and offers important advantages for the investigation of *in vitro* CC slices to quantify axon function and *in vivo* WM (selective WM ischemic by stereotaxic L-NIO injections) injury which can be assessed with behavioral tests (Nunez et al., 2016). These two WM tracts allow an excellent combined function-structure analysis of glial cells and axons after stroke.

We evaluated the expression and localization of CK2α in mouse optic nerves (MONs), using isoform-specific antibodies to support a biological basis for investigating CK2 signaling in WM (Figure 1). CK2α is expressed in axons and glial cells in

MONs demonstrated by colocalization of CK2α subunit with GFAP (+) astrocyte nuclei and some processes, NF-200 (+) axons, Olig2 (+) oligodendrocytes, and PLP (+) myelin. The robust expression pattern of CK2α suggests an extensive kinase regulation of WM structure and function (Moreno et al., 1999; Brechet et al., 2008; Yoshimura and Rasband, 2014; Rosenberger et al., 2016). Indeed, CK2 signaling is different under physiological and ischemic stress conditions. Under normal physiological conditions, CK2 signaling is important for the clustering of Na^+ channels at axon initial segments and nodes of Ranvier to enable and preserve axonal excitability (Brechet et al., 2008; Hien et al., 2014) and for oligodendrocyte development (Huillard et al., 2010). On the other hand, during ischemia, CK2 signaling mediates injury to glial cells and impairs axon function either directly and/or through Cdk5 and PTEN/AKT/GSK3β signaling regulation of downstream effectors (Figure 2). Subsequently, CK2 blockade preserves oligodendrocytes and axonal mitochondrial integrity, dynamics, and function (Baltan et al., 2018; Bastian et al., 2019b). Changes in signaling due to ischemia are achieved by

either increasing CK2 activity (Charriaut-Marlangue et al., 1991; Hu and Wieloch, 1993; Hase et al., 2005; Chao et al., 2007) or by the movement of CK2 to a different subcellular compartment (Serrano et al., 1989; Charriaut-Marlangue et al., 1991; Diaz-Nido and Avila, 1992; Faust et al., 2001; Qaiser et al., 2014). CK2 can directly interfere with mitochondrial axonal transport (Pigino et al., 2009) to ultimately alter mitochondrial dynamics (Amiri and Hollenbeck, 2008; Liu et al., 2009; Twig et al., 2010) and function (Detmer and Chan, 2007). Another signaling pathway that CK2 regulates is Cdk5 (Lim et al., 2004) (**Figure 2**). Both CK2 and Cdk5 are expressed at nodes of Ranvier (Brechet et al., 2008; Cerda and Trimmer, 2011) and by oligodendrocytes (Huillard et al., 2010; Yang et al., 2013), where CK2 can inhibit Cdk5 by contact inhibition (Lim et al., 2004). Therefore, for Cdk5 to be activated, CK2 must move away from Cdk5. Cdk5 is tethered to the membrane by its association with p35, a protein with a membrane-anchoring domain. The Cdk5/p35 complex is then fully activated by Ca^{2+} -dependent proteolytic cleavage of p35 to p25 by calpain, effectively removing its membrane-anchoring domain (Meyer et al., 2014). Local intracellular Ca^{2+} may be increased by the reversal of the Na^+ - Ca^{2+} exchanger or by activation of L-type Ca^{2+} channels (Brown, 2001; Baltan, 2009). The Cdk5 complex can then move from nodes of Ranvier to other cellular compartments to control AKT signaling (Lou et al., 2008) and axonal transport (Shea et al., 2004) to ultimately regulate mitochondrial dynamics (Amiri and Hollenbeck, 2008; Liu et al., 2009; Twig et al., 2010) and function (Detmer and Chan, 2007) (**Figure 2**). In addition, CK2 can regulate PTEN/AKT/GSK3 β (Silva et al., 2008; Silva et al., 2010) signaling. CK2 inhibits PTEN by phosphorylation, which leads to the activation of AKT. AKT phosphorylates GSK3 β to inhibit its activity (Cross et al., 1995), which could lead to changes in mitochondrial transport (Embi et al., 1980; Cohen and Frame, 2001), glycogen synthase (Embi et al., 1980; Cohen and Frame, 2001), and mitochondrial function (Detmer and Chan, 2007; Amiri and Hollenbeck, 2008; Liu et al., 2009; Twig et al., 2010).

Our recent studies, for the first time, establish that a PK mediates ischemic injury in WM by CK2 signaling leading to activation of Cdk5 and PTEN/AKT/GSK3 β pathways (Bastian et al., 2019b) (**Figure 2**). To identify the role of CK2 signaling in WM ischemic injury, we followed the preclinical recommendations of the Stroke Therapy Academic Industry Roundtable (STAIR) (Fisher et al., 2009). Based on this set of criteria, we use CX-4945 (Silmitasertib), a highly *selective* (Siddiqui-Jain et al., 2010; Son et al., 2013), *specific* (Battistutta et al., 2011), and *potent* CK2 inhibitor that can be administered *orally* (Ryan et al., 2005; Zhong et al., 2020) and *crosses the blood-brain barrier* (Vita et al., 2005; Sallam et al., 2008; Cheng et al., 2012; Zheng et al., 2013). CX-4945 is an *FDA-approved* anti-cancer drug (Martins et al., 2014). CX-4945 exerts dose-dependent protection to axon function (max protection at 5 μM) and the lack of any baseline effects of this drug on axon conduction allows comparison of recovery in *in vitro* experiments and behavioral assessments in *in vivo* experiments. Thus, we propose that CK2 inhibition protects the brain against ischemia by protecting axonal and glial compartments.

Equally important, CX-4945 confers similar protection to aging (12–14 months) and old (>20 months) WM when applied after ischemia promoting axon function recovery. The effects of aging on myelinated axons are more complicated and extensive than those in cortical GM. Despite larger and thicker aging axons, with longer and thicker mitochondria that correlate with lower ATP production, CX-4945 still provides post-ischemic protection to aging axon function by preserving mitochondrial integrity. We, therefore, suggest that CK2 signaling is a shared pathway underlying WM injury independent of age.

An important outcome measure emphasized by STAIR criteria is the consideration of the female sex. Stroke in females is associated with a decreased likelihood of excellent outcome after acute ischemic stroke, particularly in older age groups. There is a correlation between markers of WM integrity and functional outcomes in women, which implies a potential sex-specific WM injury mechanism (Etherton et al., 2017; Phan et al., 2018; Etherton et al., 2019). Therefore, evaluation of CK2 signaling in female WM injury and whether CK2 inhibition provides equal protection compared to male WM is a pending goal of our group.

Casein Kinase 2 Mediates Post-Ischemic WM Injury By Selectively Acting on the AKT Pathway

The finding that CK2 inhibition with CX-4945 when applied before or after the end of an ischemic episode promotes WM functional recovery raises the question of whether Cdk5 or AKT activation plays a distinct role in conferring post-ischemic WM protection (**Figure 2**). Inhibition of Cdk5 using Roscovitine protects axon function only when applied during ischemia, mainly acting on oligodendrocytes and axons (**Figure 2**). On the other hand, inhibition of the active conformation of AKT is beneficial when applied during or after ischemia suggesting that a window of opportunity exists in ameliorating ischemic injury in WM. AKT is involved in many neurological processes, and AKT isoforms are distinct regarding their tissue expression, pathway activation, and inhibitor sensitivity (Shaw and Kirshenbaum, 2006; Skeen et al., 2006). However, very few studies have examined AKT isoform expression at the cellular level, and cell- and age-specific AKT isoforms expression in WM remains unknown. Therefore, a systematic investigation of AKT isoforms and their contribution to axon and glia function is warranted.

Casein Kinase 2 Disrupts Axonal Mitochondria

We recently showed that the preservation of mitochondrial integrity is an essential component of post-ischemic protection of axon function in WM. (Baltan et al., 2011; Baltan, 2014a; Stahon et al., 2016). CX-4945 promotes young and aging axon function recovery following ischemia by preserving axonal mitochondria. Cdk5 directly impacts mitochondrial dynamics and function by increasing the production of ROS and phosphorylation of the mitochondrial fission protein Drp-1,

TABLE 1 | List of miRNAs with fold changes after OGD and OGD with CK2 inhibition and their cellular expression.

OGD			
MiRNA	Fold Change	p-value	Cellular Expression
A			
miR-1959	1.70	0.032	Astrocyte exosomes
miR-501-3p	1.58	0.025	Neurons
miR-146b	1.57	0.049	Neurons, Astrocytes, Oligodendrocytes
miR-201	1.50	0.027	NA
miR-335-3p	1.50	0.031	Neurons, Astrocytes
miR-1937a	−1.50	0.035	NA
miR-1937b	−1.50	0.035	Astrocyte exosomes
B			
OGD+CX-4945			
MiRNA	Fold Change	p-value	Cellular Expression
miR-1937a	1.53	0.030	NA
miR-1937b	1.53	0.030	Astrocyte exosomes
miR-m01-2	−1.63	0.002	NA
miR-501-3p	−1.65	0.047	Neurons
miR-200a	−1.69	0.047	Neurons, Astrocytes, Oligodendrocytes
miR-1959	−1.84	0.025	Astrocyte exosomes
miR-654-3p	−2.24	0.011	NA

(A) OGD, compared to control. (B) OGD + CK2 inhibition with CX-4945, compared to OGD., Welch's t-test. Negative sign indicates decrease. [Modified from (Baltan et al., 2021)].

leading to mitochondrial dysfunction (Sun et al., 2008; Morel et al., 2010; Cherubini et al., 2015; Jahani-Asl et al., 2015; Klinman and Holzbaur, 2015; Park et al., 2015). However, Cdk5 inhibition fails to exert post-ischemic protection to axon function, implying that Cdk5 signaling is important to alleviate oxidative injury specifically during ischemia. The finding that selective inhibition of phosphorylated AKT confers post-ischemic protection to axon function proposes a novel role for PTEN/AKT signaling in mediating mitochondrial disruption after an ischemic episode in WM. AKT activation contributes to increased glutamate release during OGD and ATP depletion, as well as enhanced excitotoxicity (Baltan et al., 2008) due to the upregulation of GLT-1 expression in astrocytes (Li et al., 2006; Ji et al., 2013; Zhang et al., 2013). As a result, the application of ARQ-092, which is a specific blocker for the active form of AKT (Yu et al., 2015; Lapierre et al., 2016), promotes axon function recovery suggesting that the active conformation of AKT is an important molecular target for post-ischemic protection of axon function (Figure 2). Moreover, the GSK3 β isoform which is a part of the AKT/GSK3 β signaling cascade has been reported to be a significant therapeutic target for cerebral ischemia (Koh S.-H. et al., 2008; Cowper-Smith et al., 2008). GSK3 β inhibition decreases mitochondrial ROS production and prevents neuronal damage establishing an interesting relationship between GSK3 β and mitochondria (Valerio et al., 2011). Because, we also observed that CK2 inhibition improved axon function recovery by decreasing the inactivation of GSK3 β in WM, these findings suggest that GSK3 β could be a common target to protect both GM and WM after ischemic stroke.

Casein Kinase 2 Mediates WM Injury By Regulating Micro RNAs (miRNAs)

The miRNAs emerge as important mediators of neuronal injury during an ischemia attack. However, the role and involvement of

miRNAs remain unestablished in WM ischemic injury. Therefore, in our recent study, we characterized miRNA profiles in optic nerve following ischemia using the NanoString nCounter[®] miRNA Expression Panel. Together with *in situ* hybridization, and *in silico* KEGG pathway analysis, we show that the most abundant miRNAs in the optic nerve are expressed in astrocytes, and oxygen-glucose deprivation (OGD) differentially regulates miRNA expression in the optic nerve (Baltan et al., 2021).

Based on our analysis, it remains challenging to define whether miRNAs regulated by ischemia in WM are beneficial or detrimental to the recovery of axon function. Some miRNAs were reciprocally regulated by OGD or OGD and CX-4945 application. For instance, OGD and CX-4945 selectively modulated miR-1937a, miR-1937b, miR-1959, miR-200a, miR-501-3p, and miR-654-3p (Table 1) (Baltan et al., 2021). We propose that these miRNAs may be associated with the beneficial effects of CX-4945. In agreement, miR-501-3p is expressed in neurons which in optic nerve (pure WM tract without neuronal cell body) infers axonal expression (Baltan et al., 2021). Because CK2 inhibition promotes axon function by preserving axonal mitochondria (Bastian et al., 2019b), we hypothesize that CK2 inhibition exerts white matter protection by regulating miR-501-3p. Particularly, because miR-501-3p is shown to mediate the regulation of GluA1 subunit expression of AMPA receptors and the subsequent mitochondrial injury (Sripada et al., 2012). Furthermore, miR-501-3p is expressed in human and reported to be a novel serum biomarker, which relates to the severity of Alzheimer's Disease (Hara et al., 2017). Hence, miR-501-3p appears as a promising target for further investigation. In addition, we determined that exosomal expression of miR-1959 and miR-1937b in astrocytes is also differentially regulated by OGD or OGD and CX-4945 (Jovićić and Gitler, 2017). Astrocytic exosomes are 50–100 nm membrane-bound vesicles, which contain and transfer a selected group of miRNAs to other

cells. This suggests that astrocytes coordinate an efficient communication among glia cells in response to OGD or CK2 inhibition during ischemia in WM. It will be intriguing to identify the role and cellular target of miR-1959 and miR-1937b in WM. Another novel finding is that CX-4945 treatment affects some common KEGG signaling pathways. One of these signaling pathways is the ErbB signaling system (Li et al., 2020) which is important to maintain axon function as well as supporting glia and myelin. Expectedly, a disruption in ErbB signaling may impair axon function by causing myelin damage (Carroll et al., 1997). Additionally, ErbB signaling in neurons and macrophages/microglia determines neuroprotection and repair capacity after ischemia (Xu and Ford, 2005). Interestingly, CX-4945 regulates Wingless/int1 (Wnt) signaling, which is involved in neurogenesis after cerebral ischemia, implicating Wnt signaling as a therapeutic target for ischemic injury (Yu et al., 2018; Qiu et al., 2019). CX-4945 also regulates mTOR and axon guidance pathways that are important for neuroprotection after an ischemic stroke (Sofer et al., 2005; Koh P.-O. et al., 2008; Foster and Fingar, 2010; Koh, 2010; Hinman, 2014). However, further experiments are needed to validate whether the mechanisms of protection of CX-4945 are indeed mediated through these signaling pathways.

DISCUSSION

WM ischemic lesions are correlated to neurological deficits (Yamada et al., 2003; Sea Lee et al., 2005) and particularly the extent and localization of WM injury may dictate functional deficits and recovery in humans. Because the rodent brain has a relatively small WM (10–15%) (Zhang and Sejnowski, 2000) and most widely used stroke models spare corpus callosum, the injury mechanisms mostly provide information about neuronal populations. Neuroprotective approaches focused solely on neuronal survival may be one of the reasons for the failure in translating experimental findings successfully to clinical applications. It is crucial to consider WM integrity in experimental models to identify ideal therapeutic targets for stroke patients.

REFERENCES

- Agrawal, S. K., and Fehlings, M. G. (1997). Role of NMDA and Non-NMDA Ionotropic Glutamate Receptors in Traumatic Spinal Cord Axonal Injury. *J. Neurosci.* 17 (3), 1055–1063. doi:10.1523/jneurosci.17-03-01055.1997
- Alberdi, E., Sánchez-Gómez, M. V., Marino, A., and Matute, C. (2002). Ca²⁺ Influx through AMPA or Kainate Receptors Alone Is Sufficient to Initiate Excitotoxicity in Cultured Oligodendrocytes. *Neurobiol. Dis.* 9 (2), 234–243. doi:10.1006/nbdi.2001.0457
- Amiri, M., and Hollenbeck, P. J. (2008). Mitochondrial Biogenesis in the Axons of Vertebrate Peripheral Neurons. *Devel Neurobiol.* 68 (11), 1348–1361. doi:10.1002/dneu.20668
- Baltan, S. (2014a). “Age-Dependent Mechanisms of White Matter Injury after Stroke,” in *White Matter Injury in Stroke and CNS Disease*. Editors S. Baltan, S. T. Carmichael, C. Matute, G. Xi, and J. H. Zhang (New York, NY: Springer New York), 373–403. doi:10.1007/978-1-4614-9123-1_16

In summary, our recent studies provide evidence that CK2 signaling activates Cdk5 and AKT/GSK3 β signaling pathways to mediate WM ischemic injury. The downstream molecular pathways are activated in a spatiotemporal way such that Cdk5 signaling becomes significant during ischemia, while AKT signaling emerges as the key pathway during the post-ischemic period. Consistent with this, inhibition of CK2 or the activated form of AKT confers post-ischemic protection to axon function and promotes recovery in young and aging WM. The protective effects of CK2 inhibition correlate with the conservation of oligodendrocytes, axon structure, and axonal mitochondria. Several miRNAs are differentially regulated by CX-4945 compared to ischemia, and these miRNAs may participate in ischemic WM injury mechanisms. MiRNAs are promising candidates for biomarkers of injury and therapeutic interventions as they are readily detected in body fluids. We also show that CX-4945 regulates a group of murine-associated viral miRNAs (for example see Table 1) which may justify the use of CX-4945 in clinical trials for Covid19 patients (Baltan et al., 2021) (ClinicalTrials.gov Identifier: NCT04663737). Finally, our findings may have mechanistic and therapeutic implications for dementia, Alzheimer’s disease, multiple sclerosis, periventricular leukomalacia, and Parkinson’s disease that involve WM injury.

AUTHOR CONTRIBUTIONS

All authors participated in writing the manuscript.

FUNDING

This work was supported by the National Institute of Aging (Grant Number AG033720) National Institute of Neurological Diseases and Stroke (NS094881).

ACKNOWLEDGMENTS

The authors thank Ngoc Wasson for editorial assistance.

- Baltan, S., Bastian, C., Quinn, J., Aquila, D., McCray, A., and Brunet, S. (2018). CK2 Inhibition Protects White Matter from Ischemic Injury. *Neurosci. Lett.* 687, 37–42. doi:10.1016/j.neulet.2018.08.021
- Baltan, S., Besancon, E. F., Mbow, B., Ye, Z., Hamner, M. A., and Ransom, B. R. (2008). White Matter Vulnerability to Ischemic Injury Increases with Age Because of Enhanced Excitotoxicity. *J. Neurosci.* 28 (6), 1479–1489. doi:10.1523/jneurosci.5137-07.2008
- Baltan, S. (2014b). Excitotoxicity and Mitochondrial Dysfunction Underlie Age-dependent Ischemic White Matter Injury. *Adv. Neurobiol.* 11, 151–170. doi:10.1007/978-3-319-08894-5_8
- Baltan, S. (2009). Ischemic Injury to White Matter: an Age-dependent Process. *Neuroscientist* 15 (2), 126–133. doi:10.1177/1073858408324788
- Baltan, S., Murphy, S. P., Danilov, C. A., Bachleda, A., and Morrison, R. S. (2011). Histone Deacetylase Inhibitors Preserve White Matter Structure and Function during Ischemia by Conserving ATP and Reducing Excitotoxicity. *J. Neurosci.* 31 (11), 3990–3999. doi:10.1523/JNEUROSCI.5379-10.2011
- Baltan, S., Sandau, U. S., Brunet, S., Bastian, C., Tripathi, A., Nguyen, H., et al. (2021). Identification of miRNAs that Mediate Protective Functions of Anti-

- cancer Drugs during White Matter Ischemic Injury. *ASN Neuro* 13, 175909142110422. doi:10.1177/17590914211042220
- Bastian, C., Quinn, J., Doherty, C., Franke, C., Faris, A., Brunet, S., et al. (2019a). "Role of Brain Glycogen during Ischemia, Aging and Cell-To-Cell Interactions," in *Brain Glycogen Metabolism*. Editors M. DiNuzzo and A. Schousboe (Cham: Springer International Publishing), 2019/11/02, 347–361. doi:10.1007/978-3-030-27480-1_12
- Bastian, C., Quinn, J., Tripathi, A., Aquila, D., McCray, A., Dutta, R., et al. (2019b). CK2 Inhibition Confers Functional Protection to Young and Aging Axons against Ischemia by Differentially Regulating the CDK5 and AKT Signaling Pathways. *Neurobiol. Dis.* 126, 47–61. doi:10.1016/j.nbd.2018.05.011
- Bastian, C., Zaleski, J., Stahon, K., Parr, B., McCray, A., Day, J., et al. (2018). NOS3 Inhibition Confers Post-Ischemic Protection to Young and Aging White Matter Integrity by Conserving Mitochondrial Dynamics and Miro-2 Levels. *J. Neurosci.* 38 (28), 6247–6266. doi:10.1523/JNEUROSCI.3017-17.2018
- Battistutta, R., Cozza, G., Pierre, F., Papinutto, E., Lolli, G., Sarno, S., et al. (2011). Unprecedented Selectivity and Structural Determinants of a New Class of Protein Kinase CK2 Inhibitors in Clinical Trials for the Treatment of Cancer. *Biochemistry* 50 (39), 8478–8488. doi:10.1021/bi2008382
- Blanquet, P. R. (2000). Casein Kinase 2 as a Potentially Important Enzyme in the Nervous System. *Prog. Neurobiol.* 60 (3), 211–246. doi:10.1016/s0301-0082(99)00026-x
- Bre'chet, A., Fache, M.-P., Brachet, A., Ferracci, G., Baude, A., Irondelle, M., et al. (2008). Protein Kinase CK2 Contributes to the Organization of Sodium Channels in Axonal Membranes by Regulating Their Interactions with Ankyrin G. *J. Cell Biol.* 183 (6), 1101–1114. doi:10.1083/jcb.200805169
- Brown, G. C. (2001). Regulation of Mitochondrial Respiration by Nitric Oxide Inhibition of Cytochrome C Oxidase. *Biochimica Biophysica Acta (BBA) - Bioenergetics* 1504 (1), 46–57. doi:10.1016/s0005-2728(00)00238-3
- Brunet, S., Emrick, M. A., Sadilek, M., Scheuer, T., and Catterall, W. A. (2015). Phosphorylation Sites in the Hook Domain of CaV β Subunits Differentially Modulate CaV1.2 Channel Function. *J. Mol. Cell. Cardiol.* 87, 248–256. doi:10.1016/j.yjmcc.2015.08.006
- Canedo-Antelo, M., Llaverio, F., Zugaza, J., Matute, C., and Sánchez-Gómez, M. V. (2018). "Inhibition of Casein Kinase 2 Reduces aMPa-Induced Oligodendrocyte Death through Jnk Signaling and Er Stress Regulation," in *XII European Meeting on Glial Cells in Health and Disease* (Spain: Bilbao).
- Canedo-Antelo, M., Matute, C., and Sánchez-Gómez, M. V. (2019). "Protein Kinase CK2 and JNK Modulate Pro-apoptotic Effector Activation in AMPA-Induced Excitotoxicity in Oligodendrocytes," in *Neurogune 2nd Basque Neuroscience Meeting* (Spain: San Sebastian).
- Carroll, S. L., Miller, M. L., Frohner, P. W., Kim, S. S., and Corbett, J. A. (1997). Expression of Neuregulins and Their Putative Receptors, ErbB2 and ErbB3, Is Induced during Wallerian Degeneration. *J. Neurosci.* 17 (5), 1642–1659. doi:10.1523/JNEUROSCI.17-05-01642.1997
- Cavallotti, C., Cavallotti, D., Pescosolido, N., and Pacella, E. (2003). Age-related Changes in Rat Optic Nerve: Morphological Studies. *Anatom Histol. Embryol.* 32 (1), 12–16. doi:10.1046/j.1439-0264.2003.00431.x
- Cavallotti, C., Pacella, E., Pescosolido, N., Tranquilli-Leali, F. M., and Feher, J. (2002). Age-related Changes in the Human Optic Nerve. *Can. J. Ophthalmol.* 37 (7), 389–394. doi:10.1016/s0008-4182(02)80040-0
- Cerda, O., and Trimmer, J. S. (2011). Activity-dependent Phosphorylation of Neuronal Kv2.1 Potassium Channels by CDK5. *J. Biol. Chem.* 286 (33), 28738–28748. doi:10.1074/jbc.M111.251942
- Chao, C. C., Ma, Y. L., and Lee, E. H. Y. (2007). Protein Kinase CK2 Impairs Spatial Memory Formation through Differential Cross Talk with PI-3 Kinase Signaling: Activation of Akt and Inactivation of SGK1. *J. Neurosci.* 27 (23), 6243–6248. doi:10.1523/JNEUROSCI.1531-07.2007
- Charriaud-Marlangue, C., Otani, S., Creuzet, C., Ben-Ari, Y., and Loeb, J. (1991). Rapid Activation of Hippocampal Casein Kinase II during Long-Term Potentiation. *Proc. Natl. Acad. Sci. U.S.A.* 88 (22), 10232–10236. doi:10.1073/pnas.88.22.10232
- Cheng, Y., Zhang, Y., Zhang, L., Ren, X., Huber-Keener, K. J., Liu, X., et al. (2012). MK-2206, a Novel Allosteric Inhibitor of Akt, Synergizes with Gefitinib against Malignant Glioma via Modulating Both Autophagy and Apoptosis. *Mol. Cancer Ther.* 11 (1), 154–164. doi:10.1158/1535-7163.MCT-11-0606
- Cherubini, M., Puigdel·l·vol, M., Alberch, J., and Ginés, S. (2015). Cdk5-mediated Mitochondrial Fission: A Key Player in Dopaminergic Toxicity in Huntington's Disease. *Biochimica Biophysica Acta (BBA) - Mol. Basis Dis.* 1852 (10 Pt A), 2145–2160. doi:10.1016/j.bbdis.2015.06.025
- Cohen, P., and Frame, S. (2001). The Renaissance of GSK3. *Nat. Rev. Mol. Cell Biol.* 2 (10), 769–776. doi:10.1038/35096075
- Cosentino-Gomes, D., Rocco-Machado, N., and Meyer-Fernandes, J. R. (2012). Cell Signaling through Protein Kinase C Oxidation and Activation. *Ijms* 13 (9), 10697–10721. doi:10.3390/ijms130910697
- Cowper-Smith, C. D., Anger, G. J. A., Magal, E., Norman, M. H., and Robertson, G. S. (2008). Delayed Administration of a Potent Cyclin Dependent Kinase and Glycogen Synthase Kinase 3 β Inhibitor Produces Long-Term Neuroprotection in a Hypoxia-Ischemia Model of Brain Injury. *Neuroscience* 155 (3), 864–875. doi:10.1016/j.neuroscience.2008.05.051
- Cross, D. A. E., Alessi, D. R., Cohen, P., Andjelkovich, M., and Hemmings, B. A. (1995). Inhibition of Glycogen Synthase Kinase-3 by Insulin Mediated by Protein Kinase B. *Nature* 378 (6559), 785–789. doi:10.1038/378785a0
- Curtze, S., Melkas, S., Sibolt, G., Haapaniemi, E., Mustanoja, S., Putaala, J., et al. (2015). Cerebral Computed Tomography-Graded White Matter Lesions Are Associated with Worse Outcome after Thrombolysis in Patients with Stroke. *Stroke* 46 (6), 1554–1560. doi:10.1161/STROKEAHA.115.008941
- Detmer, S. A., and Chan, D. C. (2007). Functions and Dysfunctions of Mitochondrial Dynamics. *Nat. Rev. Mol. Cell Biol.* 8 (11), 870–879. doi:10.1038/nrm2275
- Díaz-Nido, J., and Avila, J. (1992). Protein Kinases Associated with Isolated Mitotic Spindles from Mammalian Cells: Identification of a Casein Kinase II-like Enzyme. *Second Messengers Phosphoproteins* 14 (1–2), 39–53.
- Embi, N., Rylatt, D. B., and Cohen, P. (1980). Glycogen Synthase Kinase-3 from Rabbit Skeletal Muscle. Separation from Cyclic-AMP-dependent Protein Kinase and Phosphorylase Kinase. *Eur. J. Biochem.* 107 (2), 519–527.
- Eom, G. H., Cho, Y. K., Ko, J.-H., Shin, S., Choe, N., Kim, Y., et al. (2011). Casein Kinase-2 α Induces Hypertrophic Response by Phosphorylation of Histone Deacetylase 2 S394 and its Activation in the Heart. *Circulation* 123 (21), 2392–2403. doi:10.1161/CIRCULATIONAHA.110.003665
- Etherton, M. R., Wu, O., Cougo, P., Giese, A.-K., Cloonan, L., Fitzpatrick, K. M., et al. (2017). Structural Integrity of Normal Appearing White Matter and Sex-specific Outcomes after Acute Ischemic Stroke. *Stroke* 48 (12), 3387–3389. doi:10.1161/STROKEAHA.117.019258
- Etherton, M. R., Wu, O., Cougo, P., Lorenzano, S., Li, H., Cloonan, L., et al. (2019). Sex-specific Differences in White Matter Microvascular Integrity after Ischaemic Stroke. *Stroke Vasc. Neurol.* 4 (4), 198–205. doi:10.1136/svn-2019-000268
- Faust, M., Jung, M., Günther, J., Zimmermann, R., and Montenarh, M. (2001). Localization of Individual Subunits of Protein Kinase CK2 to the Endoplasmic Reticulum and to the Golgi Apparatus. *Mol. Cell Biochem.* 227 (1–2), 73–80. doi:10.1007/978-1-4615-1723-8_9
- Fern, R., and Ransom, B. R. (1997). Ischemic Injury of Optic Nerve Axons: the Nuts and Bolts. *Clin. Neurosci.* 4 (5), 246–250.
- Fern, R., Ransom, B. R., and Waxman, S. G. (1995). Voltage-gated Calcium Channels in CNS White Matter: Role in Anoxic Injury. *J. Neurophysiology* 74 (1), 369–377. doi:10.1152/jn.1995.74.1.369
- Fisher, M., Feuerstein, G., Howells, D. W., Hurn, P. D., Kent, T. A., Savitz, S. I., et al. (2009). Update of the Stroke Therapy Academic Industry Roundtable Preclinical Recommendations. *Stroke* 40 (6), 2244–2250. doi:10.1161/STROKEAHA.108.541128
- Fields, R. D. (2008). White Matter in Learning, Cognition and Psychiatric Disorders. *Trends Neurosci.* 31 (7), 361–370. doi:10.1016/j.tins.2008.04.001
- Follett, P. L., Rosenberg, P. A., Volpe, J. J., and Jensen, F. E. (2000). NBQX Attenuates Excitotoxic Injury in Developing White Matter. *J. Neurosci.* 20 (24), 9235–9241. doi:10.1523/jneurosci.20-24-09235.2000
- Foster, K. G., and Fingar, D. C. (2010). Mammalian Target of Rapamycin (mTOR): Conducting the Cellular Signaling Symphony. *J. Biol. Chem.* 285 (19), 14071–14077. doi:10.1074/jbc.R109.094003
- Franchin, C., Borgo, C., Cesaro, L., Zaramella, S., Vilardell, J., Salvi, M., et al. (2018). Re-evaluation of Protein Kinase CK2 Pleiotropy: New Insights provided by a Phosphoproteomics Analysis of CK2 Knockout Cells. *Cell. Mol. Life Sci.* 75 (11), 2011–2026. doi:10.1007/s00018-017-2705-8

- Hara, N., Kikuchi, M., Miyashita, A., Hatsuta, H., Saito, Y., Kasuga, K., et al. (2017). Serum microRNA miR-501-3p as a Potential Biomarker Related to the Progression of Alzheimer's Disease. *Acta Neuropathol. Commun.* 5 (1), 10. doi:10.1186/s40478-017-0414-z
- Hase, M., Depre, C., Vatner, S. F., and Sadoshima, J. (2005). H11 Has Dose-dependent and Dual Hypertrophic and Proapoptotic Functions in Cardiac Myocytes. *Biochem. J.* 388 (Pt 2), 475–483. doi:10.1042/BJ20041314
- Hauck, L., Harms, C., An, J., Rohne, J., Gertz, K., Dietz, R., et al. (2008). Protein Kinase CK2 Links Extracellular Growth Factor Signaling with the Control of p27Kip1 Stability in the Heart. *Nat. Med.* 14 (3), 315–324. doi:10.1038/nm1729
- Hien, Y. E., Montersino, A., Castets, F., Letierrier, C., Filhol, O., Vacher, H., et al. (2014). CK2 Accumulation at the Axon Initial Segment Depends on Sodium Channel Nav1. *FEBS Lett.* 588 (18), 3403–3408. doi:10.1016/j.febslet.2014.07.032
- Hinman, J. D. (2014). The Back and Forth of Axonal Injury and Repair after Stroke. *Curr. Opin. Neurol.* 27 (6), 615–623. doi:10.1097/WCO.0000000000000149
- Hu, B.-R., Ou Yang, Y.-B., and Wieloch, T. (1993). Heat-shock Inhibits Protein Synthesis and eIF-2 Activity in Cultured Cortical Neurons. *Neurochem. Res.* 18 (9), 1003–1007. doi:10.1007/BF00966760
- Hu, B. R., and Wieloch, T. (1993). Casein Kinase II Activity in the Postischemic Rat Brain Increases in Brain Regions Resistant to Ischemia and Decreases in Vulnerable Areas. *J. Neurochem.* 60 (5), 1722–1728. doi:10.1111/j.1471-4159.1993.tb13396.x
- Huillard, E., Ziercher, L., Blond, O., Wong, M., Deloulme, J.-C., Souchelnytskyi, S., et al. (2010). Disruption of CK2 β in Embryonic Neural Stem Cells Compromises Proliferation and Oligodendrogenesis in the Mouse Telencephalon. *Mol. Cell Biol.* 30 (11), 2737–2749. doi:10.1128/MCB.01566-09
- Jahani-Asl, A., Huang, E., Irrcher, I., Rashidian, J., Ishihara, N., Lagace, D. C., et al. (2015). CDK5 Phosphorylates DRP1 and Drives Mitochondrial Defects in NMDA-Induced Neuronal Death. *Hum. Mol. Genet.* 24 (16), 4573–4583. doi:10.1093/hmg/ddv188
- Ji, Y.-F., Zhou, L., Xie, Y.-J., Xu, S.-M., Zhu, J., Teng, P., et al. (2013). Upregulation of Glutamate Transporter GLT-1 by mTOR-Akt-NF- κ B Cascade in Astrocytic Oxygen-Glucose Deprivation. *Glia* 61 (12), 1959–1975. doi:10.1002/glia.22566
- Jović, A., and Gitler, A. D. (2017). Distinct Repertoires of microRNAs Present in Mouse Astrocytes Compared to Astrocytesecreted Exosomes. *PLOS ONE* 12 (2), e0171418. doi:10.1371/journal.pone.0171418
- Ka, S.-O., Hwang, H. P., Jang, J.-H., Hyuk Bang, I., Bae, U.-J., Yu, H. C., et al. (2015). The Protein Kinase 2 Inhibitor Tetrabromobenzotriazole Protects against Renal Ischemia Reperfusion Injury. *Sci. Rep.* 5, 14816. doi:10.1038/srep14816
- Kim, G. S., Jung, J. E., Niizuma, K., and Chan, P. H. (2009). CK2 Is a Novel Negative Regulator of NADPH Oxidase and a Neuroprotectant in Mice after Cerebral Ischemia. *J. Neurosci.* 29 (47), 14779–14789. doi:10.1523/JNEUROSCI.4161-09.2009
- Klinman, E., and Holzbaur, E. L. F. (2015). Stress-Induced CDK5 Activation Disrupts Axonal Transport via Lis1/Ndel1/Dynein. *Cell Rep.* 12 (3), 462–473. doi:10.1016/j.celrep.2015.06.032
- Koh, P.-O., Cho, J.-H., Won, C.-K., Lee, H.-J., Sung, J.-H., and Kim, M.-O. (2008a). Estradiol Attenuates the Focal Cerebral Ischemic Injury through mTOR/p70S6 Kinase Signaling Pathway. *Neurosci. Lett.* 436 (1), 62–66. doi:10.1016/j.neulet.2008.02.061
- Koh, P.-O. (2010). Ginkgo Biloba Extract (EGb 761) Prevents Cerebral Ischemia-Induced p70S6 Kinase and S6 Phosphorylation. *Am. J. Chin. Med.* 38 (4), 727–734. doi:10.1142/S0192415X10008196
- Koh, S.-H., Yoo, A. R., Chang, D.-I., Hwang, S. J., and Kim, S. H. (2008b). Inhibition of GSK-3 Reduces Infarct Volume and Improves Neurobehavioral Functions. *Biochem. Biophys. Res. Commun.* 371 (4), 894–899. doi:10.1016/j.bbrc.2008.05.006
- Kristensen, L. P., Larsen, M. R., Højrup, P., Issinger, O.-G., and Guerra, B. (2004). Phosphorylation of the Regulatory β -subunit of Protein Kinase CK2 by Checkpoint Kinase Chk1: Identification of the *In Vitro* CK2 β Phosphorylation Site. *FEBS Lett.* 569 (1-3), 217–223. doi:10.1016/j.febslet.2004.05.069
- Lapierre, J.-M., Eathiraj, S., Vensel, D., Liu, Y., Bull, C. O., Cornell-Kennon, S., et al. (2016). Discovery of 3-(3-(4-(1-Aminocyclobutyl)phenyl)-5-Phenyl-3h-Imidazo[4,5-B]pyridin-2-Yl)pyridin-2-Amine (ARQ 092): An Orally Bioavailable, Selective, and Potent Allosteric AKT Inhibitor. *J. Med. Chem.* 59 (13), 6455–6469. doi:10.1021/acs.jmedchem.6b00619
- Leslie, N. R., and Downes, C. P. (2002). PTEN: The Down Side of PI 3-kinase Signalling. *Cell. Signal.* 14 (4), 285–295. doi:10.1016/s0898-6568(01)00234-0
- Li, F., Liu, W.-C., Wang, Q., Sun, Y., Wang, H., and Jin, X. (2020). NG2-glia Cell Proliferation and Differentiation by Glial Growth Factor 2 (GGF2), a Strategy to Promote Functional Recovery after Ischemic Stroke. *Biochem. Pharmacol.* 171, 113720. doi:10.1016/j.bcp.2019.113720
- Li, L.-B., Toan, S. V., Zelenia, O., Watson, D. J., Wolfe, J. H., Rothstein, J. D., et al. (2006). Regulation of Astrocytic Glutamate Transporter Expression by Akt: Evidence for a Selective Transcriptional Effect on the GLT-1/EAT2 Subtype. *J. Neurochem.* 97 (3), 759–771. doi:10.1111/j.1471-4159.2006.03743.x
- Li, S., Mealing, G. A. R., Morley, P., and Stys, P. K. (1999). Novel Injury Mechanism in Anoxia and Trauma of Spinal Cord White Matter: Glutamate Release via Reverse Na⁺-dependent Glutamate Transport. *J. Neurosci.* 19 (14), RC16. doi:10.1523/jneurosci.19-14-j0002.1999
- Lim, A. C. B., Hou, Z., Goh, C.-P., and Qi, R. Z. (2004). Protein Kinase CK2 Is an Inhibitor of the Neuronal Cdk5 Kinase. *J. Biol. Chem.* 279 (45), 46668–46673. doi:10.1074/jbc.M404760200
- Liu, X., Weaver, D., Shirihai, O., and Hajnóczky, G. (2009). Mitochondrial 'kiss-And-Run': Interplay between Mitochondrial Motility and Fusion-Fission Dynamics. *EMBO J.* 28 (20), 3074–3089. doi:10.1038/emboj.2009.255
- Lolli, G., Pinna, L. A., and Battistutta, R. (2012). Structural Determinants of Protein Kinase CK2 Regulation by Autoinhibitory Polymerization. *ACS Chem. Biol.* 7 (7), 1158–1163. doi:10.1021/cb300054n
- Lou, D. Y., Dominguez, I., Toselli, P., Landesman-Bollag, E., O'Brien, C., and Seldin, D. C. (2008). The Alpha Catalytic Subunit of Protein Kinase CK2 Is Required for Mouse Embryonic Development. *Mol. Cell Biol.* 28 (1), 131–139. doi:10.1128/MCB.01119-07
- Lugus, J. J., Ngho, G. A., Bachschmid, M. M., and Walsh, K. (2011). Mitofusins Are Required for Angiogenic Function and Modulate Different Signaling Pathways in Cultured Endothelial Cells. *J. Mol. Cell. Cardiol.* 51 (6), 885–893. doi:10.1016/j.jmcc.2011.07.023
- Martins, L. R., Lúcio, P., Melão, A., Antunes, I., Cardoso, B. A., Stansfield, R., et al. (2014). Activity of the Clinical-Stage CK2-specific Inhibitor CX-4945 against Chronic Lymphocytic Leukemia. *Leukemia* 28 (1), 179–182. doi:10.1038/leu.2013.232
- Matute, C. (2010). Calcium Dyshomeostasis in White Matter Pathology. *Cell Calcium* 47 (2), 150–157. doi:10.1016/j.ceca.2009.12.004
- Matute, C., Sánchez-Gómez, M. V., Martínez-Millán, L., and Miledi, R. (1997). Glutamate Receptor-Mediated Toxicity in Optic Nerve Oligodendrocytes. *Proc. Natl. Acad. Sci. U.S.A.* 94 (16), 8830–8835. doi:10.1073/pnas.94.16.8830
- McDonald, J. W., Levine, J. M., and Qu, Y. (1998). Multiple Classes of the Oligodendrocyte Lineage Are Highly Vulnerable to Excitotoxicity. *Neuroreport* 9 (12), 2757–2762. doi:10.1097/00001756-199808240-00014
- Meggio, F., and Pinna, L. A. (2003). One-thousand-and-one Substrates of Protein Kinase CK2? *FASEB J.* 17 (3), 349–368. doi:10.1096/fj.02-0473rev
- Meyer, D. A., Torres-Altora, M. I., Tan, Z., Tozzi, A., Di Filippo, M., DiNapoli, V., et al. (2014). Ischemic Stroke Injury Is Mediated by Aberrant Cdk5. *J. Neurosci.* 34 (24), 8259–8267. doi:10.1523/JNEUROSCI.4368-13.2014
- Micu, I., Jiang, Q., Coderre, E., Ridsdale, A., Zhang, L., Woulfe, J., et al. (2006). NMDA Receptors Mediate Calcium Accumulation in Myelin during Chemical Ischaemia. *Nature* 439 (7079), 988–992. doi:10.1038/nature04474
- Miller, M. W., Knaub, L. A., Olivera-Fragoso, L. F., Keller, A. C., Balasubramaniam, V., Watson, P. A., et al. (2013). Nitric Oxide Regulates Vascular Adaptive Mitochondrial Dynamics. *Am. J. Physiology-Heart Circulatory Physiology* 304 (12), H1624–H1633. doi:10.1152/ajpheart.00987.2012
- Morel, M., Authalet, M., Dedeker, R., and Brion, J. P. (2010). Glycogen Synthase Kinase-3 β and the P25 Activator of Cyclin Dependent Kinase 5 Increase Pausing of Mitochondria in Neurons. *Neuroscience* 167 (4), 1044–1056. doi:10.1016/j.neuroscience.2010.02.077
- Moreno, F. J., Díaz-Nido, J., Jiménez, J. S., and Avila, J. (1999). Distribution of CK2, its Substrate MAP1B and Phosphatases in Neuronal Cells. *Mol. Cell Biochem.* 191 (1-2), 201–205. doi:10.1007/978-1-4419-8624-5_24
- Nunez, S., Doroudchi, M. M., Gleichman, A. J., Ng, K. L., Llorente, I. L., Sozmen, E. G., et al. (2016). A Versatile Murine Model of Subcortical White Matter Stroke

- for the Study of Axonal Degeneration and White Matter Neurobiology. *JoVE* 109, 53404. doi:10.3791/53404
- Ouardouz, M., Nikolaeva, M. A., Coderre, E., Zamponi, G. W., McRory, J. E., Trapp, B. D., et al. (2003). Depolarization-induced Ca²⁺ Release in Ischemic Spinal Cord White Matter Involves L-type Ca²⁺ Channel Activation of Ryanodine Receptors. *Neuron* 40 (1), 53–63. doi:10.1016/j.neuron.2003.08.016
- Park, J., Choi, H., Min, J.-S., Kim, B., Lee, S.-R., Yun, J. W., et al. (2015). Loss of Mitofusin 2 Links Beta-Amyloid-Mediated Mitochondrial Fragmentation and Cdk5-Induced Oxidative Stress in Neuron Cells. *J. Neurochem.* 132 (6), 687–702. doi:10.1111/jnc.12984
- Phan, H. T., Blizzard, C. L., Reeves, M. J., Thrift, A. G., Cadilhac, D. A., Sturm, J., et al. (2018). Factors Contributing to Sex Differences in Functional Outcomes and Participation after Stroke. *Neurology* 90 (22), e1945–e1953. doi:10.1212/WNL.0000000000005602
- Pigino, G., Morfini, G., Atagi, Y., Deshpande, A., Yu, C., Jungbauer, L., et al. (2009). Disruption of Fast Axonal Transport Is a Pathogenic Mechanism for Intraneuronal Amyloid Beta. *Proc. Natl. Acad. Sci. U.S.A.* 106 (14), 5907–5912. doi:10.1073/pnas.0901229106
- Pinna, L. A., and Allende, J. E. (2009). Protein Kinase CK2 in Health and Disease. *Cell. Mol. Life Sci.* 66 (11–12), 1795–1799. doi:10.1007/s00018-009-9148-9
- Poole, A., Poore, T., Bandhakavi, S., McCann, R. O., Hanna, D. E., and Glover, C. V. C. (2005). A Global View of CK2 Function and Regulation. *Mol. Cell Biochem.* 274 (1–2), 163–170. doi:10.1007/s11010-005-2945-z
- Qaiser, F., Trembley, J. H., Kren, B. T., Wu, J.-J., Naveed, A. K., and Ahmed, K. (2014). Protein Kinase CK2 Inhibition Induces Cell Death via Early Impact on Mitochondrial Function. *J. Cell. Biochem.* 115 (12), 2103–2115. doi:10.1002/jcb.24887
- Qiu, C.-W., Liu, Z.-Y., Zhang, F.-L., Zhang, L., Li, F., Liu, S.-Y., et al. (2019). Post-Stroke Gastrodin Treatment Ameliorates Ischemic Injury and Increases Neurogenesis and Restores the Wnt/ β -Catenin Signaling in Focal Cerebral Ischemia in Mice. *Brain Res.* 1712, 7–15. doi:10.1016/j.brainres.2019.01.043
- Rosenberger, A. F. N., Morrema, T. H. J., Gerritsen, W. H., van Haastert, E. S., Snkhchyan, H., Hilhorst, R., et al. (2016). Increased Occurrence of Protein Kinase CK2 in Astrocytes in Alzheimer's Disease Pathology. *J. Neuroinflammation* 13, 4. doi:10.1186/s12974-015-0470-x
- Ryan, Q. C., Headlee, D., Acharya, M., Sparreboom, A., Trepel, J. B., Ye, J., et al. (2005). Phase I and Pharmacokinetic Study of MS-275, a Histone Deacetylase Inhibitor, in Patients with Advanced and Refractory Solid Tumors or Lymphoma. *Jco* 23 (17), 3912–3922. doi:10.1200/JCO.2005.02.188
- Saab, A. S., Tzvetavona, I. D., Trevisiol, A., Baltan, S., Dibaj, P., Kusch, K., et al. (2016). Oligodendroglial NMDA Receptors Regulate Glucose Import and Axonal Energy Metabolism. *Neuron* 91 (1), 119–132. doi:10.1016/j.neuron.2016.05.016
- Sallam, H., Jimenez, P., Song, H., Vita, M., Cedazominguez, A., and Hassan, M. (2008). Age-dependent Pharmacokinetics and Effect of Roscovitine on Cdk5 and Erk1/2 in the Rat Brain. *Pharmacol. Res.* 58 (1), 32–37. doi:10.1016/j.phrs.2008.05.010
- Sánchez-Gómez, M. V., and Matute, C. (1999). AMPA and Kainate Receptors Each Mediate Excitotoxicity in Oligodendroglial Cultures. *Neurobiol. Dis.* 6 (6), 475–485. doi:10.1006/nbdi.1999.0264
- Sarno, S., Ghisellini, P., and Pinna, L. A. (2002). Unique Activation Mechanism of Protein Kinase CK2. *J. Biol. Chem.* 277 (25), 22509–22514. doi:10.1074/jbc.M200486200
- Sea Lee, J., Han, M.-K., Hyun Kim, S., Kwon, O.-K., and Hyoung Kim, J. (2005). “Fiber Tracking by Diffusion Tensor Imaging in Corticospinal Tract Stroke: Topographical Correlation with Clinical Symptoms,” in *NeuroImage*. doi:10.1016/j.neuroimage.2005.02.036
- Serrano, L., Hernández, M. A., Díaz-Nido, J., and Avila, J. (1989). Association of Casein Kinase II with Microtubules. *Exp. Cell Res.* 181 (1), 263–272. doi:10.1016/0014-4827(89)90200-0
- Shaw, J., and Kirshenbaum, L. A. (2006). Prime Time for JNK-Mediated Akt Reactivation in Hypoxia-Reoxygenation. *Circulation Res.* 98 (1), 7–9. doi:10.1161/01.RES.0000200397.22663.b6
- Shea, T. B., Zheng, Y.-L., Ortiz, D., and Pant, H. C. (2004). Cyclin-dependent Kinase 5 Increases Perikaryal Neurofilament Phosphorylation and Inhibits Neurofilament Axonal Transport in Response to Oxidative Stress. *J. Neurosci. Res.* 76 (6), 795–800. doi:10.1002/jnr.20099
- Siddiqui-Jain, A., Drygin, D., Streiner, N., Chua, P., Pierre, F., O'Brien, S. E., et al. (2010). CX-4945, an Orally Bioavailable Selective Inhibitor of Protein Kinase CK2, Inhibits Prosurvival and Angiogenic Signaling and Exhibits Antitumor Efficacy. *Cancer Res.* 70 (24), 10288–10298. doi:10.1158/0008-5472.CAN-10-1893
- Silva, A., Jotta, P. Y., Silveira, A. B., Ribeiro, D., Brandalise, S. R., Yunes, J. A., et al. (2010). Regulation of PTEN by CK2 and Notch1 in Primary T-Cell Acute Lymphoblastic Leukemia: Rationale for Combined Use of CK2- and -secretase Inhibitors. *Haematologica* 95 (4), 674–678. doi:10.3324/haematol.2009.011999
- Silva, A., Yunes, J. A., Cardoso, B. A., Martins, L. R., Jotta, P. Y., Abecasis, M., et al. (2008). PTEN Posttranslational Inactivation and Hyperactivation of the PI3K/Akt Pathway Sustain Primary T Cell Leukemia Viability. *J. Clin. Invest.* 118 (11), 3762–3774. doi:10.1172/JCI34616
- Skeen, J. E., Bhaskar, P. T., Chen, C.-C., Chen, W. S., Peng, X.-d., Nogueira, V., et al. (2006). Akt Deficiency Impairs Normal Cell Proliferation and Suppresses Oncogenesis in a P53-independent and mTORC1-dependent Manner. *Cancer Cell* 10 (4), 269–280. doi:10.1016/j.ccr.2006.08.022
- Sofer, A., Lei, K., Johannessen, C. M., and Ellisen, L. W. (2005). Regulation of mTOR and Cell Growth in Response to Energy Stress by REDD1. *Mol. Cell Biol.* 25 (14), 5834–5845. doi:10.1128/MCB.25.14.5834-5845.2005
- Son, Y. H., Song, J. S., Kim, S. H., and Kim, J. (2013). Pharmacokinetic Characterization of CK2 Inhibitor CX-4945. *Arch. Pharm. Res.* 36 (7), 840–845. doi:10.1007/s12272-013-0103-9
- Srinivasan, S., Spear, J., Chandran, K., Joseph, J., Kalyanaraman, B., and Avadhani, N. G. (2013). Oxidative Stress Induced Mitochondrial Protein Kinase A Mediates Cytochrome C Oxidase Dysfunction. *PLoS One* 8 (10), e77129. doi:10.1371/journal.pone.0077129
- Sripada, L., Tomar, D., and Singh, R. (2012). Mitochondria: One of the Destinations of miRNAs. *Mitochondrion* 12 (6), 593–599. doi:10.1016/j.mito.2012.10.009
- Stahon, K. E., Bastian, C., Griffith, S., Kidd, G. J., Brunet, S., and Baltan, S. (2016). Age-Related Changes in Axonal and Mitochondrial Ultrastructure and Function in White Matter. *J. Neurosci.* 36 (39), 9990–10001. doi:10.1523/jneurosci.1316-16.2016
- Stys, P. K., Ransom, B. R., Waxman, S. G., and Davis, P. K. (1990). Role of Extracellular Calcium in Anoxic Injury of Mammalian Central White Matter. *Proc. Natl. Acad. Sci. U.S.A.* 87 (11), 4212–4216. doi:10.1073/pnas.87.11.4212
- Stys, P. (2004). White Matter Injury Mechanisms. *Cmm* 4 (2), 113–130. doi:10.2174/1566524043479220
- Sun, K.-H., de Pablo, Y., Vincent, F., and Shah, K. (2008). Deregulated Cdk5 Promotes Oxidative Stress and Mitochondrial Dysfunction. *J. Neurochem.* 107 (1), 265–278. doi:10.1111/j.1471-4159.2008.05616.x
- Tekkök, S. B., and Goldberg, M. P. (2001). AMPA/Kainate Receptor Activation Mediates Hypoxic Oligodendrocyte Death and Axonal Injury in Cerebral White Matter. *J. Neurosci.* 21 (12), 4237–4248. doi:10.1523/jneurosci.21-12-04237.2001
- Tekkök, S. B., Ye, Z., and Ransom, B. R. (2007). Excitotoxic Mechanisms of Ischemic Injury in Myelinated White Matter. *J. Cereb. Blood Flow. Metab.* 27 (9), 1540–1552. doi:10.1038/sj.jcbfm.9600455
- Twig, G., Liu, X., Liesa, M., Wikstrom, J. D., Molina, A. J. A., Las, G., et al. (2010). Biophysical Properties of Mitochondrial Fusion Events in Pancreatic β -cells and Cardiac Cells Unravel Potential Control Mechanisms of its Selectivity. *Am. J. Physiology-Cell Physiology* 299 (2), C477–C487. doi:10.1152/ajpcell.00427.2009
- Underhill, S. M., and Goldberg, M. P. (2007). Hypoxic Injury of Isolated Axons Is Independent of Ionotropic Glutamate Receptors. *Neurobiol. Dis.* 25 (2), 284–290. doi:10.1016/j.nbd.2006.09.011
- Valerio, A., Bertolotti, P., Delbarba, A., Perego, C., Dossena, M., Ragni, M., et al. (2011). Glycogen Synthase Kinase-3 Inhibition Reduces Ischemic Cerebral Damage, Restores Impaired Mitochondrial Biogenesis and Prevents ROS Production. *J. Neurochem.* 116 (6), 1148–1159. doi:10.1111/j.1471-4159.2011.07171.x
- Vilk, G., Weber, J. E., Turowec, J. P., Duncan, J. S., Wu, C., Derksen, D. R., et al. (2008). Protein Kinase CK2 Catalyzes Tyrosine Phosphorylation in Mammalian Cells. *Cell. Signal.* 20 (11), 1942–1951. doi:10.1016/j.cellsig.2008.07.002
- Vita, M., Abdel-Rehim, M., Olofsson, S., Hassan, Z., Meurling, L., Siden, Å., et al. (2005). Tissue Distribution, Pharmacokinetics and Identification of Roscovitine Metabolites in Rat. *Eur. J. Pharm. Sci.* 25 (1), 91–103. doi:10.1016/j.ejps.2005.02.001

- Vocoli, V., Tonazzini, I., Signore, G., Caleo, M., and Cecchini, M. (2014). Role of Extracellular Calcium and Mitochondrial Oxygen Species in Psychosine-Induced Oligodendrocyte Cell Death. *Cell Death Dis.* 5, e1529. doi:10.1038/cddis.2014.483
- Wolf, J. A., Stys, P. K., Lusardi, T., Meaney, D., and Smith, D. H. (2001). Traumatic Axonal Injury Induces Calcium Influx Modulated by Tetrodotoxin-Sensitive Sodium Channels. *J. Neurosci.* 21 (6), 1923–1930. doi:10.1523/jneurosci.21-06-01923.2001
- Wrathall, J. R., Choiniere, D., and Teng, Y. D. (1994). Dose-dependent Reduction of Tissue Loss and Functional Impairment after Spinal Cord Trauma with the AMPA/kainate Antagonist NBQX. *J. Neurosci.* 14 (11 Pt 1), 6598–6607. doi:10.1523/jneurosci.14-11-06598.1994
- Xu, Z., and Ford, B. D. (2005). Upregulation of erbB Receptors in Rat Brain after Middle Cerebral Arterial Occlusion. *Neurosci. Lett.* 375 (3), 181–186. doi:10.1016/j.neulet.2004.11.039
- Yamada, K., Mori, S., Nakamura, H., Ito, H., Kizu, O., Shiga, K., et al. (2003). Fiber-Tracking Method Reveals Sensorimotor Pathway Involvement in Stroke Patients. *Stroke* 34 (9), E159–E162. doi:10.1161/01.str.0000085827.54986.89
- Yang, Y., Wang, H., Zhang, J., Luo, F., Herrup, K., Bibb, J. A., et al. (2013). Cyclin Dependent Kinase 5 Is Required for the Normal Development of Oligodendrocytes and Myelin Formation. *Dev. Biol.* 378 (2), 94–106. doi:10.1016/j.ydbio.2013.03.023
- Yoshimura, T., and Rasband, M. N. (2014). Axon Initial Segments: Diverse and Dynamic Neuronal Compartments. *Curr. Opin. Neurobiol.* 27, 96–102. doi:10.1016/j.conb.2014.03.004
- Yu, Y., Savage, R. E., Eathiraj, S., Meade, J., Wick, M. J., Hall, T., et al. (2015). Targeting AKT1-E17k and the PI3K/AKT Pathway with an Allosteric AKT Inhibitor, ARQ 092. *PLoS One* 10 (10), e0140479. doi:10.1371/journal.pone.0140479
- Yu, Z., Cheng, C., Liu, Y., Liu, N., Lo, E. H., and Wang, X. (2018). Neuroglobin Promotes Neurogenesis through Wnt Signaling Pathway. *Cell Death Dis.* 9 (10), 945. doi:10.1038/s41419-018-1007-x
- Zhang, K., and Sejnowski, T. J. (2000). A Universal Scaling Law between Gray Matter and White Matter of Cerebral Cortex. *Proc. Natl. Acad. Sci. U.S.A.* 97 (10), 5621–5626. doi:10.1073/pnas.090504197
- Zhang, X., Shi, M., Bjoras, M., Wang, W., Zhang, G., Han, J., et al. (2013). Ginsenoside Rd Promotes Glutamate Clearance by Up-Regulating Glial Glutamate Transporter GLT-1 via PI3K/AKT and ERK1/2 Pathways. *Front. Pharmacol.* 4, 152. doi:10.3389/fphar.2013.00152
- Zheng, Y., McFarland, B. C., Drygin, D., Yu, H., Bellis, S. L., Kim, H., et al. (2013). Targeting Protein Kinase CK2 Suppresses Prosurvival Signaling Pathways and Growth of Glioblastoma. *Clin. Cancer Res.* 19 (23), 6484–6494. doi:10.1158/1078-0432.CCR-13-0265
- Zhong, B., Campagne, O., Salloum, R., Purzner, T., and Stewart, C. F. (2020). LC-MS/MS Method for Quantitation of the CK2 Inhibitor Silmitasertib (CX-4945) in Human Plasma, CSF, and Brain Tissue, and Application to a Clinical Pharmacokinetic Study in Children with Brain Tumors. *J. Chromatogr. B* 1152, 122254. doi:10.1016/j.jchromb.2020.122254

Conflict of Interest: The authors declare that the research was conducted in the absence of any commercial or financial relationships that could be construed as a potential conflict of interest.

Publisher’s Note: All claims expressed in this article are solely those of the authors and do not necessarily represent those of their affiliated organizations, or those of the publisher, the editors and the reviewers. Any product that may be evaluated in this article, or claim that may be made by its manufacturer, is not guaranteed or endorsed by the publisher.

Copyright © 2022 Nguyen, Zhu and Baltan. This is an open-access article distributed under the terms of the Creative Commons Attribution License (CC BY). The use, distribution or reproduction in other forums is permitted, provided the original author(s) and the copyright owner(s) are credited and that the original publication in this journal is cited, in accordance with accepted academic practice. No use, distribution or reproduction is permitted which does not comply with these terms.



OPEN ACCESS

EDITED BY
Andrea Venerando,
University of Padua, Italy

REVIEWED BY
Varsha Gandhi,
University of Texas MD Anderson
Cancer Center, United States
Richard Eric Davis,
University of Texas MD Anderson
Cancer Center, United States

*CORRESPONDENCE
Sabrina Manni,
sabrina.manni@unipd.it
Francesco Piazza,
francesco.piazza@unipd.it

SPECIALTY SECTION
This article was submitted to Cellular
Biochemistry,
a section of the journal
Frontiers in Cell and Developmental
Biology

RECEIVED 03 May 2022
ACCEPTED 30 June 2022
PUBLISHED 11 August 2022

CITATION
Manni S, Pesavento M, Spinello Z,
Saggin L, Arjomand A, Fregnani A,
Quotti Tubi L, Scapinello G, Gurrieri C,
Semenzato G, Trentin L and Piazza F
(2022), Protein Kinase CK2 represents a
new target to boost Ibrutinib and
Venetoclax induced cytotoxicity in
mantle cell lymphoma.
Front. Cell Dev. Biol. 10:935023.
doi: 10.3389/fcell.2022.935023

COPYRIGHT
© 2022 Manni, Pesavento, Spinello,
Saggin, Arjomand, Fregnani, Quotti
Tubi, Scapinello, Gurrieri, Semenzato,
Trentin and Piazza. This is an open-
access article distributed under the
terms of the [Creative Commons
Attribution License \(CC BY\)](#). The use,
distribution or reproduction in other
forums is permitted, provided the
original author(s) and the copyright
owner(s) are credited and that the
original publication in this journal is
cited, in accordance with accepted
academic practice. No use, distribution
or reproduction is permitted which does
not comply with these terms.

Protein Kinase CK2 represents a new target to boost Ibrutinib and Venetoclax induced cytotoxicity in mantle cell lymphoma

Sabrina Manni^{1,2*}, Maria Pesavento^{1,2}, Zaira Spinello^{1,2},
Lara Saggin^{1,2}, Arash Arjomand^{1,2}, Anna Fregnani^{1,2},
Laura Quotti Tubi^{1,2}, Greta Scapinello^{1,2}, Carmela Gurrieri^{1,2},
Gianpietro Semenzato^{1,2}, Livio Trentin^{1,2} and
Francesco Piazza^{1,2*}

¹Department of Medicine-DIMED, Hematology and Clinical Immunology Section, University of Padova, Padova, Italy, ²Myeloma and Lymphoma Pathobiology Lab, Veneto Institute of Molecular Medicine, Padova, Italy

Mantle cell lymphoma (MCL) is an incurable B cell non-Hodgkin lymphoma, characterized by frequent relapses. In the last decade, the pro-survival pathways related to BCR signaling and Bcl-2 have been considered rational therapeutic targets in B cell derived lymphomas. The BTK inhibitor Ibrutinib and the Bcl-2 inhibitor Venetoclax are emerging as effective drugs for MCL. However, primary and acquired resistance also to these agents may occur. Protein Kinase CK2 is a S/T kinase overexpressed in many solid and blood-derived tumours. CK2 promotes cancer cell growth and clonal expansion, sustaining pivotal survival signaling cascades, such as the ones dependent on AKT, NF- κ B, STAT3 and others, counteracting apoptosis through a “non-oncogene” addiction mechanism. We previously showed that CK2 is overexpressed in MCL and regulates the levels of activating phosphorylation on S529 of the NF- κ B family member p65/RelA. In the present study, we investigated the effects of CK2 inactivation on MCL cell proliferation, survival and apoptosis and this kinase’s involvement in the BCR and Bcl-2 related signaling. By employing CK2 loss of function MCL cell models, we demonstrated that CK2 sustains BCR signaling (such as BTK, NF- κ B and AKT) and the Bcl-2-related Mcl-1 expression. CK2 inactivation enhanced Ibrutinib and Venetoclax-induced cytotoxicity. The demonstration of a CK2-dependent upregulation of pathways that may antagonize the effect of these drugs may offer a novel strategy to overcome primary and secondary resistance.

KEYWORDS

mantle cell lymphoma, CK2, ibrutinib, venetoclax, target therapy

Introduction

Mantle cell lymphoma (MCL) accounts for about 3–10% of all B-cell non-Hodgkin lymphomas (NHL) and is characterized by the propensity to frequent relapses and poor prognosis (Jain and Wang, 2022).

B-Cell Receptor (BCR)-linked survival signaling cascades, such as Phosphatidylinositol 3-Kinases/AKT (PI3K/AKT), mammalian Target Of Rapamycin (mTOR), Nuclear Factor kappa-light-chain-enhancer of activated B cells (NF- κ B), the Extracellular signal-Regulated Kinase (ERK) cascades and the Bcl-2 family of apoptosis regulators, are chronic active in MCL and enhance tumor proliferation, facilitating evasion of apoptosis. BCR signaling is essential for the development and function of B lymphocytes and is a key molecule for the growth of many B-NHL. In the last decade, the pro-survival pathways relying on BCR signaling and Bcl-2 family proteins have emerged as rational therapeutic targets. Chemical inhibitors directed against BCR signaling kinases, such as Ibrutinib and Acalabrutinib (BTK) and Idelalisib and Duvelisib (PI3K), have been successfully used in the therapy of B cell malignancies (Profitós-Pelejà et al., 2022). Ibrutinib is the first-in-class Bruton Tyrosine Kinase (BTK) inhibitor which acts switching off BTK-dependent BCR signaling and is currently approved for relapsed/refractory (R/R) MCL. Venetoclax is a first-in class selective Bcl-2 inhibitor with demonstrated clinical activity in MCL, in particular in combination with Ibrutinib (Davids et al., 2017; Tam et al., 2018). However, primary and acquired resistance to Ibrutinib, mainly due to BTK C481 or PLC γ mutations (Hershkovitz-Rokah et al., 2018), and to Venetoclax, mainly due to upregulation of other pro-survival Bcl-2 family members, may occur (Huang et al., 2022; Jain and Wang, 2022). Therefore, even with the introduction of these novel drugs, the development of refractoriness and resistance is still the main unsolved clinical-biological issue.

CK2 is a S/T kinase, composed by a tetramer of two catalytic CK2 α (most represented) or CK2 α' and two regulatory CK2 β subunits. CK2 promotes cancer cell proliferation and tumor progression by antagonizing extrinsic and intrinsic apoptosis in a “non-oncogene” addiction fashion (Mandato et al., 2016; Spinello et al., 2021). CK2 also regulates cellular processes central for cancer biology (p53, Wnt/ β -catenin, AKT and NF- κ B survival signaling pathways) (Spinello et al., 2021). CK2 phosphorylates BH3-Interacting Domain Death Agonist (BID) on T58, preventing its cleavage from caspase 8, protecting from apoptosis (Hellwig et al., 2010). By sustaining AKT function (Di Maira et al., 2009), CK2 contributes to BAD inactivation. CK2 also phosphorylates Apoptosis Repressor with Caspase recruitment domain (ARC) at T149 critically supporting caspase inhibition (Li et al., 2002). Lastly, being the CK2 recognition motif strikingly similar to that of caspases, the CK2-dependent phosphorylation of caspases substrates protects them from the proteolytic cleavage (Duncan et al.,

2011). We previously showed that CK2 sustains tumor progression in multiple myeloma (MM), NHL, leukemias and other haematological malignancies, being CK2 overexpressed in B cell derived tumors such as MM and MCL (Manni et al., 2013), follicular lymphoma and diffuse large B cell lymphoma (DLBCL) (Pizzi et al., 2015). Moreover CK2 regulates the levels of pro-survival activating p65 NF- κ B S529 and STAT3 S727 phosphorylations in MCL (Manni et al., 2013). More recently, we demonstrated that CK2 regulates BCR signaling in DLBCL cells since its inhibition is associated to impairment of Ca²⁺ mobilization and of phosphorylation of NF- κ B and AKT (Pizzi et al., 2015; Mandato et al., 2018). Phosphorylated AKT on S129 (Di Maira et al., 2009) and p65 NF- κ B on S529 (Wang et al., 2000) are direct CK2 targets important for the activity of these two BCR-activated pro-survival molecules. Different CK2 inhibitors have been developed, and the ATP competitive, clinical-grade CK2 inhibitor CX-4945 (Silmitasertib) (Siddiqui-Jain et al., 2010) is already used in Phase I/II clinical trial in solid tumors and R/R MM (ClinicalTrials.gov Identifier NCT01199718), and very recently in Phase II clinical trial for severe coronavirus disease 2019 -COVID 19- (ClinicalTrials.gov Identifier: NCT04668209).

Given the key role of CK2 in signaling pathways that could sustain active BCR and Bcl-2 family related cascades in MCL, we investigated this kinase's involvement in the BCR signaling and the effects of its inactivation on MCL cell proliferation and survival. We also evaluated if CK2 inactivation could enhance Ibrutinib and Venetoclax-induced cytotoxicity offering a potential strategy to overcome primary and secondary resistance to these drugs.

Materials and methods

Patients and cell cultures. Jeko-1, Rec-1, Granta-519 MCL cell lines, and primary MCL B cells were isolated and cultured as previously described (Manni et al., 2021). Human derived B cells were obtained after achieving informed consent according to the declaration of Helsinki and upon approval by the Ethic Committee of the Padova University Hospital Internal Institutional Board (protocol # 4,089/AO/17).

Chemicals. Ibrutinib, Venetoclax, Bortezomib and Z-VAD-FMK were from Selleck chemicals (United States); IPTG was from MERCK (Italy); CX-4945 was from Activate Scientific (Germany).

Evaluation of apoptosis. Apoptosis was assessed by Annexin V/Propidium Iodide (PI) staining (IMMUNOSTEP, Spain) and FACS analysis performed as in (Manni et al., 2017).

Cell cycle analysis. It was performed as described in (Manni et al., 2017).

Assessment of drug concentration-effect and calculation of the combination index (CI). Jeko-1, Rec-1 and Granta-519 cells

were plated into 96 well plates in 100 μ L of medium. CX-4945, Ibrutinib, and Venetoclax were added at different concentrations for 72 h alone or in combination. Cell viability was analyzed with 3-(4,5-dimethylthiazol-2-yl)-2,5-diphenyltetrazolium bromide (MTT) assay and the CI was calculated as performed in (Manni et al., 2012).

Western blot (WB). WB was performed as described in (Piazza et al., 2010). Antibodies used were: CK2 α , CK2 β , S129 AKT (abcam, United Kingdom), Mcl-1, S473 AKT, Y223 BTK, total BTK, PARP, S536 p65 NF- κ B (Cell signaling Technology, MA, United States); S529 p65 NF- κ B (Santa Cruz Biotechnology, Inc.; Italy), GAPDH (Millipore, Italy), β -actin (Sigma-Aldrich, Italy); Caspase 3 (Enzo Life Science, United Kingdom). Images were acquired using the Image Quant LAS 500 chemiluminescence detection system (GE Healthcare, United States) and densitometry of the bands was performed using the ImageQuantTL software.

RNA interference. We generated inducible CK2 α or CK2 β directed shRNA IPTG inducible MCL cell clones performing shRNA lentiviral transduction. Jeko-1 cells were transduced with the IPTG inducible lentiviral particles carrying CSNK2A1-specific shRNA (pLKO_IPTG_3XLacO, Sigma-Aldrich, Italy) with the sequence code TRCN0000320858 or CSNK2B directed shRNA (sequence code TRCN000003796). For cell transduction 2×10^4 cells were infected with a multiplicity of infection of 10, using the spinfection method (45 min, 1,000 rpm at 32°C), in the presence of 8 μ g/ml polybrene (Sigma-Aldrich, Italy). Puromycin selection (1 μ g/ml) was initiated 2 days after transduction. To induce CK2 α or CK2 β silencing, cells were incubated with IPTG 500 μ M every 2 days for a total of 6 days of silencing, time lapse in which the best knockdown efficacy was obtained.

CK2 α silencing *in vivo* in a human MCL xenograft murine model. NOD SCID mice were purchased from Envigo. All animal studies were conducted according to protocol # 160/2017 PR, approved by the Italian Ministry of Health. 3×10^6 CK2 α shRNA Jeko-1 and Jeko-1 WT cells were injected subcutaneously in 100 μ L of a mix of RPMI: matrigel matrix 10 mg/ml (Corning, United States, cat number 354263) (1:1 ratio) on the right and on the left flank respectively of NOD SCID mice. Once the tumor reached a measurable size (around 0.245 cm³, approximately after 10 days of injection), mice were divided into two groups (control/untreated and IPTG treated). Four mice for each condition were used. IPTG was administered at the concentration of 20 mM intraperitoneally (IP) (in 200 μ L of physiological solution 0.9% NaCl every other day) and at 4 mM in drinking water (refreshing it twice a week) for 25 days. Control mice were injected IP with 200 μ L physiological solution 0.9% NaCl every other day. Tumors were then dissected, weighed, and cut into pieces for protein analysis as per standard protocols.

Mitochondrial membrane potential (MMP) measurement. The MMP was measured by JC-10 dye (Sigma Aldrich, # number MAK160) staining. JC-10 forms reversible red-fluorescent

aggregates ($\lambda_{ex} = 540/\lambda_{em} = 590$ nm) in healthy mitochondria of cells. MMP reduction during apoptosis caused a failure to maintain JC-10 in the mitochondria and an increase of its monomeric, green, fluorescent form ($\lambda_{ex} = 490/\lambda_{em} = 525$ nm). Cells were stained following the manufacturer's instructions and analysed using flow cytometry (FACS Canto II Cell Cytometer and FACS Diva Software, BD-Beckton-Dickinson, Italy).

Quantitative real-time PCR. Performed as in (Manni et al., 2021) using the QuantStudio five detection system (Applied Biosystem, CA, United States) with the QuantStudioTM Design and Analysis Software v.1.4.3. The primers used are the following:

Bcl-2 Forward 5'-3' TGTGGATGACTGAGTACCTGAACC and Reverse 5'-3' AAAGGCATCCCAGCCTCC; BCL2L1 (BCL-XL) Forward 5'-3' GCAGGTATTGGTGAATCGGATCGC and Reverse 5'-3' CACAAAAGTATCCCAGCCGCC; CSNK2A1 Forward 5'-3' TCATGAGCACAGAAAGCTACGA and Reverse 5'-3' AATGGCTCCTTCCGAAAGATC; IL-6 Forward 5'-3' GGCAGTGGCAGAAAACAACCTG and Reverse 5'-3' TCACCAGGCAAGTCTCCTCATTGAAT; Mcl-1 Forward 5'-3' GAAAGTATCACAGACGTTCTCGTAAGG and Reverse 5'-3' AACCCATCCCAGCCTCTTTG.

GAPDH Forward 5'-3' AATGGAAATCCCATCACCATCT and Reverse 5'-3' CGCCCCACTTGATTTTGG.

Statistical analysis. Data were analyzed for statistical significance with the two-tail unpaired Student's *t* test or ANOVA analysis of variance with *post-hoc* corrections and statistical significance was considered with *p* values below 0.05.

Results

CK2 α sustains MCL cell survival through the activation of active BCR-linked survival signaling

To specifically assess the contribution of each CK2 subunit to MCL cell growth we generated Jeko-1 MCL cells stably transduced with lentiviral vectors, expressing a shRNA against CK2 α or CK2 β in an Isopropyl-b-D-1-thiogalattopyranoside (IPTG)-inducible manner. Upon 6 days of IPTG treatment, we confirmed efficient CK2 α or CK2 β protein silencing (Figure 1A). No off-target effects of IPTG *per se* were seen, as CK2 α/β protein levels remained unchanged in IPTG-treated Jeko-1 wild-type (WT) cells. Remarkably, Annexin V (AV) and Propidium Iodide (PI) labelling and FACS analysis revealed a substantial induction of apoptosis in CK2 α but not CK2 β -silenced cells, which was confirmed by the reduction of the anti-apoptotic Mcl-1 and Pro-caspase 3 proteins (Figure 1A and Supplementary Figure S1). As control, to exclude IPTG off-target induced toxicity, we treated Jeko-1 WT cells with IPTG for the same amount of time. As

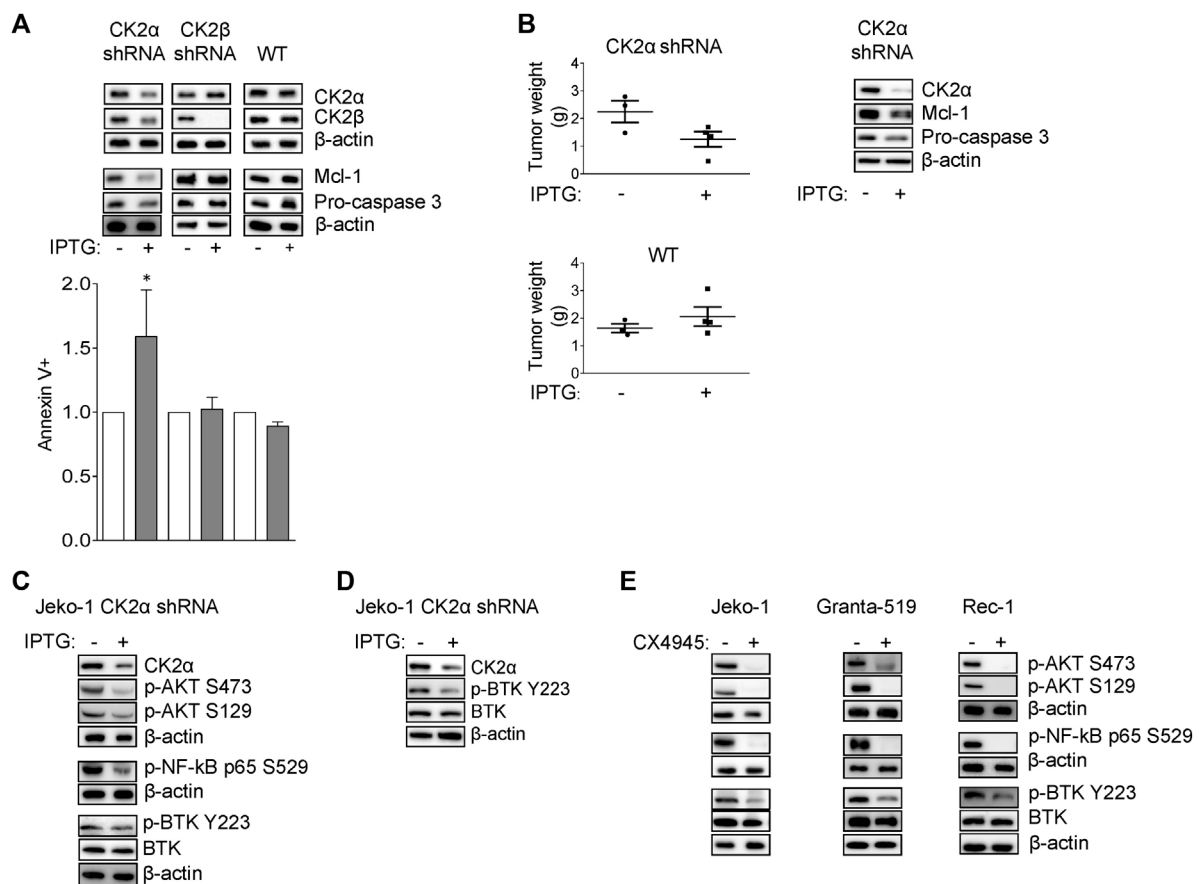


FIGURE 1

CK2α sustains MCL cell growth and survival signaling pathways downstream the BCR. **(A)** Representative WB (upper panel) of CK2α, CK2β, Mcl-1 and Pro-caspase 3 expression and histogram showing the percentage of Annexin V positive Jeko-1 CK2α shRNA, Jeko-1 CK2β shRNA and Jeko-1 WT cells (lower panel) after 6 days treatment with IPTG 500 μM. β-actin was used as loading control. Data are expressed as ratio over untreated cells, mean ± SD of $n = 8$ (Jeko-1 CK2α and CK2β shRNA) and $n = 4$ (Jeko-1 WT) independent experiments. * indicates $p < 0.05$ compared to untreated cells. **(B)** Tumor weight (grams, left panel) of Jeko-1 CK2α shRNA and Jeko-1 WT cells xenografted in NOD SCID mice and treated *in vivo* with IPTG for 25 days. Data are expressed as mean ± SD. The number of mice is indicated by the symbols. Representative WB (right panel) showing *in vivo* CK2α knock down efficacy and Mcl-1 and Pro-caspase3 reduction. β-actin was used as loading control. **(C)** Representative WB of NF-κB, PI3K/AKT and BTK dependent signaling in Jeko-1 CK2α shRNA cells after 6 days induction with IPTG 500 μM. **(D)** Representative WB showing the expression levels of phosphorylated BTK on Y223 (p-BTK Y223) *in vivo* in Jeko-1 CK2α shRNA cells xenografted, and treated with IPTG as in **(B)**. **(E)** Representative WB of NF-κB, PI3K/AKT and BTK dependent signaling in MCL cell lines Jeko-1, Granta-519 and Rec-1 after 24 h treatment with DMSO (not higher than 0.1% v/v) or CX-4945 (2.5 μM for Jeko-1 and Granta-519; 0.5 μM for Rec-1). β-actin was used as loading control. Experiments were repeated at least three times for each cell line.

expected, IPTG-treated WT cells remained viable and did not show any difference in the expression level of Mcl-1 and Pro-caspase 3 proteins, confirming the efficacy/specificity of the silencing strategy (Figure 1A and Supplementary Figure S1). We next performed *in vivo* xenotransplant experiments by implanting CK2α shRNA Jeko-1 cells in the flank of NOD-SCID mice and treating them with intraperitoneal IPTG for as long as 25 days. CK2α silencing *in vivo* was efficient (Figure 1B and Supplementary Figure S1) and associated to a trend towards a reduction in the weight of tumors, which displayed a drop in the expression of Mcl-1 and Pro-caspase 3 anti-apoptotic proteins. As a control, Jeko-1 WT cells grew to the same extent in IPTG-treated or untreated mice (Figure 1B). Next,

we analysed CK2α contribution in the regulation of pro-survival signaling pathways downstream from the BCR. First, we evaluated the expression levels of key molecules involved in the NF-κB, PI3K/AKT and BTK signaling in cultured Jeko-1 CK2α shRNA cell line. A reduction of the activating phosphorylation levels of p65/RelA on S529 (Figure 1C and Supplementary Figure S1) and consequently of the mRNA expression level of the NF-κB targets *BCL2L1* (which encodes for the BCL-XL protein), *Bcl-2* and *IL-6* (Supplementary Figure S2), and of AKT on S129 and S473 was seen in CK2α-silenced cells (Figure 1C and Supplementary Figure S1). Intriguingly, we also observed a reduction in the levels of phosphorylated BTK on Y223 in cultured cells (Figure 1C and Supplementary Figure S1)

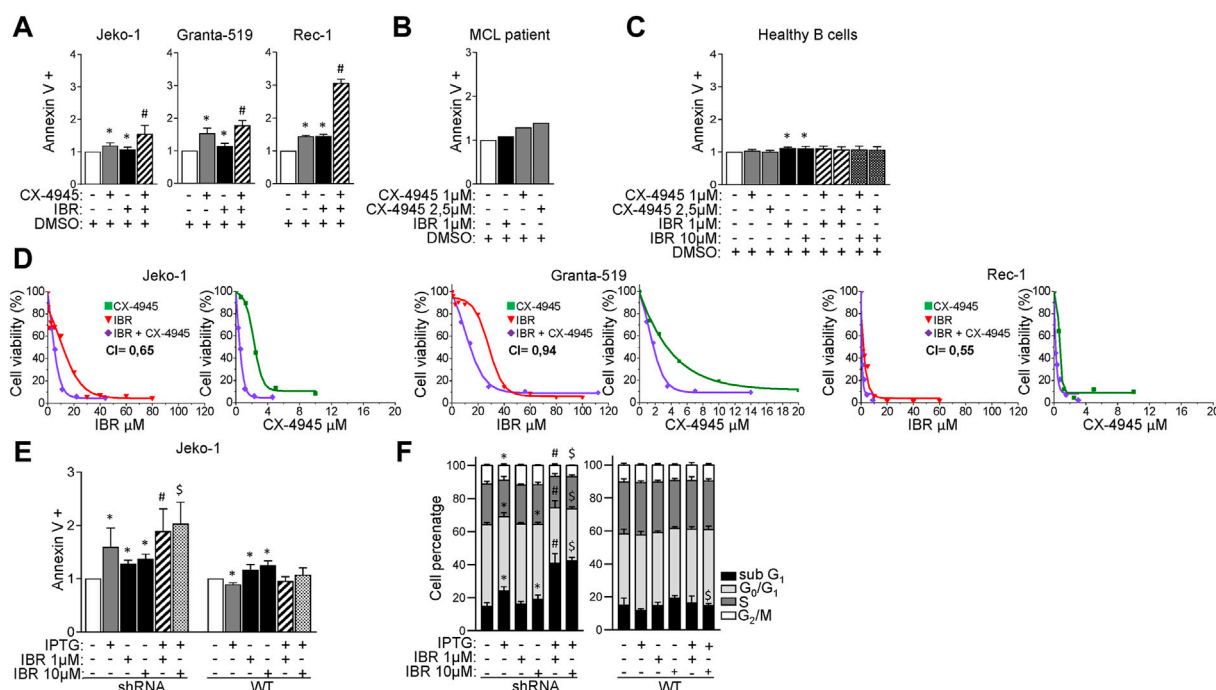


FIGURE 2

CK2α inhibition boosts Ibrutinib induced cytotoxicity. **(A)** Histograms showing the percentage of Annexin V positive Jeko-1, Granta-519 and Rec-1 cells after 24 h treatment with DMSO (not higher than 0.1% v/v; white column), CX-4945 (1 μM for Jeko-1 and Rec-1, 2.5 μM for Granta-519; grey columns), IBR (1 μM for each cell line; black columns) or their combination (striped columns). Data are expressed as ratio over DMSO treated cells, mean \pm SD of $n = 6$ (Jeko-1), $n = 5$ (Granta-519) and $n = 3$ (Rec-1) independent experiments. * indicates $p < 0.05$ compared to DMSO; # indicates $p < 0.05$ compared to both CX-4945 and IBR only treated cells. **(B)** Histogram showing the percentage of AV positive B cells derived from one Ibrutinib resistant MCL patient after 24 h treatment with DMSO (not higher than 0.1% v/v; white column), Ibrutinib (1 μM; black column), CX-4945 (1 μM and 2.5 μM; grey columns). Data are expressed as ratio over DMSO treated cells. **(C)** Histogram depicting the percentage of Annexin V positive healthy B cells after 24 h treatment with DMSO (not higher than 0.1% v/v; white column), CX-4945 (1 μM and 2.5 μM; grey columns), IBR (1 and 10 μM; black columns) or their combination (striped and dotted columns). Data are expressed as ratio over DMSO treated cells, mean \pm SD of $n = 3$ independent experiments. * indicates $p < 0.05$ compared to DMSO. **(D)** Dose response curves of Jeko-1, Granta-519 and Rec-1 cells incubated for 72 h with increasing concentrations of CX-4945 (green curves), Ibrutinib (red curves) or their combination (purple curves). Cell viability was assessed by MTT test. For Jeko-1, IC₅₀ of the single treatments were 2.3 μM for CX-4945 and 11 μM for IBR. IC₅₀ for CX-4945 used in combination with IBR was 0.5 μM, while IC₅₀ for IBR used in association with CX-4945 was 4.9 μM. The calculated CI was 0.65. For Granta-519, IC₅₀ of the single treatments were 3.5 μM for CX-4945 and 28 μM for IBR. IC₅₀ for CX-4945 used in combination with IBR was 1.67 μM, while IC₅₀ for IBR used in association with CX-4945 was 13.2 μM. The calculated CI was 0.94. For Rec-1, IC₅₀ of the single treatments were 0.76 μM for CX-4945 and 2.26 μM for IBR. IC₅₀ for CX-4945 used in combination with IBR was 0.21 μM, while IC₅₀ for IBR used in association with CX-4945 was 0.63 μM. The calculated CI was 0.55. Data are presented as averaged percentage over control of three independent experiments for each cell line. **(E)** Histogram showing the percentage of Annexin V positive Jeko-1 CK2α shRNA and Jeko-1 WT cells after 6 days induction with IPTG 500 μM (grey column), 24 h treatment with IBR (1 and 10 μM, black columns) or their combination (striped and dotted columns). Data are expressed as ratio over untreated cells, mean \pm SD of $n = 8$ (Jeko-1 CK2α shRNA) and $n = 4$ (Jeko-1 WT) independent experiments. * indicates $p < 0.05$ compared to untreated cells; # indicates $p < 0.05$ compared to both IPTG and IBR 1 μM only treated cells; \$ indicates $p < 0.05$ compared to both IPTG and IBR 10 μM only treated cells. **(F)** Cell cycle distribution of Jeko-1 CK2α shRNA and Jeko-1 WT cells treated as in **(E)**. Histograms columns sections represent mean \pm SD of $n = 4$ independent experiments for each cell line of the sub G₁ (black), G₀/G₁ (light grey), S (dark grey) and G₂/M (white) phases. * indicates $p < 0.05$ compared to untreated cells; # indicates $p < 0.05$ compared to both IPTG and IBR 1 μM only treated cells; \$ indicates $p < 0.05$ compared to both IPTG and IBR 10 μM only treated cells.

and *in vivo* in mouse xenografted IPTG-treated CK2α shRNA-expressing Jeko-1 cells (Figure 1D and Supplementary Figure S1).

To further validate the role of CK2α in BCR signaling, we treated Jeko-1, Granta-519 and Rec-1 cells with the clinical-grade CK2 inhibitor CX-4945 for 24 h. A reduction of the phosphorylation levels of p65/RelA, AKT and BTK were observed also in these conditions (Figure 1E and Supplementary Figure S1), suggesting that CK2α acts on

NF-κB, PI3K/AKT and BTK signaling, affecting the spectrum of cascades downstream from the BCR.

CK2 inactivation boosts Ibrutinib-induced cytotoxicity in MCL cells

We next sought to investigate whether CK2 inhibition could affect the responsiveness of MCL cells to Ibrutinib. To this aim,

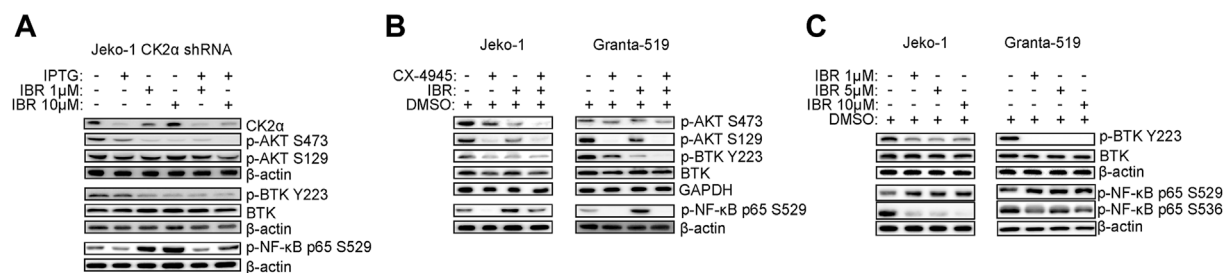


FIGURE 3

CK2 inhibition and Ibrutinib modulate BCR dependent signaling pathways. **(A,B)** Representative WB of PI3K/AKT, BTK and NF- κ B dependent signaling in Jeko-1 CK2 α shRNA cells after 6 days induction with IPTG 500 μ M, 24 h treatment with IBR (1 and 10 μ M) or their combination **(A)** and in Jeko-1 and Granta-519 cells **(B)** after 24 h treatment with DMSO (not higher than 0.1% v/v), CX4945 (1 μ M for Jeko-1 and 2.5 μ M for Granta-519), IBR (1 μ M for each cell line) or their combination. **(C)** Representative WB showing the expression levels of phosphorylated BTK on Y223 (p-BTK Y223) and NF- κ B p65 on S529 (p-NF- κ B p65 S529) and on S536 (p-NF- κ B p65 S536) in Jeko-1 and Granta-519 cells after 24 h treatment with increasing doses of IBR (ranging from 1 to 10 μ M for each cell line). β -actin and GAPDH were used as loading control. Experiments were repeated at least three times for each cell line.

MCL cells were treated for 24 h with Ibrutinib, CX-4945 or their combination. For each cell line the association of BTK and CK2 inhibitors resulted in a significantly higher frequency of apoptotic cell death as compared to that induced by the single agents (Figure 2A). Of note, CX-4945 caused apoptosis also in B cells derived from one Ibrutinib-refractory patient, (Figure 2B). CX-4945 and Ibrutinib did not cooperate in inducing apoptosis in B-cells derived from healthy donors' peripheral blood (Figure 2C) suggesting a lower sensitivity to these drugs of non-neoplastic B-cells as compared to the malignant ones. Three-(4,5-dimethylthiazol-2-yl)-2,5-diphenyltetrazolium bromide (MTT) viability assay was performed on Granta-519, Jeko-1 and Rec-1 cells treated with increasing concentrations of Ibrutinib, CX-4945 or their combination for 72 h. For each cell line, including Granta-519 (which is less sensitive to Ibrutinib as we previously published (Manni et al., 2021)), the calculated combination index (CI) was less than 1, indicating a synergistic effect between the two drugs (Figure 2D).

To exclude off-target effects of CX-4945, we repeated the experiments inactivating CK2 α by gene silencing. We treated the CK2 α -silenced Jeko-1 clone with different concentrations of Ibrutinib added 24 h before harvesting. The combination between Ibrutinib and CK2 α silencing induced a significant increase of AV positive cells as compared to the single treatments, confirming the results obtained with CX-4945 (Figure 2E). As expected, in the control IPTG-treated Jeko-1 WT cells we did not observe increased apoptosis compared to Ibrutinib-only treated cells. The synergistic growth-inhibiting/apoptosis-inducing effect was confirmed also by cell cycle analysis. CK2 α silencing combined with Ibrutinib resulted in a significant increase in the percentage of cells in sub-G1 phase (likely apoptotic) as compared to the single treatments. Additionally, the combined treatment caused also a decrease

in the percentage of cells in G0/G1 and G2/M phases as compared to the single conditions, suggesting a proliferation arrest. As expected, the cell-cycle distribution of Jeko-1 WT cells (used as control) treated with IPTG and Ibrutinib did not show any difference, confirming the specificity of the silencing strategy (Figure 2F).

At the molecular level CK2 α silencing or CX-4945 impinged on BCR dependent signaling cascades, strengthening the Ibrutinib-induced reduction of phosphorylated BTK on Y223 and AKT on S473 (Figures 3A, B and Supplementary Figure S3). Moreover, CK2 inactivation caused a marked decrease in phosphorylation of the CK2 targets AKT S129 and p65/RelA S529 (Figures 3A,B and Supplementary Figure S3). This latter, CK2 dependent phosphorylation, was surprisingly induced by Ibrutinib in a dose-dependent manner (Figure 3C and Supplementary Figure S3), indicating an Ibrutinib induced activation of CK2 which could represent a potential drawback effect possibly antagonizing the efficacy of the drug. The activity of Ibrutinib was confirmed by the reduction in phosphorylation of BTK in Y223 and p65/RelA in S536. (Figure 3C and Supplementary Figure S3).

CK2 inactivation boosts Venetoclax-induced cytotoxicity in MCL cells

Venetoclax is a BH3-mimetic already approved for the treatment of R/R Chronic Lymphocytic Leukemia and Acute Myeloid Leukemia and with clinical activity in MCL. However, also for this drug mechanisms of resistance may arise, including modulation of survival signaling cascades such as AKT (Pham et al., 2018) or increased expression of the anti-apoptotic Mcl-1 protein, buffering the inhibition of Bcl-2 (Prukova et al., 2019).

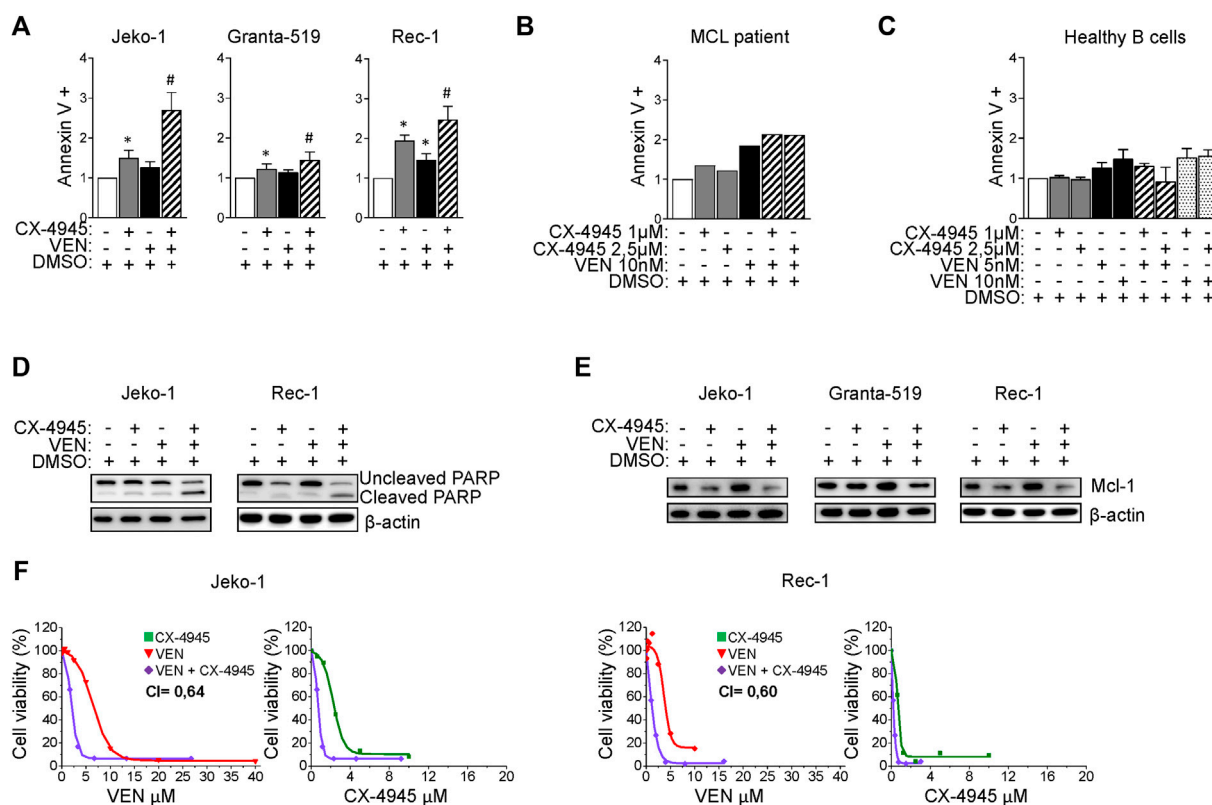
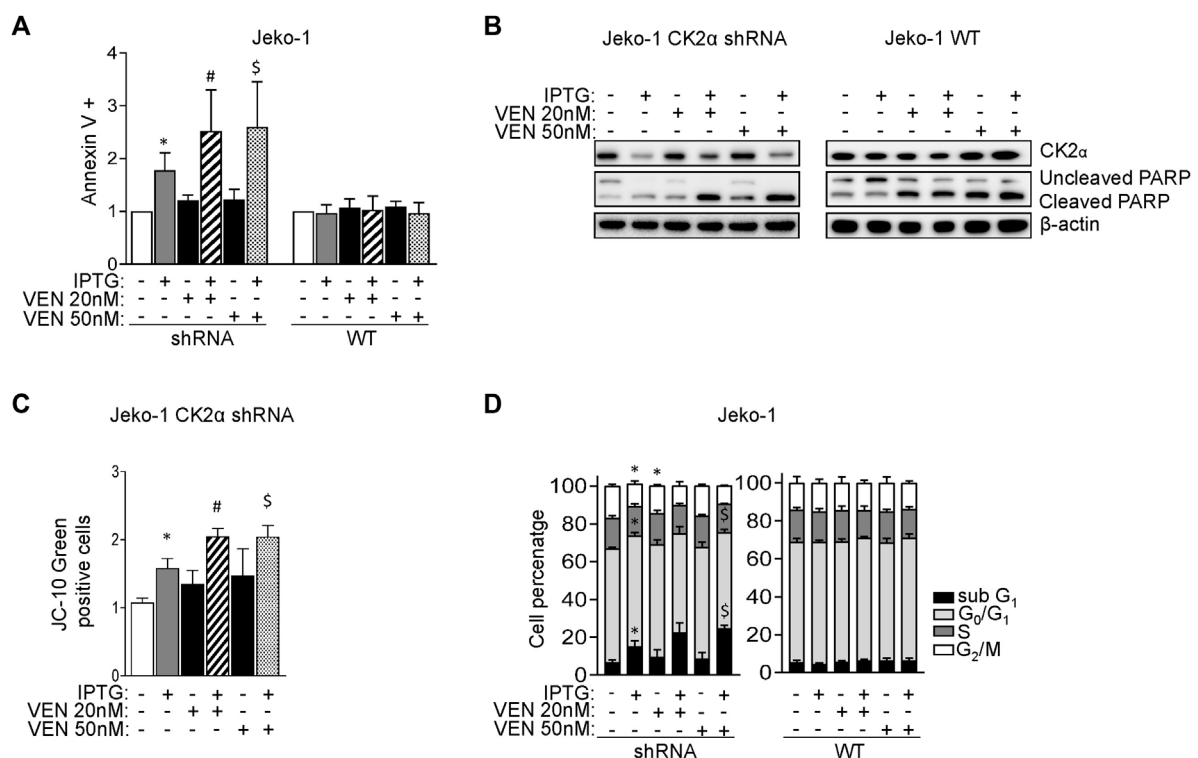


FIGURE 4

CX-4945 potentiates Venetoclax induced cytotoxicity. **(A)** Histograms depicting the percentage of Annexin V positive Jeko-1, Granta-519 and Rec-1 cells after 24 h treatment with DMSO (not higher than 0.1% v/v; white columns), CX-4945 (1 μ M for Jeko-1 and Granta-519, 0.5 μ M for Rec-1; grey columns), VEN (20 nM for Jeko-1, 1.25 nM for Granta-519 and 50 nM for Rec-1; black columns) or their combination (striped columns). Data are expressed as ratio over DMSO treated cells, mean \pm SD of $n = 10$ (Jeko-1), $n = 9$ (Granta-519) and $n = 6$ (Rec-1) independent experiments. * indicates $p < 0.05$ compared to DMSO treated cells; # indicates $p < 0.05$ compared to both CX-4945 and VEN only treated cells. **(B)** Histogram showing the percentage of Annexin V positive B cells derived from one MCL patient after 24 h treatment with DMSO (not higher than 0.1% v/v; white column), CX-4945 (1 μ M and 2.5 μ M; grey columns), VEN (10 nM; black column) or their combination (striped columns). Data are expressed as ratio over DMSO treated cells. **(C)** Histogram showing the percentage of Annexin V positive healthy B cells treated for 24 h with DMSO (not higher 0.1% v/v; white column), CX-4945 (1 μ M and 2.5 μ M; grey columns), VEN (5 and 10 nM; black columns) or their combination (striped and dotted columns). Data are normalized on DMSO treated cells and are expressed as the mean \pm SD of $n = 3$ independent experiments. **(D)** Representative WB showing the expression levels of uncleaved and cleaved PARP in Jeko-1 and Rec-1 cells treated as in **(A)**. β -actin was used as loading control. Experiments were repeated at least three times for each cell line. **(E)** Representative WB showing the expression levels of Mcl-1 in Jeko-1, Granta-519 and Rec-1 cells treated as in **(A)**. β -actin was used as loading control. Experiments were repeated at least three times for each cell line. **(F)** Dose response curves of Jeko-1 and Rec-1 cells incubated for 72 h with increasing concentrations of CX4945 (green curves), VEN (red curves) or their combination (purple curves). For Jeko-1, IC_{50} of the single treatments were 2.30 μ M for CX4945 and 6.68 μ M for VEN. IC_{50} for CX4945 used in combination with VEN was 0.74 μ M, while IC_{50} for VEN used in association with CX-4945 was 2.13 μ M. The calculated CI was 0.64. For Rec-1, IC_{50} of the single treatments were 0.76 μ M for CX-4945 and 4.0 μ M for VEN. IC_{50} for CX-4945 used in combination with VEN was 0.23 μ M, while IC_{50} for VEN used in association with CX-4945 was 1.22 μ M. The calculated CI was 0.60. Data are presented as averaged percentage over control of three independent experiments for each cell line.

Given the above-described results which proved that CK2 is a positive regulator of both AKT and the Bcl-2 family member Mcl-1 (Figure 1), we tested the effect of CK2 inactivation on Venetoclax-induced cytotoxicity. We first performed a dose response curve of Venetoclax in our MCL cell lines, treating them with increasing doses of Venetoclax for 24 h. We found that Granta-519 were the most sensitive while Jeko-1 and Rec-1 were less responsive to this drug (Supplementary Figure S4). Next, we

analyzed the effects of combining CK2 and Bcl-2 inhibitors on MCL apoptosis by labelling cells with AV. CX-4945 potentiated Venetoclax-induced apoptosis in all the MCL cell lines tested and in B cells derived from one patient (Figures 4A, B), while it had no effects on healthy B cells (Figure 4C) where cooperation between CX-4945 and Venetoclax was not observed. The increased apoptosis in MCL cells was confirmed also by the immunoblot analysis of PARP cleavage, which was enhanced in

**FIGURE 5**

CK2α silencing potentiates the cytotoxic and cytostatic effects induced by Venetoclax. **(A)** Histogram showing the percentage of Annexin V positive Jeko-1 CK2α shRNA and Jeko-1 WT cells after 6 days of CK2α silencing with IPTG 500 μM (grey columns), 24 h treatment with VEN 20 and 50 nM (black columns) or their combination (striped and dotted columns). Data are expressed as ratio over untreated cells, mean ± SD of $n = 12$ independent experiments for each cell line. * indicates $p < 0.05$ compared to untreated cells; # indicates $p < 0.05$ compared to both IPTG and VEN 20 nM only treated cells; \$ indicates $p < 0.05$ compared to both IPTG and VEN 50 nM only treated cells. **(B)** Representative WB showing the expression levels of uncleaved and cleaved PARP in Jeko-1 CK2α shRNA and Jeko-1 WT cells treated as in **(A)**. β-actin was used as loading control. Experiments were repeated at least three times for each cell line. **(C)** Histogram depicting the percentage of JC-10 green positive Jeko-1 CK2α shRNA cells treated as in **(A)**. Data are expressed as ratio over averaged untreated cells, mean ± SD of $n = 3$ independent experiments. * indicates $p < 0.05$ compared to untreated cells; # indicates $p < 0.05$ compared to both IPTG and VEN 20 nM only treated cells; \$ indicates $p < 0.05$ compared to both IPTG and VEN 50 nM only treated cells. **(D)** Cell cycle distribution of Jeko-1 CK2α shRNA and Jeko-1 WT cells treated as in **(A)**. Histograms columns sections represent mean ± SD of $n = 4$ (Jeko-1 CK2α shRNA) and $n = 6$ (Jeko-1 WT) independent experiments of the sub G₁ (black), G₀/G₁ (light grey), S (dark grey) and G₂/M (white) cell cycle phases. * indicates $p < 0.05$ compared to untreated cells; \$ indicates $p < 0.05$ compared to both IPTG and VEN 50 nM only treated cells.

the cells treated with the combination of Venetoclax and CX-4945 (Figure 4D and Supplementary Figure S5). Venetoclax treated MCL cells showed an upregulated expression of the pro-survival Bcl-2 family member Mcl-1 protein. Captivatingly, CX-4945 led to a substantial reduction of the Venetoclax-induced increase of Mcl-1, again potentially counteracting a deleterious Venetoclax-induced drawback effect (Figure 4E and Supplementary Figure S5).

Mcl-1 transcript level was unaffected in CX-4945 or Venetoclax treated cells (Supplementary Figure S6A), while its protein level was reduced in CK2 chemically inhibited cells, through a post-translational mechanism that seems to not involve caspase neither the proteasome (Supplementary Figure S6B).

To confirm the possible synergism between CK2 and Bcl-2 inhibitions, we evaluate cell growth and calculated the CI between

drugs. Remarkably, the CI between CX-4945 and Venetoclax was less than 1 even in the less Venetoclax-sensitive cell lines (Figure 4F) suggesting a synergic cytotoxic effect between CX-4945 and Venetoclax. To validate the results obtained with the CK2 chemical inhibitor and to exclude any off-target effects, we performed the same experiments using the IPTG inducible CK2α directed shRNA Jeko-1 clone. The same results were obtained upon CK2α gene silencing, as judged by the increased percentage of AV⁺ cells and extent of PARP cleavage (Figures 5A, B and Supplementary Figure S5) and JC-10 green⁺ cells (indicating mitochondrial membrane potential loss) (Figure 5C) in the combination compared to single treatments. Cell cycle analysis showed an increased percentage of apoptotic cells in the sub-G₁ phase in CK2-silenced cells and a modulation of the G₀/G₁ and G₂/M

phases indicative of a deregulation of cell proliferation (Figure 5D).

Discussion

Given the unfavourable prognosis of relapsed/refractory MCL, even in the era of novel drugs targeting cell signaling or of immunotherapy with Chimeric Antigen Receptor- T cells, the introduction of novel therapeutic approaches that might affect oncogenic survival signaling networks, is mandatory (Vose, 2017). In recent years, the pleiotropic S/T protein kinase CK2 has emerged as a potential target in solid and blood tumours (Strum et al., 2021). The overexpression of this kinase and its key role in the maintenance of the cancer phenotype have been reported in several haematological malignancies, among which MM (Manni et al., 2014), CLL (Martins et al., 2011) and B-NHL (Pizzi et al., 2015).

In accordance with the paradigm known as “non-oncogene addiction”, CK2 overexpression is believed to be responsible of propelling basic mechanisms of cell proliferation and survival (Strum et al., 2021). We previously demonstrated that CK2 is overexpressed in primary MCL samples compared to healthy ones and that treatment with CX-4945 caused not only apoptosis of MCL cell lines but also of patient derived MCL B cells (Manni et al., 2013).

In the present study we have provided strong evidence that protein kinase CK2 sustains active Bcl-2 family related and BCR signaling networks in MCL, by upregulating Mcl-1 expression and BTK, AKT and NF- κ B activation. The results showed in our work highlight the function of CK2 in protecting MCL cells from Ibrutinib and Venetoclax-induced apoptosis, therefore indicating that CK2-targeting could be envisioned as a rational therapeutic strategy to improve anti-MCL Ibrutinib and Venetoclax-induced cytotoxicity.

Importantly, the evidence of this critical role of CK2 in MCL was obtained by a dual approach, by chemical inhibition of the kinase and knock down of its expression. Manipulating CK2 expression in MCL cells, we proved that CK2 α , but not CK2 β , sustains MCL survival and proliferation, *in vitro* in cultured cells and *in vivo* in a MCL xenograft mouse model. We showed that the anti-apoptotic effect of CK2 in MCL might depend on its role on different pro-growth signaling. CK2 α silencing reduced anti-apoptotic markers expression such as Mcl-1 and Pro-caspase 3. CK2 also regulates the activating phosphorylation of three BCR downstream cascades, S129 and S473 AKT, S529 NF- κ B p65 and Y223 BTK, all of them important for MCL clonal expansion. The significance of these pathways in MCL are well-described. Overactivation of NF- κ B and PI3K/AKT is exploited in B cell tumors and in MCL (Rudelius et al., 2006; Balaji et al., 2018). Targeting BCR signaling with the BTK inhibitor Ibrutinib is an effective therapeutic option for R/R MCL cases. However, Ibrutinib resistance in MCL occurs and it may be attributable to mutations in BCR

downstream elements, such as in the NF- κ B pathway, BTK or PLC γ 2 (Hershkovitz-Rokah et al., 2018).

We showed that CK2 sustains BCR related signaling events, namely at the level of NF- κ B and PI3K/AKT activation. We also described an unanticipated role of CK2 in regulating BTK activity in cultured cells and *in vivo* in a MCL xenograft mouse model (Figures 1, 3). How CK2 chemical inactivation or gene silencing may cause a reduction of the phosphorylation of BTK on Y223 remains to be elucidated. The possibility that CK2 physically interacts with BTK or phosphorylates BTK through another kinase is presently unknown and will deserve further investigation. Targeting CK2 along with Ibrutinib modulating BTK active phosphorylation, enhanced the cytostatic and cytotoxic effect of Ibrutinib, even in the Ibrutinib less-sensitive Granta-519 cells (Figure 2). Of note, we observed that Ibrutinib increased the CK2 dependent phosphorylation of p65/RelA on S529 (Figure 3) (which is known to fully activate p65/RelA), suggesting that Ibrutinib may cause the activation of CK2. How this p65/RelA S529 increased phosphorylation is mediated needs to be defined. We performed an *in silico* search which revealed that S529 might potentially be a target for Glycogen Synthase Kinase 3 (GSK3), which is a target of AKT/PI3K signaling cascade. AKT mediated phosphorylation of GSK3 on Ser 9, 21 inhibits GSK3 and stabilizes Myc transcription factors, supporting proliferation (Mancinelli et al., 2017). Therefore, there is also the possibility that Ibrutinib, by hampering AKT activity, induces S529 p65/RelA phosphorylation through GSK3. The upregulation of phosphorylated S529 p65/RelA could represent a potential drawback effect contributing to drug resistance. In support of our data, a recent work that employed a proteomic approach to identify global kinome changes due to Ibrutinib resistance reported that Ibrutinib resistant (IR) MCL cells undergo a kinome reprogramming. Among others, the PI3K/AKT dependent cascade and CK2 α were found to be more active in IR cells compared to the parental one (Zhao et al., 2017). Collectively, this experimental evidence supports a role for CK2 over-activation in Ibrutinib resistance and suggests that this kinase may be a rational target in IR MCL cells.

In a therapeutic perspective, it can be envisioned the design of novel inhibitors, that may either target CK2 or may be dually specific against this and other BCR dependent kinases, as previously done (e.g. the PI3K δ /CK1 ϵ inhibitor Umbralisib, which showed clinical activity in CLL and lymphomas (Davids et al., 2019)).

We have also demonstrated that CK2 inhibition may synergize with another strategy used in the treatment of MCL and other haematological malignancies, i.e. the targeting of Bcl-2, through the selective, oral inhibitor Venetoclax (Cang et al., 2015; Yalniz and Wierda, 2019). CK2 has been shown to sustain Bcl-2 related family members expression in MCL (Figure 1, Supplementary Figure S1 and (Manni et al., 2013)). Therefore, we reasoned that its inhibition would affect Venetoclax mechanism of action. Indeed, this approach resulted to be synergistic with Venetoclax in all the

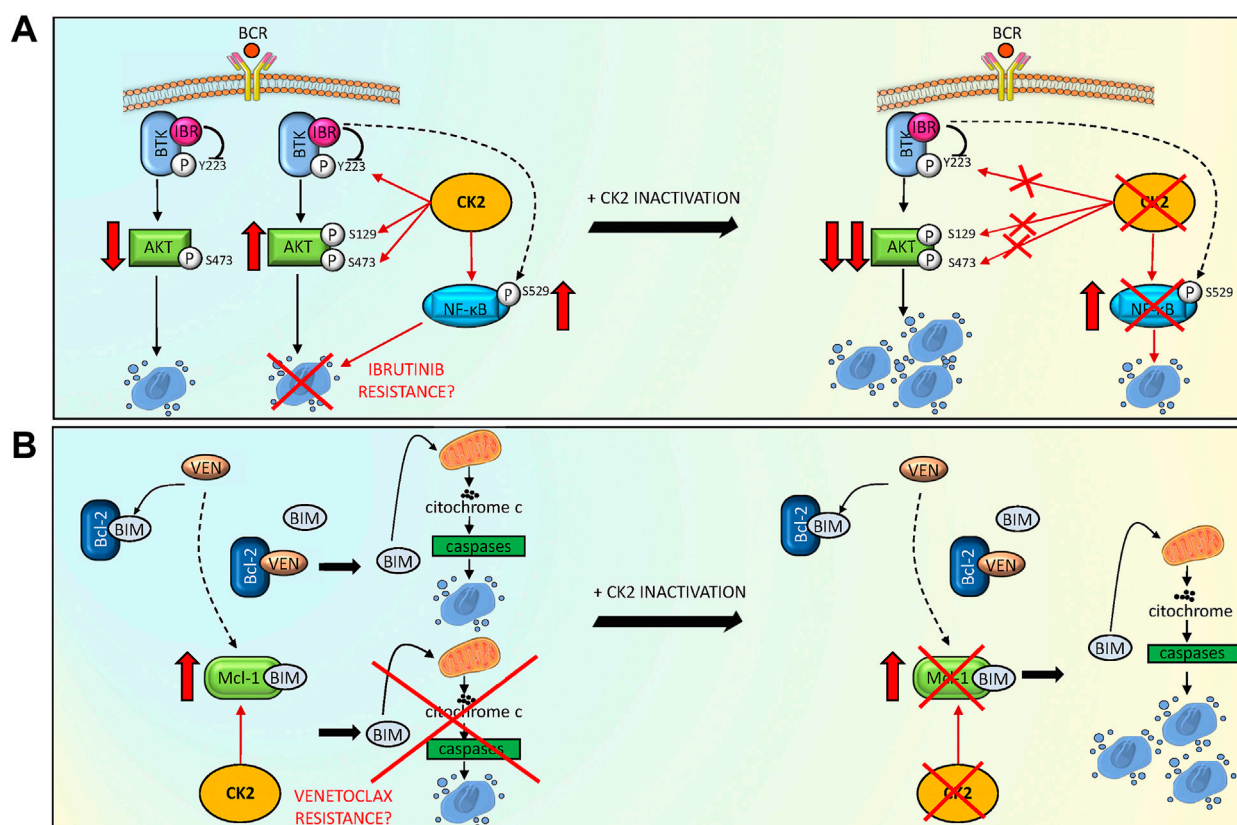


FIGURE 6

CK2 inactivation potentiates Ibrutinib and Venetoclax induced cytotoxicity, overcoming potential drug resistance mechanisms. **(A)** Model summarizing the role of CK2 inhibition to reduce the activation of MCL survival BCR dependent signaling pathways, potentiating Ibrutinib (IBR) induced cytotoxicity. Ibrutinib reduced BTK and AKT phosphorylation on Y223 and S473 respectively, causing MCL cell apoptosis. CK2 sustains the anti-apoptotic phosphorylation of BTK on Y223, of AKT on S129 and S473 (potentially contrasting the apoptosis capability of Ibrutinib) and of NF-κB on S529 (inducing a possible mechanism of resistance). The combination of CK2 inactivation and Ibrutinib potentiates the downregulation of these pro-survival signaling pathways, overcoming potential CK2 dependent mechanisms of resistance. **(B)** Model showing a possible mechanism adopted by CK2 inactivation to overcome a Venetoclax (VEN) induced mechanism of resistance. VEN binds to Bcl-2 releasing the pro-apoptotic BIM protein, causing cytochrome C/caspase mediated apoptosis. However, an increase in Mcl-1 anti-apoptotic protein can be observed, relieving VEN apoptosis inducing capability. The addition of CK2 inactivation determines a reduction in Mcl-1 protein levels, overcoming the VEN induced mechanism of resistance, ultimately potentiating MCL cell death. The figure was made using Servier Medical art templates licensed under a Creative Commons Attribution 3.0 Generic License. <http://smart.servier.com/> accessed on 25/03/2022.

cell lines studied, even in those that displayed a lower sensitivity to Bcl-2 inhibition, such as Jeko-1 and Rec-1 (Pham et al., 2018; Prukova et al., 2019). Indeed, the combination of CX-4945 and Venetoclax demonstrated higher efficacy in these cell lines anticipating a potential strategy to overcome Venetoclax resistance. To this regard, it is noteworthy that CK2 inhibition caused a dramatic reduction of Mcl-1 protein levels in MCL cells (Figure 4). The mechanism by which CX-4945 causes Mcl-1 protein decrease in the tested MCL cell lines is still unclear since it does not seem to be caspase or proteasome dependent (Supplementary Figure S6). Mcl-1 translation in the cell is finely controlled and different miRNAs have been implicated in the control of Mcl-1 translation (as an example miR29 and other miRNAs have been identified to reduce Mcl-1 protein expression) (Mott et al., 2007; Lam et al., 2010). Moreover, other pathways

such as eIF2α/stress response (Fritsch et al., 2007) or the mTORC1 (Mills et al., 2008) cascades have been implicated in the regulation of Mcl-1 translation. Therefore, the exact mechanism by which Mcl-1 protein is reduced upon CK2 inactivation is still unknown and will deserve further investigation. Mcl-1 is one of the major players involved in Venetoclax resistance and our data and others demonstrated that its expression levels could be influenced by CK2 (Manni et al., 2013; Lazaro-Navarro et al., 2021). The present work defined a synergy between CK2 inactivation and Venetoclax in inducing MCL cell death, confirming the evidence reported by others in Acute Lymphoblastic Leukemia (ALL) cells (Lazaro-Navarro et al., 2021). Remarkably, the selectivity of CX-4945 was also validated in the experiments of CK2α silencing, ascribing its apoptotic influence to CK2 inhibition and not to *off target* effects (Figure 5). In addition to its impact on Mcl-1, CK2 can modulate

mitochondrial apoptosis through the regulation of BID, a pro-apoptotic protein belonging to the Bcl-2 family. It has been reported that BID can be phosphorylated by CK2 in the proximity of the caspase-8 recognition site (T58), leading to BID insensitivity to caspase-8 cleavage and delayed apoptosis (Desagher et al., 2001). CK2 inhibition could prevent this mechanism of apoptosis-resistance, allowing the cleavage of full-length BID, the translocation of the fragment obtained to the mitochondria and the subsequent cytochrome c release. The concomitant exposure to Venetoclax would provoke an impairment of the sequestration of BID by Bcl-2, allowing a higher number of pro-apoptotic proteins to be subjected to proteolysis with consequent boosting of apoptosis. Lastly, the impact of CK2 on NF- κ B and PI3K/AKT pathways could also play a significant role in Venetoclax mechanism of action. Indeed, Venetoclax resistance mechanism may also rely on enhanced NF- κ B and AKT signaling. It has been reported that constitutively active AKT could phosphorylate the IKK α subunit on T23, inducing IKK complex activation, I κ B degradation and NF κ B translocation into the nucleus in embryonic fibroblasts (Bai et al., 2009). Additionally, Jayappa et al suggested that the activation of the NF- κ B pathway in MCL cells could lead to an enhanced expression of the anti-apoptotic proteins Bcl-xL and Mcl-1, decreasing the dependency of tumor cells on Bcl-2 and thus their sensitivity to Venetoclax (Jayappa et al., 2017). Therefore, CK2 could be an essential node in the survival signaling network that could mediate Venetoclax induced resistance.

In conclusion, our results demonstrated that CK2 sustains the activation of critical signaling pathways in MCL cells. CK2 could be a central connector in the survival signaling cascades that could interfere with Ibrutinib or Venetoclax-induced cytotoxicity (Figure 6). Its inactivation can potentiate, in a synergistic manner, the cytotoxicity induced by BTK and Bcl-2 inhibitors. We provided evidence that CK2 inactivation led to the downregulation of potential mechanism of resistance that may arise with Ibrutinib or Venetoclax, i.e. the activation of NF- κ B and Mcl-1 as summarized in Figure 6. Our data support the further testing of CK2 inhibitors in MCL in combination therapies.

Data availability statement

The original contributions presented in the study are included in the article/Supplementary Material. Further inquiries can be directed to the corresponding authors.

Ethics statement

The studies involving human participants were reviewed and approved by the Ethic Committee of the Padova University Hospital Internal Institutional Board. The patients/participants

provided their written informed consent to participate in this study. The animal study was reviewed and approved by the Italian Ministry of Health.

Author contributions

SM and FP conceived, designed the experiments, and wrote the paper. SM, MP, ZS, LS, AA, AF, and LQ performed the experiments. SM, MP, ZS, LS, and AA analyzed the data. GreS, CG provided patient samples. SM, GS, LT, and FP contributed reagents/materials/analysis tools. All authors read and approved the final manuscript.

Funding

This work was supported by Italian Gilead Oncohematology Fellowship Program (to FP and SM), Associazione Italiana per la Ricerca sul Cancro (AIRC) to FP (IG 18387) and LT (IG 25024), PRIN (Progetti di rilevante interesse nazionale)-MIUR Prot. 2017ZXT5WR to SM, Ricerca per Credere nella vita (R.C.V) ODV to LT.

Acknowledgments

We thank Prof. Antonio Rosato, Department of Surgery, Oncology and Gastroenterology, University of Padova, for the help with NOD SCID mice experiments and past and present members of the Padova Hematology Division, University-Hospital.

Conflict of interest

FP is in the Advisory Board of Roche and Janssen and reports personal fees from Roche and Janssen. LT reports grants, personal fees from Janssen and Abbvie, grants from Gilead. GS has reported consultancy or advisory board for Janssen and Celgene and has received research support from Roche and Novartis, all outside of the submitted work.

The remaining authors declare that the research was conducted in the absence of any commercial or financial relationships that could be construed as a potential conflict of interest.

The handling editor AV declared a shared parent affiliation with the authors at the time of review.

Publisher's note

All claims expressed in this article are solely those of the authors and do not necessarily represent those of

their affiliated organizations, or those of the publisher, the editors and the reviewers. Any product that may be evaluated in this article, or claim that may be made by its manufacturer, is not guaranteed or endorsed by the publisher.

References

- Bai, D., Ueno, L., and Vogt, P. K. (2009). Akt-mediated regulation of NFκB and the essentialness of NFκB for the oncogenicity of PI3K and Akt. *Int. J. Cancer* 125, 2863–2870. doi:10.1002/ijc.24748
- Balaji, S., Ahmed, M., Lorence, E., Yan, F., Nomie, K., Wang, M., et al. (2018). NF-κB signaling and its relevance to the treatment of mantle cell lymphoma. *J. Hematol. Oncol.* 11, 83. doi:10.1186/s13045-018-0621-5
- Cang, S., Iragavarapu, C., Savooji, J., Song, Y., and Liu, D. (2015). ABT-199 (venetoclax) and BCL-2 inhibitors in clinical development. *J. Hematol. Oncol.* 8, 129. doi:10.1186/s13045-015-0224-3
- Davids, M. S., Kim, H. T., Nicotra, A., Savell, A., Francoeur, K., Hellman, J. M., et al. (2019). Ubralisib in combination with ibrutinib in patients with relapsed or refractory chronic lymphocytic leukaemia or mantle cell lymphoma: A multicentre phase 1-1b study. *Lancet. Haematol.* 6, e38–e47. doi:10.1016/S2352-3026(18)30196-0
- Davids, M. S., Roberts, A. W., Seymour, J. F., Pagel, J. M., Kahl, B. S., Wierda, W. G., et al. (2017). Phase I first-in-human study of venetoclax in patients with relapsed or refractory non-hodgkin lymphoma. *J. Clin. Oncol.* 35, 826–833. doi:10.1200/JCO.2016.70.4320
- Desagher, S., Osen-Sand, A., Montessuit, S., Magnenat, E., Vilbois, F., Hochmann, A., et al. (2001). Phosphorylation of bid by casein kinases I and II regulates its cleavage by caspase 8. *Mol. Cell.* 8, 601–611. doi:10.1016/S1097-2765(01)00335-5
- Di Maira, G., Brustolon, F., Pinna, L. A., and Ruzzene, M. (2009). Dephosphorylation and inactivation of Akt/PKB is counteracted by protein kinase CK2 in HEK 293T cells. *Cell. Mol. Life Sci.* 66, 3363–3373. doi:10.1007/s00018-009-0108-1
- Duncan, J. S., Turowec, J. P., Duncan, K. E., Vilk, G., Wu, C., Lüscher, B., et al. (2011). A peptide-based target screen implicates the protein kinase CK2 in the global regulation of caspase signaling. *Sci. Signal.* 4, ra30. doi:10.1126/scisignal.2001682
- Fritsch, R. M., Schneider, G., Saur, D., Scheibel, M., and Schmid, R. M. (2007). Translational repression of MCL-1 couples stress-induced eIF2 alpha phosphorylation to mitochondrial apoptosis initiation. *J. Biol. Chem.* 282, 22551–22562. doi:10.1074/jbc.M702673200
- Hellwig, C. T., Ludwig-Galezowska, A. H., Concannon, C. G., Litchfield, D. W., Prehn, J. H. M., Rehm, M., et al. (2010). Activity of protein kinase CK2 uncouples Bid cleavage from caspase-8 activation. *J. Cell. Sci.* 123, 1401–1406. doi:10.1242/jcs.061143
- Hershkovitz-Rokah, O., Pulver, D., Lenz, G., and Shpilberg, O. (2018). Ibrutinib resistance in mantle cell lymphoma: Clinical, molecular and treatment aspects. *Br. J. Haematol.* 181, 306–319. doi:10.1111/bjh.15108
- Huang, S., Liu, Y., Chen, Z., Wang, M., and Jiang, V. C. (2022). PIK-75 overcomes venetoclax resistance via blocking PI3K-AKT signaling and MCL-1 expression in mantle cell lymphoma. *Am. J. Cancer Res.* 12, 1102–1115.
- Jain, P., and Wang, M. L. (2022). Mantle cell lymphoma in 2022-A comprehensive update on molecular pathogenesis, risk stratification, clinical approach, and current and novel treatments. *Am. J. Hematol.* 97, 638–656. doi:10.1002/ajh.26523
- Jayappa, K. D., Portell, C. A., Gordon, V. L., Capaldo, B. J., Bekiranov, S., Axelrod, M. J., et al. (2017). Microenvironmental agonists generate de novo phenotypic resistance to combined ibrutinib plus venetoclax in CLL and MCL. *Blood Adv.* 1, 933–946. doi:10.1182/bloodadvances.2016004176
- Lam, L. T., Lu, X., Zhang, H., Lesniewski, R., Rosenberg, S., Semizarov, D., et al. (2010). A microRNA screen to identify modulators of sensitivity to BCL2 inhibitor ABT-263 (navitoclax). *Mol. Cancer Ther.* 9, 2943–2950. doi:10.1158/1535-7163.MCT-10-0427
- Lazaro-Navarro, J., Pimentel-Gutiérrez, H. J., Gauert, A., Hagemann, A. I. H., Eisenschmid, J. L., Goekbuget, N., et al. (2021). Inhibiting casein kinase 2 sensitizes Acute lymphoblastic leukemia cells to venetoclax via MCL1 degradation. *Blood Adv.* 5, 5501–5506. doi:10.1182/bloodadvances.2021004513
- Li, P.-F., Li, J., Müller, E.-C., Otto, A., Dietz, R., von Harsdorf, R., et al. (2002). Phosphorylation by protein kinase CK2: A signaling switch for the caspase-inhibiting protein ARC. *Mol. Cell.* 10, 247–258. doi:10.1016/s1097-2765(02)00600-7
- Mancinelli, R., Carpino, G., Petrungraro, S., Mammola, C. L., Tomaipitina, L., Filippini, A., et al. (2017). Multifaceted roles of GSK-3 in cancer and autophagy-related diseases. *Oxid. Med. Cell. Longev.* 2017, 4629495. doi:10.1155/2017/4629495
- Mandato, E., Manni, S., Zaffino, F., Semenzato, G., and Piazza, F. (2016). Targeting CK2-driven non-oncogene addiction in B-cell tumors. *Oncogene* 35, 6045–6052. doi:10.1038/onc.2016.86
- Mandato, E., Nunes, S. C., Zaffino, F., Casellato, A., Macaccaro, P., Tubi, L. Q., et al. (2018). CX-4945, a selective inhibitor of casein kinase 2, synergizes with B cell receptor signaling inhibitors in inducing diffuse large B cell lymphoma cell death. *Curr. Cancer Drug Targets* 18, 608–616. doi:10.2174/1568009617666170427110450
- Manni, S., Brancalion, A., Mandato, E., Tubi, L. Q., Colpo, A., Pizzi, M., et al. (2013). Protein kinase CK2 inhibition down modulates the NF-κB and STAT3 survival pathways, enhances the cellular proteotoxic stress and synergistically boosts the cytotoxic effect of bortezomib on multiple myeloma and mantle cell lymphoma cells. *PLoS ONE* 8, e75280. doi:10.1371/journal.pone.0075280
- Manni, S., Brancalion, A., Tubi, L. Q., Colpo, A., Pavan, L., Cabrelle, A., et al. (2012). Protein kinase CK2 protects multiple myeloma cells from ER stress-induced apoptosis and from the cytotoxic effect of HSP90 inhibition through regulation of the unfolded protein response. *Clin. Cancer Res.* 18, 1888–1900. doi:10.1158/1078-0432.CCR-11-1789
- Manni, S., Carrino, M., Manzoni, M., Ganesin, K., Nunes, S. C., Costacurta, M., et al. (2021). Inactivation of CK1α in multiple myeloma empowers drug cytotoxicity by affecting AKT and β-catenin survival signaling pathways. *Oncotarget* 8, 14604–14619. doi:10.18632/oncotarget.14654
- Manni, S., Fregani, A., Quotti Tubi, L., Spinello, Z., Carraro, M., Scapinello, G., et al. (2021). Protein kinase CK1α sustains B-cell receptor signaling in mantle cell lymphoma. *Front. Oncol.* 11, 733848. doi:10.3389/fonc.2021.733848
- Manni, S., Toscani, D., Mandato, E., Brancalion, A., Quotti Tubi, L., Macaccaro, P., et al. (2014). Bone marrow stromal cell-fueled multiple myeloma growth and osteoclastogenesis are sustained by protein kinase CK2. *Leukemia* 28, 2094–2097. doi:10.1038/leu.2014.178
- Martins, L. R., Lúcio, P., Silva, M. C., Gameiro, P., Silva, M. G., Barata, J. T., et al. (2011). On CK2 regulation of chronic lymphocytic leukemia cell viability. *Mol. Cell. Biochem.* 356, 51–55. doi:10.1007/s11010-011-0947-6
- Mills, J. R., Hippo, Y., Robert, F., Chen, S. M. H., Malina, A., Lin, C.-J., et al. (2008). mTORC1 promotes survival through translational control of Mcl-1. *Proc. Natl. Acad. Sci. U. S. A.* 105, 10853–10858. doi:10.1073/pnas.0804821105
- Mott, J. L., Kobayashi, S., Bronk, S. F., and Gores, G. J. (2007). mir-29 regulates Mcl-1 protein expression and apoptosis. *Oncogene* 26, 6133–6140. doi:10.1038/sj.onc.1210436
- Pham, L. V., Huang, S., Zhang, H., Zhang, J., Bell, T., Zhou, S., et al. (2018). Strategic therapeutic targeting to overcome venetoclax resistance in aggressive B-cell lymphomas. *Clin. Cancer Res.* 24, 3967–3980. doi:10.1158/1078-0432.CCR-17-3004
- Piazza, F., Manni, S., Tubi, L. Q., Montini, B., Pavan, L., Colpo, A., et al. (2010). Glycogen Synthase Kinase-3 regulates multiple myeloma cell growth and bortezomib-induced cell death. *BMC Cancer* 10, 526. doi:10.1186/1471-2407-10-526
- Pizzi, M., Piazza, F., Agostinelli, C., Fuligni, F., Benvenuti, P., Mandato, E., et al. (2015). Protein kinase CK2 is widely expressed in follicular, Burkitt and diffuse large B-cell lymphomas and propels malignant B-cell growth. *Oncotarget* 6, 6544–6552. doi:10.18632/oncotarget.3446
- Profitós-Pelejá, N., Santos, J. C., Marín-Niebla, A., Roué, G., and Ribeiro, M. L. (2022). Regulation of B-cell receptor signaling and its therapeutic relevance in aggressive B-cell lymphomas. *Cancers (Basel)* 14, 860. doi:10.3390/cancers14040860

Supplementary material

The Supplementary Material for this article can be found online at: <https://www.frontiersin.org/articles/10.3389/fcell.2022.935023/full#supplementary-material>

- Prukova, D., Andera, L., Nahacka, Z., Karolova, J., Svaton, M., Klanova, M., et al. (2019). Cotargeting of BCL2 with venetoclax and MCL1 with S63845 is synthetically lethal *in vivo* in relapsed mantle cell lymphoma. *Clin. Cancer Res.* 25, 4455–4465. doi:10.1158/1078-0432.CCR-18-3275
- Rudelius, M., Pittaluga, S., Nishizuka, S., Pham, T. H., Fend, F., Jaffe, E. S., et al. (2006). Constitutive activation of Akt contributes to the pathogenesis and survival of mantle cell lymphoma. *Blood* 108, 1668–1676. doi:10.1182/blood-2006-04-015586
- Siddiqui-Jain, A., Drygin, D., Streiner, N., Chua, P., Pierre, F., O'Brien, S. E., et al. (2010). CX-4945, an orally bioavailable selective inhibitor of protein kinase CK2, inhibits prosurvival and angiogenic signaling and exhibits antitumor efficacy. *Cancer Res.* 70, 10288–10298. doi:10.1158/0008-5472.CAN-10-1893
- Spinello, Z., Fregnani, A., Quotti Tubi, L., Trentin, L., Piazza, F., Manni, S., et al. (2021). Targeting protein kinases in blood cancer: Focusing on CK1 α and CK2. *Int. J. Mol. Sci.* 22, 3716. doi:10.3390/ijms22073716
- Strum, S. W., Gyenis, L., and Litchfield, D. W. (2021). CSNK2 in cancer: Pathophysiology and translational applications. *Br. J. Cancer* 126, 994–1003. doi:10.1038/s41416-021-01616-2
- Tam, C. S., Anderson, M. A., Pott, C., Agarwal, R., Handunnetti, S., Hicks, R. J., et al. (2018). Ibrutinib plus venetoclax for the treatment of mantle-cell lymphoma. *N. Engl. J. Med.* 378, 1211–1223. doi:10.1056/NEJMoa1715519
- Vose, J. M. (2017). Mantle cell lymphoma: 2017 update on diagnosis, risk-stratification, and clinical management. *Am. J. Hematol.* 92, 806–813. doi:10.1002/ajh.24797
- Wang, D., Westerheide, S. D., Hanson, J. L., and Baldwin, A. S. (2000). Tumor necrosis factor α -induced phosphorylation of RelA/p65 on Ser529 is controlled by casein kinase II. *J. Biol. Chem.* 275, 32592–32597. doi:10.1074/jbc.M001358200
- Yalniz, F. F., and Wierda, W. G. (2019). Targeting BCL2 in chronic lymphocytic leukemia and other hematologic malignancies. *Drugs* 79, 1287–1304. doi:10.1007/s40265-019-01163-4
- Zhao, X., Lwin, T., Silva, A., Shah, B., Tao, J., Fang, B., et al. (2017). Unification of de novo and acquired ibrutinib resistance in mantle cell lymphoma. *Nat. Commun.* 8, 14920. doi:10.1038/ncomms14920



OPEN ACCESS

EDITED BY
Lorenzo Alberto Pinna,
National Research Council, Italy

REVIEWED BY
Vittoria Colotta,
University of Florence, Italy
Dwijendra K. Gupta,
Allahabad University, India

*CORRESPONDENCE
Marc Flajolet,
flajolm@rockefeller.edu,
flajolet.marc@gmail.com

SPECIALTY SECTION
This article was submitted to Molecular
Diagnostics and Therapeutics,
a section of the journal
Frontiers in Molecular Biosciences

RECEIVED 08 April 2022
ACCEPTED 19 July 2022
PUBLISHED 24 August 2022

CITATION
Sunkari YK, Meijer L and Flajolet M
(2022), The protein kinase CK1:
Inhibition, activation, and possible
allosteric modulation.
Front. Mol. Biosci. 9:916232.
doi: 10.3389/fmolb.2022.916232

COPYRIGHT
© 2022 Sunkari, Meijer and Flajolet. This
is an open-access article distributed
under the terms of the [Creative
Commons Attribution License \(CC BY\)](#).
The use, distribution or reproduction in
other forums is permitted, provided the
original author(s) and the copyright
owner(s) are credited and that the
original publication in this journal is
cited, in accordance with accepted
academic practice. No use, distribution
or reproduction is permitted which does
not comply with these terms.

The protein kinase CK1: Inhibition, activation, and possible allosteric modulation

Yashoda Krishna Sunkari¹, Laurent Meijer² and Marc Flajolet^{1*}

¹Laboratory of Molecular and Cellular Neuroscience, The Rockefeller University, New York, NY, United States, ²Perha Pharmaceuticals, Hôtel de Recherche, Roscoff, France

Protein kinases play a vital role in biology and deregulation of kinases is implicated in numerous diseases ranging from cancer to neurodegenerative diseases, making them a major target class for the pharmaceutical industry. However, the high degree of conservation that exists between ATP-binding sites among kinases makes it difficult for current inhibitors to be highly specific. In the context of neurodegeneration, several groups including ours, have linked different kinases such as CK1 and Alzheimer's disease for example. Strictly CK1-isoform specific regulators do not exist and known CK1 inhibitors are inhibiting the enzymatic activity, targeting the ATP-binding site. Here we review compounds known to target CK1, as well as other inhibitory types that could benefit CK1. We introduce the DNA-encoded library (DEL) technology that might represent an interesting approach to uncover allosteric modulators instead of ATP competitors. Such a strategy, taking into account known allosteric inhibitors and mechanisms, might help designing modulators that are more specific towards a specific kinase, and in the case of CK1, toward specific isoforms.

KEYWORDS

casein kinase 1 (CK1), kinase inhibitor, allosteric, Alzheimer's disease (AD), Neurodegeneration, DNA-encoded library (DEL)

Background

Improvements in disease diagnostics, scientific progress in therapeutic target identification, and advances in highly specific and safe therapeutic drugs represent relentless engines to address the need of new medicinal treatments, especially in the field of neurodegeneration such as Alzheimer's disease. Behind the scenes, in the back end of the pharmaceutical world, drug screening represents the backbone of a very active industry focusing on identifying new drug-like molecules. While, new treatments are certainly needed, novel therapeutic strategies and tools are also needed.

Protein kinases play a vital role in biology by catalyzing the transfer of a phosphate group, onto protein substrates, at the hydroxy position of specific amino acids, modifying their activity or function (Johnson and Lewis, 2001; Ardito et al., 2017). Deregulation of kinases and their substrates is implicated in numerous diseases, and for that reason alone kinases represent a major target class for developing novel therapeutics (Zhou et al., 2010; Rebholz et al., 2013; Roskoski, 2015; Yuan et al., 2019; Cohen et al., 2021; De Pins et al.,

2021; Roskoski, 2021). In the context of neurodegeneration, and for Alzheimer's disease in particular, a number of protein kinases have been involved with relevance to different key pathways (Flajolet et al., 2007; Bustos et al., 2017a; Bustos et al., 2017b). For example, tau hyper-phosphorylation is directly linked to tau pathology and a great deal of effort is being devoted to reduce tau hyperphosphorylation (Rubenstein et al., 2019; Wakeman et al., 2022); for a recent review see (Wegmann et al., 2021). About 30 phosphorylation sites have been found to be phosphorylated only in normal brain samples and the specific nature of the sites involved might be less important than the overall level of phosphorylation, the overall net charge of tau. Therefore, blocking or reducing the kinase activity of a kinase such as CK1 potentially targeting numerous sites, directly and indirectly *via* kinase priming, could be highly beneficial.

Casein kinase 1 (CK1) isoforms are involved in diseases and disorders

The role of CK1 in numerous diseases ranging from host-parasite interactions, to highly complex diseases such as cancer and neurodegeneration, has been well established (Knippschild et al., 2005b; Flajolet et al., 2007; Zhou et al., 2010; Schitteck and Sinnberg, 2014; Bustos et al., 2017a; Bustos et al., 2017b; Chen et al., 2017; Zhou et al., 2020; Rachidi et al., 2021). Strictly CK1-isoform specific regulators have not been described (Qiao et al., 2019; Du et al., 2021), and most CK1 small molecular weight regulators are inhibiting the enzymatic activity (Li et al., 2021). Only a limited number of CK1 modulators have been fully validated and none of the currently known CK1 inhibitors have reached clinical stage (at the exception of PF05251749 that may enter clinical evaluation in the near future).

CK1, one of the very first identified protein kinases, is ubiquitously expressed and defines a family of serine/threonine kinases, highly conserved in all eukaryotic organisms (Knippschild et al., 2005a). In mammals, seven CK1 isoforms (α , β , $\gamma 1$, $\gamma 2$, $\gamma 3$, δ and ϵ) with various splice variants have been characterized. Little is known about the regulation of CK1 *in-vivo*. It is believed that CK1 is basally active and at least some isoforms (e.g., CK1 δ and CK1 ϵ) are regulated by inhibitory autophosphorylation at their C-terminal regions. Importantly, the various isoforms are not equally distributed and their regionalized expression in various organs makes it an attractive target for disorders and diseases. In the brain, isoforms might be expressed in different neuronal and non-neuronal populations, localized in various regions (e.g., cellular membrane vs. cytoplasm; cytoplasm vs. nucleus) of the cell presenting different pools of substrates. Importantly, not all isoforms are equally distributed and expressed in different organs, and the existence of CK1 brain specific isoforms makes it an attractive target class for brain disorders and diseases.

In the context of neuronal dysfunctions, CK1 has been abundantly linked to the regulation of the dopaminergic pathway with repercussions on the action of psychostimulants and ADHD (Zhou et al., 2010; Zhou et al., 2020) among others. CK1 is also highly relevant for neurodegeneration, and especially Alzheimer's disease (AD) (Flajolet et al., 2007). Several studies, from our group and others, have linked CK1 and AD, both in relation to amyloid-Abeta peptide and the protein tau (Walter et al., 1998; Schwab et al., 2000; Yasojima et al., 2000; Pastorino et al., 2002; Flajolet et al., 2007). Briefly, after realizing that CK1 expression was increased in AD brains, we demonstrated that overexpression of CK1 ϵ increased amyloid-Abeta peptide production. Furthermore, three CK1 inhibitors (Figure 2), compounds 1–3 significantly reduced endogenous Abeta peptide production in cultured cells without affecting Notch cleavage (Flajolet et al., 2007).

CK1 might act directly by phosphorylating a target as reviewed above but it can also act indirectly via other kinases by activating or priming them, such as GSK3 for which CK1 is a priming kinase together with CK2, CDK5, DYRK1A and PKA (Meijer et al., 2004). CK1 also has the potential to act as an upstream regulator of CDK5 which is also implicated in AD (Liu et al., 2001; Walter et al., 2001). In addition, CK1 δ is regulated by CDK2 and CDK5 (Ianes et al., 2016).

In summary, the presence of numerous CK1 consensus sites on important therapeutic targets, the existence of organ and tissue regionality of CK1 isoforms, and the possibility that CK1 can prime other important kinases such as GSK3 β , give CK1 family a significant advantage to meaningfully affect important diseases and disorders.

Casein kinase 1 inhibitors target the ATP-binding site

Current CK1 inhibitors are targeting the ATP-binding site and functioning as ATP-competitive molecules. The ATP-binding site is the most conserved site in protein kinases and even more so among homologous family members. The ATP-binding site or orthosteric site is a well-defined pocket which forms a rigid and deep binding cavity. It represents an ideal structure for drug-like molecules aiming at ATP-competitive inhibition (Gray et al., 1999; Ardito et al., 2017). For these reasons, the ATP-binding site represents a highly coveted target option for kinase inhibition even though challenging (Ayala-Aguilera et al., 2022). However, inhibitors targeting a specific ATP-binding site can easily bind to other ATP-dependent enzymes, including kinases, and especially homologous family members. In the case of two brain isoforms, CK1 δ and CK1 ϵ , it is difficult to target specifically the ATP-binding site of just one isoform due to their highly conserved sequence as demonstrated in Figure 1 (Du et al., 2021). The adenine region involves GLU 83 and LEU 85 in both cases

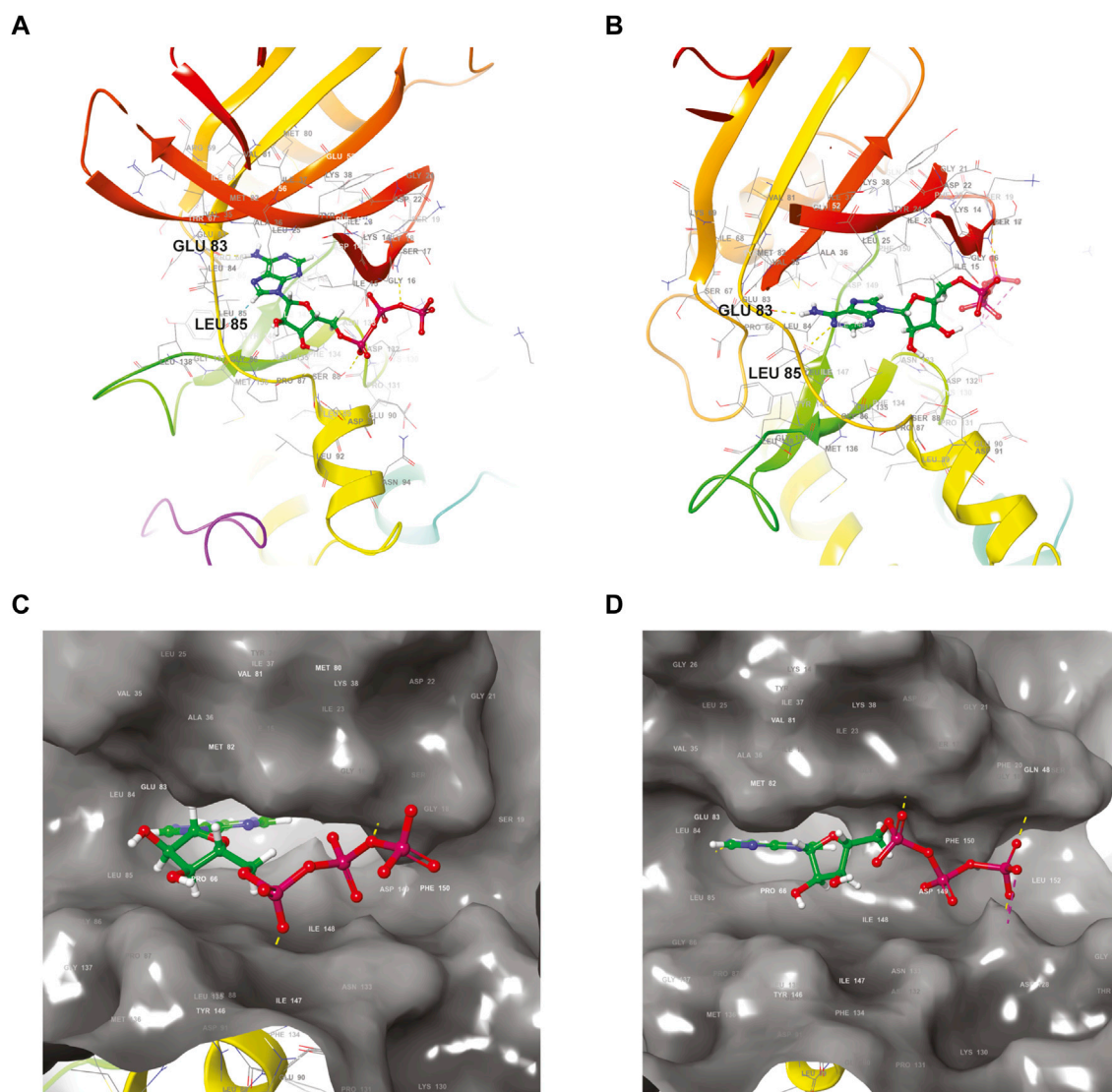


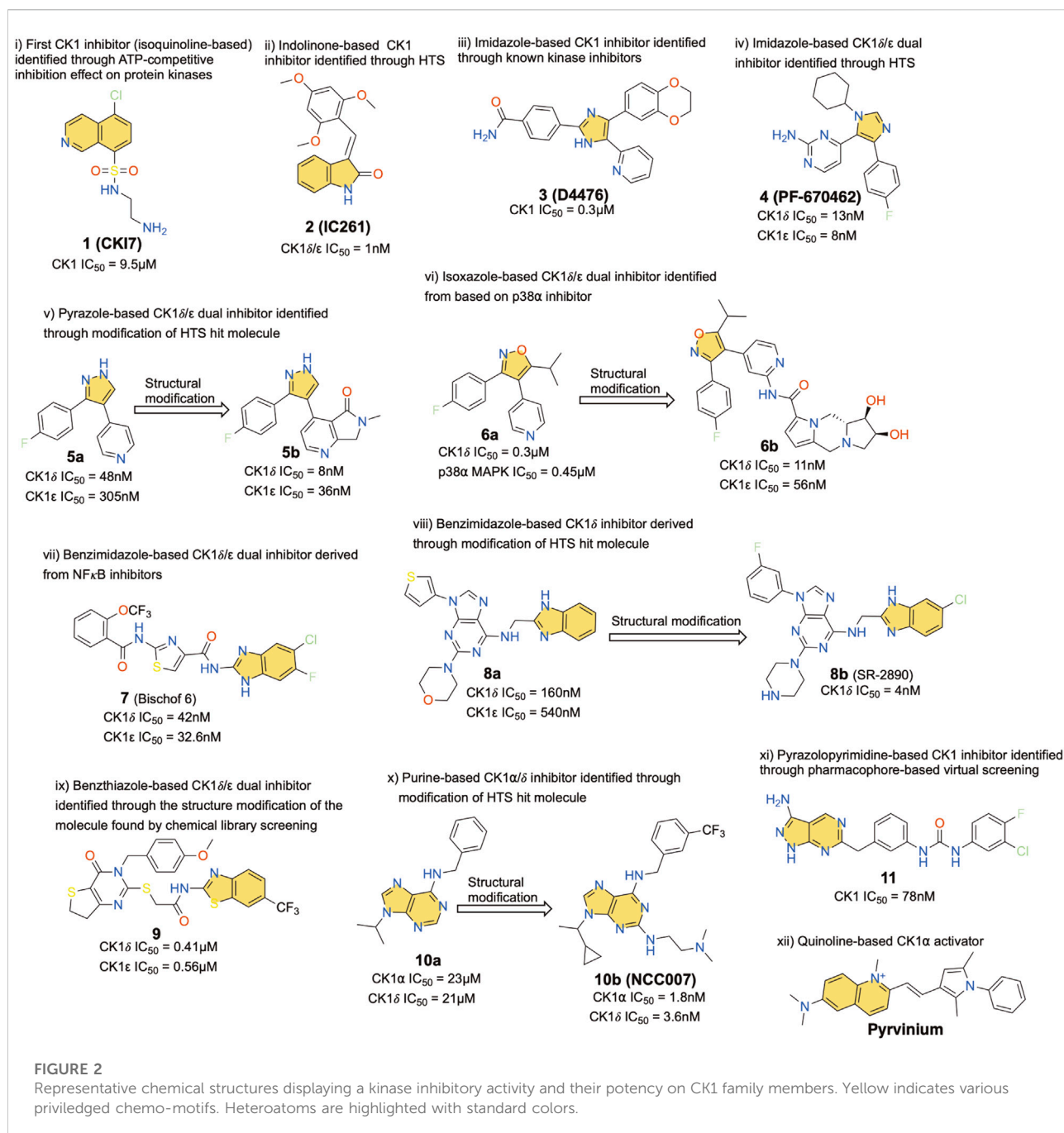
FIGURE 1

Structural comparison of the ATP-binding site of the two closely related CK1 isoforms delta and epsilon. (A,B) Ribbon diagrams of the polypeptidic backbones of CK1 delta (A) (PDB accession code 6RCG) and CK1 epsilon (B) (PDB accession code 4HNI). Ball-and-stick representations of an ATP molecule docked in the active site of CK1 delta (C) and CK1 epsilon (D) shown as surface models. The ATP tri-phosphate moieties are highlighted in red. PDB: Protein Data bank.

(Figures 1A,B) and is well conserved among CK1 isoforms in general. The overall ATP molecule is positioned very similarly in both isoforms (Figures 1C,D). Any undesired off-targeting activity can be associated with higher side-effects and deleterious clinical consequences.

Kinases adopt either a structurally active (DFG-in) or inactive (DFG-out) state conformation for their binding state and nearly all described kinase inhibitors are based on one of these two conformational configurations, which are also known as Type I and type II respectively (Kanev et al., 2019; Attwood et al., 2021).

CK1 inhibitors described in the literature can be grouped into various classes based on their basic chemical scaffold. The different compound types are presented in Figure 2. For each scaffold type, the most active compound has been selected as a representative member of the family. These compounds were identified over the last 25 years using various technologies ranging from high-throughput screening (HTS) to fragment-based drug discovery and structure-based virtual screening (Du et al., 2021; Li et al., 2021). The IC_{50} of each compound is also indicated and corresponds to different types of assays and systems, mostly obtained from *in-vitro* studies.



Compound **1**, well known as CKI7, is an isoquinoline-based derivative, and it was the first CK1 inhibitor identified historically (Xu et al., 1996). Compound **2**, or IC261, another early stage CK1 inhibitor, is an indolinone-based derivative, and it was found as a dual CK1δ/ε specific inhibitor through HTS (Mashhoon et al., 2000). Compounds **3** (D4476) and **4** (PF-670462) are imidazole-based molecules which were derived from known kinase inhibitors and HTS respectively (Badura et al., 2007; Cheong et al., 2015). The inhibitory effect of

compound **3** does not present any degree of specificity toward CK1 isoforms (perhaps slightly CK1δ), it also targets other kinases such as P38α and PDK1. Inhibitor four at the contrary is CK1δ/ε specific and is active in the low nanomolar range. Compound **5b** is a pyrazole-based molecule identified by modifications of hit molecule found through HTS as CK1δ/ε inhibitors with an IC₅₀ of 8 and 36 nM, respectively (Wager et al., 2017a; Wager et al., 2017b). Compound **6b** is an isoxazole-based derivative that also inhibits both CK1δ/ε in the nanomolar range;

this compound was derived from a p38 α kinase inhibitor (Peifer et al., 2009; Luxemburger et al., 2019). Compound 7 and 8a,b are benzimidazole-based compounds. Compound 7 is a dual CK1 δ/ϵ inhibitor that was derived from an NF κ B inhibitor, whereas hit molecule 8a was obtained by HTS and used after structural modifications to derive 8b (Bischof et al., 2012; Bibian et al., 2013). Of note, 8b also inhibits six other kinases (>90%) out of a panel of 442 kinases tested (Bischof et al., 2012). Compound 9, a benzothiazole derivative, was identified as a dual CK1 δ/ϵ inhibitor and resulted from structural modification of an initial hit molecule identified from low throughput screening (Salado et al., 2014; Garcia-Reyes et al., 2018). Compound 10a, a purine-based derivative, was identified by HTS as a dual CK1 α/δ and structure activity relationship-based optimization led to a very potent inhibitor 10b (Lee et al., 2019). Compound 11 is a pyrazolopyrimidine-based scaffold and was identified from pharmacophore-based screening. It inhibits CK1 (nanomolar range) but does not present isoform-specific inhibition (Yang et al., 2012).

In addition to selectivity related issues, there is some resistance to the development of current inhibitors targeting the ATP-binding site and its immediate vicinity including the gate keeper position(s) (Lovly and Shaw, 2014; Kim et al., 2021). Several studies demonstrated a higher mutagenicity of those regions in response to chemotherapies. Such mutations, especially frequent in various types of cancers, lead quickly to treatment resistance by by-passing classical signaling pathways. For example, the Receptor Tyrosine Kinase (RTK) EGFR (Epidermal Growth Factor Receptor) is a key regulator for important biological processes. Abnormal expression of this receptor is associated with a wide range of cancer types. FDA-approved drugs targeting the kinase activity are available and they mostly target the ATP-competitive orthosteric site. Resistance is often observed due to mutations in the vicinity of the ATP-binding site. Furthermore, the rigid and conserved nature of this orthosteric binding region makes drug design more complicated in general, and even more so when isoform specificity is required.

CK1 activator

It is legendary difficult to develop kinase activators, and in many cases, it might even be impossible. Interestingly, one CK1 activator has been reported. Indeed, known kinase activators are extremely rare and not always identified based on a rational design. Kinases can be constitutively active, activated by another protein (e.g., cyclins for CDKs), activated upon intracellular relocation or modified by alteration of their post-translational modification profile. None of these properties are particularly easy to manipulate with drug-like compounds.

Interestingly, pyrvinium, a reported CK1 activator is believed to activate CK1 α , and leading to Wnt signaling pathway

inhibition (Thorne et al., 2010) [Figure 2 (xii)]. Although several reports mentioned pyrvinium as a CK1 α activator, the mechanism underlying this activation remains controversial. A recent detailed biochemical analysis by Chen et al. supports that pyrvinium enhances CK1 α kinase activity through allosteric modulation (Shen et al., 2019).

Successful allosteric kinase inhibitors

Allosteric sites are crucial to regulate the activity of a biological target in a dynamic way requiring an inducible structural rearrangement. A drug-like compound acting as a CK1 allosteric inhibitor could be promising for several medical applications. Allosteric sites are less constraint, present a larger diversity with reduced off-target issues, resulting in an increased selectivity and/or specificity. Identifying putative allosteric sites is challenging including when benefiting from the existence of a crystal structure. A co-crystal structure with a specific ligand uncovering the allosteric site is ideal but not simple to obtain. Cryptic pockets are rarely visible by definition, unless a specific conformation of the protein target is induced, either chemically or biologically. Allosteric modulators are classified as Type III and Type IV allosteric regulators based on the distance from the ATP-binding domain of the kinase domain. Type III modulators bind to a site adjacent to the ATP-binding site and Type IV to a site located further away (see schematic representations Figures 3A, 4A).

Despite the difficulties, several kinase allosteric modulators were successfully developed and even approved for clinical use by the FDA, clearly demonstrating the value and feasibility of identifying kinase allosteric modulators. Trametinib is the first non-ATP-competitive (allosteric) FDA-approved drug that was identified as MEK inhibitor in 2013 (Wright and McCormack, 2013). MEK, a member of the mitogen-activated protein kinase family, is a dual specificity threonine/tyrosine kinase that plays a critical role in the Ras - Raf (MAPKKK) - MEK1/2 (MAPKK) - ERK1/2 (MAPK) signaling pathway. Cobimetinib (Garnock-Jones, 2015), Binimetinib (Rose, 2019) and Selumetinib (Casey et al., 2021) were three others FDA-approved Type III allosteric inhibitors for MEK1/2 (Figure 3B) and others are in clinical development (Shang et al., 2016).

Those FDA-approved allosteric drugs were identified using different technologies mostly centered on HTS and taking advantage of cellular or biochemical assays. Besides MEK, the most allosterically studied kinase is AKT and some of AKT allosteric regulators are currently being tested in clinical trials (Revathidevi and Munirajan, 2019; Martorana et al., 2021).

Compound EAI001 [Figure 3C (i)] was identified as Type III allosteric inhibitor by HTS and structural modifications led to more potent inhibitors (EAI045 and JBJ-04-125-02) (Jia et al., 2016; To et al., 2019). Sulfonamide-derivative was identified as LIMK2 Type III allosteric inhibitor through HTS hit molecule [Figure 3C (ii)] and

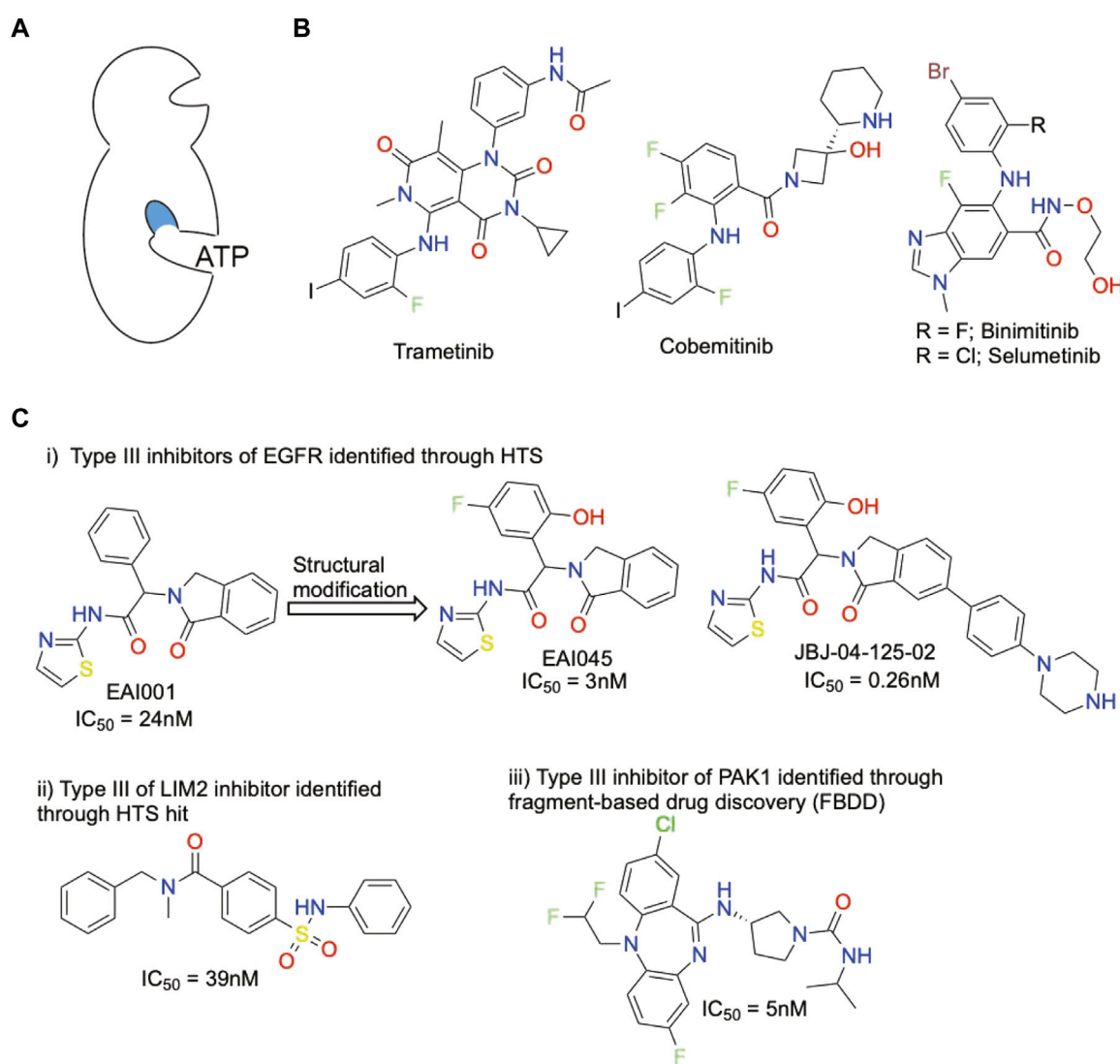


FIGURE 3

Representative chemical structures displaying a kinase inhibitory activity of Type III and their potency toward specific kinases. (A) Schematic representation of Type III allosteric site. Blue color indicates targeted site. (B) FDA-approved Type III HEK inhibitors (C) Type III kinase inhibitors.

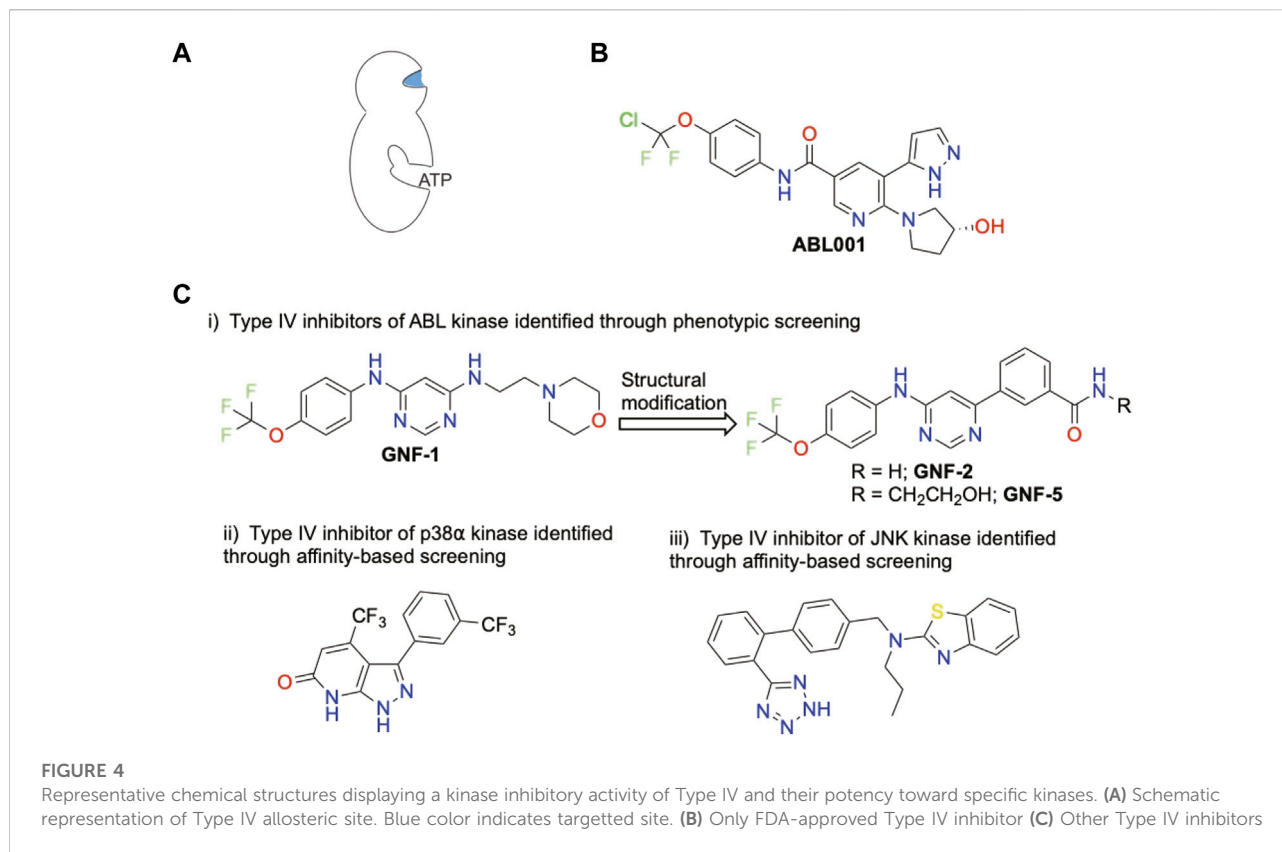
this derivative has good selectivity over its closely related kinase LIMK1 (Goodwin et al., 2015). Based on fragment-based drug discovery a dibenzodiazepine compound was derived as Type III allosteric inhibitor for PAK1 kinase (Karpov et al., 2015) [Figure 2C (iii)]. Type III allosteric inhibitors were also reported for the kinases IRE1 and RIP1 (Wu et al., 2015).

Finally, type IV allosteric inhibitors correspond to molecules which bind a distal allosteric site from the ATP-binding site (Figure 4A). At this date, Asciminib (ABL001) is the only FDA-approved Type IV inhibitor (Deeks, 2022) (Figure 4B). ABL001 was identified initially through phenotypic screening targeting ABL kinase and further optimized by fragment-based NMR (Wylie et al., 2017). Type IV modulators are typically

identified by conventional technologies such as phenotypic screening (Adrian et al., 2006) and affinity-based screenings (Comess et al., 2011) (Figure 4C).

Recently, Lu et al. categorized two other types of kinase allosteric regulators that bind outside the kinase domain. Type VI binds to the catalytic inactive site of a pseudokinase domain while Type VII binds elsewhere outside the kinase domain, for example in the extracellular region of a receptor tyrosine kinase (Lu et al., 2020).

The absence of CK1 allosteric inhibitors probably results from the convergence of the high degree of conservation between isoforms and the absence of an assay compatible with high throughput allosteric testing. Regarding the degree of



similarity between isoforms, differences do exist in the primary sequences and those could allow drug-like molecules to bind with some degree of specificity. Regarding the screening assay, the DNA-encoded library (DEL) technology does not require a functional assay. Indeed, DEL offers the possibility to search for molecules binding to the target very efficiently (hundreds of millions to billions of compounds). Allosteric regulation of the binding molecules can then be evaluated as a validation step or secondary assay, in a low throughput and well controlled enzymatic assay. Furthermore, the possibility to perform DEL screens in parallel (e.g., two or more isoforms, or wild type versus mutant) allows early on in the process, at the very first step, to select specific binders.

DNA-encoded libraries and non-biased approaches to tackle allostery

For the reasons mentioned previously, alternative therapeutic strategies directed towards the development of molecules targeting non-ATP binding sites have emerged and are becoming more popular (Wu et al., 2015; Lu et al., 2019; Lu et al., 2020). The DEL technology might be particularly adapted to identify allosteric modulators and to target cryptic pockets in general, due to its screening concept that is based solely on

binding affinity (Schwab et al., 2000; Gironde-Martinez et al., 2021; Huang et al., 2022). With this approach, a very large number of compounds this was mentioned just before covalently tagged with a unique and specific DNA sequence are mixed with the immobilized protein target in a single tube. Following the incubation step, several washes are performed and at the end of the process, compounds binding to the target are identified through PCR amplification and next generation sequencing. The DNA tag sequences allow for the hit molecules to be identified. Validation of the hit binders can then be performed individually ON-DNA and OFF-DNA. Validated binders can then be investigated for their function.

This screening approach is totally independent of a specific activity, and therefore does not require any type of assay. Furthermore, due to the practicality of such screening campaigns, several conditions can be tested in parallel and subtractive approaches can be utilized. For example, an existing inhibitor known to fit in the active site could be added during the DEL screening incubation in order to saturate the active site and block its accessibility to DEL molecules, favoring the binding of DEL compounds at other sites. A wild-type kinase could be screened in parallel to a dead kinase mutant, a single target protein could be screened in parallel to the same kinase associated to a co-factor if folding is known to be affected, a desired isoform could be compared to a

non-desired isoform for specificity reasons, etc . . . DEL might prove useful to distinguish them in a non-biased approach. Using the DEL technology, kinase inhibitors and allosteric inhibitors for GPCRs have already been identified (Petersen et al., 2016; Ahn et al., 2017; Chang et al., 2017; Ahn et al., 2018; Kim et al., 2018; Kim et al., 2019; Guilinger et al., 2021). Finally, a validated compound binding to a target, even if ineffective at modulating the activity *per se*, could be used as a PROTAC anchor or alternatively as a biotracer or research tool.

Conclusion

CK1 kinases regulate a wide variety of cellular processes and dysfunction of several members of this family have been involved in serious pathological conditions. In the context of AD, the multiple links connecting CK1 to various pathophysiological issues, its dual capacity to act on the two most important pathways (tau and amyloid beta), and the existence of well-defined neuronal specific isoforms, makes it a special and highly relevant target. We summarized here the compounds known to inhibit CK1 and for each privileged scaffold we present the most active compound as well as the method used to identify those compounds. All known CK1 inhibitors are targeting the ATP-binding site and the only activator known might do so via allosteric regulation. None of those drug-like molecules reached clinical stage. Due to the high degree of conservation between CK1 isoforms, and kinases in general, allosteric inhibitors might

be more suited for therapeutic interventions. Identifying allosteric modulators is challenging but we believe that DNA-encoded library technologies, due to their absence of strong screening requirements and their unprecedented library size, are particularly well suited for the task.

Author contributions

YS and MF wrote and revised the manuscript; YS and MF designed and realized figures; LM revised the manuscript and figures; YS, LM, and MF incorporated references.

Conflict of interest

The authors declare that the research was conducted in the absence of any commercial or financial relationships that could be construed as a potential conflict of interest.

Publisher's note

All claims expressed in this article are solely those of the authors and do not necessarily represent those of their affiliated organizations, or those of the publisher, the editors and the reviewers. Any product that may be evaluated in this article, or claim that may be made by its manufacturer, is not guaranteed or endorsed by the publisher.

References

- Adrian, F. J., Ding, Q., Sim, T., Velentza, A., Sloan, C., Liu, Y., et al. (2006). Allosteric inhibitors of bcr-abl-dependent cell proliferation. *Nat. Chem. Biol.* 2, 95–102. doi:10.1038/nchembio760
- Ahn, S., Kahsai, A. W., Pani, B., Wang, Q. T., Zhao, S., Wall, A. L., et al. (2017). Allosteric "beta-blocker" isolated from a dna-encoded small molecule library. *Proc. Natl. Acad. Sci. U. S. A.* 114, 1708–1713. doi:10.1073/pnas.1620645114
- Ahn, S., Pani, B., Kahsai, A. W., Olsen, E. K., Husemoen, G., Vestergaard, M., et al. (2018). Small-molecule positive allosteric modulators of the β 2-adrenoceptor isolated from DNA-encoded libraries. *Mol. Pharmacol.* 94, 850–861. doi:10.1124/mol.118.111948
- Ardito, F., Giuliani, M., Perrone, D., Troiano, G., and Lo Muzio, L. (2017). The crucial role of protein phosphorylation in cell signaling and its use as targeted therapy (Review). *Int. J. Mol. Med.* 40, 271–280. doi:10.3892/ijmm.2017.3036
- Attwood, M. M., Fabbro, D., Sokolov, A. V., Knapp, S., and Schioth, H. B. (2021). Trends in kinase drug discovery: Targets, indications and inhibitor design. *Nat. Rev. Drug Discov.* 20, 839–861. doi:10.1038/s41573-021-00252-y
- Ayala-Aguilera, C. C., Valero, T., Lorente-Macias, A., Baillache, D. J., Croke, S., and Unciti-Broceta, A. (2022). Small molecule kinase inhibitor drugs (1995–2021): Medical indication, pharmacology, and synthesis. *J. Med. Chem.* 65, 1047–1131. doi:10.1021/acs.jmedchem.1c00963
- Badura, L., Swanson, T., Adamowicz, W., Adams, J., Cianfrogna, J., Fisher, K., et al. (2007). An inhibitor of casein kinase I epsilon induces phase delays in circadian rhythms under free-running and entrained conditions. *J. Pharmacol. Exp. Ther.* 322, 730–738. doi:10.1124/jpet.107.122846
- Bibian, M., Rahaim, R. J., Choi, J. Y., Noguchi, Y., Schurer, S., Chen, W. M., et al. (2013). Development of highly selective casein kinase 1 δ /1 ϵ (CK1 δ /1 ϵ) inhibitors with potent antiproliferative properties. *Bioorg. Med. Chem. Lett.* 23, 4374–4380. doi:10.1016/j.bmcl.2013.05.075
- Bischof, J., Leban, J., Zaja, M., Grothey, A., Radunsky, B., Othersen, O., et al. (2012). 2-Benzamido-N-(1H-benzodimidazol-2-yl)thiazole-4-carboxamide derivatives as potent inhibitors of CK1 δ /1 ϵ . *Amino Acids* 43, 1577–1591. doi:10.1007/s00726-012-1234-x
- Bustos, V., Pulina, M. V., Bispo, A., Lam, A., Flajolet, M., Gorelick, F. S., et al. (2017a). Phosphorylated presenilin 1 decreases beta-amyloid by facilitating autophagosome-lysosome fusion. *Proc. Natl. Acad. Sci. U. S. A.* 114, 7148–7153. doi:10.1073/pnas.1705240114
- Bustos, V., Pulina, M. V., Kelahmetoglu, Y., Sinha, S. C., Gorelick, F. S., Flajolet, M., et al. (2017b). Bidirectional regulation of A β levels by Presenilin 1. *Proc. Natl. Acad. Sci. U. S. A.* 114, 7142–7147. doi:10.1073/pnas.1705235114
- Casey, D., Demko, S., Sinha, A., Mishra-Kalyani, P. S., Shen, Y. L., Khasar, S., et al. (2021). Fda approval summary: Selumetinib for plexiform neurofibroma. *Clin. Cancer Res.* 27, 4142–4146. doi:10.1158/1078-0432.CCR-20-5032
- Chang, A. I., McGregor, L. M., Jain, T., and Liu, D. R. (2017). Discovery of a covalent kinase inhibitor from a DNA-encoded small-molecule library \times protein library selection. *J. Am. Chem. Soc.* 139, 10192–10195. doi:10.1021/jacs.7b04880
- Chen, C. Y., Gu, J. L., Basurto-Islas, G., Jin, N. N., Wu, F., Gong, C. X., et al. (2017). Up-regulation of casein kinase 1 epsilon is involved in tau pathogenesis in alzheimer's disease. *Sci. Rep.* 7, 13478. doi:10.1038/s41598-017-13791-5
- Cheong, J. K., Zhang, F., Chua, P. J., Bay, B. H., Thorburn, A., and Virshup, D. M. (2015). Casein kinase 1 α -dependent feedback loop controls autophagy in RAS-driven cancers. *J. Clin. Invest.* 125, 1401–1418. doi:10.1172/JCI78018

- Cohen, P., Cross, D., and Janne, P. A. (2021). Kinase drug discovery 20 Years after imatinib: Progress and future directions. *Nat. Rev. Drug Discov.* 20, 551–569. doi:10.1038/s41573-021-00195-4
- Comess, K. M., Sun, C. H., Abad-Zapatero, C., Goedken, E. R., Gum, R. J., Borhani, D. W., et al. (2011). Discovery and characterization of non-atp site inhibitors of the mitogen activated protein (map) kinases. *ACS Chem. Biol.* 6, 234–244. doi:10.1021/cb1002619
- De Pins, B., Mendes, T., Giralt, A., and Girault, J. A. (2021). The non-receptor tyrosine kinase Pyk2 in brain function and neurological and psychiatric diseases. *Front. Synaptic Neurosci.* 13, 749001. doi:10.3389/fnsyn.2021.749001
- Deeks, E. D. (2022). Asciminib: First approval. *Drugs* 82, 219–226. doi:10.1007/s40265-021-01662-3
- Du, C. X., Yang, H. Y., Feng, F., Liu, W. Y., Chen, Y., and Sun, H. P. (2021). Achieving effective and selective Ck1 inhibitors through structure modification. *Future Med. Chem.* 13, 505–528. doi:10.4155/fmc-2020-0215
- Flajolet, M., He, G., Heiman, M., Lin, A., Nairn, A. C., and Greengard, P. (2007). Regulation of alzheimer's disease amyloid-beta formation by casein kinase I. *Proc. Natl. Acad. Sci. U. S. A.* 104, 4159–4164. doi:10.1073/pnas.0611236104
- Garcia-Reyes, B., Witt, L., Jansen, B., Karasu, E., Gehring, T., Leban, J., et al. (2018). Discovery of inhibitor of Wnt production 2 (IWP-2) and related compounds as selective ATP-competitive inhibitors of casein kinase 1 (CK1) δ/ϵ . *J. Med. Chem.* 61, 4087–4102. doi:10.1021/acs.jmedchem.8b00095
- Garnock-Jones, K. P. (2015). Cobimetinib: First global approval. *Drugs* 75, 1823–1830. doi:10.1007/s40265-015-0477-8
- Gironda-Martinez, A., Donckele, E. J., Samain, F., and Neri, D. (2021). Dna-encoded chemical libraries: A comprehensive review with successful stories and future challenges. *ACS Pharmacol. Transl. Sci.* 4, 1265–1279. doi:10.1021/acspstci.1c00118
- Goodwin, N. C., Cianchetta, G., Burgoon, H. A., Healy, J., Mabon, R., Strobel, E. D., et al. (2015). Discovery of A type iii inhibitor of lim kinase 2 that binds in A dfg-out conformation. *ACS Med. Chem. Lett.* 6, 53–57. doi:10.1021/ml500242y
- Gray, N., Detivaud, L., Doerig, C., and Meijer, L. (1999). Atp-site directed inhibitors of cyclin-dependent kinases. *Curr. Med. Chem.* 6, 859–875. doi:10.2174/092986730609220401152358
- Gullinger, J. P., Archana, A., Augustin, M., Bergmann, A., Centrella, P. A., Clark, M. A., et al. (2021). Novel irreversible covalent BTK inhibitors discovered using DNA-encoded chemistry. *Bioorg. Med. Chem.* 42, 116223. doi:10.1016/j.bmc.2021.116223
- Huang, Y., Li, Y., and Li, X. (2022). Strategies for developing dna-encoded libraries beyond binding assays. *Nat. Chem.* 14, 129–140. doi:10.1038/s41557-021-00877-x
- Ianes, C., Xu, P. F., Werz, N., Meng, Z. G., Henne-Bruns, D., Bischof, J., et al. (2016). Ck1 delta activity is modulated by Cdk2/E- and Cdk5/P35-mediated phosphorylation. *Amino Acids* 48, 579–592. doi:10.1007/s00726-015-2114-y
- Jia, Y., Yun, C. H., Park, E., Rcan, D. E., Manuia, M., Juarez, J., et al. (2016). Overcoming egfr(t790m) and egfr(C797s) resistance with mutant-selective allosteric inhibitors. *Nature* 534, 129–132. doi:10.1038/nature17960
- Johnson, L. N., and Lewis, R. J. (2001). Structural basis for control by phosphorylation. *Chem. Rev.* 101, 2209–2242. doi:10.1021/cr000225s
- Kanev, G. K., De Graaf, C., De Esch, I. J. P., Leurs, R., Wurdinger, T., Westerman, B. A., et al. (2019). The landscape of atypical and eukaryotic protein kinases. *Trends Pharmacol. Sci.* 40, 818–832. doi:10.1016/j.tips.2019.09.002
- Karpov, A. S., Amiri, P., Bellamacina, C., Bellance, M. H., Breitenstein, W., Daniel, D., et al. (2015). Optimization of A dibenzodiazepine hit to A potent and selective allosteric Pak1 inhibitor. *ACS Med. Chem. Lett.* 6, 776–781. doi:10.1021/acsmchemlett.5b00102
- Kim, D., Sun, Y. X., Xie, D., Denton, K. E., Chen, H., Lin, H., et al. (2019). Application of A substrate-mediated selection with C-src tyrosine kinase to A dna-encoded chemical library. *Molecules* 24, 2764. doi:10.3390/molecules24152764
- Kim, J., Grotegut, C. A., Wisler, J. W., Li, T. Y., Mao, L., Chen, M. Y., et al. (2018). Beta-arrestin 1 regulates beta 2-adrenergic receptor-mediated skeletal muscle hypertrophy and contractility. *Skelet. Muscle* 8, 39. doi:10.1186/s13395-018-0184-8
- Kim, P., Li, H., Wang, J., and Zhao, Z. (2021). Landscape of drug-resistance mutations in kinase regulatory hotspots. *Brief. Bioinform.* 22, bbaa108. doi:10.1093/bib/bbaa108
- Knippschild, U., Gocht, A., Wolff, S., Huber, N., Lohler, J., and Stoter, M. (2005a). The casein kinase 1 family: Participation in multiple cellular processes in eukaryotes. *Cell. Signal.* 17, 675–689. doi:10.1016/j.cellsig.2004.12.011
- Knippschild, U., Wolff, S., Giamas, G., Brockschmidt, C., Wittau, M., Wurl, P. U., et al. (2005b). The role of the casein kinase 1 (Ck1) family in different signaling pathways linked to cancer development. *Onkologie* 28, 508–514. doi:10.1159/000087137
- Lee, J. W., Hirota, T., Ono, D., Honma, S., Honma, K. I., Park, K., et al. (2019). Chemical control of mammalian circadian behavior through dual inhibition of casein kinase α and δ . *J. Med. Chem.* 62, 1989–1998. doi:10.1021/acs.jmedchem.8b01541
- Li, S. S., Dong, Y. H., and Liu, Z. P. (2021). Recent advances in the development of casein kinase 1 inhibitors. *Curr. Med. Chem.* 28, 1585–1604. doi:10.2174/0929867327666200713185413
- Liu, F., Ma, X. H., Ule, J., Bibb, J. A., Nishi, A., Demaggio, A. J., et al. (2001). Regulation of cyclin-dependent kinase 5 and casein kinase 1 By metabotropic glutamate receptors. *Proc. Natl. Acad. Sci. U. S. A.* 98, 11062–11068. doi:10.1073/pnas.191353898
- Lovly, C. M., and Shaw, A. T. (2014). Molecular pathways: Resistance to kinase inhibitors and implications for therapeutic strategies. *Clin. Cancer Res.* 20, 2249–2256. doi:10.1158/1078-0432.CCR-13-1610
- Lu, S., He, X., Ni, D., and Zhang, J. (2019). Allosteric modulator discovery: From serendipity to structure-based design. *J. Med. Chem.* 62, 6405–6421. doi:10.1021/acs.jmedchem.8b01749
- Lu, X., Smaill, J. B., and Ding, K. (2020). New promise and opportunities for allosteric kinase inhibitors. *Angew. Chem. Int. Ed. Engl.* 59, 13764–13776. doi:10.1002/anie.201914525
- Luxemburger, A., Schmidt, D., Ianes, C., Pichlo, C., Kruger, M., Von Drathen, T., et al. (2019). Design, synthesis and biological evaluation of isoxazole-based Ck1 inhibitors modified with chiral pyrrolidine scaffolds. *Molecules* 24, E873. doi:10.3390/molecules24050873
- Martorana, F., Motta, G., Pavone, G., Motta, L., Stella, S., Vitale, S. R., et al. (2021). Akt inhibitors: New weapons in the fight against breast cancer? *Front. Pharmacol.* 12, 662232. doi:10.3389/fphar.2021.662232
- Mashhoon, N., Demaggio, A. J., Tereshko, V., Bergmeier, S. C., Egli, M., Hoekstra, M. F., et al. (2000). Crystal structure of A conformation-selective casein kinase-1 inhibitor. *J. Biol. Chem.* 275, 20052–20060. doi:10.1074/jbc.M001713200
- Meijer, L., Flajolet, M., and Greengard, P. (2004). Pharmacological inhibitors of glycogen synthase kinase 3. *Trends Pharmacol. Sci.* 25, 471–480. doi:10.1016/j.tips.2004.07.006
- Pastorino, L., Ikin, A. F., Nairn, A. C., Pursnani, A., and Buxbaum, J. D. (2002). The carboxyl-terminus of bace contains A sorting signal that regulates bace trafficking but not the formation of total A beta. *Mol. Cell. Neurosci.* 19, 175–185. doi:10.1006/mcne.2001.1065
- Peifer, C., Abadleh, M., Bischof, J., Hauser, D., Schattel, V., Hirner, H., et al. (2009). 3, 4-Diaryl-isoxazoles and -imidazoles as potent dual inhibitors of p38alpha mitogen activated protein kinase and casein kinase 1delta. *J. Med. Chem.* 52, 7618–7630. doi:10.1021/jm9005127
- Petersen, L. K., Blaksjaer, P., Chaikuad, A., Christensen, A. B., Dietvorst, J., Holmkvist, J., et al. (2016). Novel p38a MAP kinase inhibitors identified from yoctoReactor DNA-encoded small molecule library. *Medchemcomm* 7, 1332–1339. doi:10.1039/c6md00241b
- Qiao, Y. T., Chen, T. K., Yang, H. Y., Chen, Y., Lin, H. Z., Qu, W., et al. (2019). Small molecule modulators targeting protein kinase Ck1 and Ck2. *Eur. J. Med. Chem.* 181, 111581. doi:10.1016/j.ejmech.2019.111581
- Rachidi, N., Knippschild, U., and Spath, G. F. (2021). Dangerous duplicity: The dual functions of casein kinase 1 in parasite biology and host subversion. *Front. Cell. Infect. Microbiol.* 11, 655700. doi:10.3389/fcimb.2021.655700
- Rebholz, H., Zhou, M., Nairn, A. C., Greengard, P., and Flajolet, M. (2013). Selective knockout of the casein kinase 2 in D1 medium spiny neurons controls dopaminergic function. *Biol. Psychiatry* 74, 113–121. doi:10.1016/j.biopsych.2012.11.013
- Revathidevi, S., and Munirajan, A. K. (2019). Akt in cancer: Mediator and more. *Semin. Cancer Biol.* 59, 80–91. doi:10.1016/j.semcancer.2019.06.002
- Rose, A. A. N. (2019). Encorafenib and binimetinib for the treatment of braf V600e/K-mutated melanoma. *Drugs Today (Barc)* 55, 247–264. doi:10.1358/dot.2019.55.4.2958476
- Roskoski, R., Jr. (2015). A historical overview of protein kinases and their targeted small molecule inhibitors. *Pharmacol. Res.* 100, 1–23. doi:10.1016/j.phrs.2015.07.010
- Roskoski, R., Jr. (2021). Properties of fda-approved small molecule protein kinase inhibitors: A 2021 update. *Pharmacol. Res.* 165, 105463. doi:10.1016/j.phrs.2021.105463
- Rubenstein, R., Sharma, D. R., Chang, B., Oumata, N., Cam, M., Vaucelle, L., et al. (2019). Novel mouse tauopathy model for repetitive mild traumatic brain injury: Evaluation of long-term effects on cognition and biomarker levels after therapeutic inhibition of tau phosphorylation. *Front. Neurol.* 10, 124. doi:10.3389/fneur.2019.00124

- Salado, I. G., Redondo, M., Bello, M. L., Perez, C., Liachko, N. F., Kraemer, B. C., et al. (2014). Protein kinase ck-1 inhibitors as new potential drugs for amyotrophic lateral sclerosis. *J. Med. Chem.* 57, 2755–2772. doi:10.1021/jm500065f
- Schitteck, B., and Sinnberg, T. (2014). Biological functions of casein kinase 1 isoforms and putative roles in tumorigenesis. *Mol. Cancer* 13, 231. doi:10.1186/1476-4598-13-231
- Schwab, C., Demaggio, A. J., Ghoshal, N., Binder, L. I., Kuret, J., and Mcgeer, P. L. (2000). Casein kinase 1 delta is associated with pathological accumulation of tau in several neurodegenerative diseases. *Neurobiol. Aging* 21, 503–510. doi:10.1016/s0197-4580(00)00110-x
- Shang, J., Lu, S., Jiang, Y., and Zhang, J. (2016). Allosteric modulators of Mek1: Drug design and discovery. *Chem. Biol. Drug Des.* 88, 485–497. doi:10.1111/cbdd.12780
- Shen, C., Li, B., Astudillo, L., Deutscher, M. P., Cobb, M. H., Capobianco, A. J., et al. (2019). The CK1 α activator pyrrinium enhances the catalytic efficiency (kcat/Km) of CK1 α . *Biochemistry* 58, 5102–5106. doi:10.1021/acs.biochem.9b00891
- Thorne, C. A., Hanson, A. J., Schneider, J., Tahinci, E., Orton, D., Cselenyi, C. S., et al. (2010). Small-molecule inhibition of Wnt signaling through activation of casein kinase 1 α . *Nat. Chem. Biol.* 6, 829–836. doi:10.1038/nchembio.453
- To, C., Jang, J., Chen, T., Park, E., Mushajiang, M., De Clercq, D. J. H., et al. (2019). Single and dual targeting of mutant egfr with an allosteric inhibitor. *Cancer Discov.* 9, 926–943. doi:10.1158/2159-8290.CD-18-0903
- Wager, T. T., Chappie, T., Horton, D., Chandrasekaran, R. Y., Samas, B., Dunn-Sims, E. R., et al. (2017a). Dopamine D3/D2 receptor antagonist pf-4363467 attenuates opioid drug-seeking behavior without concomitant D2 side effects. *ACS Chem. Neurosci.* 8, 165–177. doi:10.1021/acschemneuro.6b00297
- Wager, T. T., Galatsis, P., Chandrasekaran, R. Y., Butler, T. W., Li, J., Zhang, L., et al. (2017b). Identification and profiling of A selective and brain penetrant radioligand for *in vivo* target occupancy measurement of casein kinase 1 (Ck1) inhibitors. *ACS Chem. Neurosci.* 8, 1995–2004. doi:10.1021/acschemneuro.7b00155
- Wakeman, D. R., Weed, M. R., Perez, S. E., Cline, E. N., Viola, K. L., Wilcox, K. C., et al. (2022). Intrathecal amyloid-beta oligomer administration increases tau phosphorylation in the medial temporal lobe in the african green monkey: A nonhuman primate model of alzheimer's disease. *Neuropathology Appl. Neurobiol.* 48 (4), e12800. doi:10.1111/nan.12800
- Walter, J., Fluhrer, R., Hartung, B., Willem, M., Kaether, C., Capell, A., et al. (2001). Phosphorylation regulates intracellular trafficking of beta-secretase. *J. Biol. Chem.* 276, 14634–14641. doi:10.1074/jbc.M011116200
- Walter, J., Grunberg, J., Schindzielorz, A., and Haass, C. (1998). Proteolytic fragments of the alzheimer's disease associated presenilins-1 and -2 are phosphorylated *in vivo* by distinct cellular mechanisms. *Biochemistry* 37, 5961–5967. doi:10.1021/bi971763a
- Wegmann, S., Biernat, J., and Mandelkow, E. (2021). A current view on tau protein phosphorylation in alzheimer's disease. *Curr. Opin. Neurobiol.* 69, 131–138. doi:10.1016/j.conb.2021.03.003
- Wright, C. J. M., and McCormack, P. L. (2013). Trametinib: First global approval. *Drugs* 73, 1245–1254. doi:10.1007/s40265-013-0096-1
- Wu, P., Clausen, M. H., and Nielsen, T. E. (2015). Allosteric small-molecule kinase inhibitors. *Pharmacol. Ther.* 156, 59–68. doi:10.1016/j.pharmthera.2015.10.002
- Wylie, A. A., Schoepfer, J., Jahnke, W., Cowan-Jacob, S. W., Loo, A., Furet, P., et al. (2017). The allosteric inhibitor Abl001 enables dual targeting of bcr-abl1. *Nature* 543, 733–737. doi:10.1038/nature21702
- Xu, R. M., Carmel, G., Kuret, J., and Cheng, X. D. (1996). Structural basis for selectivity of the isoquinoline sulfonamide family of protein kinase inhibitors. *Proc. Natl. Acad. Sci. U. S. A.* 93, 6308–6313. doi:10.1073/pnas.93.13.6308
- Yang, L. L., Li, G. B., Yan, H. X., Sun, Q. Z., Ma, S., Ji, P., et al. (2012). Discovery of N6-phenyl-1h-pyrazolo[3, 4-D]Pyrimidine-3, 6-diamine derivatives as novel Ck1 inhibitors using common-feature pharmacophore model based virtual screening and hit-to-lead optimization. *Eur. J. Med. Chem.* 56, 30–38. doi:10.1016/j.ejmech.2012.08.007
- Yasojima, K., Kuret, J., Demaggio, A. J., Mcgeer, E., and Mcgeer, P. L. (2000). Casein kinase 1 delta mrna is upregulated in alzheimer disease brain. *Brain Res.* 865, 116–120. doi:10.1016/s0006-8993(00)02200-9
- Yuan, J., Amin, P., and Ofengeim, D. (2019). Necroptosis and ripk1-mediated neuroinflammation in cns diseases. *Nat. Rev. Neurosci.* 20, 19–33. doi:10.1038/s41583-018-0093-1
- Zhou, M., Gresack, J., Cheng, J., Uryu, K., Brichta, L., Greengard, P., et al. (2020). CK1 δ over-expressing mice display ADHD-like behaviors, frontostriatal neuronal abnormalities and altered expressions of ADHD-candidate genes. *Mol. Psychiatry* 25, 3322–3336. doi:10.1038/s41380-018-0233-z
- Zhou, M., Rebholz, H., Brocia, C., Warner-Schmidt, J. L., Fienberg, A. A., Nairn, A. C., et al. (2010). Forebrain overexpression of Ck1delta leads to down-regulation of dopamine receptors and altered locomotor activity reminiscent of adhd. *Proc. Natl. Acad. Sci. U. S. A.* 107, 4401–4406. doi:10.1073/pnas.0915173107



OPEN ACCESS

EDITED BY
Andrea Venerando,
University of Padua, Italy

REVIEWED BY
Alison Axtman,
University of North Carolina at Chapel
Hill, United States
Chandrika Gowda,
College of Medicine, Pennsylvania State
University, United States

*CORRESPONDENCE
Andrea Baier,
andrea.baier@kul.pl
Ryszard Szyszka,
szyszkar@kul.pl

SPECIALTY SECTION
This article was submitted to Molecular
Diagnostics and Therapeutics,
a section of the journal
Frontiers in Molecular Biosciences

RECEIVED 08 April 2022
ACCEPTED 02 August 2022
PUBLISHED 06 October 2022

CITATION
Baier A and Szyszka R (2022), CK2 and
protein kinases of the CK1 superfamily
as targets for
neurodegenerative disorders.
Front. Mol. Biosci. 9:916063.
doi: 10.3389/fmolb.2022.916063

COPYRIGHT
© 2022 Baier and Szyszka. This is an
open-access article distributed under
the terms of the [Creative Commons
Attribution License \(CC BY\)](#). The use,
distribution or reproduction in other
forums is permitted, provided the
original author(s) and the copyright
owner(s) are credited and that the
original publication in this journal is
cited, in accordance with accepted
academic practice. No use, distribution
or reproduction is permitted which does
not comply with these terms.

CK2 and protein kinases of the CK1 superfamily as targets for neurodegenerative disorders

Andrea Baier* and Ryszard Szyszka*

Institute of Biological Sciences, The John Paul II Catholic University of Lublin, Lublin, Poland

Casein kinases are involved in a variety of signaling pathways, and also in inflammation, cancer, and neurological diseases. Therefore, they are regarded as potential therapeutic targets for drug design. Recent studies have highlighted the importance of the casein kinase 1 superfamily as well as protein kinase CK2 in the development of several neurodegenerative pathologies, such as Alzheimer's disease, Parkinson's disease, Huntington's disease, and amyotrophic lateral sclerosis. CK1 kinases and their closely related tau tubulin kinases as well as CK2 are found to be overexpressed in the mammalian brain. Numerous substrates have been detected which play crucial roles in neuronal and synaptic network functions and activities. The development of new substances for the treatment of these pathologies is in high demand. The impact of these kinases in the progress of neurodegenerative disorders, their bona fide substrates, and numerous natural and synthetic compounds which are able to inhibit CK1, TTBK, and CK2 are discussed in this review.

KEYWORDS

neurodegenerative diseases, CK1, CK2, phosphorylation, TTBK, inhibitors

Introduction

Due to the fact that the world population is getting progressively older, the risk of neurodegenerative disorders (NDDs) is increasing. Those disorders occur when neurons lose their structure and function which finally leads to their death. Noteworthy, by 2000 it was estimated that the number of patients suffering from dementia in developed countries reached 13.5 million and will rise up to 36.7 million in 2050 (Zheng and Chen, 2022). Alzheimer's disease (AD) and Parkinson's disease (PD) are the most prevalent NDDs worldwide.

NDDs are classified according to their major clinical symptoms, altered proteins, and cellular/subcellular pathology. On the molecular level, typical features include protein misfolding and the formation of protein aggregates. The exact mechanisms for that are still unknown. These aggregates are the result of protein modification, like phosphorylation, sumoylation, and ubiquitination (Kovacs et al., 2010).

Typical characteristics of AD are senile plaques of amyloid-beta (A β) peptide precipitated in the space between neurons and the neurofibrillary tangles (NFTs) of fibrillar hyperphosphorylated tau protein (Glennier and Wong, 1984; Grundke-Iqbal et al.,

1986). The A β peptide is the product of the proteolytic cleavage by β - and γ -secretases of the amyloid precursor protein (APP) (Vassar et al., 1999). In AD patients typical clinical features are the progressive loss of mental abilities, e.g., increasing forgetfulness, changes in personality, and cognitive difficulties. Additionally, as result of an immune response in the brain, nerve cells lose their function and die.

Huntington's disease (HD) is caused by an autosomal dominant genetic defect. Mutations in the *huntingtin* gene (HTT) encoding huntingtin are responsible for the onset of HD. Typical features of this disease are movement disorders, like chorea and loss of coordination, as well as cognitive decline. Furthermore, common psychiatric symptoms are psychosis, depression, and obsessive-compulsive disorder (Rosenblatt, 2007). In HD patients a degeneration of the striatum and general shrinkage of the brain can be observed (Reiner et al., 1988). Loss of cortical mass is regionally selective and proceeds from posterior to anterior cortical regions during HD progression. Other symptoms are weight loss, cardiac failure, and skeletal-muscle wasting (Arenas et al., 1998; Aziz et al., 2008).

PD is a neurodegenerative disease characterized by progressive loss of neuromelanin containing dopaminergic neurons in the substantia nigra pars compacta. There is evidence for the relation between a small volume of this brain region and the weaker or less controlled motor movements of PD patients resulting in the often observed tremors (Menke et al., 2010). The pathological picture of PD includes motor impairments, like resting tremors, bradykinesia, postural instability, and rigidity. Due to the loss of norepinephrine non-movement related symptoms, like psychiatric problems, low blood pressure, and constipation, are seen. The cause of PD might be a combination of environmental and genetic factors.

Amyotrophic lateral sclerosis (ALS) is a fast progressive NDD affecting lower and upper neurons in the brain stem, spinal cord, and the motor cortex (Robberecht and Philips, 2013). It is the most common motor neuron disease in adults and the third most NDD worldwide (Renton et al., 2013). Typical features of ALS are atrophy and paralysis of skeletal muscles resulting from neuron loss and lack of communication between voluntary muscles of the body and the nervous system. Besides these symptoms, in most cases also cognitive and behavioral dysfunctions are present. ALS patients generally die within 3–5 years after first symptoms (Regal et al., 2006). The great majority of cases are classified as sporadic ALS, whereas only 10% are familial. Abnormal aggregations of transactive response DNA-binding protein 43 (TDP-43) are detected in almost all ALS cases (Neumann et al., 2006; Mackenzie et al., 2010). Mutations in the *TARDBP* gene encoding TDP-43 are associated with ALS (Sreedharan et al., 2008).

Protein kinases are encoded by about 2% of all human genes and are capable of phosphorylating up to 20% of all proteins. The counterplay of protein kinases and phosphatases regulates many

processes in living cells through modification of serine, threonine and tyrosine residues (Hunter, 1995, 2012; Cohen, 2002; Schwartz and Murray, 2011; Nishi et al., 2014). As a result of phosphorylation protein activities, their stability, localization and interaction with other proteins are controlled. This posttranslational modification is capable of changing protein functions either by allosteric interaction or binding to regulatory domains (Jin and Pawson, 2012; Ardito et al., 2017). It has an important impact on processes, such as DNA replication, transcription and translation, cell metabolism, apoptosis, as well as stress and immunological response (Hunter, 1995; Cohen, 2002; Tarrant and Cole, 2009; Karve and Cheema, 2011). Proteins mainly undergo phosphorylation in the cytosol or in the nucleus (Duan and Walther, 2015).

Currently, there are no drugs available which cure or prevent NDDs, only acute disorders and symptoms are treated.

Numerous protein kinases have been described to play an important role in NDDs (Benn and Dawson, 2020). Unfortunately, most kinase inhibitors are not able to cross the blood-brain-barrier and are, therefore, only suitable for non central nervous disorders. During last decades, there is an increasing interest in the field to develop brain penetrant kinase inhibitors using the approaches from cancer research.

CK2 and protein kinases of the CK1 superfamily

Human protein kinases have been divided into 10 groups, 9 of them contain an eukaryotic kinase domain (ePK) and the last group is classified as atypical kinases. The majority of protein kinases phosphorylate serine and threonine residues (Ser/Thr kinases), others phosphorylate tyrosine (Tyr kinases). Few kinases are able to modify all three amino acids (dual-specificity kinases). Eukaryotic protein kinases share similarities in the primary sequences and structural features (Hanks and Hunter, 1995; Taylor et al., 1995; Taylor and Kornev, 2011).

CK1 isoforms together with the closely related vaccinia-related kinases (VRKs) and tau tubulin kinases (TTBKs) are classified in a separated group within the Ser/Thr kinase superfamily, whereas CK2 isoforms constitute a subclass of the CMGC group (Knippschild et al., 2005; Perez et al., 2011; Venerando et al., 2014; Fulcher and Sapkota, 2020). Protein kinases of the CK1 group and CK2 completely differ in their structure. At the beginning, they were named according to the phosphorylated *in vitro* protein substrate, casein. They were purified for the first time from soluble extracts of lactating bovine mammary (Waddy and Mackinlay, 1971). Natively isolated enzymes were purified on DEAE-cellulose and called casein kinase 1 and 2 depending on their elution profile (Hathaway and Traugh, 1979). G-CK or Fam20C shows high similarity to the casein kinase found in lactating mammary

glands. It has been found in rat liver and brain and phosphorylates casein in the Golgi bodies (Bingham and Farrel, 1974; Lasa et al., 1997). Fam20C is characterized as a secretory kinase phosphorylating secreted proteins, from milk to bone proteins. This is important in the process of biomineralization of bones and teeth (Tagliabracci et al., 2015).

The role of CK1 in NDDs

CK1 is an evolutionarily conserved and ubiquitously expressed protein kinase. It belongs to second-messenger-independent and constitutively active kinases. CK1 exists in monomeric form with seven isoforms (α , β , γ 1, γ 2, γ 3, δ , and ϵ) and their alternative splicing forms, which are encoded by different genes (Fulcher and Sapkota, 2020). The CK1 isoforms differ in their kinase activities, functions, subcellular localization, and biochemical properties (Zhang et al., 1996; Burzio et al., 2002; Takano et al., 2004; Xu et al., 2019). They vary in their molecular weights between 37 and 51 kDa with CK1 α being the smallest and CK1 γ 3 the largest protein. The analysis of the substrate specificity of CK1 isoforms initially determined pS/pT-X₁₋₂-S/T as their consensus sequence. This led to the assumption that phosphorylation by CK1 depends on the prior phosphorylation of position -2 or -3 (Meggio et al., 1991; Meggio et al., 1992). Further studies have shown that this hypothesis did not hold true when proteins were efficiently phosphorylated without prephosphorylated residues (Flotow and Roach, 1991; Marin et al., 1994; Pulgar et al., 1999). Later, novel substrates were described containing a non-canonical motif (S-L-S) with acidic residues downstream of the phosphorylation site. Over 140 substrates are described for CK1. Most of them are involved in various cell processes, e.g., membrane transport and trafficking, microtubule-associated dynamics, apoptosis, and cell cycle progression (Yang et al., 2017; Xu et al., 2019). In diverse studies the important role of CK1 in NDDs was shown, emphasizing on tauopathies, such as AD. A distribution study of all CK1 isoforms comparing AD and control brains revealed that CK1 can be found in fibrillar lesions and, additionally, within the matrix of granulovacuolar degeneration bodies (Ghoshal et al., 1999; Kannanayakal et al., 2006). Contrary to CK1 α which is linked to fibrillar lesions, CK1 δ is linked to granulovacuolar degeneration bodies (Kannanayakal et al., 2006). It is possible that alteration of CK1 δ function is aligned with dysregulation of circadian rhythms in AD. Elevated expression levels of CK1 δ (33-fold) and CK1 ϵ (9-fold) has been described in AD post-mortem brain tissue and ALS (Ghoshal et al., 1999; Yasojima et al., 2000; Salado et al., 2014; Palomo et al., 2020; Carter et al., 2021). Many proteins related to neurological disorders are modified by CK1 α , e.g., β -secretase (Walter et al., 2001), α -synuclein (Mbefo et al., 2015), and parkin (Yamamoto et al., 2005). Similarly, it has been discovered that CK1 δ phosphorylates several proteins that are associated with

different NDDs *in vitro*. CK1 δ phosphorylates the tau protein leading to its aggregation and finally the formation of neurofibrillary tangles (Li et al., 2004). Increased CK1 activity is associated with tau aggregation (Schwab et al., 2000). CK1 δ -dependent phosphorylation has been also shown for other proteins connected with neurodegenerative diseases, e.g., presenilin-2, β -secretase, parkin, TDP43, α -synuclein, LRRK2, and tau (Okochi et al., 2000; Walter, 2000; Rubio de la Torre et al., 2009; Alquezar et al., 2016; Nonaka et al., 2016; Morales-Garcia et al., 2017; De Wit et al., 2018). Therefore, inhibition of CK1 δ/ϵ has been described to possess favorable effects on ALS, frontotemporal dementia (FTD), and PD phenotypes *in vivo* (Perez et al., 2011; Salado et al., 2014; Alquezar et al., 2016; Cozza and Pinna, 2016; Jiang et al., 2018; Palomo et al., 2020).

The role of TTBK in NDDs

Within the CK1 superfamily a small family of brain-specific kinases phosphorylating microtubule-associated proteins tau and tubulin is classified (Ikezu and Ikezu, 2014). TTBK is a Ser/Thr and Tyr dual-kinase conducting multiple functions inside the cell. It comprises two isoforms: TTBK1 and TTBK2. TTBK1 was characterized as a neuron-specific kinase phosphorylating tau which leads to its aggregation, while TTBK2 was purified from the bovine brain (Takahashi et al., 1995; Sato et al., 2006). Both isoforms are encoded by distinctive genes, and furthermore, their localization in tissues is diverse (Nozal and Martinez, 2019). The sequence of TTBK1, consisting of 1321 amino acids, can be divided into kinase domain (residues 34-297), and a regulatory domain, which contains a characteristic 39 amino acids poly-Glu motif (Ikezu and Ikezu, 2014). The comparison of the TTBK1 and CK1 δ kinase domain sequences revealed a 38% identity and 52% similarity (Sato et al., 2006). TTBK1 is primarily expressed in the human brain, notably in the adult brain cortex, cerebellum, and fetal brain. When mouse brain was analysed, TTBK1 was also detected in the frontal cortical layers, the hippocampus, and the granular layer of the cerebellum. Studies using antibodies confirmed the colocalization with tubulin in neurons (Sato et al., 2006). TTBK1 is upregulated in AD cases (Takashima et al., 1993).

TTBK2 consists of 1244 amino acids, and contrary to TTBK1, is ubiquitously expressed in the whole body. Highest TTBK2 mRNA expression levels are monitored in cerebellum Purkinje cells, granular cell layer, hippocampus, midbrain, and substantia nigra, whereas lower levels were found in the cortex of human, rat, and mouse brains (Houlden et al., 2007). In analyses of the protein expression in the brain and testis higher amounts of TTBK2 were found which correlates with higher activities of TTBK2 in these tissues (Bouskila et al., 2011). Mutations in the TTBK2 gene are responsible for the onset of spinocerebellar ataxia type 11, an NDD characterized by progressive ataxia and atrophy of the cerebellum and brainstem.

Both isoforms contain highly similar catalytic domains (88% identity and 96% similarity), but diverse C-terminal domains of 43% identity and 58% similarity (Ikezu and Ikezu, 2014; Nozal and Martinez, 2019). TTBK1/2 were described as kinases which show higher phosphorylation activity in case of a prephosphorylated substrate at position -3 (S/T-X-X-S/T/Y). On the surface of TTBK1 two positive sequences have been identified, which might act as putative binding sites for the prephosphorylated substrate (Xue et al., 2013; Kosten et al., 2014). Phosphorylation of tau was shown at Y197, S198, S199, S202, and S422, the critical sites in paired helical filaments (Grundke-Iqbal et al., 1986; Sato et al., 2006; Tomizawa et al., 2001). Interestingly, both isoforms differ in the aa sites which they phosphorylate. Due to tau phosphorylation in neurons at S422, TTBK1 is responsible for neurofibrillary pretangle formation and subsequent tau aggregation (Sato et al., 2008; Vazquez-Higuera et al., 2011; Yu et al., 2011; Lund et al., 2013). In knock-down experiments it has been demonstrated that TTBK1, not TTBK2, is the main isoform responsible for tau phosphorylation at S422 (Bao et al., 2021). Overexpression of TTBK1 in mice resulted in increased phosphorylation and oligomerization of tau in the brain (Xu et al., 2010).

Besides the phosphorylation of tau and tubulin by TTBK2, further substrates include centrosomal proteins CEP164 and CEP97, SV2A as well as neurodegeneration-associated protein TDP-43 (Takahashi et al., 1995; Tomizawa et al., 2001; Ikezu and Ikezu, 2014; Liachko et al., 2014; Liao et al., 2015; Zhang et al., 2015). Additionally, TTBK2 is crucial for the regulation of the growth of axonemal microtubules in ciliogenesis (Liao et al., 2015).

Especially TTBK1 is a promising candidate as target for NDDs treatment. It is mainly expressed in brain tissue, and therefore, possesses limited off-pathway roles. The phosphorylation of tau and TDP-43 makes it an ideal kinase in the case of these two proteinopathies.

The role of CK2 in NDDs

Together with CK1, CK2 was identified as phosphotransferase using casein as protein substrate for enzymes able to catalyze phosphate transfer from ATP to proteins (Burnett and Kennedy, 1954). Native protein kinase CK2 exists as a heterotetrameric holoenzyme consisting of two catalytic subunits, α and α' , and a dimer of regulatory subunits β (Hathaway and Traugh, 1979). The two isoforms of the CK2 catalytic subunit are highly homologous, but they are products of two different genes (Wirkner et al., 1994; Yang-Feng et al., 1994; Ackermann et al., 2005). CK2 subunits may build different active holoenzymes in three different conformations ($\alpha\alpha'$, α_2 , or α'_2) or exist as free catalytic subunits. Each CK2 isoform possesses characteristics common for CK2, but differences in their substrate specificity and sensitivity to inhibitors have been

described. They may also regulate different cellular processes (Pinna, 2002; Domańska et al., 2005; Janeczko et al., 2012).

CK2 is a constitutively active protein kinase, independent from second messengers, and is able to use both, ATP and GTP, as phosphoryl donors (Litchfield, 2003). Analysis of the eukaryotic phosphoproteome revealed that CK2 is responsible for the phosphorylation of almost one-quarter of phosphoproteins (Meggio and Pinna, 2003; Salvi et al., 2009; Franchin et al., 2015).

The minimal consensus sequence of CK2 was estimated as S/T-X-X-D/E/pS/pY, which is present in numerous proteins (Meggio et al., 1994; Venerando et al., 2014).

After the detection of the critical role in various disease states, like cancers and neurodegenerative disorders research groups worldwide focussed their attention on CK2 as a potential therapeutic target (Blanquet, 2000; Perez et al., 2011; Castello et al., 2017; Borgo et al., 2021a).

Several CK2 targets in NDDs were described. α -synuclein is phosphorylated at S129 that leads to aggregates which are the main component of Lewy bodies. In 90% of PD samples this phosphorylation is found, whereas in only 4% of normal tissue. As shown, this site is affected by several kinases and dependent on which one the biological effects might differ (Oueslati, 2016).

In different reports the diverse role of CK2 in AD is described. CK2 phosphorylates presenilin-2 at S7 and S9 *in vitro* while not altering APP cleavage by γ -secretase (Walter et al., 1996; Sannerud et al., 2016). Additionally, it was shown that CK2 phosphorylates SET, a phosphatase PP2A inhibitor, at position S9 which leads to its translocation to the cytoplasm (Zhang et al., 2018).

Numerous reports reveal that CK2 possesses a protective role in HD. The phosphorylation of huntingtin at S13 and S16 alters its location. Phospho-huntingtin is found in the nucleus which reduces its cellular toxicity (Atwal et al., 2011). Similarly, TDP-43 phosphorylation may prevent protein aggregation of truncated forms (Li et al., 2011).

Proteins involved in neurodegenerative diseases

A lot of NDD-associated proteins playing an important role in the onset of these disorders were identified (Kovacs et al., 2010): (1) the tubulin-associated unit (tau) protein; (2) amyloid- β (A β), peptides which result from cleavage of a large transmembrane precursor protein (A β -precursor protein or APP); (3) α -synuclein; (4) prion protein; (5) TDP-43 (Ou et al., 1995); (6) fused in sarcoma protein, Ewing's sarcoma RNA-binding protein 1, and TATA-binding protein-associated factor 15, also known as FET proteins (Neumann et al., 2011). Other proteins are associated with neurological disorders caused by mutations leading to trinucleotide repeats (e.g., huntingtin, ataxins, atrophin-1).

TABLE 1 Selected proteins involved in neurodegenerative diseases and their phosphomodifications by casein kinases.

Protein	Disease	Protein kinase	Phosphorylated residue	References
α -synuclein	Parkinson's disease, Alzheimer's disease, Lewy Body Dementia	CK1 δ	S87, S129	Okochi et al. (2000)
		CK2	S129	Okochi et al. (2000); Fujiwara et al. (2002); Ishii et al. (2007); Paleologou et al. (2008); Waxman and Giasson, (2008); Xu et al. (2015)
Amyloid-beta precursor protein (APP)	Parkinson's disease, Alzheimer's disease	CK1 δ/ϵ , CK2	S198, S206	Walter et al. (2000); Sundaram et al. (2019)
β -Secretase	Alzheimer's disease	CK1 δ/ϵ	S498	Walter et al. (2000)
Tau protein	Alzheimer's disease, Parkinson dementia syndrome, Pick disease of the brain	CK1 δ/ϵ	T17, S46, T50, T95, T101, T102, S113, S131, T149, T169, S184, S198, S208, S210, S212, S237, S238, S262, T263, S285, S289, S293, S305, S341, S352, S356, S361, S373, S386, S396, S404, S412, S413, T414, S416, S433, S435	Chen G et al. (2017); Oliveira et al. (2017)
		TTBK1/2	Y197, S198, S199, S202, S205, S208, S210, S416, S422, T427	Tomizawa et al. (2001); Sato et al. (2006); Oliveira et al. (2017); Taylor et al. (2018); Ikezu et al. (2020)
		CK2	T39, T52, S56, S199, S386, S396, S400, S404, S412, S413, S414, S416	Hanger et al. (2007); Greenwood et al. (1994); Oliveira et al. (2017)
TDP-43	Amyotrophic lateral sclerosis (ALS), Frontotemporal lobar degeneration	TTBK1/2	S409/410	Hasegawa et al. (2008); Liachko et al. (2014); Taylor et al. (2018); Taylor et al. (2019)
		CK1 δ , CK2	S379, S403/404, S419/410	Kametani et al. (2009); Taylor et al. (2019)
Parkin	Parkinson's disease	CK1 δ	S101, S127, S378	Chakraborty et al. (2017); Yamamoto et al. (2005); Rubio Rubio de la Torre et al. (2009)
Huntingtin	Huntington's disease	CK2	S13, S16	Atwal et al. (2011)
Ataxin-3	Spinocerebellar ataxia 3 (SCA3)	CK2	S340, S352	Mueller et al. (2009)
Presenilin -2	Alzheimer's disease	CK2	S7, S9	Walter et al. (1996); Sannerud et al. (2016); Borgo et al. (2021b)
		CK1	S19	Walter et al. (1996); Sannerud et al. (2016)
I $_2$ ^{PP2A}	Alzheimer's disease	CK2	S9	Zhang et al. (2018)

Neurodegenerative proteinopathies can be classified according to the major protein involved in the disease: tauopathies, α -synucleinopathies, TDP-43 proteinopathies, FUS/FET proteinopathies, prion diseases, trinucleotide repeat diseases, neuroserpinopathy, ferritinopathy, and cerebral amyloidoses.

Several of these proteins were identified as substrates for CK1, TTBK, and CK2 and are further described below. Table 1 summarizes information about these proteins phosphorylated by CK1, TTBK, and CK2 and their respective phosphorylation sites.

α -synuclein

The name of this protein is derived from synaptic vesicles (syn-) and the nuclear envelope (-nuclein), both places where α -synuclein was first identified (Maroteaux et al., 1988). As we

know now, this was probably the effect of a contaminated antibody that was used in this study. It is involved in PD, dementia with Lewy bodies, and multiple system atrophy (Spillantini et al., 1997; Wakabayashi et al., 1997; Gai et al., 1998). α -synuclein is a ubiquitously expressed protein with the highest levels in neurons, especially in presynaptic terminals. Other localizations for α -synuclein have been also identified, mainly based on overexpression experiments, but its function there remains unclear.

α -synuclein is a protein built of 140 amino acids that undergo posttranslational modification, especially at its C-terminus, e.g., phosphorylation, oxidation, ubiquitination, acetylation, and glycosylation. The major phosphorylation sites are S87 and S129 (Okochi et al., 2000; Fujiwara et al., 2002; Ishii et al., 2007). It was also shown that tyrosine residues are phosphorylated: Y125, Y133, and Y136 (Ellis et al., 2001; Nakamura et al., 2001; Negro et al., 2002). In pathological

states, α -synuclein adopts a β -sheet conformation, which consequently leads to α -synuclein aggregation, fibril formation, and deposition into Lewy bodies (Conway et al., 1998; El-Agnaf et al., 1998; Narhi et al., 1999; Uversky, 2007; Yonetani et al., 2009). In PD, Lewy bodies, point mutations, and duplications/triplication of α -synuclein gene are the main pathological hallmark (Burré et al., 2018). Lewy bodies containing α -synuclein were also detected in samples from familial AD patients (Lippa et al., 1998). Furthermore, in senile plaques in AD a short fragment of α -synuclein (aa residues 61–95) was found and termed non-A β -amyloid component, a region that is necessary for α -synuclein aggregation and fibrillogenesis (Ueda et al., 1993). Phosphorylation prevents or at least decreases the aggregation and toxicity of α -synuclein (Waxman and Giasson, 2008). Within all identified phosphorylation sites *in vivo* and *in vitro* only S87 lies in the non-A β -amyloid component (El-Agnaf et al., 1998).

Amyloid-beta precursor protein

APP was isolated and purified from cerebral A β deposits in 1984 (Glenner and Wong, 1984). It is found in different tissues, particularly in the brain, as a type I transmembrane protein located predominantly in the endoplasmic reticulum (Zheng and Koo, 2006). In 1992, Hardy and Higgins presented the amyloid cascade hypothesis as their theory of AD pathophysiology (Hardy and Higgins, 1992). Proteases from the secretase family (β -secretase and γ -secretase) cleave APP into A β peptides of different lengths, mainly A β 38, A β 40, and A β 42, whereas α - and γ -secretases produce P3 peptides (LaFerla et al., 2007; O'Brien and Wong, 2011). Although the most abundant form is A β 40 (80%–90%), A β 42 is mainly responsible for protein aggregations and the formation of oligomers, amyloid fibrils, and amyloid plaques (Chen C et al., 2017). Those amyloid plaques are the cause of neurotoxicity in AD progression (Citron et al., 1996; Murphy and LeVine, 2010). Effects of A β 40/A β 42 aggregation, especially A β oligomers, are calcium dishomeostasis, disturbance of ion channels, alteration of glucose regulation and oxidative damage (Tiwari et al., 2019). Furthermore, it was described that A β aggregation promotes tau phosphorylation and aggregation. Out of 30 mutations described in the APP gene, 25 are involved in the deposition of insoluble A β , like KM670/671NL (Swedish), V717I (London), V717F (Indiana).

Tau protein

The tau protein was firstly discovered in porcine brain and isolated as heat-stable protein. The function of tau is the stabilization of internal microtubules (Weingarten et al., 1975). It is particularly highly expressed in axons of neuronal cells of the central nervous system (Binder et al., 1985). Studies

have shown that tau is a phosphoprotein that then negatively influences the microtubule assembly by changes of the molecule shape (Jameson et al., 1980; Lindwall and Cole, 1984). Phosphorylation of tau is often accompanied by other posttranslational modifications, e.g., O-glycosylation, ubiquitination, and methylation. Tau inclusions occur in AD, Pick's disease, progressive supranuclear palsy, corticobasal degeneration, argyrophilic grain disease, Parkinsonism-dementia complex of Guam, and FTD (Lee et al., 2001).

Tau primary transcript generates six isoforms by alternative splicing resulting in proteins of 352–441 amino acids and MW of 45–65 kDa (Boyarko and Hook, 2021). Tau protein possesses 80 S/T and 5 Y residues of which at least 46 have been found to be phosphorylated in AD (Hanger et al., 2009). The total phosphorylation level of tau in AD and other tauopathies is several times higher than in control samples (Gong and Iqbal, 2008). The ability of tau to polymerize tubulin and to promote microtubule assembly is reduced through hyperphosphorylation (Yoshida and Ihara, 1993). A correlation between the level of hyperphosphorylation at multiple sites and the severity of NFT pathology was found which also correlates with the degree of neuronal loss and cognitive deficit (Grundke-Iqbal et al., 1986; Braak and Braak, 1991; Augustinack et al., 2002).

TDP-43

TDP-43 is a ubiquitous protein belonging to the ribonucleoprotein family and is normally localized in the nucleus where it takes part in RNA regulation (Nakielnny and Dreyfuss, 1997; Geuens et al., 2016). Firstly, it was identified as a transcriptional repressor of HIV-1 transactivator response (TAR) long terminal repeats (Ou et al., 1995). Later, it was demonstrated that it is the major component of ubiquitinated inclusions in ALS and frontotemporal lobar degeneration (FTLD). Posttranslational modifications, such as cleavage, hyperphosphorylation, and ubiquitination lead to cytoplasmic accumulation and aggregation of TDP-43 (Arai et al., 2006; Neumann et al., 2006; Hasegawa et al., 2008). The sequence of TDP-43 is divided into three parts: an N-terminal domain (residues 1–103), two RNA recognition motifs (residues 104–200 and 191–262), and a C-terminal domain (residues 274–413). TDP-43 possesses 64 potential phosphorylation sites. Phosphorylation at S403/404 and S409/410 at the C-terminus results in pathological inclusions (Hasegawa et al., 2008; Inukai et al., 2008; Zhang et al., 2009). The N-terminus contains a nuclear localization sequence that is prone to mutations leading to cytoplasmic localization of TDP-43 and aggregation, whereas the C-terminus is necessary for solubility and cellular localization (Ayala et al., 2008; Barmada et al., 2010).

Parkin

Parkin possesses an activity of an E3 ubiquitin ligase (Shimura et al., 2000). Insoluble parkin, resulting from point mutations, plays a major role in the inactivation of the protein in PD (Cookson et al., 2003; Sriram et al., 2005; Hampe et al., 2006). Phosphorylation of S101, S127, and S378 was identified using CK1 *in vitro* and *in vivo* with HEK293T cells transiently transfected with parkin (Yamamoto et al., 2005; Rubio de la Torre et al., 2009). Treatment of those cells with IC261, a selective CK1 inhibitor, significantly decreased the phosphorylation level of parkin (Mashhoon et al., 2000; Bain et al., 2007; Rubio de la Torre et al., 2009). Another potent CK1 inhibitor, D4476, was used, which confirmed the hypothesis that S101 and S378 are phosphorylated *in vivo*. Besides CK1, parkin is phosphorylated by CDK5 at S121 (Avraham et al., 2007). Experiments *in vivo* and *in vitro* have shown that the interplay of CK1 and CDK5 is necessary for efficient phosphorylation by both kinases. A phospho-mimetic mutant on the phosphorylation site of one kinase increased the phosphorylation level by the second kinase. Supporting evidence is the finding that roscovitine, a selective CDK5 inhibitor, reduced the phosphorylation of parkin by CK1 resulting from inhibition of S121 phosphorylation (Meijer et al., 1997; Rubio de la Torre et al., 2009). In further experiments, the influence of parkin phosphorylation on its activity and its effect on the formation of inclusions was examined. The results indicate that the phospho-mimetic mutant for compound phosphorylation possesses slightly enhanced enzymatic activity and showed a significantly higher tendency for aggregation (Rubio de la Torre et al., 2009).

Huntingtin

Huntingtin is a ubiquitously expressed protein with a molecular weight of 350 kDa. It possesses a poly-Glu sequence at the N-terminus containing up to 35 CAG repeats in wild-type, whereas HD patients carry 36 or more repeats (Rubinstein et al., 1996). There is evidence for an inverse correlation between the age of onset of symptoms and the number of CAG repeats (Andrew et al., 1993). In 65%–71% of cases, larger CAG repeats led to earlier ages of onset. Genetic and environmental factors are also playing an important role in the age of onset. Huntingtin is localized in the cytoplasm, partially in the nucleus. Its nuclear localization sequence is also found in the N-terminus and in the C-terminus a nuclear export sequence is found (Xia et al., 2003; Desmond et al., 2012). The prolonged poly-Glu sequence in HD patients inhibits the interaction between the N-terminus with the nuclear pore protein translocated promotor region which is involved in nuclear export. As a result, huntingtin is accumulated in the nucleus (Cornett et al., 2005). Noteworthy, toxic fragments of huntingtin present in the nucleus are mainly from the mutated protein due to their higher concentration in the nucleus than in the cytoplasm (Hackam et al., 1998; Lunkes et al., 2002). One therapeutic strategy is the inhibition of the formation of these

fragments by modification of huntingtin (e.g., phosphorylation) to prevent the cleavage of the protein (Atwal et al., 2011).

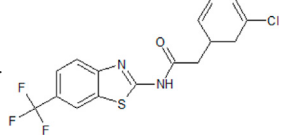
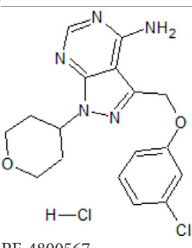
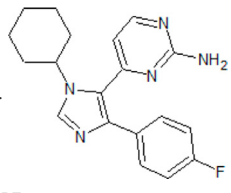
Ataxin-3

Ataxin-3 is a ubiquitin protease involved in transcriptional regulation and the disease protein in spinocerebellar ataxia type 3 (Burnett et al., 2003; Evert et al., 2006). It possesses nuclear and cytoplasmic functions. Its subcellular distribution is regulated through phosphorylation. As in the case of huntingtin, the nuclear presence of ataxin-3 represents a key element in the accumulation of toxic fragments (Bichelmeier et al., 2007). Analysis of 15 putative serine phosphorylation site mutants revealed that S236 in the first ubiquitin-interacting motif (UIM), S256 and S260/261 in the second UIM, as well as S340 and S352 in the third UIM, are the major phosphorylation sites of CK2 (Mueller et al., 2009). Phosphorylation of those serines determines the subcellular location of ataxin-3. Modulation of S340, S352, and S236 increases the nuclear presence of ataxin-3, while phosphorylation of S256 and S260/261 provides preferential cytoplasmic localization (Mueller et al., 2009). Apart from the influence on the cellular distribution of ataxin-3, phosphorylation plays also an important role in the solubility of the protein. As shown *in vivo* experiments phospho-mimetic mutants formed aggregates in the nucleus (Mueller et al., 2009). The effect of two selective CK2 inhibitors (DMAT and TBB) on the localization and presence of inclusions was examined in cell culture (Pagano et al., 2008). Inhibition of CK2 resulted in lower nuclear localization of ataxin-3 and less formation of protein aggregates (Mueller et al., 2009).

Presenilin-2

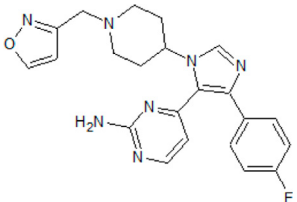
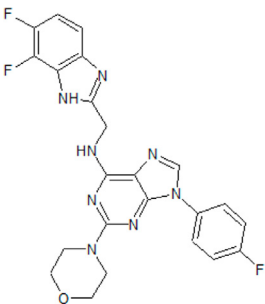
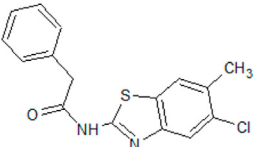
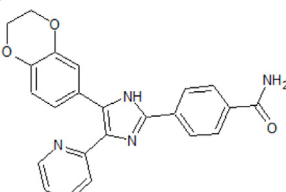
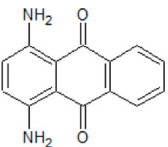
PSEN1 and *PSEN2* genes, containing 10 exons, encode presenilin-1 and presenilin-2, respectively, which play important roles in AD pathogenesis. Presenilin is a part of the γ -secretase complex responsible for the cleavage of APP to generate A β peptides. Mutations in *PSEN1/2* and deletions leading to alternative transcripts are associated with AD and FTD (Raux et al., 2000; Evin et al., 2002; Marcon et al., 2009). Incorrect transcripts, like *PS2V* lacking exon 6, are related to different diseases, e.g., AD (Braggin et al., 2019). *PS2V* produces truncated presenilin-2 containing 124 amino acids and only 1 of 9 transmembrane domains. This isoform was identified in the brain of AD patients with elevated levels leading to an increased amount of A β peptide (Sato et al., 1999; Smith et al., 2004). Two phosphorylation sites for CK2 (S7 and S9) and one for CK1 (S19) were identified (Walter et al., 1996). S19 phosphorylation elevated the binding of AP-1 protein to presenilin-2, whereas S7 and S9 phosphorylation did not show any change in the

TABLE 2 Inhibitors of CK1, TTBK, and CK2.

Inhibitor name and structure	Biological activity	References
CK1 inhibitors		
 IGS-2.7	<ul style="list-style-type: none"> - heterocyclic, central nervous system (CNS)-penetrating, and ATP-competitive inhibitors of CK1δ (IC₅₀ values of 23 nM and 47 nM) - selective over a 456 kinases panel - decrease of TDP-43 phosphorylation in cell culture assays - able to prolongate the <i>Drosophila</i> lifespan by inhibition of TDP-43 neurotoxicity - IGS-2.7 possesses protective activity on dopaminergic neurons induced by 6-hydroxy dopamine (6-OHDA) and reduces the lipopolysaccharide inflammatory activation in primary cell cultures of astrocytes and microglia - effect on cell proliferation, TDP-43 phosphorylation, and subcellular localization - effect on TDP-43 dependent repression of <i>CDK6</i> expression - progranulin-deficient cells treated with 5 μM IGS-2.7 led to a potent inhibition of TDP-43 phosphorylation and normalization of the abnormal cytosolic TDP-43 accumulation - expression of <i>CDK6</i> mRNA and the amount of TDP-43 was decreased by IGS-2.7 - IGS-2.7 prevented cytosolic TDP-43 accumulation in a human neuroblastoma SH-SY5Y cell model through CK1δ inhibition - able to reduce TDP-43 phosphorylation in human cells derived from FTD and ALS patients - IGS-2.7 is active in a TDP-43 transgenic mouse (A315T) model and in a human cell-based model of ALS 	Alquezar et al. (2016) ; Martínez-González et al. (2020) ; Morales-Garcia et al. (2017) ; Posa et al. (2019) ; Salado et al. (2014)
 PF-4800567	<ul style="list-style-type: none"> - selective ATP-competitive CK1ε inhibitor - higher inhibitory activity towards CK1ε than towards CK1δ with IC₅₀ values of 32 and 711 nM as well as IC₅₀ values of 2.65 and 20.38 μM in whole cells, respectively - blocks period protein 3 (PER3) nuclear localization mediated by CK1ε (0.01–10 μM) and suppresses PER2 degradation at μM - rapid absorption and distribution in the plasma and brain of mice - extension of the period for single phases of the molecular clockwork, especially the duration of PER2-mediated transcriptional feedback 	Meng et al. (2010) ; Walton et al. (2009)
 PF-670462	<ul style="list-style-type: none"> - effective and selective inhibitor of CK1ε and CK1δ (IC₅₀ values of 7.7 nM and 14 nM, respectively) - influence on the localization of the GFP signal back to the cytoplasm dependent on the inhibitor concentration, with an EC₅₀ of 290±39 nM in CK1ε-transfected COS7 cells - a potent inhibitor of the Wnt/β-catenin signaling pathway with an IC₅₀ of ~17 nM - weak inhibition of cell proliferation and only moderately inhibition of HEK293 and HT1080 cell growth (1 μM) - potential to repeal hippocampal proteomic changes in several AD-related and clock-regulated pathways, e.g., synaptic plasticity and APP cleavage - able to reverse effects of working memory deficits and lead to the improvement of disturbances in behavioral circadian rhythm - inhibition of CK1δ/ε increases the cognitive-affective behavior and inhibits the amyloid amount in the APP-PS1 mouse model of AD 	Adler et al. (2019) ; Badura et al. (2007) ; Cheong et al. (2011) ; Sundaram et al. (2019)

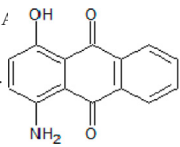
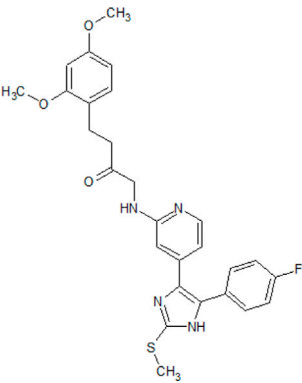
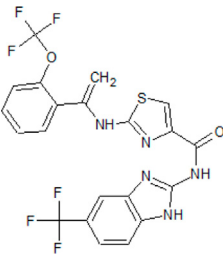
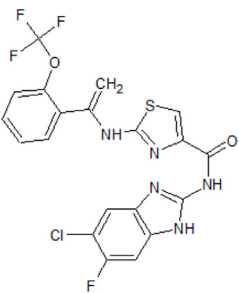
(Continued on following page)

TABLE 2 (Continued) Inhibitors of CK1, TTBK, and CK2.

Inhibitor name and structure	Biological activity	References
 <p>PF-5006739</p>	<ul style="list-style-type: none"> - possesses strong and selective potency against CK1δ and CK1ϵ in enzymatic assays (3.9 nM and 17 nM, respectively) and in whole-cell screening (EC_{50} = 15.2 and 83 nM, respectively) - in a panel of 59 kinases, only JNK2 and MAP4K6 are inhibited at a concentration of 1 μM with IC_{50} values of 6.1 and 1.5 μM, respectively - used in the treatment of several psychiatric disorders - lowers the effect on opioid drug-seeking behavior in a rodent operant reinstatement animal model dependent on the inhibitor dose - daily treatment of diet-induced obese and ob/ob mice increase expression of clock genes and improved the glucose tolerance 	Cunningham et al. (2016); Wager et al. (2014)
 <p>SR-3029</p>	<ul style="list-style-type: none"> - effective ATP-competitive CK1 inhibitor (IC_{50} values of 44 nM for CK1δ and 260 nM for CK1ϵ) - EC_{50} value below 100 nM estimated in a MTT assay against human melanoma cell line A375 - a binding assay analysis of 442 kinases showed that only CK1δ and CK1ϵ are strongly inhibited - reduction of the activities of CDK6/cyclin D3, CDK6/cyclin D1, CDK4/cyclin D3, CDK4/cyclin D1, and FLT3 (IC_{50} values between 368 and 3,000 nM) - decrease of TPA-induced skin tumor formation in carcinogen-initiated mouse skin cells, most likely by the inhibition of the Wnt/β-catenin signaling 	Bibian et al. (2013); Su et al. (2018)
 <p>LH846</p>	<ul style="list-style-type: none"> - selective, cell-permeable, ATP-site-targeting inhibitor (IC_{50} values of 290 nM, 1.3 μM and 2.5 μM for CK1δ, ϵ, and α, respectively) - inhibition of PER1 phosphorylation by CK1δ and its degradation - able to prolongate the circadian period in U2OS cells, but only minimally effects the amplitude 	Lee et al. (2011)
 <p>D4476</p>	<ul style="list-style-type: none"> - effective, reversible, and weakly specific ATP-competitive inhibitor of CK1δ and ALK5 with IC_{50} values of 0.3 and 0.5 μM, respectively - modest inhibitory activity against other kinases, including p38α MAP kinase, PKB, SGK, and GSK-3β - potently kills leukemia stem cells (LSCs) with high selectivity when compared to normal HSPCs - CK1α inhibition causes a decrease of ribosomal protein S6 phosphorylation and activates p53 resulting in the selective removal of leukemia cells - inhibition or down-regulation of CK1α, efficiently reduced glioblastoma multiforme (GBM) cell proliferation in both Tp53 wild-type and Tp53-mutant GBM cells - significant reduction of Aβ40 peptide production in N2A cells expressing APP-695 - effect towards γ-secretase cleavage activity in mammalian cells transfected with the C-terminal fragment of APP 	Flajolet et al. (2007); Järås et al. (2014); Liu et al. (2021); Rena et al. (2004)
	<ul style="list-style-type: none"> - compound 1: ATP-competitive and isoform CK1δ selective inhibitor (K_i = 125 nM) - compound 2: inhibitory activity against CK1δ (IC_{50} = 0.6 μM) - cytotoxicity of compound 1 on human ovarian carcinoma cell line 2008 (IC_{50} = 14.4 μM) and on its cisplatin-resistant clone C13 (IC_{50} = 87.9 μM) - cytotoxicity of compound 2 on human ovarian carcinoma cell 	Cozza et al. (2008)

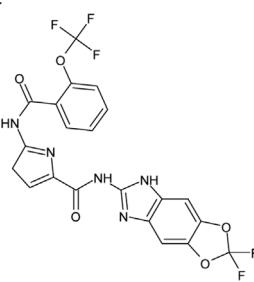
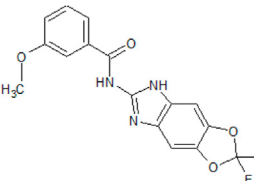
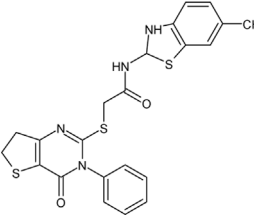
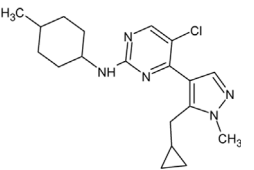
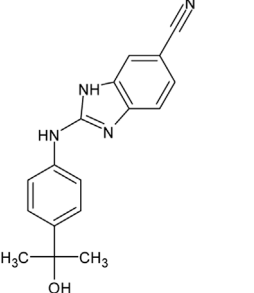
(Continued on following page)

TABLE 2 (Continued) Inhibitors of CK1, TTBK, and CK2.

Inhibitor name and structure	Biological activity	References
 Amino-antraquinone 2	<p>line 2008 ($IC_{50} = 122.4 \mu M$) and on its cisplatin-resistant clone C13 ($IC_{50} = 8.0 \mu M$)</p>	
 Compound 11b	<ul style="list-style-type: none"> - highly effective ATP-competitive inhibitor of CK1δ (IC_{50} CK1δ=4 nM, IC_{50} CK1ϵ=25 nM) - highly selective towards CK1δ when tested against more than 321 protein kinases - high efficiency against p38α MAPK with an IC_{50} value three-fold higher compared to CK1δ - inhibitory effect on human pancreatic cancer cell lines Colo357 and Panc89 (EC_{50} of 3.5 and 1.5 μM, respectively) 	Halekotte et al. (2017)
 Bischof-5	<ul style="list-style-type: none"> - potent ATP-competitive and specific inhibitors of CK1δ (IC_{50} values of 40 and 42 nM, respectively) - Bischof-5 exhibits a 5-fold higher affinity towards CK1δ than to CK1ϵ (IC_{50}=199 nM) - Bischof-6 inhibits both isoforms in similar range (IC_{50}=33 nM for CK1ϵ) - Bischof-5 is highly potent and selective towards CK1δ in a panel of 442 kinases - Bischof 5 and 6 negatively influence the proliferation of several tumor cell lines 	Bischof et al. (2012)
 Bischof-6		

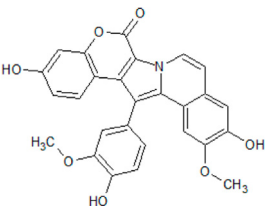
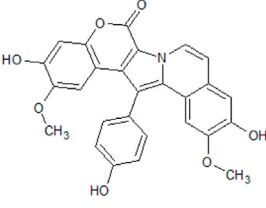
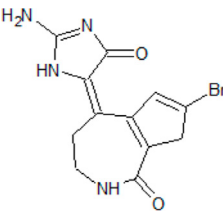
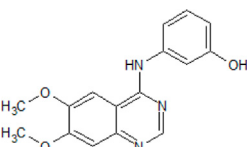
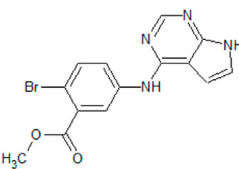
(Continued on following page)

TABLE 2 (Continued) Inhibitors of CK1, TTBK, and CK2.

Inhibitor name and structure	Biological activity	References
 <p>Compound 1</p>	<ul style="list-style-type: none"> - potent ATP-competitive and selective CK1δ/ε inhibitors (IC₅₀ values of 0.07–0.81 μM and 0.13–1.36 μM) - inhibition of growth analysed by cell viability assays and cell cycle distribution on 82 different tumor cell lines 	Richter et al. (2014)
 <p>Compound 2</p>		
 <p>IWP-2</p>	<ul style="list-style-type: none"> - ATP-competitive and CK1 specific - specifically inhibits CK1δ when compared to 320 other kinases (IC₅₀ values of 0.317 and 4 μM for CK1δ and CK1ε, respectively) - inhibition of the gatekeeper mutant^{M82F}CK1δ (IC₅₀ = 40 nM) - inhibition of the viability of various cancer cell lines 	García-Reyes et al. (2018)
 <p>BTX-A51</p>	<ul style="list-style-type: none"> - multi-kinase inhibitor (IC₅₀ values between 0.5 and 20 nM for CK1 isoforms, CDK7, and CDK9) - specifically blocks leukemic stem cell target CK1α as well as CDK7 and CDK9 preventing transcription of key oncogenic genes. - activation of p53 and its sustained stabilization by a super-enhancer shutdown of Mdm2 in combination with the transcriptional shutdown of leukemia oncogenes, including <i>Myc</i> and <i>Mcl1</i> 	Ball et al. (2020)
 <p>Compound 1h</p>	<ul style="list-style-type: none"> - highly selective and CK1 isoform-specific (IC₅₀ = 14 nM for CK1γ) - excellent selectivity over other CK1 isoforms, like CK1α (IC₅₀ = 9.18 μM) and CK1δ (IC₅₀ = 2.32 μM) - no inhibitory activity against 48 kinases including GSK3β (IC₅₀ = 60 μM) 	Hua et al. (2012)
	<ul style="list-style-type: none"> - stable in the rat and human microsomes and show good effects on cells and modest pharmacokinetic properties in rats 	

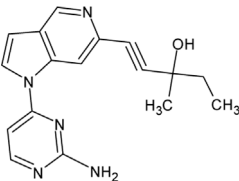
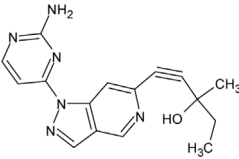
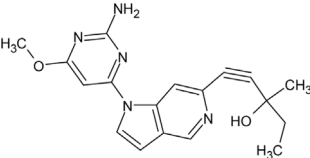
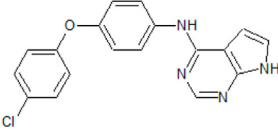
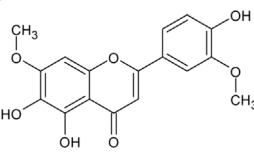
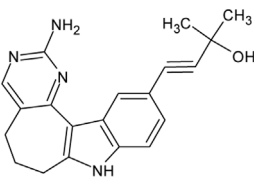
(Continued on following page)

TABLE 2 (Continued) Inhibitors of CK1, TTBK, and CK2.

Inhibitor name and structure	Biological activity	References
 <p>Lamellarin 3</p>	<p>- inhibitory activity against CK1δ and CK1ε (IC₅₀ values of 0.41 and 0.8 μM, respectively)</p>	Baunbæk et al. (2008); Iwao et al. (2011)
 <p>Lamellarin 6</p>	<p>- inhibition of other kinases (CDKs, DYRK1A, GSK3α/β, and PIM1) with IC₅₀ values from 0.06–0.6 μM</p> <p>- inhibition of cell survival of human neuroblastoma SH-SY5Y cells (IC₅₀ values of 0.56 and 0.11 μM for lamellarin 3 and 6, respectively)</p>	
 <p>Hymenialdisine</p>	<p>- inhibitory activity in nanomolar range against few AD-related protein kinases, e.g., CK1δ, GSK3β, and CDK5/p25 (IC₅₀ values of 35, 10, and 28 nM, respectively)</p> <p>- numerous kinases were inhibited only in the micromolar range, e.g., Aurora-A, Her1/2, IKKα, PKA, and PKB</p> <p>- CK1 dose-dependent inhibition of presenilin-2 phosphorylation using presenilin-2-maltose-binding protein</p> <p>- debromohymenialdisine inhibits the activities of diverse protein kinases including CK1δ, CDK5/p25, and GSK3β (IC₅₀ values of 0.1–0.4 μM)</p>	Meijer et al. (2000); Plisson et al. (2014); Wan et al. (2004); Zhang et al. (2012)
TTBK1/2 inhibitors		
 <p>AZ-1</p>	<p>- potent and selective ATP-competitive inhibitors (IC₅₀ values of 4.4 μM and 6.8 μM (AZ-1), 2.6 μM and 3.2 μM (AZ-2) for TTBK1 and TTBK2, respectively)</p> <p>- neuroprotective profile on phospho-TDP-43 induced cell death in cellular human neuroblastoma models</p>	Xue et al. (2013); Kiefer et al. (2014); Palomo et al. (2020)
 <p>AZ-2</p>		

(Continued on following page)

TABLE 2 (Continued) Inhibitors of CK1, TTBK, and CK2.

Inhibitor name and structure	Biological activity	References
 <p>TTBK1-IN-1</p>	<ul style="list-style-type: none"> - potent, selective and brain-penetrant TTBK1 inhibitor (IC_{50} = 2.7 nM) - in <i>in vivo</i> selectivity study with a panel of 150 kinases only 4 kinases (including TTBK1/2) are inhibited more than 50% - dose-dependent inhibition of tau phosphorylation levels at Ser422 (IC_{50} of ~9.5 nM) in isoflurane-induced hypothermia mice model - reduction of TDP-43 phosphorylation and formation of high molecular species in N2a cells 	Dillon et al. (2020); Halkina et al. (2021); Tian et al. (2021)
 <p>Compound 8</p>	<ul style="list-style-type: none"> - potent, selective and brain penetrant inhibitors of TTBK1 (IC_{50} of 60 nM (compound 8) and 2.7 nM (compound 31)) - compound 31 inhibits tau phosphorylation at S422 in mouse hypothermia and a rat developmental model (IC_{50} of 315 nM) 	Halkina et al. (2021)
 <p>Compound 31</p>		
 <p>Pyrropridine 29</p>	<ul style="list-style-type: none"> - cell-permeable, ATP-competitive TTBK1/2 inhibitor (IC_{50} values of 0.24 μM and 4.2 μM for TTBK1 and TTBK2, respectively) - inhibition of TDP-43 phosphorylation <i>in vitro</i> and <i>in vivo</i>, in cell cultures and in the spinal cord of transgenic TDP-43 mice 	Nozal et al., (2022)
 <p>5-TDMF</p>	<ul style="list-style-type: none"> - possesses good CNS penetrating properties and potent antioxidant and anti-inflammatory activities - inhibition of LPS-induced NF-κB translocation and expression of iNOS and COX-2 blocking MAP kinase and Erk signaling pathways 	Jana and Singh, (2020); Wang et al. (2016)
 <p>AMG-28</p>	<ul style="list-style-type: none"> - inhibition of TTBK1 and TTBK2 (1 μM) with remaining activity of 8% and 12% (MRC Kinase Profiling Inhibitor Database) - inhibition of tau phosphorylation at S422 in a biochemical and cellular assay with IC_{50} values of 199 nM and 1.85 μM, respectively - new analogs are more potent inhibitors of TTBK2 than TTBK1 - assayed in NanoBRET test in permeabilized HEK293 cells and compound 9 shows IC_{50} values of 2.5 and 1.8 μM for TTBK1 and TTBK2, respectively - in an enzymatic test derivative 9 possesses inhibitory activity (IC_{50} values between 150 and 400 nM) - derivative 9 shows highest kinome-wide selectivity towards the TTBK activities 	Potjewyd et al. (2022)

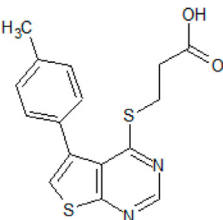
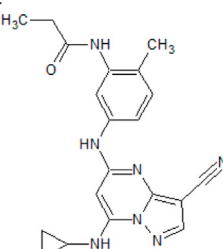
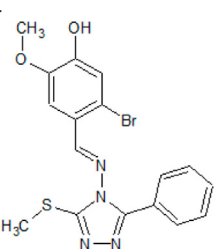
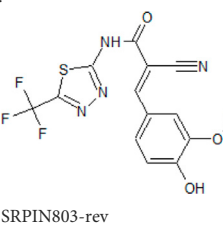
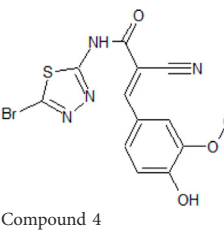
(Continued on following page)

TABLE 2 (Continued) Inhibitors of CK1, TTBK, and CK2.

Inhibitor name and structure	Biological activity	References
CK2 inhibitors		
<p>TBB</p>	<ul style="list-style-type: none"> - cell-permeable, highly selective, and ATP/GTP-competitive inhibitor of CK2 (IC₅₀ values of 0.9 and 1.6 μM for rat liver and human recombinant CK2, respectively) - discrimination between CK2 subunits (K_i values ranging from 80 nM to 210 nM) - strong inhibition of several other kinases (DYRK1-3, HIPK2, and PIM1-3) at a concentration of 10 μM - effect on human prostate cancer PC-3 cell viability is dependent on the time of administration - inhibition of okadaic acid-induced monomeric and oligomeric phospho-tau in both, N2a and CTX culture - prevention of I₂^{PP2A} phosphorylation at Ser9 in neurons and animal models 	<p>Pagano et al. (2008); Sarno et al. (2001); Szyszka et al. (1995); Yadikar et al. (2020); Zhang et al. (2018)</p>
<p>DMAT</p>	<ul style="list-style-type: none"> - ATP-competitive CK2 inhibitor (IC₅₀ = 130 nM) - inhibition of PIM1-3, HIPK2-3, DYRK1-3, PKD1, and CDK2 (IC₅₀ values between 0.07–3.7 μM) - possesses anti-neoplastic effect on the growth and hormonal activity of human adrenocortical carcinoma cell line (H295R) <i>in vitro</i> - able to induce cell death in antiestrogen-resistant human breast cancer cells - inhibition of TDP-43 phosphorylation which is necessary for the decrease of the ND251 or ND207 aggregation 	<p>Li et al. (2011); Ławnicka et al. (2010); Pagano et al. (2008); Yde et al. (2007)</p>
<p>Simitasertib (CX4945)</p>	<ul style="list-style-type: none"> - orally bioavailable, highly selective, and potent CK2 inhibitor (IC₅₀ value of 13 nM against CK2α and CK2α') - in cancer cells, causes cell-cycle arrest and selectively induces apoptosis when compared to normal cells. - correlation between the antiproliferative activity and the expression of CK2α as well as inhibition of the PI3K/Akt signaling - synergistic effects on cell death in combination with other inhibitors - synergistic cytotoxic effects of bortezomib (20S proteasome inhibitor with K_i of 0.6 nM) and CX-4945 in acute lymphoblastic leukemia resulting in turning off the prosurvival ER chaperone BIP/Grp78 and turning on the pro-apoptotic NF-κB - dose-dependent inhibition of the IL-1β/TNF-α induced secretion of the inflammatory cytokines MCP-1 and IL-6 in human primary astrocytes and U373 astrocytoma cells - strong inhibition of CLK activity - inhibition of CDC2-like kinases in nanomolar range leading to the inhibition of the phosphorylation of serine/arginine-rich proteins in mammalian cells - induction of abnormal alternative splicing of CK2α' pre-mRNA - orphan drug status by the US FDA for therapy of hard-to-treat bile duct cancers, known as cholangiocarcinomas - first described orally bioavailable CK2 inhibitor that advanced into clinical trials 	<p>Buontempo et al. (2016); Chon et al. (2015); Cozza et al. (2012); Lee et al. (2019); Kim et al. (2014); Pierre et al. (2011); Rosenberger et al. (2016); Siddiqui-Jain et al. (2010);</p>

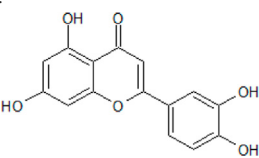
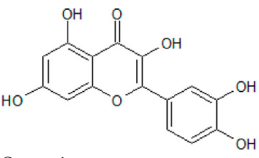
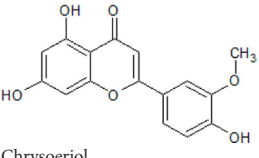
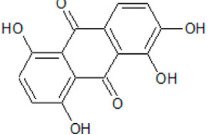
(Continued on following page)

TABLE 2 (Continued) Inhibitors of CK1, TTBK, and CK2.

Inhibitor name and structure	Biological activity	References
 TTP22	<ul style="list-style-type: none"> - inhibition of CK2 with a K_i of 40 nM - high selectivity towards CK2 confirmed using serine/threonine (ASK1, JNK3, Aurora A, and Rock 1) and tyrosine protein kinases (FGFR1, Met, and Tie2) - inhibition of CK2 decreases caspase-1-dependent MLL1 processing leading to higher MLL1 stability, and finally displace the MLL chimeras from chromatin - suppression of CK2 retard the leukemic progression in a MLL-AF9 leukemia mouse model 	Golub et al. (2011); Zhao et al. (2018)
 SGC-CK2-1	<ul style="list-style-type: none"> - potent inhibitor of CK2 with activity on both isoforms, CK2α and CK2α' (IC_{50} values of 4.2 nM and 2.3 nM, respectively) - inhibition of DYRK2 (IC_{50} of 440 nM) - potent suppression of CK2-mediated neuroinflammatory response inhibiting the expression of the proinflammatory cytokines IL-6 and IL-1β 	Wells et al. (2021); Mishra et al. (2022)
 GO289	<ul style="list-style-type: none"> - potent and selective inhibitor of CK2 (IC_{50} of 7 nM) and minor effects on CK1δ and CK1α activities - inhibition of PIM2 (IC_{50} of 13 nM) - inhibition of the phosphorylation of clock proteins, including PER2 - cell type-dependent inhibition of cancer cell growth that correlated with cellular clock function - <i>in vitro</i> potency and selectivity comparable to CX4945 	Borgo et al. (2021b); Oshima et al. (2019)
 SRPIN803-rev	<ul style="list-style-type: none"> - potent and selective dual inhibitor of CK2 and serine-arginine protein kinase 1 (SRPK1) - activity in mouse model of age-related macular degeneration due to the involvement of SRPK1 in angiogenesis and CK2 in neovascularization 	Dalle Vedove et al. (2020); Morooka et al. (2015)
 Compound 4	<ul style="list-style-type: none"> - the most potent SRPIN803-rev derivative (IC_{50} = 0.28 μM) - significant selectivity when tested on 320 kinases (inhibits only CK2 catalytic subunits by more than 50% at 1 μM concentration) - good cell permeability, inhibiting endocellularly CK2 - significant reduction of Jurkat and CEM cells viability 	Dalle Vedove et al. (2020)

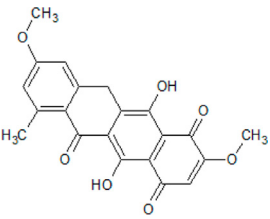
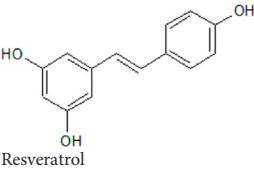
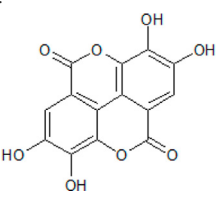
(Continued on following page)

TABLE 2 (Continued) Inhibitors of CK1, TTBK, and CK2.

Inhibitor name and structure	Biological activity	References
 Luteolin	<ul style="list-style-type: none"> - antioxidant, anti-cancer, and anti-inflammatory activities - ATP-competitive inhibition of CK1 ($IC_{50} = 1.6 \mu M$) - inhibition of CK2 holoenzyme and CK2α (IC_{50} 0.5 and 0.35 μM, respectively) - prevention of NDDs by reducing oxidative stress, inflammation, and Aβ production - protection against lipopolysaccharide-induced lethal toxicity and a reduction of the expression of pro-inflammatory intermediate in mice (0.2 mg/kg) - reduction of 6-hydroxy-dopamine-derived toxicity leading to neuroprotection in rat pheochromocytoma PC12 cells (3.13–50 μM) - neuroprotective effects on stroke patients undergoing neurorehabilitation as a component of a co-ultramicrosized composite (140 mg/day for 60 days) and palmitoylethanolamine - improvement of brain insulin resistance as well as inflammation protecting against the development of AD and the gut microbiota-liver-brain axis 	Caltagirone et al. (2015); Daily et al. (2021); Guo et al. (2013); Kang et al. (2004); Kotanidou et al. (2002); Kwon, (2017); Lolli et al. (2012); Lopez-Lazaro, (2009); Rezai-Zadeh et al. (2009); Sharma et al. (2007)
 Quercetin	<ul style="list-style-type: none"> - antioxidant and anti-inflammatory activities - potent inhibition of all CK2 isoforms with IC_{50} values below 1 μM - affects ROS-producing enzymes and protects neurons from oxidative stress-induced damage - potential up- and/or down-regulation of cytokines <i>via</i> Nrf2, ERK1/2, PI3K/Akt, JNK, MAPK pathways - Improvement of cognitive performance and cognitive functions in patients with neurological diseases or neurobehavioral disorders - inhibition of Aβ production <i>in vitro</i> and protection against cognitive impairments in a mouse model 	Baier et al. (2018); Nakagawa and Ohta, (2019); Selvakumar et al. (2012); Zaplatic et al. (2019)
 Chrysoeriol	<ul style="list-style-type: none"> - inhibition with IC_{50} values in low nanomolar range - administration alleviates the damage caused by cerebral ischemia and reperfusion in MCAO model rats - administration reduces the area of brain infarction and relief of neurobehavioral deficits - inhibition of the production of pro-inflammatory cytokines, - reduction of neuronal apoptosis and promotion of nerve growth - neuroprotective mechanism is strongly linked to the activation of the Wnt/β-catenin signaling pathway 	Baier et al. (2017); Shao et al. (2021)
 Quinalizarin	<ul style="list-style-type: none"> - potent, selective, ATP-competitive, and cell-permeable inhibitor of CK2 ($K_i = 50 \text{ nM}$) - able to discriminate between the free catalytic subunits and the CK2 holoenzymes - downregulation of transcription factors and modulation of microRNA in 3T3-L1 cells leading to inhibition of adipogenesis - inhibition of cell viability, especially in adenocarcinoma cells harboring EGFR sensitive mutation and interruption of migration - stimulation of apoptosis in different human lung cancer cell lines 	Cozza et al. (2009); Cozza et al. 2015; Schwind et al. (2017); Zhou et al. (2015)
	<ul style="list-style-type: none"> - moderate ATP-directed inhibitor of the CK2 holoenzyme (IC_{50} of 1.24 μM) - reduction of cell viability and proliferation in cancer cell lines, like MCF7, A427, and A431 (10 μM) TTBK1/2 inhibitors 	Haidar et al. (2019); Nirmaladevi et al. (2014); Hinojosa-Ventura et al. (2019)

(Continued on following page)

TABLE 2 (Continued) Inhibitors of CK1, TTBK, and CK2.

Inhibitor name and structure	Biological activity	References
 <p>Bikaverin</p>	<ul style="list-style-type: none"> - cytotoxic and antitumor effect on L5178Y lymphoma cells (IC₅₀ of 0.23 µg/ml) and on BALB/c mice inoculated with L5178Y - capable to recover the nuclear and mitochondrial integrity in H₂O₂-induced damaged cells 	
 <p>Resveratrol</p>	<ul style="list-style-type: none"> - antioxidant, anti-cancer, anti-inflammatory, and anti-aging properties - CNS penetrating molecule - increases the activity of antioxidant enzymes - reduction of the cell viability of human breast carcinoma cells (MCF-7) dependent on the concentration (IC₅₀ = 106 µM) - inhibition of CK2 activity by 1.6-fold - decrease of the potential of the mitochondrial membrane - increases ROS levels by 1.7-fold - protection of the central nervous system against symptoms of disorders, like stroke, spinal cord injury-induced inflammation, AD, PD, or HD - activation of SIRT1, Nrf2, and AMP-activated kinase 	<p>Ahmed et al. (2017); Costa et al. (2021); Gomes et al. (2018); Farkhondeh et al. (2020); Kim et al. (2018); Komorowska et al. (2020); Kumar et al. (2011); Turner et al. (2015); Liu et al. (2015); Zhao et al. (2021); Maher et al. (2010); Yu et al. (2016); Su et al. (2021); Yang et al. (2021)</p>
 <p>Ellagic acid</p>	<ul style="list-style-type: none"> - potent ATP-competitive CK2 inhibitor (IC₅₀ = 40 nM, K_i = 20 nM) - inhibitory effects towards the activity of many kinases such as LYN, PKA, SYK, GSK3, PKC, FGR, or CK1 (IC₅₀ values between 2.9 and 13 µM) - normalization of the lipid metabolism and the lipidemic profile - regulation of proinflammatory mediators, such as IL-6, IL-1β, and TNF-α - upregulation of Nrf2 and the inhibition NF-κB - neuroprotection due to antioxidant properties, ability to iron chelating, the induction of signaling pathways, and the reduction of mitochondrial dysfunction - neuroprotective contribution towards several neurotoxins in numerous animal models - neuroprotective effect in the 6-OHDA rat model of PD (50 mg/kg/day for one week) - neuroprotective potential by the reduction of apoptosis and oxidative stress, and inhibition of MAO-B. - effect on the ERβ/Nrf2/HO-1 signaling cascade - protective influence on DA neurons from rotenone-induced neuronal damage by activating Nrf2 signaling - induction of Nrf2 and HO-1 expression and inhibition of the NF-κB signaling pathway - protection of rats (6-OHDA rat model) against MTX-induced apoptosis and mitochondrial dysfunction - significant reduction of the volume of cerebrum infarction and the neurological deficit scores of the rats in an experimental rat model based on oxygen-glucose deprivation and reoxygenation in primary cultured cortical rat neurons. - increase of the number of Bcl-2-positive cells and the ratio of Bcl-2-positive to Bax-positive neurons in the semidarkness zone near the brain ischemic focus in the photothrombotic cerebral ischemia model - higher neuron viability, cell nuclear integrity, and a higher ratio of Bcl-2/Bax expression in the primary cultured neuron model - decrease of the number of apoptotic cells 	<p>Baluchnejadmojarad et al. (2017); Cozza et al. (2006); Dheen et al. (2005); Ebrahimi et al. (2019); Lastres-Becker et al. (2016); Liu et al. (2017); Rios et al. (2018); Vargas et al. (2006); Wang et al. (1998); Wei et al. (2020)</p>

binding of activator protein 1 (Sannerud et al., 2016). Further experiments are necessary to examine the role of phosphorylation in the case of presenilin-2.

Inhibitor-2 PP2A

The phosphorylation of tau is regulated by phosphoserine/threonine phosphatase PP2A and its activity is decreased in AD brain. PP2A is regulated by two endogenous inhibitory proteins called I_1^{PP2A} and I_2^{PP2A} (Gong et al., 1993; Li et al., 1996). Typically, I_2^{PP2A} is mainly located in the nucleus regulating DNA replication, gene transcription, cell-cycle progression, DNA repair and migration as well as chromatin remodeling. In AD patients, I_2^{PP2A} is overexpressed and translocated from the nucleus into the cytoplasm, where PP2A and significantly hyperphosphorylated tau is localized forming the NFTs in the neuronal cytoplasm (Tanimukai et al., 2005). In PC12 cells, stably transfected with tau and transiently transfected with human I_2^{PP2A} , accumulation of the inhibitor in the cytoplasm was observed (Chohan et al., 2006). CK2 was identified as one of two kinases responsible for the phosphorylation of S9 (Vera et al., 2007). This phosphorylation affects the ability of I_2^{PP2A} to bind to importin proteins (importin- α and importin- β). Phosphorylated I_2^{PP2A} does not form a complex with importin, therefore, it is localized in the cytoplasm instead of being transported into the nucleus (Yu et al., 2013).

Kinase inhibitors used in NDD pathway interrogation

In the literature synthetic and natural substances are described inhibiting protein kinases CK1, TTBK, and CK2. Table 2 gives an overview of several inhibitors with *in vitro* and/or *in vivo* activities on these kinase targets. Many of them do not selectively inhibit kinases, but might be a good starting point for drug design. Many research results on cancers and cancer cell lines involving protein kinase inhibitors were published, but only a few reports towards NDDs, especially in the case of CK2. Cancer and NDDs are both characterized by the dysregulation of the same signalling pathways, but with opposite effects. In cancers the cell survival and proliferation is increased, whereas, in NDDs those alterations lead to cell death and apoptosis. The most altered signal pathways in cancer, e.g., Nrf2 pathway and Wnt/ β -catenin pathway, are also implicated in NDDs, like AD and PD (Varela and Garcia-Rendueles, 2022).

The development of specific CK1 inhibitors capable to cross the blood-brain-barrier is a promising target for the treatment of TDP-43 proteinopathies, e.g., ALS. Small brain-penetrating molecules were described which block the neurotoxicity of TDP-43 in cell culture experiments through inhibition of its phosphorylation (Perez et al., 2011; Salado et al., 2014; Morales-Garcia et al., 2017). Up to now, few CK1-specific compounds

have been synthesised and a small part of them has been also examined in animal models. Kinetic studies of these compounds revealed an ATP-competitive mode of action in the case of almost all molecules.

In several studies, it has been proven that CK1 activity is necessary for molecular pacemaking. It was shown that CK1 δ is the main regulatory element of the clock period: inhibition of CK1 δ remarkably prolonged the circadian rhythms in locomotor activity *in vivo* and molecular oscillations in the suprachiasmatic nucleus (SCN) and peripheral tissue slices *in vitro*. Additionally, cumulation of PER2 protein in the nucleus was observed, *in vitro* and *in vivo* (Meng et al., 2010).

Cell proliferation is increased and colony formation is promoted through overexpression of CK1 α . Effects of CK1 α inhibition include the increase of the sensitivity to radiotherapy and reduction of the production and secretion of pro-inflammatory factors (Liu et al., 2021).

Several benzimidazole-based inhibitors displayed significant inhibition of CK1 δ , e.g., Bischof-5 and -6. Other potent ATP-competitive and selective CK1 δ/ϵ inhibitors are represented by difluoro-dioxolo-benzimidazole derivatives, compounds 1 and 2 (Richter et al., 2014). Substances derived from inhibitors of Wnt production (IWP) are structurally similar to benzimidazoles. Such inhibitors have been characterized as ATP-competitive and CK1 specific.

Another potent inhibitor, compound 1h, which is highly selective and CK1 isoform-specific was identified from a high-throughput screen of the Amgen compound library (Hua et al., 2012).

Many modulators of CK1 presently under investigation are isolated from natural environment or are derivatives of natural products. Nowadays, compounds from marine organisms are getting more attention and are now being investigated in clinical tests, essentially against cancer, inflammation, chronic pain, and NDDs. Among the promising drug candidates is the family of lamellarins, which are marine alkaloids with fused 14-phenyl-6H-[1]benzopyrano[4',3':4,5]pyrrolo[2,1-a]isoquinoline or non-fused 3,4-diarylpyrrole-2-carboxylate ring systems (Baunbaek et al., 2008; Bailly, 2015; Fukuda et al., 2020). So far, over 50 lamellarins have been purified from different marine organisms, e.g., mollusks, tunicates, and sponges. In 2008, protein kinases have been identified as new molecular targets of anticancer lamellarins (Baunbaek et al., 2008). 22 lamellarins were screened for cancer- and Alzheimer's disease-relevant protein kinases.

Until now, only a few protein kinases were described, which are associated with abnormal TDP-43 hyperphosphorylation, including both TTBK isoforms (Versluys et al., 2022). Both are known to colocalize with TDP-43 inclusions in spinal cords of ALS patients. TTBK2 is involved in crucial cellular mechanisms, e.g., ciliogenesis, microtubule dynamics, and neurotransmitter trafficking. Thus, its reduced activity may have negative effects for the patients (Jackson, 2012; Bowie and Goetz, 2020). Only a small number of TTBK1/2 inhibitors have been described, but unfortunately they do not show selectivity for one isoform (Xue et al., 2013; Kiefer et al., 2014).

A set of TTBK1 azaindazole inhibitors has been examined (Halkina et al., 2021). Two of them are characterized by high potency, selectivity and they are brain penetrant: compound 8 (4-(1-(2-Aminopyrimidin-4-yl)-1H-pyrazolo[4,3-c]pyridin-6-yl)-2-methylbut-3-yn-2-ol) with an IC_{50} of 60 nM and compound 31 ((S)-1-(1-(2-Amino-6-methoxypyrimidin-4-yl)-1H-pyrrolo[3,2-c]-pyridin-6-yl)-3-methylpent-1-yn-3-ol) with an IC_{50} of 2.7 nM.

Lately, receptor-based pharmacophore models were developed applying three TTBK1 protein structures. The combination of integrated e-pharmacophore based virtual screening and molecular dynamics simulation resulted in four hits: ZINC14644839 (5,6,4'-Trihydroxy-7,3'-Dimethoxyflavone, 5-TDMF), ZINC00012956 (3-phenyl-2-(9H-purin-6-ylamino)propan-1-ol), ZINC91332506 (1-[3-(6-aminopurin-9-yl)propyl]-3-methylpyridin-2-one), and ZINC69775110 (N-[(4-ethoxy-3-fluoro-phenyl)methyl]-7H-purin-6-amine). AMG-28 (4-(2-amino-5,6,7,8-tetrahydropyrimido [4',5':3,4]cyclohepta[1,2-b]indol-11-yl)-2-methylbut-3-yn-2-ol) was originally designed as an inhibitor of a Ser/Thr protein kinase essential for the activation of the NF- κ B pathway (NIK) (Li et al., 2013). A co-crystal structure of this inhibitor with the kinase domain of human TTBK1 showed binding of the aminopyrimidine ring with the hinge region of protein kinase. On the basis of AMG-28 11 new indolyl pyrimidine compounds were synthesized. New analogs are more potent inhibitors of TTBK2 than TTBK1 (Potjewyd et al., 2022).

Compounds that may inhibit CK2 activities were described in numerous publications. Since research results on the role of CK2 in NDD are diverse, there are only a few reports about CK2 inhibitors on NDDs available. The observation that CK2 is either overactive or overexpressed in patient brains supports kinase inhibition as a therapeutic approach for multiple neurodegenerative diseases. A large group of CK2 inhibitors, known for more than 20 years, are benzimidazoles, e.g., TBB and DMAT (Szyszka et al., 1995).

Data propose the influence of CK2 on astrocytes in the neuroinflammatory response in AD. In astrocytes in the hippocampus and temporal cortex of AD patients levels of CK2 α/α' are increased. Those astrocytes are linked to amyloid deposits in the AD brain. In human primary astrocytes and U373 astrocytoma cells, the IL-1 β /TNF- α induced secretion of the inflammatory cytokines MCP-1 and IL-6 is potently inhibited by CX-4945 dependent on the dose (Rosenberger et al., 2016). CX-4945 is the first described orally bioavailable CK2 inhibitor that advanced into clinical trials (Pierre et al., 2011; Cozza et al., 2012).

Quite recently SRPIN803-rev (6-(4-hydroxy-3-methoxybenzylidene)-5-imino-2-(trifluoromethyl)-5H-[1,3,4]thiadiazolo[3,2-a]pyrimidin-7(6H)-one), a new dual inhibitor of CK2 and serine-arginine protein kinase 1, was identified (Dalle Vedove et al., 2020). SRPIN803-rev and its new synthesized derivatives bind to the open conformation of the hinge/ α D region within the ATP-binding pocket of CK2 α .

The MLL/COMPASS stability is regulated by caspase1 cleavage and might be a possible target for clinical therapy of leukemia. Destabilized MLL and unprocessed version MLL1 associated with

chromatin results in the displacement of MLL chimeras from chromatin in leukemic cells. The CK2 phosphorylation site is next to the caspase1 cleavage site, and enables its cleavage. Inhibition of CK2 by specific inhibitors (CX-4945 or TTP22) decrease caspase1-dependent MLL1 processing, which leads to higher MLL1 stability, and finally displace the MLL chimeras from chromatin. In a MLL-AF9 leukemia mouse model the suppression of CK2 retard the leukemic progression (Zhao et al., 2018).

Naturally occurring compounds might act as antioxidant, anti-inflammatory, antiviral, antimicrobial, and anticancer agents (Baier and Szyszka, 2020). They have shown neuroprotective effects in many clinical trials (Ullah et al., 2020; Akter et al., 2021; Kim and Park, 2021; Wang et al., 2021).

It has been proven that flavonoids are most effective in the treatment of NDDs, including AD. First analyses with flavonoids against CK2 were reported by Li et al. (2009), Lolli et al. (2012). As we described in our own publications, flavonoids naturally occurring in plants are highly potent CK2 inhibitors. A set of more than 20 compounds (e.g., apigenin, pedalitin, and chrysoeriol) was tested for their inhibitory effect on four human CK2 isoforms. The results reveal that CK2 α' was most sensitive to the examined compounds (Baier et al., 2017; Baier et al., 2018).

Quercetin (3,5,7,3',4'-pentahydroxyflavone) belongs to the polyphenolic compounds with powerful antioxidant and anti-inflammatory activities. Polyphenolic compounds are often applied in the treatment and protection against severe diseases, like diabetes, cancer, neurodegenerative and cardiovascular diseases.

In time-course experiments it was shown that CK2 is crucial at early time points just after the induction of cell differentiation (Schwind et al., 2017).

In several studies it was observed that Nrf2 signaling is involved in PD pathogenesis (Dheen et al., 2005). The increase of Nrf2 induced dopamine (DA) neuroprotection and, at the same time, the decrease of Nrf2 altered DA neurons to get sensitive to oxidative stress damage (Lastres-Becker et al., 2016). It was shown that the progress of PD is linked to an incomplete activation of Nrf2 (Vargas et al., 2006).

Conclusion

During past decades many research groups provided new information to better understand the molecular aspects of cancerogenesis and neurodegenerative diseases. Protein kinases play an important role in the regulation of the activity of a huge amount of proteins involved in the control of different cell functions. Nevertheless, in many cases of NDDs, protein aggregation often caused by (hyper-)phosphorylation is observed. Therefore, the inhibition of these reactions is a promising therapeutic target. Unfortunately, whereas for the treatment of cancers several compounds were successfully developed, there does not exist a therapy for NDDs being a kinase inhibitor. Until September 2021, 73 small molecule kinase

inhibitors were approved by FDA but only a small amount of them are for noncancer-related diseases (Ayala-Aguilera et al., 2022). The main obstacle in the design of substances targeting the CNS is the effective crossing of the blood-brain-barrier which is necessary in the treatment of NDDs, but also in the case of oncology. CK1 superfamily and CK2 play essential roles in the regulation of cell processes, like in signaling pathways. With respect to this fact, it is not surprising that their deregulation might be associated to numerous disorders, e.g., inflammations, cancer, and NDDs. The starting point for CK1 inhibitors could be described as poorly selective and weakly potent molecules necessary to be improved for application in pharmacological treatment. Subsequently, compounds were developed, which show significant preference between the functionally different CK1 isoforms. Noteworthy, Pfizer designed two ATP-competitive compounds (PF-4800567 and PF-0670462), which possess selectivity towards the CK1 δ and CK1 ϵ isoforms. TG Therapeutics discovered umbralisib (UKONIQ™), an orally available dual inhibitor for PI3K δ and CK1 ϵ applied in the treatment of adults with relapsed or refractory marginal zone lymphoma, which received its FDA approval in 2021 (Burris et al., 2018). Despite this, there are no CK1 inhibitors reaching the clinical stage in neurodegenerative disorders. Those first successes raise the hope for the design of more selective and potent inhibitors of CK1 isoforms to improve the therapeutic opportunities.

In the case of TTBK1/2, up to date, only a small amount of molecules are known, which show potent inhibitory activity towards TTBK1/2. The undisputable advantage of TTBK1 over other kinases is its specific expression in neurons, and therefore, it seems to be a favorable target for NDDs.

Many kinds of CK2 inhibitors have been reported by using different methods, e.g., computer-aided drug design or structure-based reconstitution. Most of them lack cell permeability, high

selectivity, but possess off-target potential. The latter might be explained by the fact that this kinase phosphorylates a huge amount of protein substrates. The principle characteristics for a satisfactory molecule are, furthermore, metabolic stability and a good pharmacokinetic profile. Even the best compound CX-4945, already in clinical use, is not devoid of unspecific effects. Nevertheless, the number of newly developed inhibitors (GO289, SGC-CK2-1, and the SRPIN803-rev derivatives), may increase the chance of developing highly selective and CNS penetrating molecules for CK2 in the near future.

Author contributions

AB and RS conceived, wrote, and submitted this manuscript.

Conflict of interest

The authors declare that the research was conducted in the absence of any commercial or financial relationships that could be construed as a potential conflict of interest.

Publisher's note

All claims expressed in this article are solely those of the authors and do not necessarily represent those of their affiliated organizations, or those of the publisher, the editors and the reviewers. Any product that may be evaluated in this article, or claim that may be made by its manufacturer, is not guaranteed or endorsed by the publisher.

References

- Ackermann, K., Neidhart, T., Gerber, J., Waxmann, A., and Pyerin, W. (2005). The catalytic subunit α' gene of human protein kinase CK2 (CSNK2A2): Genomic organization, promoter identification and determination of Ets1 as a key regulator. *Mol. Cell. Biochem.* 274, 91–101. doi:10.1007/s11010-005-3076-2
- Adler, P., Mayne, J., Walker, K., Ning, Z., and Figeys, D. (2019). Therapeutic targeting of casein kinase 1 δ/ϵ in an Alzheimer's disease mouse model. *J. Proteome Res.* 18, 3383–3393. doi:10.1021/acs.jproteome.9b00312
- Ahmed, T., Javed, S., Javed, S., Tariq, A., Šamec, D., Tejada, S., et al. (2017). Resveratrol and Alzheimer's disease: Mechanistic insights. *Mol. Neurobiol.* 54, 2622–2635. doi:10.1007/s12035-016-9839-9
- Akter, R., Rahman, H., Behl, T., Chowdhury, M. A. R., Manirujjaman, M., Bulbul, I. J., et al. (2021). Prospective role of polyphenolic compounds in the treatment of neurodegenerative diseases. *CNS Neurol. Disord. Drug Targets* 20, 430–450. doi:10.2174/1871527320666210218084444
- Alquezar, C., Salado, I. G., de la Encarnación, A., Pérez, D. I., Moreno, F., Gil, C., et al. (2016). Targeting TDP-43 phosphorylation by casein kinase-1 δ inhibitors: A novel strategy for the treatment of frontotemporal dementia. *Mol. Neurodegener.* 11, 36. doi:10.1186/s13024-016-0102-7
- Andrew, S. E., Goldberg, Y. P., Kremer, B., Telenius, H., Theilmann, J., Adam, S., et al. (1993). The relationship between trinucleotide (CAG) repeat length and clinical features of Huntington's disease. *Nat. Genet.* 4, 398–403. doi:10.1038/ng0893-398
- Arai, T., Hasegawa, M., Akiyama, H., Ikeda, K., Nonaka, T., Mori, H., et al. (2006). TDP-43 is a component of ubiquitin-positive tau-negative inclusions in frontotemporal lobar degeneration and amyotrophic lateral sclerosis. *Biochem. Biophys. Res. Commun.* 351, 602–611. doi:10.1016/j.bbrc.2006.10.093
- Ardito, F., Giuliani, M., Perrone, D., Troiano, G., and Muzio, L. L. (2017). The crucial role of protein phosphorylation in cell signaling and its use as targeted therapy (Review). *Int. J. Mol. Med.* 40, 271–280. doi:10.3892/ijmm.2017.3036
- Arenas, J., Campos, Y., Ribacoba, R., Martín, M. A., Rubio, J. C., Ablanedo, P., et al. (1998). Complex I defect in muscle from patients with Huntington's disease. *Ann. Neurol.* 43, 397–400. doi:10.1002/ana.410430321
- Atwal, R. S., Desmond, C. R., Caron, N., Maiuri, T., Xia, J., Sipione, S., et al. (2011). Kinase inhibitors modulate huntingtin cell localization and toxicity. *Nat. Chem. Biol.* 7, 453–460. doi:10.1038/nchembio.582
- Augustinack, J. C., Schneider, A., Mandelkow, E. M., and Hyman, B. T. (2002). Specific tau phosphorylation sites correlate with severity of neuronal cytopathology in Alzheimer's disease. *Acta Neuropathol.* 103, 26–35. doi:10.1007/s004010100423
- Avraham, E., Rott, R., Liani, E., Szargel, R., and Engender, S. (2007). Phosphorylation of parkin by the cyclin-dependent kinase 5 at the linker region modulates its ubiquitin-ligase activity and aggregation. *J. Biol. Chem.* 282, 12842–12850. doi:10.1074/jbc.M608243200

- Ayala, Y. M., Zago, P., D'Ambrogio, A., Xu, Y.-F., Petrucelli, L., Buratti, E., et al. (2008). Structural determinants of the cellular localization and shuttling of TDP-43. *J. Cell Sci.* 121, 3778–3785. doi:10.1242/jcs.038950
- Ayala-Aguilera, C. C., Valero, T., Ivaro Lorente-Macias, Á., Baillache, D. J., Croke, S., and Unciti-Broceta, A. (2022). Small molecule kinase inhibitor drugs (1995–2021): Medical indication, pharmacology, and synthesis. *J. Med. Chem.* 65, 1047–1131. doi:10.1021/acs.jmedchem.1c00963
- Aziz, N. A., van der Burg, J. M. M., Landwehrmeyer, G. B., Brundin, P., Stijnen, T., EHDI Study Group, et al. (2008). Weight loss in Huntington disease increases with higher CAG repeat number. *Neurology* 71, 1506–1513. doi:10.1212/01.wnl.0000334276.09729.0e
- Badura, L., Swanson, T., Adamowicz, W., Adams, J., Cianfrogna, J., Fisher, K., et al. (2007). An inhibitor of casein kinase I induces phase delays in circadian rhythms under free-running and entrained conditions. *J. Pharmacol. Exp. Ther.* 322, 730–738. doi:10.1124/jpet.107.122846
- Baier, A., Galicka, A., Nazaruk, J., and Szyszka, R. (2017). Selected flavonoid compounds as promising inhibitors of protein kinase CK2 α and CK2 α' , the catalytic subunits of CK2. *Phytochemistry* 136, 39–45. doi:10.1016/j.phytochem.2016.12.018
- Baier, A., Nazaruk, J., Galicka, A., and Szyszka, R. (2018). Inhibitory influence of natural flavonoids on human protein kinase CK2 isoforms: Effect of the regulatory subunit. *Mol. Cell. Biochem.* 444, 35–42. doi:10.1007/s11010-017-3228-1
- Baier, A., and Szyszka, R. (2020). Compounds from natural sources as protein kinase inhibitors. *Biomolecules* 10 (11), 1546. doi:10.3390/biom10111546
- Bailly, C. (2015). Anticancer properties of lamellarins. *Mar. Drugs* 13, 1105–1123. doi:10.3390/md13031105
- Bain, J., Plater, L., Elliott, M., Shpiro, N., Hastie, C. J., McLauchlan, H., et al. (2007). The selectivity of protein kinase inhibitors: A further update. *Biochem. J.* 408, 297–315. doi:10.1042/BJ20070797
- Ball, B. J., Stein, A. S., Borthakur, G., Murray, C., Kook, K., Chan, K. W. H., et al. (2020). Trial in progress: A phase I trial of BTX-A51 in patients with relapsed or refractory aml or high-risk mds. *Blood* 136, 18–19. doi:10.1182/blood-2020-142557
- Baluchnejadmojarad, T., Rabiee, N., Zabihejad, S., and Roghani, M. (2017). Ellagic acid exerts protective effect in intrastriatal 6-hydroxydopamine rat model of Parkinson's disease: Possible involvement of ER β /Nrf2/HO-1 signaling. *Brain Res.* 1662, 23–30. doi:10.1016/j.brainres.2017.02.021
- Bao, C., Bajrami, B., Marcotte, D. J., Chodaparambil, J. V., Kerns, H. M., Henderson, J., et al. (2021). Mechanisms of regulation and diverse activities of tau-tubulin kinase (TTBK) isoforms. *Cell. Mol. Neurobiol.* 41, 669–685. doi:10.1007/s10571-020-00875-6
- Barmada, S. J., Skibinski, G., Korb, E., Rao, E. J., Wu, J. Y., and Finkbeiner, S. (2010). Cytoplasmic mislocalization of TDP-43 is toxic to neurons and enhanced by a mutation associated with familial amyotrophic lateral sclerosis. *J. Neurosci.* 30, 639–649. doi:10.1523/jneurosci.4988-09.2010
- Baunbaek, D., Trinkler, N., Ferandin, Y., Lozach, O., Ploypradith, P., Rucirawat, S., et al. (2008). Anticancer alkaloid lamellarins inhibit protein kinases. *Mar. Drugs* 6, 514–527. doi:10.3390/md20080026
- Benn, C. L., and Dawson, L. A. (2020). Clinically precedented protein kinases: Rationale for their use in neurodegenerative disease. *Front. Aging Neurosci.* 12, 242. doi:10.3389/fnagi.2020.00242
- Bibian, M., Rahaim, R. J., Choi, J. Y., Noguchi, Y., Schürer, S., Chen, W., et al. (2013). Development of highly selective casein kinase 1 δ /1 ϵ (CK1 δ/ϵ) inhibitors with potent antiproliferative properties. *Bioorg. Med. Chem. Lett.* 23, 4374–4380. doi:10.1016/j.bmcl.2013.05.075
- Bichelmeier, U., Schmidt, T., Hübener, J., Boy, J., Rüttiger, L., Häbig, K., et al. (2007). Nuclear localization of ataxin-3 is required for the manifestation of symptoms in SCA3: *In vivo* evidence. *J. Neurosci.* 27, 7418–7428. doi:10.1523/JNEUROSCI.4540-06.2007
- Binder, L. I., Frankfurter, A., and Rebhun, L. I. (1985). The distribution of tau in the mammalian central nervous system. *J. Cell Biol.* 101, 1371–1378. doi:10.1083/jcb.101.4.1371
- Bingham, E. W., and Farrel, H. M., Jr. (1974). Casein kinase from the Golgi apparatus of lactating mammary gland. *J. Biol. Chem.* 249, 3647–3651. doi:10.1016/S0021-9258(19)42622-7
- Bischof, J., Leban, J., Zaja, M., Grothey, A., Radunsky, B., Othersen, O., et al. (2012). 2-Benzamido-N-(1H-benzol[d]imidazol-2-yl)thiazole-4-carboxamide derivatives as potent inhibitors CK1 δ/ϵ . *Amino Acids* 43, 1577–1591. doi:10.1007/s00726-012-1234-x
- Blanquet, P. R. (2000). Casein kinase 2 as a potentially important enzyme in the nervous system. *Prog. Neurobiol.* 60, 211–246. doi:10.1016/s0301-0082(99)00026-x
- Borgo, C., Cesaro, L., Hirota, T., Kuwata, K., D'Amore, C., Ruppert, T., et al. (2021a). Comparing the efficacy and selectivity of CK2 inhibitors. A phosphoproteomics approach. *Eur. J. Med. Chem.* 214, 113217. doi:10.1016/j.ejmech.2021.113217
- Borgo, C., D'Amore, C., Sarno, S., Salvi, M., and Ruzzene, M. (2021b). Protein kinase CK2: A potential therapeutic target for diverse human diseases. *Signal Transduct. Target. Ther.* 6, 183. doi:10.1038/s41392-021-00567-7
- Bouskila, M., Esoof, N., Gay, L., Fang, E. H., Deak, M., Begley, M. J., et al. (2011). TTBK2 kinase substrate specificity and the impact of spinocerebellar-ataxia-causing mutations on expression, activity, localization and development. *Biochem. J.* 437, 157–167. doi:10.1042/bj20110276
- Bowie, E., and Goetz, S. C. (2020). TTBK2 and primary cilia are essential for the connectivity and survival of cerebellar Purkinje neurons. *Elife* 9, e51166. doi:10.7554/eLife.51166
- Boyarko, B., and Hook, V. (2021). Human tau isoforms and proteolysis for production of toxic tau fragments in neurodegeneration. *Front. Neurosci.* 15, 702788. doi:10.3389/fnins.2021.702788
- Braak, H., and Braak, E. (1991). Neuropathological staging of Alzheimer-related changes. *Acta Neuropathol.* 82, 239–259. doi:10.1007/BF00308809
- Braggin, J. E., Bucks, S. A., Course, M. M., Smith, C. L., Sopher, B., Osnis, L., et al. (2019). Alternative splicing in a presenilin 2 variant associated with Alzheimer disease. *Ann. Clin. Transl. Neurol.* 6, 762–777. doi:10.1002/acn3.755
- Buontempo, F., Orsini, E., Lonetti, A., Capellini, A., Chiarini, F., Evangelisti, C., et al. (2016). Synergistic cytotoxic effects of bortezomib and CK2 inhibitor CX-4945 in acute lymphoblastic leukemia: Turning off the prosurvival ER chaperone BIP/Grp78 and turning on the pro-apoptotic NF- κ B. *Oncotarget* 7, 1323–1340. doi:10.18632/oncotarget.6361
- Burnett, B., Li, F., and Pittman, R. N. (2003). The polyglutamine neurodegenerative protein ataxin-3 binds polyubiquitylated proteins and has ubiquitin protease activity. *Hum. Mol. Genet.* 12, 3195–3205. doi:10.1093/hmg/ddg344
- Burnett, G., and Kennedy, E. P. (1954). The enzymatic phosphorylation of proteins. *J. Biol. Chem.* 211, 969–980. doi:10.1016/S0021-9258(18)71184-8
- Burré, J., Sharma, M., and Südhof, T. C. (2018). Cell biology and pathophysiology of α -synuclein. *Cold Spring Harb. Perspect. Med.* 8, a024091. doi:10.1101/cshperspect.a024091
- Burris, H. A., Flinn, I. W., Patel, M. R., Fenske, T. S., Deng, C., Brander, D. M., et al. (2018). Umbralisib, a novel PI3K δ and casein kinase-1 ϵ inhibitor, in relapsed or refractory chronic lymphocytic leukaemia and lymphoma: An open-label, phase 1, dose-escalation, first-in-human study. *Lancet. Oncol.* 19, 486–496. doi:10.1016/s1470-2045(18)30082-2
- Burzio, V., Antonelli, M., Allende, C. C., and Allende, J. E. (2002). Biochemical and cellular characteristics of the four splice variants of protein kinase CK1 α from zebrafish (*Danio rerio*). *J. Cell. Biochem.* 86, 805–814. doi:10.1002/jcb.10263
- Caltagirone, C., Cisari, C., Schievano, C., Di Paola, R., Cordaro, M., Bruschetta, G., et al. (2015). Co-Ultramicronized palmitoylethanolamide/luteolin in the treatment of cerebral ischemia: From rodent to man. *Transl. Stroke Res.* 7, 54–69. doi:10.1007/s12975-015-0440-8
- Carter, B., Justin, H. S., Gulick, D., and Gamsby, J. J. (2021). The molecular clock and neurodegenerative disease: A stressful time. *Front. Mol. Biosci.* 8, 644747. doi:10.3389/fmolb.2021.644747
- Castello, J., Ragnauth, A., Friedman, E., and Rebholz, H. (2017). CK2—an emerging target for neurological and psychiatric disorders. *Pharmaceuticals* 10, 7. doi:10.3390/ph10010007
- Chakraborty, J., Basso, V., and Ziviani, E. (2017). Post translational modification of Parkin. *Biol. Direct* 12, 6. doi:10.1186/s13062-017-0176-3
- Chen, C., Gu, J., Basurto-Islas, G., Jin, N., Wu, F., Gong, C.-X., et al. (2017). Up-regulation of casein kinase 1 ϵ is involved in tau pathogenesis in Alzheimer's disease. *Sci. Rep.* 7, 13478. doi:10.1038/s41598-017-13791-5
- Chen, G.-F., Xu, T.-H., Yan, Y., Zhou, Y.-R., Jiang, Y., Melcher, K., et al. (2017). Amyloid beta: Structure, biology and structure-based therapeutic development. *Acta Pharmacol. Sin.* 38, 1205–1235. doi:10.1038/aps.2017.28
- Cheong, J. K., Hung, N. T., Wang, H., Tan, P., Voorhoeve, P. M., Lee, S. H., et al. (2011). IC261 induces cell cycle arrest and apoptosis of human cancer cells via CK1 δ/ϵ and Wnt/ β -catenin independent inhibition of mitotic spindle formation. *Oncogene* 30, 2558–2569. doi:10.1038/onc.2010.627
- Chohan, M. O., Khatoun, S., Iqbal, I.-G., and Iqbal, K. (2006). Involvement of I2PP2A in the abnormal hyperphosphorylation of tau and its reversal by Memantine. *FEBS Lett.* 580, 3973–3979. doi:10.1016/j.febslet.2006.06.021

- Chon, H. J., Bae, K. J., Lee, Y., and Kim, J. (2015). The casein kinase 2 inhibitor, CX-4945, as an anti-cancer drug in treatment of human hematological malignancies. *Front. Pharmacol.* 6, 70. doi:10.3389/fphar.2015.00070
- Citron, M., Diehl, T. S., Gordon, G., Biere, A. L., Seubert, P., and Selkoe, D. J. (1996). Evidence that the 42- and 40-amino acid forms of amyloid β protein are generated from the β -amyloid precursor protein by different protease activities. *Proc. Natl. Acad. Sci. U. S. A.* 93, 13170–13175. doi:10.1073/pnas.93.23.13170
- Cohen, P. (2002). The origins of protein phosphorylation. *Nat. Cell Biol.* 4, E127–E130. doi:10.1038/ncb0502-e127
- Conway, K. A., Harper, J. D., and Lansbury, P. T. (1998). Accelerated *in vitro* fibril formation by a mutant alpha-synuclein linked to early-onset Parkinson disease. *Nat. Med.* 4, 1318–1320. doi:10.1038/3311
- Cookson, M. R., Lockhart, P. J., McLendon, C., O'Farrell, C., Schlossmacher, M., and Farrer, M. J. (2003). RING finger 1 mutations in parkin produce altered localization of the protein. *Hum. Mol. Genet.* 12, 2957–2965. doi:10.1093/hmg/ddg328
- Cornett, J., Cao, F., Wang, C. E., Ross, C. A., Bates, G. P., Li, S. H., et al. (2005). Polyglutamine expansion of huntingtin impairs its nuclear export. *Nat. Genet.* 37, 198–204. doi:10.1038/ng1503
- Costa, P. S. D., Ramos, P. S., Ferreira, C., Silva, J. L., El-Baha, T., and Fialho, E. (2021). Pro-oxidant effect of resveratrol on human breast cancer MCF-7 cells is associated with CK2 inhibition. *Nutr. Cancer* 14, 1–10. doi:10.1080/016355581.2021.1977834
- Cozza, G., Bonvini, P., Zorzi, E., Poletto, G., Pagano, M. A., Sarno, S., et al. (2006). Identification of ellagic acid as potent inhibitor of protein kinase CK2: A successful example of a virtual screening application. *J. Med. Chem.* 49, 2363–2366. doi:10.1021/jm060112m
- Cozza, G., Gianoncelli, A., Montopoli, M., Caparrotta, L., Venerando, A., Meggio, F., et al. (2008). Identification of novel protein kinase CK1 delta (CK1delta) inhibitors through structure-based virtual screening. *Bioorg. Med. Chem. Lett.* 18, 5672–5675. doi:10.1016/j.bmcl.2008.08.072
- Cozza, G., Mazzorana, M., Papinutto, E., Bain, J., Elliott, M., di Maira, G., et al. (2009). Quinalizarin as a potent, selective and cell-permeable inhibitor of protein kinase CK2. *Biochem. J.* 421, 387–395. doi:10.1042/bj20090069
- Cozza, G., and Pinna, L. A. (2016). Casein kinases as potential therapeutic targets. *Expert Opin. Ther. Targets* 20, 319–340. doi:10.1517/14728222.2016.1091883
- Cozza, G., Pinna, L. A., and Moro, S. (2012). Protein kinase CK2 inhibitors: A patent review. *Expert Opin. Ther. Pat.* 22, 1081–1097. doi:10.1517/13543776.2012.717615
- Cozza, G., Venerando, A., Sarno, S., and Pinna, L. A. (2015). The selectivity of CK2 inhibitor quinalizarin: A reevaluation. *Biomed. Res. Int.* 2015, 734127. doi:10.1155/2015/734127
- Cunningham, P. S., Ahern, S. A., Smith, L. C., da Silva Santos, C. S., Wager, T. T., and Bechtold, D. A. (2016). Targeting of the circadian clock via CK1 δ/ϵ to improve glucose homeostasis in obesity. *Sci. Rep.* 6, 29983. doi:10.1038/srep29983
- Daily, J. W., Kang, S., and Park, S. (2021). Protection against Alzheimer's disease by luteolin: Role of brain glucose regulation, anti-inflammatory activity, and the gut microbiota-liver-brain axis. *Biofactors* 47, 218–231. doi:10.1002/biof.1703
- Dalle Vedove, A., Zonta, F., Zanforlin, E., Demitri, N., Ribaldo, G., Cazzanelli, G., et al. (2020). A novel class of selective CK2 inhibitors targeting its open hinge conformation. *Eur. J. Med. Chem.* 195, 112267. doi:10.1016/j.ejmech.2020.112267
- De Wit, T., Baekelandt, V., and Lobbstaal, E. (2018). Inhibition of LRRK2 or casein kinase 1 results in LRRK2 protein destabilization. *Mol. Neurobiol.* 56, 5273–5286. doi:10.1007/s12035-018-1449-2
- Desmond, C. R., Atwal, R. S., Xia, J., and Truant, R. (2012). Identification of a karyopherin $\beta 1/\beta 2$ proline-tyrosine nuclear localization signal in huntingtin protein. *J. Biol. Chem.* 287, 39626–39633. doi:10.1074/jbc.M112.412379
- Dheen, S. T., Jun, Y., Yan, Z., Tay, S. S. W., and Ang Ling, E. (2005). Retinoic acid inhibits expression of TNF- α and iNOS in activated rat microglia. *Glia* 50, 21–31. doi:10.1002/glia.20153
- Dillon, G. M., Henderson, J. L., Bao, C., Joyce, J. A., Calhoun, M., Amaral, B., et al. (2020). Acute inhibition of the CNS-specific kinase TTBK1 significantly lowers tau phosphorylation at several disease relevant sites. *PLOS ONE* 15 (4), e0228771. doi:10.1371/journal.pone.0228771
- Domńska, K., Zieliński, R., Kubiński, K., Sajna, E., Maslyk, M., Bretner, M., et al. (2005). Different properties of four molecular forms of protein kinase CK2 from *Saccharomyces cerevisiae*. *Acta Biochim. Pol.* 52, 947–952. doi:10.18388/abp.2005_3413
- Duan, G., and Walther, D. (2015). The roles of post-translational modifications in the context of protein interaction networks. *PLoS Comput. Biol.* 11, e1004049. doi:10.1371/journal.pcbi.1004049
- Ebrahimi, R., Sepand, M. R., Seyednejad, S. A., Omid, A., Akbariani, M., Gholami, M., et al. (2019). Ellagic acid reduces methotrexate-induced apoptosis and mitochondrial dysfunction via up-regulating Nrf2 expression and inhibiting the I κ B α /NF κ B in rats. *DARU* 27, 721–733. doi:10.1007/s40199-019-00309-9
- El-Agnaf, O. M., Jakes, R., Curran, M. D., and Wallace, A. (1998). Effects of the mutations Ala30 to Pro and Ala53 to Thr on the physical and morphological properties of α -synuclein protein implicated in Parkinson's disease. *FEBS Lett.* 440, 67–70. doi:10.1016/s0014-5793(98)01419-7
- Ellis, C. E., Schwartzberg, P. L., Grider, T. L., Fink, D. W., and Nussbaum, R. L. (2001). α -Synuclein is phosphorylated by members of the Src family of protein-tyrosine kinases. *J. Biol. Chem.* 276, 3879–3884. doi:10.1074/jbc.M010316200
- Evert, B. O., Araujo, J., Vieira-Saecker, A. M., de Vos, R. A., Harendza, S., Klockgether, T., et al. (2006). Ataxin-3 represses transcription via chromatin binding, interaction with histone deacetylase 3, and histone deacetylation. *J. Neurosci.* 26, 11474–11486. doi:10.1523/JNEUROSCI.2053-06.2006
- Evin, G., Smith, M. J., Tziotis, A., McLean, C., Canterford, L., Sharples, R. A., et al. (2002). Alternative transcripts of presenilin-1 associated with frontotemporal dementia. *Neuroreport* 13, 917–921. doi:10.1097/00001756-200205070-00036
- Farkhondeh, T., Folgado, S. L., Pourbagher-Shahri, A. M., Ashrafzadeh, M., and Samarghandian, S. (2020). The therapeutic effect of resveratrol: Focusing on the Nrf2 signaling pathway. *Biomed. Pharmacother.* 127, 110234. doi:10.1016/j.biopha.2020.110234
- Flajolet, M., He, G., Heiman, M., Lin, A., Nairn, A. C., and Greengard, P. (2007). Regulation of Alzheimer's disease amyloid-beta formation by casein kinase I. *Proc. Natl. Acad. Sci. U. S. A.* 104, 4159–4164. doi:10.1073/pnas.0611236104
- Flotow, H., and Roach, P. J. (1991). Role of acidic residues as substrate determinants for casein kinase I. *J. Biol. Chem.* 266, 3724–3727. doi:10.1016/S0021-9258(19)67854-3
- Franchin, C., Cesaro, L., Salvi, M., Million, R., Iori, E., Cifani, P., et al. (2015). Quantitative analysis of a phosphoproteome readily altered by the protein kinase CK2 inhibitor quinalizarin in HEK-293T cells. *Biochim. Biophys. Acta* 1854, 609–623. doi:10.1016/j.bbapap.2014.09.017
- Fujiwara, H., Hasegawa, M., Dohmae, N., Kawashima, A., Masliah, E., Goldberg, M. S., et al. (2002). α -Synuclein is phosphorylated in synucleinopathy lesions. *Nat. Cell Biol.* 4, 160–164. doi:10.1038/ncb748
- Fukuda, T., Ishibashi, F., and Iwao, M. (2020). Lamellarin alkaloids: Isolation, synthesis, and biological activity. *Alkaloids. Chem. Biol.* 83, 1–112. doi:10.1016/bs.alkal.2019.10.001
- Fulcher, L. J., and Sapkota, G. P. (2020). Functions and regulation of the serine/threonine protein kinase CK1 family: Moving beyond promiscuity. *Biochem. J.* 477, 4603–4621. doi:10.1042/BCJ20200506
- Gai, W. P., Power, J. H., Blumbergs, P. C., and Blessing, W. W. (1998). Multiple-system atrophy: A new α -synuclein disease? *Lancet* 352, 547–548. doi:10.1016/s0140-6736(05)79256-4
- García-Reyes, B., Witt, L., Jansen, B., Karasu, E., Gehring, T., Leban, J., et al. (2018). Discovery of inhibitor of Wnt production 2 (IWP-2) and related compounds as selective ATP-competitive inhibitors of casein kinase 1 (CK1) δ/ϵ . *J. Med. Chem.* 61, 4087–4102. doi:10.1021/acs.jmedchem.8b00095
- Geuens, T., Bouhy, D., and Timmerman, V. (2016). The hnRNP family: Insights into their role in health and disease. *Hum. Genet.* 135, 851–867. doi:10.1007/s00439-016-1683-5
- Ghoshal, N., Smiley, J. F., DeMaggio, A. J., Hoekstra, M. F., Cochran, E. J., Binder, L. I., et al. (1999). A new molecular link between the fibrillar and granulovacuolar lesions of Alzheimer's disease. *Am. J. Pathol.* 155, 1163–1172. doi:10.1016/s0002-9440(10)65219-4
- Glenner, G. G., and Wong, C. W. (1984). Alzheimer's disease: Initial report of the purification and characterization of a novel cerebrovascular amyloid protein. *Biochem. Biophys. Res. Commun.* 120, 885–890. doi:10.1016/s0006-291x(84)80190-4
- Golub, A. G., Bdzhol, V. G., Briukhovetska, N. V., Balanda, A. O., Kukhareno, O. P., Kotey, I. M., et al. (2011). Synthesis and biological evaluation of substituted (thieno[2, 3-d]pyrimidin-4-ylthio)carboxylic acids as inhibitors of human protein kinase CK2. *Eur. J. Med. Chem.* 46, 870–876. doi:10.1016/j.ejmech.2010.12.025
- Gomes, B. A. Q., Silva, J. P. B., Romeiro, C. F. R., dos Santos, S. M., Rodrigues, C. A., Gonçalves, P. R., et al. (2018). Neuroprotective mechanisms of resveratrol in

- Alzheimer's disease: Role of SIRT1. *Oxid. Med. Cell. Longev.* 2018, 8152373. doi:10.1155/2018/8152373
- Gong, C.-X., and Iqbal, K. (2008). Hyperphosphorylation of microtubule-associated protein tau: A promising therapeutic target for alzheimer disease. *Curr. Med. Chem.* 15, 2321–2328. doi:10.2174/092986708785909111
- Gong, C.-X., Singh, T. J., Grundke-Iqbal, I., and Iqbal, K. (1993). Phosphoprotein phosphatase activities in Alzheimer disease brain. *J. Neurochem.* 61, 921–927. doi:10.1111/j.1471-4159.1993.tb03603.x
- Greenwood, J. A., Scott, C. W., Spreen, R. C., Caputo, C. B., and Johnson, G. V. (1994). Casein kinase II preferentially phosphorylates human tau isoforms containing an amino-terminal insert. Identification of threonine 39 as the primary phosphate acceptor. *J. Biol. Chem.* 269, 4373–4380. doi:10.1016/S0021-9258(17)41790-x
- Grundke-Iqbal, I., Iqbal, K., Tung, Y. C., Quinlan, M., Wisniewski, H. M., and Binder, L. I. (1986). Abnormal phosphorylation of the microtubule-associated protein tau (tau) in Alzheimer cytoskeletal pathology. *Proc. Natl. Acad. Sci. U. S. A.* 83, 4913–4917. doi:10.1073/pnas.83.13.4913
- Guo, D.-J., Li, F., Yu, P. H.-F., and Chan, S.-W. (2013). Neuroprotective effects of luteolin against apoptosis induced by 6-hydroxydopamine on rat pheochromocytoma PC12 cells. *Pharm. Biol.* 51, 190–196. doi:10.3109/13880209.2012.716852
- Hackam, A. S., Singaraja, R., Wellington, C. L., Metzler, M., McCutcheon, K., Zhang, T., et al. (1998). The influence of huntingtin protein size on nuclear localization and cellular toxicity. *J. Cell Biol.* 141, 1097–1105. doi:10.1083/jcb.141.5.1097
- Haidar, S., Aichele, D., Birus, R., Hielscher, J., Laitinen, T., Poso, A., et al. (2019). *In vitro* and *in silico* evaluation of bikaverin as a potent inhibitor of human protein kinase CK2. *Molecules* 24, 1380. doi:10.3390/molecules24071380
- Halekotte, J., Witt, L., Ianes, C., Krüger, M., Bührmann, M., Rauh, D., et al. (2017). Optimized 4, 5-diarylimidazoles as potent/selective inhibitors of protein kinase CK1δ and their structural relation to p38α MAPK. *Molecules* 22, 522. doi:10.3390/molecules22040522
- Halkina, T., Henderson, J. L., Lin, E. Y., Himmelbauer, M. K., Jones, J. H., Nevalainen, M., et al. (2021). Discovery of potent and brain-penetrant tau tubulin kinase 1 (TTBK1) inhibitors that lower tau phosphorylation *in vivo*. *J. Med. Chem.* 64, 6358–6380. doi:10.1021/acs.jmedchem.1c00382
- Hampe, C., Ardila-Osorio, H., Fournier, M., Brice, A., and Corti, O. (2006). Biochemical analysis of Parkinson's disease-causing variants of parkin, an E3 ubiquitin-protein ligase with monoubiquitylation capacity. *Hum. Mol. Genet.* 15, 2059–2075. doi:10.1093/hmg/ddl131
- Hanger, D. P., Anderton, B. H., and Noble, W. (2009). Tau phosphorylation: The therapeutic challenge for neurodegenerative disease. *Trends Mol. Med.* 15, 112–119. doi:10.1016/j.molmed.2009.01.003
- Hanger, D. P., Byers, H. L., Wray, S., Leung, K.-Y., Saxton, M. J., Seereeram, A., et al. (2007). Novel phosphorylation sites in tau from alzheimer brain support a role for casein kinase 1 in disease pathogenesis. *J. Biol. Chem.* 282, 23645–23654. doi:10.1074/jbc.M703269200
- Hanks, S. K., and Hunter, T. (1995). The eukaryotic protein kinase superfamily: Kinase (catalytic) domain structure and classification¹. *FASEB J.* 9, 576–596. doi:10.1096/fasebj.9.8.7768349
- Hardy, J. A., and Higgins, G. A. (1992). Alzheimer's disease: The amyloid cascade hypothesis. *Science* 256, 184–185. doi:10.1126/science.1566067
- Hasegawa, M., Arai, T., Nonaka, T., Kametani, F., Yoshida, M., Hashizume, Y., et al. (2008). Phosphorylated TDP-43 in frontotemporal lobar degeneration and amyotrophic lateral sclerosis. *Ann. Neurol.* 64, 60–70. doi:10.1002/Ana.21425
- Hathaway, G. M., and Traugh, J. A. (1979). Cyclic nucleotide-independent protein kinases from rabbit reticulocytes. Purification of casein kinases. *J. Biol. Chem.* 254, 762–768. doi:10.1016/S0021-9258(17)37871-7
- Hinojosa-Ventura, G., Puebla-Pérez, A. M., Gallegos-Arreola, M. P., Chávez-Parga, M.-C., Romero-Estrada, A., and Delgado-Saucedo, J. I. (2019). Cytotoxic and antitumoral effects of bikaverin from *Gibberella fujikuroi* on L5178Y lymphoma murine model. *J. Mex. Chem. Soc.* 63, 115–122. doi:10.29356/jmcs.v63i4.729
- Houlden, H., Johnson, J., Gardner-Thorpe, C., Lashley, T., Hernandez, D., Worth, P., et al. (2007). Mutations in TTBK2, encoding a kinase implicated in tau phosphorylation, segregate with spinocerebellar ataxia type 11. *Nat. Genet.* 39, 1434–1436. doi:10.1038/ng.2007.43
- Hua, Z., Huang, X., Bregman, H., Chakka, N., DiMauro, E. F., Doherty, E. M., et al. (2012). 2-Phenylamino-6-cyano-1H-benzimidazole-based isoform selective casein kinase 1 gamma (CK1γ) inhibitors. *Bioorg. Med. Chem. Lett.* 22, 5392–5395. doi:10.1016/j.bmcl.2012.07.046
- Hunter, T. (1995). Protein kinases and phosphatases: The yin and yang of protein phosphorylation and signaling. *Cell* 80, 225–236. doi:10.1016/0092-8674(95)90405-0
- Hunter, T. (2012). Why nature chose phosphate to modify proteins. *Philos. Trans. R. Soc. Lond. B Biol. Sci.* 367, 2513–2516. doi:10.1098/rstb.2012.0013
- Ikezu, S., and Ikezu, T. (2014). Tau-tubulin kinase. *Front. Mol. Neurosci.* 7, 33. doi:10.3389/fnmol.2014.00033
- Ikezu, S., Ingraham Dixie, K. L., Koro, L., Watanabe, T., Kaibuchi, K., and Ikezu, T. (2020). Tau-tubulin kinase 1 and amyloid-β peptide induce phosphorylation of collapsin response mediator protein-2 and enhance neurite degeneration in Alzheimer disease mouse models. *Acta Neuropathol. Commun.* 8, 12. doi:10.1186/s40478-020-0890-4
- Inukai, Y., Nonaka, T., Arai, T., Yoshida, M., Hashizume, Y., Beach, T. G., et al. (2008). Abnormal phosphorylation of ser409/410 of TDP-43 in FTL-D and ALS. *FEBS Lett.* 582, 2899–2904. doi:10.1016/j.febslet.2008.07.027
- Ishii, A., Nonaka, T., Taniguchi, S., Saito, T., Arai, T., Mann, D., et al. (2007). Casein kinase 2 is the major enzyme in brain that phosphorylates Ser129 of human alpha-synuclein: Implication for alpha-synucleinopathies. *FEBS Lett.* 581, 4711–4717. doi:10.1016/j.febslet.2007.08.067
- Iwao, M., Fukuda, T., and Ishibashi, F. (2011). Synthesis and biological activity of lamellarin alkaloids: An overview. *HETEROCYCLES* 83, 491. doi:10.3987/rev-10-686
- Jackson, P. K. (2012). TTBK2 kinase: Linking primary cilia and cerebellar ataxias. *Cell* 151, 697–699. doi:10.1016/j.cell.2012.10.027
- Jameson, L., Frey, T., Zeeberg, B., Dalldorf, F., and Caplow, M. (1980). Inhibition of microtubule assembly by phosphorylation of microtubule-associated proteins. *Biochemistry* 19, 2472–2479. doi:10.1021/bi00552a027
- Jana, S., and Singh, S. K. (2020). Identification of human tau-tubulin kinase 1 inhibitors: An integrated e-pharmacophore based virtual screening and molecular dynamics simulation. *J. Biomol. Struct. Dyn.* 38, 886–900. doi:10.1080/07391102.2019.1590242
- Janeczko, M., Orzeszko, A., Kazimierzczuk, Z., Szyszka, R., and Baier, A. (2012). CK2α and CK2α' subunits differ in their sensitivity to 4, 5, 6, 7-tetrabromo- and 4, 5, 6, 7-tetraiodo-1H-benzimidazole derivatives. *Eur. J. Med. Chem.* 47, 345–350. doi:10.1016/j.ejmech.2011.11.002
- Järås, M., Miller, P. G., Chu, L. P., Puram, R. V., Fink, E. C., Schneider, R. K., et al. (2014). Csnk1a1 inhibition has p53-dependent therapeutic efficacy in acute myeloid leukemia. *J. Exp. Med.* 211, 605–612. doi:10.1084/jem.20131033
- Jiang, S., Zhang, M., Sun, J., and Yang, X. (2018). Casein kinase 1α: Biological mechanisms and therapeutic potential. *Cell Commun. Signal.* 16, 23. doi:10.1186/s12964-018-0236-z
- Jin, J., and Pawson, T. (2012). Modular evolution of phosphorylation-based signalling systems. *Philos. Trans. R. Soc. Lond. B Biol. Sci.* 367, 2540–2555. doi:10.1098/rstb.2012.0106
- Kametani, F., Nonaka, T., Suzuki, T., Arai, T., Dohmae, N., Akiyama, H., et al. (2009). Identification of casein kinase-1 phosphorylation sites on TDP-43. *Biochem. Biophys. Res. Commun.* 382, 405–409. doi:10.1016/j.bbrc.2009.03.038
- Kang, S. S., Lee, J. Y., Choi, Y. K., Kim, G. S., and Han, B. H. (2004). Neuroprotective effects of flavones on hydrogen peroxide-induced apoptosis in SH-SY5Y neuroblastoma cells. *Bioorg. Med. Chem. Lett.* 14, 2261–2264. doi:10.1016/j.bmcl.2004.02.003
- Kannanayakal, T. J., Tao, H., Vandre, D. D., and Kuret, J. (2006). Casein kinase-1 isoforms differentially associate with neurofibrillary and granulovacuolar degeneration lesions. *Acta Neuropathol.* 111, 413–421. doi:10.1007/s00401-006-0049-9
- Karve, T. M., and Cheema, A. K. (2011). Small changes huge impact: The role of protein posttranslational modifications in cellular homeostasis and disease. *J. Amino Acids* 2011, 207691. doi:10.4061/2011/207691
- Kiefer, S. E., Chang, C. J., Kimura, S. R., Gao, M., Xie, D., Zhang, Y., et al. (2014). The structure of human tau-tubulin kinase 1 both in the apo form and in complex with an inhibitor. *Acta Crystallogr. F. Struct. Biol. Commun.* 70, 173–181. doi:10.1107/S2053230X14000144
- Kim, E. N., Lim, J. H., Kim, M. Y., Ban, T. H., Jang, I., Yoon, H. E., et al. (2018). Resveratrol, an Nrf2 activator, ameliorates aging-related progressive renal injury. *Aging (Albany NY)* 10, 83–99. doi:10.18632/aging.101361
- Kim, H., Choi, K., Kang, H., Lee, S.-Y., Chi, S.-W., Lee, M.-S., et al. (2014). Identification of a novel function of CX-4945 as a splicing regulator. *PLoS One* 9, e94978. doi:10.1371/journal.pone.0094978
- Kim, J. K., and Park, S. U. (2021). Flavonoids for treatment of Alzheimer's disease: An up to date review. *EXCLI J.* 20, 495–502. doi:10.17179/excli2021-3492
- Knippschild, U., Gocht, A., Wolff, S., Huber, N., Löhler, J., and Stöter, M. (2005). The casein kinase 1 family: Participation in multiple cellular processes in eukaryotes. *Cell. Signal.* 17, 675–689. doi:10.1016/j.cellsig.2004.12.011
- Komorowska, J., Wątroba, M., and Szukiewicz, D. (2020). Review of beneficial effects of resveratrol in neurodegenerative diseases such as Alzheimer's disease. *Adv. Med. Sci.* 65, 415–423. doi:10.1016/j.advms.2020.08.002

- Kosten, J., Binolfi, A., Stuver, M., Verzini, S., Theillet, F.-X., Bekei, B., et al. (2014). Efficient modification of alpha-synuclein serine 129 by protein kinase CK1 requires phosphorylation of tyrosine 125 as a priming event. *ACS Chem. Neurosci.* 5, 1203–1208. doi:10.1021/cn5002254
- Kotaniidou, A., Xagorari, A., Bagli, E., Kitsanta, P., Fotsis, T., Papapetropoulos, A., et al. (2002). Luteolin reduces lipopolysaccharide-induced lethal toxicity and expression of proinflammatory molecules in mice. *Am. J. Respir. Crit. Care Med.* 165, 818–823. doi:10.1164/ajrccm.165.6.2101049
- Kovacs, G. G., Botond, G., and Budka, H. (2010). Protein coding of neurodegenerative dementias: The neuropathological basis of biomarker diagnostics. *Acta Neuropathol.* 119, 389–408. doi:10.1007/s00401-010-0658-1
- Kumar, A., Singh, C. K., LaVoie, H. A., DiPette, D. J., and Singh, U. S. (2011). Resveratrol Restores Nrf2 Level and Prevents Ethanol-Induced Toxic Effects in the Cerebellum of a Rodent Model of Fetal Alcohol Spectrum Disorders. *Mol. Pharmacol.* 80, 446–457. doi:10.1124/mol.111.071126
- Kwon, Y. (2017). Luteolin as a potential preventive and therapeutic candidate for Alzheimer's disease. *Exp. Gerontol.* 95, 39–43. doi:10.1016/j.exger.2017.05.014
- LaFerla, F. M., Green, K. N., and Oddo, S. (2007). Intracellular amyloid- β in Alzheimer's disease. *Nat. Rev. Neurosci.* 8, 499–509. doi:10.1038/nrn2168
- Lasa, M., Marin, O., and Pinna, L. A. (1997). Rat liver Golgi apparatus contains a protein kinase similar to the casein kinase of lactating mammary gland. *Eur. J. Biochem.* 243, 719–725. doi:10.1111/j.1432-1033.1997.00719.x
- Lastres-Becker, I., García-Yagüe, A. J., Scannevin, R. H., Casarejos, M. J., Kügler, S., Rábano, A., et al. (2016). Repurposing the NRF2 activator dimethyl fumarate as therapy against synucleinopathy in Parkinson's disease. *Antioxid. Redox Signal.* 25, 61–77. doi:10.1089/ars.2015.6549
- Ławnicka, H., Kowalewicz-Kulbat, M., Sicińska, P., Kazimierzczuk, Z., Grieb, P., and Stępień, P. (2010). Anti-neoplastic effect of protein kinase CK2 inhibitor, 2-dimethylamino-4, 5, 6, 7-tetrabromobenzimidazole (DMAT), on growth and hormonal activity of human adrenocortical carcinoma cell line (H295R) *in vitro*. *Cell Tissue Res.* 340, 371–379. doi:10.1007/s00441-010-0960-1
- Lee, J. W., Hirota, T., Peters, E. C., Garcia, M., Gonzalez, R., Cho, C. Y., et al. (2011). A small molecule modulates circadian rhythms through phosphorylation of the period protein. *Angew. Chem. Int. Ed. Engl.* 50, 10608–10611. doi:10.1002/anie.201103915
- Lee, J. Y., Yun, J.-S., Kim, W.-K., Chun, H.-S., Jin, H., Cho, S., et al. (2019). Structural basis for the selective inhibition of cdc2-like kinases by CX-4945. *Biomed. Res. Int.* 2019, 6125068. doi:10.1155/2019/6125068
- Lee, V. M., Goedert, M., and Trojanowski, J. Q. (2001). Neurodegenerative tauopathies. *Annu. Rev. Neurosci.* 24, 1121–1159. doi:10.1146/annurev.neuro.24.1.1121
- Li, C., Liu, X., Lin, X., and Chen, X. (2009). Structure-activity relationship of 7 flavonoids on recombinant human protein kinase CK2 holoenzyme. *Zhong Nan Da Xue Xue Bao Yi Xue Ban.* 34, 20–26.
- Li, G., Yin, H., and Kurent, J. (2004). Casein kinase 1 delta phosphorylates tau and disrupts its binding to microtubules. *J. Biol. Chem.* 279, 15938–15945. doi:10.1074/jbc.M314116200
- Li, H.-Y., Yeh, P.-A., Chiu, H.-C., Tang, C.-Y., and Tu, B. P.-h. (2011). Hyperphosphorylation as a defense mechanism to reduce TDP-43 aggregation. *PLoS One* 6, e23075. doi:10.1371/journal.pone.0023075
- Li, K., McGee, L. R., Fisher, B., Sudom, A., Liu, J., Rubenstein, S. M., et al. (2013). Inhibiting NF- κ B-inducing kinase (NIK): Discovery, structure-based design, synthesis, structure-activity relationship, and co-crystal structures. *Bioorg. Med. Chem. Lett.* 23, 1238–1244. doi:10.1016/j.bmcl.2013.01.012
- Li, M., Makkinje, A., and Damuni, Z. (1996). Molecular identification of I1PP2A, a novel potent heat-stable inhibitor protein of protein phosphatase 2A. *Biochemistry* 35, 6998–7002. doi:10.1021/bi960581y
- Liachko, N. F., McMillan, P. J., Strovast, T. J., Loomis, E., Greenup, L., Murrell, J. R., et al. (2014). The tau tubulin kinases TTBK1/2 promote accumulation of pathological TDP-43. *PLoS Genet.* 10, e1004803. doi:10.1371/journal.pgen.1004803
- Liao, J.-C., Yang, T. T., Weng, R. R., Kuo, C.-T., and Chang, C.-W. (2015). TTBK2: A tau protein kinase beyond tau phosphorylation. *Biomed. Res. Int.* 2015, 575170. doi:10.1155/2015/575170
- Lindwall, G., and Cole, R. D. (1984). Phosphorylation affects the ability of tau protein to promote microtubule assembly. *J. Biol. Chem.* 259, 5301–5305. doi:10.1016/S0021-9258(17)42989-9
- Lippa, C. F., Fujiwara, H., Mann, D. M., Giasson, B., Baba, M., Schmidt, M. L., et al. (1998). Lewy bodies contain altered alpha-synuclein in brains of many familial Alzheimer's disease patients with mutations in presenilin and amyloid precursor protein genes. *Am. J. Pathol.* 153, 1365–1370. doi:10.1016/s0002-9440(10)65722-7
- Litchfield, D. W. (2003). Protein kinase CK2: Structure, regulation and role in cellular decisions of life and death. *Biochem. J.* 369, 1–15. doi:10.1042/bj20021469
- Liu, G., Li, H., Zhang, W., Yu, J., Zhang, X., Wu, R., et al. (2021). Csnk1a1 inhibition modulates the inflammatory secretome and enhances response to radiotherapy in glioma. *J. Cell. Mol. Med.* 25, 7395–7406. doi:10.1111/jcmm.16767
- Liu, J., Yi, L., Xiang, Z., Zhong, J., Zhang, H., and Sun, T. (2015). Resveratrol attenuates spinal cord injury-induced inflammatory damage in rat lungs. *Int. J. Clin. Exp. Pathol.* 8, 1237–1246.
- Liu, Q.-S., Deng, R., Li, S., Li, X., Li, K., Kebaituli, G., et al. (2017). Ellagic acid protects against neuron damage in ischemic stroke through regulating the ratio of Bcl-2/Bax expression. *Appl. Physiol. Nutr. Metab.* 42, 855–860. doi:10.1139/apnm-2016-0651
- Lolli, G., Cozza, G., Mazzorana, M., Tibaldi, E., Cesaro, L., Donella-Deana, A., et al. (2012). Inhibition of protein kinase CK2 by flavonoids and typhostins. A structural insight. *Biochemistry* 51, 6097–6107. doi:10.1021/bi300531c
- Lopez-Lazaro, M. (2009). Distribution and biological activities of the flavonoid luteolin. *Mini Rev. Med. Chem.* 9, 31–59. doi:10.2174/138955709787001712
- Lund, H., Cowburn, R. F., Gustafsson, E., Strömberg, K., Svensson, A., Dahllund, L., et al. (2013). Tau-tubulin kinase 1 expression, phosphorylation and Co-localization with phospho-ser422 tau in the Alzheimer's disease brain. *Brain Pathol.* 23, 378–389. doi:10.1111/bpa.12001
- Lunkes, A., Lindenberg, K. S., Ben-Haïem, L., Weber, C., Devys, D., Landwehrmeyer, G. B., et al. (2002). Proteases acting on mutant huntingtin generate cleaved products that differentially build up cytoplasmic and nuclear inclusions. *Mol. Cell* 10, 259–269. doi:10.1016/s1097-2765(02)00602-0
- Mackenzie, I. R., Rademakers, R., and Neumann, M. (2010). TDP-43 and FUS in amyotrophic lateral sclerosis and frontotemporal dementia. *Lancet. Neurol.* 9, 995–1007. doi:10.1016/S1474-4422(10)70195-2
- Maher, P., Dargusch, R., Bodai, L., Gerard, P. E., Purcell, J. M., and Marsh, J. L. (2010). ERK activation by the polyphenols fisetin and resveratrol provides neuroprotection in multiple models of Huntington's disease. *Hum. Mol. Genet.* 20, 261–270. doi:10.1093/hmg/ddq460
- Marcon, G., Di Fede, G., Giaccone, G., Rossi, G., Giovagnoli, A. R., Maccagnano, E., et al. (2009). A novel Italian presenilin 2 gene mutation with prevalent behavioral phenotype. *J. Alzheimers Dis.* 16, 509–511. doi:10.3233/JAD-2009-0986
- Marin, O., Meggio, F., Sarno, S., Andretta, M., and Pinna, L. A. (1994). Phosphorylation of synthetic fragments of inhibitor-2 of protein phosphatase-1 by casein kinase-1 and -2. Evidence that phosphorylated residues are not strictly required for efficient targeting by casein kinase-1. *Eur. J. Biochem.* 223, 647–653. doi:10.1111/j.1432-1033.1994.tb19037.x
- Maroteaux, L., Campanelli, J. T., and Scheller, R. H. (1988). Synuclein: A neuron-specific protein localized to the nucleus and presynaptic nerve terminal. *J. Neurosci.* 8, 2804–2815. doi:10.1523/JNEUROSCI.08-08-02804.1988
- Martínez-González, L., Rodríguez-Cueto, C., Cabezedo, D., Bartolomé, F., Andrés-Benito, P., Ferrer, I., et al. (2020). Motor neuron preservation and decrease of *in vivo* TDP-43 phosphorylation by protein CK-1 δ kinase inhibitor treatment. *Sci. Rep.* 10, 4449. doi:10.1038/s41598-020-61265-y
- Mashhoon, N., De Maggio, A. J., Tereshko, V., Bergmeier, S. C., Egli, M., Hoekstra, M. F., et al. (2000). Crystal structure of a conformation-selective casein kinase-1 inhibitor. *J. Biol. Chem.* 275, 20052–20060. doi:10.1074/jbc.M001713200
- Mbefo, M. K., Fares, M.-B., Paleologou, K., Oueslati, A., Yin, G., Tenreiro, S., et al. (2015). Parkinson disease mutant E46K enhances α -synuclein phosphorylation in mammalian cell lines, in yeast, and *in vivo*. *J. Biol. Chem.* 290, 9412–9427. doi:10.1074/jbc.M114.610774
- Meggio, F., Marin, O., and Pinna, L. A. (1994). Substrate specificity of protein kinase CK2. *Cell. Mol. Biol. Res.* 40, 401–409.
- Meggio, F., Perich, J. W., Marin, O., and Pinna, L. A. (1992). The comparative efficiencies of the Ser(P)-Thr(P)- and Tyr(P)-residues as specificity determinants for casein kinase-1. *Biochem. Biophys. Res. Commun.* 182, 1460–1465. doi:10.1016/0006-291x(92)91898-z
- Meggio, F., Perich, J. W., Reynolds, E. C., and Pinna, L. A. (1991). A synthetic β -casein phosphopeptide and analogues as model substrates for casein kinase-1, a ubiquitous, phosphate directed protein kinase. *FEBS Lett.* 283, 303–306. doi:10.1016/0014-5793(91)80614-9

- Meggio, F., and Pinna, L. A. (2003). One-thousand-and-one substrates of protein kinase CK2? *FASEB J.* 17, 349–368. doi:10.1096/fj.02-0473rev
- Meijer, L., Borgne, A., Mulner, O., Chong, J. P., Blow, J. J., Inagaki, N., et al. (1997). Biochemical and cellular effects of roscovitine, a potent and selective inhibitor of the cyclin-dependent kinases cdc2, cdk2 and cdk5. *Eur. J. Biochem.* 243, 527–536. doi:10.1111/j.1432-1033.1997.t01-2-00527.x
- Meijer, L., Thunnissen, A.-M., White, A., Garnier, M., Nikolic, M., Tsai, L.-H., et al. (2000). Inhibition of cyclin-dependent kinases, GSK-3 β and CK1 by hymenialdisine, a marine sponge constituent. *Chem. Biol.* 7, 51–63. doi:10.1016/S1074-5521(00)00063-6
- Meng, Q.-J., Maywood, E. S., Bechtold, D. A., Lu, W.-Q., Li, J., Gibbs, J. E., et al. (2010). Entrainment of disrupted circadian behavior through inhibition of casein kinase 1 (CK1) enzymes. *Proc. Natl. Acad. Sci. U. S. A.* 107, 15240–15245. doi:10.1073/pnas.1005101107
- Menke, R. A., Jbabdi, S., Miller, K. L., Matthews, P. M., and Zarei, M. (2010). Connectivity-based segmentation of the substantia nigra in human and its implications in Parkinson's disease. *Neuroimage* 52, 1175–1180. doi:10.1016/j.neuroimage.2010.05.086
- Mishra, S., Kinoshita, Ch., Axtman, A. D., and Young, J. E. (2022). Evaluation of a selective chemical probe validates that CK2 mediates neuroinflammation in a human induced pluripotent stem cell-derived microglial model. *Front. Mol. Neurosci.* 15, 824956. doi:10.3389/fnmol.2022.824956
- Morales-Garcia, J. A., Salado, I. G., Sanz-San Cristobal, M., Gil, C., Pérez-Castillo, A., Martínez, A., et al. (2017). Biological and pharmacological characterization of benzothiazole-based CK-1 δ inhibitors in models of Parkinson's disease. *ACS Omega* 2, 5215–5220. doi:10.1021/acsomega.7b00869
- Morooka, S., Hoshina, M., Kii, I., Okabe, T., Kojima, H., Inoue, N., et al. (2015). Identification of a dual inhibitor of SRPK1 and CK2 that attenuates pathological angiogenesis of macular degeneration in mice. *Mol. Pharmacol.* 88, 316–325. doi:10.1124/mol.114.097345
- Mueller, T., Breuer, P., Schmitt, I., Walter, J., Evert, B. O., and Wüllner, U. (2009). CK2-dependent phosphorylation determines cellular localization and stability of ataxin-3. *Hum. Mol. Genet.* 18, 3334–3343. doi:10.1093/hmg/ddp274
- Murphy, M. P., and LeVine, H. (2010). Alzheimer's disease and the amyloid- β peptide. *J. Alzheimer's Dis.* 19, 311–323. doi:10.3233/jad-2010-1221
- Nakagawa, T., and Ohta, K. (2019). Quercetin regulates the integrated stress response to improve memory. *Int. J. Mol. Sci.* 20, 2761. doi:10.3390/ijms20112761
- Nakamura, T., Yamashita, H., Takahashi, T., and Nakamura, S. (2001). Activated Fyn phosphorylates alpha-synuclein at tyrosine residue 125. *Biochem. Biophys. Res. Commun.* 280, 1085–1092. doi:10.1006/bbrc.2000.4253
- Nakielly, S., and Dreyfuss, G. (1997). Nuclear export of proteins and RNAs. *Curr. Opin. Cell Biol.* 9, 420–429. doi:10.1016/S0955-0674(97)80016-6
- Narhi, L., Wood, S. J., Steavenson, S., Jiang, Y., Wu, G. M., Anafi, D., et al. (1999). Both familial Parkinson's disease mutations accelerate alpha-synuclein aggregation. *J. Biol. Chem.* 274, 9843–9846. doi:10.1074/jbc.274.14.9843
- Negro, A., Brunati, A. M., Donella-Deana, A., Massimino, M. L., and Pinna, L. A. (2002). Multiple phosphorylation of alpha-synuclein by protein tyrosine kinase Syk prevents eosin-induced aggregation. *FASEB J.* 16, 210–212. doi:10.1096/fj.01-0517je
- Neumann, M., Bentmann, E., Dormann, D., Jawaid, A., DeJesus-Hernandez, M., Ansorge, O., et al. (2011). FET proteins TAF15 and EWS are selective markers that distinguish FTLD with FUS pathology from amyotrophic lateral sclerosis with FUS mutations. *Brain* 134, 2595–2609. doi:10.1093/brain/awr201
- Neumann, M., Sampathu, D. M., Kwong, L. K., Truax, A. C., Micsenyi, M. C., Chou, T. T., et al. (2006). Ubiquitinated TDP-43 in frontotemporal lobar degeneration and amyotrophic lateral sclerosis. *Science* 314, 130–133. doi:10.1126/science.1134108
- Nirmaladevi, D., Venkataramana, M., Chandranayaka, S., Ramesha, A., Jameel, N. M., and Srinivas, C. (2014). Neuroprotective effects of bikaverin on H₂O₂-induced oxidative stress mediated neuronal damage in SH-SY5Y cell line. *Cell. Mol. Neurobiol.* 34, 973–985. doi:10.1007/s10571-014-0073-6
- Nishi, H., Shaytan, A., and Panchenko, A. R. (2014). Physicochemical mechanisms of protein regulation by phosphorylation. *Front. Genet.* 5, 270. doi:10.3389/fgene.2014.00270
- Nonaka, T., Suzuki, G., Tanaka, Y., Kametani, F., Hirai, S., Okado, H., et al. (2016). Phosphorylation of TAR DNA-binding protein of 43 kDa (TDP-43) by truncated casein kinase 1 delta triggers mislocalization and accumulation of TDP-43. *J. Biol. Chem.* 291, 5473–5483. doi:10.1074/jbc.M115.695379
- Nozal, V., and Martinez, A. (2019). Tau Tubulin Kinase 1 (TTBK1), a new player in the fight against neurodegenerative diseases. *Eur. J. Med. Chem.* 161, 39–47. doi:10.1016/j.ejmech.2018.10.030
- Nozal, V., Martínez-González, L., Gomez-Almeria, M., Gonzalo-Consuegra, C., Santana, P., Chaikuad, A., et al. (2022). TDP-43 modulation by tau-tubulin kinase 1 inhibitors: A new avenue for future amyotrophic lateral sclerosis therapy. *J. Med. Chem.* 65, 1585–1607. doi:10.1021/acs.jmedchem.1c01942
- O'Brien, R. J., and Wong, P. C. (2011). Amyloid precursor protein processing and Alzheimer's disease. *Annu. Rev. Neurosci.* 34, 185–204. doi:10.1146/annurev-neuro-061010-113613
- Okochi, M., Walter, J., Koyama, A., Nakajo, S., Baba, M., Iwatsubo, T., et al. (2000). Constitutive phosphorylation of the Parkinson's disease associated alpha-synuclein. *J. Biol. Chem.* 275, 390–397. doi:10.1074/jbc.275.1.390
- Oliveira, J., Costa, M., de Almeida, M. S. C., da Cruz e Silva, O. A. B., and Henriques, A. G. (2017). Protein phosphorylation is a key mechanism in Alzheimer's disease. *J. Alzheimer's Dis.* 58, 953–978. doi:10.3233/jad-170176
- Oshima, T., Niwa, Y., Kuwata, K., Srivastava, A., Hyoda, T., Tsuchiya, Y., et al. (2019). Cell-based screen identifies a new potent and highly selective CK2 inhibitor for modulation of circadian rhythms and cancer cell growth. *Sci. Adv.* 5, eaau9060. doi:10.1126/sciadv.aau9060
- Ou, S. H., Wu, F., Harrich, D., Garcia-Martinez, L. F., and Gaynor, R. B. (1995). Cloning and characterization of a novel cellular protein, TDP-43, that binds to human immunodeficiency virus type 1 TAR DNA sequence motifs. *J. Virol.* 69, 3584–3596. doi:10.1128/JVI.69.6.3584-3596.1995
- Oueslati, A. (2016). Implication of alpha-synuclein phosphorylation at S129 in synucleinopathies: What have we learned in the last decade? *J. Park. Dis.* 6, 39–51. doi:10.3233/JPD-160779
- Pagano, M. A., Bain, J., Kazmierczuk, Z., Sarno, S., Ruzzene, M., Di Maira, G., et al. (2008). The selectivity of inhibitors of protein kinase CK2: An update. *Biochem. J.* 415, 353–365. doi:10.1042/bj20080309
- Paleologou, K. E., Schmid, A. W., Rospigliosi, C. C., Kim, H.-Y., Lamberto, G. R., Fredenburg, R. A. et al. (2008). Phosphorylation at ser-129 but not the phosphomimics S129E/D inhibits the fibrillation of α -synuclein. *J. Biol. Chem.* 283, 16895–16905. doi:10.1074/jbc.M800747200
- Palomo, V., Nozal, V., Rojas-Prats, E., Gil, C., and Martinez, A. (2020). Protein kinase inhibitors for amyotrophic lateral sclerosis therapy. *Br. J. Pharmacol.* 178, 1316–1335. doi:10.1111/bph.15221
- Perez, D. L., Gil, C., and Martinez, A. (2011). Protein kinases CK1 and CK2 as new targets for neurodegenerative diseases. *Med. Res. Rev.* 31, 924–954. doi:10.1002/med.20207
- Pierre, F., Chua, P. C., O'Brien, S. E., Siddiqui-Jain, A., Bourbon, P., Haddach, M., et al. (2011). Pre-clinical characterization of CX-4945, a potent and selective small molecule inhibitor of CK2 for the treatment of cancer. *Mol. Cell. Biochem.* 356, 37–43. doi:10.1007/s11010-011-0956-5
- Pinna, L. A. (2002). Protein kinase CK2: A challenge to canons. *J. Cell Sci.* 115, 3873–3878. doi:10.1242/jcs.00074
- Plisson, F., Prasad, P., Xiao, X., Piggott, A. M., Huang, X., Khalil, Z., et al. (2014). Callyspongins A–D: Bromopyrrole alkaloids from an Australian marine sponge, callyspongia sp. *Org. Biomol. Chem.* 12, 1579–1584. doi:10.1039/c4ob00091a
- Posa, D., Martinez-Gonzalez, L., Bartolome, F., Nagaraj, S., Porras, G., Martinez, A., et al. (2019). Recapitulation of pathological TDP-43 features in immortalized lymphocytes from sporadic ALS patients. *Mol. Neurobiol.* 56, 2424–2432. doi:10.1007/s12035-018-1249-8
- Potjewyd, F. M., Marquez, A. B., Chaikuad, A., Howel, S., Dunn, A. S., Beltran, A. A., et al. (2022). Modulation of tau tubulin kinases (TTBK1 and TTBK2) impacts ciliogenesis. *bioRxiv* 2022, 06490937. doi:10.1101/2022.05.06.490937
- Pulgar, V., Marin, O., Meggio, F., Allende, C. C., Allende, J. E., and Pinna, L. A. (1999). Optimal sequences for non-phosphate-directed phosphorylation by protein kinase CK1 (casein kinase-1)--a re-evaluation. *Eur. J. Biochem.* 260, 520–526. doi:10.1046/j.1432-1327.1999.00195.x
- Raux, G., Gantier, R., Martin, C., Pothin, Y., Brice, A., Frebourg, T., et al. (2000). A novel presenilin 1 missense mutation (L153V) segregating with early-onset autosomal dominant Alzheimer's disease. *Hum. Mutat.* 16, 95. doi:10.1002/1098-1004(200007)16:1<95::AID-HUMU28>3.0.CO;2-H
- Regal, L., Vanopdenbosch, L., Tilkin, P., Van den Bosch, L., Thijs, V., Sciot, R., et al. (2006). The G93C mutation in superoxide dismutase 1: Clinicopathological phenotype and prognosis. *Arch. Neurol.* 63, 262–267. doi:10.1001/archneur.63.2.262
- Reiner, A., Albin, R. L., Anderson, K. D., D'Amato, C. J., Penney, J. B., and Young, A. B. (1988). Differential loss of striatal projection neurons in Huntington disease. *Proc. Natl. Acad. Sci. U. S. A.* 85, 5733–5737. doi:10.1073/pnas.85.15.5733
- Rena, G., Bain, J., Elliott, M., and Cohen, P. (2004). D4476, a cell-permeant inhibitor of CK1, suppresses the site-specific phosphorylation and nuclear exclusion of FOXO1a. *EMBO Rep.* 5, 60–65. doi:10.1038/sj.embor.7400048

- Renton, A. E., Chiò, A., and Traynor, B. J. (2013). State of play in amyotrophic lateral sclerosis genetics. *Nat. Neurosci.* 17, 17–23. doi:10.1038/nn.3584
- Rezai-Zadeh, K., Shytle, R. D., Bai, Y., Tian, J., Hou, H., Mori, T., et al. (2009). Flavonoid-mediated presenilin-1 phosphorylation reduces Alzheimer's disease beta-amyloid production. *J. Cell. Mol. Med.* 13, 574–588. doi:10.1111/j.1582-4934.2008.00344.x
- Richter, J., Bischof, J., Zaja, M., Kohlhof, H., Othersen, O., Vitt, D., et al. (2014). Difluoro-dioxolo-benzoimidazol-benzamides as potent inhibitors of CK1δ and ε with nanomolar inhibitory activity on cancer cell proliferation. *J. Med. Chem.* 57, 7933–7946. doi:10.1021/jm500600b
- Rios, J.-L., Giner, R., Marin, M., and Recio, M. (2018). A pharmacological update of ellagic acid. *Planta Med.* 84, 1068–1093. doi:10.1055/a-0633-9492
- Robberecht, W., and Philips, T. (2013). The changing scene of amyotrophic lateral sclerosis. *Nat. Rev. Neurosci.* 14, 248–264. doi:10.1038/nrn3430
- Rosenberger, A. F. N., Morrema, T. H. J., Gerritsen, W. H., van Haastert, E. S., Snkhchyan, H., Hilhorst, R., et al. (2016). Increased occurrence of protein kinase CK2 in astrocytes in Alzheimer's disease pathology. *J. Neuroinflammation* 13, 4. doi:10.1186/s12974-015-0470-x
- Rosenblatt, A. (2007). Neuropsychiatry of Huntington's disease. *Dialogues Clin. Neurosci.* 9, 191–197. doi:10.31887/DCNS.2007.9.2/arsenblatt
- Rubinstein, D. C., Leggo, J., Coles, R., Almqvist, E., Biancalana, V., Cassiman, J. J., et al. (1996). Phenotypic characterization of individuals with 30–40 CAG repeats in the Huntington disease (HD) gene reveals HD cases with 36 repeats and apparently normal elderly individuals with 36–39 repeats. *Am. J. Hum. Genet.* 59, 16–22.
- Rubio de la Torre, E., Luzon-Toro, B., Forte-Lago, I., Minguez-Castellanos, A., Ferrer, I., and Hilfiker, S. (2009). Combined kinase inhibition modulates Parkin inactivation. *Hum. Mol. Genet.* 18, 809–823. doi:10.1093/hmg/ddn407
- Salado, I. G., Redondo, M., Bello, M. L., Perez, C., Liachko, N. F., Kraemer, B. C., et al. (2014). Protein kinase CK-1 inhibitors as new potential drugs for amyotrophic lateral sclerosis. *J. Med. Chem.* 57, 2755–2772. doi:10.1021/jm500065f
- Salvi, M., Sarno, S., Cesaro, L., Nakamura, H., and Pinna, L. A. (2009). Extraordinary pleiotropy of protein kinase CK2 revealed by weblogo phosphoproteome analysis. *Biochim. Biophys. Acta* 1793, 847–859. doi:10.1016/j.bbamcr.2009.01.013
- Sannerud, R., Esselens, C., Ejsmont, P., Mattera, R., Rochin, L., Tharkeshwar, A. K., et al. (2016). Restricted location of PSEN2/γ-secretase determines substrate specificity and generates an intracellular Aβ pool. *Cell* 166, 193–208. doi:10.1016/j.cell.2016.05.020
- Sarno, S., Reddy, H., Meggio, F., Ruzzene, M., Davies, S. P., Donella-Deana, A., et al. (2001). Selectivity of 4, 5, 6, 7-tetrabromobenzotriazole, an ATP site-directed inhibitor of protein kinase CK2 ("casein kinase-2"). *FEBS Lett.* 496, 44–48. doi:10.1016/S0014-5793(01)02404-8
- Sato, N., Hori, O., Yamaguchi, A., Lambert, J. C., Chartier-Harlin, M. C., Robinson, P. A., et al. (1999). A novel presenilin-2 splice variant in human Alzheimer's disease brain tissue. *J. Neurochem.* 72, 2498–2505. doi:10.1046/j.1471-4159.1999.0722498.x
- Sato, S., Cerny, R. L., Buescher, J. L., and Ikezu, T. (2006). Tau-tubulin kinase 1 (TTBK1), a neuron-specific tau kinase candidate, is involved in tau phosphorylation and aggregation. *J. Neurochem.* 98, 1573–1584. doi:10.1111/j.1471-4159.2006.04059.x
- Sato, S., Xu, J., Okuyama, S., Martinez, L. B., Walsh, S. M., Jacobsen, M. T., et al. (2008). Spatial learning impairment, enhanced CDK5/p35 activity, and downregulation of NMDA receptor expression in transgenic mice expressing tau-tubulin kinase 1. *J. Neurosci.* 28, 14511–14521. doi:10.1523/jneurosci.3417-08.2008
- Schwab, C., DeMaggio, A. J., Ghoshal, N., Binder, L. I., Kuret, J., and McGeer, P. L. (2000). Casein kinase I delta is associated with pathological accumulation of tau in several neurodegenerative diseases. *Neurobiol. Aging* 21, 503–510. doi:10.1016/S0197-4580(00)00110-X
- Schwartz, P. A., and Murray, B. W. (2011). Protein kinase biochemistry and drug discovery. *Bioorg. Chem.* 39, 192–210. doi:10.1016/j.bioorg.2011.07.004
- Schwind, L., Nalbach, L., Zimmer, A. D., Kostelnik, K. B., Menegatti, J., Grässer, F., et al. (2017). Quinalizarin inhibits adipogenesis through down-regulation of transcription factors and microRNA modulation. *Biochim. Biophys. Acta. Gen. Subj.* 1861, 3272–3281. doi:10.1016/j.bbagen.2017.09.018
- Selvakumar, K., Bavithra, S., Suganthi, M., Benson, C. S., Elumalai, P., Arunkumar, R., et al. (2012). Protective role of quercetin on PCBs-induced oxidative stress and apoptosis in hippocampus of adult rats. *Neurochem. Res.* 37, 708–721. doi:10.1007/s11064-011-0661-5
- Shao, G., Chen, S., Sun, Y., Xu, H., and Ge, F. (2021). Chrysoeriol promotes functional neurological recovery in a rat model of cerebral ischemia. *Phcog. Mag.* 17, 802–810. doi:10.4103/pm.pm_329_21
- Sharma, V., Mishra, M., Ghosh, S., Tewari, R., Basu, A., Seth, P., et al. (2007). Modulation of interleukin-1β mediated inflammatory response in human astrocytes by flavonoids: Implications in neuroprotection. *Brain Res. Bull.* 73, 55–63. doi:10.1016/j.brainresbull.2007.01.016
- Shimura, H., Hattori, N., Kubo, S., Mizuno, Y., Asakawa, S., Minoshima, S., et al. (2000). Familial Parkinson disease gene product, parkin, is a ubiquitin-protein ligase. *Nat. Genet.* 25, 302–305. doi:10.1038/77060
- Siddiqui-Jain, A., Drygin, D., Streiner, N., Chua, P., Pierre, F., O'Brien, S. E., et al. (2010). CX-4945, an orally bioavailable selective inhibitor of protein kinase CK2, inhibits prosurvival and angiogenic signaling and exhibits antitumor efficacy. *Cancer Res.* 70, 10288–10298. doi:10.1158/0008-5472.CAN-10-1893
- Smith, M. J., Sharples, R. A., Evin, G., McLean, C. A., Dean, B., Pavey, G., et al. (2004). Expression of truncated presenilin 2 splice variant in Alzheimer's disease, bipolar disorder, and schizophrenia brain cortex. *Brain Res. Mol. Brain Res.* 127, 128–135. doi:10.1016/j.molbrainres.2004.05.019
- Spillantini, M. G., Schmidt, M. L., Lee, V. M., Trojanowski, J. Q., Jakes, R., and Goedert, M. (1997). Alpha-synuclein in Lewy bodies. *Nature* 388, 839–840. doi:10.1038/42166
- Sreedharan, J., Blair, I. P., Tripathi, V. B., Hu, X., Vance, C., Rogelj, B., et al. (2008). TDP-43 mutations in familial and sporadic amyotrophic lateral sclerosis. *Science* 319, 1668–1672. doi:10.1126/science.1154584
- Sriram, S. R., Li, X., Ko, H. S., Chung, K. K., Wong, E., Lim, K. L., et al. (2005). Familial-associated mutations differentially disrupt the solubility, localization, binding and ubiquitination properties of parkin. *Hum. Mol. Genet.* 14, 2571–2586. doi:10.1093/hmg/ddi292
- Su, C.-F., Jiang, L., Zhang, X. W., Iyaswamy, A., and Li, M. (2021). Resveratrol in rodent models of Parkinson's disease: A systematic review of experimental studies. *Front. Pharmacol.* 12, 644219. doi:10.3389/fphar.2021.644219
- Su, Z., Song, J., Wang, Z., Zhou, L., Xia, Y., Yu, S., et al. (2018). Tumor promoter TPA activates Wnt/β-catenin signaling in a casein kinase 1-dependent manner. *Proc. Natl. Acad. Sci. U. S. A.* 115, E7522–E7531. doi:10.1073/pnas.1802422115
- Sundaram, S., Nagaraj, S., Mahoney, H., Portugues, A., Li, W., Millsaps, K., et al. (2019). Inhibition of casein kinase 1δ/ε improves cognitive-affective behavior and reduces amyloid load in the APP-PS1 mouse model of Alzheimer's disease. *Sci. Rep.* 9, 13743. doi:10.1038/s41598-019-50197-x
- Szyska, R., Grankowski, N., Felczak, K., and Shugar, D. (1995). Halogenated benzimidazoles and benzotriazoles as selective inhibitors of protein kinases CK-I and CK-II from *Saccharomyces cerevisiae* and other sources. *Biochem. Biophys. Res. Commun.* 208, 418–424. doi:10.1006/bbrc.1995.1354
- Tagliabracci, V. S., Wiley, S. E., Guo, X., Kinch, L. N., Durrant, E., Wen, J., et al. (2015). A single kinase generates the majority of the secreted phosphoproteome. *Cell* 161, 1619–1632. doi:10.1016/j.cell.2015.05.028
- Takahashi, M., Tomizawa, K., Sato, K., Ohtake, A., and Omori, A. (1995). A novel tau-tubulin kinase from bovine brain. *FEBS Lett.* 372, 59–64. doi:10.1016/0014-5793(95)00955-9
- Takano, A., Hoe, H.-S., Isojima, Y., and Nagai, K. (2004). Analysis of the expression, localization and activity of rat casein kinase Iε. *Neuroreport* 15, 1461–1464. doi:10.1097/01.wnr.0000133297.77278.81
- Takashima, A., Noguchi, K., Sato, K., Hoshimoto, T., and Imahori, K. (1993). Tau protein kinase I is essential for amyloid beta-protein-induced neurotoxicity. *Proc. Natl. Acad. Sci. U. S. A.* 90, 7789–7793. doi:10.1073/pnas.90.16.7789
- Tanimukai, H., Grundke-Iqbal, I., and Iqbal, K. (2005). Up-regulation of inhibitors of protein phosphatase-2A in Alzheimer's disease. *Am. J. Pathol.* 66, 1761–1771. doi:10.1016/S0002-9440(10)62486-8
- Tarrant, M. K., and Cole, P. A. (2009). The chemical biology of protein phosphorylation. *Annu. Rev. Biochem.* 78, 797–825. doi:10.1146/annurev.biochem.78.070907.103047
- Taylor, L. M., McMillan, P. J., Kraemer, B. C., and Liachko, N. F. (2019). Tau tubulin kinases in proteinopathy. *FEBS J.* 286, 2434–2446. doi:10.1111/febs.14866
- Taylor, L. M., McMillan, P. J., Liachko, N. F., Strovast, T. J., Ghetti, B., Bird, T. D., et al. (2018). Pathological phosphorylation of tau and TDP-43 by TTBK1 and TTBK2 drives neurodegeneration. *Mol. Neurodegener.* 13, 7. doi:10.1186/s13024-018-0237-9
- Taylor, S. S., and Kornev, A. P. (2011). Protein kinases: Evolution of dynamic regulatory proteins. *Trends biochem. Sci.* 36, 65–77. doi:10.1016/j.tibs.2010.09.006
- Taylor, S. S., Radzio-Andzelm, E., and Hunter, T. (1995). How do protein kinases discriminate between serine/threonine and tyrosine? Structural insights from the insulin receptor protein-tyrosine kinase. *FASEB J.* 9, 1255–1266. doi:10.1096/fasebj.9.13.7557015

- Tian, Y., Wang, Y., Jablonski, A. M., Hu, Y., Sugam, J. A., Koglin, M., et al. (2021). Tau-tubulin kinase 1 phosphorylates TDP-43 at disease-relevant sites and exacerbates TDP-43 pathology. *Neurobiol. Dis.* 161, 105548. doi:10.1016/j.nbd.2021.105548
- Tiwari, S., Atluri, V., Kaushik, A., Yndar, T. A., and Nair, M. (2019). Alzheimer's disease: Pathogenesis, diagnostics, and therapeutics. *Int. J. Nanomedicine* 14, 5541–5554. doi:10.2147/IJN.S200490
- Tomizawa, K., Omori, A., Ohtake, A., Sato, K., and Takahashi, M. (2001). Tau-tubulin kinase phosphorylates tau at Ser-208 and Ser-210, sites found in paired helical filament-tau. *FEBS Lett.* 492, 221–227. doi:10.1016/s0014-5793(01)02256-6
- Turner, R. S., Thomas, R. G., Craft, S., van Dyck, C. H., Mintzer, J., Reynolds, B. A., et al. (2015). A randomized, double-blind, placebo-controlled trial of resveratrol for Alzheimer disease. *Neurology* 85, 1383–1391. doi:10.1212/wnl.0000000000002035
- Ueda, K., Fukushima, H., Masliah, E., Xia, Y., Iwai, A., Yoshimoto, M., et al. (1993). Molecular cloning of cDNA encoding an unrecognized component of amyloid in Alzheimer disease. *Proc. Natl. Acad. Sci. U. S. A.* 90, 11282–11286. doi:10.1073/pnas.90.23.11282
- Ullah, A., Munir, S., Badshah, S. L., Khan, N., Ghani, L., Poulson, B. G., et al. (2020). Important flavonoids and their role as a therapeutic agent. *Molecules* 25, 5243. doi:10.3390/molecules25225243
- Uversky, V. N. (2007). Neuropathology, biochemistry, and biophysics of alpha-synuclein aggregation. *J. Neurochem.* 103, 17–37. doi:10.1111/j.1471-4159.2007.04764.x
- Varela, L., and Garcia-Rendueles, M. E. R. (2022). Oncogenic pathways in neurodegenerative diseases. *Int. J. Mol. Sci.* 23, 3223. doi:10.3390/ijms23063223
- Vargas, M. R., Pehar, M., Cassina, P., Beckman, J. S., and Barbeito, L. (2006). Increased glutathione biosynthesis by Nrf2 activation in astrocytes prevents p75NTR-dependent motor neuron apoptosis. *J. Neurochem.* 97, 687–696. doi:10.1111/j.1471-4159.2006.03742.x
- Vassar, R., Bennett, B. D., Babu-Kahn, S., Kahn, S., Mendiáz, E. A., Denis, P., et al. (1999). Beta-secretase cleavage of Alzheimer's amyloid precursor protein by the transmembrane aspartic protease BACE. *Science* 286, 735–741. doi:10.1126/science.286.5440.735
- Vazquez-Higuera, J. L., Martinez-Garcia, A., Sanchez-Juan, P., Rodriguez-Rodriguez, E., Mateo, I., Pozueta, A., et al. (2011). Genetic variations in tau-tubulin kinase-1 are linked to Alzheimer's disease in a Spanish case-control cohort. *Neurobiol. Aging* 32, e5–9. doi:10.1016/j.neurobiolaging.2009.12.021
- Venerando, A., Ruzzene, M., and Pinna, L. A. (2014). Casein kinase: The triple meaning of a misnomer. *Biochem. J.* 460, 141–156. doi:10.1042/bj20140178
- Vera, J., Estanyol, J. M., Canela, N., Llorens, F., Agell, N., Itarte, E., et al. (2007). Proteomic analysis of SET-binding proteins. *Proteomics* 7, 578–587. doi:10.1002/pmic.200600458
- Versluys, L., Pereira, P. E., Schuermans, N., De Paepe, B., De Bleecker, J. L., Bogaert, E., et al. (2022). Expanding the TDP-43 proteinopathy pathway from neurons to muscle: Physiological and pathophysiological functions. *Front. Neurosci.* 16, 815765. doi:10.3389/fnins.2022.815765
- Waddy, C. T., and Mackinlay, A. G. (1971). Protein kinase activity from lactating bovine mammary gland. *Biochim. Biophys. Acta* 250, 491–500. doi:10.1016/0005-2744(71)90249-x
- Wager, T. T., Chandrasekaran, R. Y., Bradley, J., Rubitski, D., Berke, H., Mente, S., et al. (2014). Casein kinase 1δ/ε inhibitor PF-5006739 attenuates opioid drug-seeking behavior. *ACS Chem. Neurosci.* 5, 1253–1265. doi:10.1021/cn500201x
- Wakabayashi, K., Matsumoto, K., Takayama, K., Yoshimoto, M., and Takahashi, H. (1997). NACP, a presynaptic protein, immunoreactivity in Lewy bodies in Parkinson's disease. *Neurosci. Lett.* 239, 45–48. doi:10.1016/s0304-3940(97)00891-4
- Walter, J., Capell, A., Grünberg, J., Pesold, B., Schindzielorz, A., Prior, R., et al. (1996). The Alzheimer's disease-associated presenilins are differentially phosphorylated proteins located predominantly within the endoplasmic reticulum. *Mol. Med.* 2, 673–691. doi:10.1007/BF03401652
- Walter, J., Fluhrer, R., Hartung, B., Willem, M., Kaether, C., Capell, A., et al. (2001). Phosphorylation regulates intracellular trafficking of β-secretase. *J. Biol. Chem.* 276, 14634–14641. doi:10.1074/jbc.M011116200
- Walter, J., Schindzielorz, A., Hartung, B., and Haass, C. (2000). Phosphorylation of the beta-amyloid precursor protein at the cell surface by ectocasein kinases 1 and 2. *J. Biol. Chem.* 275, 23523–23529. doi:10.1074/jbc.M002850200
- Walter, J. (2000). The phosphorylation of presenilin proteins. *Methods Mol. Med.* 32, 317–331. doi:10.1385/1-59259-195-7:317
- Walton, K. M., Fisher, K., Rubitski, D., Marconi, M., Meng, Q.-J., Sladek, M., et al. (2009). Selective inhibition of casein kinase 1 minimally alters circadian clock period. *J. Pharmacol. Exp. Ther.* 330, 430–439. doi:10.1124/jpet.109.151415
- Wan, Y., Hur, W., Cho, C. Y., Liu, Y., Adrian, F. J., Lozach, O., et al. (2004). Synthesis and target identification of hymenialdisine analogs. *Chem. Biol.* 11, 247–259. doi:10.1016/j.chembiol.2004.01.015
- Wang, B., Lu, Z., and Polya, G. (1998). Inhibition of eukaryote serine/threonine-specific protein kinases by piceatannol. *Planta Med.* 64, 195–199. doi:10.1055/s-2006-957407
- Wang, Q., Dong, X., Zhang, R., and Zhao, Ch. (2021). Flavonoids with potential anti-amyloidogenic effects as therapeutic drugs for treating alzheimer's disease. *J. Alzheimers Dis.* 84, 505–533. doi:10.3233/JAD-210735
- Wang, S.-H., Liang, C.-H., Liang, F.-P., Ding, H.-Y., Lin, S.-P., Huang, G.-J., et al. (2016). The inhibitory mechanisms study of 5, 6, 4'-trihydroxy-7, 3'-dimethoxyflavone against the LPS-induced macrophage inflammatory responses through the antioxidant ability. *Molecules* 21, 136. doi:10.3390/molecules21020136
- Waxman, E. A., and Giasson, B. I. (2008). Specificity and regulation of casein kinase/mediated phosphorylation of α-synuclein. *J. Neuropathol. Exp. Neurol.* 67, 402–416. doi:10.1097/NEN.0b013e31816fc995
- Wei, Y., Zhu, G., Zheng, C., Li, J., Sheng, S., Li, D., et al. (2020). Ellagic acid protects dopamine neurons from rotenone-induced neurotoxicity via activation of Nrf2 signalling. *J. Cell. Mol. Med.* 24, 9446–9456. doi:10.1111/jcmm.15616
- Weingarten, M. D., Lockwood, A. H., Hwo, S. Y., and Kirschner, M. W. (1975). A protein factor essential for microtubule assembly. *Proc. Natl. Acad. Sci. U. S. A.* 72, 1858–1862. doi:10.1073/pnas.72.5.1858
- Wells, C. I., Drewry, D. H., Pickett, J. E., Tjaden, A., Krämer, A., Müller, S., et al. (2021). Development of a potent and selective chemical probe for the pleiotropic kinase CK2. *Cell Chem. Biol.* 28, 546–558. e10. doi:10.1016/j.chembiol.2020.12.013
- Wirkner, U., Voss, H., Lichter, P., Ansorge, W., and Pyerin, W. (1994). The human gene (CSNK2A1) coding for the casein kinase II subunit alpha is located on chromosome 20 and contains tandemly arranged Alu repeats. *Genomics* 19, 257–265. doi:10.1006/geno.1994.1056
- Xia, J., Lee, D. H., Taylor, J., Vandelft, M., and Truant, R. (2003). Huntingtin contains a highly conserved nuclear export signal. *Hum. Mol. Genet.* 12, 1393–1403. doi:10.1093/hmg/ddg156
- Xu, J., Sato, S., Okuyama, S., Swan, R. J., Jacobsen, M. T., Strunk, E., et al. (2010). Tau-tubulin kinase 1 enhances prefibrillar tau aggregation and motor neuron degeneration in P301L FTDP-17 tau-mutant mice. *FASEB J.* 24, 2904–2915. doi:10.1096/fj.09-150144
- Xu, P., Ianes, C., Gärtner, F., Liu, C., Burster, T., Bakulev, V., et al. (2019). Structure, regulation, and (patho-)physiological functions of the stress-induced protein kinase CK1 delta (CSNK1D). *Gene* 715, 144005. doi:10.1016/j.gene.2019.144005
- Xu, Y., Deng, Y., and Qing, H. (2015). The phosphorylation of α-synuclein: Development and implication for the mechanism and therapy of the Parkinson's disease. *J. Neurochem.* 135, 4–18. doi:10.1111/jnc.13234
- Xue, Y., Wan, P. T., Hillertz, P., Schweikart, F., Zhao, Y., Wissler, L., et al. (2013). X-ray structural analysis of tau-tubulin kinase 1 and its interactions with small molecular inhibitors. *ChemMedChem* 8, 1846–1854. doi:10.1002/cmdc.201300274
- Yadikar, H., Torres, I., Aiello, G., Kurup, M., Yang, Z., Lin, F., et al. (2020). Screening of tau protein kinase inhibitors in a tauopathy-relevant cell-based model of tau hyperphosphorylation and oligomerization. *PLOS ONE* 15, e0224952. doi:10.1371/journal.pone.0224952
- Yamamoto, A., Friedlein, A., Imai, Y., Takahashi, R., Kahle, P. J., and Haass, Ch. (2005). Parkin phosphorylation and modulation of its E3 ubiquitin ligase activity. *J. Biol. Chem.* 280, 3390–3399. doi:10.1074/jbc.M407724200
- Yang, A. J. T., Bagit, A., and MacPherson, R. E. K. (2021). Resveratrol, metabolic dysregulation, and Alzheimer's disease: Considerations for neurodegenerative disease. *Int. J. Mol. Sci.* 22, 4628. doi:10.3390/ijms22094628
- Yang, Y., Xu, T., Zhang, Y., and Qin, X. (2017). Molecular basis for the regulation of the circadian clock kinases CK1δ and CK1ε. *Cell. Signal.* 31, 58–65. doi:10.1016/j.cellsig.2016.12.010
- Yang-Feng, T. L., Naiman, T., Kopatz, I., Eli, D., Dafni, N., and Canaani, D. (1994). Assignment of the human casein kinase II alpha' subunit gene (CSNK2A1) to chromosome 16p13.2-p13.3. *Genomics* 19, 173. doi:10.1006/geno.1994.1032
- Yasojima, K., Schwab, C., McGeer, E. G., and McGeer, P. L. (2000). Human neurons generate C-reactive protein and amyloid P: Upregulation in Alzheimer's disease. *Brain Res.* 887, 80–89. doi:10.1016/s0006-8993(00)02970-x
- Yde, C. W., Frogne, T., Lykkesfeldt, A. E., Fichtner, I., Issinger, O.-G., and Stenvang, J. (2007). Induction of cell death in antiestrogen resistant human breast cancer cells by the protein kinase CK2 inhibitor DMAT. *Cancer Lett.* 256, 229–237. doi:10.1016/j.canlet.2007.06.010

- Yonetani, M., Nonaka, T., Masuda, M., Inukai, Y., Oikawa, T., Hisanaga, S., et al. (2009). Conversion of wildtype alpha-synuclein into mutant-type fibrils and its propagation in the presence of A30P mutant. *J. Biol. Chem.* 284, 7940–7950. doi:10.1074/jbc.M807482200
- Yoshida, H., and Ihara, Y. (1993). Tau in paired helical filaments is functionally distinct from fetal tau: Assembly incompetence of paired helical filament-tau. *J. Neurochem.* 61, 1183–1186. doi:10.1111/j.1471-4159.1993.tb03642.x
- Yu, G., Yan, T., Feng, Y., Liu, X., Xia, Y., Luo, H., et al. (2013). Ser9 phosphorylation causes cytoplasmic detention of I_2^{PP2A}/SET in Alzheimer disease. *Neurobiol. Aging* 34, 1748–1758. doi:10.1016/j.neurobiolaging.2012.12.025
- Yu, N.-N., Yu, J.-T., Xiao, J.-T., Zhang, H.-W., Lu, R.-C., Jiang, H., et al. (2011). Tau-tubulin kinase-1 gene variants are associated with Alzheimer's disease in Han Chinese. *Neurosci. Lett.* 491, 83–86. doi:10.1016/j.neulet.2011.01.011
- Yu, P., Wang, L., Tang, F., Zeng, L., Zhou, L., Song, X., et al. (2016). Resveratrol pretreatment decreases ischemic injury and improves neurological function via sonic hedgehog signaling after stroke in rats. *Mol. Neurobiol.* 54, 212–226. doi:10.1007/s12035-015-9639-7
- Zaplatic, E., Bule, M., Shah, S. Z. A., Uddin, M. S., and Niaz, K. (2019). Molecular mechanisms underlying protective role of quercetin in attenuating Alzheimer's disease. *Life Sci.* 224, 109–119. doi:10.1016/j.lfs.2019.03.055
- Zhang, H., Khalil, Z., Conte, M. M., Plisson, F., and Capon, R. J. (2012). A search for kinase inhibitors and antibacterial agents: Bromopyrrolo-2-aminoimidazoles from a deep-water Great Australian Bight sponge *Axinella* sp. *Tetrahedron Lett.* 53, 3784–3787. doi:10.1016/j.tetlet.2012.05.051
- Zhang, J., Gross, S. D., Schroeder, M. D., and Anderson, R. A. (1996). Casein kinase I α and αL : Alternative splicing-generated kinases exhibit different catalytic properties. *Biochemistry* 35, 16319–16327. doi:10.1021/bi9614444
- Zhang, N., Gordon, S. L., Fritsch, M. J., Esoof, N., Campbell, D. G., Gourlay, R., et al. (2015). Phosphorylation of synaptic vesicle protein 2A at Thr84 by casein kinase 1 family kinases controls the specific retrieval of synaptotagmin-1. *J. Neurosci.* 35, 2492–2507. doi:10.1523/JNEUROSCI.4248-14.2015
- Zhang, Q., Xia, Y., Wang, Y., Shentu, Y., Zeng, K., Mahaman, Y. A. R., et al. (2018). CK2 phosphorylating I_2^{PP2A}/SET mediates tau pathology and cognitive impairment. *Front. Mol. Neurosci.* 11, 146. doi:10.3389/fnmol.2018.00146
- Zhang, Y.-J., Xu, Y.-F., Cook, C., Gendron, T. F., Roettges, P., Link, C. D., et al. (2009). Aberrant cleavage of TDP-43 enhances aggregation and cellular toxicity. *Proc. Natl. Acad. Sci. U. S. A.* 106, 7607–7612. doi:10.1073/pnas.0900688106
- Zhao, H., Mei, X., Yang, D., and Tu, G. (2021). Resveratrol inhibits inflammation after spinal cord injury via SIRT-1/NF- κ B signaling pathway. *Neurosci. Lett.* 762, 136151. doi:10.1016/j.neulet.2021.136151
- Zhao, Z., Wang, L., Volk, A. G., Birch, N. W., Stoltz, K. L., Bartom, E. T., et al. (2018). Regulation of MLL/COMPASS stability through its proteolytic cleavage by taspase1 as a possible approach for clinical therapy of leukemia. *Genes Dev.* 33, 61–74. doi:10.1101/gad.319830.118
- Zheng, H., and Koo, E. H. (2006). The amyloid precursor protein: Beyond amyloid. *Mol. Neurodegener.* 1, 5. doi:10.1186/1750-1326-1-5
- Zheng, J. C., and Chen, S. (2022). Translational Neurodegeneration in the era of fast growing international brain research. *Transl. Neurodegener.* 11, 1. doi:10.1186/s40035-021-00276-9
- Zhou, Y., Li, K., Zhang, S., Li, Q., Li, Z., Zhou, F., et al. (2015). Quinalizarin, a specific CK2 inhibitor, reduces cell viability and suppresses migration and accelerates apoptosis in different human lung cancer cell lines. *Indian J. Cancer* 52, e119–e124. doi:10.4103/0019-509X.172508



OPEN ACCESS

EDITED BY
Andrea Venerando,
University of Padua, Italy

REVIEWED BY
Maria Ruzzene,
University of Padua, Italy
Irman Forghani,
University of Miami Hospital,
United States

*CORRESPONDENCE
Isabel Dominguez,
isdoming@bu.edu

SPECIALTY SECTION
This article was submitted to Molecular
Diagnostics and Therapeutics,
a section of the journal
Frontiers in Molecular Biosciences

RECEIVED 10 January 2022

ACCEPTED 29 June 2022

PUBLISHED 13 October 2022

CITATION

Unni P, Friend J, Weinberg J, Okur V,
Hochscherf J and Dominguez I (2022),
Predictive functional, statistical and
structural analysis of *CSNK2A1* and
CSNK2B variants linked to
neurodevelopmental diseases.
Front. Mol. Biosci. 9:851547.
doi: 10.3389/fmolb.2022.851547

COPYRIGHT

© 2022 Unni, Friend, Weinberg, Okur,
Hochscherf and Dominguez. This is an
open-access article distributed under
the terms of the [Creative Commons
Attribution License \(CC BY\)](#). The use,
distribution or reproduction in other
forums is permitted, provided the
original author(s) and the copyright
owner(s) are credited and that the
original publication in this journal is
cited, in accordance with accepted
academic practice. No use, distribution
or reproduction is permitted which does
not comply with these terms.

Predictive functional, statistical and structural analysis of *CSNK2A1* and *CSNK2B* variants linked to neurodevelopmental diseases

Prasida Unni¹, Jack Friend¹, Janice Weinberg², Volkan Okur³,
Jennifer Hochscherf⁴ and Isabel Dominguez^{1*}

¹Department of Medicine, Boston University School of Medicine and Boston Medical Center, Boston University, Boston, MA, United States, ²Department of Biostatistics, Boston University School of Public Health, Boston University, Boston, MA, United States, ³New York Genome Center, New York, NY, United States, ⁴Department of Chemistry, Institute of Biochemistry, University of Cologne, Cologne, Germany

Okur-Chung Neurodevelopmental Syndrome (OCNDS) and Poirier-Bienvenu Neurodevelopmental Syndrome (POBINDS) were recently identified as rare neurodevelopmental disorders. OCNDS and POBINDS are associated with heterozygous mutations in the *CSNK2A1* and *CSNK2B* genes which encode CK2 α , a serine/threonine protein kinase, and CK2 β , a regulatory protein, respectively, which together can form a tetrameric enzyme called protein kinase CK2. A challenge in OCNDS and POBINDS is to understand the genetic basis of these diseases and the effect of the various CK2 α and CK2 β mutations. In this study we have collected all variants available to date in *CSNK2A1* and *CSNK2B*, and identified hotspots. We have investigated CK2 α and CK2 β missense mutations through prediction programs which consider the evolutionary conservation, functionality and structure of these two proteins, compared these results with published experimental data on CK2 α and CK2 β mutants, and suggested prediction programs that could help predict changes in functionality of CK2 α mutants. We also investigated the potential effect of CK2 α and CK2 β mutations on the 3D structure of the proteins and in their binding to each other. These results indicate that there are functional and structural consequences of mutation of CK2 α and CK2 β , and provide a rationale for further study of OCNDS and POBINDS-associated mutations. These data contribute to understanding the genetic and functional basis of these diseases, which is needed to identify their underlying mechanisms.

KEYWORDS

CK2 α , CK2 β , protein kinase CK2, Okur-Chung neurodevelopmental syndrome (OCNDS), Poirier-Bienvenu neurodevelopmental syndrome (POBINDS), autism spectrum disorder (ASD), epilepsy, non-random mutation clustering (NMC)

Introduction

Okur-Chung Neurodevelopmental Syndrome (OCNDS; OMIM #617062) and Poirier-Bienvenu Neurodevelopmental Syndrome (POBINDS; OMIM # 618732) are rare, novel congenital autosomal-dominant neurodevelopmental conditions. Recently identified by whole exome sequencing, OCNDS and POBINDS are attributed mostly to *de novo* (germline non-inherited) variants in the genes *CSNK2A1* and *CSNK2B*, respectively (Iossifov et al., 2014; Okur et al., 2016; Poirier et al., 2017). Common clinical features of patients with OCNDS include intellectual disability, developmental delay, autism spectrum disorder (ASD), language impairment, ataxia, attention deficit hyperactivity disorder, microcephaly and craniofacial dysmorphisms (Iossifov et al., 2014; Okur et al., 2016; Trinh et al., 2017; Yuen et al., 2017; Akahira-Azuma et al., 2018; Chiu et al., 2018; Owen et al., 2018; Duan et al., 2019; Nakashima et al., 2019; Martinez-Monseny et al., 2020; van der Werf et al., 2020; Wang et al., 2020; Wu R et al., 2020; Xu et al., 2020; Dominguez et al., 2021; Wu et al., 2021). Typical clinical features of patients with POBINDS include early onset seizures, intellectual disability and developmental delay, although some patients are also characterized by ASD, attention deficit hyperactivity disorder, language impairment and facial dysmorphisms (Poirier et al., 2017; Sakaguchi et al., 2017; Fernández-Marmiesse et al., 2019; Li et al., 2019; Nakashima et al., 2019; Ernst et al., 2021; Rahman and Fatema 2021; Selvam et al., 2021; Valentino et al., 2021; Yang et al., 2021).

CSNK2A1 and *CSNK2B* genes encode CK2 α , a highly conserved serine/threonine protein kinase, and CK2 β , a

regulatory protein, respectively. CK2 α is present in cells in monomeric form and in a heterotetrameric form composed of two CK2 α subunits bound to a dimer of two CK2 β subunits (CK2 β) (Figure 1). Monomeric CK2 α kinase and CK2 α holoenzyme phosphorylate common and distinct substrates, as docking to CK2 β is required for some substrates to be phosphorylated (reviewed in (Roffey and Litchfield 2021)). The CK2 α -paralog CK2 α' is encoded by the *CSNK2A2* gene and differs mainly in the length and sequence of the C-terminus (Pyrin and Ackermann 2003).

CK2 α and CK2 β are linked to physiological and cellular functions in unicellular and pluricellular eukaryotes and are indispensable for embryonic development of animal and plants; they are also linked to cancer and neurodegenerative diseases, among others (Litchfield 2003; Meggio and Pinna 2003; Ahmad et al., 2008; Duncan and Litchfield 2008; Guerra and Issinger 2008; Dominguez et al., 2009; Ruzzene and Pinna 2010; Trembley et al., 2010; Macias Alvarez et al., 2013; Chua et al., 2017; Gotz and Montenarh 2017; Borgo et al., 2021). CK2 α and CK2 α' mouse knockouts had different phenotypes (reviewed in (Macias Alvarez et al., 2013)). CK2 α (Lou et al., 2008) and CK2 β (Buchou et al., 2003) knockouts are embryonic lethal while CK2 α' knockout mice are viable but have impaired spermatogenesis (Xu et al., 1999). *In vitro*, the isoenzymes display partial functional redundancy, however there are examples that indicate different functions: the C-terminal phosphorylation sites of CK2 α which are phosphorylated in a cell cycle dependent manner are absent in CK2 α' (St-Denis et al., 2009). The affinity of CK2 α' to CK2 β is lower than the affinity between CK2 α and CK2 β (Bischoff et al., 2011a), and isoform

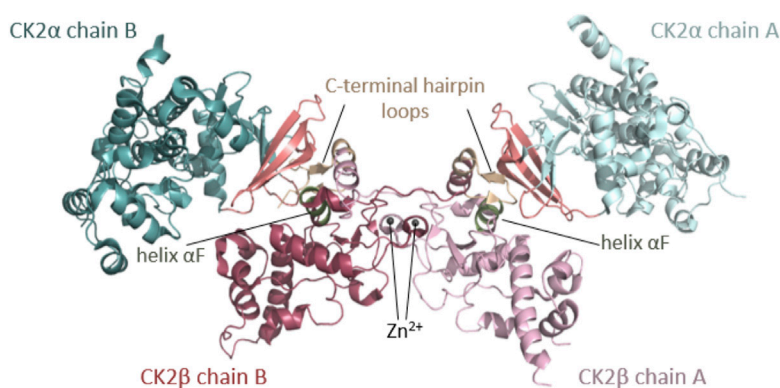


FIGURE 1

Architecture of the heterotetrameric CK2 holoenzyme. CK2 α has two lobes: a N-terminal domain based on a central 5-stranded β -sheet and an α -helical C-terminal domain. CK2 β has two domains: an α -helical domain and a zinc finger domain that serves as a dimerization interface. CK2 β forms dimers via the zinc finger, hydrophobic core residues, and the crossover of the C-terminal tails over the other CK2 β subunit. Due to the crossover of the C-terminal tails of the CK2 β dimer, both CK2 β chains are involved in the interaction with both CK2 α chains. The contact of the CK2 β dimer to the two spatially separated CK2 α subunits is mediated via the C-terminal hairpin loop of one CK2 β chain (α/β tail contact, coloured wheat) and the area around helix αF of the other CK2 β chain (α/β body contact, coloured dark green). The subunit interaction interface of CK2 α is located at the outer surface of the β -sheet of the N-terminal lobe (coloured salmon) (Niefind et al., 2001). The Figure was drawn with PyMOL (Schrödinger, 2013) using the CK2 holoenzyme structure (PDB_ID: 4DGL (Lolli et al., 2012)). Detailed figures of functional domains in the structural section.

specific binding partners have been described (Hériché et al., 1997; Bosc et al., 2000; Litchfield et al., 2001).

CK2 α has the kinase-typical bilobal architecture with a N-terminal domain with a central β -sheet and a α -helical C-terminal domain (Figure 1, detailed schemes of functional domains are found in subsequent figures), which harbor common structural and functional elements of eukaryotic protein kinases (EPKs), such as the Gly-rich loop, the hinge region, the catalytic loop, the activation loop and the P+1 loop (all analyzed in this study). CK2 α belongs to the CMGC family of EPKs—with cyclin dependent kinases (CDKs), mitogen-activated kinases (MAPKs), glycogen synthase kinase-3 (GSK-3) and cell division control 2 (CDC2)-like kinases (CLKs)—which is characterized by a helical insert after helix α G in the C-terminal lobe—(Manning et al., 2002). Unlike its highly regulated relatives within the CMGC family and the majority of other EPKs, CK2 α is constitutively active (Niefind et al., 1998; Niefind et al., 2007; Borgo et al., 2021; Roffey and Litchfield 2021). Typically, EPKs are activated or inactivated in response to an extracellular signal and undergo large conformational changes. For example, often upon activation, the activation loop opens to allow the substrate to bind and the helix α C is re-oriented leading to the formation of a salt bridge between a conserved lysine and glutamine, which is critical for the coordination of the α - and β -phospho-groups of the cosubstrate ATP (Huse and Kuriyan 2002). The structural plasticity of most EPKs that enables the rearrangements of these regulatory key elements is absent in CK2 α . On the contrary, the active conformation is fixed by internal structural constraints. Firstly, the N-terminal segment stabilizes the activation loop and helix α C in the canonical active kinase conformation (Niefind et al., 1998). Secondly, the Phe residue in the DFG-motif at the beginning of the activation loop is replaced by a Trp residue in CK2 α . This unique DWG motif in CK2 α is internally stabilized by an additional hydrogen bond and therefore disfavors the inactive “DFG-out” conformation known from other EPKs (Pargellis et al., 2002). Compared to the other EPKs, CK2 α shows different epicentres of plasticity: in particular, the hinge region and the helix α D (Niefind and Issinger 2010) and the glycine-rich loop display a high degree of flexibility (Raaf et al., 2009). A number of publications describe many unconventional mechanisms of regulation for CK2 which have been recently reviewed (Borgo et al., 2021; Roffey and Litchfield 2021).

Unlike most other protein kinases, CK2 α can efficiently use both ATP or GTP as cosubstrates. The arrangement of water molecules in the active site is crucial to switch from an ATP- to a GTP-compatible state explaining the dual cosubstrate specificity (Niefind et al., 1999). CK2 α has an acidophilic substrate profile with the minimal consensus sequence S/T-D/E-X-D/E (Marchiori et al., 1988). The preference to phosphorylate its substrate at acidic clusters is determined by two anion binding sites (P+3 site and P+1 site) at the activation segment and is

strongly interconnected with the enzyme’s constitutive activity. The function of the equivalent anion binding sites in the CMGC kinase family ranges from regulation to substrate recognition (Niefind et al., 2007). For example, during activation in MAP kinases the positive charge of the P+1 pocket is neutralized by a phosphorylated residue accompanied by large conformational rearrangements (Bellon et al., 1999), and in GSK-3 the positive charge is neutralized by an auto-inhibitory phosphorylation in its N-terminus (Cross et al., 1995) or by a primarily phosphorylated substrate (Frame et al., 2001). However, in CK2 α , the anion binding sites solely serve substrate recognition and are not involved in regulation (Niefind et al., 2007). An additional determinant of CK2 α ’s preference for acidic substrate is the polybasic stretch.

Rigidly fixed in its active form, CK2 α can only be regulated by more unconventional or subtle mechanisms (Niefind et al., 2007). In this context, the regulatory subunit CK2 β comes into play: although it does not serve as an on/off-switch, it modulates CK2 α substrate specificity and its stability against denaturation forces (Issinger et al., 1992; Meggio et al., 1992). CK2 β has an absolutely conserved zinc finger motif that serves as a dimerization interface (Figures 1, 7F). Due to the zinc finger, hydrophobic core residues, and the crossover of the C-terminal tails, the dimerization surface is highly effective and causes CK2 β to form permanent dimers (Chantalat et al., 1999). Integrated in the CK2 holoenzyme, the contact of the CK2 β dimer with the two spatially separated CK2 α subunits is mediated via the C-terminal hairpin loop of one chain (α/β tail contact) and the area around helix α F of the other chain (α/β body contact). The subunit interaction interface of CK2 α is located at the outer surface of the β -sheet of N-terminal lobe (Niefind et al., 2001).

We are beginning to gather information about the genetic basis of OCNDS and POBINDS. To date, thirty six CSNK2A1 variants (mostly *de novo*) are published in both male and female individuals with OCNDS (Iossifov et al., 2014; Okur et al., 2016; Trinh et al., 2017; Yuen et al., 2017; Akahira-Azuma et al., 2018; Chiu et al., 2018; Owen et al., 2018; Duan et al., 2019; Nakashima et al., 2019; Martinez-Monseny et al., 2020; van der Werf et al., 2020; Wang et al., 2020; Wu W et al., 2020; Xu et al., 2020; Dominguez et al., 2021; Wu et al., 2021). Most published gene variants are missense, and the rest are nonsense, splice and frameshift variants. Forty CSNK2B variants (*de novo*) are published in both male and female individuals with POBINDS (Poirier et al., 2017; Sakaguchi et al., 2017; Fernández-Marmiesse et al., 2019; Li et al., 2019; Nakashima et al., 2019; Ernst et al., 2021; Rahman and Fatema 2021; Selvam et al., 2021; Valentino et al., 2021; Yang et al., 2021). A small subset of the identified CSNK2B variants are missense, and the rest are nonsense, splice and frameshift variants. In addition to the published data, CSNK2A1 and CSNK2B variants have also been deposited in data repositories, although these data have not been analyzed so far.

While NGS-based methods have improved clinical diagnosis of rare genetic diseases and accelerated the discovery rate of

causative genes, there is a growing gap between the identification of rare-disease-causing genes and the medical and scientific knowledge leading to the formulation of effective therapies (Boycott et al., 2013). For CK2 α and CK2 β , published studies and databases have used programs to predict whether mutants are pathogenic, likely pathogenic or variants of unknown significance (VUS); sometimes these predictions have led to conflicting results. We are starting to learn the biochemical effects of the mutations in CK2 α and CK2 β . There is experimental evidence that the CK2 α and CK2 β mutations associated with OCNDS and POBINDS can cause biochemical changes in the proteins. Eighteen CK2 α missense mutants have decreased kinase activity *in vitro* kinase assays and some have low expression levels, when recombinant and cell line-expressed mutant CK2 α are analyzed (Dominguez et al., 2021). In addition, some of the CK2 α mutant proteins show changes in subcellular localization compared to the wild-type protein (Dominguez et al., 2021). There is also experimental evidence that one CK2 β mutant has low expression levels and another does not interact with CK2 α (Nakashima et al., 2019). Recently, altered substrate specificity has been reported for CK2 α variant K198R (Caefer et al., 2022; Werner et al., 2022). However, we still have no knowledge of the signaling, cellular and biological mechanism of action of the mutations in CK2 α and CK2 β that are associated with OCNDS and POBINDS, respectively.

The aims of this study are threefold: 1) provide an integrated list of all identified *CSNK2A1* and *CSNK2B* variants to date by leveraging multiple resources—scientific articles and data repositories—to have a broader understanding of the mutation hotspots and the protein domains affected; 2) analyze all mutations collected using the same diverse *in silico* functional predictions tools and assess their concordance with experimental data, and 3) hypothesize on the potential effects of the mutations on protein structure and function.

Materials and methods

CSNK2A1 and *CSNK2B* variants

CSNK2A1 and *CSNK2B* variants were compiled from the OCNDS literature (Iossifov et al., 2014; Okur et al., 2016; Trinh et al., 2017; Yuen et al., 2017; Akahira-Azuma et al., 2018; Chiu et al., 2018; Owen et al., 2018; Duan et al., 2019; Nakashima et al., 2019; Martinez-Monseny et al., 2020; van der Werf et al., 2020; Wang et al., 2020; Wu R et al., 2020; Xu et al., 2020; Dominguez et al., 2021; Wu et al., 2021), and the POBINDS literature (Poirier et al., 2017; Sakaguchi et al., 2017; Fernández-Marmiesse et al., 2019; Li et al., 2019; Nakashima et al., 2019; Ernst et al., 2021; Rahman and Fatema 2021; Selvam et al., 2021; Valentino et al., 2021; Yang et al., 2021). We also compiled *CSNK2A1* and *CSNK2B* variants from the DECIPHER database v11.6 (<https://www.deciphergenomics.org>; last accessed 1/5/22)

(Firth et al., 2009), Simons Searchlight Single Gene Dataset v8.0, AutDB Autism Informatics Portal (<http://autism.mindspec.org/autDB/>; last accessed 1/5/22) (Basu et al., 2009), and website/url to ClinVar, “(<https://www.ncbi.nlm.nih.gov/clinvar/>)” (last accessed 1/5/22) (Landrum et al., 2018).

To review the literature, we used the queries: OCNDS, POBINDS, *CSNK2A1*, *CSNK2B*. These queries identified papers focused on the two disorders, large-scale sequencing efforts, and other articles that did not contain OCNDS and POBINDS variants. In addition, we used the AutDB Autism Informatics Portal to find additional research articles that contain variants in *CSNK2A1* and *CSNK2B*. For the gene variants described in the literature, we recorded each patients’ variant on *CSNK2A1* or *CSNK2B*. For the ClinVar database, we compiled the gene variants described as OCNDS, POBINDS and also variants described as “neurodevelopmental syndrome/ inborn genetic disease,” provided that the phenotypic description closely-related to OCNDS or POBINDS. Some of the patients in the DECIPHER database were published in research articles. These patients were identified by comparing clinical manifestations and/or sequencing facilities, to ensure that each patient data was only counted once.

We applied for and obtained the Simons Searchlight Single Gene Dataset v8.0 which includes *CSNK2A1* gene variants of patients. The collection of gene variants was reviewed and deemed non-human subjects research by the Institutional Review Board (IRB) of Boston University Medical Campus and Boston Medical Center (IRB # H-41033). To avoid duplicates, we selected variants from the Simons database not already included in ClinVar, as it was highly possible that the variants were already submitted to ClinVar by the original sequencing teams. These variant data were combined and presented in Tables.

CK2 α and CK2 β sequences, protein domains and alignment

CK2 α and CK2 β gene and protein data were obtained from UniProt (Accession P68400; Accession P67870). Protein domains were determined based on the most consequent domain definition (according to the CATH database) given in (Niefind and Battistutta 2013), the crystal structure of protein kinase CK2 α from *Zea mays* at 2.1 Å resolution (Niefind et al., 1998), and the crystal structure of CK2 β (Chantalat et al., 1999). For schemes and histograms, we utilized similar color palettes to facilitate reading and understanding of the data.

We utilized R (v4.0.3) and the Ggplot package (v3.3.5) to plot the number of unique patients per residue in the primary protein sequences, including data for missense, nonsense, and frameshift mutations (excluding splice-site variants). To determine the average number of point mutations per residue in each domain we calculated the number of

unique patients per domain (End Residue – Start Residue + 1), and divided the total number of unique patients in each domain by the domain length in Microsoft Excel (v16.16.27).

To determine the probability of finding the number of patients with a particular mutation(s) in each residue, we calculated an exact chi-square test statistic comparing the observed mutation probabilities to those expected by chance and present the corresponding *p*-value. For this, we assumed that each of the 9 variants per codon are equally likely to occur, thus the counts across the 9 mutations will follow a multinomial distribution with the probability of observing each variant = 1/9 (=0.11).

The nonrandom mutation clustering (NMC) algorithm was utilized to identify nonrandom clusters of mutated residues on each protein (Ye et al., 2010). This probability model assumes that mutations along a protein follow a uniform distribution, that mutations are independent of each other in and within samples, and that the number of samples exceeds the number of mutations. NMC utilizes the differences between pair-wise order statistics to derive probabilities. In the original study, NMC was performed on missense mutations to identify activating mutations in cancers that could be targeted for pharmacological intervention. We have expanded the statistical method to identify residues that are found mutated non-randomly among the point mutations that we collected. We utilized all mutations, except splice, as our study differs from cancer studies where missense mutations are key for disease development and progression. All the mutation analyzed in CK2 α and CK2 β in this study appear in the patient populations that we are studying and therefore, all may have a role in disease (note that it has not been yet demonstrated that any of these mutations causes disease *in vivo*). For each analysis we obtained clusters ranging from 1 residue to almost full-length protein. Out of these data, significant (*p* < 0.05) clusters of only one residue were depicted in a table. R code used to generate histograms and NMC analysis is provided in R markdown upon request.

To determine the conservation of the changed residues across eukaryotic species through evolutionary alignment, the primary sequences of CK2 α and CK2 β from diverse eukaryotic organisms were downloaded. We utilized the species selected in Homologene, and utilized their curated sequences, except for *Xenopus laevis* and *Danio rerio*, for which we found sequences with high similarity to the human sequence using BLASTP. Multiple sequence alignment of the sequences utilized was built with MUSCLE (<https://www.ebi.ac.uk/>) (Edgar 2004) and displayed in HTML format. In this format, conserved residues appeared in blue (conservation across most species), gray (conservation across some species) or white (no conservation).

Prediction tools

In silico tools were used to obtain predictions of the impacts of CK2 α and CK2 β missense mutations based on their

evolutionary conservation (PANTHER, MutationTaster2), functional impact (SIFT, PROVEAN, Polyphen-2, I-Mutant 3.0 Disease, MutationAssessor, SNAP2), and importance in protein stability (PremPS, Kinact, I-Mutant $\Delta\Delta G$). Two consensus programs (PredictSNP, REVEL) were also used for functional predictions. Our classification of these programs into categories of evolutionary conservation, functional impact, and effect on protein stability are not strict classifications, as many of these programs generate their predictions based on many of these factors. Rather, these classifications are used to more easily compare programs that consider similar protein characteristics when evaluating mutations. The following steps (exemplified for CSNK2A1) were followed to obtain predictions from each of these prediction programs:

- 1) PANTHER is a protein classification system that predicts the functional consequence of a single-nucleotide polymorphism (SNP) based on the preservation time of the mutated amino acid (Tang and Thomas 2016). Click on the cSNP Scoring tab. Input the FASTA sequence for CSNK2A1 and a list of all missense substitutions. Select “*Homo sapiens*” for the organism and submit. Prediction outputs are “Benign,” “Possibly Damaging,” or “Probably Damaging.”
- 2) MutationTaster2 uses a Bayes classifier model to predict whether a mutation is disease-causing and examines conservation of amino acids across vertebrate and invertebrate species (Schwarz et al., 2014). Enter the gene name “CSNK2A1.” Select transcript “ENST00000217244 (protein_coding, 4416 bases) NM_177559.” Enter Position/snippet, which refers to “coding sequence ORF” nucleotide position. Enter the mutated base. Prediction outputs are “Polymorphism” or “Disease Causing.”
- 3) SIFT predicts the effect of missense mutations on protein function by assessing the evolutionary conservation as well as the physical characteristics of the wild type and variant amino acids (Sim et al., 2012). Input the FASTA sequence for CSNK2A1 and the list of all missense substitutions. Keep default parameters (search in UniProt-SwissProt 2010_09, Median conservation of sequences: 3.00, Remove sequences more than 90 percent identical to query) and submit. Use the SIFT Amino Acid Predictions Tables to obtain predictions and the Scales Probabilities for Entire Protein Table for prediction scores. Prediction outputs are “Tolerated” or “Not Tolerated,” and scores range from 0 to 1, with a damaging score ≤ 0.05 and a tolerated score >0.05 .
- 4) Polyphen-2 predicts damaging missense mutations based on sequence and structure changes that could result from them (Adzhubei et al., 2010). Enter gene name or FASTA sequence. Enter the residue position of the missense mutation. Click the reference amino acid and mutant amino acid, and submit. Prediction outputs are “Benign” if score is <0.5 , “Possibly Damaging” if score is 0.5–0.95, and

- “Probably Damaging” if score is >0.95 , with scores ranging from 0 to 1.
- 5) PROVEAN assesses the effects of amino acid substitutions, insertions, and deletions on protein function by utilizing sequence homology and comparing with variants that have known functional consequences (Choi et al., 2012). Enter FASTA sequence. Enter the list of missense mutations and submit. Prediction outcomes are “Deleterious” if score is <-2.5 or “Neutral” if score is >-2.5 .
 - 6) I-Mutant 3.0 Disease predicts whether a single-site mutation is disease-causing based on the change in protein sequence (Capriotti et al., 2005). Select “Protein Sequence” under “Prediction of Disease associated single point mutation from.” Enter protein sequence. Enter the residue position of mutation and the new residue. Select “sequence-based” prediction and submit. Prediction outcomes are “Neutral” or “Disease Causing.”
 - 7) MutationAssessor provides a functional impact score for missense mutations based on sequence homology (Reva et al., 2011). Input the missense mutations with “CSK21_HUMAN or CSK2B_HUMAN” before each mutation and submit. Prediction outcomes are “Neutral” if Functional Impact (FI) score is 0.8, “Low” if FI score is between 0.8 and 1.9, “Medium” if FI score is between 1.9 and 3.5, or “High” if FI score is >3.5 .
 - 8) SNAP2 predicts whether a missense mutation will have a functional effect based on sequence homology and possible alterations to protein structure (Hecht et al., 2015). Enter FASTA sequence for protein of interest and click “Run Prediction.” This will produce a chart with all of the possible variants for each amino acid of the protein. Search for residue position of interest and locate the prediction for each missense mutation in the chart. Prediction outputs are “Negative/Neutral” or “Positive/Effect”
 - 9) PremPS computes the change in Gibbs free energy produced by a variant, using a 3D structure model of the protein, to predict its impact on protein stability (Chen et al., 2020). Enter PDB code and upload PDB file (we used 2PVR for CK2 α and 3EED for CK2 β) and click next. Select protein chains (Chain A) and click next. Select “Chain A” for “Chain to Mutate,” select residue to be mutated, and select the mutant residue. Click submit. Prediction outputs are “Negative/Stabilizing” or “Positive/Destabilizing.”
 - 10) Kinact specifically assesses the impact of missense mutations on the activity of kinases by using structure and sequence characteristics to predict changes in protein stability (Rodrigues et al., 2018). Upload CK2 α PDB file (2PVR). Enter the missense mutations and specify the chain (Chain A). Enter the FASTA sequence and submit. Prediction outputs are “Positive/Stabilizing” or “Negative/Destabilizing.”
 - 11) I-Mutant $\Delta\Delta G$ predicts the effect of a single-site mutation on protein stability by calculating the difference between the unfolding Gibbs free energy of wild type and mutant protein structures (Capriotti et al., 2005). There are two options for generating an output: 1) Enter protein sequence, residue position of mutation, and the new residue. Enter temperature (37°C) and pH (7.4). Select “ $\Delta\Delta G$ Value and Binary Classification” and submit. 2) Select “protein structure” under “Prediction of protein stability changes upon single point mutation from.” Upload the PDB file for the protein of interest (2PVR for CK2 α and 3EED for CK2 β). Enter the residue position of mutation and the new residue. Enter temperature (37°C) and pH (7.4). Select “ $\Delta\Delta G$ Value and Binary Classification” and submit. Prediction outputs are “Positive/Stabilizing” or “Negative/Destabilizing.”
 - 12) PredictSNP is a consensus program that compiles predictions from MAPP, PhD-SNP, Polyphen-1, Polyphen-2, SIFT, SNAP, nsSNPAnalyzer, and PANTHER to predict which missense mutations may be related to disease (Bendl et al., 2014). Load the FASTA sequence. Select positions of interest and the corresponding mutant residues. Select tools for evaluation (PredictSNP, MAPP, PhD-SNP, Polyphen-1, Polyphen-2, SIFT, SNAP), and click evaluate. Prediction outputs are “Neutral” or “Deleterious” along with a percentage indicating the confidence of the prediction.
 - 13) REVEL is a consensus program that compiles predictions from MutPred, FATHMM v2.3, VEST 3.0, PolyPhen-2, SIFT, PROVEAN, MutationAssessor, MutationTaster, LRT, GERP++, SiPhy, phyloP, and phastCons to generate an overall prediction of pathogenicity for missense mutations (Ioannidis et al., 2016). Download the REVEL spreadsheet which corresponds to the genomic position of CSNK2A1 (clicking on the link for gene segment of interest will automatically download the REVEL spreadsheet for that segment). Search for the GRCh38 position of each variant to find corresponding predictions. Prediction outputs are “Non-disease causing” if score is <0.5 or “Disease causing” if score is >0.5 .

The McNemar’s test was used to compare the categorical outputs of the functional programs (SIFT, Polyphen-2, PROVEAN, Mutation Assessor, SNAP2, I-Mutant3.0 Disease, REVEL, and PredictSNP) and the stability programs (PremPS, Kinact mCSM, Kinact SDM, Kinact DUET, and I-Mutant3.0 $\Delta\Delta G$). The Kinact suite of tools is only available for kinases such as CK2 α therefore for CK2 β we only compared PremPS and I-Mutant3.0 $\Delta\Delta G$. We calculated two values to compare each pair of tests that were performed on the mutations. First, the Kappa Coefficient (which calculates the degree of agreement beyond what would be expected by chance.) Second, the p -value from McNemar’s test, an assessment of whether there is a significant difference between tests in the ratings or “benign” vs. “effect”. Third, the p -value from McNemar’s test, an

assessment of whether there is a significant difference between tests in the ratings or “benign” vs. “effect.”

For prediction of changes in protein-protein binding affinity on mutations we utilized BeAtMuSiC (<http://babylone.ulb.ac.be/beatmusic>). BeatMusic predicts changes in binding free energy ($\Delta\Delta G$) induced by point mutations (Dehouck et al., 2013) based on known protein structures, the strength of interactions at the interface and the overall stability of the complex. As input for this prediction we used the CK2 holoenzyme structure (PDB ID: 4DGL; (Lolli et al., 2012)).

Structural analysis

The CK2 α ¹⁻³³⁵ structure (PDB ID: 2PVR (Niefind et al., 2007)) or CK2 β ¹⁻¹⁹³ structure (PDB ID: 3EED (Raaf et al., 2008)) were used as reference structures. The protein structures were downloaded from the RCSB Protein Data Bank (Berman et al., 2000). To visualize the conserved residues of CK2 α and CK2 β the ConSurf server (Glaser et al., 2003; Landau et al., 2005; Ashkenazy et al., 2010; Celniker et al., 2013; Ashkenazy et al., 2016) was used. Multiple Sequence Alignments were built using MAFFT (Katoh et al., 2018). The Homologues were collected from UNIREF90 using the homolog search algorithm HMMER (Eddy 2011) (E-value: 0.0001; No. of HMMER Iterations: 1). As maximal identity between sequences 95% and as minimal identity for homologs 40% were chosen. The calculation was performed on a sample of 150 sequences that represent the list of homologues to the query (Supplementary Table S3). Conservation scores were calculated using the Bayesian method (Mayrose et al., 2004). For structural analysis the programs COOT (Emsley et al., 2010) and PyMOL were used. Figures 1, 4A,C, 6, 7 were drawn using PyMOL (Schrödinger 2013).

Results and discussion

Update on CSNK2A1 and CSNK2B variants

The first publications for OCNDS and POBINDS associated these syndromes with variants in *CSNK2A1* and *CSNK2B*, respectively, and provided clinical manifestations that defined the syndromes. Since then, other variants in these two genes have been published and classified as OCNDS and POBINDS. In addition, a number of unpublished *CSNK2A1* and *CSNK2B* variants have been placed in data repositories which include clinical manifestations similar to the published variants. In view of the spread of the data, we collected all of the *CSNK2A1* and *CSNK2B* variants from publications and data repositories. Chromosomal variants were not collected in this study. The results of this data collection are found in Tables 1, 2, where the data is divided into non-conservative amino acid mutations and

splice mutations. Table 1 includes the 36 published *CSNK2A1* variants (some of which were also in data repositories), and 32 unique variants from data repositories (Simons, DECIPHER, ClinVar, AutDB). Table 2 includes 40 published *CSNK2B* variants (some of which were also in data repositories) and 27 unique variants from data repositories. By pooling these diverse variant data resources, we have increased the number of variants analyzed by 89% in CK2 α and by 68% in CK2 β . Interestingly, no genetic diseases are known so far to be associated with mutants of *CSNK2A2*, a *CSNK2A1* paralog, located on a different chromosome (Yang-Feng et al., 1991).

For *CSNK2A1*, we collected 7 splice variants and 61 single nucleotide variants (SNVs) (Table 1). The SNVs were: 1 start site, 47 missense variants (S51R was coded by 2 different variants), 9 nonsense, and 4 frameshift variants. For *CSNK2B*, we collected 14 splice variants and 49 SNVs: 4 different start site variants, 20 missense, 13 nonsense (Y101* was coded by 2 different variants), 11 frameshift, and 1 codon duplication variant (Table 2). Most of the SNVs in *CSNK2A1* were substitutions leading to missense mutations while in *CSNK2B* there was a high number of duplications and deletions, which resulted in a larger number of nonsense and frameshift mutants compared to *CSNK2A1*. Figure 2 depicts the location of the CK2 α and CK2 β mutants along their primary protein structures. Indicated in the Figure are distinct structural domains, highly conserved functional domains and putative functional residues from the literature and from PhosphositePlus (Hornbeck et al., 2012) that we will analyze and discuss below.

CK2 α and CK2 β mutation frequency and hotspots

We collected the number of patients with each variant to identify hotspots (excluding splice sites). First, we represented the total number of unique patients per mutation in each residue (Figure 3). Then, we utilized a non-random mutation clustering (NMC) approach to determine clusters of mutated residues that cannot be explained by random mutation in the nucleotide sequence. We found a number of significant clusters of residues of varying lengths (Supplementary Table S1), of which we selected single-residue clusters (Table 3). For CK2 α , these were (in order of significance): K198, Y50, R47, R80, R191, R312, H160, D156, S51, Y39, R195 and D175. For CK2 β , these were D32, R47, M1, C137 and R86. Since mutations in these residues were determined to be non-random in the NMC analysis, these residues may be potential mutational hotspots.

For some residues, all the patient mutations were the same (e.g., K198R in CK2 α , and R47* in CK2 β) while for others, there were multiple different mutations in the same residue (Supplementary Table S2). For CK2 α , 24% of residues had 2 or more distinct mutations (11 of 45 residues), and 18% for CK2 β (7 of 39 residues) (Supplementary Table S2). Therefore, we

TABLE 1 CK2α mutants associated with OCNDs phenotypes. Tables include nucleotide mutation, amino acid residue change (when applicable), number of patients per mutation and source. (A) includes variants that affect amino acid residues and (B) includes splice variants. Total number of patients for CK2α was 129. For samples found duplicated in different sets, we included all sources separated with a "/".

Position	Nucleotide change	Mutation	Ref	Residue	Mut	Number of patients	Source
1	c.1A>G	p.Met1?	M	1	?	1	Chiu et al., 2018/Wang et al., 2020/ClinVar (1)
21	c.62G>A	p.Arg21Gln	R	21	Q	1	ClinVar (1)
27	c.79G>A	p.Glu27Lys	E	27	K	2	Lelieveld et al., 2017/Chiu et al., 2018 (1); (1)
32	c.96delA	p.Glu32Aspfs*14	E	32	Dfs*14	1	ClinVar (1)
36	c.106C>T	p.Gln36*	Q	36	*	1	DECIPHER (1)
39	c.116A>G	p.Tyr39Cys	Y	39	C	1	Wang et al., 2020 (1)
39	c.116A>C	p.Tyr39Ser	Y	39	S	1	DECIPHER (1)
39	c.117C>A	p.Tyr39Ter	Y	39	*	1	ClinVar (1)
46	c.137G>T	p.Gly46Val	G	46	V	1	ClinVar (1)
47	c.139C>G	p.Arg47Gly	R	47	G	2	ClinVar (1); SFARI (1)
47	c.140G>A	p.Arg47Gln	R	47	Q	8	Okur et al., 2016 (1); Chiu et al., 2018 (1) Owen et al., 2018/DECIPHER (1); DECIPHER (1); ClinVar (4)
50	c.149A>G	p.Tyr50Cys	Y	50	C	9	Martinez-Monseny et al., 2020 (1); Wu R et al., 2020 (1); ClinVar (5); DECIPHER (2)
50	c.149A>T	p.Tyr50Phe	Y	50	F	1	Dominguez et al., 2021 (1)
50	c.149A>C	p.Tyr50Ser	Y	50	S	1	Okur et al., 2016 (1)
51	c.152G>A	p.Ser51Asn	S	51	N	1	Owen et al., 2018/DECIPHER (1)
51	c.151A>C	p.Ser51Arg	S	51	R	2	Chiu et al., 2018 (1); ClinVar (1)
51	c.153T>A	p.Ser51Ile	S	51	I	1	Wang et al., 2020 (1)
51	c.152G>T	p.Ser51Ile	S	51	I	1	Wang et al., 2020 (1)
52	c.154G>A	p.Glu52Lys	E	52	K	1	ClinVar (1)
53	157G>C	p.Val53Leu	V	53	L	1	SFARI (1)
73	c.218T>A	p.Val73Glu	V	73	E	1	Chiu et al., 2018 (1)
80	c.238C>T	p.Arg80Cys	R	80	C	1	Wang et al., 2020/Wu et al., 2021 (1)
80	c.239G>A	p.Arg80His	R	80	H	5	Owen et al., 2018/DECIPHER (1); ClinVar (4)
107	c.319C>T	p.Arg107*	R	107	*	2	Wang et al., 2020 (1); ClinVar (1)
126	c.376delC	p.Gln126Argfs*2	Q	126	Rfs*2	1	ClinVar (1)
127	c.380C>T	p.Thr127Met	T	127	M	1	Wang et al., 2020 (1)
128	c.383T>A	p.Leu128*	L	128	*	1	ClinVar (1)
147	c.440G>A	p.Cys147Tyr	C	147	Y	1	Wang et al., 2020 (1)
153	c.458T>G	p.Met153Arg	M	153	R	1	ClinVar (1)
156	c.466G>C	p.Asp156His	D	156	H	1	Trinh et al., 2017/ClinVar (1)
156	c.468T>A	p.Asp156Glu	D	156	E	2	ClinVar (2)
156	c.466G>T	p.Asp156Tyr	D	156	Y	1	ClinVar/SFARI (1)
158	c.472A>G	p.Lys158Glu	K	158	E	1	ClinVar (1)
158	473A>G	p.Lys158Arg	K	158	R	1	ClinVar (1)
160	c.479A>G	p.His160Arg	H	160	R	4	van der Werf et al., 2020 (1); Wu et al., 2021 (1); ClinVar (2)
161	c.482A>G	p.Asn161Ser	N	161	S	1	DECIPHER (1)
161	c.481A>G	p.Asn161Asp	N	161	D	1	ClinVar (1)
174	c.522A>G	p.Ile174Met	I	174	M	1	Owen et al., 2018/DECIPHER (1)
175	c.524A>G	p.Asp175Gly	D	175	G	2	Okur et al., 2016/ClinVar (1); Duan et al., 2019 (1)
175	c.596G>A	p.Asp175Glu	D	175	E	1	ClinVar (1)
177	529G>A	p.Gly177Ser	G	177	S	1	ClinVar (1)
178	c.533T>G	p.Leu178Trp	L	178	W	1	DECIPHER (1)
191	c.572G>A	p.Arg191Gln	R	191	Q	2	Owen et al., 2018/DECIPHER (1); DECIPHER (1)

(Continued on following page)

TABLE 1 (Continued) CK2 α mutants associated with OCNDS phenotypes. Tables include nucleotide mutation, amino acid residue change (when applicable), number of patients per mutation and source. (A) includes variants that affect amino acid residues and (B) includes splice variants. Total number of patients for CK2 α was 129. For samples found duplicated in different sets, we included all sources separated with a "/".

Position	Nucleotide change	Mutation	Ref	Residue	Mut	Number of patients	Source
191	c.571C>T	p.Arg191*	R	191	*	3	Nakashima et al., 2019 (1); Wang et al., 2020 (1); ClinVar (1)
194	581C>T	p.Ser194Phe	S	194	F	1	SFARI (1)
195	c.583C>T	p.Arg195*	R	195	*	3	Wang et al., 2020 (1); ClinVar (2)
197	c.589T>A	p.Phe197Ile	F	197	I	1	Owen et al., 2018/DECIPHER (1)
198	c.593A>G	p.Lys198Arg	K	198	R	24	Iossifov et al., 2014 (1); Okur et al., 2016 (1) Akahira-Azuma et al., 2018 (1); Chiu et al., 2018 (1) Owen et al., 2018/DECIPHER (4); Nakashima et al., 2019 (1); van der Werf et al., 2020 (1); Xu et al., 2020 (1); ClinVar (9); TGen (3)
199	c.596G>A	p.Gly199Asp	G	199	D	1	ClinVar (1)
210	c.628G>A	p.Asp210Asn	D	210	N	1	Wang et al., 2020 (1)
231	c.692C>G	p.Pro231Arg	P	231	R	1	Lelieveld et al., 2017/Chiu et al., 2018 (1)
261	c.783C>A	p.Tyr261Ter	Y	261	*	1	ClinVar (1)
306	c.916C>T	p.Arg306*	R	306	*	1	Wang et al., 2020 (1)
312	c.935G>A	p.Arg312Gln	R	312	Q	2	Chiu et al., 2018 (1); ClinVar (1)
312	c.934C>T	p.Arg312Trp	R	312	W	3	Owen et al., 2018/DECIPHER (1); ClinVar (2)
325	c.972_973dupCAG	p.Tyr325Serfs*5	Y	325	Sfs*5	1	Wang et al., 2020 (1)
326	c.976_977insG	p.T326Serfs*13	T	326	Sfs*13	2	DECIPHER (2)
333	c.997C>T	p.Arg333*	R	333	*	1	ClinVar (1)
356	c.1066T>A	p.Ser356Thr	S	356	T	1	ClinVar (1)
363	c.1088C>A	p.Pro363His	P	363	H	1	ClinVar (1)
382	c.1145C>T	p.Pro382Leu	P	382	L	2	ClinVar (2)

Position	Nucleotide change	Variant	Number of patients	Source
55	c.165G>A	Splice variant	2	ClinVar (2)
122	c.366_366+3del	Splice variant	1	DECIPHER (1)
122	c.367-1G>A	Splice variant	1	ClinVar (1)
142	c.426 + 1G>T (IVS6+1G>T)	Splice variant	1	ClinVar/SFARI (1)
274	c.824 + 2T>C	Splice variant	1	Okur et al., 2016/ClinVar (1)
324	c.973 + 1G>A	Splice variant	1	Wang et al., 2020 (1)
324	c.973 + 1G>C	Splice variant	1	Wang et al., 2020 (1)

calculated the probability of finding the number of patients with mutation(s) in each residue. If we assume that each of the 9 variants per codon are equally likely, then the counts across the 9 mutations will follow a multinomial distribution with the probability of observing each variant once in nine ($1/9 = 0.11$). We calculated an exact chi-square test statistic comparing the observed mutation probabilities to those expected by chance and present the corresponding *p*-value (Supplementary Table S2). For CK2 α , significant results were found for R47G/Q, Y50C/F/S, R80C/H, H160R, R191Q/*, R195*, K198R and R312Q/W; and for CK2 β for D32A/N, R47*, R86C, R111P, and H165R.

Understanding the genetic mechanisms (population, gene characteristics, etc.) underlying the higher mutability of these

sites may lead to important insights that could help us understand the etiology of these diseases.

Mutation clusters

Studies on neurodevelopmental diseases (NDD) find that missense mutations cluster in or near the functional domains of NDD-associated proteins, in contrast with rare missense mutations found in the 1000 Genomes project (Geisheker et al., 2017). CK2 α and CK2 β missense mutants were found in both functional domains and interdomain sequences (Figures 2, 3).

TABLE 2 CK2 β mutants associated with POBINDS phenotypes. Table includes nucleotide and amino acid residue changes, number of patients per mutation and reference/source. (A) includes variants that affect amino acid residues and (B) includes splice variants. Total number of patients for CK2 α was 90. For samples found in different sets, we included all sources separated with a “/”.

Position	Nucleotide change	Mutation	Ref	Residue	Mut	Number of patients	Source
1	c.1A>G	p.Met1?	M	1	?	3	Ernst et al., 2021 (1); ClinVar (2)
1	c.2T>A	p.Met1?	M	1	?	1	Ernst et al., 2021 (1)
1	c.3G>A	p.Met1?	M	1	?	1	Yang et al., 2021 (1)
1	c.2T>G	p.Met1?	M	1	?	1	ClinVar (1)
5	c.13G>T	p.Glu5Ter	E	5	*	1	Li et al., 2019 (1)
9	c.27del	p.Trp9Ter	W	9	*	2	Ernst et al., 2021 (1); ClinVar (1)
20	c.58G>T	p.Glu20Ter	E	20	*	1	Ernst et al., 2021 (1)
21	c.63C>A	p.Phe21Leu	F	21	L	1	DECIPHER (1)
27	c.78_83dup	p.Glu27_Asp28dup	E	27	_D28dup	1	Ernst et al., 2021 (1)
31	c.91C>T	p.Gln31Ter	Q	31	*	1	ClinVar (1)
32	c.94G>A	p.Asp32Asn	D	32	N	6	Ernst et al., 2021 (3); ClinVar (2); DECIPHER (1)
32	c.95A>C	p.Asp32Ala	D	32	A	1	DECIPHER
34	c.101T>C	p.Phe34Ser	F	34	S	1	Ernst et al., 2021 (1)
34	c.101T>G	p.Phe34Cys	F	34	C	1	ClinVar (1)
35	c.105T>A	p.Asn35Lys	N	35	K	1	Ernst et al., 2021 (1)
37	c.108dupT	p.Thr37TyrfsTer5	T	37	Yfs*5	2	Sakaguchi et al., 2017 (1); ClinVar (1)
42	c.124C>T	p.Gln42Ter	Q	42	*	2	Fernández-Marmiesse et al., 2019 (1); Ernst et al., 2021 (1)
47	c.139C>T	p.Arg47Ter	R	47	*	6	Selvam et al., 2021 (1); Ernst et al., 2021 (1); ClinVar (4)
57	c.170del	p.Glu57Glyfs*15	E	57	Gfs*15	1	Valentino et al., 2021 (1)
61	c.181G>T	p.Glu61Ter	E	61	*	1	Ernst et al., 2021/ClinVar (1)
77	c.229G>A	p.Glu77Lys	E	77	K	2	Ernst et al., 2021 (1); ClinVar (1)
77	c.229G>T	p.Glu77Ter	E	77	*	1	ClinVar (1)
80	c.238T>A	p. Tyr80Asn	Y	80	N	1	ClinVar (1)
82	c. 245T>A	P.Leu82Ter	L	82	*	1	ClinVar (1)
86	c.256C>T	p.Arg86Cys	R	86	C	4	Li et al., 2019 (1); Ernst et al., 2021 (1); ClinVar (2)
88	c.264delC	p.Ile88Ilefs*46	I	88	Ifs*46	1	Li et al., 2019 (1)
90	c.268dupA	p.Thr90Asnfs*24	T	90	Nfs*24	1	ClinVar (1)
97	c.291G>A	p.Met97Ile	M	97	I	1	Ernst et al., 2021 (1)
101	c.303C>A c.303C>G	p.Tyr101Ter	Y	101	*	3	Ernst et al., 2021 (2); ClinVar (1)
106	c.316T>G	p.Phe106Val	F	106	V	1	Ernst et al., 2021 (1)
111	c.332G>C	p.Arg111Pro	R	111	P	3	Li et al., 2019 (2); ClinVar (1)
117	c.349C>T	p.Gln117Ter	Q	117	*	1	DECIPHER (1)
132	c.394_404del	p.Met132LeufsTer110	M	132	Lfs*110	1	Ernst et al., 2021 (1)
137	c.409T>C	p.Cys137Arg	C	137	R	1	Ernst et al., 2021 (1)
137	c.409T>G	p.Cys137Gly	C	137	G	1	Li et al., 2019 (1)
137	c.410G>T	p.Cys137Phe	C	137	F	2	Li et al., 2019 (1); Yang et al., 2021 (1)
158	c.472del	p.Tyr158fs	Y	158	fs	1	ClinVar (1)
164	c.491C>G	p.Pro164Arg	P	164	R	1	ClinVar (1)
165	c.494A>G	p.His165Arg	H	165	R	3	Nakashima et al., 2019 (1), Yang et al., 2021 (1), ClinVar (1)
167	c.499delC	Leu167Serfs*60	L	167	Sfs*60	1	Yang et al., 2021 (1)
179	c.533_534insGT	p.Pro179TyrfsTer49	P	179	Yfs*49	1	Nakashima et al., 2019/ClinVar (1)
181	c.542del	p.Asn181ThrfsTer46	N	181	Tfs*46	1	Ernst et al., 2021 (1)
186	c.554_555dupCC	p.Arg186fs	R	186	fs	1	ClinVar (1)

(Continued on following page)

TABLE 2 (Continued) CK2 β mutants associated with POBINDS phenotypes. Table includes nucleotide and amino acid residue changes, number of patients per mutation and reference/source. (A) includes variants that affect amino acid residues and (B) includes splice variants. Total number of patients for CK2 α was 90. For samples found in different sets, we included all sources separated with a "/".

Position	Nucleotide change	Mutation	Ref	Residue	Mut	Number of patients	Source
187	c.560T>C	p.Leu187Pro	L	187	P	1	ClinVar (1)
187	c.560T>G	p.Leu187Arg	L	187	R	1	Li et al., 2019 (1)
188	c.564del	p.Tyr188Ter	Y	188	*	1	Rahman and Fatema 2021 (1)
189	c.566G>T	p.Gly189Val	G	189	V	1	ClinVar (1)
207	c.620_621insC	p.Phe207Phefs*39	F	207	Ffs*39	1	Li et al., 2019 (1)

Position	Nucleotide change	Variant	Number of patients	Source
24	c.72 + 1G>A	Splice variant	1	ClinVar (1)
24	c.73-2A>G	Splice variant	1	Ernst et al., 2021/ClinVar (1)
58	c.175 + 2T>G	Splice variant	1	Poirier et al., 2017/ClinVar (1)
97	c.292-2A>C	Splice variant	2	Yang et al., 2021 (1); ClinVar (1)
97	c.292-2A>G	Splice variant	1	ClinVar (1)
122	c.367 + 1G>A	Splice variant	1	ClinVar (1)
122	c.367 + 2T>C	Splice variant	1	Poirier et al., 2017/ClinVar (1)
122	c.367+5del	Splice variant	2	ClinVar (2)
122	c.367 + 6T>C	Splice variant	1	ClinVar (1)
122	c.368-2A>G	Splice variant	1	Li et al., 2019/ClinVar (1)
185	c.557 + 2T>C	Splice variant	1	DECIPHER (1)
185	c.557 + 1G>A	Splice variant	1	Ernst et al., 2021 (1)
186	c.558-2A>G	Splice variant	1	Ernst et al., 2021 (1)
186	c.558-3T>G	Splice variant	1	Yang et al., 2021 (1)

We compiled the number of patients in the different functional domains (excluding splice sites) and calculated the ratio of mutations to residues (number of mutations in a protein domain divided by the number of residues in the protein domain) (Table 4; Supplementary Table S1). All functional domains had mutations, albeit at different ratios. None of the Ser and Thr phosphorylated sites in CK2 α or CK2 β were mutated, but as we will discuss in the structural section, phosphorylation may be affected. For CK2 α , the highest ratio was found in the Gly-rich-loop (4.3) followed by the P+1 loop (3.2) while the lowest ratio was found in the activation loop (0.08, with a similar ratio to interdomain sequences). For CK2 β , the highest ratios were in the Cys bound to Zinc (1), putative destruction box (0.75) and interface one to CK2 α (0.71) while the lowest was in the acidic loop (0.13). Intriguingly, the ratio of the N-terminal segment was among the four highest, suggesting that this region contains functional domains. The interdomain sequences in CK2 β showed a higher ratio (0.17) than one known functional domain, suggesting that there may be unidentified functional domains in CK2 β located in these sequences. Both these hypotheses are supported by the fact that most of the clusters of one residue in the NMC analysis for CK2 β fall in known functional domains, except for D32 and

R47 in the N-terminal segment, and R86 in interdomain sequences.

Therefore, as the regulation of CK2 α and CK2 β is still not fully understood, we examined the NMC data to identify short clusters of mutations outside the known functional domains that could be novel functional domains (Supplementary Table S1). For CK2 α , we found clusters including the known functional domains (or shorter versions), except for the hinge region that appears in clusters including the activation segment. Residues in the N-terminal segment were found at minimum in clusters that included at least the Gly-rich loop (e.g.: cluster 21-53), suggesting a functional interaction between the N-terminal and the Gly-rich loop. We also found clusters from residue 107 until the second CK2 β binding domain, and from residue 147 to the catalytic loop, the activation segment and residues 312/326. These residues (107, 147 and 312/326) are outside of the known functional domains. This suggests that these residues have functional interactions with known functional domains and/or form part of novel functional domains, particularly the Ct residues that are essential for CK2 α 's tertiary structure. This is supported by the fact that most of the clusters of one residue in the NMC analysis fall in known functional domains, except for R312 in CK2 α (discussed in our structural analysis).

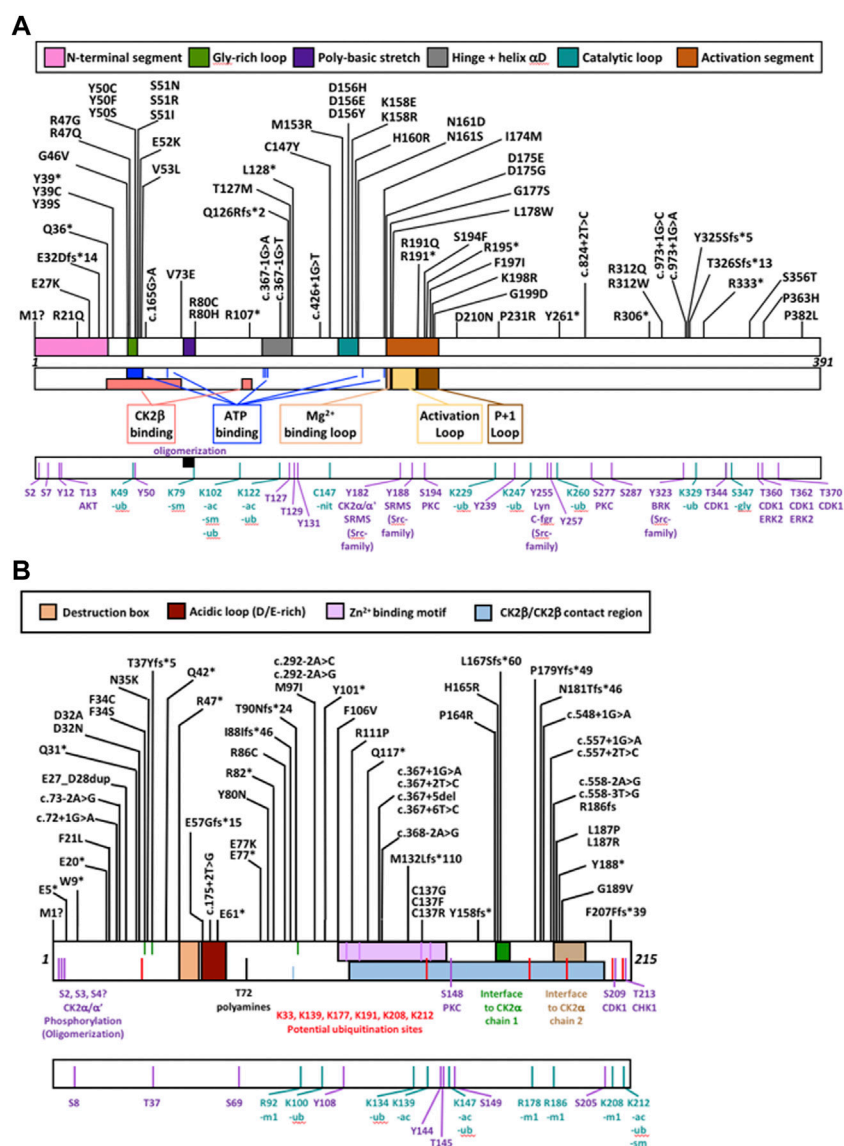


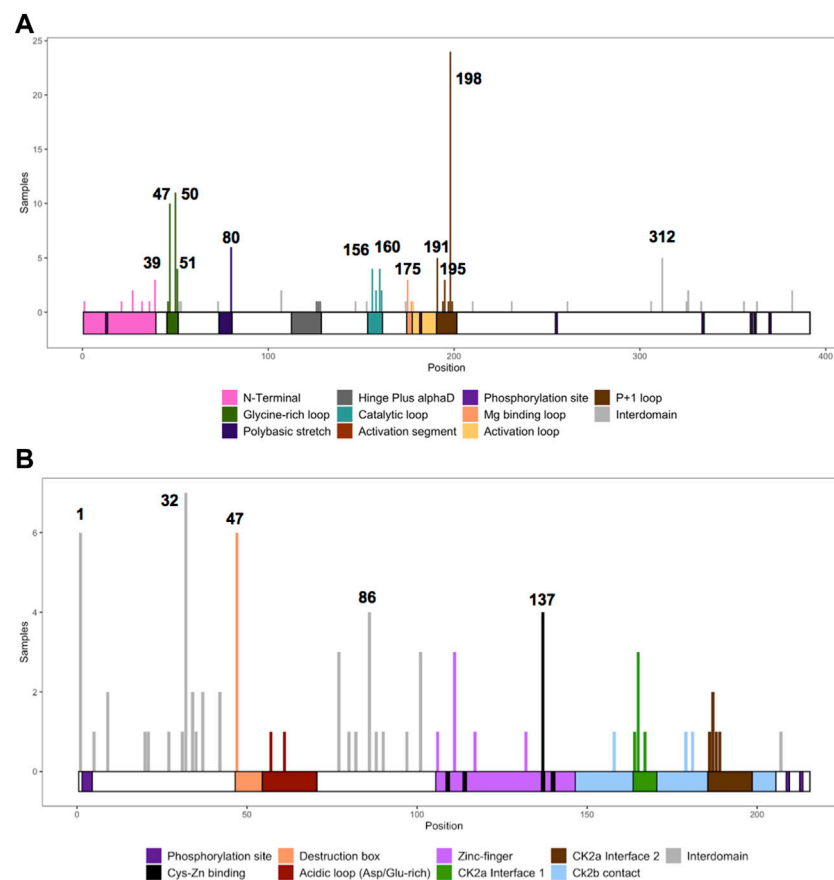
FIGURE 2

Protein diagram of CK2α and CK2β including the location of mutations to date. CK2α (A) and CK2β (B) mutants (nonsense, missense, start site variants, frameshift and splice) are represented on a diagram of the primary structure of the proteins. The diagrams include distinct structural and functional domains, and putative functional residues for each protein. For CK2β, the acidic loop domain has also function as pseudosubstrate, and for oligomerization, polyamine binding and polybasic peptide binding. The four Cys (residues 109, 114, 137, 140) key for zinc binding are highlighted in the Zn²⁺ binding motif. Ac, acetylation; gly, glycosylation; m1, monomethylation; nit, nitrosylation; sm, sumorylation.

For CK2β, the significance found in the NMC analysis was lower than in CK2α, most likely due to the limited sample number. We did not find short clusters that included the residues of the known functional domains. A number of clusters started at residues 1, 20, 21 and 27 of different lengths (highest significance ending in 32–47). We found significant short clusters around residue 32 (e.g., 31–35), and clusters including residues 47 (34/42–47) and 86 (86–88). These data suggest that these may be one to three novel functional

domains, which will be further discussed in our structural analysis.

Overall, these data suggest that protein function will be affected at least by some of these mutations. We will need experimental data to show that the identified potential domains in CK2α and CK2β are *bona fide* functional domains. If so, NMC analysis could be used to identify novel potential functional domains for NDD-associated proteins. Our next analyses will assess, via diverse methods, the potential

**FIGURE 3**

Histogram representing the number of mutations along the primary sequence of CK2 α and CK2 β . The X-axis represents the primary sequence and the functional domains of CK2 α (A) and CK2 β (B). The Y axis represents the number of patients with missense, nonsense, and frameshift mutations along the primary structure of CK2 α and CK2 β . Numbers in the histogram represent single residues found significant in the non-random mutation cluster (NMC) analysis.

impact of these mutations in protein structure and function, and will indicate potential biochemical mechanisms.

Evolutionary conservation

Disease-causing mutations are more likely to occur in evolutionary conserved positions in proteins (Michaelson et al., 2012; Yuen et al., 2016; Geisheker et al., 2017; Lelieveld et al., 2017; Wang et al., 2020); therefore, we assessed whether the residues mutated in CK2 α and CK2 β in OCNDS and POBINDS were conserved across species including vertebrates, invertebrates, plants, yeast and fungi. [Supplementary Figures S1, S2](#) show an alignment of a subset of species using MUSCLE (highest conserved residues highlighted in blue), with the residues mutated in OCNDS and POBINDS highlighted in red. [Supplementary Figures S3, S4](#) show an alignment of 150 species (highest conserved residues

highlighted in raspberry red) using MUSCLE. The accession numbers of the 150 sequences can be found in [Supplementary Table S3](#). [Figure 4](#) shows a 3D representation of alignment of 150 species using a 3D surface representation of the conserved residues calculated using the ConSurf server (Glaser et al., 2003; Landau et al., 2005; Ashkenazy et al., 2010; Celniker et al., 2013; Ashkenazy et al., 2016), and [Supplementary Figure S5](#) shows the 3D surface representation using the subset of sequences in [Supplementary Figures S1, S2](#). The alignments showed that the highest conservation across species was found in the first 324 CK2 α residues. The CK2 β sequence is less conserved than the CK2 α sequence and there was a higher degree of conservation between vertebrate and invertebrate sequences and between plant and unicellular organisms ([Supplementary Figure S5](#)). Chantalat et al. ([Chantalat et al., 1999](#)) found 40 identical residues in the seven species they investigated, which are highlighted in [Supplementary Figure S2](#). Among these conserved residues, 32, 34, 35 and 86 have missense mutations in POBINDS

TABLE 3 Nonrandom mutation clustering (NMC) for CK2 α and CK2 β mutations. Analysis was performed on the total number of patients with mutations in each amino acid residue (excluding splice site mutations). Table only includes significant clusters with a cluster size of one amino acid residue.

CK2 α residue	Number samples	<i>p</i> -value	Functional domain or description
39	3	3.12×10^{-2}	N-terminal segment; CK2b binding
47	10	4.16×10^{-11}	Gly-rich loop; ATP binding; CK2b binding
50	11	1.28×10^{-12}	Gly-rich loop; ATP binding; CK2b binding
51	4	3.03×10^{-3}	Gly-rich loop; ATP binding; CK2b binding
80	6	1.64×10^{-5}	Polybasic stretch
156	4	3.03×10^{-3}	Catalytic loop
160	4	3.03×10^{-3}	Catalytic loop
175	3	3.12×10^{-2}	Activation segment; Mg ²⁺ binding loop
191	5	2.60×10^{-4}	Activation segment (P+1 loop)
195	3	3.12×10^{-2}	Activation segment (P+1 loop)
198	24	2.73×10^{-34}	Activation segment (P+1 loop)
312	5	2.60×10^{-4}	Interdomain
CK2 β residue	Number samples	<i>p</i> -value	Functional domain or description
1	6	3.12×10^{-4}	N-terminal segment (Truncated protein)
32	7	1.04×10^{-4}	N-terminal segment (Chantalat's Conserved surface cluster 1)
47	6	3.02×10^{-4}	N-terminal Segment (Destruction box; Truncated protein)
86	4	2.08×10^{-2}	Chantalat's Conserved surface cluster 1
137	4	2.08×10^{-2}	Zinc finger (Cys bound to Zinc), CK2 α contact region

(defined by Chantalat as surface cluster 1, and discussed in the structural section). As discussed above, based on the NMC analysis, these residues could form part of novel functional domain(s).

Prediction programs based on evolutionary conservation are frequently used to determine the possible consequences associated with mutations. We used two well-known prediction programs, MutationTaster2 and PANTHER, to analyze CK2 α and CK2 β mutations (Supplementary Table S4). In MutationTaster2, all CK2 α mutants were classified as disease causing and in PANTHER, all mutants were classified as probably damaging except for S356T (possible damaging). For CK2 β mutants, both MutationTaster2 and PANTHER classified the mutants as disease causing/probably damaging. There was a concordance between the two prediction programs even for residues not fully conserved across species.

Functional predictions

We assessed the functional effects of CK2 α and CK2 β mutations with six functional prediction programs (SIFT, PROVEAN, I-Mutant 3.0 Disease, MutationAssessor, Polyphen-2, and SNAP2) and two consensus prediction programs (REVEL and PredictSNP). The majority of the programs only analyze missense mutations; therefore, the

computational analyses below are restricted to these mutations. Figure 5 represents the residues and number of patients with missense mutations.

For CK2 α , the mutations predicted to be functionally impacted across all programs were D156H, D156E, D156Y, K158E, N161S, N161D, P231R, R312Q, and R312W (Table 5A). Mutations Y50C, Y50S, S51I, S51R, V53L, C147Y, K158R, G177S, S194F, and F197I may also be highly affected as none of the programs predicted these mutations to be neutral, tolerated, or benign. In addition to these mutations, M1?, G46V, M153R, D175G, D175E, and L178W were predicted to be damaging by both consensus programs. Mutations S356T, P363H and P382L were predicted neutral/benign/non-disease causing in most of the programs. For the rest of the mutations there were discrepancies between the programs. For CK2 β , the mutations predicted to be functionally impacted across all programs were D32A, N35K, R86C, R111P, C137R, C137G, C137F, and H165R (Table 5B). The mutations D32N, F34S, F106V, L187P, and L187R may also be highly affected because none of the programs predicted these mutations to be neutral/tolerated/benign. Six prediction programs also provided numerical values associated with the predictions (Supplementary Table S5).

We performed McNemar's tests to determine whether there were statistically significant differences in the categorical values between the programs. For this, each

TABLE 4 Number of mutations per CK2 α and CK2 β functional and structural domain. Table summarizes the numbers of CK2 α (A) and CK2 β (B) mutants in each functional domain and the # mutations/# number of residues (excluding splice sites).

Domain	Residues	Total residues	Number of patients	#Patients/#residues
N-terminal segment	1–39	39	9	0.23
Gly-rich loop	46–51	6	26	4.33
Polybasic stretch	74–80	7	6	0.86
Hinge plus α D	113–128	16	3	0.19
Catalytic loop	154–161	8	12	1.5
Activation segment	175–201	27	40	1.48
CK2 β binding	36–73, 103–108	44	35	0.8
ATP binding	46–51, 66, 114, 115, 116, 163, 174	12	27	2.25
Mg ²⁺ binding loop	175–177	3	4	1.33
Activation loop	178–190	13	1	0.08
P+1 loop	191–201	11	35	3.18
Phosphorylation sites	13, 182, 255, T344, T360, S362, S370	7	0	0.00
Interdomain	—	247	19	0.08
N-terminal segment	1–54	54	33	0.61
Phosphorylation sites	2,3,4, S209, T213	5	0	0.00
Destruction box	47–54	8	6	0.75
Acidic loop (Asp/Glu-rich)	55–70	16	2	0.13
Zinc-finger	106–146	41	10	0.24
Cys bound to Zinc	109, 114, 137, 140	4	4	1.00
CK2 β /CK2 β contact region	110–205	96	22	0.23
Interface to CK2 α 1	164–170	7	5	0.71
Interface to CK2 α 2	186–198	13	5	0.38
C-terminal segment	179–215	37	8	0.22
Interdomain	39–45 & 71–105	86	15	0.17

categorical value was coded as either as “benign” (neutral, benign, tolerated, non-disease causing) or “effect” (deleterious, effect, probably damaging, possibly damaging, not tolerated, disease, low/medium/high impact, disease causing). We then calculated percent agreement, the Kappa coefficient (to address agreement beyond what would be expected by chance) and the *p*-value in McNemar’s test (Table 6A,B). For CK2 α functional predictions, REVEL had the least agreement with most other programs followed by Mutation Assessor Functional Impact, while SIFT and PredictSNP had agreement with the most number of programs. For CK2 β there were fewer significant agreements between programs, probably due to limited sample size.

Since disease-causing mutations are more likely to have common structural features, these computational analyses could identify the best mutant candidates for experimental testing of the functional impact. A complexity in using these programs is that they each have their own thresholds for determining what is damaging and the extent to which a mutation is damaging. For example, some programs predict nearly all mutations to be damaging, while other programs categorize mutations based on predicted severity. In addition,

not all programs consider other factors, such as position of the mutation, which have a significant impact on the consequence of the mutation. For instance, in the case of M1?, some of the programs predicted this mutation to be neutral/benign/tolerated and did not take into consideration that this is a mutation at the start codon, and therefore cannot not be neutral. Therefore,

Our next aim was to compare the results from these computation analyses with experimental data to determine which prediction program(s) can best help guide us in understanding the potential consequences of CK2 α and CK2 β mutations. We acknowledge that we have limited experimental data to date, particularly for CK2 β , nonetheless, we correlated experimental data, in particular, kinase activity and subcellular localization with the functional predictions. The *in vitro* kinase activity of 18 CK2 α recombinant mutant proteins purified from bacteria ranges from 0% to 50% of wild-type protein (Dominguez et al., 2021). Table 5C displays the CK2 α mutants sorted from low (0% for D175G, S51R and F197I) to medium activity (50% for V73E and R191Q) compared with the wild type protein. Given that all of these mutants had less than 50% activity, PROVEAN and

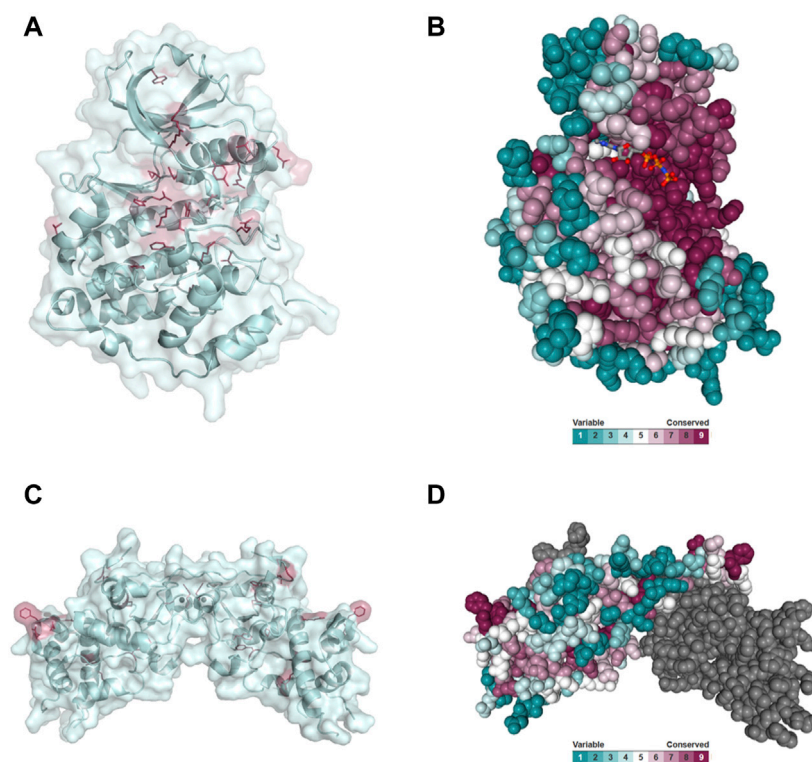


FIGURE 4

Conserved residues in CK2α and CK2β across 150 species. **(A)** General clustering of the mutation sites in CK2α including surface representation. The structure of the CK2α¹⁻³³⁵ monomer is shown as a pale cyan cartoon representation, the OCNDS related mutation sites are shown as sticks and are coloured raspberry red. The CK2α¹⁻³³⁵ structure (PDB_ID: 2PVR (Niefind et al., 2007)) was used for the figure. The figure was drawn using PyMOL (Schrödinger 2013). **(B)** Conserved residues of CK2α. Conserved residues of CK2α in spacefill representation. The figure was created using the ConSurf server (Glaser et al., 2003; Landau et al., 2005; Ashkenazy et al., 2010; Celniker et al., 2013; Ashkenazy et al., 2016) with the CK2α¹⁻³³⁵ structure (PDB_ID: 2PVR (Niefind et al., 2007)). Multiple Sequence Alignment was built using MAFFT (Katoh et al., 2018). The Homologues were collected from UNIREF90 using the homolog search algorithm HMMER (Eddy 2011) (E-value: 0.0001; No. of HMMER Iterations: 1). As maximal identity between sequences 95% and as minimal identity for homologs 40% were chosen. The calculation was performed on a sample of 150 sequences (see [Supplementary Data Sheet S3](#)) that represent the list of homologues to the query. Conservation scores were calculated using the Bayesian method (Mayrose et al., 2004). **(C)** General clustering of the mutation sites in CK2β including surface representation. The structure of the CK2β¹⁻¹⁹³ dimer is shown as a pale cyan cartoon representation, the mutation sites related to neurodevelopmental disability and epilepsy are shown as sticks and are coloured raspberry red. The CK2β¹⁻¹⁹³ structure (PDB_ID: 3EED (Raaf et al., 2008)) was used for the figure. The figure was drawn using PyMOL (Schrödinger 2013). **(D)** Conserved residues in chain A of the CK2β dimer in spacefill representation. The figure was created analogously to [Figure 3B](#) with the ConSurf server (Glaser et al., 2003; Landau et al., 2005; Ashkenazy et al., 2010; Celniker et al., 2013; Ashkenazy et al., 2016). The CK2β¹⁻¹⁹³ structure (PDB_ID: 3EED (Raaf et al., 2008)) was used as input file. Multiple Sequence Alignment was built using MAFFT (Katoh et al., 2018). The Homologues were collected from UNIREF90 using the homolog search algorithm HMMER (Eddy 2011) (E-value: 0.0001; No. of HMMER Iterations: 1). As maximal identity between sequences 95% ID and as minimal identity for homologs 40% ID were chosen. The calculation was performed on a sample of 150 sequences (see [Supplementary Data Sheet S4](#)) that represent the list of homologues to the query. Conservation scores were calculated using the Bayesian method (Mayrose et al., 2004).

SNAP2 could be used to find mutants that have impacted activity since these two programs properly categorized all of these mutants as having an effect (except M1?). For the rest of the programs, we assessed whether their categorical values may have discrimination power between mutants with the less activity (0%–25%) compared to those with higher activity (25%–50%) (bold line in the table). Based on this cut-off, PredictSNP appears to most accurately predict most of the 0%–25% range to be deleterious (eight out of nine mutations) and it predicts less of the 25%–50% to be deleterious (only

2 out of five mutations). This suggests that predictSNP may be able to pinpoint the mutants most affected and may be utilized to predict large activity changes. We also investigated the numerical predictions to determine whether we can set a range of values for mutants more or less affected ([Supplementary Table S5](#)). For CK2α, SNAP2 and REVEL showed somewhat overlapping ranges. For SNAP2: mutants with 0%–25% activity were in the range 96–6 and those with 25%–50% activity in the range: 79–31, suggesting that the most affected mutants could be found in the 96–79 range. For

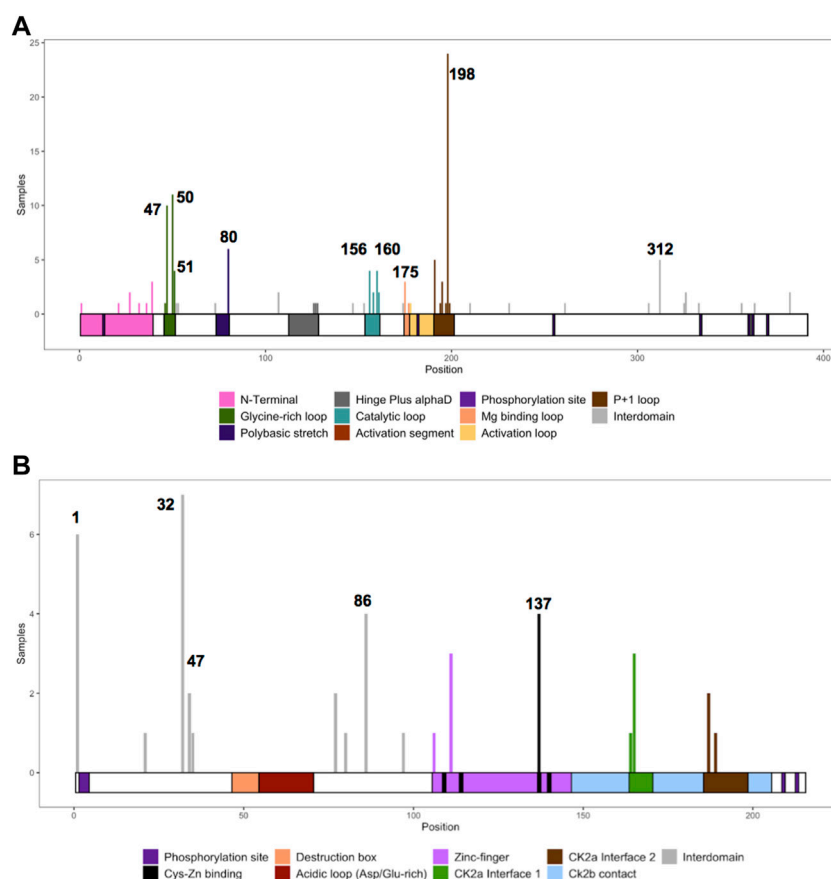


FIGURE 5

Histogram representing the number of missense mutations along the primary sequence of CK2α and CK2β. The Y axis represents the number of patients with missense mutations in each amino acid residue along the primary structure of CK2α (**A**) and CK2β (**B**). The X-axis represents the primary sequence and the functional domains of CK2α (**A**) and CK2β (**B**). Numbers mark single residues found significant in the non-random mutation cluster (NMC) analysis.

REVEL: mutants with 0%–25% activity were in the range 0.902–0.361 and mutants with 25%–50% activity were in the range: 0.552–0.357, suggesting that the most affected mutants could be found in the 0.902–0.552 range.

We also compared these prediction results with experimental data on nuclear/cytoplasmic distribution of CK2α mutant proteins (Dominguez et al., 2021) as the subcellular distribution could be an indicator of the similarity to the wild-type protein structure (e.g., folding). CK2α wild-type is predominantly nuclear in 80% of cells. To assess the predictions, we categorized the mutants into three groups: high, medium and low similarity to wild-type depending on the percentage of cells with predominantly nuclear distribution. High similarity mutants to wild-type had approximately 80% nuclear distribution (E27K, R80H, I174M, D175G, R191Q, K198R, P231R), medium similarity mutants had 50%–70% nuclear distribution (R47G, R47Q, Y50S, S51R, V73E, D156H and F197I), and low similarity mutants had 20%–30% nuclear distribution (R321Q/W). Table 5D displays the CK2α mutants

from low to high similarity to wild-type nuclear distribution. There does not seem to be a clear correlation between the categorical predictions and CK2α subcellular distribution for any of the programs. We also investigated the numerical predictions to determine whether we can find a range of values to distinguish mutants more or less affected (Supplementary Table S5). SNAP2 and MutationAssessor showed somewhat overlapping ranges, as follows. For SNAP2, these were the range 96–90 (20%–30% nuclear distribution); range: 91–31 (50%–70% nuclear distribution), and range 89–6 (80% nuclear distribution) suggesting that the most affected mutants could be found in the 96–91 range. For MutationAssessor, these were range >4.61 (20%–30% nuclear distribution), range 4.21–0.525 (50%–70% nuclear distribution), and range 3.865–0.095 (80% nuclear distribution), suggesting that the most affected mutants would be ranked >4.61 and the less affected mutants ranked <0.525.

More data is needed to determine the predictive power of these programs as it relates to CK2α and CK2β, including

TABLE 5 Analysis of CK2 α and CK2 β protein mutations using functional prediction programs. Predictions for CK2 α (A) and (B) CK2 β . Colors in the cells reflect the effect from neutral (white) to high effect (red). The numbers obtained in the analysis can be found in [Supplementary Table S4](#). (C, D) Comparison between CK2 α predictions and experimental data on CK2 α from [Dominguez et al., 2021](#). (C) kinase activity of the recombinant CK2 α protein mutants purified from bacteria; from 0% to 25% (top rows) to 25%–50% (bottom rows) compared to wild-type purified protein. (D) Degree of similarity between nuclear/cytoplasmic localization CK2 α protein mutants to wild-type proteins expressed in cell lines; from low to high. N/A (= not applicable) indicates residues that could not generate a prediction. [Note: MutationAssessor has been down precluding us from analyzing 7 mutants, indicated with (—)].

A

CK2 α	Functional						Consensus	
Mutations	PROVEAN	SNAP2	Polyphen-2	SIFT	I-Mutant 3.0 Disease	Mutation Assessor Functional Impact	PredictSNP	REVEL
M1?	neutral	neutral	probably damaging	not tolerated	neutral	N/A	deleterious	disease causing
R21Q	neutral	neutral	probably damaging	tolerated	disease	-	neutral	non-disease causing
E27K	deleterious	effect	probably damaging	not tolerated	disease	medium	deleterious	non-disease causing
Y39C	deleterious	effect	probably damaging	not tolerated	disease	high	deleterious	non-disease causing
Y39S	deleterious	effect	probably damaging	not tolerated	disease	high	deleterious	non-disease causing
G46V	deleterious	effect	probably damaging	not tolerated	disease	-	deleterious	disease causing
R47G	deleterious	effect	probably damaging	not tolerated	disease	low	neutral	disease causing
R47Q	deleterious	effect	probably damaging	tolerated	disease	neutral	neutral	non-disease causing
Y50C	deleterious	effect	probably damaging	not tolerated	disease	medium	deleterious	disease causing
Y50F	deleterious	effect	probably damaging	tolerated	neutral	neutral	deleterious	non-disease causing
Y50S	deleterious	effect	probably damaging	not tolerated	disease	low	deleterious	disease causing
S51N	deleterious	effect	possibly damaging	tolerated	neutral	medium	deleterious	non-disease causing
S51R	deleterious	effect	possibly damaging	not tolerated	disease	high	deleterious	disease causing
S51I	deleterious	effect	probably damaging	not tolerated	disease	medium	deleterious	disease causing
E52K	deleterious	effect	possibly damaging	tolerated	disease	neutral	neutral	disease causing
V53L	deleterious	effect	possibly damaging	not tolerated	disease	medium	deleterious	disease causing
V73E	deleterious	effect	probably damaging	not tolerated	neutral	neutral	neutral	non-disease causing
R80C	deleterious	effect	probably damaging	not tolerated	disease	high	deleterious	non-disease causing
R80H	deleterious	effect	possibly damaging	not tolerated	disease	medium	deleterious	non-disease causing
T127M	deleterious	effect	probably damaging	not tolerated	disease	low	neutral	non-disease causing
C147Y	deleterious	effect	probably damaging	not tolerated	disease	medium	deleterious	disease causing
M153R	deleterious	effect	probably damaging	not tolerated	disease	-	deleterious	disease causing
D156H	deleterious	effect	probably damaging	not tolerated	disease	high	deleterious	disease causing
D156E	deleterious	effect	probably damaging	not tolerated	disease	high	deleterious	disease causing
D156Y	deleterious	effect	probably damaging	not tolerated	disease	high	deleterious	disease causing
K158E	deleterious	effect	probably damaging	not tolerated	disease	high	deleterious	disease causing
K158R	deleterious	effect	probably damaging	not tolerated	disease	medium	deleterious	disease causing
H160R	deleterious	effect	probably damaging	tolerated	disease	neutral	neutral	disease causing
N161S	deleterious	effect	probably damaging	not tolerated	disease	high	deleterious	disease causing
N161D	deleterious	effect	probably damaging	not tolerated	disease	high	deleterious	disease causing
I174M	deleterious	effect	probably damaging	not tolerated	neutral	medium	deleterious	non-disease causing
D175G	deleterious	effect	benign	not tolerated	disease	medium	deleterious	disease causing
D175E	deleterious	effect	possibly damaging	not tolerated	neutral	high	deleterious	disease causing
G177S	deleterious	effect	probably damaging	not tolerated	disease	medium	deleterious	disease causing
L178W	deleterious	effect	probably damaging	not tolerated	neutral	medium	deleterious	disease causing
R191Q	deleterious	effect	probably damaging	tolerated	disease	low	deleterious	non-disease causing
S194F	deleterious	effect	probably damaging	not tolerated	disease	medium	deleterious	disease causing
F197I	deleterious	effect	probably damaging	not tolerated	disease	low	deleterious	disease causing
K198R	deleterious	effect	possibly damaging	tolerated	neutral	neutral	neutral	non-disease causing
G199D	deleterious	effect	possibly damaging	not tolerated	disease	neutral	deleterious	non-disease causing
D210N	deleterious	effect	probably damaging	tolerated	disease	low	neutral	non-disease causing
P231R	deleterious	effect	probably damaging	not tolerated	disease	high	deleterious	disease causing
R312Q	deleterious	effect	probably damaging	not tolerated	disease	high	deleterious	disease causing
R312W	deleterious	effect	probably damaging	not tolerated	disease	high	deleterious	disease causing
S356T	neutral	neutral	benign	not tolerated	neutral	neutral	neutral	non-disease causing
P363H	neutral	neutral	benign	not tolerated	neutral	neutral	deleterious	non-disease causing
P382L	neutral	effect	benign	not tolerated	neutral	neutral	deleterious	non-disease causing

TABLE 5 Analysis of CK2 α and CK2 β protein mutations using functional prediction programs. Predictions for CK2 α (A) and (B) CK2 β . Colors in the cells reflect the effect from neutral (white) to high effect (red). The numbers obtained in the analysis can be found in [Supplementary Table S4](#). (C, D) Comparison between CK2 α predictions and experimental data on CK2 α from [Dominguez et al., 2021](#). (C) kinase activity of the recombinant CK2 α protein mutants purified from bacteria; from 0% to 25% (top rows) to 25%–50% (bottom rows) compared to wild-type purified protein. (D) Degree of similarity between nuclear/cytoplasmic localization CK2 α protein mutants to wild-type proteins expressed in cell lines; from low to high. N/A (= not applicable) indicates residues that could not generate a prediction. [Note: MutationAssessor has been down precluding us from analyzing 7 mutants, indicated with (—)].

B								
CK2 β	Functional						Consensus	
Mutations	PROVEAN	I-Mutant 3.0 Disease	Mutation Assessor Functional Impact	SNAP2	SIFT	Polyphen-2	REVEL	PredictSNP
F21L	deleterious	disease	-	effect	not tolerated	probably damaging	non-disease causing	neutral
D32N	deleterious	disease	medium	effect	not tolerated	probably damaging	disease causing	deleterious
D32A	deleterious	disease	high	effect	not tolerated	probably damaging	disease causing	deleterious
F34S	deleterious	disease	medium	effect	not tolerated	probably damaging	disease causing	deleterious
F34C	deleterious	disease	-	effect	not tolerated	probably damaging	disease causing	deleterious
N35K	deleterious	disease	high	effect	not tolerated	probably damaging	disease causing	deleterious
E77K	deleterious	disease	medium	effect	tolerated	benign	non-disease causing	neutral
Y80N	deleterious	disease	-	effect	not tolerated	probably damaging	disease causing	deleterious
R86C	deleterious	disease	high	effect	not tolerated	probably damaging	disease causing	deleterious
M97I	deleterious	disease	medium	neutral	not tolerated	benign	non-disease causing	deleterious
F106V	deleterious	disease	medium	effect	not tolerated	possibly damaging	disease causing	deleterious
R111P	deleterious	disease	high	effect	not tolerated	probably damaging	disease causing	deleterious
C137R	deleterious	disease	high	effect	not tolerated	probably damaging	disease causing	deleterious
C137G	deleterious	disease	high	effect	not tolerated	probably damaging	disease causing	deleterious
C137F	deleterious	disease	high	effect	not tolerated	probably damaging	disease causing	deleterious
P164R	deleterious	disease	-	effect	not tolerated	probably damaging	disease causing	deleterious
H165R	deleterious	disease	high	effect	not tolerated	probably damaging	disease causing	deleterious
L187P	deleterious	disease	medium	effect	not tolerated	possibly damaging	disease causing	deleterious
L187R	deleterious	disease	medium	effect	not tolerated	possibly damaging	disease causing	deleterious
G189V	deleterious	disease	-	effect	not tolerated	probably damaging	disease causing	deleterious

computing of more complex characteristics that can be affected by changes in the primary structure of these proteins, such as interaction and oligomerization.

Protein stability predictions

We utilized PremPS, Kinact, and I-Mutant 3.0 $\Delta\Delta G$ to predict protein stability changes of missense mutations. All three of these programs were utilized for CK2 α mutations.

Only PremPS and I-Mutant 3.0 $\Delta\Delta G$ were used for CK2 β mutations since Kinact is specifically for kinase proteins. The prediction programs provide the Gibbs Free energy (kcal/mol) for change in protein stability. As in the above analyses only missense mutations were analyzed ([Table 7](#)).

For CK2 α , mutations Y39S, G199D, and R312Q were predicted to be highly destabilizing across all programs ([Table 7A](#); [Supplementary Table S6](#)). Mutations Y39C, Y50S, R80C, R80H, K158E, L178W, and P231R may also be destabilizing as several programs predicted them to be highly

TABLE 5 Analysis of CK2 α and CK2 β protein mutations using functional prediction programs. Predictions for CK2 α (A) and (B) CK2 β . Colors in the cells reflect the effect from neutral (white) to high effect (red). The numbers obtained in the analysis can be found in [Supplementary Table S4](#). (C, D) Comparison between CK2 α predictions and experimental data on CK2 α from [Dominguez et al., 2021](#). (C) kinase activity of the recombinant CK2 α protein mutants purified from bacteria; from 0% to 25% (top rows) to 25%–50% (bottom rows) compared to wild-type purified protein. (D) Degree of similarity between nuclear/cytoplasmic localization CK2 α protein mutants to wild-type proteins expressed in cell lines; from low to high. N/A (= not applicable) indicates residues that could not generate a prediction. [Note: MutationAssessor has been down precluding us from analyzing 7 mutants, indicated with (—)].

C

CK2 α	Functional						Consensus		Experimental
Mutations	PROVEAN	SNAP2	Polyphen-2	SIFT	I-Mutant 3.0 Disease	Mutation Assessor Functional Impact	PredictSNP	REVEL	Kinase activity
D175G	deleterious	effect	benign	not tolerated	disease	medium	deleterious	disease causing	0-25% of Wild-type
S51R	deleterious	effect	possibly damaging	not tolerated	disease	high	deleterious	disease causing	
F197I	deleterious	effect	probably damaging	not tolerated	disease	low	deleterious	disease causing	
R80H	deleterious	effect	possibly damaging	not tolerated	disease	medium	deleterious	non-disease causing	
R312W	deleterious	effect	probably damaging	not tolerated	disease	high	deleterious	disease causing	
I174M	deleterious	effect	probably damaging	not tolerated	neutral	medium	deleterious	non-disease causing	
P231R	deleterious	effect	probably damaging	not tolerated	disease	high	deleterious	disease causing	
Y50F	deleterious	effect	probably damaging	tolerated	neutral	neutral	deleterious	non-disease causing	
K198R	deleterious	effect	possibly damaging	tolerated	neutral	neutral	neutral	non-disease causing	25-50% of Wild-type
R47G	deleterious	effect	probably damaging	not tolerated	disease	low	neutral	disease causing	
R47Q	deleterious	effect	probably damaging	tolerated	disease	neutral	neutral	non-disease causing	
E27K	deleterious	effect	probably damaging	not tolerated	disease	medium	deleterious	non-disease causing	
V73E	deleterious	effect	probably damaging	not tolerated	neutral	neutral	neutral	non-disease causing	
R191Q	deleterious	effect	probably damaging	tolerated	disease	low	deleterious	non-disease causing	

D

CK2 α	Functional						Consensus		N/C distribution
Mutations	PROVEAN	SNAP2	Polyphen-2	SIFT	I-Mutant 3.0 Disease	Mutation Assessor Functional Impact	PredictSNP	REVEL	similarity to wild-type
R312Q	deleterious	effect	probably damaging	not tolerated	disease	high	deleterious	disease causing	low
R312W	deleterious	effect	probably damaging	not tolerated	disease	high	deleterious	disease causing	low
F197I	deleterious	effect	probably damaging	not tolerated	disease	low	deleterious	disease causing	mid
V73E	deleterious	effect	probably damaging	not tolerated	neutral	neutral	neutral	non-disease causing	mid
R47G	deleterious	effect	probably damaging	not tolerated	disease	low	neutral	disease causing	mid
Y50S	deleterious	effect	probably damaging	not tolerated	disease	low	deleterious	disease causing	mid
R47Q	deleterious	effect	probably damaging	tolerated	disease	neutral	neutral	non-disease causing	mid
S51R	deleterious	effect	possibly damaging	not tolerated	disease	high	deleterious	disease causing	mid
D156H	deleterious	effect	probably damaging	not tolerated	disease	high	deleterious	disease causing	mid
R191Q	deleterious	effect	probably damaging	tolerated	disease	low	deleterious	non-disease causing	high
P231R	deleterious	effect	probably damaging	not tolerated	disease	high	deleterious	disease causing	high
D175G	deleterious	effect	benign	not tolerated	disease	medium	deleterious	disease causing	high
I174M	deleterious	effect	probably damaging	not tolerated	neutral	medium	deleterious	non-disease causing	high
E27K	deleterious	effect	probably damaging	not tolerated	disease	medium	deleterious	non-disease causing	high
R80H	deleterious	effect	possibly damaging	not tolerated	disease	medium	deleterious	non-disease causing	high
K198R	deleterious	effect	possibly damaging	tolerated	neutral	neutral	neutral	non-disease causing	high

destabilizing and none of the programs gave them a stabilizing prediction. Predictions were somehow different between the programs. Kinact mCSM and I-Mutant 3.0 $\Delta\Delta G$ predicted all mutants to be destabilizing at some level, and PremPS predicted all mutants to be destabilizing at some level except for E27K and D156Y. Both Kinact SDM and Kinact DUET predicted all mutations to be destabilizing except for a few, including G46V, S51I, T127M and D175G that both programs predicted stabilizing. For CK2 β , both PremPS and I-Mutant 3.0 $\Delta\Delta G$ predicted all CK2 β mutations to be destabilizing at some level (Table 7B; Supplementary Table S6). Mutations F34S, F34C, F106V, C137G, L187P, and L187R were predicted to be highly destabilizing by both programs while D32A and E77K were predicted to have a lower destabilizing effect. We performed McNemar's tests for the differences in the categorical values between the programs (Tables 6C,D). For CK2 α stability, Kinact SDM $\Delta\Delta G$ and Kinact DUET $\Delta\Delta G$ had the least agreement with other programs (significant *p*-value).

A complexity of the use of these programs is that these prediction programs required a structure input, except for I-Mutant 3.0 $\Delta\Delta G$ that used protein sequence. Overall, there are 287 CK2 α structures in the PDB; 228 of them are from the two human paralogs CK2 α and CK2 α . Selecting the structure to use may be difficult for the newcomer to the field. Indeed, we obtained varied results when using three different structures for human CK2 α to run Kinact (PDB ID's 2PVR, 5OMY, 2ZJW) (not shown). For the data in the table, we used PDB ID 2PVR as it was the structure with the highest resolution.

There is no experimental study of the stability of CK2 α mutants to be compared with the results from these program analyses. However, there is data on expression levels from a subset of CK2 α mutant proteins that were expressed in cell lines (Dominguez et al., 2021). Three mutants appear less expressed than others in cell lines: R312Q, R312W and R47Q. As we will discuss below, R312 is a key residue to maintain the 3D structure of CK2 α as it forms an ion pair with Q201 in α -EF helix, coupling the α -GHI-subdomain with the α -EF-helix; therefore, it is predicted to be less stable. The mutant with the lowest expression, R312Q, was predicted to be destabilizing by all programs (Table 7C). We also investigated the numerical predictions to determine whether we can find a range of values to distinguish mutants more or less affected (Supplementary Table S6). For CK2 α , the three less expressed mutants had I-Mutant 3.0 $\Delta\Delta G$ scores from -1.27 to 0.73 . For CK2 β , T37Yfs*5 had low expression levels (Nakashima et al., 2019). However, we could not assess this mutant, as the prediction programs only analyze missense mutations. More experimental data is needed to determine specific programs that are better at predicting stability properties of the CK2 α and CK2 β mutants.

Prediction of changes in binding free energy induced by point mutations

The binding free energy change between the wild type and mutant complex ($\Delta\Delta G$) was predicted using BeAtMuSiC (<http://babylone.ulb.ac.be/beatmusic>) (Dehouck et al., 2013). For this, the binding of one CK2 α chain to a CK2 β dimer was evaluated, using the CK2 holoenzyme structure (PDB ID: 4DGL; (Lolli et al., 2012)) as input file. Individual side chains whose contributions strongly dominate the binding affinity of protein-protein interactions—so-called “hotspots”—(Clackson and Wells 1995) are usually defined as positions which cause an increase of binding free energy of more than 2.0 kcal/mol upon mutation. BeAtMuSiC identifies a residue as part of the protein-protein interface if its solvent accessibility in the complex is at least 5% lower than in the individual partner (Dehouck et al., 2013). First, $\Delta\Delta G$ values for experimentally characterized CK2 α and CK2 β mutants were predicted and compared to the experimental data (Table 8A,B). Indeed BeAtMuSiC predicted the highest $\Delta\Delta G$ values for the exchanges to Ala for the described hotspots of the CK2 α /CK2 β interaction, namely Leu41 and Phe54 of CK2 α (Raaf et al., 2011) as well as Tyr188 and Phe190 of CK2 β (Laudet et al., 2007) (Table 8A,B).

Among the OCNDS-linked CK2 α mutants, Tyr39Ser, Tyr39Cys and Arg47Gly have the highest $\Delta\Delta G$ values (1.76 kcal/mol, 1.12 kcal/mol and 1.69 kcal/mol) but are not considered binding hotspots as they are close but not directly involved in the interaction site (although the BeAtMuSiC algorithm recognizes them as interface residues) (Table 8C). Residues not in the interface were not predicted to change the affinity for CK2 β . This hypothesis is supported by the literature, at least in the case of Lys198Arg (Werner et al., 2022).

For CK2 β , the interface mutation Leu187Pro has a predicted $\Delta\Delta G$ value of 2.25 kcal/mol (Table 8D). Laudet et al. included Leu187 in a CK2 β -derived cyclic peptide mimicking the C-terminal CK2 β hairpin loop (Arg186 to His193) essential for binding of CK2 α (Laudet et al., 2007). In this study, each amino acid of the cyclic peptide was individually replaced by Ala and the derivatives of the original peptide were explored regarding their antagonistic activity in a CK2 α /CK2 β -binding assay. The exchange to Ala of the Leu187 equivalent position in the peptide caused a marginal reduction of CK2 α /CK2 β -binding and the role of this residue was interpreted as passive. Indeed, the Leu187Ala mutation is predicted to induce a smaller change in binding free energy (1.94 kcal/mol; Table 8B) than the POBINDS-related mutation Leu187Pro (Table 8D). Compared to the Leu187Arg variant with a predicted $\Delta\Delta G$ value of 1.04 kcal/mol, the Leu187Pro variant is predicted to have a stronger impact on the CK2 subunit interaction. It has to be noted that other variants of CK2 β with a predicted $\Delta\Delta G$ value higher than 2 kcal/mol are not located in the interface, namely Tyr80Asn, Cys137Arg and Cys137Gly. As described later, Tyr80 and Cys137 are important for the global architecture of CK2 β and hence,

the high $\Delta\Delta G$ values for the exchange of these residues may be due to changes in folding free energy.

Therefore, this analysis identified Leu187Pro in CK2 β as a potential mutation with consequences for CK2 holoenzyme formation. Further analyses could test the influence of mutations on the oligomerization of the holoenzyme, pseudosubstrate region or the binding to other partners.

A structural perspective on the OCNDS-related CSNK2A1 mutations

As we discussed above, the majority (57%) of the CK2 α variants linked to OCNDS lead to missense mutations which cluster in highly conserved functional domains and key structural regions, such as the Gly-rich loop, the basic cluster, the activation loop and the P+1 loop (Figures 2A, 4, 6). Accordingly, the catalytic and structural key elements share a high score of conservation as represented in Supplementary Figures S1, Supplementary Data Sheet S3. Apart from residues involved in catalysis, certain mutations are located in the N- and C-terminal segments, which are important for the global fold of the kinase and are critical at stabilizing the constitutively active conformation (Figures 6B,H). Other mutations, such as Tyr39Cys, are located in the CK2 β subunit interaction site (Figure 6F). Two of the reported mutations, Thr127Met and Cys147Tyr, are not located in functional domains. Thr127 is located in the helix αD and is exposed to the solvent, so its exchange with the hydrophobic Met might disturb solubility of CK2 α .

The side chain of Cys147 is directed to the inside of the kinase and its replacement with the bulkier Tyr is likely sterically incompatible with the protein fold. These sites could be functional as Thr127 has been found phosphorylated (Phosphosite Plus) and Cys147 to be nitrosylated (Wu et al., 2020; Borgo et al., 2021). For the nitrosylation at Cys147, however, the side chain must get exposed.

Missense mutations in the N-terminal segment

The N-terminal segment (residues 1–39) stabilizes the helix αC and the activation loop in their active conformations, and it is therefore a decisive element for the constitutive activity of CK2 α (Niefind et al., 1998). Indeed, the deletion of the first 30 residues leads to loss of kinase activity (Sarno et al., 2002). The Met1? Mutation will affect the start codon, and is predicted to lead to an N-terminal truncation of the protein until amino acid 137, the position of the next in-frame start codon (Chiu et al., 2018). The mutation site Arg21 is directed towards the surface however, from a structural point of view, the consequences of the exchange with Gln cannot be anticipated. The likewise critical position Glu27 (Chiu et al., 2018) is in close contact to the basic cluster of helix αC and its exchange to Lys may have a repellent electrostatic effect (Figure 6B).

Missense mutations in the Gly-rich loop

The mutations Gly46Val, Arg47Gln/Gly, Tyr50Cys/Ser/Phe, Ser51Arg/Asn/Ile, Glu52Lys and Val53Leu reside in the highly

flexible, Gly-rich loop (Figure 6C). Gly-rich loops are highly conserved among kinases and many other nucleotide-binding proteins. Gly residues are highly conserved in nucleotide positioning loops (NPLs) because of their minimal steric repulsion and their contribution to high backbone flexibility. In the protein kinase family the Gly-rich loop connects the β strands 1 and 2, and its sequence is Gly-X-Gly-X-X-Gly-X-Val (Grant et al., 1998). In CK2 α however, the third Gly is replaced by a Ser residue: Gly₄₆-Arg-Gly₄₈-Lys-Tyr-Ser₅₁-Glu-Val. The spatially undemanding Gly residues allow a close proximity of the loop backbone and the β - and γ -phosphates of ATP (and GTP in the case of CK2) (Niefind and Battistutta 2013). A systematic literature review revealed that mutations altering the Gly-rich loop are more likely to cause the widest range of phenotypes (Wu et al., 2021). Gly46 interacts with the ribose moiety of ATP/GTP (as shown in maize CK2 α structures in complex with AMPPNP (Niefind et al., 1998) and GMPPNP (Niefind et al., 1999). Mutation of the equivalent position in PKA (Gly50) showed a 10-fold decrease of affinity for ATP (Grant et al., 1998), therefore Gly46Val may lead to a decreased affinity to ATP/GTP. Structural studies revealed that this particular loop can collapse so that Arg47 blocks the active site (Raaf et al., 2009). Tyr50 is of topological interest because cyclin-dependent kinases (CDKs) also carry a Tyr residue at the equivalent position. This tyrosine is an important phosphorylation site in CDKs because its dephosphorylation in a CDK/cyclin complex is necessary for full catalytic activity (Dorée and Galas 1994). In CK2 α , there has been speculation about the regulatory significance of Tyr50 (Allende and Allende 1995). Mass spectrometry studies found Tyr50 to be phosphorylated (Gu et al., 2010; Schreiber et al., 2010) however, if putative phosphorylation of Tyr50 plays a role in the regulation of CK2 remains unresolved.

Val53 is a highly conserved residue in the catalytic spine (C-spine; residues: Leu41, Val53, Phe54, Val66, Val162, Met163, Ile164, Phe121, Met221, Met225) (Kornev et al., 2008; Taylor and Kornev 2011), and is located in the β_2 strand at the end of the Gly-rich loop. The C-spine and its counterpart, the regulatory spine (R-spine; residues: Leu85, Leu97, His154, Trp176), are two stacks of hydrophobic side chains within the catalytic core of eukaryotic protein kinases (EPKs) extending from the C-lobe to the N-lobe of the kinase (Kornev et al., 2008). Unlike the R-spine, the C-lobe requires an external supplementation: it needs to be completed by the purine ring of ATP/GTP. Val53 is one of the residues sandwiching the purine moiety; hence, the introduction of Leu, another hydrophobic amino acid with a bulkier side chain, may subtly affect ATP/GTP cosubstrate binding.

The Gly-rich loop is in close proximity to the CK2 α /CK2 β subunit interface. Therefore, mutations in this loop might alter the flexibility of the Gly-rich loop or affect the assembly of the CK2 holoenzyme. GST-tagged CK2 α Ser51Arg was inactive in an *in vitro* activity assay, while the Arg47Gln/Gly mutants showed 40%–50% activity compared to WT (Dominguez et al., 2021). The activity of these three GST-CK2 α mutants remained

TABLE 6 McNemar's test of categorical values. Each categorical value was coded as either a benign or effect. We calculated percent agreement, the Kappa coefficient and performed McNemar's test to determine statistically significant differences in categorical values.

	PROVEAN	SNAP2	Polyphen-2	SIFT	I-Mutant 3.0 disease	MAFI	PredictSNP
SNAP2	$\kappa = 0.8773$ ($p = 0.5637$)						
Polyphen-2	$\kappa = 0.6319$ ($p = 0.5637$)	$\kappa = 0.4535$ ($p = 0.999$)					
SIFT	$\kappa = 0.0070$ ($p = 0.2482$)	$\kappa = 0.0408$ ($p = 0.1317$)	$\kappa = -0.1336$ ($p = 0.1655$)				
I-Mutant 3.0 Disease	$\kappa = 0.4382$ ($p = \mathbf{0.0027}$)	$\kappa = 0.3597$ ($p = \mathbf{0.0016}$)	$\kappa = 0.2316$ ($p = \mathbf{0.0039}$)	$\kappa = 0.1496$ ($p = 0.1967$)			
MAFI	$\kappa = 0.3968$ ($p = \mathbf{0.0082}$)	$\kappa = 0.2773$ ($p = \mathbf{0.0047}$)	$\kappa = 0.3410$ ($p = \mathbf{0.0339}$)	$\kappa = 0.4397$ ($p = 0.4795$)	$\kappa = 0.4788$ ($p = >0.999$)		
PredictSNP	$\kappa = 0.1455$ ($p = 0.1317$)	$\kappa = 0.1869$ ($p = 0.0578$)	$\kappa = 0.0242$ ($p = 0.0833$)	$\kappa = 0.5386$ ($p = 0.7055$)	$\kappa = 0.1132$ ($p = 0.3173$)	$\kappa = 0.5275$ ($p = 0.7055$)	
REVEL	$\kappa = 0.1983$ ($p = \mathbf{0.0005}$)	$\kappa = 0.1399$ ($p = \mathbf{0.0003}$)	$\kappa = 0.8773$ ($p = 0.5637$)	$\kappa = 0.3244$ ($p = \mathbf{0.0075}$)	$\kappa = 0.3081$ ($p = 0.1967$)	$\kappa = 0.3886$ ($p = \mathbf{0.0209}$)	$\kappa = 0.2828$ ($p = \mathbf{0.0201}$)
SNAP2	$\kappa = *$ ($p = 0.3173$)						
Polyphen-2	$\kappa = *$ ($p = 0.1573$)	$\kappa = 0.6429$ ($p = 0.3173$)					
SIFT	$\kappa = *$ ($p = 0.3173$)	$\kappa = -0.0526$ ($p = >0.999$)	$\kappa = 0.6429$ ($p = 0.3173$)				
I-Mutant 3.0 Disease	**	$\kappa = *$ ($p = 0.3173$)	$\kappa = *$ ($p = 0.1573$)	$\kappa = *$ ($p = 0.3173$)			
MAFI	**	$\kappa = *$ ($p = 0.3173$)	$\kappa = *$ ($p = 0.1573$)	$\kappa = *$ ($p = 0.3173$)	**		
PredictSNP	$\kappa = *$ ($p = 0.1573$)	$\kappa = -0.0714$ ($p = 0.5637$)	$\kappa = 0.4444$ ($p = >0.999$)	$\kappa = 0.6429$ ($p = 0.3173$)	$\kappa = *$ ($p = 0.1573$)	$\kappa = *$ ($p = 0.3173$)	
REVEL	$\kappa = *$ ($p = 0.0833$)	$\kappa = 0.4595$ ($p = 0.1573$)	$\kappa = 0.7727$ ($p = 0.3173$)	$\kappa = 0.4595$ ($p = 0.1573$)	$\kappa = *$ ($p = 0.0833$)	$\kappa = *$ ($p = 0.1573$)	$\kappa = 0.7727$ ($p = 0.3173$)
	PremPS	Kinact mCSM $\Delta\Delta G$		Kinact SDM $\Delta\Delta G$		Kinact DUET $\Delta\Delta G$	
Kinact mCSM $\Delta\Delta G$	$\kappa = -0.0320$ ($p = 0.5637$)						
Kinact SDM $\Delta\Delta G$	$\kappa = -0.0854$ ($p = \mathbf{0.0126}$)	$\kappa = 0.1296$ ($p = \mathbf{0.0016}$)					
Kinact DUET $\Delta\Delta G$	$\kappa = 0.1357$ ($p = \mathbf{0.0339}$)	$\kappa = 0.1887$ ($p = \mathbf{0.0082}$)	$\kappa = 0.2621$ ($p = 0.3657$)				
I-Mutant 3.0 $\Delta\Delta G$	$\kappa = *$ ($p = 0.1573$)	$\kappa = *$ ($p = 0.3173$)	$\kappa = *$ ($p = \mathbf{0.0009}$)	$\kappa = *$ ($p = \mathbf{0.0047}$)			
	PremPS						
I-Mutant 3.0 $\Delta\Delta G$	**						

κ = Kappa coefficient, MAFI = Mutation Assessor Functional Impact, p = p -value from McNemar's test. * Could not be computed, ** Could not compute κ or p -value. p -values in bold are significant ($p \leq 0.05$).

unchanged in the presence of GST-CK2 β . In contrast GST CK2 α Tyr50Phe was partially rescued from 10% to 40% of *in vitro* kinase activity by addition of GST-CK2 β , suggesting a potential conformation change due to the binding of CK2 β . Noteworthy, the C-spine of CK2 α has a remarkable extension that interacts with the interaction "hot spots" in CK2 β : Leu41 and Phe54 (Bischoff et al., 2011b). Considering this, it makes even sense to test whether the mutation Val53Leu has an indirect effect on CK2 β binding.

Missense mutations in the basic cluster

Val73 is located N-terminal of the CK2 α typical KKKKIKRE-sequence which is important for substrate recognition and binding (Figure 6B). The exchange from Val to the negatively charged Glu in OCNDS may interfere with binding of the typically negatively charged substrates. Indeed, GST-CK2 α Val73Glu had half the activity of the wildtype protein towards a synthetic negative charged peptide substrate, and could not be rescued by adding GST-CK2 β . Arg80 is part of the RE-motif

TABLE 7 Analysis of the CK2 protein mutations using stability prediction tools. Predictions for each mutant in CK2 α (A) and CK2 β (B) according to each program. Highlight colors in the cells reflect the effect from stabilizing (white) to high destabilizing (red). The numbers obtained in the analysis can be found in [Supplementary Table S5](#). (C) Comparison between predictions and experimental data from [Dominguez et al., 2021](#). Table includes CK2 α mutants whose expression in cell lines is significantly altered.

A

CK2 α Mutations	PremPS	Kinact mCSM $\Delta\Delta G$	Kinact SDM $\Delta\Delta G$	Kinact DUET $\Delta\Delta G$	I-Mutant 3.0 $\Delta\Delta G$
M1?	N/A	N/A	N/A	N/A	destabilizing
R21Q	weak effect	weak effect	weak effect	stabilizing	destabilizing
E27K	stabilizing	weak effect	weak effect	stabilizing	destabilizing
Y39C	destabilizing	destabilizing	weak effect	destabilizing	destabilizing
Y39S	destabilizing	destabilizing	destabilizing	destabilizing	destabilizing
G46V	weak effect	weak effect	stabilizing	stabilizing	weak effect
R47G	weak effect	weak effect	stabilizing	weak effect	destabilizing
R47Q	weak effect	weak effect	weak effect	stabilizing	destabilizing
Y50C	destabilizing	weak effect	weak effect	weak effect	destabilizing
Y50F	weak effect	weak effect	stabilizing	weak effect	weak effect
Y50S	destabilizing	destabilizing	weak effect	weak effect	destabilizing
S51N	weak effect	weak effect	weak effect	weak effect	destabilizing
S51R	weak effect	weak effect	weak effect	weak effect	weak effect
S51I	weak effect	weak effect	stabilizing	stabilizing	weak effect
E52K	weak effect	weak effect	weak effect	weak effect	destabilizing
V53L	weak effect	weak effect	weak effect	weak effect	destabilizing
V73E	weak effect	weak effect	destabilizing	weak effect	destabilizing
R80C	weak effect	destabilizing	weak effect	destabilizing	destabilizing
R80H	destabilizing	destabilizing	weak effect	destabilizing	destabilizing
T127M	weak effect	stabilizing	stabilizing	stabilizing	weak effect
C147Y	destabilizing	weak effect	destabilizing	weak effect	weak effect
M153R	destabilizing	destabilizing	destabilizing	weak effect	destabilizing
D156H	weak effect	weak effect	weak effect	weak effect	weak effect
D156E	weak effect	weak effect	weak effect	weak effect	weak effect
D156Y	stabilizing	weak effect	weak effect	weak effect	weak effect
K158E	destabilizing	destabilizing	weak effect	weak effect	destabilizing
K158R	weak effect	destabilizing	stabilizing	weak effect	weak effect
H160R	weak effect	weak effect	stabilizing	weak effect	weak effect
N161S	weak effect	weak effect	weak effect	weak effect	weak effect
N161D	destabilizing	destabilizing	weak effect	weak effect	weak effect
I174M	weak effect	weak effect	weak effect	weak effect	destabilizing
D175G	weak effect	weak effect	stabilizing	stabilizing	destabilizing
D175E	weak effect	weak effect	stabilizing	weak effect	weak effect
G177S	weak effect	destabilizing	weak effect	weak effect	destabilizing
L178W	destabilizing	destabilizing	weak effect	weak effect	destabilizing
R191Q	weak effect	weak effect	weak effect	stabilizing	destabilizing
S194F	weak effect	weak effect	stabilizing	weak effect	weak effect
F197I	destabilizing	destabilizing	stabilizing	weak effect	destabilizing
K198R	weak effect	weak effect	weak effect	weak effect	weak effect
G199D	destabilizing	destabilizing	destabilizing	destabilizing	destabilizing
D210N	weak effect	weak effect	weak effect	weak effect	destabilizing

TABLE 7 Analysis of the CK2 protein mutations using stability prediction tools. Predictions for each mutant in CK2 α (A) and CK2 β (B) according to each program. Highlight colors in the cells reflect the effect from stabilizing (white) to high destabilizing (red). The numbers obtained in the analysis can be found in [Supplementary Table S5](#). (C) Comparison between predictions and experimental data from [Dominguez et al., 2021](#). Table includes CK2 α mutants whose expression in cell lines is significantly altered.

P231R	destabilizing	weak effect	destabilizing	weak effect	destabilizing
R312Q	destabilizing	destabilizing	destabilizing	destabilizing	destabilizing
R312W	weak effect	weak effect	weak effect	weak effect	weak effect
S356T	N/A	N/A	N/A	N/A	destabilizing
P363H	N/A	N/A	N/A	N/A	destabilizing
P382L	N/A	N/A	N/A	N/A	weak effect

B

CK2 β Mutations	PremPS	I-Mutant 3.0 $\Delta\Delta G$
F21L	destabilizing	destabilizing
D32N	weak effect	destabilizing
D32A	weak effect	weak effect
F34S	destabilizing	destabilizing
F34C	destabilizing	destabilizing
N35K	destabilizing	weak effect
E77K	weak effect	weak effect
Y80N	destabilizing	destabilizing
R86C	weak effect	destabilizing
M97I	destabilizing	weak effect
F106V	destabilizing	destabilizing
R111P	destabilizing	weak effect
C137R	destabilizing	weak effect
C137G	destabilizing	destabilizing
C137F	destabilizing	weak effect
P164R	destabilizing	destabilizing
H165R	destabilizing	weak effect
L187P	destabilizing	destabilizing
L187R	destabilizing	destabilizing
G189V	weak effect	weak effect

C.

CK2 α	Stability predictions					Protein expression (experimental) % of WT
Mutations	PremPS	Kinact mCSM $\Delta\Delta G$	Kinact SDM $\Delta\Delta G$	Kinact DUET $\Delta\Delta G$	I-Mutant 3.0 $\Delta\Delta G$	
R47Q	weak effect	weak effect	weak effect	stabilizing	destabilizing	30%
R312Q	destabilizing	destabilizing	destabilizing	destabilizing	destabilizing	10%
R312W	weak effect	weak effect	weak effect	weak effect	weak effect	40%

(Arg80-Glu81) which is characteristic for EPKs in the CMGC family. Arg80 resides in helix αC and is followed by Glu81. Glu81 forms a characteristic salt bridge with a conserved Lys68 ([Figure 6B](#)). Through this salt bridge, Lys68 is positioned in the correct conformation to bind the α and β phospho-groups of the ATP/GTP cosubstrate ([Huse and Kuriyan 2002](#)). Spatially, Arg80 is in close proximity to Arg155 to create a positively charged anion binding site required for substrate recognition at

the P+3 position ([Niefind et al., 2007](#)) ([Figure 6E](#)). Therefore, loss of the positive charge upon exchange from Arg80 to His ([Owen et al., 2018](#)) or Cys ([Wu et al., 2021](#)) likely interferes with substrate binding, and might also disturb the conformation of the critical residue Glu81. Experimentally, GST-tagged CK2 α Arg80His was only minimally active and the GST-Val73Glu mutant showed 40–50% activity compared to WT *in vitro* activity assays. Neither mutant is rescued by addition of

TABLE 8 Binding free energy changes between the wild type and mutant complexes. $\Delta\Delta G$ values were predicted using BeAtMuSiC (Dehouck et al., 2013). For this structure based approach, the binding of one CK2 α chain (chain C) to the CK2 β dimer (chains A/B) was evaluated, using the CK2 holoenzyme structure (PDB_ID 4DGL; (Lolli et al., 2012)) as input file. Mutations which cause an increase of binding free energy of more than 2.0 kcal/mol upon mutation are highlighted in red in the first column. Positive $\Delta\Delta G$ values indicate that the mutation decreases binding affinity (in red), and negative $\Delta\Delta G$ values indicate that the mutation increases binding affinity (in green). BeAtMuSiC (Dehouck et al., 2013) identifies a residue as interface residue if its solvent accessibility in the complex is at least 5% lower than in the unbound form. (A) $\Delta\Delta G$ values for previously experimentally characterized CK2 α variants (Raaf et al., 2011). (B) $\Delta\Delta G$ values for previously experimentally characterized CK2 variants or corresponding exchanges in a CK2 β -derived cyclic peptide including CK2 β residues Arg186 to His193 (Laudet et al., 2007). (C) $\Delta\Delta G$ values for OCNDS-related CK2 α variants. (D) $\Delta\Delta G$ values for POBINDS-related CK2 β variants.

CK2 α Mutations	$\Delta\Delta G_{\text{Bind}}$ (kcal/mol)	Solvent accessibility (in partner(s))	Solvent accessibility (in complex)	Interface
L41A	3.52	53.34%	0%	Yes
F54A	2.92	21.10%	0%	Yes
I69A	2.35	27.07%	2.76%	Yes

CK2 β Mutations	$\Delta\Delta G_{\text{Bind}}$ (kcal/mol)	Solvent accessibility (in partner(s))	Solvent accessibility (in complex)	Interface
M166A	1.53	22.62%	11.55%	yes
R186A	1.35	43.95%	36.13%	yes
L187A	1.94	12.69%	6.99%	yes
Y188A	2.45	71.58%	46.03%	yes
G189A	1.74	46.54%	23.84%	yes
F190A	3.63	68.45%	33.21%	yes
K191A	0.87	61.78%	46.50%	yes
I192A	1.49	17.13%	14.36%	
H193A	1.34	60.99%	37.78%	yes

CK2 α Mutations	$\Delta\Delta G_{\text{Bind}}$ (kcal/mol)	Solvent accessibility (in partner(s))	Solvent accessibility (in complex)	Interface
R21Q	-0.01	58.20%	58.20%	
E27K	0.24	40.82%	40.82%	
Y39C	1.12	11.82%	2.96%	Yes
Y39S	1.76	11.82%	2.96%	Yes
G46V	-0.1	34.05%	34.05%	
R47G	1.69	69.92%	29.30%	Yes
R47Q	0.79	69.92%	29.30%	Yes
Y50C	0.7	50.25%	43.07%	Yes
Y50F	0.21	50.25%	43.07%	Yes
Y50S	0.51	50.25%	43.07%	Yes
S51N	0.31	24.65%	24.65%	
S51R	0.27	24.65%	24.65%	
S51I	0.01	24.65%	24.65%	
E52K	0.45	31.15%	11.28%	Yes
V53L	0.24	14.59%	14.59%	
V73E	0.75	32.83%	25.53%	Yes
R80C	0.7	10.94%	10.94%	
R80H	0.36	10.94%	10.94%	
T127M	0.21	54.43%	54.43%	
C147Y	0.27	0%	0%	
M153R	0.41	0.49%	0.49%	
D156H	0.01	11.34%	11.34%	
D156E	0.38	11.34%	11.34%	
D156Y	0.13	11.34%	11.34%	

(Continued on following page)

TABLE 8 (Continued) Binding free energy changes between the wild type and mutant complexes. $\Delta\Delta G$ values were predicted using BeAtMuSiC (Dehouck et al., 2013). For this structure based approach, the binding of one CK2 α chain (chain C) to the CK2 β dimer (chains A/B) was evaluated, using the CK2 holoenzyme structure (PDB_ID 4DGL; (Lolli et al., 2012)) as input file. Mutations which cause an increase of binding free energy of more than 2.0 kcal/mol upon mutation are highlighted in red in the first column. Positive $\Delta\Delta G$ values indicate that the mutation decreases binding affinity (in red), and negative $\Delta\Delta G$ values indicate that the mutation increases binding affinity (in green). BeAtMuSiC (Dehouck et al., 2013) identifies a residue as interface residue if its solvent accessibility in the complex is at least 5% lower than in the unbound form. (A) $\Delta\Delta G$ values for previously experimentally characterized CK2 α variants (Raaf et al., 2011). (B) $\Delta\Delta G$ values for previously experimentally characterized CK2 variants or corresponding exchanges in a CK2 β -derived cyclic peptide including CK2 β residues Arg186 to His193 (Laudet et al., 2007). (C) $\Delta\Delta G$ values for OCNDS-related CK2 α variants. (D) $\Delta\Delta G$ values for POBINDS-related CK2 β variants.

CK2 α Mutations	$\Delta\Delta G_{\text{Bind}}$ (kcal/mol)	Solvent accessibility (in partner(s))	Solvent accessibility (in complex)	Interface
K158E	0.38	20.81%	20.81%	
K158R	0.06	20.81%	20.81%	
H160R	-0.03	74.07%	74.07%	
N161S	0.49	2.42%	2.42%	
N161D	0.49	2.42%	2.42%	
I174M	0.42	13.26%	13.26%	
D175G	0.16	39.07%	39.07%	
D175E	0.5	39.07%	39.07%	
G177S	0.16	13.62%	13.62%	
L178W	-0.08	21.75%	21.75%	
R191Q	0.01	68.75%	68.75%	
S194F	0.18	20.80%	20.80%	
F197I	0.76	6.28%	6.28%	
K198R	0.2	9.30%	9.30%	
G199D	0.21	0%	0%	
D210N	0.25	5.04%	5.04%	
P231R	0.86	12.26%	12.26%	
R312Q	0.41	1.17%	1.17%	
R312W	0.21	1.17%	1.17%	
S356T	n.d.	n.d.	n.d.	n.d.
P363H	n.d.	n.d.	n.d.	n.d.
P382L	n.d.	n.d.	n.d.	n.d.
D				
CK2 α Mutations	$\Delta\Delta G_{\text{Bind}}$ (kcal/mol)	Solvent accessibility (in partner(s))	Solvent accessibility (in complex)	Interface
F21L	1.23	1.80%	1.80%	
D32N	0.12	50.72%	48.83%	
D32A	0.22	50.72%	48.83%	
F34S	0.39	75.85%	51.17%	Yes
F34C	0.88	75.85%	51.17%	yes
N35K	0.66	24.17%	22.36%	
E77K	0.03	49.95%	49.95%	
Y80N	2.4	0%	0%	
R86C	0.96	28.91%	28.12%	
M97I	0.37	0%	0%	
F106V	1.42	0.45%	0.45%	
R111P	0.56	8.79%	8.79%	
C137R	2.25	0%	0%	
C137G	2.04	0%	0%	

(Continued on following page)

TABLE 8 (Continued) Binding free energy changes between the wild type and mutant complexes. $\Delta\Delta G$ values were predicted using BeAtMuSiC (Dehouck et al., 2013). For this structure based approach, the binding of one CK2 α chain (chain C) to the CK2 β dimer (chains A/B) was evaluated, using the CK2 holoenzyme structure (PDB_ID 4DGL; (Lolli et al., 2012)) as input file. Mutations which cause an increase of binding free energy of more than 2.0 kcal/mol upon mutation are highlighted in red in the first column. Positive $\Delta\Delta G$ values indicate that the mutation decreases binding affinity (in red), and negative $\Delta\Delta G$ values indicate that the mutation increases binding affinity (in green). BeAtMuSiC (Dehouck et al., 2013) identifies a residue as interface residue if its solvent accessibility in the complex is at least 5% lower than in the unbound form. (A) $\Delta\Delta G$ values for previously experimentally characterized CK2 α variants (Raaf et al., 2011). (B) $\Delta\Delta G$ values for previously experimentally characterized CK2 variants or corresponding exchanges in a CK2 β -derived cyclic peptide including CK2 β residues Arg186 to His193 (Laudet et al., 2007). (C) $\Delta\Delta G$ values for OCNDS-related CK2 α variants. (D) $\Delta\Delta G$ values for POBINDS-related CK2 β variants.

CK2 α Mutations	$\Delta\Delta G_{\text{Bind}}$ (kcal/mol)	Solvent accessibility (in partner(s))	Solvent accessibility (in complex)	Interface
C137F	0.96	0%	0%	
P164R	-0.43	0%	0%	
H165R	0.29	1.23%	1.23%	
L187P	2.25	12.69%	6.99%	yes
L187R	1.04	12.69%	6.99%	yes
G189V	1.59	46.54%	23.84%	yes

GST-CK2 β (Dominguez et al., 2021). This region of the protein is also involved in holoenzyme oligomerization however a mutation in the KKKKIKRE sequence would not have a big impact on oligomerization as the KKKKIKRE sequence is close to CK2 β but the P+1 residues of the substrate binding site are significantly much closer.

Missense mutations in the active site

Met153 is a buried residue. Although its function is structural, it has been assigned to the active site in this study as it is located just before the beginning of the catalytic loop. Met153 is part of a hydrophobic cluster, and resides in close proximity to Leu213 and the aromatic rings of Tyr188, Tyr209, Tyr211 (Figure 6H). Met153 is located close to Arg155, which is involved in substrate binding at the P+3 site (Figure 6E). The exchange of Met153 to an Arg would significantly disrupt this hydrophobic arrangement and therefore the global folding of the protein.

Asp156 is located in the active site (Figure 6D). It is the catalytic base of the kinase, therefore the Asp156His or Asp156Tyr mutations likely abolish activity, as it was shown for the kinase dead mutant CK2 α Asp156Ala (Korn et al., 1999). Even though the mutation Asp156Glu is electrostatically conservative, the exchange at this critical catalytic position may greatly affect kinase activity. The catalytic key residue Lys158 is highly conserved among EPKs and stabilizes the transition state of the phosphorylation reaction. An exchange of Lys158 to Glu/Arg may interfere with this stabilizing effect. In addition to their catalytic functions, it was shown that Asp156 and Lys158 contribute to heparin binding in a structure of CK2 α complexed with the substrate competitive inhibitor heparin (Schnitzler and Niefind 2021). Analogously, both residues could be involved in substrate binding. His160 was shown to interact with the acidic residue of the substrate at the P-

3 site (Schnitzler and Niefind 2021) (Figure 6E), therefore the substitution of His160 with Arg may sterically interfere with substrate binding. Asn161 coordinates Mg^{2+} , which is essential for balancing the negative charges of ATP (or GTP). In addition to this, it forms a hydrogen bond to the catalytic base Asp156 (see Figure 6D). Exchange from the highly conserved Asn to Ser or Asp may interfere with these functions. Ile174 is a critical residue of the active site as well (Figure 6D). Together with the residues Met163, Val53 and Ile66 it forms a hydrophobic area to fix the adenine/guanine group of ATP/GTP (Niefind et al., 1998). Exchange with Met might interfere with ATP/GTP binding (Owen et al., 2018).

The Mg^{2+} binding Asp175 (Figure 6D) is a highly conserved residue among protein kinases and is involved in the coordination of both Mg^{2+} ions. GST-tagged CK2 α Ile174Met showed 10% activity compared to WT, while GST-CK2 α Asp175Gly was no longer catalytically active at all; Ile174Met showed a slight rescue by GST-CK2 β (Dominguez et al., 2021). Gly177 is in close proximity to the Lys68-Glu81 salt bridge. A replacement with Ser might disturb the salt bridge and thereby alter catalytic activity. The intact Lys68-Glu81 salt bridge is critical for catalytic activity, and the formation of the corresponding salt bridges is involved in regulation of many EPKs. In the inactive state of many regulated EPKs, this critical salt bridge is broken and the helix αC is rotated. As part of coupled conformational rearrangements upon inactivation, the so-called DFG-motif at the beginning of the activation loop can rotate into the active site and block nucleotide and substrate binding (Huse and Kuriyan 2002). In CK2 α , however, Gly177 is part of the equivalent DWG-motif (see Figure 6D) which—compared to the canonical DFG-motif—is internally stabilized by an additional hydrogen bond. Consistent with CK2 α 's constitutive activity, the aforementioned rearrangements for inactivation have never been observed in

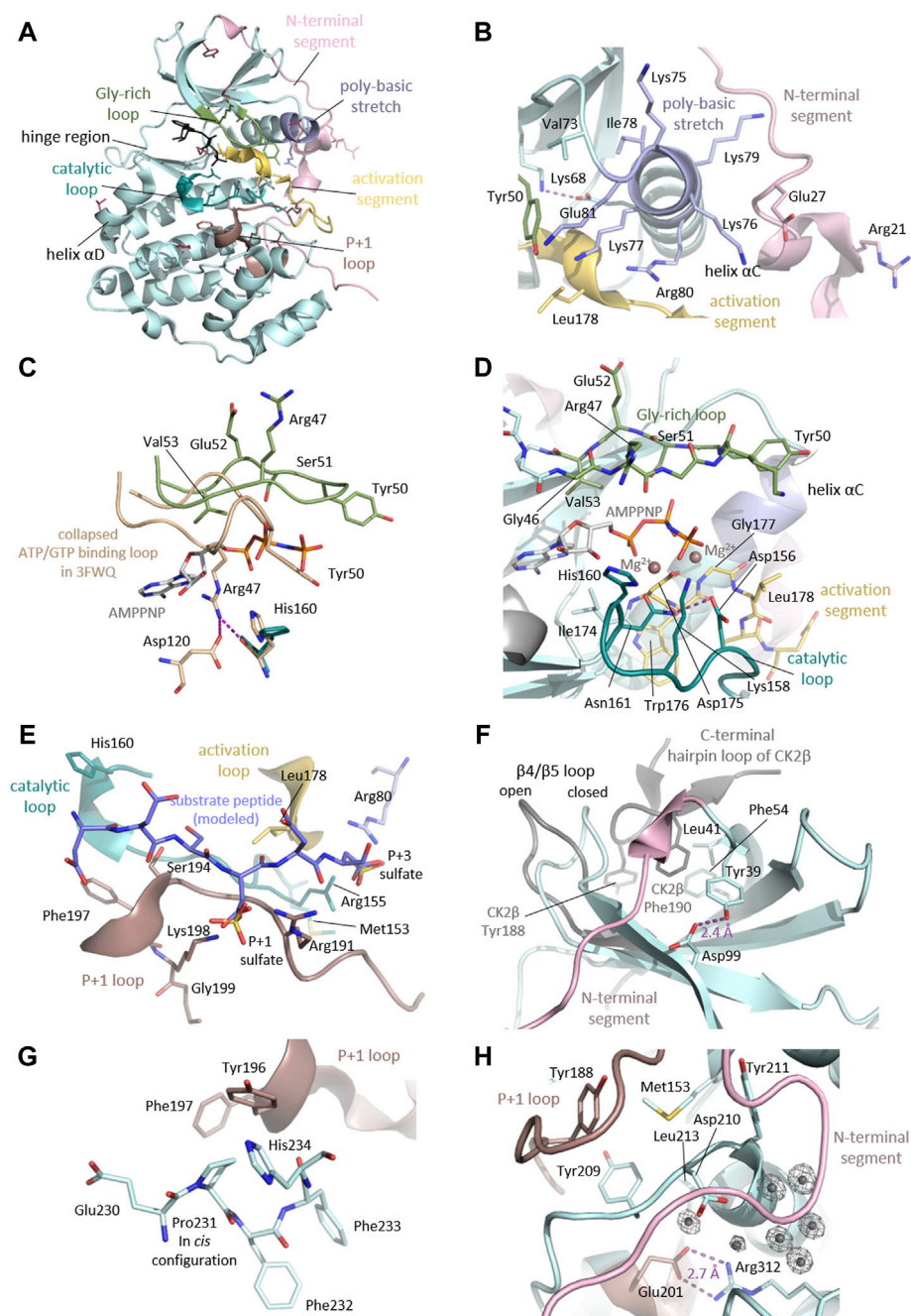


FIGURE 6

Detailed CK2α functional and structural domains. (A) Clustering of mutation sites in the catalytic and structural key elements of CK2α. The side chains of the mutated residues are shown as sticks and are coloured according to the different elements as described in the figure. Mutation sites not residing in these elements are highlighted in raspberry red. The CK2α¹⁻³³⁵ structure in complex with AMPPNP (PDB_ID: 2PVR (Niefind et al., 2007)) was used for the figure. (B) Mutation sites in the N-terminal segment and the helix αC. The N-terminal region of CK2α with the mutation sites Arg21 and Glu27 drawn in light pink. The helix αC, which is located adjacent to mutation site Val73, harbors the basic cluster (light blue) including the mutation sites Lys68 and Glu81. The critical salt bridge between Lys68 and Glu81 is shown as well as the mutation sites residing in proximity such as Tyr50 from the Gly-rich loop (pale green) and Leu178 of the activation loop (yellow). The CK2α¹⁻³³⁵ structure PDB_ID: 2PVR (Niefind et al., 2007) was used for the figure. (C) Mutation sites in the Gly-rich loop. The Gly-rich loop is shown in its open conformation (pale green, PDB_ID: 2PVR (Niefind et al., 2007)) and collapsed conformation (wheat, PDB_ID: 3FWQ (Raaf et al., 2009)). The mutation sites of the Gly-rich loop Arg47, Tyr50, Ser51, Glu52 and Val53 are shown as sticks, as well as AMPPNP. In the collapsed conformation, Arg47 forms hydrogen bonds to Asp120 and His160, which are depicted as purple dashed lines. (D) Mutation sites in the active site of CK2α. The mutation sites in the catalytic loop (Asp156, Lys158, His160 and Asn161) are drawn as dark cyan sticks. The activation loop is shown as stick representation, the respective mutation sites are Gly177 and Leu178. The Gly-rich loop is drawn as sticks and the mutation sites Arg47, Tyr50, Ser51, Glu52 and Val53 are labelled. Magnesium ions are shown as dark salmon spheres. (Continued)

FIGURE 6

maize CK2 α structure in complex with AMPPNP and magnesium ions (PDB ID: 1LP4 (Yde et al., 2005)) served as a reference for the binding mode of AMPPNP and magnesium ions in this figure. **(E)** Mutation sites involved in substrate binding. To illustrate the substrate binding mode, a peptide substrate (coloured blue) was modelled into the substrate binding site as described (Niefind et al., 2007). Sulfate ions present in the structure mark the anion binding sites for the substrate. Mutation sites which are relevant for substrate binding from the P+1 loop (Arg191 and Ser194, Phe197, Lys198 and Gly199, dark salmon), catalytic loop (Met153 and His160, dark cyan), activation loop (Leu178, yellow) and the basic cluster (Arg80, light blue) are shown as stick representations. In addition to the mutated residues, Arg155 is shown as stick representation, as it creates a positively charged anion binding site together with Arg80 which is required for substrate recognition at the P+3 position. The CK2 α^{1-335} structure (PDB_ID: 2PVR (Niefind et al., 2007)) was used for the figure. **(F)** Mutation sites in the subunit interaction interface. Critical residues for binding on the CK2 α (Leu41 and Phe54, pale cyan) and CK2 β (Tyr188 and Phe190, grey) surface are shown as sticks. The mutation site Tyr39 is not directly involved in the interaction but stabilizes the protein fold through a hydrogen bond to Asp99. To illustrate the movement of the β 4 β 5 loop upon assembly of the CK2 holoenzyme, the closed conformation of the CK2 α monomer (pale cyan) and the open conformation of CK2 α with bound CK2 β (grey) are shown. The CK2 α^{1-335} structure monomer (PDB_ID: 2PVR (Niefind et al., 2007)) and the CK2 holoenzyme structure (PDB_ID: 4DGL (Lolli et al., 2012)) were used for the figure. **(G)** *Cis*-configuration of the Pro231. The mutation site Pro231 is located in the C-terminal segment of CK2 α . Pro231 was found as a *cis*-peptide in all CK2 α structures published so far. Pro231 is located in proximity to the P+1 loop and its mutation to a non-proline residue lacking *cis*-peptide propensity may disturb the local or even global fold of the protein. The CK2 α^{1-335} structure (PDB_ID: 2PVR (Niefind et al., 2007)) was used for the figure. **(H)** Mutation sites in the hydrophobic cluster around Met153 and the C-terminal region. The mutation site Met153 is part of a hydrophobic cluster and resides in close proximity to Leu213 and the aromatic rings of Tyr188, Tyr209, Tyr211. The mutation site Arg312 forms a critical salt bridge with Glu201 of the P+1 loop/activation segment. Position Arg312 is in close proximity to the mutation site Asp210 and to a critical water cluster, which mediates the contact of the N-terminal segment (light pink), the activation loop, and the α C helix, which keeps them in the active conformation. The CK2 α^{1-335} structure (PDB_ID: 2PVR (Niefind et al., 2007)) was used for the figure. Electron densities around water molecules have a cutoff level of 2 σ .

CK2 α . Leu178 is located close to the P+3 site of the substrate (Figure 6E), and replacement with the bulkier Trp residue might interfere with substrate binding.

Missense mutations in the P + 1 loop

The OCNDS-sensitive positions Arg191, Ser194, Phe197, Lys198 and Gly199 belong to the P+1 loop of the activation segment and are important for substrate recognition (Figure 6E). Mutational studies in which the combination of Arg191, Arg195 and Lys198 were replaced by alanines showed defective substrate recognition at the P+1 position and decreased inhibition by the substrate competitive inhibitor heparin (Sarno et al., 1996; Vaglio et al., 1996). In a complex structure of CK2 α with heparin, it was shown that Arg191, Ser194, Phe197 and Lys198 are involved in heparin binding (Schnitzler and Niefind 2021). Changes in side chain charges in this region could alter the formation of regulatory holoenzyme oligomers.

Protein kinase C (PKC)-mediated phosphorylation at CK2 α residues Ser194 and Ser277, and at CK2 β residue Ser148 stimulate CK2 activity (Lee et al., 2016). Accordingly, the Ser194Phe mutation should interfere with the phosphorylation by PKC. Further phosphorylation sites in the proximity of the mutated residues are Tyr182 and Tyr188. Phosphorylation of Tyr182 and Tyr188 by Src-related kinase SRMS was shown to increase CK2 α activity (Goel et al., 2018). Mutations near the phosphorylation sites may disturb the recognition by SRMS (Roffey and Litchfield 2021).

The Lys198Arg mutation is the most frequently observed variant in OCNDS patients and is considered as a mutation hotspot (Okur et al., 2016; Akahira-Azuma et al., 2018; Chiu et al., 2018; Owen et al., 2018; Nakashima et al., 2019; Xu et al., 2020). Lys198 was described as the key residue determining the anion binding potential of the P+1 loop (Sarno et al., 1995; Sarno et al. 1996; Sarno et al. 1997). The crystal structure of the CK2 α Lys198Arg variant discloses a significant shift of a sulfate

ion marking the anion binding site in the P+1 position (Werner et al., 2022). This observation supports the notion by Cafer et al. that the Lys198Arg mutation causes an alteration of substrate specificity (Cafer et al., 2022). In this recent publication (Cafer et al., 2022), a Proteomic Peptide Library Approach (ProPel) using CK2 α Lys198Arg expressed in *E. coli* revealed that the mutation shifts substrate specificity by decreasing the preference for acidic residues in the P+1 position. Furthermore, the Lys198Arg mutation alters the phosphoacceptor preference: in contrast to the WT, CK2 α Lys198Arg strongly disfavoured Thr phosphorylation and showed an increased preference for Tyr phosphorylation. The Lys198 equivalent position in protein kinase A (PKA-C) is Leu205 and, interestingly, the mutation Leu205Arg is linked to cortisol-secreting adrenocortical adenomas responsible for Cushing's Syndrome. It was reported that the Leu205Arg mutation disrupts the binding of R (regulatory)-subunits; thereby, it renders the enzyme constitutively active (Calebiro et al., 2014) and it drastically changed the phosphorylation profile in a phosphoproteomic mapping (Lubner et al., 2018). Using NMR spectroscopy, thermodynamics, kinetic assays, and molecular dynamics simulations, Walker et al. (Walker et al., 2019) found that the Leu205Arg mutation causes global changes in PKA-C: it rewires the intra- and intermolecular interactions, and causes losses in nucleotide/pseudo-substrate binding cooperativity. By rewiring its internal allosteric network, PKA-C Leu205Arg is able to bind and phosphorylate non-canonical substrates. An additional interesting structural observation concerning Lys198 is that it stabilizes Arg193 in an unfavourable backbone conformation via hydrogen bonds. Similar tensions in the P+1 loop can be found in other CMGC Kinases, where tension and release are factors in the control mechanism (Huse and Kuriyan 2002). For CK2 α , the tension at Ala193 is without any evident function (Niefind et al., 2007). GST-tagged CK2 α Lys198Arg showed 20%–30% activity and CK2 α

Arg191Gln showed 40%–50% activity compared to wild type using a standard peptide (Dominguez et al., 2021).

The mutation Gly199Asp most likely changes the main characteristics of the P+1 loop and, therefore, the ability to bind substrates due to steric clashes of the larger residue may result in rearrangements of the P+1 loop. The substitution for an acidic residue will have a repulsive effect on the binding of acidic substrates.

Missense mutations in the C-terminal segment

This study defines the C-terminal segment as the sequence after the P+1 loop (residues 202–391). The OCNDS-associated mutations Asp210Asn, Pro231Arg, Arg312Gln/Trp, Ser356Thr, Pro363His, Pro382Leu and the C-terminal truncation Arg333* occur in the C-terminal segment. The GST-tagged variants of CK2 α Pro231Arg and CK2 α Arg312Gln lost 90% of their catalytic activity compared to WT, and Pro231Arg was rescued by CK2 β (Arg312Gln was not tested) (Dominguez et al., 2021). A *cis*-peptide was found at Pro231, a in all CK2 α structures published so far. The role of the Pro231 *cis*-peptide bond in CK2 α (Figure 6G) is not known yet, but possibly the mutation to a non-proline residue lacking *cis*-peptide propensity destabilizes the local or even global fold of the protein. Position Arg312 forms a critical salt bridge with Glu201 of the activation segment. Arg312 is in close proximity to Asp210 which was substituted for Asn in OCNDS (Figure 6H). Both residues are located near a critical cluster of water molecules -observed in high-resolution CK2 α structures- that mediates the close contact of the N-terminal segment, the activation loop, and the α C helix, keeping them in the active conformation. The C-terminus of CK2 α is an important site of posttranslational modifications and mediates the interaction with peptidyl-prolyl isomerase Pin1 (Messenger et al., 2002). However, structural information about this region is not available except for a CK2 α -derived peptide in complex with O-GlcNAc transferase (Lazarus et al., 2011). CK2 α is phosphorylated in a cell cycle dependent manner by Cdk1/cyclin B at the positions Thr344, Thr360, Ser362 and Ser370 (Bosc et al., 1995) and can be O-GlcNAc-modified on Ser347 by O-GlcNAc transferase (Tarrant et al., 2012). Mutations in proximity to critical residues can potentially interfere with recognition motifs or binding site; for example, P363H may affect Thr360/Ser362 phosphorylation by CDK1 and MAPK1 (Ji et al., 2009).

Truncating and frameshift mutations

The majority of the truncating mutations (nonsense and frameshifts) likely result in the complete loss of the normal protein folding. Interestingly, the C-terminal truncated variant Arg333 resembles the CK2 α ¹⁻³³⁵ construct commonly used for crystallization and other *in vitro* experiments. This variant is less prone to C-terminal degradation under *in vitro* conditions (Ermakova et al., 2003). Some frameshift mutants may also be an exception to miss-folding/destabilization, as we describe below for CK2 β . This indicates that each mutant must be individually studied to address stability and function.

A structural perspective of the POBINDS-related CSNK2B mutations

In contrast to the CSNK2A1 mutations in OCNDS, most mutations of the CSNK2B gene linked to POBINDS or related syndromes are frameshift, truncating, and splice site mutations. Missense mutations cluster in highly conserved regions (Figures 2B, 4D; Supplementary Figure S2), including regions important for CK2 β dimerization or CK2 α subunit interaction and therefore for the assembly of the CK2 holoenzyme (Figure 1). Many of the missense mutations are located at buried residues important for the global architecture of the protein: Phe21Leu, Tyr80Asn, Met97Ile, Arg111Pro, Phe106Val, Cys137Arg/Gly/Phe, Pro164Arg and His165Arg. These missense mutations likely destabilize the protein. Still, there are surface exposed residues in the N-terminal segment (Asp32Asn/Ala/His, Phe34Ser/Cys, Asn35Lys, Arg86Cys), in the acidic loop (Glu77Lys), and in the CK2 α interaction site, Leu187Arg/Pro and Gly189Val.

Missense mutations in Chantalat's clusters and N-terminal segment (residues 1-54)

In the first published structure of CK2 β (CK2 β ¹⁻¹⁸²), Chantalat et al. described two clusters of exposed, conserved residues (Chantalat et al., 1999). Since CK2 β functions as a docking platform, it has been suggested that these conserved surface regions play a role in ligand binding (Chantalat et al., 1999). The first conserved surface cluster is composed of Asp32, Phe34, Asn35 and Arg86 and is directed away from the rest of the protein (Chantalat et al., 1999) (Figures 4C, 7B). Interestingly, the missense mutations of each of the residues (Asp32Asn/Ala/His, Phe34Ser/Cys, Asn35Lys and Arg86Cys) have been linked to neurodevelopmental disability and/or early onset epilepsy in POBINDS and in a new CK2 β -linked intellectual disability-craniodigital syndrome (Asif et al., 2022). As discussed above, this could be a novel functional domain of CK2 β . One possibility is that this region controls protein stability as Lys33 is found ubiquitinated; therefore, mutations in this region may affect protein half-life (Borgo et al., 2021). It has to be noted that in the CK2 holoenzyme, mutations of this surface cluster will be located in the neighbourhood of the Gly-rich loop and the basic stretch of CK2 α —in particular, next to Tyr50, Lys49 and Val73 (Figure 7B). This proximity to the holoenzyme catalytic machinery could mean that mutations in the conserved surface cluster of CK2 β may impact the catalytic properties and/or binding of substrate proteins of the CK2 holoenzyme.

The second cluster of conserved surface residues is a helical groove wrapping around the dimer, containing identical residues in 6 species: residues Ile10, Glu20, Phe21, Phe22, Cys23, Glu24, Lys100, Asp105, Gly107, and Pro110 in chain A, and Tyr144, Pro146, Lys147, and Ser148 in chain B of the CK2 β dimer (Chantalat et al., 1999) (Figure 7C; Supplementary Figure S2). However, the side chains of residues Ile10, Phe21, Phe22, Cys23,

Pro146 and Tyr144 point to the inside of the protein according to their hydrophobic nature. Two of the residues of this groove are reportedly linked to POBINDS: residues 20 (Glu20Ter) and 21 (Phe21Leu). Although the hydrophobic character is retained by the exchange of Phe21 with Leu, the aromatic stacking with His151 can no longer be established. Interestingly, His151 is one of the three His residues of the karyophilic cluster (¹⁴⁷KSSRHHH¹⁵³) proposed to serve as a nuclear localization signal (NLS) (Filhol et al., 2003). Residues adjacent to the ones in this second cluster (Met97Ile, Phe106Val, and Arg111Pro) were found mutated in POBINDS, which may affect the cluster's structure.

Missense mutations in the acidic stretch

CK2 β is characterized by an acidic stretch consisting of an acidic loop (Asp55 - Asp70) and an extended acidic groove with residues from helices α A, α C and the N-terminus of helix α D (Chantalat et al., 1999). It is noteworthy that the acidic loop plays a role in the modulation of CK2 activity. It was shown that mutation of residues 55-57 to alanine results in the neutralization of the acidic loop, and hyperactivates CK2 *in vitro* (Boldyreff et al., 1993). Furthermore, the crystal structure of the CK2 holoenzyme showed that crystal contacts between neighbouring CK2 heterotetramers are mediated by the CK2 β acidic loop that binds to the positively charged substrate binding region of CK2 α (Niefind and Issinger 2005). Among the residues located in helix α D is Glu77 (Figure 7E), which is mutated to Lys in CK2 β -related neurodevelopmental disability (Ernst et al., 2021). The replacement with positively charged Lys changes the electrostatics of the acidic stretch and could alter the interactions with other proteins as well as it might affect the formation of oligomeric forms of the CK2 holoenzyme.

Missense mutations in the zinc-binding and CK2 β dimerization domain

Many mutations in POBINDS patients occur in CK2 β 's dimerization region (Figure 7F). Cys137 is one of the four cysteines in CK2 β 's zinc finger/dimerization motif (Cys109, Cys114, Cys137 and Cys140). Three different POBINDS-associated mutations at position 137 have been reported (Cys137Arg/Gly/Phe). Lys139 has been proposed as a ubiquitination site as it is an exposed residue (Zhang et al., 2002; French et al., 2007), and we hypothesize that the ubiquitination may serve as a signal to degrade non-dimerized CK2 β proteins. Mutation of Cys109 and Cys114 to Ser disrupted CK2 β dimerization and CK2 holoenzyme formation *in vitro* and *in vivo* in previous studies (Canton et al., 2001). Arg111 is involved in an inter-subunit salt bridge with Asp142 of the other CK2 β chain (Niefind et al., 2001). In addition to the loss of the salt bridge, the Arg111Pro (Li et al., 2019) mutation may lead to a structural rearrangement incompatible with zinc complexation. His165 is a part of the hydrophobic cluster in the dimerization interface (Niefind et al., 2001) (see Figure 7G). Exchange to Arg may

induce steric clashes. The neighbouring residue Pro164 resides at the beginning of helix α F and has the function of a helix breaker. The exchange of Pro164 with Arg interferes with function and leads to steric clashes (see Figure 7G).

Missense and frameshift mutations in the C-terminal segment (residues: 179-215) and CK2 α interaction site

POBINDS-related mutations were found also in the C-terminal region of CK2 β harbouring the CK2 α interaction site (see Figure 7H). Leu187 and Gly189 are important for CK2 α binding and were included in a CK2 β -derived cyclic peptide mimicking the highly conserved CK2 β hairpin loop essential for binding of CK2 α (Laudet et al., 2007). A Gly residue at this position is essential for the close contacts of the hairpin structure, therefore, Leu187/Arg or Pro and Gly189 Val are very likely to disturb the CK2 α /CK2 β interaction. In this segment, Arg186 is found methylated and Lys191 ubiquitinated, suggesting that mutations in neighbouring residues may affect these two posttranslational modifications (Phosphosite Plus) (Hornbeck et al., 2012).

The Pro179Tyrfs*49 mutation leads to an altered CK2 β mutant with a prolonged C-terminus which in co-IP experiments lacks the ability to bind CK2 α (Nakashima et al., 2019). Similarly, other frameshift variants with altered sequence of the C-terminal hairpin loop are lacking the main determinant for the subunit interaction and, consequently, may not be able to interact with CK2 α .

Truncating mutations

The majority of the reported truncating mutations should affect the global fold of CK2 β and its dimerization. Exceptions to this are truncating mutations in the C-terminal region. The crystal structure of the C-terminal deletion mutant CK2 β ¹⁻¹⁸² showed that the global fold of the protein remains intact (Chantalat et al., 1999). All C-terminal deletion variants with complete loss of C-terminal hairpin loop (main determinant for CK2 α interaction) may not interact with CK2 α .

Concluding remarks

We collected these data on *CSNK2A1* and *CSNK2B* variants with the aim to provide a consolidated resource on *CSNK2A1* and *CSNK2B* variants, and analyzed all the mutants using diverse methods to provide integrated information on their potential functional effects that can be used to inform researchers of OCNDS and POBINDS syndromes. We analysed both syndromes together, as the proteins encoded, CK2 α and CK2 β , can form a functional unit in the cell (protein kinase CK2). We acknowledge that there may be other variants yet to be identified that could modify some of the discussion and conclusions in this study.

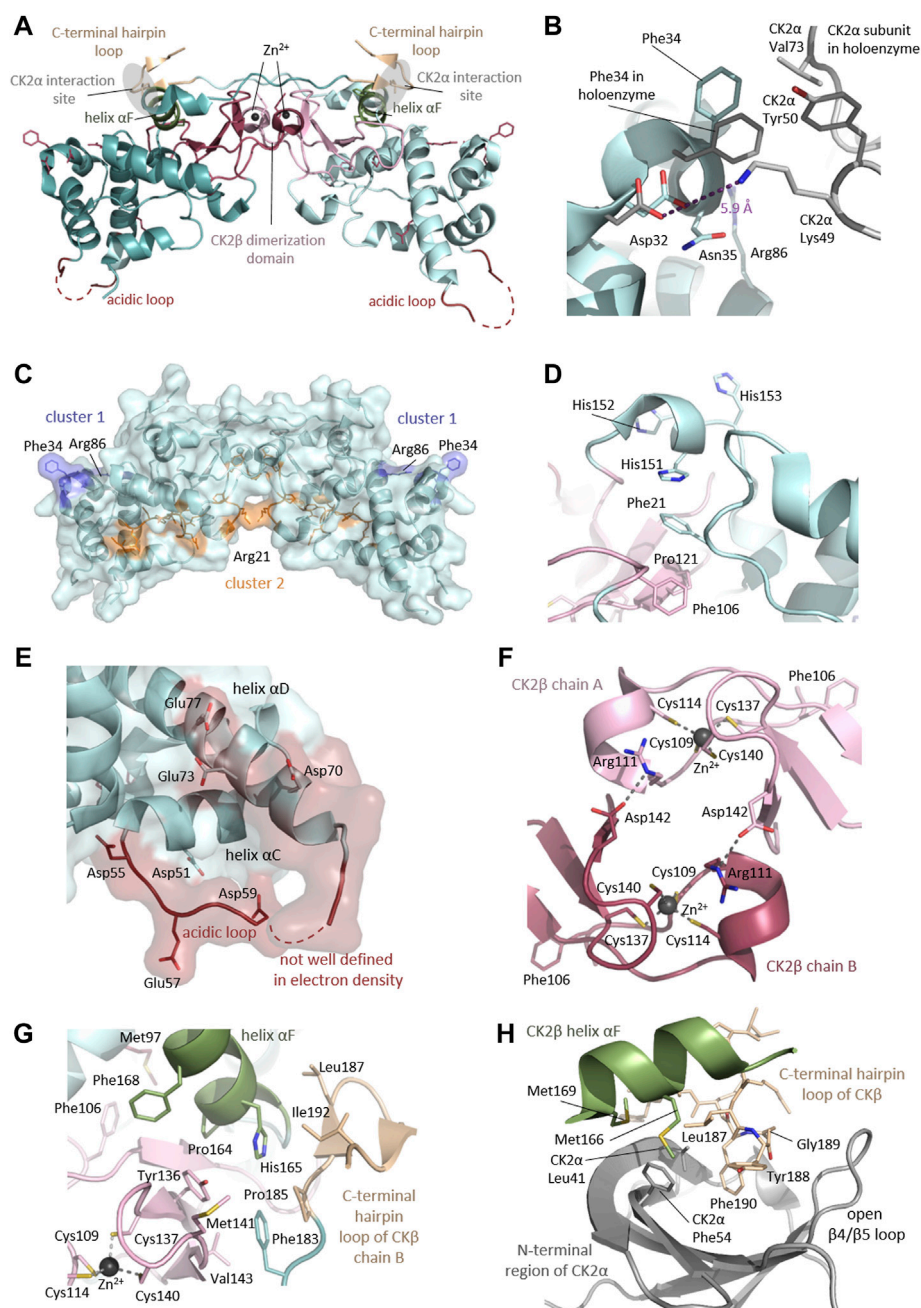


FIGURE 7

Detailed CK2 β functional and structural domains. (A) Clustering of mutation sites in structural and functional key elements of the CK2 β dimer. The mutated residue side chains are shown as sticks and are coloured according to the different elements as described in the figure. Mutation sites residing outside of the highlighted elements are shown in raspberry red. The CK2 β^{1-193} structure (PDB_ID: 3EED (Raaf et al., 2008)) was used for the figure. Parts of chain A of the CK2 β^{1-193} dimer, which are not belonging to the highlighted elements, are drawn in light cyan and the dimerization domain is drawn in light pink. Analogously, parts of chain B are drawn in dark cyan and the dimerization domain is drawn in raspberry red. The acidic loops were not defined by electron density and are therefore indicated as dashed lines. (B) Mutation sites in the N-terminal region forming a conserved surface exposed cluster. The structure of the CK2 β^{1-193} dimer (PDB_ID: 3EED (Raaf et al., 2008)) is drawn in light cyan and the structures of the CK2 β and CK2 α subunit assembled in the CK2 holoenzyme (PDB_ID: 4DGL (Lolli et al., 2012)) are drawn in grey. The CK2 β mutation sites Asp32, Phe34, Asn35 and Arg86 are drawn as sticks, as well as CK2 α residues, which are located near the CK2 β mutation sites in the assembled CK2 holoenzyme. The distance between CK2 β Asp32 and CK2 α Lys49 is shown as a purple dashed line to illustrate that the distance is too far to establish a close contact via a salt bridge. (C) Conserved surface clusters as described by Chantalat (Chantalat et al., 1999). The first conserved surface exposed cluster is composed of Asp32, Phe34, Asn35 and Arg86 (drawn in blue). The second surface cluster is composed of: Ile10, Glu20, Phe21, Phe22, Cys23, Glu24, Lys100, Asp105, Gly107, Pro110, Tyr144, Pro146, Lys147 and Ser148 (drawn in orange). The side chains of residues Ile10, Cys23, Phe21, Phe22, Pro146 and Tyr144 point into the inside of the protein. The mutation site Phe21 is highlighted. (D) Environment of the Chantalat's (Continued)

FIGURE 7

cluster 2 mutation site Phe21. Phe21 and His151 are interacting through π - π stacking. The other His-residues of the of the karyophilic cluster (residues 147–153) as well as Pro121 and the mutation site Phe106 are highlighted. (E) Mutation site Glu77 residing in the helix α D of the e acidic groove. Further acidic residues are shown as sticks. The acidic loop is indicated as a red dashed line. The CK2 β ¹⁻¹⁹³ structure (PDB_ID: 3EED (Raaf et al., 2008)) was used for the figure. (D) Mutation sites in the dimerization domain of the CK2 β ¹⁻¹⁹³ dimer (PDB_ID: 3EED (Raaf et al., 2008)). The dimerization domain of CK2 β ¹⁻¹⁹³ chain A is drawn in light pink and the dimerization domain of CK2 β ¹⁻¹⁹³ chain B is drawn in raspberry red respectively. The mutation sites Phe106, Arg111 and Cys137, as well as the remaining Cys residues of the zinc binding motif and Asp142, which is involved in an inter-subunit salt bridge with Arg111 of the other CK2 β chain are shown as sticks. Zinc ions are drawn as spheres and the interactions between Zn²⁺ and the coordinating Cys residues are indicated as purple dashed lines. The CK2 β ¹⁻¹⁹³ structure (PDB_ID: 3EED (Raaf et al., 2008)) was used for the figure. (E) Mutation sites located inside of CK2 β and the contact area to the CK2 β chain A body and the CK2 β chain B C-terminal tail/hairpin loop. The mutation sites Met97, Phe106, Cys137 and His165 are buried inside of CK2 β chain A and are shown as sticks as well as the mutation site Leu187 of the C-terminal hairpin loop of chain B. Further residues of the hydrophobic cluster such as Met141, Val143, Tyr136 and Phe168 of CK2 β chain A and Phe183, Pro185 and Ile192 residing in CK2 β chain A are shown as sticks. The Cys residues coordinating the Zn²⁺ ion in chain A are shown as sticks as well. The CK2 β ¹⁻¹⁹³ structure (PDB_ID: 3EED (Raaf et al., 2008)) was used for the figure. (F) Mutation sites Leu187 and Gly189 are residing in the subunit interaction interface of CK2 β . Critical residues for the subunit interaction of the C-terminal hairpin loop (coloured wheat) of CK2 β chain A (Tyr188 and Phe190) and the helix α F (coloured green) of CK2 β chain B (Met166 and Met169) surface are shown as sticks the CK2 α (Leu41 and Phe54, pale cyan). The N-terminal region of CK2 α subunit in the assembled CK2 holoenzyme is shown in grey and residues important for the subunit interaction (Leu41 and Phe54) are shown as sticks. The CK2 holoenzyme structure (PDB_ID: 4DGL (Lolli et al., 2012)) was used for the figure.

Our study has opened additional research questions, including addressing the genetic mechanisms leading to hotspots in CSNK2A1 SNVs. The ratio of #mutations/#residues could serve to prioritize domains/mutations to study experimentally (e.g., Gly-rich loop in CK2 α). Our study indicates that NMC analysis can be used to identify potential novel functional domains in the primary sequence of NDD-associated genes (e.g., N-terminal sequences in CK2 α). Our approach in this study, combining NMC analyses with structural analysis (i.e., residues exposed or forming clusters) and evolutionary analyses (highly conserved residues), results in a more solid identification of novel domains that should be further studied experimentally.

A number of key residues involved in substrate recognition are found mutated majorly to a specific amino acid (e.g., Lys198Arg, Arg80His, His160Arg, Arg47Gln and Tyr50Cys). It is possible that mutations in these codons that lead to other amino acids result in embryonic lethality, and thus are not identified in patients. For example, for Lys198 and Arg80 the other potential mutations in the codon are less conservative. It is conceivable that the exchange of these residues involved in substrate recognition to a less conserved residue may result in a defect other than reduced CK2 α activity. This hypothesis is supported by the fact that several mutations that strongly interfere with CK2 kinase activity (Dominguez et al., 2021) are present in patients.

For the mutations identified, potential mechanisms of action include: 1) change of substrate specificity but still a strong overlap with canonical CK2 substrates leading to phosphorylation of non-canonical substrates, as is likely the case for Lys198Arg as supported by the literature (Caefer et al., 2022; Werner et al., 2022); 2) change in substrate specificity with no overlap to CK2 canonical substrates (e.g., Lys198 exchange to Thr, Gln, Glu Asn, Ile) which we hypothesize is deleterious as proteins will be phosphorylated in an unregulated way; 3) interference with substrate phosphorylation; 4) the global fold of CK2 α is disrupted

whenever the amino acid is involved in stabilizing part of the architecture (e.g., Arg312 mutations). We do not expect a loss on the ability to bind substrates, as substrate recognition is not determined by one single residue.

Regarding the correlation of experimental to prediction data for CK2 α , we found ranges in the numerical scores from some prediction programs that relate to the mutants with the lowest activity in kinase assays, with the most altered N/C distribution, and with the lowest expression levels. Future work should experimentally address the stability of the mutant proteins. Mutant stability will have implications for treatment; mutants that are destabilizing and degrade rapidly may lead to haploinsufficient phenotypes.

This study utilized prediction programs that analyze missense mutants. Nonsense, frameshift and splice variants that are also found in CK2 α and CK2 β are typically deemed as *de facto* loss-of-function. Determining the impact of these types of mutants is complex as the prediction programs are still under development (Abrahams et al., 2021; Lord and Baralle 2021). For CK2 α and CK2 β , it will be key to develop predictions programs that include computing of more complex characteristics that can be affected by changes in the primary structure (e.g., binding to each other or other proteins, post-translational modifications, subcellular localization or the formation of oligomeric forms that inhibit activity (Glover 1986; Valero et al., 1995; Borgo et al., 2021; Roffey and Litchfield 2021). The NMC analysis assumes that each residue has an independent and equal likelihood of mutation (i.e., homogeneous mutation probability across all base positions), and calculates the probability that mutations (or clusters of mutations) are non-random. Both population and gene characteristics can affect site mutability. Published studies estimate the genome-wide average mutation rate at $\sim 1\text{--}1.5 \times 10^{-8}$ mutations per base pair per generation (Carlson et al., 2018), and that *de novo* missense mutations in patients with neurodevelopmental diseases are not randomly distributed,

and cluster in fewer genes compared to controls ([The Deciphering Developmental Disorders Study 2015](#)). A potential explanation is that for mutations associated with neurodevelopmental disease, embryonic lethality will impact on the variants that are found in patients. This will result in a non-homogeneous distribution of patient mutations.

Genotype data for many of the patients included in this study is absent or partial. However, Wu et al. indicate that mutations in protein-coding *CK2a* regions appear to influence the phenotypic spectrum of OCNDS. In particular mutations residing in the Gly-rich loop were more likely to cause the widest range of phenotypes ([Wu et al., 2021](#)). For POBINDS, Bonanni et al. very recently reviewed the available literature, where they correlate the neurodevelopmental abnormalities to epilepsy severity and highlight the heterogeneity of the clinical phenotypes that have been associated with the *CSNK2B* gene ([Bonanni et al., 2021](#)). A recent article has reviewed both diseases ([Ballardin et al., 2022](#)). Broader phenotype-genotype correlation data will help us understand the severity of the diseases and may lead to a specific differential diagnosis to clearly identify OCNDS and POBINDS patients. These types of correlations will help us understand other diseases where these genes are mutated or functionally affected ([Castello et al., 2017](#); [Colavito et al., 2018](#)).

Further experimental data is necessary to determine the impact (if any) of each identified mutation in protein structure and biochemistry, subcellular localization and molecular mechanism of disease in embryonic development and in adulthood, which will lead to insights to the severity and nature of reported symptoms. *CSNK2A1* and *CSNK2B* variants could lead to mutants with reduced or increased activity, or dominant negative or gain of function effects. Defining these effects will help indicate therapeutic approach strategies that may be needed.

Data availability statement

The original contributions presented in the study are included in the article/[Supplementary Material](#), further inquiries can be directed to the corresponding author.

Author contributions

ID and JH conceived and designed the study. ID and PU compiled the variant database and obtained IRB determination. PU performed the evolutionary, functional and stability prediction analyses. JF plotted variant and patient numbers on the primary protein structures, performed NMC and number of patients per residue analyses. JH performed the analysis of conserved residues using the ConSurf server, and the protein-protein affinity and structural analyses and diagrams. ID performed the MUSCLE alignments. JW performed the Exact chi-square Test of a Proportion and percent agreement, the Kappa coefficient and

performed McNemar's tests. VO helped identify duplicated patients and to utilize the numerical predictions to rank the effect of mutation. ID wrote the first draft of the manuscript. All authors contributed to the writing of the manuscript, read, finalized, and approved the submitted version.

Funding

This work was funded by the CSNK2A1 foundation, San Francisco, United States (to ID). JH was supported by the CSNK2A1 foundation, San Francisco, United States, and by the Deutsche Forschungsgemeinschaft (DFG) (grant NI 643/4-2). PU and JF were supported by scholarships from the Boston University Undergraduate Research Opportunities Program (UROP). JF was also supported by a scholarship from the STaRS program (NHLBI 5R25HL118693). JW was supported by the National Center for Advancing Translational Sciences, NIH, through BU-CTSI Grant Number 1UL1TR001430. Publication fees were supported by the Hematology and Medical Oncology Section/Department of Medicine/BUSM, the Library Department of the University of Cologne. Funding for the DECIPHER project was provided by Wellcome.

Acknowledgments

The authors would like to thank Dr. Karsten Niefind for scientific discussions and suggestions to the manuscript, and Zeyuan Zhong for help setting up the code for statistical analysis. We are grateful to all the families who gave consent to the centers that submitted *CSNK2A1* and *CSNK2B* variant data to ClinVar, the professionals at ClinVar that curate the data, and for access to this database. This study makes use of data generated by the DECIPHER community. A full list of centres who contributed to the generation of the data is available from <https://deciphergenomics.org/about/stats> and via email from contact@deciphergenomics.org. Professionals who carried out the original analysis and collection of the DECIPHER Data bear no responsibility for the further analysis or interpretation of the data. We thank the professionals at the AutDB site for collecting and sharing with the community publications on OCNDS and POBINDS. We are grateful to all of the families at the participating Simons Searchlight sites as well as the Simons Searchlight Consortium, formerly the Simons VIP Consortium. We appreciate obtaining access to genetic data on SFARI Base. Approved researchers can obtain the Simons Searchlight population dataset described in this study (<https://www.simonssearchlight.org/research/what-we-study/csnk2a1/>) by applying at <https://base.sfari.org>. Our deepest thanks to Jennifer Sills for the extraordinary work that she does in

reaching out and helping OCNDs families, and in supporting and bringing together researchers and clinicians to work on mechanisms of disease and potential therapies.

Conflict of interest

The authors declare that the research was conducted in the absence of any commercial or financial relationships that could be construed as a potential conflict of interest.

Publisher's note

All claims expressed in this article are solely those of the authors and do not necessarily represent those of their affiliated organizations, or those of the publisher, the editors and the reviewers. Any product that may be evaluated in this article, or claim that may be made by its manufacturer, is not guaranteed or endorsed by the publisher.

References

- Abrahams, L., Savisaar, R., Mordstein, C., Young, B., Kudla, G., Hurst, L. D., et al. (2021). Evidence in disease and non-disease contexts that nonsense mutations cause altered splicing via motif disruption. *Nucleic Acids Res.* 49 (17), 9665–9685. doi:10.1093/nar/gkab750
- Adzhubei, I. A., Schmidt, S., Peshkin, L., Ramensky, V. E., Gerasimova, A., Bork, P., et al. (2010). A method and server for predicting damaging missense mutations. *Nat. Methods* 7 (4), 248–249. doi:10.1038/nmeth0410-248
- Ahmad, K. A., Wang, G., Unger, G., Slaton, J., and Ahmed, K. (2008). Protein kinase CK2 – a key suppressor of apoptosis. *Adv. Enzyme Regul.* 48 (1), 179–187. doi:10.1016/j.advenzreg.2008.04.002
- Akahira-Azuma, M., Tsurusaki, Y., Enomoto, Y., Mitsui, J., and Kurosawa, K. (2018). Refining the clinical phenotype of Okur-Chung neurodevelopmental syndrome. *Hum. Genome Var.* 5 (December), 18011. doi:10.1038/hgv.2018.11
- Allende, J. E., and Allende, C. C. (1995). Protein kinases. 4. Protein kinase CK2: An enzyme with multiple substrates and a puzzling regulation. *FASEB J.* 9 (5), 313–323. doi:10.1096/fasebj.9.5.7896000
- Ashkenazy, H., Abadi, S., Martz, E., Chay, O., Mayrose, I., Pupko, T., et al. (2016). ConSurf 2016: An improved methodology to estimate and visualize evolutionary conservation in macromolecules. *Nucleic Acids Res.* 44 (W1), W344–W350. doi:10.1093/nar/gkw408
- Ashkenazy, H., Erez, E., Martz, E., Pupko, T., and Ben-Tal, N. (2010). ConSurf 2010: Calculating evolutionary conservation in sequence and structure of proteins and nucleic acids. *Nucleic Acids Res.* 38 (Suppl. 2), 529–533. doi:10.1093/nar/gkq399
- Asif, M., Kaygusuz, E., Shinawi, M., Nickelsen, A., Hsieh, T.-C., Wagle, P., et al. (2022). De novo variants of CSNK2B cause a new intellectual disability-craniodigital syndrome by disrupting the canonical Wnt signaling pathway. *HGG Adv.* 3 (3), 100111. doi:10.1016/j.xhgg.2022.100111
- Ballardin, D., Cruz-Gamero, J. M., Bienvenu, T., and Rebholz, H. (2022). Comparing two neurodevelopmental disorders linked to CK2: Okur-chung neurodevelopmental syndrome and poirier-bienvenu neurodevelopmental syndrome—two sides of the same coin? *Front. Mol. Biosci.* 9, 850559. doi:10.3389/fmolb.2022.850559
- Basu, S. N., Kollu, R., and Banerjee-Basu, S. (2009). AutDB: A gene reference resource for autism research. *Nucleic Acids Res.* 37 (Suppl. 1_1), D832–D836. doi:10.1093/nar/gkn835
- Bellon, S., Fitzgibbon, M. J., Fox, T., Hsiao, H. M., and Wilson, K. P. (1999). The structure of phosphorylated p38gamma is monomeric and reveals a conserved activation-loop conformation. *Structure* 7 (9), 1057–1065. doi:10.1016/s0969-2126(99)80173-7
- Bendl, J., Stourac, J., Salanda, O., Pavelka, A., Wieben, E. D., Zendulka, J., et al. (2014). PredictSNP: Robust and accurate consensus classifier for prediction of disease-related mutations. *PLoS Comput. Biol.* 10 (1), e1003440. doi:10.1371/journal.pcbi.1003440
- Berman, H. M., Westbrook, J., Feng, Z., Gilliland, G., Bhat, T. N., Weissig, H., et al. (2000). The protein Data Bank. *Nucleic Acids Res.* 28, 235–242. doi:10.1093/nar/28.1.235
- Bischoff, N., Olsen, B., Raaf, J., Bretner, M., Issinger, O.-G., Niefind, K., et al. (2011a). Structure of the human protein kinase CK2 catalytic subunit CK2 α' and interaction thermodynamics with the regulatory subunit CK2 β . *J. Mol. Biol.* 407 (1), 1–12. doi:10.1016/j.jmb.2011.01.020
- Bischoff, N., Raaf, J., Olsen, B., Bretner, M., Issinger, O.-G., Niefind, K., et al. (2011b). Enzymatic activity with an incomplete catalytic spine: Insights from a comparative structural analysis of human CK2 α and its paralogous isoform CK2 α' . *Mol. Cell. Biochem.* 356 (1–2), 57–65. doi:10.1007/s11010-011-0948-5
- Boldyreff, B., Meggio, F., Pinna, L. A., and Issinger, O. G. (1993). Reconstitution of normal and hyperactivated forms of casein kinase-2 by variably mutated β -subunits. *Biochemistry* 32 (47), 12672–12677. doi:10.1021/bi00210a016
- Bonanni, P., Baggio, M., Duma, G. M., Negrin, S., Danieli, A., Giorda, R., et al. (2021). Developmental and epilepsy spectrum of Poirier-Bienvenu neurodevelopmental syndrome: Description of a new case study and review of the available literature. *Seizure* 93, 133–139. doi:10.1016/j.seizure.2021.10.019
- Borgo, C., D'Amore, C., Cesaro, L., Sarno, S., Pinna, L. A., Ruzzene, M., et al. (2021). How can a traffic light properly work if it is always green? The paradox of CK2 signaling. *Crit. Rev. Biochem. Mol. Biol.* 56 (4), 321–359. doi:10.1080/10409238.2021.1908951
- Bosc, D. G., Graham, K. C., Saulnier, R. B., Zhang, C., Prober, D., Gietz, R. D., et al. (2000). Identification and characterization of CKIP-1, a novel pleckstrin homology domain-containing protein that interacts with protein kinase CK2. *J. Biol. Chem.* 275 (19), 14295–14306. doi:10.1074/jbc.275.19.14295
- Bosc, D. G., Slominski, E., Sichler, C., and Litchfield, D. W. (1995). Phosphorylation of casein kinase II by p34(cdc2). Identification of phosphorylation sites using phosphorylation site mutants *in vitro*. *J. Biol. Chem.* 270 (43), 25872–25878. doi:10.1074/jbc.270.43.25872
- Boycott, K. M., Vanstone, M. R., Bulman, D. E., and Mackenzie, A. E. (2013). Rare-disease genetics in the era of next-generation sequencing: Discovery to translation. *Nat. Rev. Genet.* 14 (10), 681–691. doi:10.1038/nrg3555

Author disclaimer

The contents of this article are solely the responsibility of the authors and do not necessarily represent the official views of the NIH.

Supplementary material

The Supplementary Material for this article can be found online at: <https://www.frontiersin.org/articles/10.3389/fmolb.2022.851547/full#supplementary-material>

SUPPLEMENTARY FIGURE 1

Alignment showing conservation in CK2a mutated residues across eukaryotic species.

SUPPLEMENTARY FIGURE 2

General statistics about orthologous gene groups.

SUPPLEMENTARY TABLE 2

General statistics about orthologous gene groups.

SUPPLEMENTARY TABLE 2

General statistics about orthologous gene groups.

- Bouchou, T., Vernet, M., Blond, O., Jensen, H. H., Pointu, H., Olsen, B. B., et al. (2003). Disruption of the regulatory beta subunit of protein kinase CK2 in mice leads to a cell-autonomous defect and early embryonic lethality. *Mol. Cell. Biol.* 23 (3), 908–915. doi:10.1128/mcb.23.3.908-915.2003
- Caefer, D. M., Phan, N. Q., Liddle, J. C., Balsbaugh, J. L., O'Shea, J. P., Tzingounis, A. V., et al. (2022). The okur-chung neurodevelopmental syndrome mutation CK2K198R leads to a rewiring of kinase specificity. *Front. Mol. Biosci.* 9, 850661. doi:10.3389/fmolb.2022.850661
- Calebiro, D., Hannawacker, A., Lyga, S., Bathon, K., Zabel, U., Ronchi, C., et al. (2014). Pka catalytic subunit mutations in adrenocortical cushing's adenoma impair association with the regulatory subunit. *Nat. Commun.* 5 (5680). doi:10.1038/ncomms6680
- Canton, D. A., Zhang, C., and Litchfield, D. W. (2001). Assembly of protein kinase CK2: Investigation of complex formation between catalytic and regulatory subunits using a zinc-finger-deficient mutant of CK2beta. *Biochem. J.* 358 (1), 87–94. doi:10.1042/0264-6021:3580087
- Capriotti, E., Fariselli, P., and Casadio, R. (2005). I-Mutant2.0: Predicting stability changes upon mutation from the protein sequence or structure. *Nucleic Acids Res.* 33, W306–W310. doi:10.1093/nar/gki375
- Carlson, J., Locke, A. E., Flickinger, M., Zawistowski, M., Levy, S., Myers, R. M., et al. The BRIDGES Consortium (2018). Extremely rare variants reveal patterns of germline mutation rate heterogeneity in humans. *Nat. Commun.* 9 (1), 3753. doi:10.1038/s41467-018-05936-5
- Castello, J., Ragnauth, A., Friedman, E., and Rebholz, H. (2017). CK2-An emerging target for neurological and psychiatric disorders. *Pharm. (Basel)* 10 (1), E7. doi:10.3390/ph10010007
- Celniker, G., Nimrod, G., Ashkenazy, H., Glaser, F., Martz, E., Mayrose, I., et al. (2013). ConSurf: Using evolutionary data to raise testable hypotheses about protein function. *Isr. J. Chem.* 53 (3–4), 199–206. doi:10.1002/ijch.201200096
- Chantalat, L., Leroy, D., Filhol, O., Nueda, A., Benitez, M. J., Chambaz, E. M., et al. (1999). Crystal structure of the human protein kinase CK2 regulatory subunit reveals its zinc finger-mediated dimerization. *EMBO J.* 18 (11), 2930–2940. doi:10.1093/emboj/18.11.2930
- Chen, Y., Lu, H., Zhang, N., Zhu, Z., Wang, S., and Li, M. (2020). PremPS: Predicting the impact of missense mutations on protein stability. *PLoS Comput. Biol.* 16 (12), e1008543. doi:10.1371/journal.pcbi.1008543
- Chiu, A. T. G., Pei, S. L. C., Mak, C. C. Y., Leung, G. K. C., Yu, M. H. C., Lee, S. L., et al. (2018). Okur-Chung neurodevelopmental syndrome: Eight additional cases with implications on phenotype and genotype expansion. *Clin. Genet.* 93 (4), 880–890. doi:10.1111/cge.13196
- Choi, Y., Sims, G. E., Murphy, S., Miller, J. R., and Chan, A. P. (2012). Predicting the functional effect of amino acid substitutions and indels. *PLoS ONE* 7 (10), e46688. doi:10.1371/journal.pone.0046688
- Chua, M. M. J., Ortega, C. E., Sheikh, A., Lee, M., Abdul-Rassoul, H., Hartshorn, K. L., et al. (2017). CK2 in cancer: Cellular and biochemical mechanisms and potential therapeutic target. *Pharmaceuticals* 10, 18. doi:10.3390/ph10010018
- Clackson, T., and Wells, J. A. (1995). A hot spot of binding energy in a hormone-receptor interface. *Science* 267 (5196), 383–386. doi:10.1126/science.7529940
- Colavito, D., Del Giudice, E., Ceccato, C., Dalle Carbonare, M., Leon, A., Suppiej, A., et al. (2018). Are CSNK2A1 gene mutations associated with retinal dystrophy? Report of a patient carrier of a novel de novo splice site mutation. *J. Hum. Genet.* 63 (6), 779–781. doi:10.1038/s10038-018-0434-y
- Cross, D. A., Alessi, D. R., Cohen, P., Andjelkovich, M., and Hemmings, B. A. (1995). Inhibition of glycogen synthase kinase-3 by insulin mediated by protein kinase B. *Nature* 378 (6559), 785–789. doi:10.1038/378785a0
- Dehouck, Y., Kwasigroch, J. M., Rooman, M., and Gilis, D. (2013). BeAtMuSiC: Prediction of changes in protein-protein binding affinity on mutations. *Nucleic Acids Res.* 41 (Web Server issue), W333–W339. doi:10.1093/nar/gkt450
- Dominguez, I., Cruz-Gamero, J. M., Corasolla, V., Dacher, N., Rangasamy, S., Urbani, A., et al. (2021). Okur-Chung neurodevelopmental syndrome-linked CK2a variants have reduced kinase activity. *Hum. Genet.* 140, 1077–1096. doi:10.1007/s00439-021-02280-5
- Dominguez, I., Sonenshein, G. E., and Seldin, D. C. (2009). Protein kinase CK2 in health and disease: CK2 and its role in wnt and NF-kappaB signaling: Linking development and cancer. *Cell. Mol. Life Sci.* 66 (11–12), 1850–1857. doi:10.1007/s00018-009-9153-z
- Dorée, M., and Galas, S. (1994). The cyclin-dependent protein kinases and the control of cell division. *FASEB J.* 8 (14), 1114–1121. doi:10.1096/fasebj.8.14.7958616
- Duan, H. L., Peng, J., Pang, N., Chen, S. M., Xiong, J., Guang, S. Q., et al. (2019). [A case of Okur-Chung syndrome caused by CSNK2A1 gene variation and review of literature]. *Zhonghua Er Ke Za Zhi* 57 (5), 368–372. doi:10.3760/cma.j.issn.0578-1310.2019.05.010
- Duncan, J. S., and Litchfield, D. W. (2008). Too much of a good thing: The role of protein kinase CK2 in tumorigenesis and prospects for therapeutic inhibition of CK2. *Biochim. Biophys. Acta* 1784 (1), 33–47. doi:10.1016/j.bbapap.2007.08.017
- Eddy, S. (2011). Accelerated profile HMM searches. *PLoS Comput. Biol.* 7 (10), e1002195. doi:10.1371/journal.pcbi.1002195
- Edgar, R. C. (2004). Muscle: Multiple sequence alignment with high accuracy and high throughput. *Nucleic Acids Res.* 32 (5), 1792–1797. doi:10.1093/nar/gkh340
- Emsley, P., Lohkamp, B., Scott, W. G., and Cowtan, K. (2010). *Features and Development of Coot*, 66, 486–501. doi:10.1107/S0907444910007493Acta Crystallogr. Sect. D - Biol. Crystallogr.
- Ermakova, I., Boldyreff, B., Issinger, O.-G., and Niefind, K. (2003). Crystal structure of a C-terminal deletion mutant of human protein kinase CK2 catalytic subunit. *J. Mol. Biol.* 330 (5), 925–934. doi:10.1016/s0022-2836(03)00638-7
- Ernst, M. E., Baugh, E. H., Thomas, A., Bier, L., Lippa, N., Stong, N., et al. (2021). CSNK2B: A broad spectrum of neurodevelopmental disability and epilepsy severity. *Epilepsia* 62 (7), e103–e109. doi:10.1111/epi.16931
- Fernández-Marmiesse, A., Roca, I., Diaz-Flores, F., Cantarin, V., Pérez-Poyato, M. S., Fontalba, A., et al. (2019). Rare variants in 48 genes account for 42% of cases of epilepsy with or without neurodevelopmental delay in 246 pediatric patients. *Front. Neurosci.* 13, 1135. doi:10.3389/fnins.2019.01135
- Filhol, O., Nueda, A., Martel, V. V., Gerber-Scokaert, D., Benitez, M. J. M. J., Souchier, C., et al. (2003). Live-cell fluorescence imaging reveals the dynamics of protein kinase CK2 individual subunits. *Mol. Cell. Biol.* 23 (3), 975–987. doi:10.1128/mcb.23.3.975-987.2003
- Firth, H. V., Richards, S. M., Bevan, A. P., Clayton, S., Corpas, M., Rajan, D., et al. (2009). Decipher: Database of chromosomal imbalance and phenotype in humans using ensembl resources. *Am. J. Hum. Genet.* 84 (4), 524–533. doi:10.1016/j.ajhg.2009.03.010
- Frame, S., Cohen, P., and Biondi, R. M. (2001). A common phosphate binding site explains the unique substrate specificity of GSK3 and its inactivation by phosphorylation. *Mol. Cell* 7 (6), 1321–1327. doi:10.1016/s1097-2765(01)00253-2
- French, A. C., Luscher, B., and Litchfield, D. W. (2007). Development of a stabilized form of the regulatory CK2beta subunit that inhibits cell proliferation. *J. Biol. Chem.* 282 (40), 29667–29677. doi:10.1074/jbc.M706457200
- Geisheker, M. R., Heymann, G., Wang, T., Coe, B. P., Turner, T. N., Stessman, H. A. F., et al. (2017). Hotspots of missense mutation identify neurodevelopmental disorder genes and functional domains. *Nat. Neurosci.* 20 (8), 1043–1051. doi:10.1038/nn.4589
- Glaser, F., Pupko, T., Paz, I., Bell, R. E., Bechor-Shental, D., Martz, E., et al. (2003). ConSurf: Identification of functional regions in proteins by surface-mapping of phylogenetic information. *Bioinformatics* 19 (1), 163–164. doi:10.1093/bioinformatics/19.1.163
- Glover, C. V. (1986). A filamentous form of Drosophila casein kinase II. *J. Biol. Chem.* 261 (30), 14349–14354. doi:10.1016/s0021-9258(18)67025-5
- Goel, R. K., Meyer, M., Paczkowska, M., Reimand, J., Frederick, V., Franco, V., et al. (2018). Global phosphoproteomic analysis identifies SRMS-regulated secondary signaling intermediates. *Proteome Sci.* 16, 16. doi:10.1186/s12953-018-0143-7
- Gotz, C., and Montenarh, M. (2017). Protein kinase CK2 in development and differentiation. *Biomed. Rep.* 6 (2), 127–133. doi:10.3892/br.2016.829
- Grant, B. D., Hemmer, W., Tsigelny, I., Adams, J. A., and Taylor, S. S. (1998). Kinetic analyses of mutations in the glycine-rich loop of cAMP-dependent protein kinase. *Biochemistry* 37 (21), 7708–7715. doi:10.1021/bi972987w
- Gu, T. L., Cherry, J., Tucker, M., Wu, J., Reeves, C., Polakiewicz, R. D., et al. (2010). Identification of activated Tnk1 kinase in Hodgkin's lymphoma. *Leukemia* 24 (4), 861–865. doi:10.1038/leu.2009.293
- Guerra, B., and Issinger, O.-G. (2008). Protein kinase CK2 in human diseases. *Curr. Med. Chem.* 15 (19), 1870–1886. doi:10.2174/092986708785132933
- Hecht, M., Bromberg, Y., and Rost, B. (2015). Better prediction of functional effects for sequence variants. *BMC Genomics* 16 (S8), S1. doi:10.1186/1471-2164-16-S8-S1
- Hériché, J.-K., Lebrin, F., Rabilloud, T., Leroy, D., Chambaz, E. M., Goldberg, Y., et al. (1997). Regulation of protein phosphatase 2A by direct interaction with casein kinase 2alpha. *Science* 276, 952–955. doi:10.1126/science.276.5314.952

- Hornbeck, P. V., Kornhauser, J. M., Tkachev, S., Zhang, B., Skrzypek, E., Murray, B., et al. (2012). PhosphoSitePlus: A comprehensive resource for investigating the structure and function of experimentally determined post-translational modifications in man and mouse. *Nucleic Acids Res.* 40 (Database issue), D261–D270. doi:10.1093/nar/ghr1122
- Huse, M., and Kuriyan, J. (2002). The conformational plasticity of protein kinases. *Cell* 109 (3), 275–282. doi:10.1016/s0092-8674(02)00741-9
- Ioannidis, N. M., Rothstein, J. H., Pejaver, V., Middha, S., McDonnell, S. K., Baheti, S., et al. (2016). Revel: An ensemble method for predicting the pathogenicity of rare missense variants. *Am. J. Hum. Genet.* 99 (4), 877–885. doi:10.1016/j.ajhg.2016.08.016
- Iossifov, I., O’Roak, B. J., Sanders, S. J., Ronemus, M., Krumm, N., Levy, D., et al. (2014). The contribution of de novo coding mutations to autism spectrum disorder. *Nature* 515 (7526), 216–221. doi:10.1038/nature13908
- Issinger, O. G., Brockel, C., Boldyreff, B., and Pelton, J. T. (1992). Characterization of the alpha and beta subunits of casein kinase 2 by far-UV CD spectroscopy. *Biochemistry* 31 (26), 6098–6103. doi:10.1021/bi00141a020
- Ji, H., Wang, J., Nika, H., Hawke, D., Keezer, S., Ge, Q., et al. (2009). EGF-induced ERK activation promotes CK2-mediated disassociation of alpha-Catenin from beta-Catenin and transactivation of beta-Catenin. *Mol. Cell* 36 (4), 547–559. doi:10.1016/j.molcel.2009.09.034
- Katoh, K., Rozewicki, J., and Yamada, Kazunori D. (2018). MAFFT online service: Multiple sequence alignment, interactive sequence choice and visualization. *Brief. Bioinform.* 4 (20), 1160–1166. doi:10.1093/bib/bbx108
- Korn, I., Gutkind, S., Srinivasan, N., Blundell, T. L., Allende, C., Allende, J. E., et al. (1999). Interactions of protein kinase CK2 subunits. *Mol. Cell. Biochem.* 191, 75–83. doi:10.1023/a:1006818513560
- Kornev, A. P., Taylor, S. S., and Ten Eyck, L. F. (2008). A helix scaffold for the assembly of active protein kinases. *Proc. Natl. Acad. Sci. U. S. A.* 105 (38), 14377–14382. doi:10.1073/pnas.0807988105
- Landau, M., Mayrose, I., Rosenberg, Y., Glaser, F., Martz, E., Pupko, T., et al. (2005). ConSurf 2005: The projection of evolutionary conservation scores of residues on protein structures. *Nucleic Acids Res.* 33 (Suppl. 2), 299–302. doi:10.1093/nar/gki370
- Landrum, M. J., Lee, J. M., Benson, M., Brown, G. R., Chao, C., Chitipiralla, S., et al. (2018). ClinVar: Improving access to variant interpretations and supporting evidence. *Nucleic Acids Res.* 46 (D1), D1062–D1067. doi:10.1093/nar/gkx1153
- Laudet, B., Barette, C., Dulery, V., Renaudet, O., Dumy, P., Metz, A., et al. (2007). Structure-based design of small peptide inhibitors of protein kinase CK2 subunit interaction. *Biochem. J.* 408 (3), 363–373. doi:10.1042/BJ20070825
- Lazarus, M. B., Nam, Y., Jiang, J., Sliz, P., and Walker, S. (2011). Structure of human O-GlcNAc transferase and its complex with a peptide substrate. *Nature* 469 (7331), 564–567. doi:10.1038/nature09638
- Lee, Y.-H., Park, J.-W., and Bae, Y.-S. (2016). Regulation of protein kinase CK2 catalytic activity by protein kinase C and phospholipase D2. *Biochimie* 121, 131–139. doi:10.1016/j.biochi.2015.12.005
- Lelieveld, S. H., Wiel, L., Venselaar, H., Pfundt, R., Vriend, G., Veltman, J. A., et al. (2017). Spatial clustering of de Novo missense mutations identifies candidate neurodevelopmental disorder-associated genes. *Am. J. Hum. Genet.* 101 (3), 478–484. doi:10.1016/j.ajhg.2017.08.004
- Li, J., Gao, K., Cai, S., Liu, Y., Wang, Y., Huang, S., et al. (2019). Germline de novo variants in CSNK2B in Chinese patients with epilepsy. *Sci. Rep.* 9 (1), 17909. doi:10.1038/s41598-019-53484-9
- Litchfield, D. W., Bosc, D. G., Canton, D. A., Saulnier, R. B., Vilks, G., Zhang, C., et al. (2001). Functional specialization of CK2 isoforms and characterization of isoform specific binding partners. *Mol. Cell. Biochem.* 227, 21–29. doi:10.1023/a:1013188101465
- Litchfield, D. W. (2003). Protein kinase CK2: Structure, regulation and role in cellular decisions of life and death. *Biochem. J.* 369 (Pt 1), 1–15. doi:10.1042/BJ20021469
- Lolli, G., Pinna, L. A., and Battistutta, R. (2012). Structural determinants of protein kinase CK2 regulation by auto-inhibitory polymerization. *ACS Chem. Biol.* 7, 1158–1163. doi:10.1021/cb300054n
- Lord, J., and Baralle, D. (2021). Splicing in the diagnosis of rare disease: Advances and challenges. *Front. Genet.* 12, 689892. doi:10.3389/fgene.2021.689892
- Lou, D. Y., Dominguez, I., Toselli, P., Landesman-Bollag, E., O’Brien, C., Seldin, D. C., et al. (2008). The alpha catalytic subunit of protein kinase CK2 is required for mouse embryonic development. *Mol. Cell. Biol.* 28 (1), 131–139. doi:10.1128/MCB.01119-07
- Lubner, J. M., Dodge-kafka, K. L., Carlson, C. R., Church, G. M., Chou, M. F., Schwartz, D., et al. (2018). Cushing’s Syndrome mutant PKA L205R exhibits altered substrate specificity. *FEBS Lett.* 591 (3), 459–467. doi:10.1002/1873-3468.12562
- Macias Alvarez, L., Revuelta-Cervantes, J., and Dominguez, I. (2013). “CK2 in embryonic development,” in *The wiley-IUBMB series on biochemistry and molecular biology: Protein kinase CK2*. Editor L. A. Pinna (Wiley-Blackwell Publishing, John Wiley & Sons, Inc).
- Manning, G., Whyte, D. B., Martinez, R., Hunter, T., and Sudarsanam, S. (2002). The protein kinase complement of the human genome. *Sci. (New York, NY)* 298 (5600), 1912–1934. doi:10.1126/science.1075762
- Marchiori, F., Meggio, F., Marin, O., Borin, G., Calderan, A., Ruzza, P., et al. (1988). Synthetic peptide substrates for casein kinase 2. Assessment of minimum structural requirements for phosphorylation. *Biochim. Biophys. Acta* 971 (3), 332–338. doi:10.1016/0167-4889(88)90149-8
- Martinez-Monseny, A. F., Casas-Alba, D., Arjona, C., Bolasell, M., Casano, P., Muchart, J., et al. (2020). Okur-Chung neurodevelopmental syndrome in a patient from Spain. *Am. J. Med. Genet. A* 182 (1), 20–24. doi:10.1002/ajmg.a.61405
- Mayrose, I., Graur, D., Ben-Tal, N., and Pupko, T. (2004). Comparison of site-specific rate-inference methods for protein sequences: Empirical Bayesian methods are superior. *Mol. Biol. Evol.* 9 (21), 1781–1791. doi:10.1093/molbev/msh194
- Meggio, F., Boldyreff, B., Marin, O., Pinna, L. A., and Issinger, O. G. (1992). Role of the beta subunit of casein kinase-2 on the stability and specificity of the recombinant reconstituted holoenzyme. *Eur. J. Biochem.* 204 (1), 293–297. doi:10.1111/j.1432-1033.1992.tb16636.x
- Meggio, F., and Pinna, L. A. (2003). One-thousand-and-one substrates of protein kinase CK2? *FASEB J.* 17 (3), 349–368. doi:10.1096/fj.02-0473rev
- Messenger, M. M., Saulnier, R. B., Gilchrist, A. D., Diamond, P., Gorbosky, G. J., Litchfield, D. W., et al. (2002). Interactions between protein kinase CK2 and Pin1. Evidence for phosphorylation-dependent interactions. *J. Biol. Chem.* 277 (25), 23054–23064. doi:10.1074/jbc.M200112000
- Michaelson, J. J., Shi, Y., Gujral, M., Zheng, H., Malhotra, D., Jin, X., et al. (2012). Whole-genome sequencing in autism identifies hot spots for de novo germline mutation. *Cell* 151 (7), 1431–1442. doi:10.1016/j.cell.2012.11.019
- Nakashima, M., Tohyama, J., Nakagawa, E., Watanabe, Y., Siew, C. G., Kwong, C. S., et al. (2019). Identification of de novo CSNK2A1 and CSNK2B variants in cases of global developmental delay with seizures. *J. Hum. Genet.* 64 (4), 313–322. doi:10.1038/s10038-018-0559-z
- Niefind, K., and Battistutta, R. (2013). “Structural bases of protein kinase CK2 function and inhibition protein kinase CK2,” in *The wiley-IUBMB series on biochemistry and molecular biology: Protein kinase CK2*. Editor L. A. Pinna (Wiley-Blackwell Publishing, John Wiley & Sons, Inc).
- Niefind, K., Guerra, B., Ermakowa, I., and Issinger, O. G. (2001). Crystal structure of human protein kinase CK2: Insights into basic properties of the CK2 holoenzyme. *EMBO J.* 20 (19), 5320–5331. doi:10.1093/emboj/20.19.5320
- Niefind, K., Guerra, B., Pinna, L. A., Issinger, O. G., and Schomburg, D. (1998). Crystal structure of the catalytic subunit of protein kinase CK2 from *Zea mays* at 2.1 Å resolution. *EMBO J.* 17 (9), 2451–2462. doi:10.1093/emboj/17.9.2451
- Niefind, K., and Issinger, O.-G. (2010). Conformational plasticity of the catalytic subunit of protein kinase CK2 and its consequences for regulation and drug design. *Biochim. Biophys. Acta* 1804 (3), 484–492. doi:10.1016/j.bbapap.2009.09.022
- Niefind, K., and Issinger, O.-G. (2005). Primary and secondary interactions between CK2alpha and CK2beta lead to ring-like structures in the crystals of the CK2 holoenzyme. *Mol. Cell. Biochem.* 274 (1–2), 3–14. doi:10.1007/s11010-005-3114-0
- Niefind, K., Pütter, M., Guerra, B., Issinger, O. G., and Schomburg, D. (1999). GTP plus water mimic ATP in the active site of protein kinase CK2. *Nat. Struct. Biol.* 6 (12), 1100–1103. doi:10.1038/70033
- Niefind, K., Yde, C. W., Ermakova, I., and Issinger, O.-G. (2007). Evolved to be active: Sulfate ions define substrate recognition sites of CK2alpha and emphasise its exceptional role within the CMGC family of eukaryotic protein kinases. *J. Mol. Biol.* 370 (3), 427–438. doi:10.1016/j.jmb.2007.04.068
- Okur, V., Cho, M. T., Henderson, L., Retterer, K., Schneider, M., Sattler, S., et al. (2016). De novo mutations in CSNK2A1 are associated with neurodevelopmental abnormalities and dysmorphic features. *Hum. Genet.* 135 (7), 699–705. doi:10.1007/s00439-016-1661-y
- Owen, C. I., Bowden, R., Parker, M. J., Jo, Patterson, Patterson, Joan, Price, S., et al. (2018). Extending the phenotype associated with the CSNK2A1-related okur-chung syndrome—a clinical study of 11 individuals. *Am. J. Med. Genet. A* 176 (5), 1108–1114. doi:10.1002/ajmg.a.38610
- Pargellis, C., Tong, L., Churchill, L., Cirillo, P. F., Gilmore, T., Graham, A. G., et al. (2002). Inhibition of p38 MAP kinase by utilizing a novel allosteric binding site. *Nat. Struct. Biol.* 9 (4), 268–272. doi:10.1038/nsb770

- Poirier, K., Hubert, L., Viot, G., Rio, M., Billuart, P., Besmond, C., et al. (2017). CSNK2B splice site mutations in patients cause intellectual disability with or without myoclonic epilepsy. *Hum. Mutat.* 38 (8), 932–941. doi:10.1002/humu.23270
- Pyrin, W., and Ackermann, K. (2003). The genes encoding human protein kinase CK2 and their functional links. *Prog. Nucleic Acid. Res. Mol. Biol.* 74, 239–273. doi:10.1016/S0079-6603(03)01015-8
- Raaf, J., Bischoff, N., Klopffleisch, K., Brunstein, E., Olsen, B. B., Vilk, G., et al. (2011). Interaction between CK2 α and CK2 β , the subunits of protein kinase CK2: Thermodynamic contributions of key residues on the CK2 α surface. *Biochemistry* 50 (4), 512–522. doi:10.1021/bi1013563
- Raaf, J., Brunstein, E., Issinger, O., and Niefind, K. (2008). The interaction of CK2 α and CK2 β , the subunits of protein kinase CK2, requires CK2 β in a preformed conformation and is enthalpically driven. *Protein Sci.* 17, 2180–2186. doi:10.1110/ps.037770.108
- Raaf, J., Issinger, O.-G., and Niefind, K. (2009). First inactive conformation of CK2 α , the catalytic subunit of protein kinase CK2. *J. Mol. Biol.* 386 (5), 1212–1221. doi:10.1016/j.jmb.2009.01.033
- Rahman, M. M., and Fatema, K. (2021). Genetic diagnosis in children with epilepsy and developmental disorders by targeted gene panel analysis in a developing country. *J. Epilepsy Res.* 11 (1), 22–31. doi:10.14581/jer.21004
- Reva, B., Antipin, Y., and Sander, C. (2011). Predicting the functional impact of protein mutations: Application to cancer genomics. *Nucleic Acids Res.* 39 (17), e118. doi:10.1093/nar/gkr407
- Rodrigues, C. H., Ascher, D. B., and Pires, D. E. (2018). Kinact: A computational approach for predicting activating missense mutations in protein kinases. *Nucleic Acids Res.* 46 (W1), W127–W132. doi:10.1093/nar/gky375
- Roffey, S. E., and Litchfield, D. W. (2021). CK2 regulation: Perspectives in 2021. *Biomedicines* 9 (10), 1361. doi:10.3390/biomedicines9101361
- Ruzzene, M., and Pinna, L. A. (2010). Addiction to protein kinase CK2: A common denominator of diverse cancer cells? *Biochim. Biophys. Acta* 1804 (3), 499–504. doi:10.1016/j.bbapap.2009.07.018
- Sakaguchi, Y., Uehara, T., Suzuki, H., Kosaki, K., and Takenouchi, T. (2017). Truncating mutation in CSNK2B and myoclonic epilepsy. *Hum. Mutat.* 38 (11), 1611–1612. doi:10.1002/humu.23307
- Sarno, S., Boldyreff, B., Marin, O., Guerra, B., Meggio, F., Issinger, O. G., et al. (1995). Mapping the residues of protein kinase CK2 implicated in substrate recognition: Mutagenesis of conserved basic residues in the α -subunit. *Biochem. Biophys. Res. Commun.* 206 (1), 171–179. doi:10.1006/bbrc.1995.1024
- Sarno, S., Ghisellini, P., and Pinna, L. A. (2002). Unique activation mechanism of protein kinase CK2. The N-terminal segment is essential for constitutive activity of the catalytic subunit but not of the holoenzyme. *J. Biol. Chem.* 277 (25), 22509–22514. doi:10.1074/jbc.M200486200
- Sarno, S., Vaglio, P., Marin, O., Issinger, O. G., Ruffato, K., Pinna, L. A., et al. (1997). Mutational analysis of residues implicated in the interaction between protein kinase CK2 and peptide substrates. *Biochemistry* 36 (39), 11717–11724. doi:10.1021/bi9705772
- Sarno, S., Vaglio, P., Meggio, F., Issinger, O. G., and Pinna, L. A. (1996). Protein kinase CK2 mutants defective in substrate recognition: Purification and kinetic analysis. *J. Biol. Chem.* 271 (18), 10595–10601. doi:10.1074/jbc.271.18.10595
- Schnitzler, A., and Niefind, K. (2021). Structural basis for the design of bisubstrate inhibitors of protein kinase CK2 provided by complex structures with the substrate-competitive inhibitor heparin. *Eur. J. Med. Chem.* 214, 113223. doi:10.1016/j.ejmech.2021.113223
- Schreiber, T. B., Mäusbacher, N., Kéri, G., Cox, J., and Daub, H. (2010). An integrated phosphoproteomics work flow reveals extensive network regulation in early lysophosphatidic acid signaling. *Mol. Cell. Proteomics* 9 (6), 1047–1062. doi:10.1074/mcp.M900486-MCP200
- Schrödinger, L. (2013). *The PyMOL molecular graphics system, version 1.7*. Available at: <https://pymol.org/>.
- Schwarz, J. M., Cooper, D. N., Schuelke, M., and Seelow, D. (2014). MutationTaster2: Mutation prediction for the deep-sequencing age. *Nat. Methods* 11 (4), 361–362. doi:10.1038/nmeth.2890
- Selvam, P., Jain, A., Cheema, A., Atwal, H., Forghani, I., Atwal, P. S., et al. (2021). Poirier-bienvenue neurodevelopmental syndrome: A report of a patient with a pathogenic variant in CSNK2B with abnormal linear growth. *Am. J. Med. Genet. A* 185 (2), 539–543. doi:10.1002/ajmg.a.61960
- Sim, N.-L., Kumar, P., Hu, J., Henikoff, S., Schneider, G., Ng, P. C., et al. (2012). SIFT web server: Predicting effects of amino acid substitutions on proteins. *Nucleic Acids Res.* 40 (W1), W452–W457. doi:10.1093/nar/gks539
- St-Denis, N. A., Derksen, D. R., and Litchfield, D. W. (2009). Evidence for regulation of mitotic progression through temporal phosphorylation and dephosphorylation of CK2 α . *Mol. Cell. Biol.* 29 (8), 2068–2081. doi:10.1128/MCB.01563-08
- Tang, H., and Thomas, P. D. (2016). PANTHER-PSEP: Predicting disease-causing genetic variants using position-specific evolutionary preservation. *Bioinformatics* 32 (14), 2230–2232. doi:10.1093/bioinformatics/btw222
- Tarrant, M. K., Rho, H.-S., Xie, Z., Jiang, Y. L., Gross, C., Culhane, J. C., et al. (2012). Regulation of CK2 by phosphorylation and O-GlcNAcylation revealed by semisynthesis. *Nat. Chem. Biol.* 8 (3), 262–269. doi:10.1038/nchembio.771
- Taylor, S. S., and Kornev, A. P. (2011). Protein kinases: Evolution of dynamic regulatory proteins. *Trends biochem. Sci.* 36 (2), 65–77. doi:10.1016/j.tibs.2010.09.006
- The Deciphering Developmental Disorders Study (2015). Large-scale discovery of novel genetic causes of developmental disorders. *Nature* 519 (7542), 223–228. doi:10.1038/nature14135
- Trembley, J. H., Chen, Z., Unger, G., Slaton, J., Kren, B. T., Van Waes, C., et al. (2010). Emergence of protein kinase CK2 as a key target in cancer therapy. *BioFactors* 36 (3), 187–195. doi:10.1002/biof.96
- Trinh, J., Hünig, I., Budler, N., Hingst, V., Lohmann, K., Gillesen-Kaesbach, G., et al. (2017). A novel de novo mutation in CSNK2A1: Reinforcing the link to neurodevelopmental abnormalities and dysmorphic features. *J. Hum. Genet.* 62 (1–1), 1005–1006. doi:10.1038/jhg.2017.73
- Vaglio, P., Sarno, S., Marina, O., Meggio, F., Issinger, O. G., Pinna, L. A., et al. (1996). Mapping the residues of protein kinase CK2 α subunit responsible for responsiveness to polyanionic inhibitors. *FEBS Lett.* 380 (1–2), 25–28. doi:10.1016/0014-5793(95)01542-6
- Valentino, F., Bruno, L. P., Doddato, G., Giliberti, A., Tita, R., Resciniti, S., et al. (2021). Exome sequencing in 200 intellectual disability/autistic patients: New candidates and atypical presentations. *Brain Sci.* 11 (7), 936. doi:10.3390/brainsci11070936
- Valero, E., Bonis, S. D., Filhol, O., Wade, R. H., Langowski, J., Chambaz, E. M., et al. (1995). Quaternary structure of casein kinase 2. Characterization of multiple oligomeric states and relation with its catalytic activity. *J. Biol. Chem.* 270 (14), 8345–8352. doi:10.1074/jbc.270.14.8345
- van der Werf, I. M., Jansen, S., de Vries, P. F., Gerstmanns, A., van de Vorst, M., Van Dijk, A., et al. (2020). Overrepresentation of genetic variation in the AnkyrinG interactome is related to a range of neurodevelopmental disorders. *Eur. J. Hum. Genet.* 28 (12), 1726–1733. doi:10.1038/s41431-020-0682-0
- Walker, C., Wang, Y., Olivieri, C., Karamafrooz, A., Casby, J., Bathon, K., et al. (2019). Cushing's syndrome driver mutation disrupts protein kinase A allosteric network, altering both regulation and substrate specificity. *Sci. Adv.* 5 (8), eaaw9298. doi:10.1126/sciadv.aaw9298
- Wang, T., Hoekzema, K., Vecchio, D., Wu, H., Sulovari, A., Coe, B. P., et al. (2020). Large-scale targeted sequencing identifies risk genes for neurodevelopmental disorders. *Nat. Commun.* 11 (1), 4932. doi:10.1038/s41467-020-18723-y
- Werner, C., Gast, A., Lindenblatt, D., Nickelsen, A., Niefind, K., Jose, J., et al. (2022). Structural and enzymological evidence for an altered substrate specificity in okur-chung neurodevelopmental syndrome mutant CK2 α (Lys198Arg). *Front. Mol. Biosci.* 9, 831693. doi:10.3389/fmolb.2022.831693
- Wu, R., Tang, W., Liang, L., Li, X., Ouyang, N., Meng, Z., et al. (2020). [Identification of a novel de novo variant of CSNK2A1 gene in a boy with Okur-Chung neurodevelopmental syndrome]. *Zhonghua Yi Xue Yi Chuan Xue Za Zhi* 37 (6), 641–644. doi:10.3760/cma.j.issn.1003-9406.2020.06.011
- Wu, R., Tang, W., Qiu, K., Li, X., Tang, D., Meng, Z., et al. (2021). Identification of novel CSNK2A1 variants and the genotype–phenotype relationship in patients with okur-chung neurodevelopmental syndrome: A case report and systematic literature review. *J. Int. Med. Res.* 49 (5), 1. doi:10.1177/0300060521101706310.1177/03000605211017063
- Wu, W., Sung, C. C., Yu, P., Li, J., and Chung, K. K. K. (2020). S-Nitrosylation of G protein-coupled receptor kinase 6 and Casein kinase 2 α modulates their kinase activity toward α -synuclein phosphorylation in an animal model of Parkinson's disease. *PLoS ONE* 15 (4), e0232019. doi:10.1371/journal.pone.0232019
- Xu, S., Lian, Q., Wu, J., Li, L., and Song, J. (2020). Dual molecular diagnosis of tricho-rhino-phalangeal syndrome type I and okur-chung neurodevelopmental syndrome in one Chinese patient: A case report. *BMC Genet.* 21 (1), 158. doi:10.1186/s12881-020-01096-w10.1186/s12881-020-01096-w
- Xu, X., Toselli, P. A., Russell, L. D., and Seldin, D. C. (1999). Globozoospermia in mice lacking the casein kinase II α ' catalytic subunit. *Nat. Genet.* 23 (1), 118–121. doi:10.1038/12729

Yang, S., Wu, L., Liao, H., Lu, X., Zhang, X., Kuang, X., et al. (2021). Clinical and genetic analysis of six Chinese children with Poirier-Bienvenu neurodevelopmental syndrome caused by CSNK2B mutation. *Neurogenetics* 22 (4), 323–332. doi:10.1007/s10048-021-00649-2

Yang-Feng, T. L., Zheng, K., Kopatz, I., Naiman, T., and Canaanil, D. (1991). Mapping of the human casein kinase II catalytic subunit genes: Two loci carrying the homologous sequences for the alpha subunit. *Nucleic Acids Res.* 19 (25), 7125–7129. doi:10.1093/nar/19.25.7125

Ye, J., Pavlicek, A., Lunney, E. A., Rejto, P. A., and Teng, C-H. (2010). Statistical method on nonrandom clustering with application to somatic mutations in cancer. *BMC Bioinforma.* 11 (1), 11. doi:10.1186/1471-2105-11-11

Yuen, R. K., Merico, D., Cao, H., Pellicchia, G., Alipanahi, B., Thiruvahindrapuram, B., et al. (2016). Genome-wide characteristics of de novo mutations in autism. *NPJ Genom. Med.* 1 (1), 160271–1602710. doi:10.1038/npgenmed.2016.27

Yuen, R. K. C., Merico, D., Bookman, M., Howe, L. J., Thiruvahindrapuram, B., Patel, R. V., et al. (2017). Whole genome sequencing resource identifies 18 new candidate genes for autism spectrum disorder. *Nat. Neurosci.* 20 (4), 602–611. doi:10.1038/nn.4524

Zhang, C., Vilk, G., Canton, D. A., and Litchfield, D. W. (2002). Phosphorylation regulates the stability of the regulatory CK2beta subunit. *Oncogene* 21 (23), 3754–3764. doi:10.1038/sj.onc.1205467

Frontiers in Molecular Biosciences

Explores biological processes in living organisms
on a molecular scale

Focuses on the molecular mechanisms
underpinning and regulating biological processes
in organisms across all branches of life.

Discover the latest Research Topics

[See more →](#)

Frontiers

Avenue du Tribunal-Fédéral 34
1005 Lausanne, Switzerland
frontiersin.org

Contact us

+41 (0)21 510 17 00
frontiersin.org/about/contact



Frontiers in Molecular Biosciences

